# Air Pollution Modeling and its Application XXI

# NATO Science for Peace and Security Series

This Series presents the results of scientific meetings supported under the NATO Programme: Science for Peace and Security (SPS).

The NATO SPS Programme supports meetings in the following Key Priority areas: (1) Defence Against Terrorism; (2) Countering other Threats to Security and (3) NATO, Partner and Mediterranean Dialogue Country Priorities. The types of meeting supported are generally "Advanced Study Institutes" and "Advanced Research Workshops". The NATO SPS Series collects together the results of these meetings. The meetings are co-organized by scientists from NATO countries and scientists from NATO's "Partner" or "Mediterranean Dialogue" countries. The observations and recommendations made at the meetings, as well as the contents of the volumes in the Series, reflect those of participants and contributors only; they should not necessarily be regarded as reflecting NATO views or policy.

**Advanced Study Institutes (ASI)** are high-level tutorial courses intended to convey the latest developments in a subject to an advanced-level audience

**Advanced Research Workshops (ARW)** are expert meetings where an intense but informal exchange of views at the frontiers of a subject aims at identifying directions for future action

Following a transformation of the programme in 2006 the Series has been re-named and re-organised. Recent volumes on topics not related to security, which result from meetings supported under the programme earlier, may be found in the NATO Science Series.

The Series is published by IOS Press, Amsterdam, and Springer, Dordrecht, in conjunction with the NATO Emerging Security Challenges Division.

**Sub-Series**

| | | |
|---|---|---|
| A. | Chemistry and Biology | Springer |
| B. | Physics and Biophysics | Springer |
| C. | Environmental Security | Springer |
| D. | Information and Communication Security | IOS Press |
| E. | Human and Societal Dynamics | IOS Press |

http://www.nato.int/science
http://www.springer.com
http://www.iospress.nl

**Series C: Environmental Security**

# Air Pollution Modeling and its Application XXI

edited by


## Douw G. Steyn
Department of Earth and Ocean Sciences,
The University of British Columbia, Vancouver, BC, Canada

and

## Silvia Trini Castelli
Institute of Atmospheric Sciences and Climate National Research Council CNR
Torino, Italy



Published in Cooperation with NATO Emerging Security Challenges Division

Proceedings of the 31st NATO/SPS International Technical Meeting on
Air Pollution Modeling and its Application
Torino, Italy
September 27 – October 1, 2010

Library of Congress Control Number: 2011933839

ISBN 978-94-007-1361-1 (PB)
ISBN 978-94-007-1358-1 (HB)
ISBN 978-94-007-1359-8 (e-book)
DOI 10.1007/978-94-007-1359-8

Published by Springer,
P.O. Box 17, 3300 AA Dordrecht, The Netherlands.

*www.springer.com*

*Cover illustration:* © Archivio Fotografico della Città di Torino e di Turismo Torino e Provincia

*Printed on acid-free paper*

*This volume is dedicated to the memory of Daewon Byun, friend, colleague and extraordinary air pollution modeller who attended the 31st ITM and many before that. He was taken from our midst on February 10th, 2011.*

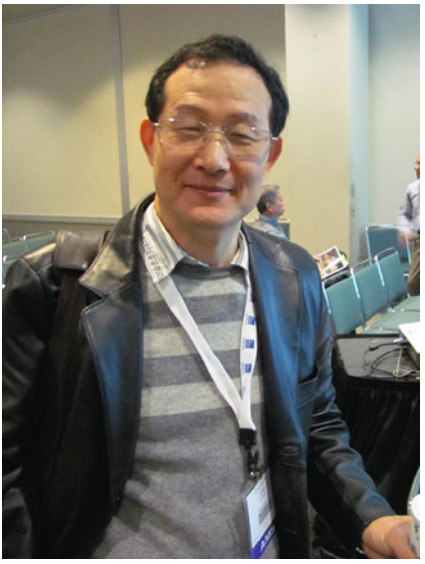

# Previous Volumes in this Mini-Series

Volumes I–XII were included in the NATO Challenges of Modern Society Series

Air Pollution Modeling and Its Applications I
Edited by C. de Wispelaere

Air Pollution Modeling and Its Applications II
Edited by C. de Wispelaere

Air Pollution Modeling and Its Applications III
Edited by C. de Wispelaere

Air Pollution Modeling and Its Applications IV
Edited by C. de Wispelaere

Air Pollution Modeling and Its Applications V
Edited by C. de Wispelaere, Francis A. Schiermeier, and Noor V. Gllani

Air Pollution Modeling and Its Applications VI
Edited by Han van Dop

Air Pollution Modeling and Its Applications VII
Edited by Han van Dop

Air Pollution Modeling and Its Applications VIII
Edited by Han van Dop and Douw G. Steyn

Air Pollution Modeling and Its Applications IX
Edited by Han van Dop and George Kallos

Air Pollution Modeling and Its Applications X
Edited by Sven-Erik Gryning and Millán M. Millán

Air Pollution Modeling and Its Applications XI
Edited by Sven-Erik Gryning and Francis A. Schiermeier

Air Pollution Modeling and Its Applications XII
Edited by Sven-Erik Gryning and Nadine Chaumerliac

Air Pollution Modeling and Its Applications XIII
Edited by Sven-Erik Gryning and Ekaterina Batchvarova

Air Pollution Modeling and Its Applications XIV
Edited by Sven-Erik Gryning and Francis A. Schiermeier

Air Pollution Modeling and Its Applications XV
Edited by Carlos Borrego and Guy Schayes

Air Pollution Modeling and Its Applications XVI
Edited by Carlos Borrego and Selahattin Incecik

Air Pollution Modeling and Its Applications XVII
Edited by Carlos Borrego and Ann-Lise Norman

Air Pollution Modeling and Its Applications XVIII
Edited by Carlos Borrego and Eberhard Renner

Air Pollution Modeling and Its Applications XIX
Edited by Carlos Borrego and Ana Isabel Miranda

Air Pollution Modeling and Its Applications XX
Edited by Douw G. Steyn and S. Trivikrama Rao

Air Pollution Modeling and Its Applications XXI
Edited by Douw G. Steyn and Silvia Trini Castelli

# Preface

In 1969, the North Atlantic Treaty Organization (NATO) established the Committee on Challenges of Modern Society (CCMS). From inception, the subject of air pollution was established as one of the priority problems for study within the framework of various pilot studies undertaken by this committee. The main activity relating to air pollution is the periodic organization of a conference series called **International Technical Meeting on Air Pollution Modeling and its Application** (ITM). Pilot Countries organizing these meetings have been: United States of America; Federal Republic of Germany; Belgium; The Netherlands; Denmark; Portugal and Canada.

This volume contains the abstracts of papers and posters presented at the 31st NATO/SPS ITM, held in Torino, Italy, from September 27 to October 1, 2010. This ITM was organized by the Institute of Atmospheric Sciences and Climate of the Italian National Research Council (Host Country) and The University of British Columbia (Pilot Country). Key topics presented at this ITM included: Local and urban scale modelling; Regional and intercontinental modelling; Data assimilation and air quality forecasting; Model assessment and verification; Aerosols in the atmosphere; Interactions between climate change and air quality; Air quality and human health.

The ITM was attended by 157 participants representing 36 countries. Invited papers were presented by Andrea Flossmann, France (Aerosols in the Atmosphere); Stefano Galmarini, Italy (Data Assimilation and Air Quality Forecasting); Joakim Langner, Sweden (Interactions between climate change and air quality) and Lawrence Reiter, USA (Air pollution and human health).

On behalf of the ITM Scientific Committee and as organizers and editors, we would like to thank all the participants who contributed to the success of the meeting. We especially recognize the organizational and support efforts of the chairpersons and rapporteurs, the staff at ISAC-CNR and Vincent Jeanson for the 31st ITM logo.

Finally, special thanks to the sponsoring institutions: ISAC CNR (Italy) and The University of British Columbia (Canada), and the sponsoring organizations NATO Science for Peace and Security; Environment Canada; Regione Piemonte; Camera di Commercio, Industria, Artigianato e Agricoltura di Torino; Torino Convention Bureau; Consiglio Regionale del Piemonte and European Association for the Science of Air Pollution (EURASAP). Regione Piemonte and Provincia di Torino gave their patronage to the Congress. A special grant was given by EUR-ASAP to award prizes to young researchers for the best paper or poster.

The next meeting will be held in May 2012 in Utrecht, The Netherlands.

Silvia Trini Castelli
Douw G. Steyn

# Members of the Scientific Committee for the 31st NATO/SPS International Technical Meeting (ITM) on Air Pollution Modelling and Its Application

| | |
|---|---|
| Ana Isabel Miranda | Portugal |
| Clemens Mensink | Belgium |
| Ekaterina Batchvarova | Bulgaria |
| Douw Steyn | Canada (Chair) |
| Sven-Erik Gryning | Denmark |
| Nadine Chaumerliac | France |
| Eberhard Renner | Germany |
| George Kallos | Greece |
| Domenico Anfossi | Italy |
| Trond Iversen | Norway |
| Carlos Borrego | Portugal |
| Josè Baldasano | Spain |
| Peter Builtjes | The Netherlands |
| Selahattin Incecik | Turkey |
| Anthony Dore | United Kingdom |
| S. Trivikrama Rao | United States of America |
| Werner Klug | Germany, Honorary Life Member |
| Han van Dop | The Netherlands, Honorary Life Member |
| Frank Schiermeier | United States of America, Honorary Life Member |

# History of NATO/CCMS (SPS) Air Pollution Pilot Studies

**Pilot Studies on Air Pollution International Technical Meetings (ITM) on Air Pollution Modelling and its Application**

**Dates and Locations of Completed Pilot Studies**

| | |
|---|---|
| 1969–1974 | Air Pollution Pilot Study (Pilot Country: United States of America) |
| 1975–1979 | Air Pollution Assessment Methodology and Modelling (Pilot Country: Germany) |
| 1980–1984 | Air Pollution Control strategies and Impact Modelling (Pilot Country: Germany) |

**Dates and Locations of Pilot follow-Up Meetings**

*Pilot Country - United States of America (R.A. McCormick, L.E. Niemeyer)*

| | | | |
|---|---|---|---|
| February | 1971 | Eindhoven, The Netherlands | First Conference on Low Pollution Power Systems Development. |
| July, | 1971 | Paris, France | Second Meeting of the Expert Panel on Air Pollution Modelling |

All subsequent meetings were supported by the NATO Committee for Challenges to Modern Society, and were designated NATO/CCMS International Technical Meetings (ITM) on Air Pollution Modelling and its Application, until 2007 when the designation changed to NATO/SPS with the creation of the NATO Committee on Science for Peace and Security.

| | | | |
|---|---|---|---|
| October | 1972 | Paris, France | 3rd ITM |
| May | 1973 | Oberursel, Federal Republic of Germany | 4th ITM |
| June | 1974 | Roskilde, Denmark | 5th ITM |

*Pilot Country - Germany (Erich. Weber)*

| | | | |
|---|---|---|---|
| September | 1975 | Frankfurt, Federal Republic of Germany | 6th ITM |
| September | 1976 | Airlie House, USA | 7th ITM |
| September | 1977 | Louvain-la-Neuve, Belgium | 8th ITM |

| | | | |
|---|---|---|---|
| August | 1978 | Toronto, Canada | 9th ITM |
| October | 1979 | Rome, Italy | 10th ITM |
| *Pilot Country - Belgium (C. De Wispelaere)* | | | |
| November | 1980 | Amsterdam, The Netherlands | 11th ITM |
| September | 1981 | Menlo Park, California, USA | 12th ITM |
| September | 1982 | Ile des Embiez, France | 13th ITM |
| September | 1983 | Copenhagen, Denmark | 14th ITM |
| April | 1985 | St. Louis, Missouri, USA | 15th ITM |
| *Pilot Country - The Netherlands (Han van Dop)* | | | |
| April | 1987 | Lindau, Federal Republic of Germany | 16th ITM |
| September | 1988 | Cambridge, United Kingdom | 17th ITM |
| May | 1990 | Vancouver, BC, Canada | 18th ITM |
| September | 1991 | Ierapetra, Greece | 19th ITM |
| *Pilot Country - Denmark (Sven-Erik Gryning)* | | | |
| November | 1993 | Valencia, Spain | 20th ITM |
| November | 1995 | Baltimore, Maryland, USA | 21st ITM |
| May | 1997 | Clermont-Ferrand, France | 22nd ITM |
| September | 1998 | Varna, Bulgaria | 23rd ITM |
| May | 2000 | Boulder, Colorado, USA | 24th ITM |
| *Pilot Country - Portugal (Carlos Borrego)* | | | |
| September | 2001 | Louvain-la-Neuve, Belgium | 25th ITM |
| May | 2003 | Istanbul, Turkey | 26th ITM |
| October | 2004 | Banff, Canada | 27th ITM |
| May | 2006 | Leipzig, Germany | 28th ITM |
| September | 2007 | Aveiro, Portugal | 29th ITM |
| *Pilot Country - Canada (Douw Steyn)* | | | |
| May | 2009 | San Francisco, California, USA | 30th ITM |
| September | 2010 | Torino, Italy | 31st ITM |

# List of Participants

The 31st NATO/SPS International Technical Meeting on Air Pollution Modeling and Its Application, Torino, Italy, September 27th - October 1st, 2010

**Argentina**

**Ulke Ana Graciela**
Ph. +54 11 4576 3356
Mail: ulke@at.fcen.uba.ar
Department of Atmospheric Sciences
University of Buenos Aires
Pabellon II - Piso 2° Ciudad Universitaria - 1428, Buenos Aires

**Australia**

**Lee Sunhee**
Ph. +61 3 9239 4551
Mail: sunhee.lee@csiro.au
CSIRO, Marine and Atmospheric Research
107–121 Str. - VIC 3150, Aspendale

**Austria**

**Arnold Delia**
Ph. +34 600057111
Mail: delia.arnold@boku.ac.at
Institute of Meteorology
University of Natural Resources and Applied Life Sciences
Peter-Jordan Str. 82–1190, Vienna

**Belgium**

**Cosemans Guido**
Ph. +32 1433 5511 / 5599
Mail: guido.cosemans@vito.be
VITO, TAP
Boeretang 200 - B2400 Mol

**Delcloo Andy**
Ph. 32 23730593
Mail: andy.delcloo@meteo.be
Royal Meteorological Institute of Belgium, Observations
Ringlaan 3 - B-1180 Ukkel

**Janssen Stijn**
Ph. +32 14336702
Mail: stijn.janssen@vito.be
VITO NV, RMA
Boeretang 200–2400 Mol

**Lefebvre Wouter**
Ph. +32 14336748
Mail: wouter.lefebvre@vito.be
VITO NV, RMA
Boeretang 200–2400 Mol

**Mensink Clemens**
Ph. +32 14336700
Mail: clemens.mensink@vito.be
VITO NV, RMA
Boeretang 200–2400 Mol

**Michiels Hans**
Ph. +32 14 33 58 91
Mail: hans.michiels@vito.be
VITO – Department of Transport & Mobility
Boeretang 200 – 2400 Mol

**Bulgaria**

**Batchvarova Ekaterina**
Ph. +359 887507283
Mail: ekaterina.batchvarova@meteo.bg
National Institute of Meteorology and Hydrology
Tzarigradsko Chaussee 66–1784, Sofia

**Todorova Angelina**
Ph. +359 2 9793708
Mail: imdnme@gmail.com
Department of Atmospheric Physics
Bulgarian Academy of Sciences
3, Acad. G. Bonchev str. - 1113, Sofia

**Canada**

**Antonopoulos Stavros**
Ph. +1 514 421 4772
Mail: stavros.andronopoulos@ec.gc.ca
Environment Canada
Canadian Meteorological Center
2121 Trans-Canada Highway - H9P 1J3 Dorval

**Bourgouin Pierre**
Ph. +1 514 421 5297
Mail: pierre.bourgouin@ec.gc.ca
Meteorological Service of Canada
CMC - EERS
2121 Trans - Canadienne - H9P 1J3 Dorval Quebec

**Daggupaty Sreerama**
Ph. 416 739 4451/4281
Mail: sam.daggupaty@ec.gc.ca
Environment Canada
4905 Dufferin Street - M3H 5T4 Toronto

**Davignon Didier**
Ph. +1 514 421 7242 / 4679
Mail: didier.davignon@ec.gc.ca
Environment Canada
Canadian Meteorological Center
2121 Trans-Canada Highway - H9P 1J3 Dorval

**Gong Wanmin**
Ph. 1 416 739 4883 / 4288
Mail: wanmin.gong@ec.gc.ca
Department of Science and Technology Branch
Environment Canada
4905 Dufferin Street - M3H 5T4 Toronto

**Moran Michael**
Ph. 416 739 5762
Mail: mike.moran@ec.gc.ca
Air Quality Research Division
Environment Canada
4905 Dufferin Street - M3H 5T4, Toronto, Ontario

**Steyn Douw G.**
Ph.+1 604 1827 5517
Mail: dsteyn@eos.ubc.ca
Department of Earth and Ocean Sciences
The University of British Columbia
6339 Stores Road V6T 1Z4, Vancouver, BC

**Chile**

**Ulloa Priscilla**
Ph. +56-2-2405768
Mail: pulloa@conama.cl
Department of Air Quality Management
Chilean Environmental protection agency (CONAMA)
Teatinos 258, piso 8–8340434, Santiago

**Croatia**

**Jericevic Amela**
Ph. +385 1 4565 787 / 630
Mail: jericevic@cirus.dhz.hr
Air Quality Research Department
Croatian Meteorological and Hydrological Service
Gric 3–10000, Zagreb
Cyprus

**Alexander de Meij**
Ph. +357 22 208 631 / 625
Mail: a.demeij@cyi.ac.cy
The Cyprus Institute, Energy, Environment and Water Research Center
15 Kypranoros Street – 1061, Nicosia

**Czech Republic**

**Fuka Vladimir**
Mail: vladimir.fuka@gmail.com
Faculty of Mathematics and Physics, Department of Meteorology
and Environmental Protection
Charles University
V. Holesovickach 2–18000, Prague

**Halenka Tomas**
Ph. +420 2 2191 2514 / 2533
Mail: Tomas.halenka@mff.cuni.cz
Faculty of Mathematics and Physics, Department of Meteorology
and Environmental Protection
Charles University
V Holesovickach 2–18000, Prague

**Kukacka Libor**
Ph. +420 266053203
Mail: kukacka@it.cas.cz
Institute of Thermomechanics AS CR, v.v.i, Environmental Aerodynamics
Dolejskova 1402/5 - 18020, Prague

**Denmark**

**Gryning Sven-Erik**
Ph. +45 46775005
Mail: sveg@risoe.dtu.dk
Risø National Laboratory for Sustainable Energy – DTU
Frederiksborgvej 399–4000 Roskilde, Denmark

**Silver Jeremy David**
Ph. +4546301154
Mail: jds@dmu.dk
Department of Atmospheric Environment
National Environmental Research Institute, Aarhus University
Frederikborgvej, 399 4000, Roskilde

**Egypt**

**Salem Mohamed Fathy Mahmoud**
Ph. +20 106639267
Mail: salemkairo@gmail.com
Department of Environmental Biology
Genetic Engineering and Biotechnology Research Institute, Minufiya University
GEBRI - P.O.Box: 79, Sadat City, Minufiya

**Estonia**

**Kaasik Marko**
Ph. +37 27355563
Mail: marko.kaasik@ut.ee
Institute of Physics
University of Tartu
Riia 142 – 51014, Tartu

**Loot Ardi**
Ph. +37 27355563
Mail: marko.kaasik@ut.ee
Institute of Physics
University of Tartu
Riia 142–51014, Tartu

**Ots Riinu**
Ph. +37 27355563
Mail: marko.kaasik@ut.ee
Institute of Physics
University of Tartu
Riia 142–51014, Tartu

**Finland**

**Kukkonen Jaakko**
Ph. +358505202684
Mail: jaakko.kukkonen@fmi.fi
Department of Air Quality Reasearch
Finnish Meteorological Institute
Erik Palmenin aukio1, P.O.Box 503, FI-00101 Helsinki

**Prank Marje**
Ph. +358 466841270
Mail: marje.prank@fmi.fi
Air Quality Research
Finnish Meteorological Institute
Erik Palmenin Aukio 1–00560, Helsinki

**Soares Joana**
Ph. +358 919 295 4 59
Mail: joana.soares@fmi.fi
Department of Air Quality
Finnish Meteorological Institute
Erik Palminen Aukio 1 00101, Helsinki

**Sofiev Mikhail**
Ph. +358 91919 5433
Mail: mikhail.sofiev@fmi.fi
Air Quality Research
Finnish Meteorological Institute
Erik Palmenin Aukio 1–00560, Helsinki

**Vira Julius**
Ph. +358 50 3746 246
Mail: julius.vira@fmi.fi
Air Quality Research
Finnish Meteorological Institute
Erik Palmenin Aukio 1–00560, Helsinki

**France**

**Carissimo Bertrand**
Ph. +33 0130877615
Mail: carissimo@cerea.enpc.fr
Ecole de Ponts, Paritech, CEREA
6–8 Avenue Blaise Pascal, Cite Descartes - 77455 Champs Sur Marne,
Marne La Valée

**Chaumerliac Nadine**
Ph. +33473407372
Mail: N.Chaumerliac@opgc.univ-bpclermont.fr
LaMP CNRS
Universitè Blaise Pascal
24, Av. des Landais 63177, Aubière

**Flossmann Andrea**
Ph. +33473407351
Mail: a.flossmann@opgc.univ-bpclermont.fr
Laboratoire de Météorologie Physique
Universitè Blaise Pascal
24, Av. des Landais 63171, Aubière Cedex

**Malherbe Laure**
Ph. +33 (0)3 44 55 62 18
Mail: laure.malherbe@ineris.fr
INERIS, CIVS
Parc Technologique Alata - BP7 - 60050 Verneuil en Halatte

**Qu Yongfeng**
Ph. +33 0130877217
Mail: yongfeng.qu@cerea.enpc.fr
Ecole de Ponts, Paritech, CEREA
6–8 Avenue Blaise Pascal, Cite Descartes - 77455, Champs Sur Marne

**Salizzoni Pietro**
Ph. +33 4 72186508
Mail: pietro.salizzoni@ec-lyon.fr
Laboratoire de Mecanique des Fluides et Acoustique
Ecole Centrale de Lyon
36, Av. Guy de Collogne - 69134, Ecully

**Tedeschi Gilles**
Ph. +33 494 142 589
Mail: tedeschi@univ-tin.fr
Department of LSEET
University of Toulon-Var
Av. G. Pompidou - 83162, La Vallette du Var

**Zaidi Hanane**
Ph. +33 0130877246
Mail: hanane.zaidi@edf.fr
Ecole de Ponts, Paritech, CEREA
6–8 Avenue Blaise Pascal, Cite Descartes - 77455 Champs Sur Marne

**Germany**

**Banzhaf Sabine**
Ph. +49 030 83871124
Mail: sabine.banzhaf@met.fu-berlin.de
Institute of Meteorology
Freie Universitaet Berlin
Carl-Heinrich-Becker-Weg 6–10 - 12165 Berlin

**Bieser Johannes**
Ph. +49 4152 87 2334
Mail: johannes.bieser@gkss.de
Institute for Coastal Research
GKSS Research
Max-Plank Str. - 21502 Geesthacht

**Graff Arno**
Ph. +49 340211032323
Mail: arno.graff@uba.de
Umweltbundesamt
Worlitzer Platz 1–06841, Dessau

**Kerschbaumer Andrea**
Ph. +49 030 83871129
Mail: andreas.kerschbaumer@fu-berlin.de
Institute of Meteorology
Freie Universitaet Berlin
Carl-Heinrich-Becker-Weg 6–10 - 12165 Berlin

**Renner Eberhard**
Ph. +49(341)2352320
Mail: renner@tropos.de
Department of Modelling
Leibniz Institut for Tropospheric Research
Permoserstrasse 15–04318 Leipzig

**Sandig Beate**
Ph. +49(341)2352860
Mail: saendig@tropos.de
Leibniz Institut for Tropospheric Research Leipzig
Permoserstrasse 15–04318, Leipzig

**Matthias Volker**
+49-40-4152-872346
Mail: Volker.matthias@gkss.de
GKSS Research Center
Institute for Coastal Research
Max Plank Strasse 1–21502 Gesthacht

**Wolke Ralf**
Ph. +49(341)2352860
Mail: wolke@tropos.de
Department of Modelling
Leibniz Institut for Tropospheric Research
Permoserstrasse 15–04318, Leipzig

**Greece**

**Douros Ioannis**
Ph. +30 2310996054
Mail: jdouros@aix.meng.auth.gr
Laboratory of Heat Transfer and Environmental Engineering
Aristotle University of Thessaloniki
University Campus - 54124, Thessaloniki

**Kallos George**
Ph. +30 210 7276835
Mail: kallos@mg.uoa.gr
School of Physics
University of Athens
University Campus Bldg. - PHYS – 15784, Athens

**Karatzas Kostas**
Ph. +30 2310996054
Mail: kkara@eng.auth.gr
Aristotle University of Thessaloniki
University Campus - 54124, Thessaloniki

**Solomos Stavros**
Ph. +30 210 7276835
Mail: stavros@mg.uoa.gr
School of Physics
University of Athens
University Campus Bldg. - PHYS - 15784, Athens

**Israel**

**Anteby Ido**
Ph. (972) 8 6518894
Mail: ido@bgu.ac.il
SOREQ
81800 Yavne

**Haikin Nitsa**
Mail: nitsah@nrcn.org.il
NRCN
P.O.B. 9001–84190 Beer Sheva

**Kaplan Hadassah**
Ph. 972 8 9381440
Mail: khadas1@gmail.com
IIBR, Applied Mahematics
Reuven Lerer 24, 99999, Ness-Ziona

**Kischa Pavel**
Ph. +972 54 5483217
Mail: pavel@cyclone.tau.ac.il
Geophysics and Planetary Sciences
Tel-Aviv University
Ramat Aviv - 69978 Tel-Aviv

**Lacser Avraham**
Ph. 97289381432
Mail: avilac@zahav.net.il
IIBR
POB 19–74100, Ness Ziona

**Levitin Yosef**
Ph. +972 3 9682133
Mail: jlevitin@yahoo.com
Research and Development
Israel Meteorological Service
P.O. Box 25–52050 Bet Dagan

**Mamane Yaacov**
Ph. +972 4 6360657
Mail: mamane@technion-ac.il
Department of Civil and Environmental Engineering
Technion - Israel Institute of Technology
32000, Haifa

**Reisin Tamir Gustavo**
Ph. (972) 89434287
Mail: treisin@soreq.gov.il
Department of Physics and nuclear engineering
Soreq Nuclear Research Center
81800 Yavne, Israel

**Tsadik Zamir**
Ph. 972252962562
Mail: tsadik@dsw.co.il
Department of Environment & Ecology
Dead Sea Works LTD
Potash House POB 75 – 84100, Be'er Sheva

**Italy**

**Alessandrini Stefano**
Ph. +39 02 39924624
Mail: stefano.alessandrini@erse-web.it
Department of ASV Environment and Sustainable Development
RSE S.p.A.
Via Rubattino 54, 20134, Milano

**Anfossi Domenico**
Ph. +39 0113839826
Mail: d.anfossi@isac.cnr.it
Italian National Research Council
Institute of Atmospheric Sciences and Climate
Corso Fiume 4–10133, Torino

**Angelino Elisabetta**
Ph. +39 02 69666721
Mail: e.angelino@arpalombardia.it
Environmental Protection Agency of Lombardy (ARPA Lombardia)
Viale Restelli 3/1 - 20124, Milano

**Balanzino Alessia**
Ph. +39 0131360151
Mail: alessia.balanzino@mfn.unipmn.it
Dipartimento di Scienze e Tecnologie Avanzate
Univeristà del Piemonte Orientale
Viale Teresa Michel 11–15121 Alessandria

**Baldi Marina**
Ph. +39 06 49937680
Mail: m.baldi@ibimet.cnr.it
IBIMET - CNR
Via Taurini, 19 – 00185, Roma

**Bedogni Marco**
Ph. +39 39733384
Mail: marco.bedogni@amat-mi.it
IBS Engineering sas
Via Isonzo, 24 – 20052, Monza

**Bianconi Roberto**
Ph. +39 039 6293636
Mail: info@enviroware.com
Enviroware srl
Via Dante,142-20049 Concorezzo

**Brusasca Giuseppe**
Ph. +39 02 2700 7255/8084
Mail: g.brusasca@aria-net.it
ARIANET SRL
ia Gillino 9–20128, Milano

**Carlino Giuseppe**
Ph. +39 011 9717302
Mail: g.carlino@simularia.it
Simularia S.r.L.
Via Principe Tommaso 39–10125, Torino

**Carnevale Claudio**
Ph. +39 0303715449
Mail: Carneval@ing.unibs.it
Department of Information Engineering
University of Brescia
Via Branze, 38 – 25123, Brescia

**Curci Gabriele**
Ph. +39 3295337701
Mail: gabriele.curci@aquila.infn.it
Department of Physics-Cetemps
University of L'Aquila
Via Vetoio, Coppito - 67010, L'Aquila

**De Maria Roberta**
Ph. +39 01119680286
Mail: r.demaria@arpa.piemonte.it
ARPA Piemonte
SC05 Sistemi Previsionali - SS03 Qualità dell'aria
Via Pio VII, 9–10135, Torino

**D'Isidoro Massimo**
Ph. +39 0151 6098905
Mail: massimo.disidoro@enea.it
Italian National Agency for New Technologies, Energy and Sustainable Economic Development
UTVALAMB - AIR
Via Martiri di Monte Sole, 4–40129 Bologna

**Falabino Simona**
Ph. +39 0113839828
Mail: simona.falabino@gmail.com
Institute of Atmospheric Sciences and Climate,
Italian National Research Council
Corso Fiume 4–10133 Torino

**Ferrero Enrico**
Ph. +39 0131360151
Mail: enrico.ferrero@mfn.unipmn.it
Dipartimento di Scienze e Tecnologie Avanzate
Univeristà del Piemonte Orientale
Viale Teresa Michel 11–15121 Alessandria

**Finardi Sandro**
Ph. +39 02 2700 7255/8084
Mail: s.finardi@aria-net.it
ARIANET SRL
Via Gillino 9–20128, Milano

**Galmarini Stefano**
Mail: stefano.galmarini@jrc.ec.europa.eu
Joint Research Centre
Institute for Environment and Sustainability
TP441 - 21027, ISPRA

**Garbero Valeria**
Ph. +39 011 5647556
Mail: valeria.garbero@polito.it
Department of Mathematics
Politecnico di Torino
Corso Duca degli Abruzzi 24–10129 Torino

**Laino Elisa**
Ph. +39 0252034988
Mail: elisa.laino@saipem.eni.it
SAIPEM S.p.A.
Via Martiri di Cefalonia 67–20098, San Donato Milanese

**Mircea Mihaela**
Ph. +39 0151 609 8650/8675
Mail: mihaela.mircea@enea.it
Italian National Agency for New Technologies, Energy
and Sustainable Economic Development
UTVALAMB - AIR
Via Martiri di Monte Sole, 4–40129 Bologna

**Mortarini Luca**
Ph. +39 0113839835
Mail: l.mortarini@isac.cnr.it
Institute of Atmospheric Sciences and Climate,
Italian National Research Council
Corso Fiume 4–10133 Torino

**Nanni Alessandro**
Ph. +39 02 2700 7255/8084
Mail: a.nanni@aria-net.it
ARIANET SRL
Via Gillino 9–20128, Milano

**Pernigotti Denise**
Ph. +39 0332 78 6574
Mail: denise.pernigotti@jrc.ec.europa.eu
European Commission
Joint Research Center
Department of Institute for Environment and Sustainability Action H4
Air Quality and Transport Modelling
Via E. Fermi 1 - I-21207, ISPRA Varese

**Radice Paola**
Ph. +39 02 2700 7255/8084
Mail: p.radice@aria-net.it
ARIANET SRL
Via Gillino 9–20128, Milano

**Solazzo Efisio**
Mail: efisio.solazzo@jrc.ec.europa.eu
Joint Research Centre-Institute for Environment and Sustainability
Via Enrico Fermi, 2749 21027, ISPRA

**Tinarelli Gianni**
Ph. +39 02 2700 7255/8084
Mail: g.tinarelli@aria-net.it
Arianet S.R.L
Via Gillino 9–20128, Milano, Italy

**Trini Castelli Silvia**
Ph. +39 0113839828
Mail: s.trinicastelli@isac.cnr.it
Institute of Atmospheric Sciences and Climate, National Research Council
Corso Fiume 4–10133, Torino, Italy

**Tuccella Paolo**
Ph. +39 3295337701
Mail: paolo.tuccella@aquila.infn.it
Department of Physics-Cetemps
University of L'Aquila
Via Vetoio, Coppito - 67010, L'Aquila

**Japan**

**Hama Takehide**
Ph. 075 753 6155
Mail: hama@kais.kyoto-u.ac.jp
Graduate School of Agriculture
Kyoto University
Kitashirakawa Oiwake-cho, Sakyo.ku - 606–8502, Kyoto

**Kitada Toshihiro**
Ph. +81 532 44 6902
Mail: kitada@earth.ens.tut.ac.jp
Department of Environmental and Life Sciences
Toyohashi University of Technology
Tempaku - cho - 441–8580, Toyohashi

**Shigeto Kavashima**
Ph. 90 6532 6328
Mail: sig@kais.kyoto-u.ac.jp
Graduate School of Agriculture
Kyoto University
Kitashirakawa Oiwake-cho, Sakyo.ku - 606–8502 Kyoto

**The Netherlands**

**Builtjes Peter**
Ph. +31 088 866 2017 / 2044
Mail: peter.builtjes@tno.nl
TNO, Air Quality and Climate
P.O. Box 8005–3508 TA, Utrecht

**Denier Vand Der Gon Hugo**
Ph. +31 088 8662024
Mail: hugo.deniervandergon@tno.nl
TNO
Princetonlaan 6–3584 CB, Utrecht

**Eskes Henk**
Ph. 31 30 2206352
Mail: eskes@knmi.nl
Deparment of Climate and Seismology
KNMI
P.O. Box 201–3730 AE, De Bilt

**Schaap Martijn**
Mail: martijn.schaap@tno.nl
TNOPO
BOX 80015–3508 TA Utrecht

**Van der Swaluw Eric**
Ph. +31 30 2748531
Mail: eric.van.der.swaluw@rivm.nl
National Institute for public Health and The Environment
Centre for Environmental Monitoring
P.O.Box 1 – Bilthoven

**Timmermans Renske**
Ph. +31 088 8662080
Mail: renske.timmermans@tno.nl
TNO
Princetonlaan 6–3508 TA, Utrecht

**New Zealand**

**Dirks Kim Natasha**
Ph. +64 9 3737 599 Ext. 89755
Mail: k.dirks@auckland.ac.nz
School of Population Health, Faculty of Medical and Health Sciences
University of Auckland
Private Bag 92019 – Auckland

**Norway**

**Denby Bruce Rolstad**
Ph. +47 63896164
Mail: bruce.denby@nilu.no
Norwegian Institute for Air Research (NILU)
PO Box 100–2027, Kjeller

**Iversen Trond**
Ph. +47 922 83 626
Mail: trond.iversen@met.no
Research Department and Department of Geosciences
Norwegian Meteorological Institute and University of Oslo,
P.O.Box 43, Blindern - 0313, Oslo

**Poland**

**Kryza Maciej**
Ph. +48-71348-54-41
Mail: kryzam@meteo.uni.wroc.pl.
Department of Climatology and Atmosphere Protection
Wroclaw University
Kosiby 6/8 51–670, Wroclaw

**Portugal**

**Borrego Carlos**
Ph. +351 234 400 800
Mail: c.borrego@ua.pt
CESAM and Department of Environment and Planning
University of Aveiro
Campus Universitario de Santiago, 3800–193, Aveiro

**Carvalho Anabela**
Ph. +35 1234370200
Mail: avc@ua.pt
Environment and Planning
University of Aveiro
Campus Universitario de Santiago - 3800–193, Aveiro

**Martins Helena**
Ph. +35 1234370220
Mail: hmartins@ua.pt
Environment and Planning
University of Aveiro
Campus Universitario de Santiago - 3800–193, Aveiro

**Miranda Ana Isabel**
Phone: +351 234 370200
Mail: miranda@ua.pt
University of Aveiro
3800–193, Aveiro

**Monteiro Alexandra**
Ph. +351 234 370 220
Mail: alexandra.monteiro@ua.pt
Environment and Planning
University of Aveiro
3800–193, Aveiro

**Russia**

**Genikhovich Eugene**
Ph. +7 812 297 8664
Mail: ego@main.mgo.rssi.ru
Department Air Pollution Modelling and Forecasting Lab
Voeikov Main Geophysical Observatory
Karbyshev St. 7, 194021, St. Petersburg

**Rakitin Anton**
Ph. +7 812 428 4347 / 7240
Mail: anton.v.rakitin@gmail.com
Faculty of Physics, Department of Atmospheric Physics
Saint-Petersburg State University
Ulyanovskaya 1–198504, Saint Petersburg

**Saudi Arabia**

**Al-Qahtani Jumaan**
Ph. 00966-3-8760406
Mail: Jumaan.qahtani@aramco.com
Saudi Aramco Department EPD
31311, Dhahran

**Serbia**

**Podrascanin Zorica**
Ph. 38 1637837815
Mail: zorica.podrascanin@gmail.com
Faculty of Science, Department of Physics
Dositej Obradovic Sq. 4–21000, Novi Sad

**Rajkovic Borivoj**
Mail: bora@ff.bg.ac.rs
Physics Faculty, Department of Meteorology
Dobracina 16–11000, Belgrade

**Slovenia**

**Boznar Marija Zlata**
Ph. +386 1 366 3226 / 3227
Mail: marija.zlata.boznar@meis.si
MEIS environmental consulting d.o.o
Mali Vrh pri Smarju 78–1293, Smarje-Sap

**Grasic Bostjan**
Ph. +386 1 366 3226 / 3227
Mail: bostjan.grasic@meis.si
MEIS environmental consulting d.o.o
Mali Vrh pri Smarju 78–1293, Smarje-Sap

**Spain**

**Arrizabalaga Ibarzabal Jon**
Ph. +34 94 607 33 00 / 49
Mail: jarrizabalaga@labein.es
Environment Unit
LABEIN – TECNALIA
Geldo - Parque Tecnologico de Bizkaia Ed. 700–48160, Derio

**Baldasano Jose M.**
Ph. +34 670282432
Mail: jose.baldasano@bsc.es
Department of Earth Sciences
Barcelona Supercomputing center (BSC - CNS)
c/ Jordi Girona 29–08034, Barcelona

**Dios Maria**
Ph. +34 981 563 100 ext. 16756
Mail: maria.dios@civusc.es
Chemical Engineering
University of Santiago de Compostela
ETSE, Lopez Gomez de Marzoa Str., Campus VIda - E-15782,
Santiago de Compostela

**Souto José A.**
Ph. +34 981 563 100 ext. 16757
Mail: ja.souto@usc.es
Chemical Engineering
University of Santiago de Compostela
ETSE, Lopez Gomez de Marzoa Str., Campus
VIda - E-15782 Santiago de Compostela

**Sweden**

**Langner Joakim**
Ph. +46 1149584
Mail: joakim.langner@smhi.se
Swedish Meteorological and Hydrological Institute
Folkborgsvagen 1 - SE-601, Norrkoping

**Switzerland**

**Aksoyoglu Sebnem**
Ph. +41 563102969
Mail: sebnem.aksoyoglu@psi.ch
Laboratory of Atmospheric Chemistry
Paul Scherrer Institute
5232 Villigen PSI

**Turkey**

**Incecik Selahattin**
Ph. +90 212 285 31 84
Mail: incecik@itu.edu.tr
Department of Meteorology
Instanbul Technical University
34469, Sariyer

**Toros Huseyin**
Ph. +90 212 285 31 84
Mail: toros@itu.edu.tr
Department of Meteorology
Instanbul Technical University
34469 Sariyer

**Ukraine**

**Biliaev Mykola**
Ph. +3-0956776957
Mail: envteam@ukr.net
Fluid Dynamics Department
Dnipropetrovsk National University of Railway Engineering
Lazaryana Str. 2, Dnepropetrovsk, Ukraine Dnipropetrovsk 49000

**Nochvai Volodymyr**
Ph. +38 044 4249168
Mail: fhvortex@yahoo.com
Pukhov Institute of Modelling Problems in Power Engineering
National Academy of Sciences of Ukraine
General Naumov str., 15–03164, Kiev

**United Kingdom**

**Cai Xiaoming**
Ph. 44 121 4145533
Mail. x.cai@bham.ac.uk
Geography, Earth and Environmental Sciences
University of Birmingham
B15 2TT Edgbaston, Birmingham

**Dore Anthony**
Ph. +44 131 445 8525
Mail: todo@ceh.ac.uk
Centre for Ecology and Hydrology
Bush Estate
EH26 9HF Penicuik, Midlothian

**Fisher Bernard**
Ph. +44 1189 535244
Mail: bernard.fisher@environment-agency.gov.uk
Department of Modelling and Risk
Environment Agency
Kings Meadow Road - RG1 8DQ Reading

**Heaviside Clare**
Ph. +44(0)1235827435
Mail: clare.heaviside@hpa.org.uk
Health Protection Agency
Centre for Radiation, Chemical & Environmental Hazards
Oxon OX 11 0RQ, Chilton, Didcot

**Savage Nicholas**
Ph. +44 01392 886519
Mail: nicholas.savage@metoffice.gov.uk
Met Office, Weather Science
Fitzroy Road, EX1 3PB Exeter

**Vardoulakis Sotiris**
+44(0)1235827435
Mail: sotiris.vardoulakis@hpa.org.uk
Health Protection Agency
Centre for Radiation, Chemical & Environmental Hazards
Oxon OX 11 0RQ, Chilton, Didcot

**USA**

**Appel Keith Wyat**
Ph. +1 919 541 0757
Mail: appel.wyat@epa.gov
Office of Research and Development
U.S. Environmental Protection Agency
109 T.W. Alexander Drive - 27711 Durham

**Arunachalam Saravanan**
Ph. 919-966-2126
Mail: sarav@email.unc.edu
Institute for the Environment
University of North Carolina
137, E.Franklin St., suite #656 27599–6116 Chapel Hill

**Garcia Valerie**
Ph. +1 919 541 2649 / 1379
Mail: garcia.val@epa.gov
Atmospheric Modeling & Analysis Division
U.S. Environmental Protection Agency
MD-E243-02, 109 T.W. Alexander Drive - 27711,
Research Triangle Park, NC

**Hanna Steven**
Ph. +1 207 967 4478
Mail: hannaconsult@roadrunner.com
Hanna Consultants
7 Crescent Ave - 04046 Kennebunkport Maine

**Hogrefe Christian**
Ph.+1 518-402-8402-
Mail: chogrefe@asrc.cestm.albany.edu
Department of Atmospheric Sciences Research Center
University of Albany
251 Fuller Road-NY 12203 Albany

**Isakov Vlad**
Ph. +1 919 541 2494 / 1379
Mail: isakov.vlad@epa.gov
Atmospheric Modeling & Analysis Division
U.S. Environmental Protection Agency
MD-E243-02, 109 T.W. Alexander Drive - 27711
Research Triangle Park, NC

**Lee Pius**
Ph. 301-713-0295 Ext 111
Mail: pius.lee@noaa.gov
Department of Air Resources Laboratory,
Office of Oceanic and Atmospheric Research
National Oceanic and Atmospheric Administration USA
1315 East-West Highway, SSMC3-Room 3316, MD 20910 Silver Spring

**Mathur Rohit**
Ph. +1 919 541 1483 / 1379
Mail: mathur.rohit@epa.gov
U.S. Environmental Protection Agency
Atmospheric Modeling & Analysis Division
MD-E243-03, 109 T.W. Alexander Drive - 27711,
Research Triangle Park, NC

**Mobley David**
Ph. +1 919 541 4676 / 1379
Mail: mobley.david@epa.gov
Atmospheric Modeling & Analysis Division
U.S. Environmental Protection Agency
MD-E243-02, 109 T.W. Alexander Drive - 27711,
Research Triangle Park, NC

**Napelenok Sergey**
Ph. +1 919 541 1135 / 1379
Mail: napelenok.sergey@epa.gov
National Exposure Research Laboratory
U.S. Environmental Protection Agency
MD-E243-04, 109 T.W. Alexander Drive - 27711,
Research Triangle Park, NC

**Pierce Thomas**
Ph. +1 919 541 1375 / 1379
Mail: pierce.tom@epa.gov
Atmospheric Modeling & Analysis Division
U.S. Environmental Protection Agency
MD-E243-04, 109 T.W. Alexander Drive - 27711,
Research Triangle Park, NC

**Pleim Jonathan**
Ph. +1 919 541 1336 / 1379
Mail: pleim.jon@epa.gov
Atmospheric Modeling & Analysis Division
U.S. Environmental Protection Agency
MD-E243-03, 109 T.W. Alexander Drive - 27711,
Research Triangle Park, NC

**Porter Steven P.**
Ph. +1 208 282 7974
Mail: porter@if.uidaho.edu
Department of Civil Engineering
University of Idaho
1776 Science Center - 83402, Idaho Falls, ID

**Ran Limei**
Ph. 1 919 966 2245
Mail: lran@unc.edu
Institute for the Environment
University of North Carolina at Chapel Hill
137 E.Franklin Str. Room 654–27599 - 6116, Chapel Hill

**Rao S.T.**
Ph. +1 919 541 4542 / 1379
Mail: rao.st@epa.gov
Atmospheric Modeling & Analysis Division
U.S. Environmental Protection Agency
MD-E243-02, 109 T.W. Alexander Drive - 27711,
Research Triangle Park, NC

**Reiter Lawrence W.**
Ph. +1 919 541 2106
Mail: reiter.larry@epa.gov
National Exposure Research Laboratory
U.S. Environmental Protection Agency
D305-01 4930 Page Road - 27711 Research Triangle Park, NC

**Schere Kenneth**
Ph. +1 919 541 3795 / 1379
Mail: schere.ken@epa.gov
Atmospheric Modeling & Analysis Division
U.S. Environmental Protection Agency
MD-E243-02, 109 T.W. Alexander Drive - 27711,
Research Triangle Park, NC

**Schiermeier Francis**
Ph. 919-467-5120
Mail: schiermeier@msn.com
EPA/NOAA Retired
303 Glasgow Road 27511, Cary, North Carolina

**Stajner Ivanka**
Ph. 1 703 610 2495
Mail: ivanka.stajner@noblis.org
NOAA/NWS and Noblis
3150 Fairview Park Drive South - 22042–4519, Falls Church VIrginia

**Tassone Caterina**
Ph. 301 7638000 ext 7723
Mail: caterina.tassone@noaa.gov
NOAA/NCEP/IMSG
5200 Auth Rd - MD 20746, Camp Springs

**Weil Jeff**
Ph. +1 303 497 8907
Mail: weil@ucar.edu
Research Application Lab
National Center for Atmospheric Research
3450 Mitchell Lane - 80301, Boulder Colorado

**Venkatram Akula**
Ph. +1 981 827 2195
Mail: venky@engr.ucr.edu
Riverside Department of Mechanical Engineering
University of California
3401 Watkins Dr. Bourns Hall B342 - 92521, Riverside

# Contents

**Part I Local and Urban Scale Modelling**

**1 Atmospheric Modelling Under Urban Land Use Changes: Meteorological and Air Quality Consequences** ..... 3
Helena Martins, Ana Isabel Miranda, and Carlos Borrego

**2 Comparison of RAMS, RMS and MSS Modelling Systems for High Resolution Simulations in Presence of Obstacles for the MUST Field Experiment** ..... 9
Silvia Trini Castelli, Tamir Gustavo Reisin, and Gianni Tinarelli

**3 The Role of Vegetation in Local and Urban Air Quality**..... 15
Clemens Mensink, B. De Maerschalck, B. Maiheu, S. Janssen, and J. Vankerkom

**4 Using a Coupled Meteorological and Chemical Transport Modelling Scheme to Evaluate the Impact of the Aerosol Direct Effect on Pollutant Concentration Fields in Paris** ..... 21
Gerold Halmer, Ioannis Douros, George Tsegas, and Nicolas Moussiopoulos

**5 CFD Simulations of Air Pollution in Urban Micro Environments** ..... 27
Stijn Janssen, Bart De Maerschalck, Irina Nikolova, Bino Maiheu, Jean Vankerkom, and Peter Vos

**6 Dispersion of Buoyant Emissions from Low Level Sources in Urban Areas**..... 33
Akula Venkatram, Sam Pournazeri, Marko Princevac, David Pankratz, and Qiguo Jing

**7 Comparison Between a Building Resolving Micro-Meteorogical Model and Measurements at SIRTA** ..... 39
Hanane Zaidi, X. Zhang, E. Dupont, M. Milliez, L. Musson-Genon, and Bertrand Carissimo

**8 A New Method for Buoyant Plume Rise Computation in Lagrangian Particle Models** ..... 45
Stefano Alessandrini, Domenico Anfossi, and Enrico Ferrero

**9 Influence of Wall Heating in a Street Canyon on Kinetic Energy and Scalar's Exchange: A Large-Eddy Simulation** ..... 51
Xiaoming Cai

**10 Stable Boundary Layer Modeling for Air Quality Applications** ..... 57
Jeffrey C. Weil

**11 Street Canyon Atmospheric Composition: Coupling Dynamics and Chemistry** ..... 63
Vivien Bianca Bright, William James Bloss, and Xiaoming Cai

**12 New Methods for Improvement of the Computational Efficiency of the Lagrangian Particle Dispersion Model** ..... 69
Boštjan Grašič, Marija Zlata Božnar, and Primož Mlakar

**13 Development of a Building Resolving Atmospheric CFD Code Taking into Account Atmospheric Radiation in Complex Geometries** ..... 75
Yongfeng Qu, Maya Milliez, Luc Musson-Genon, and Bertrand Carissimo

**14 A New Approach to Building Downwash Modelling** ..... 81
Guido Cosemans and Wouter Lefebvre

**15 Numerical Simulation of Indoor Air Pollution and Atmosphere Pollution for Regions Having Complex Topography** ..... 87
Mykola Mykolayevich Biliaiev and Mykola Mykolayevich Kharytonov

**16 The Canadian Urban Dispersion Modeling (CUDM) System: Prototype Evaluation over Vancouver 2010** ..... 93
Pierre Bourgouin, Richard Hogue, Najat Benbouta, Nils Ek, Jean-Philippe Gauthier, Nathalie Gauthier, Matthew Holly, Alexandre Leroux, Gilles Mercier, Serge Trudel, Calin Zaganescu, Stéphane Bélair, Eugene Yee, and Fue-Sang Lien

**17 Fast Model to Compute the Concentration Covariance of Two Passive Scalars from Their Mean Concentration Field** ..... 97
Luca Mortarini and Enrico Ferrero

**18 The Impact of Anthropogenic and Biogenic Emissions on Surface Ozone Concentrations in Istanbul: A Modeling Study** ..... 103
Ulaş İm, Anastasia Poupkou, Selahattin İncecik, Kostandinos Markakis, Tayfun Kindap, Dimitros Melas, Orhan Yenigün, Sema Topcu, Mehmet Talat Odman, Mete Tayanc, and Meltem Guler

**19 An Integrated System to Forecast PM10 Concentrations in an Urban Area, Using MODIS Satellite Data** ..... 107
Claudio Carnevale, Giovanna Finzi, Enrico Pisoni, Vikas Singh, Marialuisa Volta, Alessandra Cacciari, and Walter Di Nicolantonio

**20 Analysis of Scalar Fluxes and Flow Within Modelled Intersection Depending on the Approach Flow Direction** ..... 113
Libor Kukačka, Radka Kellnerová, Klára Jurčáková, and Zbyněk Jaňour

**21 Analysis of HIRLAM NWP Model During an Air Pollution Episode in Istanbul in 2009** ..... 119
Hüseyin Toros, Gertie Geertsema, Gerard Cats, and Selahattin İncecik

**22 WRF-ARW Simulation: Urban Area Scale Forecast for the Tel Aviv Metropolitan Area** ..... 125
Yosef Levitin

**23 Dispersion of Bioaerosols from a Wastewater Plant: An Experimental – Modellistic Approach** ..... 133
Roberta Bertari, Marco Achilli, and Marco Bedogni

**24 Dispersion and Deposition of Radioactive Particulate Matter from an Explosion** ..... 137
Vladimír Fuka and Josef Brechler

**25 Calculation of Standard Deviation of Concentration Using a Second-Order Closure Theory** ..... 143
Zorica Milivoj Podrascanin and Borivoj Rajkovic

**26 Simulating Building Downwash of Heavy Metals by Using Virtual Sources: Methodology and Results** ..... 147
Wouter Lefebvre, Guido Cosemans, Karen Van de Vel, Stijn Janssen, Clemens Mensink, David Celis, Frank Sleeuwaert, Hendrik Van Rompaey, and Frea Blommaert

**Part II Regional and Intercontinental Modelling**

**27 Air Quality Modelling and Source Apportionment Studies for Aerosols in Switzerland** ..... 155
Sebnem Aksoyoglu, J. Keller, C. Haeni, D. Oderbolz, A.S.H. Prevot, and U. Baltensperger

**28 High Ozone Levels in a Rural Mountainous Area: Where Does It Come from?** ..... 161
Carlos Borrego, Alexandra Monteiro, Anabela Carvalho, Helena Martins, Oxana Tchepel, Ana Isabel Miranda, A. Strunk, H. Elbern, Santiago Saavedra, Angel Rodríguez, José A. Souto, and J. Casares

**29 Development and Evaluation of an Ammonia Bi-Directional Flux Model for Air Quality Models** ..... 169
Jonathan E. Pleim, John Walker, Jesse Bash, and Ellen Cooter

**30 Extending the Applicability of the Community Multiscale Air Quality Model to Hemispheric Scales: Motivation, Challenges, and Progress** ..... 175
Rohit Mathur, Robert Gilliam, O. Russell Bullock Jr., Shawn Roselle, Jonathan Pleim, David Wong, Francis Binkowski, and David Streets

**31 The Urban Impact on the Regional Climate of Dresden** ..... 181
Beate Sändig and Eberhard Renner

**32 Incremental Development of Air Quality Forecasting System with Off-Line/On-Line Capability: Coupling CMAQ to NCEP National Mesoscale Model** ..... 187
Pius Lee, Fantine Ngan, Hyuncheol Kim, Daniel Tong, Youhua Tang, Tianfeng Chai, Rick Saylor, Ariel Stein, Daewon Byun, Marina Tsidulko, Jeff McQueen, and Ivanka Stajner

**33 Measuring and Modeling Wet Deposition Fluxes in the Netherlands and Europe** ..... 193
Eric Van der Swaluw, Martijn Schaap, Ferd Sauter, Sabine Banzhaf, and Astrid Manders

**34 Discrepancies Between Top-Down and Bottom-Up Emission Inventories of Megacities: The Causes and Relevance for Modeling Concentrations and Exposure** ..... 199
Hugo Denier Van der Gon, Sean Beevers, Alessio D'Allura, Sandro Finardi, Cécile Honoré, Jeroen Kuenen, Olivier Perrussel, Paola Radice, Jochen Theloke, Melinda Uzbasich, and Antoon Visschedijk

**35 Making High Resolution Air Quality Maps for Flanders, Belgium** ..... 205
Wouter Lefebvre, Stijn Janssen, Jean Vankerkom, Felix Deutsch, Nele Veldeman, Frans Fierens, Wim Peelaerts, Stijn Van Looy, Natacha Claeys, Tania Van Mierlo, and Filip Lefebre

**36 Development of an Agricultural Fertilizer Modeling System for Bi-Directional Ammonia Fluxes in the CMAQ Model** ..... 213
Limei Ran, Ellen Cooter, Verel Benson, and Qun He

**37 Air Quality Forecasting with LOTOS-EUROS in the Context of the MACC Project**..... 221
Henk Eskes, Martijn Schaap, Renske Timmermans, Lyana Curier, and Daan Swart

**38 Examining the Impact of an Updated Toluene Mechanism on Air Quality in the Eastern US** ..... 227
Golam Sarwar, K. Wyat Appel, Rohit Mathur, and Kenneth Schere

**39 Episodic High Surface Ozone in Central Japan in Warm Season: Relative Importance of Local Production and Long Range Transport** ..... 233
Toshihiro Kitada

**40 A European Chemical Weather Forecasting Portal** ..... 239
Kostas Karatzas, Jaakko Kukkonen, Tassos Bassoukos, Victor Epitropou, and Taru Balk

**41 Modeling the Impact of Urban Emissions in Russia on Air Quality in Northern Europe** ..... 245
M. Makarova, A. Rakitin, and D. Ionov

**42 Aerosol Load and Characteristics in Buenos Aires: Relationships with Dispersion Mechanisms and Sources in South America** ..... 251
Ana Graciela Ulke, Saulo Ribeiro Freitas, and Karla Maria Longo

**43 A Numerical Investigation of Endosulfan Impact to the Great Lakes Ecosystem** ..... 257
Sreerama M. Daggupaty and Jianmin Ma

**44 Bulgarian Emergency Response System for Release of Hazardous Pollutants – Design and First Tests** ..... 263
Angelina D. Todorova, Kostadin G. Ganev, Dimiter E. Syrakov, Maria Prodanova, Georgi J. Georgiev, Nikolai G. Miloshev, and Georgi K. Gadzhev

**45 Towards High-Resolution Environmental Modelling in the Alpine Region** ..... 269
Delia Arnold, Irene Schicker, and Petra Seibert

**46 Modelling the Impact of Best Available Techniques for Industrial Emissions Control in Air Quality** ..... 275
Angel Rodríguez, Santiago Saavedra, Maria Dios, Carmen Torres, Jose A. Souto, Juan J. Casares, Belen Soto, and Jose L. Bermúdez

**47 Changes in Sulphur and Nitrogen Deposition in Poland due to Domestic and European Emission Abatement** ..... 279
Maciej Kryza, Małgorzata Werner, Anthony James Dore, and Marek Błaś

**48 A Methodology for Quantifying the Contribution of Volcanic Ash to Urban Air Pollution** ..... 285
Kim Natasha Dirks, N. Singhal, G.L. Austin, M.A. Elangasinghe, and Alessandro Nanni

**49 Impact of Saharan Dust on PM10 Daily Exceedances over Italy During 2003–2005** ..... 289
Anna Pederzoli, Mihaela Mircea, Sandro Finardi, and Gabriele Zanini

**50 Intercomparison Between Two Air Pollution Simulations in Northern Italy Based on Different Emission Inventories** ..... 293
Alessia Balanzino, Enrico Ferrero, Guido Pirovano, Giuseppe M. Riva, and Mauro Causà

**51 Sea-Salt Aerosol Forecasts Compared with Wave Height and Sea-Salt Measurements in the Open Sea** ..... 299
Pavel Kishcha, B. Starobinets, R. Bozzano, S. Pensieri, E. Canepa, S. Nickovic, A. di Sarra, R. Udisti, S. Becagli, and P. Alpert

**52 Comparison of EMEP Emissions Inventory and Limited Area Bottom-Up Inventory in the Simulation of Air Quality by Means of CHIMERE** ..... 305
María Dios, C.M. Torres, A. Rodríguez, S. Saavedra, José A. Souto, and J.J. Casares

**53 Forecasting $O_3$, $PM_{25}$ and $NO_2$ Hourly Spot Concentrations Using an Updatable MOS Methodology** ..... 309
Stavros Antonopoulos, Pierre Bourgouin, Jacques Montpetit, and Gerard Croteau

**54 Coupling of the CTM CHIMERE to the High Resolution LAM ALADIN for Belgium** ..... 315
Andy W. Delcloo, Alex Deckmyn, Rafiq Hamdi, Herman Van Langenhove, Gilles Foret, and Hugo De Backer

**55 Impact of Saharan Dust on PM10 Concentrations in Farm model** ..... 321
Anna Pederzoli, Mihaela Mircea, Sandro Finardi, and Gabriele Zanini

**56 Contribution of Aviation Emissions on the Air Pollution Levels of the Mediterranean Region with the Use of an Online Coupled, Fully Integrated Modeling System** ..... 327
Jonilda Kushta, Stavros Solomos, and George Kallos

**57 Mixed Deterministic-Statistical Modelling of Regional Ozone Air Pollution** ..... 333
Stoitchko Dimitrov Kalenderski and Douw G. Steyn

**Part III Data Assimilation and Air Quality Forecasting**

**58 Efficacy of Incremental Reduction of Input Uncertainties to Improve Air Quality Prediction** ..... 341
Daewon W. Byun, Dae-Gyun Lee, Hyun-Cheol Kim, Soontae Kim, Fong Ngan, Beata Czader, Bernhard Rappenglueck, Shobha Kondragunta, and Brad Pierce

**59 LOTOS-EUROS Air Quality Forecasts by Assimilation of OMI Tropospheric NO2 Columns** ..... 347
Renske Timmermans, Henk Eskes, Peter Builtjes, Arjo Segers, Daan Swart, and Martijn Schaap

**60 Integrating $PM_{25}$ Observations, Model Estimates and Satellite Signals for the Eastern United States by Projection onto Latent Structures** ..... 353
P. Steven Porter, James J. Szykman, S.T. Rao, Edith L. Gégo, Christian Hogrefe, and Valerie Garcia

**61 Operational Chemical Weather Forecasting Models on a Regional Scale in Europe** ..... 359
J. Kukkonen, T. Balk, D.M. Schultz, A. Baklanov, T. Klein, A.I. Miranda, A. Monteiro, M. Hirtl, V. Tarvainen, M. Boy, V.-H. Peuch, A. Poupkou, I. Kioutsioukis, S. Finardi, M. Sofiev, R. Sokhi, K.E.J. Lehtinen, K. Karatzas, R.S. José, M. Astitha, G. Kallos, M. Schaap, E. Reimer, H. Jakobs, and K. Eben

**62 Forecasting Urban Air Quality over Cities by Statistical Adaptation of Deterministic Chemistry Transport Model Outputs** ..... 367
Laure Malherbe, Charlotte Songeur, Cécile Honoré, Anthony Ung, and Frédérik Meleux

**63 Scale Interaction in Air Quality Simulations by Means of a Nudging Technique** ..... 373
Massimo D'Isidoro, Alberto Maurizi, Felicita Russo, and Francesco Tampieri

**64 US National Air Quality Forecast Capability: Expanding Coverage to Include Particulate Matter** ..... 379
Ivanka Stajner, Paula Davidson, Daewon Byun, Jeffery McQueen, Roland Draxler, Phil Dickerson, and James Meagher

**65 On a Contribution of Wild-Land Fires on Atmospheric Composition in Arid Regions** ..... 385
Joana Soares, Janne Hakkarainen, Tatjana Ermakova, and Mikhail Sofiev

**66 An Assessment of a Real-Time Analysis and Its Impact on Dispersion Modeling** ..... 391
Caterina Tassone, Marina Tsidulko, Yanqiu Zhu, Lidia Cucurull, Geoff Manikin, Jeff McQueen, and Geoff DiMego

**67 An Air Quality Forecasting Tool over Italy (ForeChem)** ..... 397
Gabriele Curci

**68 Comparing Air Quality Forecast and a Reanalysis: Improvements Due to Chemical Data Assimilation and Better NWP Forcing** ..... 403
Julius Vira and Mikhail Sofiev

**69 Simulation of the Sensitivity of Rural Tropospheric Ozone Levels to BVOCs Emissions over a European Atlantic Coastal Region (Galicia, NW of Spain)** ..... 407
Angel Rodríguez, Santiago Saavedra, Jose A. Souto, and Juan J. Casares

**70 Ensemble Air Quality Forecasting: Effects of Perturbations in Meteorology and Emissions** ..... 411
Christian Hogrefe, Prakash Doraiswamy, Brian Colle, Kenneth L. Demerjian, Winston Hao, Mark Beauharnois, Michael Erickson, Matthew Souders, Jia-Yeong Ku, and Gopal Sistla

**Part IV Model Assessment and Verification**

**71 Multi-model Ensembles: Metrics, Indexes, Data Assimilation and All That Jazz** ..... 419
Stefano Galmarini and Slowomir Potempski

**72 Diagnostic Evaluation of Complex and Simple Atmospheric Chemical Transport Models by Considering Single Source Impacts in the UK** ..... 427
Bernard A. Fisher, Charles Chemel, Xavier V. Francis, Rong-Ming Hu, Ranjeet S. Sokhi, Garry D. Hayman, Keith J. Vincent, Tony Dore, Stephen Griffiths, Paul Sutton, and Ray D. Wright

**73 Construction and Performance Analysis of a Limited-Size Ensemble of Atmospheric Dispersion Simulations** ..... 433
Marje Prank, Mikhail Sofiev, Julius Vira, and Mirjam Paales

**74 On the Use of Principal Component and Spectral Density Analyses to Evaluate the Community Multiscale Air Quality (CMAQ) Model** ..... 439
Brian Eder, Wyat Appel, and Thomas Pierce

**75 Dynamic Model Evaluation of $NO_x$ Emissions Reductions on Ozone Concentrations in the Presence of Uncertain Emission Inventories** ..... 447
Sergey L. Napelenok, Kristen M. Foley, Daiwen Kang, Thomas Pierce, Rohit Mathur, and S. Trivikrama Rao

**76 Influence of Meteorological Input Parameters on Urban Dispersion Modelling for Traffic Scenario Analysis** ..... 453
Paolo Giambini, Pietro Salizzoni, Lionel Soulhac, and Andrea Corti

**77 Wet Deposition: Model Development and Evaluation** ..... 459
Sabine Banzhaf, Peter Builtjes, Andreas Kerschbaumer, Martijn Schaap, Eric van der Swaluw, Rainer Stern, and Eberhard Reimer

**78 Detailed Modeling of Dry Deposition over Germany** ..... 467
A. Kerschbaumer, T. Gauger, E. Hendriks, and P. Builtjes

**79 The Impact of Meteorological Uncertainties on the Prediction of PM in Urban Areas** ..... 473
Ralf Wolke, Jens Stoll, Alexander Smalla, Roland Schroedner, Oswald Knoth, and Eberhard Renner

**80 Setting Acceptance Criteria for Air Quality Models** ..... 479
Steven R. Hanna and Joseph Chang

**81 The Impact of Meteorology on Air Quality Simulations over the Po Valley in Northern Italy** ..... 485
Denise Pernigotti, Emilia Georgieva, Philippe Thunis, Cornelius Cuvelier, and Alexander de Meij

**82 Modeling Air Quality over Italy with MINNI Atmospheric Modeling System: From Regional to Local Scale** ..... 491
Mihaela Mircea, Gabriele Zanini, Gino Briganti, Andrea Cappelletti, Anna Pederzoli, Lina Vitali, Giandomenico Pace, Pietro Marri, Camillo Silibello, Sandro Finardi, and Giuseppe Calori

**83 Evaluation of Vertical Profiles in Mesoscale Meteorological Models Based on Observations for the COST728 Study of Winter 2003 PM Episodes in Europe** ..... 499
Sven-Erik Gryning, Ekaterina Batchvarova, Markus Quante, and Volker Matthias

**84 Performance Summary of the 2006 Community Multiscale Air Quality (CMAQ) Simulation for the AQMEII Project: North American Application** ..... 505
K. Wyat Appel, Shawn Roselle, George Pouliot, Brian Eder Thomas Pierce, Rohit Mathur, Kenneth Schere, Stefano Galmarini, and S.T. Rao

**85 Comparative Evaluation of Model Simulations of Regional Ozone and Particulate Matters for Two Distinct Summers over Eastern North America** ..... 513
Wanmin Gong, Junhua Zhang, Paul A. Makar, Michael D. Moran, Craig Stroud, Sylvie Gravel, Sunling Gong, and Balbir Pabla

**86 Dynamic Evaluation of Long-Term Air Quality Model Simulations over the Northeastern U.S.** ..... 519
Christian Hogrefe, Kevin Civerolo, Winston Hao, Eric E. Zalewsky, Jia-Yeong Ku, P. Steven Porter, S.T. Rao, and Gopal Sistla

**87 Aerosol Analysis and Forecast in the ECMWF Integrated Forecast System: Evaluation by Means of Case Studies** ..... 525
Alexander Mangold, Hugo De Backer, Andy Delcloo, Bart De Paepe, Steven Dewitte, Isabelle Chiapello, Yevgeny Derimian, Meloe Kacenelenbogen, Jean-Francois Léon, Nicolas Huneeus, Michael Schulz, Darius Ceburnis, Colin O'Dowd, Harald Flentje, Stefan Kinne, Angela Benedetti, Jean-Jacques Morcrette, and Olivier Boucher

**88 Objective Discrimination and Pooling Models in the Ensemble** ..... 529
Eugene Genikhovich, Tatiana Pavlova, and Alexander Ziv

**89 Implementation and Evaluation of a Comprehensive Emission Model for Europe** ..... 533
Johannes Bieser, A. Aulinger, V. Matthias, and M. Quante

**90 A Wintertime Local-to-Regional Scale Test Case Study of SILAM Model** ..... 539
Riinu Ots, Ardi Loot, and Marko Kaasik

**91 Air Pollution Dispersion Modeling Around Thermal Power Plant Šoštanj in Complex Terrain: Model Validation and Regulatory Planning** ..... 543
Marija Zlata Božnar, Boštjan Grašič, and Primož Mlakar

**Part V Aerosols in the Atmosphere**

**92 Will Pollution Reduce Precipitation?** ..... 549
Andrea I. Flossmann and Wolfram Wobrock

**93 Aerosol Simulation with Fully Coupled "Online" Meteorology-Chemistry Model WRF/Chem over Europe: Preliminary Results** ..... 559
Paolo Tuccella, Gabriele Curci, and Guido Visconti

**94 Human Health Impacts of PM2.5 and $NO_x$ Transport Air Pollution in Belgium** ..... 565
Hans Michiels, Felix Deutsch, Leo De Nocker, Steven Broekx, Leen Van Esch, and Luc Int Panis

**95 Effects of Airborne Particles on Cloud Formation and Precipitation: A Modeling Study** ..... 571
Stavros Solomos, Jonilda Kushta, and George Kallos

**96 Simulation of the Indirect Radiative Forcing of Climate Due to Aerosols by the Two-Way Coupled WRF-CMAQ over the Eastern United States** ..... 579
Shaocai Yu, Rohit Mathur, Jonathan Pleim, David Wong, Annmarie G. Carlton, Shawn Roselle, S.T. Rao, and Yang Shao

**97 Assessing the Anthropogenic Fugitive Dust Emission Inventory and Temporal Allocation Using an Updated Speciation of Particulate Matter** ..... 585
George Pouliot, Heather Simon, Prakash Bhave, Daniel Tong, David Mobley, Tom Pace, and Thomas Pierce

**98 Improvements to Wintertime Particulate-Matter Forecasting With GEM-MACH15** ..... 591
Michael D. Moran, Paul A. Makar, Sylvain Ménard, Radenko Pavlovic, Mourad Sassi, Paul-Andre Beaulieu, David Anselmo, Curtis J. Mooney, Wanmin Gong, Craig Stroud, Sunling Gong, and Junhua Zhang

**99 Improved CTM Boundary Conditions Using DREAM Desert Dust Forecasts: A Case Study over the Po Valley** ..... 599
Claudio Carnevale, Giovanna Finzi, Enrico Pisoni, Marialuisa Volta, Pavel Kishcha, Gabriele Curci, and P. Alpert

**100 Desert Dust Particle Distribution: From Global to Regional Scales** ..... 607
Marina Astitha, Alexander de Meij, Jos Lelieveld, and Andrea Pozzer

**101 Study of Vertical Transport of Marine Aerosol Using an Unsteady 2D Model** ..... 613
Gilles Tedeschi and J. Piazzola

**102 Comparing Monitoring-Based and Modeling-Based Approaches for Evaluating Black Carbon Contributions from a U.S. Airport** ..... 619
Saravanan Arunachalam, Alex Valencia, Dongmei Yang, Neil Davis, Bok Haeng Baek, Robin E. Dodson, Andres E. Houseman, and Jonathan I. Levy

**Part VI Interactions Between Air Quality and Climate Change**

**103 Modelling the Impact of Climate Change on Air Pollution over Europe Using the MATCH CTM Linked to an Ensemble of Regional Climate Scenarios** ..... 627
Joakim Langner, Magnuz Engardt, and Camilla Andersson

**104 Urban Impact on Air Quality in RegCM/CAMx Couple for MEGAPOLI Climate Change Study in High Resolution** ..... 637
Tomas Halenka, Peter Huszar, and Michal Belda

**105 Impact of Climate Change on Ozone Pollution in the Lower Fraser Valley, Canada** ..... 641
Christian Reuten, Bruce Ainslie, Peter Jackson, Ian McKendry, and Douw Steyn

**106 Impact of Global Warming on the Regional Climate Adjacent to the Great Lake Biwa** ..... 647
Takehide Hama, Shigeto Kawashima, and Koji Sato

**Part VII Air Quality and Human Health**

**107 Advancing Exposure Science and Its Applications** ..... 655
Lawrence W. Reiter

**108 An Investigation of the Impacts of Aviation Emissions on Future Air Quality and Health** ..... 663
Saravanan Arunachalam, Matthew Woody, Bok Haeng Baek, Uma Shankar, and Jonathan I. Levy

**109 Nitrogen Deposition in the UK: The Influence of Grid-Space and Time on the Exceedance of Critical Loads and Levels** ..... 669
Anthony James Dore, Małgorzata Werner, Stephen Hallsworth, Jane Hall, Christopher Dore, Maciej Kryza, Ron Smith, Ulrike Dragosits, Sim Tang, Massimo Vieno, and Mark Sutton

**110 Modelling of Particulate Matter: A Detailed Analysis of Sources and Abatement Strategies** ..... 675
Peter Builtjes, Wolfram Jörss, Rainer Stern, and Jochen Theloke

**111 Development and Evaluation of Alternative Metrics of Ambient Air Pollution Exposure for Use in Epidemiologic Studies** ..... 681
Vlad Isakov, James Crooks, Joe Touma, M. Valari, Halûk Özkaynak, Stefanie Ebelt Sarnat, Jeremy Sarnat, Priya Kewada, and James Mulholland

**112 Sub-grid Variability and Its Impact on Air Quality Exposure Assessment** ..... 687
Bruce Rolstad Denby, Massimo Cassiani, Jan Horálek, Peter de Smet, and Frank de Leeuw

**113 Cost-Effective Plans to Mitigate Air Quality Effects on Human Health in Northern Italy** ..... 693
Claudio Carnevale, Giovanna Finzi, Enrico Pisoni, Marialuisa Volta, and Fabian Wagner

**114 Enhanced Aerosol Formation and Nutrient Deposition by Ship Emissions in North Sea Coastal Regions** ..... 699
Volker Matthias, Ines Bewersdorff, Armin Aulinger, and Markus Quante

**115 Multi-objective Optimization of Emission Parameters for Air Pollution Models** ..... 705
Volodymyr Nochvai

**116 Characterizing the Exposure of Regional-Scale Air Quality in the Northeastern United States** ..... 711
Valerie C. Garcia, J. Crooks, E. Gego, S. Lin, and S.T. Rao

**117 Development and Evaluation of Land-Use Regression Models Using Modeled Air Quality Concentrations** ..... 717
Vlad Isakov, Markey Johnson, Joe Touma, and Halûk Özkaynak

**118 Pollen Dispersal and Hybridization Model for Risk Assessment of Genetically Modified Crops** ..... 723
Shigeto Kawashima and Takehide Hama

**119 The Impact of the Urban Air Pollution on the Human Health: A Case-Study in Turin** ..... 729
Valeria Garbero, A. Montalto, N. Lazovic, Pietro Salizzoni, S. Berrone, and Lionel Soulhac

**120 A New Canadian Modeling Platform for Policy Emission Reduction Scenarios: Year 2006 Configuration** ..... 733
Sophie Cousineau, Didier Davignon, Jack Chen, Annie Duhamel, Samuel Gilbert, Valérie Ménard, Radenko Pavlovic, Jacinthe Racine, Mourad Sassi, and Mehrez Samaali

**121 flexRISK – Flexible Tools for Assessment of Nuclear Risk in Europe** ..... 737
Delia Arnold, Klaus Gufler, Wolfgang Kromp, Helga Kromp-Kolb, Gabriele Mraz, Petra Seibert, Steven Sholly, Philipp Sutter and Antonia Wenisch

**122 Novel Approaches for Estimating Human Exposure to Air Pollutants** ..... 741
Tim Watkins, Lisa Baxter, Haluk Özkaynak, Vlad Isakov, and David Mobley

**123 Air Quality Trends in the U.S. Rocky Mountain Area** ..... 747
Steven R. Hanna, Dan Jaffe, P. Steven Porter, and Douglas Blewitt

**124 The Potential of Biofumigation in Solving Air Pollution in Developing Countries** ..... 753
Mohamed Fathy M. Salem

**Author Index** ..... 761

# Part I
# Local and Urban Scale Modelling

# Chapter 1
# Atmospheric Modelling Under Urban Land Use Changes: Meteorological and Air Quality Consequences

**Helena Martins, Ana Isabel Miranda, and Carlos Borrego**

**Abstract** Urban sprawl is altering the landscape and leading to changes in emissions and air quality. This study analyses the impacts of alternative urban growth patterns on air quality, through a 1-year application of a modeling system to Porto urban region (Portugal). MM5-CAMx was evaluated to define an adequate setup for the purpose of the study, namely the land use dataset and the spatial distribution of emissions. Two land use scenarios for Porto urban area were defined (SPRAWL and COMPACT). Modeling results revealed that SPRAWL leads to an aggravation of PM10 concentrations. For $O_3$, differences between scenarios were smaller. Finally, population exposure to pollutants is higher for COMPACT because more inhabitants are found in areas of higher concentrations.

**Keywords** Air quality • Modeling • Urban • Land use

## 1.1 Introduction

The last two centuries have seen a transformation of cities from relatively contained to widespread over kilometers of suburban land with commercial areas, office parks and housing developments. Urban planners have focused their attention on the type of urban structure that is more sustainable: compact or dispersed? Several empirical and modeling studies integrate land use and transport issues and its relation with urban structure; however, few explore the connection to air quality and human exposure. This study starts by identifying an adequate urban area, followed by the definition of two alternative urban development scenarios. An adequate air quality modeling system was selected and a suitable modeling configuration defined.

H. Martins (✉) • A.I. Miranda • C. Borrego
CESAM and Department of Environment and Planning, Campus Universitario de Santiago, University of Aveiro, Aveiro 3800-193, Portugal
e-mail: hmartins@ua.pt

D.G. Steyn and S. Trini Castelli (eds.), *Air Pollution Modeling and its Application XXI*, NATO Science for Peace and Security Series C: Environmental Security 4,
DOI 10.1007/978-94-007-1359-8_1, 

The land use scenarios were then tested through the application of the modeling system and the main findings discussed.

## 1.2 Porto Case Study Presentation

Southern Europe's urban areas are experiencing a change towards more dispersed growth. Porto, in Northern Portugal, is currently cited as an example of this trend [1]. Also, Porto area presents a poor air quality, with $O_3$ thresholds and PM10 limit values exceeded. The reference situation (BASE) of Porto urban area was analyzed regarding urban expansion, population and mobility, and established the basis for the development of two urban development scenarios: SPRAWL representing urban expansion, and COMPACT, symbolizing urban containment. The scenarios were developed over the CLC2000 land use, with the following results: in SPRAWL, built-up areas increased from 18% to 25%; in COMPACT, all urban growth is accommodated within already existent urban areas. Both scenarios were developed for a population of 2.2 million people.

## 1.3 Modelling System Setup

The simulations for the reference situation and for the scenarios were performed with the numerical models MM5 and CAMx. Figure 1.1 shows the domains setup and the location of the meteorological stations to be used in the validation.

For the sensitivity analysis to land use and emissions spatial distribution, an air pollution episode occurring from 3 to 6 June 2006 was selected. The analysis of the MM5 land use dataset (USGS24) and the CLC2000 datasets for the simulation domains, revealed significant differences, with the latter presenting a more realistic representation of urban areas. Therefore, the USGS24 land use was replaced by CLC2000, and simulations were conducted for both datasets. The simulations skill was evaluated through the quantitative error analysis by Keyser and Anthes [2], showing that CLC2000 yields better results, both for temperature and zonal wind component, with higher correlations and smaller errors.

For the air quality simulation the national emission inventory was disaggregated using: (i) population and fuel consumption data (traditional setup), and (ii) spatial surrogates calculated using land use and population data, according to [3] (improved setup). CAMx was applied for both spatial disaggregation schemes. Results were evaluated through comparison with data from the region's monitoring network and calculation of statistical parameters: correlation factor, bias and mean quadratic error; these parameters yielded higher skills for the improved setup.

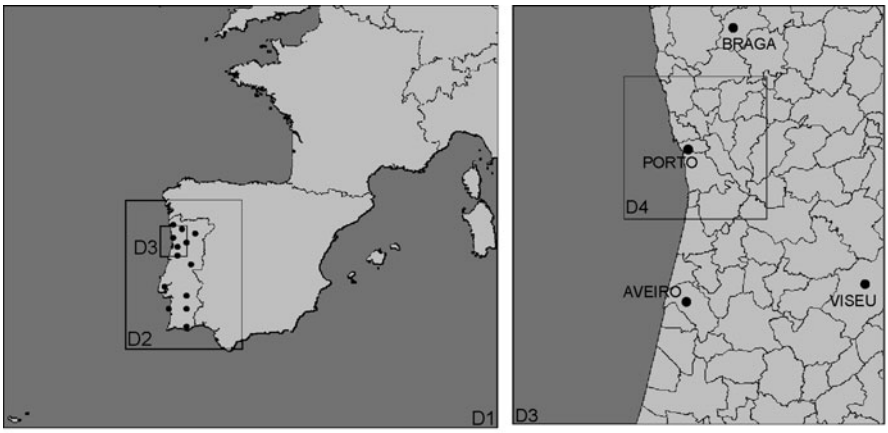


| Domain | No.cells in x | No.cells in y | Z levels | Resolution (km) |
|---|---|---|---|---|
| D1 | 91 | 77 | 25 | 27 |
| D2 | 63 | 81 | | 9 |
| D3 | 45 | 51 | | 3 |
| D4 | 51 | 51 | | 1 |

**Fig. 1.1** Modeling domains specification

## 1.4 Land Use – Air Quality Modelling Application

For the study of the impacts of land use changes in the Porto urban area the air quality modeling simulation was extended over a full-year of different meteorological conditions to cover a wide range of air pollution conditions. Meteorological modeling for the three cases (BASE, SPRAWL and COMPACT) was performed for 2006. SPRAWL produced a domain-averaged annual temperature increase of approximately 0.4°C, due to the increased share of built-up areas, which convert incoming radiation to sensible heat rather than to latent heat. As a result of the population growth and land use changes for each scenario, new emission totals and spatial distribution were calculated. A methodology accounting for land use and population changes was devised and implemented, resulting in SPRAWL emissions 9–17% higher than BASE emissions, and COMPACT emissions 4–6% higher than BASE. Figure 1.2 presents the spatial distribution of PM10 annual average concentrations, highlighting the areas for which the legislated annual limit value (40 μg $m^{-3}$) is exceeded.

BASE and COMPACT present a larger area of high PM10 annual averages over Porto municipality and its immediate surroundings. This is because the SPRAWL scenario implies a further decrease in Porto's population, and therefore emissions, and a consequent increase in neighboring municipalities. Considering the entire simulation domain, SPRAWL shows the highest PM10 annual concentrations and

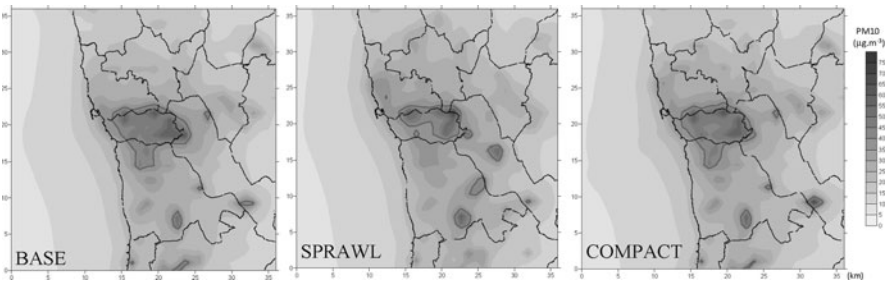


**Fig. 1.2** PM10 annual average for BASE, SPRAWL and COMPACT (The *grey lines* surround the areas for which the legislated annual limit value is exceeded)

larger areas above the annual limit value. Regarding the daily limit value a general aggravation of the situation is found for SPRAWL. $O_3$ summer average concentration differences are much smaller than those for PM10, ranging from −6 to +4 µg $m^{-3}$ between SPRAWL and BASE, from −1.5 to +2 µg $m^{-3}$ between COMPACT and BASE. Under the combined effects of increased urbanization and emissions, $O_3$ decreases are not unexpected due to $O_3$ removal by titration [4, 5].

The number of individuals affected by high concentrations was also determined, since the population distribution across the study area is quite different between scenarios. The maps of annual average concentrations were crossed with population data per grid cell. COMPACT presents the greatest share of population affected by PM10 concentrations above 40 µg $m^{-3}$ (17%) and the highest share of inhabitants affected by $O_3$ summer average concentrations above 70 µg $m^{-3}$ (48.5%). Notwithstanding the existence of higher concentrations in SPRAWL, results indicate that the dispersion of the population along the study region withdraws people from the areas of higher concentrations.

## 1.5 Conclusions

While the environmental implications of transport and industrial activities have been recognized and studied for decades, the study of the influence of urban structure on air quality is still in its early steps. Results from this study, conducted for a 1-year period for three distinct situations, indicate clearly that changes in land use patterns in urban areas lead to changes in meteorology, emissions, air quality, and population exposure. Sprawling urban areas, when compared to contained urban development, are responsible by higher temperatures, higher emissions of pollutants to the atmosphere, and higher atmospheric pollutants concentrations. However, compact urban developments imply a higher number of individuals exposed to the higher concentrations.

## References

1. Kasanko M, Barredo JI, Lavalle C, McCormick N, Demicheli L, Sagris V, Brezger A (2006) Are European cities becoming dispersed? A comparative analysis of fifteen European urban areas. Landscape Urban Plan 77:111–130
2. Keyser D, Anthes RA (1977) The applicability of a mixed-layer model of the planetary boundary layer to real-data forecasting. Mon Weather Rev 105:1351–1371
3. Maes J, Vliegen J, Vel KV, Janssen S, Deutsch F, Ridder K, Mensink C (2009) Spatial surrogates for the disaggregation of CORINAIR emission inventories. Atmos Environ 43:1246–1254
4. Civerolo KL, Sistla G, Rao ST, Nowak DJ (2000) The effects of land use in meteorological modelling: implications for assessment of future air quality scenarios. Atmos Environ 34:1615–1621
5. De Ridder K, Lefebre F, Adriaensen S et al (2008) Simulating the impact of urban sprawl on air quality and population exposure in the German Ruhr area. Part II: Development and evaluation of an urban growth scenario. Atmos Environ 42(30):7070–7077

## Questions and Answers

**Q**: The sprawling and compact urban distributions imply changes in activities distribution and traffic modification. How were those taken into account?

**A**: Since road transport emissions are highly dependent not only on population distribution but mainly on the mobility of the population, ideally a traffic model should be applied, however these modeling techniques fall out of the scope of the present work and therefore are not used. Instead, to calculate transport emissions resulting from land use changes, a methodology is developed taking into account the population growth, the urban area expansion and the mobility attractiveness/repulsion rates between municipalities:

i. The growth of the population causes an increase in the number of trips. For each municipality it was assumed that the emissions are proportional to the number of trips, which in turn is proportional to the number of residents.
ii. The growth of the urban area causes an increase in the mean distance from home to employments and leisure destinations. The residents in new urbanized areas find themselves more distant from locations where most employments are concentrated, while the residents in already existent urban areas will find possible employment and leisure destinations in the newly built areas in the periphery. For each municipality it was assumed that the emissions are proportional to the mean travel distance, which in turn is proportional to the urban area's radius.
iii. An additional factor related to attraction/repulsion rates between municipalities has to be considered since traffic emissions are not only dependent on the population and urban area, but also on the mobility of people between municipalities. The attraction/repulsion rates calculated for BASE were used for both scenarios.

**Q**: Did you consider changes in biogenic VOC emissions? If so, what was the magnitude of the effect on overall emissions and air quality?

**A**: Yes. The calculated differences in biogenic emissions result from the conversion of forested areas to artificial areas, and also from temperature changes induced by land use changes. As a result of land use changes biogenic SPRAWL emissions are 20% lower for monotherpene and 16% lower for isoprene when compared to BASE (and COMPACT). It's individual effect on air quality could not be estimated, since emission changes in the antropogenic activities also took place.

**Q**: With all those land use changes what about the dry deposition processes? How to they change and how are they important to results?

**A**: The modeling systems accounts for dry and wet deposition processes, however its changes were not analyzed in this study.

# Chapter 2
# Comparison of RAMS, RMS and MSS Modelling Systems for High Resolution Simulations in Presence of Obstacles for the MUST Field Experiment

**Silvia Trini Castelli, Tamir Gustavo Reisin, and Gianni Tinarelli**

**Abstract** The goal of this work is to investigate, compare and evaluate three different modelling approaches to describe pollutant dispersion at the microscale and in presence of obstacles. The observed data used as reference for the comparison are those of the Mock Urban Setting Test (MUST) field campaign, providing flow and dispersion data measured within an idealized urban roughness. A case in neutral conditions was chosen.

**Keywords** Urban flow • Eulerian and Lagrangian models • MUST experiment

## 2.1 The Case Study

Three modelling systems were tested on the case n. 2681829 of MUST field experiment, characterized by a neutral stratification [2]: (1) a version of the RAMS6.0 atmospheric model modified by us, RAMS6-mod, able to reproduce the meteorology at the microscale in presence of obstacles, working in an Eulerian frame; (2) the μRMS modelling system, a microscale version of the regional modelling system RMS composed by the interface of RAMS6-mod with MIRS

S.T. Castelli (✉)
Institute of Atmospheric Sciences and Climate, National Research Council,
Corso Fiume 4, Torino 10133, Italy
e-mail: s.trinicastelli@isac.cnr.it

T.G. Reisin
Department of Physics and Nuclear Engineering, Soreq Nuclear Research Center,
Yavne 81800, Israel
e-mail: treisin@soreq.gov.il

G. Tinarelli
Arianet – S.r.l, Via Gillino 9, Milan 20128, Italy
e-mail: g.tinarelli@aria-net.it

D.G. Steyn and S. Trini Castelli (eds.), *Air Pollution Modeling and its Application XXI*,
NATO Science for Peace and Security Series C: Environmental Security 4,
DOI 10.1007/978-94-007-1359-8_2, 

boundary layer and turbulence parameterization code and μSpray Lagrangian particle model; and (3) the MSS modelling system, where μSpray is driven by the diagnostic model μSwift and obstacles can be included.

The MUST data set provides flow and dispersion data measured within an idealized urban roughness, composed by an array of 120 containers (12.2 m long, 2.42 m wide, 2.54 m high), during an extensive field test carried out in the Great Basin Desert in 2001 test site. The terrain of the field site is characterized as 'flat open terrain' with a horizontally homogenous roughness, 0.5–1 m high. The observation fields were averaged over a reference period 300–500 s after the start of the observational period.

The applicability of RAMS6-mod in describing the dynamics and pollutant dispersion at high resolutions with obstacles was evaluated in Reisin and Trini Castelli [1]. This further work aims at (1) comparing the Lagrangian dispersion dynamics and the concentration fields with the outputs from the Eulerian run, using the same meteorological RAMS6-mod driving fields and (2) investigating the effect on the Lagrangian model performances induced by the meteorological processor driving the dispersion model, diagnostic (μSwift) or prognostic (RAMS6-mod), thus solving in a different way the boundary layer and turbulence parameterisations (Fig. 2.1).

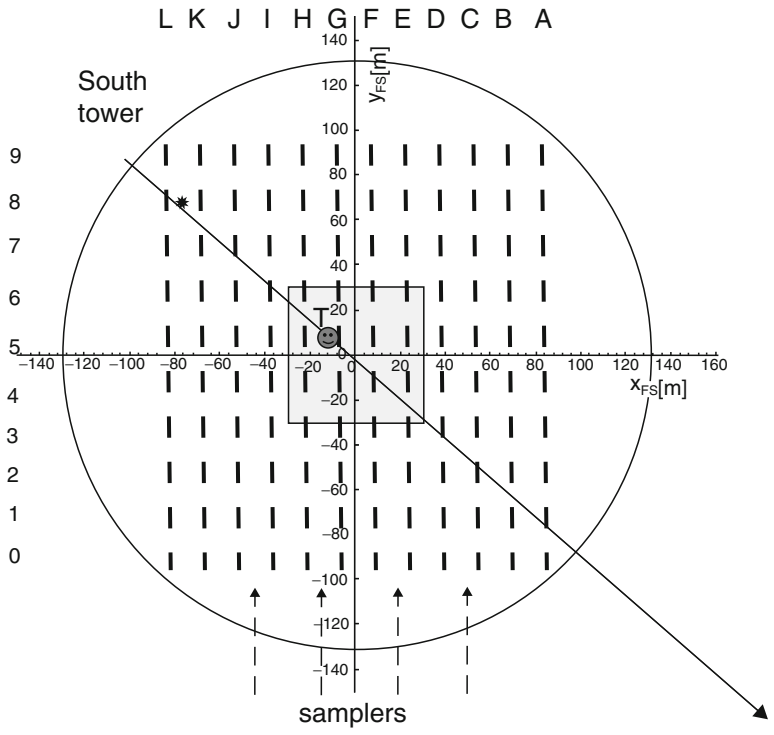


**Fig. 2.1** Geometry of MUST experiment (courtesy of Prof. B. Leitl for COST 732 Action), showing the direction of the incoming flow (*arrow*), the T tower location, the 119 containers and the service van. Note the labeling of the obstacles rows where samplers were placed

RAMS6-mod simulation domain extends 265 m in longitude and 321 m in latitude ($\Delta x = 0.8$ m, $\Delta y = 1.6$ m), with 35 stretched vertical levels ($\Delta z$ from 0.2 m up to 3.3 m), till a total height of 36 m. The timestep was $4 \times 10^{-3}$ s. The mean wind profile for the inflow was logarithmically extrapolated from the measured data available at three levels up to 16 m from the South tower. No initial profile was set for the turbulent kinetic energy (tke) and the $k$-ε turbulence closure scheme was used. The dispersion simulation was conducted using a passive tracer, released with a continuous emission at a height $z = 1.8$ m as in the case selected, after the model reached its quasi-steady condition.

In the μRMS system, the outputs of RAMS6-mod are processed through MIRS parameterization code and given as input to μSpray Lagrangian dispersion model. Thus, the same mean flow and turbulence as in RAMS6-mod are used but the dispersion is simulated with a Lagrangian-particle approach.

Instead, in the simulation performed with MSS the flow dynamics is built by μSwift from the same initial wind profile. The total turbulence is obtained summing the local one, produced by the flow distortion around the obstacles, plus a background level obtained by standard boundary layer parameterizations ([3], for neutral conditions). The local turbulence is estimated on the basis of a mixing-length closure, with the mixing length a function of the distance to the obstacle or the ground. It is assumed a homogeneity in the equation for the tke, imposing that its production and dissipation are in balance. In both μRMS and MSS simulations, the same emission conditions were used in μSpray runs: 400 particles per second were emitted and 13,000 particles moved during the stationary phase inside the computational domain; particles were sampled every 1 s after 500 s; the sampling period to compute concentrations corresponds to the 200 s of the experiment; ground level concentrations were computed between 0 and 0.5 m height.

## 2.2 Results and Discussion

In Fig. 2.2 the vertical profiles of speed and tke for RAMS6.0/μRMS and MSS runs and concentration for RAMS6.0, μRMS and MSS runs are plotted for tower T. We notice that the differences in the flow and turbulence fields are not negligible: μSwift tends to speed up the flow more than RAMS6-mod, its tke profile does not capture the observed maximum but better matches the measurements at higher levels, which might correspond to the background turbulence values. The predicted concentrations values are higher than the observed ones close to the surface and the maximum is found at different heights. In spite of the differences previously discussed, MSS concentration profile does not differ substantially from RAMS6-mod one. Instead, μRMS simulation better captures the concentrations above 10 m height, indicating that, with the same meteorology, μSpray Lagrangian plume spread is closer to the observed than with the Eulerian RAMS6-mod approach.

In Fig. 2.3 predictions are plotted versus the observations at the sensors displaced along the rows of the container arrays, at 1.6 m height. In general, simulations better match the observed data at the surface samplers than at the

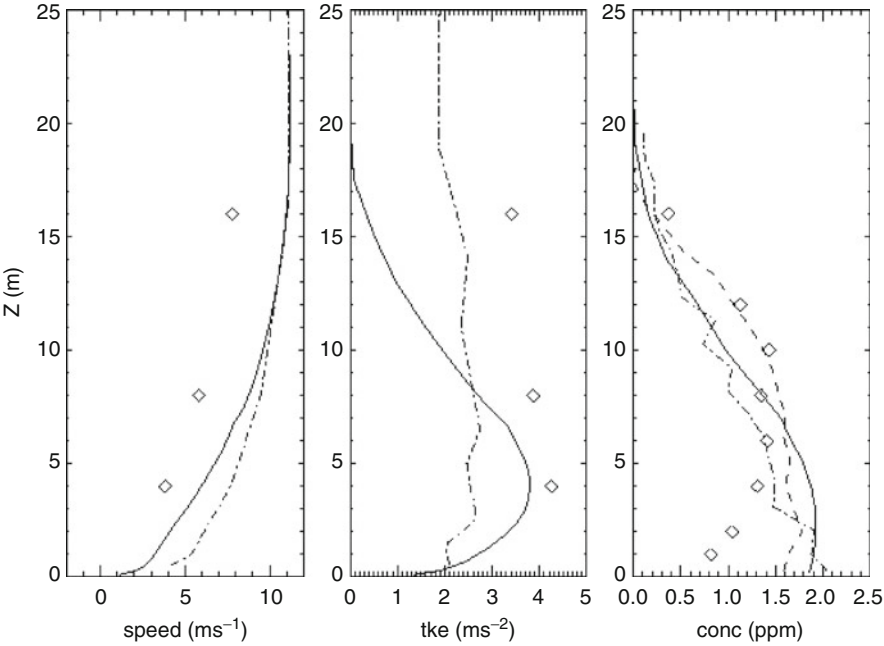


**Fig. 2.2** Wind speed, turbulence and concentration profiles at T tower. Diamonds: observations; *solid line*: RAMS6-mod; *dashed line*: μRMS; *dash-dotted line*: MSS

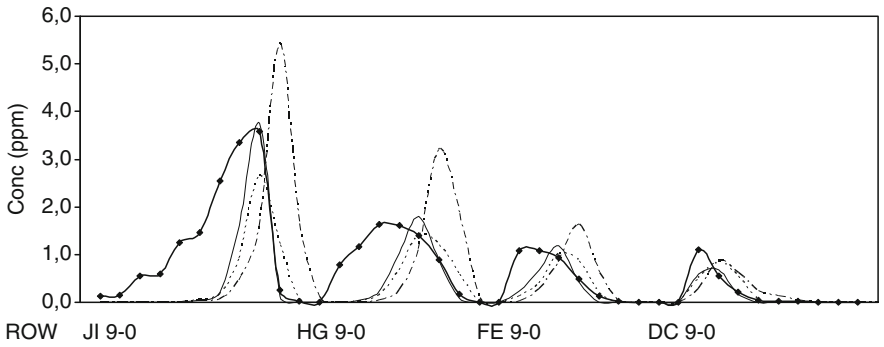


**Fig. 2.3** Concentration at the samplers along the obstacles array rows. Diamonds + line: observations, *solid line*: RAMS6-mod; *dashed line*: μRMS; *dash-dotted line*: MSS

vertical profiles. RAMS6-mod well captures the maximum, μRMS underestimates it while MSS overestimates it. In all simulations the plume spread is smaller than observed, especially at the rows closer to the source. This is probably due to a lesser deviation of the plume centreline with respect to the upwind direction than in the reality. This effect is enhanced in MSS run, which shows a displacement of the concentration field and of its maximum.

We conclude highlighting that, on the operational point of view, the fastest modelling system MSS ran the chosen case in a few minutes, while a full simulation of RAMS6-mod took several days.

## References

1. Reisin TG, Trini Castelli S (2010) Application of the atmospheric model RAMS to simulate high resolution urban flow – validation with the MUST Case. In: Steyn D, Rao ST (eds) Air pollution modeling and its application XX. Springer, Dordrecht (NL), pp 9–13
2. Yee E, Biltoft CA (2004) Concentration fluctuation measurements in a plume dispersing through a regular array of obstacles. Bound-Lay Meteorol 111:363–415
3. Hanna S (1982) Applications in air pollution modelling. In: Nieuwstadt F, Van Dop H (eds) Atmospheric turbulence and air pollution modelling. Reidel, Dordrecht (NL), pp 275–310

## Questions and Answers

**Questioner Name**: Mykola Biliaiev

**Q**: Any building is a "bluff body". It is known that k-ε model is not good for this turbulent flow. Why do not use, for example, "Large Eddy Simulations" procedure?

**A**: Of course you can use different modeling approaches. Our proposal and rationale here is to modify and apply an atmospheric model for using it in presence of obstacles. The atmospheric model applied here, RAMS, is a RANS model, where basically first-order closures are used. Therefore, we implemented in RAMS the k-ε turbulence closure scheme as done in CFD models, which also are RANS and are largely used in complex geometries such as the urban fabric.

**Questioner Name**: Steven Hanna

**Q**: Can you explain why the observed maximum concentration occurred at a height of 10 m, even though the source release height was much closer to the ground.

**A**: I am not able at present to provide a final answer, since we have been studying up to now a single case among the MUST experiments. It might be related to the presence of the obstacles, however we noticed that the concentrations measured at the samplers, placed close to the surface inside the array rows, may take rather different values with respect to the ones recorded at the masts at similar heights. In our runs for the concentration we found a better agreement of the predictions with the observations at the samplers than with the mast profiles. Dr. Bertrand Carissimo has a much larger experience in MUST case and considered different cases, so he may have a definitive answer.

**Bertrand Carissimo**: The plume is following the wind direction above the canopy but inside the canopy it is deflected by the buildings, following more the 'street canyons'. Therefore we can observe an elevated concentration maximum in the wind direction from the source, the higher concentrations below being deflected by the canopy in another direction.

# Chapter 3
# The Role of Vegetation in Local and Urban Air Quality

**Clemens Mensink, B. De Maerschalck, B. Maiheu, S. Janssen, and J. Vankerkom**

**Abstract** We present the outcome of the international conference 'Local Air Quality and its Interactions with Vegetation', which took place in Antwerp, Belgium on January 21-22, 2010. Results of international CFD studies, measurement campaigns and experimental studies show that vegetation can have an important effect on dispersion patterns determining local air quality. However, there are many parameters involved (vegetation structure, local meteorology, urban canopy characteristics, mechanical turbulence properties) and the results show that the complexity of the mechanisms of vegetation affecting local air quality are often underestimated.

**Keywords** Air pollution • Vegetation • Trees • CFD modeling • Street canyons • Highways

## 3.1 Introduction

While cities are expanding and population density within urbanized areas is increasing, more and more people are exposed to high levels of air pollution. This demographic evolution urges for accurate understanding of all processes affecting local air quality. One of these processes, which recently gained a lot of interest, both from scientists and policy makers, is the role of vegetation within urbanized areas. An important question posed by policy makers to scientists is whether or not vegetation can become an important instrument to improve local air quality.

The general perception is that trees and other forms of vegetation play important roles in our urban environment, although few attempts have been made to quantify the benefits they provide and to weigh these against any costs they may incur (Hewitt [8]). On the benefit side, it is known that trees and urban vegetation can

C. Mensink (✉) • B. De Maerschalck • B. Maiheu • S. Janssen • J. Vankerkom
VITO, Boeretang 200, Mol B-2400, Belgium
e-mail: clemens.mensink@vito.be

D.G. Steyn and S. Trini Castelli (eds.), *Air Pollution Modeling and its Application XXI*,
NATO Science for Peace and Security Series C: Environmental Security 4,
DOI 10.1007/978-94-007-1359-8_3, 

provide shade and cooling effects (by evapotranspiration), can increase thermal comfort, increase biodiversity, have aesthetic appeal, can provide heat insulation for buildings, can enhance water retention and provide humidity, can stimulate noise mitigation, can serve for recreation and community purposes, reduce $CO_2$ and enhance carbon storage, provide a habitat for birds and other fauna, and can remove pollutants from the atmosphere.

On the cost side, trees and urban vegetation require maintenance, can cause damage to buildings and roads and may contribute to the formation of ozone and secondary particulate matter by means of NMVOC emissions.

Today we know that vegetation can affect local air quality in various ways: e.g. by aerodynamic effects on local wind and turbulence fields, by absorption of gases and deposition of (ultra) fine particles, by cooling and shadowing effects in our densely urbanized areas. And although some of the *individual* interaction processes between air quality and vegetation are more or less well understood, it is still very difficult to understand the *overall* impacts of the vegetation on local air quality.

## 3.2 Methodology

We present the main findings on this topic presented at the *1st International Conference on Local Air Quality and its Interaction with Vegetation*, which took place on January 21–22, 2010 in Antwerp, Belgium and attracted 80 participants from 20 countries. The main focus is on the role of Computational Fluid Dynamics (CFD) modeling in supporting the state-of-the-art knowledge of plant-atmosphere interactions. Results are presented on three different scales: at the *plant level or micro-scale*, focusing on the direct interactions of air pollution and plants; at the *local scale*, focusing on air quality impacts of trees and vegetation on air quality near *highways* and in *street canyons*; and finally at the *urban or city scale*, focusing on air quality in entire cities and city quarters.

## 3.3 Results and Discussion

### *3.3.1 Interactions at the Plant Level (Micro Scale)*

Anatomical and morphological leaf parameters, and in particular stomatal characteristics, are very sensitive to air quality. A key modeling parameter is the stomatal resistance (Rs) expressesing the extent of the inhibition of gas diffusion through stomata. Changes in stomatal density and stomatal pore surface have an opposite influence on stomatal resistance. Rs is found to be significantly higher in polluted urban areas than at a background locations. Plants growing in more polluted environments adapt by forming more but smaller stomata, causing a net increase in stomatal resistance (Wuytack et al. [15]). The dependence of Rs on ambient air pollution concentrations is generally not reflected in deposition models.

Trees that don't emit the most reactive volatile organic compounds but do have large leaf surface areas have the best effects on air quality. Scots pine, common alder,

larch, Norway maple, field maple, ash and silver birch remove the most pollutants without contributing to the formation of new pollutants. Oak, poplar and willow can have detrimental effects through their NMVOC emissions (Hewitt [8]). In their assessment of the impact of biogenic and anthropogenic emissions on the urban Houston air, Leuchner and Rappenglück [11] find that biogenic sources mainly from isoprene play only a minor role at the urban site with 4.4% of the total measured NMHC mass. However during the afternoon, the ratio of biogenic to anthropogenic factors can be as high as 27%, and thus play an important role in the formation of photochemically produced secondary compounds and the production of radicals.

### 3.3.2 Interactions at the Local Scale: Near Highways

Hofschreuder et al. [9] reported on an extensive modeling and monitoring campaign along the A50 highway close to the village of Vaasen in the Netherlands. They concluded that vegetation along a road obstructs the wind, giving rise to less dilution and higher concentrations of NO and $NO_x$ at short distances from the road. The $NO_2$ concentration is however lower than in a situation without vegetation. Not only because of deposition of $NO_2$ but also because of less mixing in of ozone and hence lower production of $NO_2$ from NO. For $PM_{10}$ an increase in mass of 21% was found. This was related to an increase in relative humidity caused by the vegetation resulting in an increase in aerosol mass by water vapour uptake. Overall simulations using the ENVI-met model (De Maerschalck et al. [3] www.envi-met.com) were able to predict an increase of concentration close to the vegetation up to a few meters behind it, in agreement with measurements. Away from the vegetation a decrease in concentration was found (De Maerschalck et al. [4]).

### 3.3.3 Interactions at the Local Scale: In Street Canyons

In an overview on tree effects in street canyons, Di Sabatini et al. [6] report that some of the tree effects on flow and dispersion have been considered individually in previous works, such as deposition, filtration, blockage etc. but we are still far from a comprehensive understanding of the overall role plaid by vegetation on urban air quality. Although particle deposition on plant surfaces removes particles from the air, plants also represent obstacles to airflow which can reduce air mass exchange. Tree canopy models based on the k-ε model add extra terms in the transport equations to simulate these aerodynamic effects of trees, both on velocity decrease and increase in the turbulence and energy dissipation rate. Crown porosity, tree positioning and arrangement were identified as the major components affecting pollutant concentrations in urban street canyons.

The obstacle effect of trees was confirmed in a monitoring study performed in some street canyons in Amsterdam by Keuken et al. [10]. They concluded that reduced ventilation by trees dominates over absorption of air pollution to leaves. Wind tunnel studies performed by Gromke and Ruck [9] show a more complex situation. For the street canyons with trees of high crown porosity, they found an

increased concentration at the leeward wall (+58%) and a decrease at the windward wall (−30%) in comparison to the tree-free reference case.

In the extensive CFD study of Maiheu et al. [12], several street configurations with trees were compared. Next to an obvious reduction in wind velocity, they found a clear enhancement of the turbulent energy behind and above the tree buffers. This effect induces an increased vertical mixing of the pollutants. The effect of pollutant deposition is found to be relatively limited in comparison to the aerodynamic effects. They observed quite significant effects in the simulation on the pollutant concentrations at the leeward side of the canyon and a small decrease in concentrations at the windward side in the presence of the tree line.

### *3.3.4 Interactions at the Urban and City Scale*

Computer simulations for a large park area in Madrid (Spain) using CHIMERE showed that the presence of the park constitutes a sink of ambient ozone, due to the stomata up-taking of ozone by vegetation (Vivanco et al. [14]). The positive effect of vegetation on a larger urban scale was also confirmed by a monitoring study in Tel Aviv (Israel) (Cohen and Potchter [2]), showing that urban green spaces improve local climatic conditions and air quality (CO, $NO_x$ and $PM_{10}$).

A study for the city of Rome performed by Manes et al. [13] highlighted that both evergreen and deciduous species appeared to work well in the removal of urban air pollutants; however, the seasonal trends of $O_3$ and $PM_{10}$, and the year to year climatic variability may influence the efficiency of removal among the different leaf-types. A CFD study for the city of Lisbon (Amorin et al. [1]) using the URVE model focusing on CO concentrations revealed that the effect of trees on air quality is depending on meteorological conditions (e.g. wind direction), the aspect-ratio of the street-canyons, and the presence of vegetation.

Hewitt [8] reported the overall effects on air quality of very large scale planting of almost all tree species in cities would be highly positive. He demonstrated that doubling the amount of trees in the 900 $km^2$ West Midlands conurbation would reduce the concentration of fine particles by 25%, and would lead to a reduction of 140 deaths caused by airborne particles each year.

Gorbachevskaya and Schreiter [6] assessed the air pollution mitigation by extensive green roof systems in Berlin city centre (Germany). They found that these greening roof systems accumulate heavy metals and PAH, associated with fine dust particles of $PM_{2.5}$ and $PM_{10}$. The retention of the vegetation systems can be enhanced by adding substances which amplify the binding capacity of substrates (e.g. Bentonite-like Friedlander Ton).

Morani et al. (2010) discussed the MillionTreesNYC initiative. The City of New York has the ambitious goal to plant and care for one million new trees over the next decade. They found air quality improvements to increase with increased percent tree cover. They estimate that the new million trees planted in New York City will uptake an average of 7,300 metric tons of carbon for the total tree population per year and remove 9.7 g of air pollution per square meter of canopy cover ($g/m^2$) per year with a value of $ 527 per hectare of tree cover.

## 3.4 Conclusions

Results of international CFD studies presented at the international conference 'Local Air Quality and its Interactions with Vegetation' show that vegetation can have a significant effect on dispersion patterns determining local air quality. This is supported by the experimental studies and the results of the measurement campaigns presented at the conference. However, there are many parameters involved (vegetation structure, local meteorology, urban canopy characteristics, mechanical turbulence properties) and the CFD results show that the complexity of the mechanisms of vegetation affecting local air quality is often underestimated.

Plants can act as porous barriers. This barrier slows down the wind, depending on the size, type and porosity of the plant. However, less is known on the spatial range of this effect and how it is depending on atmospheric turbulence. Also the complex interaction of vegetation and turbulent energy is less understood.

Vegetation parameters like stomatal resistance are strongly depending on stomatal density and stomatal pore surface. These parameters are strongly influenced by air pollution. However in most of the known actual deposition models these feedback mechanisms are not taken into account.

## References

1. Amorin JH, Rodrigues V, Borrego C, Costa AM (2010) A CFD analysis of the vegetative canopy effect on urban air pollutants dispersion, in: Proceedings of the CLIMAQS Workshop 'Local Air Quality and its Interactions with Vegetation' January 21–22, 2010, Antwerp, Belgium, 104–108
2. Cohen P, Potchter O (2010) Daily and seasonally air quality characteristics of urban parks in the Mediterranean city of Tel Aviv, in: Proceedings of the CLIMAQS Workshop 'Local Air Quality and its Interactions with Vegetation' January 21–22, 2010, Antwerp, Belgium, 17–21
3. De Maerschalck B, Janssen S, Vankerkom J, Mensink C, van den Burg A, Fortuin P (2009) CFD simulations of the impact of a line vegetation element along a motorway on local air quality. Proc. 12th Int. Conf. on Harmonisation within Atmospheric Dispersion Modelling for Regulatory Purposes, Cavtat (Croatia), October 6–9
4. De Maerschalck B, Maiheu B, Janssen S, Vankerkom J (2010) CFD-modeling of complex plant-atmosphere interactions: direct and indirect effects on local turbulence, in: Proceedings of the CLIMAQS Workshop 'Local Air Quality and its Interactions with Vegetation' January 21–22, 2010, Antwerp, Belgium, 119–123
5. Di Sabatini S, Buccolieri R, Gromke C (2010) CFD modelling of tree-atmosphere interaction and assessment of air quality in street canyons, in: Proceedings of the CLIMAQS Workshop 'Local Air Quality and its Interactions with Vegetation' January 21–22, 2010, Antwerp, Belgium, 83–87
6. Gorbachevskaya O, Schreiter H (2010) Contribution of extensive building naturation to air quality improvement, in: Proceedings of the CLIMAQS Workshop 'Local Air Quality and its Interactions with Vegetation' January 21–22, 2010, Antwerp, Belgium, 137–141
7. Gromke C, Ruck B (2010) Interaction of traffic pollutant dispersion with trees in urban street canyons, in: Proceedings of the CLIMAQS Workshop 'Local Air Quality and its Interactions with Vegetation' January 21–22, 2010, Antwerp, Belgium, 93–97
8. Hewitt N (2010) Trees and urban air quality, in: Proceedings of the CLIMAQS Workshop 'Local Air Quality and its Interactions with Vegetation' January 21–22, 2010, Antwerp, Belgium, 7–8

9. Hofschreuder P, Kuypers V, de Vries B, Janssen S, De Maerschalck B, Erbrink H, de Wolff J (2010) Effect of vegetation on air quality and fluxes of NOx and PM-10 along a highway, in: Proceedings of the CLIMAQS Workshop 'Local Air Quality and its Interactions with Vegetation' January 21–22, 2010, Antwerp, Belgium, 11–16
10. Keuken, M. and van der Valk, K. (2010) The effects of trees and hedges on air quality in a street-canyon in Amsterdam, in: Proceedings of the CLIMAQS Workshop 'Local Air Quality and its Interactions with Vegetation' January 21–22, 2010, Antwerp, Belgium, 88–92
11. Leuchner, M. and Rappenglück, B. (2010) The role of biogenic and anthropogenic NMHCs in the local air quality of a highly polluted urban area, in: Proceedings of the CLIMAQS Workshop 'Local Air Quality and its Interactions with Vegetation' January 21–22, 2010, Antwerp, Belgium, 75–79
12. Maiheu, B., De Maerschalck, B., Vankerkom, J. and Janssen, S. (2010) Local air quality and its interaction with vegetation in the urban environment, a numerical simulationusing ENVI-met, in: Proceedings of the CLIMAQS Workshop 'Local Air Quality and its Interactions with Vegetation' January 21–22, 2010, Antwerp, Belgium, 98–103
13. Manes, F. Vitale, M., Incerti, G. and Salvatori, E. (2010) Modeling the uptake of air pollutants by urban green in the city of Rome, in: Proceedings of the CLIMAQS Workshop 'Local Air Quality and its Interactions with Vegetation' January 21–22, 2010, Antwerp, Belgium, 70–74
14. Vivanco, M.G., Alonso, R., Bermejo, V, Palomino, I., Garrido, J.L., Elvira, S., Salvador, P. and Artíñano, B. (2010) Ozone pollution removal by peri-urban trees in Madrid city (Spain) in: Proceedings of the CLIMAQS Workshop 'Local Air Quality and its Interactions with Vegetation' January 21–22, 2010, Antwerp, Belgium, 65–69
15. Wuytack, T., Verheyen, K., Wuyts, K., Kardel, F., Adriaenssens, S. and Samson, R (2010) The potential of bio-monitoring of air quality using leaf characteristics of white willow (Salix alba L.) in: Proceedings of the CLIMAQS Workshop 'Local Air Quality and its Interactions with Vegetation' January 21–22, 2010, Antwerp, Belgium, 36–40

## Questions and Answers

**Questioner Name**: S. Aksoyoglu

**Q**: You said needle leaved trees improve air quality. But they are main sources for terpenes which are precursors for SOA. Aren't particles considered in this study?

**A**: As stated in the introduction trees can have both positive and negative impacts on air quality. Coniferous trees are known to be efficient in removing particulate matter through the deposition process, but on the other hand may indeed contribute to the formation of secondary particulate matter by means of NMVOC emissions.

**Questioner Name**: J. Kukkonen

**Q**: The trees and other vegetation in urban areas have also one effect that was not mentioned in your presentation: the release of allergenic pollen. That should be taken into account, when evaluating the role of vegetation on urban air quality, do you not agree?

**A**: The release of pollen is indeed an effect which might be considered negative from a health perspective. It might be added to the list of negative effects, mentioned in the introduction. However, this contribution focuses on the aerodynamic effects versus the effects of deposition at the various levels ranging from the micro scale to the urban or city scale.

# Chapter 4
# Using a Coupled Meteorological and Chemical Transport Modelling Scheme to Evaluate the Impact of the Aerosol Direct Effect on Pollutant Concentration Fields in Paris

**Gerold Halmer, Ioannis Douros, George Tsegas, and Nicolas Moussiopoulos**

**Abstract** Aerosols have a significant impact on the Earth's radiation budget by scattering and absorbing solar radiation thus decreasing the radiation absorbed at the surface and increasing low-level static stability. Recent developments in urban air pollution modelling have focused on the introduction of two-way coupling between aerosol modules and the driving meteorological models, aiming to a more accurate description of aerosol-induced radiative forcings in the atmosphere. In this study, the feedback mechanism due to the aerosol direct effect is examined with the aid of a mesoscale Eulerian meteorological model and a chemical transport model, as part of an on-line coupled scheme. For the assessment of the performance of the coupled model system, pollutant dispersion over the Paris area is simulated over a summer period in 2005 identified in the framework of the MEGAPOLI project. A comparison between the standalone and coupled calculations reveals that the radiative forcing due to the direct effect has a substantial impact on the calculated meteorological fields and leads to an improved representation of the pollutant concentration patterns.

**Keywords** Aerosol direct effect • Urban air pollution modelling • Aerosol modelling • Two-way coupling

## 4.1 Introduction

Modelling is becoming an important tool for investigating the intricate feedback mechanisms involved in the aerosol direct and indirect effects, further driving the ongoing evolution of computational tools towards the integration of meteorological

G. Halmer
Institut für Technische Thermodynamik, University of Karlsruhe, Karlsruhe, Germany

I. Douros (✉) • G. Tsegas • N. Moussiopoulos
Laboratory of Heat Transfer and Environmental Engineering, Aristotle University of Thessaloniki, University Campus, Thessalonika 54124, Greece
e-mail: jdouros@aix.meng.auth.gr

D.G. Steyn and S. Trini Castelli (eds.), *Air Pollution Modeling and its Application XXI*, NATO Science for Peace and Security Series C: Environmental Security 4,
DOI 10.1007/978-94-007-1359-8_4, 

and chemical-dispersion models. Aiming at an accurate description of the feedbacks involved in the direct aerosol effect, an on-line coupled system was developed consisting of the mesoscale Eulerian meteorological model MEMO and the chemical transport model MARS-aero.

There are some limitations to be noted for this study. First, only the direct effect is taken into account. According to IPCC [4] the first indirect effect is comparable and can be larger than the direct aerosol effect in global scale, however it is more uncertain to what extend this holds true in smaller spatial scales. In any case, the simulated period had relatively clear skies, thus significantly reducing indirect effects due to cloud properties. Another limitation is that the length of the simulation presented in the study is not sufficiently long to establish a conclusive signal of the aerosol radiative forcing in the Paris area. Finally, the current study is focused solely on the effect of anthropogenic aerosols, not taking into account other sources such as windblown dust and sea salt.

## 4.2 Methodology

In the present study, mesoscale wind flow pattern and concentration fields in the Paris area are examined by means of model simulations using the MEMO and MARS-aero models. MEMO is a 3D non-hydrostatic mesoscale meteorological model [5, 6] and MARS-aero is a 3D Eulerian dispersion model for reactive species in the local-to-regional scale [1, 7].

In the coupled model configuration used in this work, the 3D aerosol concentration fields calculated by MARS-aero are introduced back as input in the enhanced radiation module of MEMO by means of the OPAC (Optical Properties of Aerosols and Clouds) software library [3]. For the calculation of the absolute optical properties, number densities for several of the OPAC aerosol component types are obtained from the concentration fields of appropriate aerosol aggregates calculated by MARS-aero [2].

The performance of the coupled MEMO-MARS-aero model system was assessed using a 3-day case between 9 July and 11 July 2005 for the Paris area. The anticyclonic synoptic conditions prevailing over the area during most of the period of interest, in combination with the weak local circulation, favoured stagnation conditions and accumulation of pollutants over the central urban area. The computational grid extended to $50 \times 50$ km$^2$ with a resolution of 1,000 m, covering the metropolitan area of Paris.

## 4.3 Results

The patterns of the aerosol induced changes in wind speed and turbulent kinetic energy (TKE) at the first computational layer of MEMO (Fig. 4.1) indicate a clear dynamical effect of aerosols on local meteorology.

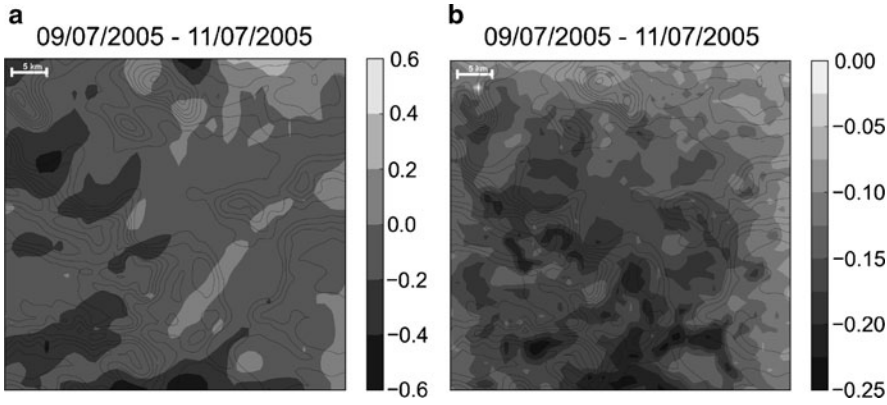


**Fig. 4.1** Difference fields between the control and the coupled runs for (**a**) wind speed and (**b**) turbulent kinetic energy, at a height of 10 m

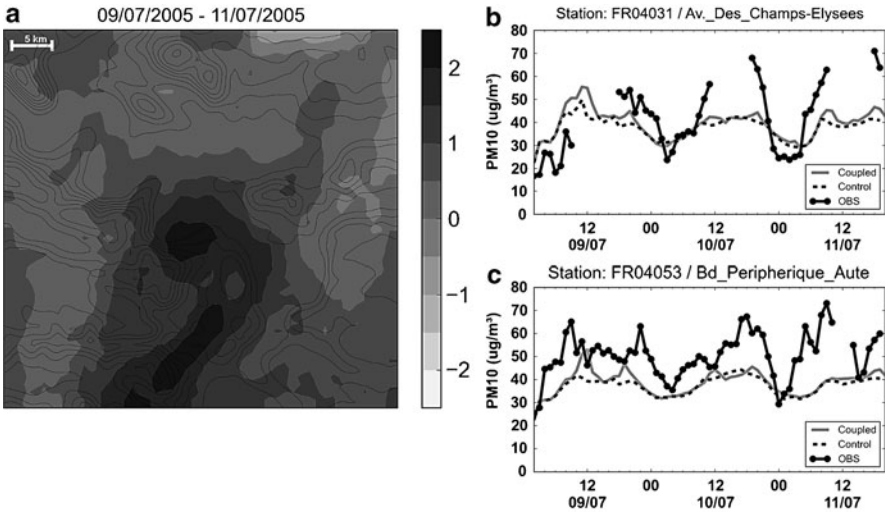


**Fig. 4.2** Difference field between the control and the coupled runs for average $PM_{10}$ concentrations (**a**), and concentration timeseries calculated for the Bd. Peripherique (**b**) and the Av. des Champs Elysees (**c**) measurement locations

Taking into account the direct effect leads to a reduction trend of the predicted mean wind speed over most of the domain, while a notable decrease of the TKE production at the first layer of the model is also evident, indicating the influence of reduced thermal forcings on the surface.

The difference field for $PM_{10}$ concentrations (Fig. 4.2a) on the other hand, reveals a clear increase over almost the entire domain, reaching up to 2.5 μg $m^{-3}$

in the central Paris area and the southern part of the computational area, with a higher pollution load due to the prevailing wind flow during the simulation period. Comparison between time series of predicted $PM_{10}$ concentrations and measurements at the locations of AIRPARIF stations within the domain (Fig. 4.2b), indicate satisfactory agreement, with the coupled system being able to better reproduce both the mean values and the diurnal evolution of the concentrations.

## 4.4 Conclusions

A two-way coupled meteorological and chemical transport modelling scheme was implemented and tested for simulating the effect of the direct aerosol effect on mesoscale meteorological and dispersion fields over the urban area of Paris, France. The performance of the new formulation was evaluated by observing the response of the primary meteorological variables governing the transport and dispersion of pollutants, as well as trends in particulate matter concentrations. The impact of the direct aerosol effect was found to be substantial with regard the turbulent characteristics of the flow near the surface, while the performance of the coupled model in predicting urban air quality was improved.

## References

1. Arvanitis A, Moussiopoulos N, Kephalopoulos S (2001) Development and testing of an aerosol module for regional/urban scales. In: Proceedings of the 2nd conference on air pollution modelling and simulation, APMS '01, Champs-sur-Marne, 8–12 April 2001, pp 277–288
2. Halmer G (2011) Ph.D. thesis (in preparation)
3. Hess M, Koepke P, Schult I (1998) Optical properties of aerosols and clouds: the software package OPAC. Bull Am Meteorol Soc 79(5):831–844
4. IPCC (2007) Climate change 2007: the physical science basis. In: Solomon S, Qin D, Manning M, Chen Z, Marquis M, Averyt KB, Tignor M, Miller HL (eds) Contribution of working group I to the fourth assessment report of the Intergovernmental Panel on Climate Change. Cambridge University Press, Cambridge/New York, 996 pp
5. Kunz R, Moussiopoulos N (1997) Implementation and assessment of one-way nesting technique for high resolution wind flow simulations. Atmos Environ 31:3167–3176
6. Moussiopoulos N (1995) The EUMAC zooming model, a tool for local-to-regional air quality studies. Meteorol Atmos Phys 57:115–133
7. Moussiopoulos N, Sahm P, Kunz R, Vögele T, Schneider Ch, Kessler Ch (1998) High resolution simulations of the wind flow and the ozone formation during the Heilbronn ozone experiment. Atmos Environ 31:3177–3186

## Questions and Answers

**Q**: Do you see any "straightforward" correlation in difference maps of meteorological and chemical fields?

**A**: The most evident correlation is between wind speed and the concentration of species that have a strong primary component, such as $PM_{10}$. As expected, lower wind speeds lead to higher concentration levels near the surface. Yet another correlation is between surface temperature and concentrations of $NO_2$, where higher temperatures apparently lead to higher pollutant concentrations. This is principally due to the fact that $NO_2$ formation takes place through thermal reactions.

# Chapter 5
# CFD Simulations of Air Pollution in Urban Micro Environments

**Stijn Janssen, Bart De Maerschalck, Irina Nikolova, Bino Maiheu, Jean Vankerkom, and Peter Vos**

**Abstract** This paper presents the results of two recent case studies which were evaluated with the CFD model ENVI-met. In a first case, the impact of a vegetation barrier along a highway on the local air quality is studied. In a second case, the dispersion of total UFP concentrations within a street canyon is examined. In both cases, ENVI-met model output is compared with measurements resulting in an overall acceptable agreement of the model performance.

**Keywords** CFD • Local air pollution • Ultra fine particles • Vegetation barriers

## 5.1 Introduction

CFD-based air quality models can be used to describe the complex dispersion phenomena in urban micro environments. This makes them useful tools to assess local air pollution levels and to assess the (local) impact of mitigation strategies. In this paper results of the CFD-based model ENVI-met are presented. ENVI-met [1] simulates atmospheric parameters (wind field, concentrations) with a typical resolution between 0.5 and 10 m. ENVI-met distinguishes itself from other CFD-models due to the implementation of a detailed meteorological and vegetation module. The meteorological module for example takes into account the effect of temperature differences due to solar radiation and shadows and is coupled with a soil model to account for the effects of heat and vapour exchange. The vegetation module describes the interaction of local vegetation with the atmosphere, not only on the wind and

S. Janssen (✉) • B. De Maerschalck • I. Nikolova • B. Maiheu • J. Vankerkom • P. Vos
VITO – Flemish Institute for Technological Research, Boeretang 200,
Mol B-2400, Belgium
e-mail: stijn.janssen@vito.be

D.G. Steyn and S. Trini Castelli (eds.), *Air Pollution Modeling and its Application XXI*,
NATO Science for Peace and Security Series C: Environmental Security 4,
DOI 10.1007/978-94-007-1359-8_5, 

turbulence fields, but also on the thermodynamic processes and the deposition of gases and particulate matter. In addition the model contains a chemistry module describing the fast chemical reactions between nitrogen oxides and ozone. As such ENVI-met is a suitable tool to examine urban scale air quality phenomena.

In this paper, two recent case studies are presented in which the ENVI-met model was used to assess air pollution levels at the micro scale and in which model results were validated with in-situ measurements.

## 5.2 Case 1: Impact of Vegetation Barriers Along Highways

The Air Quality Innovation Project (IPL), initiated by the Dutch ministries for Transport, Public Works and Water Management (Rijkswaterstaat), aimed to find concrete strategies to improve the air quality in the vicinity of highways. One of the seven tracks of the project was the investigation, both experimentally and numerically, of the effect of vegetation along the motorway. Therefore, a number of measurement campaigns have been set up between 2006 and 2009 along various tracks of the A50 motorway in the Netherlands. Two of the campaigns were setup by ECN at a location close to the village Vaassen, The Netherlands. During these campaigns [2] nitrogen oxides and particulate matter were measured at different distances (10, 45 and 90 m) downwind from the highway in two fields next to the A50, one without vegetation and one separated from the motorway by a line of trees and bushes of about 10 m high and wide.

For the A50-Vaassen location, the ENVI-met model was setup and the five most successful days of the measurement campaign were simulated. Figure 5.1 shows the normalized mean $NO_2$ concentrations at 2 m height. These are the mean concentrations averaged over the five measurement days and normalized with the value of the concentration just in front of the vegetation barrier. The plots present both the modelled concentrations as full lines, and the measured mean values as dots with error bars. The red dots and lines represent the measurements and model results in the reference field, while the green dots and lines represent the measurements and model results in front of and behind the vegetation. The green bar indicates the location of the vegetation barrier and the red blocks at the bottom the location of the traffic emissions.

In front of and just behind the vegetation an increase in $NO_2$ concentrations is observed. This increase is caused by the reduced wind speed at these locations and due to extra $NO_2$ production by the ozone chemistry compared to the free reference field. However, at some further distances behind the vegetation (10–100 m – downwind) both the measurements and the ENVI-met model results show that a vegetation barrier along a motorway can have a 5–10% local positive effect on the $NO_2$ concentrations.

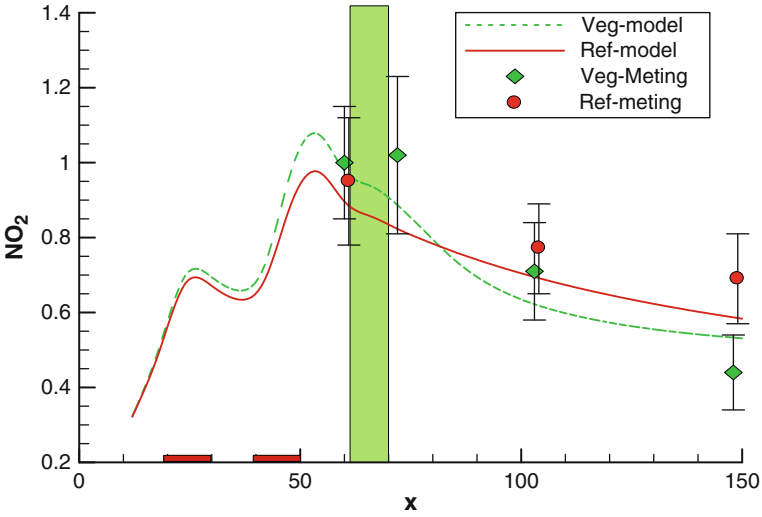


**Fig. 5.1** Normalised mean NO2 concentrations at 2 m height. The high bar indicates the location of the vegetation, the two small boxes indicate the line sources. Diamonds and dots represent the ECN AU1 measurements, the lines represent the model results. Solid line: along the reference line, dashed line: in front of and behind the vegetation barrier. Mean wind is blowing from the left.

## 5.3 Case 2: UFP Concentrations in a Street Canyon

In a second case, the dispersion of ultrafine particles (UFP) in a street canyon was studied. In the Summer of 2009, a measurement campaign was setup in the Wolfstraat, a street canyon in the city of Antwerp, Belgium. At four different locations in the canyon (at the beginning, the end and at the left and right hand side in the middle – see Fig. 5.2) total number of UFP was measured during 2 weeks. For five single days, measurement data is available simultaneously at all four location in the canyon. Four those 5 days, the ENVI-met model is setup. In order to take into account the complex urban micro structure, not only the canyon is modelled but also the surrounding neighbourhood is included in the model domain. Note that a present, no size resolving information of the UFP and related transformation processes are taken into account in ENVI-met. The total number of particles emitted by the traffic is simulated as a tracer which can disperse in the micro environment and depose on the surfaces and the walls. In Fig. 5.2, the simulated total number UFP at 1.5 m height is present for the whole study domain. The Wolfstraat is the canyon in the middle of the plot. In the North, the Wolfstraat starts at the much more traffic intensive Plantin & Moretus boulevard (South-East to North-West).

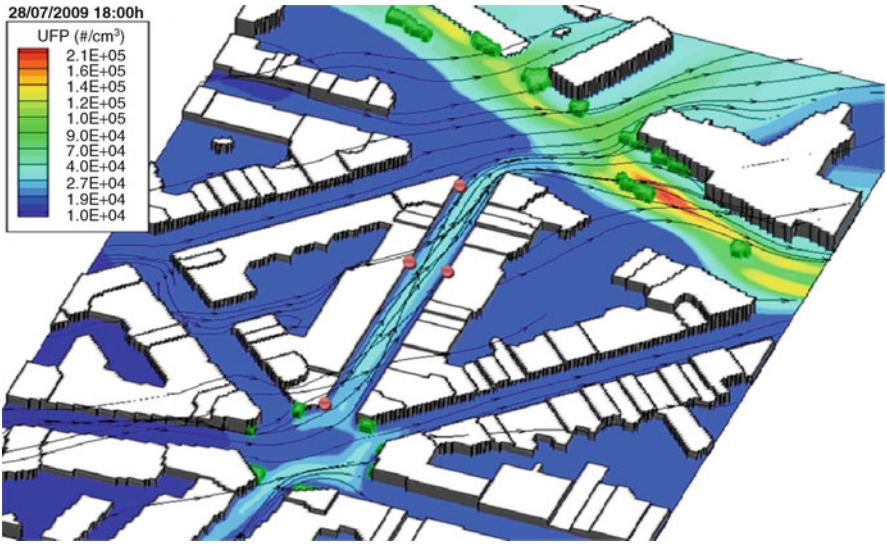


**Fig. 5.2** UFP concentrations and wind direction at 1.5 m height in the Wolfstraat and Plantin and Moretuslei in Antwerp, Belgium. The *dots* indicate the measurement locations

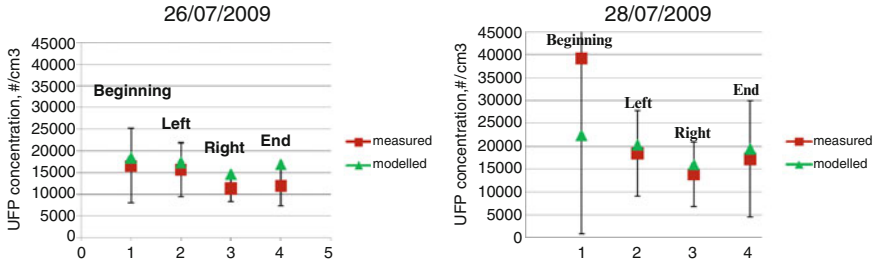


**Fig. 5.3** Comparison of modelled (*triangles*) and measured (*squares*) total number UFP concentrations for two different days in July 2009. Measurements and model results are compared at four different locations in the Wolfstraat street canyon: beginning (*1*); *left* (*2*) and *right* (*3*) in the middle of the street and at the end (*4*) of the canyon

In Fig. 5.3, two selected days are presented for which the modelled UFP concentration are compared with the measured ones at four locations in the street canyon. On July 26, the modelled trend in the UFP concentrations well resembles the measured ones and within the uncertainties of the measurements showing an overall good agreement. In particular the observed left right asymmetry in the middle of the canyon is well represented by the ENVI-met model. On July 28, the model is able to describe the same asymmetry in the middle of the canyon but during this particular day, very high UFP concentrations ($4.10^4$#/cm$^3$) were measured at the beginning of

the canyon, close to the busy boulevard. Under the give meteorological conditions (South-Eastern wind), the model is unable to account for such high concentrations.

## References

1. Bruse M, Fleer H (1998) Simulating surface–plant–air interactions inside urban environments with a three dimensional numerical model. Environ Model Software 13:373–384
2. Weijers EP, Kos GPA, van den Bulk WCM, Vermeulen AT (2007) Onderzoek naar de luchtkwaliteit rondom een vegetatiestrook langs de snelweg. Technical report ECN-E–07-011, Energy Research Center of the Netherlands

## Questions and Answers

**Questioner Name**: M. Biliaiev

**Q**: In the case of vegetation, to use the numerical model it is necessary to know the coefficients of pollutant absorption by plants. How did you determine these coefficients?

**A**: ENVI-met uses a classical resistance scheme for the calculation of the deposition velocity. It takes into account the aerodynamic and quasi-laminar resistances for particulate matter. For gaseous species such as $NO_2$, the stomatal resistance is also taken into account. Details of ENVI-met's deposition scheme can be found at www.envi-met.com.

**Questioner Name**: E. Genikhovich

**Q**: On one of the pictures, the boundary of the computational grid looked like steps with 90° angles. It means that you should have an additional recirculation and eddy generation at those boundaries. How did you avoid this problem?

**A**: ENVI-met is by construction limited to a regular mesh. This means that irregular or curved boundaries of the model domain (e.g. terrain or buildings) always have to be represented as stepwise structures. In the case of the highway elevation, the slope is also modelled in this was. Those artificial steps increase the roughness of the surface but it is verified that they do not give rise to unrealistic turbulence production.

# Chapter 6
# Dispersion of Buoyant Emissions from Low Level Sources in Urban Areas

**Akula Venkatram, Sam Pournazeri, Marko Princevac, David Pankratz, and Qiguo Jing**

**Abstract** The projected increase in distributed power generation has given rise to the need for a model to examine the air quality impact of small power plants located in urban areas. This model needs to treat plume rise and dispersion of a buoyant release in an inhomogeneous urban boundary layer whose structure is governed by complex surface characteristics. Models such as AERMOD [Cimorelli AJ, Perry SG, Venkatram A, Weil JC, Paine RJ, Wilson RB, Lee RF, Peters WD, Brode RW (2005) AERMOD: A dispersion model for industrial source applications. Part I: General model formulation and boundary layer characterization. J Appl Meteorol 44(5):682–693] are not designed for such sources, although they do include methods to account for the effects of isolated buildings on dispersion. This paper describes progress in developing a dispersion model that treats the governing processes relevant to an urban boundary layer. The model is being developed using data from a field study conducted in the vicinity of a distributed generator (DG). The data from the field study was supplemented with data from simulations conducted in a water channel.

**Keywords** Plume rise • Buoyant emissions • Urban areas • Dispersion • Urban canopy • Vertical mixing • Field study • Water channel • Tracer study • Modeling

## 6.1 Field Study

A field study was conducted in Palm Springs, California in summer 2008, in which sulfur hexafluoride ($SF_6$) was released from a 9.3 m DG stack. The tracer was sampled at ground-level with 49 monitors located on 5 different arcs at distances ranging from

A. Venkatram (✉) • S. Pournazeri • M. Princevac • D. Pankratz • Q. Jing
Department of Mechanical Engineering, University of California,
3401 Watkins Dr. Bourns Hall B342, Riverside, CA 92521, USA
e-mail: venky@engr.ucr.edu

D.G. Steyn and S. Trini Castelli (eds.), *Air Pollution Modeling and its Application XXI*,
NATO Science for Peace and Security Series C: Environmental Security 4,
DOI 10.1007/978-94-007-1359-8_6, 

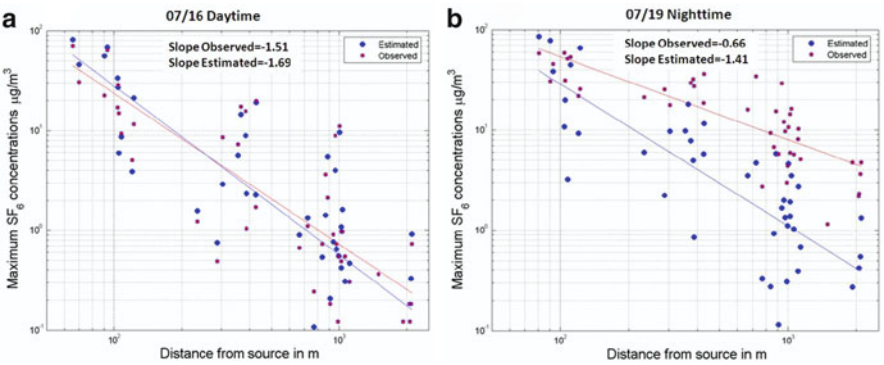


**Fig. 6.1** Observed (small circles) and AERMOD (big circles) estimated concentration, with the relative straight lines, as a function of downwind distance on (a) 16th (Daytime) and (b) 19th (Nighttime) July, 2008

60 m to 2 km from the release location. The study consisted of seven experiments, three during the day, and four during the night, each experiment lasting 6 h. Velocity and temperature measurements were made with sonic anemometers at heights of 3 and 11 m.

Figure 6.1 shows that daytime ground level concentrations drop off rapidly with distance as a result of vigorous mixing in the convective boundary layer. Near source nighttime concentrations are comparable to daytime concentrations indicating rapid mixing of the plume towards the ground. However, they decrease more slowly with ground level concentrations even as far as 2 km from the source being several times those observed during the daytime. This suggests strong vertical mixing within a shallow mixed layer during the night.

Figure 6.1 also shows the performance of AERMOD in explaining the observed tracer concentrations; the effects of the DG building are included in the simulations. We see that while AERMOD explains the distributions of concentrations observed during the daytime, it underestimates the concentrations during the nighttime. We suspect that this discrepancy is related to inadequate modeling of the nighttime urban boundary layer height, and its interaction with the buoyant plume. Figure 6.2 shows that we can describe the observed behavior of concentrations with plausible choices of mixed layer height and Lagrangian time scale for horizontal plume spread. This is an area that needs more attention in AERMOD. The field study did not provide information on ground-level impact within meters of the source. This was investigated using laboratory experiments, described next.

## 6.2 Water Channel Experiments

The laboratory experiments were conducted in a custom-designed re-circulating water channel. The water channel is equipped with the Particle Image Velocimetry (PIV) system for velocity measurements which is able to measure mean and

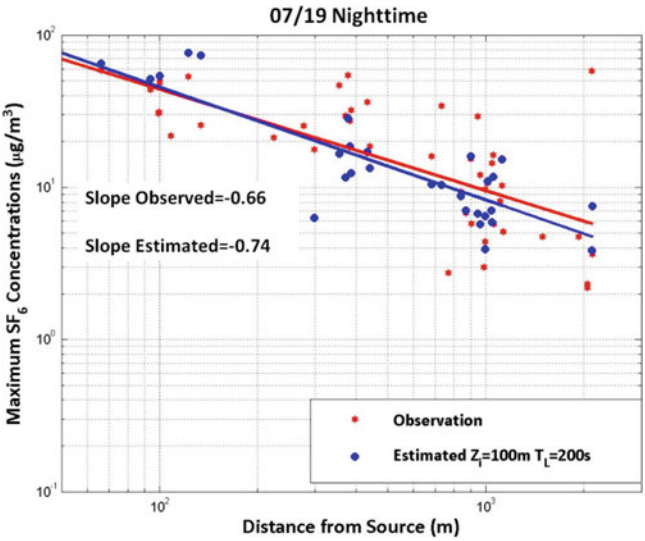


**Fig. 6.2** The effect of Lagrangian time scale $T_L$ and mixing layer height $Z_i$ on nighttime predictions in a Gaussian dispersion model

turbulent velocities in the vertical and horizontal planes. A mixture of water, alcohol and fluorescent dye, Uranine, was used for plume visualization.

Experiments were conducted in water channel using scaled down (100:1) replicas of the Palm Springs DG and the surrounding buildings. Ground-level concentrations were measured using a custom built device that correlated laser induced fluorescence to dye concentrations. To examine the mixing induced by the urban canopy, we conducted experiments to understand the behavior of the plume in the presence of upstream buildings. Plume visualizations (Fig. 6.3) indicate that upstream buildings decrease the wind speed near the stack and increase plume rise. However, at the same time, upstream buildings increase turbulent intensities near the stack resulting in rapid vertical mixing. Thus, the presence of buildings results in effects that counteract each other in changing the ground-level concentrations. A higher plume rise lowers the concentrations while increased vertical mixing increases ground level concentrations. It was necessary to include vertical mixing induced by the canopy to obtain realistic concentrations, especially during the night when atmospheric turbulence is subdued.

## 6.3 Urban Canopy Layer Model (UCLM)

We conducted a preliminary examination of the effects of canopy induced mixing by simply averaging the concentrations associated with the Gaussian dispersion model (including the reflection term) over the height of the urban canopy layer:

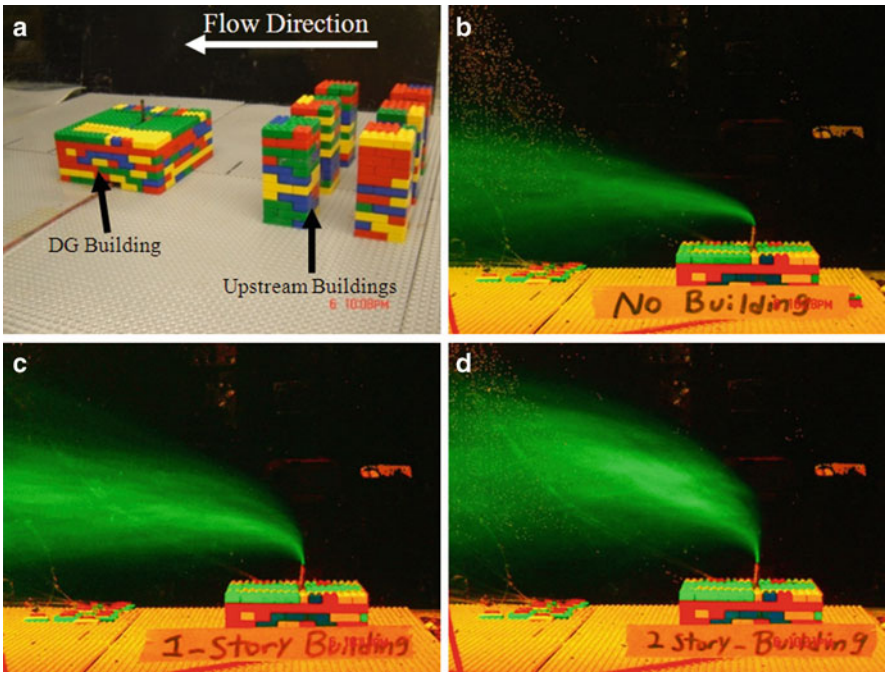


**Fig. 6.3** (**a**) DG and upstream buildings modeled in water channel using Lego and Plume visualizations for (**b**) No Upstream Buildings (**c**) Single Storey Upstream Buildings (**d**) Double Storey Upstream Buildings

$$C(x,y,0) = \frac{1}{2\pi\sigma_y\sigma_z U} exp\left(-\frac{y^2}{2\sigma_y^2}\right)\frac{1}{h_c}\int_o^{h_c}\left[exp\left(-\frac{(z-h_e)^2}{2\sigma_z^2}\right) + exp\left(-\frac{(z+h_e)^2}{2\sigma_z^2}\right)\right]dz \tag{6.1}$$

where $U$ is the wind speed, $h_e$ is the effective plume height, $h_c$ is the height of the urban canopy layer and $\sigma_y$, $\sigma_z$ are the lateral and vertical spreads of the plume. Equation 6.1 yields

$$C(x,y,0) = \frac{1}{2\sqrt{2\pi}\sigma_y U h_c} exp\left(-\frac{y^2}{2\sigma_y^2}\right)\left[erf\left(\frac{h_e+h_c}{\sqrt{2}\sigma_z}\right) - erf\left(\frac{h_e-h_c}{\sqrt{2}\sigma_z}\right)\right] \tag{6.2}$$

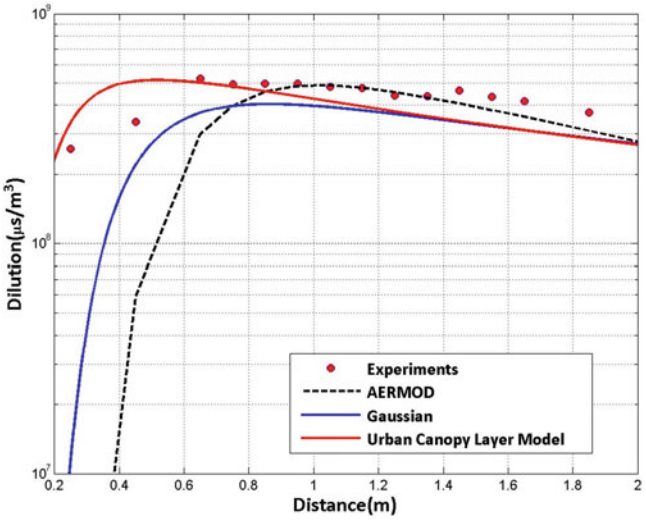


**Fig. 6.4** The effect of including canopy induced mixing in a Gaussian dispersion model

The urban canopy height, $h_c$, was set equal to the height of the Palm Springs DG model building, and the plume spreads were estimated using the measured turbulent velocities.

Figure 6.4 shows that this simple treatment of urban canopy mixing provides a better description of concentrations close to the source than a Gaussian dispersion model does. Note that even AERMOD, with its treatment of building effects, underestimates the concentrations close to the source.

## 6.4 Summary and Conclusions

Results from a field study conducted in the vicinity of a DG situated in Palm Springs and water tank laboratory experiments indicate that a model for dispersion of a low level buoyant release in an urban boundary layer requires two essential ingredients: (1) a realistic treatment of the interaction between the nighttime urban mixed layer and the buoyant plume, and (2) urban canopy induced mixing close to the source. We have modified a simple dispersion model to account for these effects. The encouraging results from this model suggest modifications to AERMOD to allow its application to buoyant low level releases in urban areas.

**Acknowledgments** The California Energy Commission (CIEE MAQ-07-03) supported this research.

## Reference

1. Cimorelli AJ, Perry SG, Venkatram A, Weil JC, Paine RJ, Wilson RB, Lee RF, Peters WD, Brode RW (2005) AERMOD: A dispersion model for industrial source applications. Part I: General model formulation and boundary layer characterization. J Appl Meteorol 44(5):682–693

## Questions and Answers

**Question (Tom Pierce)**: Historically, Gaussian plume dispersion models were conservative as they were applied for protecting human health. Based on your field results, should AERMOD be modified to be more conservative as predicted extremes were lower than that observed?
**Response (Akula Venkatram)**: AERMOD was designed to be unbiased rather than conservative. It is not possible to estimate the concentrations at the upper end of the observed distribution. However, we can estimate the upper end of the observed distribution, say the 98th percentile, making plausible assumptions about the concentration distribution.

**Question (S.M. Daggupaty)**: Is it not common to include initial dispersion depending upon obstacle dimension for short range dispersion models? This is what we do for night and daytime conditions. What is your opinion on this with respect to buoyant plumes you are talking about?
**Response (Akula Venkatram)**: I would include initial dispersion, proportional to building dimensions, only for a surface release in the vicinity of the building, or when the plume is entrained into the building cavity. I would not include initial spread for a buoyant plume that is not affected by the building.

**Question (D. Anfossi)**: In your water tank, how did you fix the time scale for wind meandering?
**Response (Akula Venkatram)**: We do not control the frequency of meandering in the water tank. It is determined by the frequency of the axial pump that is forcing the water through the water channel.

# Chapter 7
# Comparison Between a Building Resolving Micro-Meteorogical Model and Measurements at SIRTA

**Hanane Zaidi, X. Zhang, E. Dupont, M. Milliez, L. Musson-Genon, and Bertrand Carissimo**

**Abstract** This numerical work presents a computational fluid dynamics (CFD) model to simulate wind flow over complex site SIRTA which is located in Palaiseau, 20 km south of Paris (France) in a semi urban environment. The purpose is to study the ability of an atmospheric CFD model (Code_Saturne) to reproduce the micro scale heterogeneities of wind and turbulent kinetic energy (TKE), using a 16 month data set collected at SIRTA site. The forested areas were modeled either according to the classical roughness law or with a drag porosity model, in which trees effects are modeled with additional terms in momentum, TKE and dissipation rate equations. The results obtained in this work show that the drag porosity model represents well the special heterogeneities of the site and gives results much closer to experimental results than the classical roughness law in the sector where the influence of forested areas is predominant.

**Keywords** Computational Fluid Dynamic • Turbulence • Forest • Canopy model

## 7.1 Numerical Setup

### *7.1.1 CFD Code*

The numerical simulations of the atmospheric flow were performed with the atmospheric module of *Code_Saturne*. This code is based on the finite volume co-localized method [1, 6] to solve the system of equation governing the atmospheric flow.

H. Zaidi (✉) • X. Zhang • E. Dupont • M. Milliez • L. Musson-Genon • B. Carissimo
Joint laboratory ENPC-EDF R&D, Ecole de Ponts, Paritech, CEREA,
Teaching and Research Centre in Atmospheric Environment, 6-8 Avenue Blaise Pascal,
Cite Descartes, Champs Sur Marne, Marne la Vallee/Chatou, France
e-mail: hanane.externe-zaidi@edf.fr; carissimo@cerea.enpc.fr

D.G. Steyn and S. Trini Castelli (eds.), *Air Pollution Modeling and its Application XXI*,
NATO Science for Peace and Security Series C: Environmental Security 4,
DOI 10.1007/978-94-007-1359-8_7, 

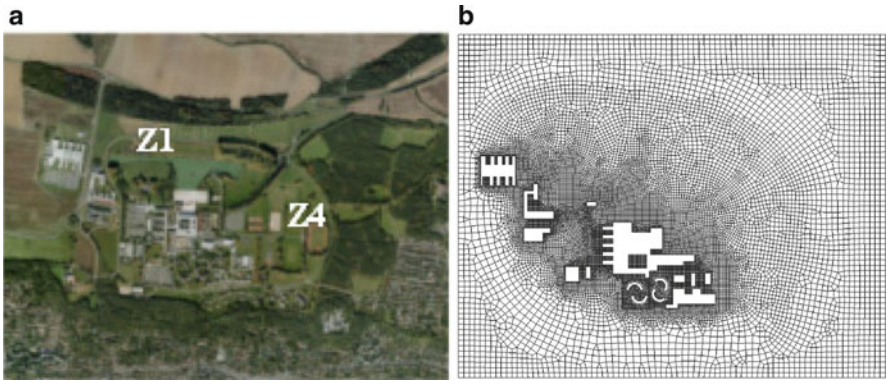


**Fig. 7.1** (**a**) Satellite view showing the two instrumented zones, (**b**) horizontal cross section at ground level

### *7.1.2 Computational Domain and Meshing*

Computations were performed on a tree-dimensional domain 2,200 m long, 1,800 m wide and 2,500 m high. The number of computational cells used for all simulations is about 2100468 cells and the number of vertical levels along the axis z is 90 (Fig. 7.1). The buildings are explicitly taken into account [8].

### *7.1.3 Boundary Conditions*

The boundary conditions imposed in this study are as follows:

- Input condition:the Dirichlet condition is defined with an academic logarithmic profile for the surface layer [7].
- Outlet conditions: all gradients are null (outflow).
- Upper limit of the domain: Symmetry condition.
- At the surface (roof, sides of buildings): a constant roughness of 0.03 m is applied.

## 7.2 Modelling

Forested areas were modeled with two approaches: either with the classical roughness law or with a drag-porosity model. Other land use types present on the site (low vegetation, water, houses) are taken into account with the roughness law approach using a land use cover file provided by the French Institute of Geography (IGN) with an horizontal resolution of 50 m.

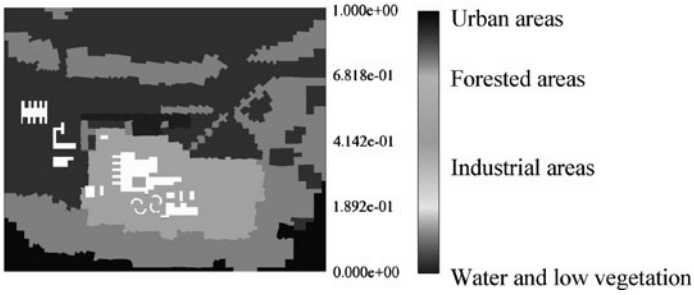


**Fig. 7.2** Roughness map (m) projected onto the mesh

### *7.2.1 Classical Roughness Law*

In this approach, a roughness length of 0.75 is assigned to the trees (forested areas). Figure 7.2 shows the roughness map projected onto the mesh.

### *7.2.2 Drag Porosity Model*

The drag model which has been implemented in *Code_Saturne* is based on the model of Lopes da Costa et al. [4]. The canopy creates a drag force against the flow, it causes a decrease in speed and changes the turbulence. The pressure and viscous forces due to the vegetation are modelled by a single force Fi added as a source term in the Navier-Stokes equation:

$$F_i = -\frac{1}{2}\rho \, \alpha \, C_D \, |U| \, \overline{U}_i \tag{7.1}$$

where U is the wind speed, α: is the leaf foliage area per unit of volume (0.5), $C_D$ is the canopy drag coefficient and ρ is the air density. The modification of the TKE is modelled with an additional term ($S_k$,$S_\varepsilon$) both in k and ε equations:

$$S_k = \frac{1}{2}\rho \, \alpha \, C_D |U|^3 \tag{7.2}$$

$$S_\varepsilon = \frac{\varepsilon}{2\,k} \, C_{4\varepsilon}\rho \, \alpha \, C_D \, |U|^3 \tag{7.3}$$

C4ε is a constant related to the drag porosity model, fixed at 1.95 [4].
For SIRTA site : H = 15 m, $C_D = 0.2$ and $\alpha = 0.5$.

## 7.3 Results

Numerical simulations were performed for all wind directions every 10° with both drag porosity model and classical roughness law and are compared with the measurements.

First, the experimental data collected by the CEREA for 16 months (October 2006–January 2008) are classified according to conditions of stability by calculating the difference in temperature ΔT between the altitudes 10 m and 30 m at the zone 4. Then, the cases close to neutral stability ($-0.1°C < \Delta T < -0.3°C$) are selected. The data obtained from sonic anemometers at 10 m are classified by direction sector of 10°. For each sector, the averaged ratio $TKE/U^2$ is calculated. Figure 7.3 shows the ratio $TKE/U^2$ (where U is the wind speed), obtained numerically and experimentally for Zone 1 and Zone 4 as a function of the wind direction. The measured values indicate that in Zone 1 the effects of the northern forested area are predominant (sector 330° to 80°). In Zone 4, the ratio takes more homogenous values according to the wind direction. The results of numerical simulations performed with the drag porosity model are qualitatively similar to experimental results. It can be stated that the drag porosity model accurately represents the heterogeneity of the site of SIRTA but discrepancies remain for some wind directions in the north-east sector and the south-west sector. In Zone 1, the drag porosity model overestimates the normalized TKE for wind directions ranging from 340° to 30° and underestimates it for directions between 50° and 90°. In Zone 4, the drag-porosity model gives a reasonable agreement with the measurements for the sectors of north-east and south-east (wind directions between 20° and 130°). In the sectors of north-west and south-west, the drag porosity model underestimates the ratio ($TKE/U^2$). Possible sources of improvement are:

- The land use map does not reflect accurately the heterogeneities that exist at the site of SIRTA, especially those located near the measurement tower located in zone 4 (the map shall be modified).
- The parameters of drag porosity model (leaf index, drag coefficient, trees height) which require sensitivity analysis to determine their impact.

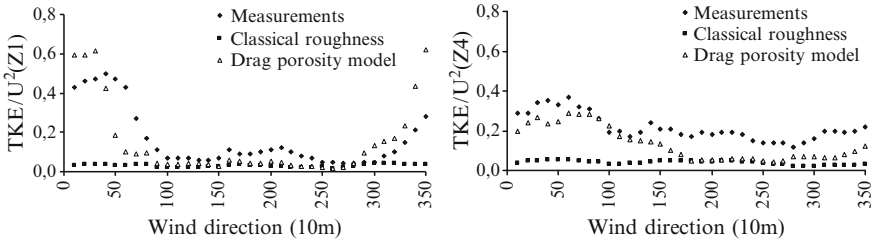


**Fig. 7.3** Comparison of measured and calculated ratio (TKE//U) for Zone 1 (*left*) and Zone 4 (*right*), as a function of wind direction

For the classical roughness law model, the ratio $TKE/U^2$ remains constant in Zone 1 and Zone 4, for all wind directions. As a conclusion, this model is less appropriate to represent heterogeneities of the SIRTA site.

## 7.4 Conclusions and Perspective

A CFD model was used to simulate the air flow on the SIRTA site. The forested areas were represented with two models: the classical roughness law and a drag-porosity model. The standard k-ε turbulence model is used, in which source terms were added to the governing equations to represent the effect of trees. The drag porosity model leads to encouraging results; it qualitatively better simulates the effects of spatial heterogeneities, especially in Zone1, but still underestimates the normalized turbulent kinetic energy in a large west sector in Zone 4.

The ongoing work consists in improving this model:

- A modified formulation of the model (Katul's model), with an additional term in the equations of turbulent energy and its dissipation rate.
- An adaptation of the model constants (trees height, leaf area index and drag coefficient) for the SIRTA.
- A modification of the land use map.

## References

1. Archambeau F, Mechitoua N, Sakiz M (2004). A finite volume method for the computation of turbulent incompressible flows - industrial applications. Int. J. Finite 1:1–62.
2. Dalpé B, Masson C (2009) Numerical simulation of wind flow near a forest edge. J Wind Eng Ind Aerodyn 97:228–241
3. Katul GG, Mahrt L, Poggi D, Sanz C (2004) One- and two-equation models for canopy turbulence. Bound-Lay Meteorol 113:81–109
4. Lopes da Costa JC, Castro FA, Palma JMLM, Stuart P (2006) Computer simulation of atmospheric flows over real forests for wind energy resource assessment. J Wind Eng Ind Aerodyn 111:603–620
5. Sanz C (2003) A note on k-ε modelling of vegetation canopy air-flows. Bound-Lay Meteorol 108:191–197
6. Saturne_User Guide (2008)
7. Stull RB (1988) An introduction into boundary layer meteorology. Kluwer, Dordrecht, 670
8. Zaidi H, Dupont E, Carissimo B, Milliez M, Musson-Genon L (2010) Realistic simulation of spatial heterogeneities of wind and turbulence at microscale with an atmospheric CFD code. In: The fifth international symposium on Computational Wind Engineering (CWE2010), Chapel Hill, North Carolina, 23–27 May 2010

## Questions and Answers

**Peter Builtjes**: Can you explain why the Katul model is less sensitive to changes in coefficients than the Costa model? Is there a physical reason?
The two canopy models, Lopes da Costa et al. [4] and Katul et al. [3], are used to represent the effects of forested areas. Both use the same formulation for Fi (Eq. 7.1) but two different formulations for additional terms $S_K$ and Sε.

Costa's model uses the additional terms $S_K$ and $S_\varepsilon$ defined by Eqs. 7.2 and 7.3 and Katul's model uses the following formulations:

$$S_k = \frac{1}{2}\rho\ \alpha\ C_D B_p\ |U|^3 - \frac{1}{2}\ \rho\ \alpha\ C_D B_d k |U| \tag{7.4}$$

$$S_\varepsilon = \frac{\varepsilon}{2\,k}\ C_{4\varepsilon}\rho\ \alpha\ C_D\ |U|^3 - C_{\varepsilon 5} B_d \varepsilon\, |U| \tag{7.5}$$

Where: $C_{4\varepsilon}$, $C_{5\varepsilon}$, $B_p$ and $B_d$ are the model constants. Using $B_p = 1$ [2, 3, 5], the constants are calculated with formulations proposed by Katul et al. [3]. Table 7.1 presents the constants values of Katul's model.

**Table 7.1** Katul constants model

| Bp | Bd | $C_{4\varepsilon}$ | $C_{5\varepsilon}$ |
|---|---|---|---|
| 1 | 5.03 | 0.9 | 0.9 |

Numerical results obtained in 2D with Katul model for different values of Bp (1, 0.7 and 0.5) are very similar but those obtained with Costa's model are strongly affected by the choice of $C_{\varepsilon 4}$.

The Katul's model is less sensitive to variation of coefficients than the Costa's model because both additional terms $S_K$ and $S_\varepsilon$ of Katul's model consist in two terms which are of opposite sign and of the same order of magnitude.

The vegetation elements break the mean flow motion and generate wake turbulence ($\alpha\ C_D.U^3$). However, such wakes dissipate rapidly because of a "short-circuiting" of the Kolmogorov cascade [3]. The canonical form for $S_K$ reflecting such mechanisms (Eqs. 7.4 and 7.5) is given by Sanz [5].

With Katul model, $S_K$ is modelled by the sum of the wake k production rate ($\alpha\ C_D.U^3$) and a sink ($\alpha\ C_D.U.k$) to account for the short-circuiting of the turbulence cascade [3].

A more detailed discussion about Costa and Katul models will be found in a future publication.

# Chapter 8
# A New Method for Buoyant Plume Rise Computation in Lagrangian Particle Models

**Stefano Alessandrini, Domenico Anfossi, and Enrico Ferrero**

**Abstract** An alternative method for the buoyant plume rise computation is proposed. It is based on the same idea described in a recent paper related with chemical reactions in Lagrangian particle models (Alessandrini S and Ferrero E, Phys A 388:1375–1387, 2009) for simulating the ozone background concentration. A fictitious scalar transported by the particles, the temperature difference between the plume portions and the environment air temperature, is introduced. As a consequence no more particles than those inside the plume have to be released to simulate the entrainment of the background air temperature. In this way the entrainment is properly simulated and the plume rise is calculated from the local property of the flow.

**Keywords** Lagrangian particle model • Plume rise

## 8.1 Introduction

An accurate estimation of a buoyant plume rise is one of the basic aspects for a correct estimation of the ground level concentration emitted by an industrial stack. The introduction of the plume rise computation in a Lagrangian particle model

S. Alessandrini (✉)
Department of ASV Environment and Sustainable Development, RSE S.p.A.,
Via Rubattino 54, Milan, 20134, Italy
e-mail: stefano.alessandrini@rse-web.it

D. Anfossi
Institute of Atmospheric Sciences and Climate, Italian National Research Council,
Corso Fiume 4, Torino 10133, Italy
e-mail: d.anfossi@isac.cnr.it

E. Ferrero
Dipartimento di Scienze e Tecnologie Avanzate, Università del Piemonte Orientale,
Viale Teresa Michel 11, Alessandria 15121, Italy
e-mail: enrico.ferrero@mfn.unipmn.it

D.G. Steyn and S. Trini Castelli (eds.), *Air Pollution Modeling and its Application XXI*,
NATO Science for Peace and Security Series C: Environmental Security 4,
DOI 10.1007/978-94-007-1359-8_8, 

is not straightforward. In fact the buoyant forces acting on the plume portions depend on the difference between their temperature and that of the background air that can be computed only considering the entrainment phenomenon. To do that, this model should take into account all the fluid simultaneously, i.e. by filling the whole domain with a large amount of particles. Several authors have suggested to overcome this problem by introducing a vertical velocity whose values come from analytical solution of Eulerian equations [4] or solving a set of differential equations describing the time and space evolution of bulk plume quantities [3, 6, 8]. This approach is accurate and very efficient from the computational time point of view but some problems may arise in those situations where the analytical equation for the vertical velocity is difficult to define, i.e. where several plumes, released by different stacks located close to each other, mix themselves together.

## 8.2 The Plume Rise Model

The new plume rise model, based on a similar approach but for chemical reactions [1], is introduced in the Lagrangian stochastic model SPRAY [7]. In the model each particle carries a quantity which specifies the difference between the temperature and the momentum of the plume and the environment air. To this aim we assign to any emitted particle in the time interval $\Delta t$ the "equivalent mass" $m_T$, defined as follows:

$$m_{T_i} = \frac{\left[T_{pinit} - T_a(H_s)\right] w_u S \, \Delta t}{N_p}$$

where $T_{pinit}$ is the initial plume temperature, $T_a(H_S)$ is the environment air temperature at the stack height, $S$ is the stack section, $N_P$ is the total number of particles released in the time interval $\Delta t$ and $w_u$ the plume exit velocity. The air-plume temperatures difference for the cell is:

$$\Delta T_c\,(t_0) = \frac{\sum_i^M m_{T_i}(t_0)}{V_c},$$

where M is the number of particles in the cell and $V_c$ is the cell volume. The new temperature difference $\Delta T_c(t_1)$ (where $t_1 = t_0 + \Delta t$) is calculated by the equations:

$$\Delta T_c(t_1) = \Delta T_c(t_0) + T_a(t_0) - T_a(z_c)$$

where $z_c$ is the cell height and $T_a(t_0)$ is the mean of the temperature "memory" carried by each particle. Afterwards, the value of $w_b$ is computed in every cell using the following equation:

$$w_b = \frac{\Delta T_c}{T_a(z_c) + \Delta T_c}\ g\ \Delta t,$$

Then, the "equivalent mass" is computed for each particle following the method proposed by Chock and Winkler [5]:

$$m_{T_i}(t_1) = \frac{m_{Ti}(t_0) \cdot \Delta T_c(t_1)}{\Delta T_c(t_0)}.$$

Furthermore, to each particle is assigned the "memory" of the air temperature through the equation:

$$T_{a_i}(t_1) = T_a(z_c)$$

A similar procedure (not shown for sake of brevity) is applied to calculate the plume vertical velocity due to the initial momentum and damped by the entrainment.

## 8.3 Simulation Results

Some preliminary results in isothermal (stable) condition are presented in Fig. 8.1. The plume barycenter height trend is compared with those obtained using the Briggs formula for neutral conditions [4] that can be assumed correct for the first rise stage

$$h(t) = \frac{1.6 F_b^{1/3} \cdot t^{2/3}}{u^{1/3}}$$

and with the previous method implemented in the model SPRAY [2]. The equilibrium height (depicted with the horizontal line) is computed following Briggs [4]:

$$h_{\max} = 2.6 \cdot \left(\frac{F_b}{u \cdot s}\right)^{1/3}$$

Figure 8.1 shows that both the equilibrium height and the trend are correctly predicted by the new plume rise model for the wind velocity different from zero. In the case of low wind velocity (U = 0.01 m/s) the theoretical formula cannot give reliable results. Further, it is worth noticing that the neutral Briggs formula applies only close to the source.

The encouraging results suggest the application of this method also in different atmospheric stability conditions.

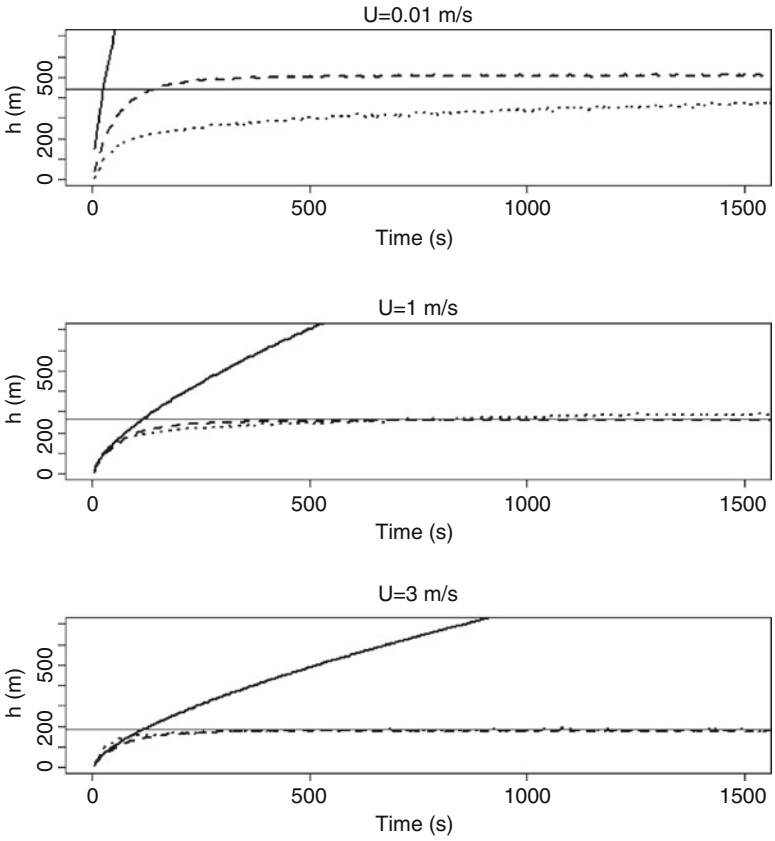


**Fig. 8.1** Plume barycenter height vs time from the emission computed for three different horizontal velocities in isothermal condition. New method (*dotted line*), old SPRAY method (*dashed line*), Briggs formula (*continuous line*), $h_{max}$ (*horizontal continuous line*)

**Acknowledgments** This work has been financed by the Research Fund for the Italian Electrical System under the Contract Agreement between RSE and the Ministry of Economic Development – General Directorate for Energy and Mining Resources stipulated on July 29, 2009 in compliance with the Decree of March 19, 2009.

## References

1. Alessandrini S, Ferrero E (2009) A hybrid lagrangian-eulerian particle model for reacting pollutant dispersion in non-homogeneous non-isotropic turbulence. Phys A 388:1375–1387
2. Anfossi D, Ferrero E, Brusasca G, Marzorati A, Tinarelli G (1993) A simple way of computing buoyant plume rise in a Lagrangian stochastic dispersion model for airborne dispersion. Atmos Environ 27A:1443–1451
3. Anfossi D, Tinarelli G, Trini Castelli S, Nibart M, Olry C, Commanay J (2009) A new Lagrangian particle model for the simulation of dense gas dispersion. Atmos Environ 44 (2010):753–762

4. Briggs GA (1975) Plume rise predictions. In: Haugen D (ed) Lectures on air pollution and environmental impact analyses. Workshop proceedings, Boston. AMS Publications, Boston, pp 59–111
5. Chock DP, Winkler SL (1994) A particle grid air quality modeling approach, 2. Coupling with chemistry. J Geophys Res 99D1:1033–1041
6. Hurley PJ (2005) The Air Pollution Model (TAPM) Version 3. Part1: Technical Description. CSIRO Atmospheric Research Technical Paper No. 71
7. Tinarelli G, Anfossi D, Bider M, Ferrero E, Trini Castelli S (2000) A new high performance version of the Lagrangian particle dispersion model SPRAY, some case studies. In: Gryning SE, Batchvarova E (eds) Air pollution modelling and its applications XIII. Plenum Press, New York, pp 499–506
8. Webster HN, Thomson DJ (2002) Validation of a Lagrangian model plume rise scheme using the Kincaid data set. Atmos Environ 36:5031–5042

## Questions and Answers

**Questioner Name**: Steve Hanna

**Q**: Earlier, your group shoved applications of your model to dense gases. I would think that the same equations should apply to both dense and buoyant gases. Is your model equally applicable to plumes with positive and negative buoyancy?

**A**: Yes, the equations developed earlier by our group apply to dense and buoyant gas. However, they are Eulerian in principle and pose some questions in applying them in a Lagrangian context. Moreover they are based, as all the existing plume rise equations, on the entrainment hypothesis. The present plume rise derivation is completely Lagrangian and does not make use of any entrainment hypothesis but verifies it and may be applied to both dense and light emissions.

**Questioner Name**: Jeff Weil

**Q**: The trajectory of the two-stacks plume looked quite different from the single-stack trajectory, which is $\Delta h = c_1 F^{\frac{1}{3}} x^{\frac{2}{3}}$. But the ultimate rise for the 2-stacks plume should be $\Delta h = c_1 (2F)^{\frac{1}{3}} x^{\frac{2}{3}}$ and $2^{\frac{1}{3}} = 1.26$ so the rise of the 2-stacks case could at most be 26% higher than the single-stack case. You should check to make sure that your 2-stacks rise is $\leq 1.26 \Delta h(1stack)$

**A**: During the presentation it has been shown the example of the rise of two-stack plume. There are 2 stacks at a distance of 100 m whose plumes collide and rise together. In neutral conditions the total plume rise of the single plume is around 400 m while the two plumes total rise is around of 500 m. So the condition is verified.

**Questioner Name**: Eugene Genikhovich

**Q**: One of the scalars carried by the particle in your model is the atmospheric temperature memory. How could one parameterize with no measurements data describing it?

**A**: In our model the use of the scalar "temperature memory" is introduced only to take into account non-isothermal conditions. It is just the temperature of the atmosphere at the position of each particle at the previous time step. In this way it is possible to know, inside each computational cell, which is the average atmospheric temperature condition at the level where the temperature difference of each particle was computed at the previous time step.

# Chapter 9
# Influence of Wall Heating in a Street Canyon on Kinetic Energy and Scalar's Exchange: A Large-Eddy Simulation

**Xiaoming Cai**

**Abstract** A large-eddy model is developed for a street canyon flow and dispersion of scalars when building/street surfaces are heated by solar radiation. A wall function for temperature and scalar is proposed at the building/street surfaces. The model is applied to a canyon, with the aspect ratio of unity and background wind blowing across the canyon axis, for two idealised heating scenarios: (1) the roof and the upstream wall (UW) are heated, and (2) the roof and the downstream wall (DW) are heated. In Case (1), the mean primary vortex (MPV) driven by the boundary layer wind is *assisted* by the thermal updrafts near the heated UW and the turbulent kinetic energy (TKE) inside the canyon is also enhanced with the increasing wall temperature. In Case (2), however, the MPV is *opposed* by the thermal updrafts near the heated DW and its intensity is inhibited remarkably. On the other hand, the TKE inside the canyon for Case (2) increases with the wall temperature, more significantly in comparison with that for Case (1). Consequently the advective flux driven by the MPV is comparable to the turbulent flux driven by TKE at the roof level for Case (1), but the advective flux is negligible for Case (2). These results are useful for proposing a new parameterisation scheme for a street canyon air quality model.

**Keywords** Urban street canyon • Large-eddy simulation • Wall heating

## 9.1 Introduction

In an urban street canyon, transport of air pollutants to the boundary layer (BL) aloft is subject to air flow and turbulent structure inside and above the canyon. In the presence of solar radiation, the surface temperatures on the street/wall/roof may be much higher

X. Cai (✉)
School of Geography, Earth and Environmental Sciences,
University of Birmingham, Edgbaston, Birmingham B15 2TT, UK
e-mail: x.cai@bham.ac.uk

D.G. Steyn and S. Trini Castelli (eds.), *Air Pollution Modeling and its Application XXI*,
NATO Science for Peace and Security Series C: Environmental Security 4,
DOI 10.1007/978-94-007-1359-8_9, 

than that of the air and this can significantly affect the air flow and turbulent structure, and therefore the transport of pollutants. Specifically, when solar radiation heats one side of the canyon, the thermally driven updrafts may interact with the primary vortex inside the canyon which is driven by the BL wind if there were no solar radiation. In this study, a large-eddy simulation (LES) model is adopted in order to reveal such effects. Two idealized scenarios are considered: (1) the roof and the upstream wall (UW) are heated, and (2) the roof and the downstream wall (DW) are heated. The BL wind blows from the UW to the DW perpendicularly.

## 9.2 Model Configurations

### *9.2.1 Domain Setting*

The dynamical part of the LES model adopted in the present study is similar to that in an early paper by Cai et al. [1], in which dispersion and transfer of surface scalars for the neutral case with various street canyon aspect ratios ($H/W$) has been validated against wind tunnel experiments, in which $H$ is the building height and $W$ is the canyon width. The wind above the canyon blows from the left to the right. Cyclic boundary condition is applied to all wind components and temperature in both $x$- and $y$-directions, but for a passive scalar, an advective constraint is specified at the outlet of the domain. Because the flow behaves periodically in the $x$- and $y$-directions, only one canyon with a finite length is configured for the simulations. Left boundary of the domain is at the middle of the upstream building and right boundary at the middle of the downstream building so that the domain width $L_x$ equals to $W + B$. In the present study, $H = 18$ m, $B = 6$ m and $W = 18$ m; a length of the modelling domain, $L_y = 40$ m. The domain is covered by $80 \times 40 \times 91$ grid points with grid spacing of 0.3 m $\times$ 0.3 m $\times$ 1.0 m inside the canyon. Above the canyon top, the vertical grid spacing is stretched gradually to about 5 m at the top of the domain. The maximum wind speed at the top of the domain is 2.5 m $s^{-1}$.

### *9.2.2 Roughness Length for Temperature and Scalar*

In order to apply this LES model to non-neutral cases such as the wall-heating scenarios, a wall function for temperature is developed for all canyon facets. This function allows a calculation of heat flux when surface temperature is given (readily available through direct measurements or remote sensing observations in reality). It is well known that in the framework of the Reynolds analogy, heat/scalar transfer is much less efficient than momentum transfer; in other words, resistance to heat/scalar transfer, $\ln\frac{(z_1/z_{0T})}{(\kappa u^*)}$, is greater than that to momentum transfer, $\ln\frac{(z_1/z_{0T})}{(\kappa u^*)}$, by a percentage of $\ln\frac{z_0/z_{0T}}{(z_1/z_0)}$, in which $z_0$ is the roughness length, $z_{0T}$ is that

for temperature and $z_1$ is a reference distance to the surface. In this study a value of $\ln(z_0/z_{0T}) = 5.0$ is adopted in a modified Louis scheme [5]. The boundary condition is used for temperature on the heated facets and for a passive scalar imposed as an area source on the street surface (a constant value of $C_0 = 1.0$ on the surface).

### 9.2.3 *Wall Heating Scenarios*

Two categories of wall heating scenarios are simulated: upstream-wall heating (UWH) cases (namely, Cases 'd00') and downstream-wall heating (DWH) cases (namely, Cases '00d'), where the value 'd' is the temperature difference between the surface and the air (when 'd' $>$ 10, 'A' $=$ 10, 'B' $=$ 11, etc.). The three numbers in a case name represent the temperature difference between the UW, the street surface, and the DW, respectively, and the air. The temperature difference for the roof is the same as that for the heated wall.

## 9.3 Results and Discussion

Figure 9.1a displays the mean kinetic energy (MKE) and TKE for the UWH cases in which the thermally driven updrafts *assist* the mechanically driven mean primary vortex (MPV). The results of MKE indicate that the intensity of the MPV is enhanced by the wall heating; meanwhile, TKE also increases. For the DWH cases, however, MKE is depressed by the increasing wall heating mainly because the thermally driven updrafts *oppose* the mechanically driven MPV (Fig. 9.1b). TKE is generally higher than that of the corresponding UWH case.

An important parameter quantifying the exchange between the urban BL and urban canopy layer (CL) is the *exchange velocity*, or *transfer velocity*, denoted by

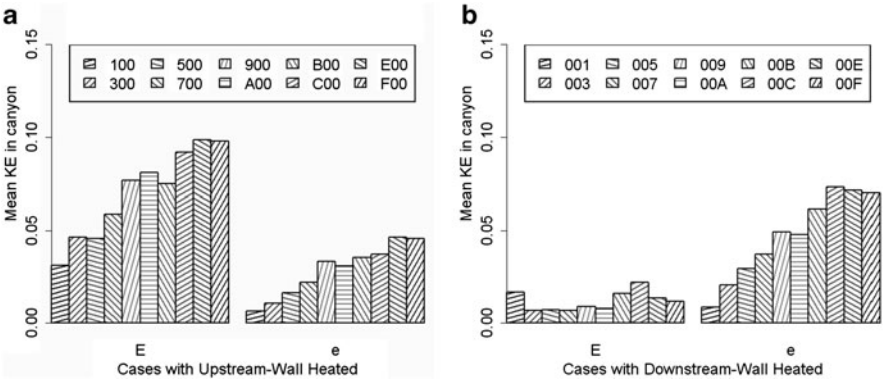


**Fig. 9.1** Mean kinetic energy (MKE) and turbulent kinetic energy (TKE) for all cases

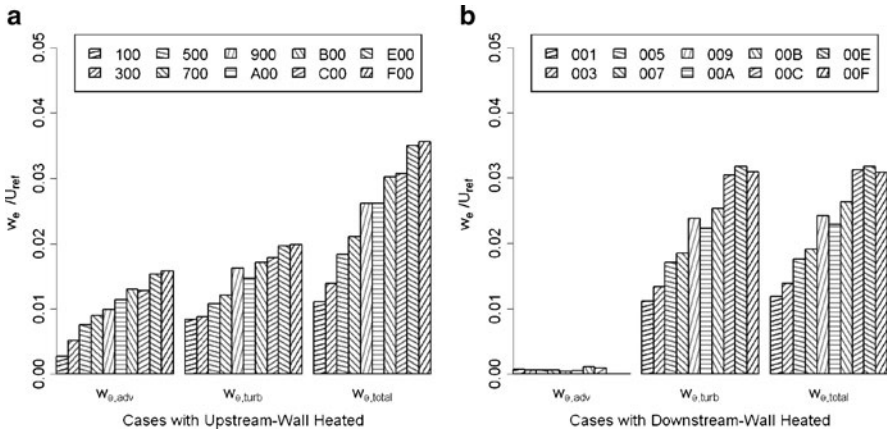


**Fig. 9.2** Normalised exchange velocities $\frac{W_e}{U_{ref}}$ derived from the advective, turbulent, and total flux of the scalar for all cases

$W_e$ hereafter. Its definition in a bulk form for a scalar $C$ is $W_e = \frac{F_{CLT}}{\langle C_{CL} \rangle - C_{BL}}$, in which $F_{CLT}$ is the flux at the canopy layer top (CLT), $\langle C_{CL} \rangle$ is the averaged concentration in the CL, and $C_{BL}$ is the concentration is the BL. It is noted that the exchange of air between the street canyon and the BL is contributed by two mechanisms: advection by mean flow and mixing by turbulence; the exchange velocities respective to these two are denoted by $W_{e,adv}$ and $W_{e,turb}$. In general, $W_{e,adv} (= \langle C_{CL} \rangle)$ is non-zero due to the spatial inhomogeneity of $\bar{w}_{CLT}(x)$ and $\bar{C}_{CLT}(x)$ at the CLT. Figure 9.2a shows that the magnitude of $W_{e,adv}$ can be as large as that of $W_{e,turb}$ for the UWH cases. Furthermore, both $W_{e,adv}$ and $W_{e,turb}$ are enhanced by UWH. For the DWH cases, however, the contributions from $W_{e,adv}$ to $W_{e,total}$ is negligible compared with $W_{e,turb}$; in other words, turbulent mixing dominates. It must be noted that the $W_e$ defined here is based on $\langle C_{CL} \rangle$ rather than $C_0 (= 1.0)$; using the latter, $W_e$ would be much smaller, representing the exchange velocity between the *street surface* and the BL.

## 9.4 Conclusion

This study has obtained a unique finding that the decomposition of the exchange velocity into $W_{e,adv}$ and $W_{e,turb}$ possesses very different features for the UWH and DWH cases. This is mainly caused by the interaction between the mechanically driven MPV and thermally driven updrafts. This new finding is useful for proposing a new parameterisation scheme for a street canyon air quality model.

**Acknowledgments** The computations described in this paper were performed using the University of Birmingham's BlueBEAR HPC service, which was purchased through HEFCE SRIF-3 funds. See http://www.bear.bham.ac.uk for more details.

## References

1. Cai XM, Barlow JF, Belcher SE (2008) Dispersion and transfer of passive scalars in and above street canyons – large-eddy simulations. Atmos Environ 42(23):5885–5895
2. Li XX et al. (2010) Large-eddy simulation of flow and pollutant transport in urban street canyons with ground heating. Bound-Lay Meteorol 137:187–204
3. Kim JJ, Baik JJ (2001) Urban street-canyon flows with bottom heating. Atmos Environ 35:3395–3404
4. Xie XM, Liu CH, Leung DYC (2007) Impact of building facades and ground heating on wind flow and pollutant transport in street canyons. Atmos Environ 41:9030–9049
5. Uno I, Cai XM, Steyn DG, Emori S (1995) A simple extension of the Louis method for rough surface layer modelling. Bound-Lay Meteorol 76(4):395–409

## Questions and Answers

**S. Vardoulaki**: What would be the influence of a heated pavement and/or carriageway on the average flow and TKE generated within the street canyon?
**X.-M. Cai**: There have been a few modelling studies on this topic (e.g. Li et al. [2]; Kim and Baik [3]; Xie et al. [4]). In general, these results demonstrate a strong influence of ground heating on the flow and TKE within the street canyon as well as the exchange between the canyon air and the boundary layer above.

**M. Biliaiev**: What was the boundary condition for heat flux on the heated wall? Was it an unsteady heat flux?
**X.-M. Cai**: The boundary condition on the heated wall was not given to heat flux but to temperature. There are two types of boundary conditions on building surfaces for temperature (or any scalar): (1) a given flux at the facets (e.g. heat flux at the walls), and (2) a given value at the facets (e.g. temperature at the walls). For the cases studied here in which some facets are heated, the data of surface temperature are readily available through direct measurements or remote sensing observations. Therefore the boundary condition of a given value of temperature is used in this study. The novelty of this study is to adopt a modified Louis scheme [5] as the wall function, using a smaller roughness length for temperature (or scalar) than that for momentum. The heat flux at the walls will be calculated based on the wall function.

**A. Venkatram**: How did you use the LES simulations to interpret the data you showed at the beginning of your talk?
**X.-M. Cai**: I need to clarify that the data showed at the beginning of my talk serve as the motivation to this study. I do not intend to interpret the data using the LES output at this stage.

# Chapter 10
# Stable Boundary Layer Modeling for Air Quality Applications

**Jeffrey C. Weil**

**Abstract** The stable boundary layer (SBL) is one of the key modeling problems for air quality predictions at local and regional scales. This paper presents an SBL model for the mean wind, temperature, and turbulent flux profiles over a range of stability based on an eddy-diffusivity approach. Model results agree well with large-eddy simulations and observations in both weakly- and very-stable boundary layers.

**Keywords** Eddy diffusion • Mean wind • Stable boundary layer • Turbulence

## 10.1 Introduction

Modeling of the stable boundary layer (SBL) is one of the outstanding challenges for air quality applications at local and regional scales. A recent study by Cuxart et al. [3] showed that SBL models used in regional-scale wind-field models overestimated the SBL depth and surface friction velocity, which characterizes the SBL turbulence. This led to weaker stability and stronger turbulence in the modeled SBLs than in reality, and would lead to under-predicted concentrations for a surface release in the SBL. However, the concentrations due to a surface source are highest in the SBL by comparison to other stabilities (e.g., unstable conditions), and thus it is important to correct this problem.

As suggested by Mahrt [4], it is useful to think about the SBL by considering two extreme states: (1) the weakly stable boundary layer (WSBL) driven by moderate-to-strong winds and weak thermal stratification, and (2) the very stable

J.C. Weil (✉)
CIRES, University of Colorado, Boulder, CO 80309, USA

Research Application Lab, National Center for Atmospheric Research,
3450 Mitchell Lane, Boulder, CO 80303, USA
e-mail: weil@ucar.edu

D.G. Steyn and S. Trini Castelli (eds.), *Air Pollution Modeling and its Application XXI*,
NATO Science for Peace and Security Series C: Environmental Security 4,
DOI 10.1007/978-94-007-1359-8_10, 

boundary layer (VSBL) characterized by light winds, strong radiative cooling, and very stable stratification. Of the two, we know less about the VSBL owing to complications caused by the weak wind forcing, strong stratification, and intermittent turbulence. In the modeling below, we address both SBL cases and the continuous variation from one to the other.

## 10.2 SBL Modeling and Parameterization

A one-dimensional model is presented for predicting the shapes of vertical profiles of the mean wind, potential temperature, and turbulent fluxes in the SBL. The model consists of the differential equations for the mean horizontal wind components and potential temperature and are closed using an eddy-diffusivity ($K(z)$) parameterization of the turbulent momentum and heat fluxes, where $z$ is height above the surface. The approach is justified because of the small turbulence length scales in the SBL. The $K(z)$ form adopted here is that of Brost and Wyngaard (BW) [2] because it: (1) accounts for the surface layer behavior wherein the Monin-Obukhov (MO) similarity expressions are valid, (2) has an appropriate decrease of $K$ with $z$ throughout the SBL, and (3) agrees well with large-eddy simulation (LES) results of a WSBL [1] and observations. As shown below, this diffusivity depends on the stability parameter $h/L$, where $h$ and $L$ are the SBL height and MO length, respectively.

We briefly present the analysis and solution method for obtaining the potential temperature ($\theta$) and heat flux ($H$); a similar approach is used for finding the mean wind and stresses. The SBL is considered to be horizontally homogeneous so that the above variables are only functions of $z$, time $t$, and the boundary conditions. Thus, the $H$ and stresses ($\tau_{xz}$ and $\tau_{yz}$) are prescribed by $H = -K_h\ (\partial\theta/\partial z)$, $\tau_{xz} = K_m\ (\partial U/\partial z)$, and similarly for $\tau_{yz}$, where subscripts $h$ and $m$ denote the diffusivities for heat and momentum, and $U$ is the mean wind in the $x$ or east-west direction.

The Brost and Wyngaard form for the heat diffusivity in dimensionless form is given by $K_h/(u_* h) = k \cdot (z/h)(1 - az/h)^p / [1 + \beta(h/L)(z/h)]$, where $k$ (= 0.4) is the von Karman constant, and $u_*$ is the surface friction velocity; BW adopted $a = 1$, $p = 3/2$, and $\beta = 4.7$ based on their second-order closure model results. For $z/h << 1$, the diffusivity reduces to the MO surface-layer similarity expression for stable conditions. In addition, the $h/L$ in the $K_h$ expression serves as a stability index where small values, $h/L \leq 3$, correspond to a WSBL and large values, e.g., $h/L > 10$, to a VSBL. BW [2] found that the above form for $K_h$ also fit their $K_m$ results, but with $K_m$ averaging about 0.8 $K_h$ over the SBL.

The potential temperature was found by first deriving an expression for the vertical heat flux, and then solving for $\theta$ using the flux-gradient relationship, $H(z,t)$, and $K_h(z)$. This performed much better than the usual method of substituting the flux-gradient expression directly into the heat or $\theta$ equation. The overall solution was obtained by reducing the partial differential equation for $H$ to an ordinary differential equation using a similarity variable, $\eta = \int d\xi/[2K_h(\xi)t]^{1/2}$

where $\xi$ is a dummy variable for $z$. This led to $H(\eta) = H_0(1 - \mathrm{erf}(\eta/\sqrt{2}))$, where $H_0$ is the surface flux and also to a reasonably simple form for $\theta(\eta)$. The variations of $H$ and $\theta$ with $z$ and $t$ were then obtained by inverting the $\eta(z,t)$ relationship.

## 10.3 Results

Figure 10.1a shows profiles of the dimensionless potential temperature change with time following evening transition in a WSBL with $h/L = 1.6$, where $\theta_h$ and $\theta_0$ denote the temperatures at the SBL top and surface, respectively; this is the WSBL case explored by Beare et al. [1]. The $\theta$ at evening transition is assumed to be uniform with $z$, whereas the $\theta_h$ and $\theta_0$ are independent of $t$ and a function of $t$, respectively. The profiles exhibit a rapid development with time over the period shown – 0.5–8 h, and the profile shape at 8 h agrees well with that from the LES at 9 h. Note that at $t = 8$ h there is a weak stability over much of the SBL with an inversion developing at the SBL top.

Figure 10.1b shows that the heat flux profiles for the same WSBL case also have a systematic development with time. Moreover, the profile at 8 h agrees well with the LES results and the mean of the field data (points) obtained by Nieuwstadt [6], which correspond to an average $h/L = 1.5$. The field measurements began about 2–3 h after evening transition and continued until sunrise. The field data have a broad variability as indicated by the horizontal bars, with the left-most limit being close to the model curve at $t = 2.5$ h, the approximate starting time of the measurements. Thus, the time varying nature of the modeled profiles suggests that there may be a systematic component to the field data variability.

For a VSBL with $h/L = 40$, the modeled temperature profiles in Fig. 10.2a demonstrate a systematic, but much slower development with time than for the WSBL.

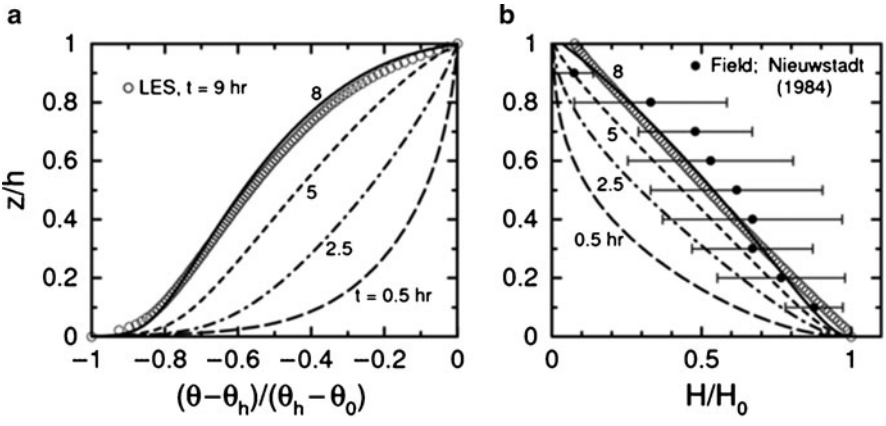


**Fig. 10.1** Variation of vertical profiles of potential temperature and heat flux with time in a weakly stable boundary layer with model results given by lines. The LES results were provided by P.P. Sullivan and E.G. Patton and are the "NCAR" case in Beare et al. [1]

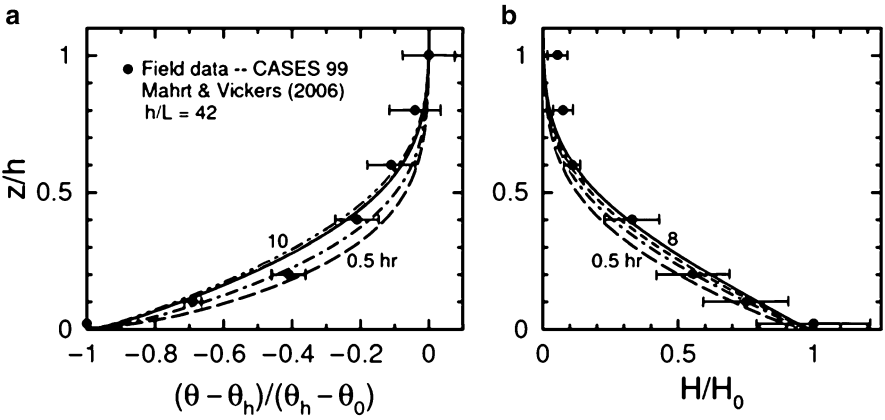


**Fig. 10.2** Variation of vertical profiles of potential temperature and heat flux with time in a very stable boundary layer

The general shape of the profiles is consistent with the CASES 99 field data analyzed by Mahrt and Vickers [5]. Figure 10.2b shows that the modeled heat fluxes also agree well with the CASES 99 measurements. As with the temperature, the variation of the flux profiles with time is much less than that found for the WSBL. This is probably due to the smaller diffusivity ($K_h$) in the VSBL. Overall, the behavior and shapes of the temperature profiles in both the VSBL and WSBL are in agreement with observations reported by van Ulden and Holtslag [8].

## 10.4 Applications to Dispersion

In order to apply this model to local-scale dispersion, it must be completed with predictions of the turbulent velocity variance profiles. Such profiles can be obtained by solving a simplified form of the turbulent kinetic energy equation along with those for the mean winds, θ, etc. The full set of predicted profiles could then be used to drive a Lagrangian particle dispersion model (LPDM) for the SBL. The results of the LPDM predictions could be tested by comparison with those of an LPDM driven by LES fields, which has already been done for a WSBL and tested against the Prairie Grass data for WSBLs, i.e., $h/L < 4$. An advantage of the LPDM driven by predicted or parameterized mean wind and turbulence profiles is that it also could be used for a VSBL, where LES currently does not apply.

**Acknowledgements** I thank Drs. P.P. Sullivan and E.G. Patton for providing the LES results used in Fig. 10.1 and Dr. Y. Kimura for helpful discussions on the solution method for the wind profiles. This work was sponsored by the MACTEC Corporation under funding from the U.S. Environmental Protection Agency and by the Army Research Office under Grant W911NF-09-0572.

## References

1. Beare RJ et al (2006) An intercomparison of large-eddy simulations of the stable boundary layer. Bound-Layer Meteorol 118:247–272
2. Brost RA, Wyngaard JC (1978) A model study of the stably stratified planetary boundary layer. J Atmos Sci 35:1427–1440
3. Cuxart J et al (2006) Single-column model intercomparison for a stably stratified atmospheric boundary layer. Bound-Layer Meteorol 118:273–303
4. Mahrt L (1999) Stratified atmospheric boundary layers. Bound-Layer Meteorol 90:375–396
5. Mahrt L, Vickers D (2006) Extremely weak mixing in stable conditions. Bound-Layer Meteorol 119:19–39
6. Nieuwstadt FTM (1984) The turbulent structure of the stable nocturnal boundary layer. J Atmos Sci 41:2202–2216
7. Strang EJ, Fernando HJS (2001) Turbulence and mixing in stratified shear flows. J Fluid Mech 428:349–386
8. van Ulden AAP, Holtslag AAM (1985) Estimation of atmospheric boundary layer parameters for diffusion applications. J Clim Appl Meteorol 24:1196–1207

## Questions and Answers

**Question (Enrico Ferrero)**: Is your model able to predict turbulence for Richardson numbers greater than its critical value?

**Response (Jeffrey Weil)**: The answer depends on which Richardson number – gradient $Ri$ or bulk $Ri_b$ – is considered and the critical value taken: $Ri_c = 0.25$ from linear stability theory or 1 from nonlinear theory [7]. The $Ri$ has not yet been computed from the model profiles for mean wind and potential temperature but could be and will be in the future. However, for the WSBL case ($h/L = 1.6$) used here, the $Ri$ within the SBL from the LES profiles is $Ri \leq 0.23$ and the $Ri_{bh} \approx 0.2$. That is, they are both less than the $Ri_c = 0.25$ value as expected based on Nieuwstadt's [6] analysis and results for a WSBL and those of Beare et al. [1]. Here, $Ri_{bh}$ is the bulk Richardson number for the SBL as a whole and is $Ri_{bh} = g\Delta\theta_h h/(\theta_0 U_h{}^2)$, where $g$ is the gravitational acceleration, $\Delta\theta_h$ is the potential temperature change ($= \theta_h - \theta_0$), and $U_h$ is the wind speed at the SBL top.

For the VSBL ($h/L \approx 40$) and the CASES 99 data, the $Ri_{bh} = 1.2$ and thus is at or near the $Ri_{bc} = 1$ limit. For the FLOSS VSBL data analyzed by Mahrt and Vickers [5], the model did not work well for the wind and flux profile predictions; at FLOSS, the $Ri_{bh}$ was 51 and hence much greater than 1. The $U_h$ ($= 0.35$ m/s) at FLOSS was so low that the mechanically-forced turbulence was extremely weak and dominated by other forcings, e.g., density-driven flows and turbulence, horizontal inhomogeneities in landscape, roughness, and winds, etc. Based on this discussion, the current model is expected to apply for an $Ri_{bh} \leq \lambda$, where $\lambda$ is of the order of 1; further work is necessary for a better determination of $\lambda$.

# Chapter 11
# Street Canyon Atmospheric Composition: Coupling Dynamics and Chemistry

**Vivien Bianca Bright, William James Bloss, and Xiaoming Cai**

**Abstract** The composition of air within a street canyon is determined by the composition of background air mixed in from above, advection of air into and out of the canyon, emissions from within the street, and the mixing and chemical processing of pollutants within the canyon. This paper describes a modelling study of street canyon atmospheric composition, integrating the combined effects of emissions, dynamics and chemistry. The research builds upon an existing dynamical model of canyon atmospheric motion (Large Eddy Simulation model) by adding a detailed chemical reaction scheme.

**Keywords** Street canyon • LES • RCS • Air quality • Composition • Chemistry

## 11.1 Introduction

A modelling study of street canyon atmospheric composition is outlined, integrating the combined effects of emissions, dynamics and chemistry. The interaction of these factors determines both the pollutant concentrations experienced within the canyon, their spatial and temporal variation, and the extent to which emissions are pre-processed within the street before escaping to the wider boundary layer. The timescale of both the chemistry ($NOx$-$O_3$ steady state and $HO_2$/$RO_2$ reactions) and dynamics are of the same order of magnitude (a few seconds to minutes). Within-canyon dynamical processes can have a significant effect on atmospheric chemical processing on such timescales.

A Large Eddy Simulation (LES) model is used to accurately simulate the atmospheric motion and mixing which result from background air flowing over a

V.B. Bright • W.J. Bloss • X. Cai (✉)
Department of Geography, Earth and Environmental Sciences,
University of Birmingham, Edgbaston, Birmingham B15 2TT, UK
e-mail: x.cai@bham.ac.uk

D.G. Steyn and S. Trini Castelli (eds.), *Air Pollution Modeling and its Application XXI*,
NATO Science for Peace and Security Series C: Environmental Security 4,
DOI 10.1007/978-94-007-1359-8_11, 

street canyon and the chemical interaction between the various chemical species present. The existing LES model is enhanced through the development and application of a more detailed chemical reaction scheme. This will provide a powerful tool to further investigate the non-linearity of mixing and chemical processing and to assess the extent to which emissions are processed within the canyon before escaping to the wider urban boundary layer.

## 11.2 Modelling Approach

A zero-dimensional box model was used to develop a suitable (computationally affordable) reduced chemical scheme to apply to the LES model. As a basis for scheme development, the Common Representatives Intermediates mechanism version (CRI V2-R5) [5, 6] (a subset of a near explicit chemical mechanism, the Master Chemical Mechanism (MCM) [4]) was used. This was further reduced by considering daytime processes alone and removing those species and reactions that result in minimal changes in the concentration of important chemical species (including OH). The final reduced chemical scheme (RCS) includes 51 chemical species and 136 reactions.

The RCS was compared to the MCM, the latter providing a benchmark to evaluate the accuracy of the developed mechanism. The box model was initially run with chemistry alone. Over a 4 h period the maximum difference in OH between the RCS and the MCM is $\approx 6\%$ i.e. within the bounds of the smallest errors associated with the measurement of OH. The RCS is therefore is suitable to incorporate into a dynamical model such as the LES.

The LES model used (from Cui et al. [3]), simulates turbulent flow in and above an idealised street canyon with an aspect (H/W) ratio of one (Fig. 11.1). This has been previously used to investigate dispersion and $NO_X$-$O_3$ chemistry with three chemical reactions applied [1]. Following the implementation of the RCS, the LES model was run without chemistry for 30 min in order to establish dynamical equilibrium. At this time, a set of concentrations of all chemical species (derived from the enclosed box model) is inserted in the whole model domain; this set of values is also used as the inlet boundary conditions above the upwind building.

## 11.3 Results and Discussion

Spatially averaged 'within canyon' concentrations of NO, $NO_2$, $O_3$, OH and $HO_2$ were calculated using the LES model and compared to the box model (BOX) with equivalent emissions and external mixing (exchange velocity, $\omega_t \approx 0.020$ m $s^{-1}$) after 30 min and without chemical deposition (Fig. 11.2). The results illustrate the effect of the inhomogeneous emissions within the LES model on species concentration when compared to the box model and the instantaneous mixing of pollutants.

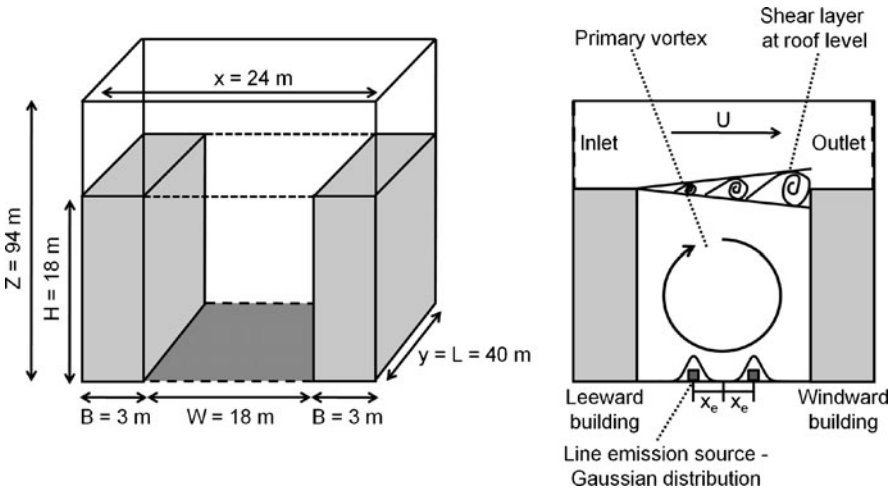


**Fig. 11.1** A schematic illustration of the LES model configuration and canyon characteristics. Emissions within the canyon are represented by two line sources at 2.5 m to the *left* and the *right* of the canyon centre. Emission rates represent moderate weekday traffic (1,500 veh $h^{-1}$) travelling at an average speed of 30 mph (Adapted after Baker et al. [1])

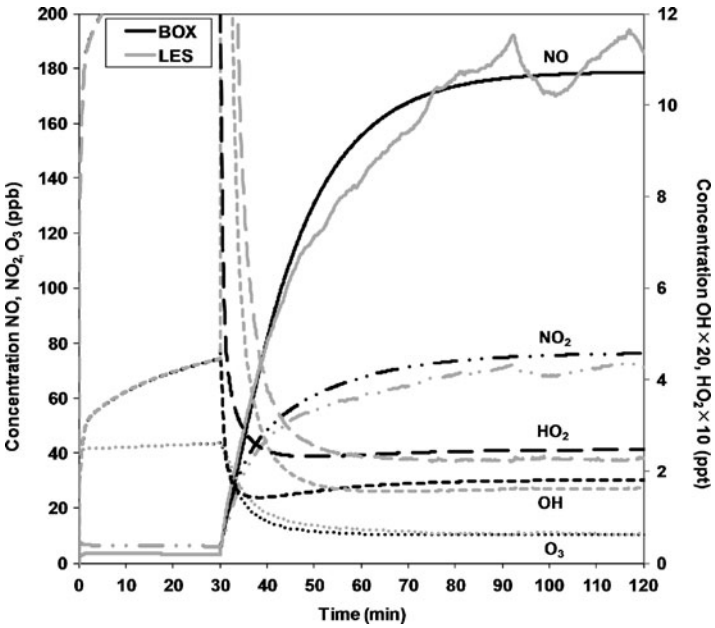


**Fig. 11.2** Time evolution of modelled NO, $NO_2$, $O_3$ (ppb), OH and $HO_2$ (ppt) mixing ratios

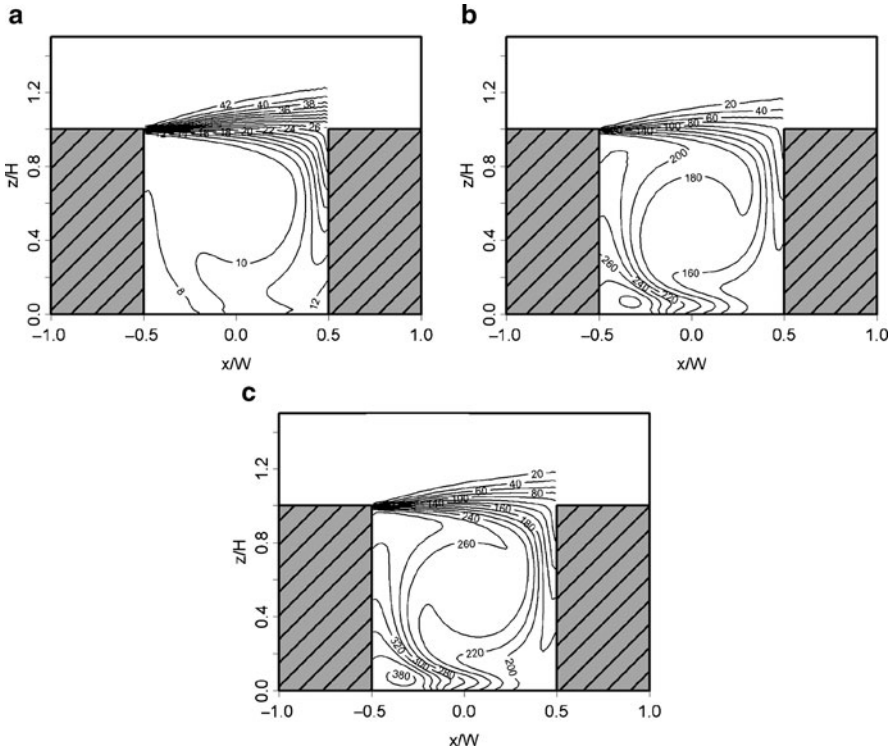


**Fig. 11.3** Mean (**a**) [$O_3$], (**b**) [NO], and (**c**) (a passive scalar) in ppb between t = 90–120 min

Figure 11.3 illustrates the mean concentrations of $O_3$, NO and a passive scalar between t = 90–120 min (by which time quasi-equilibrium is established). The highest concentrations of NO and the lowest concentration of $O_3$ occur toward the leeward wall due to NO + $O_3$ titration. Elevated levels of $NO_x$ occur within the canyon compared to the background air, with the highest levels toward the leeward wall. Pollutants are effectively trapped at roof level due the presence of a shear layer. This becomes increasingly turbulent toward the windward wall, allowing pollutants to escape at this point and background air to enter the canyon.

Exchange velocity is defined as, $\omega_t = F_c/(C\text{-}C_b)$, where $F_c$ is pollutant flux at roof level and the denominator is the difference between the pollutant concentration within (C) and above the canyon ($C_b$). For the passive scalar the average flux across roof level for $t = 90$–120 min is ca. 4.52 ppb m $s^{-1}$. Where $C \approx 248$ ppb and $C_b \approx 0.04$ ppb a value of $\omega_t \approx 0.018$ m $s^{-1}$ is obtained, an approximation to within 11% of the 0.020 m $s^{-1}$ value applied to the box model. As air is exchanged with background air in the upper part of the canyon using an average canyon concentration of pollutants may be inaccurate. A value of $\omega_t \approx 0.020$ m $s^{-1}$ is determined using a lower, near roof level (z/H = 0.9 − 1.0), concentration (C) of 224 ppb. In this case $\omega_t$ is in excellent agreement with that of the box model. $\omega_t$ here is

based on the canyon-mean C, representing the exchange velocity between the canyon and the air above and is much smaller than the values in Cai et al. [2] which represent the exchange velocity between the street surface and the air above the canyon.

This study demonstrates that the enhanced model is a suitable tool to investigate atmospheric composition. The importance of using a suitable technique to deduce $\omega_t$ based on LES output has been highlighted. Future work will refine these simulations which will then be used to determine the variance in canyon pollutant levels experienced by receptors, and the extent of chemical ageing of exhaust emissions.

**Acknowledgments** The authors would like to thank Dr. Mike Jenkin and Professor Dudley Shallcross for the provision of the Common Representatives Intermediates mechanism version 2-R5. VB also thanks the University of Birmingham for award of a Ph.D. scholarship.

## References

1. Baker J, Walker HL, Cai XM (2004) A study of the dispersion and transport of reactive pollutants in and above street canyons – a large eddy simulation. Atmos Environ 38(39):6883–6892. doi:10.1016/j.atmosenv.2004.08.051
2. Cai XM, Barlow JF, Belcher SE (2008) Dispersion and transfer of passive scalars in and above street canyons – large-eddy simulations. Atmos Environ 42(23):5885–5895. doi:10.1016/j.atmosenv.2008.03.040
3. Cui ZQ, Cai XM, Baker CJ (2004) Large-eddy simulation of turbulent flow in a street canyon. Q J R Meteorol Soc 130(599):1373–1394. doi:10.1256/qj.02.150
4. Saunders SM, Jenkin ME, Derwent RG, Pilling MJ (1997) World wide web site of a master chemical mechanism (mcm) for use in tropospheric chemistry models. Atmos Environ 31(8):1249–1249
5. Jenkin ME, Watson LA, Utembe SR, Shallcross DE (2008) A common representative intermediates (cri) mechanism for voc degradation. Part 1: Gas phase mechanism development. Atmos Environ 42(31):7185–7195. doi:10.1016/j.atmosenv.2008.07.028
6. Watson LA, Shallcross DE, Utembe SR, Jenkin ME (2008) A common representative intermediates (cri) mechanism for voc degradation. Part 2: Gas phase mechanism reduction. Atmos Environ 42(31):7196–7204. doi:10.1016/j.atmosenv.2008.07.034

# Chapter 12
# New Methods for Improvement of the Computational Efficiency of the Lagrangian Particle Dispersion Model

**Boštjan Grašič, Marija Zlata Božnar, and Primož Mlakar**

**Abstract** Paper presents three new methods to improve the computational performances of air-pollution modelling methodology based on Lagrangian particle dispersion model. New methods are developed in such a manner that properties of the original air-pollution model are preserved in their original form. All methods are complementary one to another and each one can be integrated into existing methodology separately as a standalone method. The first method is application of the clustering method for a reduction of the computational cost. The second method is the cell concentration kernel density estimation method adaptation that is used to substitute the box counting concentration estimation method. The Lagrangian particle-dispersion control method based on artificial neural networks is presented as third method to control the parameters of the Lagrangian particle model. All methods are applied to Spray Lagrangian particle model (product of Arianet s.r.l.) and validated on two field data sets on highly complex terrain in Slovenia. The validations proved the hypothesis that controlling the number of particles in the simulation using proposed new methods is actually preserving the quality of results at a constant level.

**Keywords** Lagrangian particle air pollution dispersion model • Computational efficiency • Clustering • Cell concentration kernel density estimation method • Artificial neural networks

B. Grašič (✉) • M.Z. Božnar • P. Mlakar
MEIS Environmental Consulting d.o.o., Mali Vrh pri Šmarju 78,
SI-1293 Šmarje – Sap, Slovenia
e-mail: bostjan.grasic@meis.si; marija.zlata.boznar@meis.si; primoz.mlakar@meis.si

D.G. Steyn and S. Trini Castelli (eds.), *Air Pollution Modeling and its Application XXI*,
NATO Science for Peace and Security Series C: Environmental Security 4,
DOI 10.1007/978-94-007-1359-8_12, 

## 12.1 Introduction

The aim of an air-pollution model is to simulate the dispersion of air pollutants in the ambient atmosphere. The impact of the air pollution from different well-known sources is studied on the basis of simulation results. In this paper three new methods are presented to improve the computational performance of the air-pollution modelling methodology. They are developed based on the limit capacities, properties and performance of the Lagrangian particle dispersion model [1]. The new methods are developed in a manner such that the original methods in the air-pollution modelling methodology are not modified at all. The parameters, methods and structure of the original air-pollution model are preserved in their original form and no additional adjustments are performed. The methods that determine and optimize the reconstruction of the computationally expensive air-pollution situations are integrated into the existing air-pollution modelling methodology [7].

## 12.2 Methods for Computational Improvements

### *12.2.1 Clustering of Virtual Particles*

First method for a reduction of the computational cost is usage of clustering for decrease of number of virtual particles in the simulations [4]. The computational expenses can be reduced by using this method by at least 50%. It has a minor influence on the quality of the results only when the final number of particles after clustering in the domain remains above a certain threshold.

According to the finally acquired results it is concluded that the hierarchical clustering method with additional parameters can be used in practice only for the limitation of a very large number of particles. In such a case the number of particles exceeds the normal values because of the occurrence of extreme situations: like the failure of the desulphurization plant when the emissions increase by an order of magnitude or when a very stable meteorological situation with low winds occurs and the air pollution starts to accumulate in the domain.

The strong limitation of the number of particles in the reconstructions during typical situations with the clustering method is not recommended because the quality of the results becomes very poor. A comparison of the original results and the results obtained with the clustering method showed that the results obtained with the clustering method can become bubbled and less smooth than the original.

An example of clustering method effectiveness in presented on Fig. 12.1. The upper left graph shows comparison of time used for the simulations between original model and model with integrated clustering. The lower two pictures of the domain show 3D situation. The clustering method is very effective in the case of low-wind conditions when the air pollution accumulates in the domain.

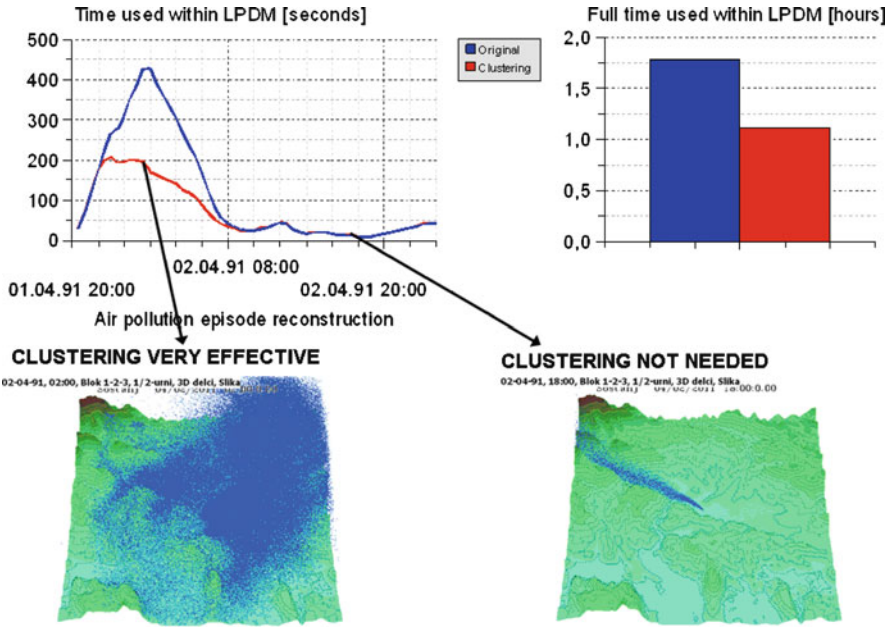


**Fig. 12.1** Effectiveness of clustering method

### *12.2.2 Kernel Density Estimation Method*

The cell concentration kernel density estimation method adaption is presented to substitute the box counting concentration estimation method. It is used to improve the poor quality of the results when a smaller number of particles is used in the simulations [2]. To evaluate the performance of the contributed method and the dependence on the input parameters, several simulations have been performed. In these experiments three cases of the optimal input parameters $\sigma_x$, $\sigma_y$ and $\sigma_z$ are determined for the experimental field data set according to the correlation with the reference. The comparisons simulation results of these three different optimal points show that the final optimal parameters are set from the example where the correlation with the original result is very good. The final comparisons prove that the correlation coefficient and the root mean square error are significantly improved. The fractional bias comparison showed that there are practically no underestimations in the results of the advanced simulation, which is crucial for long-term evaluations of air pollution.

This final comparison proved that the poor quality of the simulation results in situations when a relatively small number of particles is used can be improved by using the kernel density concentration estimation method.

### *12.2.3 Artificial Neural Networks*

The Lagrangian particle-dispersion control method based on artificial neural networks [5] also contributes to the control of the particle density parameter and the clustering parameter of the Lagrangian particle model. The rule for particle density control is the following: when high emissions occur the particle density should be decreased, and when low emissions occur the particle density can be increased. In special situations when the smallest possible particle density is used and it is still expected that the computational resources will be exceeded, the clustering must be activated to reduce the number of particles from a previous air-pollution episode reconstruction. This is very important for situations when extreme air pollution is expected. Such a common situation occurs in calm meteorological conditions when air pollution starts to accumulate in the domain for a longer time interval. The proposed method consists of two main subsequent methods: in the first step the percentage of lost particles is predicted using the artificial neural network based on meteorology, emissions and the situation of the air pollution at the end of the previous episode reconstruction and in the second step the clustering parameters are determined using a decision-making method.

## 12.3 Conclusions

Effective implementation of the proposed methods improves significantly computational efficiency of the Lagrangian models [6]. Therefore it enables better long term simulations of the air pollution over most complex cases. Several very complex areas with a lot of industry exist in Slovenia, because there is very little flat terrain, so the industry was placed in meteorologically non-suitable areas. More effective modelling will contribute to better understanding of such phenomena [3]. The new methods have a great scientific value because the air pollution detail reconstruction over complex terrain for longer periods is presently still one of the only partially solved challenges.

**Acknowledgements** The study was financed by Ministry of Higher Education, Science and Technology of Republic of Slovenia, Grant No. 3211-05-000552 and Slovenian Research Agency, Project No. L1-2082.

## References

1. Brusasca G, Tinarelli G, Anfossi D (1992) Particle model simulation of diffusion in low windspeed stable conditions. Atmos Environ 26:707–723
2. De Haan P (1999) On the use of density kernels for concentration estimations within particle and puff dispersion models. Atmos Environ 33:2007–2022

3. Grašič B, Božnar MZ, Mlakar P (2007) Re-evaluation of the Lagrangian particle modelling system on an experimental campaign in complex terrain. Il Nuovo Cimento C 30(6):557–575
4. Melheim JA (2005) Cluster integration method in Lagrangian particle dynamics. Comput Phys Commun 171:155–161
5. Mlakar P, Božnar M (1996) Analysis of winds and SO2 concentrations in complex terrain. Air pollution IV: monitoring, simulation and control. Computational Mechanics Publications, Southampton/Boston, pp 455–464
6. Schwere S, Stohl A, Rotach MW (2002) Practical considerations to speed up Lagrangian stochastic particle models. Comput Geosci 28:143–154
7. Tinarelli G, Anfossi D, Bider M, Ferrero E, Trini Castelli (2000) A new high performance version of the Lagrangian particle dispersion model SPRAY, some case studies. NATO Chall Mod Soc 23A:499–508

# Chapter 13
# Development of a Building Resolving Atmospheric CFD Code Taking into Account Atmospheric Radiation in Complex Geometries

**Yongfeng Qu, Maya Milliez, Luc Musson-Genon, and Bertrand Carissimo**

**Abstract** In order to take into account atmospheric radiation and the thermal effects of the buildings in simulations of atmospheric flow and pollution dispersion in urban areas, we have developed a three-dimensional atmospheric radiative scheme in the atmospheric module of the open-source CFD model *Code_Saturne*. This paper describes our ongoing work on the development of this model. The radiative scheme has been previously validated with idealized cases and the results of a real case. Here we present results of the full coupling of the radiative and thermal schemes with the 3D dynamical flow model and compare the results with simpler approaches found in the literature.

**Keywords** Urban surface modeling • 3D Radiative transfers • Surface temperature • Computational fluid dynamics

## 13.1 Introduction

Interest in urban micro-climatology has increased in the recent decade. It corresponds to the thermal airflow response to the urban system solicitations resulting in radiative transfers and convective exchanges within the urban air and with the building walls. In order to more accurately model the airflow in the urban canopy in non neutral conditions and take into account the three-dimensional convective exchanges, we have developed a three-dimensional microscale atmospheric radiative scheme in a Computational Fluid Dynamics (CFD) code adapted

Y. Qu (✉) • M. Milliez • L. Musson-Genon • B. Carissimo
Joint Laboratory of Ecole des Ponts ParisTech/EDF R&D, Ecole de Ponts, Paritech, CEREA, Teaching and Research Centre in Atmospheric Environment, 6-8 Avenue Blaise Pascal, Cite Descartes, Champs Sur Marne 77455, Marne la Vallee, France
e-mail: yongfeng.qu@cerea.enpc.fr; milliez@cerea.enpc.fr; luc.musson-genon@edf.fr; carissim@cerea.enpc.fr

D.G. Steyn and S. Trini Castelli (eds.), *Air Pollution Modeling and its Application XXI*, NATO Science for Peace and Security Series C: Environmental Security 4,
DOI 10.1007/978-94-007-1359-8_13, 

to complex geometry. The radiative scheme has been validated with idealized cases and the results of a real case [6, 9]. Here we present the model and discuss the results of the full coupling.

## 13.2 Equations and Models

### *13.2.1 CFD Model*

The simulations are performed with the 3D CFD model *Code_Saturne* capable of handling complex geometry and physics. In this work, we use the atmospheric module, which takes into account the larger scale meteorological conditions and the stratification of the atmosphere. In our simulations, we use a RANS approach with a k-ε turbulence closure. The numerical solver is based on a finite-volume approach for co-located variables on an unstructured grid. Time discretization is achieved through a fractional step scheme, with a prediction-correction step [1, 7, 8].

### *13.2.2 Radiative Model*

We have adapted to the atmosphere a radiative heat transfer scheme available in *Code_Saturne* for complex geometry. This model, based on the Discrete Ordinate Method (DOM), solves the radiative transfer equation for a grey semi-transparent media [6, 9]. As a key parameter, the surface temperature is determined by the surface energy balance and is related in a fundamental way to each of its component fluxes. We obtained it with a simple approach: the Force-restore method, widely used for soil modeling in meteorological models:

$$\frac{\partial T_w}{\partial t} = \frac{\sqrt{2\omega}}{\mu_w} Q_w^* - \omega(T_w - T_{g/b}) \tag{13.1}$$

where $T_w$ is the surface temperature, ω is the earth angular frequency, $\mu_w$ is the thermal admittance, $T_{g/b}$ is either deep soil or internal building temperature, $Q_w^*$ is the total net flux received by the wall, which can be expressed as:

$$Q_w^* = Q_S^* + Q_L^* - Q_H - Q_{LE} - Q_F \tag{13.2}$$

with $Q^*_L$ and $Q^*_S$ being net long and short wave flux, respectively, $Q_H$ the sensible heat flux, $Q_{LE}$ the latent heat flux, $Q_F$ the anthropogenic heat flux.

## 13.3 Results

Our validation is based on the Mock Urban Setting Test (MUST) field experiment [2]. MUST has already been used to validate the dynamics and dispersion model [7, 8]. Since temperature data are available, we used the MUST experiment to study in detail the dynamic-radiative coupling. We are just interested in one container within the array, the domain has been reduced to 3 by 3 containers with an optimum domain size. The variation of the deep soil temperature is neglected. The internal building temperature is updated by computing the average surface temperature from the previous radiative time step. The values of albedo, emissivity and thermal admittance are obtained from the literature. The diurnal evolutions of the temperatures at top face, S-E face, (and N-E face, not shown here) are correctly reproduced by our coupling model (Fig. 13.1a) using the force-restore scheme. For the N-W face (and S-W face, not shown here) there is a delay in warming in the simulation results. This may be due to the conduction between the walls that is not taken into account in the simulations. Assuming an insulation inside the building, a wall thermal model is able to reduce the delay in warming (Fig. 13.1b).

The simulation results show a large amplitude difference between the coupled model and the only radiative model, showing the importance of accurately modeling the dynamics in microscale modeling.

## 13.4 Discussion: Comparison of Three Schemes for Predicting Surface Sensible Heat Flux

In this section, we compare three schemes used for predicting surface sensible heat flux by changing transfer coefficient. The simulated case is based on the previous one: it takes place from 12 to 12 h 30 the same day, with an upstream wind direction of $-45°$. The air temperature is 18°C, the reference 10 m-wind speed is $U_{ref} = 4\ ms^{-1}$.

Figure 13.2 summarizes the three convective schemes by visualizing the surface temperatures. The constant $h_f$ scheme (Fig. 13.2 (1)), which is usually used in architecture simulation tools [5] considers a constant heat transfer coefficient. In 1D $h_f$ scheme (Fig. 13.2 (2)), the heat transfer coefficient is calculated based on a simple relationship [3] which is a function of the 1D wind profile inside the canopy. In our case, we used Macdonald [4] exponential profile. In the 3D $h_f$ model (Fig. 13.2 (3)) hf is computed by solving the 3D Reynolds Averaged Navier-Stokes equations in the entire fluid domain.

For this study case, the three convective schemes gave a difference of the sensible flux around 100–240 $Wm^{-2}$ for the S-E face and N-E face. The average surface temperatures calculated by the three convective schemes are similar. Since the building array is not dense in the MUST configuration, the effects of the shadow and the multi reflections are small. That is the reason why the temperatures in the

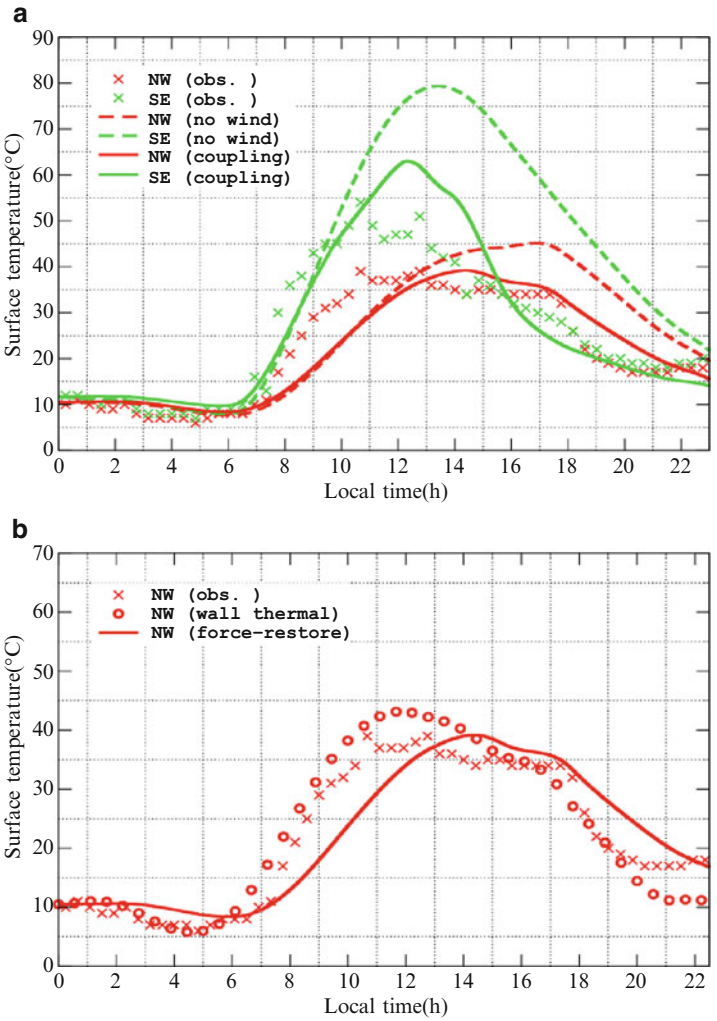


**Fig. 13.1** Diurnal evolution of surface temperatures (obs: measurements; no wind: simulation with radiation only; coupling: simulation with the dynamic-radiative coupling; wall thermal: wall thermal model; force-restore: force-restore model)

constant $h_f$ approach show little difference on each wall. With the 1D $h_f$ model, we can obviously see the 1D inhomogeneity of the surface temperatures which is linked to the exponential law. The 3D $h_f$ model results show the 3D inhomogeneity of the surface temperatures, linked to the inhomogeneity of the 3D wind. On the same face, we can have a difference of temperature of about 4 K. These results demonstrate the effect of the computation of the convection fluxes on the surface temperatures in urban areas.

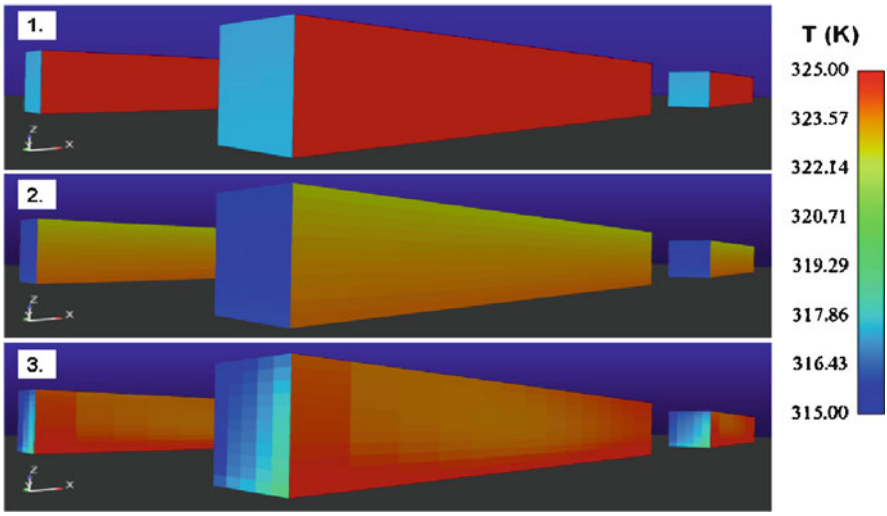


**Fig. 13.2** Comparison of three convective models with visualization SE and NE wall at 12 h 30: (*1*. Constant $h_f$ model; *2*. 1D $h_f$ model; *3*. 3D $h_f$ model)

## 13.5 Conclusions and Perspectives

Evaluation of a microscale 3D dynamic-radiative coupling model using field observations from an ideal urban area, the MUST case, suggests that dynamic-radiative coupling model performs overall well. The model is able to reproduce the evolution of the surface temperatures for different faces of a container during a diurnal cycle. The impact of convective effect on the surface temperature is significant. The 3D calculation of the sensible heat fluxes allows predicting more accurately the non uniform surface temperatures. Uncertainties associated with the thickness and the physical properties of the building wall limit our ability to validate the results. Thus, the perspective of this work is to improve the thermal model. Moreover the coupled dynamic-radiative model will then be used on a real urban area with the CAPITOUL experiment (City of Toulouse, France).

## References

1. Archambeau F, Mechitoua N, Sakiz M (2003) Code_Saturne: a finite volume code for the computation of turbulent incompressible flows-industrial applications, Int J Finite Volumes 1:1–62
2. Biltoft CA (2001) Customer report for mock urban setting test, DPG Document No. WDTC-FR-01-121, West Desert Test Center, U.S. Army Dugway Proving Ground, Dugway, Utah
3. Krayenhoff ES, Voogt JA (2007) A microscale three-dimensional urban energy balance model for studying surface temperatures. Bound-Lay Meteorol 123:433–461

4. Macdonald RW (2000) Modelling the mean velocity profiles in the urban canopy layer. Bound-Lay Meteorol 97:25–45
5. Miguet F, Groleau D (2002) A daylight simulation tool for urban and architectural spaces – application to transmitted direct and diffuse light through glazing. Build Environ 37:833–843
6. Milliez M (2006) Modélisation micro-météorologique en milieu urbain: dispersion des polluants et prise en compte des effets radiatifs, Ph.D. thesis, Ecole Nationale des Ponts et Chaussées
7. Milliez M, Carissimo B (2007) Numerical simulations of pollutant dispersion in an idealized urban area, for different meteorological conditions. Bound-Lay Meteorol 122:321–342
8. Milliez M, Carissimo B (2008) CFD modelling of concentration fluctuations in an idealized urban area, for different meteorological conditions. Bound-Lay Meteorol 127:241–259
9. Milliez M, Musson-Genon L, Carissimo B (2006) Validation of a radiative scheme for CFD modelling of heat transfers between buildings and flow in urban canopies. In: Preprints of the 6th international conference on urban climate, Goteborg, June 12–16

## Questions and Answers

**Questioner Name**: Boliaieo M

**Q**: You presented a very good work, high-level numerical simulations. But, I think you could use more simple models in your case. Why you do not use them?

**A**: Indeed, the complexity of the model depends on the scale of the study and the application domain and in idealized cases, simpler models could be used. Nevertheless, whereas our model was validated on simple configurations it is aimed to be used at micro-scale, to model the energy exchanges in the roughness sub layer, for real urban areas. Our model is also aimed to be used as a research tool which could help parameterizing simpler models.

**Questioner Name**: Bourgouin P

**Q**: Have you looked at the effect of differential heating on the wind patterns?

**A**: Yes. As an extension to this study, we simulated a low wind speed case to see the impact on the wind patterns of radiative transfers. We compared the results to the neutral case and the stratified case with uniform wall heating. In comparison to the uniform wall heating case, taking into account the radidative transfers, and more specifically the position of the sun and the shading effects, modifies the dynamics patterns.

# Chapter 14
# A New Approach to Building Downwash Modelling

**Guido Cosemans and Wouter Lefebvre**

**Abstract** Thompson (1991, 1993) measured ground-level concentrations profiles (GLCPs) for 330 combinations of stack height, building type and distance between stack and building. Cosemans and Lefebvre (Dispersion parameters in a wind tunnel and in the field: analysing Thompson's 1991 wind tunnel data for isolated stacks with IFDM, and its application to building downwash. In: Preprints of the 13th international conference on harmonisation within atmospheric dispersion for regulatory purposes, Paris, pp 304–308, 2010) derived dispersion parameters needed by the bi-Gaussian transport and dispersion equation to reproduce the GLCPs measured for nine isolated stacks. Now, we present a formula to reproduce the 321 other GLCPs, measured. Basically, the plume affected by building downwash is replaced by a set of plumes that have a modified lognormal distribution of height and pollutant mass. The different phenomena that influence plume growth subject to building downwash are modelled by virtual origin functions. Incorporating this in a regulatory plume model could strongly increase the capacity of such model to predict the pollutant concentrations in the vicinity of buildings neighbouring emission sources

**Keywords** Bultynck-Malet • Stability parameters • Atmospheric dispersion experiments • Ground-level concentrations • Building downwash • Wind tunnel

## 14.1 Introduction

Thompson [3, 4] measured ground-level concentrations profiles (GLCPs) for 330 combinations of stack height, building type and distance between stack and building. Cosemans and Lefebvre [2] analysed the GLCPs measured downwind

G. Cosemans (✉) • W. Lefebvre
VITO NV, RMA, Boeretang 200, Mol 2400, Belgium
e-mail: guido.cosemans@vito.be; wouter.lefebvre@vito.be

D.G. Steyn and S. Trini Castelli (eds.), *Air Pollution Modeling and its Application XXI*,
NATO Science for Peace and Security Series C: Environmental Security 4,
DOI 10.1007/978-94-007-1359-8_14, 

nine isolated stacks ranging from 38 to 450 mm height. We assumed a scale of 1 mm in the wind tunnel equal to 1 m in the field. The dispersion parameters needed to reproduce these GLCPs, using the measured wind speed profile $u(z)$ and the standard bi-Gaussian transport and dispersion equation with $\sigma_y(x) = ax^{\alpha}$ and $\sigma_z(x) = bx^{\beta}$ were found to be:

$$a(H_s) = a(E_3) - 0.0001(4.5H_s + 500) \tag{14.1}$$

$$b(H_s) = b(E_2) + 0.0001(4.5\,H_s - 0.0005(H_s - 150)^2) \tag{14.2}$$

$$u(z) = 2.2(z/10)^{0.136} \quad \text{or} \quad u(z) = 0.35\ln[(z - 2.62)/0.015] \tag{14.3}$$

where $H_s$ is the stack height (m), $a(E2)$, $a(E3)$, $\alpha$ and $\beta$ are defined by the Bultynck-Malet dispersion system [1]. The dispersion in the wind tunnel is comparable to that for lightly stable to neutral stability conditions for the park-like terrain of the Nuclear Energy Research Centre in Mol, Belgium.

## 14.2 Components of the New Formula

*The following equation* is able to reproduce the other 321 measured GLCPs:

$$C(x,0,0) = \int_{-\infty}^{+\infty} \frac{Q_{z_p}}{\pi\, u(h_{z_p})\sigma_y(x^*)\sigma_z(x^*)} \exp\left(\frac{-1}{2}\left(\frac{h_{z_p}}{\sigma_z(x^*)}\right)^2\right) dz_p \tag{14.4}$$

This equation says that the GLC under the plume axis of a building downwashed plume is the sum of the GLCs caused by a set of plumes where each sub-plume has its own (virtual) height $h_{z_p}$ and source strength $Q_{z_p}$ (Fig. 14.1). Symbols:

$x^*$: the virtual distance between the origin of the plume set and the receptor;
$u(h_{z_p})$: the wind speed at sub-plume height according to Eq. 14.3;
$\sigma_y(x^*)$ and $\sigma_z(x^*)$: the dispersion parameters (Eqs. 14.1 and 14.2) where the sub-plume height is to be used;
$z_p$: the variable of the normal (Gaussian) probability distribution;
$h_{z_p}$: follows a folded lognormal[1] probability distribution defined by:

$$h_{z_p} = \exp\left(\mu - \left|z_p\right|\sigma\right) \tag{14.5}$$

*The evaluation of Eq.* 14.3 is a two-step procedure because it relies upon a proportionality between $h_{z_p}(x^*)$ and $C(x,0,0)$. *In step 1*, $x^*$, $h_{z_p}$ and $\sigma$ are (tabulated)

[1] The lognormal distribution prevents that some plume are situated below the wind tunnel floor whereas the absolute value of $z_p$, avoids that some plumes go through the wind tunnel ceiling.

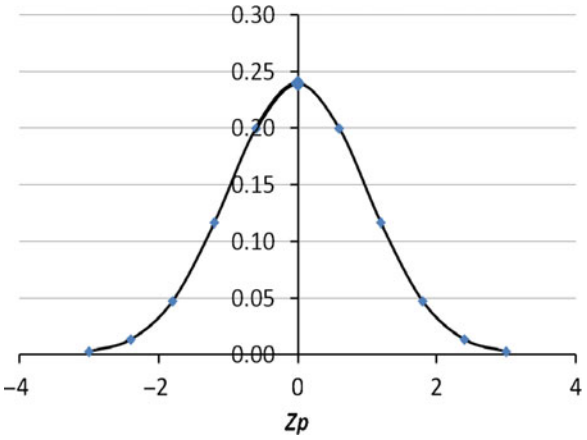


**Fig. 14.1** Mass-distribution over the 'folded lognormal' plumes

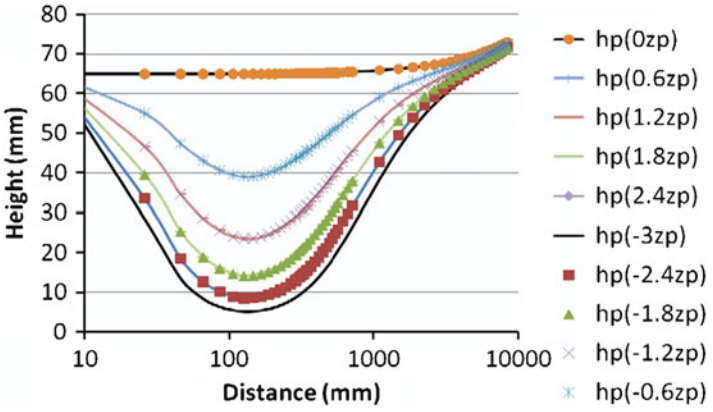


**Fig. 14.2** Folded log-normal plume heights, defined by $H_{\mu} = 65$ mm and $\Sigma_{max} = 37$ mm

constants. Let $x^*_{0,i,j,k}$ be the upwind displacement[2]; $h_{z,i,j,k}$ the virtual origin height and $\sigma_{z,i,j,k}$ (used in Eq. 14.5) be the 'spread' of the plume set for the $GLC_{i,j,k}$ one wants to reproduce. Using these constants, evaluate Eq. 14.3 and determine the location $x_{Cmax}$ and maximum concentration $C_{max}$. (One could use the secant method for this). Next, take the tabulated value $\zeta_{i,j,k}$ . The function $h_{z_p}(x)$ (Fig. 14.2) is now defined by:

$$\zeta(x) = C(x, 0, 0)\zeta_{i,j,k}/C_{max} \tag{14.6}$$

[2] The 321 measured GLC profiles differ in building type $i$, stack height $h_s$ and/or distance stack-building $x_s$. Using the index-triplet $i,j,k$ to denote these three dimensions, functions such as $x^*(x)$ use constants such as the upwind displacement $x^*_0$, whose value $x^*_{0,i,j,k}$ for a particular GLC-profile has been tabulated for use in Eq. 14.3. The tables of all $i,j,k$-parameters needed can not be given here, some values however are at the end of this section.

$$H_\mu = \exp(\mu) = h_{z_p}(0) \quad \text{and} \quad \zeta(\mathrm{x}) = H_\mu - \exp(\mu - \sigma(\mathrm{x})) \tag{14.7}$$

$$h_{z_p}(x) = \exp\left(\mu - \left|z_p\right|\sigma(x)\right) \tag{14.8}$$

where $H_\mu$ : the height of the virtual origin common to all sub-plumes. *The tabulated values*[3] for $x_0^*, i, j, k$, $h_{z,i,j,k}$ and $\zeta_{i,j,k}$ have been determined using an application-specific Newton-Raphson based root finder.

## 14.3 Some Results

Figure 14.3 shows the measured GLCPs for five plumes of several stack heights located on top of a building and their reproduction of with Eq. 14.4. The stacks range in height from 1 to 2.5 times the (cubicle) building height (150 mm). They are located on the downwind side of the building. Using $x_0^*$ for the initial virtual source displacement, the ($h_{z,i,j,k}$, $\zeta_{i,j,k}$, $x^*{}_{0,i,j,k}$) triplets $T_{hs}$ used to compute the shown GLCP's are: $T_{150} = (94, 37.4, -471)$, $T_{188} = (98.5, 31.9, -440)$, $T_{225} = (127.5, 22.1, -127)$, $T_{300} = (238.9, 18, 59)$ and $T_{375} = (345, 13.9, 473)$.

For reproducing all 321 measured GLC profiles, $x^*$ becomes $x^*(x)$ with additional terms that account for:

1. plume dilution when the plume passes over the building;
2. plume dilution when descending streamlines hit the ground, can be reproduced by a local increase of the virtual origin $x^*$ over a distance equal to the building height after $x_{Cmax}$;
3. the inclination of the streamlines after $x_{Cmax}$, which is of the form $H_\mu(x) = H_\mu + \alpha X$, where $\alpha$ is a small value less than 0.0003.

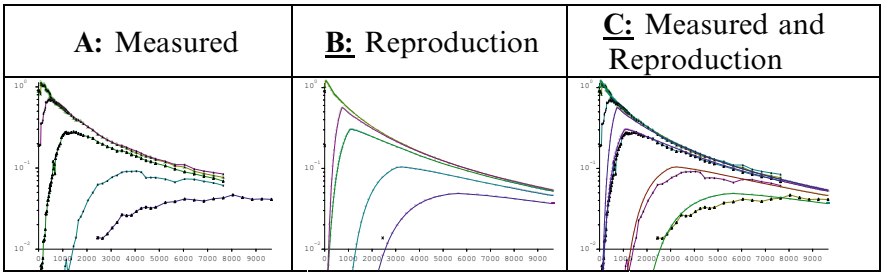


**Fig. 14.3** Ground-level concentration profile for emissions through stacks of 150, 188, 225, 300 and 375 mm on roof of cubical building

[3] Equation 14.7 can be used to calculate $\sigma_{z,i,j,k}$ given the value of $\zeta_{i,j,k}$.

## 14.4 Conclusions

We presented an extended bi-Gaussian equation that allows to reproduce the ground-level concentrations measured in a wind tunnel under the axis of a plume subject to building downwash. Leaving some details apart, the plume is replaced by a set of plumes having a lognormal-type distribution of height and pollutant mass. Incorporating this in a regulatory plume model could strongly increase the capacity of such model to predict the pollutant concentrations in the vicinity of buildings neighbouring emission sources.

## References

1. Bultynck H, Malet L (1972) Evaluation of atmospheric dilution factors for effluents diffused from an elevated continuous point source. Tellus 24:445–472
2. Cosemans G, Lefebvre W (2010) Dispersion parameters in a wind tunnel and in the field: analysing Thompson's 1991 wind tunnel data for isolated stacks with IFDM, and its application to building downwash. In: Preprints of the 13th international conference on harmonisation within atmospheric dispersion for regulatory purposes, Paris, pp 304–308
3. Thompson RS (1991) Data report. Project: Building amplification factors.US EPA
4. Thompson RS (1993) Building amplification factors for sources near buildings – a wind-tunnel study. Atmos Environ A 27:2313–2325

# Chapter 15
# Numerical Simulation of Indoor Air Pollution and Atmosphere Pollution for Regions Having Complex Topography

**Mykola Mykolayevich Biliaiev and Mykola Mykolayevich Kharytonov**

**Abstract** In Ukraine, to predict the area of chemical pollution after accidents with toxic substances standard model which is adopted by Government is used. This is the empirical model which possibilities are very restricted. This paper presents numerical models to simulate the flow field and pollutant concentrations in the regions with complex topography. The hydrodynamic model of inviscid flow is used to predict the velocity field over complex terrain and that is the reason of main advantage of these models, because of they do not consume much of computing time. The models can be used for express (quickly ) air quality modeling for cases of air pollution after accidents when there is lack of initial information about meteorological parameters, mass of ejection, etc.

**Keywords** Air pollution • Numeric simulation • Local and urban scale

M.M. Biliaiev (✉)
Fluid Dynamics Department, Dnipropetrovsk National University of Railway Engineering, Lazaryana St. 2, Dnipropetrovsk, Ukraine
e-mail: envteam@ukr.net

M.M. Kharytonov
Soil Science & Ecology Department, Dnipropetrovsk State Agrarian University, Voroshilav St. 25, Dnipropetrovsk, 49600 Ukraine
e-mail: mykola_kh@yahoo.com

D.G. Steyn and S. Trini Castelli (eds.), *Air Pollution Modeling and its Application XXI*, NATO Science for Peace and Security Series C: Environmental Security 4,
DOI 10.1007/978-94-007-1359-8_15, 

## 15.1 Mathematical Model of Pollutant Dispersion

To simulate the pollutant transport in the atmosphere the gradient transport model is used

$$\frac{\partial C}{\partial t}+\frac{\partial uC}{\partial x}+\frac{\partial vC}{\partial y}+\frac{\partial wC}{\partial z}+\sigma C=\frac{\partial}{\partial x}\left(\mu_x\frac{\partial C}{\partial x}\right)+\frac{\partial}{\partial y}\left(\mu_y\frac{\partial C}{\partial y}\right)+\frac{\partial}{\partial z}\left(\mu_z\frac{\partial C}{\partial z}\right)+\sum Q_i(t)\delta(x-x_i)\delta(y-y_i)\delta(z-z_i) \quad (15.1)$$

where $C$ is mean concentration; $u$, $v$, $w$ are the wind velocity components; $\sigma$ is the parameter taking into account the process of pollutant decay; $\mu = (\mu_x, \mu_y, \mu_z)$ are the diffusion coefficients; $Q$ is intensity of point source ejection ; $\delta(r - r_i)$ are Dirak's delta function; $r_i = (x_i, y_i, z_i)$ are the coordinates of the point source.

The transport equation is used with the following boundary conditions:

inlet boundary: $C|_{inlet} = C_E$, where $C_E$ is the known concentration (very often $C_E = 0$);

- outlet boundary: in numerical model the condition $C(i+1,j,k) = C(i,j,k)$ is used (this boundary condition means that we neglect the process of diffusion on this plane);
- top boundary and ground surface $\frac{\partial C}{\partial n} = 0$.

In the numerical model developed the following approximations for wind speed and diffusion coefficient are used:

$$u = u_1\left(\frac{z}{z_1}\right)^n, \quad \mu_z = 0,11z, \quad \mu_y = k_0 \cdot u, \quad \mu_y = \mu_x$$

where $u_1$ is wind speed at the height $z_1 = 10\,\text{m}$; n = 0,15; $k_0$ is parameter.

### *15.1.1 Numerical Model*

The calculation of pollutant dispersion is carried out on the rectangular grid. To create the form of complex terrain the procedure of approximating the boundary by a broken surface with segments parallel to the coordinate lines is used [2]. In Ukraine this method is often called the "markers method". Markers are used to separate the computational cells from cells which correspond to terrain.

Main features of the implicit finite difference scheme to solve transport equation are discussed in [1].

To simulate the wind flow over complex terrain the model of potential flow is used. In this case the governing equation is

$$\frac{\partial^2 P}{\partial x^2} + \frac{\partial^2 P}{\partial y^2} + \frac{\partial^2 P}{\partial z^2} = 0 \tag{15.2}$$

where P is the potential of velocity.

The components of velocity are calculated as follows

$$u = \frac{\partial P}{\partial x}, \quad v = \frac{\partial P}{\partial y}, \quad w = \frac{\partial P}{\partial z}$$

Instead of Eq. 15.2 the 'time-dependent' equation for the potential of velocity is used in the model

$$\frac{\partial P}{\partial \eta} = \frac{\partial^2 P}{\partial x^2} + \frac{\partial^2 P}{\partial y^2} + \frac{\partial^2 P}{\partial z^2} \tag{15.3}$$

where $\eta$ is 'fictitious' time.

For $\eta \to \infty$ the solution of Eq. 15.3 tends to the solution of Eq. 15.2.

To solve Eq. 15.3 A.A. Samarskii's change-triangle difference scheme is used.

To take into account the effects of flow separation over the complex terrain another hydrodynamic model is used. This is the 2D model of inviscid separated flows [1]. The governing equations of this model are equation of vortex transport:

$$\frac{\partial \omega}{\partial t} + \frac{\partial u\omega}{\partial x} + \frac{\partial v\omega}{\partial y} = 0, \tag{15.4}$$

where $\omega = \frac{\partial v}{\partial x} - \frac{\partial u}{\partial y}$.

Poisson's equation for flow function $\psi$:

$$\frac{\partial^2 \psi}{\partial x^2} + \frac{\partial^2 \psi}{\partial y^2} = -\omega. \tag{15.5}$$

Components of wind velocity are calculated as follows:

$$u = \frac{\partial \psi}{\partial y}; \quad v = -\frac{\partial \psi}{\partial x}.$$

The assumption is made that the separation of flow takes part at the "corner" points of terrain which are appeared in the numerical model when the procedure of terrain approximation with markers is carried out. Main features of the vortex intensity

determination near corner points is discussed in [1]. For this hydrodynamic model the 2D gradient transport model is used. To simulate pollutant transfer in industrial rooms both Eqs. 15.1 and 15.2 are used.

## 15.2 Results

Two codes based on the numerical models considered were developed. One of these codes was used to predict the atmosphere pollution after accidents with toxic substances on rail way near Dnepropetrovsk city ( Ukraine). In Fig. 15.1 the results of numerical simulation are shown. This picture illustrates the pollutant field near the railway hill. It's well seen that the toxic gas rapidly moves into the cave in the hill (Fig. 15.1).

The second code was used to calculate the pollution of the air in the industrial room after NH3 ejection. The numerical experiment was carried out when the neutralizing is going on in the room. In this case the H3PO4 solution was supplied using special opening. We see from Fig. 15.2 that the neutralizing allows reduce the pollution area in the room very rapidly.

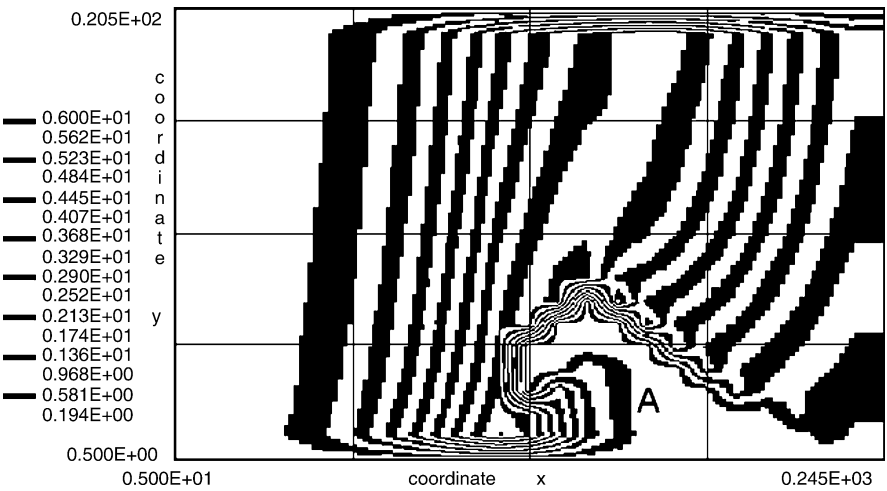


**Fig. 15.1** Concentration field near the hill at time t = 22 s after accident

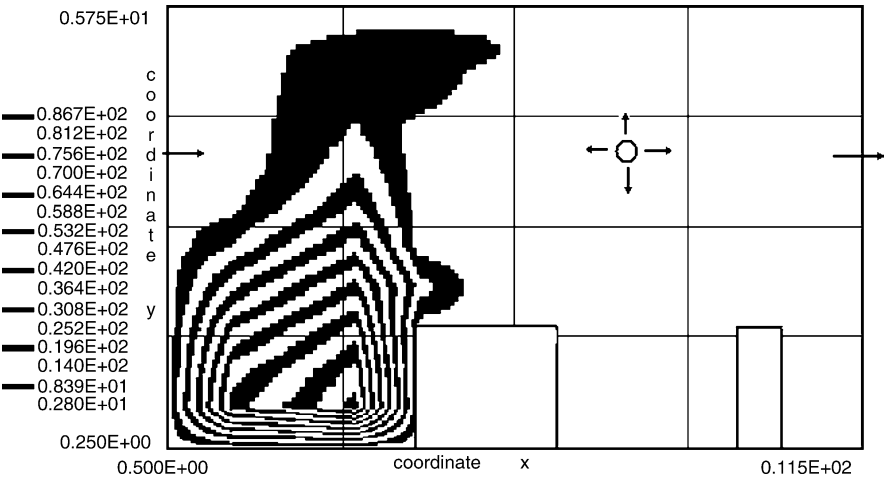


**Fig. 15.2** Field of pollutant concentrations in the room, $t = 11\,s$ (section y = 5.5 m, with neutralizing)

## References

1. Belayev NN, Kazakevitch MI, Khrutch VK (1999) Computer simulation of the pollutant dispersion among buildings. // Wind Engineering into 21st century. In: Proceedings of the tenth international conference on wind engineering. Copenhagen/Denmark/A. A.Balkema/ Rotterdam/Brookfield, pp 1217–1220
2. Kadja M, Anagnostopoulos J et al. (2001) Computation of wind flow and air pollution for regions having a complex topography. In: Proceedings of 3rd European and African conference on wind engineering. Eindhoven University of Technology, the Netherlands, 2–6 July 2001, pp 355–358

# Chapter 16
# The Canadian Urban Dispersion Modeling (CUDM) System: Prototype Evaluation over Vancouver 2010

**Pierre Bourgouin, Richard Hogue, Najat Benbouta, Nils Ek, Jean-Philippe Gauthier, Nathalie Gauthier, Matthew Holly, Alexandre Leroux, Gilles Mercier, Serge Trudel, Calin Zaganescu, Stéphane Bélair, Eugene Yee, and Fue-Sang Lien**

**Abstract** The CUDM system provides transport and dispersion modeling capability at the urban scale. It simulates the mean flow, turbulence and concentration fields in urban areas. The system involves a cascade of meteorological models from the operational regional model to an urbanized meso-scale model that in turn drives a CFD flow model running at the urban scale. This CFD model simulates mean wind and turbulence fields that can feed dispersion models. The presentation will briefly describe the current state of the CUDM system, present results obtained over Vancouver during the Olympics and over Toronto during the G8/G20 summit meetings, and compare the different configurations.

**Keywords** Urban dispersion • CFD • Sensitivity • CBRN

There is an increasing concern over the possibility of a terrorist release of a chemical, biological, radiological or nuclear (CBRN) agent in a large and densely populated urban area. To respond effectively to such an attack, rapid decisions need to be made concerning the transport, dispersion, deposition and fate of the CBRN agent and its concomitant effects on the exposed population. As a consequence, there is an urgent need to develop a comprehensive modeling system to predict the

P. Bourgouin (✉) • R. Hogue • N. Benbouta • N. Ek • J.-P. Gauthier • N. Gauthier • M. Holly • A. Leroux • G. Mercier • S. Trudel • C. Zaganescu
Canadian Meteorological Centre, Meteorological Service of Canada, Montreal, QC, Canada
e-mail: pierre.bourgouin@ec.gc.ca

S. Bélair
Meteorological Research Division, Environment Canada, Dorval, QC, Canada

E. Yee
Defence R&D Canada, Suffield, AB, Canada

F.-S. Lien
Department of Mechanical Engineering, University of Waterloo, Waterloo, ON, Canada

D.G. Steyn and S. Trini Castelli (eds.), *Air Pollution Modeling and its Application XXI*, NATO Science for Peace and Security Series C: Environmental Security 4,
DOI 10.1007/978-94-007-1359-8_16, 

consequences arising from releases of hazardous materials in the atmosphere for use in real-time emergency response, pre-event planning, and post-incident assessment. The Canadian Urban Dispersion Modeling (CUDM) system was developed with these considerations in mind. It is a multiscale system that can be used to predict the mean flow and turbulence in the urban environment (and beyond) and the dispersion of contaminants released into these highly disturbed flows across a wide range of space and time scales. The system was developed over the past 5 years, through funding from the **C**BRN **R**esearch and **T**echnology **I**nitiative (CRTI) program. The CUDM system was developed in two major phases. The first phase produced the core modeling components and was completed in 2008. The second (follow-on) phase is focused on the seamless integration of the different modeling components in order to produce an operational prototype. The proposed operational modeling system will have four main components; namely, the nested set of environmental flow models for the prediction of flow across multiple scales of motion, the building-aware computational fluid dynamics (CFD) model, the model for atmospheric dispersion driven by the environmental and CFD model, and the integrating framework used to organize and structure all the modeling components to provide a system-of-systems simulation system that can be used for integrated assessment modeling. The different components were validated during the first phase of the project, using primarily the high-quality experimental data acquired during the Joint Urban 2003 field campaign in Oklahoma City.

The first component of the system involves a cascade of meteorological models from the operational regional model to an urbanized mesoscale model. The Canadian short-range regional forecasting system is based on the Global Environmental Multiscale (GEM) model [1]. This model gives the initial conditions for a cascade of a number of limited-area versions of GEM (GEM-LAM) starting from the 15 km spatial resolution of GEM and progressing downwards in scale to 2.5 km, 1 km and finally to 250 m. This model cascade uses an urbanized version of GEM-LAM (urbanGEM) to simulate the urban micrometeorology [2]. The second component includes urbanSTREAM [3], a building-aware computational fluid dynamics model which resolves the highly disturbed flow down to the street or building scale. This model predicts the mean flow and turbulence fields in a built-up environment and is based on an unsteady Reynolds-averaged Navier-Stokes (URANS) approach with either a standard or modified two-equation $k$-$\varepsilon$ model used for the turbulence closure. The numerical framework used in urbanSTREAM employs a fully-collocated, cell-centered storage arrangement for all transported properties. Diffusive volume-face fluxes are discretized using a second-order central differencing scheme. The higher-order quadratic upwind interpolation for convective kinematics (QUICK) scheme (or, alternatively, a total variation diminishing (TVD) variant of QUICK) is used to approximate the convective volume-face fluxes. Mass conservation is enforced indirectly by solving a pressure correction equation. The iterative scheme used here to enforce mass conservation is the Semi-Implicit Method for Pressure-Linked Equations Consistent (SIMPLEC). The inflow and lateral boundary conditions required for urbanSTREAM are

obtained from urbanGEM at 250-m resolution. Building-aware modeling requires high-fidelity digital models of buildings as input. We have acquired to date, building databases for Vancouver, Montréal, Ottawa, Toronto and, shortly, Québec City and Calgary. The goal is to be able to run the modeling system for any large Canadian city. The third component is the urban dispersion model. A Lagrangian stochastic (LS) model for urban dispersion referred to as urbanLS [4] has been implemented in the integrative multiscale urban modeling system. This LS particle trajectory model computes forward or reverse time paths of "marked" fluid parcels released from transient or continuous sources and is driven using the fully three-dimensional building-resolving wind field provided by urbanSTREAM. The fourth component is the informatics framework (referred to as SPI) allowing all the other model components and sub-components to interact seamlessly with each other to form a truly integrated system. SPI also provides a graphical user interface to execute all the operations required for pre-processing and for launching the various modeling components in the suite. SPI is a key component required to transition the modeling system into an operational capability.

As mentioned above, the focus of the second phase of the project is to develop a prototype that will be operational at Canadian Meteorological Centre (CMC). CMC is Canada's national meteorological centre, operating on 24/7 around the clock schedule. An operational implementation of the CUDM system at CMC would benefit from the Centre's operational facilities and tools. Much work was needed to integrate the different components into one modeling suite and to adapt the different programs to meet CMC requirements. This work was accomplished by the Environmental Emergency Response Section (EERS) in order to produce a first version of the prototype for use in support of the 2010 Vancouver Winter Olympics. This prototype was extensively tested during the Vancouver Winter Olympics and Paralympics. Following modeling support for the Olympics, upgrades to the modeling system were included in preparation for support during the G8/G20 summit meetings in Toronto in June 2010. The CUDM system with its meteorological cascade and CFD model is computationally intensive. However, for an operational system, it is desirable to have the system run as quickly as possible. Towards that objective, we will explore alternative configurations for improving the execution time, thereby increasing the potential usefulness of the system. Specifically, we want to evaluate the following configurations:

- Value-added of urbanGEM 250 m vs. urbanGEM 1 km vs. urbanGEM 2.5 km
- Value-added of urbanGEM 250 m vs. a non-urbanized version of GEM-LAM 250 m
- Value-added of urbanLS vs. a non-urban dispersion model
- Sensitivity of urbanSTREAM to specification of inflow and lateral boundary conditions
- Possibility of pre-calculation of urban flow (wind field library)

This is not a simple task because of the difficulties involved in the validation very high resolution models (meteorological, CFD). The difficulty resides in the

sparsity of data available to validate the model predictions and therefore to quantify the benefits associated with the different configurations.

The presentation will briefly describe the current state of the CUDM system, present results obtained over Vancouver during the Olympics and over Toronto during the G8/G20 summit meetings, and compare the different configurations.

## References

1. Bélair S, Crevier LP, Mailhot J, Bilodeau B, Delage Y (2003) Operational implementation of the ISBA land surface scheme in the Canadian Regional Weather Forecast Model. Part I: Warm season results. J Hydrometeorol 4:352–370
2. Leroyer S, Mailhot J, Bélair S, Lemonsu A, Strachan IB (2010) Modeling the surface energy budget during the thawing period of the 2006 montreal urban snow experiment. J Appl Meteorol Clim 49:68–84
3. Lien F-S, Yee E (2004) Numerical modelling of the turbulent flow developing within and over a 3-D building array, Part I: A highresolution Reynolds-averaged Navier–Stokes approach. Bound Lay Meteorol 112:427–466
4. Wilson JD, Yee E, Ek N, d'Amours R (2009) Lagrangian simulation of wind transport in the urban environment. Q J R Meteorol Soc 135:1586–1602

# Chapter 17
# Fast Model to Compute the Concentration Covariance of Two Passive Scalars from Their Mean Concentration Field

**Luca Mortarini and Enrico Ferrero**

**Abstract** The modeling of chemical reactions between two species at small scales where the chemical equilibrium is not yet attained and the segregation effect may not be negligible depends on the knowledge of the covariance of the concentration field. Unfortunately, while the mean concentration field determination is almost a settled matter, the evaluation of the second moments of the concentration field is still an open problem. In this framework, the fluctuating plume model has proved to be a versatile and powerful tool to evaluate the whole concentration field, nevertheless the Lagrangian simulation of the plume barycenter meandering in real cases is still a challenging task. Following Cassiani and Giostra (Atmos Environ 36:4717–4724, 2002) we use the hypotheses of the fluctuating plume model to develop a simple and fast method to derive the concentration field in real situations without using a Stochastic Lagrangian model, but using a mean concentration field, either measured or numerically simulated. The model is tested against a wind tunnel experiment data-set and the results are presented and discussed.

**Keywords** Lagrangian stochastic models • Concentration fluctuations • Fluctuating plume • Chemical reactions • Segregation

L. Mortarini (✉)
Institute of Atmospheric Sciences and Climate, Italian National Research Council (CNR), Corso Fiume 4, Torino, 10100, Italy
e-mail: l.mortarini@isac.cnr.it

E. Ferrero
Dipartimento di Scienze e Tecnologie Avanzate (DISTA), Università del Piemonte Orientale, Viale Teresa Michel 11, Alessandria 15121, Italy
e-mail: enrico.ferrero@mfn.unipmn.it

D.G. Steyn and S. Trini Castelli (eds.), *Air Pollution Modeling and its Application XXI*, NATO Science for Peace and Security Series C: Environmental Security 4,
DOI 10.1007/978-94-007-1359-8_17, 

## 17.1 Introduction

It is generally recognized that the segregation of the chemical reactants cannot be neglected in the short-term concentration prediction [6], when the chemical reactions take place before the pollutants are well mixed by the turbulence. Recently we developed a Lagrangian stochastic one-particle model with chemical reactions [1], where the segregation coefficient, depending on the covariance of the species concentrations, is calculated through a parameterisation. An alternative approach is the fluctuating plume model [7], which is able to estimate the concentration fluctuations in non-homogeneous turbulence, like in the convective or canopy layers [4, 10]. To predict the reactive airborne compounds concentration we followed an original approach: we re-wrote the fluctuating plume model using a bi-variate probability density function [8], obtaining a new model able to simulate the simultaneous dispersion of two reactive species and to account for the segregation coefficient. The fluctuating plume model is generally coupled with a Lagrangian Stochastic model that simulates the motion of the barycenter position [4, 9, 10] or with an analytical model [7, 12] that simulate the motion of the barycenter position; following Cassiani and Giostra [3] we propose to evaluate the barycenter position from the mean concentration field. Afterwards, the relative dispersion PDFs of the two contaminants is parameterized with a bi-variate gamma PDF [8].

## 17.2 The Fluctuating Plume Model

The Fluctuating Plume model is based on the idea that the absolute dispersion can be thought as a result of two different processes: the mean meandering of the plume and the relative dispersion inside the plume. Dividing the turbulence scales allow us to valuate the concentration moments as:

$$\langle c^n \rangle = \int \langle c_r^n \rangle p_m dz_m \tag{17.1}$$

where $p_m$ is the barycenter PDF and $\langle c_r^n \rangle$ are the concentration moments relative to the centroid position. This approach can be easily extended to two passive scalars, i.e. to the covariances of the concentration PDF:

$$\langle c_A^n c_B^m \rangle = \int \langle c_{rA}^n c_{rB}^m \rangle p_m dz_m \tag{17.2}$$

$$\langle c_{Ar}^n c_{rB}^m \rangle = \int c^n c^m p_{cr}(c_A, c_B | x, z, z_m) dc \tag{17.3}$$

to solve these equations it is necessary to provide $p_m(z, zm)$ and $p_{cr}(c_A, c_B | x, z, z_m)$.

**The barycenter PDF.** Cassiani and Giostra [3] suggest to extract the barycenter position PDF from the mean concentration field. Known $\langle c(x,z)\rangle$ the probability density for the position z is:

$$p_z(x,z) = \frac{\langle c(x,z)\rangle}{\int \langle c(x,z)\rangle dz} \tag{17.4}$$

and the resulting PDF for $z_m$ is:

$$p_m = \begin{cases} 0 & \text{(outside the compressed field)} \\ p_z \dfrac{\Delta z}{\Delta z_m} & \text{(inside the compressed field)} \end{cases} \tag{17.5}$$

where $\Delta z_m$is obtained from a linear transformation of $p_z(x,z)$.

**The relative concentration PDF.** For a single passive tracer Gailis et al. [5] measured that $p_{cr}(c|x,z,zm)$ is a Gamma PDF and Luhar et al. [9], Mortarini et al. [10] parameterized it as:

$$p_{cr}(c|z,z_m) = \frac{c^{\lambda-1}}{\Gamma(\lambda)b^{\lambda}} \exp\left(-\frac{c}{b}\right) \tag{17.6}$$

with $\lambda = 1/i_r^2$ and $b = \langle c_r\rangle/\lambda$. Known λ and $\langle c_r\rangle$, Eq. 17.6 allows to evaluate all the moments of the concentration PDF. The form we need for $p_{cr}(c_A, c_B|x,z,z_m)$ is a PDF whose marginal distributions are of the form (17.6). The only PDF that fulfills this requirement in the literature is the bi-variate Gamma PDF proposed by Loaiciga and Leipnik [8]:

$$p_{cr}(c_A,c_B|x,z,z_m) = \sum_{n=0}^{\infty} (-1)^n \binom{-1}{n} \left(\frac{\beta}{b_A b_B}\right)^n \frac{\left(\frac{c_A}{b_A}\right)^{\Lambda_A-1}\left(\frac{c_B}{b_B}\right)^{\Lambda_B-1} e^{-\left(\frac{c_A}{b_A}+\frac{c_B}{b_B}\right)}}{\Gamma(\Lambda_A)\Gamma(\Lambda_B)b_A b_B} C_n\left(\Lambda_A-1, \frac{c_A}{b_A}\right) C_n\left(\Lambda_B-1, \frac{c_B}{b_B}\right) \tag{17.7}$$

where $\Lambda_i = \lambda_i(n+1)$ and $\beta = \rho b_A b_B \sqrt{\lambda_A \lambda_B} = \rho \sigma_{crA}\sigma_{crB}$, with $\rho$ correlation coefficients between the two concentrations and $\sigma_{cri}$ the concentration standard deviation in the relative frame. Substituting Eq. 17.7 in Eqs. 17.3 and 17.4 with $n = m = 1$ we obtain:

$$\langle c_A c_B\rangle = \int \rho i_{rA} i_{rB} \langle c_{rA}\rangle \langle c_{rB}\rangle p_m dz_m \tag{17.8}$$

## 17.3 Results and Conclusions

For sake of comparison a wind tunnel experiment carried out by Brown and Bilger [2] has been considered. In this experiment a NO point source emission was placed inside an airflow doped with a uniform $O_3$ concentration. Thus in the fluctuating plume model described above the simple chemical reaction: $NO + O_3 \rightarrow NO_2 + O_2$ has been introduced. In order to determine the correct reaction rate, the concentration covariance between NO and $O_3$ has to been evaluated. The mean concentration fields for each species were computed with a 1-d single particle Lagrangian model [11], the barycenter PDF is extracted with Eq. 17.5 and $\langle c_{NO} c_{O_3} \rangle$ is evaluated with Eq. 17.8. The Fig. 17.1 shows the comparison between the plume centerline $NO_x$ concentrations and the experimental data [2]. Note that the "frozen limit" corresponds to the dispersion of a conserved scalar ($NO_x$, in the present case).

In spite of its simple formulation and low computational cost the coupling of the fluctuating plume model with Cassiani and Giostra [3] PDF contraction is able to reproduce the concentration covariances, and showed a very good agreement with the data. Further efforts are necessary to extend this approach to a full three dimensional case.

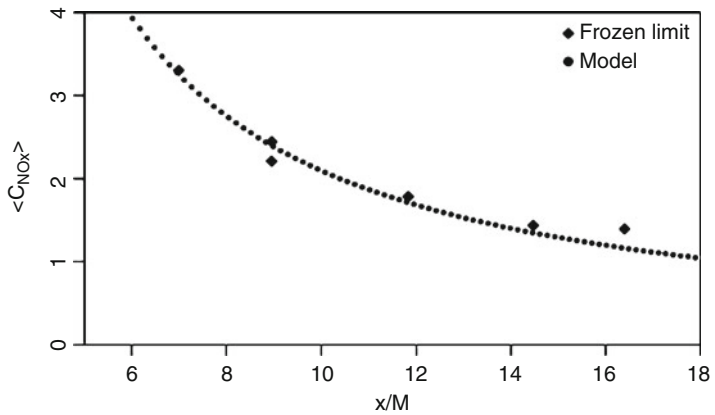


**Fig. 17.1** Comparison of the frozen limit plume centerline concentrations, data refer to Brown and Bilger [2] experiment

## References

1. Alessandrini S, Ferrero E (2009) A hybrid lagrangian–eulerian particle model for reacting pollutant dispersion in non-homogeneous non-isotropic turbulence. Phys A 388:1375–1387
2. Brown RJ, Bilger RW (1996) An experimental study of a reactive plume in grid turbulence. J Fluid Mech 312:373–407

3. Cassiani M, Giostra U (2002) A simple and fast model to compute concentration moments in a convective boundary layer. Atmos Environ 36:4717–4724
4. Franzese P (2003) Lagrangian stochastic modeling of a fluctuating plume in the convective-boundarylayer. Atmos Environ 37:1691–1701
5. Gailis RM, Hill A, Yee E, Hilderman T (2007) Extension of a fluctuating plume model of tracer dispersion to a sheared boundary layer and to a large array of obstacles. Bound-Lay Meteorol 122:577–607
6. Garmory A, Richardson ES, Mastorakos E (2006) Micromixing effects in a reacting plume by the stochastic fields method. Atmos Environ 40:1078–1091
7. Gifford F (1959) Statistical properties of a fluctuating plume dispersion model. Adv Geophys 6:117–137
8. Loaiciga HA, Leipnik RB (2005) Correlated gamma variables in the analysis of microbial densities in water. Adv Water Resour 28:329–335
9. Luhar A, Hibberd M, Borgas M (2000) A skewed meandering-plume model for concentration statistics in the convective boundary layer. Atmos Environ 34:3599–3616
10. Mortarini L, Franzese P, Ferrero E (2009) A fluctuating plume model for concentration fluctuations in a plant canopy. Atmos Environ 43:921–927
11. Thomson DJ (1987) Criteria for the selection of stochastic models of particle trajectories in turbulent flows. J Fluid Mech 180:529–556
12. Yee E, Wilson D (2000) A comparison of the detailed structure in dispersing tracer plumes measured in grid-generated turbulence with a meandering plume model incorporating internal fluctuations. Bound-Lay Meteorol 94:253–296

# Chapter 18
# The Impact of Anthropogenic and Biogenic Emissions on Surface Ozone Concentrations in Istanbul: A Modeling Study

**Ulaş İm, Anastasia Poupkou, Selahattin İncecik, Kostandinos Markakis, Tayfun Kindap, Dimitros Melas, Orhan Yenigün, Sema Topcu, Mehmet Talat Odman, Mete Tayanc, and Meltem Guler**

**Abstract** Ground level ozone levels were simulated for Istanbul during a summer episode in June 2008, using MM5/CMAQ model system. Two sets of base runs were carried out in order to investigate the impact of biogenic emissions on ozone concentrations in Istanbul. The inclusion of biogenic emissions significantly improved the performance of the model, particularly the temporal variation of ozone concentrations. It was found out that biogenic NMVOCs emissions enhanced maximum ozone concentrations in the GIA up to 25 ppb. The sensitivity analysis pointed to $NO_x$-sensitive chemistry in the region

**Keywords** Istanbul • Ozone • Biogenic emissions • CMAQ

U. İm
Department of Chemistry, Environmental Chemical Processes Laboratory, University of Crete, Heraklion, Greece

A. Poupkou • K. Markakis • D. Melas
Department of Physics, Laboratory of Atmospheric Physics, Aristotle University of Thessaloniki, Thessaloniki, Greece

S. İncecik (✉) • S. Topcu
Department of Meteorology, Istanbul Technical University, Istanbul, Turkey
e-mail: incecik@itu.edu.tr

T. Kindap
Eurasia Institute of Earth Sciences, Istanbul Technical University, Istanbul, Turkey

O. Yenigün • M. Guler
Institute of Environmental Sciences, Boğazici University, Istanbul, Turkey

M.T. Odman
School of Civil and Environmental Engineering, Georgia Institute of Technology, Atlanda, GA, USA

M. Tayanc
Department of Environmental Engineering, Marmara University, Istanbul, Turkey

D.G. Steyn and S. Trini Castelli (eds.), *Air Pollution Modeling and its Application XXI*, NATO Science for Peace and Security Series C: Environmental Security 4,
DOI 10.1007/978-94-007-1359-8_18, 

## 18.1 Introduction

In the present study, the influence of biogenic emissions on ozone concentrations is assessed and the sensitivity of ozone levels to various anthropogenic emission scenarios is examined. There have been some previous studies focusing on ozone formation in the urban atmosphere of Istanbul that were based on observational data and showed that the high emissions of $NO_x$ and VOCs, concurrent with high radiation and temperature in ozone season, leaded to elevated ozone concentrations [3]. The impact of emission sources on ozone levels in Istanbul have never been studied before.

## 18.2 Materials and Methods

### *18.2.1 Measurements and Simulation Period*

In the framework of the COST728 Action and the TUJJB projects, two ozone monitoring stations have been established in Istanbul. Kandilli station is located few kilometers away from the Bosporus, at a highly ventilated suburban site. Büyükada air quality station is situated at the crest of Prince Island of Istanbul. Büyükada is considered as representative station for the background air quality levels in Istanbul. A 7 day period from 13th to 19th of June, 2008, has been simulated, during which the highest concentrations of the 3-year period (2007–2009) were observed at both measurement stations (90 ppb). The episode was mostly characterized by southerly winds originated from the land-see breeze circulation.

### *18.2.2 Meteorology and Chemistry Modeling*

The mesoscale, non-hydrostatic meteorological model PSU/NCAR MM5 V3.7 [2] was used in this study. The initial and boundary conditions are provided from the National Centers for Environmental Prediction (NCEP) Final Analyses (FNL) data of $1 \times 1^{\circ}$. The physical options used in MM5 study were the mix phase moisture scheme, Kain-Fritsch 2 cumulus scheme, MRF (medium range forecast) boundary layer parameterization, and RRTM (rapid radiative transfer model) radiation scheme.

The US EPA Community Multiscale Air Quality (CMAQ) model, version 4.6 was used in this study as the chemistry and transport model (CCTM; [1]). The chemical mechanism used for the gaseous species was CB-IV, whereas AERO4 was employed as the aerosol mechanism. The CCTM was used to simulate the ozone concentrations in 10 different scenarios to investigate the impact of biogenic emissions and the sensitivity of ozone levels on different emission scenarios for anthropogenic NO, $NO_2$, $NO_x$ and NMVOC emissions.

An anthropogenic emission inventory was compiled on 2 km resolution for the Greater Istanbul Area, where the details are given in Im et al. [4]. A Biogenic Emission Model (BEM) was used for the calculation of spatially and temporally resolved biogenic NMVOCs emissions [5].

## 18.3 Results and Discussion

The lowest ozone concentrations were calculated at the urban center and around the big industrial complexes of İstanbul and Kocaeli region, where high amounts of $NO_x$ emissions are emitted. The highest ozone concentrations were found over the maritime areas of the GIA, due to the transport of ozone precursors emitted that are transported over the sea, which together with the low deposition velocity of ozone over the sea allow elevated ozone levels to appear over the maritime areas of the GIA.

The comparison of calculated ozone levels for both scenarios with observations at the Büyükada and Kandilli air quality stations are presented in Fig. 18.1. The model was not able to capture the diurnal variation successfully with anthropogenic emissions only ($r = 0.22$ and 0.30, respectively). The comparison of the modeled ozone levels by including biogenic emissions show that mean ozone levels are still slightly overestimated by the model at both stations, however with better temporal

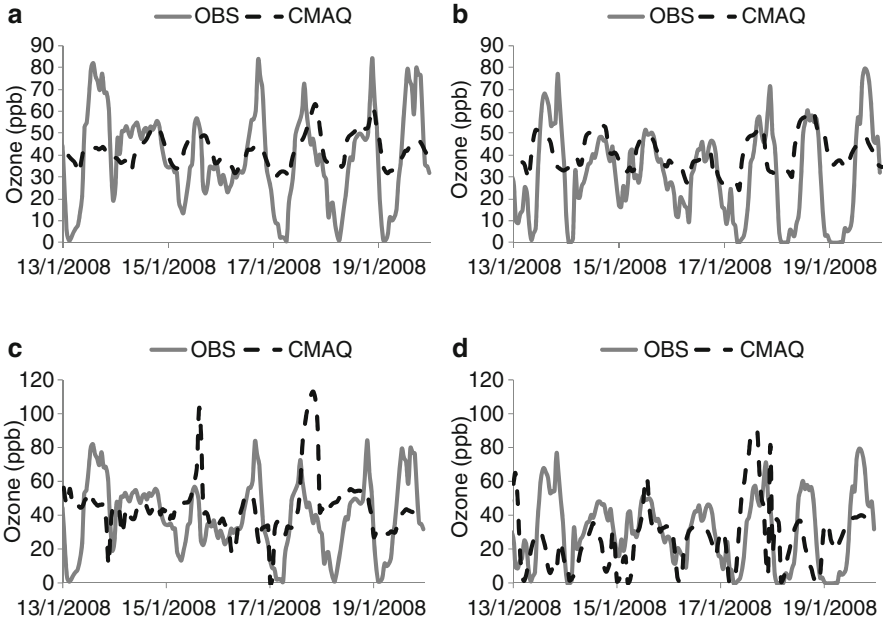


**Fig. 18.1** Observed and simulated ozone concentrations using (*1*) anthropogenic emissions (**a** and **b**) and (*2*) anthropogenic + biogenic emissions (**c** and **d**) at Büyükada and Kandilli air quality stations

agreement (0.53 and 0.55). The minimum ozone levels at night time are much better captured by the model when biogenic emissions are accounted for.

The inclusion of biogenic NMVOCs emissions resulted in a spatial average increase up to 25 ppb of the maximum ozone concentrations during the whole modeling time period. The impact of biogenic emissions on ozone concentrations is more pronounced on the north of the city. This is due to the south winds that prevailed throughout the time period studied allowing the transportation of ozone precursors that had both anthropogenic and biogenic origin, to the north resulting to an urban plume with more enhanced ozone values. The results of model simulations implemented under different emission scenarios showed that the $NO_x$-sensitive chemistry was dominant in Istanbul during the time period studied.

## 18.4 Conclusions

A high resolution MM5/CMAQ air quality modeling system was used in order to investigate the high ozone levels in Istanbul. The inclusion of biogenic NMVOC emissions resulted in improved values of the statistical measures used to evaluate model calculated ozone results. The temporal variations of simulated ozone levels as well as the resolution of nighttime chemistry were improved. More realistic nighttime ozone concentrations were achieved attributed to the destruction of ozone by monoterpene emissions. Sensitivity runs also showed that the chemistry was $NO_x$-sensitive.

**Acknowledgments** The authors would like to thank for the financial support by the COST Action 728, Scientific and Technological Research Council of Turkey (TUBITAK, project no: 105Y005) and Bogazici University Research Fund projects 07HY101D and 05Y105.

## References

1. Byun DW, Ching JKS (1999) Science algorithms of the EPA model-3 community multi-scale air quality (CMAQ) modeling system. US EPA Report No. EPA/600/R-99/030, Office of Research and Development, Washington, DC
2. Grell GA, Dudhia J, Stauffer DR (1994) A description of the fifth – generation Penn State/NCAR mesoscale model (MM5). NCAR Technical Note, NCAR/TN-398+STR
3. Im U, Tayanc M, Yenigun O (2008) Interaction patterns of major photochemical pollutants in İstanbul, Turkey. Atmos Res 89:382–390
4. Im U, Poupkou A, Incecik S, Markakis K, Kindap T, Unal A, Melas D, Yenigun O, Topcu S, Odman MT, Tayanc M, Guler M (2011) The impact of anthropogenic and biogenic emissions on surface ozone concentrations in Istanbul. Sci Total Environ 409:1255–1265
5. Poupkou A, Giannaros T, Markakis K, Kioutsioukis I, Curci G, Melas D, Zerefos C (2010) Development of a biogenic volatile organic compound emissions: software development and first validation. Environ Modell Softw 25:1845–1856. doi:10.1016/j.envsoft.2010.05.004

# Chapter 19
# An Integrated System to Forecast PM10 Concentrations in an Urban Area, Using MODIS Satellite Data

**Claudio Carnevale, Giovanna Finzi, Enrico Pisoni, Vikas Singh, Marialuisa Volta, Alessandra Cacciari, and Walter Di Nicolantonio**

**Abstract** An integrated forecasting system, using artificial neural networks (ANNs) and cokriging technique, has been developed to forecast daily mean PM10 concentrations 2 days in advance. The test case has been performed over Milan metropolitan area in northern Italy where PM10 concentrations are continuously monitored by 14 monitoring stations. In the first step, ANNs are identified for each monitoring stations to forecast and in the second step, the forecasted values are interpolated using cokriging algorithms over the whole domain. The use of the MODIS derived PM concentration maps as a secondary variable for cokriging, account for the local spatial patterns of PM10 where no measurements are available. The results are validated in terms of statistical and forecast exceedance indexes. The validation has been performed in two steps: first, the Neural Network model performances have been investigated comparing the point forecast with observations, and then the cokriging algorithm has been validated using leave one out cross validation method. The validation results show good agreement in terms of statistical indexes. The proposed forecasting methodology represents a fast and reliable way to provide decision makers and general public with PM10 forecast over an urban area.

**Keywords** Forecasting systems • Neural networks • Satellite measurements

C. Carnevale (✉) • G. Finzi • E. Pisoni • V. Singh • M. Volta
Department of Information Engineering, University of Brescia, Via Branze, 38, Brescia 25123, Italy
e-mail: carneval@ing.unibs.it

A. Cacciari • W. Di Nicolantonio
CGS, Bologna, Italy

D.G. Steyn and S. Trini Castelli (eds.), *Air Pollution Modeling and its Application XXI*, NATO Science for Peace and Security Series C: Environmental Security 4,
DOI 10.1007/978-94-007-1359-8_19, 

## 19.1 Introduction

Over recent years, higher concentrations of particulate matter have become an important environmental problem due to the direct impact on the environment and on human health. Because of the health risks due to pollution exposure, EU 2008 directive recommends member states to ensure that timely information about actual or forecasted exceedances of pollutants threshold values are provided to the public [4]. In order to follow these guidelines, prevent critical episodes and inform the public, real time alarm forecasting systems have to be set up.

Moreover, within this frame, the capabilities of Earth observation satellites have greatly improved over the last few years, with gradual improvements in temporal and spatial resolutions and enhancements in radiometric accuracy, thus encouraging further studies on the use of satellite data to assess air quality. Satellite-based measurements strengthen the potential for monitoring air pollution transport and directly evaluating the spatial distribution of various air pollutant concentrations, [5]. In this paper, we describe a modeling system [1] to forecast the daily mean PM10 concentration 2 days ahead over a metropolis using ANNs [2] and cokriging algorithms [6] using MODIS derived maps of $PM_{2.5}$ concentration at the ground as a secondary variable. The proposed methodology provides real time interpolated pollution maps starting from the station forecasted values.

## 19.2 Methodology

The developed forecasting system is composed of two parts. First uses ANNs to perform point-wise forecast at each station location, up to 2 days in advance. Different networks have been identified for each measurement station and forecast lag using the measurement data. The inputs to the networks are mean PM10 concentration of the previous day, NOx hourly concentration measured in the first 12 h of the present day and the third input is forecasted temperature for the corresponding days. Temperature forecast input is only used for the stations also having temperature measurement data. In the second part, cokriging has been used to interpolate the forecasted PM10 concentrations all over the domain. Cokriging methodology allows improving the pollutant concentration estimate by using a secondary correlated variable, which is more intensely sampled than the primary one. In present case, since the number of monitoring station is not sufficient to represent the spatial pattern, bimonthly averaged PM2.5 concentrations, derived from MODIS satellite data, have been used as secondary to provide additional information about the distribution of pollution over the domain. Taking advantage of the satellite synoptic view and of the MODIS repetition cycle, nearly 1 map of PM2.5 concentration at the ground was available per day over Northern Italy for bimonthly averaging. These daily maps have been obtained fusing MODIS level 2 aerosol data, corresponding meteorological files computed for the same domain and PM2.5 samplings in several sites of the Po valley, [3].

## 19.3 Results and Discussion

Test case has been performed for the entire year 2004, over Northern Italy domain, including Milan metropolitan area. The domain has a dimension of 60 × 60 km$^2$, divided in 144 cells of 5 × 5 km$^2$. The domain is monitored by 14 PM10 monitoring stations (Fig. 19.1) and the measurement data of years 2000–2006 have been obtained from Lombardia Regional Environmental Protection Agency (ARPA). For the test case, the data has been divided into a training data set spanning from 2000 to 2003 and from 2005 to 2006 and a validation data set containing daily measurement of year 2004. The training data have been used to identify the artificial neural network models. Leave one out cross validation has been performed to assess the performance of the forecasting system.

In the test case, successive forecast of daily mean PM10 concentrations has been performed all over the domain, 2 days in advance. The predicted values at corresponding validation monitoring stations have been compared with historical time series measured in the year 2004 and a set of standard performance indexes have been calculated. In order to check the ability of the model to reproduce legislation requirements, a threshold of 50 μg/m$^3$ has been considered to evaluate the forecast performance as to exceedances in terms of success index (SI) [7]. The box plots of the calculated statistical indexes for cross validation are shown in Fig. 19.2. The performance results show a general good agreement mainly related to satisfying correlations, low bias and positive success index. With respect to the overall considered period, it can be seen that the quality of forecast decreases as forecast horizon increases. Moreover, it has been found that model performs better for urban background station than the traffic station because of the local emissions and meteorological condition which is difficult to predict by the model.

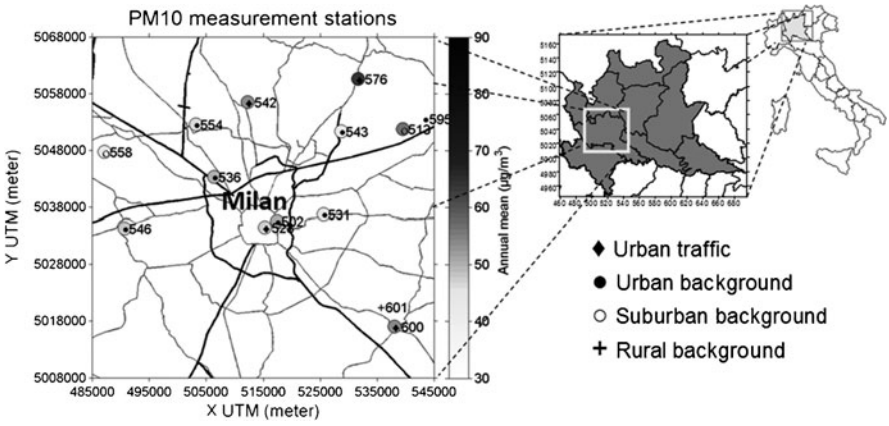


**Fig. 19.1** Test case domain in Northern Italy including Milan metropolitan area showing PM10 monitoring stations

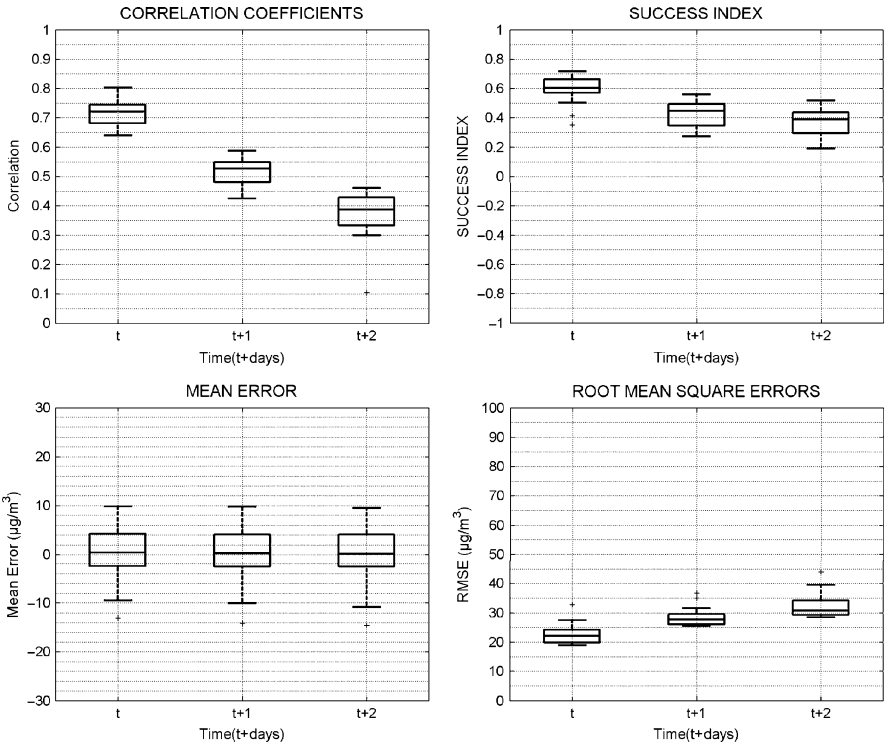


**Fig. 19.2** Box plots of leave-one-out cross validation performance results for PM10

## 19.4 Conclusions

The proposed methodology, integrating artificial neural networks and cokriging techniques is able to forecast daily mean PM10 concentration up to 2 days in advance. This methodology is able to reproduce the spatial patterns of the pollutants over the domain by integrating MODIS satellite data. The results of the presented application over Northern Italy show good agreement in terms of performance indexes although the quality of forecast gets worse for the next days of forecast. Nevertheless the implemented forecasting methodology represents a fast and reliable way to provide decision makers and general public with a spatial distribution of forecasted possible exceedances.

**Acknowledgments** The research has been developed in the framework of the Pilot Project QUITSAT (http://www.quitsat.it), sponsored and funded by the Italian Space Agency (ASI).

## References

1. Carnevale C, Finzi G, Pisoni E, Singh V, Volta M (2008) Neural networks and co-kriging techniques to forecast ozone concentrations in urban areas. In: Proceedings of the iEMSs fourth biennial meeting, Barcelona
2. Corani G (2005) Air quality prediction in Milan: feed-forward neural networks, pruned neural networks and lazy learning. Ecol Modell 185:513–529
3. Di Nicolantonio W, Cacciari A, Tomasi C (2009) Particulate matter at surface: Northern Italy monitoring based on satellite remote sensing, meteorological fields, and in-situ samplings. IEEE J Sel Top Appl Earth Observ Remote Sens 2:284–292
4. EU Directive. 2008/50/EC. (2008) Ambient air quality and cleaner air for Europe. L152, 51
5. Hoff RM, Christopher SA (2009) Remote sensing of particulate pollution from space: have we reached the promised land? J Air Waste Manage Assoc 59:645–675
6. Isaaks EH, Srivastava RM (1990) An introduction to applied geostatistics. Oxford University Press, New York
7. Van Aalst R, de Leeuw F (1997) National ozone forecasting systems and international data exchange in Northwest Europe. Report of the Technical Working Group on Data Exchange and Forecasting for Ozone Episodes in Northwest Europe (TWG-DFO)

# Chapter 20
# Analysis of Scalar Fluxes and Flow Within Modelled Intersection Depending on the Approach Flow Direction

**Libor Kukačka, Radka Kellnerová, Klára Jurčáková, and Zbyněk Jaňour**

**Abstract** The influence of the approach flow direction on contaminant spreading and ventilation within an intersection in an idealised symmetrical urban area was investigated in this study. Advective horizontal and vertical scalar fluxes are computed from measured data for five flow directions. The highest advective contaminant fluxes are measured in the bottom parts of street-canyons. The important role of the vertical turbulent scalar flux in ventilation of intersection is expected. Quadrant analysis of vertical flux of longitudinal momentum is used to determine a domination of sweep or ejection events above the intersection.

**Keywords** Air pollution • Boundary layer • Wind tunnel modelling • Contaminant spreading • Scalar fluxes • Street canyon • Intersection

## 20.1 Introduction

Vehicle traffic pollutants emitted directly to street-canyons represent serious health hazard for people in large cities. As shown in Robins et al. [5] and Wang and McNamara [7], geometry of street intersections plays an important role in pollutant

L. Kukačka (✉) • R. Kellnerová
Department of Meteorology and Environment Protection, Charles University, Prague, Czech Republic

Environmental Aerodynamics, Institute of Thermomechanics, Academy of Sciences of the Czech Republic, v.v.i, Dolejškova 1402/5, Prague 18200, Czech Republic
e-mail: kukacka@it.cas.cz

K. Jurčáková • Z. Jaňour
Environmental Aerodynamics, Institute of Thermomechanics, Academy of Sciences of the Czech Republic, v.v.i, Dolejškova 1402/5, Prague 18200, Czech Republic

D.G. Steyn and S. Trini Castelli (eds.), *Air Pollution Modeling and its Application XXI*, NATO Science for Peace and Security Series C: Environmental Security 4,
DOI 10.1007/978-94-007-1359-8_20, 

dispersion and ventilation in urban areas. The objective of this study is to investigate the influence of the approach flow direction on contaminant spreading and ventilation within an intersection in an idealised urban area.

## 20.2 Experimental Set-up

The model of idealised urban area with apartment houses was designed after the common European inner-city area. Regular blocks of apartment houses with pitched roofs form a perpendicular arrangement of street canyons and intersections, see Fig. 20.1. Wind tunnel model has been scaled down to 1:200. We consider characteristic obstacle high $H = 20$ m as a height of building walls to the bottom edge of the roofs. The experiment was conducted in low-speed aerodynamic tunnel of Institute of Thermomechanics in Nový Knín. Fully turbulent boundary layer was developed by spires and roughness elements. 2-D Laser Doppler Anemometry (LDA) was used for flow measurements. Concentration was measured by slow-response Flame Ionisation Detector (FID). Tracer gas ethane was emitted from a point source placed in the street canyon in front of the intersection, see Fig. 20.1.

Vertical profile of measured turbulent approach flow characteristics data was fitted by the logarithmic and the power law with following parameters: roughness length $z_0 = 0.53$ m, displacement $d_0 = 14.4$ m and power law exponent $\alpha = 0.25$ in full scale. This corresponds according to Britter and Hanna [2] to parameters for neutrally stratified boundary layer flow above a densely built-up area without much obstacle height variation. Validity of the Townsend hypothesis [6] was verified during the experiment. Free stream velocity was 3 m.s$^{-1}$.

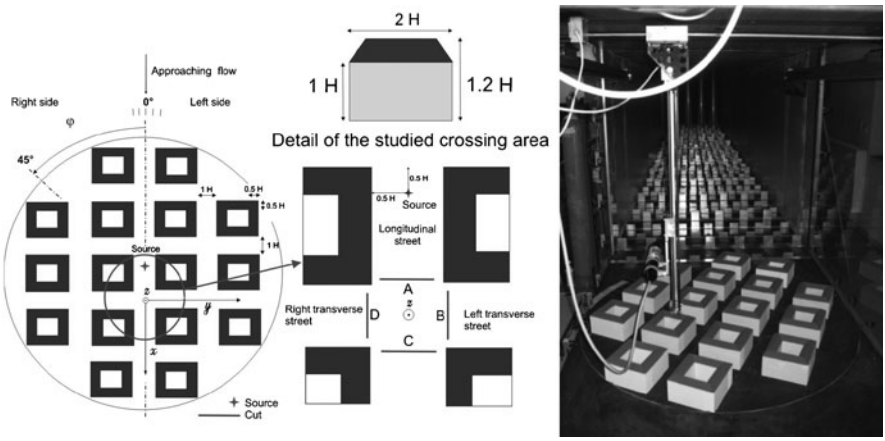


**Fig. 20.1** Scheme of the built-up area model, the studied X-shaped intersection and the photograph of the model placed in the wind tunnel

## 20.3 Results

We determined dimensionless quantities to quantify spreading of pollutants within the studied intersection: concentration of tracer gas $C^*$, horizontal velocity of flow $U^*$ in vertical cross-sections placed at outfalls street canyons connected to the intersection and vertical velocity $W^*$ of flow in a horizontal cross-section at roof level ($z = 1.2\,H$) above the intersection. Results were obtained for 5 values of the approach flow angle $\varphi = 0°$, 5°, 15°, 30° and 45°.

A relative dimensionless flux of passive contaminant $F^*$ was computed by $F^* = U^*C^*$, see similar approach in Belcher [1] and Robins [4]. For getting an information about absolute values of dimensionless flux of passive contaminant in different parts of studied area we computed an absolute dimensionless flux of passive contaminant $F_A^*$ by $F_A^* = A^*U^*C^*$, where $A^*$ is dimensionless area.

The relative flux and absolute flux expresses a rate of emissions spreading through an unit area and area $A^*$, respectively. Computed fluxes characterize advective transfer with following convention of signs: the positive sign means flux outwards and the negative sign means flux inwards the intersection. Values of computed fluxes for three approach flow directions are plotted in Fig. 20.2a–c.

The quadrant analysis was applied to the velocity fluctuation time series to obtain contributions of vertical flux of longitudinal momentum $<u'w'>$ from particular quadrants defined as: 1st quadrant "outward interaction" ($u' > 0$, $w' > 0$), 2nd quadrant "sweep" ($u' > 0$, $w' < 0$), 3rd quadrant "inward interaction" ($u' < 0$, $w' < 0$), 4th quadrant "ejection" ($u' < 0$, $w' > 0$). The particular contribution from $i$th quadrant to the total momentum flux $<u'w'>$ is given by $S_i = <u'w'>_i N_i/N_{total}$, where $<u'w'>_i$ is the average stress and $N_i$ is the number of events in the $ith$ quadrant, number of all measured events is $N_{total}$, see Kellnerová [3].

The relative contributions from ejections $S_4$ and sweeps $S_2$ to the total momentum flux dominated the other two interactions. The difference $\Delta S = S_4 - S_2$ indicates prevailing mechanism of vertical momentum transport in the area, see Fig. 20.3. Ejections characterize the upward transport of longitudinal momentum deficit ($\Delta S > 0$), sweeps correspond to the downward transport of longitudinal momentum excess ($\Delta S < 0$). Ejections and sweeps are approx. of the same magnitude for the approach flow direction $\varphi \sim 0°$, see Fig. 20.3a. Large areas of sweeps increase for directions $\varphi \geq 15°$, see Fig. 20.3b, c.

## 20.4 Conclusions

The described wind tunnel experiment quantified traffic pollutant dispersion within the X-shaped intersection in an idealised symmetric urban area depending on the approach flow direction. Computed scalar fluxes of contaminant showed spreading of pollution mostly within the longitudinal street for the approach flow angles $\varphi \leq 5°$ and to the transverse street by angles $\varphi \geq 15°$. We determined the highest

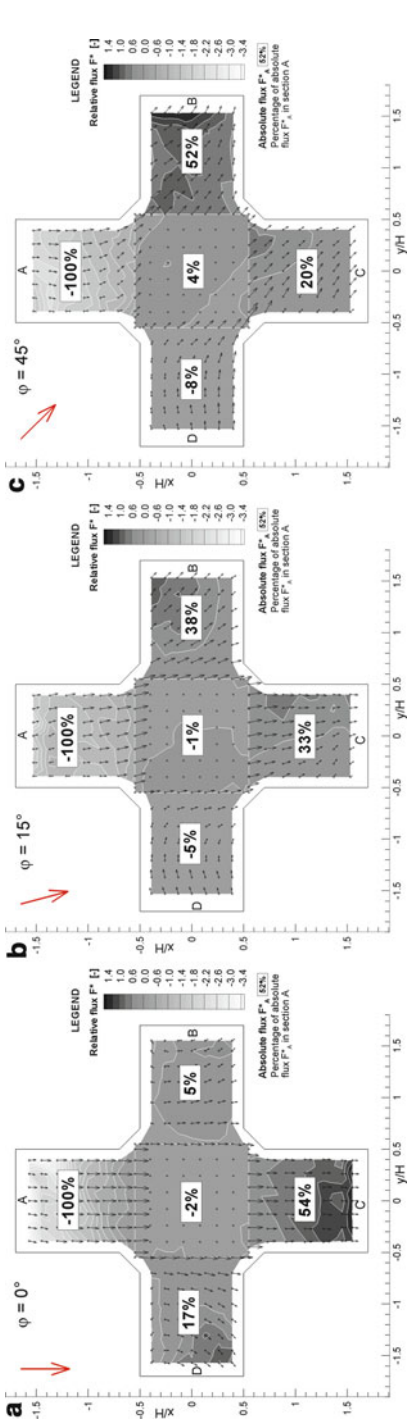


**Fig. 20.2** Relative and absolute dimensionless flux of passive contaminant fields for three approach flow directions in the intersection with horizontal velocity vectors. Numbers in the *white boxes* mean the absolute flux in each cross-section as a percentage of the absolute flux in section A

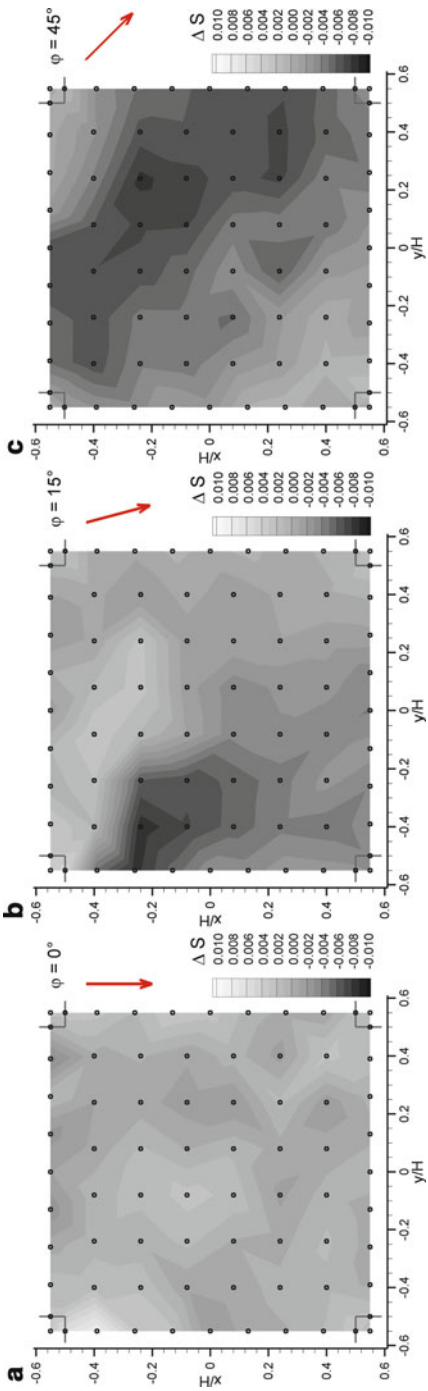


**Fig. 20.3** Difference ΔS between sweeps and ejection events in vertical momentum flux distribution in a horizontal plane at roof level above the studied intersection for three approach flow directions

absolute fluxes in bottom parts of street canyons. Significant vertical turbulent ventilation is expected because of non-zero sum of all measured fluxes within the intersection. Quadrant analysis determined dominating sweeps events by angles $\varphi \geq 15^{\circ}$ that probably extensively influences ventilation of the area by transporting clean air from free stream downwards.

**Acknowledgments** Authors kindly thank Charles University for support by grant GAUK No. 136609 (115-10/259266), the Ministry of Education, Sports and Youth of the Czech Republic for support by AVOZ20760514 and support of the Academy of Sciences of the Czech Republic.

## References

1. Belcher ES (2005) Mixing and transport in urban areas. Philos Trans R Soc A 363:2947–2968
2. Britter RE, Hanna SR (2003) Flow and dispersion in urban areas. Annu Rev Fluid Mech 35:469–496
3. Kellnerová R (2009) Quadrant analysis of boundary layer above pitched and flat roofs. Acta Tech 54:401–413
4. Robins A (2009) Short range dispersion in urban areas. NCAS Urban Meteorology Workshop, Reading
5. Robins A, Savory E, Scaperdas A, Grigoriadis D (2002) Spatial variability and Source-receptor relations at a street intersection. Water Air Soil Pollut 2:381–393
6. Townsend AA (1976) A structure of turbulent shear flow. Cambridge University Press, New York
7. Wang X, McNamara KF (2007) Effects of street orientation on dispersion at or near urban street intersections. J Wind Eng Ind Aerodyn 95:1526–1540

# Chapter 21
# Analysis of HIRLAM NWP Model During an Air Pollution Episode in Istanbul in 2009

**Hüseyin Toros, Gertie Geertsema, Gerard Cats, and Selahattin İncecik**

**Abstract** Meteorological forecasts have been analyzed in detail during an episode involving substantially high concentrations of PM10 that occurred in Istanbul on 18–20 November 2009. The episode addressed here is associated with areas of high pressure over the Northwest of Turkey. These conditions caused poor air quality, especially in the Istanbul Metropolitan Area. Simulations were executed with version 7.2.1 of the HIRLAM model. The simulations were able to predict the temperatures, wind speeds and relative humidity at near surface.

**Keywords** Air quality • Episode • Meteorology • NWP • HIRLAM • Istanbul

## 21.1 Introduction

The megacity Istanbul air quality improved after the 1990s due to the increasing use of natural gas but still experiences episode days. The main reason for these episodic levels was the use of coal and traffic emissions especially from diesel vehicles in the city. The burning of the lignite in the past caused high sulfur and ash levels which persisted due to the anti-cyclonic pressure patterns over Istanbul and surrounding areas [1–3]. Following the fuel switching in the city in mid 1990s, $SO_2$ levels were decreased, but PM10 levels still problem due to the increasing number of vehicles. In this study, the PM10 levels in the greater area of Istanbul are analyzed using monitoring PM10 data measured at the urban areas and significant episodic events

H. Toros (✉) • S. İncecik
Department of Meteorology, Faculty of Aeronautics and Astronautics, Istanbul Technical University, Maslak, 34469 Istanbul, Turkey
e-mail: toros@itu.edu.tr; incecik@itu.edu.tr

G. Geertsema • G. Cats
Weather Research, Royal Netherlands Meteorological Institute, De Bilt, The Netherlands
e-mail: gertie.geertsema@knmi.nl; cats@knmi.nl

D.G. Steyn and S. Trini Castelli (eds.), *Air Pollution Modeling and its Application XXI*, NATO Science for Peace and Security Series C: Environmental Security 4,
DOI 10.1007/978-94-007-1359-8_21, 

**Table 21.1** Description of the HIRLAM model setup

| | |
|---|---|
| Number of levels, grid points in x, y | 60, 406, 400 |
| Coordinates (lon, lat and south pole) | −4.39S, −4.46W, 4.39N, 4.46E, −49.0, 28.8 |
| Time step fc and lower resolution DA | 80 s, 300s |
| Dynamics, physics, surface, analysis, bound | Hydrostatic, HIRLAM, ISBA, 4DVAR, ECMWF |

are selected for case studies in the framework of the project Hirlam ISTanbul 2009 (HIST09). We have analyzed selected episode days involving substantially high concentrations of PM10 that occurred in Istanbul using the HIRLAM mesoscale modeling system.

## 21.2 Materials and Methods

Air quality data were obtained from the Environment Department of Istanbul Greater Metropolitan and the Ministry of Environment and Forestry of Turkey. We have used measurement data from ten air quality stations in the Istanbul Metropolitan Area. Meteorological observations are obtained from the Turkish State Meteorological Service (TSMS). The HIRLAM project (www.hirlam.org) develops and maintains a state-of-the-art NWP model for analysis and short-range forecasting. The HIRLAM model version 7.2.1 is used as the basis for operational short-range prediction in the participating national meteorological services. The HIRLAM model is a hydrostatic limited area grid-point model with lateral boundary values given by a large-scale ECMWF model. The HIRLAM run is initialized at 00 UTC on 16 November with 24-h forecasts every 12 h until 00 UTC 20 November. The model was run at ECMWF using the default settings with a 2.5 km horizontal resolution. The model main characteristics, features of numerics, physics and analysis initialization for the case study is presented (Table 21.1).

## 21.3 Results

Time series of the daily average PM10 concentrations are used to select a peak pollution episode. One of the episodes is seen on 18–20 November 2009. In order to evaluate the episode days, the corresponding synoptic maps, radiosonde measurements, surface wind, precipitation and relative humidity observations were analyzed. During the episode on 18–20 November 2009 there is a high

pressure center with a central sea level pressure of 1,025 hPa over Istanbul and in the 500 hPa map a ridge can be identified leading to divergence and subsidence (not shown here). The radiosonde measurements for 18–20 November at 00 UTC made at the Kartal meteorological station (Fig. 21.1) show a strong surface inversion and a dry air layer between 800 and 900 hPa, caused by the subsidence. Such synoptic conditions result in weak dispersion at the surface.

The surface winds measured at the Goztepe station during these days are shown in Fig. 21.2. At Goztepe station the daily minimum and maximum temperatures are decreasing until 19 November 2009. The winds were light (around 1 m/s) on 18–20 November. There is no rain in the area. Relative humidity is increasing from beginning 13th November to 21 November. As a consequence, the pollutants were accumulated during these days due to stagnant conditions.

Figure 21.3 shows HIRLAM 24-h forecasts during the episode. Observed maximum temperature is 10–13°C and 24-h forecast is 8–10°C. The model mispredicts minimum temperature: observation is 0–2°C whereas the 24-h forecasts are 4–8°C. Both observation and 24-h forecast wind speed is about 1 m/s. The model result is also good at relative humidity because observation and 24-h forecast values are

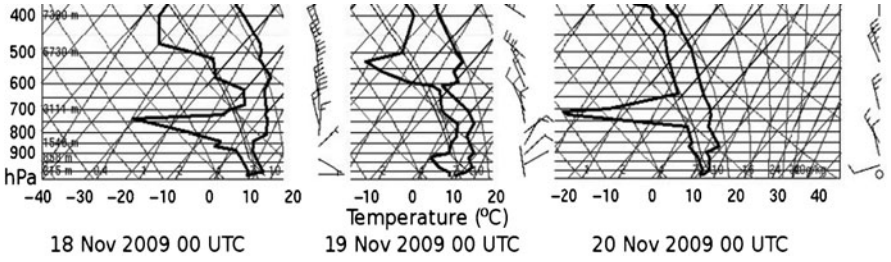


**Fig. 21.1** Radiosonde ascent from the station of Kartal showing temperature *T* and dewpoint *Td* (Radiosonde graph obtained from http://weather.uwyo.edu/upperair/)

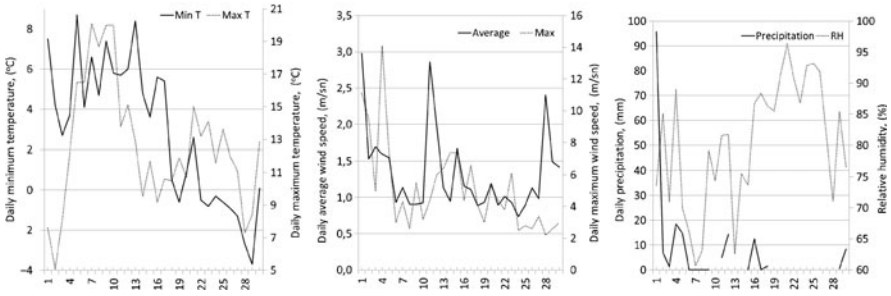


**Fig. 21.2** Daily maximum (*dashed*) and minimum (*solid*) temperature, average (*solid*) and maximum (*dashed*) wind speed and the precipitation (*solid*) and relative humidity (*dashed*) time series measured at station Goztepe on November 2009

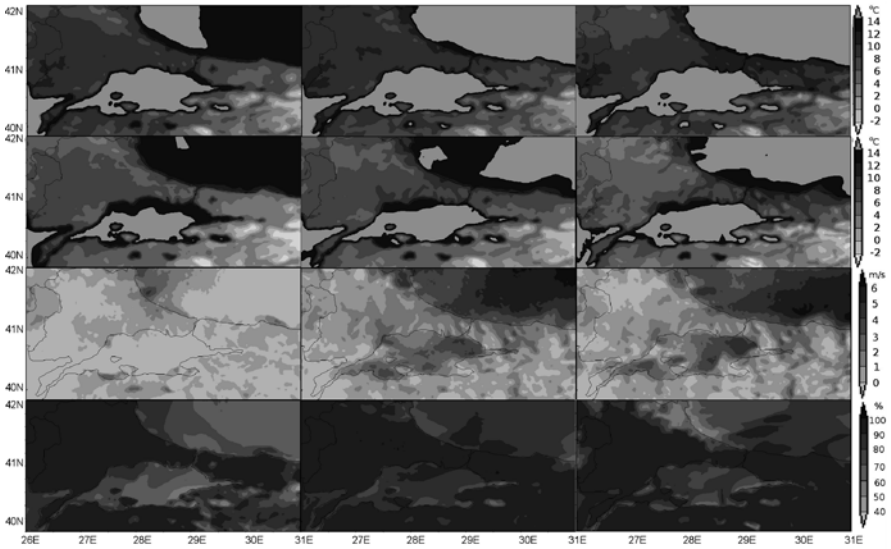


**Fig. 21.3** The 24-h forecast for maximum temperature (1st Panel), minimum temperature (2nd panel), wind speed $u_{10}$ (3 rd panel) and relative humidity (4th panel) on 18 (*left*), 19 (*center*) and 20 (*right*) November 2009

about 90% during the episode days. Observed surface pressure is about 1,025 hPa and model result values are between 1,023 and 1,028 hPa. In summary, all parameters except minimum temperature are well forecast.

## 21.4 Conclusion

High pressure with strong inversion and light winds created favorable conditions for high concentration air pollution in Istanbul during 18–20 November 2009. The high PM10 concentrations during the episode considered here probably originated from the heating of residences due to low temperature and heating need. Accuracy in forecasting air pollution levels depends critically on the ability of the numerical weather prediction models to compute the relevant meteorological parameters like pressure, temperature, wind speed and relative humidity. We have therefore tested the performance of the limited area weather forecasting model HIRLAM. This study showed that the 24 h forecast from HIRLAM was able to forecast the high pressure, low wind speed, low temperature and high relative humidity.

**Acknowledgments** The authors are grateful to Turkish State Meteorological Service, Environment Department of Istanbul Greater Metropolitan and the Ministry of Environment and Forestry of Turkey for the PM10 data.

## References

1. Erçelebi SG, Toros H (2009) Extreme value analysis of Istanbul air pollution data. Clean 37(2):122–131. doi:10.1002/clen.200800041
2. İncecik S (1996) An investigation of the atmospheric conditions in Istanbul leading to air pollution episodes. Atmos Environ 30:101–111
3. Topçu S, İncecik S, Ünal YS (2003) The influence of meteorological conditions and stringent emission control on high episodes in Istanbul. Environ Sci Poll Res 10(1):24–32

# Chapter 22
# WRF-ARW Simulation: Urban Area Scale Forecast for the Tel Aviv Metropolitan Area

**Yosef Levitin**

**Abstract** WRF Modelling System (ver. 2.2) was running for several days during summer and winter seasons within four nested domains with horizontal resolution of 36, 12, 4 and 1.33 km, respectively. Short-term 24 h simulations, as the input meteorological data for operative air quality forecast, were realized using the NCEP global model forecast data. Simulations were fulfilled for different PBL schemes. The calculated standard meteorological parameters, such as wind speed and direction, temperature and relative humidity, were compared with the ground-level observation data from automatic meteorological stations within the urban area and outside the city. The main object of the study was the urban heat island (UHI) effect and, as its consequence, modification of the wind field and surface layer turbulent structure within and over the urban canopy. The intensity of the UHI effect as function of urban surface characteristics, anthropogenic heat release and season meteorological conditions was evaluated.

**Keywords** Weather forecast • Urban canopy • Heat island

As known from many investigations, there is a significant urban heat island (UHI) in large cities with the temperature difference between internal urban territory and surrounding rural areas about 5°C and over. The UHI effect is able to intensify some of environmental problems, such as air quality and visibility, so it is interesting to study this effect also for the Tel Aviv conurbation where the air quality situation is very aggravated.

The Great Tel Aviv urban area includes Tel Aviv itself, Yafo, Ramat Gan, Givataim, Bene Braq and several smaller towns (Fig. 22.1). The urban area lies

Y. Levitin (✉)
Research and Development, Israel Meteorological Service, P.O. Box 25,
Bet Dagan 50250, Israel
e-mail: jlevitin@yahoo.com

D.G. Steyn and S. Trini Castelli (eds.), *Air Pollution Modeling and its Application XXI*,
NATO Science for Peace and Security Series C: Environmental Security 4,
DOI 10.1007/978-94-007-1359-8_22, 

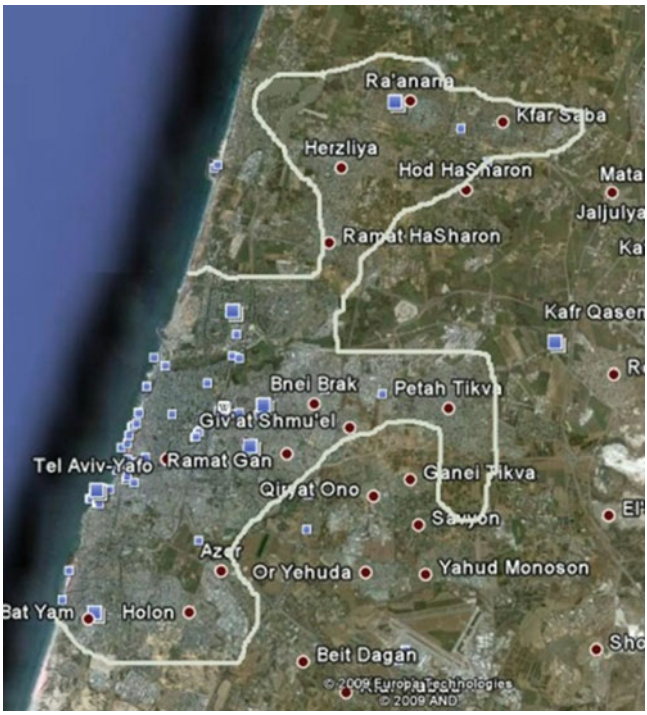


**Fig. 22.1** Configuration of the modelling domains

about 20 km along the Mediterranean shoreline at coastal plain and extends about 10 km eastward without any meaningful topography features. Mountains to the east limit the coastal plain to width of about 20 km. The Tel Aviv climate is Mediterranean; the average daily temperature is of 25°C during summer and 14°C during winter; relative humidity is of 69% and 66% in summer and winter, respectively. The mean global irradiance reaches 28 MJ $m^{-2}day^{-1}$ in summer and 13 MJ $m^{-2}day^{-1}$ in winter [4]. Precipitation occurs from November to March, mainly in December-February (~500−600 mm per year). The summer wind rose reflects the daily sea-land breeze circulation with some influence of the summer trough; in winter, the winds caused by different pressure systems play a significant role.

The UHI effect have been investigated using the Weather Research and Forecasting (WRF) mesoscale model coupled with the Noah land surface and Urban Canopy models (WRF-Noah-UCM) [1, 3, 5]. The WRF model (version 2.2) was running in a nested mode involving four domains with horizontal resolution of 36, 12, 4 and 1.33 km and with 27 vertical levels. The largest domain runs over Mediterranean and Middle East regions, ~4,000 km × 4,000 km (Fig. 22.2). The finest domain with 1.33 km resolution (~40 km × 52 km) involves the Tel Aviv urban area. The set of physical options includes Yonsei University (YSU)

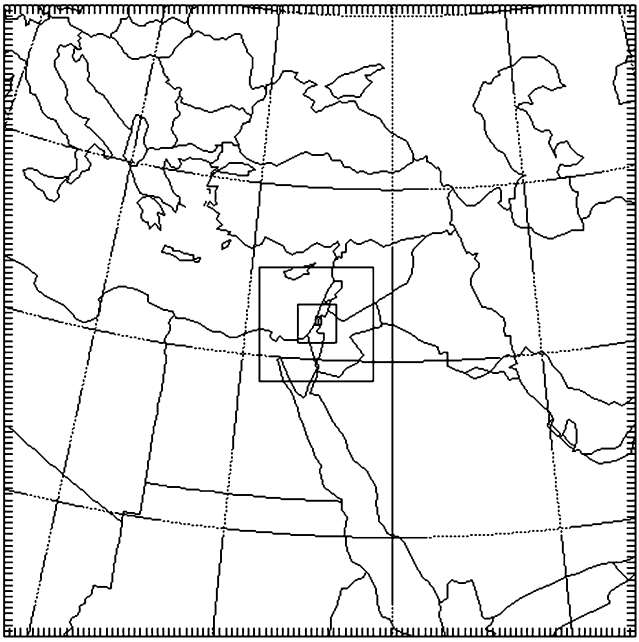

**Fig. 22.2** Map of the Tel-Aviv conurbation (domain 4)

PBL scheme, Ferrier microphysics, Kain-Fritsch cumulus parameterization (for domains 1 and 2), RRTM long wave and Dudhia short wave radiation schemes.

Two days with calm weather conditions, 15 July 2008 and 24 February 2009, were used to examine the UHI effect. During the daytime of the both days, wind direction was mainly the west-southwest. The model ran from 00:00 GMT (02:00 LST) 14 July 2008 and 23 February 2009 with the forecast period for 48 h. The initial and boundary conditions for WRF were taken from the global GFS model at a frequency of 6-h intervals. At present Israel Meteorological Service runs WRF as an operative mesoscale model twice per day (from 00:00 GMT and 12:00 GMT) on two domains (36 and 12 km resolution) for 72-h forecast.

For the date 15 July 2008 Fig. 22.3a–d shows profiles of a predicted surface temperature for the finest domain with two different land use options: UCM and the original USGS 25-category land use data (1st category and 16th one correspond to urban area and sea surface, accordingly). Two curves on the pictures correspond to the cross-section along the longitude across centre of the urban area and the third curve corresponds to the longitude crossed rural territory just north of the Tel-Aviv conurbation. Pictures (a–d) correspond to forecast for different GMT, namely, Z06, Z12, Z18 and Z00 (the difference from GMT to LST is +2 h). Schematic profile of land use for the urban cross-section also is shown, the lowest flat segment corresponds the building zone.

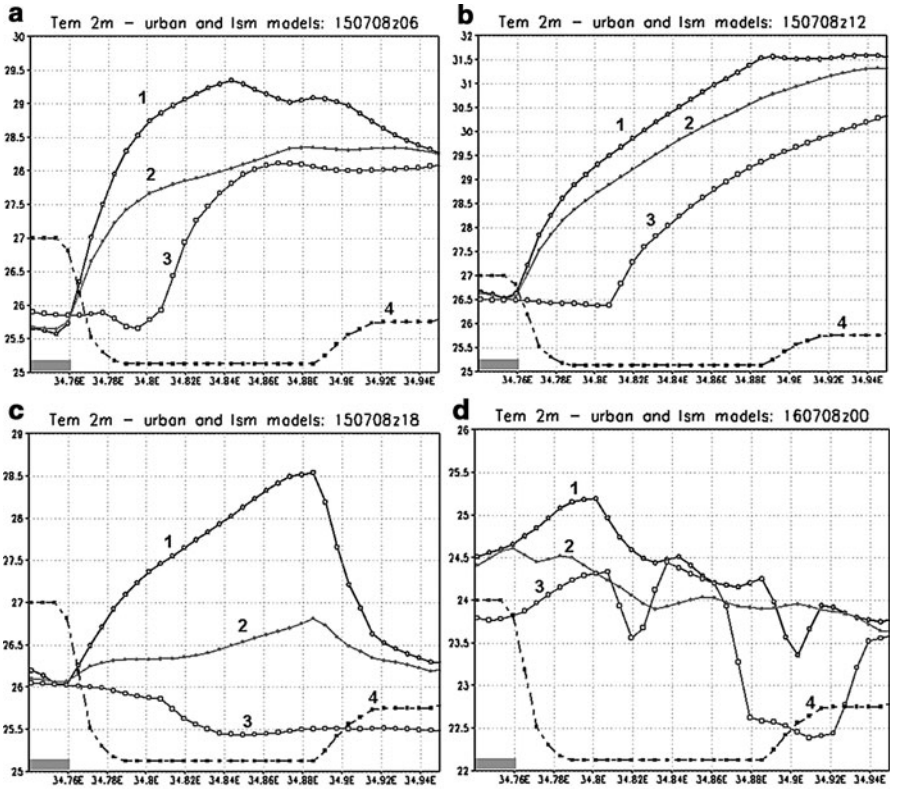


**Fig. 22.3** Temperature at 2 m level along longitude at 08:00 (**a**), 14:00 (**b**), 20:00 (**c**), 02:00 (**d**) LST on 15–16 July 2008. Temperature across urban area center for UCM (1), USGS land use (2), USGS land use across rural area (3), schematic profile of USGS land use (from the urban category 1 to the water category 16) (4), sea surface (*grey strip*)

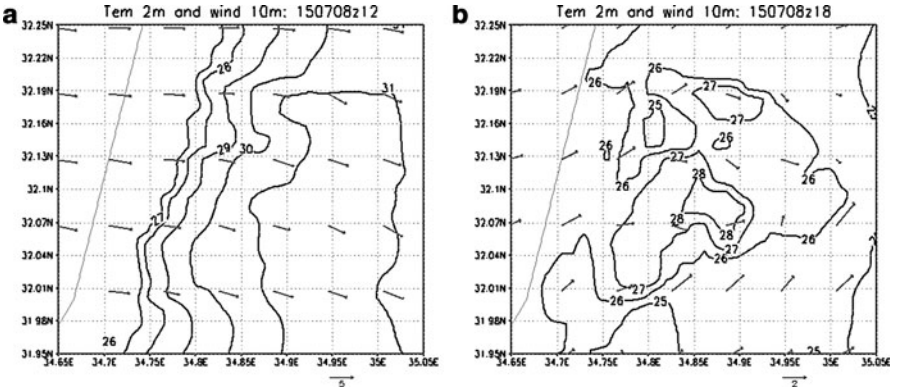


**Fig. 22.4** Wind field at 10 m and surface temperature at 14:00 LST (**a**) and 20:00 LST (**b**) on 15 July 2008. The *grey line* shows the shoreline

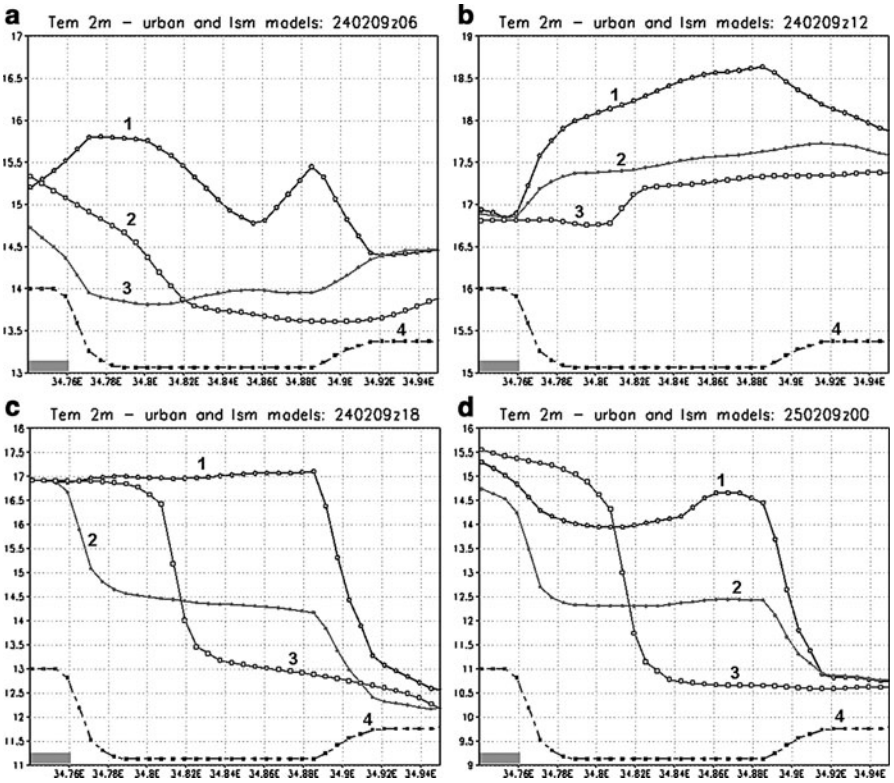


**Fig. 22.5** Temperature at 2 m level along longitude at 08:00 (**a**), 14:00 (**b**), 20:00 (**c**), 02:00 (**d**) LST on 24–25 February 2009. Temperature across urban area center for UCM (1), USGS land use (2), USGS land use across rural area (3), schematic profile of USGS land use (from urban category 1 to water category 16) (4), sea surface (*grey strip*)

Figure 22.4a, b shows surface wind fields (see breeze) and surface temperature isopleths at 14:00 LST (a) and at 20:00 LST (b). As may be seen from Fig. 22.4, deformation of the wind field increases in the evening that may be caused by UHI effect, which reaches its maximum at 17:00–18:00 LST, as well as decrease of the sea breeze intensity in the evening.

Figure 22.5a–d shows the analogous to Fig. 22.3 data for the winter day 24 February 2009. For this day surface wind fields and surface temperature isopleths at 14:00 LST (a) and at 20:00 LST (b) are shown in Fig. 22.6a, b. As may be seen from Fig. 22.6, deformation of the wind field increases in the evening that may be caused mainly by the UHI effect as in winter the sea breeze intensity is small and wind direction and wind speed are more stable.

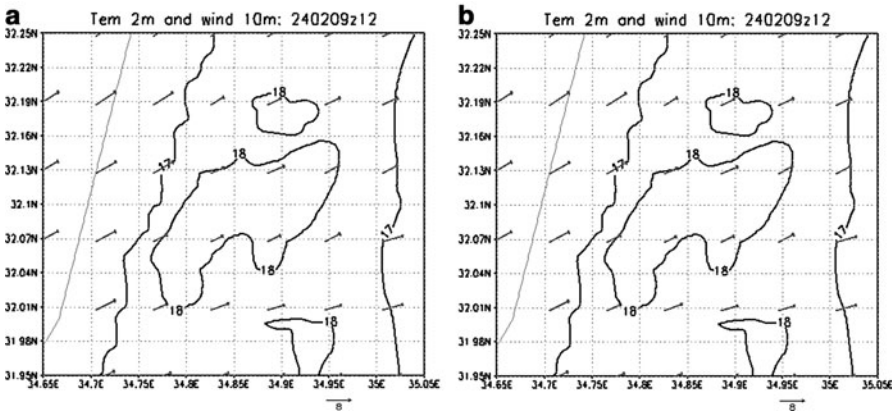


**Fig. 22.6** Wind field at 10 m and surface temperature at 14:00 LST (**a**) and 20:00 LST (**b**) on 24 February 2009. The *grey line* shows the shoreline

## 22.1 Summary

Among many factors, the anthropogenic heat flux (AH) plays an important role in UHI intensity. For example, in the megapolises as Tokyo and Taipei the AH could exceed 400 $Wm^{-2}$ in the daytime; an increase in AH by 100 $Wm^{-2}$ could increase the surface temperature by several tenth degree [2]. In our study we use a rough value of 200 $Wm^{-2}$ for the AH similarly to the value used for Taipei [2]. During the next stage of our study, we are going to evaluate the AH range for the Tel Aviv area conditions.

The predicted intensity of UHI, which is air temperature difference between urban and rural areas, amounts to 3°C in summer and 4°C in winter, during 14:00–18:00 LST. In summer, UHI appears in the morning and decreases to 1°C in the late evening. In winter, UHI appears at the later hours, keeping its intensity to late night. Results of the run with original USGS land use for urban area and turned off UCM (green lines on Fig. 22.3 and 22.5) mainly are between UCM values and rural surface temperatures (yellow lines). In consequence of the prevailing onshore wind direction during the tested days, surface air temperatures for the runs with different land use start with the close values over the sea surface and then diverge along with the airflow movement over the urban territory. The heat trace of the city stretches to 3–7 km leeward.

## References

1. Ek MB, Mitchell KE, Lin Y et al (2003) Implementation of Noah land surface model advances in the NCEP operational mesoscale Eta model. J Geophys Res 108:8851
2. Lin C-Y, Chen F, Huang JC et al (2008) Urban heat island effect and its impact on boundary layer development and land-sea circulation over northern Taiwan. Atmos Environ 42:5635–5649

3. Skamarock WC, Klemp JB, Dudhia J et al (2005) A description of the advanced research WRF version 2. NCAR technical note. National Center for Atmospheric Research, Boulder, CONCAR/0054N-468 + STR
4. Stanhill G, Ianetz A (1997) Long-term trend in, and the spatial variation of, global irradiance in Israel. Tellus 49B:112–122
5. Tevari M, Chen F, Kusaka H (2006) Implementation and evaluation of a single-layer urban model in WRF/Noah. In: Proceedings of the 7th WRF User's workshop, June 2006, Boulder, CO

# Chapter 23
# Dispersion of Bioaerosols from a Wastewater Plant: An Experimental – Modellistic Approach

**Roberta Bertari, Marco Achilli, and Marco Bedogni**

**Abstract** Degradation processes of organic substances in wastewater treatment plants give rise to aerosolised microorganisms (bioaerosols) that are generated mainly during aeration phases. The dispersion of such bioaerosols in the air may cause adverse health effects not only to the workers in wastewater plants but also to the population living or working in the adjacent areas. In order to prevent health risks to the population, Italian national laws prescribe a buffer zone (at least 100 m from the plant) regardless of the local situation, i.e. not considering the dimension of the plant, local meteorological conditions etc. In this paper an evaluation of the actual impact of bioaerosols produced by a small wastewater plant located in Northern Italy is reported. The main aim of the study is an estimation of the real extent of the areas affected by the bioaerosols dispersion.

**Keywords** Wastewater treatment plant • Bioaerosol model dispersion • Bioaerosol emissions

## 23.1 Introduction

A mixed experimental – modellistic approach, characterized by three main phases, was adopted for this study:

- a meteorological analysis of the winds blowing over the investigated area;
- a monitoring campaign of the bioaerosols released by the main sources within the plant (aeration basins, sanding basin, etc.), with measurements carried out in several points of the domain of study, inside and outside the plant;

R. Bertari (✉) • M. Achilli • M. Bedogni (✉)
IBS Engineering sas, Via Isonzo 24, 20052 Monza, Italy
e-mail: info@ibs-eng.it

D.G. Steyn and S. Trini Castelli (eds.), *Air Pollution Modeling and its Application XXI*,
NATO Science for Peace and Security Series C: Environmental Security 4,
DOI 10.1007/978-94-007-1359-8_23, 

- a long-term validation and application of a computer-based atmospheric dispersion model (CALPUFF).

By means of this methodology, a map of the areas involved with the bioaerosol dispersion around the wastewater plant was delineated in relation to the real emissions of the plant and the local meteorological conditions.

## 23.2 Area of Study and Facility

The wastewater plant is located in a flat area of the Po River Valley, in Northern Italy. The terrain in the area of study is flat for at least 4 km from the plant, and no obstacles are present near the wastewater plant except for a wood westward. Excluding the wood area from the computational domain, it was possible to apply a mathematical dispersion model for flat terrain.

The facility is a medium-size (designed for a maximum of 28.800 Population Equivalent) activated sewage sludge treatment plant processing municipal wastewater. Influent sewage is subjected to a primary grid treatment and then is pumped into a sanding basin by separation of sand. Cleared raw sewage is distributed to denitrification basins followed by oxidation/nitrification basins and at last to the final secondary sedimentation phase. Except for primary grid clearing and pumping, the described processes take place outdoors, included sludge dewatering.

## 23.3 Meteorological Analysis

Long term meteorological analysis was carried out evaluating the data measured by all the nearest stations, situated in a range of 2–20 km from the wastewater plant. These data show conditions which are typical for the Po River Valley: low temperatures during winter, sometimes with fog, hot temperatures summertime with poor rain, and variable intermediate seasons. Winds are generally very low (Fig. 23.1), with 50% of 1-h mean wind speed values lower than 1 m/s and, in particular, almost 20% of calms (i.e. wind speed lower than 0.3 m/s) or variable directions. Winds generally blow from the south daytime and from the north during the night; the latter are usually mountain breezes with very low speeds.

## 23.4 Monitoring Activities

Very little scientific information about bioaerosol flux emissions from a wastewater plant is available. In order to better characterise the actual facility emissions and their impact beyond its boundaries, bioaerosol concentrations were monitored in five points inside the plant (near the most important bioaerosol sources) and

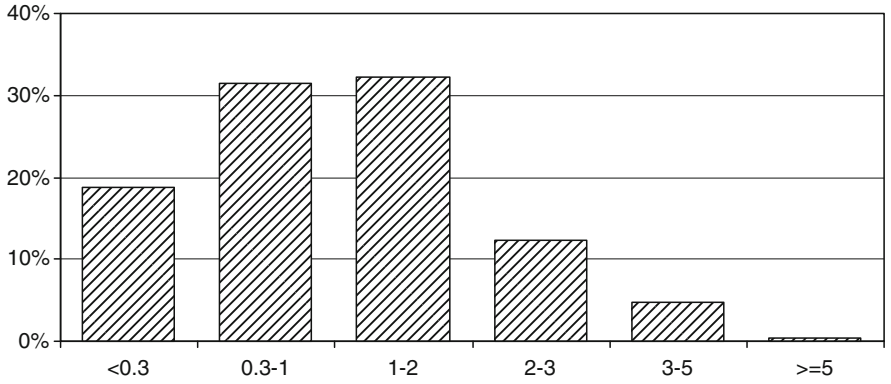


**Fig. 23.1** Distribution of hourly measured wind speed data (m/s) in 2007

in seven points outside the plant, along and perpendicularly to the direction of winds blowing at the moment of the measurement.

Air sampling was performed in June 2008 and in February 2010, with low speed winds (less than 1 m/s) in the first case and with stronger winds (2 m/s) in the latter case. The samples were taken upwind, close to the sewage treatment installations (at less than 1 m) for the measurements inside the plant, and at 140 cm above the ground in the other points.

Air samples were taken by means of a Strainbuster Aquaria sampler, with an air volume of 0.3 $m^3$. In each sampling site, total mesophilic bacteria, total coliform, *Escherichia coli*, *Enterobacters*, *Streptococcus faecalis*, *Pseudomonas aeruginosa*, *Enterococcus* and *Salmonella* were analysed.

## 23.5 Model Calibration and Validation

After the experimental characterization of the plant, a computer-based dispersion model was applied in order to estimate the extent of the area involved with the bioaerosol dispersion. Due to the high frequency of low winds characterising the area, a model able to manage calm conditions is usually recommended for applications over Northern Italy. For this reason, CALPUFF version 5.8 mathematical model [2] was used.

Bioaerosols were treated as particulate matter with aerodynamic diameter up to 2 μm [1]. As a conservative choice in relation to the possible public health impact, bacterial survival aspects were not taken into account, i.e. modelled particulate matter didn't include any decay time of the aerosolised bacteria.

Emission sources were described as area sources. Special care was taken in preparing the numerical parameters describing the area sources, in particular emission fluxes. Very little information about numerical values of the emission fluxes from the different parts of the plant is available: this is the reason why the "classic" technique to determine the flux values for which the mathematical dispersion model

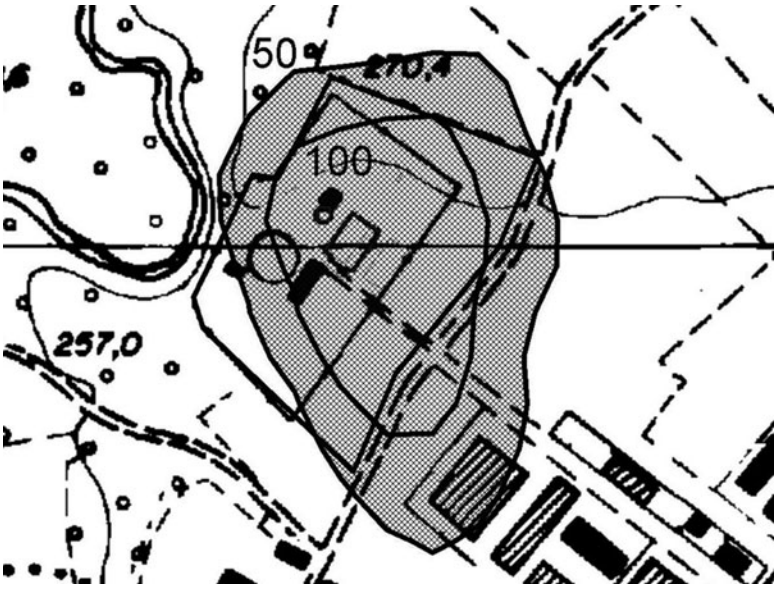


**Fig. 23.2** Example of the mean annual calculated bioaerosol concentration map

predicts the measured downwind bacterial concentrations inside the plant, was applied. Daily bacteria aerosols emission factor estimated for the plant as a whole is $4.5 \times 10^5$ CFU $d^{-1}$ $PE^{-1}$, that is of the same order of magnitude of the values reported in [1].

Downwind bioaerosol concentrations measured outside the plant were used for the validation of the model.

## 23.6 Model Application

After the validation, long-term (1 year) simulations were carried out on the base of hourly meteorological data measured by the nearest monitoring stations. In this way, model results gave interesting information about the probable extent of areas involved with the bioaerosol dispersion. Figure 23.2 shows an example of the mean annual distribution of bioaerosol concentrations due to the wastewater plant.

## References

1. Bauer H, Fuerhacker M, Zibuschka F, Schmid H, Puxbaum H (2002) Bacteria and fungi in aerosols generated by two different types of wastewater treatment plants. Water Res 36(16):3965–3970
2. Scire JS, Strimaitis DG, Yamartino RJ (2000) A user's guide for the CALPUFF dispersion model (version 5). Technical report Earth Tech Inc., Concord

# Chapter 24
# Dispersion and Deposition of Radioactive Particulate Matter from an Explosion

**Vladimír Fuka and Josef Brechler**

**Abstract** Several experiments of dispersion of radioactive particulate matter after an explosion have been performed by the National Radiation Protection Institute of the Czech Republic. These experiments were set up to simulate an attack by a so-called "dirty bomb". Many pieces of experimental equipment were used to measure aerosol concentration, deposited activity, dose rates and basic meteorological parameters. In this contribution we perform a computer simulation of this experiment using our in-house CFD (LES) code. We mainly concentrate on deposition of activity in the area of interest and the time evolution of concentration. These experiments are also used as a model short scale scenario for Working group 9 of project EMRAS II coordinated by the IAEA.

**Keywords** Radioactive aerosol • Dirty bomb • Large eddy simulation

## 24.1 Introduction

The National Radiation Protection Institute (NRPI) of the Czech Republic performed a series of experiments of dispersion of radioactive tracer (solution of $^{99}$Tc) after an explosion [5]. This explosion should have simulated a terrorist act using a radioactive dispersion device. An area of approx. 50 × 50 m was covered by paper detectors for measurement of deposited activity. Several pieces of other equipment was installed at the site, namely Dusttraks (measuring PM10 concentration in time), cascade impactor (measuring average particle size distribution) and a small meteorological probes measuring wind speed and direction in 2 m,

V. Fuka (✉) • J. Brechler
Department of Meteorology and Environment Protection, Faculty of Mathematics and Physics, Charles University in Prague, V Holešovičkách 2, 180 00, Prague 8, Czech Republic
e-mail: vladimir.fuka@mff.cuni.cz; josef.brechler@mff.cuni.cz

D.G. Steyn and S. Trini Castelli (eds.), *Air Pollution Modeling and its Application XXI*, NATO Science for Peace and Security Series C: Environmental Security 4,
DOI 10.1007/978-94-007-1359-8_24, 

atmospheric pressure and temperature. Said experiments are also used by a Working group 9 – Urban areas of project EMRAS II under International Atomic Energy Agency.

## 24.2 Numerical Methods

Our simulation software is an LES code developed by the authors (e.g. [2]) using common numerical methods. It solves Navier-Stokes equations for incompressible flows and is aimed mainly at flows and pollution dispersion in the atmospheric boundary layer in complex geometry. It uses an orthogonal grid for spatial discretization to keep the code simple and computationally effective.

The time marching scheme is based on a fractional step (or pressure correction) method for incompressible Navier-Stokes equations. In this method momentum equations are solved first without the incompressibility constraint (continuity equation). In the next step the computed velocity field is corrected to be non-divergent and pressure for the next time step is computed at the same time. For the spatial discretization of the (nonlinear) advection terms we use central difference scheme for momentum, because low numerical diffusion of the method is desirable. For the advection of pollutants this method is not appropriate, because it can lead to numerical instability and negative values can occur. Therefore we use a partial linear method with a slope limiter [6], that preserves monotonicity (prevents creation of new extremes) of the solution. The subgrid terms are modelled using an eddy-viscosity model by Vreman [7].

Very important issues are the sinks and sources of contaminants. In the present study the contaminant is inserted in the computational domain by an initial condition, which approximates the concentration just after the explosion. We choose a simple uniform distribution in a volume $7 \times 7 \times 12$ m for the first computations. The only sink considered is a dry deposition. We employed a semi-empirical scheme Kharcheno [3] for dry deposition on moderately rough surfaces. The deposition depends largely on the particle size distribution, which is based on measurements by a cascade impactor. Because of the large scatter in measurements we choose a fixed initial distribution for all cases as (Table 24.1):

The code treats the each category in Table 24.1 as an independent scalar field with a fixed particle diameter.

**Table 24.1** Percentage of activity contained in different particle size classes used by the model

| Particle diameter [μm] | Activity (%) |
|---|---|
| 0.2 | 10 |
| 1 | 13 |
| 6 | 64 |
| 20 | 13 |

## 24.3 Boundary Conditions

The experimental domain was the same for all computed cases with a pair of obstacles placed downwind from the explosion in some tests. The computational area has dimensions $100 \times 80 \times 50$ m$^3$ in most computations. We used roughness length 1 mm for the gravel surface of the site.

The inflow wind speed and direction was based on a 5 min average of the measurements. The average profile was logarithmic. The actual turbulent inflow condition was then computed using a scheme based on random numbers by Klein et al. [4] in a more effective variant by Xie and Castro [8].

The solid obstacles were computed using a first approximation of the immersed boundary method (e.g. $u = 0$ inside bodies). This was found by Bodnar et al. [1] not to produce significant difference to a boundary fitted grid.

## 24.4 Results

We computed the dispersion and deposition for several experiments. Because of the position of the experimental site in a small valley with forests on its flanks, the wind was in all computed cases almost aligned with the prepared axis of the experiments (i.e. position of detectors and obstacles). The results agree with most of the experiments plus minus one order of magnitude but the exact shapes are different. The differences can be attributed mostly to many unknowns in initial and boundary conditions. The explosion itself was directed by metal plates which makes the initial formation of the cloud even harder to predict. Examples of computed depositions are in Fig. 24.1. More details to individual tests are in Prouza et al. [5].

In Fig. 24.2 are time histories of non-dimensional concentrations in three positions along the centerline (in front of the main obstacle, just behind it and

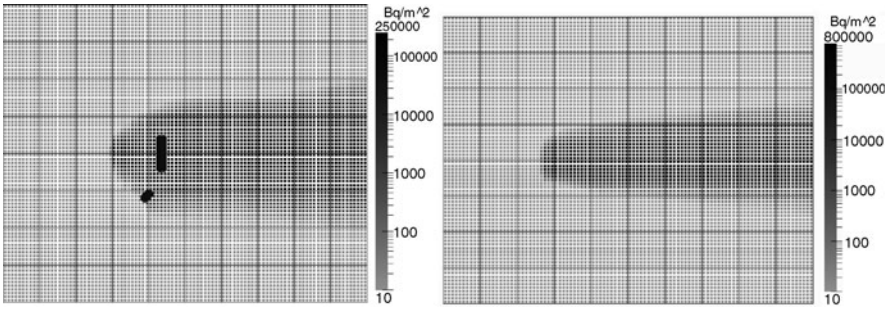


**Fig. 24.1** Computed deposition of activity for two tests 17.07.2009 (*left*) and 15.05.2008 (*right*). *Grid lines* every 10 m

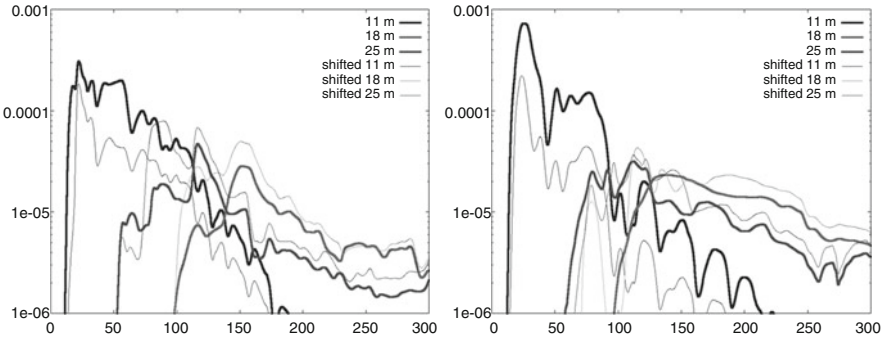


**Fig. 24.2** Time histories of non-dimensional concentrations of aerosol in three different positions along the centerline for the test from 21.10.2008 (computations with same input parameters)

22 m farther) for test of 21. 10. 2008. The most interesting feature is the order of the peaks in different positions, which differs from experiment. We did not succeed in explaining this discrepancy.

## 24.5 Conclusions

We performed numerical simulation of several explosion and dispersion tests of radioactive tracer. The method proved to be useful and give reasonable predictions, despite incomplete knowledge of input data.

**Acknowledgments** The work was supported by grant SVV-2010-261308 and by the Czech Ministry of Education, Youth and Sports under the framework of research plan MSM0021620860

## References

1. Bodnar T, Benes L, Kozel K (2008) Numerical simulation of flow and pollution dispersion in the area of opencast coal mine. In: Numerical analysis and applied mathematics. American Institute of Physics, Melville, New York, pp 100–103
2. Fuka V, Brechler J (2008) Finite volume microscale air-flow modelling using the immersed boundary method. In: Borrego C, Miranda AI (eds) Air pollution modeling and its application XIX. Springer, Dordrecht
3. Kharcheno AI (1997) Parameterization of dry deposition velocity in the atmospheric surface layer. J Aerosol Sci 28(Suppl 1):589–590
4. Klein M, Sadiki A, Janicka J (2003) A digital filter based generation of inflow data for spatially developing direct numerical or large eddy simulations. J Comp Phys 32:652–665
5. Prouza Z, Beckova V, Cespirova I, Helebrant J, Hulka J, Kuca P, Michalek V, Rulik P, Skrkal J, Hovorka J (2010) Field tests using radioactive matter. Radiat Prot Dosim 139(4):519–531

6. Van Leer B (1979) Towards the ultimate conservative difference scheme, V. A second order sequel to Godunov's method. J Comp Phys 32:101–136
7. Vreman AV (2004) An eddy-viscosity subgrid-scale model for turbulent shear flow: algebraic theory and applications. Phys Fluids 16:3670–3681
8. Xie Z-T, Castro IP (2008) Efficient generation of inflow conditions for large-eddy simulation of street-scale flows. Flow Turbul Combust 81(3):449–470

# Chapter 25
# Calculation of Standard Deviation of Concentration Using a Second-Order Closure Theory

**Zorica Milivoj Podrascanin and Borivoj Rajkovic**

**Abstract** The quality of the simulation of the motion and spread of a passive substance in a puff model depends on the ability to estimate the speed of the wind at the source height and standard deviation of concentration both in time and space. The wind profile is calculated using the standard Monin-Obukhov similarity theory and standard deviation of concentration, ("sigmas" in the further text) is calculated using a scheme based on the second-order closure theory. To asses the success of the model comparison was made with two other approaches for the calculation of the "sigmas", the Briggs empirical method and a semi-empirical scheme based on the statistical theory. All of these methods are based on the various parameters of turbulence which were calculated from standard measurements using the so called meteorological pre-processing. Finally the results were compared with the results from the measurements from Tracer Dispersion Experiments in the Copenhagen Area during 1978/1979. First we have analyzed the wind extrapolation results and when we were satisfied with those we did comparisons with the observed concentration.

**Keywords** Standard deviation of concentration • Puff model • Wind profile • The second-order closure theory

Z.M. Podrascanin (✉)
Center for Meteorology and Environmental Predictions
University of Novi Sad, Novi Sad, Serbia
e-mail: zorica.podrascanin@gmail.com

B. Rajkovic
Faculty of Science, University of Belgrade, Belgrade, Serbia
e-mail: bora@ff.bg.ac.rs

D.G. Steyn and S. Trini Castelli (eds.), *Air Pollution Modeling and its Application XXI*,
NATO Science for Peace and Security Series C: Environmental Security 4,
DOI 10.1007/978-94-007-1359-8_25, 

## 25.1 Introduction

At the beginning of Gaussian type models development, standard deviation of concentration was calculated using empirical formulas where the "sigmas" were only function of distance and stability categories. One of the most popular empirical set of such formulas is the one suggested by Briggs [1]. With the development of statistical theory of turbulence a new approach appeared. However, statistical theory was too complex to be easily applied in modeling of passive substance and because of that it has been simplified in combination with measurements. That combination gives a set of semi-empirical schemes [2] for stable, unstable and neutral atmospheric stability.

On the other hand Sykes et al. [5–7] developed a new way for "sigmas" calculations based on second order turbulence closure theory. Their approach is to start with the transport equitation for integrated mean scalar concentration in the plane transverse to the transport direction. The problem is that the system consist of second-order correlation and needs to be closed. The closure was suggested by Lewellen [3], which led to the system that could be solved for "sigmas". Unlike in the case of semi-empirical theories, here the stability is taken into account through the turbulent parameters which could be either estimated from the standard measurements or directly measured with the new automatic weather stations.

## 25.2 Model Description

For testing "sigmas" based on second order turbulence closure theory the two new parts of model were inserted in a puff type model that has been previously developed and extensively used for various ecological problems for dispersion of various passive substances as well as for radiation dose estimates [4]. The main feature of this model is that the emissions from sources were regarded as a continuous series of consecutive puffs released within a certain period of time (1 min). The center of each puff is carried by wind. Concentration in each cell is the sum of puffs released until a given moment.

The first added part is meteorological pre-processing, where all turbulence parameter are calculated. There are two ways to estimate friction velocity, Monin-Obukhov length and temperature scale needed for wind profile calculation: (a) the standard profile method, which we used, and (b) the energy budget method [8].The first method requires temperature gradient which could not be obtained from the standard meteorology measurements. The second method avoided this problem by calculating heat flux from the energy budget at surface for day time and calculating temperature scale as a simple function of total cloud amount for night time. The friction velocity is then obtained via Monin-Obukhov theory through standard iterative procedure. With those two scales in "hand", wind profile was

obtained. After that standard deviation of wind and relevant length and time scale are estimated.

When the all needed turbulence parameter were estimated it was easy to add another part. In the second part the spatial distribution of concentration is calculated using "sigmas" based on second order turbulence closure theory. In that way the previous empirical set of equation was chanced with only one equation for "sigmas" in one direction.

## 25.3 Results

The results from the above described model were compared with real time measurements obtained during the Tracer Dispersion Experiments in the Copenhagen Area during 1978/1979. The wind speed is compared with measured at altitude of 120 m and 200 m. Results in terms of the wind bias score obtained during experiment performed on 19.07.1979 are given in Fig. 25.1. The agreement between measured and calculated wind data is good for stable and unstable regime but it is less good in transition between those two. The root mean square comparison was made for 7 days. For altitude of 120 m it was in the range between 0.74 and 1.94 m/s and for altitude of 200 m it was in the range between 0.98 and 2.16 m/s. It is clear that the agreement is better for altitude of 120 m.

The agreement between second-order "sigmas" and measured ones are in the range from 1% to 45% percents and depends on the source distance and experiment. In Fig. 25.2 there are presented "sigmas" calculated during experiment performed on 19.07.1979 using three different methods: (a) calculations using Briggs formulas, (b) standard semi-empirical calculations and (c) calculations using results from the second-order turbulence closure method. To see the model accuracy calculated

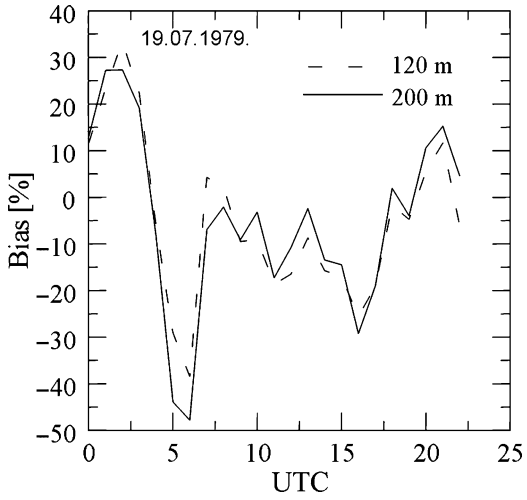


**Fig. 25.1** Wind bias on altitude of 120 m and 200 m

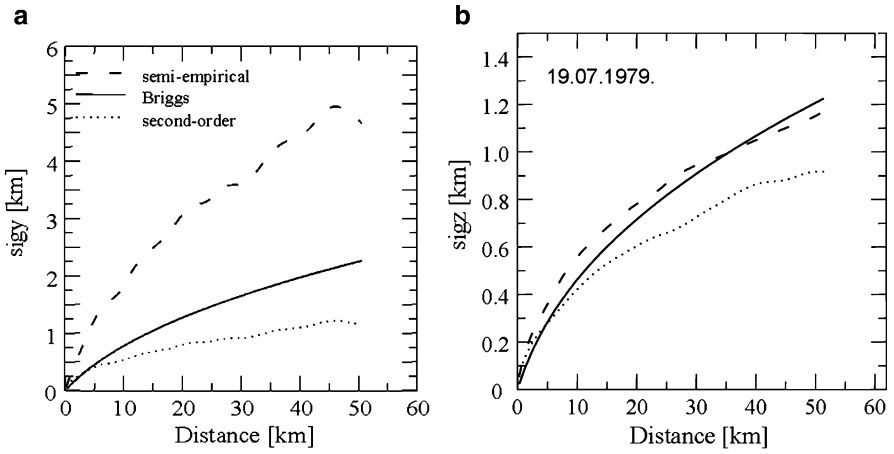


**Fig. 25.2** Standard deviation of concentration in y (**a**) and z (**b**) direction

and observed concentration are compared. Agreement of calculated and observed concentration decreases with the distance between the source and receptors. The agreement is also better with receptors which are near central puff line.

**Acknowledgments** This work has been partially funded by the Republic of Serbia, Ministry of Science, grants no. 1197 and 141035, Italian ministry of Environment and territories through its two projects, SINTA and ADRICOSM-STAR

## References

1. Briggs GA (1973) Diffusion estimates for small emissions. NOAA, ERL Report. ATDL-79, 59 pp
2. Carruthers DJ, Weng WS, Hunt JCR, Holroyd RJ, McHugh CA, Dyster SJ (2003) Atmopheric dispersion modelling system (UK-ADMS). Plume/puff spread and mean concentration module specifications document UK ADMS 1.0; P10/01 T/03; P12/01 T/03 12.03. from UK-ADMS 1.3 technical specification
3. Lewellen WS (1977) Use of invariant modeling. In: Frost W, Moulden TH (eds) Handbook of turbulence. Plenum Press, New York, pp 237–280
4. Rajkovic B, Arsenic I, Grsic Z (2008) Point source atmospheric diffusion. In: Gualtieri C, Mihailovic DT (eds) Fluid mechanics of environmental interfaces. Taylor and Francis, London, pp 1–17
5. Sykes RI, Gabruk RS (1997) A second-order closure model for the effect of averaging time on turbulent plume dispersion. J Appl Meteorol 36:165–184
6. Sykes RI, Lewellen WS, Parker SF (1986) A Gaussian plume model of atmospheric dispersion based on second-order closure. J Clim Appl Meteorol 25:322–331
7. Sykes RI, Parker SF, Henn DS, Cerasoli CP, Santos LP (2000) PC-SCIPUFF Version 1.3 technical documentation. A.R.A.P Report No. 725. Titan Corporation, ARAP Group
8. Van Ulden AP, Holtslag AAM (1985) Estimation of atmospheric boundary layer parameters for diffusion applications. J Clim Appl Meteorol 24:1196–1207

# Chapter 26
# Simulating Building Downwash of Heavy Metals by Using Virtual Sources: Methodology and Results

**Wouter Lefebvre, Guido Cosemans, Karen Van de Vel, Stijn Janssen, Clemens Mensink, David Celis, Frank Sleeuwaert, Hendrik Van Rompaey, and Frea Blommaert**

**Abstract** There is a discrepancy in data quality between the highly detailed concentration measurements in the surroundings of industrial plants emitting heavy metals and the registered emission data at these sites. When simulating the concentration fields in the direct vicinity of the emitting plants by using the bi-gaussian model IFDM and the reported emissions, the simulated concentrations were much lower than the measured concentrations. Originally, this was thought to be due to diffuse, wind-fugitive emissions not reported in the official inventories. Therefore, inverse modeling was performed to get the emission data and wind dependency of these emissions. It was expected that the emissions coming out of the inverse modeling would follow a power law of the wind speed except for very low and very high wind speeds. In the latter case, a constant emission was expected, while in the former case, no emissions were expected to be found. However, this lower threshold did not seem to exist in the modeled emissions. Furthermore, these emissions seemed to have their source in spots not used for storage of heavy metals such as parking lots. Detailed analysis of these results showed that another effect, known as building downwash, is responsible for this behavior. Thereafter, it was shown that it is possible for a bi-gaussian model that lacks a building downwash module, to simulate correct concentration levels by putting in virtual sources just behind the buildings causing the building downwash phenomenon. By using half of the available concentration data for the inverse modeling and half for the validation, it was shown that this technique can be used to produce detailed and validated

W. Lefebvre (✉) • G. Cosemans • K. Van de Vel • S. Janssen • C. Mensink • F. Sleeuwaert • H.V. Rompaey
Department of Environmental Modelling, Flemish Institute for Technological Research (VITO), Boeretang 200, 2400 Mol, Belgium
e-mail: wouter.lefebvre@vito.be; guido.cosemans@vito.be; stijn.janssen@vito.be; clemens.mensink@vito.be

D. Celis • F. Blommaert
Afdeling Lucht, Milieu en Communicatie, Vlaamse Milieumaatschappij, Kronenburgstraat 45, B-2000, Antwerpen, Belgium

D.G. Steyn and S. Trini Castelli (eds.), *Air Pollution Modeling and its Application XXI*, NATO Science for Peace and Security Series C: Environmental Security 4,
DOI 10.1007/978-94-007-1359-8_26, 

concentration maps of the surroundings of the industrial site. Finally, it was shown that in this case study building downwash has an important effect on local concentrations and that a better representation of building downwash is needed in bi-gaussian models to describe the complex dispersion patterns in the wake of industrial sites.

**Keywords** Building downwash • Virtual sources • Gaussian plume model • Local scale

## 26.1 Introduction

There is a discrepancy in data quality between the highly detailed concentration measurements in the surroundings of industrial plants emitting heavy metals and the registered emission data at these sites. When simulating the concentration fields in the direct vicinity of the emitting plants by using the bi-gaussian model IFDM and the reported emissions, the simulated concentrations were much lower than the measured concentrations. This discrepancy was thought to be originated from diffuse, wind-driven emissions not reported in the official inventories. This study describes the methodology and the results of a study which tries to determine these sources.

## 26.2 Model

The model used in this study is IFDM. IFDM is a bi-Gaussian air pollution model, designed to simulate non-reactive pollutant dispersion on a local scale. The dispersion parameters are dependent on the stability of the atmosphere and the wind speed following the Bultynck and Malet formulation [1]. The meteorological input for this model is taken from measurements made in Antwerp (Luchtbal) or in Mol. More information on the IFDM model can be found in the European Model Database (http://air-climate.eionet.europa.eu/databases/MDS/index_html).

In order to determine the unknown sources, which were supposed here to come from diffuse emissions, the following procedure is developed. The measurement dataset is split up in two, with half of it used for the determination of the sources and half for the validation of the results. The measurements contained in the former half are noted by $M_{i,t}$ with $i$ the location of the measurement and $t$ the time step. In order to determine the unknown sources, it is necessary to eliminate the effect of the known sources. Therefore, a corrected measurement series $M'_{i,t}$ is created as follows:

$$M'_{i,t} = M_{i,t} - B - \mu_{i,t}, \tag{26.1}$$

with B the known background of the pollutant and $\mu_{i,t}$ the modelled value of the concentration at the measurement location $i$ and at time step $t$, by taking into

account the known sources. However, it was shown that the $M'_{i,t}$ was close to $M_{i,t}$, showing that the known sources are less important than the unknown. Therefore, a list of possible sources $s_j$ is compiled. This is done as follows:

- At places where one would expect diffuse emissions, several sources $s_j$ are placed. These sources differ for instance in their treatment of the emission dependence on the wind speed (see below).
- To incorporate for unexpected sources, several grids of sources (for different wind dependences) are placed on the company terrain.

This leads to a list of possible sources $s_j$ which can contain up to 200 possible sources.

The wind dependence is treated by determining four parameters: the basic emission strength of the source $s_j$: $Q_j$, a minimum wind value $u_{min}$, a maximum wind value $u_{max}$ and a factor describing the form of the wind dependence $p$. The emission at a time t for this source is then determined by the following equations:

- If $u<u_{min} : Q_{j,t} = 0$
- If $u_{min}<u<u_{max} : Q_{j,t} = Q_j(u - u_{min})^p$
- If $u>u_{max} : Q_{j,t} = Q_j(u_{max} - u_{min})^p$.

For each of the possible sources $s_j$, their effect, assuming a unit value $U$ for the emission, is calculated on the measurement locations $i$ at every time step $t$. We call this values $\sigma_{i,j,t}$. Then, for every measurement location and time step (which can amount easily to values over 20.000) an equation is composed:

$$M'_{i,t} = \Sigma_j Q_j \sigma_{i,j,t} \tag{26.2}$$

This set of equations is then solved for $Q_j$ using the Gram-Schmidt algorithm [2]. In the results, all the sources with negative values of $Q_j$ are eliminated. The remaining set of equations is then solved again. This is reiterated until only positive emission values remain.

The Gram-Schmidt algorithm determines not only the value of $Q_j$, but also the standard deviation on this value. Following procedure is now reiterated:

- The set of equations for the remaining sources is solved using the Gram-Schmidt algorithm.
- The source for which the standard deviation divided by $Q_j$ is the largest is eliminated.

This procedure continues until all emission strengths are at least three times their standard deviation. The final set of sources is composed by the combining the known sources with the remaining unknowns, assigning them a source strength of $UQ_j$. In general, less than ten sources are needed to describe most of the variability of the measurement data.

Finally, the results calculated using these final sources are checked for having the same pollution roses, cumulative frequency distributions, ... as the measurements.

## 26.3 Results

When applying the procedure described above on data for three industrial sites in Belgium, the results showed that the found sources could not be due to fugitive emissions. On the one hand, with fugitive emissions, one would expect to get a threshold value $u_{min}$ different from 0, as for very low winds, no fugitive emissions are expected. On the other hand, one would expect the emissions to be found at locations with storage of heavy metals. However, here, we got emissions located for instance at parking spots.

Detailed analysis of the data then lead to the conclusion that it were not the fugitive emissions that played an important role, but building downwash. The plume of the known sources plummets to the ground behind some of the buildings. In our model, this leads to the placement of a source just behind the building. This source is wind dependent with a lower threshold $u_{min}$ of 0.

Using now the data that was kept out of the calculations for validation, we can show that the major measurement characteristics can easily be reproduced by the model. For instance, in Fig. 26.1, the validation plot for one pollutant (Nickel) near a copper-lead recycling plant in the Northern part of Belgium is shown. It is seen that the model captures very well the yearly mean concentration values. In Fig. 26.2, for one station, a time series plot is shown. In this plot, it can be seen that the model is correct not only for the yearly mean values, but also for the time dependency of

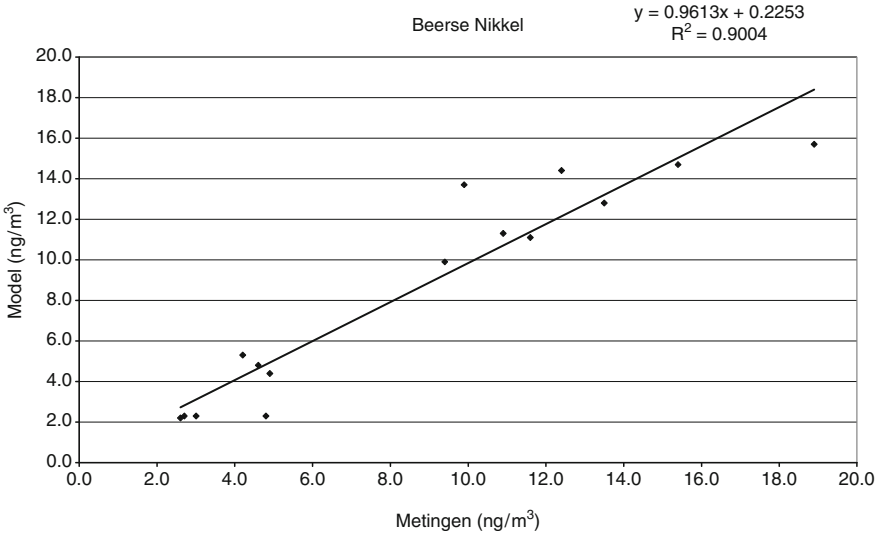


**Fig. 26.1** The validation plot for the Nickel concentration at the village of Beerse. On the *x-axis*: the yearly mean measurements of Nickel are shown (in ng/m$^3$). On the *Y-axis*: the yearly mean model values of Nickel are shown (in ng/m$^3$). Every *dot* represents a yearly mean value at one measurement location (4 years for 3 stations, 3 year for 1 station, both determination and validation data) in the vicinity of the company

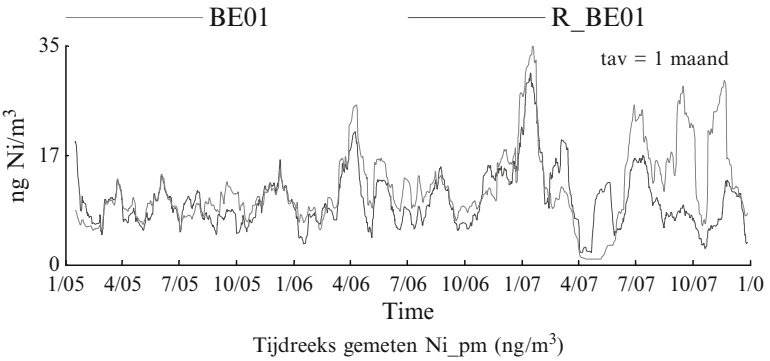


**Fig. 26.2** The running mean (over 1 month) measurement and model values at the location BE01, covering 3 years. In grey: the measured concentrations. In black: the modelled concentrations using the four remaining sources. On the x-axis: the time denoted in format month/year. On the y-axis: the concentration values in ng/m$^3$. The period on which the sources are determined extends from the 31st of May 2006 up to the 19th of October 2007. The rest of the period is used for validation

the measurements. This is not only true for the periods used in the inverse modelling but also for the periods which were deliberately left out for validation. Finally, it is then possible to assess the geographical distribution of the yearly mean model value. By connecting these results to a satellite image, the exposure of the population can be estimated.

## 26.4 Conclusions

In this study, it is shown that building downwash plays an important role in the measured occurrence of high pollutant concentrations near some heavy metals plants. Furthermore, it is shown that using virtual sources can lead to an accurate model re-creation of the measurement data. However, an improved building downwash algorithm for bi-gaussian plume models would be welcome in order to better study these cases.

## References

1. Bultynck H, Malet LM (1972) Evaluation of atmospheric dilution factors for effluents diffused from an elevated continuous point source. Tellus, XXIV.5, pp 465–471
2. Wampler RH (1979) Algorithm 544: L2A and L2B, weighted least squares solutions by modified Gram–Schmidt with iterative refinement [F4]. ACM Trans Math Softw 5(4):494–499

# Part II
# Regional and Intercontinental Modelling

# Chapter 27
# Air Quality Modelling and Source Apportionment Studies for Aerosols in Switzerland

**Sebnem Aksoyoglu, J. Keller, C. Haeni, D. Oderbolz, A.S.H. Prevot, and U. Baltensperger**

**Abstract** We modelled the air quality in Switzerland for summer and winter periods in 2006 using the CAMx model with the focus on aerosols. The contributions of various source regions to aerosol concentrations at receptor sites were investigated using the Particulate Matter Source Apportionment Technology (PSAT) tool of CAMx. The source regions were defined as Switzerland, surrounding countries and other countries in Europe. Organic aerosols (OA) and particulate nitrate ($PNO_3$) are the main components of winter aerosols in the modeled domain. In summer, organic aerosols dominate the aerosol composition and they are mainly secondary. In general more than 50% of PM2.5 was predicted to come from Swiss sources except for a few sites at the border regions. Primary particles originate mostly from local sources in both seasons, except at Basel where significant contribution from France and Germany was predicted. In the south, Italy is the main contributor to aerosols. On the other hand, about half of the secondary aerosols originate from Germany and France for receptors in the north and from Italy for receptors in the south.

**Keywords** Source apportionment • CAMx • Aerosols • Summer • Winter

## 27.1 Method

We used the Comprehensive Air Quality Model with extensions (CAMx, version 4.5) to simulate the air quality in January and June 2006 [1]. The meteorological parameters were calculated using the meso-scale model MM5 version 3.7.4 [3].

S. Aksoyoglu (✉) • J. Keller • C. Haeni • D. Oderbolz •
A.S.H. Prevot • U. Baltensperger
Laboratory of Atmospheric Chemistry, Paul Scherrer Institut,
Villigen PSI 5232, Switzerland
e-mail: sebnem.aksoyoglu@psi.ch

D.G. Steyn and S. Trini Castelli (eds.), *Air Pollution Modeling and its Application XXI*,
NATO Science for Peace and Security Series C: Environmental Security 4,
DOI 10.1007/978-94-007-1359-8_27, 

There were three nested model domains with horizontal resolutions of 27 km × 7 km, 9 km × 9 km, and 3 km × 3 km. We used 31 and 14 layers in MM5 and CAMx, respectively. The initial and boundary conditions were prepared using data from the global model MOZART [2]. The simulations were performed for 1–31 January 2006 and 1–30 June 2006, to calculate concentrations of particles smaller than 2.5 μm using CAMx with PSAT. The source regions were defined as Switzerland, Germany, France, Italy, Austria and other European countries. Various receptor sites covering whole Switzerland were evaluated.

## 27.2 Results and Discussion

Both measurements and model predictions showed that organic aerosols and particulate nitrate are the main components of winter aerosols (Fig. 27.1). In summer, OA dominates the aerosol composition at all sites (Fig. 27.2). Model performance was reasonably good. The model results suggest that the secondary organic aerosols (SOA) mainly come from the oxidation of biogenic precursors such as monoterpenes and sesquiterpenes as well as from oligomerization of particles. The highest levels were predicted in the north both in winter and summer. The contribution from abroad

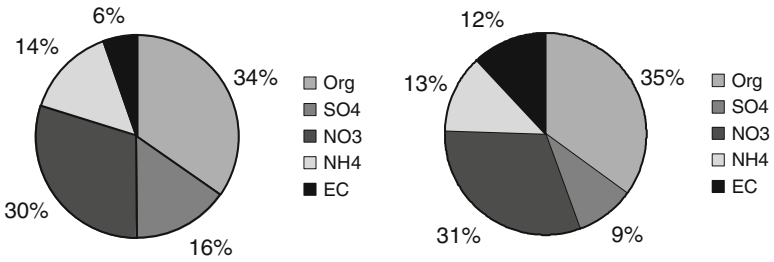


**Fig. 27.1** Relative contribution of aerosol species to the measured (*left*) and modeled (*right*) PM2.5 composition at Zurich in January 2006

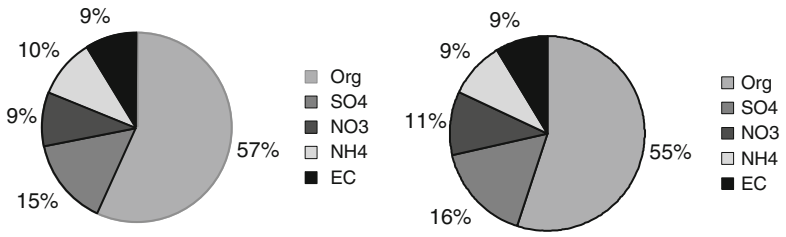


**Fig. 27.2** Relative contribution of aerosol species to the measured (*left*) and modeled (*right*) PM2.5 composition at Payerne in June 2006

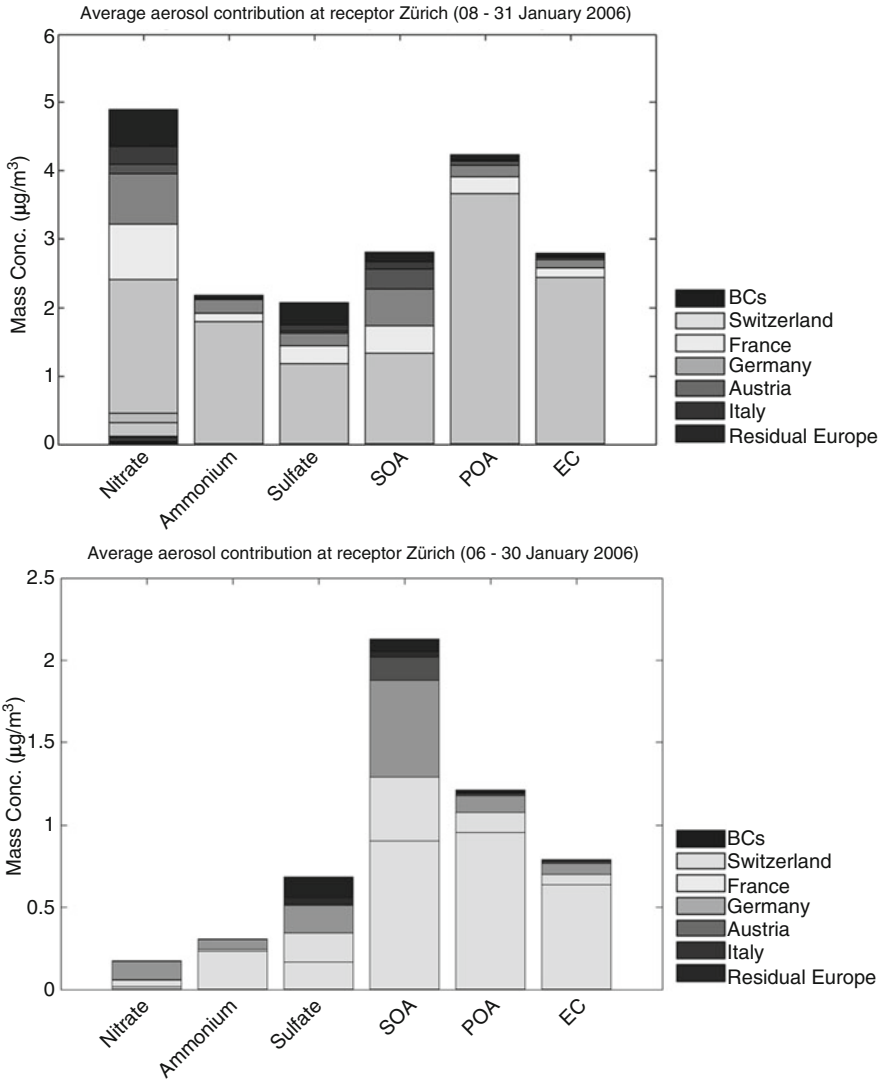


**Fig. 27.3** Average source attribution in January (*top*) and June (*bottom*) 2006 at Zurich (north)

varied as 31–69% and 33–76% in winter and summer, respectively. The sites close to borders had higher foreign contribution.

Contributions from source regions to aerosol species at Zurich (north) and Lugano (south) are shown in Figs. 27.3 and 27.4, respectively. In general primary particles originate mainly from domestic sources but about half of SOA and

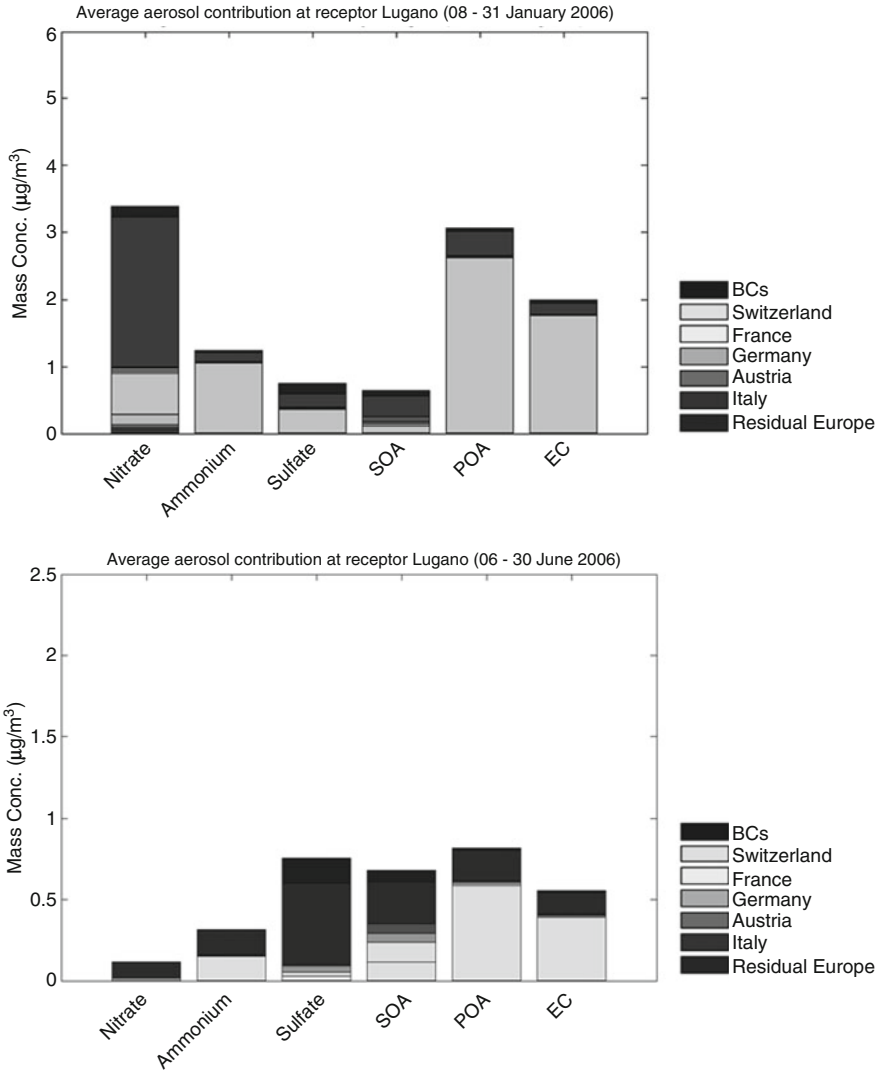


**Fig. 27.4** Average source attribution in January (*top*) and June (*bottom*) 2006 at Lugano (south)

particulate nitrate come from abroad; at Zurich mainly from France and Germany, at Lugano from Italy. Sulfate was predicted to originate mainly from abroad in summer. Other European countries contribute in smaller fractions. In order to estimate the contribution not only from other countries but also from various emission sectors, we will run PSAT with emission sources such as traffic, wood burning and biogenic emissions in a future study.

**Acknowledgments** This work was financially supported by the Federal Office of Environment.

## References

1. Environ (2006) User's guide, comprehensive air quality model with extensions (CAMx), version 4.4. Environ International Corporation, California
2. Horowitz LW, Walters S, Mauzerall DL, Emmons LK, Rasch PJ, Granier C, Tie X, Lamarque J-F, Schultz MG, Tyndall GS, Orlando JJ, Brasseur GP (2003) A global simulation of tropospheric ozone and related tracers: description and evaluation of MOZART, version 2. J Geophys Res 108:4784. doi:doi:4710.1029/2002JD002853
3. PSU/NCAR (2004): MM5 version 3. Tutorial Presentations

## Questions and Answers

**Questioner Name**: M. Biliaiev

**Q**: There are mountains between Switzerland and Italy which form the obstacle on the way of pollutants. How do you take into account this factor?

**A**: We are using a 3-dimensional air quality model. The model domain covers whole Europe and it uses a terrain following coordinates. Alps between Switzerland and Italy certainly cause differences in weather patterns, however, meteorological and chemical models take care of all physical transport processes as well as chemistry.

**Questioner Name**: M. Biliaiev

**Q**: To predict concentrations it is necessary to know the intensity of sources of ejection. How did you obtain the data about these sources of ejection in Germany, France, Italy?

**A**: Emissions are one of the basic inputs in air quality models. There are hourly gridded emission rates of gaseous as well as particulate pollutants from stationary and mobile sources in whole Europe in the emission inventories we are using. These emission rates are calculated based on data provided by various countries and institutes.

**Questioner Name**: Tony Dore

**Q**: Modelled boundary condition contributes to particulate concentration in Switzerland was significant only for nitrate aerosol. Can this be attributed to higher boundary concentrations of nitrate (than sulphate or ammonium) or to longe range transport?

**A**: It is most likely due to the boundary concentrations.

# Chapter 28
# High Ozone Levels in a Rural Mountainous Area: Where Does It Come from?

**Carlos Borrego, Alexandra Monteiro, Anabela Carvalho, Helena Martins, Oxana Tchepel, Ana Isabel Miranda, A. Strunk, H. Elbern, Santiago Saavedra, Angel Rodríguez, José A. Souto, and J. Casares**

**Abstract** During July 2005, a particularly high ozone episode (values above 350 μg $m^{-3}$) occurred at Lamas d'Olo, a rural station in northern Portugal. The main objective of the work is to identify the origin of this ozone-rich episode. Data analysis together with air quality numerical simulations were applied. The results indicate that long-range transport of ozone and its precursors instead of local chemical production is responsible for the high ozone concentrations. The sea-breeze circulation turns out to be the driving force for the transport of pollutants from the coastal urban and industrialized areas.

**Keywords** Ozone • Modelling • Synoptic flow • Sea-breeze • Long-range transport

## 28.1 Introduction

Some studies performed in the last decade showed high ozone levels in rural areas far from the anthropogenic emission sources. This is the case for Lamas de Olo (LOL), a rural air quality monitoring station located at the North of Portugal, at 1,086 m, where ozone ($O_3$) exceedences are numerous [1]. This specific episode will be in the focus of the present paper. The distribution of ozone in mountainous

C. Borrego (✉) • A. Monteiro • A. Carvalho • H. Martins • O. Tchepel • A.I. Miranda
CESAM & Department of Environment and Planning, University of Aveiro, Aveiro, Portugal
e-mail: cborrego@ua.pt

A. Strunk
The Royal Netherlands Meteorological Institute, KNMI, de Bilt, The Netherlands

H. Elbern
Rhenish Institute for Environmental Research, University of Cologne, Cologne, Germany

S. Saavedra • A. Rodríguez • J.A. Souto • J. Casares
Department of Chemical Engineering, University of Santiago de Compostela, Santiago de Compostela, Spain

D.G. Steyn and S. Trini Castelli (eds.), *Air Pollution Modeling and its Application XXI*, NATO Science for Peace and Security Series C: Environmental Security 4,
DOI 10.1007/978-94-007-1359-8_28, 

regions has been studied already in specific areas and results show on the whole positive relationships between site altitude and $O_3$ mixing ratios [2]. Regarding the main objective of this paper, both statistical and modeling approaches will be used to investigate the origin and formation of the referred ozone episode.

## 28.2 Description and Analysis of the Episode

Both air quality and meteorological variables were monitored at LOL (Fig. 28.1). There is a clear overlap of the peaks for the several gaseous pollutants – ozone ($O_3$), nitrogen dioxide ($NO_2$) and sulphur dioxide ($SO_2$), which can indicate a long-range transport of these pollutants. Besides that, the ozone peaks are registered after 17 UTC, suggesting that local chemical production is not the only origin of ozone. The $O_3$ peaks have other particularities: they develop within 1 h (an increase of 150 $\mu g.m^{-3}$) and their duration is only about 4 h. The analysis of the temperature and wind and its relationship with $O_3$ levels is presented in Fig. 28.2. The highest values of temperature were registered during the 3 days ($11^{th}$–$13^{th}$ July). Nevertheless, there is a time lag (1–2 h) between the temperature and the $O_3$ peaks. This highlights the hypothesis of transport of pollutants. Regarding the wind, there is an identical and repetitive pattern in the 3 days, characterized by the eastern synoptical forcing with a change to the western direction during specific hours in the afternoon. This west wind pattern has its origin in the sea-breeze circulation that develops at the coast in the morning and reaches LOL in the afternoon. $O_3$ episodes occur within this west direction change followed by a wind velocity peak. The synoptical conditions during the episode are characterised by a large-scale high pressure area during anti-cyclone conditions (Azores High pressure centre, placing its centre over the British Isles), with stagnant air masses above a large part of Europe (URL1).

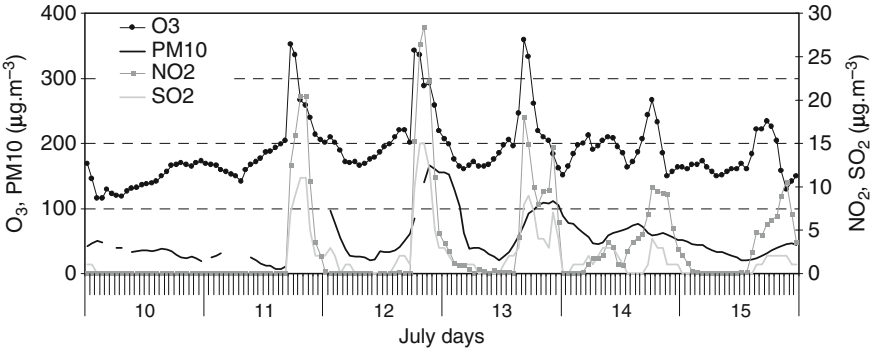


**Fig. 28.1** Monitored hourly concentrations of $O_3$, $NO_2$, $SO_2$ and $PM_{10}$ from $10^{th}$ to$15^{th}$ July 2005

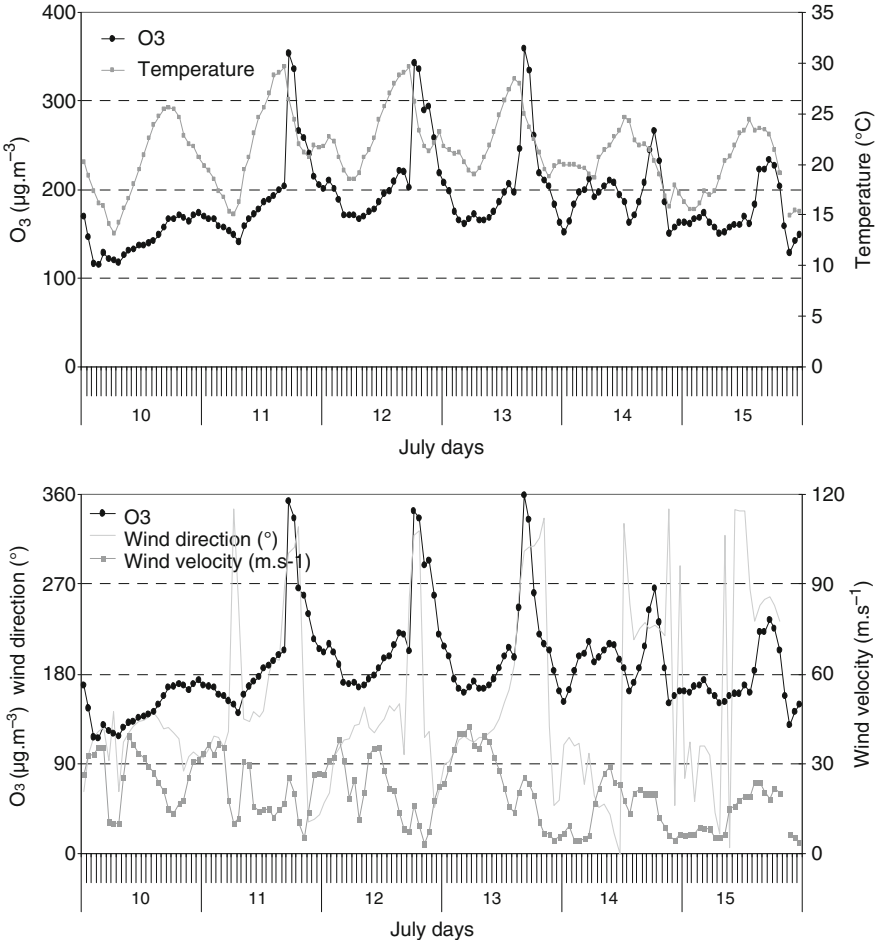


**Fig. 28.2** Meteorological parameters *vs* ozone concentration measured during the study episode

## 28.3 Air Quality Modelling Application

The air quality modelling system selected and applied in this study uses the chemistry-transport model EURAD-IM [3] driven by the mesoscale model MM5 using the Zangl extension [4]. The model domains were defined in order to fulfill both high grid resolution (over northern Portugal ($1 \times 1$ km$^2$)) and the integration of a larger area to simulate large-scale transport processes, using a nesting approach. There is a very good correspondence between modeled and observed values for both wind direction and wind speed (not shown). MM5-Zangl is able to reproduce the eastern synoptic forcing as well as the thermal western circulation shaped by the sea-breeze. Vertical phenomena involved were analysed and vertical profiles of potential temperature and *w*-wind component are plotted in Fig. 28.3,

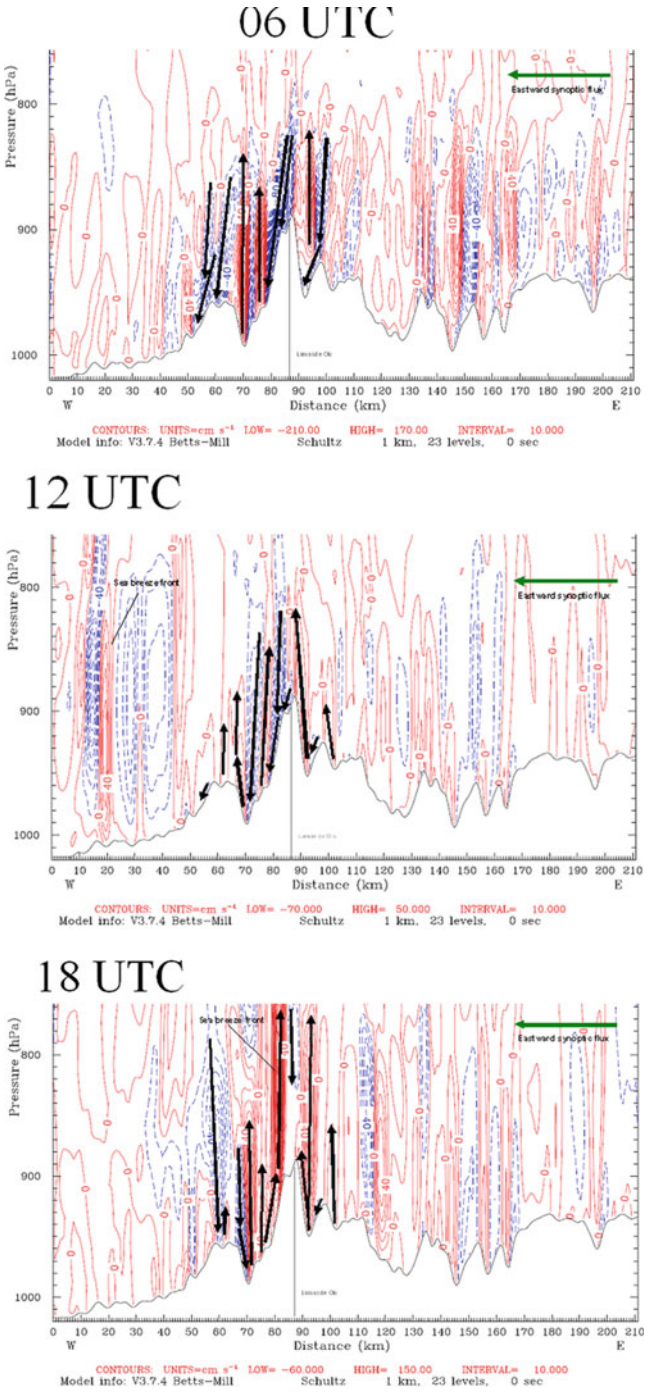


**Fig. 28.3** MM5 vertical profiles of potential temperature and w-wind component (the solid line represents ascending wind and the dashed line descending wind) cross-section at LOL – at 06, 12 and 18 UTC for the 12th of July. Synoptic wind flow is represented in the upper right corner

over LOL cross-section. The simulated vertical patterns reveal that the complex topography and the sea breeze development (from W) are the main features that influence the local circulation patterns. The subsidence flow caused by the synoptic conditions and land breeze help the downward transport of high-altitude $O_3$-rich air masses leading to the high $O_3$ concentrations. This recirculation process is responsible for the increase of the $O_3$ levels over this region.

A first evaluation of the chemical simulation results, both observations and model simulation show a strong increase of ozone levels during this week, including a fast decline at the end of this episode. The model shows only a small overestimation of the ozone values at the 16 existent stations during this period. In contrast to this promising simulation skill, the comparison at LOL exhibits a strong underestimation throughout the whole episode (not shown), besides the time of occurrence can be reproduced almost perfectly. To test the hypothesis of a possible underestimation of the $O_3$ precursor's emissions, different scenarios were evaluated: 2x NOx; 2x VOC, 2x NOx and VOC emissions. The peaks' magnitudes increase significantly (up to 25% on the latter scenario), but the strong underestimation of the $O_3$ background did not vanish. The limited sophistication of these tests cannot reflect the complex interaction of processes that are needed to produce the high observed $O_3$ levels. Notwithstanding, the model is able to capture and reproduce the daily pattern, namely the peaks occurrence. In accordance with the steep initiation of the observed peaks, the EURAD-IM results show a very sharp spatial gradient of $O_3$ concentrations, given in Fig. 28.4b for 19 UTC on 12th of July.

## 28.4 Discussion and Conclusions

Results pointed out that observed $O_3$ peaks at LOL in July 2005 were not produced locally but a result of transport phenomena. A very high correlation of ozone peaks with the arrival of westerly winds, suggested that sea breeze circulation was transporting $O_3$ and its precursors to LOL, where the polluted air masses arrive around 17 UTC. The air quality modelling was able to reproduce the occurrence of the observed $O_3$ peaks at LOL very well. Several tests with $O_3$ precursor emissions indicate that the discrepancies are not due to emission estimates only. The too low background level of $O_3$ in the model at LOL may be attributed to unresolved processes and insufficiently known input parameters, some of them related to the special location of LOL. Nevertheless, the origin of those air masses, which are responsible for the exceptional peaks, could be tracked.

**Acknowledgements** The authors wish to thank the financial support of the Comissão Coordenadora de Desenvolvimento Regional do Norte (CCDR-N). Thanks are extended to the Portuguese Science Foundation for the financial support through the Project ENSEMBLAIR (PTDC/AMB/69599/2006) and for the PhD grant of S. Saavedra (Project CTQ2006-15481/PPQ, R&D Spanish Programme) and A. Rodríguez ("María Barbeito" Programme, Xunta de Galicia).

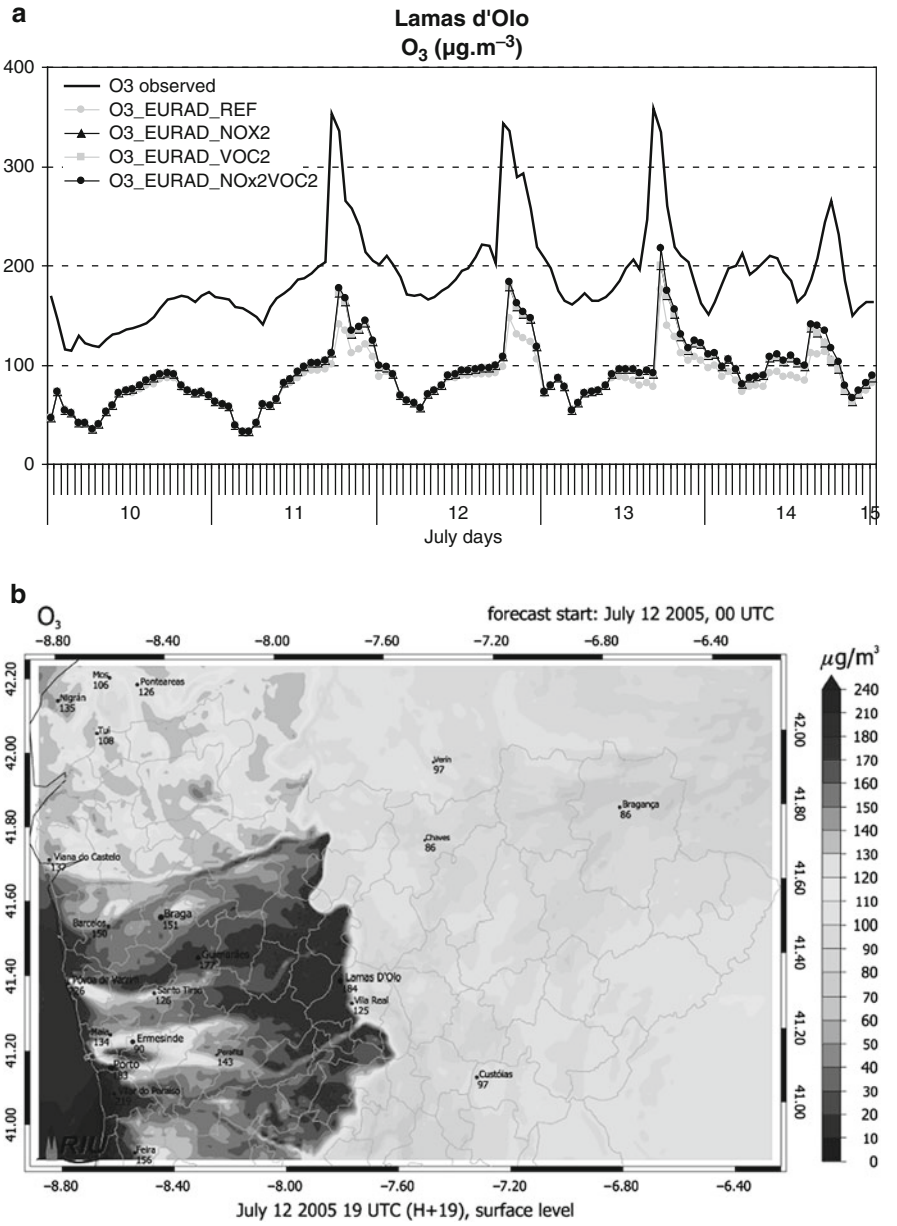


**Fig. 28.4** (**a**) Comparison of $O_3$ values modeled and observed at LOL for different scenarios: reference (REF); 2xNOx (NOX2); 2xVOC (VOC2) and 2x (NOx + VOC) emissions. (**b**) EURAD-IM surface $O_3$ concentrations at 19 UTC on 12th of July 2005

## References

1. Carvalho A, Monteiro A, Ribeiro I, Tchepel O, Miranda AI, Borrego C, Saavedra S, Souto JA, Casares JJ (2010) High ozone levels in the Northeast of Portugal: analysis and characterization. Atmos Environ 44:1020–1031
2. Chevalier A, Gheusi F, Delmas R, Ordonez C, Sarrat C, Zbinden R, Thouret V, Athier G, Cousin JM (2007) Influence of altitude on ozone levels and variability in the lower troposphere: a ground-based study for Western Europe over the period 2001–2004. Atmos Chem Phys 7:4311–4326
3. Elbern H, Strunk A, Schmidt H, Talagrand O (2007) Emission rate and chemical state estimation by 4-dimensional variational inversion. Atmos Chem Phys 7:3749–3769
4. Zangl G (2003) A generalized sigma coordinate system for the MM5. Mon Weather Rev 131:2875–2884, www.wetterzentrale.de

## Questions and Answers

**Questioner Name**: Bolioiev, Ukrania

**Q**: You compare the results of numerical simulation with observations. Where is the observation point situated on numerical model?

**A**: Observed data are compared with the modeled data, using the central point of each model grid cell.

**Questioner Name**: Steven Hanna

**Q**: Did you have any vertical profile observations of ozone near your site?

**A**: No, we don't. That's the reason why we could not validate our modeled vertical profiles and to confirm the hypothesis of underestimation of the vertical ozone layer.

**Questioner Name**: Clare Heaviside

**Q**: Were elevated ozone levels observed to the west of the main station before 17:00 UTC?

**A**: Yes, in fact, also at the rural stations located in the west coast, high levels of ozone were observed during the 3 days episode. Nevertheless, the magnitude of these concentration values (below 200 ug.m$^{-3}$) were much lower comparing to the registered at Lamas d'Olo station.

# Chapter 29
# Development and Evaluation of an Ammonia Bi-Directional Flux Model for Air Quality Models

**Jonathan E. Pleim, John Walker, Jesse Bash, and Ellen Cooter**

**Abstract** Ammonia is an important contributor to particulate matter in the atmosphere and can significantly impact terrestrial and aquatic ecosystems. Surface exchange between the atmosphere and biosphere is a key part of the ammonia cycle. Agriculture, in particular, is a large source of ammonia emitted to the atmosphere, mostly from animal operations and fertilized crops, while dry and wet deposition are the primary sinks of atmospheric ammonia. Although, current air quality models consider all of these source and sink processes, algorithms for emissions from fertilized crops and dry deposition are too simplistic to provide accurate accounting of the net surface fluxes. New modeling techniques are being developed that replace current ammonia emission from fertilized crops and ammonia dry deposition with a bi-directional surface flux model. Comparisons of the ammonia bi-direction flux algorithm to field experiments involving both lightly fertilized soybeans and heavily fertilized corn are presented and discussed. Initial tests and evaluation of CMAQ modeling results for a full year (2002) at 12 km grid resolution including implementation of a soil nitrification model and the ammonia bi-directional flux algorithm result in improved $NH_x$ wet deposition.

**Keywords** Ammonia • Bi-directional flux • Fertilizer

J.E. Pleim (✉) • J. Bash • E. Cooter
Atmospheric Modeling and Analysis Division, U.S. EPA,
Research Triangle Park, NC 27711, USA
e-mail: pleim.jon@epa.gov

J. Walker
National Risk Management Research Laboratory,
Air Pollution Prevention and Control Division, U.S. EPA,
Research Triangle Park, NC 27711, USA

D.G. Steyn and S. Trini Castelli (eds.), *Air Pollution Modeling and its Application XXI*,
NATO Science for Peace and Security Series C: Environmental Security 4,
DOI 10.1007/978-94-007-1359-8_29, 

## 29.1 Introduction

Ammonia is an important precursor to fine-scale particulate matter ($PM_{2.5}$) which is known to be a serious human health hazard [5] and is subject to regulation through the National Ambient Air Quality Standards (NAAQS). Increased PM due to ammonia emissions also significantly affects climate forcing by direct scattering of shortwave solar radiation and indirect alteration of cloud albedos and lifetimes through increased cloud condensation nuclei concentrations [6]. Atmospheric ammonia and ammonium aerosol also contribute a large fraction of reactive nitrogen deposition that is a source of nutrient enrichment and one of the sources of acidification that cause deleterious impacts on terrestrial and aquatic ecosystems such as eutrophication and forest health decline [3]. Currently, about 85% of the ammonia emissions in the US are from agricultural sources with about 35% of that coming from fertilizer application. Thus, a more accurate and responsive method for modeling ammonia emissions from fertilizer is needed to improve atmospheric modeling of ammonia and ammonium concentrations and deposition.

## 29.2 The Bi-Directional Flux Model

When exposed to liquid water ammonia gas will dissolve and dissociate in solution and establish equilibrium between ammonia gas, ammonium ion, and hydroxide ion. When combined with the equilibrium dissociation of water, the net equilibrium is between ammonia gas plus hydrogen ion and ammonium ion. Such equilibria can exist in leaves where $NH_{3(g)}$ in the stomatal cavity is in equilibrium with $NH_4^+$ and $H^+$ in the water contained in the apoplast tissue within the leaf and in the soil where $NH_{3(g)}$ in the soil pore air space is in equilibrium with $NH_4^+$ and $H^+$ dissolved in soil water. The concentration of $NH_{3(g)}$ in the stomatal cavities $(\chi_s)$ and the soil air space $(\chi_g)$ can be related to the aqueous concentrations of $NH_4^+$ and $H^+$ in the leaves and soil water as [4]:

$$\chi_{s,g} = \frac{A}{T_{s,g}} 10^{-B/T_{s,g}} \Gamma_{s,g} \tag{29.1}$$

where $\chi_{s,g}$ is the compensation point-based concentration of $NH_3$ in the air space inside the leaf stomata and soil pores (μg $m^{-3}$), A ($2.746 \times 10^{15}$) and B (4507) are constants derived from the equlibria constants, $T_{s,g}$ is the leaf and soil temperature (K), and $\Gamma_{s,g}$ is the dimensionless $NH_3$ emission potential from the leaf stomata and soil ($\Gamma = NH_4^+/H^+$). The direction of ammonia flux to or from the leaf apoplast and soil water depends on the compensation points compared to the air concentration in the canopy, $\chi_c$, such that ammonia will volatilize (emission) when, $\chi_{s,g} > \chi_c$ and deposit when $\chi_{s,g} < \chi_c$.

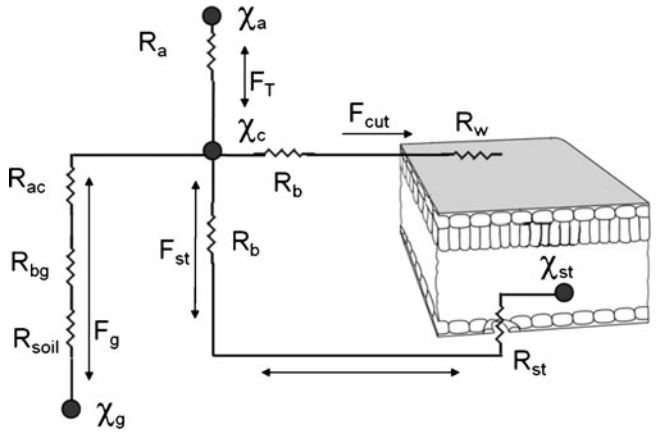


**Fig. 29.1** Schematic of bi-direction flux for soil and leaf

Like most dry deposition models the bi-directional flux model is based on an electrical resistance analog where flux is analogous to current and concentration difference is analogous to voltage as shown in Fig. 29.1. The total flux between the plant canopy and the overlying atmosphere ($F_T$) is sum of two bi-directional pathways, to the leaf stomata ($F_{st}$) and the soil ($F_g$), and one uni-directional deposition pathway to the leaf cuticle ($F_{cut}$).

## 29.3 Comparison to Field Studies

The bi-directional model has been evaluated and improved through comparisons to two field studies. Although both field experiments were performed in agricultural fields their conditions for ammonia fluxes were very different. The first experiment was in a soybean field in Warsaw, NC in the summer of 2002 [7] and the second was in a corn field in Lillington, NC during the spring and summer of 2007. In addition to obvious differences in canopy height and leaf structure between soybeans and corn, the most important difference was in the amount of fertilizer that was applied. Soybeans, being nitrogen fixing legumes, require very little fertilization while corn needs large amounts of fertilizer. Thus, for soybeans the ammonia fluxes were truly bi-directional with deposition generally occurring in the morning, peaking at about 830 LT, and evasion from late morning through the mid afternoon as shown in Fig. 29.2. The model was able to replicate this behavior with rather low values of $\Gamma$ ($\Gamma_s = 1{,}000$ and $\Gamma_g = 800$) and most of the flux followed the stomatal pathway.

In contrast to the soybean experiment, the ammonia fluxes in the corn field were entirely evasion because of the massive amount of fertilizer that was applied on June 6, just 2 weeks before the measurements shown in Fig. 29.3. Also note that the daily peak fluxes were around 1 $\mu g\, m^{-2}\, s^{-1}$, which is about one order-of-magnitude

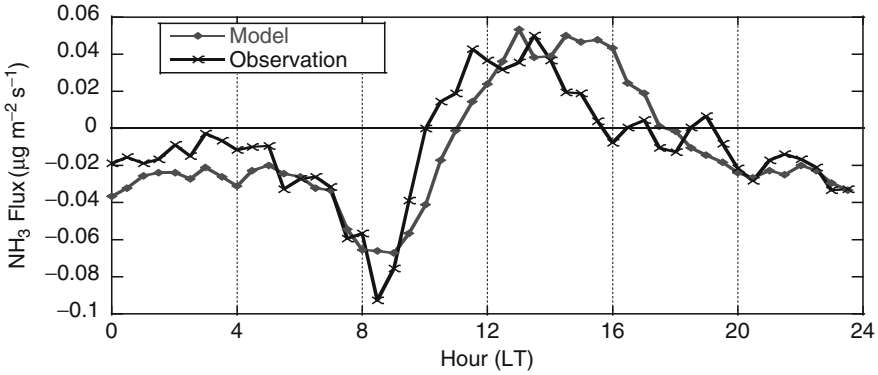


**Fig. 29.2** Ammonia flux over soybeans in Warsaw, NC averaged over 2 months in summer 2002

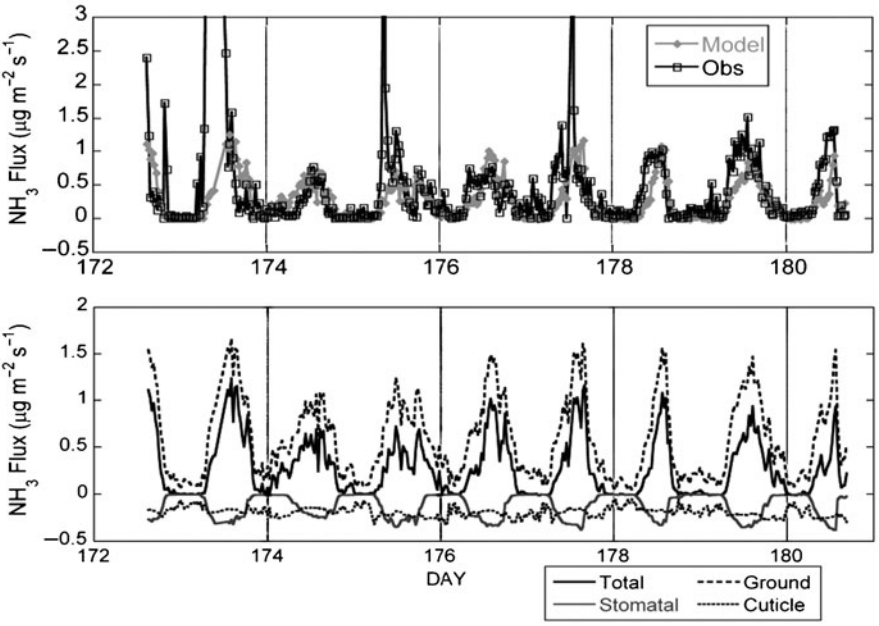


**Fig. 29.3** Ammonia fluxes over a corn field at Lillington, NC, June 21–30. Modeled and measured total fluxes (*top*) and modeled flux components (*bottom*)

greater than measured in the soybean field. As shown in the lower panel of Fig. 29.3, the large upward flux was from the soil because the soil $\Gamma$ ranged from about 100,000–200,000. The fluxes for the stomatal and cuticle pathways were always negative indicating that a portion of the ground flux was taken-up by the canopy. Model simulations about a month later suggest that about half of the ground flux was intercepted by the canopy, which agrees with an analysis of in-canopy ammonia measurements made by Bash et al., [1].

## 29.4 Conclusions

The two agricultural flux experiments demonstrate that a comprehensive bi-directional flux model must have realistic treatments of the ground, stomatal, and cuticle pathways. Different pathways are dominant in different conditions with complex interactions among them. Critical resistances for the soil and leaf cuticle needed to be developed to create a model capable of reasonable agreement with the measured fluxes for both experiments.

The bi-directional flux model has been applied in the Community Multiscale Air Quality (CMAQ) model along with a fertilizer application tool and a soil nitrification and acidification model to compute soil gamma values [2]. Preliminary annual model simulations show improved estimates of $NH_x$ wet deposition over the eastern US as a whole (reduction in mean error), with regions of significant reduction in bias and regions of moderate increase in bias.

## References

1. Bash JO, Walker JT, Katul GG, Jones MR, Nemitz E, Robarge W (2010) Estimation of in-canopy ammonia sources and sinks in a fertilized Zea Mays field. Environ Sci Technol 44:1683–1689
2. Cooter EJ, Bash JO, Walker JT, Jones MR, Robarge W (2010) Estimation of $NH_3$ bi-directional flux from managed agricultural soils. Atmos Environ 44:2107–2115
3. Dennis R, Haeuber R, Blett T, Cosby J, Driscoll C, Sickles J, Johnston J (2007) Sulfur and nitrogen deposition on ecosystems in the United States. Environ Manag 2007:12–17
4. Farquhar GD, Firth PM, Wetselaar R, Weir B (1980) On the gaseous exchange of ammonia between leaves and the environment: determination of the ammonia compensation point. Plant Physiol 66:710e714
5. Pope CA, Dockery DW (2006) Health effects of fine particulate air pollution: lines that connect. J Air Waste Manage Assoc 56:709–742
6. Ramanathan V, Crutzen PJ, Kiehl JT, Rosenfeld D (2001) Aerosols, climate, and the hydrological cycle. Science 294(5549):2119–2124
7. Walker JT, Robarge WP, Wu Y, Meyers TP (2006) Measurement of bi-directional ammonia fluxes over soybean using the modified Bowen-ratio technique. Agric For Meteorol 138:54–68

## Questions and Answers

**Questioner Name**: Bernard Fisher

**Q**: Could the large flux spikes of ammonia in the early morning be caused by ammonia dissolved in evaporating dew?

**A**: We wondered about that also, so we measured the aqueous concentrations of ammonia in dew on the leaves and there was not enough to cause the large flux spikes. However, perhaps ammonia from the soil water somehow mixes into the dew on the ground. If this happens then the soil resistance is essentially short-circuited resulting in big flux spikes when the dew evaporates.

**Questioner Name**: Jeff Weil

**Q**: What is the importance or sensitivity of the modeled flux to the term in the exponential term that is raised to the 5th power? Was that term a physically-derived quantity or was it empirical?

**A**: The equation for soil resistance is based on analogy to an empirical expression for soil moisture evaporation and includes an exponential of the 5th power of one minus relative soil moisture. This resistance is very sensitive to soil moisture especially when very dry. The ammonia flux is also quite sensitive to soil moisture but to a lesser degree because the value of gamma also increases as the soil dries.

# Chapter 30
# Extending the Applicability of the Community Multiscale Air Quality Model to Hemispheric Scales: Motivation, Challenges, and Progress

**Rohit Mathur, Robert Gilliam, O. Russell Bullock Jr., Shawn Roselle, Jonathan Pleim, David Wong, Francis Binkowski, and David Streets**

**Abstract** The adaptation of the Community Multiscale Air Quality (CMAQ) modeling system to simulate $O_3$, particulate matter, and related precursor distributions over the northern hemisphere is presented. Hemispheric simulations with CMAQ and the Weather Research and Forecasting (WRF) model are performed for the year 2006 using identical projections and grid configurations. The ability of the model to represent long-range transport of air pollutants is analyzed for selected cases through comparison with available surface, aloft and remotely sensed observations. These demonstrate the feasibility of extending the applicability of the CMAQ modeling system to hemispheric scales to provide a conceptual framework to examine interactions between atmospheric processes occurring at various spatial and temporal scales in a consistent manner.

## 30.1 Introduction

Atmospheric chemistry-transport models must address the increasing complexity arising from emerging applications that treat multi-pollutant interactions at urban to hemispheric spatial scales and hourly to annual temporal scales. To assist with the design of emission control strategies that yield compliance with more stringent air quality standards, models must possess the fidelity to accurately simulate ambient pollutant levels across the entire spectrum ranging from background to extreme

R. Mathur (✉) • R. Gilliam • O.R. Bullock Jr. • S. Roselle • J. Pleim • D. Wong
Atmospheric Modeling & Analysis Division, U.S. Environmental Protection Agency, MD-E243-03, 109 T.W. Alexander Drive, 27711 Research Triangle Park, NC, USA
e-mail: mathur.rohit@epa.gov; pleim.jon@epa.gov

F. Binkowski
University of North Carolina, Chapel Hill, NC, USA

D. Streets
Argonne National Laboratory, Argonne, IL, USA

D.G. Steyn and S. Trini Castelli (eds.), *Air Pollution Modeling and its Application XXI*, NATO Science for Peace and Security Series C: Environmental Security 4,
DOI 10.1007/978-94-007-1359-8_30, 

concentrations. Regional model calculations over annual cycles have pointed to the need for accurately representing impacts of long-range transport. Efforts linking regional and global scale models have met with mixed success as biases in the global model can propagate and influence regional calculations and often confound interpretation of model results. Since transport is efficient in the free-troposphere and since simulations over Continental scales and annual cycles provide sufficient opportunity for "atmospheric turn-over", i.e., exchange between the free-troposphere and the boundary-layer, a conceptual framework is needed wherein interactions between processes occurring at various spatial and temporal scales can be consistently examined. The expansion of detailed regional models to the hemispheric scale provides opportunities for consistently representing various atmospheric processes at the disparate scales.

## 30.2 Model Setup

The Community Multiscale Air Quality (CMAQ) modeling system [1] was applied over a domain encompassing the northern hemisphere. The horizontal domain, set on a polar stereographic projection was discretized using grid cells with a 108 km resolution, while the vertical extent ranging from the surface to 50 mb was discretized with 35 layers of variable thickness with a 20 m deep lowest layer. 3-D meteorological fields were derived from the Weather Research and Forecasting (WRF) modeling system operating on the exact same projection and grid configuration as CMAQ. Observations from NCAR's global upper air observation data set combined with the GFS 1-degree analysis provided the reanalysis fields every 6 h for grid nudging in the WRF simulations. CMAQ v4.7.1 was configured with CB05 chemical mechanism and the AER05 aerosol module. In addition, $O_3$ mixing ratios in the top most model layer (~50 mb) were modulated based on scaling to the spatially and temporally varying potential vorticity fields to represent possible effects associated with stratosphere-troposphere exchange [2]. Emissions of $NO_x$, $SO_2$, CO, volatile organic compounds, and particulate matter from anthropogenic and biomass burning sources were derived from the ARCTAS global emission inventory recently compiled by David Streets (http://www.cgrer.uiowa.edu/arctas/emission.html). Monthly varying biogenic emissions of isoprene and terpene were based on the Precursors of Ozone and their Effects on the Troposphere (POET) inventory.

## 30.3 Results and Discussion

Model simulations were conducted for the entire 2006 calendar year with a 20 day spin-up. During the spring and summer of 2006 extensive measurements on the vertical structure of $O_3$ distributions are available from the INTEX Ozonesonde

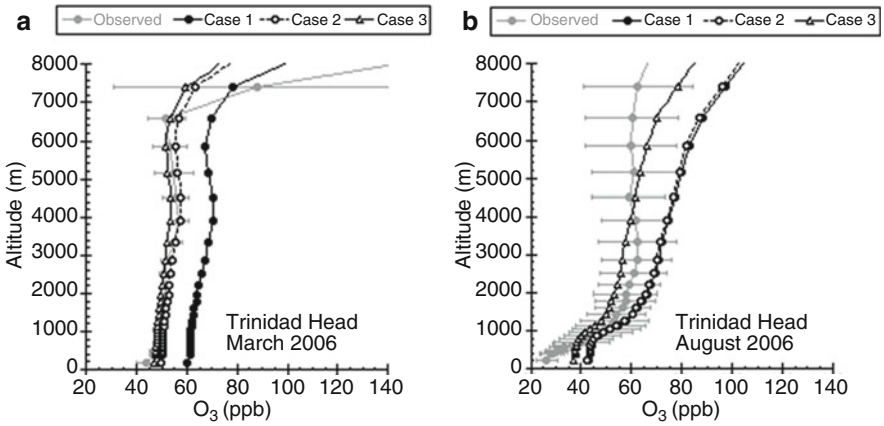


**Fig. 30.1** Comparisons of simulated average vertical profiles of $O_3$ with ozonesonde measurements at Trinidad Head, CA: (**a**) for March, 2006 and (**b**) for August, 2006. Also shown is the $\pm 1$ standard deviation of the observed mixing ratios

Network Study (IONS). Figure 30.1 presents a comparison of mean profiles of simulated $O_3$ mixing ratios for various cases with these measurements at Trinidad Head, CA, a site nominally representing inflow conditions to North America. Large overestimations in $O_3$ through the troposphere are noted for the base case simulation (Case 1). These were found to arise from the profile used to initialize $O_3$ in the mid-troposphere. Case 2 represents a simulation wherein the model was initialized to "clean" tropospheric background values and allowed to build up based on the model physics and chemistry. This resulted in much better agreement with the measured profile during Spring (Fig. 30.1a); however, by summer, overestimations still persisted. In the CB05 mechanism, the species NTR is used to represent organic nitrates and serves as a reservoir for oxides of nitrogen ($NO_x$; through photolysis and reaction with OH). On the hemispheric scale, organic nitrates formed from isoprene are the largest contributor to the simulated tropospheric NTR burden and can consequently modulate the simulated tropospheric $O_3$ burden. An additional simulation (Case 3) was performed wherein the physical sinks of NTR were enhanced by mimicking its dry deposition and wet scavenging to $HNO_3$. The comparisons shown in Fig. 30.1 illustrate the relatively large effects of the modulation of the resultant NTR burden on the simulated $O_3$ burden through much of the lower to mid-troposhere. In limited area calculations with the CB05 mechanism it is likely that the NTR produced is advected out of the regional domains before it can significantly alter $O_3$ production. However, over the space and time-scales of northern hemispheric calculations, $NO_x$ recycled from NTR can modulate the simulated background $O_3$; consequently accurate characterization of its sources and sinks becomes critical. The hemispheric calculations, thus provides a framework for examining the role of various physical and chemical processes on atmospheric chemical budgets in a consistent manner.

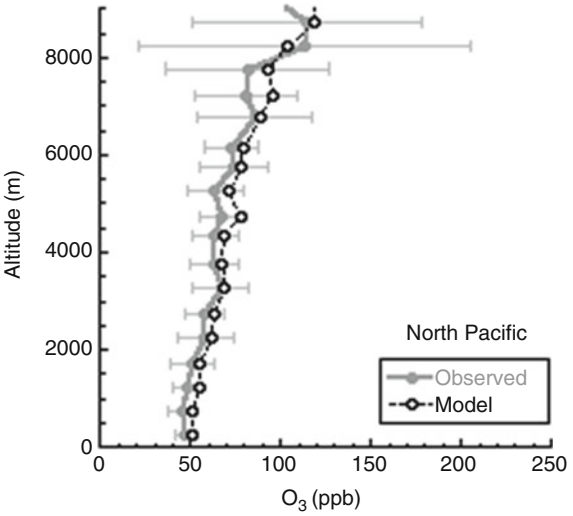


**Fig. 30.2** Comparisons of simulated average vertical profiles of $O_3$ with measurements from the NASA DC-8 aircraft over the North Pacific. Averages based on comparison of model and measured values for all flights during May 1–15, 2006

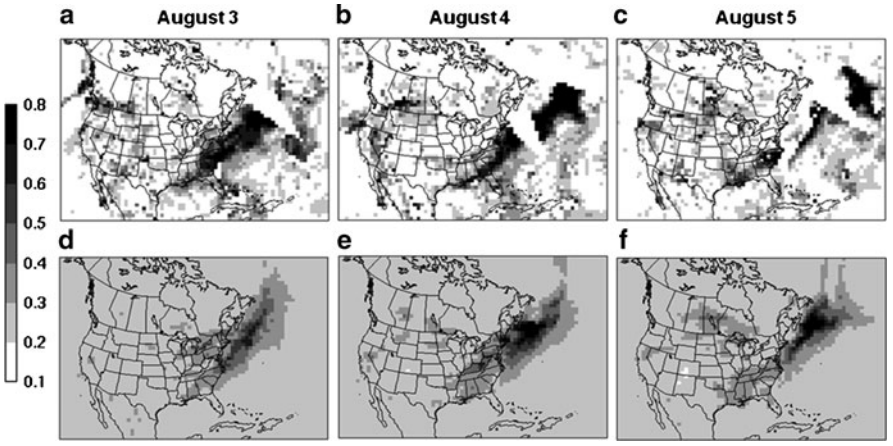


**Fig. 30.3** Characterizing the export of air pollution from North America during August 3–5, 2006: comparison of simulated aerosol optical depth (**d**–**f**) with MODIS retrievals (**a**–**c**)

Figure 30.2 presents similar comparisons of simulated composite vertical profiles of $O_3$ (from Case 3) with measurements from the DC-8 aircraft during the INTEX-B field campaign [3] and indicate that the model exhibits good skill in replicating the 3-D tropospheric $O_3$ structure over the Pacific.

The ability of the model to simulate the transport and distributions of fine particulate matter is illustrated in Fig. 30.3 which presents comparisons of the simulated aerosol optical depth with those from the MODIS retrievals and further indicates that the model is able to capture the long-range transport and export of air pollution from North America to the remote Atlantic.

**Disclaimer** Although this paper has been reviewed by EPA and approved for publication, it does not necessarily reflect EPA's policies or views.

## References

1. Byun DW, Schere KL (2006) Review of the governing equations, computational algorithms, and other components of the Models-3 Community multiscale air quality (CMAQ) modeling system. Appl Mech Rev 59:51–77
2. Mathur R, Lin H-M, McKeen S, Kang D, Wong D (2008) Three-dimensional model studies of exchange processes in the troposphere: use of potential vorticity to specify aloft $O_3$ in regional models. 2008 CMAS conference. Available at: http://www.cmascenter.org/conference/2008/slides/mathur_three-dimension_model_cmas08.ppt
3. Singh HB, Brune WH, Crawford JH, Flocke F, Jacob DJ (2009) Chemistry and transport of pollution over the Gulf of Mexico and the Pacific: spring 2006 INTEX-B campaign overview and first results. Atmos Chem Phys 9:2301–2318

## Questions and Answers

**Questioner Name**: A. Venkatram

**Q**: Conservation of mixing ratio in regional models has been a long standing problem, which is important for results on transport of tracers. How have you addressed this problem?

**A**: CMAQ is formulated with a 3-D mass consistent tracer advection algorithm. Through rediagnosis of the vertical wind velocity, the scheme ensures that the Continuity equation is strictly satisfied, thereby ensuring tracer mass conservation as well as conservation of a well mixed tracer.

**Questioner Name**: A. Venkatram

**Q**: How do you compare aircraft measurements with model results which have an implied averaging time?

**A**: The raw aircraft measurements are typically at different time resolutions for different species and also at temporal scales finer than the model output time step. In the comparisons presented here, we "flew" the aircraft through the model domain and sampled the simulated 3-D field based on time and location of the aircraft. All observed values for each hour within a model grid cell were averaged to ensure that the model and measured values were averaged over similar space and time scales; these are the values were then used to construct the vertical profile comparisons plots.

# Chapter 31
# The Urban Impact on the Regional Climate of Dresden

**Beate Sändig and Eberhard Renner**

**Abstract** The building effect parameterization (BEP) module [3] was implemented in a high resolution version of the COSMO model (DWD) in order to take into account the urban impact on the airflow and the radiation budget. Based on urban structure data of Dresden, relevant input parameters of the BEP module were developed. By means of this model setup it is possible to investigate the interactions between the city structure and the meteorological variables with different types of artificial cities, ranging from densely built-up areas to suburban areas in order to illuminate the impact of the city type on the dynamical and thermal properties of the atmosphere.

## 31.1 Introduction

This project is aimed to simulate aerosol distributions for Dresden with an urbanized version of the COSMO model coupled online with the CTM MUSCAT (Multiscale Chemical Aerosol Transport). It is important to use the urbanized COSMO version for high resolution chemical simulations because thermal and dynamical conditions are strongly influenced by the city. The model setup and the input parameter are presented in Sect. 31.2. The results from a case study with the urbanized COSMO model for Dresden are presented in Sect. 31.3. The urbanized COSMO model with resolutions up to 180 m is used to calculate an autumn episode of 10 days for the valley of the river Elbe and the city of Dresden driven by reanalysis data (DWD) with a resolution of 28 km. As downscaling technique a one way nesting with a five step (7 km, 2.8 km, 1 km, 420 m, 180 m) nesting chain is used.

B. Sändig (✉) • E. Renner
Department of Modelling, Leibniz Institute for Tropospheric Research,
Permoserstraße 15, 04318 Leipzig, Germany
e-mail: saendig@tropos.de; renner@tropos.de

D.G. Steyn and S. Trini Castelli (eds.), *Air Pollution Modeling and its Application XXI*,
NATO Science for Peace and Security Series C: Environmental Security 4,
DOI 10.1007/978-94-007-1359-8_31, 

## 31.2 The Urban Module BEP

The urban module BEP parameterizes the urban structure with a simplified type of morphology. In this simpler framework urban grid cell characteristics like typical street directions, typical street and buildings width and height dependent probability distribution of finding a house at a special urban grid level are used to define building blocks, which are as long as the grid cell. These blocks have a height dependent width, resulting from the typical buildings width scaled with height dependent probability function. The distance between the house blocks is the typical street width and they lying perpendicular to the typical street directions. They are able to reproduce real sky-view factors better than a simple 3D approach [2]. The classical MOST surface-layer formulae [1] are used to compute additional turbulent momentum and latent heat fluxes due to horizontal surfaces of these building blocks. The exchange of momentum on the vertical house block surfaces is parameterized with a drag approach [4]. These additional turbulent flux terms are calculated on each "urban" grid level and are scaled with the urban area fraction. The surface temperature of urban areas is calculated with a heat diffusion equation, which is solved in several layers at the interior of the building and street material. The implementation of the urban module in the COSMO model was done by O. Fuhrer. In the framework of the project this BEP code has been adapted for the use with higher grid resolutions.

## 31.3 Input Parameters for the Urban Module BEP

The basic vector dataset consisting of perimeters of all buildings and their respective heights of the City of Dresden was provided by the IOER (Leibniz Institute of Ecological and Regional Development) in Dresden. The calculations of the typical street- and house width and the typical street direction as well as the height distribution of buildings for every grid cell are done with the open source GRASS GIS on a grid with a resolution of about 180 m. Input parameters for grid resolutions of 420 m and 1,100 m are calculated by the means of taking the most frequently value of the first three input parameter. The height dependent probability distribution is directly calculated for each resolution.

## 31.4 Results

A 10 day simulation (11.10.2006–20.10.2006) with a complex city morphology input dataset for Dresden was done with a resolution of 420 m. A setup of 16 artificial city structures are constructed to answer the question, how important is the complexity of the urban morphology. The 16 setups vary four parameter, the width

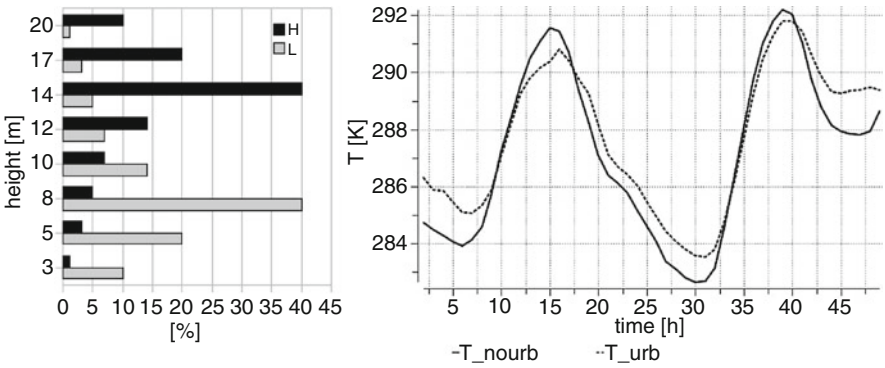


**Fig. 31.1** Two artificial building height distributions (*left*) and Temperature time series for model with urban module(*urb*) and model without urban module (*nourb*) (*right*)

of the buildings (5 m; 10 m), the width of the street(25 m; 50 m), the characteristic street direction (45°/135°; 0°/90°) and the artificial height distributions labeled with H and L for high and low buildings, which are shown in detail in Fig. 31.1 (left). Figure 31.1 (right) shows temperature time series for the urbanized and non-urbanized model with a resolution of 1,100 m over the City of Dresden at the lowest model level (15 m). The impact of the City is clearly visible at midnight, with temperature differences up to 2 K. The heat island effect is visible at night. The Bohemian wind coming from south-east increases in the second night and induces stronger ventilation and lesser temperature differences relative to the first and third night.

The temperature of the lowest model layer (15 m) differ in simulations with an artificial city maximal by +/− 1.5 K in comparison to city simulations with an complex urban morphology input dataset. Mean differences are about +/− 0.5 K.

Within a 10 day simulation period, there are strong wind events which result in strong temperature differences, which could be seen in the morning and some weaker differences are visible in the evening and at night. The strongest positive temperature deviations from the complex run are observable in the run 0-5-50-L and 0-10-50-L, that means the lowest model layer of a city with wide streets with north-south and east-west orientations and low houses is cooler as in a complex city. In contrast to this result warmer temperatures are observable in a city with high buildings in small streets, which are rotated around 45° and 135° (45-5-25-H,45-10-25-H). The smallest deviations from a complex town simulation are detectable in the simple setups with wide streets and high buildings or with small streets and low houses. It is a hint, that the aspect ratio (building height to street width) is important for the magnitude of the additional turbulent production. In weak wind situations the minor temperature difference pattern are comparable in the morning, in the evening and at night. Almost all setups show a diurnal cycle in the temperature deviation with a minimum at noon during the whole 10 day simulation period. Its remarkable that the only exception of that rule makes a city with small streets and small low houses, which has its maximum temperature differences at noon and is

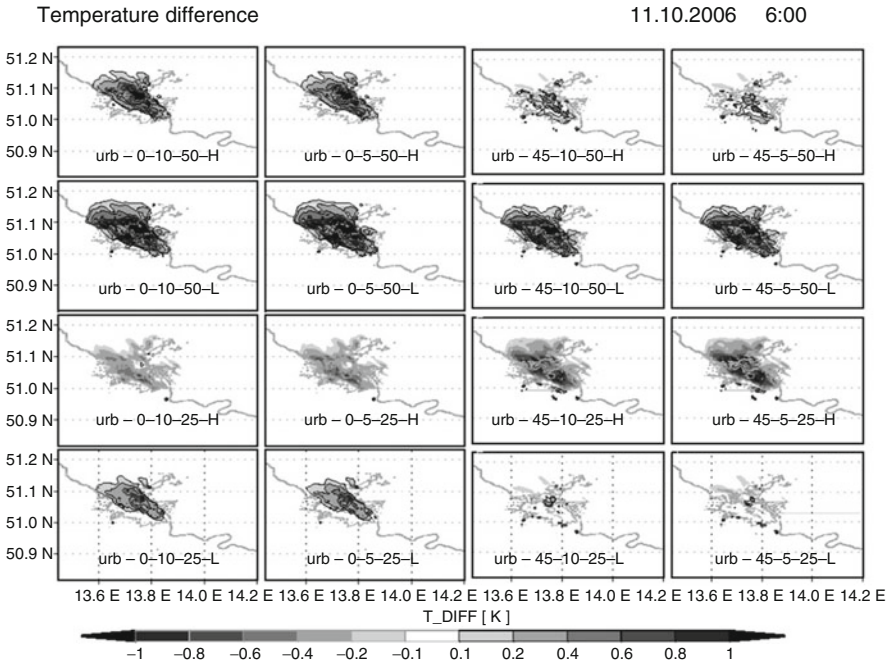


**Fig. 31.2** Temperature differences between a city with complex structure (*urb*) and very simple characteristics (16 different runs)

cooler as a complex city at this time. It is deducible from Fig. 31.2, that a simple city geometry with wide streets and high buildings comes as close as possible to the complex city structure with respect to the temperature development of the lowest model layer. These results show that model simulations at high resolution are sensible to the characteristic city morphology.

**Acknowledgments** This study was supported by the Bundesministerium für Bildung und Forschung (BMBF) within the REGKLAM project (FKZ 01LR0802).

## References

1. Louis JF (1979) A parametric model of vertical eddies fluxes in the atmosphere. Bound-Lay Meteorol 17:187–202
2. Martilli A (2009) On the derivation of input parameters for urban canopy models from urban morphological datasets. Bound-Lay Meteorol 130:301–306
3. Martilli A, Clappier A et al (2002) An urban surface exchange parameterisation for mesoscale models. Bound-Lay Meteorol 104(2):261–304
4. Raupach MR, Antonia RA, Rajagoplan S (1991) Rough-Wall turbulent boundary layers. Appl Mech Rev 44:1–25

## Questions and Answers

**Questioner Name**: Sunshee Lee

**Q**: Among 4 urban factors, street width, building height, building width and street direction, do you find any dominant in your simulation of temperature difference?

**A**: The most important impact could be seen if street width and building heights are changed. The street direction could have an impact and the building width plays a minor role.

**Questioner Name**: Stijn Janssen

**Q**: Why you selected one particular date and hour of the szenario analysis and what would be the impact of other hours of the day (e.g. late afternoon)?

**A**: The date is chosen arbitrarily. Detailed studies are planned in future. The shown hour is the one with the striking differences.

# Chapter 32
# Incremental Development of Air Quality Forecasting System with Off-Line/On-Line Capability: Coupling CMAQ to NCEP National Mesoscale Model

**Pius Lee, Fantine Ngan, Hyuncheol Kim, Daniel Tong, Youhua Tang, Tianfeng Chai, Rick Saylor, Ariel Stein, Daewon Byun, Marina Tsidulko, Jeff McQueen, and Ivanka Stajner**

**Abstract** The National Air Quality Forecast Capability (NAQFC) is based on the EPA Community Multiscale Air Quality (CMAQ) model driven by meteorological data from the NOAA North American Mesoscale (NAM) Non-hydrostatic Mesoscale Model (NMM). Currently, NMM meteorological data on Arakawa E-grid are interpolated on a CMAQ's Arakawa C-grid using the processors PRODGEN and PREMAQ to handle map-projection transform, vertical layer collapsing, and other emission and meteorological data feed issues. The FY11 pre-implementation version of NAM has undergone significant changes in the vertical layering, horizontal grid projection and improved science components for its FY11 upcoming major upgrade release. This provides an opportunity to improve the coupling methodology between NMM and CMAQ that reduces uncertainties both in the meteorological and emission inputs for the off-line air quality modeling and helps

P. Lee (✉) • R. Saylor • D. Byun
Department Air Resources Laboratory, Office of Oceanic and Atmospheric Research, National Oceanic and Atmospheric Administration USA, 1315 East-West Highway, SSMC3-Room 3316, Silver Spring 20910, MD, USA
e-mail: pius.lee@noaa.gov

F. Ngan
University Corporation for Atmospheric research, Boulder, CO, USA

H. Kim • D. Tong • T. Chai • A. Stein
Earth Resources Technology, Annapolis Junction, MD, USA

Y. Tang • M. Tsidulko
IMSG Corp., Silver Spring, MD 20190, USA

J. McQueen
Environmental Modeling Center, National Centers for Environmental Prediction, Camp Springs, MD, USA

I. Stajner
Noblis Inc., Fairfax, VA, USA
e-mail: ivanka.stajner@noblis.org

D.G. Steyn and S. Trini Castelli (eds.), *Air Pollution Modeling and its Application XXI*, NATO Science for Peace and Security Series C: Environmental Security 4,
DOI 10.1007/978-94-007-1359-8_32, 

development of on-line NMM-CMAQ version. Three major tasks are needed to achieve a tighter coupling between them: (1) Adapt to NAM's vertical hybrid pressure and grid structure; (2) Change CMAQ to use the same rotated latitude longitude B staggered horizontal grid structure as NAM, (3) Modify emission model to provide generic inputs for the B staggered grid and hybrid vertical structure of NAM. The first task achieves consistent matching of dynamics between the two systems, despite the possible necessity of layer-collapsing to fit within operational time-lines. The second task removes unnecessary interpolation of meteorology data for air quality simulations. The third task involves modification of the U.S. EPA Sparse Matrix Object Kernel Emission (SMOKE) model to handle the staggered B grid. At this time only the first of these three steps has been accomplished, and the test result from this test focusing on the selected test period has been compared to that produced by the operational NAQFC. Further work with all these three modifications concurrently in place is underway.

**Keywords** Fine horizontal resolution • Rotated Lat-Long projection • Hybrid vertical grid

## 32.1 Introduction

Air Quality modelers place emphasis on the accuracy of meteorological drivers of air quality forecast models. The current National Air Quality Forecasting Capability (NAQFC) in the U.S. is based on coupling the National Centers for Environmental Prediction (NCEP) North American Mesoscale Model (NAM) [4] with the Community Multi-scale Air Quality (CMAQ) model [1] in an off-line manner. Both components are currently running at 12 km horizontal grid spacing. As the Eta model, NAM's predecessor, the horizontal coupling required interpolation from Rotated Latitude-Longitude (rll) map projection with Arakawa E staggered grid to CMAQ's Lambert Conformal Conics (lcc) projection with Arakawa C staggered grid [5]. Inherent to the bilinear or nearest neighbor schemes of the horizontal interpolations involved, accuracy of the meteorological fields are compromised.

With NCEP retiring the E grid system in its next major NAM implementation, corresponding NAQFC upgrade aims to rid of these interpolations in coupling NAM and CMAQ. As NAM will be configured to run rll with Arakawa B staggered grid, so will CMAQ. This future system associated with the FY11 NAM implementation will hereafter be referenced in this study as NAM-β coupled with rll-CMAQ. This entails the following changes in CMAQ: (a) All inputs to CMAQ including emission files are required to be prepared in rll projection; and (b) All processes assuming uniform grid-cell areas under CMAQ's customary lcc projection need modification to account for the varying grid-cell areas of rll map projection. NAQFC is configured with 22 vertical layers, and has adopted a "tight" vertical coupling approach [2] since September 2007. In contrary to interpolating NAM's vertical structure to a 22 layers sigma-p vertical grid for CMAQ prior to

September 2007, the "tight" coupling approach enable CMAQ to retain NAM's hybrid upper-pure-pressure and lower-pure-sigma-p structure as is, but selectively choose the 22 layers. This process also needs some modification as the hybrid vertical co-ordinate of NAM-β will be a mixed hybrid with no pure pressure part or pure terrain following sigma-p part.

Finally to address the fine horizontal resolution fidelity of emission processing, emission inventories and emission factor surrogate files must be generated utilizing fine resolution Geographical Information System (GSI) and shapes files. Results from other smaller limited domain air quality modeling studies showed the finer grids could enable higher fidelity in capturing transient and local features (e.g. [3]).

## 32.2 Map Projection

The current NAQFC in 12 km horizontal resolution depends on a string of horizontal map projection transformations to link its meteorological and chemical components. The fourteen 3-D and thirty two 2-D meteorological fields fed from NAM to CMAQ undergo a two-steps horizontal map projection interpolation from rll Arakawa E staggered grid: (1) to lcc A grid, and then (2) to lcc projection with Arakawa C staggered grid (Fig. 32.1). This study represents the first task of a series of tasks aiming to modify CMAQ so that its scalar and wind vector quantities are casted in rll map projection and Arakawa B staggered grid. In essence, this will achieve identical horizontal grid structure between NAM-β and rll-CMAQ in the next NCEP major implementation of NAQFC. As such, preservation of the dynamics of air flows is assured by ridding the numerical diffusion inherent to numerical interpolation operations that dumps out fine features of meteorological fields. This is important for finer horizontal resolution modeling.

In order to make CMAQ to handle rll map projection, there are three groups of modules must be modified: (a) Advection routines, (b) Emission flux strength

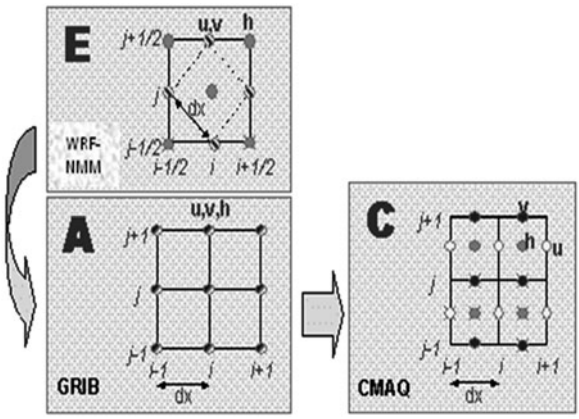


**Fig. 32.1** Two steps grid transformation of the current operational NAQFC that couples NAM and CMAQ: (*1*) rotated latitude-longitude map projection and Arakawa E grid staggering to Lambert Conformal Conics (*lcc*) projection with A grid staggering, and (*2*) lcc A grid staggering to CMAQ's C grid staggering

routines, and (c) horizontal deformation and diffusivity routines. They all dealt with varying grid-cell area of rll projection.

## 32.3 Hybrid Vertical Co-ordinate

The delineation of the pure-pressure-upper part and pure-lower-σ-$p$ part in the current NAM will be change to a mixed hybrid vertical co-ordinate system. As discussed by Byun et al. [2] the so-call continuous methodology utilizes $\sigma_\pi$, an equivalent sigma, as shown in Fig. 32.2 and Eq. 32.1, is used throughout the vertical and the methodology is independent of whether the hybrid layers are delineated as pure parts or not.

$$J_{\hat{x}^3} = \left|\frac{\partial z}{\partial \hat{x}^3}\right| = \left|\frac{\partial z}{\partial p}\frac{\partial p}{\partial \hat{x}^3}\right| = \frac{1}{\rho g}(PD + P_{TOP}) \quad \text{for all layers} \tag{32.1}$$

where $\hat{x}^3 \equiv 1 - \sigma_\pi$, And $\hat{x}^3$ denotes the general vertical coordinate, $J_{\hat{x}^3}$ is the Jacobian for vertical coordinate transformation, $z$is height AGL, $p$ is pressure, $\rho$ denotes air density, $g$is gravitational acceleration, $PD$ indicates difference between the pressure at the surface and at the top of the model atmosphere, and

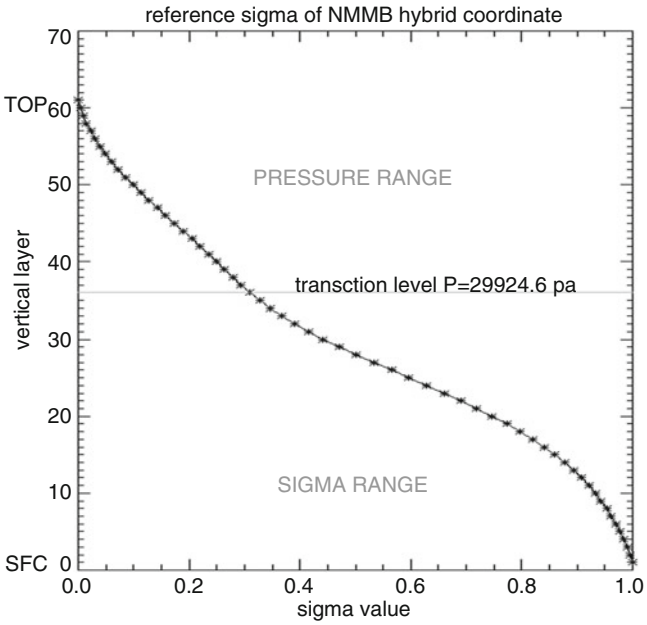


**Fig. 32.2** Application of the continuous method presented in Byun et al. [2] to derive a reference sigma as discussed in Sect. 32.3 at the initial time for the standard atmospheric column

$P_{TOP}$ is the model top pressure, where the vertical coordinate is expressible as its sole function; namely, $\sigma_\pi \equiv (P - P_{TOP})/PD$. Figure 32.2 shows a sample $\sigma_\pi$ with prescribed $PD = 29924.6$ Pa. Equation 32.1 has been implemented to the lcc-CMAQ.

## 32.4 High Surface Ozone Episode in Ca Late June, 2010

With the preparation work described in Sects. 32.2 and 32.3 in place, lcc-CMAQ is ready to be tested. However, the speed limiting step of the preparation is often the generation of emission surrogate files that requires the processing of hundreds of emission surrogates with GSI based tools such as US EPA's Spatial Allocator. For the interest of time of this study, a selected region in Western U.S. was chosen. Meteorology is obtained by running NAM-β for a region considerable larger than CONUS in 12 km resolution and nested in the selected region in 4 km resulted as indicated in Fig. 32.3. An elevated surface Ozone concentration episode between June 22 and 24 was selected. Figure 32.4 shows a sample upper air pressure and air flow over the 4 km resolution nested domain.

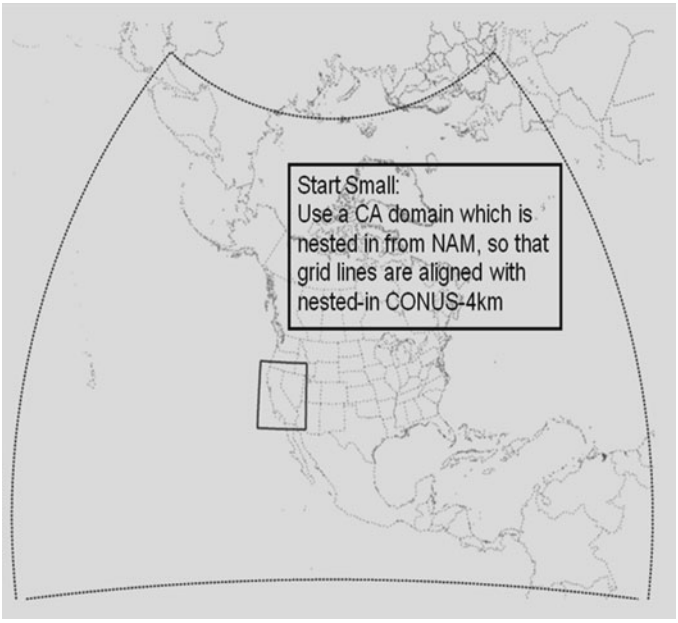


**Fig. 32.3** A nested application of the NAM model in launcher mode is used to generated meteorology fields for a parent domain in 12 km and a child domain in 4 km horizontal grid spacing, respectively. The child domain depicted is the testing domain for this study's development of a NAM-β coupled rll-CMAQ modeling system

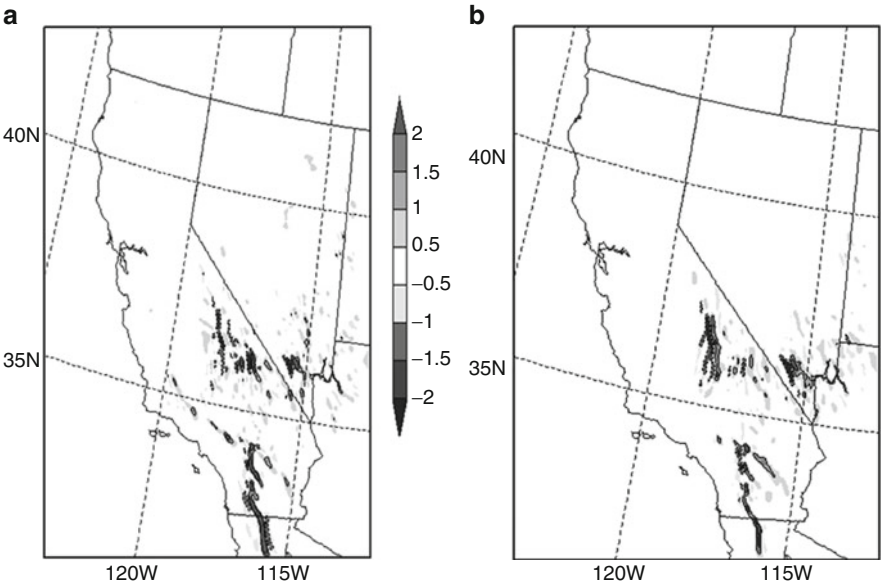


**Fig. 32.4** Sample upper vertical wind velocity [m $s^{-1}$] of the nested-in domain at about 100 hPa valid at: (**a**) 11 UTC, and (**b**) 19 UTC, June 22, 2010; respectively. The perturbation evident at location of complex terrain reflects convergent and divergent flows expected of orographic effects thereof

## References

1. Byun D, Schere KL (2006) Review of the governing equations, computational algorithms, and other components of the Models-3 community multiscale air quality (CMAQ) modeling system. Appl Mech Rev 59:51–77
2. Byun D, Percell P, Ngan F, Kim S (2008) Final report: Testing the linkage between WRF-NMM and CMAQ Models, prepared for K. Schere and R. Mathur, Atmospheric Resources laboratory, NOAA, pp 1–84
3. Hogrefe C, Rao ST, Kasibhatla P, Hao W, Sistla G, Mathur R, McHenry J (2001) Evaluating the performance of regional-scale photochemical modeling systems: part II—ozone predictions. Atmos Environ 35(24):4175–4188. doi:10.1016/S1352-2310(01)00183-2
4. Janjic ZI (2003) A nonhydrostatic model based on a new approach. Meteorol Atmos Phys 82:271–285. doi:10.1007/s00703-001-0587-6
5. Otte TL, Pouliot G, Pleim JE, Young JO, Schere KL, Wong DC, Lee PCS, Tsidulko M, McQueen JT, Davidson P, Mathur R, Chuang HY, DiMego G, Seaman NL (2005) Linking the Eta model with the community multiscale air quality (CMAQ) modeling system to build a national air quality forecasting system. Weather Forecasting 20(3):367–384

# Chapter 33
# Measuring and Modeling Wet Deposition Fluxes in the Netherlands and Europe

**Eric van der Swaluw, Martijn Schaap, Ferd Sauter, Sabine Banzhaf, and Astrid Manders**

**Abstract** The Dutch National Precipitation Chemistry Monitoring Network measures the wet deposition fluxes of acidifying and eutrophying compounds and heavy metals over the Netherlands since 1978. Recent measurements of sulfate, ammonium and nitrate of this precipitation network are used to validate the outcome of the new wet deposition module implemented into the regional air quality model LOTOS-EUROS. The old wet deposition module only included below-cloud scavenging, whereas the new wet deposition module takes into account below-cloud *and* in-cloud scavenging. Both processes are implemented such that the effect of the saturation of rain droplets on the scavenging efficiency is included. A simple parameterization, based on the liquid water content data from ECMWF, is used to distinguish between regions in which respectively below-cloud or in-cloud scavenging occurs. In general, it is found that the combination of below-cloud and in-cloud scavenging increases the net scavenging process in the LOTOS-EUROS model simulations; hence the wet deposition fluxes are increased. These increased wet deposition fluxes in the model simulations are evaluated at the sites of the precipitation network in the Netherlands and show a better agreement as compared to results of simulations performed with the old wet deposition module.

E. van der Swaluw (✉) • F. Sauter
National Institute for Public Health and the Environment, Centre for Environmental Monitoring, P.O. Box 1, 3720 BA Bilthoven, The Netherlands
e-mail: eric.van.der.swaluw@rivm.nl

M. Schaap • A. Manders
TNO, Business Unit Environment, Health and Safety, P.O. Box 80015, 3508 TA Utrecht, The Netherlands
e-mail: martijn.schaap@tno.nl

S. Banzhaf
Institute of Meteorology, Freie Universitaet Berlin, Carl-Heinrich-Becker-Weg 6–10, 12165 Berlin, Germany
e-mail: sabine.banzhaf@met.fu-berlin.de

D.G. Steyn and S. Trini Castelli (eds.), *Air Pollution Modeling and its Application XXI*, NATO Science for Peace and Security Series C: Environmental Security 4,
DOI 10.1007/978-94-007-1359-8_33, 

Finally the wet deposition fluxes are also evaluated at the sites of the European EMEP monitoring stations: a similar improvement is found again between the measurements and model results.

**Keywords** Wet deposition • Modelling • Monitoring

## 33.1 Introduction

Since 1978, the Dutch National Precipitation Chemistry Monitoring Network has been operational in the Netherlands. With this network the wet deposition of ammonium ($NH_4$), nitrate ($NO_3$) and sulfate ($SO_4$) has been continuously monitored at 11 permanent sites in the Netherlands since 1992 (Fig. 33.1 left panel). The samples of rain water are collected with wet-only samplers in the network, thereby ensuring that there is no contribution from dry deposition to the collector. Because of the long time series available at these 11 sites, a trend analysis was performed in van der Swaluw et al. [3] for $NH_4$, $NO_3$ and $SO_4$. In this paper we use the data from the Dutch Precipitation Network to validate the outcome of the new wet deposition module implemented into the regional air quality model LOTOS-EUROS.

LOTOS-EUROS (LE) is a 3D chemical transport model driven by anthropogenic emissions on a grid bound at 35° and 70° North and 10° West and 60° East with a grid resolution of approximately 25 × 25 km. In the vertical direction there are three dynamic layers up to 3.5 km above sea level and an optional surface layer. The meteorological data used to drive the model runs presented in this paper are 3-h data from ECMWF. See Schaap et al. [1] for further technical details of the LE model.

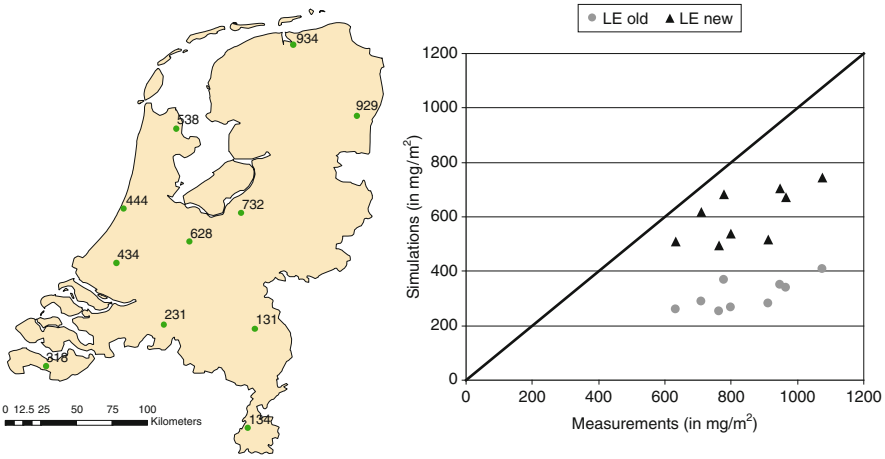


**Fig. 33.1** The Dutch National Precipitation Chemistry Monitoring Network in 2005 for the components $NH_4$, $NO_3$, and $SO_4$ (*left panel*). A comparison between observed and modeled total wet deposition fluxes of ammonium for 2005 in the Netherlands (*right panel*)

A new wet deposition module was implemented in LE which models below-cloud and in-cloud scavenging with a scavenging coefficient $\Lambda$ which scales linearly with the amount of precipitation $P$:

$$\Lambda = C \cdot P, \tag{33.1}$$

here $C$ is a coefficient which depends on the type of component and the type of scavenging (below-cloud or in-cloud). We use the scavenging coefficient as used in the EMEP model [2]. The values for $C$ are larger for in-cloud scavenging than for below-cloud scavenging. Hence, including in-cloud scavenging is expected on average to increase the amount of wet deposition for a rain event. A simple parameterization, based on the liquid water content data from ECMWF, is used to distinguish between regions in which respectively in-cloud or below-cloud scavenging occurs. In the old wet deposition module of LE wet scavenging occurred in *all* the vertical layers above the surface of a grid cell during a rain event. In the new wet deposition module this is no longer the case: from the liquid water content profiles the position of the cloud is determined, hence in regions above the cloud there is no wet scavenging during a rain event. This new method decreases the total volume in which wet deposition occurs with respect to the old method.

## 33.2 Results

The LE model was run for the year 2005 with the old and the new wet deposition module. First the obtained simulation results are compared with the observations at the 11 monitoring sites of the Dutch Precipitation Network. Figure 33.1 (right panel) depicts the result for ammonium, which shows that the new wet deposition module yields a better agreement for the observations with the precipitation network as compared to the old module. The components $SO_4$ and $NO_3$ also show an increase of the wet deposition fluxes with the new wet deposition module.

Figure 33.2 shows a comparison between the modeled and observed wet deposition of ammonium at the sampling frequency of the Dutch Precipitation Network at the site of De Bilt (628), the location of the Dutch MET office KNMI. The variability of the deposition flux is well captured by the LE simulations. Furthermore the regression coefficient is going up from 0.39 to 0.73 with the new wet deposition module. The peak values of the wet deposition levels during the summer of 2005 are however still underestimated.

Finally, Fig. 33.3 shows a first scan of the comparison between measurements of wet deposition of ammonium at the EMEP stations in Europe and the modeled deposition fluxes for 2005 with the LE simulations with both the old and new module. On average, the regression coefficient is moving closer to unity with the new wet deposition module; the scattering is, however, still quite large.

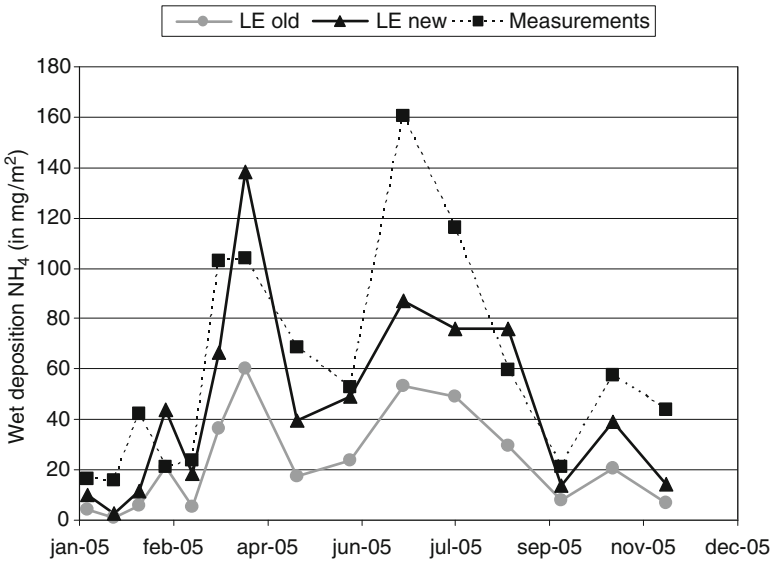


**Fig. 33.2** Comparison of ammonium wet deposition between measurements and simulations with the LE model for the 15 sampling periods in 2005

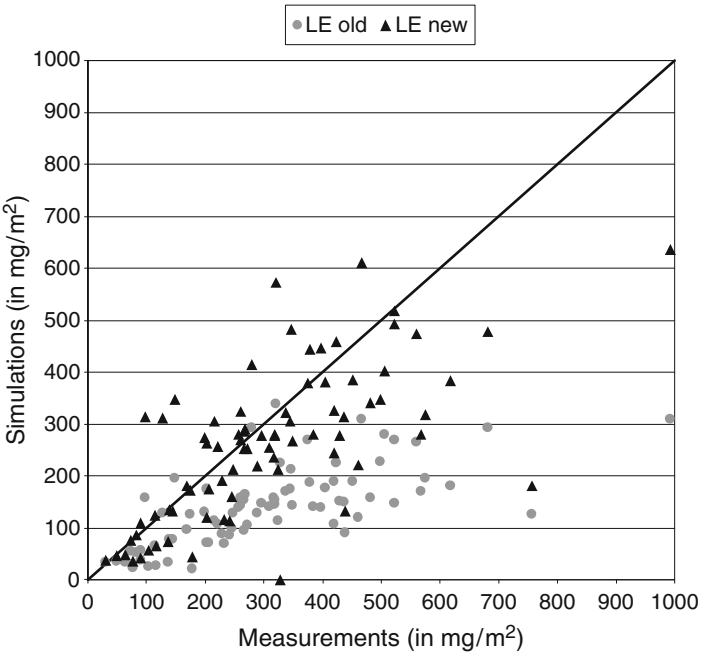


**Fig. 33.3** The comparison of the total ammonium wet deposition in 2005 from observations at EMEP stations with the LE model results

Studies have been performed on the effect of the saturation of rain droplets on the scavenging efficiency. First results with the LE model indicate that the results as presented here will not change significantly due to this additional effect of saturation.

## References

1. Schaap M, Sauter F, Timmermans RMA, Roemer M, Velders G, Beck J, Builtjes PJH (2008) The LOTOS-EUROS model: description, validation and latest developments. Int J Environ Pollut 32(2):270–290
2. Simpson D, Fagerli H, Jonson JE, Tsyro S, Wind P, Tuovinen J-P (2003) Transboundary acidification, eutrophication and ground level ozone in Europe. EMEP status report I
3. van der Swaluw E, Asman WA, van Jaarsveld H, Hoogerbrugge R (2011) Wet deposition of ammonium, nitrate and sulfate in the Netherlands over the period 1992–2008. Atmos Environ, doi:10.1016/j.atmosenv.2011.04.017

## Questions and Answers

**Questioner Name**: Steven Hanna

**Q**: The inclusion of in-cloud processes seems to have removed the model underpredictions. But how can you be sure that there are not other physical reasons for the underpredictions, such as underestimation of emissions?

**A**: We do not exclude the possibility that that there might be other physical reasons for the underpredictions. However, since in-cloud processes were not included in the wet deposition scheme of the LE model, its inclusion seemed to us the **first** logical step to be made.

**Questioner Name**: Akula Venkatram

**Q**: You are using measured precipitation to estimate your modeled deposition of $NH_4$. So both your measured and modeled contain a common variable that might improve the correlation between the modeled and measured depositions. You might want to compare concentrations in rain to remove this artificial correlation.

**A**: Interesting suggestion! After the conference I made a calculation using the data shown in Fig. 33.1 (right panel) with concentration of $NH_4$ instead of wet deposition of $NH_4$. The correlation between measured and simulated concentration of $NH_4$ is *higher* than the correlation between measured and simulated wet deposition of $NH_4$.

**Questioner Name**: Anthony Dore

**Q**: Ammonium aerosol is associated with long range transport and ammonia gas with local emissions. What is the relative importance in the Netherlands of $NH_3$ and $NH_4^+$ to total reduced nitrogen wet deposition.

**A**: A preliminary study with *the LE model* shows that most of the reduced nitrogen wet deposition in the Netherlands comes from the ammonium aerosol.

**Questioner Name**: Gabriele Curci

**Q**: Did you have a look at convective processes? If you have an underestimate of wet deposition maybe not enough air is pumped from the surface to upper levels in updrafts.

**A**: No, we improved the wet deposition processes. No work was performed for this paper on the transport part of the code (in order) to improve the modeled wet deposition levels.

# Chapter 34
# Discrepancies Between Top-Down and Bottom-Up Emission Inventories of Megacities: The Causes and Relevance for Modeling Concentrations and Exposure

**Hugo Denier van der Gon, Sean Beevers, Alessio D'Allura, Sandro Finardi, Cécile Honoré, Jeroen Kuenen, Olivier Perrussel, Paola Radice, Jochen Theloke, Melinda Uzbasich, and Antoon Visschedijk**

**Abstract** A state-of-the-art regional European emission data base is combined and cross-checked with bottom-up emission inventories of Paris, London, Rhine-Ruhr area (Germany) and the Po-valley (Italy). It is shown that the allocation of the emission in the regional top-down inventory can deviate substantially from the megacity bottom-up inventories. For example, the PM10 and NOx in local inventories are respectively 26% and 62% (London), 33% and 95% (Paris), 55% and 108% (Rhine-Ruhr) and 110% and 107% (Po valley) of the emission allocated to the same area in the regional inventory. The match for the Po Valley is reasonable but if we zoom in on a city level (Milan) similar problems as seen in Paris and London surface. We conclude that the European scale inventory is consistent with official reported national emissions but local-national-regional scale inventories are not consistent. Since the discrepancies are large, predicted concentrations and population exposure estimates may be significantly different.

H. Denier van der Gon (✉) • J. Kuenen • A. Visschedijk
Climate, Air quality, and Sustainability, TNO, Princetonlaan 6,
3584 CB Utrecht, The Netherlands
e-mail: hugo.deniervandergon@tno.nl

S. Beevers
King's College London, The Strand, London WC2R 2LS, UK
e-mail: sean.beevers@kcl.ac.uk

A. D'Allura • S. Finardi • P. Radice
Arianet, via Gilino 9, 20128 Milano, Italy
e-mail: s.finardi@aria-net.it

C. Honoré • O. Perrussel
AirParif, 7, rue Crillon, 75004 Paris, France
e-mail: cecile.honore@airparif.asso.fr

J. Theloke • M. Uzbasich
University Stuttgart, IER, Heßbrühlstraße 49a, 705656 Stuttgart, Germany
e-mail: jt@ier.uni-stuttgart.de

D.G. Steyn and S. Trini Castelli (eds.), *Air Pollution Modeling and its Application XXI*,
NATO Science for Peace and Security Series C: Environmental Security 4,
DOI 10.1007/978-94-007-1359-8_34, 

Our work shows the importance of regionalization of emissions for model input and argues that consistency between emission inventories at different scales deserves more attention.

**Keywords** Emission inventories • Air pollutants • Mega cities • Particulate matter

## 34.1 Introduction

Emissions of air pollutants cause air quality degradation and result in climate change. Reducing emissions is one of the most important options for abating these negative impacts. A proper knowledge of emission sources and their location in time and space is a crucial component of being able to model air quality and climate, predict their future change, and design feasible mitigation scenarios. Moreover, a major scientific challenge is to understand how the rapid urbanization, resulting in megacities, affects air quality and climate (e.g., [4]). The first critical step in improving our understanding of how megacities impact air quality, atmospheric composition and climate on different scales is the development of high-quality emission inventories (EI) of relevant gases and aerosols and their precursors. The generation of a high resolution emission inventory for selected European megacities is the scope of this paper.

## 34.2 Regional Emission Inventory and Emissions of Selected Mega Cities

Recently Denier van der Gon et al. [3] prepared a high resolution (1/8 longitude × 1/16 latitude) European emission inventory for the base year 2005 which includes the substances NOx, $SO_2$, NMVOC, $CH_4$, $NH_3$, CO and primary PM10 and PM2.5. This emission inventory is used as a starting point in the present study. The four megacities (MCs) of focus in this study are Paris, London, Rhine-Ruhr area, and Po Valley. The Rhine-Ruhr and Po Valley are not cities but are urban conglomerations with megacity features. The Po Valley domain is much larger than e.g. the Greater London Area (Fig. 34.1). The fraction of the national population living in the MC varies between 14% (London; population 7.7 million) and 45% (Po-Valley; population 24.3 million). Emission inventories for these MCs are compiled by local agencies to support the local authorities in environmental policy making. The European inventory and the local MC inventories have different resolutions and different source sector splits. Through a collaborative effort we defined the domains of the local inventories and worked towards the nesting of the local inventories into a consistent European emission map.

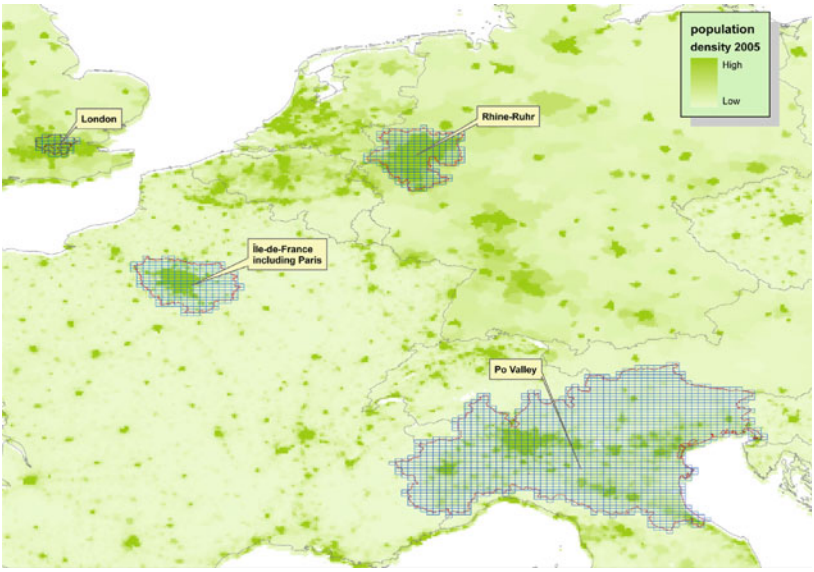


**Fig. 34.1** Domain of selected 1st level Megacities for EU IP MEGAPOLI and population density pattern

## 34.3 Comparison of the Down-Scaled and Bottom-Up Inventories

The local MC inventories use local statistics and activity data to estimate the emissions within their domain. Since the domains are accurately defined (Fig. 34.1) we can "cut-out" the MC emission from the regional inventory and compare them to the local MC emission estimates (Table 34.1). The differences were quite dramatic. The discrepancy for NOx is limited but not for uncertain pollutants like PM, NMVOC and CO. For example, the PM10 emission allocated to London or Paris by the down-scaled regional inventory is a factor 3–4 higher than the local inventories. The match for the Po valley appears reasonable but if we zoom in on a city level (Milan) similar problems as seen in Paris and London surface. So, the smaller the domain, the larger the discrepancies are. A remarkable feature is the ten-fold overestimating of $SO_2$ emission from London (Table 34.1). This was due to uncertainties of the exact location of some point sources. Such misplacements can be understood and repaired but some more complex discrepancies need further study. To analyse the discrepancies closer, national regionalized inventories are also included and a comparison is made at the sector level (Fig. 34.2). In our final European + MC inventory, the MC inventories made

**Table 34.1** Ratio of the MC emission from the Regional European scale inventory over the local MC emission inventory

| | $NO_x$ | PM10 | PM2.5 | $NH_3$ | $SO_2$ | NMVOC | CO |
|---|---|---|---|---|---|---|---|
| London | 1.6 | 3.9 | na | na | 9.4 | 1.5 | 3.6 |
| Paris | 1.1 | 3.0 | 3.2 | 2.2 | 1.9 | 1.9 | 4.1 |
| Rhine Ruhr | 0.9 | 1.6 | 1.2 | 1.6 | 1.1 | 2.4 | 0.7 |
| Po Valley | 0.9 | 0.9 | na | 1.0 | 1.2 | 0.8 | 1.4 |

na = not available

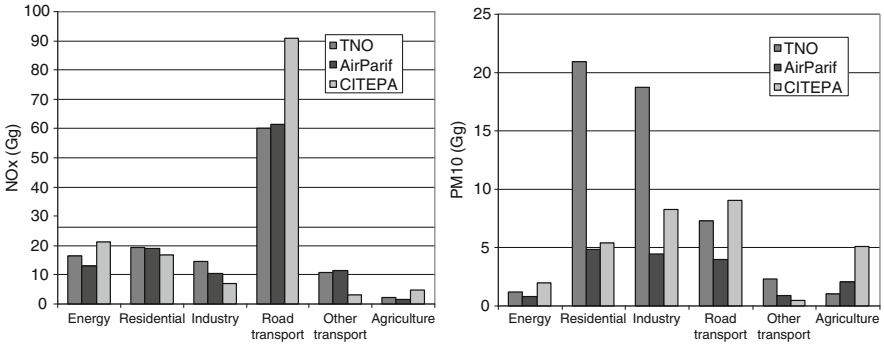


**Fig. 34.2** Emissions of NOx (*left*) and PM10 (*right*) from three inventories; European regional (*TNO*), France national [2] and France provincial [1] for the Ile de France region (Paris) by source sector for 2005

by the local authorities are nested in the European domain (Fig. 34.1). To ensure that the national reported emissions are maintained, any difference in emissions is compensated in the national domain outside the respective MC domain.

## 34.4 Conclusions

The European scale inventory is consistent with official reported national emissions but local-national-regional scale inventories were not consistent. In general, the megacity inventories have more detailed local information and a cause of discrepancy is the spatial distribution of emissions in the down-scaled regional inventory. Since the discrepancies are large, especially for an important pollutant like PM10, the predicted concentrations and population exposure may be significantly different when using a local EI. Modelling combined with observational data may help to validate the emission estimates, confirm distribution patterns and/or identify gaps in emission inventories.

**Acknowledgments** The research leading to these results has received funding from the EU's FP7 2007–2011 under grant agreement n°212520 MEGAPOLI

## References

1. Airparif (2010) Ile-de-France gridded emission inventory 2005 (version2008). http://www.airparif.asso.fr/
2. CITEPA (2010) Inventaire départementalisé des émissions de polluants atmosphériques en France. http://www.citepa.org/publications/. Accessed Feb 2010
3. Denier van der Gon HAC, Visschedijk A, van der Brugh H, Dröge R (2010) A high resolution European emission data base for the year 2005 – A contribution to UBA- Projekt PAREST: particle Reduction Strategies. report TNO-034-UT-2010-01895_RPT-ML, Utrecht
4. Gurjar BR, Butler TM, Lawrence MG, Lelieveld J (2008) Evaluation of emissions and air quality in megacities. Atmos Environ 42:1593–1606

## Questions and Answers

**Questioner Name**: Alexandra Monteiro

**Q**: Are you thinking to use air quality modelling to evaluate these different "top-down" and "bottom-up" approaches?

**A**: Yes, that is certainly the intention. However, the models will have to be able to deal with high resolutions to pick-up the gradients and be able to use local urban background measurement data for validation.

**Questioner Name**: V. Nochvai

**Q**: What is your vision of future "bottom-up" emission inventory in Europe? What should it be, some centralized database? Do you know steps in this direction?

**A**: It would be good if such a scientific "shadow" emission inventory would be maintained at an European institution. I am not aware of any steps in such a direction.

**Questioner Name**: Johannes Bieser

**Q**: How comparable are local emission inventories from one area (e.g., Milano, Torino) Are the methodologies behind these inventories consistent?

**A**: In this case (Milano, Torino) the same methodologies are used but still it is possible that the application of the methodology is not exactly the same. This should be checked through consultation with the local agencies. One step further; for example comparing Paris and Milano the methodologies will certainly be different.

**Questioner Name**: Thomas Pierce

**Q**: Why not constrain the "mass balance" within an urban area with the national total and use activity data from the local authorities; this might achieve consistency between scales (urban - > regional) and reasonable spatial distribution within the city?

**A**: This would be the other alternative solution. However, there are two main reasons why we do not do this at present. First, we have seen that from our down-scaled (regional / national) inventory we significantly overestimate the residential emissions in a city because some of the more polluting fuels are not or only little used in the city. Only improving the spatial distribution within the city would not solve this problem. Second, we want a dialogue with the city planners and policy makers. By starting with the same city emissions they use in their current planning – and as constructed by the responsible agency – we create a common starting point. This will make our results more valuable and acceptable to them. Next, if we find major discrepancies or uncertainties it will be easier to get these on the agenda as it will be our common interest to make further improvements.

# Chapter 35
# Making High Resolution Air Quality Maps for Flanders, Belgium

**Wouter Lefebvre, Stijn Janssen, Jean Vankerkom, Felix Deutsch, Nele Veldeman, Frans Fierens, Wim Peelaerts, Stijn Van Looy, Natacha Claeys, Tania Van Mierlo, and Filip Lefebre**

**Abstract** Using a combination of models, high resolution air quality maps for Flanders (Belgium) have been made. First of all, the Eulerian air quality model AURORA has simulated for a complete year the air pollutant concentrations over the region on a 3 × 3 km resolution. These results are calibrated using the RIO-interpolation model on air quality station data. Thereafter, an extra simulation using the bi-Gaussian IFDM model is made on a resolution of 1 × 1 km, with a finer resolution (up to 25 m) close to the major roads. The nesting methodology of IFDM in AURORA is designed to avoid double counting of the roads. The results are highly detailed $PM_{10}$, $PM_{2.5}$, $NO_2$ and EC maps for Flanders. Using station data and data from several measurement campaigns, the maps have been validated and it has been shown that the maps show indeed a highly detailed picture of the air quality in Flanders. These data will be used in assessing the air quality and human exposure to it in Flanders, and in assessing policy scenarios designed to improve the air quality.

**Keywords** Regional modelling • Air quality standards • Exposure • High resolution

W. Lefebvre (✉) • S. Janssen • J. Vankerkom • F. Deutsch • N. Veldeman • W. Peelaerts • S. Van Looy • F. Lefebre
Department of Environmental Modelling, Flemish Institute for Technological Research (VITO), Boeretang 200, 2400 Mol, Belgium
e-mail: wouter.lefebvre@vito.be; stijn.janssen@vito.be

F. Fierens
Belgian Interregional Environment Agency, Kunstlaan 10–11, 1210 Brussels, Belgium

N. Claeys • T. Van Mierlo
Departement Leefmilieu, Natuur en Energie, Afdeling Lucht, Hinder, Risicobeheer, Milieu & Gezondheid, Koning Albert II-laan 20, bus 8, 1000 Brussel, Belgium

D.G. Steyn and S. Trini Castelli (eds.), *Air Pollution Modeling and its Application XXI*, NATO Science for Peace and Security Series C: Environmental Security 4,
DOI 10.1007/978-94-007-1359-8_35, 

## 35.1 Introduction

The European Union requires its member states to protect the health of their citizens by obtaining good air quality and thus keeping air pollution under predefined limits. Since particulate matter and nitrogen dioxide are some of the most important air pollutants in Flanders (Northern part of Belgium), mitigation strategies are evaluated on the basis of PM and $NO_2$ concentration decreases. As IPPC is well implemented, current and future measures are mainly focused to abate the traffic pollution. In order to assess the effectiveness of measures, assessing the air quality is necessary. However, it is impossible to monitor the air quality at every single place in the country. This paper describes an effort in combining monitoring data with modelled data for Flanders, in order to obtain high resolution maps.

## 35.2 Methodology

For the road traffic emissions, MIMOSA4 has been used. MIMOSA4 is the most recent version of the MIMOSA traffic model (original version: [9]; current version: [10]), which generates hourly output for different types of emissions, such as $NO_x$, $NO_2$, EC, $PM_{10}$ and $PM_{2.5}$ at individual road level for Flanders using COPERT-IV methodology [1].

For Flanders, the non-traffic emissions are those based on the inventory made by the Flemish Environment Agency. For Brussels, Wallonia and the neighbouring countries, the EMAP tool is used [7].

Meteorological fields, required as input for AURORA and IFDM, were simulated using the Advanced Regional Prediction System (ARPS), a non-hydrostatic meso-scale atmospheric model developed by the University of Oklahoma [11, 12]. The ARPS model is nested into ECMWF data.

The regional air quality model used in this study is AURORA (Air quality modelling in urban regions using an optimal resolution approach, Mensink et al. [8]). More information on the AURORA model can be found in the European Model Database (http://air-climate.eionet.europa.eu/databases/MDS/index_html).

The AURORA model simulates, in three successive nesting steps, the air quality over the region of Flanders at a resolution of respectively $25 \times 25$, $9 \times 9$ and $3 \times 3$ km$^2$. The boundary conditions for the outermost 25 km resolution simulation are taken from the BelEUROS model which simulated the whole of Europe at a resolution of 60 km [2]. More information on the BelEUROS model can be found in the European Model Database (http://air-climate.eionet.europa.eu/databases/MDS/index_html).

The available measurements are interpolated over Flanders with the RIO-corine-tool [4]. This interpolation is done on a grid of $3 \times 3$ km$^2$.

In the calibration step, the $3 \times 3$ km$^2$ AURORA results are calibrated with the RIO-data, which are also available on a $3 \times 3$ km$^2$ grid. For the pollutants

for which no or few measurements were available (EC), the modelled data were not calibrated.

In order to increase the spatial resolution of the AURORA-calibrated results in the direct vicinity to major roads, the bi-Gaussian IFDM model is applied at a regular resolution grid of $1 \times 1$ km$^2$ and at a road following irregular grid with a maximum resolution of 25 m. More information on the IFDM model can be found in the European Model Database (http://air-climate.eionet.europa.eu/databases/MDS/index_html).

AURORA and IFDM have been coupled by using a simple algorithm to avoid double counting of the traffic emissions [6].

## 35.3 Results

Figures 35.1 and 35.2 show some examples of maps obtained in this study. It can be seen that the local EC-concentration gradient is high around the major roads, while for the number of exceedances of the $PM_{10}$ daily mean limit value, this gradient is small. The observed west-east gradient in $PM_{10}$ exceedance days is also clearly visible in the results. These results describe the situation for 2007. With measures taken both in Flanders and the neighbouring regions, the situation is expected to improve drastically.

These results can also be used to get a more detailed image of the population exposure to air pollution in Flanders, when detailed information on the population

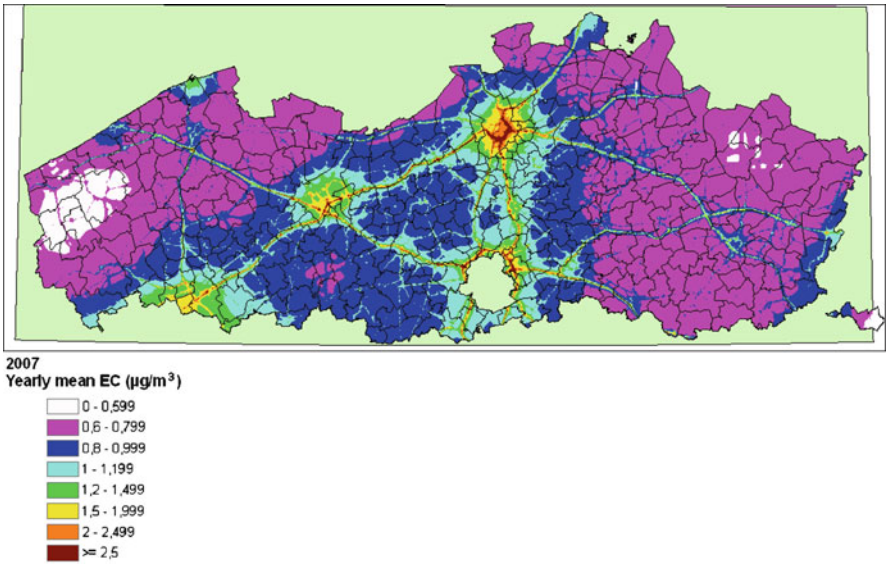


**Fig. 35.1** Annual mean simulated EC-concentration (in µg/m$^3$) for the year 2007

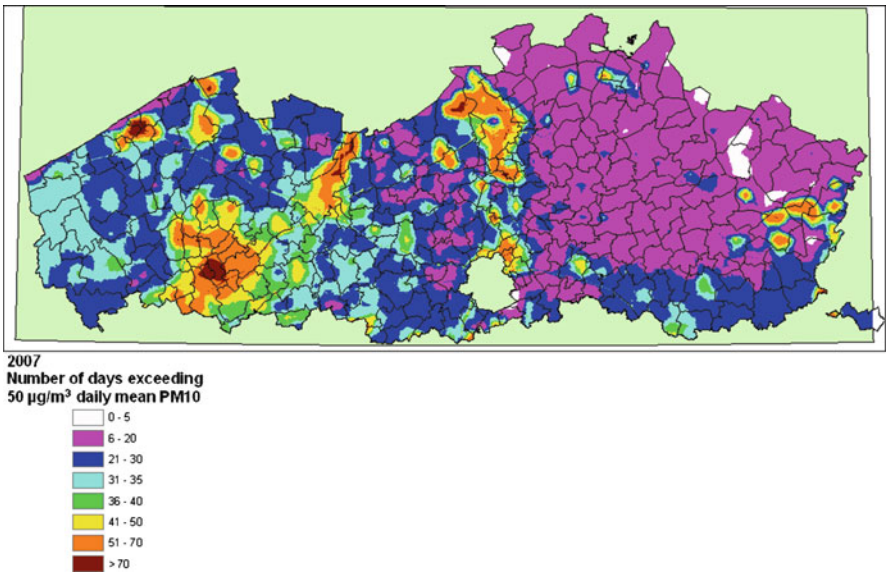


**Fig. 35.2** Number of days in 2007 for which the daily mean $PM_{10}$-concentration exceeds the European limit of 50 µg/m$^3$

density is known. Thanks to the Flemish Environment Agency, such data was made available for this study. For instance, we have found that almost 35% of the population in Flanders is exposed to daily mean $PM_{10}$ concentrations higher than 50 µg/m on more than 35 days. Removing the primary traffic emissions reduces this percentage of the Flemish population slightly to around 30%.

## 35.4 Conclusions

By using both model results and measurement data, it is possible to get a much more precise spatial view of the air quality in a certain region. This was done here for Flanders, but the methodology can be extended to other regions, when all necessary data is available. This information can help local governments to assess air quality on a higher spatial resolution. With the methodology the impact of regional action plans that reduce emissions can be estimated together with the attainability of the current and future European air quality standards.

It was pointed out that the impact of traffic on the PM concentrations ($PM_{10}$ and $PM_{2.5}$) is rather limited, while the impact on the $NO_2$ concentrations is much more significant. Furthermore, it was shown that traffic can have a significant impact on the elemental carbon (EC) concentrations. This is important because there is growing evidence that EC is one of the most toxic components of particulate

matter (see references in Lefebvre et al. [5]). The contribution of EC to the total mass concentrations of $PM_{10}$ (and $PM_{2.5}$) however is rather small (only a few %). As such, policy makers are facing the situation that traffic mitigation strategies will have a small impact on the total mass PM concentration and thus on meeting the EU air quality limit values, but they might be relevant in reducing the health impact of the exposed population (see also Lefebvre et al. [5]).

## References

1. COPERT IV (2007) Emission inventory guidebook, Chapter Road Transport, Activities 070100–070500, version 6.0 of 23 August 2007, Aristotle University Thessaloniki, Thessaloniki
2. Deutsch F, Viaene P, Janssen S, Maes J, Vankerkom J, Janssen L, Vliegen J, Peelaerts W, Mensink C (2009). Validation of the completely renewed BelEUROS model. Final report for project by order of the Flemish Environment Agency (in Dutch)
3. Deutsch F, Vankerkom J, Veldeman N, Peelaerts W, Fierens F, Vanpoucke C, Trimpeneers E, Vancraeynest L, Buysse H (2010) Verklarende factoren voor evoluties in luchtkwaliteit. Studie uitgevoerd in opdracht van MIRA, Milieurapport Vlaanderen, Oktober 2010, 2010/RMA/R/234, www.milieurapport.be (in Dutch)
4. Janssen S, Dumont G, Fierens F, Mensink C (2008) Spatial interpolation of air pollution measurements using CORINE land cover data. Atmos Environ 42:4884–4903. doi:10.1016/j.atmosenv.2008.02.043
5. Lefebvre W, Fierens F, Trimpeneers E, Janssen S, Van de Vel K, Deutsch F, Viaene P, Vankerkom J, Dumont G, Vanpoucke C, Mensink C, Peelaerts W, Vliegen J (2011a) Modelling the effects of a speed limit reduction on traffic-related elemental carbon (EC) concentrations and population exposure to EC. Atmos Environ 45(1):197–207
6. Lefebvre W, Vercauteren J, Schrooten L, Janssen S, Degraeuwe B, Maenhaut W, de Vlieger I, Vankerkom J, Cosemans G, Mensink C, Veldeman N, Deutsch F, Van Looy S, Peelaerts W, Schepens J, Lefebre F (2011b) Validation of the MIMOSA-AURORA-IFDM model chain for policy support: modeling concentrations of elemental carbon in Flanders, submitted to Atmos Environ
7. Maes J, Vliegen J, Van de Vel K, Janssen S, Deutsch F, De Ridder K, Mensink C (2009) Spatial surrogates for the disaggregation of CORINAIR emission inventories. Atmos Environ 43(6):1246–1254
8. Mensink C, De Ridder K, Lewyckyj N, Delobbe L, Janssen L, Van Haver P (2001) Computational aspects of air quality modelling in urban regions using an optimal resolution approach (AURORA). In: Large-scale scientific computing, vol 21791, Lecture notes in computer science. Springer, Berlin, pp 299–308
9. Mensink C, De Vlieger I, Nys J (2000) An urban transport emission model for the Antwerp area. Atmos Environ 34:4595–4602
10. Vankerkom J, De Vlieger I, Schrooten L, Vliegen J, Styns K (2009) Beleidsondersteunend onderzoek: Aanpassingen aan het emissiemodel voor wegtransport MIMOSA. Studie uitgevoerd in opdracht van VMM – MIRA, 2009/TEM/R/084
11. Xue M, Droegemeier KK, Wong V (2000) The Advanced Regional Prediction System (ARPS) – a multiscale non-hydrostatic atmospheric simulation and prediction tool. Part I: Model dynamics and verification. Meteorol Atmos Phys 75:161–193

12. Xue M, Droegemeier KK, Wong V, Shapiro A, Brewster K, Carr F, Weber D, Liu Y, Wang D-H (2001) The Advanced Regional Prediction System (ARPS) – a multiscale non-hydrostatic atmospheric simulation and prediction tool. Part II: Model physics and applications. Meteorol Atmos Phys 76:134–165

## Questions and Answers

**Questioner Name**: Elisabetta Angelino (ARPA Lombardia)

**Q**: On which temporal base did you make validation with AOD data and did validation results differ in relation with the time of the day or of the year?

**A**: The comparison with the AOD data was done on the annual mean maps. Therefore, no relation with the time of the day or of the year could be discerned.

**Questioner Name**: Peter Builtjes (TNO)

**Q**: You stated that primary PM-emission by traffic on roads are not the main cause of exceedances of $PM_{10}$ levels of EU-limit. What is then causing these exceedances?

**A**: Large part of the $PM_{10}$-concentrations are imported from outside Flanders (up to 75%). However, exports from Flanders to our neighboring regions are also high. For the sources in Flanders, a source apportionment study with the BelEUROS-model (Deutsch et al. [3]) showed that agriculture is responsible for about 54% of the Flemish contribution to $PM_{10}$. Transport, industry and the domestic sector are the following most important sectors with respectively 16, 16 and 10% of the Flemish contribution. Furthermore, only part of this transport contribution is due to direct PM-emissions.

**Questioner Name**: S.T. Rao

**Q**: (a) Who is using these high-resolution air quality maps and for which purpose?
(b) Did you perform cross-validation to judge the quality of the map?
(c) Have you looked into the false positives if these data are being used to estimate exceedances of the European standards?

**A**: (a) These high resolution air quality maps are made for the Flemish Government. They use them to assess the exceedances of the European standards in Flanders. They are also used to determine the number of people living in regions that exceed the European standards. An interesting possible future use is for determination of exposure and health effects.
(b) RIO has been cross-validated [4]. Furthermore, this model has been validated by comparing it to different independent datasets, as the ChemKar-campaign (Lefebvre et al. [6]) and a measurement campaign in Rumst along a major highway. Cross-validation of the entire methodology would be extremely expensive in computer time and has therefore not been done.

(c) We have not specifically looked into false positives in this study. However, the method is as sensitive to false negatives as it is to false positives. Furthermore, a small negative bias is apparent in the model results. Currently, a study is been made looking into the possible false positives, in order to be able to correct for them.

# Chapter 36
# Development of an Agricultural Fertilizer Modeling System for Bi-Directional Ammonia Fluxes in the CMAQ Model

**Limei Ran, Ellen Cooter, Verel Benson, and Qun He**

**Abstract** Atmospheric ammonia ($NH_3$) plays an important role in fine-mode aerosol formation. Accurate estimates of ammonia from both human and natural emissions can reduce uncertainties in air quality modeling. The majority of ammonia anthropogenic emissions come from the agricultural practices, such as animal operations and fertilizer applications. The current emission estimates at the U.S. Environmental Protection Agency (U.S. EPA) are based on the annual National Emission Inventory (NEI). However, accurate estimation of ammonia emissions in space and time has been a challenge. For instance, fertilizer applications vary in the date of application and amount by crop types and geographical area. With the support of the U.S. EPA, we have responded by an agricultural fertilizer modeling system for use with a newly developed ammonia bi-directional flux algorithm in the Community Multiscale Air Quality (CMAQ) model. This modeling system will simulate $NH_3$ emissions from fertilizer applications on agricultural lands rather than from emission estimates based on pre-defined emission factors. The goal for this paper is to demonstrate how this agricultural fertilizer modeling system is developed for a continental U.S. CMAQ 12-km modeling domain and the tools we developed in this system.

L. Ran (✉) • Q. He
Institute for the Environment, University of North Carolina at Chapel Hill,
137 E.Franklin Str. Room 654, 27599 - 6116 Chapel Hill, NC, USA
e-mail: lran@unc.edu

E. Cooter
Atmospheric Modeling and Analysis Division, U.S. EPA, Research Triangle Park,
NC 27711, USA

V. Benson
Benson Consulting, 200 Haywood Ct, Columbia, MO 65203, USA

D.G. Steyn and S. Trini Castelli (eds.), *Air Pollution Modeling and its Application XXI*,
NATO Science for Peace and Security Series C: Environmental Security 4,
DOI 10.1007/978-94-007-1359-8_36, 

**Keywords** Atmospheric ammonia ($NH_3$) • CMAQ • Ammonia bi-directional flux modeling • EPIC • $NH_3$ emissions from fertilizer applications • Agricultural fertilizer modeling system • BELD4 • NLCD • MODIS

## 36.1 Introduction

Human activities have significantly altered the nitrogen cycle [2]. The majority of ammonia anthropogenic emissions come from agricultural practices, about 51% from animal husbandry and about 28% from agricultural fertilizer applications based on the 2002 NEI. Atmospheric ammonia ($NH_3$) is a precursor for ammonium nitrate, ammonium sulfate, and ammonium bisulfate aerosol formation. Nitrogen aerosols have significant and deleterious impacts on human health (e.g. [11]). In addition, deposition of excess N in the form of ammonia and ammonium can have serious impacts on aquatic and terrestrial ecosystems (e.g. [4, 9]). Therefore, accurately estimating ammonia from both anthropogenic and biogenic emissions is important not only for air quality studies but also for ecosystem N deposition impact assessments. Currently, $NH_3$ emissions from fertilizer applications are estimated using the Carnegie Mellon University (CMU) Ammonia Model version 3.6 which relies on county-level fertilizer sales data or estimates. Application timing is based on state-level climatological averages that are constant in time. Fertilizer applications are distributed monthly to agriculture land area estimated from satellite land cover data representing the early 1990's. Emissions are then estimated as a function of these estimates and a set of fixed emission factors. Thus, current methods do not account for more recent land use changes or variations in the dates and amounts of fertilizer applications by crop types and geographical area.

The study by Cooter et al. [1] demonstrated that bi-directional $NH_3$ flux from managed agricultural soils can be reasonably estimated through integration of the resistance-based flux model of Nemitz et al. [5] and CMAQ deposition [6] with components of the Environmental Policy Integrated Climate (EPIC) model [10]. The results of Cooter et al. [1] showed good temporal (daily) and accumulated monthly $NH_3$ estimates and provided a sound foundation for building an agricultural fertilizer modeling system at the regional scale for use with a newly developed ammonia bi-directional flux algorithm in the CMAQ model [7]. This modeling system has a mechanistic description of the fertilizer application method, timing, amount, and rate for specific pastures and crops. This is different from previous emission estimates because it can be used to simulate scenarios with different agricultural operation and management techniques. Thus, future scenarios, such as increased bio-fuel production that may impact fertilizer use, can be simulated to assess their impacts on air quality. The purpose of this paper is to describe how this agricultural fertilizer modeling system is developed for a continental U.S. 12 km grid-resolution CMAQ modeling domain.

## 36.2 Agricultural Fertilizer Modeling System

The agricultural fertilizer modeling system contains three main components within the dash line box in Fig. 36.1: (1) the EPIC model, (2) tools in the Spatial Allocator to convert mesoscale meteorology Weather Research and Forecasting (WRF) model data and CMAQ N deposition data for EPIC fertilizer modeling and to convert EPIC fertilizer output for CMAQ air quality modeling, and (3) a simple Java-based interface which air quality modelers can use to generate and visualize fertilizer application data for different modeling scenarios. In this modeling system with WRF and CMAQ, accurate and consistent land use information is important for agricultural fertilizer application modeling, meteorological land surface processes, biogenic emissions, and chemical surface fluxes. Land use data (called BELD4), computed from the most recent 2001 National Land Cover Data (NLCD) products at 30 m cell resolution for the U.S., Moderate Resolution Imaging Spectroradiometer (MODIS) for areas outside the U.S., and U.S. Department of Agriculture (USDA) Forest Inventory and Analysis (FIA) tree species and National Agricultural Statistics Service (NASS) pasture/crop categories at county level will be used in this modeling system. The gridded NLCD/MODIS land cover data has been applied in the PX land surface model for WRF/CMAQ modeling [8]. The tool to generate the BELD4 data is under the development with the support from the US EPA.

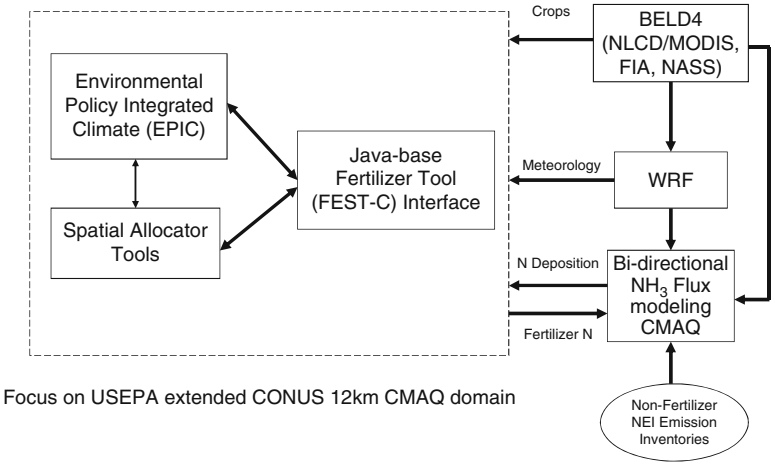


**Fig. 36.1** The agricultural fertilizer modeling system for the CMAQ

### 36.2.1 EPIC Modeling

The EPIC model is a cropping simulation system developed during the 1980's and is being continuously enhanced [3]. It simulates drainage areas that are characterized by homogeneous weather, soil, landscape, crop rotation, and management conditions at field/site scale on a daily time step. It has been used by the USDA and researchers around the world from field to national scale to simulate crop growth, fertilization, erosion, water quality, climate change, and carbon/nitrogen cycling. The development of the EPIC modeling data files is displayed in Fig. 36.2. We have developed programs to build EPIC soil and site crop management data sets at the 8-digit hydrologic cataloging unit (HUC) level. The programs use a combination of expert knowledge and data compiled for the USDA CRP Evaluation, USDA Conservation Technical Assistance Evaluation, and soil and management data compiled for future USDA and FAPRI analyses. Initially, the system is built for the 8-digit HUC geographic level; however, 12 km grid elevation, slope, land use, and weather data are used to modify the site and heat unit scheduled management to incorporate some attributes of each 12 km grid cell. After the evaluation and analysis of the generated EPIC data files at the 8-digit HUC level, we developed programs to create EPIC site data files for the continental CMAQ 12 km grid-resolution domain. Only grid cells with NLCD/MODIS agricultural pasture or crop lands will be used in EPIC modeling. We have

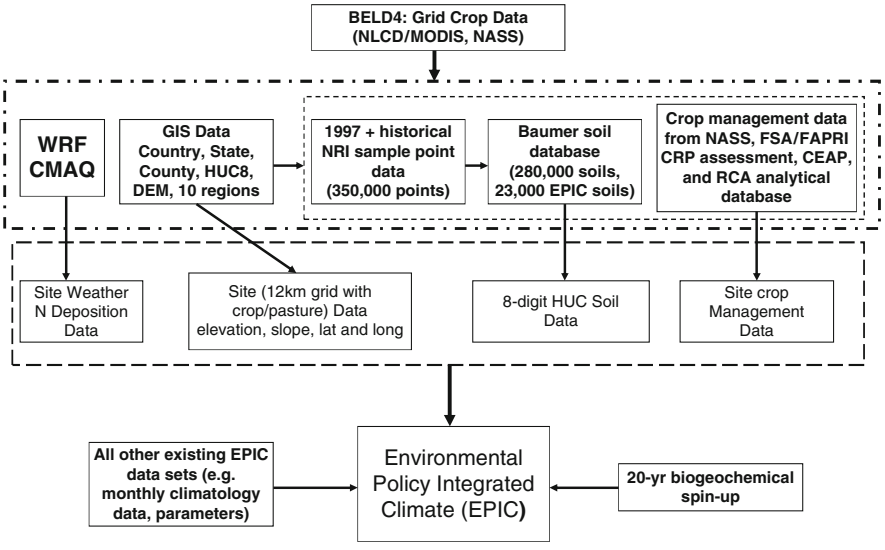


**Fig. 36.2** Modified EPIC modeling for the continental CMAQ 12 km domain grids

completed the development of the EPIC data files for thirty eight NASS irrigated and rainfed pasture and crops in the CMAQ grids over the U.S. Currently, we are evaluating 20-year biogeochemical spin-up runs for all pasture and crops for evaluation and modification.

### *36.2.2 Tools to Connect EPIC and CMAQ*

The tools to connect EPIC and WRF/CMAQ were developed in the Spatial Allocator Raster Tools system (http://www.ie.unc.edu/cempd/projects/mims/spatial/). The WRF/CMAQ-to-EPIC tool extracts weather and N deposition data needed for EPIC modeling from the WRF and CMAQ modeling output. The EPIC model requires as input daily weather data on radiation, maximum temperature, minimum temperature, rain, relative humidity, and wind speed. The EPIC model is to be modified to take into consideration CMAQ dry and wet N deposition estimates during the fertilizer demand estimation process. The EPIC-to-CMAQ tool extracts EPIC output files at each grid cell to generate NetCDF files containing information on soil conditions, daily or monthly time step EPIC output, and fertilizer applications. Thus, CMAQ can obtain each crop N application data from the NetCDF files and aggregate total applied N in each grid for all crops based on grid BELD4 NASS crop fractions for the bi-directional $NH_3$ flux modeling.

### *36.2.3 Fertilizer Emission Scenario Tool for CMAQ (FEST-C) Interface*

The Java-based FEST-C interface provides integrated capabilities of running the EPIC model, Spatial Allocator Raster Tools, and VERDI visualization for input and output NetCDF files. The interface contains five components: (1) process WRF weather and CMAQ N deposition data for EPIC modeling, (2) modify management scenario and EPIC run files, (3) run the EPIC model, (4) process EPIC output data into the CMAQ ready format, and (5) visualize input and output data using VERDI. The interface can be launched from a local machine or remote Linux server where the EPIC model and Spatial Allocator Tools are located.

## 36.3 Future Work

We are working to complete the EPIC modeling data files for grids outside the U.S. Then, the complete EPIC model will be tested on a Linux server for whole system evaluation. The FEST-C interface components 2 and 3 will be fully implemented.

We will modify and enhance site, soil, and crop management programs to build EPIC site, soil, and management data files for other domains with different grid resolutions. We will develop and model crop rotation and biofuel scenarios for air quality impact assessment. In addition, we will prepare for climate change applications (e.g., multi-year time slices) and integrate with the coupled WRF-CMAQ for climate, air quality, and agricultural productivity studies.

**Acknowledgments** This research was supported by the U.S. EPA under contract numbers EP-W-09-023 and EP-D-07-102.

## References

1. Cooter EJ, Bash JO, Walker JT, Jones MR, Robarge W (2010) Estimation of $NH_3$ bi-directional flux over managed agricultural soils. Atmos Environ 44:2107–2115
2. Galloway JN et al (2004) Nitrogen cycles: past, present, and future. Biogeochemistry 70:153–226
3. Gassman PW et al (2010) The Agricultural Policy/Environmental Extender (APEX) model: an emerging tool for landscape and watershed environmental analyses. Trans Am Soc Agric Biol Eng 53(3):711–740
4. Lovett GM et al (2009) Effects of air pollution on ecosystems and biological diversity in the eastern United States. Ann N Y Acad Sci 1162:99–135
5. Nemitz E, Milford C, Sutton MA (2001) A two-layer canopy compensation point model for describing bi-directional biosphere-atmosphere exchange of ammonia. Q J R Meteorol Soc 127:815–833
6. Pleim JE, Xiu A, Finkelstein PL, Otte TL (2001) A coupled land-surface and dry deposition model and comparison to field measurements of surface heat, moisture, and ozone fluxes. Water Air Soil Pollut Focus 1:243–252
7. Pleim JE, Walker J, Bash J, Cooter E (2011) Development and evaluation of an ammonia bi-directional flux model for air quality models. In: Steyn DG, Castelli ST (eds) Air pollution modeling and its application XXI. Springer, Dordrecht
8. Ran L, Pleim J, Gilliam AR (2010) Impact of high resolution land-use data in meteorology and air quality modeling systems. In: Air pollution modeling and its application XX. Springer, Dordrecht, pp 3–7
9. Smith VH, Tilman GD, Nekola JC (1998) Eutrophication: impacts of excess nutrient inputs on freshwater, marine, and terrestrial ecosystems. Environ Pollut 100(1–3):179–196
10. Williams JR (1995) The EPIC model. In: Singh VP (ed) Computer models in watershed hydrology. Water Resources Publications, Highlands Ranch, pp 909–1000
11. Wolfe AH, Patz JA (2002) Reactive nitrogen and human health: acute and long-term implications. Ambio 31:120–125

## Questions and Answers

**Questioner Name**: Dr. B. Fisher

**Q**: Does the EPIC model include the runoff of nitrogen after heavy precipitation. This is another pathway for the transfer of nitrogen (to be compared with the atmospheric pathway in CMAQ)?

**A**: EPIC does simulate the complete N cycle in soils and N loss from surface runoff and subsurface flow. However, since the model is at single field level, it does not have information about N flow from other EPIC modeling sites. If you want to know N flow information from multiple fields or within a watershed, you may use APEX or SWAT models. For emissions-driven air quality analyses, knowledge regarding field-scale fertilizer applications for 12 km grids is sufficient.

**Questioner Name**: Dr. Mohamed Salem

**Q**: What are the sources of organic phosphorus fertilizers you use in your study?
**A**: Organic phosphorus is based on soil organic matter (carbon) initially and then organic phosphorus is added from plant residues or manure. Grazing is set up to apply the manure excreted daily by livestock. Manure can be applied as fertilizer. We don't have it yet for our pasture, but we may have it in the future

# Chapter 37
# Air Quality Forecasting with LOTOS-EUROS in the Context of the MACC Project

**Henk Eskes, Martijn Schaap, Renske Timmermans, Lyana Curier, and Daan Swart**

**Abstract** The European project MACC (Monitoring Atmospheric Composition and Climate) is developing a pre-operational system for forecasting the chemical composition of the atmosphere, both on a global scale and on a regional scale for Europe. The regional scale forecasts in MACC are based on an ensemble of seven regional air quality (RAQ) models, including the Dutch LOTOS-EUROS model. These RAQ models have been set up independently to deliver forecasts of trace gases on a daily basis, up to three days ahead. In the presentation I will introduce the MACC approach to air quality forecasting for Europe. The performance of the LOTOS-EUROS model will be compared with the other contributing models (EMEP, EURAD, MATCH, SILAM, MOCAGE, CHIMERE), and the evaluation procedure in MACC will be discussed. Within MACC a data assimilation capability is built for all seven models. We will show first results of the assimilation of both European surface observations as well as OMI $NO_2$ satellite observations.

**Keywords** Air quality • Forecast • Lotos-Euros • Data assimilation • Ensemble Kalman filter • Ozone • Nitrogen dioxide • Satellite • OMI • MACC

H. Eskes (✉)
Deparment of Climate and Seismology, KNMI, Royal Meteorological Institute Netherlands, P.O. Box 201, 3730 AE De Bilt, The Netherlands
e-mail: henk.eskes@knmi.nl

M. Schaap • R. Timmermans • L. Curier
TNO, Netherlands Organisation for Applied Scientific Research, Utrecht, The Netherlands
e-mail: martijn.schaap@tno.nl

D. Swart
RIVM, National Institute for Public Health and the Environment, Bilthoven, The Netherlands

D.G. Steyn and S. Trini Castelli (eds.), *Air Pollution Modeling and its Application XXI*, NATO Science for Peace and Security Series C: Environmental Security 4,
DOI 10.1007/978-94-007-1359-8_37, 

## 37.1 Lotos-Euros Contribution to the MACC Project

MACC (Monitoring Atmospheric Composition and Climate, 2009–2011) is the current pre-operational atmospheric service of the European GMES programme. MACC provides data records on atmospheric composition for recent years, data for monitoring present conditions and forecasts of the distribution of key constituents for a few days ahead. MACC combines state-of-the-art atmospheric modelling with Earth observation data to provide information services covering European Air Quality, Global Atmospheric Composition, Climate, and UV and Solar Energy.

Seven regional air-quality analysis and forecasting systems are operated routinely for MACC (CHIMERE, EMEP, EURAD, LOTOS-EUROS, MATCH, MOCAGE and SILAM). The regional service draws not only on what has been developed in GEMS but also on the Integrated Air Quality assessment and forecasting service operated by PROMOTE. The forecasts produced by the seven models are collected centrally at Meteo-France. The products provided on the MACC website (http://www.gmes-atmosphere.eu/) are: Daily air-quality analyses (hourly) for the day before from each model; Daily air-quality forecasts up to 72 h (hourly) from each model; Daily ensemble air-quality analyses (hourly) for the day before; Daily ensemble air-quality forecasts up to 72 h (hourly); Ensemble air-quality reanalyses for the years 2007, 2008 and 2009. An example of a forecast of the ozone distribution is shown in Fig. 37.1.

The LOTOS-EUROS model [6] is a 3D chemistry transport model aimed to simulate air pollution in the lower troposphere. The model has been used for the assessment of particulate air pollution in a number of studies directed to total PM10 (e.g. [3, 5]), secondary inorganic components (e.g. [1]), primary carbonaceous components and trace metals. The model has participated frequently in international model comparisons addressing ozone (e.g. [8]) and particulate matter (e.g. [7]).

The Dutch LOTOS-EUROS model teams are contributing forecasts, analyses and reanalyses to the MACC regional subproject cluster, where TNO and KNMI are

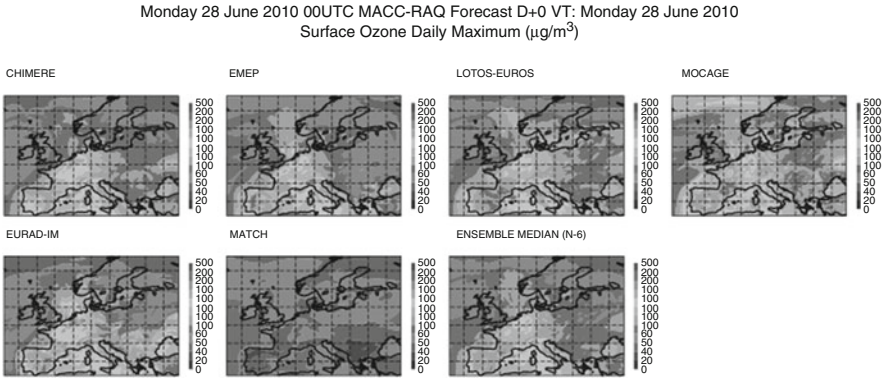


**Fig. 37.1** Example of an ozone forecast for 28 June 2010, combined with the ensemble median

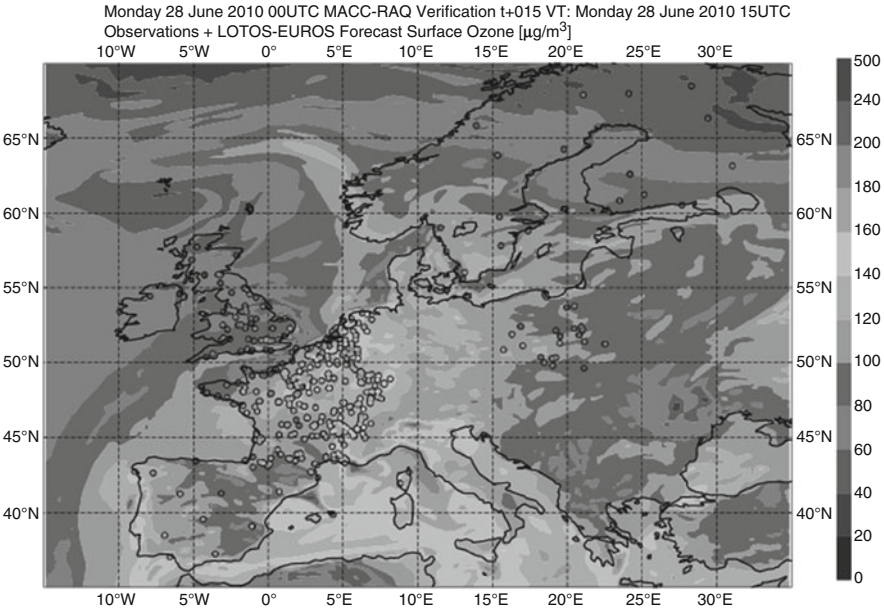


**Fig. 37.2** Verification of the LOTOS-EUROS ozone field for Monday 28 June, 15 UTC, with the available surface observations

MACC project members. LOTOS-EUROS is currently developed by TNO, RIVM and KNMI. The RIVM is both model developer and user of the forecasts, and they have the legal obligation to provide real-time air quality measurements and pollution forecasts to the Dutch public, see http://www.lml.rivm.nl/. In Fig. 37.2 we show an example of the verification of the LOTOS-EUROS ozone forecasts with near-real time surface measurements that are made available to the MACC project.

## 37.2 Assimilation of Surface O3 and OMI NO2 Satellite Observations

The LOTOS-EUROS model is equipped with a data assimilation package based on the ensemble Kalman filter technique (e.g. [1, 3]). At this moment data assimilation is performed for ozone in the zoom region over the Netherlands in the context of the Dutch SmogProg project. Assimilation of surface ozone measurements is applied Europe-wide to the MACC domain for the 2007 reanalysis. The use of other observational datasets of PM10, $NO_2$, AOD from surface networks and satellite missions is under investigation.

A data assimilation run was performed for the period 1 April–1 November based on European surface observations of ozone. As is shown in Fig. 37.3, the analysis improved the comparison with the surface observations considerably. The biggest

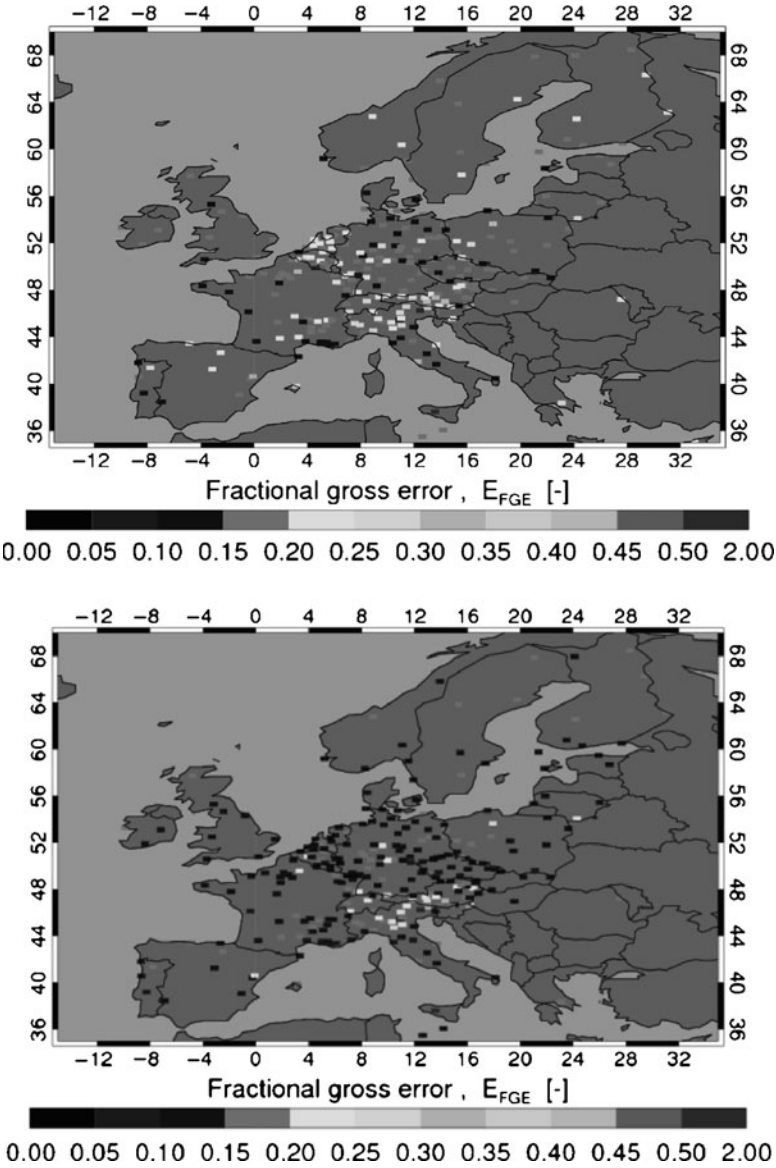


**Fig. 37.3** Impact of European ozone surface measurements on the LOTOS-EUROS v1.6 model. *Above*: Fractional gross error for the ozone daily maximum for a model only run. *Below*: Same, but now for the analysis produced by assimilating surface ozone data. Period 1 April–30 October 2007

improvements were observed at the assimilated stations, but a positive impact was also seen at stations which were not used in the assimilation.

Experiments have also been performed with the assimilation of $NO_2$ tropospheric column data measured by the OMI instrument [2, 4] on EOS-Aura. OMI data over Europe was assimilated for the period of 1 month with the ensemble Kalman filter assimilation approach. In this approach several model parameters were adjusted, namely the $NO_x$ emission strength, the VOC emissions, and the ozone boundary conditions.

The OMI data had the largest impact on the $NO_x$ emissions, which is not surprising given the direct link between $NO_x$ emissions and $NO_2$ concentrations observed. Biases observed have in the past initiated a model update where the $NO_y$ chemistry has been improved. The bias between the latest version 1.6 and OMI is much reduced, and at the same time an improvement in ozone was found. New assimilation experiments with LOTOS-EUROS are now conducted and the first results have been discussed at the ITM-2010 meeting.

## References

1. Barbu A, Segers A, Schaap M, Heemink A, Builtjes PJH (2008) A multi-component data assimilation experiment directed to sulphur dioxide and sulphate over Europe. Atmos Environ 43(9):1622–1631. doi:10.1016/j.atmosenv.2008.12.005
2. Boersma KF, Eskes HJ, Veefkind JP, Brinksma EJ, van der A RJ, Sneep M, van den Oord GHJ, Levelt PF, Stammes P, Gleason JF, Bucsela EJ (2007) Near-real time retrieval of tropospheric $NO_2$ from OMI. Atmos Chem Phys 7:2103–2118. doi:10.5194/acp-7-2103-2007
3. Denby B, Schaap M, Segers A, Builtjes P, Horalek J (2008) Comparison of two data assimilation methods for assessing PM10 exceedances on the European scale. Atmos Environ 42:7122–7134
4. Levelt PF, van den Oord GHJ, Dobber MR, Mälkki A, Visser H, de Vries J, Stammes P, Lundell JOV, Saari H (2006) The ozone monitoring instrument. IEEE Trans Geosci Remote Sens 44(5):1199–1207. doi:10.1109/TGRS.2006.872333
5. Manders AMM, Schaap M, Hoogerbrugge R (2009) Testing the capability of the chemistry transport model LOTOS-EUROS to forecast PM10 levels in the Netherlands. Atmos Environ 43(26):4050–4059. doi:10.1016/j.atmosenv.2009.05.006
6. Schaap M, Timmermans RMA, Roemer M, Boersen GAC, Builtjes PJH, Sauter FJ, Velders GJM, Beck JP (2008) The LOTOS–EUROS model: description, validation and latest developments. Int J Environ Pollut 32:270–290
7. Stern R, Builtjes P, Schaap M, Timmermans R, Vautard R, Hodzic A, Memmesheimer M, Feldmann H, Renner E, Wolke R, Kerschbaumer A (2008) A model inter-comparison study focussing on episodes with elevated PM10 concentrations. Atmos Environ 42:4567–4588. doi:10.1016/j.atmosenv.2008.01.068
8. van Loon M, Vautard R, Schaap M, Bergstrom R, Bessagnet B, Brandt J, Builtjes PJH, Christensen JH, Cuvelier C, Graff A, Jonson JE, Krol M, Langner J, Roberts P, Rouil L, Stern R, Tarrason L, Thunis P, Vignati E, White L (2007) Evaluation of long-term ozone simulations from seven regional air quality models and their ensemble. Atmos Environ 41:2083–2097. doi:10.1016/j.atmosenv.2006.10.073

## Questions and Answers

**Questioner Name**: Thomas Pierce

**Q**: Using the KF approach with surface ozone observations, which of the four model-components (NOx emissions, VOC emissions, ozone boundary conditions, ozone deposition) was most modified? Was this modification physically realistic?

**A**: All four model parameters are considerably modified during the assimilation process, but the NOx emission strength is typically one which is prominently influenced. The Kalman filter will adjust the four model parameters within the uncertainty allowed by the implementation of the error covariance initialisation/evolution. In our case this will be of order 0–50% which seems a reasonable estimate of uncertainties in these parameters. In our ensemble Kalman filter approach one single dataset (surface ozone observations) will influence the entire model state, (e.g. also NO2 or PM10) and this impact is often negative. A careful optimisation of the covariance modelling is needed to optimise the overall performance of the model.

# Chapter 38
# Examining the Impact of an Updated Toluene Mechanism on Air Quality in the Eastern US

**Golam Sarwar, K. Wyat Appel, Rohit Mathur, and Kenneth Schere**

**Abstract** Model simulations were performed using the CB05 chemical mechanism containing the base and updated toluene mechanisms for the eastern US. The updated toluene mechanism increased monthly mean 8-h ozone by 1.0–2.0 ppbv in urban areas of Chicago, the northeast US, Detroit, Cleveland, and Cincinnati compared to those with the base toluene chemistry. The updated chemistry reduced mean bias and root mean square error in ozone predictions when compared with observations greater than 85 ppbv and increased mean secondary organic aerosol from toluene by a maximum of 4%.

## 38.1 Introduction

Toluene is an important aromatic compound that can affect ozone ($O_3$) and secondary organic aerosol (SOA) in the atmosphere. However, there is currently a great deal of uncertainty about toluene chemistry [3]. Whitten et al. [7] recently proposed an updated condensed mechanism for toluene for use with the Carbon Bond 2005 (CB05) chemical mechanism. The updated toluene mechanism can better explain results of environmental chamber experiments involving toluene and oxides of nitrogen ($NO_x$). This study examines the impact of the updated toluene mechanism on air quality modeling results for the eastern US.

G. Sarwar (✉) • K.W. Appel • R. Mathur • K. Schere
Atmospheric Modeling & Analysis Division, U.S. Environmental Protection Agency, MD-E243-03, 109 T.W. Alexander Drive, Research Triangle Park, NC 27711, USA
e-mail: sarwar.golam@epa.gov; appel.wyat@epa.gov; mathur.rohit@epa.gov; schere.keneth@epa.gov

D.G. Steyn and S. Trini Castelli (eds.), *Air Pollution Modeling and its Application XXI*, NATO Science for Peace and Security Series C: Environmental Security 4,
DOI 10.1007/978-94-007-1359-8_38, 

## 38.2 Method

The study uses the Community Multiscale Air Quality (CMAQ) modeling system (version 4.7) [2] to simulate air quality. Evaluations for the CMAQ modeling system have been conducted by comparing model predictions with measured ambient pollutants [1]. The modeling domain consisted of 213 × 188 horizontal grid-cells covering the eastern US with 12-km grid spacings and 14 vertical layers; the surface layer thickness was approximately 36 m. The CMAQ chemical transport model was configured to use the mass continuity scheme to describe 3-D advection, the Asymmetric Convective Model Version 2 (ACM2) [5] to describe vertical diffusion processes, the multiscale method to describe horizontal diffusion processes, and an adaptation of the ACM algorithm for convective cloud mixing. Aqueous chemistry, aerosol processes, and dry/wet deposition were included. The meteorological driver for the CMAQ modeling system was the PSU/NCAR MM5 system (version 3.5) [4]. Initial and boundary conditions for this study were obtained from model simulation results of a larger modeling domain. Anthropogenic emissions were derived from the 2001 National Emissions Inventory and biogenic emissions were estimated using the Biogenic Emissions Inventory System (version 3.13) [6]. Two model simulations were performed using the CB05 mechanism [8] for a summer month. One simulation used the base toluene mechanism in CB05 (CB05-Base) and the other simulation used the updated toluene mechanism in CB05 (CB05-TU) [7]. The CB05-TU contains 26 chemical reactions involving 13 species for toluene oxidation while the CB05-Base contains ten chemical reactions involving five chemical species. The use of CB05-TU increased computational time of the model by approximately 3–5% compared to those with the CB05-Base.

## 38.3 Results and Discussion

The monthly mean of daily 8-h maximum $O_3$ with CB05-Base and changes in mean 8-h $O_3$ between CB05-TU and CB05-Base are displayed in Fig. 38.1. CB05-TU increased monthly mean 8-h $O_3$ by a maximum of 2.0 ppbv in Chicago, IL; 1.9 ppbv in Cleveland, OH; 1.7 ppbv in the northeastern US; 1.3 ppbv in Detroit, MI; and 1.0 ppbv in Cincinnati, OH and Louisville, KY compared to those obtained with the CB05-Base. CB05-TU also increased mean 8-h $O_3$ by 0.5 ppbv or more in several other urban areas. The monthly mean toluene to total VOC concentration ratio is also shown in Fig. 38.1. CB05-TU enhanced $O_3$ in areas with higher toluene to total VOC concentration ratios. Although not shown here, modeled VOC/$NO_x$ ratios in these areas were less than 8.0; thus these areas were VOC-limited for $O_3$ production. The impact of CB05-TU on $O_3$ occurred only in VOC-limited areas.

Day-to-day variation of the changes in the daily maximum 8-h $O_3$ is presented in Fig. 38.2 for three representative areas: Chicago, northeastern US, and Detroit. For each area, changes in daily 8-h maximum $O_3$ between CB05-TU and CB05-

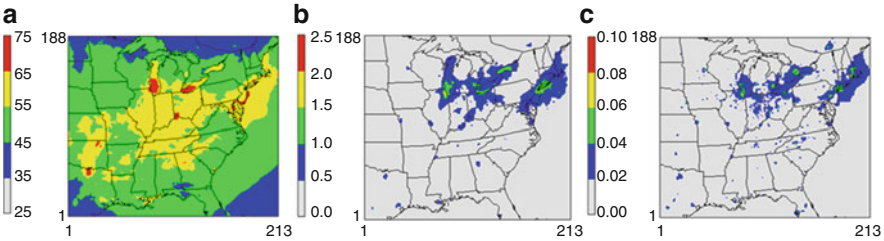


**Fig. 38.1** (**a**) Monthly mean of daily 8-h maximum $O_3$ with CB05-Base (**b**) increases in monthly mean 8-h $O_3$ between CB05-TU and CB05-Base (**c**) mean toluene to VOC concentrations ratio for CB05-Base (unit for **a** and **b** = ppbv. unit for **c** = none)

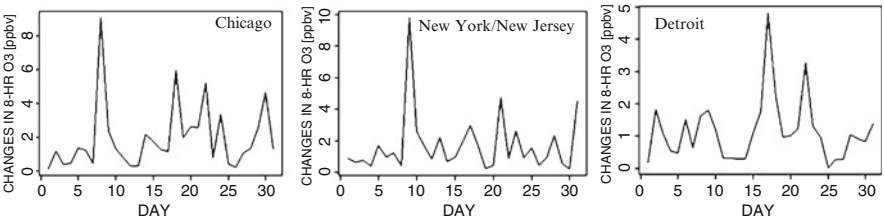


**Fig. 38.2** Variation of increases in daily 8-h max $O_3$ with the two mechanisms

Base varied from day to day. While increases were relatively high on some days, they were modest on many other days. Increases in Chicago and northeastern US were comparable while increases in Detroit were lower than those in Chicago or northeastern US.

Ozone production efficiency (OPE) is defined as the number of $O_3$ molecules formed from each $NO_x$ molecule oxidized to $NO_z$ and can be calculated from a regression of the $O_3$-$NO_z$ relationship. OPE values with CB05-TU in Chicago, the northeast US, Detroit, Cleveland, and Cincinnati were marginally lower (<0.1) compared to those with CB05-Base.

Mean bias (MB) for $O_3$ changed from 9.1 to 10.7 ppbv in Chicago, −0.53 to +0.52 ppbv in New York/New Jersey, and −4.1 to −3.1 ppbv in Detroit with CB05-Base and CB05-TU, respectively. Root mean square error (RMSE) for $O_3$ changed from 18.6 to 20.0 ppbv in Chicago, 12.7 to 12.5 ppbv in New York/New Jersey, and 12.9 to 12.5 ppbv in Detroit with CB05-Base and CB05-TU, respectively. Predictions with CB05-TU reduced both MB and RMSE at these locations when observed data were greater than 85 ppbv.

Monthly mean SOA from toluene with CB05-Base and the ratio of mean SOA obtained with CB05-TU to that from CB05-Base are shown in Fig. 38.3. The CB05-TU increased monthly mean SOA from toluene by a maximum of 4% compared to that with the CB05-Base. Locations of SOA increases generally coincided with the locations of $O_3$ increases; the largest impact occurred in the

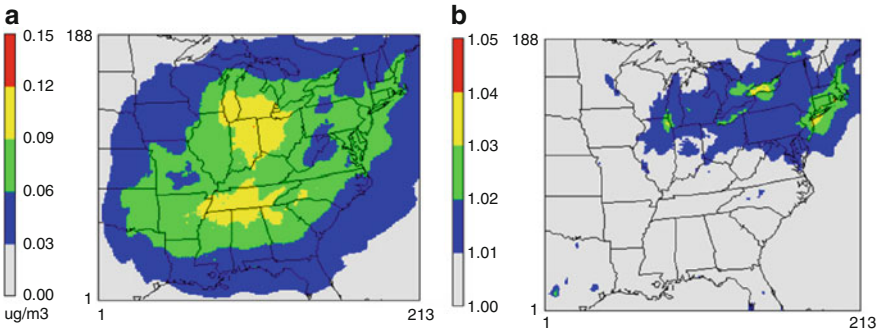


**Fig. 38.3** (**a**) Monthly mean SOA from toluene with the CB05-Base (**b**) ratio of mean SOA obtained with CB05-TU and CB05-Base

northeastern US. CB05-TU increased monthly mean hydroxyl and hydroperoxy radicals by a maximum of 19% and 20%, respectively. The impact on $PM_{2.5}$ was smaller (largest increase 1%).

## 38.4 Summary

CB05-TU enhanced the monthly mean of daily maximum 8-h $O_3$ in some urban areas in the eastern US by up to 2.0 ppbv. Results obtained with CB05-TU did not substantially change the MB and RMSE for $O_3$. CB05-TU increased SOA from toluene by a maximum of 4% compared to results obtained with CB05-Base. Next we plan to evaluate the impact of CB05-TU on air quality in the western US.

**Disclaimer** Although this paper has been reviewed by EPA and approved for publication, it does not necessarily reflect EPA's policies or views.

## References

1. Appel KW, Gilliland AB, Sarwar G, Gilliam RC (2007) Evaluation of the Community Multiscale Air Quality (CMAQ) model version 4.5: Sensitivities impacting model performance Part I-Ozone. Atmos Environ 41:9603–9615
2. Byun D, Schere KL (2006) Review of the governing equations, computational algorithms, and other components of the Models-3 Community Multiscale Air Quality (CMAQ) modeling system. Appl Mech Rev 59:51–77
3. Calvert JG, Atkinson R, Becker KH, Kamens RM, Seinfeld JH, Wallington TJ, Yarwood G (2002) The mechanisms of atmospheric oxidation of aromatic hydrocarbons. Oxford University Press, New York, 566pp
4. Grell G, Dudhia J, Stauffer D (1994) A description of the fifth-generation Penn State/NCAR Mesoscale model (MM5). NCAR Technical Note NCAR/TN-398 + STR

5. Pleim JE (2007) A combined local and nonlocal closure model for the atmospheric boundary layer. Part I: Model description and testing. J Appl Meteor Climatol 46:1383–1395
6. Schwede D, Pouliot G, Pierce T (2005) Changes to the biogenic emissions inventory system version 3 (BEIS3). In: 4th annual CMAS Models-3 Users' conference, 26–28 Sept 2005, UNC-Chapel Hill. Available at http://www.cmascenter.org/html/2005_conference/abstracts/2_7.pdf
7. Whitten GZ, Heo G, Kimura Y, McDonald-Buller E, Allen D, Carter WPL, Yarwood G (2010) A new condensed toluene mechanism for Carbon Bond: CB05-TU. Atmos Environ 44(40):5346–5355
8. Yarwood G, Rao S, Yocke M, Whitten G (2005) Updates to the carbon bond chemical mechanism: CB05. Final report to the U.S. EPA, RT-0400675. Available at www.camx.com

## Questions and Answers

**Questioner Name**: Ivanka Stajner

**Q**: The impacts on ozone in the coastal areas were mostly increases. Are these desired changes, improving the model performance?

**A**: It depends upon the circumstances. The effects of the toluene mechanism were mostly in radical-limited areas with high aromatics emissions. At high ozone concentrations (above 60–70 ppb) we saw small improvements in the model bias for ozone, while at lower concentrations the model performance showed small increases in the bias.

**Questioner Name**: Sebnem Aksoyoglu

**Q**: Will the new toluene mechanism be available for other air quality models besides CMAQ?

**A**: The new chemical mechanism is being published and is currently in an article in press in Atmospheric Environment. The publication makes the mechanism available to all modelers. We can expect to see it in new versions of the CMAQ and CAMx models within a year.

# Chapter 39
# Episodic High Surface Ozone in Central Japan in Warm Season: Relative Importance of Local Production and Long Range Transport

**Toshihiro Kitada**

**Abstract** Because of rapidly growing emission sources of photochemical smog precursors in continental countries in East Asia, people are concerned about possible strong contribution of long range transport to episodic high ozone in Japan. This study evaluates relative importance of the long range transport and local production to the episodic high surface ozone in Central Japan by using high resolution chemical transport calculation with 1 km horizontal grid.

**Keywords** Ozone • Episode • Japan • CTM • LRT

## 39.1 Introduction

Photochemical oxidant (hereafter, abbreviated as Ox, which is nearly equal to $O_3$) is air pollutant of the lowest rate, almost 0%, of compliance with the Environmental Standard in Japan. In addition, long term trend of Ox in Aichi Pref., located on the Pacific Ocean side in Central Japan, shows increase at about 0.2 ppb/y from 1979 to 2006. Under this situation, from May to July, 2007 (from April in the northern Kyushu), "warning" of high Ox (>120 ppb) was issued over the new area in eastern part of Aichi Pref., the cities of Toyohashi & Tahara in which the "warning" was never given for the last 30 years. On its reason, there may be the following two extreme views. One is (a) that the long range transport of ozone-rich air mass from the continental countries, where emissions of photochemical precursors have rapidly increased for the last decades, is the only reason, and the other one is (b) that the local (domestic) photochemical production of $O_3$ in Japan is the only reason since Japanese mega-cities still discharge huge amount of pollutants though the emissions have been

T. Kitada (✉)
President, Gifu National College of Technology, Motosu City,
Kami-Makuwa 2236-2 Gifu Pref. 501-0495, Japan
e-mail: kitada@earth.ens.tut.ac.jp

D.G. Steyn and S. Trini Castelli (eds.), *Air Pollution Modeling and its Application XXI*,
NATO Science for Peace and Security Series C: Environmental Security 4,
DOI 10.1007/978-94-007-1359-8_39, 

gradually reduced". In this paper, we will try to answer this problem, which, (a) or (b), is the main reason for high Ox concentration in the area of Central Japan on the Pacific Ocean side.

## 39.2 Observation of High $O_3$ Episode

Ozone (with ultraviolet absorption method; Model 1150 by Dylec Co. Ltd.) and NOx (with chemi-luminescence method; ECL-880US by Anatec-Yanaco Co. Ltd.) have been monitored at Nanasato-Isshiki in mountainous central Japan (see Fig. 39.1) since November, 2006; the site at 34°40′48″N, 137°57′56″E, and 404 m high above mean sea level is on the ridge of the mountains dividing Aichi and Shizuoka Prefectures. Nanasato-Isshiki is about 36 km far from Toyohashi in Aichi Pref. and 30 km from Hamamatsu in Shizuoka Pref. Toyohashi and Hamamatsu are coastal industrial cities with population of 380,000 and 800,000, respectively. In this section, on an episodic high oxidant day, 27 July 2007, local transport of O rich air mass in Hamamatsu, Toyohashi, Nanasato-Isshiki area will be discussed by comparing with those in Toyohashi, Hamamatsu, and Norikura in Gifu Pref. (see Fig. 39.1). Norikura site is at 1,940 m above mean sea level (AMSL) and its $O_3$ concentration should be mainly affected by long range transport.

In 2007, cities in the central and western Japan frequently experienced high ozone concentration episodes from April to August. As expected from the

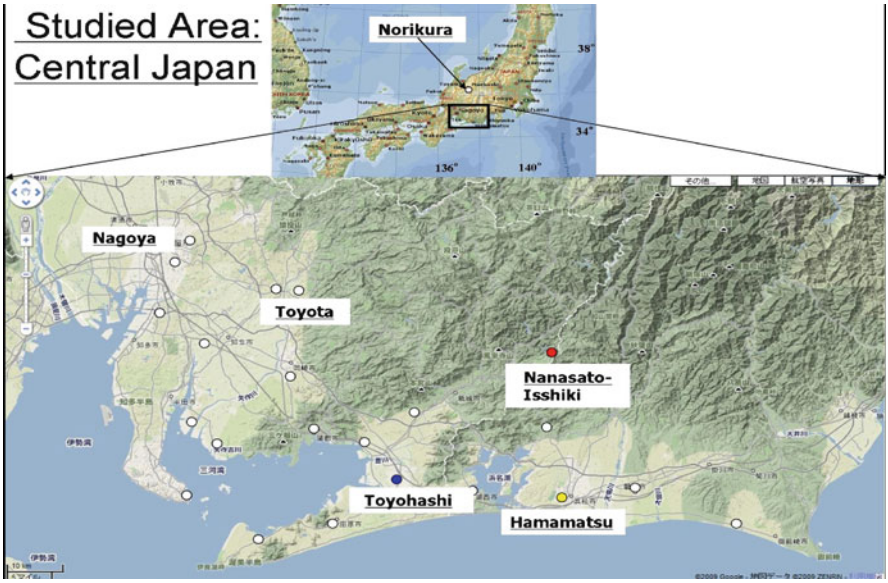


**Fig. 39.1** Area for ozone study in central Japan

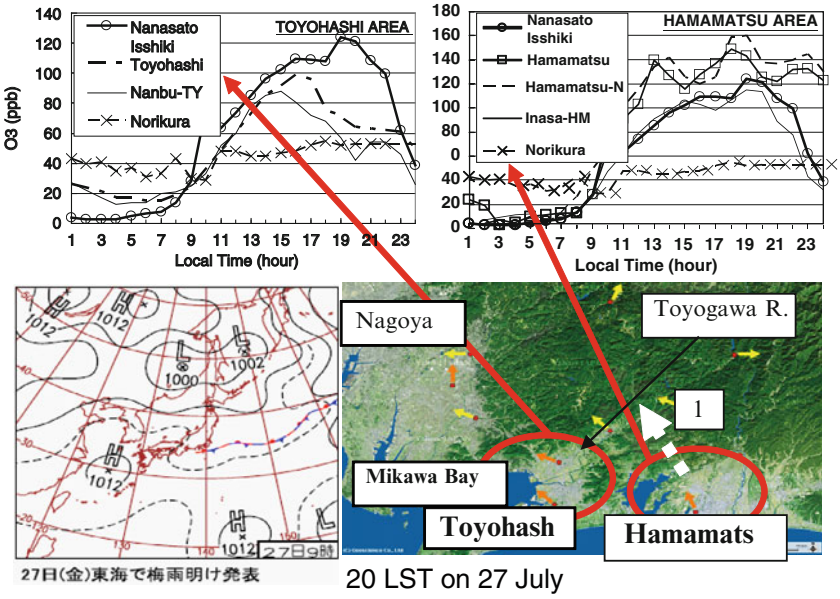


**Fig. 39.2** Diurnal variations of $O_3$ in Toyohashi and Hamamatsu areas on the episodic day; 27 July 2007, indicating $O_3$ at Nanasato-Isshiki "1" was that mainly advected from Hamamatsu

topography found in Fig. 39.1, local winds such as land/sea breeze and mountain/valley wind tend to develop in Toyohashi and Hamamatsu areas under light gradient wind and clear weather conditions dominated by high pressure system. These conditions are also suitable for photochemical smog reactions. Thus high ozone concentration episodes in this area are always associated with development of the local winds.

At Nanasato Isshiki, high $O_3$ episodes have been found to occur associated with local transport from Toyohashi or Hamamatsu (see Fig. 39.1). Extremely high $O_3$ at Nanasato-Isshiki on 27 July 2007 in Fig. 39.2 was caused mainly by transport of polluted air from Hamamatsu. As indicated in the weather map in Fig. 39.2, synoptic scale wind over the area was light northwesterly influenced by the high pressure system with its center over the East China Sea. Thus the pollutants in Nagoya area, discharged during nighttime, moved over Mikawa Bay toward Toyohashi and Hamamatsu area in the morning with land breeze enhanced by the synoptic flow. Then, in early afternoon from 12 to 16 LST, the sea breeze/valley wind along Toyokawa River transported the pollutants in Toyohashi and also originated from Nagoya to Nanasato-Isshiki with photo-chemically producing ozone (see the top-left panel in Fig. 39.2). After 1600LST, a large scale sea breeze of the southeasterly, generated by the contrast of the Pacific Ocean and the central Japan (e.g., [1–3]), brought pollutants-rich air mass in Hamamatsu area into Nanasato Isshiki (see the top-right panel in Fig. 39.2 and also the thick dotted

arrow on the bottom-right panel). Following these flow systems, it can be inferred that $O_3$ at Nanasato Isshiki was originated from Toyohashi area before 1600LST (see the top-left panel in Fig. 39.2), and was from Hamamatsu area after 1600LST. It should be noted $O_3$ at Norikura, a remote site shows only 10 ppb increase during the episode (see top panels in Fig. 39.2), suggesting long range transport in continental scale did not contribute much to this $O_3$ episode.

## 39.3 Sensitivity Study on High Ozone Episode in Coastal Mega-City, Central Japan: Local Production vs. Long Range Transport

Ozone reaching Central Japan by long range transport (from continental countries in East Asia to Japan) may have its characteristics: first, the ozone is in aged air mass with its high value and low precursors' concentrations, and thus the ozone concentration shows no significant diurnal variation (see ozone at Norikura on the top panels in Fig. 39.2); secondly, the air mass has to move over the mountains at its average height of 1–2 km to reach Japanese mega-cities on the Pacific Ocean side (see Fig. 39.3). This long-range transported ozone will be mixed with large amount of fresh NOx and NMHCs discharged in Japanese mega-cities for further photochemical smog reactions. Based on this consideration, we generated five simulation cases to evaluate relative importance of long-range transport (abbreviated as LRT) from Asian continent and local $O_3$ production in Japanese coastal city, Nagoya; Case 1, base case with no significant LRT (no-LRT) with the min $O_3$ of 30 ppb at inflow-boundary (as $(O_3)$min $=$ 30 ppb), and normal emission in Japan; Case 2, LRT case with high $(O_3) = 80$ ppb for 1–2.5 km high AMSL, and $(O_3)$min $=$ 55 ppb; Case 3, LRT case with $(O_3)$min $=$ 55 ppb only; Case 4, LRT and Japanese emissions reduced to its one-fifth (as Jpn-Emi_1/5); Case 5, same as Case 4 but Jpn-Emi_1/100 indicating almost no-Japanese emissions (Fig. 39.4).

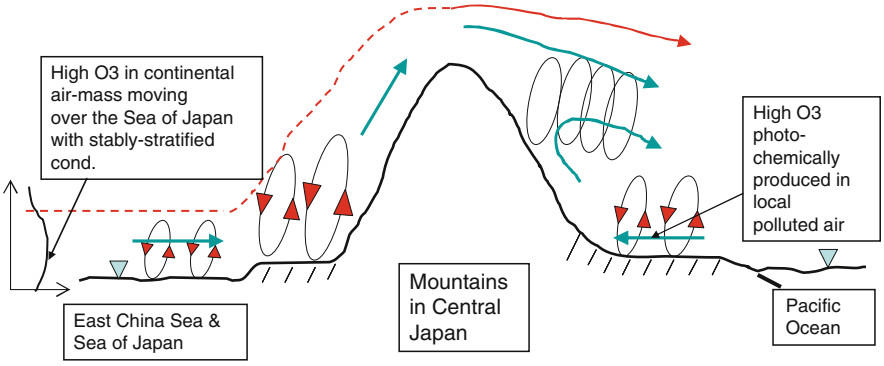


**Fig. 39.3** Schematic showing how the pollutants-rich continental air-mass migrates over East China Sea, experiences convective activity after landing on Japan, and moves over the mountains to reach the Pacific Ocean side

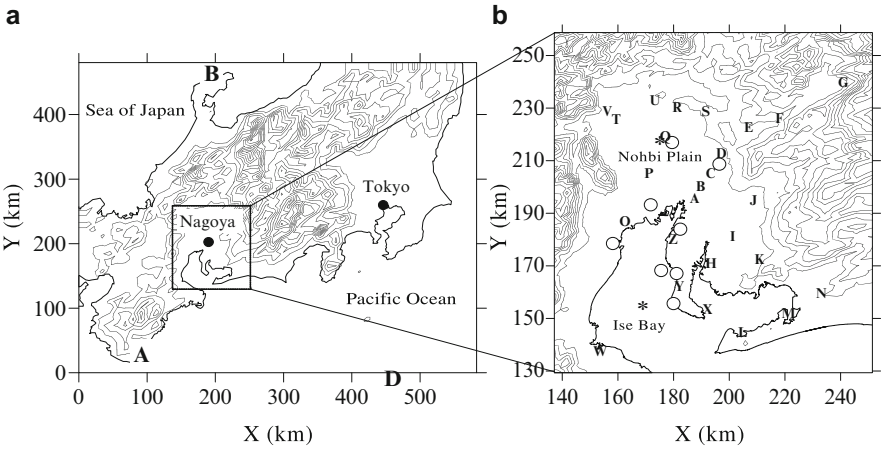


**Fig. 39.4** Domain for chemical transport simulations focused on $O_3$ concentration in five scenarios. Symbol "C" in (**b**) shows "Shidami" in northern Nagoya, where $O_3$ concentration was discussed

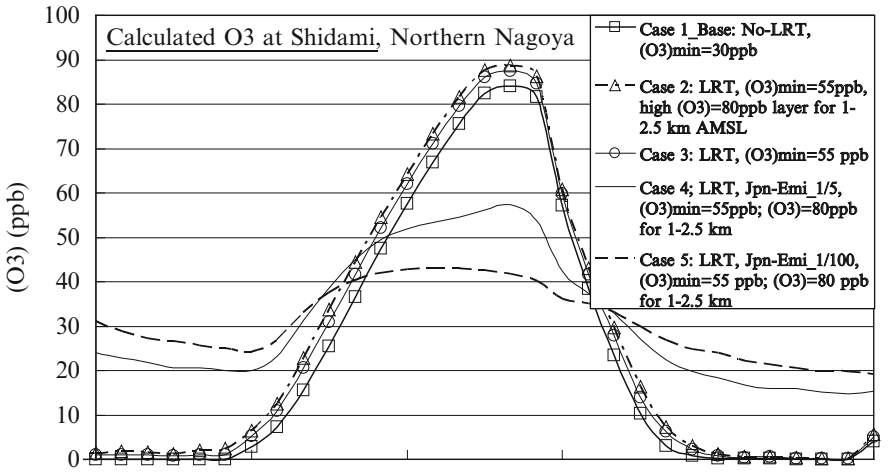


**Fig. 39.5** Calculated $O_3$ concentrations at Shidami in Case 1 (base), Case 2 & 3 for LRT conditions, and Case 4 & 5 for reduced local emissions with keeping LRT conditions. Location of "Shidami" in northern Nagoya is shown as "C" in Fig. 39.4b

Comparison of Cases 2 and 3 with Case 1 (base) in Fig. 39.5 suggests that LRT contributes to max $O_3$ by less than 10 ppb, while local $O_3$ production can explain as much as 50 ppb of daily max $O_3$. Together with Fig. 39.3, these results suggest high $O_3$ episodes in urban areas on the Pacific Ocean side, Central Japan are mainly due to local photochemical production.

## 39.4 Conclusion

Ozone monitored at Nanasato-Isshiki in mountainous rural area in Central Japan showed episodic high $O_3$ at Nanasato-Isshiki is usually associated with the transport of photochemical smog originated from the coastal urban areas of Hamamatsu and Toyohashi. Numerical simulations also quantitatively verified high $O_3$ episodes in Japanese mega-cities on the Pacific Ocean side are mainly due to local photochemical production and not due to long range transport from East Asian continental countries.

## References

1. Kitada T, Okamura K, Nakanishi H, Mori H (2000) Production and transport of ozone in local flows over central Japan – comparison of numerical calculation with airborne observation. In: Gryningand S-E, Batchvarova E (eds) Air pollution modeling and its application XIII. Kluwer/Plenum Publisher, New York, pp 95–106
2. Kitada T, Okamura K, Tanaka S (1998) Effects of topography and urbanization on local winds and thermal environment in the Nohbi Plain, coastal region of central Japan: a numerical analysis by mesoscale meteorological model with a k-ε turbulence model. J Appl Meteor 37(10):1026–1046
3. Kurita H, Sasaki K, Muroga H, Ueda H, Wakamatsu S (1986) Long-range transport of air pollution under light gradient wind conditions. J Climate Appl Meteorol 24:425–434

## Discussion

**Yosef Levitin**: What is the influence of NOx on ozone concentration in urban areas?

**Kitada**: Both NOx and NMHCs are key precursors for photochemical ozone production in urban and rural atmosphere. However, it needs several hours for ozone to be produced in boundary layer. The produced ozone comes back to the surface level by convective mixing activity, and is also transported downwind. Thus, in strong NOx emission area, discharged fresh nitric oxide rather consumes ozone and lowers its concentration temporally; our calculation also reproduced such a phenomenon in urban area.

# Chapter 40
# A European Chemical Weather Forecasting Portal

**Kostas Karatzas, Jaakko Kukkonen, Tassos Bassoukos, Victor Epitropou, and Taru Balk**

**Abstract** The European Chemical Weather Forecasting Portal (ECWFP) has been developed within the COST (European Cooperation in Science and Technology) ES0602 action, "Towards a European Network on Chemical Weather Forecasting and Information Systems". The portal provides access to the predictions of a substantial number of chemical weather forecasting systems and may be used to find out which services are available for specific (1) areas, (2) time periods and (3) pollutants. The portal serves as a "one stop shop" of chemical weather modeling services and associated information, and is currently expanding its functionalities to allow for a harmonized presentation and inter-comparison of the various available forecasts, as well as for the computation of model ensemble predictions.

**Keywords** Air quality forecasts • Environmental information portal • Model intercomparison • Image processing • Harmonization

## 40.1 Introduction

Atmospheric modeling services and methods that include a combination of weather forecasting and atmospheric chemistry simulations are here referred to as chemical weather (CW) forecasting (CWF) [7]. Relevant modeling systems are usually comprised of Atmospheric Chemistry Transport Models (ACTM) that are coupled with, or driven by Numerical Weather Prediction Models (NWPM).

K. Karatzas (✉) • T. Bassoukos • V. Epitropou
Department of Mechanical Engineering, Informatics Systems and Applications Group, Aristotle University, GR-54124 Thessaloniki, Greece
e-mail: kkara@eng.auth.gr

J. Kukkonen • T. Balk
Finnish Meteorological Institute, Erik Palmenin aukio 1, P.O. Box 503, FI-00101 Helsinki, Finland

D.G. Steyn and S. Trini Castelli (eds.), *Air Pollution Modeling and its Application XXI*, NATO Science for Peace and Security Series C: Environmental Security 4,
DOI 10.1007/978-94-007-1359-8_40, 

The definition of chemical weather therefore extends the concept of air quality forecasting [5].

Following the mandates of the EU legislation like the CAFÉ Directive (2008/50/EC), it is evident that harmonizing CW forecast and information systems would be cost-effective and beneficial for citizens, society and decision-makers across Europe. On this basis, the COST ES0602 action (www.chemicalweather.eu) has focused on the evaluation and assessment of modeling and information systems for chemical weather and air quality forecasting [5, 6]. One of the main goals of the ES0602 action is the development of mesoscale modeling capability for air pollution and dispersion applications. The Action has already collected information on the operational CWF models on a regional and continental scale in a structured form, and inter-compared and evaluated the physical and chemical structure of these models [5]. Nevertheless, there are some important steps that need to be completed before achieving the goal for providing timely CWF information to all affected users: the presentation, communication and interpretation of air quality (AQ) and CW information can be substantially improved on a European level. We have previously presented recommendations on best practices concerning the presentation and dissemination of chemical weather information [3, 8], as well as an assessment of the web – based technologies that are applied in relevant information systems [4]. The ECWFP is providing seamless access to CW information in a harmonized way, thus supporting better AQ management and the Clean Air For Europe (CAFÉ) initiative, and enhancing environmental information provision, in line with the Directive on Public Access to Environmental Information (Dir. 2003/4/EC). On this basis, the portal may also be considered as a contribution towards a Shared Environmental Information System (http://ec.europa.eu/environment/seis/index.htm).

## 40.2 An Overview of the ECWFP

Currently there is no comprehensive review of available CWF services in the internet, for the various European regions and urban areas. Even for expert users, it is therefore far from evident to find out, e.g., (1) which services are available for a specific geographic domain, (2) which of these services would be best applicable for any specific requirements, and (3) how accurate, and reliable are the forecasts of any given system. We have thus developed a European chemical weather forecasting portal that includes links to a substantial number of CW forecasts in Europe in a user-friendly graphical format. This interactive application (http://www.chemicalweather.eu/Domains), is a public domain forum, in which the forecasts can easily be viewed, accessed and added. The system is continuously updated, to incorporate various related information and services. All selected models are CWF models, i.e., these include a combination of numerical weather forecasting and atmospheric chemistry modelling. The portal includes primarily

CWF models on European and regional scales; although some urban, local and global scale models and model applications have also been included.

We have implemented the service based on Google Maps, using its default interface: by clicking on any point of interest on the map, users are presented with the CWF systems that cover the specific geographic location, and by select one of them (if many), they are presented with an overview of that system. This feature provides, e.g., with the opportunity to find all the available CWF services that cover an area of interest in Europe. The actual CW forecasts can be viewed through by selecting the name of the system, which is hyperlinked to the homepage of the specific CWF system. In addition, the ECWFP takes advantage of the Model Documentation System of the European Environment Agency (http://air-climate.eionet.europa.eu/databases/MDS/), for providing additional information concerning the various CW models used.

In submitting a CWF system to the portal, no registration is required, but the service operators need to accept the new contribution. The procedure has three stages: (1) the creation of a description of a CWF system, which is then saved in the portal, (2) to be checked, revised if necessary, and (3) approved by the system administrator. Adding a new CWF system is straightforward, and only requires the provision of basic information on the CWF system.

For all the considered CW forecasting systems, the forecasts are presented in the form of an image or a set of images, with the aid of various web-based image presentation technologies, and including various artefacts. The result is that CW forecasts are presented in a wide range of heterogeneous forms, and there is no direct way to inter-compare them even if they refer to the same geographic area of interest, for the same pollutant and period. There is also no way to combine information coming from different CWF systems, unless access is provided directly to the numerical output of the models. We have therefore developed an image harmonisation method, based on image interpolation and transformation algorithms that were developed for environmental image processing, data extraction and reuse [2]. This method allows for the proper transformation, harmonization and presentation of different CW forecasts, thus providing to the user an opportunity to compare them, or even formulate a model ensemble. The developed algorithms have been implemented as additional functions in the research version of the portal. The user may initially identify the CW forecasting systems that cover the area of interest, by clicking of the coverage map. Then, the user may select the pollutant and the CWF forecasting systems that he or she would like to include. The ECWF will subsequently parse the data, make the necessary transformation and harmonization, and present it to the user. The main advantage is that the above mentioned new services allow for a harmonized presentation, inter-comparison and combination of CW predictions, originated from independent sources. This is a unique characteristic of the ECWFP in comparison with other available corresponding portals. The ECWFP may therefore be used as a service for the harmonization and comparison of the independently available CW forecasts, as well as any other spatially attributed environmental information [1].

Regarding future developments, the ECWFP could also serve as platform, upon which various additional user- and region-customized services may be developed and operated. The portal may also be extended to include more detailed meta-information concerning the CWF models and the available forecasts in a structured manner. The COST ES0602 action is currently compiling detailed up-to-date information regarding, e.g., the categories of models, the advantages and limitations of the models, the modelled pollutants of each CWF system, the pollution source categories included, and various details of the operational implementation of the modelling systems. The provision of such supplementary information in structured format would make it feasible for the users to make more informed decisions on, for instance, which model or models respond in the best way to any specific user requirements.

**Acknowledgments** This paper has been part of the action COST ES0602 and the EU funded projects MEGAPOLI and TRANSPHORM. The authors wish to thank the whole COST ES0602 consortium, and especially those partners, who have submitted CWF systems to the portal.

## References

1. Balk T, Kukkonen J, Karatzas K, Bassoukos A, Epitropou V (2010) A European open access chemical weather forecasting portal. Atmos Environ. In Press. Available online, ISSN 1352-2310. doi:10.1016/j.atmosenv.2010.09.058
2. Epitropou V, Karatzas K, Bassoukos A (2010) A method for the inverse reconstruction of environmental data applicable at the Chemical Weather portal. In: Car A, Griesebner G, Strobl J (eds) Geospatial Crossroads @GI_Forum'10: Proceedings of the GeoInformatics Forum Salzburg. Wichmann Verlag, Berlin, pp 58–68. ISBN 978-3-87907-496-9
3. Karatzas K (2009) Informing the public about atmospheric quality: air pollution and pollen. Allergo J 18(3/09):212–217
4. Karatzas K, Kukkonen J (eds) (2009) COST Action ES0602: quality of life information services towards a sustainable society for the atmospheric environment. Sofia Publishers, Thessaloniki, 118pp. ISBN 978-960-6706-20-2
5. Kukkonen J, Klein T, Karatzas K, Torseth K, Fahre Vik A, San Jose R, Balk T, Sofiev M (2009a) COST ES0602: towards a European network on chemical weather forecasting and information systems. Adv Sci Res 3:27–33. www.adv-sci-res.net/3/27/2009/. Contributions of the 8th EMS annual meeting and 7th European conference on applied climatology
6. Kukkonen J, Karatzas K, Tørseth K, Fahre Vik A, Klein T, San José R, Balk T, Sofiev M (2009b) An overview of the COST action "Towards a European network on chemical weather forecasting and information systems". In: Karatzas K, Kukkonen J (eds) Quality of life information services towards a sustainable society for the atmospheric environment, COST Action ES0602, Workshop Proceedings. Sofia Publications S.A, Thessaloniki, pp 21–37. ISBN 978-960-6706-20-2
7. Lawrence MG, Hov Ø, Beekmann M, Brandt J, Elbern H, Eskes H, Feichter H, Takigawa M (2005) The chemical weather. Environ Chem 2:6–8. doi:10.1071/EN05014
8. Zhu L, Karatzas K, Lee L (2009) Urban environmental information perception and multimodal communication: the air quality example. In: Esposito A, Hussain A, Marinaro M, Martone R (eds) Multimodal signals: cognitive and algorithmic issues, vol 5398, Lecture Notes in Artificial Intelligence. Springer, Berlin/Heidelberg, pp 288–299

## Questions and Answers

**Questioner Name**: B. Fisher

**Q**: Many potential users like to have an expert opinion as well as an air quality forecast. Have you thought about ways of adding an expert system, or cautionary guidance, so that the information is user properly?

**A**: The intention of our system was not to offer an expert system related to air quality forecasting. Nevertheless, we believe that we contribute in making such a system possible. The necessary requirement in any system is the seamless access to the information itself, which serves as the "raw material" for services and applications. The current landscape of AQ forecasts does not provide with free, harmonized access to model results, and does not allow for comparisons and combinations of results, functions that are necessary for understanding, interpreting and use of environmental information. The ECWFP provides these functions as free services to its visitors-users, and actually moves one step ahead in the direction of services for the society as well as for the scientific community.

**Questioner Name**: C. Mensink

**Q**: What apriori information do you need to run the system? E.g. do you need any information on the geographical projection used?

**A**: We do not require any information for running the system, as it is capable of recognizing the geographic projection and other model domain application characteristics. Nevertheless, if such information was provided by modelers on their web site (or elsewhere), the application of the system would become easier and a bit faster.

**Questioner Name**: Nick Savage

**Q**: Does the existence of this portal potentially mean AQ forecasting will be unsupported as anyone can turn to a cheap web service instead of a modeling system? Who will pay for AQ forecasts?

**A**: The ECWFP depends on the existence of AQ modeling systems of high quality, so it facilitates the understanding, dissemination and use of their results but it does not replace them.

# Chapter 41
# Modeling the Impact of Urban Emissions in Russia on Air Quality in Northern Europe

**M. Makarova, A. Rakitin, and D. Ionov**

**Abstract** Accurate assessment of air quality on a regional scale and understanding the contribution of various sources is critical for developing mitigation strategies to improve air quality and protect human health. This study is a first attempt to use air quality modeling in characterizing the impact of anthropogenic emissions from urban sources in Russia on air pollution in Northern Europe. We used CMAQ to simulate concentrations of key air pollutants (CO, NO2, O3 and PM) in winter-spring of 2006. We used WRF to simulate meteorology, and SMOKE to prepare emission inputs using the official emission inventory for Russian Federation. CMAQ results were compared with the NO2 ground-based measurements of NO2, CO and O3 at Saint-Petersburg and its suburbs. We found that Saint-Petersburg is the most significant factor impacting air quality in the North-Western region of Russia. Specifically, concentrations of NO2 and CO within the lower layer in the troposphere may exceed background concentrations by 20 and 6 times (correspondingly) for St. Petersburg and its suburbs. Model results suggest that anthropogenic emissions from Saint-Petersburg can impact levels of pollutant concentrations more than 300 km away from megacity (e.g. in border countries Finland and Estonia).

## 41.1 Introduction

Air pollutants emitted into the atmosphere (CO, SO2, $NO_X$, $NH_3$, VOCs, and PM) are known to have direct and indirect effects on human health and also known to be harmful when deposited into sensitive terrestrial or aquatic ecosystems. Chemical transport models are among the primary tools used by air quality managers to assess

M. Makarova (✉) • A. Rakitin • D. Ionov
Faculty of Physics, Department of Atmospheric Physics, Saint-Petersburg State University, Ulyanovskaya 1, 198504 Saint Petersburg, Russia
e-mail: zaits@troll.phys.spbu.ru

D.G. Steyn and S. Trini Castelli (eds.), *Air Pollution Modeling and its Application XXI*, NATO Science for Peace and Security Series C: Environmental Security 4,
DOI 10.1007/978-94-007-1359-8_41, 

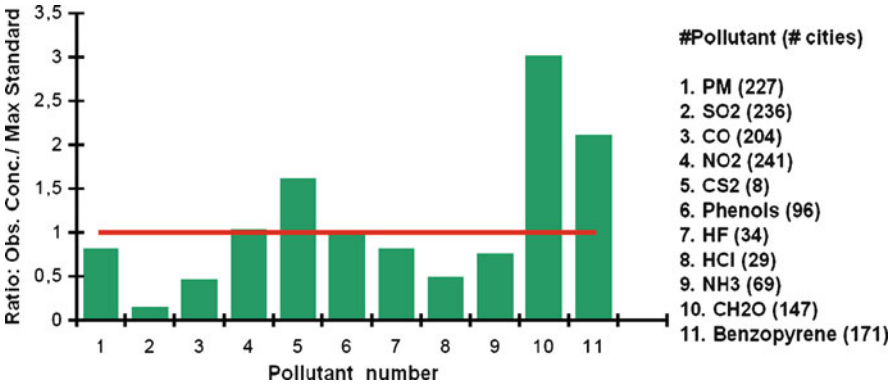


**Fig. 41.1** Relative contribution of monitored air quality concentrations for multiple pollutants in their relationship to ambient air quality standards

the impact of various sources of emissions on air quality in Europe. However, relative contribution of emissions from Russia still remains a main source of uncertainty in model simulations. Air quality monitoring data in Russia are very limited, which creates a challenge for model evaluation. This study is a first attempt to use air quality modeling in characterizing the impact of anthropogenic emissions from urban sources in Russia on air pollution in Northern Europe.

### *41.1.1 Analysis of Monitored Air Quality Concentrations in Russia*

The number of air quality monitoring stations that can be used to estimate regional levels of air pollution in central and north-western parts of Russian Federation is limited. For example, in 2008, there were only four monitoring stations in European part of Russian Federation. On the other hand, there is a large number of monitoring stations in urban areas designed to provide air quality information in highly populated areas. Two hundred and forty-eight cities in Russia have air quality stations that monitor levels of concentrations of multiple air pollutants (Fig. 41.1). Observations show that levels observed concentrations for both criteria and toxic pollutants exceed the standards in many cities across the country [3].

Analysis of measured air quality concentrations from the Russian Federal Service for Hydrometeorology and Environmental Monitoring network indicate that concentrations of several pollutants (PM, $NO_2$, and Formaldehyde) have increased over the 4-year period from 2004 to 2008. More than 67% of Russian cities (or 56.3 millions of people) show high levels of air pollution. People living in two largest urban areas of Russia, St. Petersburg and Moscow (i.e. 10% of the entire population of Russian Federation) are exposed to high levels of air pollution concentrations. There is a concern that high levels of air pollution could have a significant impact

on human health in Russia. According to the state statistics of Russian Federation [2], children morbidity increased by 20% from 2000 to 2008. There is a significant increase (more than 20%) of respiratory symptoms that can be correlated to unhealthy levels of air pollution in Russia.

### *41.1.2 Modelling Air Quality Concentrations in the North-West Region of Russian Federation*

St. Petersburg is the third largest city in Europe with population of 4.6 million people and area of 1,400 $km^2$. Therefore, accurate estimates of emissions for St. Petersburg are critical for air quality modeling. Mobile sources are one of the most significant sources of emissions in St. Petersburg. For the last 5 years, there has been a strong increase in number of vehicles in St. Petersburg (about 10% per year). In this study, we used WRF [4], SMOKE [5] and CMAQ [1] to simulate air quality concentrations in the north-western region of Russia. The simulation period was January–March 2006, when elevated levels of air pollution were observed. The modeling domain covered an area of about 800 $\times$ 800 km encompassing St. Petersburg, north-western part of Russian Federation and neighboring states.

We compared model results with observed total column CO and NO2 data from SPbSU filed measurements. The monitoring site was located in Peterhof, in the suburbs of St. Petersburg (59.88N, 29.83E). A comparison shows a good agreement between modeled and observed concentrations.

Model results indicate that the impact of anthropogenic emissions from St. Petersburg on levels of air pollution can quite high, about 40% contribution for average values of CO total column amounts. For NO2 tropospheric column, the contribution could be even more significant – up to 20 times higher as compared to its background levels. This could be an important factor to consider when measuring ambient levels of background concentrations and columns near large metropolitan areas such as St. Petersburg or Moscow. Model results show that the impact could be noticeable at long distances, up to 300 km or so. This should be taken into account when modeling air quality impact on a regional scale, considering the fact that the distance from St. Petersburg and neighboring states (Estonia and Finland) is only 150 km. Therefore, the accuracy in emission estimates for all major cities in the modeling domain (St. Petersburg, Tallinn, and Helsinki) should be comparable. The results of model sensitivity simulations indicated that the impact of emissions from St. Petersburg could result in increase of concentrations of by 0.26 ppm for CO, 22 ppb for NO2, and 2 ppb SO2 at 150 km distance, and 0.12 ppm for CO, 10 ppb for NO2, and 0.8 ppb for SO2 at 300 km distance (which is a similar distance to Tallinn and Helsinki). Examples from these sensitivity simulations are shown in Figs. 41.2 and 41.3. In these cases, air pollution due to emissions from St. Petersburg can reach its neighboring states (Estonia and Finland). Note, that westerly flow is dominant for this area, therefore, the probability of the transport of air pollution from St. Petersburg to Northern Europe is low.

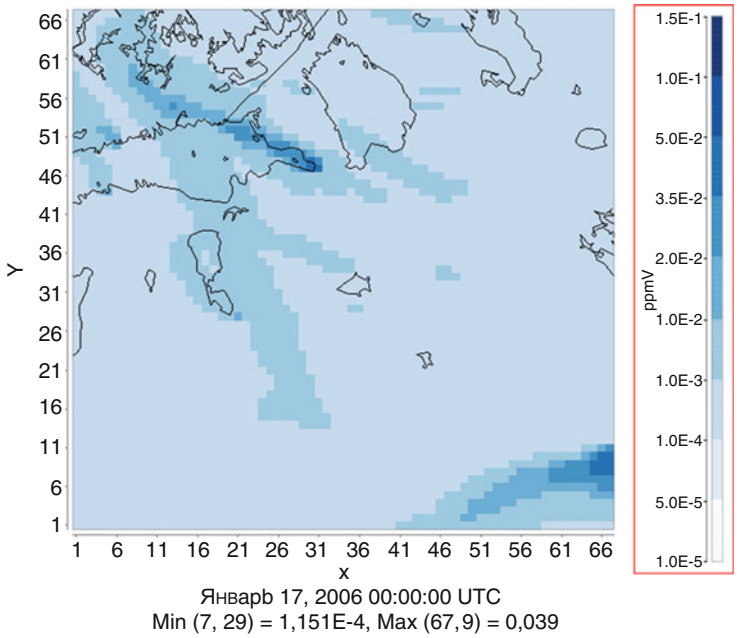


**Fig. 41.2** $NO_2$ concentrations in lowest layer on January 17, 2006 as simulated by CMAQ

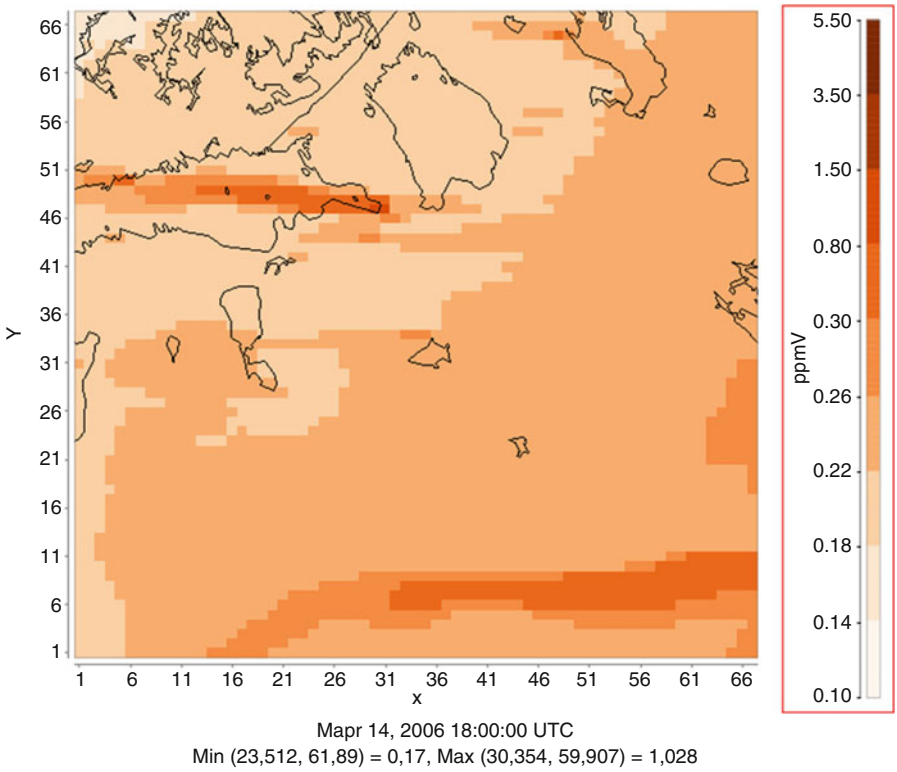


**Fig. 41.3** CO concentrations in lowest layer on March 14, 2006 as simulated by CMAQ

Air quality modeling can be a very useful tool in estimating the levels of air quality concentrations in the north-western region of Russia, where observational network is limited.

**Acknowledgements** This work was supported by the Federal Purposeful Program "Kadry" (NK-627P/17, P969).

## References

1. Byun DW, Schere K (2006) Review of the governing equations, computational algorithms, and other components of the Models-3 Community Multiscale Air Quality (CMAQ) modeling system. Appl Mech Rev 59:51–77
2. Federal State Statistics Service. http://www.gks.ru/
3. Roshydromet (Federal Service for Hydrometeorology and Environmental Monitoring) (2009) Overview of the environmental statement and pollution in Russian Federation in 2008. http://downloads.igce.ru/publications/reviews/review2008.pdf
4. Skamarock WC, Klemp JB (2008) A time-split nonhydrostatic atmospheric model for research and NWP applications. J Comp Phys 227:3465–3485
5. SMOKE Manual. http://smoke-model.org

# Chapter 42
# Aerosol Load and Characteristics in Buenos Aires: Relationships with Dispersion Mechanisms and Sources in South America

**Ana Graciela Ulke, Saulo Ribeiro Freitas, and Karla Maria Longo**

**Abstract** The aim of this contribution is to study the aerosol load in Buenos Aires in order to help characterize the contribution of distant sources and the role of the flow patterns in Southeastern South America (SESA) as dispersion mechanisms. The regional pollution in SESA is mainly due to biomass burning and the related smoke plume could be frequently observed by remote sensors from space. Observations and modeling results are combined to assess the relative importance of the biomass burning contribution to the aerosol pollution in the megacity. Buenos Aires aerosol load and derived quantities have episodic contributions from biomass burning. An increase in aerosol optical depth and Ångström coefficient and an impact in the particle size distribution are observed. A dispersion model coupled on-line with a regional atmospheric model is able to reproduce the plume pattern and evolution and the mean aerosol load.

**Keywords** Aerosol • Biomass burning • Regional pollution • Dispersion modeling

A.G. Ulke (✉)
Department of Atmospheric and Oceanic Sciences, Faculty of Sciences, University of Buenos Aires, Pabellon II - Piso 2° Ciudad Universitaria, 1428 Buenos Aires, Argentina
e-mail: ulke@at.fcen.uba.ar

S.R. Freitas
Center for Weather Forecasts and Climate Studies (CPTEC), INPE, Cachoeira Paulista, Brazil

K.M. Longo
Center for Space and Atmospheric Sciences, INPE, São Jose dos Campos, Brazil

D.G. Steyn and S. Trini Castelli (eds.), *Air Pollution Modeling and its Application XXI*, NATO Science for Peace and Security Series C: Environmental Security 4,
DOI 10.1007/978-94-007-1359-8_42, 

## 42.1 Introduction

Biomass burning activities during the dry season in central South America release to the atmosphere a considerable amount of gaseous and particle material. These pollutants are responsible for important effects in many scales, which range from the radiative budget to the hydrological cycle and population welfare. The pollution problem in South America is thus characterized by the presence of a regional plume from biomass burning, which has a seasonal pattern, and, in the megacities, the local air pollution mostly due to mobile sources. The knowledge of the apportionment of local and regional contributions to air pollution is of utmost importance to advance in the development of integrated air quality control strategies. The transport of the emitted material from central South America towards Buenos Aires, is driven by the interaction of the semi permanent flow systems with the Andes range. The variability of the flow patterns and the superimposed effects of transient perturbations result in different configurations on a daily basis. A well known feature of the regional circulation, the South American Low Level Jet (SALLJ), is responsible for the transport of substances from tropics to mid-latitudes [5]. A subset of the SALLJ, known as Chaco Jet (CJ), has a main role in the long range transport from the source region to Buenos Aires, as documented in some case studies [2, 4]. This current is normally located east of the Andes at low latitudes, is oriented NW-SE, and extends farther 30ºS. Its exit region to the Atlantic Ocean occurs generally near the Rio de la Plata. The CJ events have a baroclinic environment associated with the approach of a cold front from southern Argentina. The channeled flow east of the Andes accelerates behind the frontal surface and transports the smoke products to the megacity.

## 42.2 Data and Methodology

In order to assess the contribution from regional pollution to Buenos Aires, a 5 year period (2001–2005) is considered. The information about fire spots over South America is obtained with remote sensors and after processing, it is freely available at http://www.cptec.inpe.br. The observations of particulate matter in Buenos Aires that could give evidence of the intrusion of the regional smoke plumes consist on measurements of columnar aerosol content and derived quantities at the CEILAP-BA (34.5°S, 58°W) site of the AErosol RObotic NETwork (AERONET) from National Atmospheric and Science Administration (NASA) (http://aeronet.gfsc.nasa.gov). The regional transport mechanism (SALLJ) is diagnosed using the Global Data Assimilation System (GDAS) analyses from the National Centers for Environmental Prediction (NCEP) and a modification of Bonner's criteria [1]. The dates of occurrence of CJ in which Buenos Aires has a pre-frontal location are identified. Outputs from a high resolution modeling system (Coupled Aerosol and Tracer Transport model to the Brazilian developments on the Regional Atmospheric Modeling System (CATT-BRAMS)) for the 2002 biomass burning season are used

to explore the ability of the system to capture the events. The dispersion model includes the biomass burning emissions and their diurnal cycle and considers the different land cover types over South America to estimate the emission strength of the main gaseous and particle pollutants released during the different stages of the burning process. Wet and dry deposition removals are included and the material is considered as a passive tracer. The model is part of an air quality prediction system with two nested grids, the inner one encompassing South America with 40 km resolution.

## 42.3 Discussion

Figure 42.1 depicts the monthly evolution of the fire spots over central South America, with an increase during the burning season, from August to October.

In the considered period, the SALLJ events occurred 30% of the time, from which the CJ had a 35% frequency. The monthly mean aerosol optical thicknesses (AOT500nm), for the whole period and for the CJ events are presented in Fig. 42.2. The CJ events are associated with an increase in AOT500nm that is clearly greater during the biomass burning season. The overall climatological value for the site is 0.12. The mean AOT500nm for the CJ events during the burning season is 0.35, whereas that for the CJ during the other months is 0.13.

Figure 42.3 shows the relation between the Ångström coefficient (440–870 nm) and the AOT500nm, for the sub samples CJ and no CJ. The higher Ångström exponents during CJ show a logarithmic variation with the AOT500nm. According to the literature, this indicates an increase in the fine fraction of the aerosol load [3].

The composite field for the AOT500nm obtained with the CATT-BRAMS model for the CJ events during the 2002 burning season is shown in Fig. 42.4. The streamlines illustrate the flow at 1,500 m (the mean height of the SALLJ).

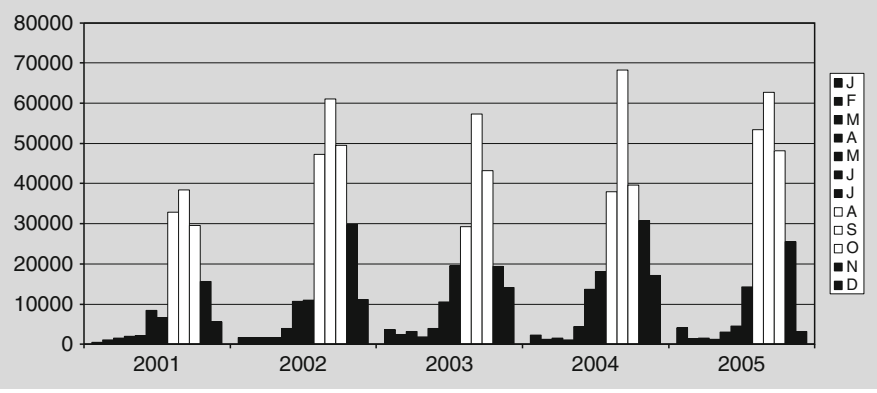


**Fig. 42.1** Evolution of the number of fires in central South America in 2001–2005

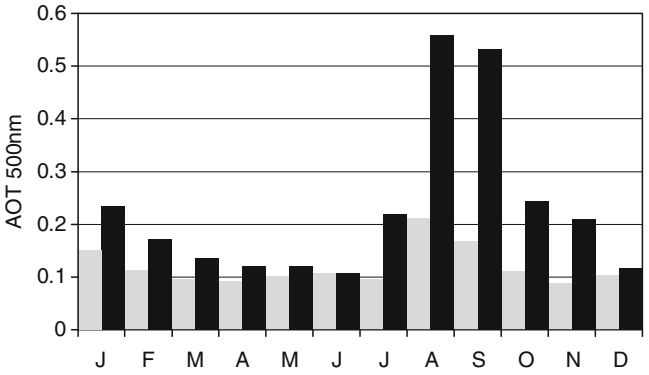


**Fig. 42.2** Evolution of the AOT500nm at CEILAP-BA in 2001–2005 (total sample: *grey bar*, CJ events: *black bar*)

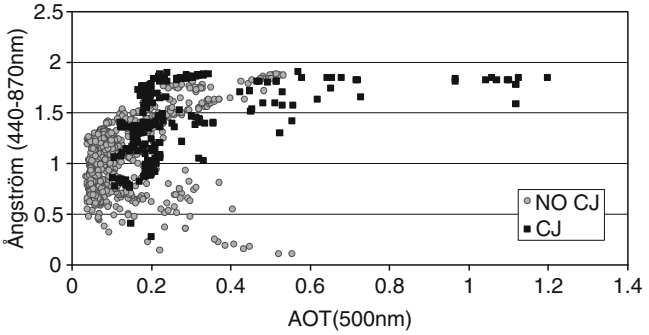


**Fig. 42.3** Variation of Ångström exponent (440–870 nm) with the AOT500nm

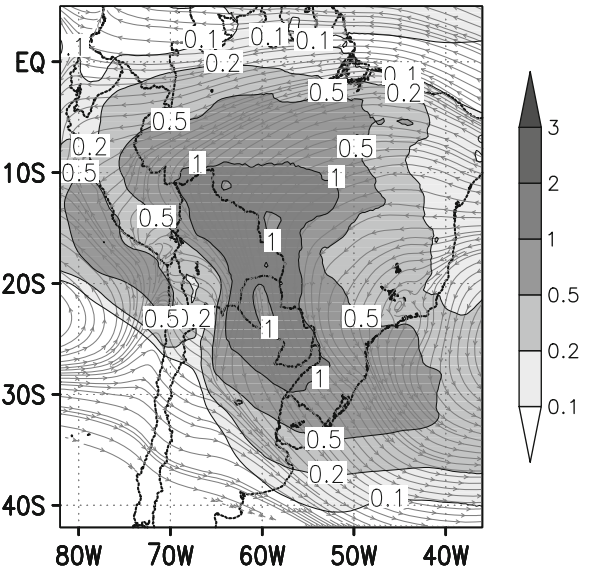


**Fig. 42.4** CATT-BRAMS composite field of AOT500nm and airflow at 1,500 m for CJ events in the 2002 burning season

During the CJ events, the modeled regional plume covers a great extent of South America and values ranging from 0.2 to 0.5 in the composite field reach Buenos Aires. This is in accordance with the mean observed AOT500nm at CEILAP-BA.

**Acknowledgments** Thanks are due to Brent Holben for the AERONET data. NCEP is acknowledged for the meteorological fields and the Center for Weather Forecast and Climate Prediction for the outputs of the CATT-BRAMS model. This research was funded by UBACyT X224 and ANPCyT PICT 1739.

## References

1. Bonner WD (1968) Climatology of the low level jet. Mon Weather Rev 119:1575–1589
2. Freitas SR, Longo KM, Silva Dias MAF, Silva Dias PL, Chatfield R, Prins E, Artaxo P, Grell GA, Recuero FS (2005) Monitoring the transport of biomass burning emissions in South America. Environ Fluid Mech 5:135–167
3. Kambezidis HD, Kaskaoutis DG (2007) Aerosol climatology over four AERONET sites: an overview. Atmos Environ 42(8):1892–1906
4. Ulke AG, Longo KM, Freitas SR, Hierro RF (2007) Regional pollution due to biomass burning in South America. Cien Nat 10:201–204
5. Vera CS et al (2006) The South American low level jet experiment. Bull Am Meteorol Soc 87(1):63–77

## Questions and Answers

**Questioner Name**: Marija Zlata Božnar, Slovenia

**Q**: Can you explain the reason for this biomass burning? Is this part of sugar cane production or other? Is it before or after the crops are collected?

**A**: Biomass burning in South America is mainly of anthropogenic origin, related to land use and land cover change, such as deforestation for agricultural use (e.g. soy); grassland management as pasture, land clearing for human settlements or pests control.

# Chapter 43
# A Numerical Investigation of Endosulfan Impact to the Great Lakes Ecosystem

**Sreerama M. Daggupaty and Jianmin Ma**

**Abstract** The Canadian Model for Environmental Transport of Organochlorine Pesticides (CanMETOP) is used to simulate concentration and deposition of Endosulphan for a period of 2 years over North American region. The preliminary model results are compared with the surface based monitored air measurements around the Great Lakes. The interannual variation and seasonal variation of endosulphan concentration are reasonably simulated and possible explanation is offered.

## 43.1 Introduction

Endosulfan is used in agriculture around the world as a wide-range pesticide with acaricide properties against a variety of insects and some mites. It is used to disinfect seeds and to kill pests over vegetable, fruit crops, cashew, tea, tobacco, and cotton crops. Endosulfan is acutely neurotoxic to both insects and mammals. It causes reproductive and developmental damage in both animals and humans. It has been banned in several countries in Europe and Asia. Endosulfan and endosulfan-bearing products were used and are still being used in North America, mostly in the United States. Given its persistence in environments and toxicity, endosulfan has been listed as a potential candidate for the inclusion into the UN-ECE Protocol on persistent organic pollutants (POPs) and the UNEP Stockholm Convention on POPs.

Significant amount of endosulfan in the atmosphere and other environment media has been observed in environmental sensitive ecosystems in North America such as the Great Lakes and pristine regions such as the Arctic. This contamination by endosulfan has raised serious concern on sources and pathways of the chemical. Numerical modeling and emission inventory studies have been carried out to assess potential sources, pathways, and source-receptor relationships.

S.M. Daggupaty (✉) • J. Ma
Air Quality Research Division, Environment Canada, 4905 Dufferin Street,
Toronto ON M3H 5 T4, Canada
e-mail: sam.daggupaty@ec.gc.ca

D.G. Steyn and S. Trini Castelli (eds.), *Air Pollution Modeling and its Application XXI*,
NATO Science for Peace and Security Series C: Environmental Security 4,
DOI 10.1007/978-94-007-1359-8_43, 

## 43.2 Emission and Environmental Fate Modeling

To establish the endosulfan inventory, a method to estimate the use of endosulfan was developed. First, information of crops on which endosulfan is applied and average endosulfan use and annual application frequencies were collected. Secondly with the help of GIS (geographic information system), the usage data of this insecticide on each crop and cropland area for each province was allocated to a grid system, with a 1/4° longitude by 1/6° latitude resolution, with a size for each grid cell of approximately 25 km by 25 km. Finally, the gridded usages are converted to air emissions using documented emission factors [5, 6].

Canadian Model for Environmental Transport of Organochlorine Pesticides (CanMETOP) was employed in the present modeling investigation. The origin of CanMETOP lies in two air pollution prediction systems one is a mesoscale model [1, 3] and the other is a regional scale model, [2] both were used for studies on atmospheric transport and deposition of trace metals. The regional model is modified for application with pesticides with the inclusion of fugacity based programs for chemical exchange and volatilization across media. CanMETOP [7] is a three-dimensional regional-scale atmospheric dispersion model coupled with a dynamic, three soil layers, Level IV fugacity-based soil/air exchange model and a water-air exchange model. Because extensive application of endosulfan in the US starts from late spring and early summer, the CanMETOP was used to simulate endosulfan transport and deposition from April 1st 2000 to December 31st 2001. For this study, the air emission inventory data developed for the year 2000 is kept invariant with actual application limited to two intermittent air emissions for 2 days (April 1 and June 1st) in each year in the modeling assessment. Chemical/physical properties of endosulfan used in the modeling study are referred to [9] and [5].

## 43.3 Results and Discussion

Higher air concentrations of endosulfan have been observed for the summer season as compared with the springtime and other seasons [9]. This has been attributed to the timing of the agricultural use of endosulfan in the U.S. [9]. Figure 43.1 shows modeled daily air concentration at the 10 m height averaged over each lake of the Great Lakes. As seen, the modeled mean concentration exhibits clear seasonality, showing higher level during warm period of years. This pattern is associated not only with the timing of application of this insecticide, but also with partitioning between air and soils which, in turn, is associated with air temperature.

Although the same emission strength in 2000 and 2001 was assumed in this study, considerable lower concentrations were predicted for 2001. In a recent analysis of measured air concentration of endosulfan over the Great Lakes region [4] found that there is a positive relationship between lower spring air temperature extending from the Midwest US to the Great Lakes and lower summer atmospheric level of the

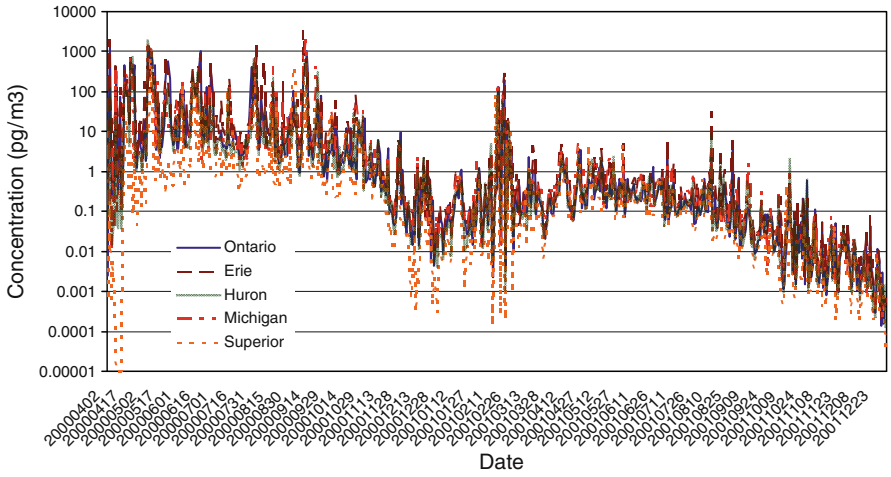


**Fig. 43.1** Modeled daily mean air concentrations averaged over each of the Great Lakes from April 1st 2000 to December 31st 2001

chemical over the Great Lakes. This relationship suggests that the lower air concentrations of endosulfan in the summertime are likely attributable to lower agricultural application of endosulfan during the summertime under lower spring air temperatures. In the present study, however, modeled lower air concentration in 2001 is related largely to lower air temperature and weaker meridional winds during the spring – summer of 2001. The former reduced re-volatilization of the chemical from soil to air, and the latter led to weaker atmospheric transport from the major source regions to the Great Lakes.

Modeled results are evaluated using measured air concentrations every 12 days over the Great Lakes by the Integrated Atmospheric Deposition Network (IADN). The IADN operates five master sampling stations for POPs on the shores of each lake [9]. Sampled atmospheric concentrations of endosulfan at Burnt Island, in northern Lake Huron, and Sturgeon point on Lake Erie were compared with the modeled concentrations at the corresponding time and at 1.5 m height and at the nearest grid point to the station locations. Figure 43.2a, b displayed modeled and sampled air concentrations in 2000 at these stations. Overall, the modeled air concentrations agree very well with the measurements at a correlation coefficient of 0.8. The time series show remarkable phase similarity with peaks and low values however magnitude wise the model underestimates atmospheric level of endosulfan as compared with the measurements. This is likely due to underestimated emission inventory and large uncertainty of chemical and physical properties of the chemical. Further Figs. 43.1 and 43.2 show a peak concentration during September 10–12, 2000 and this is due to an episodic transport of endosulfan from the southern U.S.A. to the Great Lakes. A circulation event occurred with a strong confluent zone extending from southern U.S.A to the Great Lakes. This episodic event was thoroughly studied with a case of Toxaphene transport in an earlier paper [8].

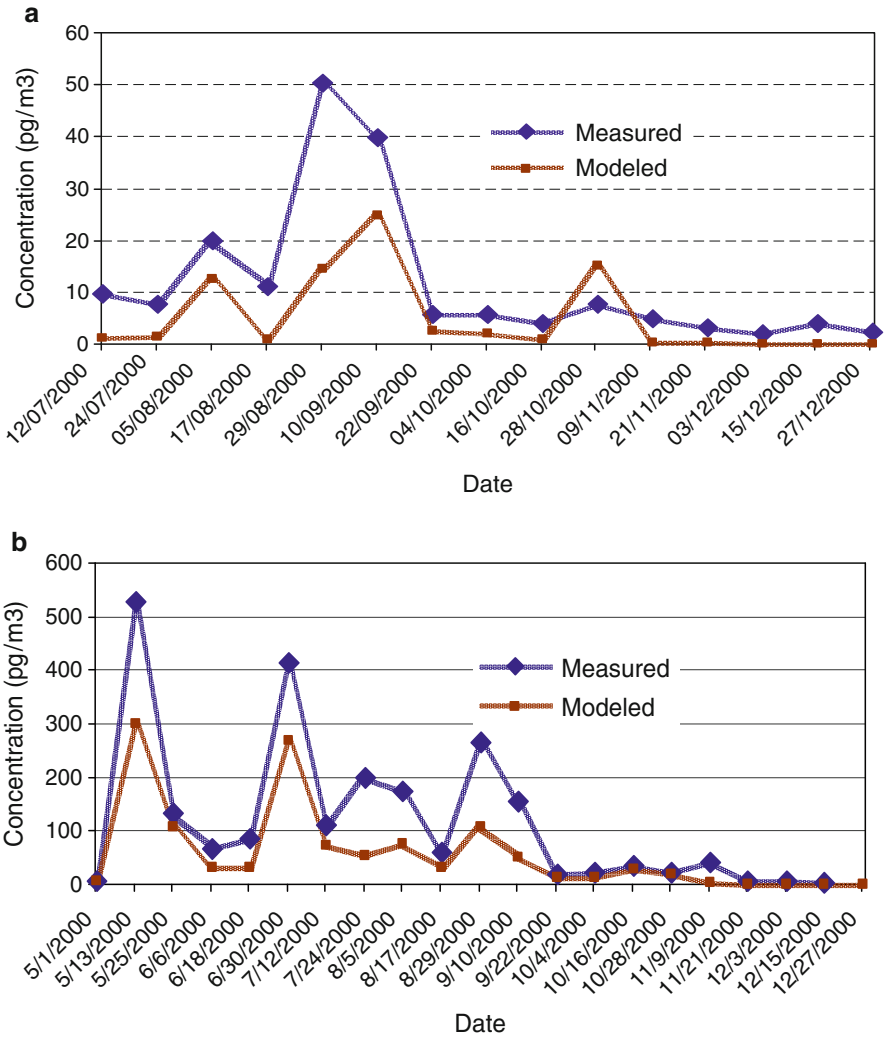


**Fig. 43.2** (**a**) Modeled and measured air concentrations at Burnt Island (Lake Huron) on IADN sampling days. (**b**). Same as (**a**) except for Sturgeon Point on Lake Erie

## 43.4 Conclusions

Modelled air concentrations of endosulfan agree reasonably well with the measured air concentrations at IADN sites. However the model underestimates measured air concentrations. It is possible that uncertainty in the amount and periodicity of emission used in the simulation could be reasons. Study of episodic events and a thorough review of emission inventory should be given a special attention.

## References

1. Daggupaty SM (2001) A case study of the simultaneous development of multiple lake breeze fronts with a boundary layer forecast model. J Appl Meteorol 40:289–311
2. Daggupaty SM, Ma J (2002) Numerically simulated atmospheric transboundary Contribution of lead loading to the Great Lakes. In: Borrego C, Schayes G (eds) Air pollution modelling and its application XV. Kluwer/Plenum Publishers, New York, pp 69–77
3. Daggupaty SM, Banic CM, Cheung P, Ma J (2006) Numerical simulation of air concentration and deposition of particulate metals around a copper smelter in northern Quebec, Canada. Geochem Explor Environ Anal 6:139–146
4. Gao H, Ma J, Cao Z, Dove A, Zhang L (2010) Trend and climate signals in seasonal air concentration of organochlorine pesticides over the Great Lakes. J Geophys Res. doi:2009jd013627
5. Jia H, Li Y, Wang D, Cai D, Yang M, Ma J, Hu J (2009) Endosulfan in China 1 – gridded usage inventories. Environ Sci Pollut Res 16:295–301
6. Li Y (2009) Endosulfan-gridded usage inventories for North America (personal communication)
7. Ma J, Daggupaty SM, Harner T, Li Y (2003) Impacts of lindane usage in the Canadian prairies on the Great Lakes ecosystem – 1: coupled atmospheric transport model and modeled concentrations in air and soil. Environ Sci Technol 37:3774–3781
8. Ma J, Venkatesh S, Li YF, Cao Z, Daggupaty SM (2005) Tracking toxaphene in the North American Great Lakes basin – 2. A strong episodic long-range transport event. Environ Sci Technol 39:8132–8141
9. Sun P, Blanchard P, Brice K, Hites RA (2006) Atmospheric organochlorine pesticide concentrations near the Great Lakes: temporal and spatial trends. Environ Sci Technol 40:6587–6593, http://pubs.acs.org/doi/abs/10.1021/es060858%2B - es0608581AF3#es0608581AF3

## Questions and Answers

**Questioner Name**: Volker Matthias

**Q**. Endosulfan has long half life time of 9 months to 6 years. Therefore you should consider Endosulfan from outside your domain at the boundaries. How did you do this?

**A**. You are right if your intent is to know the overall effect due to global sources. But we are not planning that in this study. We are interested only to know the impact due to North American sources. This will help in regulating North American sources.

A monitoring station might be recording due to sources outside the domain, but it does not matter as long as we repeat the experiments with and without particular sources in the domain. Then we will be identifying the relative influence of each and every significant source in the domain.

# Chapter 44
# Bulgarian Emergency Response System for Release of Hazardous Pollutants – Design and First Tests

**Angelina D. Todorova, Kostadin G. Ganev, Dimiter E. Syrakov, Maria Prodanova, Georgi J. Georgiev, Nikolai G. Miloshev, and Georgi K. Gadzhev**

**Abstract** The present paper demonstrates some preliminary results of the set up and testing of a system for modelling of toxic air pollution due to possible accidents in industrial sites. Risk assessment for the region of "Vereya Him" factory, Yambol, Bulgaria is performed. The modelling tools used for this study are: WRF, CMAQ and SMOKE. The CB05 toxic chemical mechanism, including chlorine reactions, is used. The shown numerical results demonstrate the practical value of the preparedness mode of the planned emergency response system.

**Keywords** Modelling • Emergency response • Chlorine • US EPA models-3 system

## 44.1 Introduction

The present work demonstrates some preliminary results produced by the Bulgarian system for emergency response. The system should supply the authorities, the relevant international organizations and the public with information, which will make possible proper measures for diminishing the damages, caused by accidental harmful releases in the atmosphere, to be planned. The planned modelling system will have the potential to assist emergency managers in three stages:

A.D. Todorova (✉) • K.G. Ganev • G.J. Georgiev • N.G. Miloshev, • G.K. Gadzhev
Geophysical Institute, Bulgarian Academy of Sciences, 3, Acad. G. Bonchev str., 1113 Sofia, Bulgaria
e-mail: imdnme@gmail.com

D.E. Syrakov • M. Prodanova
National Institute of Meteorology and Hydrology, Bulgarian Academy of Sciences, Sofia, Bulgaria

D.G. Steyn and S. Trini Castelli (eds.), *Air Pollution Modeling and its Application XXI*, NATO Science for Peace and Security Series C: Environmental Security 4,
DOI 10.1007/978-94-007-1359-8_44, 

In preparedness mode, "risk analysis" will be performed. It will result in a set of risk assessments for different emergency scenarios for selected "hot spots". These assessments can be of a direct use for immediate emergency response (for example evacuation of people from the pollution exposed regions, proper assignment of medical teams) in order to minimize the pollution impact on human health.

In the operational mode the system will produce fast short-term forecast of the pollutant propagation in local and regional scale. This information will help the authority decisions about the immediate measures and activities to be carried out. This information will also warn the international community of possible trans-boundary harmful pollutant transport.

In the off-line mode the modelling system will produce a more detailed and comprehensive analysis of the possible longer-term impact of the harmful releases on the environment and human health in local to regional scales, including the whole Balkan region.

The intension is to elaborate a system based on up-to date and complex meteorological and pollution transport models with proved high-quality simulation performance and possibility to follow the accidentally released harmful gases from local to European scale, accounting for the mesoscale dynamic phenomena, to 'zoom-in' and obtain a detailed air pollution evaluation in the particularly damaged regions.

The work on the system is still going on, so some results from the system preparedness mode will be demonstrated in this paper.

## 44.2 Modeling Tools

It was decided the system to be based on the following models: **WRF** – [3], used as meteorological pre-processor; **CMAQ** [1] – the Chemical Transport Model (CTM) of the system. A chlorine chemical mechanism has been added to CMAQ based on [4]. **SMOKE** [2] – the emission pre-processor.

### *44.2.1 Some Examples of the System Risk Assessment Simulations*

#### 44.2.1.1 Brief Description of the Numerical Experiments

The risk may generally be defined as a product of probability (recurrence) of happening of a given event and the impact of this event (in the particular case on human health). Applying this definition to the problem of air pollution impact this

means that an event occurring with high probability, even with relatively low impact, may result in higher risk than a rare event with stronger impact. For the needs of the emergency response preparedness mode a map of the risk (the product of probability and impact) around potential sources of emergency toxic gas releases should be constructed. The impact should be evaluated by some metrics directly giving the effect of toxic gas on human health – in this case the national regulatory threshold values (defined for $Cl_2$ and HCl), so the risk is simply the probability these thresholds to be exceeded. Following this definition of risk it is clear that a large number of simulations of the toxic gases (primary as well as secondary) dispersion around the potentially dangerous site should be made under comprehensive set of meteorological conditions and for different accidental release times. The averaged over this ensemble concentration fields should be treated as an assessment of the potential risk.

The simulations are made for year 2008 for an instantaneous release of 25 t chlorine ($Cl_2$) released at the site of "VEREYA-HIM" Yambol between 3 and 4 o'clock in the morning. The simulations are carried out in three nested domains for downscaling the problem to a horizontal resolution of 1 km around the site

#### 44.2.1.2 Brief Discussion of the Numerical Results

The probabilities surface concentration fields of $Cl_2$ (the primary pollutant) and HCl (one of the secondary pollutants) to exceed the respective threshold values are demonstrated for the four seasons and for the whole year (the annual probability for $Cl_2$ is shown in Fig. 44.1). There are several things about the probability fields that should be mentioned:

1. The secondary pollutant concentrations may also exceed the regulatory threshold;
2. The probability fields are quite different for the different seasons (the HCl concentrations during winter never exceed the threshold), which yet again demonstrates the importance of the meteorological conditions for the pollution field pattern. The probability field pattern is pretty complex for both $Cl_2$ and HCl, still a tendency for spreading the pollution in SW-NE direction could be seen, which probably reflects some local circulation specifics;
3. Non-zero probabilities could cover a big domain around the "VEREYA-HIM" site. This is a good demonstration why the risk assessment is necessary. It can be seen that significant risk could happen far from the site and with temporal delay, that some of the roads (evacuation of the population) at certain time could be rather risky, etc.

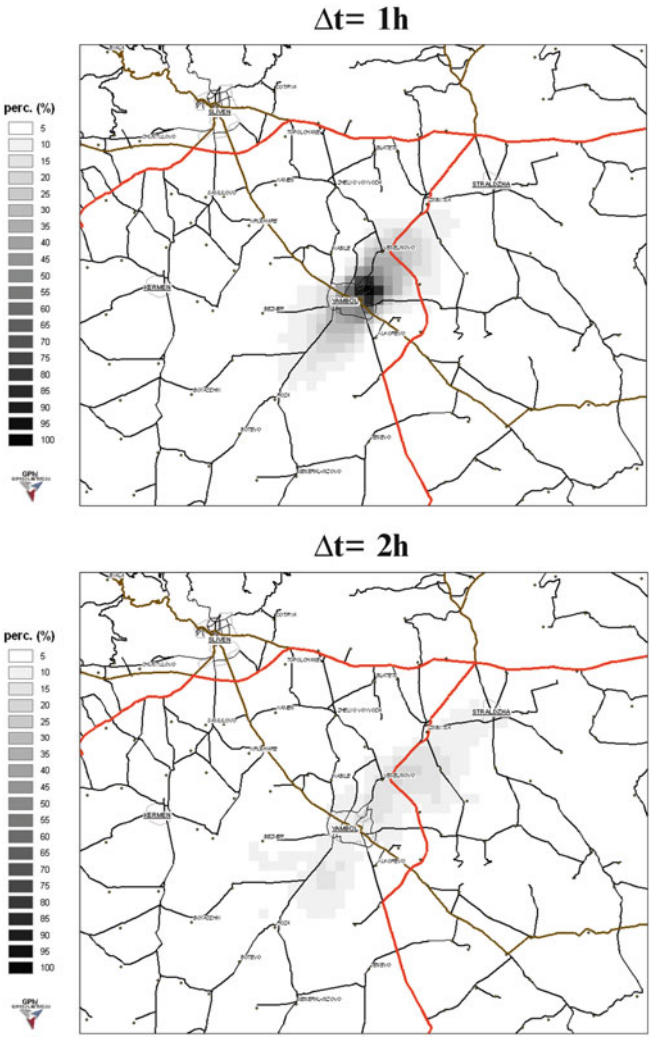


**Fig. 44.1** Annual fields of probability surface $Cl_2$ concentrations to exceed the threshold value for times $\Delta t = 1$ h and 2 h after the release

## 44.3 Conclusions

The shown results are very preliminary. In order to achieve a real assessment of the risk simulations should be made for a much larger set of meteorological conditions (probably several years in order to account for the seasonal variability) and for

much more release times in order to account for diurnal variability. At this stage of the system development, however, it can be concluded that:

1. The chosen modelling tools are probably suitable for this particular task and the obtained preliminary results are quite realistic and promising;
2. The shown numerical results very well demonstrate the practical value of the preparedness mode of the system.

**Acknowledgments** The present work is supported by the projects NATO ESP.EAP.SFPP 981393, SEE-GRID-SCI – contract No FP7 –RI-211338, as well as by the Bulgarian National Science Fund (grants No Д002-161/2008 and Д002-115/2008).

Deep gratitude is due to US EPA, US NCEP and EMEP for providing free-of-charge data and software. Special thanks to the Netherlands Organization for Applied Scientific research (TNO) for providing us with the high-resolution European anthropogenic emission inventory.

The work of the young scientists A. Todoriva, G. Jordanov and G. Gadzhev is also supported by the ESF project No BG51PO001-3.3.04-33/28.08.2009. G. Gadzhev is World Federation of Scientists grant holder.

## References

1. Byun D, Ching J (1999) Science algorithms of the EPA Models-3 Community Multiscale Air Quality (CMAQ) modeling system. EPA Report 600/R-99/030, Washington DC
2. CEP (2003) Sparse Matrix Operator Kernel Emission (SMOKE) modeling system. University of Carolina, Carolina Environmental Programs, Research Triangle Park
3. Shamarock et al. (2007) A description of the Advanced Research WRF Version 2. http://www.mmm.ucar.edu/wrf/users/docs/arw_v2.pdf Accessed 15 June 2010
4. Tanaka PL, Allen DT, McDonald-Buller EC, Chang S, Kimura Y, Yarwood G, Neece JD (2003) Development of a chlorine mechanism for use in the carbon bond IV chemistry model. J Geophys Res 108:4145

## Questions and Answers

**Questioner Name**: Steven Hanna

**Q**: Do you have a plan to use a smaller-scale plume model , since the major effects of chlorine release (even 90 t from a railcar) are observed to be limited to downwind distances of less than 10 km

**A**: In the National Environmental Agency (as far as I know), they have already made such assessments for "VEREYA-HIM" Yambol. In our study we want to have chemical reactions and secondary pollutants.

**Questioner Name**: Gabriele Cura

**Q**: Do you have suggestions for a strategy to validate your "emergency response" system?
**A**: We haven't had an accident in Bulgaria yet. I hope that we will never have to validate it.

**Questioner Name**: Prof. M. Biliaiev

**Q**: What was the domain resolution? Maybe your artificial viscosity will suppress the physical one.
**A**: The innermost domain has a resolution of 1 km.

**Questioner Name**: Prof. M. Biliaiev

**Q**: Do you take into account in the model, that HCl is a heavy gas?
**A**: I haven't examined the chlorine mechanism in such details. In order to find the answer, one has to look at the values of the deposition velocity for HCl, which is calculated inline in the model.

# Chapter 45
# Towards High-Resolution Environmental Modelling in the Alpine Region

**Delia Arnold, Irene Schicker, and Petra Seibert**

**Abstract** An evaluation of mesoscale meteorological simulations using MM5 and WRF in respect to air pollution conditions during a winter episode in January/February 2004 in a steep Alpine valley, the Inn Valley, is carried out. Static input fields, e.g. landuse, delivered with the model have been evaluated and compared to latest available data. Comparison of e.g. landuse data indicate that an update to the existing CORINE landuse data would be useful. Results of the MM5 simulations show that grid resolutions of at least 1 km or higher are needed to realistically represent the meteorological conditions in steep and narrow valleys.

**Keywords** MM5 • WRF • Alpine valley • CORINE

## 45.1 Introduction

The highly populated areas and main traffic pathways in the Alpine region are mainly located at the valley floors which are seldom wider than a few kilometres. The surrounding topography, with steep slopes and high mountains, together with the high emission density in the valleys, are a major factor for poor air quality conditions with repeated exceedance of limits in these regions. In order to asses and evaluate in

D. Arnold (✉)
Institute of Meteorology, University of Natural Resources and Life Sciences,
Peter-Jordan Str. 82, 1190 Vienna, Austria

Institute of Energy Technologies, Technical University of Catalonia,
Diagonal 647, 08028 Barcelona, Spain
e-mail: delia.arnold@boku.ac.at

I. Schicker • P. Seibert
Institute of Meteorology, University of Natural Resources and Life Sciences,
Peter-Jordan Str. 82, 1190 Vienna, Austria

D.G. Steyn and S. Trini Castelli (eds.), *Air Pollution Modeling and its Application XXI*,
NATO Science for Peace and Security Series C: Environmental Security 4,
DOI 10.1007/978-94-007-1359-8_45, 

a realistic way the influence of complex topography on the transport patterns in such regions, high resolution meteorological and atmospheric transport modelling is required. However, higher horizontal resolution results in steeper model surfaces, which introduces additional errors, since most models have not been developed for the use in steep and complex topography. Typical effects of such problems are wrong spatial distribution and/or wrong amount of precipitation, and inability to properly reproduce the temperature and wind regimes inside valleys. Approaches where only some components are treated at high resolution are insufficient as this does not remove numerical errors and does not consider the dynamical linkage between the scales. In some non-hydrostatic meteorological models improvements for steep topography have been introduced in the past years. Further improvements, especially a possibility to easily use DEM and land-use data at corresponding high resolution (e.g. the SRTM 3″ DEM), still need to be implemented.

Within this context the project HiRmod (High-Resolution Atmospheric Modelling in Complex Terrain for Future Climate Simulations) [3] has appeared as an attempt to give better background and improved model capabilities for climate studies in regions with complex topography, such as the Inn valley, which require horizontal resolutions of ~1 km. The results if this project may be applied not only in a climate context but also in air quality studies.

## 45.2 Models and Methods

The Pennsylvania State University/NCAR Mesoscale Model MM5 [2] and its daughter model, the Advanced Research Weather Research and Forecasting model [5] have been selected as the appropriate models for the scales and complexity involved in this project. As a first step, an evaluation of their performance when both the vertical and horizontal resolution is increased (with innermost domains down to 0.2 km and up to 90 vertical levels) is carried out in three main target areas, the Black Forest, the Inn Valley and the Vienna basin. Following this first evaluation, the introduction of better digital elevation, such as the SRTM 3″ data, and land use data, such as the CORINE data. A configuration of five nested domains has then been arranged in the Inn Valley ROI. For the three innermost domains, WPS has been run with and without the two new datasets to compare the differences. As summarised in Table 45.1 the number of pixels that differ in landuse when using CLC2000 is close to 70%. This underlines the importance of using the non-standard land-use data set, even if it would not be needed for resolution. The use of a high resolution elevation model (DEM) gives higher maximums and lower minimums since the orographic features are less smoothed. The RMSE is exceeding 100 m even at a model resolution of 2.4 km which would indicate that the SRTM data should be important.

In order to assess the influence of the improved meteorological modelling in the dispersion calculations typically used in air quality applications, further simulations

**Table 45.1** WPS output with GTOPO30 and SRTM, and with USGS and CLC2000 land use data, for Innsbruck. The percentage of grid cells that change the landuses, the maximum and minimum elevations and the elevation RMSE. Switzerland is not included in CLC2000 data; Swiss grid points have therefore been considered as missing and do not contribute to the percentage of differing pixels

| | | Land use | Elevation | | |
|---|---|---|---|---|---|
| Domain | Grid distance | % grid points that differ | SRTM (max/min) | GTOPO30 (max/min) | RMSE |
| D3 | 2.4 km | 65 | 31/3,544 | 26/3,619 | 105 |
| D4 | 0.8 km | 74 | 244/3,534 | 222/3,525 | 126 |
| D5 | 0.27 km | 78 | 448/3,608 | 449/3,505 | 157 |

**Table 45.2** Number of domains and their respective sizes for three different domain configurations

| | Grid spacing in km | | | | | |
|---|---|---|---|---|---|---|
| Run # | D1 | D2 | D3 | D4 | D5 | D6 |
| Run 2 | 64.8 | 21.6 | 7.2 | 2.4 | – | – |
| Run 3 | 64.8 | 21.6 | 7.2 | 2.4 | 0.8 | – |
| Run 4 | 64.8 | 21.6 | 7.2 | 2.4 | 0.8 | 0.27 |

with the FLEXPART Lagrangian particle dispersion model in its MM5 [4]and WRF [1] versions will be performed. The obtained different source receptor sensitivities for stations within the target regions will then be compared. Additionally, dispersion calculations, if folded with the appropriate emission inventory, can be directly compared with monitoring data of radon and other trace gases at the stations and provide a useful tool to give a deeper insight on the influence of the resolution and input data in the whole modelling procedure.

### *45.2.1 Example: The Inn Valley*

The evaluation procedure has already started in the three main target areas. As an example, it is shown here the meteorological MM5 simulations with different domain configurations for the Inn Valley with increasing number of domains and resolutions (Table 45.2) but keeping the main set-up of the model regarding parameterizations. Run 2, with just four domains, is unable to represent properly the 2-m temperature diurnal cycle within the valley (Fig. 45.1) although at 2.4 km the valley starts being resolved. Runs 3 and 4 show clear improvement when looking at the D5 (0.8 km) temperature time series, and slightly better results are achieved when a 6th domain with higher resolution is added even without the improved input data regarding land uses and elevation.

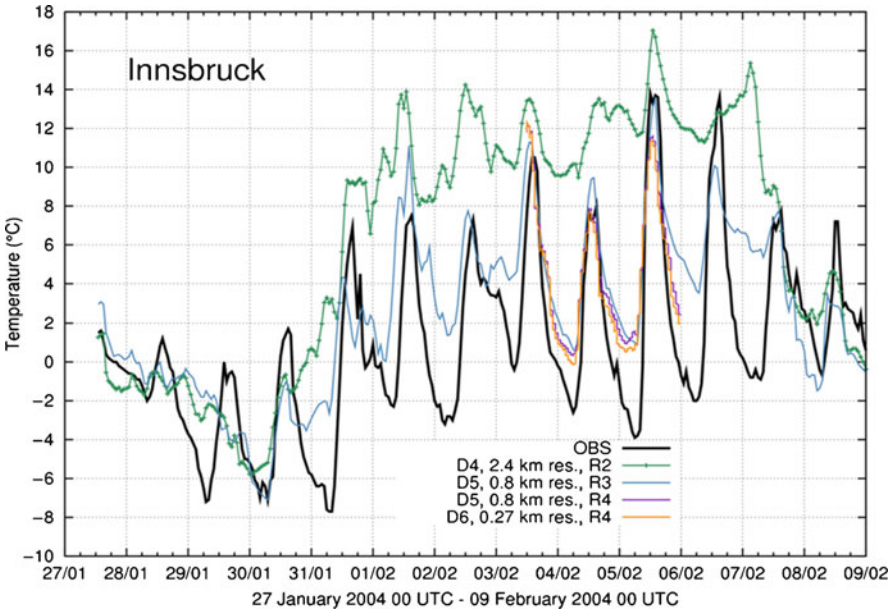


**Fig. 45.1** Comparison of observed (*OBS*) and modelled temperature for Innsbruck University (577 m) for the innermost domains of the runs specified in Table 45.2

## 45.3 Conclusions and Outlook

Several issues have already been addressed in the first evaluation runs. Amongst them the most important are that increasing the horizontal resolution gives more realistic model results in places with complex topography even without adding high resolution elevation data and CORINE land uses. Especially areas like narrow valleys require the inclusion of orographic shading in the simulations.

The evaluation procedure continues with the analysis of WRF model performance in the target areas. Additionally, introduction of the aforementioned better input data is being done for both models.

A final set of recommendations and optimal set-ups and modelling tools will be provided as outcome of the HiRmod project.

**Acknowledgments** HiRmod is funded by the Austrian This project is funded by "Klima- und Energiefonds".

The computational results presented have been achieved [in part] using the Vienna Scientific Cluster (VSC).

## References

1. Fast JD, Easter RC (2006) A lagrangian particle dispersion model compatible with WRF. 7th WRF Users' Workshop, NCAR, 19–22 June, Boulder, p 6.2
2. Grell G, Dudhia J, Stauffer D (1994) A description of the fifth-generation Penn State/NCAR Mesoscale Model (MM5). NCAR/TN-398+STR. (http://www.mmm.ucar.edu/mm5/)
3. HiRmod (2010) http://www.boku.ac.at/met/envmet/hirmod.html
4. Seibert P, Skmorowski P (2007) Untersuchung der orographischen Besonderheiten der Probennahmestellen Schauinsland und Freiburg und deren Auswirkungen auf die Genauigkeit von adjungierten atmosphärischen Ausbreitungsrechnungen. Bundesamt für Strahlenschutz, Salzgitter / Freiburg. Schriftenreihe Reaktorsicherheit und Strahlenschutz, BMU – 2008 – 713. http://www.bmu.de/strahlenschutz/schriftenreihe_reaktorsicherheit_strahlenschutz/doc/4187
5. Skamarock WC, Klemp JB, Dudhia J, Gill DO, Barker DM, Duda DM, Huang X-Y,. Wang W, Powers JG (2008) A description of the Advanced Research WRF Version 3. NCAR Technical Notes-475+STR. (http://www.mmm.ucar.edu/wrf/)

# Chapter 46
# Modelling the Impact of Best Available Techniques for Industrial Emissions Control in Air Quality

**Angel Rodríguez, Santiago Saavedra, Maria Dios, Carmen Torres, Jose A. Souto, Juan J. Casares, Belen Soto, and Jose L. Bermúdez**

**Abstract** The strategies for industrial emissions control depend on, amongst other variables, the best available techniques, their economical feasibility, and their positive impact over air quality; i.e., advances in power generation technology are making older coal and fuel oil power plants to be replaced by natural gas combined cycles. In ITM 2007, the estimation of the impact of the application of best available techniques (BATs) in industrial emissions control in Galicia (NW Spain) was presented [Rodríguez R et al (2008) Modelling the impact of best available techniques for industrial emissions control in air quality: setting up inventories and establishing projections. In: Air pollution modeling and its application XIX. Springer, Dordrecht, pp 677–678]. In this work, the effect of these changes over the tropospheric ozone levels in this region is simulated using the CAMx model, for three different ozone episodes previously characterised.

**Keywords** Industrial emissions • BATs • Tropospheric ozone episodes • CAMx model

A. Rodríguez (✉) • S. Saavedra • M. Dios • J.A. Souto • J.J. Casares
Department of Chemical Engineering, University of Santiago de Compostela, 15782 Santiago de Compostela, Spain
e-mail: angel.rodriguez@usc.es

C. Torres
Department of Chemical Engineering, University of Santiago de Compostela, 15782 Santiago de Compostela, Spain

Department of Chemical Engineering, University of Rovira i Virgili, 43007 Tarragona, Spain

B. Soto • J.L. Bermúdez
As Pontes Power Plant, Endesa, 15320 As Pontes de García Rodríguez, Spain

D.G. Steyn and S. Trini Castelli (eds.), *Air Pollution Modeling and its Application XXI*, NATO Science for Peace and Security Series C: Environmental Security 4,
DOI 10.1007/978-94-007-1359-8_46, 

**Table 46.1** NOx emission changes between year 2001 (reference inventory) and 2010 (projected inventory), in the three power plants locations

| | | NOx (Tm/year) | | |
|---|---|---|---|---|
| Source | Emission level (m) | 2001 data | 2010 projection | Change |
| Sabón | 200 (aloft) | 833 | 738 | +320% |
| | Low height | – | 2,764 | |
| Meirama | 200 (aloft) | 9,059 | 1,604 | −83% |
| As Pontes | 356 (aloft) | 20,035 | 6,863 | −52% |
| | Low height | – | 2,764 | |

## 46.1 Field Data

For the evaluation of emissions changes impact in air quality, three different tropospheric ozone episodes previously registered at Galicia were chosen: episode 1 (14–23 July 2002), episode 2 (16–24 March 2003), and episode 3 (12–22 September 2003). The characterization of these episodes [3] shows a different principal origin of ozone peaks depending on the meteorological conditions: episode 1, North of Portugal; episode 2, Castilian plateau, and episode 3, and Galicia.

Simulation domains covered the Iberian Peninsula, including the Galician region. For these domains, industrial emissions inventories were developed by the combination of top-down inventory from EMEP (Iberian Peninsula) and bottom-up industrial emissions inventory from REGADE [2]. SMOKE was applied for speciation, time and spatial segregation of industrial emissions. 2001 year was set as reference, and 2010 year was considered for projections.

BVOCs emissions were estimated by using MEGAN [1]. As the main differences in the industrial emissions of ozone precursors between 2001 inventory and 2010 projection, NMVOCs shows an increment of 6.6% and $NO_x$ a reduction of 27%. In addition, a significant spatial redistribution of $NO_x$ industrial sources is observed (Table 46.1) due to: (a) fuel changes in the three Galician high stacks power plants, which reduce in 50% their $NO_x$ emissions; (b) two planned combined cycles, with $NO_x$ emissions at lower height (less than 200 m).

## 46.2 Results

Simulations were performed using CAMx [4] with two nested grids covering the Iberian peninsula ($27 \times 27$ km$^2$ resolution) and Galicia ($9 \times 9$ km$^2$ resolution), using chemical boundary conditions provided by GOCART and MOZART data. Meteorological inputs were provided by PSUN/NCAR MM5 one-way nesting simulations at $27 \times 27$ km$^2$ and $9 \times 9$ km$^2$ resolutions, using NCEP reanalysis as initial and boundary conditions.

Changes in the industrial emissions will produce a significant reduction in the nocturnal ozone glc around the new combined cycles (As Pontes and Sabón) and their surrounding areas sporadically affected by their plumes (i.e., see Fig. 46.1b).

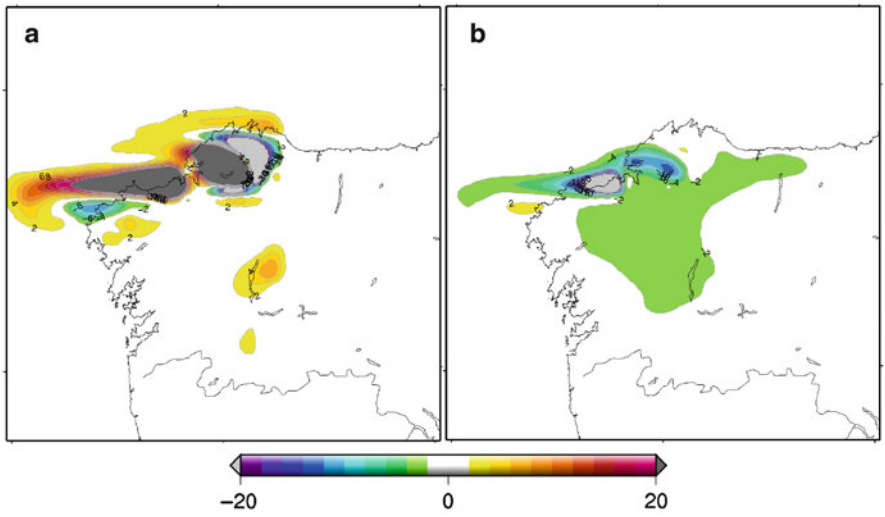


**Fig. 46.1** Relative differences (%) in nocturnal $NO_2$ (**a**) and $O_3$ (**b**) glc over Galicia between 2001 emissions inventory and 2010 emissions projection simulations at the central date of episode 3 (02 UTC, September 16th, 2003)

This reduction is due to the significant increment of $NO_x$ glc around both sources (because their stacks are lower than the old power plant stacks).There are no changes in nocturnal ozone glc in the rest of the region, even though a significant reduction of $NO_x$ emissions aloft is expected (Table 46.1). This is because aloft emissions are dispersed above the nocturnal stable layer.

No significant changes are observed in daytime ozone glc; only a small reduction over the local areas affected by the plumes from the aloft sources (As Pontes and Meirama), as the combined effect of the reduction of $NO_x$ emissions aloft (reducing daytime ozone production) and the increment of $NO_x$ surface emissions (increasing daytime ozone production and consuming nocturnal ozone).

Changes in air quality are more significant in $NO_2$ glc: increment of $NO_2$ nocturnal glc around Sabón and As Pontes sources (Figs. 46.1 and 46.2), due to the surface emissions surface. Daytime $NO_2$ glc shows a small and very changeable increment (Fig. 46.2), due to the opposite effects of the emissions aloft (reduction) and emissions surface (increment).

## 46.3 Conclusions

From the comparison of 2001 emissions inventory and 2010 emissions projection at Galician region, simulations results from CAMx model show a change on ozone distribution, remarkably decreasing its concentration downwind the combined

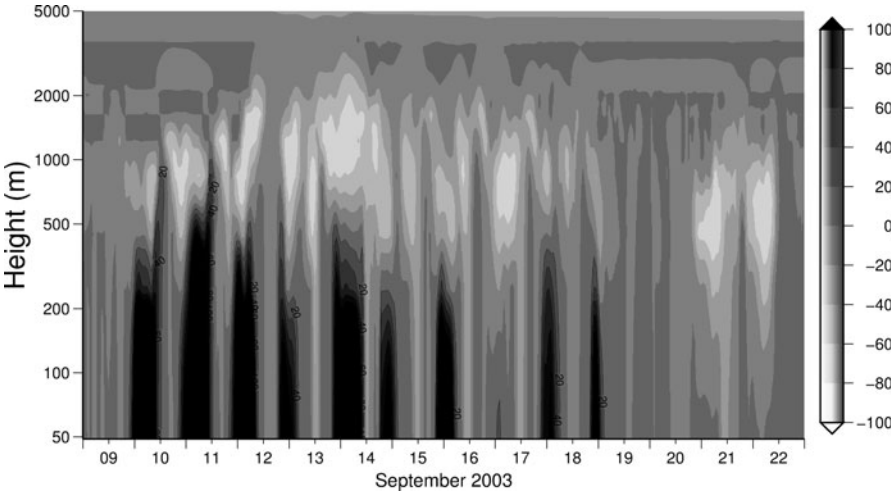


**Fig. 46.2** Aloft relative differences (%) in $NO_2$ over F2-Louseiras between 2001 emissions inventory and 2010 emissions projection simulations during episode 3

cycles because of their lower stacks (with respect to the old coal and fuel oil power plants), and slightly decreasing it in remote areas. Considering three typical air pollutants ($SO_2$, $NO_x$ and $O_3$), the overall regional air quality has improved; showing a local increment of nitrogen oxides, and on the other side, ozone concentration suffers a local reduction downwind from the new natural gas combined cycles that should be checked on a routine basis.

**Acknowledegements** This work was financially supported by the R&D Spanish Programme (CTQ2006-15481/PPQ). PhD research grant of A. Rodríguez is supported by Galician "María Barbeito" Programme (Xunta de Galicia). Air quality data were provided by Xunta de Galicia (Spain), As Pontes Power Plant (Endesa) and Ministerio do Ambiente of Portugal (web page).

## References

1. Rodríguez A, Saavedra S, Souto JA, Casares JJ (2010) Simulation of the sensitivity of rural tropospheric ozone levels to BVOCs emissions over a European Atlantic coastal region (Galicia, NW of Spain). In: 31st NATO/SPS international technical meeting on air pollution modelling and its application, Torino
2. Rodríguez R et al (2008) Modelling the impact of best available techniques for industrial emissions control in air quality: setting up inventories and establishing projections. In: Air pollution modeling and its application XIX. Springer, Dordrecht, pp 677–678
3. Saavedra S (2010) Caracterización de episodios de ozono troposférico en Galicia mediante la aplicación de distintas técnicas de simulación e interpretación de datos de campo. Ph.D. thesis, Universidade de Santiago de Compostela, Santiago de Compostela (in Spanish)
4. Song J et al (2010) Ozone response to emission changes: a modeling study during the MCMA-2006/MILAGRO Campaign. Atmos Chem Phys 10:3827–3846

# Chapter 47
# Changes in Sulphur and Nitrogen Deposition in Poland due to Domestic and European Emission Abatement

**Maciej Kryza, Małgorzata Werner, Anthony James Dore, and Marek Błaś**

**Abstract** The FRAME model was used to assess the changes in contribution of domestic emissions and transboundary transport to national deposition budget of oxidised sulphur and nitrogen in Poland during the period 2005–2020. It was found that the role of the transboundary transport will increase in 2020, especially over E and NE areas of Poland, due to relatively small decrease in emissions from eastern European countries, which are not obliged to meet EU emission standards.

**Keywords** Sulphur and nitrogen deposition • Transboundary transport • FRAME

## 47.1 Introduction

Despite the significant abatements in emissions of sulphur (S) and nitrogen (N) since 1990, Poland is still one of the European countries with the largest emissions. This results in a significant deposition of S and N compounds and leads to eutrophication, acidification and exceedance of critical loads [5]. Poland also receives large load of S and N due to transboundary transport (TT). According to the EMEP (European Monitoring and Evaluation Programme) model, 64% of oxidised S and 26% of N deposited in Poland in 2005 came from domestic sources, and the remaining was

M. Kryza (✉) • M. Werner • M. Błaś
Department of Climatology and Atmosphere Protection, University of Wroclaw,
Kosiby 6/8, 51-670 Wroclaw, Poland
e-mail: maciej.kryza@uni.wroc.pl; malgorzata.werner@uni.wroc.pl; marek.blas@uni.wroc.pl

A.J. Dore
Centre for Ecology and Hydrology, Edinburgh, Scotland, UK
e-mail: todo@ceh.ac.uk

D.G. Steyn and S. Trini Castelli (eds.), *Air Pollution Modeling and its Application XXI*,
NATO Science for Peace and Security Series C: Environmental Security 4,
DOI 10.1007/978-94-007-1359-8_47, 

attributed to emissions in other European countries. According to the emission scenario for 2020, S and N emissions from the EU countries are expected to decrease [1]. The opposite trend is projected for eastern European countries, which could be important for the amount and spatial pattern of S and N deposition in Poland.

The aim of this paper is to assess the changes in contribution of domestic emissions and TT to national deposition budget of oxidised sulphur and nitrogen in Poland during the period 2005–2020, and changes in spatial patterns of transboundary and domestic contribution to deposition of S and N.

## 47.2 Data and Methods

FRAME is a Lagrangian statistical trajectory model that describes the main atmospheric processes in a column of air moving along straight-line trajectories following specified wind directions [3]. The domain dimensions for Poland are $160 \times 160$ grids covering the country with 5 km $\times$ 5 km spatial resolution. FRAME consists of 33 vertical layers of thickness ranging from 1 m at the surface to 100 m at the top of the domain. The boundary conditions are calculated with the FRAME-Europe, a version of the model running for the entire Europe on the EMEP 50 km $\times$ 50 km grid. Details on chemistry scheme, dry and wet deposition calculations, are provided by [3] and references therein.

Meteorological data for year 2005 were used in this study. As the main interest is put on modelling of the deposition of atmospheric pollutants, the model evaluation is presented only by comparison with wet deposition measurements for year 2005. The FRAME estimated national deposition budget (NDB) is compared with EMEP model results and interpolation-based projections calculated by the Polish Chief Inspectorate of Environmental Protection (CIEP).

National emission inventory for year 2005 was available from [2] and, in a spatial form suitable for modelling, from [4]. The 2005 emissions were rescaled with the sector dependent scaling factors (SF) calculated on the basis of the EMEP expert emission inventory [6]. The SF were calculated to show the ratio of 2005–2020 emissions and were developed for $NH_3$, $SO_2$ and $NO_2$.

To assess the transboundary and domestic sources contribution to spatial pattern and NDB of oxidised S and N in Poland, for each year (2005 and 2020) FRAME was run twice. The first simulation is the base run, performed with full emission inventory available for the model domain and boundary concentrations calculated with FRAME-Europe. The second model run is performed with the emissions from Polish sources only, and with the boundary concentrations set to zero. The fraction of NDB, coming from domestic and European emissions, are calculated from the difference between the 1st and 2nd model simulation.

## 47.3 Results

FRAME modelled wet depositions of oxidised N and S for year 2005 are in good agreement with the measurements, with the correlation coefficient above 0.8. The model underestimates wet deposited oxidised N, with mean bias (MB) −0.12 kg N $ha^{-1}year^{-1}$ and overestimates for S (MB 0.09 kg S $ha^{-1}year^{-1}$).

Total deposition of S for year 2005 is in range from 3.8 to 28.2 kg S $ha^{-1}$, with the country average at 8.5 kg S $ha^{-1}$. The deposition for 2020 has similar spatial patterns to 2005, and ranging from 2.5 to 20.4 kg S $ha^{-1}$ (average 5.3 kg S $ha^{-1}$). The largest deposition of oxidised N is calculated for the mountainous areas in the south and in the largest cities. The highest total deposition calculated by the FRAME model exceeded 12.4 kg N $ha^{-1}$ in year 2005, with the country average at 5.1 kg. The respective values for year 2020 are 7.8 and 3.2 kg N $ha^{-1}$.

NDB of S and N in Poland in 2005 is 266 Gg S and 160 Gg N, which is close to the EMEP and CIEP estimates(Fig. 47.1). For year 2005, NDB for oxidised N is dominated by the TT, whereas for S domestic sources dominate (Fig. 47.1). The same is for 2020, but the contribution of TT is larger compared to 2005 for S and N.

Contribution of the TT is the largest along the country borders, and can exceed 75% of total deposition of these pollutants in the mountainous SW part of Poland (Fig. 47.2). The area that suffers from high contribution of TT extends from the western boundary farther to the centre of Poland, due to the prevailing westerly winds. The FRAME-estimated changes in TT contribution are the largest in the central and E part of Poland, which can be attributed to the expected increase in emissions from eastern European countries and abatements from the domestic sources.

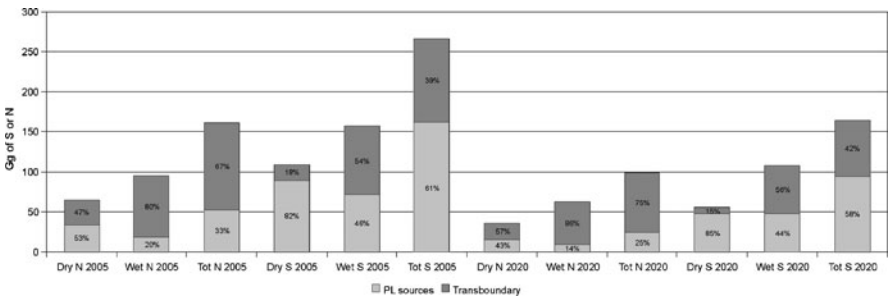


**Fig. 47.1** National deposition budget for dry, wet and total deposition of oxidised nitrogen and sulphur for years the 2005 and 2020 (*dark grey* – TT contribution, *light* – domestic)

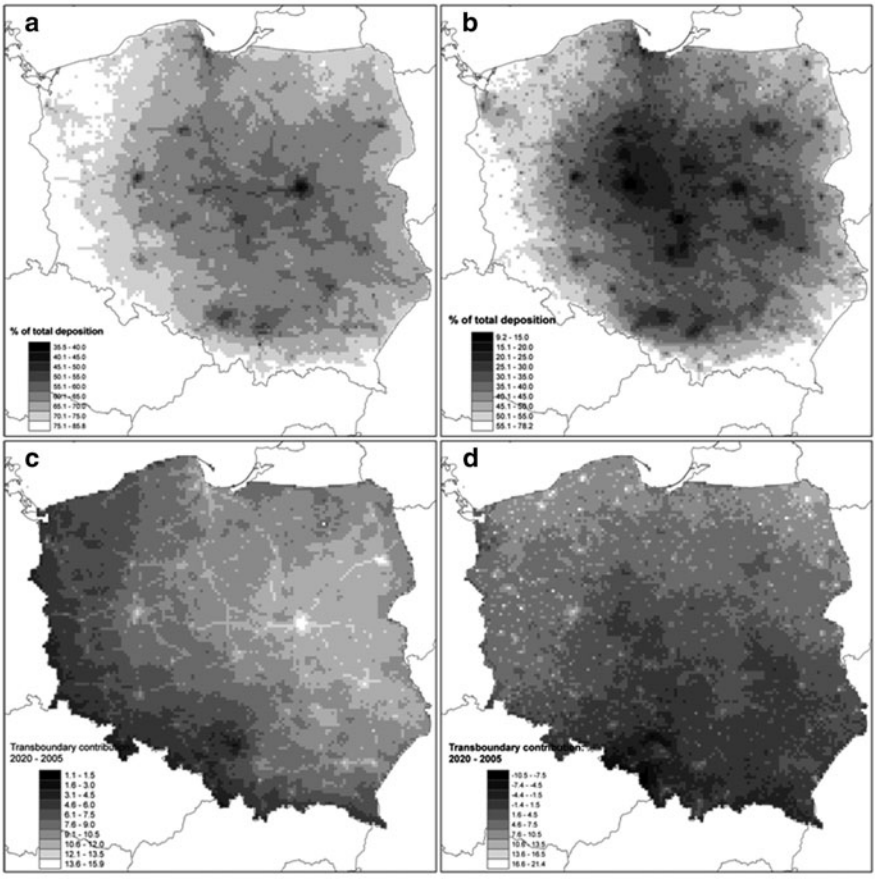


**Fig. 47.2** TT contribution to total deposition of oxidised N (**a**) and S (**b**) for year 2005 and the difference between 2020 and 2005 TT contribution to deposition of oxidised N (**c**) and S (**d**)

## 47.4 Summary

The main aim of the paper was to assess temporal and spatial changes in contribution of domestic sources and transboundary transport to deposition of oxidised S and N in Poland with the FRAME model. The model results were found to be in good agreement with measured wet deposition. FRAME estimates for national dry, wet and total deposition budget are close to EMEP-Unified model predictions and, in case of wet deposition, to interpolation-based CIEP calculations.

The transboundary transport is expected to contribute more to NDB of oxidised S and N in the year 2020, compared with 2005. The increase in relative contribution is expected to be especially large in E and NE areas of Poland. This can be attributed

to large abatements in domestic emissions of S and N and expected relatively small decrease in emissions from eastern European countries, which are not obliged to meet EU emission standards.

## References

1. Amann M, Bertok I, Cofala J, Heyes C, Klimont Z, Rafaj P, Schoepp W, Wagner F (2008) Baseline emission projections for the revision of the Gothenburg protocol up to 2020. CIAM Report 2/2008, EMEP Centre for Integrated Assessment Modelling, Geneva
2. Dębski B, Olendrzyński K, Cieślińska J, Kargulewicz I, Skośkiewicz J, Olecka A, Kania K (2009) Inwentaryzacja emisji do powietrza $SO_2$, $NO_2$, CO, $NH_3$, pyłów, metali ciężkich, NMZO i TZO w Polsce za rok 2009. Institute of Environmental Protection, Warsaw
3. Dore AJ, Vieno M, Tang YS, Dragosits U, Dosio A, Weston KJ, Sutton MA (2007) Modelling the atmospheric transport and deposition of sulphur and nitrogen over the UK and assessment of the influence of $SO_2$ emissions from international shipping. Atmos Environ 11:2355–2367
4. Kryza M, Werner M, Błaś M, Dore AJ, Sobik M (2010) The effect of emission from coal combustion in nonindustrial sources on deposition of sulphur and oxidized nitrogen to Poland. J Air Waste Manage Assoc 60(7):856–866. doi:10.3155/1047-3289.60.7.856
5. Mill W (2006) Temporal and spatial development of critical loads exceedance of acidity to Polish forest ecosystems in view of economic transformation and national environmental policy. Environ Sci Policy 9:563–567
6. Vestreng V, Mareckova K, Kakareka S, Malchykhina A, Kukharchyk T (2007) Inventory report 2007. Emission data reported to LRTAP convention and NEC Directive. MSC-W Technical Report 1/07, The Norwegian Meteorological Institute, Oslo

# Chapter 48
# A Methodology for Quantifying the Contribution of Volcanic Ash to Urban Air Pollution

**Kim Natasha Dirks, N. Singhal, G.L. Austin, M.A. Elangasinghe, and Alessandro Nanni**

**Abstract** Air quality in urban areas is often dominated by vehicle emissions but pollutants such as volcanic ash, dust from bush fires and particles from dust storms also contribute. This paper presents a semi-empirical methodology for quantifying the relative contribution of these sources. The technique is based on the underlying premise that vehicles follow a diurnal pattern of emissions (whereas the other sources do not) but that both are modulated by the surface wind flows. The methodology is evaluated using rainfall washout as a removal mechanism (rather than an additional source). Whereas gaseous pollutants are relatively insoluble in water, particulate matter is readily removed. The extent of the washout is observed as the difference between the model predicted and observed concentrations. The same methodology can be applied to quantify the relative contribution of pollution sources such as ash.

**Keywords** Urban • Modelling • Semi-empirical • Washout • Ash

K.N. Dirks (✉)
School of Population Health, Faculty of Medical and Health Sciences,
The University of Auckland, Private Bag 92019 Auckland, New Zealand
e-mail: k.dirks@auckland.ac.nz

N. Singhal • M.A. Elangasinghe
Department of Civil & Environmental Engineering, Faculty of Engineering,
The University of Auckland, Private Bag 92019 Auckland, New Zealand

G.L. Austin
Department of Physics, Faculty of Science, The University of Auckland,
Private Bag 92019 Auckland, New Zealand

A. Nanni
Arianet srl, via Gilino 9, 20128 Milan, Italy
e-mail: a.nanni@aria-net.it

D.G. Steyn and S. Trini Castelli (eds.), *Air Pollution Modeling and its Application XXI*,
NATO Science for Peace and Security Series C: Environmental Security 4,
DOI 10.1007/978-94-007-1359-8_48, 

## 48.1 Introduction and Background

Many air pollution models have been developed over the years for the purpose of predicting urban air pollution concentrations based on the emission characteristics of the pollutants of interest and their dispersion processes. In urban environments, vehicles, industry and home heating are significant sources of air pollution that are often considered. Such emissions, those from vehicles in particular, tend to follow regular emission patterns that vary throughout the day but are predictable from day to day. For example, the emissions at a particular point on a busy road at 8:00 AM on one Monday tend to be similar to the emissions at the same place on the road on the next Monday at 8:00 AM. The day-to-day variability in concentrations of pollutants at a particular site at a given time of day is largely a reflection of changes in the local surface meteorology, with the wind speed and direction being the dominant factors. This allows for the development of a simple site-optimised semi-empirical (SOSE) modelling approach (based on a box model) which relates the surface meteorology to the observed concentrations at each particular time of day (and for a particular site) using linear regression of the observed concentration on the wind speed. The regression parameters vary by time of day as the emission patterns change (due to different traffic flow rates and states of congestion) and the background concentration. While very simple, this modelling approach has been found to be reliable at predicting urban air pollution concentrations ($NO_x$, $PM_{10}$ and CO) for specific sites providing the surface wind speed and direction are known.

## 48.2 Results

Figure 48.1 shows some SOSE modeling results for a topographically-complex area in the Aosta Valley in Italy based on 1-hour averages. The SOSE modeling approach as has also been found to be reliable for sites in New Zealand [1, 2], Greece [7], India [4] and in Hong Kong [5] and has been found to be useful in many practical applications such as interpolating for missing data and looking at 'what-if' scenarios associated with changes in traffic flow patterns and surface meteorology [1–3].

Because the model produces good results (from being semi-empirical and site-specific and taking advantage of the regularity in emission patterns), it is expected that the model is able to detect any *anomalies* in the emission patterns that don't follow a consistent daily pattern. Ultimately the interest is in determining the contribution of volcanic ash to urban air pollution levels. This will involve identifying periods associated with eruption events and also using a mesoscale model (such as WRF) to determine (via back-trajectory analysis) the time periods when the wind conditions are such that, if erupting, the volcanic ash is likely to be present in the air over the urban area of interest. However, to test the methodology, a completely unrelated 'sporadic' process was used – that of the washout of pollutants as a result of rainfall. Rainfall does not follow a consistent daily pattern and has its greatest impact on particulate matter. While a removal mechanism rather than a source, it is none-the-less a useful test for the prediction of anomalies.

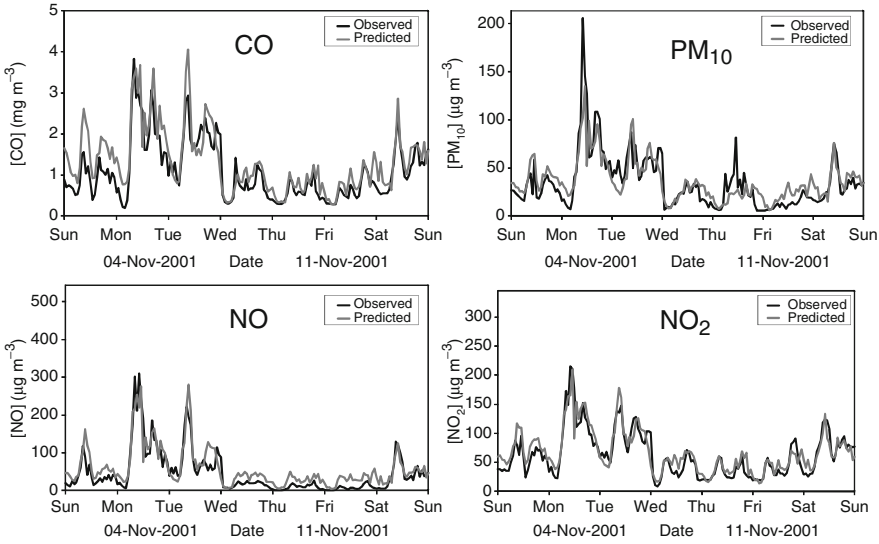


**Fig. 48.1** Example of model output for 1 week of data during winter (Data from the Piazza Plouvres Site in the Aosta Valley)

Testing of the model in terms of its ability to detect the extent of washout due to rainfall was carried out using data from the same urban site in the Aosta Valley in Italy where CO, NOx and $PM_{10}$ concentrations were measured. The model parameters were estimated using only dry periods (removing rainy periods from the dataset), and then comparing the predicted concentrations with what was observed during the wet periods.

Figure 48.2 shows the difference between the predicted and observed concentrations as a function of the rainfall rate. What is noticed is that there is significant over-prediction during rain events for $PM_{10}$ (indicating that washout has occurred) but not for the gaseous pollutants. This is consistent with our understanding of washout but, more importantly, demonstrates the ability of our modeling methodology for detecting anomalies with respect to the expected daily cycle of emissions.

Our case study is the City of Catania where the frequent eruptions of Mt Etna have a significant impact on air quality. By coupling the SOSE model with a mesoscale model such as WRF, it is expected that it will be possible to indentify the periods when the volcanic plumes have passed over Catania (using back-trajectory analysis) and estimate the contribution of volcanic ash to the total air pollution concentrations by looking at the extent of model under-prediction (using SOSE). Based on the spatial distribution of the under-predictions (the volcanic ash contribution), the source strength of the volcano may be able to be estimated, something that is expected to be of significant interest to volcanologists. The contribution of volcanic ash to urban air pollution could also be used to inform studies looking at the health impacts of volcanic ash exposure (such as discussed in [6, 8]) and used to provide information for data assimilation in air quality forecast systems.

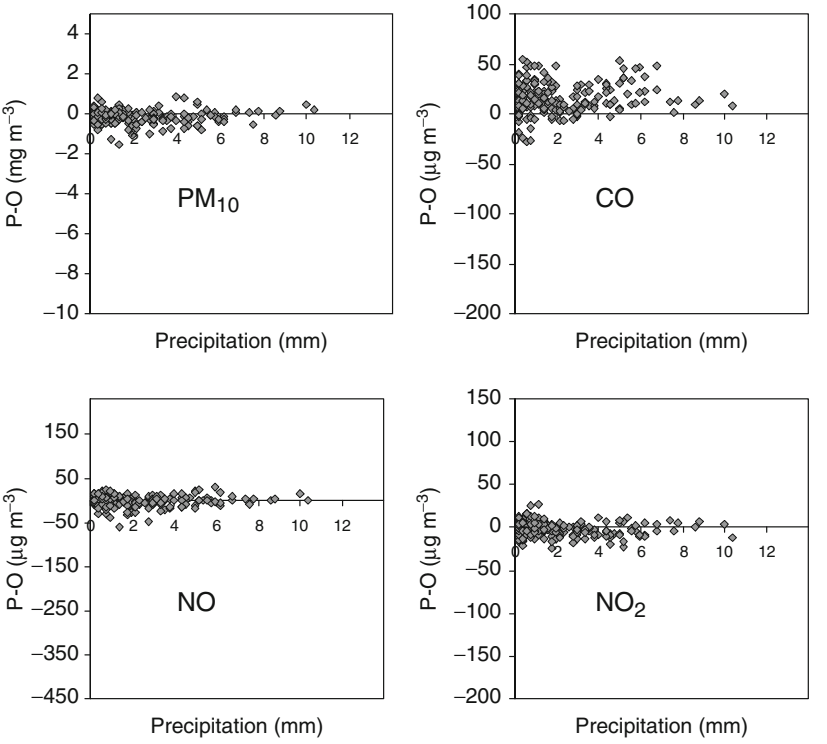


**Fig. 48.2** The impact of washout on pollution concentrations (Data from the Piazza Plouvres Site in the Aosta Valley)

## References

1. Dirks KN, Johns MD, Hay JE, Sturman AP (2002) A semi-empirical model for predicting missing carbon monoxide concentrations. Atmos Environ 36(39–40):5953–5959
2. Dirks KN, Johns MD, Hay JE, Sturman AP (2003) A semi-empirical model for predicting the effect of changes in traffic flow patterns on carbon monoxide concentrations. Atmos Environ 37:2719–2724
3. Dirks KN, Nanni A, Dirks V (2006) Modelling and predicting urban atmospheric pollutants in the Aosta Valley. Atmos Sci Lett 7:15–20
4. Gokhale S, Pandian S (2007) A semi-empirical box modelling approach for predicting the carbon monoxide concentrations at an urban intersection. Atmos Environ 41:7940–7950
5. He HD, Lu WZ, Xue Y (2009) Prediction of PM10 concentrations at urban traffic intersections using semi-empirical box modelling with instantaneous velocity and acceleration. Atmos Environ 43:6336–6342
6. Horwell CJ, Baxter PJ (2006) The respiratory health hazards of volcanic ash: a review for volcanic risk mitigation. Bull Volcanol 69:1–24
7. Kassomenos PA, Karakitsios SP, Pilidis GA (2004) A simple semi-empirical approach to modelling benzene concentration in a street canyon. Atmos Environ 38:6073–6078
8. Newnham R, Dirks KN, Samaranayake D (2010) An investigation into the long-distance health impacts of the 1996 eruption of Mt Ruapehu, New Zealand. Atmos Environ 44:1568–1578

# Chapter 49
# Impact of Saharan Dust on PM10 Daily Exceedances over Italy During 2003–2005

**Anna Pederzoli, Mihaela Mircea, Sandro Finardi, and Gabriele Zanini**

**Abstract** The assessment of the anthropogenic and natural contributions to PM10 concentrations is a key issue for the development of air quality policies in Europe. In areas such as the Mediterranean basin, a consistent fraction of the natural contribution to PM10 concentration is given by dust particles transported from Sahara. This study presents an estimate of the dust contribution to PM10 concentrations in years 2003–2005 at six Italian locations. The reduction (%) in the number of daily exceedances of the PM10 limit value (50 $\mu gm^{-3}$) after subtraction of the African dust contribution is also presented.The reduction varies with station between 20% and 50% in 2005 and between 5% and 25% in 2003 and 2004.

**Keywords** Dust • Exceedances • $PM_{10}$ • Air quality

## 49.1 Introduction

The accurate estimate of Saharan dust contribution to PM10 concentration when it exceeds the limit values of 50 $\mu gm^{-3}$ per day [1] is very important for the assessment of air quality in Europe. In fact, when these exceedances can be attributed, previous

A. Pederzoli (✉)
European Commission – DG JRC, Via E. Fermi, 2749 (TP 441),
I-21027 Ispra (VA), Italy
e-mail: anna.pederzoli@jrc.ec.europa.eu

M. Mircea • G. Zanini
Italian National Agency for New Technologies, Energy and Sustainable
Economic Development, UTVALAMB – AIR, Via Martiri di Monte Sole 4,
40129 Bologna, Italy
e-mail: mihaela.mircea@enea.it

S. Finardi
ARIANET SRL, via Gilino, 9, 20128 Milan, Italy
e-mail: s.finardi@aria-net.it

D.G. Steyn and S. Trini Castelli (eds.), *Air Pollution Modeling and its Application XXI*,
NATO Science for Peace and Security Series C: Environmental Security 4,
DOI 10.1007/978-94-007-1359-8_49, 

an accurate scientific validation, to Saharan dust outbreaks rather than anthropogenic sources, these days can be discounted by the State Members of the European Union (EU) [1]. The estimate of this contribution in mass (μg $m^{-3}$) is a hard task because of the difficulty to discriminate the anthropogenic component of dust ("fugitive" dust), which has local origin, from the natural one, usually due to long-range transport. The analysis of the chemical composition of aerosol particles can be used to accomplish this task. However, chemical speciation analysis techniques are usually time consuming and expensive [4]. Several statistical methods [2, 3, 5] have been developed in recent years in order to estimate the natural contribution without the need of PM speciation. This study reports the estimates of the Saharan dust contribution to PM10 concentrations at six locations across Italy over 3 years (2003, 2004 and 2005) as calculated by the application of a statistical method [2]. The reduction in the number of daily exceedances of the limit value (50 μg$m^{-3}$) after the subtraction of this contribution is also presented.

## 49.2 Results

The classification of dust events in 2003–2005 reported in Pederzoli et al. [6] has been used for estimating the contribution (μg $m^{-3}$) of Saharan dust to total PM10 concentration at six rural background monitoring sites (Table 49.1). The statistical method of Escudero et al. [2] is applied. Estimates of Saharan dust concentrations are reported in Table 49.2. Further details can be found in Pederzoli et al. [6].

**Table 49.1** Rural background monitoring sites measuring daily PM10 concentration in 2003–2005. All sites except Ispra are part of the Italian air quality monitoring network BRACE (http://www.brace.sinanet.apat.it). Ispra is part of the EMEP (European Monitoring and Evaluation Programme) monitoring network

| | Lat | Lon |
|---|---|---|
| Fontechiari | 41.68°N | 13.68°E |
| Gherardi | 44.84°N | 11.96°E |
| S.Antioco | 39.06°N | 8.46°E |
| La Mandria | 45.17°N | 7.56°E |
| Ispra | 45.82°N | 8.62°E |
| Passo Giovi | 44.63°N | 8.94°E |

**Table 49.2** Average dust contribution (μg $m^{-3}$) to PM10 concentration in years 2003, 2004 and 2005

| | 2003 | 2004 | 2005 |
|---|---|---|---|
| Fontechiari | 1.5 | 0.6 | 2.8 |
| Gherardi | 1.4 | 0.4 | 0.9 |
| S.Antioco | No data | No data | 1.5 |
| La Mandria | 2.8 | 1.3 | 3.8 |
| Ispra | 2.1 | 2.2 | 3.7 |
| Passo Giovi | No data | 0.5 | 2.1 |

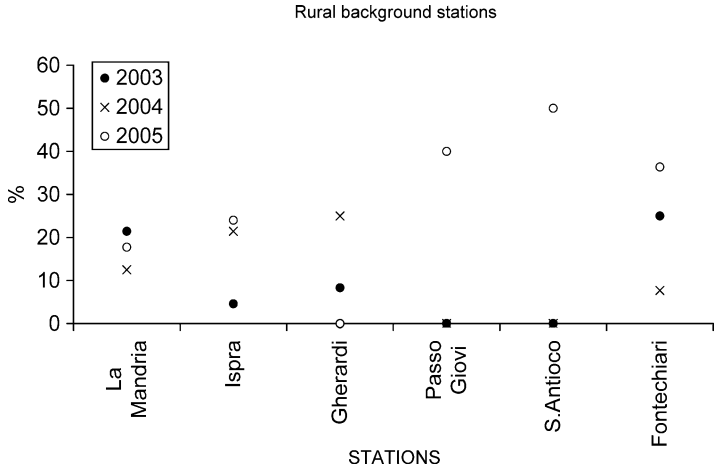


**Fig. 49.1** Reduction (%) in the number of exceedances of the limit value (50 μg $m^{-3}$) after subtraction of dust contribution in years 2005, 2004 and 2003

The reduction in the number of outbreaks of the daily limit values (50 μg $m^{-3}$) after the subtraction of the dust contribution from PM10 observations is calculated at each site. For each dust day, the dust concentration is subtracted from the PM10 concentration measured at each station. The reduction is then calculated as follows:

$$REDUCTION(\%) = \frac{N_T - N_{T-dust}}{N_T} \cdot 100$$

where $N_T$ is the total annual number of exceedances in $PM_{10}$ daily measured concentrations and $N_{T-dust}$ is the number of exceedances after subtraction of the dust contribution from observations. As expected, the impact of Sharan dust on $PM_{10}$ concentrations (Fig. 49.1) is higher over elevated areas (Passo Giovi) as well as in Centre Italy (Fontechiari) and the islands (S.Antioco) compared to Northern Italy. Fontechiari experiences a reduction by approximately 25% in 2003, 8% in 2004 and 35% in 2005. In the same year the reduction at S.Antioco and Passo Giovi is about 50% and 40% respectively. At Gherardi and Ispra it is between 20% and 25% in 2005 and 2004 and between 5% and 10% in 2003. Finally it is assessed around 20% in 2005 and 2003 and 12% in 2004 at La Mandria. A stronger impact is expected in Southerly regions (i.e. Basilicata, Sicily, Campania which are typically affected by dust intrusions during summertime). Unfortunately the lack of monitoring background stations measuring $PM_{10}$ and $PM_{25}$ in 2003–2005 did not allow to extend the analysis to these areas.

**Acknowledgments** This work is part of the MINNI (Integrated National Model in support to the International Negotiation on Air Pollution) project, funded by the Italian Ministry for Environment, Territory and Sea and carried out by ENEA. It is supported and coordinated by ENEA and ARIANET Srl.

## References

1. EC (2008) Council Directive 2008/50/EC of 21 May 2008 relating on ambient air quality and cleaner air for Europe. Off J L152:0001–0043, 11/06/2008. Available at http://eur-lex.europa.eu/LexUriServ/LexUriServ.do?uri=OJ:L:2008:152:0001:0044:EN:PDF
2. Escudero M, Querol X, Avila A, Cuevas E (2007) Origin of the exceedances of the European daily PM limit value in the regional background areas of Spain. Atmos Environ 41:730–744
3. Ganor E, Stupp A, Alpert P (2009) A method to determine the effect of mineral dust aerosols on air quality. Atmos Environ 43:5463–5468
4. Karlsson L, Henandez F, Rodriguez S, Lopez-Perez M, Hemandez-Armas J, Alonso-Perez S, Cuevas E (2008) Using $^{137}$Cs and $^{40}$K to identify natural Saharan dust contributions to PM10 concentrations and air quality impairment in the Canary Islands. Atmos Environ 42:7034–7042
5. Nicolás J, Chiari M, Crespo J, Garcia OI, Lucarelli F, Nava S, Pastor C, Yubero E (2008) Quantification of Saharan and local dust impact in an arid Mediterranean area by the positive matrix factorization (PMF) technique. Atmos Environ 42(39):8872
6. Pederzoli A, Mircea M, Finardi S, di Sarra A, Zanini G (2010) Quantification of Saharan dust contribution to PM10 concentrations over Italy in 2003-2005. Atmos Environ 44:4181–4190

# Chapter 50
# Intercomparison Between Two Air Pollution Simulations in Northern Italy Based on Different Emission Inventories

**Alessia Balanzino, Enrico Ferrero, Guido Pirovano, Giuseppe M. Riva, and Mauro Causà**

**Abstract** Preliminary results of two annul simulations of the air quality in a region of the Northern Italy are presented. The simulations, which refer to two different year, were performed using a modeling system based on a meteorological model, an interface code and a transport-chemistry model. Comparisons with measured data are presented and discussed.

**Keywords** Air pollution modeling • Photochemistry • Emission inventory

## 50.1 The Modelling System

The modeling system includes the meteorological model RAMS [3], an emission processor and the photochemical model CAMx [2]. The emission processing system was designed by our group [1] to produce emission fields according to the model needs. It is based on emission data collected from the different regional inventories. The domain chosen for the dispersion simulation extends over a 250 $\times$ 250 km$^2$ area. Two nested grids were used for the meteorological simulation in the case of the year 2005, the larger one covered a 540 $\times$ 540 km$^2$ domain and the inner grid, having a resolution of 5 km, coincided with that of the dispersion and chemical model. Considering the 1999 simulation only the inner grid was considered.

A. Balanzino (✉) • E. Ferrero
DISTA, University of Piemonte Orientale, Alessandria, Italy
e-mail: alessia.balanzino@mfn.unipmn.it; enrico.ferrero@mfn.unipmn.it

G. Pirovano • G.M. Riva
RSE, Milan, Italy

M. Causà
University of Napoli, Napoli, Italy

D.G. Steyn and S. Trini Castelli (eds.), *Air Pollution Modeling and its Application XXI*,
NATO Science for Peace and Security Series C: Environmental Security 4,
DOI 10.1007/978-94-007-1359-8_50, 

## 50.2 Simulation Results

In order to highlight the discrepancies that can arise from the change of the emission inventories, which are routinely carried out by national and local environment protection agencies, we present the results of the comparison with measured data of the main pollutants, $NO_2$, $O_3$ and PM10 (for sake of brevity $NO_2$ results are not shown), predicted by two simulations concerning the years 1999 [1] and 2005 respectively. Obviously differences can be due, besides to the emission scenarios, also to other causes as the meteorological field, the boundary conditions and the measurement uncertainty. Nevertheless we intend to give a first overview of the extent of the difference between the two simulations, leaving to further deeper analysis the task to give conclusive considerations. For PM10 daily mean values are considered, while the daily maximum 8-h average concentrations is accounted for concerning $O_3$. As far as $O_3$ is concerned, the results are presented for the hot season (from April to September), while PM10 concentrations refer to the cold season divided in two trimester (from January to March and from October to December).

In Fig. 50.1a, b it can be observed the comparison between simulated and measured daily maximum 8-h average $O_3$ concentrations at one station for 1999

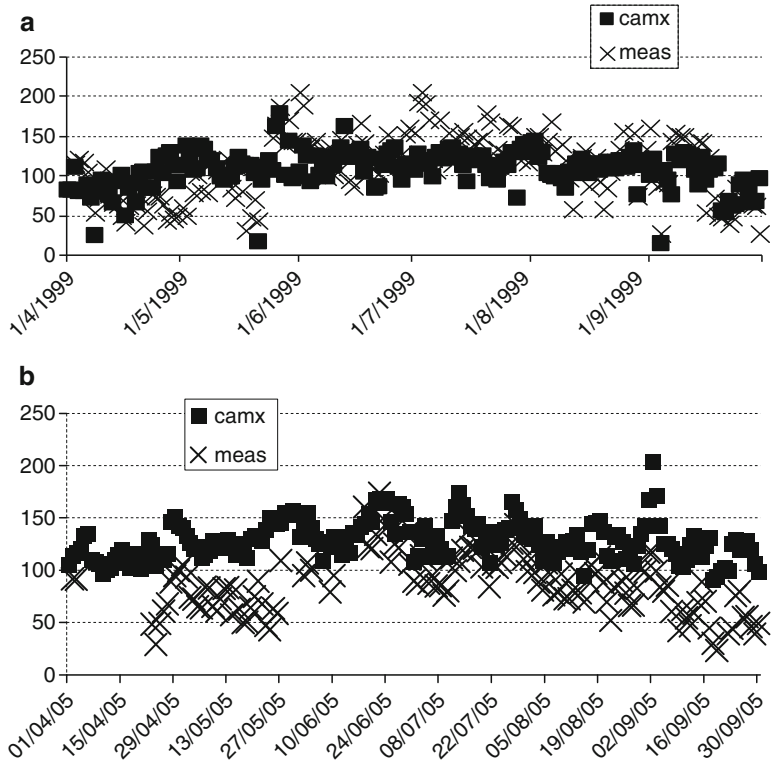


**Fig. 50.1** Six months daily maximum 8-h average $O_3$ concentrations ($\mu g/m^3$). (**a**) 1999, (**b**) 2005

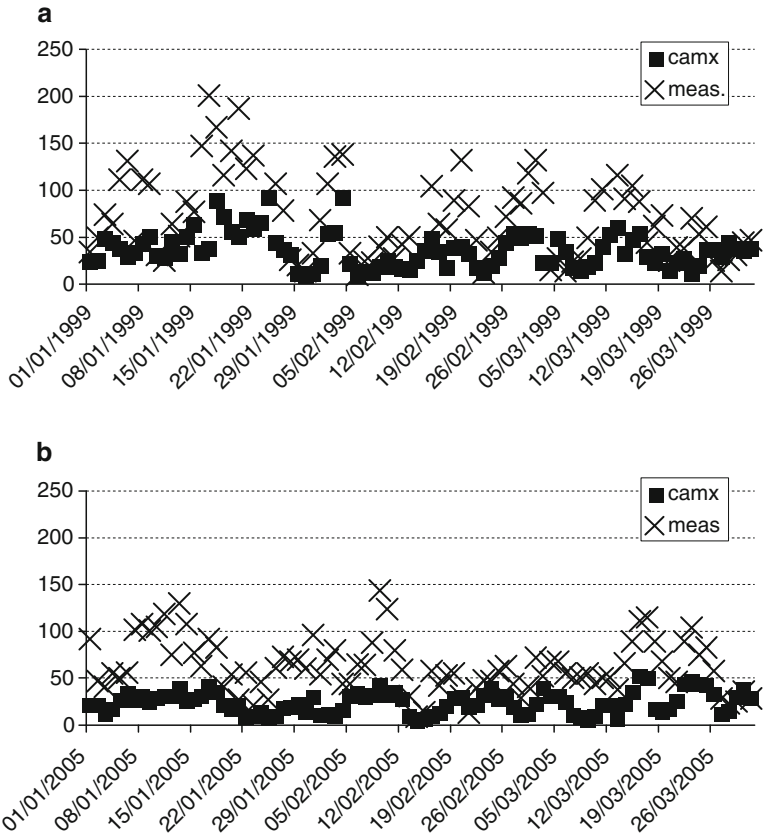


**Fig. 50.2** First quarter (*JFM*) daily mean PM10 concentrations (μg/m$^3$). (**a**) 1999, (**b**) 2005

and 2005 respectively. The predicted values seem to agree better with the measurements in the case of 1999, although some maximum is not reproduced. On the contrary the simulation of the year 2005 roughly reproduces the maxima, but generally overestimates. This result reflect the underestimation of $NO_2$ and it might be due to an uncorrected $NO_X$ emission estimation which does not allow to well reproduce the $O_3$ titration. The results of the simulation concerning PM10 compared with the measured data at a station are presented in Fig. 50.2a, b for the first quarter (JFM) and in Fig. 50.3a, b for the fourth quarter (OND). Concerning the first quarter the PM10 concentration are underestimated both for the 1999 and 2005 simulations. In particular, the predicted concentrations are in nearly every case below 60 μg/m$^3$. The results of the fourth quarter seems to be slightly better. As a matter of fact, the underestimation is reduced and the predicted concentrations have values higher than 60 μg/m$^3$, particularly for the case of 1999. This different behaviour during the two quarters could be attributed to the meteorology which yields different dispersion conditions.

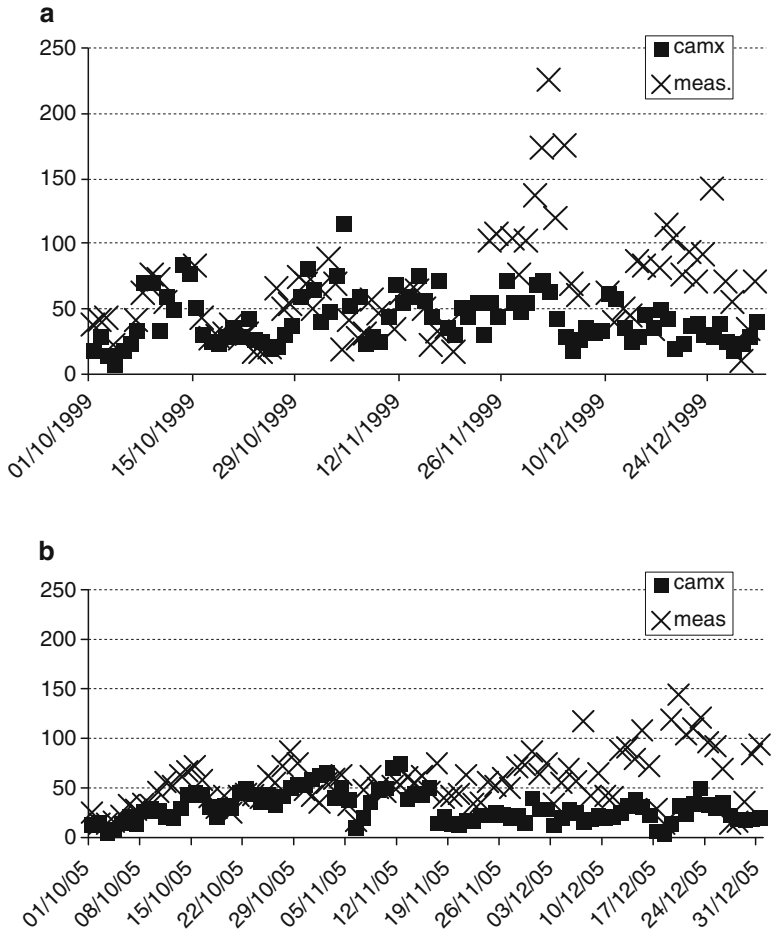


**Fig. 50.3** Fourth quarter (*OND*) daily mean PM10 concentrations ($\mu g/m^3$). (**a**) 1999, (**b**) 2005

## 50.3 Conclusions

A chemical pollution model system has been applied to simulate airborne dispersion and chemical reactions on a regional scale domain ($250 \times 250$ km$^2$) with a grid resolution of 5 km, placed in the North-West of Italy. Two simulations were carried out concerning the years 1999 and 2005, in order to evaluate the effect of the change of the emission inventory. It is found that different results are obtained as far as the $NO_2$ and $O_3$ are concerned probably because of the worst prediction of the $NO_X$ emissions in the 2005. Regarding the PM10 the performances of the model seem to be comparable in the 2 years considered, but differences are found between the first and the fourth quarter possibly due to different meteorological conditions.

**Acknowledgments** The authors wish to acknowledge ARPA Piemonte Meteorological Service for providing meteorological data and emission inventory, Regione Piemonte for supporting the project in which this work is carried out. RSE (formerly ERSE) contribution has been financed by the Research Fund for the Italian Electrical System under the Contract Agreement between RSE and the Ministry of Economic Development – General Directorate for Energy and Mining Resources stipulated on July 29, 2009 in compliance with the Decree of March 19, 2009.

## References

1. Balanzino A, Ferrero E, Pirovano G, Pertot C, Causà M, Alessandrini S, Costa MP (2011) Annual simulation of secondary pollution over northern Italy. Int J Environ Pollut 45(4):353–384
2. ENVIRON (2005) CAMx (Comprehensive Air Quality Model with extensions) User's guide Version 4.20. Internal Report, Environ International Corporation, Novato
3. Pielke RA, Cotton WR, Walko RL, Tremback CJ, Lyons WA, Grasso LD, Nicholls ME, Moran MD, Wesley DA, Lee TJ, Copeland JH (1992) A comprehensive meteorological modelling system – RAMS. Meteorol Atmos Phys 49:69–91

# Chapter 51
# Sea-Salt Aerosol Forecasts Compared with Wave Height and Sea-Salt Measurements in the Open Sea

**Pavel Kishcha, B. Starobinets, R. Bozzano, S. Pensieri, E. Canepa, S. Nickovic, A. di Sarra, R. Udisti, S. Becagli, and P. Alpert**

**Abstract** Sea-salt aerosol (SSA) could influence the Earth's weather and climate acting as cloud condensation nuclei. In spite of the importance of SSA effects on the Earth's climate and weather, there were no measurements of sea-salt aerosols in the open sea. At Tel-Aviv University, the DREAM-Salt prediction system has been producing daily forecasts of 3-D distribution of sea-salt aerosol concentrations over the Mediterranean model domain 20 W–45E, 15 N–50 N (http://wind.tau.ac.il/salt-ina/salt.html). In order to evaluate the model performance in the open sea, daily modeled sea-salt aerosol concentrations were compared directly with sea-salt ground-based measurements taken at the tiny island of Lampedusa, in the Central Mediterranean. In order to further test the robustness of the model, the model performance over the open sea was indirectly verified by comparing modeled SSA concentrations with wave height measurements collected by the ODAS Italia 1 buoy. Model-vs.-measurement comparisons show that the model is capable of

P. Kishcha (✉) • B. Starobinets • P. Alpert
Department of Geophysics and Planetary Sciences, Tel-Aviv University, 69978 Tel-Aviv, Israel
e-mail: pavelk@post.tau.ac.il

R. Bozzano • S. Pensieri
National Research Council (CNR-ISSIA), 16149 Genoa, Italy

E. Canepa
National Research Council (CNR-ISMAR), 16149 Genoa, Italy

S. Nickovic
World Meteorological Organization, Geneva, Switzerland

A. di Sarra
National Agency for New Technologies, Energy, and Economic Sustainable Development, Bologna, Italy

R. Udisti • S. Becagli
University of Florence, Florence, Italy

D.G. Steyn and S. Trini Castelli (eds.), *Air Pollution Modeling and its Application XXI*, NATO Science for Peace and Security Series C: Environmental Security 4,
DOI 10.1007/978-94-007-1359-8_51, 

producing realistic SSA concentrations and their day-to-day variations over the open sea, in accordance with observed wave height and wind speed.

**Keywords** Marine aerosol • Sea-salt aerosol forecast • Mediterranean Sea

## 51.1 Introduction

In the open sea, where sea-salt aerosol is mainly produced, its concentration and impact on the Mediterranean climate and weather could be significant under strong winds. Model-based forecasts of SSA, daily produced in Tel-Aviv University could be helpful, providing valuable information about space and time distributions of sea-salt aerosols. In this study we tested the robustness of the SSA forecasts by comparing directly with SSA measurements at the island of Lampedusa (Central Mediterranean), and indirectly by comparing SSA forecasts with sea-wave height, given that the main factors for SSA production in the open sea are sea waves and associated winds.

## 51.2 Methodology

Numerical simulations of sea-salt aerosol presented in this study were conducted using a version of the DREAM dust aerosol model [2, 5] with embedded SSA component (DREAM-Salt) [3, 4]. The DREAM-Salt prediction system has been producing daily forecasts of 3-D distribution of sea-salt aerosol concentrations over the Mediterranean model domain 20°W–45°E, 15°N–50°N (Fig. 51.1, left panel). The model has 0.3° horizontal resolution, 24 vertical levels, and eight

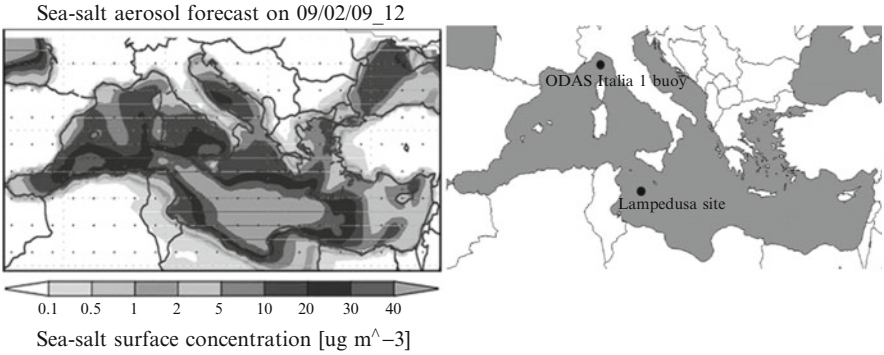


**Fig. 51.1** *Left panel* – an example of *SSA* forecast on February 9, 2009. *Right panel* – a map of the Mediterranean Sea with the monitoring site in Lampedusa and the ODAS Italia 1 buoy (the *black* place marks)

particle size bins ranging from 1–8 μm. Forecasts are made once every day, starting from the 12:00 UTC objective analyses and providing forecasts up to 72 h ahead. The NCEP/Eta regional atmospheric model drives the aerosol. The sea-salt emission scheme defines the lower boundary condition using the source function of Erickson et al. [1]. DREAM-Salt incorporates parameterizations of all other major phases of atmospheric sea-salt aerosol life such as: diffusion, advection, gravitational settling, and wet removal of sea-salt aerosols.

In order to evaluate the model performance over the open sea, the numerical simulations of sea-salt aerosol (SSA) were compared with sea-salt ground-based measurements taken at the tiny Mediterranean island of Lampedusa, Italy, during the 2-year period from 2007–2008 (Fig. 51.2) [3]. In Lampedusa, the conditions of SSA measurements are considered similar to those in the open sea, given the small dimensions of the island.

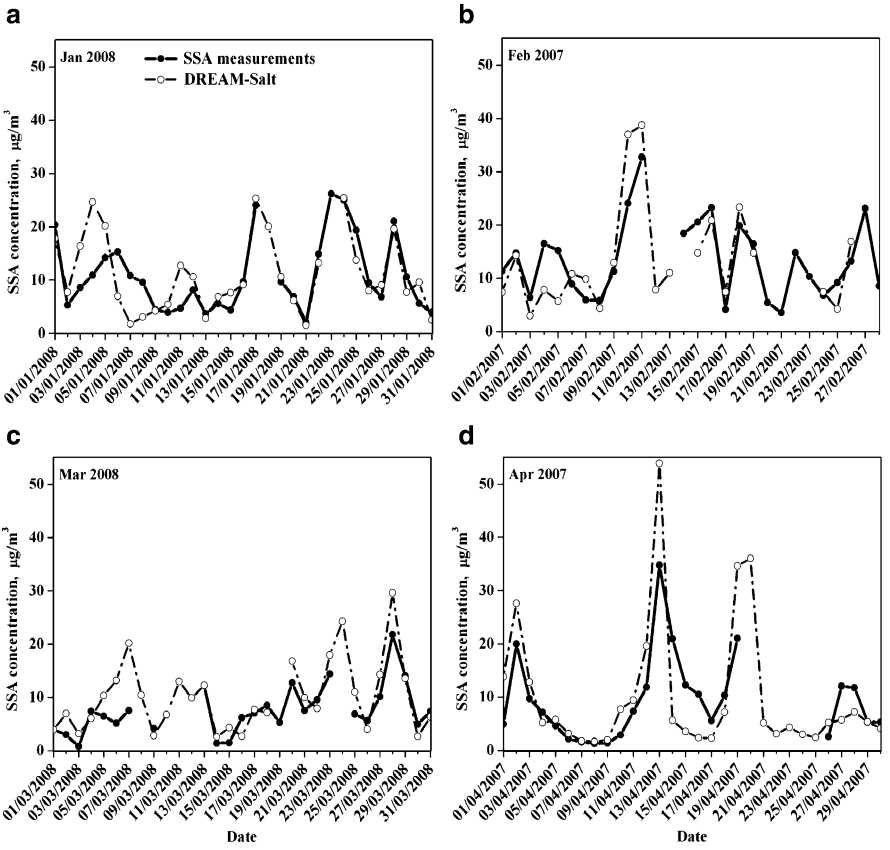


**Fig. 51.2** Examples of the comparison between modeled sea-salt concentrations and measurements in Lampedusa

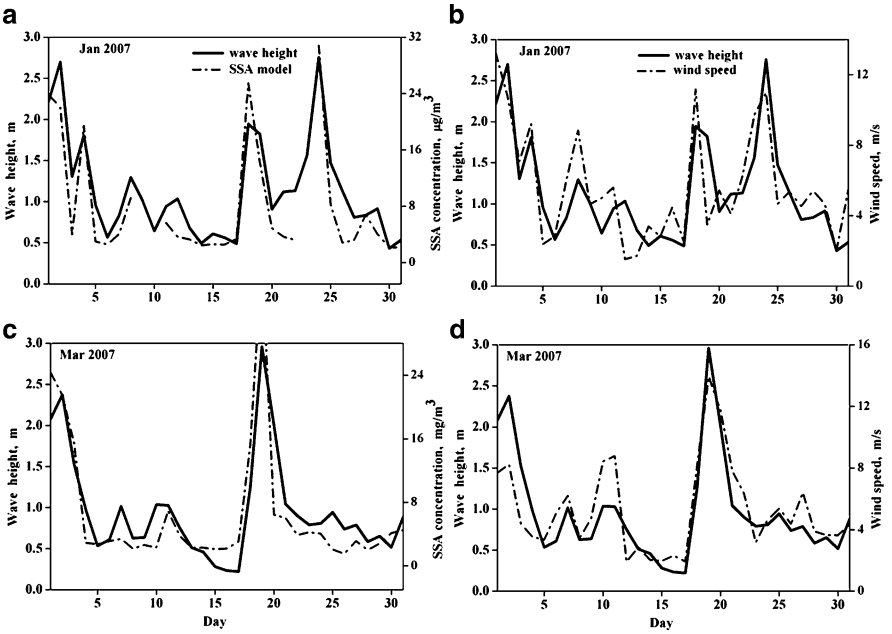


**Fig. 51.3** Examples of the comparison (*left panel*) between modeled sea-salt concentrations and wave height, and (*right panel*) between buoy-measured wind speed and wave height

The ODAS Italia 1 spar buoy in the Ligurian Sea of the Western Mediterranean basin, located at approximately 75 km far from the coast, provided us with information about wave height and sea-surface wind [7]. Since the buoy is positioned offshore, it is exposed to winds and waves without any shield by the surrounding orography [6]. Daily data are available for the periods July 2006–August 2007, August 2008–December 2008, and March 2009–September 2009. The model performance has been indirectly verified by comparing modeled SSA concentrations with observed wave height taking into account that the main factors for SSA production in the open sea are sea waves and associated winds (Fig. 51.3).

## 51.3 Results and Discussion

Direct model-vs.-measurement comparisons at Lampedusa show a relatively high correlation of 0.7 between model data and measurements for all 380 days used in the analysis; a rather low mean bias of $-0.5$ μg/m$^3$; and a mean normalized bias less than 20% [3]. Therefore, the model was capable of producing reasonable SSA concentrations and their day-to-day variations over the open sea.

Quite a good correspondence between wind speed and wave height measured at the ODAS Italia 1 buoy is clearly seen in Fig. 51.3, indicating that most sea-waves

were created by the observed strong winds. As surface winds are used as a key parameter for sea-salt production in the model SSA parameterization, one could expect that the good correspondence between wind speed and wave height should be accompanied by a good correspondence between modeled SSA concentrations and wave height. Indeed, the examples shown in Fig. 51.3 demonstrate quite a good correlation between modeled SSA – concentrations and wave height at the monitoring site. In general, as estimated for all 540 days used in the analysis, the model performance was considered acceptable: it was characterized by a relatively high correlation of 0.78 between modeled SSA – concentrations and wave height. The correlation between observed wind speed and wave height was estimated to be as much as 0.82. This is an indirect indication that, over the open sea, the model produced realistic day-to-day time variations of SSA-concentrations, in line with observed day-to-day variations of wind speed and wave height.

## References

1. Erickson DJ, Merril JT, Duce RA (1986) Seasonal estimates of global atmospheric sea-salt distribution. J Geophys Res 91:1067–1072
2. Kishcha P, Nickovic S, Ganor E, Kordova L, Alpert P (2008) Saharan dust over the Eastern Mediterranean: model sensitivity. In: Air pollution modelling and its applications XIX, chap 4.2. Springer, Dordrecht, pp 358–366. ISSN: 1874-6519, doi:10.1007/978-1-4020-8453-9_39
3. Kishcha P, Nickovic S, Starobinets B, di Sarra A, Udisti R, Becagli S, Sferlazzo D, Bommarito C, Alpert P (2011) Sea-salt aerosol forecasts compared with daily measurements at the island of Lampedusa (Central Mediterranean). Atmos Res. doi:10.1016/j.atmosres.2010.12.021
4. Nickovic S, Janjic ZI, Kishsha P, Alpert P (2007) Model for simulation of the sea salt aerosol atmospheric cycle. Research activities in Atmospheric and Oceanic Modelling, WMO, Geneva, CAS/JSC WGNE, sect 20, pp 19–20
5. Nickovic S, Kallos G, Papadopoulos A, Kakaliagou O (2001) A model for prediction of desert dust cycle in the atmosphere. J Geophys Res 106(D16):18113–18129
6. Pensieri S, Bozzano R, Schiano ME (2010) Comparison between QuikSCAT and buoy wind data in the Ligurian Sea. J Mar Syst 81:286–296
7. Picco P, Bozzano R, Schiano ME, Bordone A, Borghini M, Di Nallo G, Pensieri S, Schirone A, Sparnocchia S (2007) Marine observing system from fixed platform in the Ligurian Sea. Boll Geofis Teor Appl 48(3):227–239

# Chapter 52
# Comparison of EMEP Emissions Inventory and Limited Area Bottom-Up Inventory in the Simulation of Air Quality by Means of CHIMERE

**María Dios, C.M. Torres, A. Rodríguez, S. Saavedra, José A. Souto, and J.J. Casares**

**Abstract** The purpose of this work was to assess the influence of emission data on CHIMERE, by means of the study of episodic ozone levels in 2007 at Galicia (NW of Spain). As input data to the simulations both EMEP emissions inventory data and a detailed bottom-up inventory for the EMEP (51,14) grid cell were applied, in order to compare their impact in the air quality results.

**Keywords** EMEP/CORINAIR emissions • Bottom-up emissions inventory • CHIMERE model • Episodic ozone

## 52.1 Introduction

The assessment of emissions impacts over final air quality standards requires their qualitative and quantitative characterization. In addition, the use of these emissions as the input to an air quality model allows to simulate the transport, deposition and/or chemical transformation of pollutants emissions in the atmosphere. In order to estimate the air quality, in this work, the air quality model employed CHIMERE (version *chimere2008c*) was applied as a powerful research tool for comparing the results using different emissions input data [5].

Emissions data provided by CHIMERE are mainly from EMEP annual emissions database, which are based on annual national emissions inventories and activity data, reported every year to EMEP *(European Monitoring and Evaluation Programme)*, by each participating country of the Convention on Long-range Transboundary Air Pollution CLRTAP [2].

M. Dios (✉) • C.M. Torres • A. Rodríguez • S. Saavedra • J.A. Souto • J.J. Casares
Department of Chemical Engineering, University of Santiago de Compostela,
15782 Santiago de Compostela, Spain
e-mail: maria.dios@usc.es; ja.souto@usc.es

D.G. Steyn and S. Trini Castelli (eds.), *Air Pollution Modeling and its Application XXI*,
NATO Science for Peace and Security Series C: Environmental Security 4,
DOI 10.1007/978-94-007-1359-8_52, 

Due to the aggregating nature of the EMEP inventory, during the top-down processes of allocation and spatial distribution of the reported emissions, the resulting input data becomes slightly different and, in some ways, less accurate, from that which can be obtained directly by means of application of a bottom-up methodology. In this work, emissions inventory was performed for EMEP (51,14) grid cell, changing the original EMEP emissions. This cell is characterised by different urban, industrial and agricultural activities: a city of around 100,000 inhabitants; 51 rural councils (30 completely and 21 partially affected); and diverse industrial activities related to ceramic and food industry.

The study was completed with the application of the original EMEP emissions data and the emissions changed by this bottom-up inventory in the CHIMERE model during the simulation of a local ozone episode, on 1–2/Aug/2007; in order to estimate the impact of both emissions inventories in the ozone glc.

## 52.2 Methodology

*Bottom-up emissions inventory*: Emissions were estimated through an organized calculation procedure following EMEP/CORINAIR structure [3]. However, specific data of the activities were combined to reference data, driving to decompose the pollutant sources into individual units, which were independently quantified. Considering that, the more specific these units, the lower will be the error related to the calculation [1].

*CHIMERE simulations*: In this application, the main features in the CHIMERE model were:

- Mother domain: Covering the region of Galicia (NW of Spain) from 10.0°W to 6.0°W, and from 41.0°N to 44.0°N (see Fig. 52.1)
- Resolution: 0.08° × 0.06°
- Meteorological data: MM5 mesoscale model simulations by using NCEP reanalysis as boundary conditions (which were also applied as input to estimate BVOCs emissions using MEGAN model)

## 52.3 Results and Concluding Remarks

*Comparison between inventories*: For comparison purposes and because of the huge differences observed, the ratio between the bottom-up and EMEP emissions over EMEP (51,14) grid cell was presented (Table 52.1). Though major differences were found, especially in road and off-road transport and residential sectors, both inventories are comparable since are of the same order of magnitude.

These results show the aggregating characteristics of EMEP data. The area under study concentrates high values of traffic and agricultural activity in respect of its

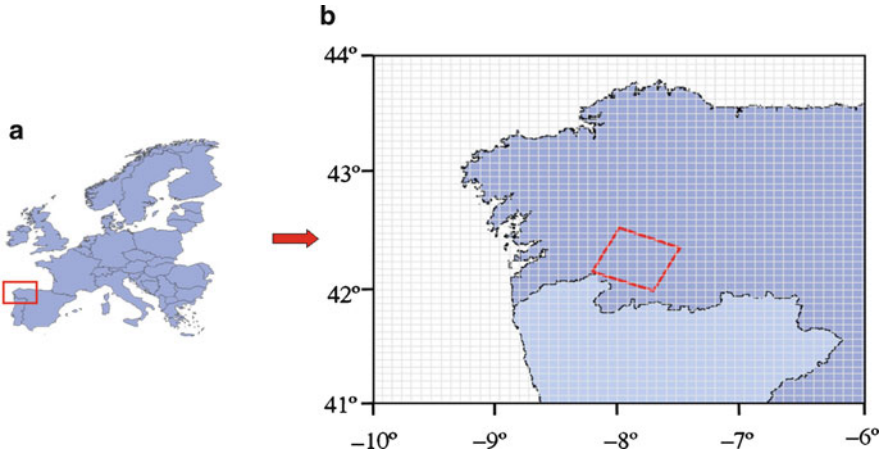


**Fig. 52.1** Mother domain (**a**) of the simulations and the highlighted area (**b**) corresponding to EMEP (51,14) grid cell, on which the bottom-up emissions inventory was done

**Table 52.1** Bottom-up inventory to EMEP inventory emissions ratio for EMEP (51,14) grid cell

| $NO_x$ | NMVOC | CO | $PM_{2.5}$ | $SO_x$ | $NH_3$ | Cd | Hg | Pb |
|---|---|---|---|---|---|---|---|---|
| 3.18 | 1.85 | 1.33 | 1.80 | 3.42 | 0.84 | 1.87 | 3.06 | 1.48 |

surroundings. Within the city involved, more than 140,000 vehicles per day can be measured [6]; and with regard to the off-road machinery, more than 4,900 agricultural engines are registered [4]. Also, the usage of diesel fuel for domestic heating plays a very significant role for certain pollutants.

*CHIMERE results*: Simulation results of the two scenarios proposed show some regional differences in ozone glc levels; especially during the 2nd day of the simulation (Fig. 52.2). Due to the higher emission values obtained the simulation of the bottom-up inventory shows higher pollution levels outside the EMEP (51,14) grid cell, with significant changes in the North of Portugal. These results do suggest a transboundary air pollution transport not detected applying EMEP emissions database.

Because of the limited period of this study, further research has to be done, in order to asses the influence and improvements that can be achieve with the detailed calculation of the emission data for air quality models. This approach requires a great deal of effort in the compilation of emission and activity factors, calculation and analysis, and air quality modeling. However, the differences observed in this simulation should justify the extra work.

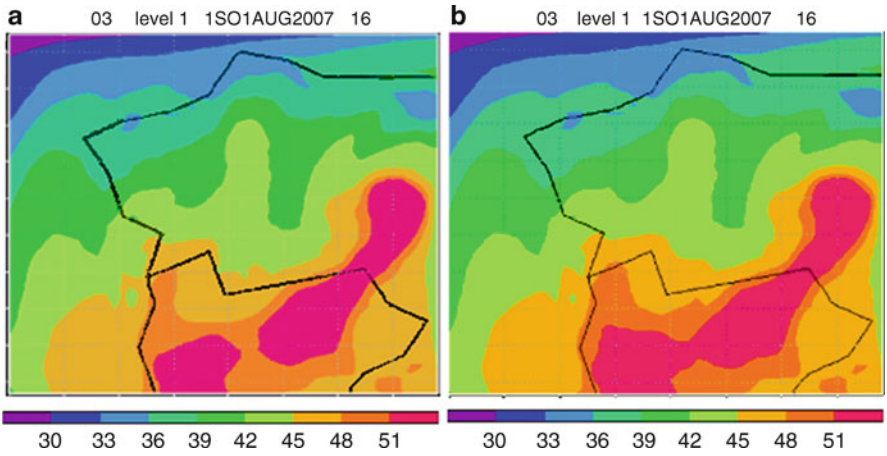


**Fig. 52.2** Simulations of hourly glc ozone concentration (ppb) with CHIMERE applying (**a**) EMEP data; (**b**) EMEP data except in (51,14) grid cell where bottom-up emissions were considered

**Acknowledgments** M. Dios and A. Rodríguez research grants have been supported by Xunta de Galicia, through the Ph.D. Programme, María Barbeito.

## References

1. Casares JJ et al (2005) Inventory, assessment and projection of Galician atmospheric industrial emissions. University of Santiago de Compostela, Santiago de Compostela (in Spanish)
2. CEIP EMEP Centre on Emission Inventories and Projections (2007) Officially reported emission data, year 2007. http://www.ceip.at/. Updated June 2009
3. EEA European Environment Agency (2007) EMEP/CORINAIR Emission Inventory Guidebook – 2007. Technical report No. 16/2007. European Environment Agency, Copenhagen
4. IGE Galician Statistical Institute (2007) Registered fleet of agricultural and forest machinery. Local database. http://www.ige.eu. Updated May 2009
5. INERIS Institut National de l'Environnement Industriel et des Risques (2008) Documentation of the chemistry-transport model CHIMERE [version chimere2008]. Institut Pierre-Simon Laplace, LISA & CNRS
6. Xunta de Galicia (2008) Traffic report about Galician roads 2007. Department of territorial policy, public works and transport. Galician Government, Spain

# Chapter 53
# Forecasting $O_3$, $PM_{25}$ and $NO_2$ Hourly Spot Concentrations Using an Updatable MOS Methodology

**Stavros Antonopoulos, Pierre Bourgouin, Jacques Montpetit, and Gerard Croteau**

**Abstract** The steps taken to expand the Updatable MOS (UMOS) methodology to air-quality forecasting (UMOS-AQ) will be presented. This methodology has shown great ability to improve direct model output with weather elements. Air-quality data (observational and numerical) are used to produce hourly spot concentration forecasts of ozone ($O_3$), particulate matter 2.5 μm($PM_{25}$) and nitrogen dioxide ($NO_2$), up to 48 h. Numerical data originating from one source, an air-quality model (GEM-MACH15), were used to produce a set of direct and calculated predictors. The UMOS-AQ system produces one equation per station, per predictand, per model run and per forecast hour. Verifications on an independent sample show encouraging results with significant improvement over the model's direct forecast. The UMOS-AQ system effectively reduces the model's bias and error while increasing its variance. Important conclusions can be derived from the order of the chosen predictors that can lead to a better understanding of site-specific conditions.

**Keywords** Particulate matter • Ozone • Nitrogen dioxide • Updatable MOS • UMOS • MLR • Post-processing

## 53.1 Introduction

The Updatable Model Output Statistics – Air Quality (UMOS-AQ) project applies Multivariate Linear Regression (MLR) statistics to forecast air-quality predictands. One of its main advantages versus other traditional MOS systems is its ability to adapt to model changes and also update its equations four times per month.

S. Antonopoulos (✉) • P. Bourgouin • J. Montpetit • G. Croteau
Weather Elements Section, Environment Canada, Dorval, QC, Canada
e-mail: stavros.andronopoulos@ec.gc.ca; pierre.bourgouin@ec.gc.ca

D.G. Steyn and S. Trini Castelli (eds.), *Air Pollution Modeling and its Application XXI*,
NATO Science for Peace and Security Series C: Environmental Security 4,
DOI 10.1007/978-94-007-1359-8_53, 

UMOS is a statistical post-processing system that takes into account statistical relations between predictors and predictands and therefore improves on the model's output Wilson and Vallée [1].

UMOS-AQ has two seasons (summer and winter) and needs a minimum of 250 observation-forecast pairs per season to create stable equations and produce spot forecasts. Its principal role is to remove the model's bias originating from systematic errors. In addition, it takes into account statistical relationships between predictors and predictands and therefore brings a general improvement in the model's output.

## 53.2 History and Evolution

The project went through several major and minor changes over the course of the last 3 years, with the following two main phases:

**Phase 1**
The project started in 2007 with a minimal database of observations (2 years).
The predictor database was built from two models : GEM-Reg (the Canadian Regional GEM) and CHRONOS, a chemical transport model. Three-hourly forecasts were issued.

**Phase 2**
In the second phase, hourly forecasts were achieved after a cloning of the Sum of Squares and Cross Products (SSCP) matrices.
In addition, a model switchover was achieved by a gradual transition towards the new Canadian air-quality model GEM-MACH15 that provides both the chemistry and meteorology for predictor production.

## 53.3 Stations

We presently have 231 stations in the dictionary and Fig. 53.1 shows their geographic distribution.

All stations belong to the National Air Pollution Surveillance Network (NAPS) and measure all or a combination of the following pollutants: ozone ($O_3$), fine particulates ($PM_{25}$) and nitrogen dioxide ($NO_2$).

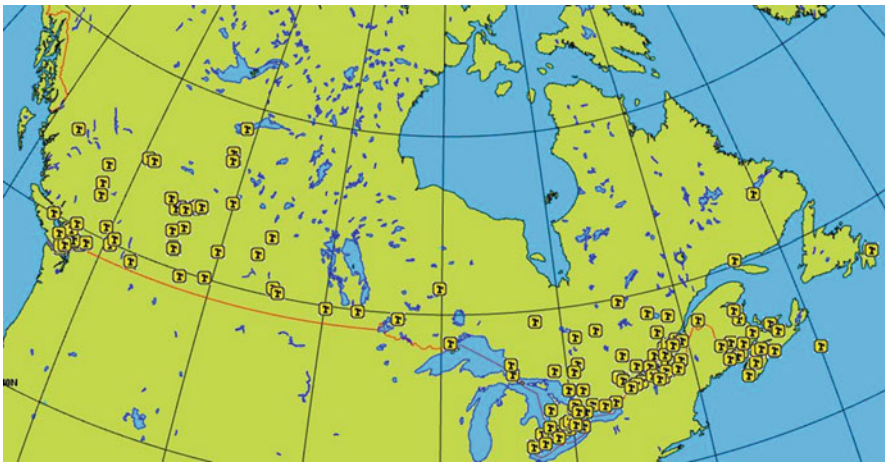

**Fig. 53.1** Geographical distribution of UMOS-AQ stations

## 53.4 Verifications

Below we show verification scores for two seasons, summer and winter, for the following periods: 15th August 2009–15th October 2009 and 14th December 2009–15th February 2010.

The scores are based on independent samples produced in a semi-operational mode.

The scores used are BIAS, RMSE and de-biased Reduction of Variance ($RV_{cmc}$) defined as:

$$RVcmc = 1 - \left[ \frac{\sum_{i=1}^{N} (Fi - BIAS - Oi)^2}{\sum_{i=1}^{N} \left(\bar{O} - Oi\right)^2} \right]$$

The scores in the graphics below are calculated for all stations that observe the predictand in question for the 00Z run (Figs. 53.2 and 53.3).

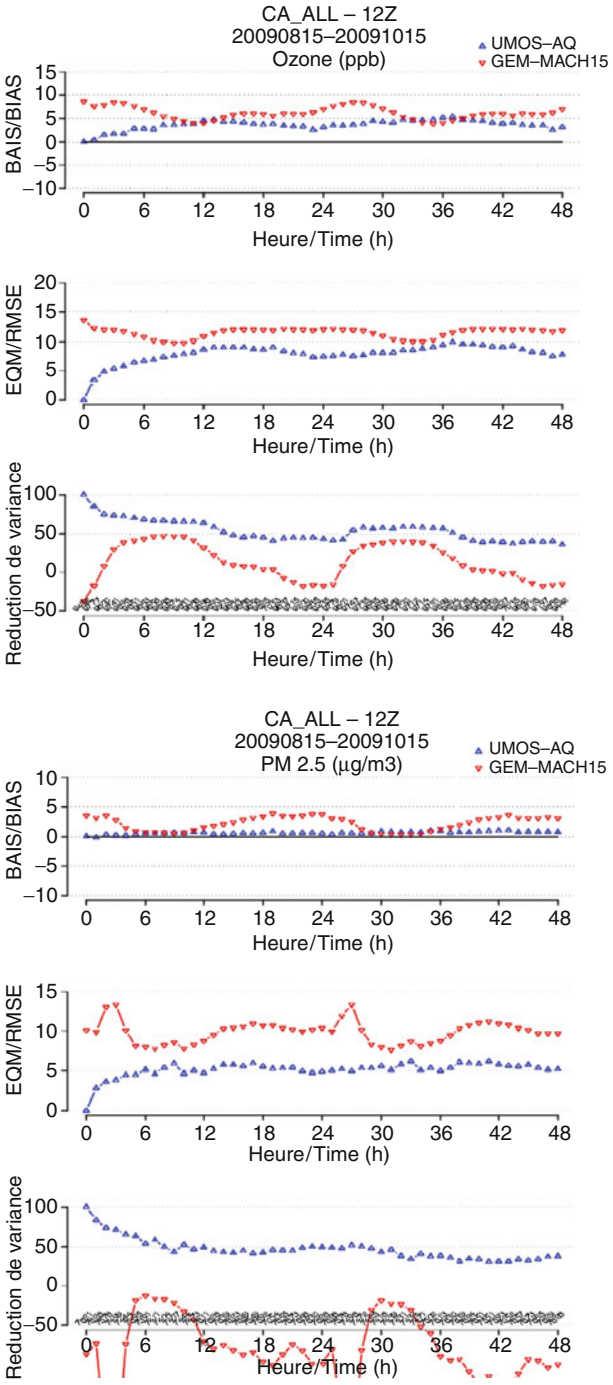


**Fig. 53.2** Ozone and $PM_{25}$ scores for the summer season

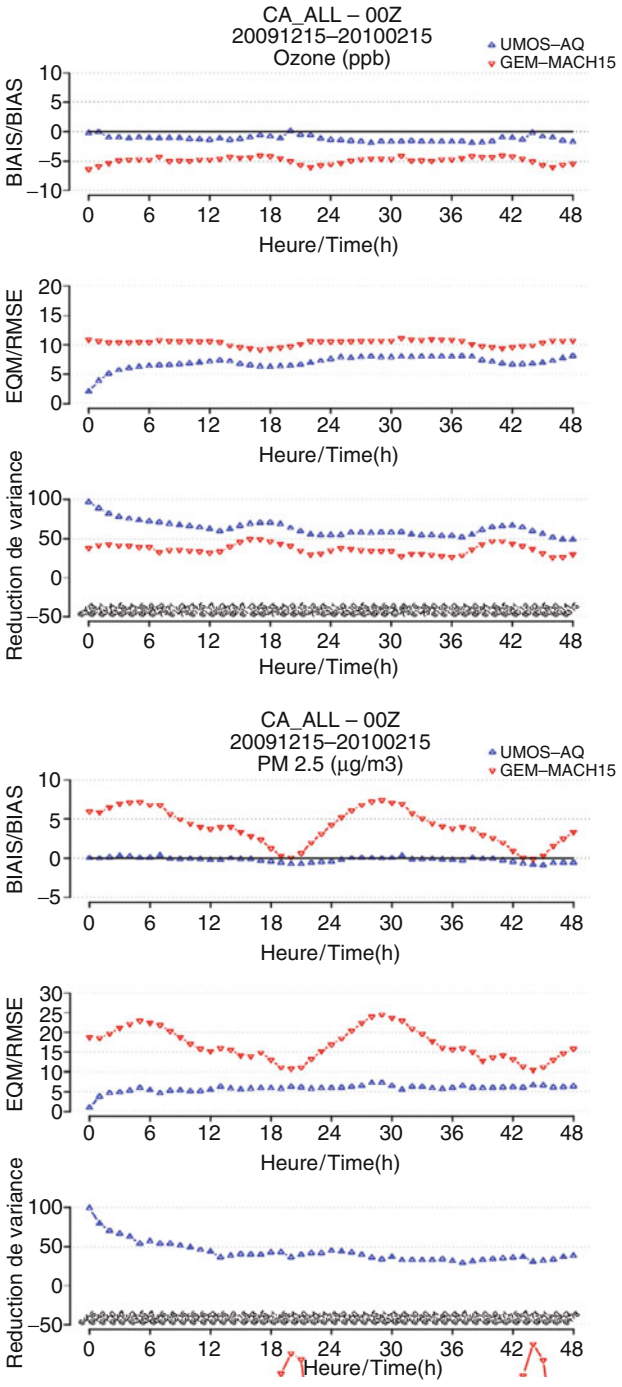


**Fig. 53.3** Ozone and $PM_{25}$ scores for the winter season

## 53.5 Conclusions

Over the last 2 years UMOS-AQ has shown a significant improvement over the direct model output for all three pollutants in both seasons. This fact has been repeatedly verified over long and short term independent verification periods.

An abrupt model switchover along with a matrix cloning operation did not noticeably affect the quality of the forecasts which demonstrates the robustness of the system.

UMOS-AQ can provide a high quality national guidance in AQ forecasting.

Future improvement is expected as more cases get accumulated and a full transition to GEM-MACH15 is completed. UMOS has shown great potential into a different field such as AQ.

## Reference

1. Wilson JW, Vallée M (2001) The Canadian updatable model output statistics (UMOS) system: design and development tests. Weather Forecast 17:206–222

# Chapter 54
# Coupling of the CTM CHIMERE to the High Resolution LAM ALADIN for Belgium

**Andy W. Delcloo, Alex Deckmyn, Rafiq Hamdi, Herman Van Langenhove, Gilles Foret, and Hugo De Backer**

**Abstract** At the Royal Meteorological Institute of Belgium we use the chemical transport model (CTM) CHIMERE. In a first phase it has been coupled to meteo fields from ECMWF. The emission database used is EMEP. The simulation domain covers Western Europe with a spatial resolution of 50 km. RMI also runs the Limited Area NWP model ALADIN operationally four times a day at a spatial resolution of 7 km. The meteorological fields from ALADIN have been used to apply a one way nesting to the CTM model running at a spatial resolution of 7 km on a domain of about $680 \times 680\ km^2$ covering Belgium and The Netherlands. The emission database used for this high resolution is the TNO/GEMS emission database. We present the first results of this coupling for ozone and PM10 for two different episodes. Also the influence of running ALADIN and its updated version ALARO with improved physical parameterizations will be investigated.

**Keywords** Ozone modelling • LAM • ALADIN

A.W. Delcloo (✉) • A. Deckmyn • R. Hamdi • H. De Backer
Royal Meteorological Institute of Belgium, Brussels, Belgium
e-mail: andy.delcloo@meteo.be

H. Van Langenhove
Research group EnVOC, Department of Sustainable Organic Chemistry and Technology, Faculty of Bioscience Engineering, Ghent University, Ghent, Belgium

G. Foret
Laboratoire Interuniversitaire des Systèmes Atmosphériques, NRS/INSU/IPSL/UPEC/Université, P7 Créteil, France

D.G. Steyn and S. Trini Castelli (eds.), *Air Pollution Modeling and its Application XXI*, NATO Science for Peace and Security Series C: Environmental Security 4,
DOI 10.1007/978-94-007-1359-8_54, 

## 54.1 Introduction

The chemical transport model CHIMERE [2] has been coupled to the IFS/ECMWF at a coarse resolution of 50 km. The CHIMERE model is able to catch most of the day-to-day variability when verified against observations for Belgium at this coarse resolution. Still, there are days where the CTM is simply not able to catch an ozone pollution event. Delcloo and Brasseur [1] showed the importance of good quality meteorological data by perturbing some meteorological parameters that are known to have a major influence on the production of ozone. Such an ensemble approach can enhance forecasts of ozone- and PM10 pollution events in a probabilistic way.

Running CHIMERE on a coarse resolution of 50 km, using a large domain (Europe) helps us understand the contribution of synoptic weather phenomena to pollution events. However, to study the ability of a CTM to capture the day-to-day variability on a local scale, it is necessary to feed the model with high-resolution meteorological data from a NWP-model. The NWP-models we use for our analysis run four times a day in an operational context at our institute; the ALADIN model and its updated version ALARO receive their boundary conditions from ALADIN France, run by Météo France.

## 54.2 Results and Discussion

To validate our results, observation data is used from IRCELINE. Two different versions of our NWP-model are used: ALADIN and ALARO. With these models, two different cloud scenarios are investigated.

When considering the production of ozone, cloud cover is one of the most important meteorological input variables together with temperature. Therefore we will study two different methods to integrate the cloud cover from the NWP model output in the CTM. The first method is to use instantaneous values valid at the coupling times (every 3 h) (CL1). A second possibility is to use 3 h mean cloud cover values (CL2). This could have an important effect on the production of ozone in the summer during peak events.

The improved physical parameterization scheme of ALARO leads to an improved precipitation-, temperature- and cloud field. A qualitative and quantitative evaluation is made between the one-way nested couplings of CHIMERE with both different LAM's. Table 54.1 gives an overview of some general statistics on the modelling of maximum ozone concentrations for 1 month during the summer (July 2008) for some specific observation stations and different scenarios. Figure 54.1 shows a time series of modelled- against observed maximum ozone concentrations for the station of Houtem for the next day for the ALARO-CL2 scenario.

**Table 54.1** Correlation, rmse (μg/m$^3$) and bias (μg/m$^3$) for the time period 01/07/2008–31/07/2008 are shown for some stations for the scenarios ALADIN-CL1, ALADIN-CL2, ALARO-CL1 and ALARO-CL2 for the analysis (D−1)

| | | Dessel | Houtem | Moerkerke | Destel-bergen | Hasselt |
|---|---|---|---|---|---|---|
| ALADIN-CL1 | corr | 0.89 | 0.83 | 0.85 | 0.87 | 0.84 |
| | rmse | 20.65 | 16.73 | 17.95 | 17.07 | 15.39 |
| | bias | 8.15 | 2.06 | 7.46 | 3.14 | 1.46 |
| ALADIN-CL2 | corr | 0.9 | 0.85 | 0.86 | 0.87 | 0.84 |
| | rmse | 18.92 | 15.92 | 17.76 | 16.47 | 15.25 |
| | bias | 6.33 | 1.35 | 6.77 | 2.38 | 1.04 |
| ALARO-CL1 | corr | 0.91 | 0.86 | 0.85 | 0.88 | 0.89 |
| | rmse | 18.95 | 15.33 | 18.49 | 16.07 | 13.49 |
| | bias | 6.5 | 2.42 | 8.59 | 3.92 | 1.56 |
| ALARO-CL2 | corr | 0.92 | 0.87 | 0.86 | 0.88 | 0.89 |
| | rmse | 18.81 | 15.19 | 18.36 | 15.9 | 13.51 |
| | bias | 4.94 | 1.9 | 7.65 | 2.97 | 1.36 |

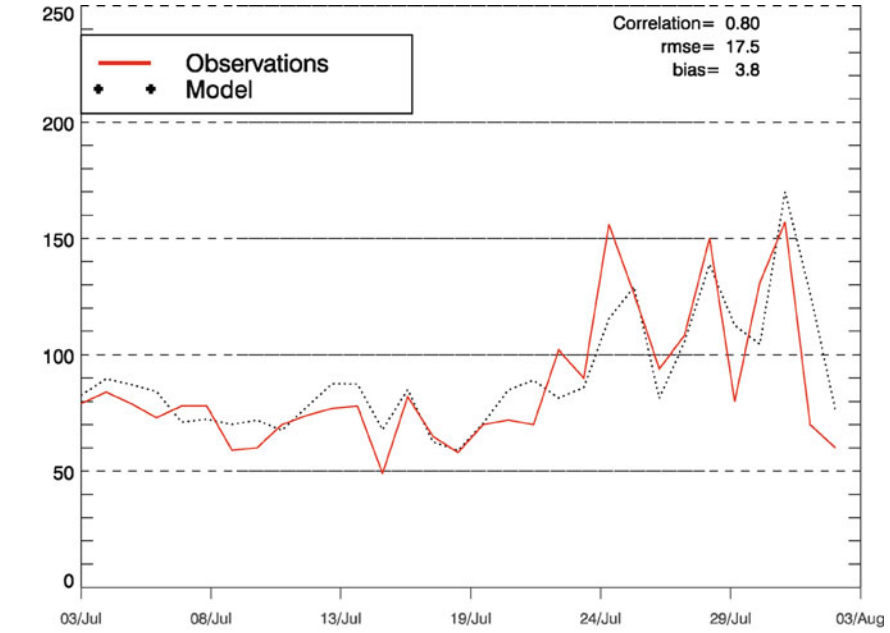


**Fig. 54.1** Time series of observed- and modelled maximum ozone concentrations for the time period 01/07/2008–31/07/2008 for the station of Houtem for the next day (D + 1)

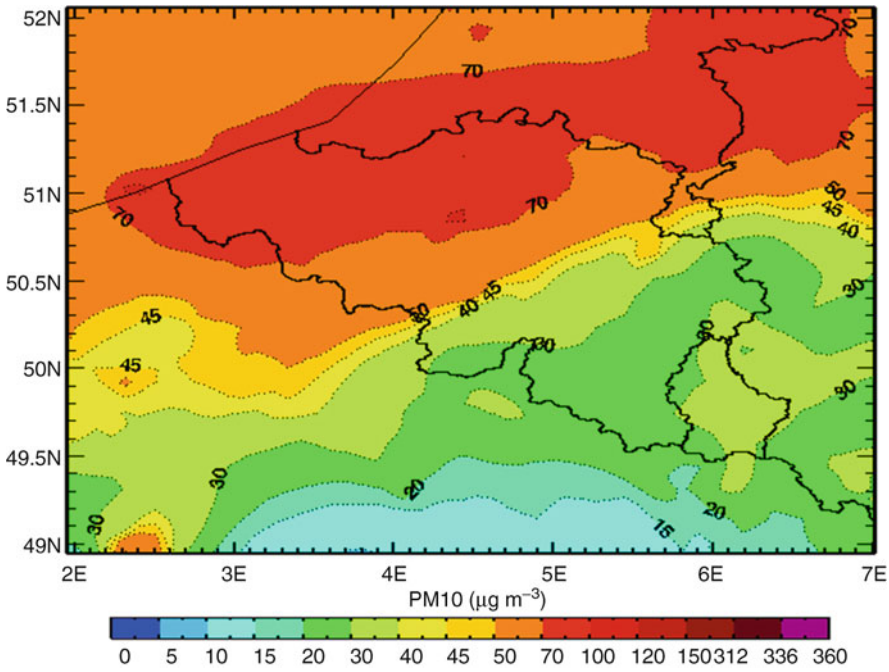


**Fig. 54.2** Averaged modelled PM10 concentrations for the Belgian domain on the 20th of February 2008 (analysis, D−1)

Table 54.1 shows that the updated version ALARO reduces the bias and improves the modelling of the day-to-day variability of the maximum ozone concentrations. Also the new integration of clouds in the CTM (CL2) improved the model results.

PM10 concentrations have been modelled during 1 month in the winter period (February 2008). Figure 54.2 shows an example of the skills of this model to catch "pollution events". On this particular day, elevated particulate matter concentrations were measured.

In general, correlations between modelled- and observed PM10 concentrations vary between 0.5 and 0.8. The statistics for PM10 also show an improvement (reduction) in the bias when coupled to the ALARO NWP model (4–5 µg/m$^3$).

## 54.3 Conclusions

When the CTM was coupled to the updated ALADIN NWP-model ALARO, the statistics significantly improved for both modelling maximum ozone- and PM10 concentrations.

The adapted implementation of cloud cover from the NWP data supplementary improved the modelling results for maximum ozone- and PM10 concentrations during summer.

**Acknowledgments** The authors would like to thank IRCELINE for providing the ozone and PM10 data.

## References

1. Delcloo A, Brasseur O (2007) Evaluation of an operational ensemble prediction system for ozone concentrations over Belgium using the CTM Chimere, Aveiro, 23–30 Sept
2. Vautard R, Beekmann M, Roux J, Gombert D (2001) Validation of a deterministic forecasting system for the ozone concentrations over the Paris area. Atmos Environ 35:2449–2461

# Chapter 55
# Impact of Saharan Dust on PM10 Concentrations in the FARM model

**Anna Pederzoli, Mihaela Mircea, Sandro Finardi, and Gabriele Zanini**

**Abstract** This study aims to improve the performance of the Flexible Air quality Regional Model FARM by including dust concentrations from a dust transport model (SKIRON) into Lateral Boundary Conditions (LBCs). A sensitivity test has been performed in order to assess the impact of SKIRON Saharan dust on $PM_{10}$ modelled concentrations. A dust episode (25th–30th July 2005) has been simulated running FARM on a $20 \times 20\,km^2$ resolution domain over Italy. Preliminary results from three simulations: NDC ("no dust" case), DC ("dust" case) and DC1.3 ("dust multiplied by a factor 1.3" case) have been compared to $PM_{10}$ ground measurements from the Italian Air Quality Network.

**Keywords** Air quality • Modeling • Dust • Scenarios • Boundary conditions

## 55.1 Models Description

The Flexible Air quality Regional Model (FARM) [11] is a three-dimensional Eulerian model which simulates the transport, dispersion and chemistry of aerosol and gaseous pollutants in the atmosphere. The gas-phase chemistry is modelled by the chemical scheme SAPRC-90 [2] coupled with the online Tropospheric Ultraviolet and Visible (TUV) Radiation Model [9]. FARM implements the aerosol module by

A. Pederzoli (✉)
European Commission – DG JRC, Via E. Fermi,
2749 (TP 441), I-21027 Ispra (VA), Italy

M. Mircea • G. Zanini
ENEA, Via Martiri di Monte Sole, 4, 40129 Bologna, Italy
e-mail: anna.pederzoli@jrc.ec.europa.eu

S. Finardi
ARIANET SRL, via Gilino, 9, 20128 Milan, Italy
e-mail: s.finardi@aria-net.it

D.G. Steyn and S. Trini Castelli (eds.), *Air Pollution Modeling and its Application XXI*,
NATO Science for Peace and Security Series C: Environmental Security 4,
DOI 10.1007/978-94-007-1359-8_55, 

Binkowski [1] for modelling the aerosol chemistry and dynamics. Meteorological fields come from the Regional Atmospheric Modelling System (RAMS) prognostic model [3] The anthropogenic emission inventory used in this study is derived from the diffuse emissions at provincial level [5].

The SKIRON/Eta system [7] is based on the Eta/NCEP atmospheric model [6]. It includes the dust cycle modules by Nickovic et al. [10] which incorporate state-of-the-art parameterizations of all the main atmospheric processes involving dust. SKIRON output data consist of gridded 3D fields of size resolved dust concentration over Northern Africa and Europe. The temporal resolution is hourly. The model horizontal resolution is $0.24^\circ \times 0.24^\circ$. The model has 38 vertical levels from surface up to 22 km.

## 55.2 Model Simulations

Three FARM simulations have been carried out on a 20 km $\times$ 20 km domain over Italy (Fig. 55.1a). A dust episode (25th–29th July 2005) has been simulated. Modelled surface $PM_{10}$ concentrations have been extracted and compared to observations from six rural background monitoring stations across Italy (Fig. 55.1b).

**NDC**. In the "No Dust Case" concentrations from the EMEP (European Monitoring and Evaluation Programme) model are used as LBCs in FARM. EMEP concentrations are interpolated from 50 $\times$ 50 $km^2$ to 20 $\times$ 20 $km^2$ and re-projected onto the four sides of the FARM domain. EMEP fields do not include dust concentration.

**DC**. In the "Dust Case" simulation, hourly SKIRON fields are interpolated to 20 $\times$ 20 $km^2$ and re-projected onto the four sides of FARM grid. Size-resolved dust concentrations by SKIRON are then added to the LBCs used in the previous case (NDC).

**DC1.3**. SKIRON dust concentrations are multiplied by a factor 1.3. According to Kallos et al. [8] the model underestimates low dust concentrations by approximately 30%. The same study suggests to multiply SKIRON dust values by a factor 1.3 in order to reduce the biases of the model. The same procedure used in the DC is then applied and new LBCs are created.

Results from the DC and DC1.3 simulations are very close for all stations. The increase of dust concentration by a factor 1.3 suggested by Kallos et al. [8] has not a significant impact on $PM_{10}$ concentrations. Differences between DC and DC1.3 concentrations are approximately less than 3 $\mu gm^{-3}$. The comparison with measurements suggests that FARM underestimates $PM_{10}$ concentration in the NDC simulation (Fig. 55.2). This underestimate is only partially reduced by the introduction of dust concentrations on the boundaries. At Gherardi station Saharan dust has not a significant impact on $PM_{10}$ concentrations. FARM underestimates $PM_{10}$ observed concentration by approximately 8 $\mu gm^{-3}$ up to 15 $\mu gm^{-3}$ in all simulations. In S. Antioco the dust contribution is more relevant, ranging from 4 $\mu gm^{-3}$ on both 26th and 27th July up to 10 $\mu gm^{-3}$ on the 28th. In Fontechiari the NDC simulation shows that FARM clearly underestimates PM10 concentration by approximately

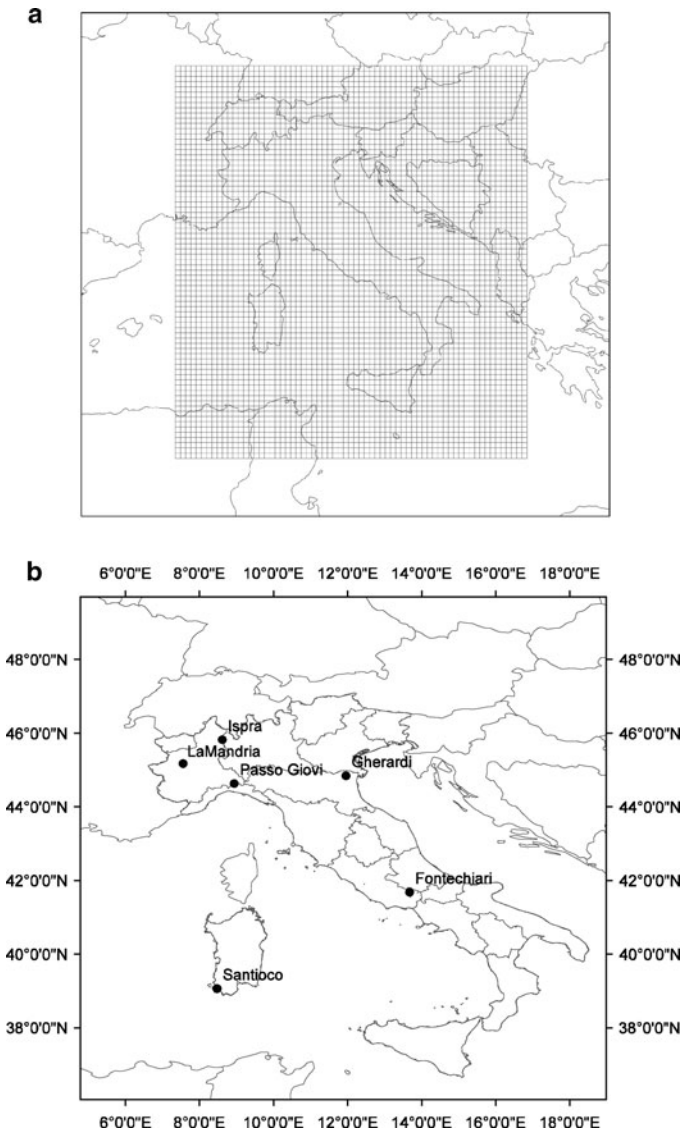


**Fig. 55.1** (**a**) Model domain at 20 × 20 km$^2$ resolution. (**b**) Rural background monitoring stations measuring PM10 concentrations on a daily basis in 2005

20 μgm$^{-3}$ up to 40 μgm$^{-3}$. This finds agreement with the results found by Gariazzo et al. [4] for the same episode over the Lazio region. SKIRON dust concentration is around 2 μgm$^{-3}$ every day apart from day 27th when the it is about 7 (DC) and 10 (DC1.3) μgm$^{-3}$. The stations in Northern Italy (Ispra, La Mandria and Passo Giovi) all show a similar behaviour. The dust contribution is always very low (about 2 μgm$^{-3}$), apart from day 29th: the underestimate shows a reduction varying between 9 and 12 μgm$^{-3}$ in the DC simulation and between 12 and 17 μgm$^{-3}$ in the DC1.3 one.

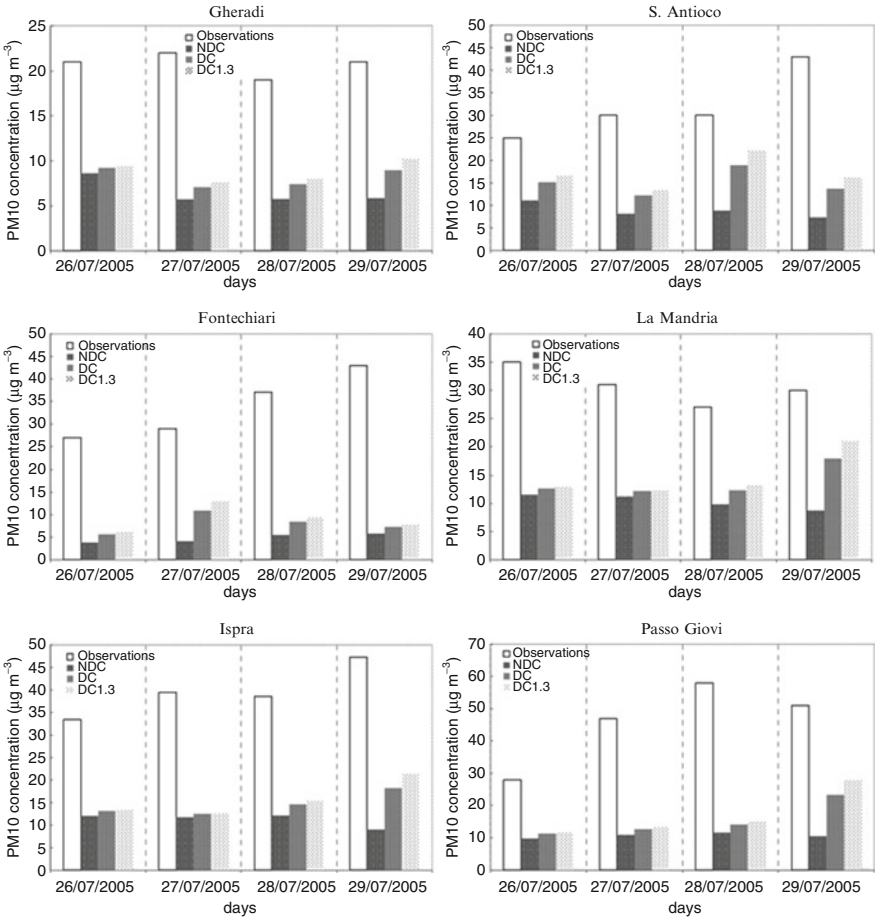


**Fig. 55.2** Comparison between modelled and measured $PM_{10}$ concentrations at six rural background monitoring sites for the simulations: NDC, DC and DC1.3

**Acknowledgments** This work is part of the MINNI project, funded by the Italian Ministry for Environment, Territory and Sea and carried out by ENEA and ARIANET Srl. A special thanks to G. Kallos and the Atmospheric Modeling and Weather Forecasting Group at the University of Athens for providing the SKIRON modelled data used in this work.

## References

1. Binkowski FS (1999) The aerosol portion of Models-3 CMAQ. In: Byun DW, Ching JKS (eds) Science algorithms of the EPA Models-3 Community Multiscale Air Quality (CMAQ) modeling system. Part II: chaps 9–18. National Exposure Research Laboratory, U.S. Environmental Protection Agency, Washington, DC. EPA- 600/R-99/030
2. Carter WPL (1990) A detailed mechanism for the gas-phase atmospheric reactions of organic compounds. Atmos Environ 24A:481–518

3. Cotton WR, Pielke RA, Walko RL, Liston GE, Tremback CJ, Jiang H, McAnelly RL, Harrington JY, Nicholls ME, Carrio GG, McFadden JP (2003) RAMS 2001: current status and future directions. Meteorol Atmos Phys 82:5–29
4. Gariazzo C, Silibello C, Finardi S, Radice P, Piersanti A, Calori G, Cecinato A, Perrino C, Nussio F, Pelliccioni A, Gobbi GP, Di Filippo P (2007) A gas/aerosol air pollutants study over the urban area of Rome using a comprehensive chemical transport model. Atmos Environ 41:7286–7303
5. ISPRA (2005) http://www.sinanet.apat.it/it/inventaria
6. Kallos G, Nickovic S, Jovic D, Kakaliagou O, Papadopoulos A, Misirlis N, Boukas L, Mimikou N, Sakellaridis G, Papageorgiou J, Anadranistakis E, Manousakis M (1997) The regional weather forecasting system SKIRON and its capability for forecasting dust uptake and transport. In: Proceedings of the WMO conference on dust storms, Damascus, 1–6 Nov 1997, p 9
7. Kallos G, Papadopoulos A, Katsafados P, Nickovic S (2005) Trans-Atlantic Saharan dust transport: model simulation and results. J Geophys Res 111:D09204. doi:10.1029/2005JD006207
8. Kallos G, Spyrou C, Papantoniou N, Mitsakou C, Astitha M (2007) Analysis of the particulate matter exceedances in Greece during the period 2003–2004. Technical report for the Ministry of Environment City planning and public works
9. Madronich S (1993) UV radiation in the natural and perturbed atmosphere. In: Tevini M (ed) UV-B radiation and ozone depletion: effects on humans, animals, plants, microorganisms, and materials. Lewis Publisher, Boca Raton, pp 17–69
10. Nickovic S, Kallos G, Papadopoulos A, Kakaliagou O (2001) A model for prediction of desert dust cycle in the atmosphere. J Geophys Res 106:18113–18129
11. Silibello C, Calori G, Brusasca G, Giudici A, Angelino E, Fossati E, Peroni E, Buganza E, Degiarde E (2005) Modelling of PM10 concentrations over Milan urban area: validation and sensitivity analysis of different aerosol modules. In: Proceedings of fifth international conference on urban air quality, Valencia, 29–31 Mar 2005

# Chapter 56
# Contribution of Aviation Emissions on the Air Pollution Levels of the Mediterranean Region with the Use of an Online Coupled, Fully Integrated Modeling System

**Jonilda Kushta, Stavros Solomos, and George Kallos**

**Abstract** In this presentation, the contribution of the European aviation on the air pollution of the Mediterranean region is discussed using the new modeling tool, the Integrated Community Limited Area Modeling System (ICLAMS). The modeling system uses the approach of "online coupling" of meteorological and chemical mechanisms which studies the processes that take place in the atmosphere in an integrated way and in the same spatial and temporal resolution. The model was tested for July 2005 for Europe and the Mediterranean Region. Two simulations have been performed, one with emissions from all anthropogenic activities and the second excluding the emissions from aviation. The area that is influenced by the emissions from aviation is very large, and the most affected region is the Eastern Mediterranean and several areas in North Africa. The typical summer circulation with the prevailing west – northwest wind field over West and Central Europe favors the transport of pollutants towards East, South East Europe and North Africa leading to perturbations in the atmospheric composition especially up to 8 km above surface. The alterations in the atmospheric concentrations of $O_3$, are discussed.

## 56.1 Introduction

The present and forecasted growth of aviation raises concerns on the environmental impacts associated with this industry. These impacts can be characterized as direct (noise, air pollution) or indirect (feedback on radiation and cloud properties) and their temporal and spatial scales can range from hours to years and from local to

J. Kushta (✉) • S. Solomos • G. Kallos
School of Physics, Atmospheric Modeling and Weather
Forecasting Group, University of Athens, University Campus Bldg PHYS-5,
15784 Athens, Greece
e-mail: kousta@mg.uoa.gr; stavros@mg.uoa.gr; kallos@mg.uoa.gr; http://forecast.uoa.gr

D.G. Steyn and S. Trini Castelli (eds.), *Air Pollution Modeling and its Application XXI*,
NATO Science for Peace and Security Series C: Environmental Security 4,
DOI 10.1007/978-94-007-1359-8_56, 

regional. The degree of impact can change from region to region, due to different circulation regimes and topographic characteristics. In order to examine the regional impacts of aviation emissions on both air quality and meteorology an integrated modelling approach is necessary.

In this study, an effort has been devoted to assess the contribution of aviation emissions from European airports on the concentration field of several pollutants in the Mediterranean Region. The modelling study is performed with the use of ICLAMS model, which is an online coupled fully integrated, meteorology – chemistry – aerosols – cloud radiation atmospheric modelling system [4] based on the atmospheric model RAMS [1, 3]. It treats gas, aqueous and aerosol phase chemistry processes, and the atmospheric cycle of natural aerosols (mineral dust, sea salt). The model includes an explicit cloud droplet nucleation scheme as well as the radiative effects of several natural and anthropogenic aerosols.

## 56.2 Case Study

For this study, a summer test case has been selected (July 2005) due to the increased photochemical activity that occurs during this season in the Greater Mediterranean Region (GMR). Strong insolation and limited precipitation are proper conditions for the study of chemical oxidants and their transport and transformation processes [2]. The model was run twice: the first time the anthropogenic emissions from all activities (including aviation) were used, while the second time the aviation emissions of BC, CO, $NO_x$, OC and $SO_2$ have been excluded from the anthropogenic emissions. During the test period the relative contribution of the aviation emissions to the total emitted mass in the domain varies from 4.5% to 7.5% in $NO_x$ depending on the time of the day. The difference on the pollutants concentration field is defined as $C_{\text{all emissions}} - C_{\text{without aviation emissions}}$. In the present study the description is limited to the changes caused by aviation emissions on the ozone concentration field.

The meteorological conditions over Europe present a wind field dominated by the extension of the Atlantic anticyclone easterly over Europe and Mediterranean (Fig. 56.1). This lower tropospheric flow pattern favours the transport of anthropogenic pollution produced over Europe and West Mediterranean towards East Mediterranean and North Africa, preventing at the same time the transport of natural aerosol pollutants like mineral dust towards higher latitudes.

During daytime, the difference in the ozone concentration field over Europe and Mediterranean comes as a result of two mechanisms: firstly, higher ozone production is noticed near airports due to elevated levels of ozone precursors (mainly $NO_x$); secondly, the transport of ozone, and to a smaller degree the transport of ozone precursors, leads to higher ozone levels in distant downwind areas (Fig. 56.2a, b). During nighttime the ozone field remains higher, when the aviation emissions are included, due to the preservation of the daytime difference (Fig. 56.2c, d). A decrease in $O_3$ concentration due to the titration of ozone by

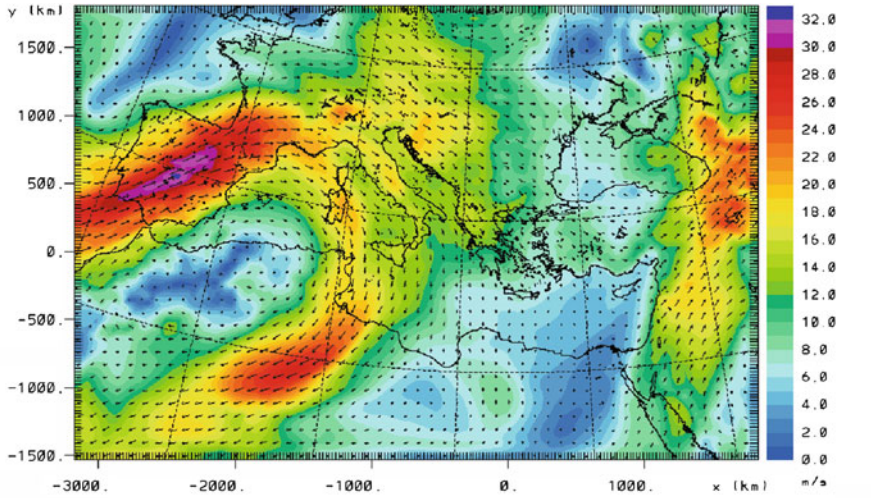


| AM&WFG | | grid 1 | | | |
|---|---|---|---|---|---|
| z = 4367.3 m | 2005-07-17-1200.00 UTC | min | max | inc | lab* |
| contours | speed (m/s) | 0.1067 | 32.30 | 1.000 | 1e 0 |
| vectors · | 8 m/s horiz | 0.1067 | 32.30 | | |

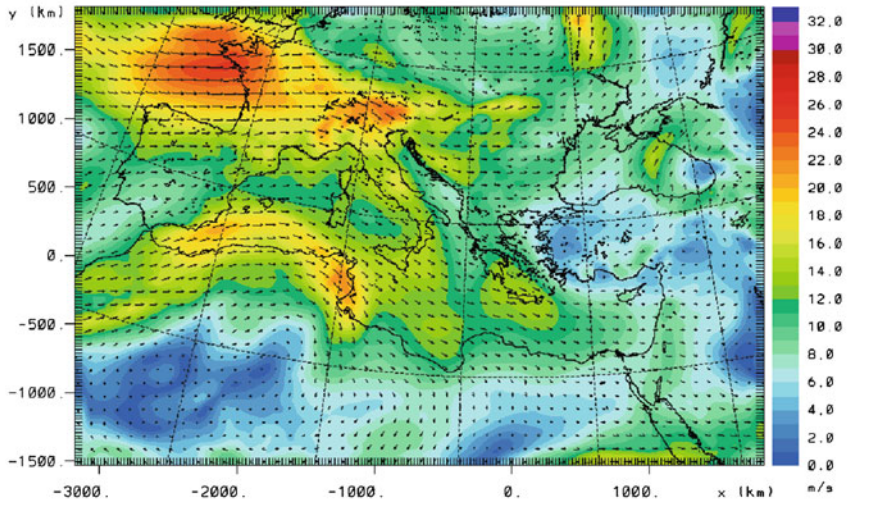


| AM&WFG | | grid 1 | | | |
|---|---|---|---|---|---|
| z = 4367.3 m | 2005-07-24-1200.00 UTC | min | max | inc | lab* |
| contours | speed (m/s) | 0.9398E-01 | 25.17 | 1.000 | 1e 0 |
| vectors · | 6 m/s horiz | 0.9398E-01 | 25.17 | | |

**Fig. 56.1** Wind speed and direction at 4,500 m over Greater Mediterranean Region for 17 and 25 July 2005

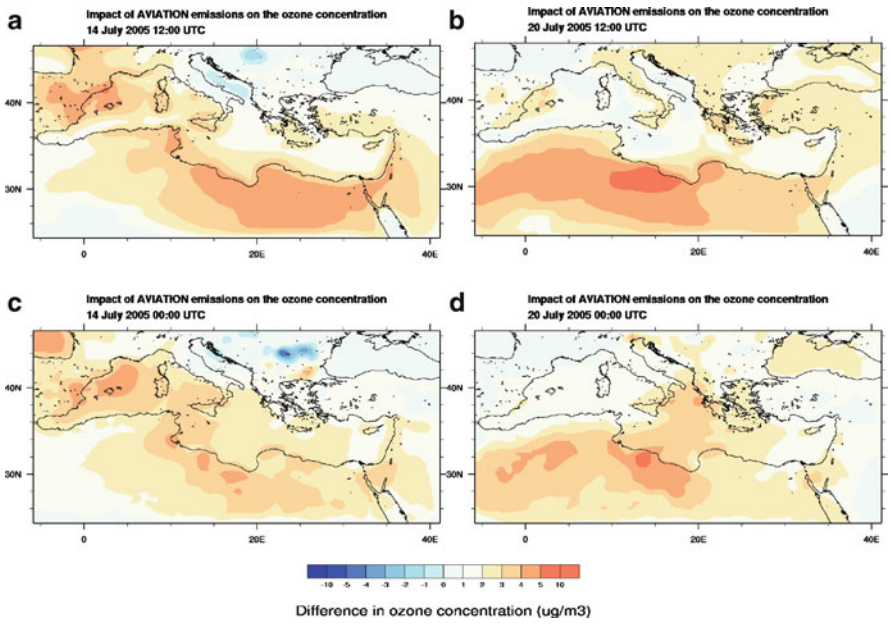


**Fig. 56.2** Difference in surface ozone concentration due to the inclusion of the aviation emissions in the emission inventory for (**a**) 14 July 2005 at 12:00 UTC, (**b**) 20 July 2005 at 12:00 UTC, (**c**) 14 July 2005 at 00:00 UTC and (**d**) 20 July 2005 at 00:00 UTC

the additional NO from aviation emissions is not present, because of the significant daytime difference. Since the ozone formation reactions are fast reactions, the ozone transport is the main factor of the modification of the air pollution field in downwind areas both during day and night. This explains the one sign difference (positive = increase of ozone concentrations when the aviation emissions are included in the inventory) in the ozone field.

The spatial patterns of the near-surface ozone difference are dictated by the circulation patterns. When the westerlies are enhanced over West Europe the pollution is transported towards East Europe and further down towards Eastern Mediterranean due to the seasonal northerly winds (trade winds) over Aegean, leading to higher ozone concentrations over East Mediterranean and North-East Africa. When the extension of the Atlantic anticyclone reaches Central Europe, an enhanced transport of pollution towards Central Mediterranean, Iberian Peninsula, North coast of Africa and even inland Africa, is noticed. Even though the difference in the ozone concentration field over Europe varies from day to day and from location to location depending on the wind field, an accumulative persistent daytime difference, constantly higher than 4 $\mu g/m^3$, is noticed over inland North Africa.

Aviation emissions represent a non-negligible source of pollution not only at the surface but at altitude also. Therefore, an analysis of the changes on the vertical ozone concentration field is performed. In altitude, the maximum impact of the aviation emissions differs from region to region. The impact during noon hours over Mediterranean is present at altitudes up to 8,000 m as illustrated from the vertical cross sections of the difference in ozone concentrations (Fig. 56.3a). At this altitude

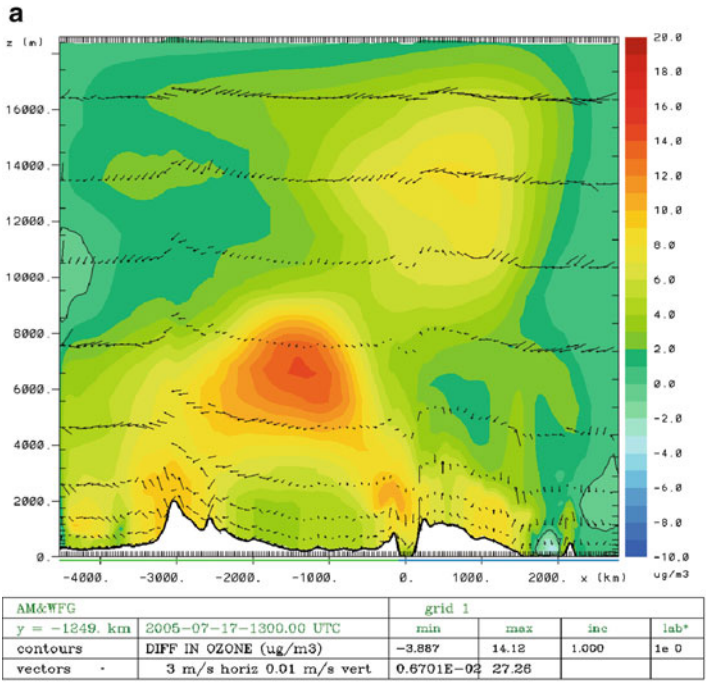


| AM&WFG | | grid 1 | | | |
|---|---|---|---|---|---|
| y = −1249. km | 2005-07-17-1300.00 UTC | min | max | inc | lab* |
| contours | DIFF IN OZONE (ug/m3) | −3.887 | 14.12 | 1.000 | 1e 0 |
| vectors · | 3 m/s horiz 0.01 m/s vert | 0.6701E-02 | 27.26 | | |

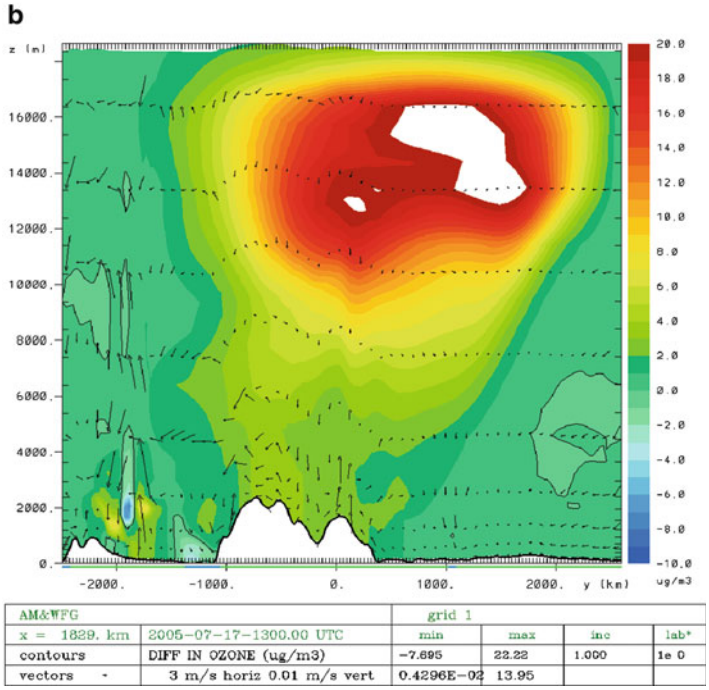


| AM&WFG | | grid 1 | | | |
|---|---|---|---|---|---|
| x = 1829. km | 2005-07-17-1300.00 UTC | min | max | inc | lab* |
| contours | DIFF IN OZONE (ug/m3) | −7.695 | 22.22 | 1.000 | 1e 0 |
| vectors · | 3 m/s horiz 0.01 m/s vert | 0.4296E-02 | 13.95 | | |

**Fig. 56.3** Difference in the vertical ozone concentration field (**a**) west-east cross section over North Africa and (**b**) south-north cross section over East Mediterranean on 17 July 2005, 12:00 UTC

the aviation emission are the only source of pollutants and therefore the difference in the ozone concentration field is a result of solely these emissions. The photolysis rates at these altitudes are higher due to higher actinic fluxes leading to enhanced ozone production than the same amount of surface emissions. Over East Mediterranean the maximum impact is a result of accumulating higher ozone at altitudes around 14,000 m (Fig. 56.3b).

## 56.3 Concluding Remarks

Under characteristic summer conditions emissions from European aviation can influence not only Europe, but the Mediterranean Region and North Africa as well. The aviation emissions can increase the surface ozone concentrations during noon time by approximately 2–10 $\mu g/m^3$ with the most affected areas being the Iberian Peninsula, Central Mediterranean and North Africa, despite the fact that the airports with higher emissions are located over West Europe. At altitudes the impact may be higher, especially over East Mediterranean. Even though global studies of the impact of aviation on air pollution give lower values, in specific circulation regimes and seasons these impacts can be significantly higher.

Future work includes the examination of other species that are affected by aviation emissions, as well as the study of these processes during different meteorological conditions. Additionally, there is an increasing need for assessment studies for aviation emission scenarios, examining the best possible link between emission reduction technologies and air quality performance of aviation.

**Acknowledgments** This work is supported by EUROCONTROL, under the terms of the Research Studentship Agreement no. C06/22048ST and the EU 6th Framework Program CIRCE IP, contract# 036961.

## References

1. Cotton WR, Pielke RA Sr, Walko RL, Liston GE, Tremback CJ, Jang H, McAnelly RL, Harrington J-Y, Nicholls ME, Carrio GG, McFadden JP (2003) RAMS 2001: Current status and future directions. Meteorol Atmos Phys 82:5–29
2. Millan MM, Sanz MJ, Salvador R, Mantilla E (2002) Atmospheric dynamics and ozone cycles related to nitrogen deposition in the western Mediterranean. Environ Pollut 118(2):167–186
3. Pielke RA, Cotton WR, Walko RL, Tremback CJ, Nicholls ME, Moran MD, Wesley DA, Lee TJ, Copeland JH (1992) A comprehensive meteorological modeling system – RAMS. Meteorol Atmos Phys 49:69–91
4. Solomos S, Kallos G, Kushta J, Astitha M, Tremback C, Nenes A, Levin Z (2011) An integrated modeling study on the effects of mineral dust and sea salt particles on clouds and precipitation. Atmos Chem Phys 11:873–892

# Chapter 57
# Mixed Deterministic-Statistical Modelling of Regional Ozone Air Pollution

**Stoitchko Dimitrov Kalenderski and Douw G. Steyn**

**Abstract** We develop a physically motivated statistical model for regional ozone air pollution by separating the ground-level pollutant concentration field into three components, namely: transport, local production, and large-scale mean trend mostly dominated by emission rates. The model is novel in the field of environmental spatial statistics in that it is a combined deterministic-statistical model, which gives novel perspectives on the modeling of air pollution. The model is presented in a Bayesian hierarchical formalism, and explicitly accounts for advection of pollutants, using the advection equation. We apply the model to a specific case of regional ozone pollution – the Lower Fraser Valley of British Columbia, Canada. As a predictive tool, we demonstrate that the model outperforms existing, simpler statistical modelling approaches. Our study highlights the importance of simultaneously considering different aspects of air pollution as well as taking into account the physical bases that govern the processes of interest.

**Keywords** Deterministic-stochastic modelling • Ozone

## 57.1 Introduction

The modelling of air pollutant concentrations in ambient air has a long and varied history. Most of this modelling occurs because of a need to estimate spatial and temporal patterns of variability in the context of air quality management or environmental impact requirements. While a wide variety of modelling approaches exists, it is possible to broadly categorize them as either *deterministic* or *statistical*. Berliner [1] points out that this classification leads to a false dichotomy, and that the

S.D. Kalenderski (✉) • D.G. Steyn
Department of Earth and Ocean Sciences, The University of British Columbia, Vancouver, BC, Canada
e-mail: stoitchko.kalenderski@kaust.edu.sa; dsteyn@eos.ubc.ca

D.G. Steyn and S. Trini Castelli (eds.), *Air Pollution Modeling and its Application XXI*, NATO Science for Peace and Security Series C: Environmental Security 4,
DOI 10.1007/978-94-007-1359-8_57, 

two approached should be considered as merely end points of a logical continuum. A broader discussion of deterministic and statistical approaches in air pollution studies is presented in [8].

In this work, we consider the spatiotemporal analysis of an air pollution field, and explicitly take into account:

- Dynamical nature of the modeled processes
- Interaction between the spatial and temporal components
- Dependence on physical processes
- Availability of deterministic relationships
- Uncertainties inherent in modelling

## 57.2 Model Development

The development of a Bayesian hierarchical model (BHM) usually approaches organizing variables in three levels [13]:

*Data model*: distribution of observations, conditional on process and model parameters.
*Process model*: distribution of process(es) of interest, conditional on parameters.
*Parameter model*: prior distribution of all model parameters.

Then BHM takes the following form:

$$[process, parameters|data] \propto$$
$$[data|process, parameters] \times [process|parameters] \times [parameters]$$

where the bracket notation [.] represents a probability distribution.

### *57.2.1 Data Model*

At the first stage of the hierarchy, we assume that the data are conditionally independent which leads to relatively easy construction of the likelihood function and thus simplified calculations. The general model considered here is for spatiotemporal data recorded at $n$ locations $s_i,\ i = 1, \ldots, n$, in a gridded spatial domain $D \subset R^2$ over a period $T$ of uniformly spaced points in time. Let $Z_t = (Z(s_1, t), \ldots, Z(s_n, t))'$ denote the $n$-dimensional observation vector at time point $t$, $t = 1, \ldots, T$. Then, given the true process of interest, the data model takes the form:

$$\mathbf{Z}_t = K\mathbf{O}_t + \varepsilon_t \tag{57.1}$$

where $O_t = (O(s_1, t), \ldots, O(s_N, t))'$ is an unobserved true process whose components represent the average pollutant concentration for each particular grid cell. $N$ is the number of grid cells in the domain and $K$ is an $n \times N$ matrix that maps averaged pollutant concentration throughout the domain to the observed concentrations.

### 57.2.2 Process Model

A natural approach to modeling $O(s,t)$ is to employ scientific arguments. Using physical reasoning the pollutant concentration field is further decomposed into three components (identified with distinct processes) namely: large-scale spatio-temporal structure, local production and transport (advection). That is:

$$O(s,t) = \mu(s,t) + O^l(s,t) + O^a(s,t) + \eta(s,t) \tag{57.2}$$

where $\eta(s,t)$ represent the unexplained variability at this stage of the hierarchical model.

In addition, it is known that meteorological variables are significant predictors of pollutant concentration [3, 9]. Thus, grouping meteorology in two categories of variables related to the above decomposition will enable us to quantify the significance of these unobservable processes. The first category ($M^l$) refers to local pollutant production, and may include for example: surface temperature, solar radiation, and humidity. The second category ($M^a$) relevant to the transport may include: wind speed and wind direction. Other important meteorological predictors are those related to airmass temperature and convective instability [3]. However, these data are not easily available and generally require coupling the pollution model to a weather prediction system.

The proposed decomposition of the pollutant field identifies the mechanisms (sources of heterogeneity) that contribute to a non-stationary covariance structure. This approach allows development of physically motivated sub-models for each of the components conditioned on different categories of meteorological variables.

### 57.2.3 Large-Scale Spatiotemporal Structure

We propose a deterministic additive model (multiplicative on the original scale if $O(s,t)$ are on the logarithmic scale) to capture the data mean structure defined by the equation

$$\mu(s,t) = \alpha(t) + \beta(s) \tag{57.3}$$

in vector form

$$\mu = \alpha \otimes 1_{Nx1} + 1_{Tx1} \otimes \beta \tag{57.4}$$

The additive form of the model is physically justifiable since the physical phenomena behind the large-scale temporal and spatial trends are independent.

The large scale temporal variability, $\alpha(t)$, mostly dominated by the seasonal and diurnal cycles is caused by planetary motion. On the other hand the large-scale spatial pattern, $\beta(s)$, is mostly dominated by the emissions rates of the pollutants or their precursors throughout the domain of interest. Heterogeneous emissions rates are one of the mechanisms that induce heterogeneity in the pollutant process and can explain different capacities of sub regions to produce pollutant concentration, all other conditions being unchanged. We assume that the emissions are relatively constant in time (i.e. $\beta(s,t) = \beta(s)$), which is in contrast to the other two types of heterogeneity modeled by transport and local production components of the model.

How we model the large-scale temporal trend, $\alpha(t)$, depends on what kind of data we have at hand. However, the hourly mean data are the most difficult to model since they contain several deterministic signals such as: annual trends, diurnal and seasonal cycles and unknown short-term fluctuations. There are several approaches to modelling $\alpha(t)$ including: Box-Jenkins models [2]; linear combination of different basic functions such as: cubic spline [6]; sine and cosine components [7] and indicator functions [5].

The large-scale spatial pattern, which is largely due to spatially varying emission rates, can have a very complex structure. That structure sometimes cannot be captured easily by traditional methods such as polynomial functions of latitude and longitude or Markov Random Fields (MRF) [12, 13]. Alternatively, the emissions structure can be estimated from the data by the first spatial pattern of a Principal Component Analysis (PCA). Calculating the spatial patterns directly from observations will include heterogeneity induced by the transport (wind). This problem can be relatively easily eliminated by selecting only observations that correspond to very light winds (e.g. $<3\,\mathrm{km/h}$) for analysis.

The important point here is that we take the mean field as a measure of the emissions rate structure and we use the first eigenfunction ($EOF_1$) in our analysis since this eigenfunction resembles the mean surface. The mean field is obtained by averaging out the different meteorological conditions on which the pollutant concentration levels depend. As a result averaging eliminates non-stationary mechanisms, which reflect local production, and what remains is a pattern caused by spatially varying emissions rates. One can use the mean field to estimate the large-scale emissions structure as well but we think that it is safer to use $EOF_1$ which allows us to not ignore other potential sources of non-stationarity. We should also notice that the emission rates could (as an alternative approach) be obtained from emissions inventory data.

The view outlined above leads us to the following model for the mean spatial structure

$$\beta(s) = b\,EOF_1(s) \tag{57.5}$$

where $b$ is a proportionality parameter that must be estimated from the data.

## 57.3 Application

The hierarchical model presented in the previous section was applied to a ground-level ozone concentration data. The dataset considered here consists of 1-h-average ozone measurements provided by the Lower Fraser Valley (LFV) Air Quality Monitoring Network operated by Metro Vancouver, covering the 24 years from 1982 to 2006 at 38 stations [10]. However, we model daily maximum 8-h average ozone concentration data obtained from hourly ozone data by calculating the maximum of rolling 8-h averages for each day. The 8-h average values are of particular interest because that is the averaging basis for the Canada-Wide Standard for ozone, based on the adverse effect of ozone and other pollutants on human health and the environment [4]. The spatial domain of study is restricted to a rectangular region of about 146 $\times$ 61 km, covering the Lower Fraser Valley of British Columbia. We also restrict the time period of analysis the most recent 3 years available (2004, 2005, and 2006). That period includes 1 year of high concentrations (2006), one of low (2005) and one of intermediate (2004), though the analysis of data from other years is not excluded.

A Gibbs sampler was applied to estimate the marginal posterior distributions for all unknowns. The MCMC plots (not presented here) show good convergence of the Gibbs sampler for all unknowns and that the results were not very sensitive to changes in the priors.

Our model provides an opportunity for partial comparison with the results obtained through simpler time series models that were employed in many previous ozone studies [9, 11]. As a benchmark we used the two best models employed by Robson and Steyn [11] namely: Temperature-Persistence (TP) model and an ARIMA model. The TP model is a linear model that relates the ozone daily maximum value to the daily maximum air temperature ($T$) and the previous day's daily maximum ozone concentration.

As in Robson and Steyn [11] we analyze data from two monitoring stations that crudely represent two distinct atmospheric situations: an urban and a rural. The comparison between TP and ARIMA model performance confirm the results in Robson and Steyn [11]. However, both models have weaker performance than the model introduced in the previous Section. The Bayesian hierarchical model outperforms the ARIMA and TP model by factor of 1.8–2.5 in the RMS error of prediction.

## 57.4 Conclusions

We have successfully developed and implemented a mixed statistical-deterministic model for regional ozone pollution within a Bayesian Hierarchical formulation. The proposed model was able to capture a number of key ozone features such as: the strong dependence of ozone levels on temperature and persistence; the highest ozone levels

are not generally associated with the strong winds; the wind's ability to transport pollutants. The model outperformed the considerably simpler univariate time series models by a factor of 1.8–2.5.

The transport component is modeled based on the advection equation. It was shown that different approximation schemes lead to different spatial autoregressive models. In our analysis we have used a lagged nearest-neighbor structure to model spatial dependency caused by the wind field. This is one of many possible parameterizations that could be investigated including simultaneous or staggered schemes. We have ignored the downward transport effect since: our dataset does not provide vertical wind fields and second intrusions of stratospheric ozone that reach the surface are rare events, though is possible that surface concentrations can be affected by mixing air between the surface layer and the free troposphere above.

It is important to emphasize two factors when modeling the transport of an air pollutant: wind field and the pollutant gradients should both be considered and they should be considered concurrently. Excluding small-scale phenomena such as diffusion means it is not possible to have transport if there are no gradients in the pollutant field and/or there is no wind. This fact is a consequence of the advection equation and has been employed by the proposed model.

## References

1. Berliner LM (2003) Physical-statistical modeling in geophysics. J Geophys Res 108 (D24):8776
2. Box G, Jenkins G (1976) Time series analysis forecasting and control. Holden-Day, Inc., San Francisco
3. Burrows WR, Benjamin M, Beauchamp S, Lord ER, McCollor D, Thomson B (1995) CART decision tree statistical analysis and prediction of summer season maximum surface ozone for the Vancouver, Montreal, and Atlantic Regions of Canada. J Appl Meteorol 34:1848–1862
4. EPA AQCD (2006) Air quality criteria for ozone and related photochemical oxidants: U.S. Environmental protection agency. Washington, DC, EPA/600/R-05/004aF-CF
5. Guillas S, Tiao G, Wuebbles D, Zubrow A (2006) Statistical diagnostic and correction of a chemistry-transport model for the prediction of total column ozone. Atmos Chem Phys 6:527–537
6. Huang HC, Hsu NJ (2004) Modeling transport effects on ground-level ozone using a non-stationary space–time model. Environmetrics 15:251–268
7. Huerta G, Sanso B, Stroud JR (2004) A spatiotemporal model for Mexico City ozone levels. Appl Stat 53(2):231–248
8. Kalenderski S (2009) Stochastic modelling of space-time processes: an air pollution problem. VDM Verlag, Saarbrücken. Available from http://hdl.handle.net/2429/7457
9. McKendry IG (2002) Evaluation of artificial neural networks for fine particulate pollution ($PM_{10}$ and $PM_{2.5}$) forecasting. J Air Waste Manage Assoc 52:1096–1101
10. Metro Vancouver (2007) Lower fraser valley air quality report. p 35
11. Robeson SM, Steyn DG (1989) A conditional probability density function for ozone air quality data. Atmos Environ 23:689–692
12. Royle JA, Berliner LM (1999) A hierarchical approach to multivariate spatial modeling and prediction. J Agric Biol Environ Stat 4:29–56
13. Wikle CK, Berliner M, Cressie N (1998) Hierarchical Bayesian space-time models. J Environ Ecol Stat 5:117–154

# Part III
# Data Assimilation and Air Quality Forecasting

# Chapter 58
# Efficacy of Incremental Reduction of Input Uncertainties to Improve Air Quality Prediction

**Daewon W. Byun*, Dae-Gyun Lee, Hyun-Cheol Kim, Soontae Kim, Fong Ngan, Beata Czader, Bernhard Rappenglueck, Shobha Kondragunta, and Brad Pierce**

**Abstract** Performance of an air quality prediction may suffer with problems due to uncertainties in meteorological forecasts, lack of event-based real-life emissions variations such as forest fires, and inaccurate dynamic boundary conditions representing effects of long-range transport events. The main objective of this article is to demonstrate the combined synergistic effect of incremental reduction of uncertainties in the model inputs for improving air quality predictions. Effects of improved meteorological inputs, emissions, and initial and boundary conditions, through the use of in-situ measurements and satellite-retrieved information are studied for the continental US domains utilizing the Community Multiscale Air

* The work was conducted at University of Houston (Posthumous authorship).

D.W. Byun • H.-C. Kim (✉) • F. Ngan
NOAA Air Resources Laboratory, 1315 East West Hwy, Silver Spring, MD 20910, USA

University of Houston, Houston, TX, USA
e-mail: hyun.kim@noaa.gov

D.-G. Lee
National Institute of Environmental Research, Incheon, South Korea

University of Houston, Houston, TX, USA

S. Kim
Ajou University, Suwon, South Korea

University of Houston, Houston, TX, USA

B. Czader • B. Rappenglueck
University of Houston, Houston, TX, USA

S. Kondragunta
NOAA Environmental Satellite, Data, and Information Service (NESDIS), Camp Springs, MD, USA

B. Pierce
NOAA NESDIS Center for Satellite Applications and Research, Madison, WI, USA

D.G. Steyn and S. Trini Castelli (eds.), *Air Pollution Modeling and its Application XXI*, NATO Science for Peace and Security Series C: Environmental Security 4,
DOI 10.1007/978-94-007-1359-8_58, 

Quality (CMAQ) model. In this extended abstract, only the impacts of improved initial and boundary conditions are discussed.

**Keywords** Air quality forecasting • Emissions • Input uncertainties • Ozone • Particulate matter

## 58.1 Introduction

Credible numerical air quality prediction requires both a well-verified, comprehensive air quality model and accurate model inputs. In addition to the meteorological inputs from a weather prediction model, initial and boundary conditions of modeled chemical species and high quality emissions data are necessary for the simulation of air quality. An air quality modeling system may have many deficiencies, such as inadequate parameterizations of atmospheric processes and missing source representations. Previously, we have studied effects of the retrospective meteorological inputs on the air quality predictions by the Community Multiscale Air Quality (CMAQ) model subject to emission uncertainties.

The main goal of the present study is to improve air quality predictions in spite of such model shortcomings through the use of observation-based model inputs, in particular: (1) improvement of boundary conditions for air quality models with global chemistry model outputs incorporating in-situ and satellite measurements, and (2) aerosol predictions with the Moderate Resolution Imaging Spectroradiometer (MODIS) satellite-derived aerosol optical depth (AOD) for the Conterminous US (CONUS) domain.

## 58.2 Lateral Boundary Conditions from Global Chemistry Transport Model

Lateral boundary conditions (LBCs) are one of the most important inputs for regional air quality modeling because they influence the temporal variations and spatial distributions of the pollutants. One of the most common methods to generate boundary condition inputs is utilization of global-scale model outputs. A global chemistry model, the NOAA NESDIS/NASA LaRC/University of Wisconsin Real-time Air Quality Modeling System (RAQMS) [7], is used in this study to provide analyzed trace gas and aerosol boundary conditions to the CMAQ simulations. The RAQMS analysis utilizes satellite trace gas measurements from the Ozone Monitoring Instrument (OMI), Tropospheric Emission Spectrometer (TES), and Microwave Limb Sounder on the NASA Aura satellite and satellite aerosol optical depth measurements from the MODIS instruments on the NASA Terra and Aqua satellites to constrain the analysis.

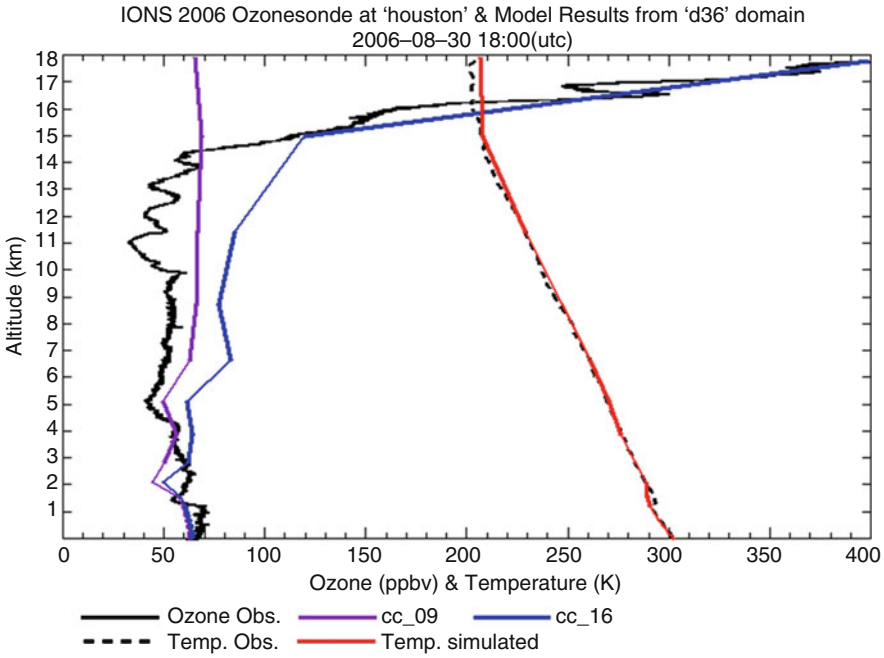


**Fig. 58.1** CMAQ simulated ozone profiles compared to ozonesonde measurements in Houston on August 30. Black solid line is the ozonesonde data. *Purple and blue lines* are the ozone concentration from CMAQ with constant and RAQMS LBCs, respectively. *Black dashed and red lines* are the observed and simulated temperature profiles, respectively

RAQMS is run at a spatial resolution of 2° longitude × 2° latitude with 36 hybrid isentropic-sigma vertical layers in a standard global assimilation mode. The CMAQ CONUS 36-km resolution domain results were nested down to the 4-km resolution Southeastern Texas domain to demonstrate how the the dynamic LBCs together with the improved meteorology and different emission inventories affect air quality predictions. Figure 58.1 shows benefits of using RAQMS boundary conditions on the CMAQ ozone predictions over the CONUS domain with ozonesonde data.

## 58.3 Initialization with Satellite-Derived Aerosol Optical Depth

Compared to ground measurements, satellite data, due to their large spatial coverage and reliable repeated measurements, provide another important opportunity to monitor distribution and transport patterns of aerosols. One important and common aerosol parameter retrieved from satellite sensors is the dimensionless aerosol optical depth (AOD), which is a function of the aerosol mass concentration, mass

extinction efficiency, hygroscopic growth factor (a function of relative humidity) and effective scale height that is mainly determined by the vertical distribution of aerosols [5]. A few studies [3, 4, 8] have revealed that the satellite-derived AOD and ground-based PM concentrations are well correlated, suggesting the high possibility of using the satellite-derived AOD for improving accuracy of air quality modeling.

We hypothesize that satellite observation data can be utilized to generate more accurate initial condition inputs for improving regional aerosol predictions even if certain source functions are missing in the modeling system. For this study, the total MODIS AOD from both the land and ocean modes at 0.55 μm and the fine mode AOD retrieved from the Aqua and Terra satellites are utilized. In order to compare MODIS AOD with CMAQ AOD, the 10 km square MODIS AOD data in latitude/longitude coordinates are mapped onto the CMAQ grid in a Lambert Conformal projection by the 'drop-in-grid' method. A MODIS AOD pixel was assigned to the CMAQ grid if the central point fell within the CMAQ grid cell, and if multiple MODIS pixels were present in a single CMAQ grid, they were averaged. With the assumptions above, CMAQ-predicted AOD due to particle scattering and absorption were calculated by multiplying the total extinction coefficients and the model layer thicknesses. A semi-empirical "reconstructed" mass extinction method suggested by Malm et al. [6] and Binkowski and Roselle [1] was used to estimate the model extinctions due to scattering and absorption. The mass concentration of each of these species was directly obtained from the CMAQ simulation. Organic mass is taken as the sum of all organic species. Fine soil is taken as the unspeciated portion of $PM_{2.5}$ emitted species. Light absorbing carbon is derived using the elemental carbon concentration.

The Cressman [2] successive correction method is used for the objective analysis of AOD to adjust aerosol initial conditions. In normal CMAQ simulations, we run the model day-by-day from 00Z to 00Z (25 h) and initial conditions are taken from the very last time-step of the previous day's simulation results. Then, as the first step, the aerosol initial conditions are adjusted by using the ratio between the calculated AOD and satellite AOD values on the grid at starting time (00Z) while keeping the relative contribution of species and vertical profile shapes as computed. In the second step, we used hourly $PM_{2.5}$ data collected from US EPA Air Quality System (AQS; http://www.epa.gov/ttn/airs/airsaqs/) monitoring stations in order to adjust ICs one more time. The Cressman objective analysis scheme was applied again to generate an analysis field by using the adjusted concentration as a first guess field and AQS $PM_{2.5}$ data as input observations. Only the surface layer concentrations were adjusted with the AQS data in the second step.

The period of the MODIS aerosol initialization study is August 30 ~ September 8, 2006 when CMAQ ozone concentrations are well compared with observations. Figure 58.2 shows that initialization with the total AOD case simulated $PM_{2.5}$ much better in the NW region of USA but, an unrealistic high peak $PM_{2.5}$ appeared (daily maximum 120 vs. 50 $\mu g\, m^{-3}$) possibly due to the effect of an elevated smoke plume on AOD and large uncertainties in coarse mass emissions. When the fine mode AOD was used for the initialization, the simulated daily peaks were reduced

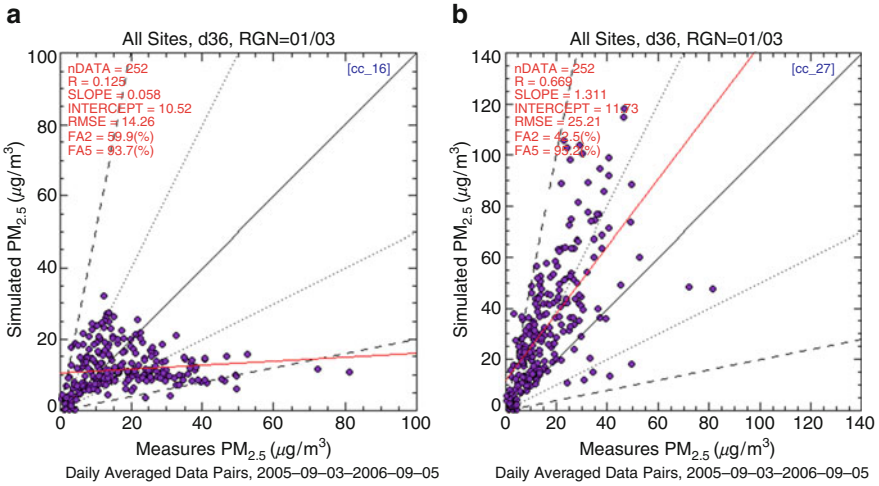


**Fig. 58.2** Scatter diagrams of daily averaged $PM_{2.5}$ concentration with (**a**) first guess initial conditions and (**b**) with those adjusted by total AOD for the western US during September 3 ~ 8, 2006 period

by $-10 \sim -50\ \mu g\ m^{-3}$ although the correlations are not necessarily better (not shown). On the other hand for the SE regions of USA that are affected by regional haze, the results between the total and fine mode AOD initializations are not much different.

## 58.4 Conclusive Remarks

The first portion of this research demonstrated the need to use proper LBCs, such as those provided by satellite-data-assimilated RAQMS output, to reproduce the general vertical ozone structure measured by ozonesondes. It was found that LBCs impact ozone simulations throughout the model layers – most significantly in the upper troposphere, moderately in the middle troposphere, but still considerable in the lower troposphere; and stronger influences can be found in the regions with high latitude and high surface elevations. The second part of this study suggests that satellite-derived AOD can be used to adjust the initial conditions of the model to improve $PM_{2.5}$ simulations although further refinements of the vertical distribution of aerosols are critically needed. In combination with reliable emission inputs representing real-time source conditions such as forest fires, the improved initial and boundary conditions are essential components for the accurate simulation of local and regional air pollution events.

## References

1. Binkowski FS, Roselle SJ (2003) Models-3 Community Multiscale Air Quality (CMAQ) model aerosol component: 1. Model description. J Geophys Res 108(D6):4183. doi:10.1029/2001JD001409
2. Cressman GP (1959) An operational objective analysis system. Mon Weather Rev 87:367–374
3. Engel-Cox JA, Holloman CH, Coutant BW, Hoff RM (2004) Qualitative and quantitative evaluation of MODIS satellite sensor data for regional and urban scale air quality. Atmos Environ 38:2495–2509
4. Gupta P, Christopher SA, Wang J, Gehrig R, Lee Y, Kumar N (2006) Satellite remote sensing of particulate matter and air quality assessment over global cities. Atmos Environ 40:5880–5892
5. Kaufman YJ, Fraser RS (1983) Light extinction by aerosols during summer air pollution. J Appl Meteorol 22:1694–1706
6. Malm WC, Sisler JF, Huffman D, Eldred RA, Cahill TA (1994) Spatial and seasonal trends in particle concentration and optical extinction in the United States. J Geophys Res 99:1347–1370
7. Pierce RB et al (2003) Regional Air Quality Modeling System (RAQMS) predictions of the tropospheric ozone budget over east Asia. J Geophys Res 108:8825. doi:10.1029/2002JD003176
8. Szykman C, White J, Pierce B, Al-Saadi J, Neil D, Kittaka C, Chu A, Remer L, Gumley L, Prins E (2004) Utilizing MODIS satellite observations in near-real-time to improve AIRNow next day forecast of fine particulate matter, PM2.5. In: Sixth conference on atmospheric chemistry: air quality in Megacities, Seattle, Washington

## Questions and Answers

**Questioner Name**: Akula Venkatram

**Q**: How do you estimate plume rise associated with fires? This has to be a large uncertainty in your modeling. How sensitive are your model results to plume rise estimates?

**A**: Because no individual heat fluxes for the satellite detected fires are available, we used a simple assumption of 80% of smoke resides within the planetary boundary layer (PBL) and 20% of plume to penetrate into free troposphere up to 5-km altitude. We performed sensitivity test with 60%/40% split but the net long range transport differences were within 5%.

**Questioner Name**: Mikhail Sofiev

**Q**: This is rather a comment to the previous question. According to the MISR dataset, over 80% of fire plumes are within the boundary layer, so only strongest fires can inject directly to free atmosphere

**A**: Thanks for the comment.

# Chapter 59
# LOTOS-EUROS Air Quality Forecasts by Assimilation of OMI Tropospheric NO2 Columns

**Renske Timmermans, Henk Eskes, Peter Builtjes, Arjo Segers, Daan Swart, and Martijn Schaap**

**Abstract** Both at the national and international level there is a large interest for improved air quality forecasts of ozone, $NO_2$ and aerosols. Data assimilation of observations into chemistry transport models is a means to achieve these improved forecasts. For improvement of the ozone and $NO_2$ forecasts over Europe tropospheric $NO_2$ columns from the OMI instrument on board the NASA's AURA satellite will be assimilated into the LOTOS-EUROS model. As a first step the tropospheric $NO_2$ columns from the model are compared with the values from the OMI satellite instrument. The results show a seasonal bias which is largest in summer and over Eastern and Southern Europe. A similar bias has been observed in an intercomparison study of 9 atmospheric chemistry models with OMI. In this paper we will discuss the results from the intercomparison between the LOTOS-EUROS model and the OMI tropospheric $NO_2$ column data. We will provide possible reasons for the detected bias and discuss suggestions for model improvements. Finally we will present some first results from the assimilation of OMI tropospheric $NO_2$ columns into the LOTOS-EUROS model.

**Keywords** Air quality • Forecasts • Assimilation • $NO_2$ columns • Satellite

R. Timmermans (✉) • P. Builtjes • A. Segers • M. Schaap
Unit Environment, Health and Safety, TNO, Netherlands Organisation for Applied Scientific Research, P.O.Box 80015, 3508 TA Utrecht, The Netherlands
e-mail: renske.timmermans@tno.nl; peter.builtjes@tno.nl; martijn.schaap@tno.nl

H. Eskes
KNMI, Royal Meteorological Institute Netherlands, De Bilt, The Netherlands
e-mail: eskes@knmi.nl

D. Swart
RIVM, National Institute for Public Health and the Environment, Bilthoven, The Netherlands

D.G. Steyn and S. Trini Castelli (eds.), *Air Pollution Modeling and its Application XXI*, NATO Science for Peace and Security Series C: Environmental Security 4,
DOI 10.1007/978-94-007-1359-8_59, 

## 59.1 Introduction

Due to the negative impact of air pollution on the health of humans, animals and vegetation there is a large interest for good air quality forecasts of ozone, $NO_2$ and aerosols. Data assimilation of observations into chemistry transport models is a means to achieve improved forecasts. Besides assimilation of surface data from groundbased networks which is in many studies proven to improve modelled fields, assimilation of satellite observations is interesting owing to the large spatial coverage of this type of observations. This coverage for example will allow the early detection of pollution plumes heading for the area of interest. Previous work showed that assimilation of AOD columns from e.g. MODIS in specific situations clearly improved the modelled and forecasted PM levels [3].

Up till now the ozone and $NO_2$ forecasts over Europe and more specifically the Netherlands have been based on model results in combination with groundbased ozone observations. Due to localisation of highest ozone concentrations in the stratosphere, ozone observations from satellites are usually restricted to a total column amount or profiles that are not very precise near the ground. However $NO_2$ concentrations are largest at the ground and tropospheric $NO_2$ column values are retrieved from a number of different satellite instruments.

In this paper we present the steps taken to assimilate tropospheric $NO_2$ columns from the OMI instrument on board the NASA's AURA satellite into the chemistry transport model LOTOS-EUROS.

## 59.2 Comparison Model and OMI $NO_2$ Values

As a first step the tropospheric $NO_2$ columns from the model were compared with the values from the OMI satellite instrument. The first results from the comparison showed that the $NO_2$ columns from the LOTOS-EUROS model were almost a factor 2 lower than the OMI values as can be seen in the left plot of Fig. 59.1 for July 2006.

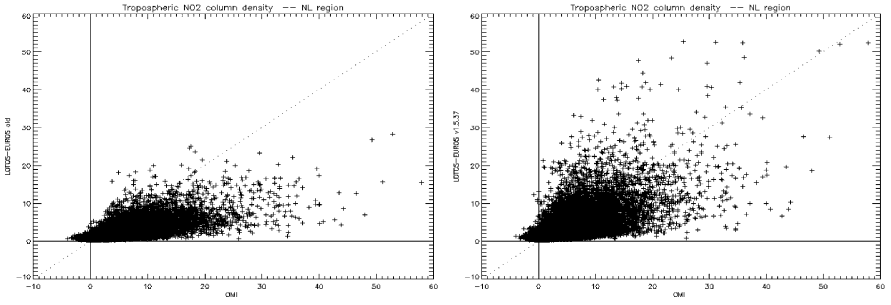


**Fig. 59.1** LOTOS-EUROS tropospheric $NO_2$ columns from old version (*left*) and new version (*right*) versus OMI $NO_2$ columns for July 2006 for region from −2W–14E to 47N–57N

At the same time it was found that LOTOS-EUROS had difficulty in reproducing the high ozone peaks within this period. Improvements in the model included new biogenic VOC emissions, decreased horizontal diffusion, updated isoprene chemistry rates and corrected reaction rates. Especially, the results are sensitive to the reactions including PAN.

The improved model now provides a much improved comparison to the observations as shown in the right plot of Fig. 59.1. The results from the updated model version do however still show a seasonal bias which is largest in summer and over Eastern and Southern Europe (see Fig. 59.2). A similar bias has been observed in an intercomparison study of nine atmospheric chemistry models with OMI [2].

The observed bias can be caused by uncertainties in both model and OMI observations. According to Boersma et al. [1] the uncertainty in the OMI observations can account for a 40% positive bias in summer over polluted regions.

Recently a new OMI NO2 product has become available produced at the EMPA institute. For this product a higher resolution albedo data set is used which has less problems with cloud and snow contamination. Certainly a good message is that the data set reduces the high bias in the OMI data set in summer.

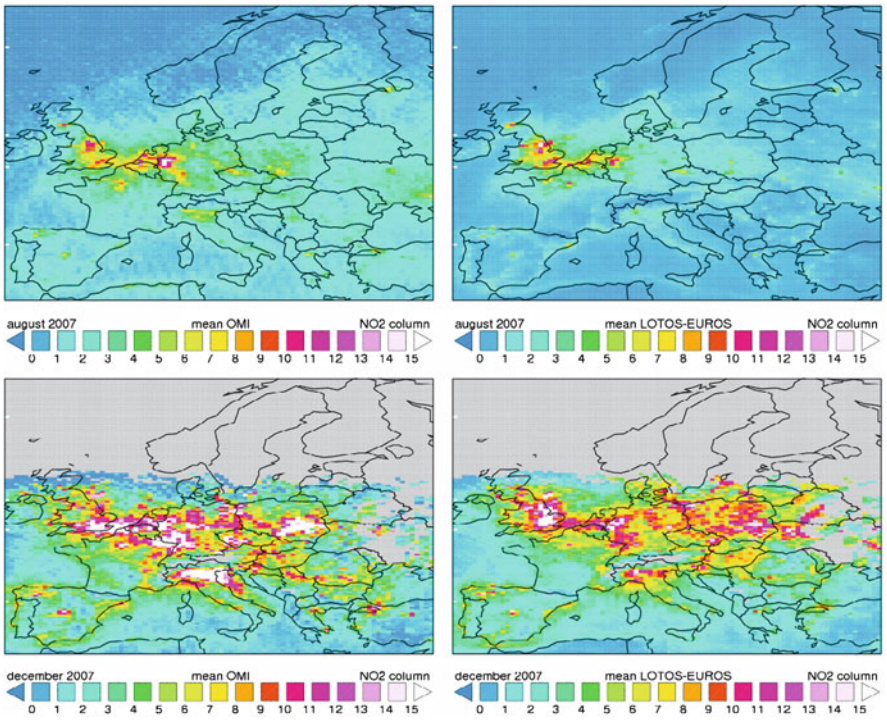


**Fig. 59.2** Mean tropospheric $NO_2$ columns from OMI gridded to LOTOS-EUROS grid (*left*) and LOTOS-EUROS (*right*). *Top row*: August 2007, *bottom row*: December 2007

The model could have a bias caused by missing emissions from e.g. the soil, biomass burning or lightning. Although some of the models in the intercomparison by Huijnen did incorporate lightning emissions and still show a negative bias in summer.

Also missing anthropogenic emissions due to unaccounted economic growth could cause the underestimation by the models.

Another issue is the lifetime of $NO_2$ that seems too short in most models

## 59.3 Assimilation of OMI $NO_2$

The assimilation system around LOTOS-EUROS is based on an Ensemble Kalman filter. For the assimilation of tropospheric OMI $NO_2$ columns, an ensemble of model states is simulated based on different emissions of NOx and VOC and different deposition velocities and boundary conditions. The ensemble specifies a realistic range of possible $NO_2$ loads in each grid cell. With this setup, assimilation of the OMI observations is performed to provide a best estimate of the $NO_2$ and $O_3$ distribution.

First assimilation exercises with OMI $NO_2$ columns where the errors of the OMI data are taken as small show promising results (see Fig. 59.3).

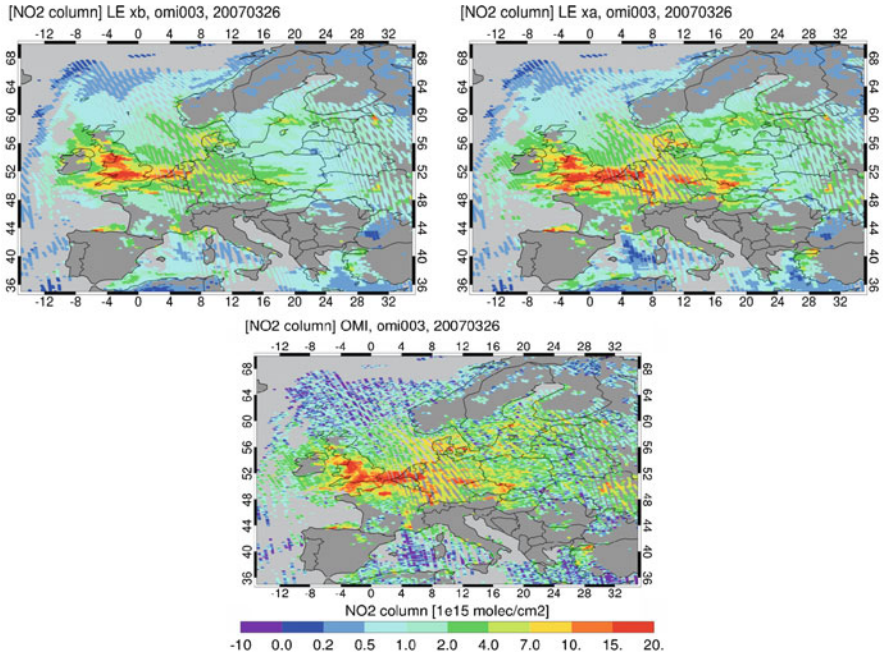


**Fig. 59.3** LOTOS-EUROS modelled tropospheric $NO_2$ columns before (*top left*) and after assimilation (*top right*) and corresponding OMI values (*bottom*) for 26 March 2007

**Acknowledgments** Some of the work presented here is part of the MACC, SMOGPROG and PASODOBLE projects. We would like to acknowledge Dominik Brunner from the EMPA institute for the provision of the EOMINO data.

## References

1. Boersma KF, Eskes HJ, Brinksma EJ (2004) Error analysis for tropospheric NO2 retrieval from space. J Geophys Res, 109(D04311). doi: 10.1029/2003JD003962
2. Huijnen V, Eskes HJ, Amstrup B, Bergstrom R, Boersma KF, Elbern H, Flemming J, Foret G, Friese E, Gross A, D'Isidoro M, Kioutsioukis I, Maurizi A, Melas D, Peuch V-H, Poupkou A, Robertson L, Sofiev M, Stein O, Strunk A, Valdebenito A, Zerefos C (2009) Comparison of OMI $NO_2$ tropospheric columns with an ensemble of global and European regional air quality models. Atmos Chem Phys Discuss 9:22271–22330
3. Schaap M, de Leeuw G, Henzing B, Builtjes PJH (2006) Assimilation of aerosol optical depth over Europe in a regional chemistry transport model. In: Proceedings of the 7th International Aerosol Conference, St. Paul, vol 2, pp 1839–1840, Abstract Book

## Questions and Answers

**Questioner Name**: Sergey L. Napelenok

**Q**: Have you considered comparing assimilated results to ground level observations of $NO_2$

**A**: Yes, we are planning to do so but are not at this stage yet.

**Questioner Name**: Akula Venkatram

**Q**: You use NOx emissions to bring modelled NO2 columns closer to observations. By increasing NOx emissions you run the risk of underestimating ozone in urban areas, which are often VOC limited.Your forecasts of ozone could be really wrong in urban areas where forecasts really matter.

**A**: Of course we need to investigate the effect of assimilation of NO2 on our ozone forecasts to see whether we have negative impacts. In our first tests we do not see a deterioration of the performance for ozone when assimilating NO2 columns. I also would like to note that we only look at the performance at rural background stations since the resolution of the model is not high enough to be representative for urban stations. In the end we are aiming at a combined assimilation of ozone and NO2.

**Questioner Name**: Elisabetta Angelino

**Q**: For OMI $NO_2$ assimilation did you use monthly averaged or daily data.

**A**: We used daily $NO_2$ data for the assimilation.

# Chapter 60
# Integrating $PM_{25}$ Observations, Model Estimates and Satellite Signals for the Eastern United States by Projection onto Latent Structures

**P. Steven Porter, James J. Szykman, S.T. Rao, Edith L. Gégo, Christian Hogrefe, and Valerie Garcia**

**Abstract** Detailed, time-varying spatial fields of air contaminant concentrations are valuable to public health professionals seeking to identify relationships between human health and ambient air quality, and policy makers interested in assessing compliance with air quality regulations. In this paper $PM_{25}$ fields are created from a linear model that predicts $PM_{25}$ at unmonitored grid points from observed $PM_{25}$ concentrations, CMAQ model outputs, and satellite estimates of aerosol optical density. The dimensionality of the input data set is first reduced using projection onto latent structures. Parameters of the linear model are mapped to the CMAQ model domain, permitting estimation of $PM_{25}$ at unmonitored sites.

**Keywords** PM25 • Remote sensing • Latent structures

P.S. Porter (✉)
University of Idaho, Idaho Falls, ID, USA
e-mail: porter@if.uidaho.edu

J.J. Szykman • S.T. Rao • V. Garcia
AMAD/NERL, U.S.E.P.A., Research Triangle Park, NC, USA
e-mail: james.j.szykman@nasa.gov; rao.st@epa.gov; garcia.val@epa.gov

E.L. Gégo
Gego and Associates, Idaho Falls, ID, USA
e-mail: e.gego@onewest.net

C. Hogrefe
New York State Department of Environmental Conservation, Albany, NY, USA

Atmospheric Sciences Research Center, University at Albany, Albany, NY, USA
e-mail: chogrefe@asrc.cestm.albany.edu

D.G. Steyn and S. Trini Castelli (eds.), *Air Pollution Modeling and its Application XXI*,
NATO Science for Peace and Security Series C: Environmental Security 4,
DOI 10.1007/978-94-007-1359-8_60, 

## 60.1 Introduction

Air quality observations are available in the US on a temporally dense but spatially sparse basis. To achieve additional spatial density, observations have been integrated (fused) with outputs of numerical air quality models. A more recent development is the integration of satellite data, used as proxies for ambient concentrations, into fused maps.

Viable integration techniques address the bias of model outputs and efficiently make use of the vast amount of available information. Here fused maps were created with *Projection onto Latent Structures*, also known as partial least-squares regression (PLSR). PLSR is a multivariate regression tool in which a response matrix (Y) is predicted from a matrix of predictors (X). With PLSR, the predictors (X) may be numerous (much greater than the dimension of Y), and correlated with each other [1, 2, 4]. The purpose of this paper is to present a technique for producing maps of ambient concentrations from these three sources of information.

## 60.2 Methods

The data used for this study were extracted from the *Remote Sensing Information Gateway* (RSIG, [3]). The goal of RSIG, an interactive web browser-based application hosted by the United States Environmental Protection Agency (USEPA), is to support researcher and analyst data gathering needs (sharing, visualization, and analysis), to extend air quality research and management to the larger air quality community. In addition to satellite data, RSIG hosts air quality observations and air quality model outputs. Multiple datasets can be visualized at the same time and downloaded. RSIG provides users the ability to integrate various data sets across different time and space scales. A valuable RSIG option is the display of different datasets on the CMAQ model grid.

We created fused maps of daily averaged $PM_{25}$ concentrations for the period 1 June 2006–31 December 2006 for the eastern U.S. at a resolution of 12 km. $PM_{25}$ concentrations at AIRS sites with continuous $PM_{25}$ monitors were downloaded from RSIG. Sites 80% complete for the period of interest were retained (103 sites). Hourly community Multiscale Air Quality (CMAQ) model estimates of $PM_{25}$ concentrations for the surface layer, and GOES EAST Aerosol/Smoke Product (GASP) Aerosol Optical Depth (AOD) remotely sensed (satellite) signals were also extracted from the RSIG site. Daily averages were formed from the hourly data. Data details can be found at the RSIG web site [3].

The AIRS $PM_{25}$ sites were randomly divided into 18 'predictor' and 85 'response' sets. The AIRS 'predictor' set, together with CMAQ and GASP, form X. The AIRS 'response' set forms Y. The dimension of X was reduced using PLSR (Matlab PLS function). PLSR transforms the numerous correlated predictors into a limited set of orthogonal (uncorrelated) latent structures defined to both capture X variability and

best explain the Y response. PLSR is similar to principal component analysis (PCA) in that the dimension of a set of variables is reduced to a smaller orthogonal set. The goal of PLSR, prediction of Y, differs from the goal of PCA, which is to predict X without consideration of any response variable Y.

Following the detailed description of PLSR found in Wold et al. [4], the set of predictor variables is expressed as the product of 'scores' and 'loads':

$$X = X_S \cdot X_L + E, \quad X = \text{predictor matrix} \tag{60.1}$$

X [dimension = $N_t$ (number of time steps) × $N_X$ (number of predictors)]
$X_S$ = X Scores [dimension = $N_t \times N_{Lv}$ (number of latent variables)]
$X_L$ = X Loads [dimension = $N_{Lv} \times N_X$]
E = portion of X not explained by $X_S \cdot X_L$

A few X scores explain X ($N_{Lv} \ll N_x$) and can be expressed as a linear combination of X:

$$X_S = X \cdot W, \quad W = \text{set of constants} \tag{60.2}$$

The response variable is predicted by $X_S$ and the Y loads ($Y_L$):

$$Y = X_S \cdot Y_L + F, \quad F = Y \text{ variability not explained by the model} \tag{60.3}$$

and $Y_L$ is found from:

$$Y = X \cdot W \cdot Y_L, \quad Y = X \cdot B, \quad B = W \cdot Y \tag{60.4}$$

Fused maps were created as follows:

1. estimate the B coefficients at monitored grid points
2. map the B coefficients over the entire domain with a 2D cubic spline
3. estimate Y at unmonitored grids using the mapped B coefficients:

$$\hat{Y}\ (\text{unmonitored grid}) = X \cdot \hat{B}(\text{mapping}) \tag{60.5}$$

where X is the collection of CMAQ, GASP, and AIRS time series described above. For our application, the model can also be written:

$$Y = Bo + B_1 \cdot X_1 + B_2 \cdot X_2 + B_3 \cdot X_3 \tag{60.6}$$

Where Y is one of the 85 AIRS sites in the response set (time series of 214 daily mean $PM_{25}$), $X_1$ consists of the other 18 AIRS sites (prediction set), $X_2$ = GASP, 3 × 3 neighborhood of the monitored grid (9 time series), and $X_3$ are time series in a CMAQ 3 × 3 neighborhood of the monitored (Y) grid (9 time series).

The map is created from:

$$\hat{Y}\ (\text{unmonitored grid}) = X \cdot \hat{B}\ (\text{mapping}) \tag{60.7}$$

## 60.3 Results and Discussion

Figure 60.1 shows X (GASP, CMAQ and AIRS) and the fused map for 1 July 2006. 'Leave one out' cross-validation examples in Figs. 60.2 and 60.3 show good agreement and poor agreement, respectively. Overall, cross-validation results summarized in Table 60.1 are not terribly impressive but are to be expected given the sparse network of observations that form the basis of the map.

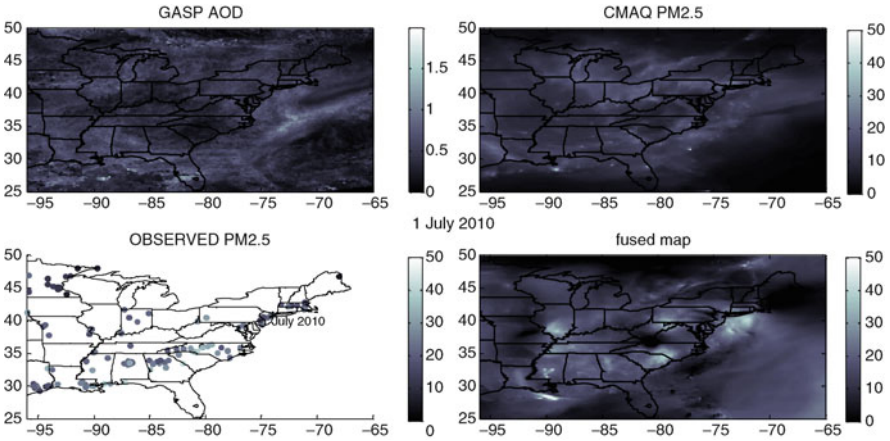


**Fig. 60.1** Fused map (36 predictors/ 5 latent variables)

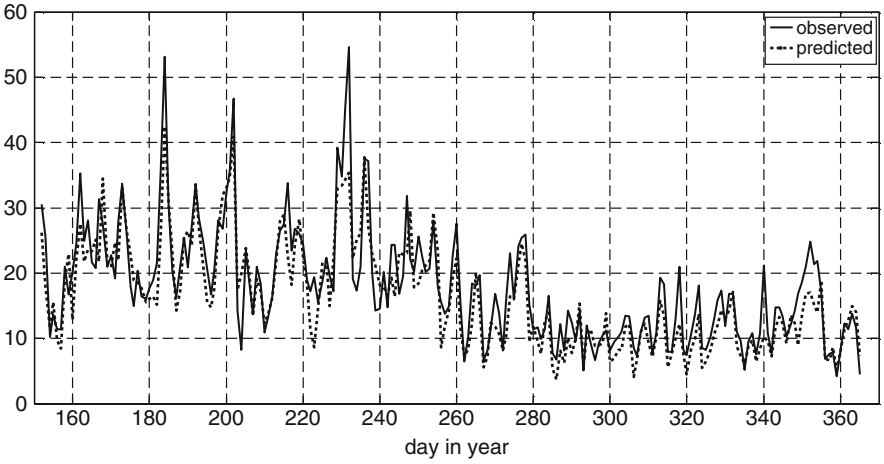


**Fig. 60.2** Example of 'good' cross-validation result ($R^2$ 0.80)

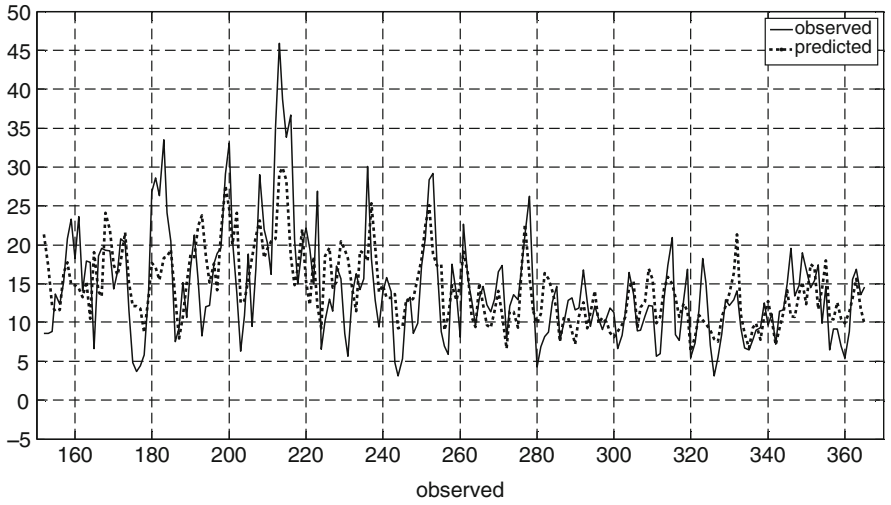


**Fig. 60.3** Example of 'poor' cross-validation result ($R^2$ 0.16)

**Table 60.1** Cross-validation results (5 latent vectors)

| Predictors | Number of predictor grids | Relative RMSE | Relative mean bias | $R^2$ |
|---|---|---|---|---|
| GASP | 9 (3×3) | 0.63 | 0.48 | 0.03 |
| CMAQ | 9 (3×3) | 0.48 | 0.48 | 0.02 |
| CMAQ | 36 (3×3) | 0.58 | 0.44 | 0.21 |
| GASP | (3×3) | | | |
| AIRS | (18 sites) | | | |

## 60.4 Summary

PLSR can be used to reduce the dimension of the very large correlated set of explanatory variables represented by observations, CMAQ, and remotely sensed information. Fused maps produced by PLSR have relief derived from spatially dense CMAQ and satellite information. PLSR prediction performance in this study is limited by the sparse $PM_{25}$ network utilized. Improvements might accrue from expansion of the set of predictor variables to other CMAQ layers, other remotely sensed parameters, and derived variables.

## References

1. Smoliak BV, Wallace JM, Stoelinga MT, Mitchell TP (2010) Application of partial least squares regression to the diagnosis of year-to-year variations in Pacific Northwest snowpack and Atlantic hurricanes. Geophys Res Lett 37:L03801. doi:10.1029/2009GL041478

2. Trygg J, Wold S (2002) Orthogonal projections to latent structures (O-PLS). J Chemometr 16:119–128
3. USEPA (2011) Remote Sensing Information Gateway (RSIG), http://badger.epa.gov/rsig/
4. Wold S, Sjostrom M, Eriksson L (2001) PLS-regression: a basic tool of chemometrics. Chemom Intell Lab Syst 58:109–130

## Questions and Answers

**Questioner Name**: Akula Venkatram

**Q**: Does your method for combining model results with observations improve upon a purely statistical technique such as Kriging of observations.
**A**: Kriged maps are too smooth for our purposes.

**Questioner Name**: Jeremy Silver

**Q**: How do you think the maps would look if the satellite data did not have areas missing due to cloudiness?
**A**: Missing data are an important issue with GASP data. A significant effort goes into preprocessing, including filling-in missing values. The maps would undoubtedly look different with complete satellite information.

# Chapter 61
# Operational Chemical Weather Forecasting Models on a Regional Scale in Europe

**J. Kukkonen, T. Balk, D.M. Schultz, A. Baklanov, T. Klein, A.I. Miranda, A. Monteiro, M. Hirtl, V. Tarvainen, M. Boy, V.-H. Peuch, A. Poupkou, I. Kioutsioukis, S. Finardi, M. Sofiev, R. Sokhi, K.E.J. Lehtinen, K. Karatzas, R.S. Josè, M. Astitha, G. Kallos, M. Schaap, E. Reimer, H. Jakobs, and K. Eben**

**Abstract** Methods that include a combination of weather forecasting and atmospheric chemistry simulations are here referred to as chemical weather forecasting (CWF). We have selected 18 operational CWF models on regional and continental scales in Europe for a more detailed analysis. We have collected the information in a

J. Kukkonen (✉) • V. Tarvainen • M. Sofiev
Finnish Meteorological Institute, Helsinki, Finland
e-mail: jaakko.kukkonen@fmi.fi

T. Balk
Finnish Meteorological Institute, Helsinki, Finland

Division of Atmospheric Sciences, Department of Physics, University of Helsinki, Finland

D.M. Schultz
Finnish Meteorological Institute, Helsinki, Finland

Division of Atmospheric Sciences, Department of Physics, University of Helsinki, Finland

Centre for Atmospheric Science, School of Earth, Atmospheric and Environmental Sciences, University of Manchester, Manchester, UK

A. Baklanov
Danish Meteorological Institute, Copenhagen, Denmark

T. Klein
Swedish Meteorological and Hydrological Institute, Norrköping, Sweden

A.I. Miranda • A. Monteiro
University of Aveiro, Aveiro, Portugal

M. Hirtl
Section of Environmental Meteorology, Central Institute for Meteorology and Geodynamics, Vienna, Austria

M. Boy
Division of Atmospheric Sciences, Department of Physics, University of Helsinki, Finland

V.-H. Peuch
Meteo-France, Toulouse Cedex, France

D.G. Steyn and S. Trini Castelli (eds.), *Air Pollution Modeling and its Application XXI*, NATO Science for Peace and Security Series C: Environmental Security 4,
DOI 10.1007/978-94-007-1359-8_61, 

structured form, and inter-compared and evaluated the mathematical structure of these models. This information makes it possible to evaluate the relative advantages and limitations of the various modeling systems, modeling approaches and sub-models. We have also surveyed the most prominent gaps of knowledge in this field, and suggested potential priorities for future research directions. There are substantial gaps of knowledge, especially in the following fields: emission inventories, the availability and exchange of observations, the evaluation of the boundary conditions for the CWF models, the integration of numerical weather prediction and atmospheric chemical transport models, the data assimilation of the various chemical species, the understanding of several chemical and physical processes, the construction of model ensembles, and the scientific evaluation of the CWF models, including their evaluation against data.

**Keywords** Chemical weather • Scientific model evaluation • Forecasting model

---

A. Poupkou • I. Kioutsioukis
Laboratory of Atmospheric Physics, Physics Department, Aristotle University of Thessaloniki, Thessaloniki, Greece

S. Finardi
ARIANET s.r.l., Milano, Italy

R. Sokhi
University of Hertfordshire, Hatfield, UK

K.E.J. Lehtinen
Finnish Meteorological Institute, Kuopio, Finland

University of Eastern Finland, Kuopio, Finland

K. Karatzas
Department of Mechanical Engineering, Aristotle University of Thessaloniki, Thessaloniki, Greece

R.S. Josè
Technical University of Madrid, Madrid, Spain

M. Astitha
Energy, Environment and Water Research Center (EEWRC), The Cyprus Institute, Cyprus

G. Kallos
Faculty of Physics, University of Athens, Athens, Greece

M. Schaap
TNO Built Environment and Geosciences, Utrecht, The Netherlands

E. Reimer
Freie Universität Berlin, Berlin, Germany

H. Jakobs
University of Cologne, Cologne, Germany

K. Eben
Institute of Computer Science, Academy of Sciences of the Czech Republic, Prague, Czech Republic

## Abbreviations

| | |
|---|---|
| ACT | Atmospheric Chemistry Transport |
| ACTM | Atmospheric Chemistry Transport Model |
| ADM | Atmospheric Dispersion Model |
| CTM | Chemical Transport Model |
| CW | Chemical Weather |
| CWF | Chemical Weather Forecasting |
| CWFIS | Chemical Weather Forecasting and Information System |
| NWP | Numerical Weather Prediction |
| VOC | Volatile Organic Compounds |

## 61.1 Introduction

This study is part of the COST ES0602 action, which provides a forum for benchmarking approaches and practices in data exchange and multi-model capabilities for chemical weather forecasting and near-real-time (NRT) information services in Europe (http://www.chemicalweather.eu/). The content of this action, its main objectives and organisation have been reviewed by Kukkonen et al. [7]. The action includes participants from 21 countries, and its duration is from 2007 to 2011.

Recently, an overview has been published on existing integrated mesoscale meteorological and chemical transport modelling systems in Europe [1]. However, this study did not aim at an intercomparison of the mathematical structure of the various modeling systems. Baklanov et al. [2] suggested a more extended definition and concept of CWF, considering the chemical weather as a two-way interaction between the meteorological and chemical composition of the atmosphere based on on-line coupled models.

There are currently several tens, possibly more than a hundred, chemical weather forecasting and information systems (CWFISs) on a local, regional and continental scale in Europe and worldwide. An extensive amount of literature exists regarding the properties of individual models, their evaluation against various datasets, and various model applications. However, the literature is scarce regarding the scientific evaluation of such models. With a scientific evaluation, we refer here to the detailed analysis and evaluation of the mathematical structure of such models or modelling systems, in terms of the underlying physics and chemistry of atmospheric pollution.

The literature is also very sparse regarding the inter-comparisons of the properties of several, or even a few, models. However, in most cases, it is far from obvious which modelling option or sub-module is the optimal solution for a specific task. A systematic review of the various available modelling alternatives is therefore urgently needed, to be able to evaluate the advantages and limitations of the various methods.

This paper is based upon a larger review article [6] that has three main aims. The first is to gather information on the selected operational CWF models in harmonized formats. The second aim is to preliminarily evaluate, and to provide information that makes it possible for the readers to evaluate the relative strengths and limitations of the various sub-models and modeling systems. The third is to highlight and survey the most prominent gaps of knowledge in this field, and to suggest potential priorities for future research directions. This extended abstract focuses on the third aim and only on some selected emerging areas and future research challenges in this area.

## 61.2 Emerging Areas and Future Challenges

The aim of this section is to highlight some selected emerging scientific areas as well as future research challenges that would be expected to lead to improving the reliability of chemical weather forecasts. These topics include emission and chemistry uncertainties, integration of NWP and ACT models, boundary conditions, assimilating chemical data into the models, the improved understanding and parameterization of physical processes, the evaluation of CWF models against data, the generation of model ensembles and the availability and exchange of observations.

The evaluation of emissions is one of the main sources of the uncertainties in the predictions of the CWF models. First of all, improvement is required for the emission inventories for aerosols, VOCs and organic species. Most of the regional emission inventories currently consider $PM_{10}$ and $PM_{2.5}$; however, primary aerosol emissions definitely need to be further specified in terms of the aerosol size distributions, chemical composition and their source origins. In particular, particulate black carbon (BC) and organic carbon (OC) should be specified. The modelling of the natural emissions of PM – for example, dust events in arid or semi-arid areas, wildland fires and sea spray – are emerging areas of further research.

Knowledge of the emissions of relevant organic species and their atmospheric chemistry limits the understanding of secondary organic aerosols, which are of importance for both air quality and climate change. Correspondingly, the models for aerosol formation and dynamics need to be implemented into CWF models, and the chemical mechanisms used in CWF models should be substantially improved to be able to simulate sufficiently accurately such processes.

The lack of harmonisation of emission inventories at European and national levels is one of the main obstacles to the quantitative inter-comparison of the predictions of operational CWF systems. The horizontal resolution of the emission inventories can currently be reasonably accurate for regional CWFs (e.g., the grid spacing for the pan-European domain is 6 km $\times$ 7 km in the emission inventory within the MEGAPOLI project). However, the temporal variability of emissions and the vertical distribution of the heights of the emission sources are not considered accurate in all cases, and these aspects of the emission inventories need to be improved.

The on-line integration of NWP or other meteorological models with atmospheric aerosol and chemical transport models has several advantages. Integration provides the opportunity (1) to use the three-dimensional fields from NWP models in ACTMs at each time step, and (2) to consider feedbacks of air pollution (e.g., those due to aerosols) on meteorological processes and climate forcing, and further on the atmospheric chemical composition. This is one future direction of research (as a part of, and a step towards, Earth Modelling Systems), and could potentially lead to a new generation of models for NWP and CWF.

An important aspect in the regional applications of the CWF models is the type of initial and boundary conditions used. The use of climatic conditions is one of the common practices, but implementing boundary conditions obtained from global air quality models is currently a significant challenge. This challenge consists of obtaining the required parameters (especially regarding the properties of particulate matter) from the global model computations within a sufficient temporal and spatial resolution.

A fast-growing research area is inverse modeling of emissions using adjoint methods and 4D-VAR. Inverse modelling is being used, especially in global modelling, for monitoring atmospheric constituents, but its benefit for weather and chemical weather forecasting has also been demonstrated. Research on both inverse modelling and data assimilation has been boosted by the availability of satellite-retrieved measurements, which have brought new aspects into assimilation of chemical components. Global spatial coverage, better representativeness of the measured area and gradually improving resolution are the main virtues of these data. In contrast, censoring by clouds, relatively poor time resolution (e.g. two times daily over one spot) and inaccuracies or even errors of the retrieval process are the main drawbacks. An overview of European research on remote sensing of tropospheric constituents has been presented by Burrows et al. [4].

Observations of chemical weather is fragmented within the existing European and global landscape of initiatives and infrastructures. This fragmentation reflects the historical development of understanding and the widening spectrum of environmental issues under investigation during the last decades, but also exists to some extent because of the limited resources and the lack of cooperation between countries [8]. As is evident from the emergence of chemical data assimilation, the limited availability of measurement data has significant consequences for the pace of progress of research and development in that area.

## 61.3 Conclusions

To summarize this paper, we focus on two areas where our community faces huge challenges: the large number of chemical species and communicating uncertainty.

First, although a relatively new field, CWF is developing quickly, touching upon research, development, and operational forecasting. Although CTM models can be

coupled to NWP models either off-line or on-line, a scientific perspective of CWF would argue for an eventual migration from off-line modelling (where the CTM is run after the NWP model is completed) to on-line modelling, allowing coupling and integration of the physical and the chemical components of CWFISs. Specifically, better and more complete representations of physical and chemical processes and interactions in the models are needed. When compared to weather forecasting, CWF has still a long way to go.

A key challenge appears to be the dimensionality and complexity of the problem itself. For example, the traditional set of prognostic state variables in weather forecasting (e.g., temperature, wind, precipitation) expands to hundreds of prognostic variables because of the number of chemical species involved. In particular, resolving, simulating, and parameterizing processes is no longer limited to relatively well-known physical processes, but is compounded by a huge amount of both chemical and physical processes (e.g., interactions between species, emission, deposition, radiation). This fact has important ramifications for predictability, data assimilation, and ensemble prediction, where scientific and technological progress in CW is slower than in traditional meteorology. Importantly, progress is also inhibited by the lack of or insufficient monitoring of many relevant species and the lack of well-established monitoring data-exchange mechanisms. It is reassuring to know that COST ES0602 and other initiatives are working to address these issues.

Second, numerous well-validated operational CWFISs operate in Europe, addressing the needs of a large spectrum of users from governmental organizations to the individual citizen (e.g., [5]). How is the output from CWF models assessed and interpreted for the end users? Moreover, how do we interact with those users to provide the needed services? With the ability to assess and explore ensemble prediction systems comes the challenge in communicating probabilistic chemical weather forecasts. Again, many lessons can be learned from the weather forecasting community who are actively facing such concerns with weather forecasts, in general (e.g., [3]).

Successful CWFIS services will also need to aggregate and integrate information and deliver it in a way that is comprehensible, user-friendly, timely, and reliable. As a first step, the COST ES0602 CWF portal (http://www.chemicalweather.eu/) integrates existing CWFISs offered by numerous institutions within Europe. This portal provides a direct gateway to the individual resources and is intended to complement and support other European initiatives, such as the GMES Atmospheric Service.

## References

1. Baklanov A, Fay B, Kaminski J, Sokhi R, Pechinger U, De Ridder K, Delcloo A, Smith Korsholm U, Gross A, Männik A, Kaasik M, Sofiev M, Reimer E, Schlünzen H, Tombrou M, Bossioli E, Finardi S, Maurizi A, Castelli ST, Finzi G, Carnevale C, Pisoni E, Volta M, Struzewska J, Kaszowski W, Godlowska J, Rozwoda W, Miranda AI, San José R, Persson C,

Foltescu V, Clappier A, Athanassiadou M, Hort MC, Jones A, Vogel H, Suppan P, Knoth O, Yu Y, Chemel C, Hu R-M, Grell G, Schere K, Manins P, Flemming J (2008a) Overview of existing integrated (off-line and on-line) mesoscale meteorological and chemical transport modelling systems in Europe, WMO TD No. 1427, Geneva
2. Baklanov A, Korsholm U, Mahura A, Petersen C, Gross A (2008b) Enviro-HIRLAM: on-line coupled modelling of urban meteorology and air pollution. Adv Sci Res 2:41–46
3. Board on Atmospheric Sciences and Climate (2006) Completing the forecast: characterizing and communicating uncertainty for better decisions using weather and climate forecasts. National Academies Press, Washington, DC, 112 pp. http://www.nap.edu/catalog.php?record_id=11699
4. Burrows J, Platt U, Borrell P (eds) (2011) The remote sensing of tropospheric composition from space. Springer Verlag, Heidelberg. ISBN 978-3-642-14790-6. http://www.ppmborrell.co.uk/RemoteSensingBook/
5. Karatzas K, Kukkonen J (eds) (2009) Quality of life information services towards a sustainable society for the atmospheric environment: COST Action ES0602, Workshop proceedings. Sofia Publications S.A., Thessaloniki, 118 pp. ISBN 978-960-6706-20-2
6. Kukkonen J, Balk T, Schultz DM, Baklanov A, Klein T, Miranda AI, Monteiro A, Hirtl M, Tarvainen V, Boy M, Peuch V-H, Poupkou A, Kioutsioukis I, Finardi S, Sofiev M, Sokhi R, Lehtinen K, Karatzas K, San José R, Astitha M, Kallos G, Schaap M, Reimer E, Jakobs H, Eben K (2011) Operational, regional-scale, chemical weather forecasting models in Europe. Atmos Chem Phys Discuss 11(2):5985–6162
7. Kukkonen J, Klein T, Karatzas K, Torseth K, Fahre Vik A, San José R, Balk T, Sofiev M (2009) COST ES0602: towards a European network on chemical weather forecasting and information systems. Adv Sci Res 3:27–33. www.adv-sci-res.net/3/27/2009/
8. Tørseth K, Fahre Vik A (2009) An overview of WG1: "Exchange of AQ Forecasts and input data". In: Karatzas K, Kukkonen J (eds) Quality of life information services towards a sustainable society for the atmospheric environment: COST Action ES0602, Workshop proceedings. Sofia Publications S.A., Thessaloniki, pp 39–42. ISBN 978-960-6706-20-2

## Questions and Answers

**Bertrand Carissimo**: You mentioned that it is more difficult to use ensemble forecasting for CWP than for NWP, because you have more than a hundred species. However, the numerical weather system is chaotic and therefore it is very sensitive to initial conditions, whereas this is not the case for CWP. Can you comment?
**Jaakko Kukkonen**: The point of the presentation was that, unlike in weather forecasting, air quality is not primarily determined by initial conditions but rather is the result of a range of processes (such as, e.g., emissions, transport, deposition and chemistry) that all provide tendencies that have similar orders of magnitude. This state of affairs requires one to develop approaches that are more complex than the well-established techniques used in numerical weather prediction. However, I agree with you on the fact that, whereas the meteorological flow system may show chaotic behaviour in some conditions, the system of chemical reaction equations commonly does not.

# Chapter 62
# Forecasting Urban Air Quality over Cities by Statistical Adaptation of Deterministic Chemistry Transport Model Outputs

**Laure Malherbe, Charlotte Songeur, Cécile Honoré, Anthony Ung, and Frédérik Meleux**

**Abstract** Within the European CITEAIR II project, deterministic and statistical forecasting approaches are combined to forecast an air quality index in European cities. The idea is to benefit both from chemistry-transport modelling, which provides large scale information about the evolution of photo-oxidizing pollution, and from local measurements of pollution levels. In addition to usual predictors, numerical outputs from the PREV'AIR system are used in multiple linear regression to forecast $O_3$, $NO_2$ and $PM_{10}$ concentrations at urban stations and derive the city-level forecast index. The methodology was applied to Rotterdam, Sevilla and Prague with 2008 data set and validated against 2009 one. It can be extended to any European city involved in CITEAIR II, in particular to those having not implemented their own forecasting system yet.

**Keywords** Urban air quality forecasting • Statistical adaptation

## 62.1 Introduction

The European CITEAIR II project (www.citeair.eu) is aimed at publishing information about air quality, greenhouse gases and emissions in European cities, promoting good practices in those fields and enhancing comparability between cities through an interactive website (www.airqualitynow.eu). One major objective is to develop and transfer good practices in the field of air quality forecasting.

L. Malherbe (✉) •
A. Ung • F. Meleux
INERIS, Parc Technologique ALATA, B.P.2, 60550 Verneuil-en-Halatte, France
e-mail: laure.malherbe@ineris.fr

C. Songeur • C. Honoré
AIRPARIF, 7 rue Crillon, 75004 Paris, France

D.G. Steyn and S. Trini Castelli (eds.), *Air Pollution Modeling and its Application XXI*,
NATO Science for Peace and Security Series C: Environmental Security 4,
DOI 10.1007/978-94-007-1359-8_62, 

Whatever the approach (deterministic or statistical modelling), a detailed forecast at the city scale requires specific inputs and skills that may not always be available. Therefore, it was decided to work out three methodologies corresponding to different levels of complexity according to the city needs, resources and experience. As a common basis, a robust methodology which combines two types of easily accessible information, large scale European forecasts from the PREV'AIR system [3] and local monitoring data, was developed and tested. It is presented in the following sections.

## 62.2 Air Quality Index Forecast: Methodology

### *62.2.1 Which Variable Is to Be Forecast?*

The Common Air Quality Index (CAQI) is a global index calculated from the daily maximum concentrations of $NO_2$ and $O_3$ and the daily average concentrations of $PM_{10}$ at a selection of monitoring stations defined by each city. Observed values of the CAQI are updated every day on www.airqualitynow.eu. Our objective is to provide forecast values as well.

### *62.2.2 Data*

The methodology combines two main sources of concentration data: large scale outputs ($0.5^\circ \times 0.5^\circ$) from CHIMERE, the chemistry – transport model implemented in PREV'AIR; daily measurements of $NO_2$, $O_3$ and $PM_{10}$ at the selected monitoring stations.

Meteorological data available at local scale were too scarce to be utilized in our developments. To test the effect of meteorology, large scale meteorological fields were also extracted from the meteorological module used in CHIMERE (MM5 model) and interpolated at the station locations.

## 62.3 Method

The **multiple linear regression** technique is chosen because of its efficiency – which bears comparison with more sophisticated methods provided relevant predictors are selected (see for instance [1, 2, 4]), its flexibility, which makes it easy to add or remove predictors, and its low computing cost. The considered model takes the form:

$$\mathbf{y_S(t)} = \beta_0 + \beta_1 \mathbf{x_1} + \beta_2 \mathbf{x_2} + \beta_3 \mathbf{x_3} + \cdots \beta_n \mathbf{x_n} + \varepsilon$$

where $\mathbf{y_S}$ denotes the pollutant concentration at station S and time t; $\{\mathbf{x}_i\}_{i=1...n}$ denote the quantitative or qualitative independent predictors; $\boldsymbol{\varepsilon}$ is the error term assumed to be uncorrelated to the predictors.

It is called "statistically adapted model" as it incorporates CHIMERE outputs into a statistical relationship to provide the final forecast. It is built for two prediction horizons: D + 0 and D + 1. For each station, each pollutant and – if necessary – each season, statistical adaptation is performed in three steps: (1) Preselection of explanatory variables from a comprehensive list of potential predictors. That list includes both quantitative variables (daily minimum, maximum, mean and range of D + 0 or D + 1 CHIMERE forecasts, D − 1 CHIMERE error, D − 1 measured concentrations, meteorological forecasts) and qualitative variables (day of the week, type of day). (2) Construction of the model (analysis of covariance) on a training data set. (3) Validation of the model against an independent data set.

Intermediate forecasting of individual concentrations at each selected station is preferred to direct forecasting of the CAQI. This approach enables better understanding of the discrepancies between forecast and measured indexes. Two indexes are computed, for urban background and traffic-related pollution respectively.

## 62.4 Application

The methodology was first applied to three cities involved in CITEAIR II: Rotterdam, Sevilla and Prague. Various issues were investigated through extensive evaluation. In particular, does the model perform better than CHIMERE raw forecast? Does the model performance depend on the forecasting horizon (D + 0 or D + 1)? Validation was performed both for pollutant concentrations and the resulting CAQI. An example of comparison between measured and forecast concentrations is displayed hereafter (Fig. 62.1).

## 62.5 Conclusion

Statistical adaptation of CHIMERE outputs using local measurements improves the model forecasting skill in many cases, and never decreases its performances. As in any statistical approach intended to show overall good performance, smoothing effects and punctual discrepancies between predicted and measured indexes are observed. However, it appears that even with a limited set of predictors, the combination of large scale CTM outputs and local measurements is sufficient to yield acceptable forecasts of the CAQI. Provided minimum validation in each city is performed, it can be reasonably generalized.

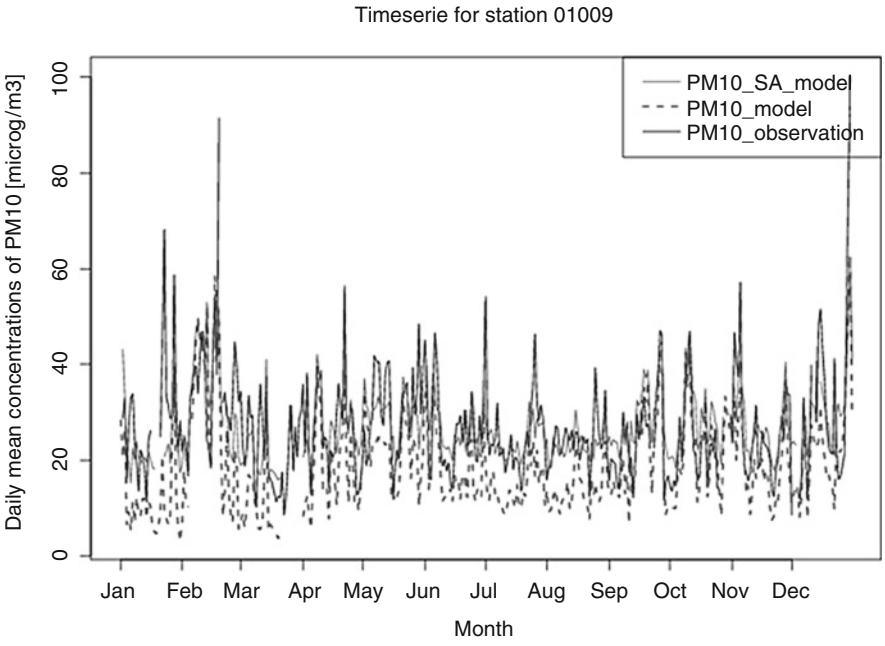


**Fig. 62.1** Example of an urban background station of Rotterdam. D + 0 forecasting of $PM_{10}$ daily mean concentrations. 2009 validation period. *Black*: measured concentration. *Dotted*: CHIMERE forecast. *Grey*: CHIMERE forecast after statistical adaptation

**Acknowledgments** This study is part of the **CITEAIR II (Common Information to European Air)** project which is co-funded under the European Commission INTERREG IVC programme.

## References

1. Barrero MA, Grimalt JO, Canto L (2006) Prediction of daily ozone concentration maxima in the urban atmosphere. Chemom Intell Lab Syst 80:67–76
2. Demuzere M, van Lipzig NPM (2009) A new method to estimate air quality levels using a synoptic-regression approach. Part I: Present-day O3 and PM10 analysis. Atmos Environ 44:1341–1355
3. Rouïl L, Honore C, Vautard R, Beekmann M, Bessagnet B, Malherbe L, Meleux F, Dufour A, Elichegaray C, Flaud J-M, Menut L, Martin D, Peuch A, Peuch V-H, Poisson N (2009) PREV'AIR: an operational forecasting and mapping system for air quality in Europe. Bull Am Meteorol Soc. doi:10.1175/2008BAMS2390.1
4. Slini T, Kaprara A, Karatzas K, Moussiopoulos N (2006) PM10 forecasting for Thessaloniki, Greece. Environ Modell Softw 21:559–565

## Questions and Answers

**Questioner Name**: Kostas Karatzas

**Q**: Linear regression is known to have limitations concerning the strong non-linearity of air pollution problems. How are you planning to deal with that? Is there a relationship between your work and the Eye on Earth project of the EEA?

**A**: It is true that non-linearity is not completely taken into account in our approach. Only logarithmic transformation of the explanatory variables is considered. Some other transformations have been tried for temperature but did not significantly increase the model performance. However, it can be noted that the CTM forecasts, which generally represent major predictors in the statistical models, account for most of the non-linearities. With those forecasts the relationship usually appears to be linear. It should also be recalled that our objective was not to define very precise models for each city but to develop a robust approach capable of improving the European wide CTM forecasts.

Our work is not related to the Eye on Earth project but has been carried out in the framework of the CITEAIRII project.

**Remark** (Eugene Genikhovich): The technique presented in your talk has been used in Russia since the 1970s. In particular, it is applied to the operational air pollution forecasts which are produced for 100 Russian cities. Some problems mentioned in your talk, e.g. non-linear dependencies have been accounted for using this technique.

**Questioner Name**: Sotiris Vardoulakis

**Q**: PREV'AIR model underpredicted pollution levels for Rotterdam? Is this a trend for other cities and other pollutants? Could you use the statistical model results to interpret the performance of PREV'AIR?

**A**: PREV'AIR predictions tend to underestimate $NO_2$ concentrations in cities, which can mainly be explained by the spatial resolution of the model ($0.5^\circ \times 0.5^\circ$ for Europe). As for the second question, it is difficult to answer at this stage. A closer look at the predictors that are most frequently selected in addition to PREV'AIR might be helpful in interpreting the model performance.

# Chapter 63
# Scale Interaction in Air Quality Simulations by Means of a Nudging Technique

**Massimo D'Isidoro, Alberto Maurizi, Felicita Russo, and Francesco Tampieri**

**Abstract** Atmospheric composition modelling requires the handling of a very wide range of scales from local, where anthropogenic emission are concentrated, to global where we are interested to study the impact of these sources. The need to allow different scales to interact stimulates a variety of approaches to bridge them. Here we describe a nudging-based method to realize such bridging. This technique permits models of different design and resolution to interact allowing, for instance, to force global models using regional or local models without a direct dynamic two-way interaction. In this study we describe the general approach, the experimental setup and the results of a numerical experiment performed looking at the Po Valley hot spot. For sake of simplicity this first experiment is performed running the same model BOLCHEM, a regional air quality model, at different spatial resolutions.

**Keywords** Nudging • Scale interaction • Air quality modeling

## 63.1 Introduction

Processes determining the atmospheric composition cover a wide interval of scales, ranging from global, which is interesting for climate and large scale transport episodes (volcanic eruptions, large forest fires, global meteorology) to the inertial range of scale the turbulence spectrum and to the molecular, where dissipation of energy takes place along with the basic transformation processes (chemical reactions).

Studying the interactions between climate and anthropogenic activities, specifically those concentrated in megacities/hot spots, suggests the development and

M. D'Isidoro (✉)
ENEA, Via Martiri di Monte Sole 4, 40129 Bologna, Italy
e-mail: massimo.disidoro@enea.it

A. Maurizi • F. Russo • F. Tampieri
CNR-ISAC, Via Gobetti 101, 40129 Bologna, Italy

D.G. Steyn and S. Trini Castelli (eds.), *Air Pollution Modeling and its Application XXI*, NATO Science for Peace and Security Series C: Environmental Security 4,
DOI 10.1007/978-94-007-1359-8_63, 

use of scale-bridging model systems capable to describe the interaction between different spatial scales [1].

Within the CityZen FP7 Project [4], for example, there is an effort in developing and applying tools to study the impact of megacities on atmospheric pollution by means of a multi-scale approach. The adopted techniques, besides the nudging approach described in this work, involve zoomed [5] and nested grids [2].

In this study we introduce the use of a nudging-based technique for scale-bridging in atmospheric composition modelling. As a test case the same regional air quality model (BOLCHEM, [3]) at coarse and fine resolution is used, but in general this method can be adopted between two different models, e.g. a global model and a regional model.

## 63.2 Bridging the Scales: The Nudging Technique

The basic idea of the nudging technique is to force the concentrations in a certain region of the model domain during a low resolution run with the fields obtained from a high resolution simulation. The technique consists in adding a term in the concentration tendency equation into the model running at low resolution. This term acts to force the computed concentrations towards the high resolution concentrations obtained from a fine scale model. In general the forcing is applied to the low resolution model in the following form:

$$C_{LR}(x, y, z, t + \Delta t) = C_{LR}(x, y, z, t) + \frac{\Delta t}{\tau}[C_{HR}(x, y, z, t) - C_{LR}(x, y, z, t)] \quad (63.1)$$

where $C_{LR}$ refers to the actual Low Resolution Concentration and $C_{hR}$ is the High Resolution Concentration computed by the fine resolution model, $\tau$ is the relaxation time, which regulates how fast the actual fields are relaxed to the high resolution, and the $\Delta t$ integration time step of $C_{LR}$.

The point to focus on is that this technique can be applied not only to the same model running at different resolution but also to two different models (e.g. a global, coarse resolution model and a regional, high resolution model).

## 63.3 Experimental Setup and Results

The nudging procedure is applied using the BOLCHEM model [3] running at different horizontal resolutions: a high resolution run is used to force the low resolution one, and the forced run is compared with the original one, to check whether is closer to the high resolution, taken as reference. We performed the three different model runs for the month of August 2009:

- A low resolution run (*LR*) over a European domain
- A high resolution run (*HR*) over the central Mediterranean region driven by boundary conditions taken from (*LR*) run

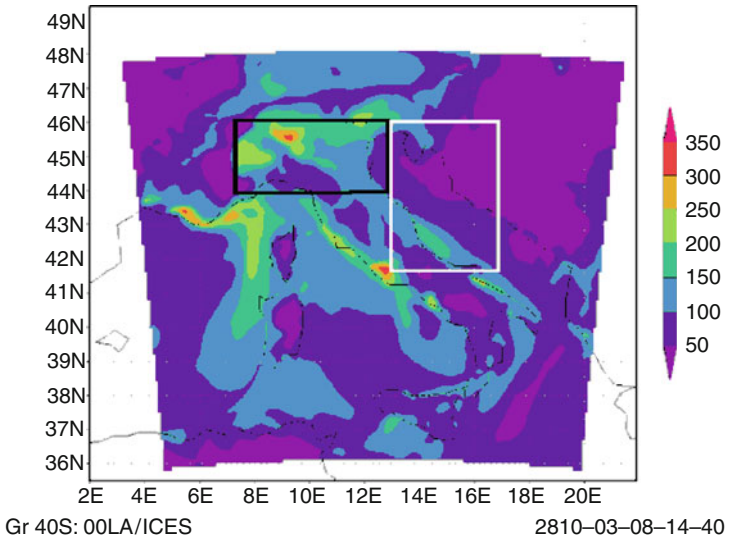


**Fig. 63.1** Illustration of the BOLCHEM domain on which the *HR* run was done. The area included within the *black lines* is the Po Valley region on which the nudging was performed. The Adriatic area, on which the diagnostic was done, is indicated by the *white rectangle*

- A low resolution run (*LR-N*) over the same domain as *LR* run applying the nudging over the Po Valley (*7.5°E–13°E, 44°N–46°N*, Fig. 63.1) every forecast hour and for all model species

In this application of the nudging technique, the relaxation time in Eq. 63.1 was set to *20* min, so that in steady conditions and for a passive tracer the *LR* run would converge to the *HR* run before the updated forcing value is used. The integration time step $\Delta t$ was set to *400 s*. The value of $C_{HR}$, that has been chosen to be the average of the *HR* values over the grid cell of *LR* run, is updated every hour which is the time interval $\Delta t_{HR}$ on which the *HR* values are saved.

It is expected that the main effects of this technique occur within the forcing area; but is also evident that the aim is an overall improvement of the skill of the low resolution run also outside of the forcing area. Therefore we also studied the effects of the nudging technique outside of the Po Valley area and the diagnostic of the method has been done on both the Po Valley region and the Adriatic area (*13°E–17°E, 41.5°N–46°N*) that are illustrated in Fig. 63.1. For each run we simulated a period of *24* days. Figure 63.2 shows as an example the time dependence of *CO* concentrations, averaged over the Po Valley, obtained with the three runs. The main feature is that the mean values of concentrations computed by *LR-N* run generally lie between run *LR* and *HR*. This can be noted also for other species.

In order to better highlight the differences between *LR* run and *LR-N* run we can use the *HR* run as a reference and the performance of the model runs *LR* and *LR-N* will be studied in reference to *HR* run.

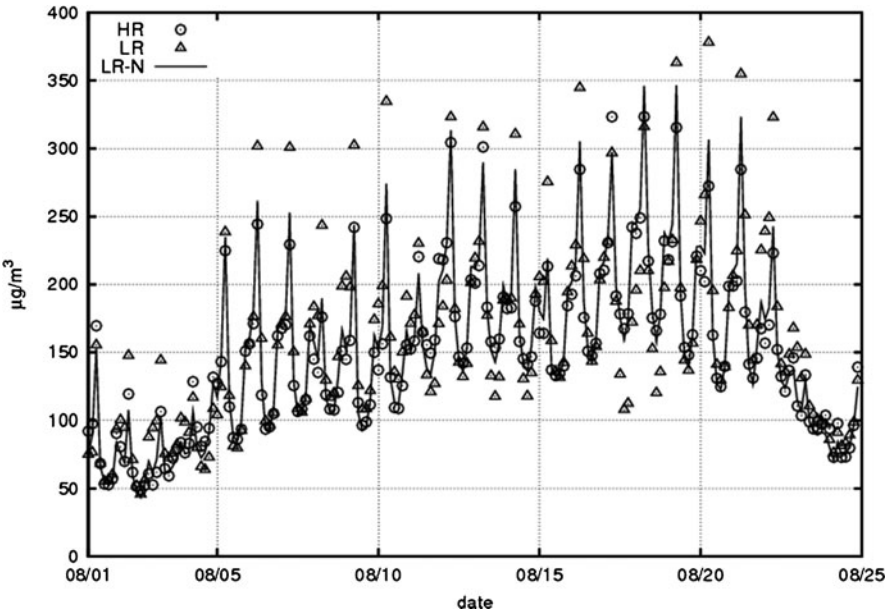


**Fig. 63.2** Time series of the surface *CO* concentrations during the *25* days simulation period. The *circles* indicate the time series obtained in the *HR* run, while the *triangles* indicate the values obtained in the *LR* run and the *black line* indicates the values of the *LR-N* forced by the *HR* run. All the time series show clearly the diurnal cycle of *CO*, which reaches a minimum during the night and has diurnal maxima due to the urban traffic peaks. As expected the values of the *LR-N* run lie mostly between the *HR* and the *LR* runs

The Taylor diagrams provide concise two-dimensional plots of statistical properties, which show how well simulated patterns match a reference [6]. In this case, the comparison between low resolution simulations (with and without nudging) and the reference (*HR* run) is made. The axes refer to the normalized standard deviation of the reference; the correlation coefficient between a given field and the reference is given by its azimuthal position while the root mean square difference between a run and the reference (in units of standard deviation) is proportional to their distance. Therefore each point plotted on the diagram defines how a simulation is close to the reference in terms of the above statistical properties. Figure 63.3 represents the Taylor diagram resulting from the comparison between run LR and HR (black symbols) and run LR-N and HR (gray symbols) for some of the modeled species. It is clear the improvement due to the nudging in terms of increase of the correlation and decrease of the centered root mean square difference.

In order to study the effects of the nudging outside of the Po Valley region we computed for the Adriatic area indicated in Fig. 63.1, a Taylor diagram similar to that done for the Po valley. This diagram, not shown here, depicts a much less pronounced change between *LR* and *LR-N* compared to the diagram in Fig. 63.3, with the exception of the *PM25* and *PM10* species for which a small improvement is noticeable.

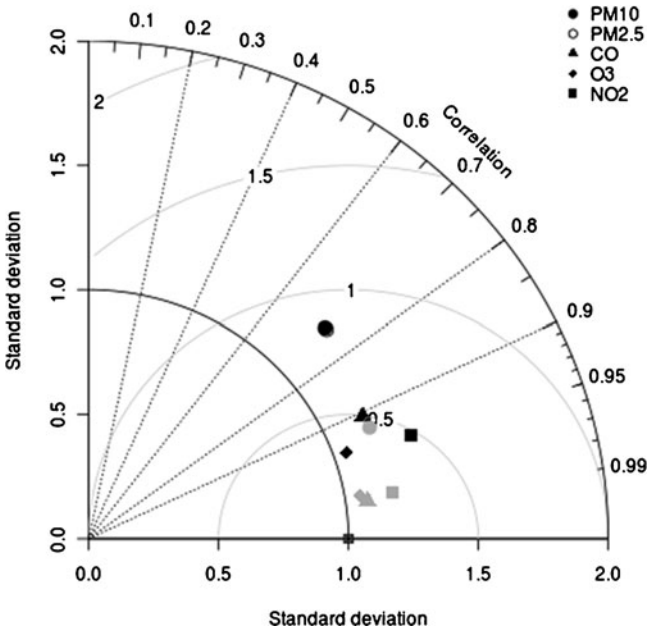


**Fig. 63.3** Taylor diagram showing the comparison between the average results of BOLCHEM in the Po Valley area before (*black symbols*) and after the nudging (*gray symbols*)

## 63.4 Conclusions

To investigate a new method for allowing different models with different spatial scales to interact, we performed a numerical experiment using two runs of BOLCHEM at different spatial resolutions focusing on the Po Valley hot spot.

As the Taylor diagrams show the application of the nudging technique to force the low resolution model to the high resolution area has two important consequences:

- The performance of the nudged coarse model is significantly closer to that of the fine resolution model within the Po Valley
- The performance of the nudged coarse model outside the forcing region is also closer to the finer resolution and is more evident in the case of *PM25* and *PM10*

The point to be stressed again is that this technique can be applied to the same model running at different resolution but more importantly to two different models (e.g. a global, coarse resolution model and a regional, high resolution model). Furthermore, different choices of the parameters ( $\Delta t_{HR}$ and $\tau$) must be investigated in order to allow the best agreement with the reference (which should be either a model or observations).

**Acknowledgments** The research leading to these results has received funding from the European Union's Seventh Framework Programme (FP7/2007-2013) project CITYZEN under grant agreement no. 212095. The support of the Special Project "Impatto degli hot spot sui cambiamenti climatici a scala regionale" financed in the frame of the activities of the Centro Euro Mediterraneo per i Cambiamenti Climatici (CMCC) is also acknowledged.

## References

1. Hodnebrog O, Stordal F, Berntsen TK (2009) Scale interactions in ozone photochemistry: impacts of urban scale variability on regional and global scales. Geophys Res Abstr 11, EGU2009-3017
2. Memmesheimer M, Jakobs HJ, Wurzler S, Friese E, Piekorz G, Ebel A (2009) Air pollution in the Benelux/Rhine-Ruhr area: numerical simulations with a multi-scale regional chemistry-transport model. Geophys Res Abstr 11, EGU2009-8762-3
3. Mircea M, D'Isidoro M, Maurizi A, Vitali L, Monforti F, Zanini G, Tampieri F (2008) A comprehensive performance evaluation of the air quality model BOLCHEM to reproduce the ozone concentrations over Italy. Atmos Environ 42(6):1169–1185
4. Rouil L, Gauss M (2009) CITYZEN partners team: the CityZen project – bridging the scales with focus on megacities. Geophys Res Abstr 11, EGU2009-13576
5. Siour G, Colette A, Bessagnet B, Coll I, Meleux F, Menut L (2010) Bridging the scales in a eulerian air quality model to assess the impact of megacity pollution export at the regional level. Geophys Res Abstr 12, EGU2010-4236-1
6. Taylor KE (2001) Summarizing multiple aspects of model performance in a single diagram. J Geophys Res 106(D7):7183–7192

## Questions and Answers

**Questioner Name**: Peter Biultjes

**Q**: In the Taylor diagram you showed that the nudged results relative to the HR results are the worst for PM10. Do you have an explanation for that?

**A**: We noticed that behavior but we don't have a clear explanation. A more complete study is going to be performed for the whole 2005 year aiming to investigate the results more in detail.

**Questioner Name**: Gabriele Curci

**Q**: Is the physical meaning of the relaxation time $\tau$ related to winds? And if yes, may it be estimated "on-line" (at each time step) using simulated winds?

**A**: In the present work we only wanted to investigate if the nudging technique can give good results applied to our problem, so that we used fixed parameters. Of course the nudging parameters, including the relaxation time, need to be tuned and for which concerns the relaxation time $\tau$ it is possible to compute its value directly during the simulation in function of the wind speed.

# Chapter 64
# US National Air Quality Forecast Capability: Expanding Coverage to Include Particulate Matter

**Ivanka Stajner, Paula Davidson, Daewon Byun*, Jeffery McQueen, Roland Draxler, Phil Dickerson, and James Meagher**

**Abstract** The US National Air Quality Forecast Capability (NAQFC), developed by the National Oceanic and Atmospheric Administration (NOAA) in partnership with the Environmental Protection Agency (EPA), currently provides next-day operational predictions for ground level ozone and smoke for 50 US states. Ozone predictions are produced with the Community Multiscale Air Quality (CMAQ) model driven by NOAA's operational North American Mesoscale weather forecast Model (NAM); routine verification is conducted with monitoring data compiled by the EPA. Smoke prediction relies on satellite detections of smoke sources, US Forest Service emission estimates, with transport and dispersion simulated by the HYbrid Single-Particle Lagrangian Integrated Trajectory (HYSPLIT) model driven by NAM; routine verification is conducted with satellite observations of smoke. Quantitative predictions of fine particulate matter (PM2.5) are in development. Inventory based simulations using CMAQ with aerosol modules show seasonal biases: overestimating in wintertime and underestimating in summertime. Current testing focuses on including intermittent aerosol sources directly emitted by wildfires and dust storms within the forecast domain; longer-range transport of dust is incorporated through lateral boundary conditions. For example, simulations of trans-Atlantic transport of Saharan dust, injected into

*Dedicated to the memory of Dr. Daewon Byun.

I. Stajner (✉)
National Oceanic and Atmospheric Administration (NOAA), Silver Spring, MD, USA

Noblis, 3150 Fairview Park Drive South, 22042-4519 Falls Church, VA, USA
e-mail: ivanka.stajner@noblis.org

P. Davidson • D. Byun* • J. McQueen • R. Draxler
National Oceanic and Atmospheric Administration (NOAA), Silver Spring, MD, USA

P. Dickerson
Environmental Protection Agency (EPA), Research Triangle Park, NC, USA

J. Meagher
National Oceanic and Atmospheric Administration (NOAA), Boulder, CO, USA

D.G. Steyn and S. Trini Castelli (eds.), *Air Pollution Modeling and its Application XXI*, NATO Science for Peace and Security Series C: Environmental Security 4,
DOI 10.1007/978-94-007-1359-8_64, 

the prediction domain, contribute enhanced surface PM2.5 concentrations in the southern US, as observed in surface monitoring. Simulated PM2.5 concentrations are being evaluated with speciated observations in order to improve seasonal biases in predictions. Research on assimilating PM2.5 surface observations shows potential to improve predictions. Furthermore, analysis of discrepancies between observations and model predictions that are produced during assimilation can provide insight on impacts of proposed improvements to PM2.5 predictions.

**Keywords** Dust • Ozone prediction • Particulate matter • Smoke prediction • Verification

## 64.1 Introduction

As directed by Congress, NOAA is building the US NAQFC to provide operational Air Quality (AQ) predictions with enough accuracy and lead-time so that people can take actions to limit harmful effects of poor AQ. NOAA is developing the NAQFC in partnership with the US EPA, and with state and local AQ agencies.

The US NAQFC currently provides next-day operational predictions of ground level ozone and smoke for 50 states (available at www.weather.gov). Ozone predictions are produced using the CMAQ model driven by NOAA's operational NAM weather model [5, 7]. Monitoring data compiled by the EPA in real-time are used for routine verification of ozone predictions. The verification assures that operational predictions meet required accuracy targets for conditions used to issue AQ alerts [4]. With respect to the current ozone warning threshold of 76 ppb, the fraction correct (Fig. 64.1a) has exceeded the target of 0.9 during

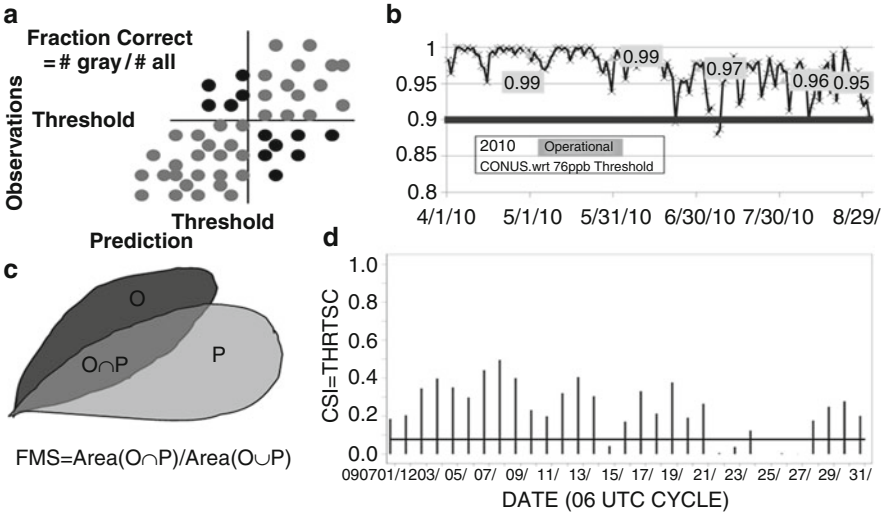


**Fig. 64.1** (**a**) Schematic representation of fraction correct metric (**b**) Fraction correct for operational ozone predictions for summer 2010 for contiguous 48 states (**c**) Schematic representation of FMS metric (**d**) FMS for smoke predictions over Alaska in July 2009

summertime ozone season in 2010, varying from 0.99 in May to 0.95 in August (Fig. 64.1b). Smoke prediction relies on satellite detections of smoke sources, US Forest Service emission estimates, and transport and dispersion simulations from the HYSPLIT model driven by NAM [9]. Satellite observations of smoke are used for routine verification of smoke predictions. Verification is reported as a threat score, also described as a figure-of-merit in space (FMS), characterizing the overlap of predicted (P) with observed (O) smoke plumes (Fig. 64.1c). The FMS for Alaska for most days in July 2009 exceeds the target of 0.08 (marked by blue line in Fig. 64.1d). Over 2.9 million acres burned during very active 2009 fire season in Alaska.

## 64.2 Development of PM2.5 Predictions

Quantitative PM2.5 predictions are being developed in phases, starting with operational smoke predictions. Testing includes prediction of airborne dust from dust storms over contiguous 48 states (Fig. 64.2a). Source regions with dust-emissions potential are estimated from monthly climatology of satellite-observed dust events during 2003–2006 [3]. When surface wind exceeds entrainment threshold, dust is emitted and transported in HYSPLIT driven by NAM meteorology to predict surface and column dust concentrations [1].

Inventory based simulations using CMAQ aerosol modules show seasonal biases: overestimation in wintertime and underestimation in summertime (Fig. 64.2b). The latter is consistent with missing intermittent sources; therefore current testing focuses on including aerosol sources directly emitted by wildfires and dust storms.

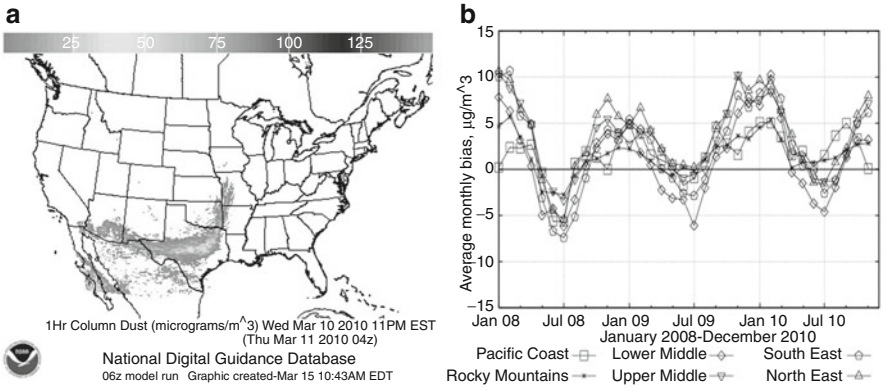


**Fig. 64.2** (**a**) Example of dust prediction showing average dust concentration in the column between surface and 5,000 m for March 10, 2010 (**b**) Monthly bias of CMAQ aerosol predictions in comparison with AIRNow surface observations of PM2.5 for six US regions

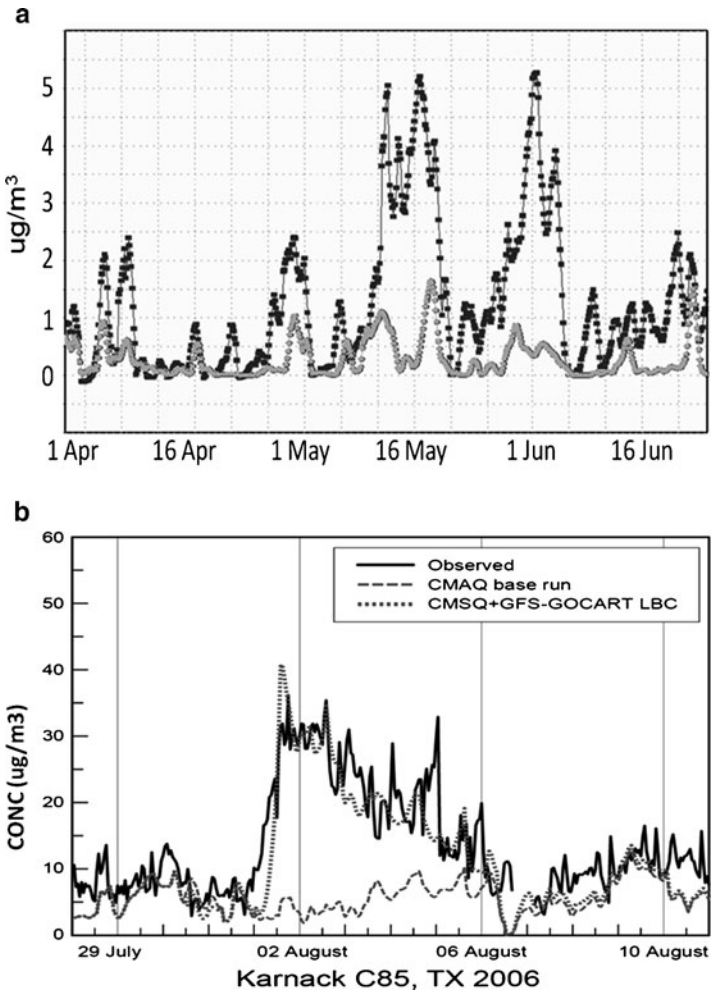


**Fig. 64.3** Long-range transport of dust (**a**) Submicron aerosol in spring 2007 at Mt. Bachelor: measurements (*black*) and model simulation of dust (*gray*) (**b**) Surface PM2.5 in Texas in August 2006: observations (*solid line*), CMAQ simulation using clean boundary conditions (*dashed line*, staying below 15 μg/m$^3$), and CMAQ with boundary conditions that include transport of Saharan dust (*dotted line*, peaking above 40 μg/m$^3$ on August 2)

Global long-range transport of dust is being incorporated. The first example shows that global simulation reproduces temporal variability of submicron aerosol at Mt. Bachelor in Oregon, at about 2.7 km altitude due to trans-Pacific transport of Asian dust (Fig. 64.3a). Modeled dust explains about 25% of total aerosol, which is in the range seen in the analysis of speciated aerosol measurements in this region. The second example shows that global simulation of trans-Atlantic transport of Saharan dust, injected into the regional prediction domain through lateral boundary

conditions [10] successfully simulates enhanced surface PM2.5 concentrations in the southern US, as observed in surface monitoring (Fig. 64.3b).

Simulated concentrations of PM2.5 and component chemical species are evaluated with speciated observations (cf. [6]) to understand and reduce prediction errors. Preliminary evaluation of CMAQ version 4.6 predictions indicates shortcomings in simulation of secondary organic aerosols (SOA). Testing of CMAQ version 4.7.1 is underway in order to improve simulation of SOA seasonal cycle, following Foley et al. [2]. Resolution increase, planned for meteorological prediction models over CONUS-wide domain, and for accompanying AQ prediction is expected to benefit ozone and PM2.5 simulations, especially in coastal regions and over complex terrain. Assimilation of PM2.5 surface observations shows potential to improve predictions [8]. Analysis of discrepancies between observations and predictions created during assimilation will provide an additional tool for evaluation of proposed model improvements.

## References

1. Draxler RR, Ginoux P, Stein AF (2010) An empirically derived emission algorithm for wind blown dust. J Geophys Res 115, D16212. doi: 10.1029/2009JD013167
2. Foley KM, Roselle SJ, Appel KW et al (2010) Incremental testing of the Community Multiscale Air Quality (CMAQ) modeling system version 4.7. Geosci Model Dev 3:205–226. doi:10.5194/gmd-3-205-2010
3. Ginoux P, Garbuzov D, Hsu NC (2010) Identification of anthropogenic and natural dust sources using Moderate Resolution Imaging Spectroradiometer (MODIS) Deep Blue level 2 data. J Geophys Res 115:D05204. doi:10.1029/2009JD012398
4. Lee P, Kang D, McQueen J et al (2008) Impact of domain size on modeled ozone forecast for the northeastern United States. J Appl Meteorol Climatol 47:443–461. doi:10.1175/2007JAMC1408.1
5. Lee P, Tang YH, Kang D et al (2009) Impact of consistent boundary layer mixing approaches between NAM and CMAQ. Environ Fluid Mech 9:23–42. doi:10.1007/s10652-008-9089-0
6. Mathur R, Yu S, Kang D et al (2008) Assessment of the wintertime performance of developmental particulate matter forecasts with the Eta-Community Multiscale Air Quality modeling system. J Geophys Res 113:D02303. doi:10.1029/2007JD008580
7. Otte TL, Pouliot G, Pleim JE et al (2005) Linking the Eta Model with the Community Multiscale Air Quality (CMAQ) modeling system to build a national air quality forecasting system. Weather Forecast 20:367–384. doi:10.1175/WAF855.1
8. Pagowski M, Grell GA, McKeen SA et al (2010) Three-dimensional variational data assimilation of ozone and fine particulate matter observations: some results using the Weather Research and Forecasting – chemistry model and Gridpoint Statistical Interpolation. Q J R Meteorol Soc 136:2013–2024. doi:10.1002/qj.700
9. Rolph GD, Draxler RR, Stein AF et al (2009) Description and verification of the NOAA smoke forecasting system: the 2007 fire season. Weather Forecast 24:361–378. doi:10.1175/2008WAF2222165.1
10. Tang Y, Mcqueen JT, Huang HC et al (2010) Coupling global and regional air quality models: influence of hemispheric transport of mineral dust and biomass burning aerosols on U.S. air quality. In: 90th AMS Annual Meeting, Atlanta, 21 Jan 2010

## Questions and Answers

**Questioner Name**: Thomas Pierce

**Q**: Impressive advances have been made with your predictions of dust and smoke. With the inclusion of Hawaii, are there plans to account for the contribution of volcanic emissions to PM2.5?

**A**: We are striving to include better information on intermittent sources of particulate matter from wildfires and wind storms. Work on inclusion of volcanic emissions in Hawaii is ongoing. Specification of real-time volcanic emission information for use in predictions is challenging.

**Questioner Name**: Massimo D'Isidoro

**Q**: What kind of data assimilation method do you use for PM concentrations?

**A**: We are currently developing assimilation of PM2.5 surface observations following Pagowski et al. [8] using the Gridpoint Statistical Interpolation (GSI) method, which is used operationally at NOAA/NCEP for assimilation of meteorological observations. We will consider other assimilation methods in the future.

# Chapter 65
# On a Contribution of Wild-Land Fires on Atmospheric Composition in Arid Regions

**Joana Soares, Janne Hakkarainen, Tatjana Ermakova, and Mikhail Sofiev**

**Abstract** The study presents the Fire Assimilation System (FAS) based on Level MODIS Collection 5 Active Fire Products. The FAS estimates the emission fluxes originated from the wild-land fires and provides this information to the atmospheric composition modelling system SILAM. Presently, the FAS incorporates the emission factors for three main land-use types (grass and agriculture, forest and mixed), which values were verified for several European episodes. Current work is a part of the FAS calibration for totally different geographical regions, Portugal and Australia, which nonetheless have several common environmental features.

## 65.1 Introduction

The biomass-burning smoke consists of both gaseous and particulate compounds. The main gaseous compounds are carbon oxides, methane, non-methane volatile organic compounds, nitrogen oxides, nitrous oxide and ammonium [7]. High concentrations of reactive species in the fire-induced plumes and presence of organic and inorganic aerosols result in intense chemical transformations while the plume is transported in the atmosphere [2]. In this study, the effect of severe fires occurred in Portugal (2003) and in Australia (2006) is evaluated and compared to in situ and remote sensing data.

J. Soares (✉) • J. Hakkarainen • M. Sofiev
Finnish Meteorological Institute, FI-00101 Helsinki, Finland
e-mail: joana.soares@fmi.fi; mikhail.sofiev@fmi.fi

T. Ermakova
Russian State Hydrometeorological University, St. Petersburg, Russian Federation

D.G. Steyn and S. Trini Castelli (eds.), *Air Pollution Modeling and its Application XXI*,
NATO Science for Peace and Security Series C: Environmental Security 4,
DOI 10.1007/978-94-007-1359-8_65, 

## 65.2 Methodology

### *65.2.1 Fire Input Data: FAS v.1.1*

The FAS provides spatially and temporally resolved emission fluxes originated from wild-land fires. The currently operational FAS v.1.1 consists of two parallel branches based on partly independent Level 2 MODIS Collection 4 and 5 active-fire products: the Temperature Anomaly (FAS-TA) and Fire Radiative Power (FAS-FRP). Their algorithms of converting the fire information to the emission fluxes of atmospheric pollutants are described in Sofiev et al. [6]. The scaling coefficients used to obtain the emission fluxes for $PM_{2.5}$ are based in different fire episodes representing three land-use types: grass, forest and mixed. The $PM_{2.5}$ emission fluxes can be converted further to total PM, as well as to other species using the factors of Andreae and Merlet [1].

The FAS-TA and FAS-FRP branches are partly independent and demonstrate somewhat different features. In particular, FAS-TA is more sensitive to small-scale fires. However, FRP is physically a better grounded quantity for the determination of the fire emissions, since the release of radiative energy is approximately proportional to the number of carbon atoms oxidised per second. Sofiev et al. [6] showed that the combination of both methods improves the representation of emission of small fires.

### *65.2.2 Modelling Tool: SILAM v.4.5.4*

The modelling tool used in this study is the Air Quality and Emergency Modelling System SILAM [4, 5]. For aerosols, the mechanisms of dry deposition varies from primarily turbulent diffusion driven removal of fine aerosols to primarily gravitational settling of coarse particles. The wet deposition distinguishes between sub- and in-cloud scavenging and between rain and snow [4]. The physical-chemical modules of SILAM cover inorganic chemistry, size-resolved primary particles of various types, radioactive nuclides and probability distribution. For the current study, the SILAM simulations included anthropogenic, fire-induced and sea salt emissions. Meteorological information and necessary geophysical and land cover maps are taken from ECMWF meteorological models. Wild-land fires source was obtained from FAS v1.1 system described above. The run for the Portuguese case was based on the European domain with a horizontal resolution of 0.2*0.2°and the Australian run was set with a resolution of 0.4*0.4°. Vertical profile was represented by 9 uneven layers reaching up to the tropopause and having the lowest layer 50 m thick. All simulations had 15 min internal time-step while the output concentration and deposition were averaged over 1 h.

### 65.2.3 Environmental Monitoring Data

The predicted concentrations of gases and aerosols have been compared with both the ground-based and remote-sensing observations. The near-surface mass concentration was compared with observations of the European air quality database (AirBase) that reported hourly concentration for $PM_{2.5}$ and $PM_{10}$ for different measurement sites in Portugal. In the Australian wild-land study case, the near-surface mass concentration was compared with $PM_{2.5}$ and $PM_{10}$ daily concentration reported by the National Environment Protection Measure for Ambient Air Quality. SILAM's resulting gaseous and particulate compounds have been converted to AOD and to total-PM column-integrated burden. The remote sensing data was obtained from merged MODIS Aqua and Terra aerosol column-integrated mass over land.

## 65.3 Results and Discussion

Portugal case study is focused in August where the persistent extreme fire conditions led to the most severe fire seasons experienced during the last decades in Southern Europe, emitting over than 1,000 kgPM/s. Australian fire season in 2003 witness one most extensive bushfire seasons in Victoria State, with December turning out to be one most intense in term of emissions, reaching emissions of ~5,000 kgPM/s. Due to very strong buoyant fluxes observed during these episodes, the plume rise was computed using the modification of the classical empirical formulations in order to accommodate the FRP as the only available input parameter. The SILAM evaluation of these episodes has well reacted to the outstanding emission rates suggested by FAS: the typical concentrations inside the fire plumes were frequently exceeding 100 μg PM m-3.

As seen in Fig. 65.1, the contribution of fires to total concentrations is substantial and evident from the sudden increase of total carbon (TC). In general, the model-measurement comparisons showed an agreement with the observations within a factor of two over the areas where the fire-originated pollution is dominating. The system tends to over-estimate the emission of the most-powerful fires and slightly underestimates for moderate cases. This suggests a non-linear character of emission fluxes of reactive species and PM with regard to FRP and a substantial dependence of the speciation on the fire intensity – the features, so far missing from all existing fire information systems. In case of Portugal, the underestimation is due to the lack of dust emission in the model. Additionally, the difference between the results seen in Fig. 65.1 is also explained by the type of station, an urban site. Unfortunately the available data for this evaluation is from urban stations.

The results in Fig. 65.2 show an example of model results comparison for $PM_{2.5}$ AOD over Australia. The SILAM results are compared with MODIS-AQUA. The simulations of the episode of the fires in Australia 2006/2007 with FAS + SILAM system reproduce fire sources and plumes accurately. The same results were seen for other studies such as Dirksen et al. [3].

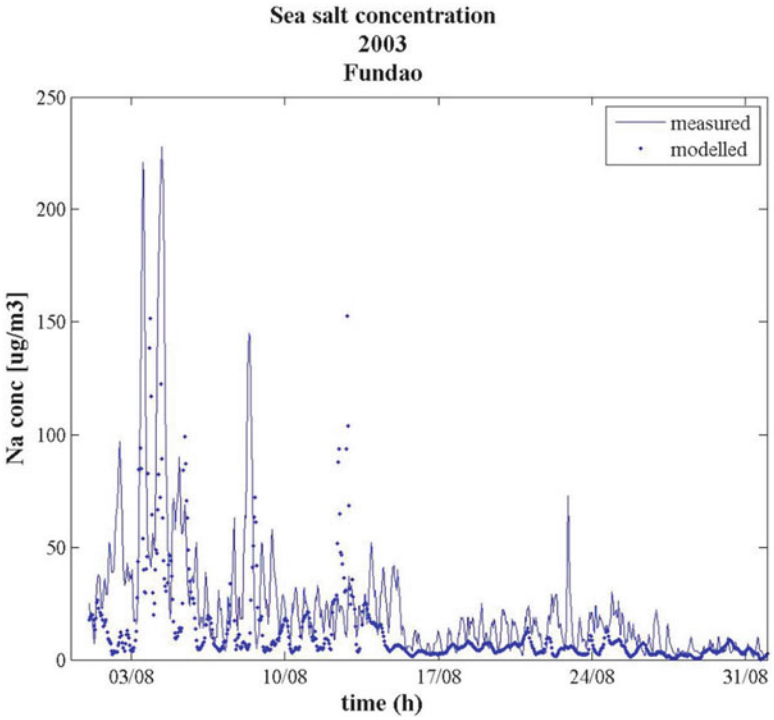


**Fig. 65.1** Model-measurement comparison of PM10 daily concentrations ($\mu g/m^3$) for the measurement site Fundão, Portugal

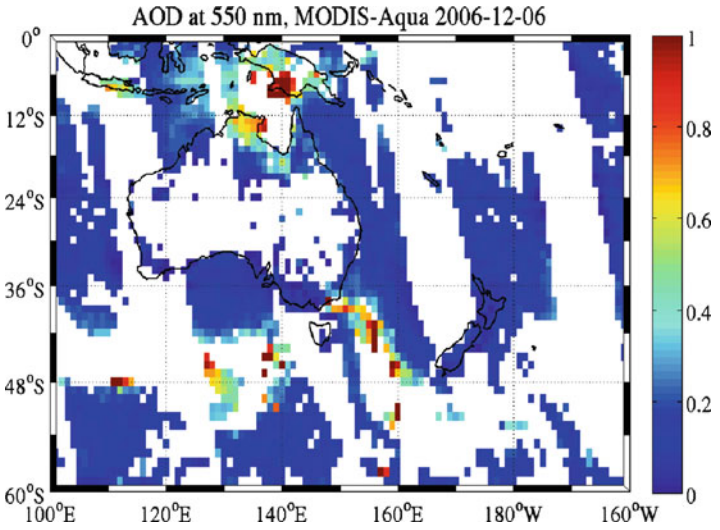


**Fig. 65.2** Model-measurement comparison of AOD $PM_{2.5}$ for December 6 2006 at 10UTC. MODIS AOD on the *left panel* SILAM AOD on the *right panel*

## 65.4 Conclusions

The results from the FAS system linked to the dispersion model SILAM tend to over-estimate the emission of the most-powerful fires and slightly underestimate for moderate cases. The system is able to identify where the fire-originated pollution is dominating, proving to be very useful for the forecasting suites.

**Acknowledgments** The study has been funded by the Academy of Finland, project IS4FIRES.

## References

1. Andreae MO, Merlet P (2001) Emission of trace gases and aerosols from biomass burning. Glob Biogeochem Cycles 15:955–966
2. Blake NJ, Blake NJ, Blake DR, Wingenter OW, Sive BS, Kang CH, Thornton DC, Bandy AR, Atlas E, Flocke F, Harris JM, Rowland FS (1999) Aircraft measurements of the latitudinal, vertical, and seasonal variations of NMHCs, methyl nitrate, methyl halides, and DMS during the First Aerosol Characterization Experiment (ACE 1). J Geophys Res 104(D17):21, 803–821
3. Dirksen RJ, Boersma KF, de Laat J, Stammes P, van der Werf GR, Val Martin M, Kelder HM (2009) An aerosol boomerang: rapid around-the-world transport of smoke from the December 2006 Australian forest fires observed from space. J Geophys Res 114, D21201
4. Sofiev M, Siljamo P, Valkama I, Ilvonen M, Kukkonen J (2006) A dispersion modeling system SILAM and its evaluation against ETEX data. Atmos Environ 40:674–685
5. Sofiev M, Galperin M, Genikhovich E (2008) Construction and evaluation of Eulerian dynamic core for the air quality and emergency modeling system SILAM. NATO Science for piece and security serties C: Environmental security. Air pollution modelling and its application, XIX, Borrego C, Miranda AI (eds), Springer, pp 699–701
6. Sofiev M, Vankevich R, Lotjonen M, Prank M, Petukhov V, Ermakova T, Koskinen J, Kukkonen J (2009) An operational system for the assimilation of the satellite information on wild-land fires for the needs of air quality modelling and forecasting. Atmos Chem Phys 9:6833
7. Ward DE, Radke LF (1993) Emissions measurements from vegetation fires: a comparative evaluation of methods and results. In: Crutzen P, Goldammer J (eds) Fire in the environment: the ecological, atmospheric, and climate importance of vegetation fires. Dahlem workshop reports, environmental sciences research report 13. Wiley, Chischester, pp 53–76

## Questions and Answers

**Questioner Name**: Ana Miranda

**Q**: What was the monitoring station used for your validation?
**A**: Reboleira station (Portugal).

**Q**: do you intend to compare your results with previously published works about the 2003 fire season inn Portugal?
**A**: Yes. In particular, we would like to compare our results with the studies done by the University of Aveiro, Portugal, where these episodes are thoroughly studied.

**Comment**: There is a list of dust Saharan episodes along the fire season in Portugal. You can use it to better understand your results.

# Chapter 66
# An Assessment of a Real-Time Analysis and Its Impact on Dispersion Modeling

**Caterina Tassone, Marina Tsidulko, Yanqiu Zhu, Lidia Cucurull, Geoff Manikin, Jeff McQueen, and Geoff DiMego**

**Abstract** The height of the Planetary Boundary Layer (PBL) is an important quantity for certain applications such as dispersion modeling. A dedicated two-dimensional PBL height analysis has been developed as an additional component of NCEP's Real-Time Mesoscale Analysis. As for other meteorological analysis applications, the quality of the output is dependent on the quality of the input, including the observation. Here we assess the quality and potential for use in the PBL height analysis of a series of candidate observations, including Radiosonde Observations (RAOBS), Aircraft Communications Addressing and Reporting System (ACARS), Cooperative Agency Profilers (CAP), COSMIC satellite Radio Occultation and NWS Next-Rad radar reflectivities. The quality is assessed both by physical plausibility of the measurements and by comparison of the observations and the resulting analysis with independent observations not used in the analysis.

**Keywords** PBL height analysis • ACARS • PBL DC-experiment

## 66.1 Introduction

Accurate estimates of the depth of the atmospheric boundary layer are crucial for applications such as dispersion modeling. In order to improve PBL height predictions used by atmospheric dispersion models, a PBL analysis has been added to the NOAA Real Time Mesoscale Analysis (RTMA). The analysis uses the Rapid Update Cycle (RUC) 13 km model boundary layer height as background for the analysis. Among the candidate observations are derived PBL heights from RAOBS, ACARS, CAP, COSMIC and RADAR data. For each type of data a careful

C. Tassone (✉) • M. Tsidulko • Y. Zhu • L. Cucurull • G. Manikin • J. McQueen • G. DiMego
NOAA/NCEP/EMC, 5200 Auth Rd, Camp Springs, MD 20746, USA
e-mail: caterina.tassone@noaa.gov

D.G. Steyn and S. Trini Castelli (eds.), *Air Pollution Modeling and its Application XXI*,
NATO Science for Peace and Security Series C: Environmental Security 4,
DOI 10.1007/978-94-007-1359-8_66, 

evaluation took place before the decision was made on whether or not to include them in the PBL analysis. In particular, ACARS derived PBL height have been evaluated to assess their temporal and spatial error characteristics. The quality of PBL heights from COSMIC radio occultations and from ground-based radar reflectivity measurements has been assessed by comparing them with collocated ACARS and RAOBS estimates. Finally, a first version of the PBL analysis is verified against independent observations such as the ones collected during the DC PBL experiment.

## 66.2 RTMA

The RTMA [2] is a 2D-VAR based Real-Time Mesoscale analysis that provides 5-km estimates of surface and near-surface conditions on an hourly basis. Based on a two-dimensional modification of NCEP's Grid-point Statistical Interpolation (GSI) analysis system, the RTMA uses the 13-km 1-h forecast from the Rapid update Cycle (RUC) downscaled to the 5-km RTMA grid as its first guess. The GSI uses surface observations together with this first guess to produce gridded analyzes of 2-m temperature, 2-m specific humidity, 10-m u and v-components of the wind and surface pressure. The PBL height of 1-h RUC forecasts generally shows good agreement with the NAM (WRF-NMM) and with observations.

## 66.3 Observations

PBL height observations that will be assimilated into the RTMA require careful screening in order to obtain a high quality analysis. ACARS, RAOBS, COSMIC and RADAR derived PBL heights were first evaluated by comparison with independent measurements from fields experiments and by examining them for their reflection of typical characteristics of PBL heights, e.g. a realistic range of values (between 100 m and 3,000 m), and an identifiable diurnal cycle.

PBL heights from ACARS, RAOBS and CAP profilers are calculated using a Richardson Number method [5]. Observations of wind, temperature, humidity are used to compute a Richardson Number with the following formula:

$$\mathrm{Ri_B} = \frac{gz(\theta(z) - \theta(s))}{\theta(s)\left[(u(z) - u(z))^2 + (v(z) - v(s))^2 + bu_*\right]} \tag{66.1}$$

The PBL height is defined to be the height where the computed Richardson number for the first time exceeds a value of 0.25 beginning from the surface. Heights derived from RAOBS are generally good and will be retained as observations for the PBL analysis. However, their use is limited by their inherently poor temporal resolution,

with the only useful measurement over CONUS made at 00Z. ACARS data are collected more frequently and therefore have the potential to capture the diurnal variation of the PBL height. In order to calculate the PBL height, a vertical profile is constructed using ACARS wind and temperature, specific humidity from RUC analysis and surface observations from a nearby METAR station. Equation 66.1 is applied using a constant $u_*$ and b = 100. Studies on data collected over extended periods of time have shown that ACARS derived PBL heights behave statistically well and show a realistic diurnal variation [4]. In order to further evaluate and possibly improve the algorithm used to derive PBL heights, ACARS estimations were also compared with measurements collected during the DC field experiment (September 2009). During this experiment, radiosondes were launched at 2 h intervals at three different locations in the DC area and PBL heights were subjectively derived from these measurements. Lidar measurements as well as estimates from ground lidar (MPLNET), are also available. Figure 66.1 shows a time series of PBL heights from ACARS at Baltimore Washington International Airport (BWI) and radiosondes measurements from the DC experiment on the 15th of September. During the hours of maximum BL development ACARS is in good agreement with PBL height derived from radiosondes. However, at 20Z, the ACARS PBL height collapses to 200 m, well below both the radiosondes and the lidar estimates (not shown). In order to obtain good agreement, Eq. 66.1 was modified by adding a term of 0.5 K to the surface temperature. This term represents a temperature excess, a measure of the strength of the convective thermals in the PBL. This modification proved to be useful in several cases.

However, the major problem in the use of the ACARS data is the fact that the data used for the Richardson Number computations do not represent a truly vertical profile. Figure 66.2 shows typical trajectories for flights landing in San Francisco and departing from Miami, respectively. In both cases the PBL is detected at several

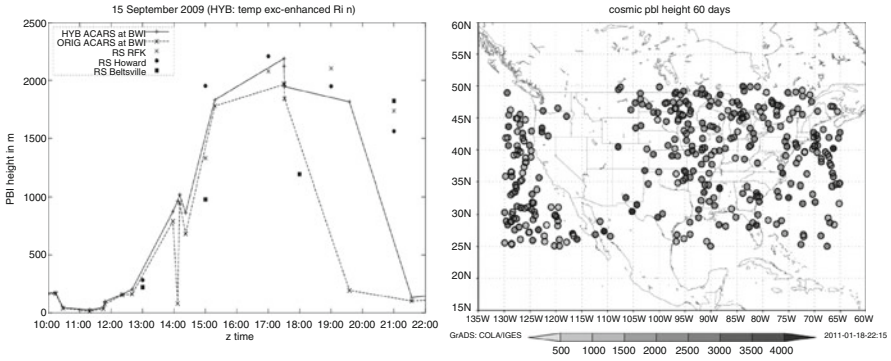


**Fig. 66.1** PBL Heights from observations. DC-experiment (*left panel*): radiosondes at Beltsville, RFK (R.F. Kennedy Stadium, Washington DC) and Howard U. ACARS at BWI (original – *solid line*; modified surface temperature – *dashed line*). COSMIC PBL height for August–September 2009 (*right panel*)

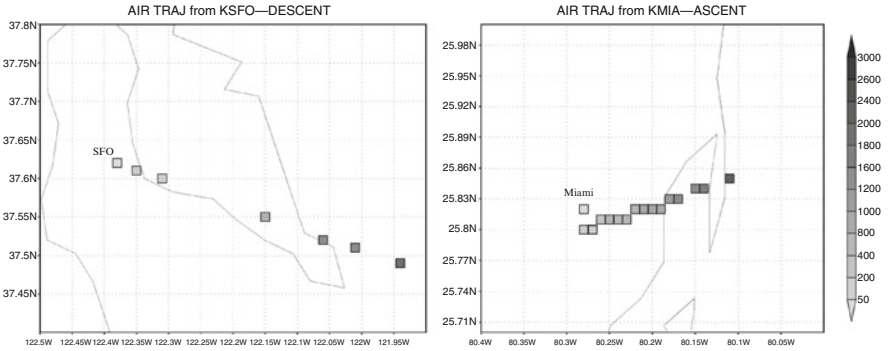


**Fig. 66.2** Examples of aircraft trajectories used for boundary layer calculation. Descent into SFO-20100308 22Z (*left panel*); ascent from Miami-20100605 21Z (*right panel*). *Gray* intensity indicates aircraft altitude at horizontal location. *Plot ends* when PBL height is reached

kilometers from the initial surface location. The characteristics of the boundary layer depend on the underlying surface, a problem exacerbated by the fact that many airports are located on the coast, close to the inhomogeneous land-sea transition. In order to address this problem and to ensure appropriate representation of the underlying surface, the surface data closest to the location of the aircraft at each level will be attached to the vertical profile. More work would be needed to ensure that ACARS estimates of PBL height are as accurate as possible, however, the current version of the ACARS estimates have already been demonstrated to be useful for the PBL analysis.

COSMIC Radio occultations (RO) can be used to determine the depth of the PBL [3]. A large lapse in the bending angle profile, which indicates strong vertical moisture gradient, is used for estimating PBL height. Calculated distributions agree well with observed climatological features and when taking into account several years of data, diurnal variations of PBL height of the ocean was detected. For our study we used 2 months worth of data (August–September 2009). Values of COSMIC derived PBL heights are within reasonable physical bounds (Fig. 66.1, data provided by Sokolovskiy), but due to insufficient data it was not possible to detect a diurnal cycle. The evaluation also included comparison of COSMIC PBL height with collocated ACARS estimates and with the DC experiment measurements. With a one-degree lat/lon collocation criterion, only 17 cases of collocated ACARS and COSMIC data were found. For the DC experiment only two COSMIC PBL heights at about 300 km from the DC area were found. For both comparisons, the COSMIC PBL heights are systematically higher, a feature to be expected because of the nature of the measurements. COSMIC data may be a useful data set for PBL analysis. However, more data is needed in order to perform a statistically significant study before including COSMIC observations in the PBL analysis.

Reflectivity collected by the network of Weather Surveillance Radar-1988 Doppler (WSR-88D) radars can also be used to estimate PBL height [1]. A preliminary study showed ambiguous results and these data were not pursued further.

## 66.4 Validation of PBL Analysis

The PBL analysis was performed using ACARS and RAOBS derived PBL height as observations and RUC 1-h forecast as a background. The observation closest in time to the analysis time is selected for assimilation and is combined with the background field according to the specification of observation and background error covariances. The PBL height analysis at the location of BWI is compared to the radiosondes PBL heights available for the DC PBL experiment and to the 1-h forecast PBLH from RUC. On September 20, a drop in the analysis at 18Z is in disagreement with the experimental data (Fig. 66.3). Triangles show the ACARS data available to the RTMA analysis. For each observation set (one for each of the three DC area airports BWI, IAD and DCA), only the one observation closest to the analysis time is selected and used by the analysis. Many of the observations from IAD at 18–19Z are given much smaller weights due to their relative times to analysis time. Although this is standard usage for objective analysis, the nature of the PBL height, with its high spatial and temporal variation is such that one might consider using all the available observations rather than just the one closest in time.

Figure 66.3 shows the PBL height analysis obtained by using all available observations. The upper cluster of observations (circles) is from IAD, while the lower one (triangles) is from BWI, and the analysis at BWI tends towards observations from BWI.

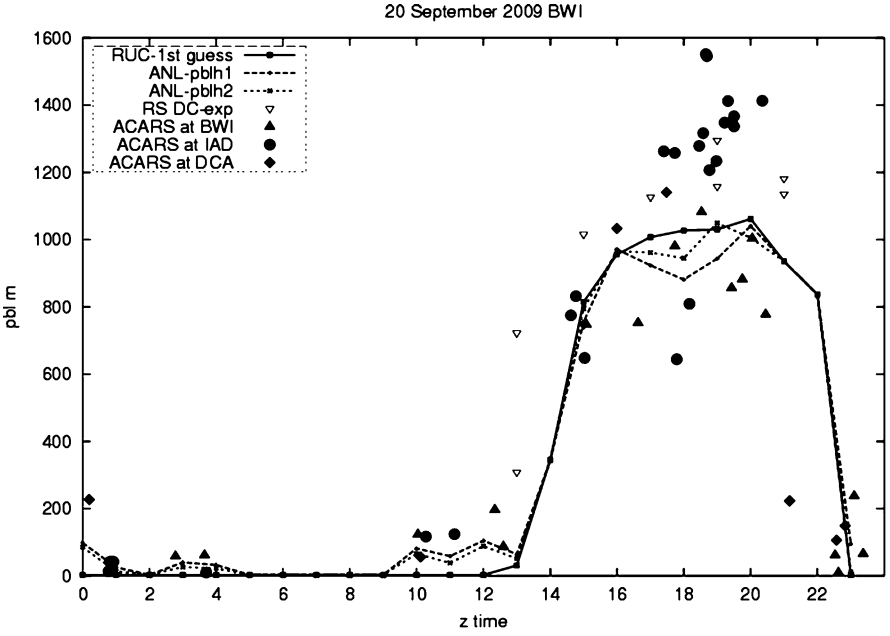


**Fig. 66.3** PBL height from DC experiment: RUC first guess (*solid line*), original analysis (*dotted line*), analysis obtained with all available observations (*dashed line*), radiosondes from DC experiment (*open triangles*) and ACARS (*dark symbols*)

## 66.5 Summary

The evaluation of data shows that ACARS-derived PBL heights are a good source of information for the RTMA analysis. Modification of internal parameters in the analysis resulted in a better performance judged by comparison with independent measurements collected during the DC PBL experiment. Validation of the modified analysis will be conducted using measurements from the wind profilers.

## References

1. Heinselman PL, Stensrud DJ, Hluchan RM, Spencer PL, Burke PC, Elmore KL (2009) Radar reflectivity-based estimates of mixed layer depth. J Atmos Oceanic Technol 26:229–239
2. Pondeca MSFV, Manikin GS, Park SY, Parrish DF, Wu WS, DiMego G, Derber C, Benjamin S, Horel JD, Lazarus SM, Anderson L, Colman B, Mann GE, Mandt G (2007) The development of the real time mesoscale analysis system at NCEP. In: 23rd Conference on IIPS, American Meteorological Society, San Antonio, P1.10
3. Sokolovskiy SV, Rocken C, Lenschow DH, Kuo Y-H, Anthes RA, Schreiner WS, Hunt DC (2007) Observing the moist troposphere with radio occultation signals from COSMIC. Geophys Res Lett 34.L18892. doi:10.1029/2007GL030458
4. Tsidulko M, McQueen J, DiMego G, Ek M (2008) PBL verification with Radiosonde and Aircraft data. AGU Fall Meeting, San Francisco, 15–19 Dec 2008
5. Vogelezang DHP, Holtslag AA (1996) Evaluation and model impacts of alternative boundary-layer height formulations. Bound-Lay Meteorol 81:245–269

# Chapter 67
# An Air Quality Forecasting Tool over Italy (ForeChem)

**Gabriele Curci**

**Abstract** The MM5-CHIMERE regional modelling system is implemented over Italy and validated against available ground-based observations of atmospheric composition in summer. MM5 meteorological model is run on two nested domain covering Europe and Italy at respectively 36 and 12 km horizontal resolution. CHIMERE chemistry transport model is used to simulate gas and aerosol composition on the two domains at 0.5° and 0.15° horizontal resolution. Anthropogenic hourly emissions of primary pollutants over Italy are derived from the CTN-ACE inventory developed by national environmental agencies. Biogenic volatile organic compound emissions are calculated with MEGAN model driven by MM5 radiation and temperature fields. Ozone ($O_3$) daily maxima are simulated with good correlation (0.76) and overestimated by 10%. Model overestimation decreases with increasing observed $O_3$, while correlation increases. $PM_{10}$ is underestimated by 30–40% and reproduced with a correlation >0.5. Over Italy, the model capture enhanced level of $O_3$, but not that of PM. Model skills in the 3-day ahead forecast do not degrade rapidly. Graphical output of forecast is operationally available on the ForeChem web site: http://pumpkin.aquila.infn.it/forechem/.

**Keywords** Air quality • Forecast • Chemical weather • Italy

## 67.1 Introduction

Air Quality forecast modelling systems are becoming more and more common throughout European countries [3, 10], particularly in response to the need for short and long term actions aimed at reducing air pollution impact on human health [4].

G. Curci (✉)
CETEMPS – Dip. Fisica, Università degli Studi dell'Aquila,
Via Vetorio, 67010 Coppito, L'Aquila, Italy
e-mail: gabriele.curci@aquila.infn.it

D.G. Steyn and S. Trini Castelli (eds.), *Air Pollution Modeling and its Application XXI*,
NATO Science for Peace and Security Series C: Environmental Security 4,
DOI 10.1007/978-94-007-1359-8_67, 

In the last decade, the availability of increased computer power allowed the development of progressively more sophisticated and resolved three-dimensional "deterministic" atmospheric models, which have now almost completely substituted the more simplified and computationally efficient "statistical" models [10]. At European scale there are many models providing operational 3-days ahead forecast at about 50 km horizontal resolution for ozone ($O_3$), nitrogen dioxide ($NO_2$), particulate matter with aerodynamic diameter less than 10 μm ($PM_{10}$), and other pollutants. Some of these forecasts are collected in an ensemble in the frame of European Monitoring Atmospheric Composition and Climate (MACC) project (http://www.gmes-atmosphere.eu/). In Italy there are several groups developing and running regional atmospheric composition models and there are three operational "chemical" weather services, two covering Europe and Italy [7, 9], and one covering Northern Italy [1]. In this work we report a first validation of the ForeChem service [7], recently developed in the frame of the QUITSAT (Air Quality with Integration of Remote Sensing from Ground and Satellite and Models, http://www.quitsat.it/) project funded by the Italian Space Agency (ASI).

## 67.2 MM5 and CHIMERE Models

Meteorological input to the system is provided by the MM5 model [5] run on two domains covering Western Europe at 36 km horizontal resolution and Italy at 12 km resolution (Fig. 67.1). In the vertical, the model has 32 terrain-following σ-levels extending up to ~100 hPa, with first four layers below 200 m altitude and first ten below 1 km altitude. The following choices of main parameterizations are adopted: Reisner 2 microphysics, Grell cumulus scheme, MRF planetary boundary layer, RRTM radiation, Noah land-surface scheme.

The CHIMERE chemistry-transport model [2] uses the meteorological input from MM5, hourly emission inventories and boundary conditions to simulate the chemical state (gas and aerosol phase) of the troposphere over the two domains of interest, Europe and Italy, at 0.5° and 0.15° horizontal resolution, respectively. In the vertical, the model has 8 terrain-following σ-levels extending up to 500 hPa,

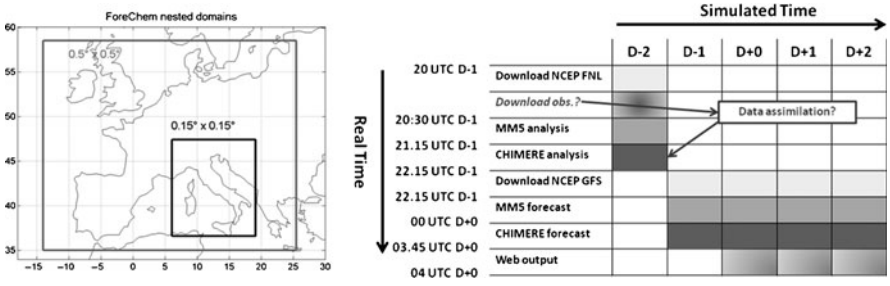


**Fig. 67.1** *Left*: ForeChem nested domains of simulation. *Right*: ForeChem data flow and timings

with first levels having an approximate height of 40, 100 and 180 m. Anthropogenic emissions (CO, NOx, SOx, NMVOCs, and $NH_3$) and particulate matter ($PM_{10}$ and $PM_{2.5}$) are taken from EMEP[1] expert emissions at continental scale and from CTN-ACE (Italian National Focal Point on Atmospheric Emissions) activity at Italian scale. Biogenic emissions for isoprene and monoterpenes are calculated with MEGAN model [8]. Aerosol primary and secondary (inorganic and organic) species are simulated in eight internally mixed bins [2].

The MM5-CHIMERE modelling system is setup over a 4-processors Linux platform and runs automatically everyday in two main steps: analysis and forecast mode. The data flow is schematically represented in Fig. 67.1. In future developments, the system may accommodate a chemical data assimilation procedure during the analysis step, in case of availability of near-real time observations.

## 67.3 Model Validation July 2007

We run the ForeChem system for the period 19 June–15 July 2007, we discard the first 2 weeks as model spin-up, and compare the results for 3–15 July with ground observations of $O_3$, $PM_{10}$ and $PM_{2.5}$ from EMEP[2] and Airbase[3] databases. We consider for comparison only rural, suburban, and urban background stations, since industrial and traffic stations are not representative of the simulated spatial scale (maximum horizontal resolution ~12 km).

In Table 67.1 we show statistics of comparison at continental scale. Ozone maximum is reproduced with a small positive bias <10% and mean correlation up to 0.76. PM levels are underestimated by 30–40% and with a mean correlation up to 0.59. In Table 67.2 we show statistics on Italian high-resolution domain.

**Table 67.1** Comparison of EMEP and AirBase observations with ForeChem results, for 3–15 July 2007 at continental scale

| | | | OBS | MOD | MB | NMB | RMSE | |
|---|---|---|---|---|---|---|---|---|
| Species | DB | N | $\mu g/m^3$ | $\mu g/m^3$ | $\mu g/m^3$ | % | $\mu g/m^3$ | CORR |
| O3 max | EMEP | 84 | 87.8 | 90.3 | 1.6 | 5.3 | 15.7 | 0.59 |
| O3 max | AirBase | 1,145 | 88.0 | 93.0 | 4.9 | 10.2 | 17.2 | 0.76 |
| PM10 daily | EMEP | 20 | 14.0 | 8.4 | −5.7 | −34.0 | 8.8 | 0.58 |
| PM10 daily | AirBase | 937 | 16.5 | 8.4 | −8.2 | −44.2 | 9.5 | 0.59 |
| PM2.5 daily | EMEP | 15 | 9.7 | 5.3 | −4.4 | −35.0 | 6.2 | 0.54 |
| PM2.5 daily | AirBase | 145 | 9.0 | 5.2 | −4.1 | −27.5 | 5.8 | 0.43 |

Indices are: *N* number of available stations, *OBS* mean observed value, *MOD* mean modelled value, *MB* Mean Bias, *NMB* Normalized Mean Bias, *RMSE* Root Mean Square Error, *CORR* temporal correlation

[1] http://www.ceip.at/emission-data-webdab/emissions-used-in-emep-models/

[2] http://tarantula.nilu.no/projects/ccc/emepdata.html

[3] http://www.eea.europa.eu/data-and-maps/data/airbase-the-european-air-quality-database-2

**Table 67.2** Same as Table 67.1, but on the Italian high-resolution domain

| | | | OBS | MOD | MB | NMB | RMSE | |
|---|---|---|---|---|---|---|---|---|
| Species | DB | N | $\mu g/m^3$ | $\mu g/m^3$ | $\mu g/m^3$ | % | $\mu g/m^3$ | CORR |
| O3 max | AirBase | 190 | 113.0 | 119.0 | 5.5 | 9.9 | 22.0 | 0.71 |
| PM10 daily | AirBase | 103 | 19.5 | 8.2 | −11.4 | −55.8 | 12.9 | 0.52 |
| PM2.5 daily | AirBase | 11 | 10.3 | 5.5 | −4.7 | −35.6 | 5.8 | 0.37 |

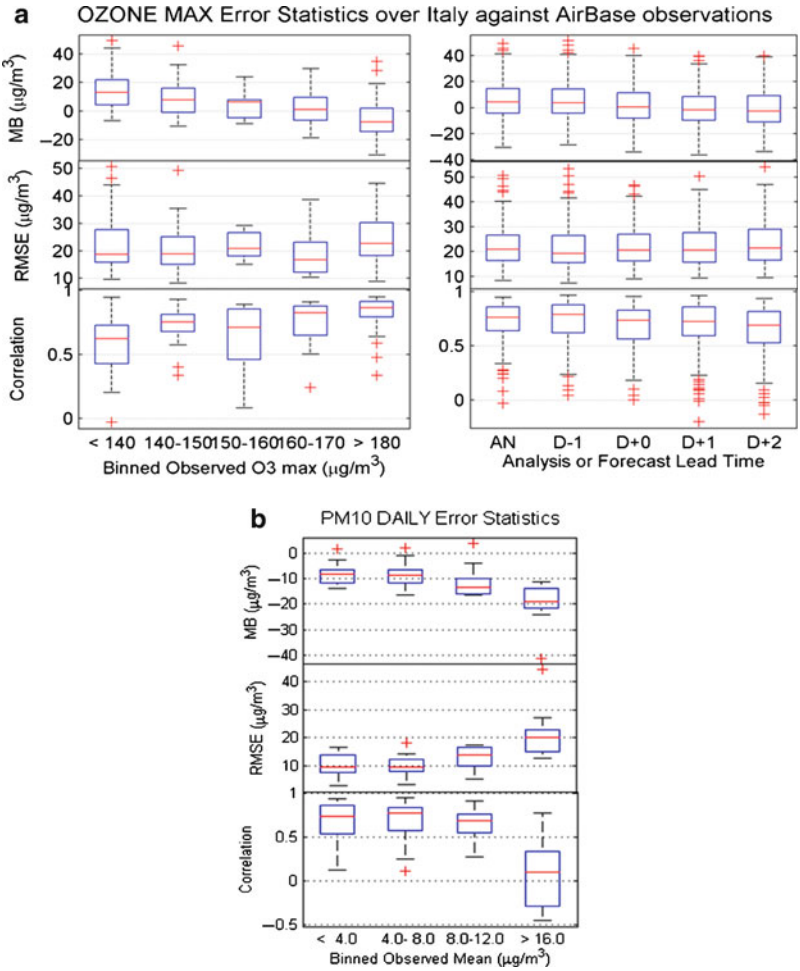


**Fig. 67.2** Error statistics of simulated (**a**) O3 max and (**b**) daily PM10 against AirBase observations over high-resolution Italian domain. Whisker plots denote median, 25th and 75th percentiles, 1.5 × (inter-quartile range), and outliers

Results for EMEP database are not shown, because only two stations are available in Italy. Average ozone maximum is much higher than continental value, and the model is able to capture this variability with a positive bias of 10% and a correlation of 0.71. PM levels are also higher than continental average, but the model does not reproduce this feature, indeed its negative bias is generally higher than that seen for the continental scale, and temporal correlation is lower.

Further analysis of the ozone bias, reveals that positive bias is mostly due to overestimation of values at lower end of distribution, while values at higher end are slightly underestimated and have an higher RMSE (Fig. 67.2a, left panel). On the other hand, the correlation increases with increasing maximum observed concentration. The model' skills degrade slowly with forecast lead time (Fig. 67.2, right panel). Regarding PM (Fig. 67.2b), it comes out that model errors increase with increasing observed PM value, being very poor at higher end of distribution.

Future work will extend this preliminary analysis to a longer simulation, including also a winter period, and will include further statistical indices to evaluate model prediction skills in terms of human health protection [6].

**Acknowledgments** The work is part of the Pilot Project QUITSAT, funded by the Italian Space Agency (ASI), contract I/035/06/0 – http://www.quitsat.it.

## References

1. ARPA (Regional Environmental Protection) Emilia Romagna. http://www.arpa.emr.it/aria/
2. Bessagnet B et al (2008) Regional modeling of carbonaceous aerosols over Europe – Focus on Secondary Organic Aerosols. J Atmos Chem 61:175–202
3. Dabbert WF et al (2006) USWRP workshop on air quality forecasting. Bull Am Meterol Soc 87:215–221
4. Directive on Ambient Air Quality and Cleaner Air for Europe (2008) Directive 2008/50/EC of the European Parliament and of the Council
5. Dudhia J (1993) A nonhydrostatic version of the Penn State/NCAR mesoscale model: Validation tests and simulation of an Atlantic cyclone and cold front. Mon Weather Rev 121:1493–1513
6. Eder B et al (2010) Using National Air Quality Forecast guidance to develop local Air Quality Index forecasts. Bull Am Meterol Soc 91:313–325
7. ForeChem. http://pumpkin.aquila.infn.it/forechem/
8. Guenther A, Karl T, Harley P, Wiedinmyer C, Palmer PI, Geron C (2006) Estimates of global terrestrial isoprene emissions using MEGAN (Model of Emissions of Gases and Aerosols from Nature). Atmos Chem Phys 6:3181–3210
9. LaMiaAria. http://www.lamiaaria.it/
10. Menut L (2010) Bessagnet, B: atmospheric composition forecasting in Europe. Ann Geophys 28:61–74

# Chapter 68
# Comparing Air Quality Forecast and a Reanalysis: Improvements Due to Chemical Data Assimilation and Better NWP Forcing

**Julius Vira and Mikhail Sofiev**

**Abstract** The paper discusses the operational experience of European-scale AQ hind- and fore-casting with the SILAM dispersion model and compares the performance of the two setups. Two parallel lines of daily AQ assessment in Europe have been established: the 72 h long stand-alone forecast and a previous-day 24 h hindcast followed by a 72 h forecast. In the hindcasting mode, 3D-VAR based data assimilation is used to refine the initial fields for $O_3$, $NO_2$ and $SO_2$. The standalone forecast, on the other hand, is initialized from the previous forecast without data assimilation. According to preliminary statistics, the best score improvement in the forecast is obtained for $O_3$, while only minor or no improvement is seen for $SO_2$ and $NO_2$. In addition, the data assimilation of gas-phase species has a visible effect on predictions of secondary inorganic aerosols.

**Keywords** Air quality forecasting • Data assimilation • 3D-Var

## 68.1 Introduction

The data assimilation problem for the air quality (AQ) assessment and forecasting has both similarities with and differences from the meteorological forecasting. Apart from the initial state of the model, which can be determined via assimilation of the observations, the evolution of the system is strongly controlled by emission fluxes and meteorological fields, which are the external parameters for the chemistry transport models (CTMs). This limits the impact of the initial state assimilation from observations because the model state evolution is quickly taken over by the emission and meteorological forcing. However, the initial state can still be a useful control variable in a short-term forecast.

J. Vira (✉) • M. Sofiev
Finnish Meteorological Institute, P.O. BOX 503, FI-00101 Helsinki, Finland
e-mail: julius.vira@fmi.fi; mikhail.sofiev@fmi.fi

D.G. Steyn and S. Trini Castelli (eds.), *Air Pollution Modeling and its Application XXI*,
NATO Science for Peace and Security Series C: Environmental Security 4,
DOI 10.1007/978-94-007-1359-8_68, 

The problem of estimating the initial state can be approached with assimilation methods including 3-dimensional variational data assimilation (3D-VAR) and optimal interpolation [1, 9]. In both studies, the effect of initial state adjustment was found to be generally limited to the first 24–36 h of the forecast.

The current work evaluates the impact of the initial model state assimilation performed with 3D-VAR at a European scale and used for the 72-h-long air quality forecasting.

## 68.2 Materials and Methods

The set of tools used in the current study includes the 3D-VAR data assimilation (DA) system and the dispersion modelling system SILAM version 4 [7, 8]. It is based on the non-diffusive advection scheme of Galperin [2] and the adaptive vertical diffusion algorithm of Sofiev [6]. The model is forced by the ECMWF meteorological fields with up to 72 h forecast length. However, the previous-day assimilation and re-analysis cycles are based on the shortest available NWP forecasts with horizon of +3 to +12 h. The emission data are taken from the TNO European emission inventory. The computational domain covers the whole of Europe (http://www.gmes-atmosphere.org) with resolution of ~25 km. Atmospheric gas-phase chemistry follows the CB4 chemical mechanism [3], while the heterogeneous chemistry and production of the secondary inorganic aerosols follow Sofiev [5].

The 3D-VAR analysis is performed every 6 h, and both the model background field and observations are picked at the end of this interval. The modelled background field is obtained from the previous analysis followed by the 6-h long SILAM forecast. The background error covariance matrix is derived from archived air quality forecasts using the NMC method [4]. Following the NMC approach, the difference between the two forecasts valid at the same time is taken as a sample of the forecast error distribution.

In the current setup, a spatially homogeneous Gaussian correlation model is assumed for each species with horizontal length scales estimated between approximately 80 and 200 km, depending on the chemical component. The correlation between the vertical levels is assumed to be separable from the horizontal correlation, and is estimated directly as the sample correlation matrix from the NMC dataset. Contrary to the spatial correlation function, the method allows the variance of background errors to depend on the grid point location without additional computational expenses. The assumption of spatial homogeneity of the correlations allows for a very efficient numerical implementation using the eigenvalue decomposition of the background error covariance matrix.

## 68.3 Results

The forecast initialized using the analysis fields is expected to perform better than the free-running one. One of the potential sources of improvements is the shorter forecast length of the meteorological fields. However, the effect appears to strongly

depend on the species. As an illustration, the RMS errors were computed for both forecasts over the period between 5 and 12 September, 2010.

Both the $SO_2$ and $NO_2$ fields show modest improvement with highly varying difference between the reference run without DA and the analysis field. For $SO_2$, the effect is lost entirely in the forecast window. This pattern is a result of the high density of the observation network, and the comparatively low correlation distance of these pollutants.

The most substantial change is seen for ozone but it is not entirely for the better. The problem may originate from the usually positive bias of the model during the night-time. While the night-time bias is reduced by the assimilation, a negative bias is correspondingly introduced in day-time levels. However, the overall effect is positive (Table 68.1).

The forecast of PM2.5 improves somewhat, despite of no direct assimilation of particulate matter. The improvement thus propagates through the aerosol formation mechanisms, i.e. it seems likely that assimilation of $SO_2$ and NOx leads to improved prediction of secondary inorganic aerosols. This is illustrated for the case of sulphates in Fig. 68.1.

**Table 68.1** Scores of the reference forecast, analysis and the initialized forecast

| RMSE (μg/m$^3$) | Forecast, no DA | Analysis | Forecast with DA |
|---|---|---|---|
| $O_3$ | 29.1 | 22.2 | 26.6 |
| $NO_2$ | 19.3 | 17.5 | 18.5 |
| $SO_2$ | 5.88 | 5.64 | 5.99 |
| PM2.5 | 10.1 | 9.21 | 9.33 |

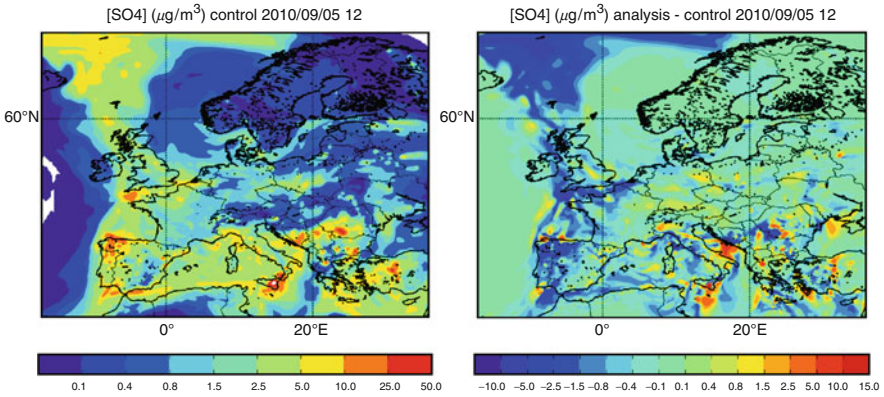


**Fig. 68.1** Impact of data assimilation on sulphates. *Left*: reference run, *right*: analysis-reference

## 68.4 Conclusions

A 3DVAR-based setup for near-real-time analyses of the pollutant concentrations for the previous day has been discussed. The analyses are used to initialise a 72 h forecast, where ozone shows significant improvement, while for $NO_2$ the RMSE is decreased only slightly. Furthermore, the setup demonstrates that assimilation of gas-phase species can have significant impact on particulate matter predictions due to secondary aerosol formation.

## References

1. Blond N, Vautard R (2004) Three-dimensional ozone analyses and their use for short-term ozone forecasts. J Geophys Res 109:D17303
2. Galperin M (2000) The approaches to correct computation of airborne pollution advection. In problems of ecological monitoring and ecosystem modelling. Gidrometeoizdat, pp 54–68
3. Gery M, Whitten G, Killus J, Dodge M (1989) A photochemical kinetics mechanism for urban and regional scale computer modelling. J Geophys Res 94:925–956
4. Parrish D, Derber J (1992) The National Meteorological Center's spectral statistical analysis system. Mon Weather Rev 120:1747–1763
5. Sofiev M (2000) A model for the evaluation of long-term airborne pollution transport at regional and continental scales. Atmos Environ 34(15):2481–2493
6. Sofiev M (2002) Extended resistance analogy for construction of the vertical diffusion scheme for dispersion models. J Geophys Res Atmos 107:D12. doi:10.1029/2001JD001233
7. Sofiev M, Galperin M, Genikhovich E (2008) Construction and evaluation of Eulerian dynamic core for the air quality and emergency modeling system SILAM. In: Borrego C, Miranda AI (eds) Air pollution modelling and its application XIX, NATO science for peace and security Series C: environmental security. Springer, Dordrecht, pp 699–701
8. Sofiev M, Siljamo P, Valkama I, Ilvonen M, Kukkonen J (2006) A dispersion modelling system SILAM and its evaluation against ETEX data. Atmos Environ 40:674–685. doi:10.1016/j.atmosenv.2005.09.069
9. Tombette M, Mallet V, Sportisse B (2009) PM10 data assimilation over Europe with the optimal interpolation method. Atmos Chem Phys 9:57–70

# Chapter 69
# Simulation of the Sensitivity of Rural Tropospheric Ozone Levels to BVOCs Emissions over a European Atlantic Coastal Region (Galicia, NW of Spain)

**Angel Rodríguez, Santiago Saavedra, Jose A. Souto, and Juan J. Casares**

**Abstract** Volatile organic compounds (VOCs) are key species for the production of tropospheric ozone, and biogenic VOCs (BVOCs) emissions are significantly important in rural areas because of their amount and the photochemical ozone creation potential (POCP) of biogenic species.Galicia is an Atlantic coastal region located in northwestern Spain, with forestry as the most important land use, including both deciduous (oak, chestnut, birch) and evergreen (pine, eucalyptus) species. In this region, because of its changeable weather conditions and its local Atlantic forest species, BVOCs emissions are highly variable, depending on meteorological (temperature, PAR and moisture) and seasonal parameters (leaf area index and daylight hours).This work is focused on the sensitivity analysis of the rural tropospheric ozone levels due to influence of BVOCs emissions from the European Atlantic forest.

**Keywords** BVOCs emissions • MEGAN model • Tropospheric ozone episodes • CAMx model

## 69.1 Field Data

Four ozone episodes with hourly maximum glc above 150 μg/m$^3$ in the north of Galicia (July 14th–23 rd, 2002, March 16th–24th, 2003, September 9th–22nd, 2003 and August 1st–6th, 2007) were taken as realistic modeling scenarios.

For this modeling experiment, in a first stage the typical BVOCs emissions range estimated in other regions of the Iberian peninsula [3] were considered.

A. Rodríguez (✉) • S. Saavedra • J.A. Souto • J.J. Casares
Department of Chemical Engineering, University of Santiago de Compostela,
15782 Santiago de Compostela, Spain
e-mail: angel.rodriguez@usc.es; ja.souto@usc.es

D.G. Steyn and S. Trini Castelli (eds.), *Air Pollution Modeling and its Application XXI*,
NATO Science for Peace and Security Series C: Environmental Security 4,
DOI 10.1007/978-94-007-1359-8_69, 

Therefore, three different scenarios with constant BVOCs emissions were simulated: no BVOC emissions, a regular 3 $Tm \cdot km^{-2} \cdot year^{-1}$ emission rate of isoprene, and an extreme 10 $Tm \cdot km^{-2} \cdot year^{-1}$ emission rate of isoprene.

In a second stage, in order to obtain a realistic comparison of the effect of both meteorological and seasonal conditions, MEGAN model [2] was applied to estimate hourly BVOCs emissions in Galicia along the modeling scenarios. Chemical speciation used by MEGAN was the corresponding to biogenic species included in Carbon Bond IV mechanism, and four functional plant types (broadleaf and needleaf trees, shrublands and herbaceous) were considered.

In the different simulations, anthropogenic emissions from EMEP were reviewed at Galicia by considering industrial emissions from the bottom-up REGADE inventory [1], using preprocessor SMOKE to temporal disaggregation, spatial distribution and speciation.

## 69.2 Results

Simulations of the four episodes were performed using CAMx with two nested grids covering the Iberian peninsula ($27 \times 27$ $km^2$ resolution) and Galicia ($9 \times 9$ $km^2$ resolution), applying GOCART and MOZART data as initial and boundary chemical conditions. Meteorological inputs were provided by PSU/NCAR MM5 simulations, using NCEP reanalysis as initial and boundary meteorological conditions.

The simulation results revealed that the rise of BVOCs emissions contributes to increasing daily ozone levels (Figs. 69.1 and 69.2), because these compounds, along with NOx, are one of the main photochemical precursors of tropospheric ozone; however, it is remarkable that ozone ground level concentrations continue to increase even with the highest constant rate of BVOCs used (10 $Tm \cdot km^{-2} \cdot year^{-1}$). This could point to a VOCs – limited regime for ozone chemical production in rural areas of the northern Galicia (i.e. $O_3$ decreases as VOC emissions are reduced), as often appears in urban areas. This regime is probably caused by large amounts of NOx available due to emissions from the power plants located at the area.

In fact, an important influence of BVOCs has been observed in photochemical generation of ozone in stations close to industrial sources of NOx. Simulations using MEGAN model have shown a 15–30% increment in episodic peak ozone concentrations in these stations with respect to the simulations results without biogenic emissions of VOCs (Figs. 69.1 and 69.2). Moreover, these results also confirm the important influence of temperature on ozone sensitivity to BVOCs due to the enhancement of BVOCs emissions with thermal increasing. Thus, on days with high temperatures (Fig. 69.2) ozone levels using emissions estimated by MEGAN model are similar to or even higher than simulated ozone levels considering a 3 $Tm \cdot km^{-2} \cdot year^{-1}$ constant emission rate of BVOCs. This effect has not been observed on days with temperatures below 25°C (Fig. 69.1).

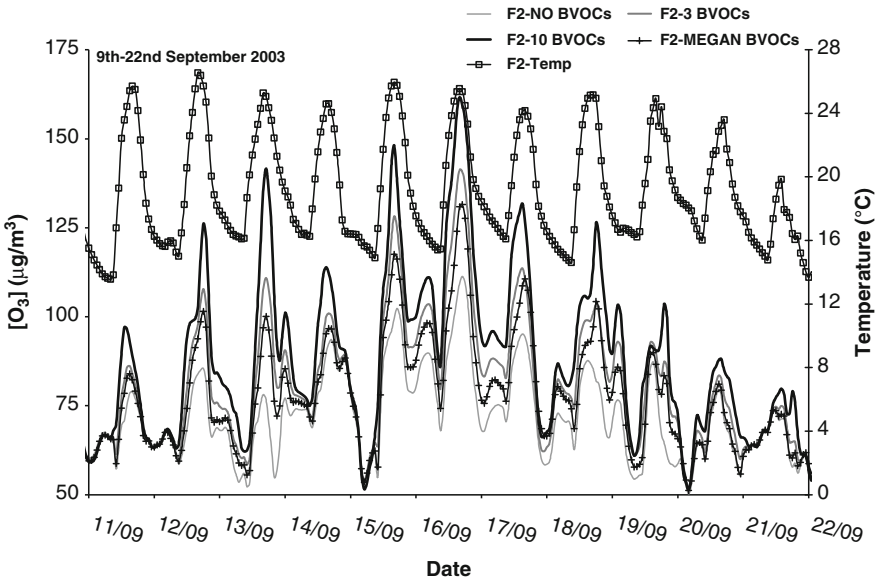


**Fig. 69.1** Time series plots of hourly averaged ozone concentrations ($\mu g/m^3$) and surface temperature (°C) in F2-Fraga Redonda rural station for 9th–22nd September 2003. Results from simulations without BVOCs (NO BVOCs), 3 $Tm \cdot km^{-2} \cdot year^{-1}$ of isoprene (3 BVOCs), 10 $Tm \cdot km^{-2} \cdot year^{-1}$ of isoprene (10 BVOCs) and with biogenic emissions from MEGAN (MEGAN BVOCs)

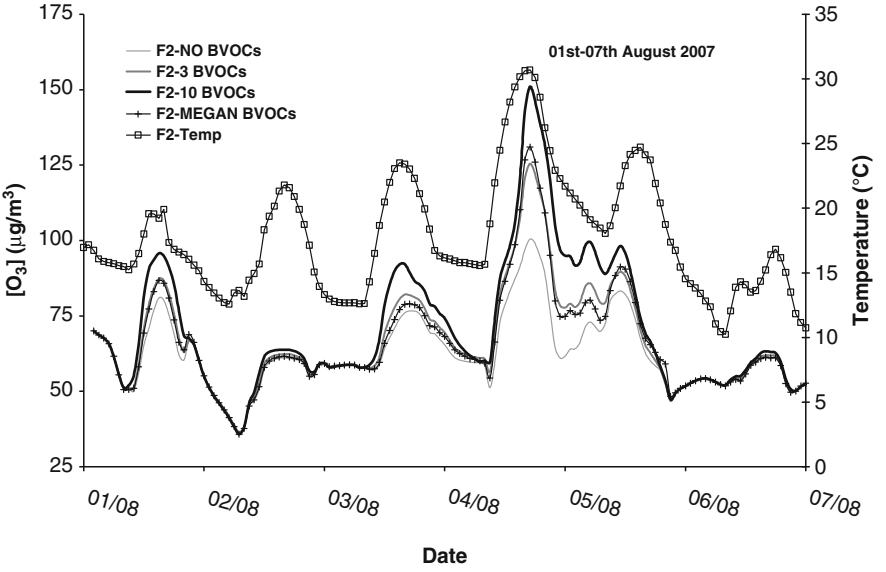


**Fig. 69.2** Time series plots of hourly averaged ozone concentrations ($\mu g/m^3$) and surface temperature (°C) in F2-Fraga Redonda rural station for 1st–7th August 2007. Results from simulations without BVOCs (NO BVOCs), 3 $Tm \cdot km^{-2} \cdot year^{-1}$ of isoprene (3 BVOCs), 10 $Tm \cdot km^{-2} \cdot year^{-1}$ of isoprene (10 BVOCs) and biogenic emissions from MEGAN (MEGAN BVOCs)

## 69.3 Conclusions

Results of the air quality simulations performed over Galicia with different levels of BVOCs emissions suggest that the major industrial emissions of NOx can change the classic rural NOx-limited regime of rural areas to a VOCs limited-regime of ozone production.

Consequently, simulations show the importance of BVOCs in ozone levels in the north of Galicia, specially at temperatures above around 25°C, when chemical mechanisms that promote ozone production (as isoprene photolysis) are fast enough. In addition, higher temperatures allow higher BVOCs emissions depending on the seasonal conditions in this region, increasing $O_3$ production.

**Acknowledgements** This work was financially supported by the R&D Spanish Programme (CTQ2006-15481/PPQ). Air quality data were provided by Xunta de Galicia (Spain), As Pontes Power Plant (Endesa) and Ministerio do Ambiente of Portugal (web page). PhD research grant of Angel Rodríguez is supported by Galician "María Barbeito" Programme (Xunta de Galicia).

## References

1. Casares JJ, Rodríguez R, Maceira P, Souto JA, Ramos S, Costoya MA, Sáez A, Vellón JM (2005) Inventario, Análisis y Proyección de las Emisiones Atmosféricas Industriales de Galicia. Servizo de Publicacións e Intercambio Científico, Universidade de Santiago de Compostela, Santiago de Compostela
2. Guenther A, Hewitt CN, Erickson D, Fall R, Geron C, Graedel T, Harley P, Klinger L, Lerdau M, Mckay WA, Pierce T, Scholes B, Steinbrecher R, Tallamraju R, Taylor J, Zimmerman PA (1995) Global-model of natural volatile organic-compound emissions. J Geophys Res 100 (D5):8873–8892
3. Parra R, Gassó S, Baldasano JM (2004) Estimating the biogenic emissions of non-methane volatile organic compounds from the North Western Mediterranean vegetation of Catalonia, Spain. Sci Total Environ 329:241–259

# Chapter 70
# Ensemble Air Quality Forecasting: Effects of Perturbations in Meteorology and Emissions

**Christian Hogrefe, Prakash Doraiswamy, Brian Colle, Kenneth L. Demerjian, Winston Hao, Mark Beauharnois, Michael Erickson, Matthew Souders, Jia-Yeong Ku, and Gopal Sistla**

**Abstract** Model-based air quality forecasts are affected by uncertainties in both meteorology and emissions. In this study, we analyze the impacts of these uncertainties on ozone ($O_3$) forecasts over the Northeastern U.S. during a 45 day period in the summer of 2008. The meteorological uncertainty is prescribed through the use of 12 different weather forecasts from a short-range ensemble forecasting system differing in their initial conditions and physics options. To quantify the effects of emission uncertainties, we computed $O_3$ sensitivities towards variations in anthropogenic $NO_x$ and VOC emissions using the Direct Decoupled Method (DDM). Results show that the perturbations in meteorology tend to have a larger impact on $O_3$ forecasts than the emission perturbations considered in this study.

**Keywords** Ensemble Air Quality Forecasting • Direct Decoupled Method

C. Hogrefe (✉)
New York State Department of Environmental Conservation, Albany, NY, USA

Atmospheric Sciences Research Center, University at Albany, Albany, NY, USA
e-mail: chogrefe@asrc.cestm.albany.edu

P. Doraiswamy • K.L. Demerjian • M. Beauharnois
Atmospheric Sciences Research Center, University at Albany, Albany, NY, USA

B. Colle • M. Erickson • M. Souders
School of Marine and Atmospheric Sciences, Stony Brook University,
Stony Brook, NY, USA

W. Hao • J.-Y. Ku • G. Sistla
New York State Department of Environmental Conservation, Albany, NY, USA

D.G. Steyn and S. Trini Castelli (eds.), *Air Pollution Modeling and its Application XXI*,
NATO Science for Peace and Security Series C: Environmental Security 4,
DOI 10.1007/978-94-007-1359-8_70, 

## 70.1 Introduction

The application of photochemical modeling systems has become an integral part of air quality forecasting in the U.S. The development of ensemble forecast systems is a promising avenue for improving air quality forecast guidance and to develop probabilistic forecast products. Most initial applications of this concept in the U.S. have relied upon ensembles of opportunities in which air quality forecasts from different modeling groups were compared for limited time periods without an attempt to compare the contributions from weather forecast uncertainties vs. emission uncertainties to the spread of the resulting ensemble predictions. The goal of this study is to address this issue by analyzing how ozone ($O_3$) forecasts depart from a base model forecast when perturbing either meteorology or anthropogenic $NO_x$ and/or VOC emissions.

## 70.2 Modeling System and Method of Analysis

The base air quality forecast modelling system used in this study consists of the MM5 meteorological model and the Community Multiscale Air Quality (CMAQ) chemical transport model. Emission inventories were compiled by the New York State Department of Environmental Conservation (NYSDEC) and processed with SMOKE. All simulations were performed for June 4–July 22, 2008. To estimate the effect of meteorological forecast uncertainties on predicted $O_3$ concentrations, CMAQ simulations were driven by seven daily MM5 and five daily WRF-ARW members from the Stony Brook University Short-Range Ensemble Forecast (SREF) system. These members differ in their choice of initial and boundary conditions as well as different convective parameterization, boundary layer, and microphysical schemes. The same set of base emission inventories processed through SMOKE was used for all of these CMAQ simulations. To estimate the effect of emission perturbations on simulated air quality, we used the Direct Decoupled Method (DDM) implemented in CMAQ. CMAQ-DDM simulations were performed with the MM5 meteorological fields from the base model configuration. Following the general approach described in Cohan et al. [1], Napelenok et al. [2], and Pinder et al. [3], the CMAQ-DDM sensitivity fields were used to develop a reduced-form model for $O_3$ using first and second order terms. For calculating $O_3$ variations caused by emission uncertainties, we varied total anthropogenic $NO_x$ and VOC emissions from −40% to +40% of their base case value.

## 70.3 Results and Discussion

Figure 70.1 compares the variability in predicted daily maximum 8-h $O_3$ (DM8HR) concentrations introduced by perturbations in meteorology vs. those introduced by perturbing anthropogenic $NO_x$ and/or VOC emissions. The histograms display the

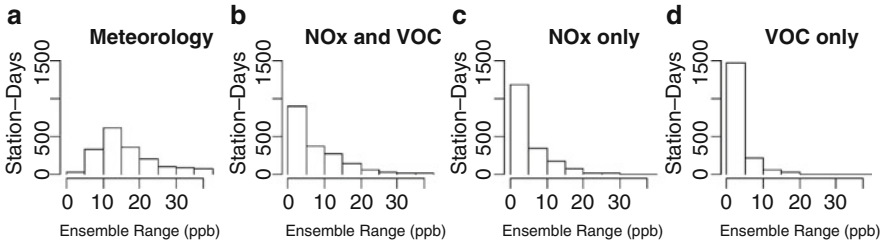


**Fig. 70.1** Histograms of the range of predicted daily maximum 8-h ozone concentrations as a result of perturbations in meteorology and emissions. The ranges were calculated for each day at each of the 38 $O_3$ monitors in New York State

range of predicted DM8HR concentrations at each of the 38 $O_3$ monitors in New York State. To develop these histograms, the difference between the highest and lowest predicted DM8HR concentrations was calculated at each monitor for each day for (a) perturbations in meteorology, (b) perturbations in both $NO_x$ and VOC emissions, (c) perturbations in $NO_x$ emissions only, and (d) perturbations in VOC emissions only. The results show that perturbations in meteorology typically cause a larger range of predicted $O_3$ concentrations than the +/− 40% perturbations in anthropogenic $NO_x$ and/or VOC emissions considered here as indicated by the larger median and wider spread of the distribution in panel (a) compared to the distributions in panels (b)–(d). The median predicted DM8HR range is 14.3 for perturbations in meteorology, 4.9 ppb for simultaneous perturbations in both $NO_x$ and VOC emissions, 3.3 ppb for perturbation in $NO_x$ emissions only, and 1.4 ppb for perturbations in VOC emissions.

While the histograms shown in Fig. 70.1 present an overall assessment of the relative impact of perturbations in meteorology vs. emissions, they do not reveal whether there are spatial differences in these impacts. To investigate this issue further, Fig. 70.2b–e show maps of the predicted ranges for a particular day (June 10). The map showing the ranges caused by perturbations in meteorology is shown in Panel (b) while the ranges caused by perturbations in $NO_x$ and VOC emissions, $NO_x$ emissions only, and VOC emissions only are shown in Panels (c), (d), and (e), respectively. Panel (a) shows a map of the predicted DM8HR $O_3$ concentrations for the base model. These panels illustrate that the effect of emission perturbations is largest in the areas of the highest concentrations predicted by the base model, and that simultaneous perturbations in both anthropogenic $NO_x$ and VOC emissions have a larger effect than perturbing these emissions individually. Meteorological perturbations also have a large impact in the areas of the highest concentrations predicted by the base model but in addition also cause variability in other areas such as the southern portion on the forecast domain, areas of upstate New York and the Atlantic Ocean.

One potential application of air quality ensemble forecast systems is to provide maps of predicted probabilities for exceeding certain threshold levels. For each grid cell, such probabilities can be calculated based on how many of the ensemble

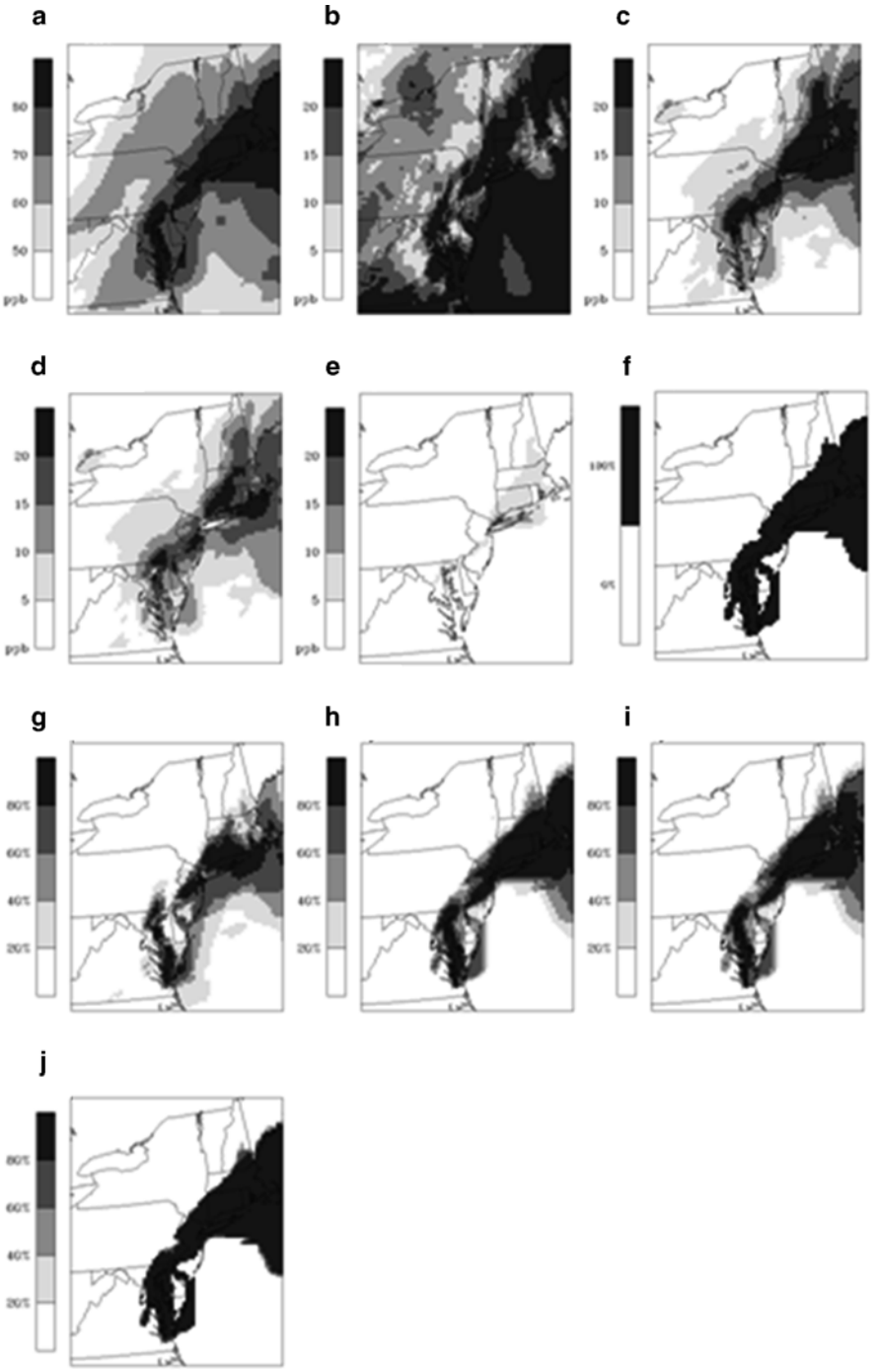


**Fig. 70.2** Maps of (**a**) DM8HR predicted by the base model, (**b**)–(**e**) ranges in DM8HR as a result of perturbations in meteorology and emissions, (**f**) exceedance probabilities for the base model, and (**g**)–(**j**) exceedance probabilities resulting from perturbations in meteorology and emissions. All maps are for June 10, 2008

members exceed a threshold level of interest. As an example, Fig. 70.2f–j shows estimated probabilities for DM8HR exceeding 75 ppb for June 10 for (f) the base model, (g) the meteorology ensemble, (h) the $NO_x$ and VOC perturbation ensemble, (i) the $NO_x$ perturbation ensemble, and (j) the VOC perturbation ensemble. The exceedance probability predicted by the base model for a given grid cell is either 0% or 100% depending on whether or not the predicted DM8HR was less than 75 ppb. All emission perturbation cases show a spatial pattern of exceedance probabilities that is very similar to the base model, i.e. the transition from regions of low predicted probabilities to high predicted probabilities occurs very rapidly. This is especially pronounced for the VOC-only perturbations which had a relatively small overall effect on the plume magnitude as already shown in panel (e), but even the perturbations of $NO_x$ emissions do not add many grid cells of "transitional" exceedance probabilities. In contrast, the map of exceedance probabilities for the meteorological perturbations exhibits a more gradual transition from regions of low exceedance probabilities to regions of higher exceedance probabilities, decreasing the exceedance probability with respect to the base model in some areas (e.g. parts of Massachusetts) and increasing it in others (e.g. southern New Jersey). These results suggest that the primary impact of emission perturbations is on the magnitude of $O_3$ plumes while meteorological perturbations affect both the magnitude and location of these plumes.

In future work, the potential of ensemble systems to provide forecasts of exceedance probabilities as illustrated in Fig. 70.2g–j will necessitate the application of probabilistic evaluation techniques as illustrated in Pinder et al. [3]. To investigate whether the relative impact of meteorology vs. emission perturbations is different for $PM_{2.5}$ forecasts, future work will include ensembles that incorporate perturbations of both primary $PM_{2.5}$ and precursor emissions for both summer and winter episodes. In addition, CMAQ-DDM simulations can be configured to track the impacts of emission perturbations from specific source sectors and regions. Employing such a configuration and performing CMAQ-DDM air quality forecasts on a routine basis would allow for the quantification of benefits stemming from potential episodic emission control measures during high pollution events. Finally, future work will also be directed at discerning differences between biases vs. uncertainties in emission inventories and combining bias adjustment techniques with ensemble systems to yield improved air quality forecasts.

## References

1. Cohan DS, Hakami A, Hu YT, Russell AG (2005) Nonlinear response of $O_3$ to emissions: source apportionment and sensitivity analysis. Environ Sci Technol 39:6739–6748
2. Napelenok SL, Cohan DS, Odman MT, Tonse S (2008) Extension and evaluation of sensitivity analysis capabilities in a photochemical model. Environ Model Softw 23:994–999
3. Pinder RW, Gilliam RC, Appel KW, Napelenok SL, Foley KM, Gilliland AB (2009) Efficient probabilistic estimates of surface ozone concentration using an ensemble of model configurations and direct sensitivity calculations. Environ Sci Technol 43(7):2388–2393

# Part IV
# Model Assessment and Verification

# Chapter 71
# Multi-model Ensembles: Metrics, Indexes, Data Assimilation and All That Jazz

**Stefano Galmarini and Slowomir Potempski**

**Abstract** We investigate the possibility of using different metrics for the evaluation of multi-model ensembles, in the attempt to find the optimal representation of the ensemble spread and bias. We present basic properties of different metrics and we discuss the consequences of applying them in atmospheric dispersion multi-model ensemble systems. We show also how we can obtain relevant information equivalent to different statistical treatments of an ensemble by combining the application of various metrics for calculating the ensemble spread and bias. A digression is presented on the use of the optimal combination of model results within an ensemble Kalman filter application for data assimilation.

**Keywords** Ensemble treatment • Metrics for ensembles of models

## 71.1 Introduction

An analogy for atmospheric dispersion ensemble modeling could be darts competition by teams. We could think of models that try to simulate a physical process as dart players in a competition and the model ensemble as a team of players. Thus the team relies on the efforts of all its members trying to hit the target. The latter known as the *bull's-eye* or *bull*, represents the measurement in a point in space and at an instant in time that characterizes a physical process. During the throwing all team members do their best to get as close as possible to the *bull*, however one way or another some

S. Galmarini (✉)
European Commission – DG Joint Research Centre, Institute for Environment and Sustainability, Ispra, Italy
e-mail: stefano.galmarini@jrc.ec.europa.eu

S. Potempski
Institute of Atomic Energy POLATOM, Otwock-Swierk, Poland

D.G. Steyn and S. Trini Castelli (eds.), *Air Pollution Modeling and its Application XXI*, NATO Science for Peace and Security Series C: Environmental Security 4,
DOI 10.1007/978-94-007-1359-8_71, 

throw above the target, some to its right and some far away from it. At the end of a round we are left with a cloud of darts and holes on the board, including maybe some that indeed hit it right in the middle. The problem we wish to tackle is how we can evaluate the team performance. If we consider all the shots equally plausible and true attempts to hit the target, we will have to consider the whole cloud on the board when assigning the final score. What kind of evaluation parameter should we use to account for all throws? The question reduces to finding the best way to condense in one or few parameters the performance of all shots, both good and bad. Visually it may be clear which of the teams is closer, but not necessarily so, therefore we want to devise a method to determine quantitatively the team result. We will start by defining, according to specific metrics, a point within the cloud that represents all throws prior to its relative position to the target. The definition of a cloud representative which will not necessarily be a dart hole is important per-se to the extent that it summarizes the characteristics of each hole and it will become the reference point to relate the ensemble to the target. We assume here that every player throws the dart without being influenced by any other team member. In fact we can assume that each of the players throws autonomously and therefore, that the team shots are uncorrelated ([9] – PG09). Out of the analogy we are interested in addressing these issues specifically for atmospheric transport and dispersion models including air quality models. The use of the ensemble technique, mainly multi-model ensembles, according to which several models concur to the estimation of a physical parameter, has become more and more popular and widely used (e.g. [1–5] and [8–12]).

## 71.2 Plausible Metrics

In PG09 an optimal linear combination of model results has been determined under the assumption that the results of models' simulations can be represented by *random variable*s with given biases and variances for each model. The optimal representative has been obtained by minimizing the mean square error, which is a commonly used approach. The question however arises as: what would be an optimal representation of multi-model ensemble results when other metrics are applied? We will concentrate on the cloud spread that we define here as the distance of all ensemble members from a point that we will call 'centre of the ensemble'. Mathematics says that in order to find this point the function representing the spread should be minimized. The determination of a distance relates however, to the specification of a metric. We selected the standard metrics usually referred to as *maximum*, *Euclidean*, and *Taxi cab*. From them the following definitions of the spread can be derived:

$$S_{\max}(x) = \max_i |x - x_i| \tag{71.1}$$

$$S_E(x) = \sqrt{\sum_i |x - x_i|^2} \tag{71.2}$$

$$S_T(x) = \sum_i |x - x_i| \tag{71.3}$$

where $x_i$ $i = 1,..,m$ are models' results (throughout the whole paper $m$ stands for the number of models) and $x$ represents the point that summarizes all the positions of the darts or of the model results. In statistics, in particular in estimation theory, it is known that different norms can be applied in optimisation problems to get various statistical indicators (for example [6, 7]). We will proceed in a similar way. To find $x^{opt}$ the centre of the cloud of results and darts, or optimal ensemble representative, we have to minimize the spread, namely: to find $x^{opt}$ such that $S(x^{opt}) = \min_x S(x)$ for all three different definitions of the spread $S$, Eqs. 71.1–71.3. The solutions to this problem for the three adopted metrics are given as:

$$S_{\max}(x^{opt}) = \min_x \max_i |x - x_i| \quad \text{for} \quad x^{opt} = \frac{\min_i (x_i) + \max_i (x_i)}{2} = \overline{x}_{\max} \tag{71.4}$$

$$S_E(x^{opt}) = \min_x \sqrt{\sum_i |x - x_i|^2} \quad \text{for} \quad x^{opt} = \frac{1}{m} \sum_i x_i = \overline{x}_E \tag{71.5}$$

$$S_T(x^{opt}) = \min_x \sum_i |x - x_i| \quad \text{for} \quad x^{opt} = Median(x_i) = \overline{x}_T \tag{71.6}$$

From now on we will use the "bar" (as in Eqs. 71.4–71.6) to identify the optimal ensemble representative and the subscripts *max*, *E* and *T* to identify the metrics Eqs. 71.1–71.3, respectively.

## 71.3 Mutual Relationships, Differences of Ensemble Representatives and the MMM Patterns

From the minimization solutions presented in Sect. 2 through Eqs. 71.4–71.6, it follows that the selection of a value chosen as the representative of multi-model ensemble results depends on the applied norm. By using the Schwarz inequality, the following general relationships among the three metrics can easily be shown:

$$S_{\max}(x) \leq S_E(x) \leq S_T(x),$$

$$S_T(x) \leq \sqrt{m} S_E(x),$$

$$S_E(x) \leq \sqrt{m} S_{\max}(x) \tag{71.7}$$

$$S_T(x) \leq m S_{\max}(x)$$

Inequalities (Eq. 71.7) are generic – in practice one can expect that typically, the ratios between the spreads are:

$$\frac{S_T(x)}{S_E(x)} \approx a_1\sqrt{m}, \quad \frac{S_E(x)}{S_{\max}(x)} \approx a_2\sqrt{m},$$

where $\alpha_1, \alpha_2 \in (0,1)$. Metric (Eq. 71.1) is often referred to as *the-worst-case metric*, as it shows the maximum possible distance between the ensemble centre and the ensemble members. The second metric, the most frequently used, is related to the Euclidian norm hence the optimal representative defined by Eq. 71.5 determines the centre of the circle in which all model predicted values are. This metric smoothes out the distances between the ensemble models and their representative. One can say that it spreads out the influence of the outliers to the other models. The third metric is known as "Taxi cab" or "city", or "Manhattan" norm as the distance is measured along a gridded street-like network. This metric is the least sensitive to outliers in comparison with two previously mentioned ones. If the values of all the three ensemble representatives determined by Eqs. 71.4–71.6 are close to each other it means that the models predicted values are distributed around the average, and this is the best situation we can expect – any chosen representative of the ensemble and ensemble member are well represented by the average of the ensemble. If additionally the spread is also small then there is a good accordance among the models, and we can expect good coherence of model predictions for the considered case.

One can also combine information from the spreads calculated in different ways into one value – for instance in what we define the average relative variation (ARV) as:

$$ARV = \frac{1}{m}\left(\frac{S_T}{2S_{\max}} - 1\right) = \frac{1}{m}\left(\sum_{k=1}^{m} \frac{|\overline{x}_T - x_k|}{\max\limits_{j=1,\ldots,m}(x_j) - \min\limits_{j=1,\ldots,m}(x_j)} - 1\right)$$

It takes the values in the interval (0,1) – number 1 (actually 1/m) is substracted otherwise the minimum value would be 1/m coming from summing the differences to maximum and minimum. The closer the ARV values are to 0, the larger is the agreement among the models.

In Fig. 71.1 we present all six basic possibilities of mutual relations among the mid-point, mean and median that we will call *MMM patterns*. The figure shows the model value versus the model identification number. For a better visualization of the differences we assumed that the model values are in ascending order and lie in the interval [0,1] with mid-point 0.5 (i.e. minimum and maximum are 0 and 1 respectively). Obviously patterns that follow in between those presented are possible.

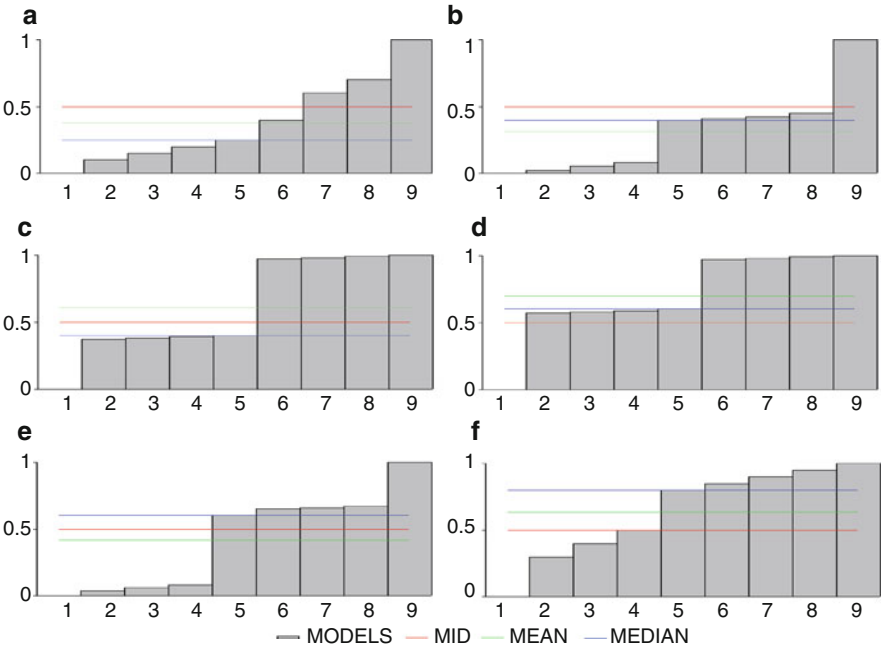


**Fig. 71.1** Different types of patterns for relations among the mid-point, mean and median: (**a**) mid > mean > median, (**b**) mid > median > mean, (**c**) mean > mid > median, (**d**) mean > median > mid, (**e**) median > mid > mean, (**f**) median > mean > mid

It is also interesting to notice that the choice of the metric implies specific definitions of other important parameters, for example, the bias. In principle we can obtain nine different biases by applying three different metrics to three representatives mentioned above, which leads to the following combinations:

| | | | |
|---|---|---|---|
| Maximum: Midpoint | $(\overline{\mathbf{X}}_{\mathbf{max}} - \mathbf{Y})$ | $(\overline{\mathbf{X}}_{\mathbf{E}} - \mathbf{Y})$ | $(\overline{\mathbf{X}}_{\mathbf{T}} - \mathbf{Y})$ |
| Euclidian: Mean | $(\overline{\mathbf{X}}_{\mathbf{max}} - \mathbf{Y})$ | $(\overline{\mathbf{X}}_{\mathbf{E}} - \mathbf{Y})$ | $(\overline{\mathbf{X}}_{\mathbf{T}} - \mathbf{Y})$ |
| Taxi: Median | $(\overline{\mathbf{X}}_{\mathbf{max}} - \mathbf{Y})$ | $(\overline{\mathbf{X}}_{\mathbf{E}} - \mathbf{Y})$ | $(\overline{\mathbf{X}}_{\mathbf{T}} - \mathbf{Y})$ |

## 71.4 Data Assimilation

Another problem related to an optimal representation of multi-model ensemble based on the minimization of the mean square error as shown in PG09 is related to data assimilation. It can be formulated as follows: which ensemble representative should be taken in ensemble Kalman filter – the usual mean or the optimal combination determined by the formulas in PG09 based on variances or covariance matrix? Formally this can be also posed as another optimization problem as

follows: assume that the vectors $\overline{\mathbf{X}}, \mathbf{Y}$ denote respectively, representatives of the ensemble (i.e. the combination of $m$ multi-model unbiased results at $n$ grid points) and observational data at $p$ points, and we want to find optimal vector $\mathbf{X}$ as:

$$\mathbf{X} = \overline{\mathbf{X}} + \mathbf{W}(\mathbf{Y} - \mathbf{H}(\overline{\mathbf{X}})) = \overline{\mathbf{X}} + \mathbf{W}\mathbf{d} \tag{71.8}$$

where $\mathbf{W}$ is the so-called weight (or gain) matrix of $n \times p$ dimension, $\mathbf{d} = \mathbf{Y} - \mathbf{H}(\overline{\mathbf{X}})$ innovation vector of $p$ dimension and the operator $\mathbf{H}$ describes transformation from $n$-dimensional model results space to $p$-dimensional observation space. We can assume that $\mathbf{H}$ is a linear operator (i.e. $p \times n$ matrix) because a linear interpolation can be used to get the combined models' results at the observational locations (or we can use tangent operator).

In order to find $\mathbf{X}$ we can formulate a general problem of finding both optimal weight matrix $\mathbf{W}$ and linear combination of multi-model results$\overline{\mathbf{X}}$ at a time by minimizing corresponding covariance error matrix. Hence the main difference between typical approach for Kalman filter and our situation is such that we have to solve system of nonlinear equations of higher dimension instead of linear system of equations for the elements of the gain matrix $\mathbf{W}$ only**.** It can be shown however, that this can be done by applying:

- Formulas for optimal linear combination for multi-model ensemble shown in PG09, and
- Normal formulas for the weight matrix as in Kalman filter.

## 71.5 Conclusions

The use of ensembles to improve the performance of individual deterministic model results is becoming more and more widespread. In this paper we have tried to address systematically and fundamentally the characterization of the ensemble by means of new parameters. The parameters identified are, the centre of the ensemble (or representative of the ensemble), the spread or minimized distance of all ensemble members from the centre. We have considered the application of all available metrics to define these parameters. In particular we have shown that using metrics known as *maximum*, *Euclidean* and *Taxi cab* we obtain as representatives of the ensemble the mid point, mean or median respectively since they optimize the ensemble spread.

Considering atmospheric dispersion multi-model ensembles we can formulate the following general hints:

- for emergency response applications the *maximum* and *Taxi cab* metrics provide the most important information for the decision making and regulatory purposes; in particular the *Taxi cab* metric (and consequently the median) is the least sensitive to the outliers,

– for the problems in air quality related to long-term simulations, for example to evaluate different emission strategies, the *Euclidean* metric describes well the averaged behavior of the ensemble.

In the present study for the first time, a clear theoretical framework is identified that includes most of the conclusions reached in the studies listed above. We clearly show that the three metrics identified are the only possible for the representation of first-order and easy-to-handle statistics.

The six *MMM patterns*, corresponding to various relationships among the ensemble mid-point, mean and median, have been presented and identified as possible basic structures of the whole ensemble description. This type of analysis can be particularly useful for the ensembles containing many members because it is based only on three ensemble representatives. The identification of analytical relationships between different parameters such as the ensemble spread or the bias can facilitate the inspection of largely populated ensembles thus summarizing in few indices their characteristics and allowing a straight forward comparison of sub sets or of different cases of applications.

The formulas for optimal linear combination of model results can be also utilized in data assimilation process based on ensemble Kalman filter. Instead of taking the mean of ensemble an optimal solution is using formulas for ensemble representative based on model covariance matrix.

## References

1. Dabbert WF, Miller E (2000) Uncertainty, ensembles and air quality dispersion modelling: applications and challenges. Atmos Environ 34:4667–4673
2. Galmarini S, Bianconi R, Bellasio R, Graziani G (2001) Forecasting consequences of accidental releases from ensemble dispersion modelling. J Environ Radioactiv 57:203–219
3. Galmarini S et al (2004) Ensemble dispersion forecasting, Part 1: concept, approach and indicators. Atmos Environ 38(28):4607–4617
4. Galmarini S et al (2004) Ensemble dispersion forecasting, Part II: application and evaluation. Atmos Environ 38(28):4619–4632
5. Hogg RV, Craig AT (1995) Introduction to mathematical statistics, 5th edn. Macmillan, New York
6. Kay SM (1993) Fundamentals of statistical signal processing, volume 1: estimation theory. Presentice-Hall, New York, 595 pp
7. Krishnamurti TN, Kishtawal CM, Zhang Z, LaRow T, Bachiochi D, Williford E, Gadgil S, Surendran S (2000) Multimodel ensemble forecasts for weather and seasonal climate. J Clim 13(23):4196–4216
8. McKeen S et al (2005) Assessment of an ensemble of seven real-time ozone forecasts over eastern North America during the summer of 2004. J Geophys Res D: Atmos 110(21):1–16
9. Potempski S, Galmarini S (2009) *Est modus in rebus*: analytical properties of multi-model ensembles. Atmos Chem Phys 9:9471–9489
10. Potempski S et al (2008) Multi-model ensemble analysis of the ETEX-2 experiment. Atmos Environ 42:7250–7265
11. Riccio A, Giunta G, Galmarini S (2007) Seeking for the rational of the Median Model: the optimal combination of multi-model ensemble. Atmos Chem Phys 7:1–14
12. Van Loon M et al (2007) Evaluation of long-term ozone simulations from seven regional air quality models and their ensemble. Atmos Environ 41:2083–2097

## Questions and Answers

**Questioner Name**: Eugene Genikhovich

**Q**: In addition to the previous discussion I would like to stress out that the models that do not contribute too much to the performance of the ensemble cannot be considered as bad. They just do not provide and independent additional information as compared to the good contributors. If however they are not excluded from the final prediction it could result in a worsening of these predictions (see my poster presentation).

**A**: I agree.

**Questioner Name**: Alexandra Monteiro

**Q**: Do you think that we should invest in ensemble approaches applications or to continue improving the Physics and Chemistry of the model?

**A**: As I presented last year, it is difficult to obtain a colorful butterfly by averaging a white and black one or to transform the phenotypical difference of sea shells in a plate of seafood spaghetti. The ensemble treatment can improve a result that is supposed to represent at best the physics and the chemistry. The phenotypical difference in model results should be representative of the complexity of a system and the multiple ways to represent it. When that condition is fulfilled then you can expect a further contribution from the ensemble treatment. So continue improving models if you want to have a yet improved ensemble result.

**Questioner Name**: Ivanka Styner

**Q**: How are the extreme events that are important for Air quality applications accounted for in the ensemble metrics? Do they adjust case by case?

**A**: The maximum metrics has been explicitly devised to account for the extremes. In particular for forecast situation the comparison of the three metrics according to us gives the best chances of spotting extreme and relevant events.

**Questioner Name**: Trond Inversen

**Q**: You showed a figure with reduced RMSE of the ensemble mean as a function of the ensemble members. Did you verify whether the models have similar quality, did you perform bias correlation in order to check if your result have ‘universal validity’.

**A**: The 25 ensemble members where individually investigated in other occasions. May be universality is a bit ambitious but the RMSE that I have showed are the minimum values of all the possible combinations as I have explained, so may be not universal but of unique validity.

# Chapter 72
# Diagnostic Evaluation of Complex and Simple Atmospheric Chemical Transport Models by Considering Single Source Impacts in the UK

**Bernard A. Fisher, Charles Chemel, Xavier V. Francis, Rong-Ming Hu, Ranjeet S. Sokhi, Garry D. Hayman, Keith J. Vincent, Tony Dore, Stephen Griffiths, Paul Sutton, and Ray D. Wright**

**Abstract** A model evaluation has been undertaken by considering a diagnostic evaluation of the distance dependent structure of a single source footprint.

**Keywords** Footprint • Diagnostic • Evaluation • Trajectory • CMAQ • PM10

B.A. Fisher (✉)
Environment Agency, Kings Meadow House, Kings Meadow Road, Reading, Berks RG1 8DQ, UK
e-mail: bernard.fisher@environment-agency.gov.uk

C. Chemel • X.V. Francis • R.-M. Hu • R.S. Sokhi
Centre for Atmospheric and Instrumentation Research, University of Hertfordshire, College Lane Campus, Hatfield, Herts AL10 9AB, UK

G.D. Hayman
CEH Wallingford, Maclean Building, Benson Lane, Crowmarsh Gifford, Wallingford, Oxfordshire OX10 8BB, UK

K.J. Vincent
AEA Energy & Environment, The Gemini Building, Fermi Avenue, Harwell International Business Centre, Didcot, Oxon OX11 0QR, UK

T. Dore
Centre for Ecology & Hydrology, Bush Estate, Penicuik, Midlothian EH26 0QB, UK

S. Griffiths
Technology Centre, E.ON New Build and Technology, Ratcliffe-on-Soar, Nottingham NG11 0EE, UK

P. Sutton • R.D. Wright
RWE npower, Windmill Hill Business Park, Whitehill Way, Swindon SN5 6PB, UK

D.G. Steyn and S. Trini Castelli (eds.), *Air Pollution Modeling and its Application XXI*, NATO Science for Peace and Security Series C: Environmental Security 4,
DOI 10.1007/978-94-007-1359-8_72, 

## 72.1 Regulation and Emulation

The regulatory assessment of industrial sources is an important factor in the design of a cost effective strategy to reduce air pollution, acid deposition, and eutrophication. Such an assessment requires appropriate modelling tools. In the past, what would be regarded as simple modelling systems have been applied for regulatory purposes in the UK. These modelling systems include one that combines a Trajectory Model with Atmospheric Chemical Kinetics (TRACK) for long-range impacts and the Atmospheric Dispersion Modelling System (ADMS) for short-range impacts (TRACK-ADMS) [6], and the Fine Resolution Atmospheric Multi-pollutant Exchange (FRAME) model [5]. However advanced air quality models, such as the Community Multi-scale Air Quality (CMAQ) modelling system are now available and the question arises as to whether the advantages of more detailed process models can be exploited as practical regulatory assessment tools. The view taken here is that the simpler models are effectively emulations of the complex fundamental models, whose choice of parameter values, on the basis of comparisons with observations and expert judgement, should approximate the results of the complex models. (In a previous paper [3] a statistical approach to emulating complex models has been described.) With this interpretation there is not one best model, but a number of possible assessment approaches. A model comparison exercise has been set up to examine the performance of simple and advanced air quality models in relation to regulatory use. Since the simpler models are effectively adding together contributions from individual sources a specific question is the response of those models to emission changes. The contribution to regional air pollution and deposition from a UK regulated power station is estimated using the CMAQ modelling system in its versions 4.6 and 4.7, TRACK-ADMS, and FRAME, for the year 2003 and annual average $PM_{10}$ concentrations have been compared. The values of parameters in the simpler models would in principle be different if the background pollution climatology were different, say for a different year or region.

### *72.1.1 Footprints and Evaluation*

The aim of a diagnostic evaluation is to identify the role of specific processes affecting the response of the model to changes in emissions. It requires choosing simple diagnostic variables whose role within the models can be clearly identified.

Figure 72.1 shows an idealised footprint with two diagnostic variables: the circumferential average concentration $C(r,\theta)$ as a function of distance $r$ from the source which implicitly includes a $1/r$ decay, ($\frac{1}{2\pi}\int_0^{2\pi} C(r,\theta)d\theta$, where $\theta$ is the angular dependence), and the average concentration along a typical trajectory which approximately removes any dilution arising from dispersion by multiplying concentration by distance ($\frac{r}{2\pi}\int_0^{2\pi} C(r,\theta)d\theta$) scaled by a concentration value near the source. Bergin et al. [1] have assessed the impact of a single source representing NOx emissions from an Ohio power plant on the levels of ozone at long distances

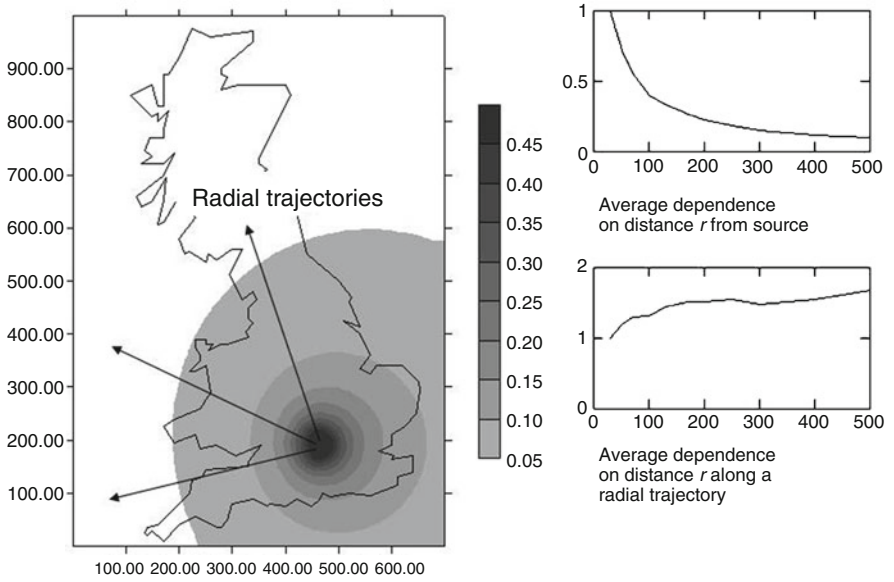


**Fig. 72.1** Typical example of the annual average $PM_{10}$ concentration footprint in μg $m^{-3}$ from a major stationary point source e.g. power station

downwind using a three dimensional air quality model. A brute force method which requires two runs of the model, taking the difference, has been used here. Vieno et al. [5] have applied the FRAME model to assess the importance of the source configuration and activity of 69 major stationary sources in the UK, to quantify footprints of regional atmospheric sulphur deposition. Here we present an example of a calculation of the contribution from a power station in the south of Britain to the air quality in surrounding regions using CMAQ, for the year 2003 (see [2] for information about the operational evaluation of the model. See also [4]). The emissions from the power station in 2003 were: for $SO_2$ 42,000 tonnes, NOx 24,700 tonnes (as $NO_2$), $PM_{10}$ 987 tonnes, and CO 3,711 tonnes. The power station's footprint for $PM_{10}$ from CMAQ v4.6 is shown in Fig. 72.2.

The trajectory dependence of CMAQ v4.7 (see second insert in Fig. 72.2), the simpler TRACK-ADMS model and of the inorganic aerosol from FRAME all show a similar shape characterised by no strong decay with distance, suggesting an approximate balance between the supply and removal of secondary $PM_{10}$.

### *72.1.2 Interpretation*

The dependence of the $PM_{10}$ concentration along a trajectory is seen not to decrease rapidly with distance. This can be explained by the gradual formation of secondary aerosol. (The distance dependence is not exact, because of edge effects outside the

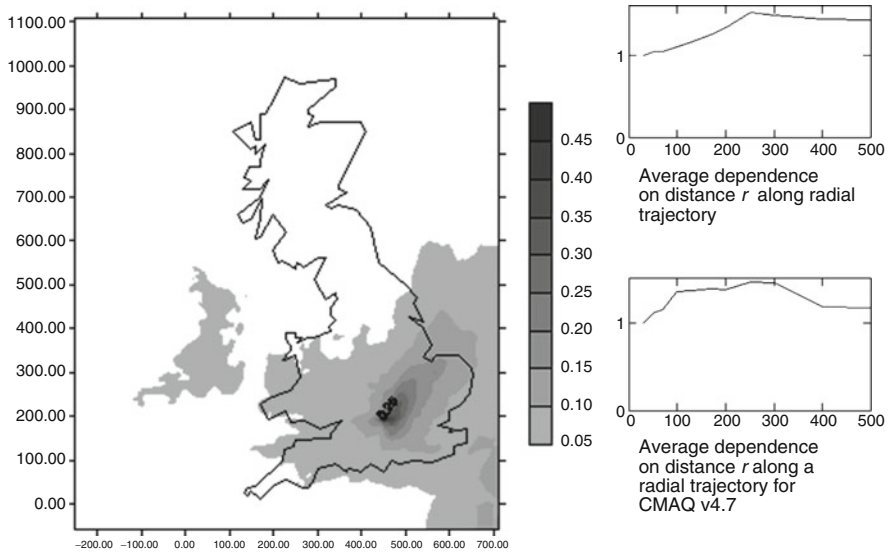


**Fig. 72.2** Annual average $PM_{10}$ concentration footprint from power station in μg $m^{-3}$ using CMAQ v4.6 (calculation at 5 km spatial resolution)

study area which have only been corrected in an approximate manner.) Using a two component linear analytical model representing sulphur oxides, one can obtain a formula for the position of the maximum $SO_4$ concentration along a trajectory from the source, which turns out to be about 800 km (It would be different for the other main inorganic components, i.e. nitrate and ammonium, and for total particulate, which contains primary particulate which can only decay with distance as a result of dispersion and removal from the atmosphere.) For CMAQ, the distance appears to be somewhat less. The distance to the maximum particulate $SO_4$ concentration along a trajectory is strongly dependent on the deposition velocity and the rate of production of $SO_4$. By comparing an emulator, whether a simpler model or just a two component model, with a complex model, it is possible to understand what are the key factors determining a power station footprint and which parameters need not be treated in detail. We have shown that an example diagnostic of a power station footprint is the scale of the variation in $PM_{10}$ as a function of distance along an average trajectory from the location of the source.

## References

1. Bergin MS, Russell AG, Odman M, Cohan DS, Chameides WL (2008) Single-source impact analysis using three-dimensional air quality models. J Air Waste Manage Assoc 58:1351–1359
2. Chemel C, Sokhi RS, Yu Y, Hayman GD, Vincent KJ, Dore AJ, Tang YS, Prain HS, Fisher BEA (2010) Evaluation of a CMAQ simulation at high resolution over the UK for the calendar year 2003. Atmos Environ 44:2927–2939

3. Fisher B, Chemel C, Hu R-M, Sokhi R (2010) Emulating complex calculations for regulatory decisions. In: Steyn DG, Rao ST (eds) Air pollution modeling and its application XX. Springer, Dordrecht, pp 195–199
4. Manders A, van der Gon HD, Boersen G, Visschedijk A, Builtjes P (2010) Contribution of power plant emissions in the UK and the Netherlands to air quality and deposition in the Netherlands. TNO report TNO-034-UT-2010-00691_RPT-ML
5. Vieno M, Dore AJ, Bealey WJ, Stevenson DS, Sutton MA (2010) The importance of source configuration in quantifying footprints of regional atmospheric sulphur deposition. Sci Total Environ 408:985–995
6. Vincent K, Abbott J (2008) Air quality and deposition benefits from Environment Agency regulation. Environment Agency Science Report SC060108, Product Code: SCHO1108BOZH-E-P, ISBN: 978-1-84432-967-0

## Questions and Answers

**Questioner Name**: Peter Builtjes

**Q**: You showed the intriguing plot with distance weighting for $PM_{10}$ for CMAQ v4.6, CMAQ 4.7 and TRACK-ADMS. But TRACK-ADMS is much better in comparison with observations of $PM_{10}$. Does that influence your results of the distance weighting plot?

**A**: The distance weighting plot of a model should tell one something about the behaviour of that model. TRACK-ADMS appears to perform better when compared with observations suggesting that the TRACK-ADMS distance weighting plot is the most reliable. However TRACK-ADMS includes some degree of tuning against measurements (correction for bias), so that it is not possible to be sure of this conclusion.

# Chapter 73
# Construction and Performance Analysis of a Limited-Size Ensemble of Atmospheric Dispersion Simulations

**Marje Prank, Mikhail Sofiev, Julius Vira, and Mirjam Paales**

**Abstract** Ensemble construction and treatment are considered in application to the atmospheric composition problem. One emergency and one air quality test case are discussed. Performances of several approaches to the ensemble treatment are compared: (a) static methods based on mean, median, upper and lower percentiles, (b) adaptive weighting based on dynamic solutions of minimization problems for selected statistical scores, (c) heuristic methods using the model scores as the weighting parameters, (d) spatially homogeneous and inhomogeneous weighting coefficients. For the adaptive weighting of ensemble members, the predictability of the scaling coefficients for the future times and the possibility of their extrapolation outside the area where they are established via model-measurement comparison are considered.

**Keywords** Air quality forecasting • Ensemble dispersion modelling

## 73.1 Introduction

According to the experience of both air quality and emergency modelling, even limited size ensembles with median as a treatment method have routinely shown better skills in comparison with observations than the individual simulations [1, 4]. However, simple averaging of the members is based on a set of assumptions about the ensemble (i.e. the methods of generating the ensemble members, the number of members, statistical features of the problem, etc.) and its optimality in terms of skill

M. Prank (✉) • M. Sofiev • J. Vira
Finnish Meteorological Institute, Helsinki, Finland
e-mail: marje.prank@fmi.fi; mikhail.sofiev@fmi.fi; julius.vira@fmi.fi

M. Paales
University of Tartu, Tartu, Estonia
e-mail: mirjam.paales@ut.ee

D.G. Steyn and S. Trini Castelli (eds.), *Air Pollution Modeling and its Application XXI*,
NATO Science for Peace and Security Series C: Environmental Security 4,
DOI 10.1007/978-94-007-1359-8_73, 

scores against measurements is often doubtful. More sophisticated approaches are under construction aiming at the optimal selection and combination of the ensemble members and at softening or lifting some of the underlying assumptions ([2, 3], etc.). Apart from the ensemble mean, the spread between the individual ensemble members indicates a range of uncertainties in the simulation results and, in some cases, hints on the predictability of the episode in general.

A comparison of several adaptive methods with the static averaging constitutes the goal of this study. Two cases are considered: the ETEX-1 as an emergency-type problem and the 2003 re-analysis of the atmospheric composition by the GEMS modelling ensemble as an air-quality example.

## 73.2 Results

The ETEX-1 ensemble was constructed of eight runs of the air quality and emergency modelling system SILAM [5, 6]: two different advection-diffusion schemes (the Eulerian and the Lagrangian ones) were forced by four different meteorological input datasets (ECMWF, HIRLAM v.2, HIRLAM v.5 and ENVIRO-HIRLAM). Seven different ensemble treatment methods were applied: (a) static methods: arithmetic average, median, upper & lower quantiles, (b) linear combinations of the ensemble members with adaptive weights following various optimization criteria: minimization of root mean square difference (RMS) of the ensemble model from the observations, inverse RMS of an individual member taken as its weighting coefficient, and the space-resolving weighting using the inverse RMS inter/extrapolated with regard to squared distance from the observational sites. With regard to the time axis, two versions of the adaptive weights were created: (a) with the coefficients attributed to the same time step when they were computed, and (b) the coefficients extrapolated forwards for the next 3 h.

Comparing the scores of the above ensemble treatment methods, one can see that already the median model regularly outperforms the single members (Fig. 73.1 left). The good performance of the lower-quantile model is caused by the high bias

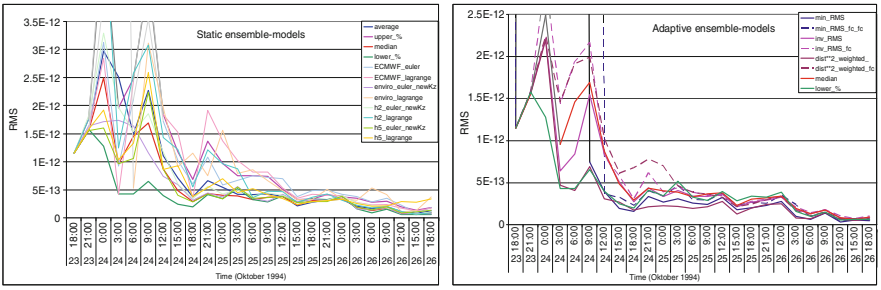


**Fig. 73.1** Scores of different ensemble models for the ETEX-1 case. *Left*: individual ensemble members and static ensemble models; *right*: adaptive ensemble models. Unit: [kg $m^{-3}$]

of all the ensemble members. The minimum RMS was reached via adaptive methods (Fig. 73.1 right) – with space-resolving weighting. However, the advantage is lost if the coefficients are extrapolated in time for just 3 h (marked with fc in Fig. 73.1 right) or space (no improvement compared to the median model was visible in control stations, which were not used for establishing the weights). The RMS minimization still works better than any individual ensemble member or the median even in the case of the forecasted and extrapolated weights. However, the method fails during the first 15 h of the case when accurate positioning of the narrow plume is of primary importance and the optimal solution may be difficult to find due to high stiffness of the system of equations.

As an example of an air quality application, we used a multi-model re-analysis ensemble constructed within the GEMS project for 2003. The ensemble consists of six members. Contrary to the above ETEX-1 case, the members were generated by different AQ models driven by same meteorological input and emission. For this study, the results for O3, NO2 and SO2 were analysed. Every month was analysed separately to study the seasonal differences in the ensemble performance. The measurement data were taken from Airbase database. The set consisted of hourly surface concentration observations from ~2,000 stations, ~1,500 of which were used as learning set and the rest as control set.

The primary problem addressed was the possibility of ensemble forecasting of air quality using optimised treatment methods. The weighting coefficients of individual ensemble members were established for each hour and then used over next 72 h to simulate the ensemble forecast. The applicability of each ensemble treatment method for the forecasting purposes was analysed.

The skill scores of the ensemble forecasts for all pollutants (Figs. 73.2 and 73.3) showed very strong diurnal variations. For the O3 forecast (Fig. 73.2), the optimal

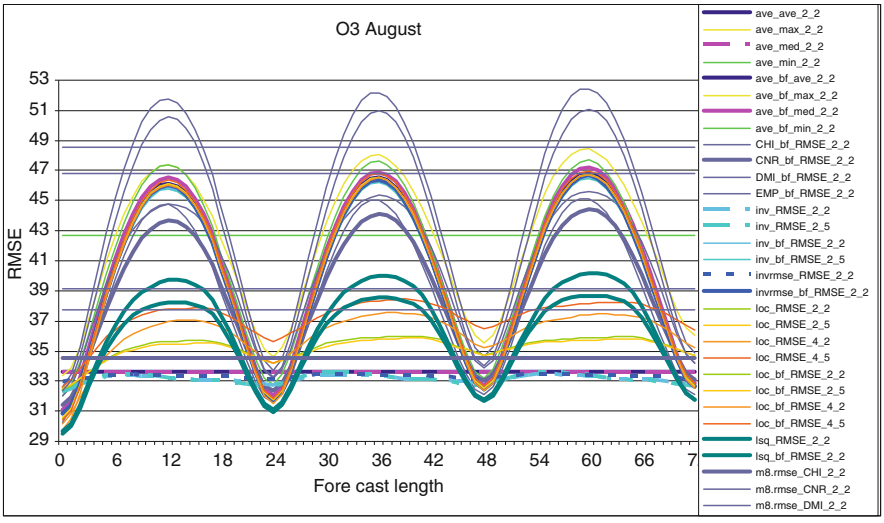


**Fig. 73.2** Root mean square error of O3 forecast

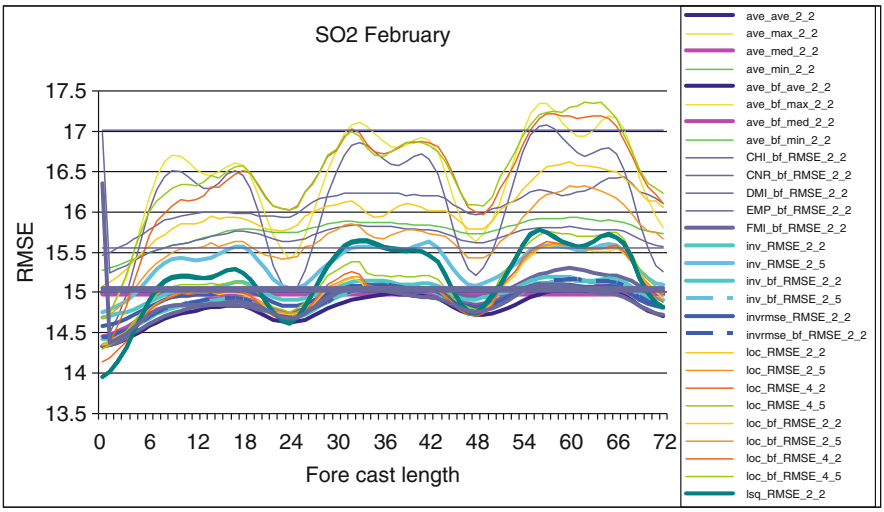


**Fig. 73.3** Root mean square error of SO2 forecast

least-square fit (LS) appeared performing the best but only during first few hours after the weights were calculated. After that, its scores drop strongly and inverse-RMS and simple averaging methods become preferable. However, after 24 h, the LS-treatment again becomes the best – and again after 48 and 72 h.

Application of the regionalised inverse-RMS (i.e., the impact of each station was set limited to its region only) resulted in even further improvement of the ensemble performance for learning dataset – but noticeably worse results for the control set, where it was outperformed by the above whole-Europe LS optimization.

The results for NO2 (not shown) manifested a strong need for the bias removal pre-processing for all ensemble members. After the de-biasing, the inverse-RMS and simple average appeared to perform similarly well. The scores of the ensemble models exhibit a strong 12-h cycle resulting from the two high-emission periods in the morning and evening of each day.

For SO2 (Fig. 73.3), the outcome resembled that of the emergency applications. The SO2 pollution pattern consists of a set of isolated plumes originated from strong point sources. This strongly diminishes the value of the optimising methods essentially reducing the ensemble treatment down to averaging of the patterns. The improved performance of the ensemble compared to its individual members is then explained by blurring of the picture, which reduces the impact of the plumes mis-location. Intriguingly, in winter the 12-h cycle was again noticeable, which is probably due to a combined effect of the emission diurnal variation and the height of the ABL.

## 73.3 Conclusions

Several methods of the ensemble treatment have been tested, including simple averaging and dynamic adaptive weighting. Possibilities to extrapolate the weighting coefficients in time and space were evaluated for the dynamic methods. Among the considered methods, the median seems to be the most-robust and useful for coping with the jumps of the individual members. The smallest RMS can be reached via adaptive methods – with coefficients varying in space and/or time.

The best estimate based on the modelling ensemble outperformed its individual members – also in forecasting mode. The optimal solution and the most-efficient methods were found to depend on the features of the specific pollutant. Well pronounced 24 h cycle was found in the skill scores of the ensemble forecast. During winter also a 12-h cycle becomes visible for all pollutants.

**Acknowledgments** This study was performed within the scope of the EU-MACC project. Support of the COST Action ES0602, Estonian National Targeted Financing Project SF0180038s08, and the Estonian Science Foundation (grant 7005) are appreciated.

## References

1. Galmarini S, Bianconi R, Addis R, Andronopoulos S, Astrup P, Bartzis JC, Bellasio R, Buckley R, Champion H, Chino M, D'Amours R, Davakis E, Eleveld H, Glaab H, Manning A, Mikkelsen T, Pechinger U, Polreich E, Prodanova M, Slaper H, Syrakov D, Terada H, Van der Auwera L (2004) Ensemble dispersion forecasting – Part II: application and evaluation. Atmos Environ 38(28): 4619–4632
2. Mallet V, Stoltz G, Mauricette B (2009) Ozone ensemble forecast with machine learning algorithms. J Geophys Res 114:D05307. doi:10.1029/2008JD009978
3. Potempski S, Galmarini S, Riccio A, Giunta G (2010) Bayesian model averaging for emergency response atmospheric dispersion multimodel ensembles: Is it really better? How many data are needed? Are the weights portable? J Geophys Res 115:D21309. doi:10.1029/2010JD014210
4. Riccio A, Giunta G, Galmarini S (2007) Seeking for the rational basis of the Median Model: the optimal combination of multi-model ensemble results. Atmos Chem Phys 7:6085–6098
5. Sofiev M, Galperin M, Genikhovich E (2008) Construction and evaluation of Eulerian dynamic core for the air quality and emergency modeling system SILAM. In: Borrego C, Miranda AI (eds) Air pollution modelling and its application, XIX, NATO science for peace and security series C: environmental security. Springer, Dordrecht, pp 699–701
6. Sofiev M, Siljamo P, Valkama I, Ilvonen M, Kukkonen J (2006) A dispersion modelling system SILAM and its evaluation against ETEX data. Atmos Environ 40:674–685. doi:10.1016/j.atmosenv.2005.09.069

## Questions and Answers

**Questioner Name**: Akula Venkatram

**Q**: Is there any justification besides empirical for assuming that even if the individual models do not work, combining the model results will somehow produce an adequate prediction?

**A**: If the individual models really didn't work, the case would be hopeless. The models included in the ensembles actually seem to be doing quite well even on their own. The fact that the combinations of the ensemble members seem to have predictive capacity shows that the ensemble methods do have some added value in eliminating the part of the error that is not correlated between the models. Also, the ensemble treatment can include other kinds of statistical post-processing like additive and multiplicative bias removal, which will also improve the forecast skill compared with the individual models.

**Questioner Name**: Stefano Galmarini

**Q**: Are you suggesting that the ensemble treatment should depend on the variable, the season or the day of the week? I guess these results are pointing toward a verification of the processes modeled rather than expecting the ensemble to solve them.

**A**: Different pollutants have different features, such as the correlation distances and lifetime in the atmosphere. Our ability to predict them also differs. Therefore, it would be natural to use the mathematical methods of post-processing that are most-adequate for the particular patterns.

# Chapter 74
# On the Use of Principal Component and Spectral Density Analyses to Evaluate the Community Multiscale Air Quality (CMAQ) Model

**Brian Eder, Wyat Appel, and Thomas Pierce**

**Abstract** A 5 year (2002–2006) simulation of CMAQ covering the eastern United States is evaluated using principle component analysis in order to identify and characterize statistically significant patterns of model bias. Such analysis is useful in that in can identify areas of poor model performance across space and time; facilitate understanding of the probable mechanisms (emissions, meteorological, and/or chemical) responsible for said poor performance; and designate specific locations that can be used in providing in depth diagnostic analysis.

**Keywords** Air quality • Model evaluation • Principal component analysis • CMAQ and CASTNet

## 74.1 Motivation

The scope of air quality model evaluation has expanded greatly recently, in both methodology development as well as the amount of modeled data that needs to be evaluated. As recently as 5 years ago, modelers would have at most a short simulation, perhaps a month in length to evaluate. As computing capabilities increased, so did the modeler's ability to simulate over greater spatial and temporal scales, with annual and even decadal, continental-scale simulations becoming possible. While such large scale simulations can be advantageous, they can also provide new challenges, as the amount of output that needs to be evaluated can become overwhelming. Rudimentary techniques and performance statistics become less elucidating, even when broken down into seasonal or monthly periods [1, 3].

B. Eder (✉) • W. Appel • T. Pierce
Atmospheric Modeling and Analysis Division, National Exposure Research Laboratory, United States Environmental Protection Agency, Research Triangle Park, NC 27711, USA
e-mail: eder.brian@epa.gov; appel.wyat@epa.gov; pierce.tom@epa.gov

D.G. Steyn and S. Trini Castelli (eds.), *Air Pollution Modeling and its Application XXI*, NATO Science for Peace and Security Series C: Environmental Security 4,
DOI 10.1007/978-94-007-1359-8_74, 

Accordingly, the purpose of this paper is to introduce and demonstrate a multivariate statistical technique called Principal Component Analysis (PCA), with the hope of motivating the evaluation community in its use. Though infrequent, the use of PCA and similar analyses in the evaluation of air quality models is not unprecedented. For example, Li et al. [4] use PCA to evaluate the Eulerian Acid Deposition and Oxidant Model (ADOM) against aerosol and gas observations in Ontario, Canada. With Li's and other similar applications, the PCA was performed separately on model output and observations, and then subsequently compared. The approach demonstrated here is different, in that we apply PCA directly to a measure of the Community Multi-scale Air Quality (CMAQ) model's performance, namely the modeled $SO_4^{2-}$ bias (CMAQ concentration – CASTNet concentration). Keep in mind that the analysis could be applied to any measure of performance (i.e. root mean square error) and for any specie concentration or deposition simulated by CMAQ.

The advantage of using such an approach is that it will identify any systematic patterns of model bias across a myriad of spatial and temporal scales (i.e. not constrained to geopolitical boundaries nor monthly/seasonal time periods). Such analysis is useful in that it: (1) provides "weight of evidence" concerning the regional-scale nature of any CMAQ bias patterns; (2) facilitates understanding of the probable mechanisms responsible for the statistically unique behavior among bias patterns; and (3) identifies stations that can be used as indicators for more diagnostic evaluation.

## 74.2 Data

### *74.2.1 CMAQ Simulation*

This evaluation used a 5-year (2002–2006) simulation of CMAQ (Version 4.7) released in December 2008 [2]. The modeling domain covered the contiguous United States using a 36 km × 36 km horizontal grid resolution (148 (columns) × 112 (rows) = 16,576 grid cells) and a 24-layer logarithmic vertical structure, extending from the surface to ~100 hPa. The meteorological fields were provided from MM5, the Fifth-Generation Pennsylvania State University/National Center for Atmospheric Research (NCAR) Meso-scale Model and were processed using the Meteorological-Chemistry Interface Program (MCIP). This 5-year simulation used the CB05 gas-phase chemistry mechanism. The emissions, which were processed using the Sparse Matrix Operator Kernel Emissions (SMOKE) processor, were based on EPA's 2002 National Emissions Inventory, with year-specific fire, mobile (from MOBILE6), biogenic (from Biogenic Emission Inventory System (BEIS) v. 3.13) and major point source Electrical Generating Unit (EGU) data.

### *74.2.2 CASTNet*

Currently operated by EPA's Clean Air Markets Division (CAMD), CASTNet is a long-term, predominately rural monitoring network designed to measure and characterize broad-scale spatial and temporal trends of pollutants contributing to acidic deposition. While the primary purpose of the Network is to assess the efficacy of emission control strategies established by EPA (i.e. the $NO_x$ "State Implementation Plan" Call), its long-term, high-quality data also makes it ideal for use in evaluation of deterministic air quality models like CMAQ. Ambient air concentrations are measured weekly (Tuesday to Tuesday) from a height of 10 m using an open faced, three-stage filter pack. The CASTNet data used in demonstration of this evaluation technique consist of ambient air concentrations of particulate $SO_4^{2-}$ ($\mu g\ m^{-3}$).

The CMAQ modeled concentrations were post-processed in order to achieve spatial (monitor to grid cell, with no interpolation) and temporal (weekly) compatibility with the CASTNet observations. A total of 45 stations were selected, focusing on the Eastern United States (locations of the CASTNet sites are shown in the left panel of Fig. 74.1). Given CMAQ's 5 year simulation period and CASTNet's weekly sampling schedule, a total of 256 weekly observations were available (Tuesday, Jan. 1, 2002 through Tuesday, Dec. 26, 2006), resulting in a total of 11,520 data pairs. Missing observation data were imputed by using a spline interpolation scheme, across time.

## 74.3 Methodology

### *74.3.1 Spatial Analysis*

The rotated principal component analysis begins with the calculation of a square, symmetrical correlation matrix **R** (having dimensions of $45 \times 45$) from CMAQ's $SO_4^{2-}$ bias matrix having dimensions of 45 (CASTNet stations) $\times$ 256

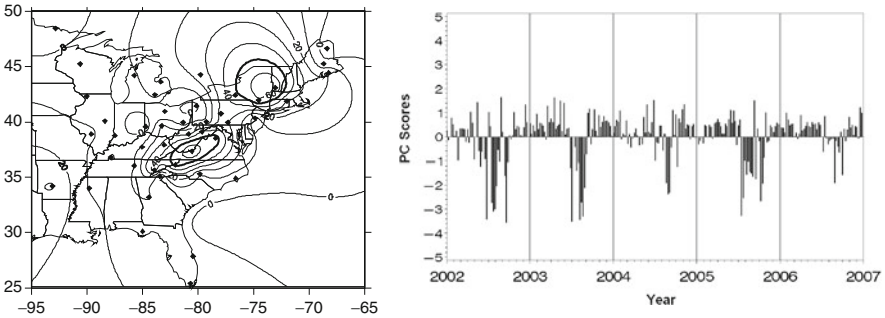


**Fig. 74.1** Component loadings (x10) at each of the 45 paired CASTNet – CMAQ locations (*left panel*) and time series of the principal component scores (*right panel*) associated with the third rotated principal component

(weekly biases) and containing 11,520 observations. By using **R** and the identity matrix (**I**) of the same dimensions, 45 eigenvalues ($\lambda$) were derived that satisfy the polynomial equation:

$$\det[{}_{45}\mathrm{R}_{45} - \lambda_{45}\mathrm{I}_{45}] = 0 \tag{74.1}$$

For each root of Eq. 74.1, which is called the *characteristic equation*, a non-zero vector (**e**) can be derived such that:

$${}_{45}\mathrm{R}_{45}\mathrm{e}_1 = \lambda_{45}\mathrm{e}_1 \tag{74.2}$$

where **e** is the eigenvector of **R**, associated with its corresponding Eigen value ($\boldsymbol{\lambda}$). The eigenvectors represent the mutually orthogonal linear combinations or "modes of variation" of the bias matrix, while their respective eigenvalues represent the amount of variance explained by each of the eigenvectors. By retaining only the first few eigenvector-eigenvalue pairs, collectively called the *principal components*, a substantial amount of the total variance of each pattern of bias can be explained while ignoring the higher order principal components which explain smaller amounts of the variance. The exact number of components that should be retained was determined by examination of a Scree plot and revealed that a 10 component solution was most appropriate.

When the elements of each eigenvector are multiplied by the square root of the associated eigenvalue ($\lambda^{0.5}$), one obtains the principal component loading (L), which represents the correlation between the bias component and the CASTNet station. The retained principal components were then "rotated", to facilitate spatial interpretation, using an orthogonal rotation. This rotation technique increases the segregation between component loadings, which in turn better defines the areas of homogenous bias. The station(s) with the highest loading in each of the bias regions can then be designated as the "bias pattern indicator", subsequently allowing more focused diagnostic analysis.

### *74.3.2 Temporal Analysis*

Having identified the spatial patterns of bias, examination of their time series was then achieved through the calculation of the rotated *principal component scores* ($\mathrm{PC_s}$). The $\mathrm{PC_s}$ for week *w* on component *i* are weighted, summed values, whose magnitudes are dependent upon the weekly bias ($\mathrm{B}_{wj}$) for week *w* at station *j* and the $\mathrm{L}_{ji}$ is the loading of station *j* on component *i* as seen below:

$$(\mathrm{PC_s})_{\mathrm{wi}} = \sum_{\mathrm{j}} \mathrm{B_{wj}L_{ji}} \tag{74.3}$$

The PCs are standardized, so they have a mean of zero and standard deviation of one. Positive scores correspond to positive CMAQ bias, while negative scores represent negative CMAQ bias. When plotted as a time series, the weekly $PC_s$ provide excellent insight into the spectrum of temporal variance experienced by each bias pattern. A 4 week moving average was applied to each time series to aid in interpretation.

Spectral Density Analysis (SDA) using the finite Fourier transformation was also applied to each of the time series. This analysis decomposes each time series into a sum of cosine and sine waves of varying amplitudes and wavelengths, yielding a measure of the distribution of the bias variance over a continuous spectrum of all possible wavelengths. The abscissa on the spectral density plots ranges from 0 to 262 weeks, which corresponds to cycles or periodicities from as little as 2 weeks to as long as trends.

## 74.4 Results

### *74.4.1 Spatial Analysis*

A total of 10 principal components were deemed significant by the Scree test, which together explained 69.8% of CMAQ's $SO_4^{2-}$ bias. For the sake of brevity, we present the results for just one of the components ($PC_3$), which, with an eigenvalue ($\lambda_3$) of 3.94, explained 8.8% (3.94/45) of CMAQ's total $SO_4^{2-}$ bias. Examination of the left of panel Fig. 74.1 reveals this bias component's unique spatial characteristic, as the component loadings (which again represent the correlation between the pattern and the CASTNet stations) clearly indentify five high-elevation locations (Lye Brook (Loading: 0.74), elev.: 730 m; Claryville (0.70), 765 m; Horton Station (0.66), 920 m; Shenandoah (0.60), 1,073 m and Cranberry (0.50), 1,219 m). Of these five stations, four are classified by CASTNet as mountain top, with the fifth (Claryville) classified as a complex terrain site.

### *74.4.2 Temporal Analysis*

Examination of this component's principal component scores time series (right panel of Fig. 74.1) is equally compelling in that a strong, systematic pattern of bias is revealed in which CMAQ tends to over-predict $SO_4^{2-}$ concentrations at these locations during the first 6 months of the year, under-predict during the months of July, August and September, then over predict from October through December. The strength of this pattern, which is strongest in 2002, 2003 and 2005, is affirmed in Fig. 74.2, which depicts a "typical year" constructed by using the median of each of the 5 years of simulations (left panel) and a SDA plot revealing a statistically

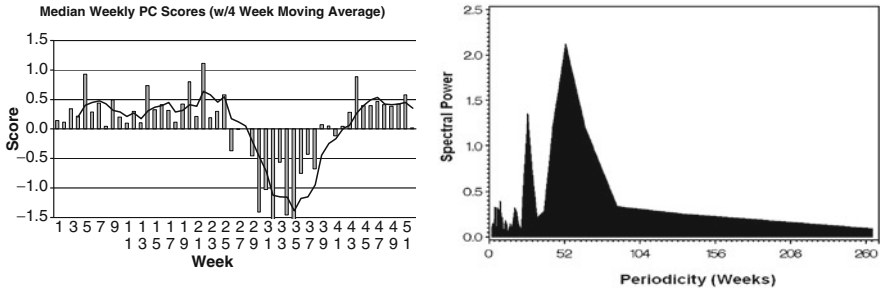


**Fig. 74.2** Weekly median values of the principal component scores (with a 4 week moving average – *left panel*) and SDA of the raw time series (*right panel*) associated with the third rotated principal component

significant cycle at 52 weeks (right panel.) Note the periodicity at 26 weeks may be a spurious alias of the 52 week and will be investigated. Having identified and characterized this statistically unique pattern of $SO_4^{2-}$ bias, the next step in the evaluation approach (not discussed) will involve a diagnostic analysis of its most representative site (Lye Brook), which should facilitate understanding into the process(es) responsible for this systematic bias. The other principal components characterized nine equally compelling systematic patterns of bias, each providing "indicator stations" that will be the focus of future diagnostic evaluation.

## 74.5 Conclusions

Examination of only one of the ten components has demonstrated the advantage of using principal component and spectral density analyses, in that they have identified systematic patterns of CMAQ $SO_4^{2-}$ bias across spatial and temporal scales unconstrained by geopolitical boundaries and calendar periods. Such analysis has provided "weight of evidence" concerning the regional-scale nature of these patterns while identifying stations that should be used for diagnostic evaluation, which will lead to a better understanding of the mechanisms responsible for the modeled bias.

## References

1. Appel W, Bhave P, Gilliland A, Sarwar G, Roselle S (2008) Evaluation of the CMAQ model *v* 4.5: sensitivities impacting model performance; Part II–particulate matter. Atmos Environ 42:6057–6066
2. Byun D, Schere K (2006) Review of the governing equations, computational algorithms, and other components of the Models-3 Community Multiscale Air Quality modeling system. Appl Mech Rev 59:51–77

3. Eder B, Yu S (2006) A performance evaluation of the 2004 release of Models-3 CMAQ. Atmos Environ 40:4811–4824
4. Li S, Anlauf K, Wiebe H, Bottenheim J, Pucket K (1994) Evaluation of a comprehensive Eulerian air quality model with multiple chemical species measurements using principal component analysis. Atmos Environ 28:3449–3461

## Questions and Answers

**Questioner Name**: Jeremy Silver

**Q**: How do you deal with missing data?

**A**: Principal component analysis should not be applied to a dataset that contains missing data. Accordingly, all missing data were imputed using a spline interpolating scheme. To limit the amount of interpolation, stations with less than 90% capture were excluded from the analysis.

**Questioner Name**: Bruce Denby

**Q**: If the PCA was based on model error at points, how were the spatial maps made?

**A**: The maps were produced by Kriging the principal component loadings. It is noted that care must be used when interpreting such results in areas where data are sparse.

# Chapter 75
# Dynamic Model Evaluation of $NO_x$ Emissions Reductions on Ozone Concentrations in the Presence of Uncertain Emission Inventories

**Sergey L. Napelenok, Kristen M. Foley, Daiwen Kang, Thomas Pierce, Rohit Mathur, and S. Trivikrama Rao**

**Abstract** The Community Multiscale Air Quality (CMAQ) model was evaluated for its ability to reproduce observed changes in ambient concentrations of ozone ($O_3$) for two seasons: the summer of 2002 and the summer of 2005 covering the eastern United States. These two summer periods were distinguished by large emissions reductions stemming from controls mandated by the $NO_x$ State Implementation Plan (SIP) after 2002. CMAQ was evaluated for the robustness of its response in ambient $O_3$ levels to changes in $NO_x$ emissions. Furthermore, uncertainties in the $NO_x$ emissions inventory were propagated through the model using a direct sensitivity approach. Considering a 50% uncertainty in the area and mobile source $NO_x$ emissions, the model was able to replicate changes in $O_3$ concentrations between 2002 and 2005 at most observation sites.

**Keywords** CMAQ • Air quality modeling • Dynamic model evaluation • Ozone • Uncertainty • Sensitivity • Direct decoupled method • DDM

## 75.1 Introduction

Previous dynamic evaluation of regional air quality models have focused on comparing the absolute change predicted by the CMAQ model with the absolute change seen in the $O_3$ observations [1]. For example, the measurements might have registered a −10.6 ppb change in $O_3$ according to some metric, while the modeling results for the same time period might have shown a −5.1 ppb change in the same metric. While much has been learned from such model evaluations, it is difficult to

S.L. Napelenok (✉) • K.M. Foley • T. Pierce • R. Mathur • S.T. Rao
United States Environmental Protection Agency, Research Triangle Park, NC 27711, USA
e-mail: napelenok.sergey@epa.gov

D. Kang
Computer Science Corporation, Research Triangle Park, NC, USA

D.G. Steyn and S. Trini Castelli (eds.), *Air Pollution Modeling and its Application XXI*,
NATO Science for Peace and Security Series C: Environmental Security 4,
DOI 10.1007/978-94-007-1359-8_75, 

assess the overall ability of the model to respond robustly to changes in emissions inputs since model input, mainly emissions, is known to be uncertain.

Consideration of uncertainty in the inputs enables us to better evaluate model's response to emission changes.

## 75.2 Method

All modeling was performed on a 12 km horizontal resolution grid covering the Eastern United States for the periods of 1 May–31 August 2002, and 1 May–31 August 2005. CMAQ version 4.7.1, instrumented with DDM-3D [3], was used to calculate $O_3$ concentrations and sensitivities to three emission sectors for $NO_x$: area sources, mobile source, and point sources. Meteorology was calculated using MM5 with standard physics options, and emissions were developed using SMOKE based on temporally and spatially resolved fire, electricity generating units, and mobile sources. Ozone observations from the AQS and CASTNET networks were used to evaluate the model predictions of ozone.

Calculated DDM-3D sensitivities were used to provide responses to the perturbations in the inputs of the three $NO_x$ emissions categories outlined above through Taylor series expansion [2]. Generally, pollutant concentration as a function of any one perturbation can be reconstructed using the following:

$$C_j(\overline{\mathbf{x}},t) = C_0(\overline{\mathbf{x}},t) + \Delta\varepsilon_j S_j^{(1)}(\overline{\mathbf{x}},t) + \frac{1}{2}\Delta\varepsilon_j^2 S_{j,j}^{(2)}(\overline{\mathbf{x}},t) + (h.o.t),$$

where $C_j(\overline{\mathbf{x}},t)$ is the concentration due to a specific perturbation $j$; $C_0(\overline{\mathbf{x}},t)$ is base simulation concentration; $\Delta\varepsilon_j$is the fractional perturbation of the parameter $j$; $S_j^{(1)}(\overline{\mathbf{x}},t)$ and $S_{j,j}^{(2)}(\overline{\mathbf{x}},t)$ are the first and second order sensitivity coefficients, and $h.o.t$ are higher order terms with little impact on the approximation. More than one perturbation to the base case would simply require additional terms in the Taylor series expansion.

Various estimates of uncertainty from each $NO_x$ emissions sector were used in the analysis, ranging from ±30–70% for ground-level area and mobile sources and ±3–5% for elevated point sources. The source of uncertainty in point sources was due mainly to measurement error in the Continuous Emissions Monitoring (CEM) technology and, hence, was set to low values.

For each uncertainty scenario evaluated, e.g. ±50% area sources, ±50% mobile sources, and ±3% point sources, a perturbation parameter, $\Delta\varepsilon_j$, was randomly chosen from a normal distribution spanning the uncertainty range using Monte-Carlo sampling. Combined with the DDM-3D calculated sensitivity coefficients, the resulting sets of uncertainty estimates were used in the Taylor Series to generate an ensemble of ozone predictions at each location in the domain during each simulation period.

In an effort to remove some of the influences of meteorology, observed and modeled data were analyzed in terms of cumulative frequency distribution at each location. The dynamic signal in ozone air quality between the two episodes (2002 and 2005) in the observations was calculated simply as the difference between the distributions for each year. Modeling results were treated similarly, but accounting for the ensemble of possible outcomes at each location. The model was then evaluated for its ability to respond to large changes in emissions inputs.

## 75.3 Results and Discussion

Ensembles of model predictions allowed for more informative comparisons of model results with the observed data. The standard CMAQ model underestimated the maximum 8 h $O_3$ concentrations in 2002 and overestimated in 2005 for middle to high ozone events, leading to the dampening of the observed $O_{3\text{-}2002}$–$O_{3\text{-}2005}$ signal (Fig. 75.1). Accounting for even a modest degree of emissions uncertainty, in the same scenario, showed that model estimates were closer to observed values.

Concentration ensembles allowed for comparison of whether or not the observed $O_{3\text{-}2002}$–$O_{3\text{-}2005}$ signal was within the ensemble of modeled signal. It was found that with 50% uncertainty in $NO_x$ emissions from mobile and area sources, the model-predicted signal in ozone encompassed that in the observations at 441 out of 684 total measurement sites (Fig. 75.2). As expected, higher levels of uncertainty corresponded to higher number of sites where predictions were correct.

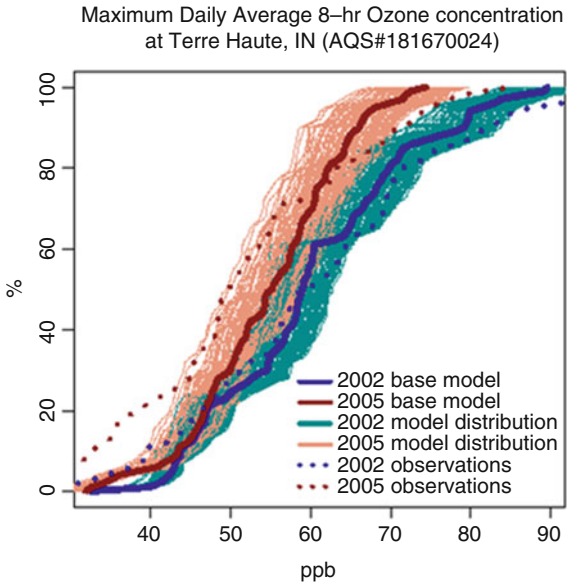


**Fig. 75.1** Modeled and observed maximum 8 h $O_3$ concentrations in 2002 and 2005 as well as possible $NO_x$ emissions uncertainty ensemble members under relatively low estimates of uncertainty. Results are shown for a monitoring site in Terre Haute, IN

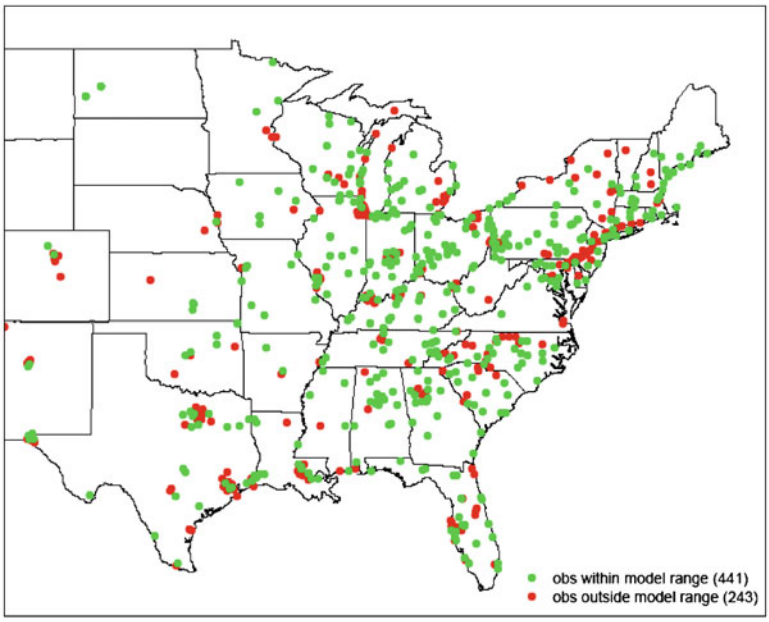


**Fig. 75.2** Measure of success of the model in predicting the measured signal of ozone change between 2002 and 2005 for the 95th percentile of data. At the majority of the sites (441), the signal was predicted correctly considering 50% uncertainty in $NO_x$ emissions

In summary, a method for dynamical evaluation of maximum 8 h $O_3$ predictions considering emissions uncertainty was applied to the large emissions reductions of $NO_x$ that occurred in accordance with the $NO_x$ SIP Call. Due to the uncertainties in inputs, the model was unable to reproduce the signal in an absolute sense. However, accounting for some of these uncertainties in the emission inventory enabled us to better assess model's response to reductions in $NO_x$ emissions.

## References

1. Gilliland AB, Hogrefe C, Pinder RW, Godowitch JM, Foley KL, Rao ST (2008) Dynamic evaluation of regional air quality models: assessing changes in O3 stemming from changes in emissions and meteorology. Atmos Environ 42:5110–5123
2. Hakami A, Odman MT, Russell AG (2003) High-order, direct sensitivity analysis of multi-dimensional air quality models. Environ Sci Technol 37:2442
3. Napelenok SL, Cohan DS, Odman MT, Tonse S (2008) Extension and evaluation of sensitivity analysis capabilities in a photochemical model. Environ Mod Soft 23:994–999

## Questions and Answers

**Q**: What is the influence of the second order sensitivity terms on prognosis accuracy?

**A**: The importance of second order sensitivity terms is varies in space. For $NO_x$ emissions sensitivity, second order terms are typically large near model grid cells with high emissions.

**Q**: How can you justify 3% accuracy for point sources emission data?

**A**: Emission rates for the $NO_x$ point source inventory used in this study were collected by measurements from continuous emission monitoring (CEM) system outfitted on the units at the point of emissions. The error on CEMs is primarily measurement error and is very low.

# Chapter 76
# Influence of Meteorological Input Parameters on Urban Dispersion Modelling for Traffic Scenario Analysis

**Paolo Giambini, Pietro Salizzoni, Lionel Soulhac, and Andrea Corti**

**Abstract** The aim of this study is to evaluate the results from using parallel observation and numerical weather prediction data as inputs to the urban dispersion model SIRANE applied to traffic scenarios of $NO_X$ in the city of Florence. A detailed sensitivity analysis of the air quality modelling system against measurements from monitoring stations of the city of Florence has been carried out in order to identify the advantage and disadvantages of the use of meteorological observation and numerical weather prediction data.

**Keywords** Urban dispersion model • Sensitivity analysis • Meteorological input

## 76.1 Introduction

The evaluation of traffic scenarios is one of the most important aspects for air quality management and assessment in urban areas. In order to evaluate the validity of emission reduction strategies, it is fundamental to reliably simulate pollutant dispersion inside the urban canopy; understanding the influence of meteorological input parameters on urban dispersion modelling is necessary for the development of adequate tools. Urban dispersion models have usually been based on input of hourly

P. Giambini (✉)
Dipartimento di Ingegneria dell'Informazione, Università degli Studi di Siena, Siena, Italy

Dipartimento di Energetica, Università degli Studi di Firenze, Firenze, Italy
e-mail: giambini@dii.unisi.it

P. Salizzoni • L. Soulhac
Ecole Central de Lyon, Écully, France
e-mail: pietro.salizzoni@ec-lyon.fr

A. Corti
Dipartimento di Ingegneria dell'Informazione, Università degli Studi di Siena, Siena, Italy

D.G. Steyn and S. Trini Castelli (eds.), *Air Pollution Modeling and its Application XXI*,
NATO Science for Peace and Security Series C: Environmental Security 4,
DOI 10.1007/978-94-007-1359-8_76, 

observation from not too distant meteorological stations. An alternative source of meteorological input data can be obtained from numerical weather prediction models; they can include heat flux, Monin-Obukhov length, friction velocity and boundary layer height, which are not routinely measured. These parameters play a fundamental role on influencing the dispersion calculations, especially when simulations are performed using new generation models that have to be driven by sophisticated meteorological pre-processors.

The aim of this study is to inter-compare the results from using parallel observation and numerical weather prediction (deriving from RAMS-CALMET modelling system) data as inputs to the urban dispersion model SIRANE. The behaviour of the model, driven by different meteorological data pre-processing, has been investigated by means of the simulation of traffic scenarios in the city of Florence. A comparison among the micro-meteorological pre-processor outputs and a sensitivity analysis of the air quality modelling system against measures from the permanent monitoring stations of Florence (including a wide range of traffic levels and different street geometries) has been carried out in order to discuss potential advantage and disadvantages of the use of different meteorological input data.

## 76.2 Case Study

In this study we simulated the atmospheric dispersion connected to traffic emission scenarios of the entire territory of the municipal district of Florence ($11 \times 6$ km$^2$ sized area). The full year 2002 time period was investigated, using a 1-h time step. Traffic emissions were carried out using CORINAIR methodology in combination with the traffic volume data carried out by the application of the mobility model VISUM 10. $NO_X$ were the chosen pollutant; the urban background concentrations were included in the simulations using the monitored concentrations of the background site of Firenze-Boboli, site acknowledged by the administration as the reference urban background. The simulations were carried out using SIRANE [5], a multi-scale model developed by the Ecole Centrale de Lyon and based on a combination of a Gaussian plume model and a box model. SIRANE has a meteorological pre-processor able to calculate wind fields and micro-meteorological variables over the considered domain using meteorological input data from a single site. The SIRANE simulation outputs consist of hourly averaged values of mixing height ($H_{mix}$), PGT stability class, Monin-Obukhov length ($L_{MO}$), friction velocity ($u^*$), sensible heat flux ($H_0$) and ground level pollutant concentration ($c$). Two different configurations have been chosen in order to perform a sensitivity analysis of the SIRANE results to the meteo input:

1. *Observations (OBS) provided by a meteorological station located inside the study area*. Firenze-Ximeniano station was chosen because it has the most complete hourly time series data of wind velocity and direction measured at 10 m a.g.l., temperature, global and net solar radiation and it is located in the central position of the study area.

2. *Numerical weather prediction (NWP) deriving from RAMS-CALMET modelling system* [2]. The NWP was achieved by means of a $4 \times 4$ km$^2$ spaced vertical profiles grid provided by the RAMS forecasting system of CNR-IBIMET/LaMMA; a scaling to the $1 \times 1$ km$^2$ resolution was performed by using the CALMET meteorological model. One of the points of the RAMS-CALMET output grid (the one located approximately at the centre of the study area) was chosen as a 'virtual' meteorological station for the meteorological pre-processor of SIRANE. The following data have been used to fed SIRANE: wind speed and direction, temperature, stability class and mixing height.

In order to compare the influence of the different meteorological input configurations, the following analysis have been carried out: graphical comparison and statistical analysis of the meteorological pre-processor outputs and of the ground level concentration values for the two input configurations. The statistical analysis was achieved comparing the concentration results to measured data by the monitoring networks of Florence (eight monitoring stations: two background and six roadside). Both long term averages (annual) as well as short term ones (hourly and historical series) were considered. The statistical indices used for the sensitivity study are derived from the BOOT software [3] and the Model Validation Kit [4]. The resulting statistical set is: mean (MEAN), fractional bias (FB), standard deviation (SD), fractional standard deviation (FS), linear correlation coefficient (COR), fraction within a factor of 2 (FA2) and normalized mean square error (NMSE). Chang & Hanna acceptability criteria ($FA2 > 0.5; -0.3 < FB < 0.3$; $NMSE < 4$ [1]) was used as reference to evaluate model sensitivities and performances.

## 76.3 Results and Conclusions

Firstly, a comparison between results provided by meteorological pre-processor of SIRANE has been carried out; for brevity only some results are reported here in Fig. 76.1. The comparison has been performed basing on calculated wind speed at 10 m, mixing height, PGT stability class, friction velocity and sensible heat flux.

As shown by the Fig. 76.1, the two configurations give different results; in particular, the wind speeds and the mixing heights deriving from NWP data are generally lower than the ones obtained from observational data and the NWP configuration tends to estimate higher frequency of stable atmospheric conditions (class F).

Concentrations statistics described previously have been calculated for each monitoring site; the results of the statistical analysis are reported in Table 76.1. Good performances are obtained both in terms of annual mean concentration and hourly mean concentrations for the two meteorological input configurations; acceptability criteria proposed by Chang and Hanna are substantially verified for all the cases. The influence of the meteorological input, and of its processing by the model, doesn't seems to be relevant on the model outputs; the statistical analysis of the concentration results doesn't show significant differences between the two configurations.

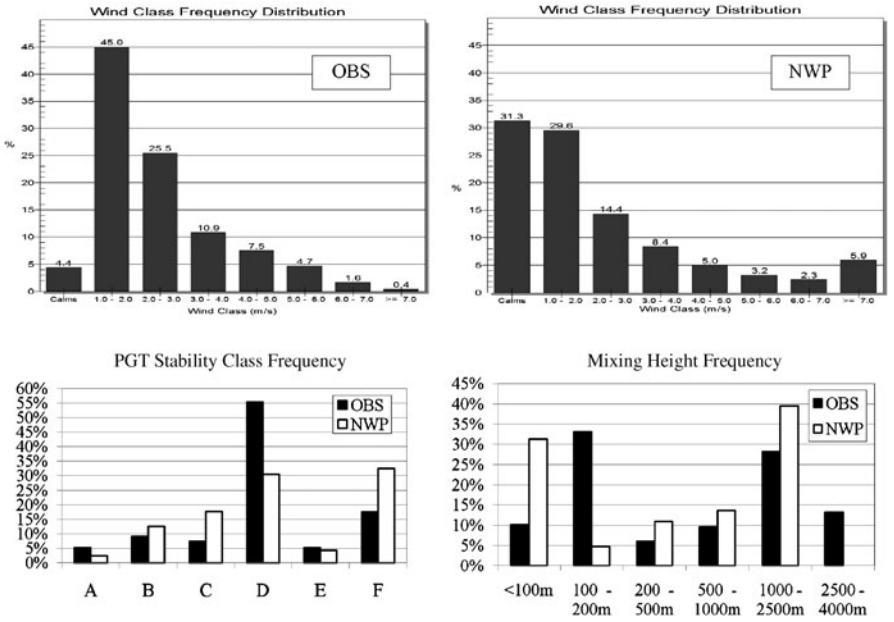


**Fig. 76.1** Wind speed at 10 m a.g.l. (*top*), PGT stability classes (*right*) and mixing height (*left*) frequency distribution for the two meteorological input configurations

**Table 76.1** Statistical indices based on the annual mean concentrations and on the maximum and the time series of hourly mean concentrations of NOx

| Time series of NOx hourly conc. | MEAN | FB | SD | FS | COR | FA2 | NMSE |
|---|---|---|---|---|---|---|---|
| Measurements | 156.3 | 0.00 | 155.3 | 0.00 | 1.00 | 1.00 | 0.00 |
| OBS | 140.4 | 0.11 | 157.5 | −0.01 | 0.73 | 0.66 | 0.62 |
| NWP | 137.0 | 0.13 | 153.6 | 0.01 | 0.69 | 0.64 | 0.72 |
| **NOx annual mean conc.** | **MEAN** | **FB** | **SD** | **FS** | **COR** | **FA2** | **NMSE** |
| Measurements | 158.9 | 0.00 | 77.3 | 0.00 | 1.00 | 1.00 | 0.00 |
| OBS | 141.9 | 0.11 | 89.8 | −0.15 | 0.87 | 1.00 | 0.10 |
| NWP | 138.3 | 0.14 | 86.3 | −0.11 | 0.85 | 1.00 | 0.11 |
| **NOx hourly mean conc.** | **MEAN** | **FB** | **SD** | **FS** | **COR** | **FA2** | **NMSE** |
| Measurements | 1316.6 | 0.00 | 435.4 | 0.00 | 1.00 | 1.00 | 0.00 |
| OBS | 843.7 | 0.44 | 252.3 | 0.53 | 0.81 | 0.83 | 0.27 |
| NWP | 929.1 | 0.35 | 341.7 | 0.24 | 0.84 | 0.83 | 0.17 |

Only for the estimation of the maximum hourly mean concentrations, it is possible to highlight an improvement of the model using numerical weather prediction; this is due to the addition of upper air information that permits to better reproduce atmospheric condition characterized by stable condition, calm wind and very low mixing height (lower than 50 m).

In conclusions, the results show that both the use of observations from a meteorological station (OBS) and the use of numerical weather prediction (NWP) can be reliable approaches to evaluate the air quality impact of future traffic

scenarios in urban areas. Due to the complexity of the implementation of consistent NWP, the use of observation seems to be preferable, although NWP can be better for the analysis of the maximum hourly mean concentration.

## References

1. Chang JC, Hanna SR (2004) Air quality model performance evaluation. Meteorol Atmos Phys 87(1–3):167–196
2. Giambini P, Carpentieri M, Corti A (2008) Inter-comparison, sensitivity and uncertainty analysis between different urban dispersion models applied to an air quality action plan in Tuscany, Italy, In: HARMO12, Cavtat, 6–9 Oct 2008
3. Hanna SR (1989) Confidence limits for air quality model evaluations as estimated by bootstrap and jackknife resampling methods. Atmos Environ 23(6):1385–1398
4. Olesen HR (2005) User's Guide to the Model Validation Kit. In: Initiative on harmonisation within atmospheric dispersion modelling for regulatory purposes. National Environmental Research Institute, Ministry of the Environment, Denmark
5. Soulhac L, Mejean P, Perkins RJ (2001) Modelling vehicle-generated atmospheric pollution in a quarter of Lyon using the model SIRANE. In: HARMO 7, Belgirate, 28–31 May 2001

## Questions and Answers

**Questioner Name**: Thomas Pierce

**Q**: To improve performance with the NWP option, perhaps an urban meteorology algorithm could reduce calm winds and decrease very stable conditions? Have the authors considered this possibility?

**A**: In this stage of the study the NWP option doesn't include an urban meteorology algorithm. Future implementations will consider the integration of such kind of algorithms and evaluate the efficacy and the usefulness of it.

**Questioner Name**: Elisabetta Angelino

**Q**: The graph comparing modelled and measured concentrations, points out the tendency by the model to underestimate observed values during daytime in both the studied meteorological conditions. This could probably due to difficulties in emission pattern and intensity reproduction. Don't you think that this probable influence meteorological input evaluation?

**A**: A detailed sensitivity study about the influence of the emission input data (see "Giambini P, Salizzoni P, Soulhac L, Corti A −2010-, Air quality modelling system for traffic scenario analysis in Florence: model validation and identification of critical issues, Proceedings of the 13th International Conference on Harmonisation within Atmospheric Dispersion Modelling for Regulatory Purposes, pp. 195–200, Ed. Armand Albergel, ARIA technologies, June 2010, Paris, France, ISBN 2-8681-5062-4") was carried out before the meteorological input data evaluation shown in the present paper. The sensitivity study of the emission input data permitted to find the most reliable model calibration that minimize the influence of the emission inputs.

# Chapter 77
# Wet Deposition: Model Development and Evaluation

**Sabine Banzhaf, Peter Builtjes, Andreas Kerschbaumer, Martijn Schaap, Eric van der Swaluw, Rainer Stern, and Eberhard Reimer**

**Abstract** The Chemistry Transport Model REM-Calgrid (RCG) has been improved by implementing a more detailed description of aqueous-phase chemistry and wet deposition processes including droplet pH. A sensitivity study on cloud and rain droplet pH has been performed to investigate its impact on model sulphate production and gas wet scavenging. Air concentrations and wet deposition fluxes of model runs applying differing droplet pH have been analysed and compared to observations. It was found that droplet pH variation within atmospheric ranges affects modelled air concentrations and wet deposition fluxes significantly.

**Keywords** Wet deposition • Aqueous-phase chemistry • Droplet pH sensitivity • RCG

S. Banzhaf (✉) • A. Kerschbaumer • R. Stern • E. Reimer
Institute of Meteorology, Free University Berlin, Carl-Heinrich-Becker-Weg 6-10, 12165 Berlin, Germany
e-mail: sabine.banzhaf@met.fu-berlin.de; andreas.kerschbaumer@fu-berlin.de; rstern@zedat.fu-berlin.de; reimer@zedat.fu-berlin.de

P. Builtjes
Institute of Meteorology, Free University Berlin, Carl-Heinrich-Becker-Weg 6-10, 12165 Berlin, Germany

TNO, P.O. Box 80015, 3508 TA, Utrecht, The Netherlands
e-mail: peter.builtjes@tno.nl

M. Schaap
TNO, P.O. Box 80015, 3508 TA, Utrecht, The Netherlands
e-mail: martijn.schaap@tno.nl

E. van der Swaluw
Centre for Environmental Monitoring, National Institute for Public Health and the Environment (RIVM), P.O. Box 1, 3720 BA, Bilthoven, The Netherlands
e-mail: eric.van.der.swaluw@rivm.nl

D.G. Steyn and S. Trini Castelli (eds.), *Air Pollution Modeling and its Application XXI*, NATO Science for Peace and Security Series C: Environmental Security 4,
DOI 10.1007/978-94-007-1359-8_77, 

## 77.1 Introduction

Enhanced deposition fluxes of sulphur and nitrogen compounds damage ecosystems eutrophying and acidifying soils and fresh water leading to a change of ecosystem diversity. International co-operations to reduce anthropogenic emissions of acidic precursors have been adopted since the 1980s. However, Critical Loads are still exceeded over large parts of Europe [5] indicating a continued need for further implementation of air pollution abatement strategies. Chemistry Transport Models (CTMs) are used to calculate sulphur and nitrogen dry and wet deposition fluxes. The description of wet deposition processes within many CTMs is often rather crude. A multi model evaluation on sulphur and nitrogen wet deposition fluxes including 23 models showed that 60–70% of the calculated wet deposition rates for Europe and North America agreed to within ±50% with measurements [2]. Model development concerning the description of cloud chemistry and scavenging processes is needed to improve modelling of wet deposition fluxes and thus the overall model performance. Sulphur and nitrogen concentrations in the atmosphere impact the pH of atmospheric water droplets. The droplet pH affects the aqueous phase chemistry within the droplet and the mass of scavenged gases by the droplet [7]. Accounting for pH dependent cloud chemistry is essential for investigating trends in sulphur concentrations and depositions [4]. However, there are only few studies on the sensitivity of model results to droplet pH. In the present study a detailed physical and chemical description of wet scavenging processes and an improved sulphate production scheme both including pH dependency were implemented in the RCG model. Several model runs were carried out to investigate the sensitivity of sulphate formation and gas wet scavenging to pH variations by analyzing the modelled air concentrations and wet deposition fluxes. Furthermore the model results were compared to observations.

## 77.2 Methods and Data

### *77.2.1 Chemistry Transport Model*

The off-line Eulerian grid model RCG simulates air pollution concentrations solving the advection-diffusion equation on a regular lat-lon-grid with variable resolution over Europe [1]. RCG was evaluated within many urban and regional applications and within the framework of several European model inter-comparison studies ([8] and references therein). For the present study model improvements concerning sulphate production and scavenging processes have been carried out. For the aqueous-phase conversion of dissolved $SO_2$ to sulphate in cloud water two pathways are considered in the model: oxidation by $H_2O_2$ and oxidation by dissolved $O_3$. The upgraded corresponding reaction rates are functions of cloud liquid water content and pH [7]. The improved RCG wet deposition scheme distinguishes

between in-cloud and below-cloud scavenging for gases and particles. The gas in-cloud scavenging coefficient is dependent on the cloud liquid water content and cloud water pH. Moreover, droplet saturation is considered for gas wet scavenging by calculating the maximum possible gas in solution as a function of pH [3].

### *77.2.2 Summary of Model Runs*

All model runs were performed on a domain covering Germany (47.2 N–55.1 N; 5.4E–15.7E) with a horizontal resolution of approx. $7 \times 7$ km$^2$ and 20 vertical layers up to 5,000 m. A large scale RCG run covering Europe provided the Boundary Conditions. Emissions for Germany were delivered from local and national inventories, while European emissions are based on EMEP data post-processed at TNO [9]. Hourly meteorological fields are provided by the analysis system TRAMPER [6]. The model sensitivity study was performed over 4 weeks in summer 2005 (5 July–2 Aug 2005). The base run was carried out forcing droplet pH to a constant value of 5 as applied within RCG operational version. Sensitivity runs were performed applying a constant droplet pH of 4.5, 5.5, 6 and 6.5 for

Case 1: sulphate production only while gas wet scavenging pH constant at 5
Case 2: gas wet scavenging only while sulphate production pH constant at 5
Case 3: sulphate production and gas wet scavenging

### *77.2.3 Observational Data*

For evaluation of TRAMPER precipitation, RCG wet deposition fluxes and RCG air concentrations Umweltbundesamt (UBA) station measurements were used.

## 77.3 Results and Discussion

### *77.3.1 Model Cloud Chemistry and Gas Wet Scavenging Sensitivity to Droplet pH*

Figure 77.1a demonstrates the sensitivity of model sulphate formation to droplet pH (=Case 1). The figure shows the vertical distribution of the domain average sulphate air concentration of the different droplet pH runs for the investigation period. Sulphate concentrations increase with increasing model droplet pH due to a higher sulphate production rate via the $O_3$ oxidation pathway. Applying a droplet pH of 6.5 average sulphate concentrations increase by up to 46% compared to the base run.

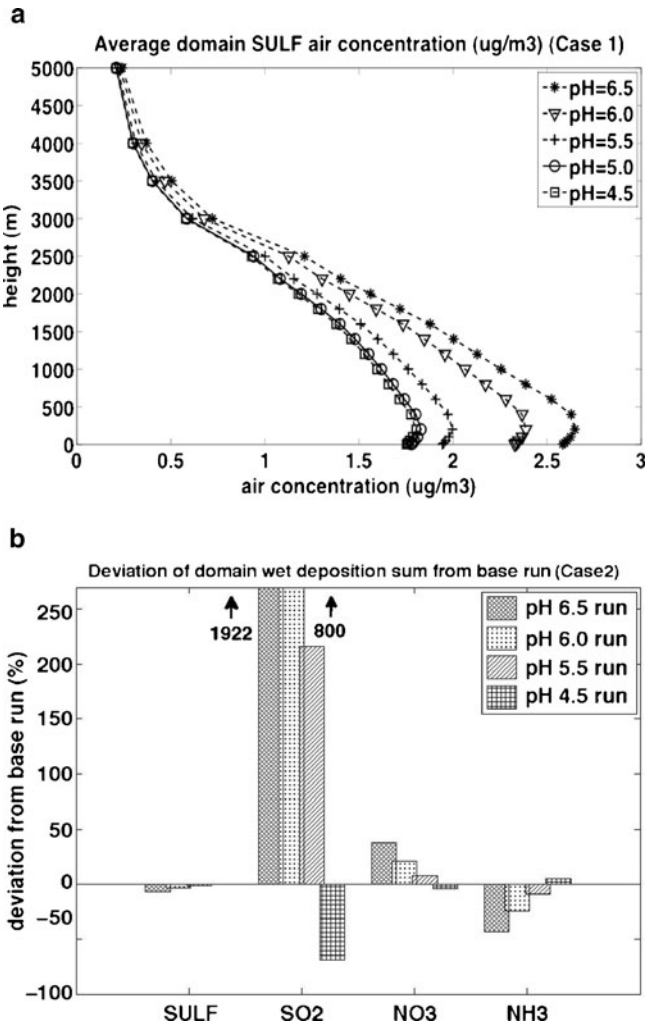


**Fig. 77.1** (**a**) Domain average sulphate air concentration and (**b**) deviation of the domain wet deposition sum from the base run of the different droplet pH runs for the investigation period

The enhancement is most significant for model runs with droplet pH greater 5. For pH lower 5 the reaction rates of oxidation via $H_2O_2$ are several magnitudes higher than those of the $O_3$ oxidation pathway. While oxidation by dissolved $O_3$ varies over wide ranges for atmospheric pH ranges, oxidation by $H_2O_2$ shows a negligible pH dependency. Since sulphate production is a $SO_2$ sink the domain average $SO_2$ (not shown here) concentration decreases with increasing pH. Figure 77.1b displays the sensitivity of model gas wet scavenging to droplet pH (=Case 2). The deviation of the domain wet deposition sum from the base run is presented for different droplet pH runs. Most significant is the increase of $SO_2$ wet deposition fluxes with increasing

model droplet pH (enhancement by a factor of ca. 20 for the pH 6.5 run). This is because more $SO_2$ can be dissolved in the droplets as the pH of the latter increases. Hence, $NH_3$ wet deposition fluxes decrease with increasing model droplet pH. The decrease is less significant than for $SO_2$ due to the high solubility of $NH_3$. The decline of $NH_3$ wet depositions fluxes leads to higher $NH_3$ air concentrations resulting in an enhanced formation of ammonium nitrate, and hence to an increase of $NO_3$ wet deposition fluxes.

### *77.3.2 Model Sensitivity to pH and Comparison to Observations*

In Fig. 77.2 results of the investigation on the overall model sensitivity on droplet pH are shown (=Case 3). Figure 77.2a presents the sulphate air concentrations of the different model runs for the investigation period at Melpitz compared to UBA observations. The impact of model droplet pH variation on the sulphate concentration is significant. RCG reproduces well the temporal devolution of the observed concentrations and the absolute values are within the right range for all droplet pH runs. Since pH of atmospheric droplets varied during the investigation period there is not one particular droplet pH run that compares best to the observations over the whole period. Weekly measured rainwater pH at Melpitz ranged from 4.7 to 5.8 for the investigation period. Figure 77.2b shows the modelled NHx wet deposition fluxes of the model sensitivity runs for the investigation period compared to observations at 17 UBA stations spread over Germany. TRAMPER precipitation (not shown here) compared well to the measurements exhibiting a correlation of 0.8. RCG simulates the wet fluxes within the right range. The analysis of the modelled fluxes demonstrates their significant dependency on pH variation.

## 77.4 Conclusion and Outlook

The present investigation demonstrates that cloud and rain droplet pH variances within model cloud chemistry and gas wet scavenging schemes have a significant impact on resultant air concentrations and wet deposition fluxes. As a next step RCG will be run applying a variable pH of cloud and rain water droplets calculated by using the dissolved species concentrations. First test runs exhibit encouraging results indicating an improvement of RCG model skill when applying a modelled droplet pH instead of a constant droplet pH of 5.

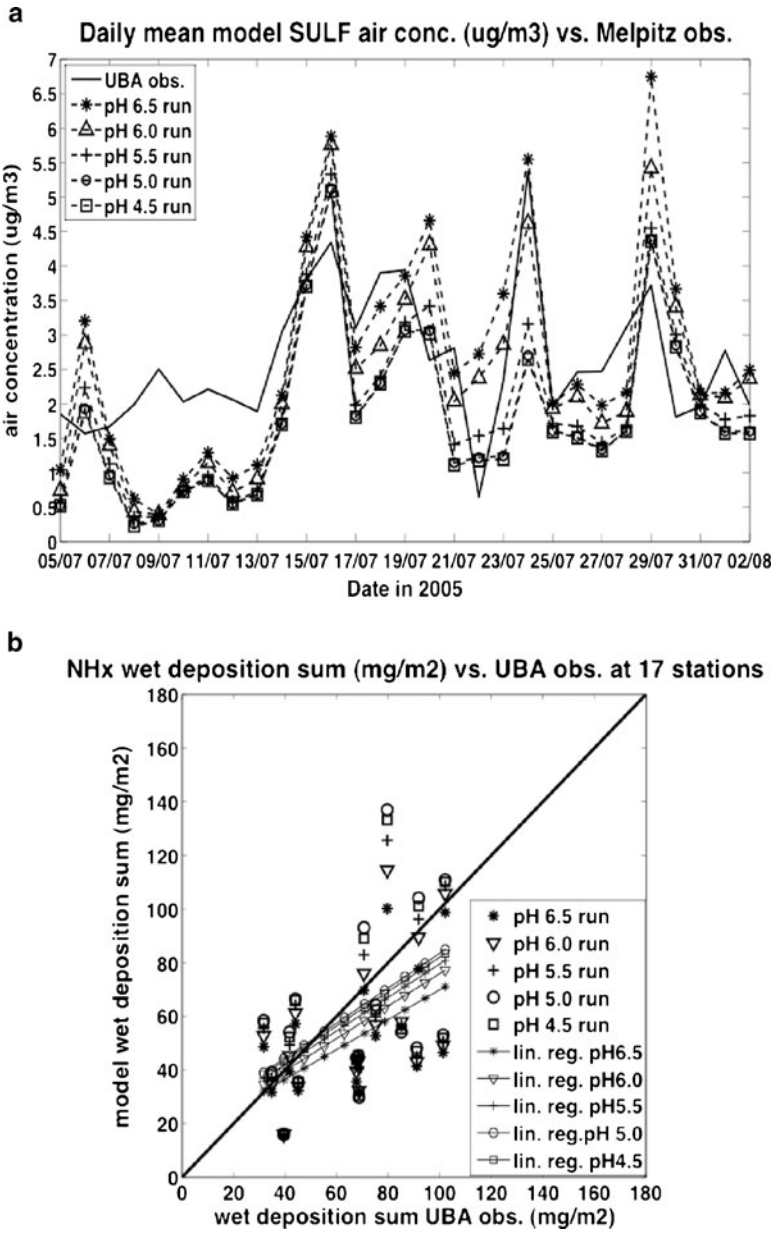


**Fig. 77.2** (**a**) Modelled and observed sulphate air concentrations at UBA station Melpitz and (**b**) modelled and observed NHx wet deposition fluxes at 17 UBA stations spread over Germany

## References

1. Beekmann M et al (2007) PM measurement campaign HOVERT in the Greater Berlin area: model evaluation with chemically specified particulate matter observations for a 1 year period. Atmos Chem Phys 7:55–68
2. Dentener F et al (2006) Nitrogen and sulfur deposition on regional and global scales: a multimodel evaluation. Glob Biogeochem Cycles 20:GB4003
3. ENVIRON (2010) CAMx User's Guide, Comprehensive air quality model with extensions, Version 5.20, ENVIRON International Corporation, Novato, 279 pp
4. Fagerli H, Aas W (2008) Trends of nitrogen in air and precipitation: model results and observations at EMEP sites in Europe, 1980–2003. Environ Pollut 154(3):448–461
5. Lorenz M et al (2008) Critical loads and their exceedances at intensive forest monitoring sites in Europe. Environ Pollut 155:426–435
6. Reimer E, Scherer B (1992) An operational meteorological diagnostic system for regional air pollution analysis and long term modeling. In: Air pollution modelling and its application IX. Kluwer Academic/Plenum Publisher, New York
7. Seinfeld JH, Pandis N (1998) Atmospheric chemistry and physics: from air pollution to climate change. Wiley, New York, 1326 pp
8. Stern R et al (2008) A model inter-comparison study focussing on episodes with elevated PM10 concentrations. Atmos Environ 42:4567–4588
9. Thiruchittampalam B et al (2010) Dokumentation des PAREST Emissionsverteilungsmodells für Deutschland, PAREST-Bericht, Juli 2010

## Questions and Answers

**Questioner Name**: S.T. Rao

**Q**: Have you corrected for bias in precipitation in looking at model evaluation results on base vs. updated chemistry (statistics)?

**A**: First test runs applying a modelled droplet pH exhibited encouraging results showing an improvement concerning model RMSE and BIAS compared to applying a constant droplet pH of 5.

To enable an assessment of model performance concerning wet deposition fluxes TRAMPER precipitation has also been evaluated. TRAMPER precipitation compared well to the measurements exhibiting a correlation of 0.8. Nevertheless, for the modelled droplet pH run it was found that precipitation error and RCG wet deposition flux error are correlated. However, a correction for BIAS in precipitation has not been done yet since in a first step we were interested in the performance of the whole modelling system RCG-TRAMPER.

# Chapter 78
# Detailed Modeling of Dry Deposition over Germany

**A. Kerschbaumer, T. Gauger, E. Hendriks, and P. Builtjes**

**Abstract** The chemistry transport models REM_Calgrid and LOTOS-EUROS have been used to simulate annual total deposition fluxes on German ecosystems for the whole year 2005. To evaluate these results only indirect measurements are available, i.e. wind turbulence, air pollution concentrations and deduced deposition fluxes over specific ecosystems. The comparison of friction velocities processed from COSMO_EU and from ECMWF has shown good agreement with measurements with correlation coefficients around 0.8. Nitrogen deposition fluxes calculated with the two models for the year 2005 were comparable giving the same spatial distribution and summed over the whole area similar amounts. Comparisons with measured values at a forest site in Augustendorf for the year 2003 have shown substantial differences between the two models, both underestimating the measured nitrogen deposition flux.

**Keywords** Dry deposition • Reactive nitrogen species • Model evaluation

## 78.1 Introduction

Deposited loads of sulfur and nitrogen compounds, stemming from anthropogenic precursors, endanger ecosystems and need to be modeled in order to assess the effectiveness of action plans. Model results have shown that approximately 40%

A. Kerschbaumer (✉)
Institut für Meteorologie, Freie Universitaet Berlin, Berlin, Germany
e-mail: andreas.kerschbaumer@fu-berlin.de

T. Gauger
Institut für Navigation, Universität Stuttgart, Stuttgart, Germany
e-mail: gauger@nav.uni-stuttgart.de

E. Hendriks • P. Builtjes
TNO, Utrecht, The Netherlands
e-mail: elise.hendriks@tno.nl; peter.builtjes@tno.nl

D.G. Steyn and S. Trini Castelli (eds.), *Air Pollution Modeling and its Application XXI*,
NATO Science for Peace and Security Series C: Environmental Security 4,
DOI 10.1007/978-94-007-1359-8_78, 

of total pollutants deposition is due to wet processes and 60% to dry deposition. At the same time dry deposition is very difficult to measure as it depends on atmospheric stability and on individual receptors of specific pollutants, altogether. The absorbed species concentration in the stomata of different plants, for example, is almost impossible to measure, or to generalize for bigger areas. Measurements are thus a combination of observed air concentrations and micrometeorological measurements and modeled absorption processes for individual ecosystems [3]. The same model approach for dry deposition processes is implemented in Chemistry-Transport-Models. The process itself determines, next to emission loads, transport and air chemistry, the quality of air pollution concentration simulations. A thorough model evaluation needs thus to account for dry deposition fluxes and their intrinsic parameters, i.e. atmospheric stability, land classification and air pollution concentration gradients. We performed a model evaluation with respect to dry deposition fluxes comparing independent meteorological measurements and total nitrogen fluxes to a forest site in Germany for two Eulerian Chemistry Transport Models for different time periods.

## 78.2 Methods

The off-line chemistry transport models (CTM) REM_Calgrid (RCG) [8] and LOTOS-EUROS (LE) [7] simulate air pollution concentrations and deposition solving the advection-diffusion equation with a horizontal resolution of approximately $7 \times 7$ km and up to 3,500 m height. Emissions for Germany were delivered from local and national inventories, while European emissions are based on EMEP data post-processed at TNO [6]. Meteorological fields were taken from COSMO-EU (DWD) for RCG and from ECMWF for LE. Both CTM were evaluated within the framework of several European model inter-comparison studies (e.g. [2]).

Dry deposition velocity is parameterised in both CTM following the resistance approach proposed by Erisman et al. [4]. The atmospheric resistance $R_a$ and the sublayer resistance $R_b$ are driven by the friction velocity $u_*$ and the atmospheric stability $\Psi_m$. which is parameterised with the Monin-Obukhov-Length (L). The canopy resistance for gases depends largely on the surface humidity and on plant physiological parameters. Friction velocity $u_*$ is one of the most prominent parameters in simulating dry deposition processes. At Lindenberg in the South-East of Berlin, DWD has been performing turbulence measurements since more than 10 years. A 28 m measurement tower at the forest site was equipped with meteorological measurement devices at different levels with sampling times for temperature, humidity, wind speed and direction of 1 s. [1]. Turbulent momentum fluxes were determined from the high resolution measurements of the three wind components by computing mean eddy covariances and used to compute the friction velocity. The nitrogen deposition measurements at the forest site in Augustendorf in the North-Western plain land of Germany, have been derived using the micrometeorological method described in Dämmgen [3] which uses the eddy covariance assumption coded in

the PLATIN-model [5]. The model calculates the exchange of trace gases and fine-particle constituents. The vertical transport between an above-canopy reference height, for which air properties and concentrations of matter must be known, and the sinks and/or sources of the plant/soil-surface system is estimated. The air pollution concentrations were measured using in series denuder tubes [3] for gaseous $NH_3$, $HNO_2$, $HNO_3$, $SO_2$ and HCL and for particles $NH_4$-N, $NO_3$-N, $SO_4$-S, Cl and Na. Wind speed and direction, air temperature and humidity were measured at 25 m as well as at 22 m above ground, with an average sampling period of 15 min.

## 78.3 Results and Discussion

Figure 78.1 shows the hourly performance of the friction velocity simulations (y-axis) compared to the forest measurement sites in Lindenberg (x-axis), derived for RCG from the dynamic model COSMO-EU (left panel) and for LE from the ECMWF-model (right panel). Taking into account that both meteorological models comprise more than one land-use-type in one cell, friction velocities are well reproduced temporally with correlation coefficients around 0.8 for both models slightly underestimating measurements (slope 0.6 and intercept 0.13 m/s for COSMO_EU and 0.76 slope and intercept 0.16 m/s for ECMWF).

Figure 78.2 shows the total nitrogen deposition fluxes simulated with the two CTM for the year 2005. The spatial distribution is very similar in both models emphasizing areas with high NOx – emissions in Germany. Also the absolute values are comparable. For the year 2003 measurements from Augustendorf were available and have been used to validate RCG and LE for this year at this forest-site.

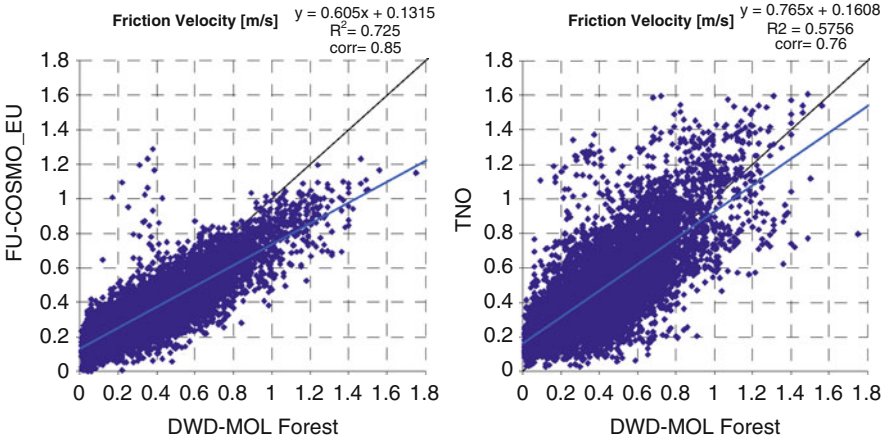


**Fig. 78.1** Model (*y-axis*) friction velocity compared to measurements (*x-axis*) for COSMO_EU (*left*) and ECMWF (*right*)

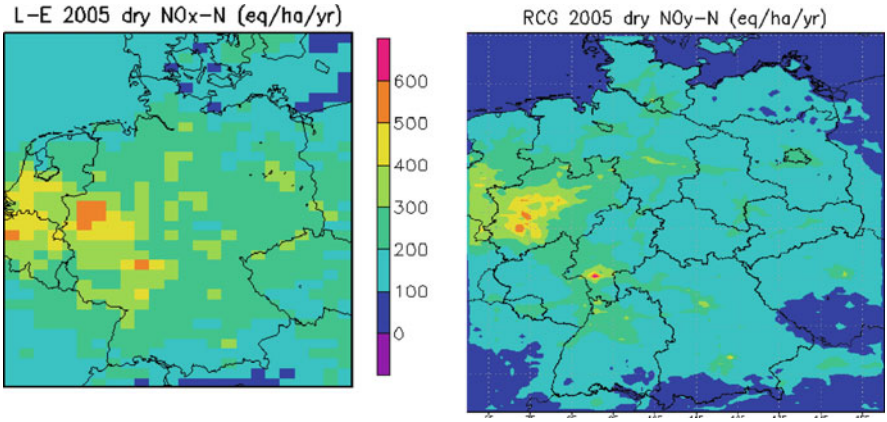


**Fig. 78.2** Total nitrogen deposition flux, accumulated for 2005, simulated with LE (*left*) and with RCG (*right*) in eq/ha-a

**Table 78.1** Simulated accumulated annual deposition fluxes for gaseous and aerosol N-species in Augustendorf – Germany

| Species [kg-N/ha-a] | Observed | RCG | LE |
|---|---|---|---|
| $NH_3$ | 16.2 | 16.1 | 26.5 |
| $NH_4$ | 14.1 | 0.1 | 3.0 |
| $NO_3$ | 8.2 | 0.1 | 2.0 |
| $HNO_3$ | 2.9 | 0.6 | 0.9 |
| $NO_2$ | 1.5 | 1.9 | 1.7 |
| $HNO_2$ | 0.8 | 0.0 | 0.0 |
| Total | 43.7 | 18.6 | 34.1 |

Table 78.1 gives the accumulated observed and simulated gaseous and solid nitrogen fluxes. RCG simulates very well $NH_3$ on a yearly basis while LE overestimates ammonia. Both models underestimate heavily aerosol ammonia and aerosol nitrate, while $NO_2$ is again reproduced correctly. The total nitrogen deposition at the observation site in the forest is depicted well with LE (ca. 20% less) and underestimated by 60% with RCG. The good performance of LE is partially due to the overestimation of $NH_3$. A point to grid comparison is difficult and not always representative, nevertheless available micrometeorological observations and measured deposition fluxes are at the same order of magnitude as modeled values.

**Acknowledgments** This work has been funded by Umweltbundesamt – Germany within the R&D-project MAPESI under Contract No. 3707 64 200.

## References

1. Beyrich F, Adam WK (2007) Site and data report for the Lindenberg Reference Site in CEOP – Phase I. Berichte des Deutschen Wetterdienstes, 230. Selbstverlag des Deutschen Wetterdienstes, 55 pp
2. Cuvelier C et al (2007) CityDelta: a model intercomparison study to explore the impact of emission reductions in European cities in 2010. Atmos Environ 41:189–207
3. Dämmgen U (ed) (2005) Bestimmung von Ammoniak-Einträgen aus der Luft und deren Wirkung auf Waldökosysteme (ANWER-Projekt). Landbauforschung Völkenrode, Special Issue 279, 128 pp
4. Erisman JW, van Pul A, Wyers P (1994) Parametrization of surface-resistance for the quantification of atmospheric deposition of acidifying pollutants and ozone. Atmos Environ 28:2595–2607
5. Grünhage L, Haenel H-D (2008) PLATIN – PLant-ATmosphere INteraction model. Landbauforschung Völkenrode, Special Issue 319, 85 pp
6. Klotz V et al (2009) An integrated measure-based approach to fulfil European air quality targets cost-effective on a national level – first results of the German PAREST-project. TFIAM Meeting, Bilthoven, 10 Juni 2009
7. Schaap M, Sauter F, Timmermans RMA, Roemer M, Velders G, Beck J, Builtjes PJH (2008) The LOTOS–EUROS model: description, validation and the latest developments. Int J Environ Pollut 32(2):270–290
8. Stern R, Yamartino R, Graff A (2003) Dispersion modelling within the European Community's air quality directives: long term modelling of $O_3$, PM10 and $NO_2$. In: 26th ITM, Turkey

## Questions and Answers

**Questioner Name**: A. Venkatram

**Q**: Your estimated dry deposition fluxes of aerosols are about a factor of 10–100 less than the observed values. Were the associated ambient aerosol concentrations also underestimated? If not, these results of underestimates are not consistent with the good estimates of the surface friction velocity because dry deposition of aerosols is governed by the surface friction velocity.

**A**: The simulated aerosol concentrations were in good agreement with the measured concentrations at the specific monitoring site. Unfortunately, micrometeorological measurements have not been compared to simulations at the same site (Augustendorf), but on a different observation site (Lindenberg). Friction velocities simulations have shown to compare well with simulations at Lindenberg. We generalized this result to the whole area which might not be correct. As particle dry deposition depends only on friction velocity in the model and as the air concentration of particles is in the same order of magnitude as observations the underestimation of particle dry deposition fluxes at Augustendorf is most probably due to a strong underestimation of friction velocities at that site. The final conclusion is corroborated by this finding: model evaluation always must include process evaluation if order to avoid misinterpretation of assumed good results.

# Chapter 79
# The Impact of Meteorological Uncertainties on the Prediction of PM in Urban Areas

**Ralf Wolke, Jens Stoll, Alexander Smalla, Roland Schroedner, Oswald Knoth, and Eberhard Renner**

**Abstract** The transport and transformation of PM is mainly forced by meteorological processes. Therefore, an appropriate description of these processes is of essential interest in chemistry transport modelling. In the paper, the influence of two different meteorological drivers on the simulated particle concentrations is analyzed. For this purpose, the chemistry transport code MUSCAT was online-coupled with WRF as well as with the COSMO model of the German Weather Service. Furthermore, WRF-Chem simulations are also considered in the model comparison. The combination of two meteorological and two chemistry-transport models has a great potential for a detailed analysis of the meteorological dependencies and its impact on the aerosol processes. The simulation results were compared with a comprehensive set of ground-based and profile measurements. The influence of several meteorological parameters (e.g., PBL height, humidity, precipitation) on the simulated concentration fields was analyzed. Main differences are caused by deviations in PBL and cloudiness.

**Keywords** Chemistry transport modelling • Meteorological forcing • Aerosol dynamics • Time integration schemes • Online coupling

## 79.1 Introduction

Recent model studies (e. g., [6]) showed that models tend to underestimate observed PM10 concentrations over Europe. There are many possible reasons for this underestimation. One of the main problems in this context is the appropriate modelling of the planetary boundary layer (PBL). The aim of this study was to look in more detail at the meteorological effects that influence the particle and gas phase concentrations at ground but also in higher altitudes. Different model configurations

R. Wolke (✉) • J. Stoll • A. Smalla • R. Schroedner • O. Knoth • E. Renner
Leibniz Institute for Tropospheric Research (IfT), Permoserstrasse 15, 04303 Leipzig, Germany
e-mail: wolke@tropos.de; renner@tropos.de

D.G. Steyn and S. Trini Castelli (eds.), *Air Pollution Modeling and its Application XXI*,
NATO Science for Peace and Security Series C: Environmental Security 4,
DOI 10.1007/978-94-007-1359-8_79, 

and grid resolutions are investigated for selected scenarios during the EUCAARI LONGREX campaign in May/June 2008. The simulation results are compared with ground-based measurements and radiosonde data. Furthermore, the influence of several meteorological parameters provided by the meteorological drivers (mixing layer height, humidity, wind direction, . . .) on the concentration fields are scrutinized.

The chemistry transport model MUSCAT (Multi-Scale Atmospheric Transport Model) performs the atmospheric transport as well as chemical transformations for several gas phase species and particle populations [4, 8]. The transport processes include advection, turbulent diffusion, sedimentation, dry and wet deposition. The atmospheric chemistry contains the gas phase mechanism of RACM-MIM2 [2] and the formation of secondary particulate matter. The description of the particle size distribution and aerosol dynamical processes is performed by an extended version of the modal aerosol model M7 [7] or, alternatively, by a simplified mass based approach.

For this study, the chemistry transport code MUSCAT was online-coupled with two different meteorological models. Both models are capable of self-nesting and offer the possibility to use different meteorological parameterizations in dependence on the spatial model resolution. Firstly, the operational forecast model COSMO[1] of the German Weather Service is a non-hydrostatic and compressible meteorological model [5]. The model includes the dynamic kernel for the atmosphere as well as the necessary parameterisation schemes for various meteorological processes, boundary conditions and surface exchange relations. Secondly, the Weather Research and Forecasting (WRF[2]) model is a numerical weather prediction and atmospheric simulation system designed for both research and operational applications. It is also fully compressible, non-hydrostatic and uses a staggered Arakawa C-grid. In difference to COSMO, a mass-conserving approach is implemented in WRF. Additionally to the WRF-MUSCAT and COSMO-MUSCAT runs, chemistry transport simulations are performed with WRF-Chem [1].

## 79.2 Online Coupling Between WRF and MUSCAT

The "sequential" online-coupling approach proposed by Lieber and Wolke [3] is adapted to the WRF-MUSCAT coupling. This approach was firstly used in COSMO-MUSCAT. Each processor is assigned to carry out one partition of the coupled codes alternately. Since the workload of each model is distributed equally over all processors, imbalances between the codes are compensated. In the "sequential" approach, all processors first calculate the meteorology over one coupling interval. Then the meteorological coupling data are exchanged and all processors continue with the calculation of chemistry-transport over the same interval. Required arrays for feedback are sent from MUSCAT to the meteorological models, before the next

[1] http://www.cosmo-model.org
[2] http://www.wrf-model.org

coupling step is performed. An essential advantage of the sequential scheme is that an a priori partitioning of the processors is not necessary. The meteorological and the chemistry-transport algorithms have their own separate time step size control. All meteorological fields are given with respect to the uniform horizontal meteorological grid. They have to be averaged or interpolated from the base grid into the block-structured chemistry-transport grid with different resolutions. The meteorological processors communicate directly with each of the corresponding MUSCAT processors.

## 79.3 Results and Discussion

The COSMO-MUSCAT, WRF-MUSCAT, and WRF-Chem simulations are performed from the European to the urban scale. In our configuration, the region of interest covers the Berlin area as well as the EUSAAR "Supersite" station Melpitz. A one-way nesting strategy is used for all model configurations. The used inventories of the anthropogenic emissions are based on the EMEP/CORINAIR data, improved by TNO. Biogenic emissions and radiation activity are calculated by MUSCAT, whereas information on the cloud cover, temperature, and other meteorological parameters are taken from the coupled meteorological model. The meteorological forcing of COSMO is performed either by reanalysed data provided by the global meteorological model GME or the operational COSMO runs for finer resolutions. WRF is driven by NCEP data.

The simulation results were compared with ground-based measurements of particulate matter as well as relevant gas phase concentrations. We observe only a moderate agreement of the concentration fields in most of the stations. Especially, the discrepancies in PM10 are considerable (Fig. 79.1). COSMO-MUSCAT tends

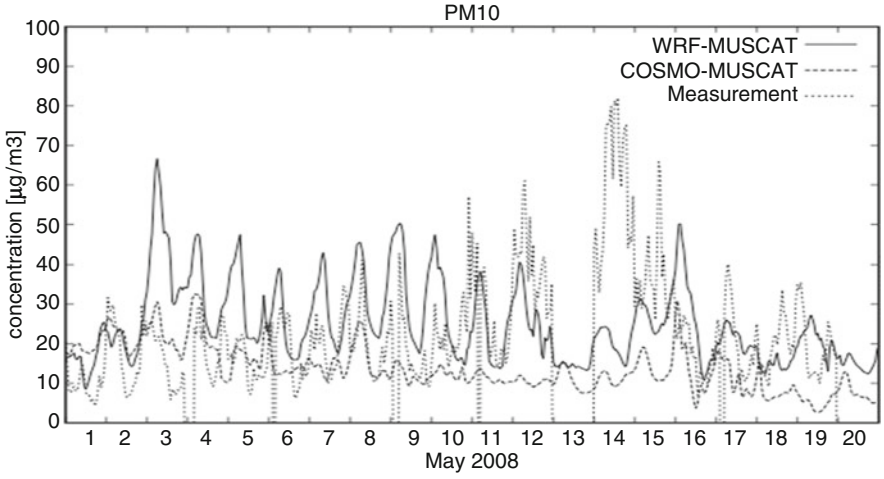


**Fig. 79.1** Comparison of simulated and measured hourly PM10 concentrations at the monitoring station Melpitz during the period 1–20 May 2008

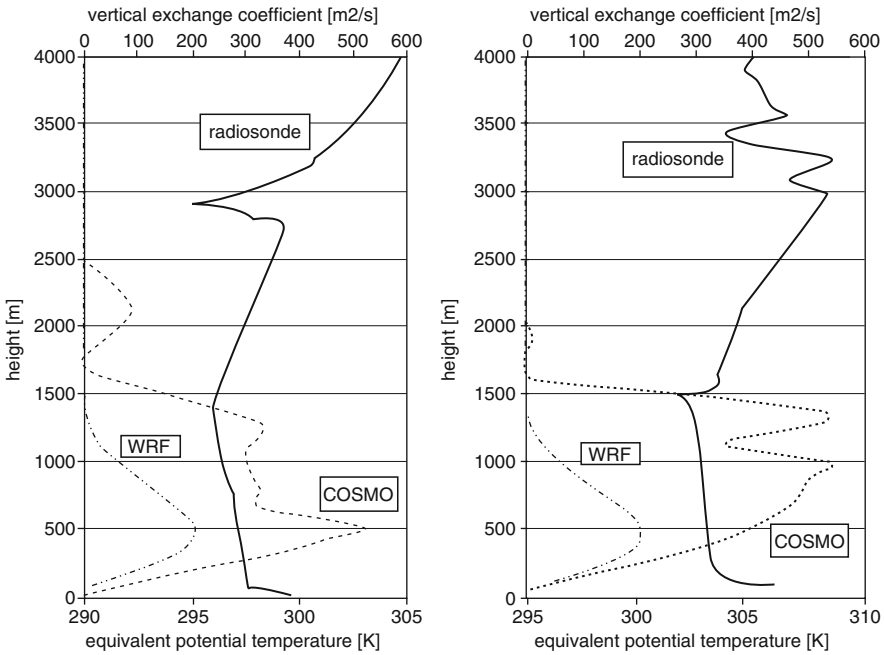


**Fig. 79.2** Comparison of the modeled profiles of the vertical exchange coefficients and the radiosonde profiles of the equivalent potential temperature in Greifswald (*left*) and Lindenberg (*right*) at 18 May 2008, 12:00 UTC

to underpredict the concentrations most of the time. WRF-MUSCAT can reproduce the range of PM10 in the second decade of May but overestimates the measured values especially during the first days. This different behaviour seems to be caused mainly by the modelled PBL height of WRF and COSMO (Fig. 79.2). Note that the measured PM10 peaks around May 14th are caused by a Saharan dust event in Central Europe. This is confirmed by the fact that the simulated sulphate and nitrate concentrations in Melpitz show a good agreement for our model runs. Dust emissions are not included in the simulations of Fig. 79.1. Currently, available aircraft and LIDAR measurements are used for model evaluation as well as the analysis of the urban-regional scale interactions.

**Acknowledgments** The work was supported by European Commission 6th Framework programme project EUCAARI (contract no. 036833–2), the ZIH Dresden and the NIC Jülich. Furthermore, we thank the DWD Offenbach and ECMWF for good cooperation.

## References

1. Grell GA, Peckham SE, Schmitz R, McKeen SAS, Frost G, Skamarock WS, Eder B (2005) Fully coupled "online" chemistry within the WRF model. Atmos Environ 39:6957–6975

2. Karl M, Dorn H-P, Holland F, Koppmann R, Poppe D, Rupp L, Schaub A, Wahner A (2006) Product study of the reaction of OH radicals with isoprene in the atmosphere simulation chamber, SAPHIR. J Atmos Chem 55:167–187
3. Lieber M, Wolke R (2008) Optimizing the coupling in parallel air quality model systems. Environ Modell Softw 23:235–243
4. Renner E, Wolke R (2010) Modelling the formation and atmospheric transport of secondary inorganic aerosols with special attention to regions with high ammonia emissions. Atmos Environ 44:1904–1912
5. Steppeler J, Doms G, Schättler U, Bitzer HW, Gassmann A, Damrath U, Gregoric G (2003) Meso-gamma scale forecasts using the nonhydrostatic model LM. Meteorol Atmos Phys 82:75–96
6. Stern R, Builtjes PJH, Schaap M, Timmermans R, Vautard R, Memmesheimer MHA, Renner EFH, Wolke R, Kerschbaumer A (2008) A model intercomparison study focussing on episodes with elevated PM10 concentrations. Atmos Environ 42:4567–4588
7. Vignati E, Wilson J, Stier P (2004) M7: an efficient size-resolved aerosol microphysics module for large-scale aerosol transport models. J Geophys Res 109:D22202. doi:10.1029/2003JD004485
8. Wolke R, Knoth O (2000) Implicit-explicit Runge-Kutta methods applied to atmospheric chemistry-transport modelling. Environ Modell Softw 15:711–719

## Questions and Answers

**Ken Schere**: Why did you allow the transport of chemical tracers to be done by MUSCAT in the coupled model system, when you could provide tracer concentrations or tendencies back to the meteorological model, so that all scalars are transported consistently?

**Ralf Wolfe**: For MUSCAT an implicit-explicit time integration scheme was developed [8] to combine in an efficient way the slow process of horizontal advection and the fast processes of vertical exchange and chemistry. Whereas the slow processes are integrated by explicit Runge-Kutta methods any suitable solver can be applied to the fast processes. The "two way" coupling between meteorology and chemistry transport takes place at each horizontal advection time step. If this coupling step is restricted to one COSMO time step, MUSCAT can be considered as a subroutine using consistent numerical schemes.

# Chapter 80
# Setting Acceptance Criteria for Air Quality Models

**Steven R. Hanna and Joseph Chang**

**Abstract** Is an air quality model acceptable for use (fit for purpose)? We now have several state-of-the-art statistical methodologies in place for calculating model performance measures and for determining the statistical significance of the results. But a more difficult question is whether, based on the calculated performance measures, the model is acceptable or not. This question is being addressed in several of the authors' recent studies, and an example carried out for the Joint Effects Model (JEM) is the focus of the current paper. The rationale for selecting acceptance criteria for air quality models is described, and the results of applications of the method to four urban field experiments are presented. The values of the acceptance criteria are based on the authors' experiences with a wide variety of air quality models and observations. For example, an acceptable FAC2 is $>0.3$ for urban scenarios. Furthermore, since a model is unlikely to fulfill all acceptance criteria at every field experiment site, we require that the model meet the individual criteria for at least 50% of the performance measures and field experiments and input options used in the study. It is shown here that the JEM model meets the 50% criterion.

**Keywords** Air quality model evaluation • Acceptance criteria • JEM • U2000 • JU2003 • MSG05 • MID05

S.R. Hanna (✉)
Hanna Consultants, Kennebunkport, ME, USA
e-mail: hannaconsult@roadrunner.com

J. Chang
Fairfax, VA, USA

D.G. Steyn and S. Trini Castelli (eds.), *Air Pollution Modeling and its Application XXI*,
NATO Science for Peace and Security Series C: Environmental Security 4,
DOI 10.1007/978-94-007-1359-8_80, 

## 80.1 Introduction

The Department of Defense (DoD) is sponsoring the development of the Joint Effects Model (JEM), whose purpose is to provide a common representation of hazard areas resulting from a variety of hazardous releases. The authors have been carrying out Independent Validation and Verification (IV&V) of the dispersion model component of JEM. We have used our BOOT model evaluation software, as described by Hanna [7] and Chang and Hanna [5]. However, the DoD requires that acceptance criteria be set for anything going through the IV&V process. The term "fitness for purpose" is sometimes also used and refers to both scientific concerns and quantitative performance measures. Chang and Hanna [5] reviewed many evaluation exercises, involving many models and many types of observations, and suggested some preliminary acceptance criteria based on some standard performance measures. These were used in evaluating JEM with five rural field experiments as reported by Chang et al. [6].

We noticed that our 2004 suggestions were being adopted by others and that some additional acceptance criteria were being suggested such as "hit rate". We agree that it is necessary to define a comprehensive acceptance criterion, similar to hit rate, in addition to the standard criteria, so as to avoid having a good model rejected just because it happened to do poorly in one or two field experiments. The discussions below use a comprehensive acceptance criterion of 50%, which can be interpreted as saying the model must pass the individual quantitative performance criteria in more than 50% of the "data sets" or categories defined as, for example, different field experiments and/or model options.

The current paper builds on the JEM rural evaluations presented by Chang et al. [6] and moves to evaluations with four U.S. urban tracer field experiments: Urban 2000 (U2000; [4]); Joint Urban [1] (JU2003; [1]); Madison Square Garden 2005 (MSG05; [2]); and Midtown Manhattan 2005 (MID05; [3]). These experiments involve moderately to highly built-up urban areas, and near-surface tracer releases. Table 80.1 gives some basic attributes of these experiments. Only near-surface samplers are used here.

The urban model evaluation study is more challenging than its rural predecessor as described in Chang et al. [6]. The model acceptance criteria for urban applications have not been well-established, as there are just not as many studies involving urban data sets. Multiple meteorological input and modeling options were involved in making JEM runs. Two urban modeling options were considered,

**Table 80.1** Attributes of four urban field experiments. Releases and samplers are at surface

| Field exp. | Location | Time of day | Tracers | Releases | Samplers |
|---|---|---|---|---|---|
| U2000 | Salt Lake City | Night | 1 | 18 | ~100 to ~6 km |
| JU2003 | Oklahoma City | Day & night | 1 | 21 | ~120 to ~4 km |
| MSG05 | New York City | Day | 5 | 20 | ~20 to ~0.5 km |
| MID05 | New York City | Day | 6 | 87 | ~160 to ~2 km |

the Urban Dispersion Model (UDM) and the urban canopy (UC) algorithm. The model's ability to predict the maximum concentrations as a function of downwind distance was examined, as well as the ability to predict the concentrations paired-in-space. The model performance measures considered are the fractional bias (FB), the normalized mean square error (NMSE), and the fraction of predictions within a factor of 2 of observations (FAC2) for the first approach; and the normalized absolute difference (NAD) for the second approach. FB, NMSE, and FAC2 were calculated using actual values of observations ($C_o$) and model predictions ($C_p$). NAD was calculated by simply counting the number of sampler locations where $C_p > C_T$ (threshold) and $C_o < C_T$; $C_p < C_T$ and $C_o > C_T$; or $C_p > C_T$ and $C_o > C_T$. It is assumed that $C_T = 3$ times the Method Limit of Quantification (MLOQ) or the tracer background concentration.

Model performance for urban applications is not expected to be as good as that for non-urban applications due to variability introduced by buildings. Therefore, it was recommended that the model acceptance criteria for urban applications be relaxed by roughly a factor of 2 from those for non-urban cases.

- $|FB| < \sim 67\%$, *i.e.*, the mean bias < a factor of ~2
- NMSE < ~6, *i.e.*, the random scatter < ~2.4 times the mean
- FAC2 > ~30%, *i.e.*, the fraction of $C_p$ within a factor of two of $C_o$
- NAD < ~50%, *i.e.*, the fractional area for errors, $A_F/(A_F + A_{OV})$, < ~50%

Note that FB, NMSE, and FAC2 are based on arc-maximum comparisons; and NAD is based on paired-in-space comparisons. A comprehensive acceptance criterion is defined as being met if at least half of the performance measure criteria are met for least half of the field experiments considered.

## 80.2 Results

Table 80.2 is an example of the summary tables prepared in order to more easily "see" whether the acceptance criteria were satisfied. The table is for the MSG05 surface samplers and for one of the PFTs used as tracers. There are three wind input options

**Table 80.2** Example of performance measures for MSG05 street-level samplers for PMCH tracer

| | | Arc-Max | | |
|---|---|---|---|---|
| Met input and urban model option | | FB | NMSE | FAC2 |
| LGA airport | UC | 0.210 | 0.76 | 0.714 |
| | UDM | 0.776 | 1.18 | 0.250 |
| Single local observed | UC | 0.155 | 1.27 | 0.375 |
| | UDM | 0.740 | 0.92 | 0.625 |
| MEDOC (MM5) | UC | −0.749 | 4.93 | 0.143 |
| | UDM | 0.533 | 0.38 | 0.625 |

Grey-shaded blocks met acceptance criteria and un-shaded blocks did not

**Table 80.3** Summary showing the number out of all of the cases considered where the acceptance criteria were met, to be compared with the comprehensive acceptance criterion of 50%

| | Performance measures | | | |
|---|---|---|---|---|
| Field data set | FB | NMSE | FAC2 | NAD |
| U2000 | 7 of 10 | 5 of 10 | 10 of 10 | 9 of 10 |
| JU2003 | 2 of 8 | 1 of 8 | 8 of 8 | 8 of 8 |
| MSG05 | 7 of 18 | 14 of 18 | 11 of 18 | 12 of 18 |
| MID05 | 6 of 24 | 14 of 24 | 17 of 24 | 10 of 24 |
| Total | 22 of 60 | 34 of 60 | 46 of 60 | 39 of 60 |

and two urban dispersion model options (UC and UDM). Grey shading indicates that the acceptance criterion was met and no shading indicates that it was not. It is easy to see that there are more grey blocks than unshaded blocks, which suggests that the comprehensive acceptance measure is greater than 50% and therefore the JEM dispersion model is "acceptable" for this field experiment and tracer.

Table 80.3 provides a summary (across each field experiment and all model options, input conditions and tracers) of the number of cases where each performance measure satisfied its respective acceptance criterion. As mentioned earlier, only surface samplers are included. Overall, more than half of the time the acceptance criteria proposed above were met (but just barely). As a result, the comprehensive acceptance measure exceeds 50% and JEM's performance is considered acceptable for urban applications.

## 80.3 Limitations

The model acceptance criteria themselves are arbitrary, and a more valid and widely-recognized set might result via an expert elicitation process, including a workshop. Clearly the evaluation results depend on the quality and extent of the field experiment and on the scenario being studied. Another issue is that it is not helpful if nearly all models fail the tests (or the converse – if nearly all models pass). We also find that using more onsite data or high-resolution mesoscale meteorological outputs does not necessarily guarantee better model performance. It is clear that JEM did not do as well for rooftop and near-field (~within one building height) samplers. These cases are outside UDM's applicability and were therefore not included in the statistics.

**Acknowledgments** This research was supported by the U.S. Defense Threat Reduction Agency (DTRA), with Rick Fry as Project Manager, and by the Joint Effects Model (JEM) IV&V program, with Brian Boyle as project manager.

## References

1. Allwine KJ, Flaherty JE (2006a) Joint urban 2003: study overview and instrument locations. Pacific Northwest National Laboratory, Report no. PNNL-15967, 92 pp
2. Allwine KJ, Flaherty JE (2006b) Urban dispersion program MSG05 field study: summary of tracer and meteorological measurements. Pacific Northwest National Laboratory, Report no. PNNL-15969, 27 pp
3. Allwine KJ, Flaherty JE (2007) Urban dispersion program overview and MID05 field study summary. Pacific Northwest National Laboratory, Report no. PNNL-16696, 63 pp
4. Allwine KJ, Shinn JH, Streit GE, Clawson KL, Brown M (2002) Overview of urban 2000. A multiscale field study of dispersion through an urban environment. Bull Am Meteorol Soc 83:521–536
5. Chang JC, Hanna SR (2004) Air quality model performance evaluation. Meteorol Atmos Phys 87:167–196
6. Chang JC, Boybeyi Z, Tang H, Cervone G, Bakosi J, Hanna S, Hendrick E, Santos L, Bowers J (2007) Independent verification and validation of joint effects model. Prepared for Naval Surface Warfare Center, Dahlgren Division, 191 pp
7. Hanna SR (1989) Confidence limits for air quality model evaluations as estimated by bootstrap and jackknife resampling methods. Atmos Environ 23:1385–1398

## Questions and Answers

**Questioner Name**: Silvia Trini-Castelli

**Q**: Considering that observations are affected by their own uncertainties, how do you take account that aspect in your comprehensive acceptance criteria approach? Can you somehow include these uncertainties as a sort of "weight" of your acceptance measures to estimate the model performance?

**A**: The observations used in the evaluations in this paper are research-grade and their thresholds and uncertainties were analyzed and reported in the data archives. However, we did not specifically include the uncertainties in our definitions of acceptance criteria. The instrument uncertainties are a component of the performance measures and obviously cannot be eliminated by even a "perfect" model. Thus, as acceptance criteria are further studied, the influence of the instrument uncertainties can be included.

**Questioner Name**: Bruce Rolstad Denby

**Q**: The criteria you have set up are for a particular application. These should not be the same for other applications. Could you comment on this?

**A**: The applications used as examples in this paper were based on the authors' experiences with models for dispersion from continuous or instantaneous point and line sources in the lowest 100 m of the boundary layer. Distances of concern are up to about 100 km for rural field studies and up to about 10 km for urban field studies. The acceptance criteria suggested here are for evaluations with research-grade field experiment data, with the sources well

known, with on-site meteorological observations, and with an extensive array of high-quality concentration samplers. The suggestions of acceptance criteria in this paper are intended to represent a start to the discussion and it is hoped that further studies can help develop acceptance criteria for other applications and types of available data.

**Questioner Name**: Stefano Galmarini

**Q**: Do you include spatial pattern evaluation? What about the evaluation of vertical distributions?

**A**: The application described in the paper did not include performance measures for spatial patterns or vertical distributions. These can be added at any time once the acceptance criteria are decided based on experience with several models and data sets.

# Chapter 81
# The Impact of Meteorology on Air Quality Simulations over the Po Valley in Northern Italy

**Denise Pernigotti, Emilia Georgieva, Philippe Thunis, Cornelius Cuvelier, and Alexander de Meij**

**Abstract** The Po valley in Northern Italy has been identified as a hot spot area in Europe where pollutant levels are expected to remain problematic in the years to come despite the application of the legislation devoted to air pollution control. High anthropogenic emissions in combination with frequently occurring stagnant atmospheric conditions cause very high PM (particulate matter) concentrations in winter. The POMI project (PO valley Model Inter-comparison exercise) has been set-up to evaluate the capabilities of current air quality models to reproduce the concentration levels reached in this area. One of the outcomes of the project has been the confirmation that air quality models do under-estimate quite significantly the observed PM concentrations in this region. A series of sensitivity test have been run in order to understand the reasons for this underestimation and in particular to highlight the impact of meteorology on modeled concentrations. Different nudging techniques of observations from regulatory networks into MM5 (meteorlogical model) are explored in an attempt to improve the simulation of frequent low wind regimes in the Po valley. The sensitivity of CHIMERE (chemical transport model) is evaluated for January 2005, a period with high PM concentrations. Strengths and weaknesses of the approaches on simulating PM in one of the most polluted and complex areas in Europe are discussed.

**Keywords** MM5 • Nudging • fdda • Chimere • Wind • PM10 • Po valley

D. Pernigotti (✉) • E. Georgieva • P. Thunis • C. Cuvelier • A. de Meij
European Commission, JRC, Institute for Environment and Sustainability, Ispra, Italy
e-mail: denise.pernigotti@jrc.ec.europa.eu; a.demeij@cyi.ac.cy

D.G. Steyn and S. Trini Castelli (eds.), *Air Pollution Modeling and its Application XXI*,
NATO Science for Peace and Security Series C: Environmental Security 4,
DOI 10.1007/978-94-007-1359-8_81, 

## 81.1 Introduction

The POMI project (http://aqm.jrc.it/POMI) outcomes confirm the difficulties of the various chemical models to reproduce the pollutants behavior in the Po valley. Among others, one of the reasons must relate to the difficulties of prognostic models to reproduce the local, generally low, ventilation. The fifth Generation Mesoscale Model (MM5) [2] gives the possibility to nudge observations into the model, so that the final analysis is more consistent with reality [5]. It is generally agreed that this technique produce more accurate low-level wind field [4], but not in all cases [1]. The effect of nudging meteorological observations on simulated PM concentrations is not clearly stated in areas with strong stagnation [3]. A sensitivity study of the nudging techniques on MM5 is made here, in the attempt to improve the analysis for the low wind regime and the PM concentration.

## 81.2 Models Used and Experimental Setting

MM5 is used on two nested grids, both centered on central Po valley. The mother domain (D1) has a resolution of 18 km and covers an area of 900 × 900 km; the daughter domain (D2) has a resolution of 6 km and covers northern Italy including the Alps (an area of 580 × 420 km, Fig. 81.2). The vertical grid has 23 levels, in sigma coordinates from surface to 100 hPa. The boundaries, initial and first guess conditions are taken every 6 h form NCEP Global Tropospheric Analysis ($1^{o} \times 1^{o}$ resolution). CHIMERE is implemented on about the same domain as D2, with 6 km spatial resolution and 8 vertical levels. The emissions come from an ad-hoc POMI inventory [6] and boundary from EMEP model.

For the year 2005, in the framework of the POMI Project, data from 70 surface meteorological stations were collected. Out of these only 56 were used (marked with + sign on Fig. 81.2) whilst the remaining 14 were rejected due to their only local spatial representativeness. Radiosounding data used were collected at the stations of Payerne, Cuneo, Milano Linate, San Pietro Capofiume and Udine.

The analysis focuses on the performance of 7 sensitivity runs of MM5 with a combination of different nudging techniques (and the corresponding 7 runs of CHIMERE) as described in Table 81.1, in the period 5–31 January.

## 81.3 Results and Discussion

As seen in Fig. 81.1 the results are very encouraging on the whole domain (mean BIAS decreases by almost 50%) as well as in the single regions.

Figure 81.2 summarizes the spatial difference between the run with the nudging of all observations (gdobsfdda) and the run with only analysis nudging (nfdda).

**Table 81.1** Experimental set-up where NCEP stands for nudging of 3D NCEP analysis every 6 h 1° resolution, GD-3D stands for radiosoundings every 6–12 h (re-gridded by MM5 preprocessor Little at R with NCEP as 1st guess), GD-SFC stands for surface data every 3 h via LittleR, OBS-SFC stands for direct nudging of surface data every 1 h

| | D1 & D2 | D1 & D2 | D2 | D2 |
|---|---|---|---|---|
| Name of run | NCEP (6 h) | GD-3D (6 h) | GD-SFC (3 h) | OBS-SFC (1 h) |
| nofdda | | | | |
| nfdda | X | | | |
| 3fdda | X | X | | |
| gdfdda | X | X | X | |
| obsfdda | X | | | X |
| 3obsfdda | X | X | | X |
| gdobsfdda | X | X | X | X |

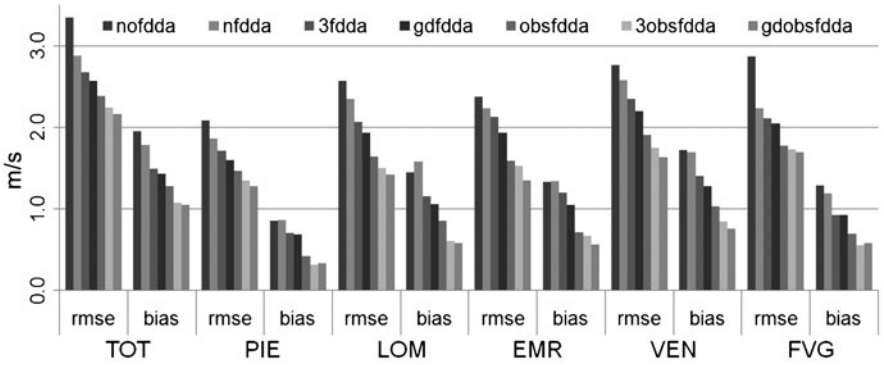


**Fig. 81.1** Statistical scores for wind speed (rmse and bias) for the 7 experiments (from *left* to *right*), for all 56 stations (*TOT*) and divided by region from West to East: Piemonte (*PIE*), Lombardia (*LOM*), Emila Romagna (*EMR*), Veneto (*VEN*), Friuli Venezia Giulia (*FVG*)

Wind speed (contours) is reduced by MM5 up to 1 m/s where the observation network is denser. Since the observed mean wind speeds for the selected period are in general around 1.5–2 m/s this shows that the nudging leads to more than 50% reduction of the surface winds. The increase in simulated PM10 concentrations produced by CHIMERE (shaded areas) is not homogeneous; in particular the effect of the reduced wind speed is more evident in central/northern Lombardy, especially in the area of Milan, and in the northern/eastern part of Veneto. On the other hand all the central/southern part of the Po valley seems not to be affected by the nudging techniques.

## 81.4 Conclusions

A set of simulations has been carried out to investigate the sensitivity of MM5 simulated wind speed and the response of CHIMERE simulated PM10 levels to different nudging techniques for meteorological observational data into MM5.

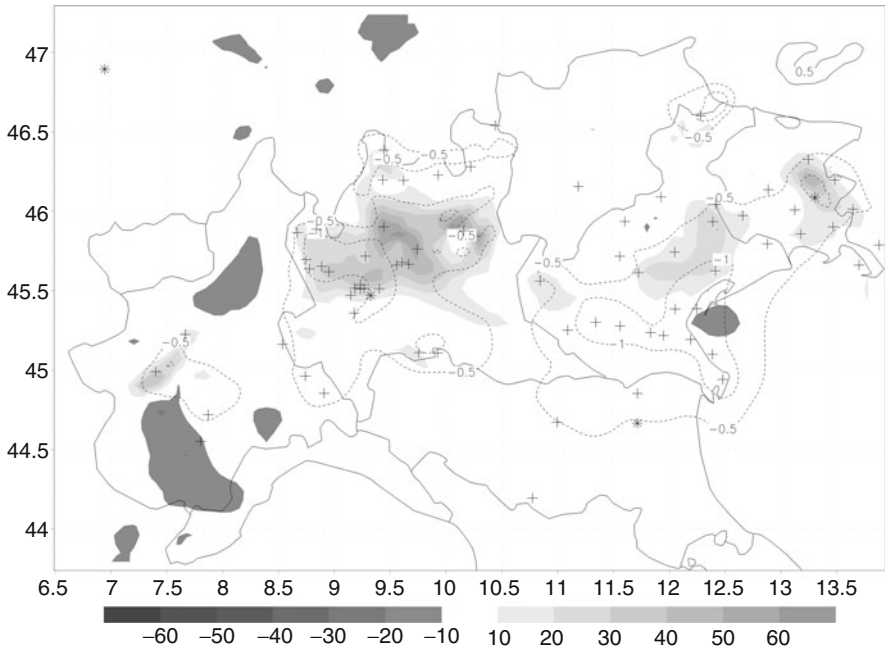


**Fig. 81.2** Difference between run gdobsfdda and nfdda for wind speed (contour in m/s, MM5) and for PM10 (*shaded areas* in percentage with respect to nfdda run, CHIMERE), first model's level (about 15 –20 m); surface meteorological stations locations are marked with +, soundings locations are marked with *

Surface wind analysis of MM5 shows a significant improvement due to nudging of observational data, whilst for PM10 the result is evident only is certain areas of the Po valley (up to 70% increase of the PM10 values in Milan area, see Fig. 81.2).

The lack of homogeneity in the variation of PM10 in the CHIMERE output will need further investigation.

## References

1. Borge R, Alexandrov V, José del Vas J, Lumbreras J, Rodríguez E (2008) A comprehensive sensitivity analysis of the WRF model for air quality applications over the Iberian Peninsula. Atmos Environ 42:8560–8574
2. Grell GA, Dudhia J, Stauffer DR (1995) A descriptionof the fifth generation Pennsylvania State/ NCARMesoscale model (MM5). National Center for Atmospheric Research, Boulder
3. Hu J, Ying Q, Chen J, Mahmud A, Zhao Z, Chen S, Kleeman MJ (2010) Particulate air quality model predictions using prognostic vs. diagnostic meteorology in central California. Atmos Environ 44:215–226
4. Stauffer DR, Seaman NL (1994) Multiscale four-dimensional data assimilation. J Appl Meteor 33:416–434

5. Stauffer DR, Seaman NL, Binkowski FS (1991) Use of four-dimensional data assimilation in a limited-area mesoscale model Part II: Effects of data assimilation within the planetary boundary layer. Mon Weather Rev 119:734–754
6. Triacchini G, Pastorello C, Gzella A, Dilara P (2009) Preparation of a spatialised emission inventory as input for modelling. In: 18th annual international emission inventory conference, Comprehensive inventories -leveraging technology and resources, EPA, Baltimore. http://www.epa.gov/ttn/chief/conference/ei18/session3/triacchini.pdf

## Questions and Answers

**Questioner Name**: Enrico Ferrero

**Q**: Does your method influence not only the mean wind but also the diffusion coefficient?

**A**: Further investigations have been carried on, showing that the variation in the vertical diffusivity in MM5 is characterized, as expected, by a decrease in the areas where wind speed is reduced (Fig. 81.3). For CHIMERE (not shown) the vertical diffusivity decreases (in correspondence to PM10 increase in Fig. 81.2) but there are also areas of increment where the wind speed is reduced. More detailed studies are needed to explain this strange behavior of vertical diffusivity in CHIMERE.

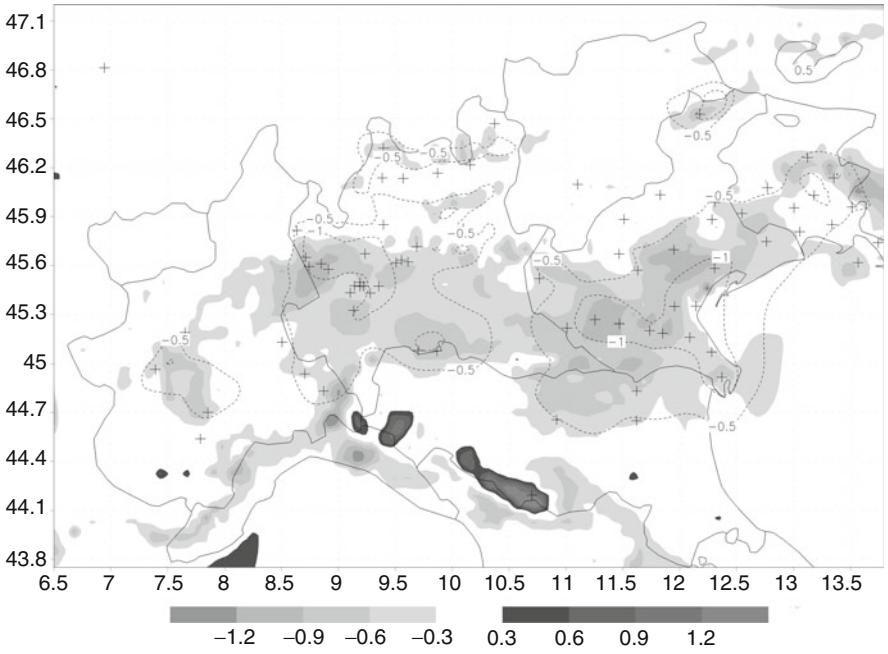


**Fig. 81.3** MM5, *shaded* is vertical diffusivity of heat ($m^2s^{-1}$) difference between the runs gdobafdda and nfdda, first model level (about 15 m). As expected vertical diffusivity decrease where wind speed (contours as in Fig. 81.2) decrease

**Questioner Name**: Elisabetta Angelino (ARPA Lombardia)

**Q**: At the beginning of the presentation you said that models underestimate by 55% PM10 concentrations (January case). The final graph compares results among different nudging test. How are they compared with the observed ones? How is the improvement in reducing underestimation?

**A**: As can be seen in Fig. 81.2 the increase in PM10 concentrations due to the decrease of wind is not uniform over the Po valley. In particular in the urban area of Milan (mean observation value for the period of 86 $\mu g/m^3$) the best result is found, with the model bias passing from 44 $\mu g/m^3$ (nfdda) to 29 $\mu g/m^3$ (gdobsfdda). However in other areas the increase in modeled PM10 concentrations with the lower wind regime is negligible.

# Chapter 82
# Modeling Air Quality over Italy with MINNI Atmospheric Modeling System: From Regional to Local Scale

**Mihaela Mircea, Gabriele Zanini, Gino Briganti, Andrea Cappelletti, Anna Pederzoli, Lina Vitali, Giandomenico Pace, Pietro Marri, Camillo Silibello, Sandro Finardi, and Giuseppe Calori**

**Abstract** This study shows part of the results obtained during the operational evaluation of MINNI atmospheric modeling system over Italy. MINNI is the Italian Integrated Assessment Modelling System for supporting the International Negotiation Process on Air Pollution and assessing Air Quality Policies at national/local level sponsored by the Italian Ministry of the Environment. The evaluation was carried out for both meteorology and air quality for the years 1999 and 2005. Changes of meteorological variables and of ozone concentrations in relation to the change of horizontal grid resolution were also investigated. The results show the capability of the modelling system to reconstruct the meteorological and ozone fields over Italy.

**Keywords** Air quality model validation • Ozone • Spatial resolution

## 82.1 Introduction

MINNI [10] is the Italian Integrated Assessment Modelling System for supporting the International Negotiation Process on Air Pollution and assessing Air Quality Policies at national/local level sponsored by the Italian Ministry of the Environment. The MINNI system is composed by an Atmospheric Modelling System (AMS) and

M. Mircea (✉) • G. Zanini • A. Pederzoli • L. Vitali • G. Pace
Italian National Agency for New Technologies, Energy and Sustainable Economic Development (ENEA) Technical Unit Models, Methods and Technologies for the Environmental Assessment (UTVALAMB), Air Quality Laboratory (AIR), Via Martiri di Monte Sole, 4, 40129 Bologna, Italy
e-mail: mihaela.mircea@enea.it; gabriele.zanini@enea.it

G. Briganti • A. Cappelletti • P. Marri
Vasco Viviani 23, 56124 Pisa, Italy

C. Silibello • S. Finardi • G. Calori
ARIANET s.r.l., Gilino, 9, 20128 Milan, Italy

D.G. Steyn and S. Trini Castelli (eds.), *Air Pollution Modeling and its Application XXI*, NATO Science for Peace and Security Series C: Environmental Security 4,
DOI 10.1007/978-94-007-1359-8_82, 

the Greenhouse Gas and Air Pollution Interactions and Synergies -Model over Italy (GAINS-Italy). The main components of AMS are the meteorological model (RAMS) and the Local Analysis and Prediction System (LAPS), for simulating the meteorological conditions, and the emission processor (EMMA) and the air quality model (FARM), for simulating the atmospheric chemistry.

This study shows part of results obtained during the operational evaluation carried out for both meteorology and air quality for the years 1999 and 2005. The simulation domain covers the Italian peninsula, including the islands: Sicily and Sardinia. The two years were simulated with two horizontal grid resolutions: 20 km $\times$ 20 km and 4 km $\times$ 4 km, the second simulations being nested in the first ones.

## 82.2 Description of AMS and of Simulations Setup

For each year, several simulations were conducted: one over the whole Italy with horizontal spatial resolution of 20 km $\times$ 20 km (IT) and five over sub-domains including respectively north of Italy (NIT), centre of Italy (CIT), south of Italy (SIT), Sardinia (SAO) and Sicily (SCO) islands with horizontal spatial resolution 4 km $\times$ 4 km.

The meteorological fields were produced with the prognostic, non-hydrostatic meteorological model RAMS [3], which was run in a 2-ways nested grid system: the outer grid covering large part of the Central Europe and the Mediterranean Sea, with a resolution of 60 km $\times$ 60 km and an inner grid including the target area for the air quality simulations and having the same horizontal resolution of 20 km $\times$ 20 km [9]. Initial and boundary conditions and data assimilation have been based on mesoscale analyses produced by mean of the RAMS pre-processor ISAN (Isentropic ANalysis) with a time frequency of 1 h. ISAN implements an optimal interpolation method based on Barnes algorithm. ECMWF analyses, available every 6 h with an horizontal space resolution of 0.5°, have been used as background fields.

The meteorological fields for the simulations on sub-domains (NIT, CIT, etc.) were downscaled from the meteorological fields predicted by RAMS at 20 km $\times$ 20 km spatial resolution by means of the diagnostic meteorological model LAPS (Local Analysis and Prediction System) [5]. The downscaling approach was chosen since it is computationally inexpensive and can provide a satisfactory representation of the local meteorology when proper meteorological observations are used.

The air quality model FARM [6] is a three-dimensional Eulerian model dealing with the transport and the multiphase chemistry of pollutants in the atmosphere. Gas-phase reactions are described by means of SAPRC-90 chemical scheme [2].

The anthropogenic emission inventory used in this study over Italy was derived from the emissions for major point sources and for the diffuse sources at provincial level provided by national emission inventories ([4]). These emissions are classified according to activity level CORINAIR/SNAP (CO-oRdinated INformation on the Environment in the European Community AIR/Simplified Nomenclature for Air Pollution). EMEP emission inventories for years 1999 and 2005 have been employed to describe the anthropogenic sources located in other countries included

in the computational domain. The biogenic emissions had also two sources: APAT 2000 over Italy and a global database for the other countries. The emissions fields also include the maritime activities, the ship emissions on the national and international sources and the port areas. The diffuse emissions and the minor point sources are distributed in the lowest model layers of FARM (below 50 m) with 80% in the first 20 m above ground. The point sources such as industries, power plants, volcanoes, etc., are treated individually in FARM, considering the plume rise effect.

The anthropogenic emission used for NIT, CIT and SIT simulations are based on a version of the national inventory scaled down to municipalities using a set of proxies. The EMEP model concentration fields at 50 km horizontal resolution provided the initial and boundary conditions for IT simulation, while NIT and CIT simulations were nested into IT grid. The same biogenic emissions were used in all simulations.

## 82.3 Results

### *82.3.1 Analysis of Meteorology at Regional and Local Scale*

Several meteorological analysis has been carried for both years over different regions. Here, the results obtained for 2005 over the area of Friuli Venezia Giulia, an Italian region located at the North-Eastern bounds of Italy are shown.

Figure 82.1 shows comparison between modelled and observed data for wind speed, temperature and relative humidity. IOA values, calculated from whole hourly

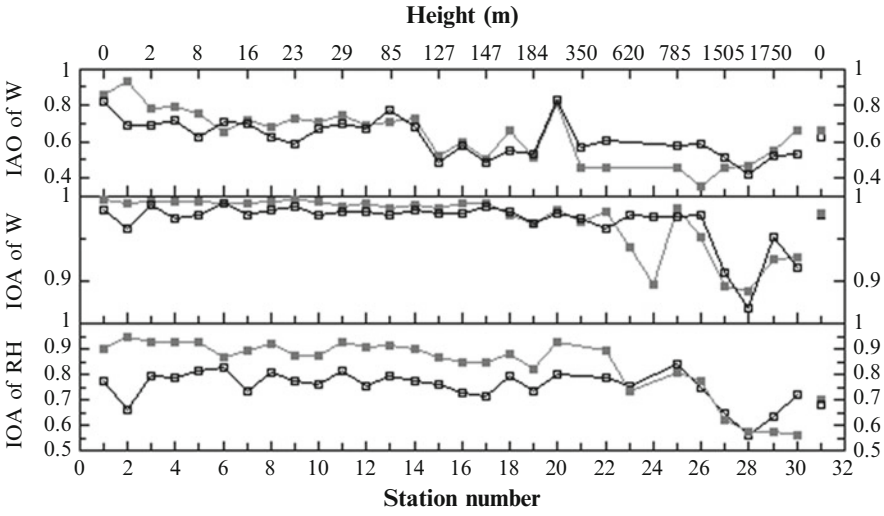


**Fig. 82.1** Poor performances over mountain areas were expected from a diagnostic modelling approach based on a limited resolution input measurements network insufficient to resolve topographic features, as it shown by similar results reported in literature

data of the year, are shown for all the available stations, ordered by increasing height a.s.l. Values of IOA very close to 1 are obtained for stations sited at coastal and internal plain locations, in particular for temperature and humidity analysis. It is worth noting that LAPS humidity fields are largely improved with respect to RAMS ones at heights lower than 500 m a.s.l., while model performances deteriorate for all variables at higher altitudes for both RAMS and LAPS data. Moreover, LAPS analyses do not improve RAMS fields at mountain stations. The data used to verify the meteorological fields reliability were provided by the regional meteorological network, managed by ARPA Friuli Venezia Giulia and were not used in LAPS analyses.

### *82.3.2 Analysis of Air Quality at Regional and Local Scale*

This section show some results from the model operational evaluation with ozone measurements from two databases: BRACE for 1999 and AirBase v3 for 2005. Figure 82.2 shows the simulated and measured hourly ozone concentrations as a function of time for July, for both years, at two background stations: urban (Quarto) and rural (Gambara). The simulations were performed with 20 km $\times$ 20 km and 4 km $\times$ 4 km spatial resolution. The figures show that the maximum hourly ozone concentrations and the daily ozone cycle are relatively well reproduced at rural station. Similar results but for more stations were shown in [1]. The increase of spatial resolution determines overall a decrease of simulated maximum ozone concentrations and an improvement of the agreement with observations for 2005, at rural station. For the year 1999, at Gambara station, the simulation with finer resolution captures better the maximum ozone concentrations on 15, 16 and 17 July 1999.

Figures 82.3 and 82.4 show the mean normalized bias error (MNBE) and mean absolute normalised gross error (MANGE) for 1999 and 2005, respectively. Only results for the northern part of Italy are shown. It can be noted that the model scores generally meets the US-EPA [7,8] criteria: MNBE is lower than 15% and MANGE is lower than 30–35%. Also, it can be noted that the increase of spatial resolution affect more MNBE than MANGE. For example, the increase of resolution lead to an increase of MNBE at Juvara station in 2005 and to a decrease at Margherita station, but MANGE does not vary.

## 82.4 Conclusions

This study shows that AMS of MINNI project is able to simulate well the meteorological parameters and ozone concentrations. LAPS improves the prediction of meteorological variables in the plains, reproduces better the temperature diurnal cycle by correcting RAMS nocturnal overestimation, and, thus, leads to a relevant improvement for humidity predictions. The daily ozone cycle and the maximum hourly ozone

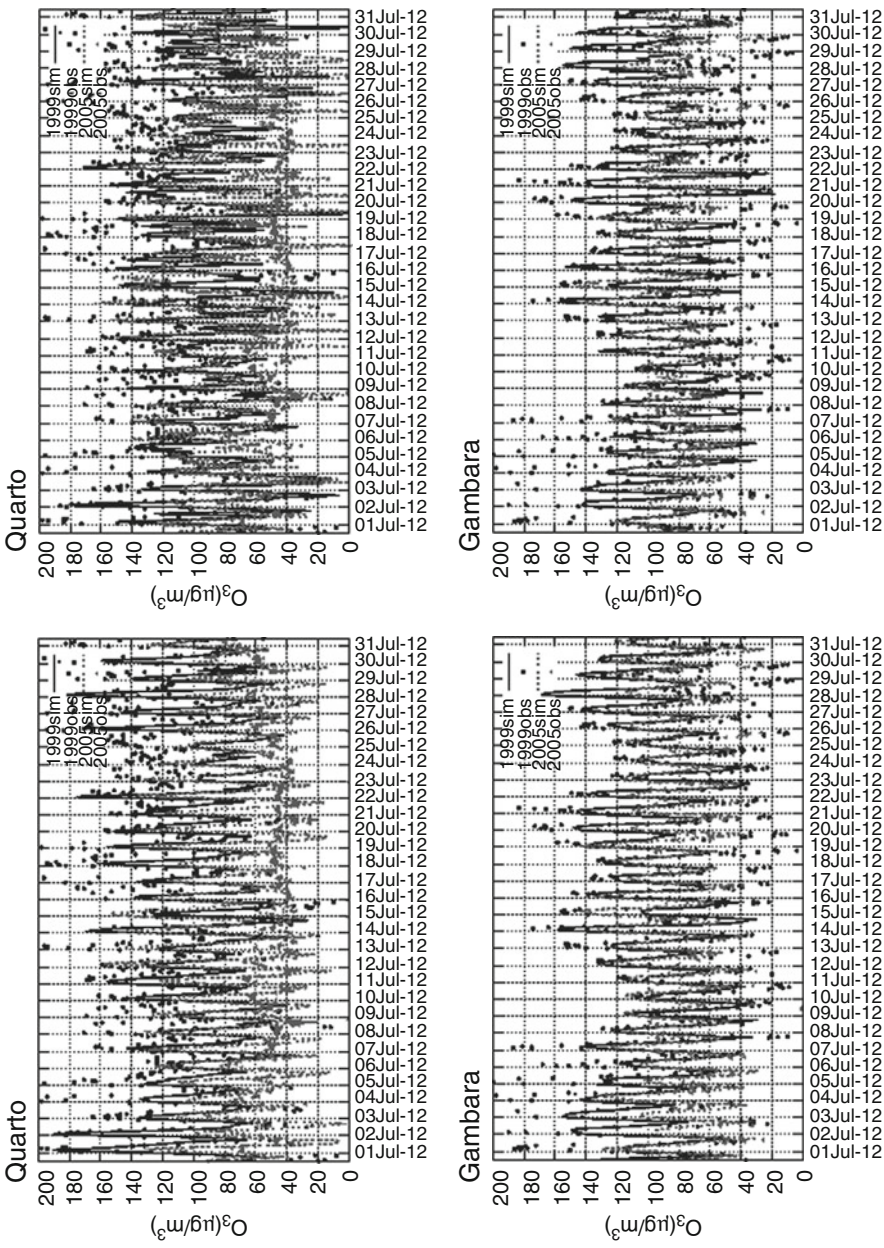


**Fig. 82.2** Hourly ozone concentrations measured (*dots*) and simulated (*lines*) for 1999 and 2005 at an background urban (Quarto) and at a background rural (Gambara) monitoring stations

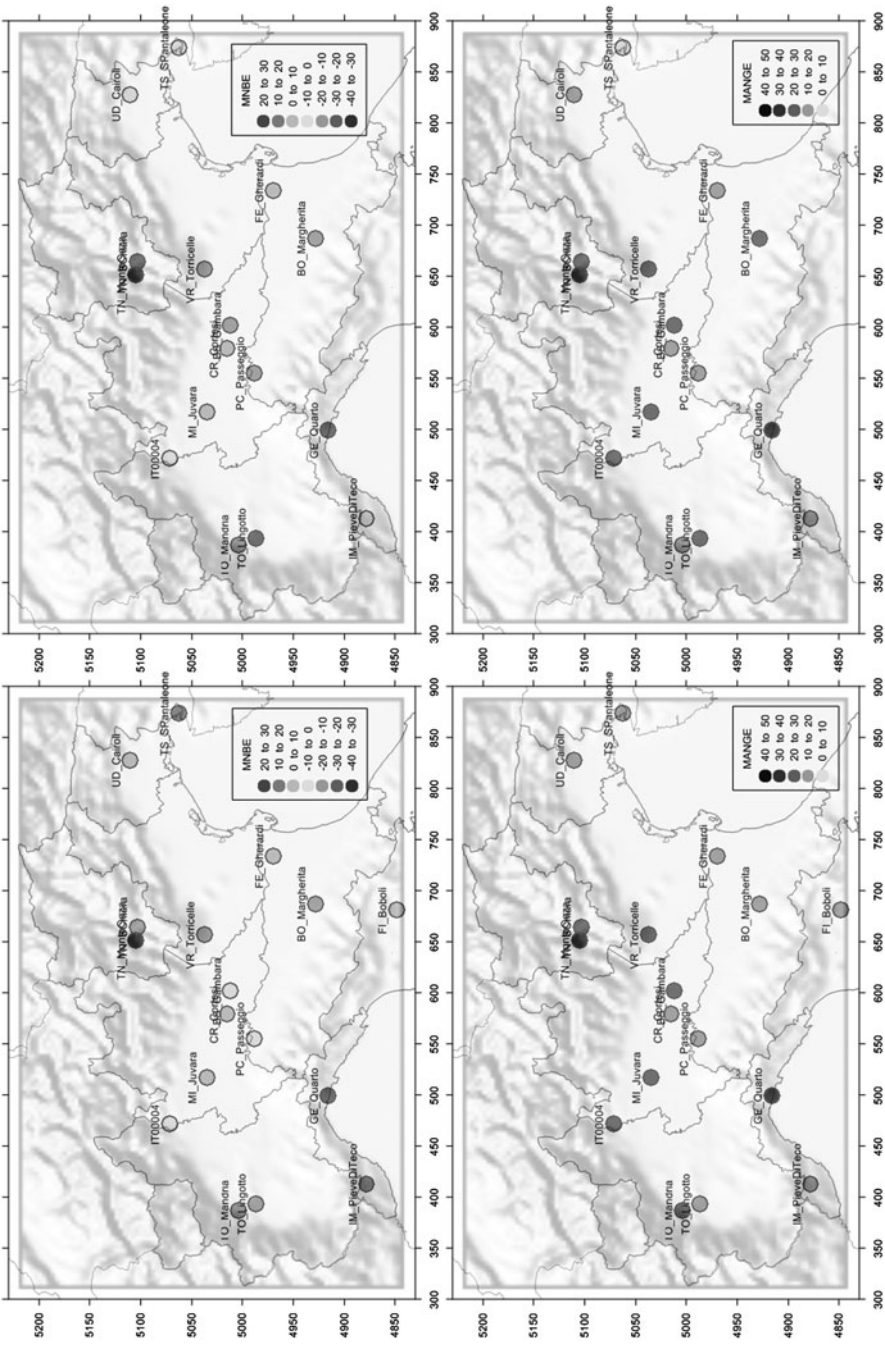


**Fig. 82.3** Statistical scores, MNBE (*upper*) and MANGE (*lower*), for the year 1999, for the simulations with 20 km × 20 km (*left*) and 4 km × 4 km (*right*) spatial resolutions

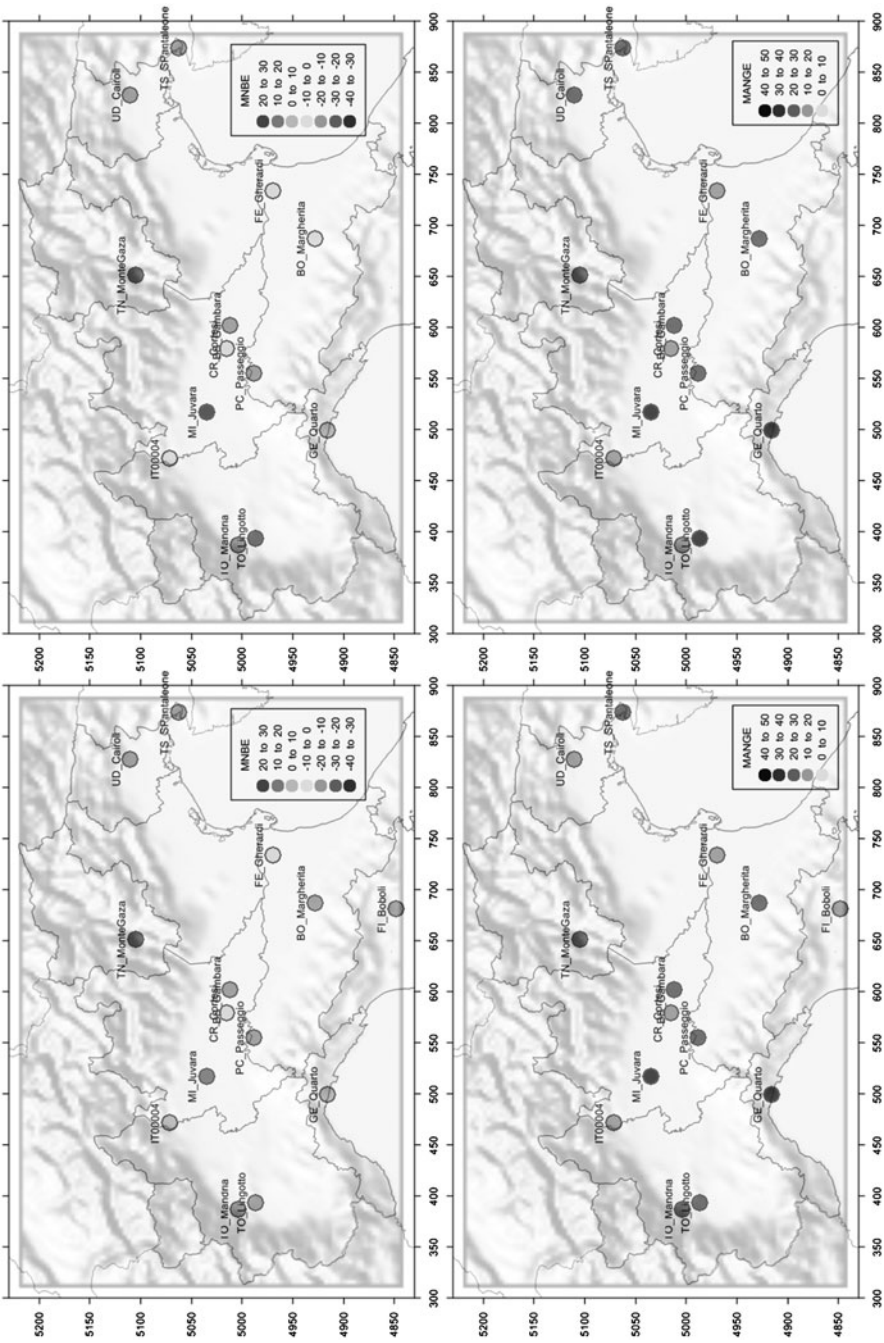


**Fig. 82.4** Statistical scores, MNBE (*upper*) and MANGE (*lower*), for the year 2005, for the simulations with 20 km × 20 km (*left*) and 4 km × 4 km (*right*) spatial resolutions

concentrations are also well reproduced by. The statistical indicators show good model performance according to US-EPA criteria. While it is obvious that finer grid resolutions are able to better resolve inhomogeneities in emission rates, land cover and dispersion, no systematic improvement of calculated statistical indicators is observed. However, the comparison of model results with observations shows that finer resolution grids can improve model predictions for some particular days.

**Acknowledgments** This work is part of the MINNI project, funded by the Italian Ministry for Environment and Territory and Sea and carried out by ENEA. The authors thank the Regional Center of Environmental Modelling of ARPA Friuli Venezia Giulia, which provided the meteorological measurements.

## References

1. Briganti G et al (2010) Testing the capability of the MINNI atmospheric modeling system. In: HARMO13 proceedings, Paris, 1–4 June 2010, pp 161–165. ISBN: 2-8681-5062-4
2. Carter WPL (1990) A detailed mechanism for gas-phase atmospheric reactions of organic compounds. Atmos Environ 24A:481–518
3. Cotton WR et al (2003) RAMS 2001 current status and future directions. Meteo Atmos Phys 82:5–29
4. ISPRA (2000, 2005) http://www.sinanet.apat.it/it/inventaria
5. McGinley JA et al (1991) Validation of a composite convective index as defined by a real-time local analysis system. Weather Forecast 6:337–356
6. Silibello C et al (2008) Modelling of PM10 concentrations over Milano urban area using two aerosol modules. Environ Model Softw 23:333–343
7. U.S. Environmental Protection Agency (1991) EPA report EPA-540/4-91-013, 98 pp
8. U.S. Environmental Protection Agency (2005) EPA report EPA-454/R-05-002, 128 pp
9. Vitali L et al (2010) Validation of simulated atmospheric. In: HARMO13 HARMO13, Paris, 1–4 June 2010, pp 609–613. ISBN: 2-8681-5062-4
10. Zanini G et al (2005) The MINNI project: an integrated assessment modeling system for policy making. MODSIM 2005, Melbourne, 12–15 Dec 2005, pp 2005–2011. ISBN: 0-9758400-2-9

## Questions and Answers

**Questioner Name**: Stavros Solomos

**Q**: What kind of data were used for the LAPS 4 km × 4 km system?

**A**: For LAPS analysis we used WMO surface observations, retrieved from ECMWF archives.

# Chapter 83
# Evaluation of Vertical Profiles in Mesoscale Meteorological Models Based on Observations for the COST728 Study of Winter 2003 PM Episodes in Europe

**Sven-Erik Gryning, Ekaterina Batchvarova, Markus Quante, and Volker Matthias**

**Abstract** An important new emphasis in meteorological models evaluation is the thorough discussion of vertical profiles of meteorological parameters. This discussion contributes to the understanding of why different mesometeorological models calculate quite different wind and temperature profiles and atmospheric boundary layer heights (even when using the same method) while all show good agreement between simulated and measured surface data. The wind, temperature and turbulence profiles influence significantly the transport and diffusion of pollutants in the air. The calculations of a number of crucial parameters in air quality models, such as deposition and biogenic emissions, also depend on meteorological parameters. The availability of 3D measured wind fields provided by wind profile radars and lidars give a new challenge for such studies. The 3D model to measurements comparisons should consider new performance statistics. This study presents few examples from the COST 728 intercomparison exercise for the winter of 2003 in Europe.

**Keywords** Atmospheric boundary-layer • Methods for model evaluation • Vertical profiles • Flux measurements • Wind profiler • Natural variability

S.-E. Gryning (✉)
National Laboratory for Sustainable Energy, RISØ DTU, Roskilde, Denmark
e-mail: sveg@risoe.dtu.dk

E. Batchvarova
National Laboratory for Sustainable Energy, RISØ DTU, Roskilde, Denmark

National Institute of Meteorology and Hydrology, Sofia, Bulgaria

M. Quante • V. Matthias
Helmholtz-Zentrum Geesthacht, Geesthacht, Germany

D.G. Steyn and S. Trini Castelli (eds.), *Air Pollution Modeling and its Application XXI*,
NATO Science for Peace and Security Series C: Environmental Security 4,
DOI 10.1007/978-94-007-1359-8_83, 

## 83.1 Introduction

Several model comparison and evaluation exercises were carried out as part of the COST 728 action (Enhancing Mesoscale Meteorological Modelling Capabilities for Air Pollution and Dispersion Applications).

One of the cases covers Central and Northern Europe in February and March 2003, when several PM10 episodes were observed. Stern et al. [4] showed that the predictions of several models differed widely.

In this study we compare model results and measurements of meteorological parameters for Lindenberg for the period of the episode. Specific runs with the same boundary conditions were performed with several models and profile output data were stored. Here we present GKSS MM5 and GKSS Cosmo modeling results.

## 83.2 Wind Profiler Data

Wind profiler data were provided for this comparison from Lindenberg. The comparisons of modelled and measured wind profiles showed significant spread.

Wind profiler data are very useful for the evaluation of meteorological models. Among other results, a study of the wind speed spectra was performed at different heights [2]. Modelled (GKSS MM5, 54 km resolution and GKSS CLM-Cosmo, 54 km resolution) and measured wind spectra based on hourly data at about 500 m height are presented in Fig. 83.1.

The spectra comparison shows that the models remove significantly the short time variability of meteorological parameters. In this case the resolution is very

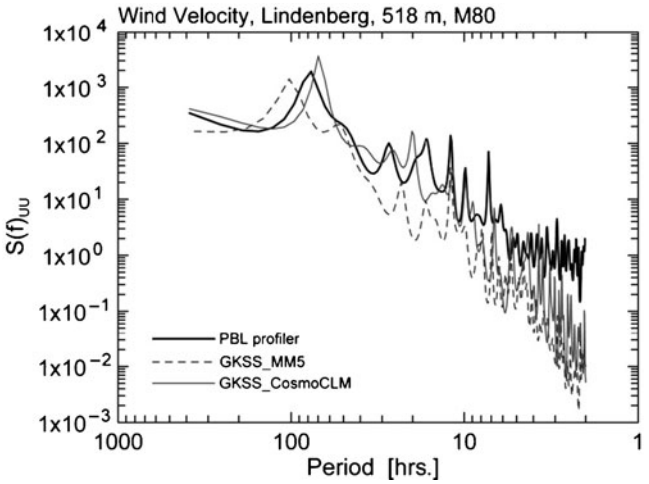


**Fig. 83.1** Power spectra of wind at about 500 m height at Lindenberg during the case study

coarse, but the feature is observed also at less than 5 km resolution of the model although the difference is smaller. From a number of comparisons performed in the study it can be concluded that the effective resolution of a mesoscale meteorological model is considerable larger than 4 times the grid resolution used.

## 83.3 Natural Variability

The natural variability (representativeness) in the measurements depend not only on the state of the atmosphere but also on the averaging time of the measurements. Here we evaluate the performance of a model by assuming that the model prediction of a given parameter represents the average (representative) value. Then the uncertainty due to the natural variability of the measurements is added as error bars on the results from the model simulation. The actual measurement represents one realization only; if the measurement is inside the error bar then it is within the expected natural variability of the model prediction.

In this paper we take the surface sensible heat flux as an example – but the method is applicable for other parameters as well [1].

An applied method proposed by Sreenivasan et al. [3] to determine the standard deviation of the sensible heat flux for a given averaging time is used:

$$\sigma_{\overline{w'\theta'},T} = 8 \sqrt{\frac{z}{Tu}} \overline{w'\theta'} \tag{83.1}$$

It can be seen that the standard deviation $\sigma_{\overline{w'\theta'},T}$ increases with height and sensible heat flux and it decreases with averaging time and wind speed. The method is illustrated for wind speed at different heights by Batchvarova and Gryning [1].

## 83.4 Mast Measurements and Models

Meteorological measurements from the Falkenberg site of Richard Assmann Observatorium near Lindenberg, Germany, have been used. The site is flat and covered with grass.In the study of the representativeness measurements of turbulent fluxes carried out with a sonic anemometer at a 12 m tall meteorological mast are used.

Cosmo and MM5 simulations performed at GKSS (now called Helmholtz-Zentrum Geestacht) are compared with measurements of surface heat flux on 24th February 2003. For MM5 simulations, the measurements fall inside the natural variability bars for very short intervals in the morning and the afternoon, Fig. 83.2 left panel. For the GKSS Cosmo simulations the heat fluxes are always lower than the measurements even when considering the natural variability, Fig. 83.2, right panel.

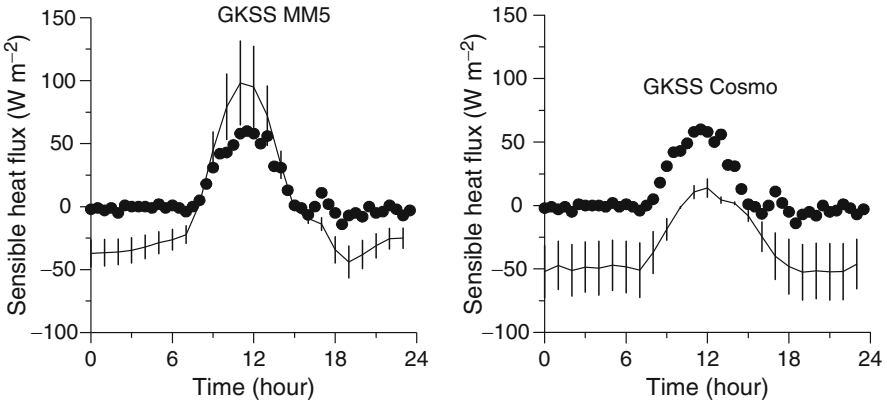


**Fig. 83.2** Sensible heat flux near the surface for 24th February 2003 at Lindenberg; *bullets* denote measurements, *full line* – model results, and *bars* show the natural variability

It should be emphasized that the present study deals with measurements from only one day which is considered too short a period to draw general conclusion on the behavior of the models.

## 83.5 Concluding Remarks

- Progress in model developments is based on comparison with data.
- It is essential to evaluate the models on profile measurements, not just traditional surface measurements.
- The natural variability of the meteorological parameters should be taken into account in any model evaluation against measurements.
- The variability is a function of the length scale of turbulence (height in the surface layer) and averaging time of the measurements.
- A good model performance does not require exact match with data.
- In other words a model cannot be improved if the measurements fall within the statistical range defined by the variability.
- Wind profiler data can be used for model evaluation.

**Acknowledgments** The data from Lindenberg are provided through the CEOP/GEWEX BALTEX (Baltic Sea Experiment) database and it is a pleasure to acknowledge the Deutscher Wetterdienst (DWD) – Meteorologisches Observatorium Lindenberg/ Richard Assmann Observatorium who originally provided the measurements for the data base. The study is supported by the Danish Council for Strategic Research, Sagsnr 2104-08-0025 and the EU FP7 Marie Curie Fellowship PIEF-GA-2009-237471-VSABLA. The work is part of collaboration within COST 728 - A. Aulinger, C. Chemel, G. Geertsema, B. Geyer, H. Jakobs, A. Kerschbaumer, M. Prank, R. San José, H. Schlünzen, J. Struzewska, B. Szintai, R. Wolke have participated in the discussions on this intercomparison exercise.

## References

1. Batchvarova E, Gryning S-E (2010) The ability of mesoscale meteorological models to predict the vertical profiles of meteorological parameters. In: Steyn DG, Rao ST (eds) Air pollution modeling and its application XX, vol 103. Springer, Dordrecht, pp 379–383
2. Quante M, Matthias V, Gryning S.-E, Batchvarova E, Aulinger A, Chemel C, Geertsema G, Geyer B, Jakobs H, Kerschbaumer A, Frank M, San José R, Schlünzen H, Struzewska J, Szintai B, Wolke R (2009) Using windprofiler data in time and frequency domain for the evaluation of meteorological drivers employed in chemistry transport modeling. In: Apituley A, Russchenberg HWJ, Monna WAA (eds) 8th International symposium on tropospheric profiling. Delft (NL), 18–23 Oct 2009. RIVM, Delft, 2009. S07-006-1-S07-006-4 p. Type: Conference paper published in book/proceeding
3. Sreenivasan KR, Chambers AJ, Antonia RA (1978) Accuracy of moments of velocity and scalar fluctuations in the atmospheric surface layer. Bound-Lay Meteorol 14:341–359
4. Stern R, Builtjes P, Schaap M, Timmermans R, Vautard R, Hodzic A, Memmesheimer M, Feldmann H, Renner E, Wolke R, Kerschbaumer A (2008) A model inter-comparison study focussing on episodes with elevated PM10 concentrations. Atmos Environ 42:4567–4588

## Questions and Answers

**Questioner Name**: Enrico Ferrero

**Q**: In the comparison between model and wind profiler data, you show the results at about the top of the boundary layer. Does the poor agreement mean that the problem of models is not only due to the parameterization of the boundary layer?

**A**: Based on profiler and radiosonde data we can evaluate the model performance within the boundary layer, the entrainment zone and the free atmosphere. The degree at which the boundary-layer parameterization influences the model results at higher altitudes is a topic for further investigations.

# Chapter 84
# Performance Summary of the 2006 Community Multiscale Air Quality (CMAQ) Simulation for the AQMEII Project: North American Application

**K. Wyat Appel, Shawn Roselle, George Pouliot, Brian Eder, Thomas Pierce, Rohit Mathur, Kenneth Schere, Stefano Galmarini, and S.T. Rao**

**Abstract** The CMAQ modeling system has been used to simulate the CONUS using 12-km by 12-km horizontal grid spacing for the entire year of 2006 as part of the Air Quality Model Evaluation International Initiative (AQMEII). The operational model performance for $O_3$ and $PM_{2.5}$ for the simulation was assessed. The model underestimates $O_3$ mixing ratios in the winter, which is likely due to low $O_3$ mixing ratios in the middle and lower troposphere from the lateral boundary conditions. $PM_{2.5}$ performance varies seasonally and geographically, with $PM_{2.5}$ overestimated in the winter and fall, while performance in the spring and summer is generally good, especially in the summer. $PM_{2.5}$ concentrations are systematically higher in the AQMEII CMAQ simulation than in previous CMAQ simulations, primarily due to higher concentrations of TC and unspeciated $PM_{2.5}$ mass, which may also be due to differences in the lateral boundary conditions.

**Keywords** CMAQ • Ozone • Particulate matter • Air quality modeling • Model evaluation

## 84.1 Introduction

The Air Quality Model Evaluation International Initiative (AQMEII) is a model evaluation project involving numerous research groups from North American and Europe with the goal of advancing the way regional scale air quality modeling

K.W. Appel (✉) • S. Roselle • G. Pouliot • B. Eder • T. Pierce • R. Mathur • K. Schere • S.T. Rao
Atmospheric Modeling and Analysis Division, National Exposure Research Laboratory, U.S. Environmental Protection Agency, Research Triangle Park, NC, USA
e-mail: appel.wyat@epa.gov

S. Galmarini
Joint Research Center (JRC), Institute for Environment and Sustainability, Ispra, Italy

D.G. Steyn and S. Trini Castelli (eds.), *Air Pollution Modeling and its Application XXI*, NATO Science for Peace and Security Series C: Environmental Security 4,
DOI 10.1007/978-94-007-1359-8_84, 

systems are evaluated. As part of the AQMEII project, the Atmospheric Modeling and Analysis Division (AMAD) of the U.S. Environmental Protection Agency (USEPA) has performed an annual 2006 Community Multiscale Air Quality (CMAQ; [4]) simulation for the continental U.S. (CONUS).

The CMAQ simulation performed for this project is unique compared to previous CMAQ simulations performed by AMAD in the past for several reasons. First, the simulation was performed over a single domain that covers the entire CONUS and a large portion of Canada using 12-km by 12-km horizontal grid spacing. In the past, two separate simulations covering the eastern and western U.S. have been used instead of single, continuous domain. Second, the simulation utilizes meteorology provided by the latest version of the Weather Research and Forecasting (WRF) model, whereas previous CMAQ annual simulations have typically utilized meteorology provided by the 5$^{th}$ Generation Mesoscale Model (MM5; [3]). Finally, the CMAQ simulation utilizes boundary conditions provided by the Global and regional Earth-system Monitoring using Satellite and in-situ data (GEMS) product.

## 84.2 Data

### *84.2.1 Model Inputs and Configuration*

The CMAQ model requires gridded meteorological and emissions data to simulate the formation, transport and fate of numerous atmospheric pollutants, including ozone ($O_3$) and fine particulate matter ($PM_{2.5}$). Meteorological data for the simulation are provided by the Weather Research and Forecast (WRF) model with a domain covering the CONUS and portions of Canada and Mexico using 12-km by 12-km horizontal grid spacing and 34-vertical layers extending up to 50 hPa. Boundary conditions for the WRF simulation were provided by the North American Model (NAM). Outputs from the WRF simulation were preprocessed for input in the CMAQ model using v3.6 of the Meteorology-Chemistry Interface Processor (MCIP).

The emission dataset used for the AQMEII modeling was based on a 12-km national U.S. domain with speciation for the CB05 mechanism. The emission inventory and ancillary files were based on the 2005 emission modeling platform (http://www.epa.gov/ttn/chief/emch/index.html#2005). The fire emissions were based on 2006 daily fire estimates using the Hazard Mapping System Fire detections and Sonoma Technology SMARTFIRE system. Continuous Emission Monitoring (CEM) data from 2006 was used for the Electric Generating Units (EGU) sector. Plume rise was calculated within the CMAQ model. Temporal allocation was done monthly for each day of the week with all holidays ignored. Emissions were preprocessed for the CMAQ model using the Sparse Matrix Operator Kernel Emissions (SMOKE).

The CMAQ model simulation utilized version 4.7.1 of the model [4] with 34 vertical layers and 12-km by 12-km horizontal grid spacing covering the CONUS, southern Canada and northern Mexico. The CB05 chemical mechanism and AERO5 aerosol module were also used. Boundary conditions for the CMAQ simulation were provided by the GEMS product, which combines modeled data and observations (surface and satellite) to provide data for meteorology and atmospheric gases including greenhouse gases, global reactive gases and global aerosols.

### *84.2.2 Observed Data*

The observed data used to assess the CMAQ model estimates are obtained from several observational networks available across the U.S. that measure a combination of gas, aerosol, dry and wet deposition and meteorological variables. The primary source of ground level ozone ($O_3$) and federal reference method (FRM) daily average $PM_{2.5}$ mass measurements is the EPA's Air Quality System (AQS). The $O_3$ and $PM_{2.5}$ networks in AQS are geographically diverse and span the entire U.S. and are an excellent source of quality assured air quality measurements. Assessment of the model performance was accomplished using the Atmospheric Model Evaluation Tool (AMET; [1]), which can perform a vast number of different analyses and produce many different plots useful for assessing model performance.

## 84.3 Results

### *84.3.1 Ozone*

Operational model performance was generally consistent with previous CMAQ simulations performed for the same time period, with several notable exceptions. Performance of maximum 8-h average $O_3$ for the eastern U.S. (east of 110°W longitude) in the winter (January–March) underperformed previous CMAQ simulations, with the simulation demonstrating a large underestimation of $O_3$ in the winter. The underestimation was largest in the Northeast and Great Lakes regions of the U.S., with smaller underestimations in the southern U.S. This is a significant deviation from previous CMAQ simulations for the same time period, where $O_3$ performance was generally good and not significantly underestimated. Figure 84.1 presents a time series comparison of results from the CMAQ simulation using WRF/GEMS data with those from a previous CMAQ simulation for the same time period that utilized GEOS-CHEM model generated boundary conditions and MM5 meteorology.

The large underestimation of $O_3$ in the current simulation that was not present in previous CMAQ model simulations is likely due to several differences between the

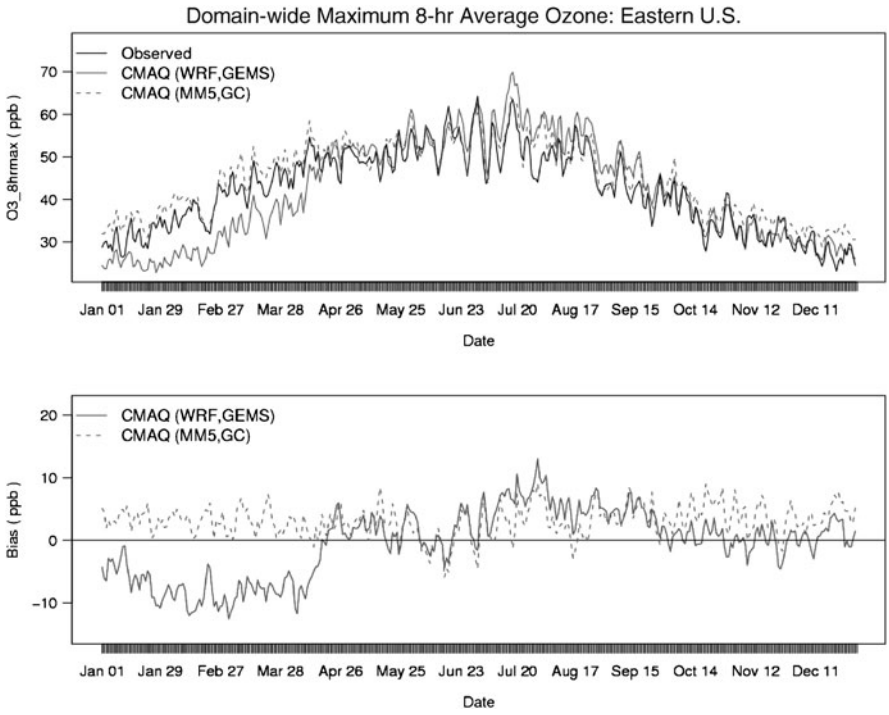


**Fig. 84.1** Time series of maximum 8-h average ozone (ppb; *top*) for AQS observed (*black*), CMAQ using WRF and GEMS data (*solid grey*) and CMAQ using MM5 and GEOS-Chem data (*dashed grey*). The *bottom* time series plot shows the corresponding bias (ppb) for each simulation

current simulation and previous simulations. First, the boundary conditions used in previous CMAQ model simulations of 2006 used were provided by the GEOS-CHEM model, unlike the current simulation which utilizes boundary conditions provided by GEMS. Estimates of $O_3$ mixing ratios in the mid to lower troposphere are much higher in the GEOS-CHEM boundary conditions than in the GEMS boundary conditions. It is likely that the lower $O_3$ mixing ratios in the troposphere in the GEMS boundary conditions result in lower ground-level $O_3$ mixing ratios, particularly in the winter when the $O_3$ provided from the boundaries comprises a significant portion of the CMAQ estimated ground-level $O_3$.

The CMAQ model estimates of maximum 8-h average $O_3$ for the rest of the year are relatively good overall, with similar performance to previous CMAQ model simulations (Fig. 84.1). The CMAQ model typically overestimates $O_3$ mixing ratios from approximately 20 ppbV to 50 ppbV and underestimates the very highest $O_3$ mixing ratios. During the summer (June through August), $O_3$ mixing ratios are significantly overestimated in the lower mid-western U.S. The exact cause of the overestimation in that region is still under investigation; however it may be related to several large $NO_x$ point sources in that region.

### 84.3.2 Particulate Matter

For the winter, $PM_{2.5}$ is typically overestimated in the eastern U.S., while in the spring (March–May) the model still overestimates $PM_{2.5}$ but to a lesser extent than in the winter (Fig. 84.2). For the summer, CMAQ estimated $PM_{2.5}$ concentrations generally compare well with observations in the eastern U.S. This is a significant improvement over previous CMAQ model simulations for the same time period, where $PM_{2.5}$ was underestimated across the entire eastern U.S. In the fall (September–November), $PM_{2.5}$ is once again overestimated in both the eastern and western U.S., with worse performance than previous CMAQ simulations for the same time period.

The CMAQ model estimated $PM_{2.5}$ is higher in all seasons and regions in the current simulation compared to previous simulations. The primary source of the higher $PM_{2.5}$ concentrations in CMAQ is higher concentrations of EC and OC (herein referred to as TC) and higher concentrations of unspeciated particulate matter ($PM_{other}$). The higher TC and $PM_{other}$ concentrations in the current simulation are likely due to differences in both the meteorology and boundary conditions used. Previous studies have shown that CMAQ estimated $PM_{2.5}$ concentrations are higher in simulations using WRF meteorology as compared to MM5 driven CMAQ simulations [2].

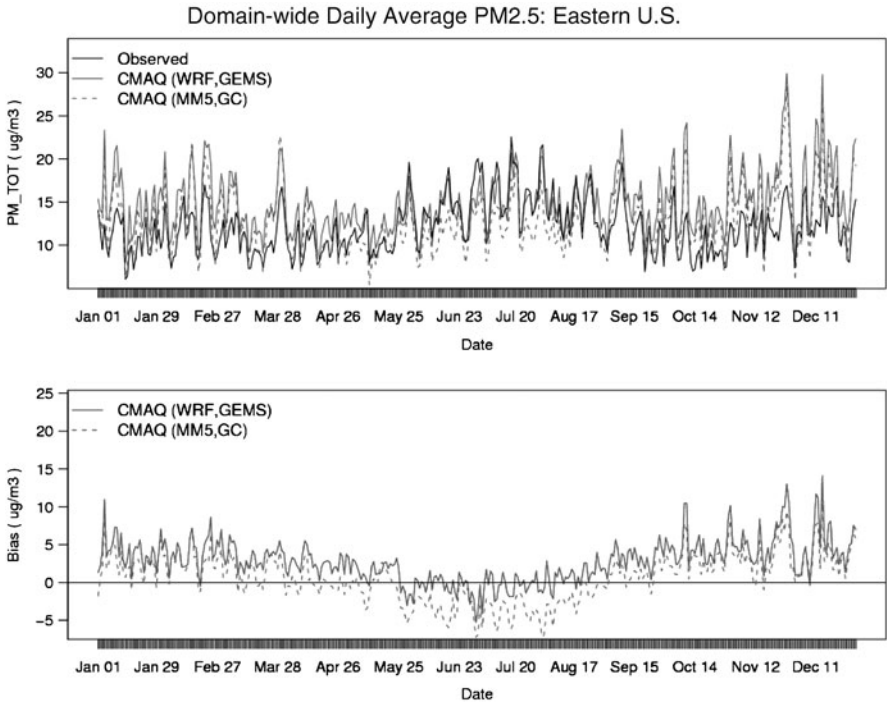


**Fig. 84.2** Time series of daily average $PM_{2.5}$ ($\mu g/m^3$; *top*) for observed (*solid black*), CMAQ using WRF and GEMS data (*solid grey*) and CMAQ using MM5 and GEOS-Chem data (*dashed grey*). The *bottom* time series plot shows the corresponding bias ($\mu g/m^3$) for each simulation

The GEMS boundary conditions used are year-specific and capture large sources of TC and $PM_{other}$ (e.g. wildfires), particularly during the summer and fall periods as detected by satellite sensors. Previous CMAQ simulations for the same period utilized climatological boundary conditions, which would not have captured wildfire events. The result is systematically higher total $PM_{2.5}$ mass throughout the year, which results in improved comparisons to observations when $PM_{2.5}$ is underestimated and degraded performance when $PM_{2.5}$ is overestimated.

## 84.4 Conclusions

The CMAQ modeling system has been used to simulate the CONUS using 12-km by 12-km horizontal grid spacing for the entire year of 2006. The operational model performance for $O_3$ varies seasonally, with the model largely underestimating $O_3$ mixing ratios in the winter. Performance for the other seasons is generally good, with the model overestimating $O_3$ mixing ratios at low observed levels and underestimating $O_3$ mixing ratios at high levels. The underestimation of $O_3$ mixing ratios in the winter represents a significant departure from previous CMAQ simulations, which generally showed little winter bias. It is believed that lower $O_3$ mixing ratios in the middle and lower troposphere from the GEMS generated boundary conditions as compared to GEOS-CHEM generated boundary conditions are primarily responsible for the lower ground-level $O_3$ mixing ratios.

As with $O_3$, $PM_{2.5}$ performance varies seasonally and geographically, with $PM_{2.5}$ overestimated in the winter and fall, while performance in the spring and summer is generally good, especially in the summer. $PM_{2.5}$ concentrations are higher in the current simulation than in past simulations, primarily due to higher concentrations of TC. The higher TC concentrations are due to differences in the WRF meteorology versus MM5 (winter) and higher concentrations coming in from the GEMS generated boundary conditions (summer).

## References

1. Appel KW, Gilliam RC, Davis N, Zubrow A, Howard SC (2011) Overview of the Atmospheric Model Evaluation Tool (AMET) v1.1 for evaluating meteorological and air quality models. Environ Modell Softw 26(4):434–443
2. Appel KW, Roselle SJ, Gilliam RC, Pleim JE (2010) Sensitivity of the community multiscale air quality (CMAQ) model v4.7 results for the eastern United States to MM5 and WRF meteorological drivers. Geosci Model Dev 3:169–188
3. Grell GA, Dudhia AJ, Stauffer DR (1994) A description of the Fifth-Generation PennState/NCAR Mesoscale Model (MM5). NCAR technical note NCAR/TN-398 + STR. Available at http://www.mmm.ucar.edu/mm5/doc1.html

4. Foley KM, Roselle SJ, Appel KW, Bhave PV, Pleim JE, Otte TL, Mathur R, Sarwar G, Young JO, Gilliam RC, Nolte CG, Kelly JT, Gilliland AB, Bash JO (2010) Incremental testing of the community multiscale air quality (CMAQ) modeling system version 4.7. Geosci Model Dev 3:205–226

## Questions and Answers

**Questioner Name**: Henk Eskes

**Q**: Does the capping of ozone in the stratosphere influence radiation and reaction rates in the troposphere?

**A**: No, the capping of ozone in the upper troposphere and stratosphere in these simulations has no impact on the radiation or reactions rates in the model.

**Questioner Name**: Jaako Kukkonen

**Q**: There are some PM2.5 source categories that are poorly known, such as residential combustion and non-exhaust vehicular sources. How did you allow for those sources? The residential combustion emissions have a substantial seasonal variation, which could potentially have an influence on the agreement of predictions and data seasonally?

**A**: These emissions sources are included in the emission inventory used in the simulations. The seasonable variability in residential combustion is accounted for in the emissions inventory.

# Chapter 85
# Comparative Evaluation of Model Simulations of Regional Ozone and Particulate Matters for Two Distinct Summers over Eastern North America

**Wanmin Gong, Junhua Zhang, Paul A. Makar, Michael D. Moran, Craig Stroud, Sylvie Gravel, Sunling Gong, and Balbir Pabla**

**Abstract** The Environment Canada regional air quality modelling system, AURAMS, is used to simulate two summer periods in 2004 and 2007, coinciding with two air quality measurement campaigns over eastern North America. The two summers are quite distinct in weather and air quality conditions. The model results are compared with various surface based monitoring air and precipitation chemistry measurements to examine model's capability in capturing the impact of meteorology on air quality and explore the roles of different processes affecting ozone and PM in the region.

**Keywords** Air quality modelling • Dynamic model evaluation • Regional $O_3$ and $PM_{2.5}$ • Meteorological influence

## 85.1 Introduction

The Environment Canada regional air quality modelling system, AURAMS, has been used to provide real-time forecasts for several recent field campaigns. Two of the campaigns were conducted over eastern North America: the International Consortium for Atmospheric Research on Transport and Transformation (ICARTT) field study during the summer of 2004 [2] and the Border Air-Quality Study – Meteorology (BAQS-Met) during the summer of 2007 over southwestern Ontario [6].

The two summers are quite different, in the sense that the summer of 2004 was characterized as being cooler and wetter than average over eastern North America whereas the summer of 2007 was closer to average over the region.

W. Gong (✉) • J. Zhang • P.A. Makar • M.D. Moran • C. Stroud • S. Gravel • S. Gong • B. Pabla
Air Quality Research Division, Environment Canada, Downsview, ON, Canada
e-mail: wanmin.gong@ec.gc.ca

D.G. Steyn and S. Trini Castelli (eds.), *Air Pollution Modeling and its Application XXI*, NATO Science for Peace and Security Series C: Environmental Security 4,
DOI 10.1007/978-94-007-1359-8_85, 

Ozone monitoring data show an average of 4 ppb difference between the ICARTT period (lower) and the BAQS-Met period (higher), both in terms of 1-h daily maximum and daily mean. A preliminary study [4] based on existing retrospective model runs for the two field campaign periods showed that this difference was correctly simulated by the model, although the model-predicted ozone was in general biased high for both periods. For $PM_{2.5}$ mass, similar concentration levels were observed over the region for the two periods, whereas the model predicted significantly higher concentrations for the BAQS-Met period. In this paper, analysis is carried out based on new model runs of the periods and more extensive monitoring data, exploring the causes for the differences in model performance between the two periods, the impact of meteorology, and the roles of different processes affecting ozone and PM in the region.

## 85.2 Simulation Setup and Evaluation Dataset

AURAMS is a multi-pollutant, regional air-quality modeling system with size segregated and chemically speciated representation of aerosols (see [3, 7, 8]). For this study, AURAMS version 1.4 was used to simulate the two field study periods in a cascading fashion, from 42- to 15-km resolutions, by one-way nesting. For the ICARTT study, runs were carried out for July 1–August 31, 2004 and for BAQSMet, for June 1–August 31, 2007. The same set of grids was used for both periods with the 42-km resolution model domain covering most of the North American continent and the 15-km resolution domain covering most of the eastern North America (see [6]). The simulations were configured so that the only difference between the two periods is in modeled meteorology, provided by the Canadian weather forecasting model (GEM: [1]). For this study, GEM version 3.2.2 with additional parameterization for anthropogenic heat islands [5] was used in a regional configuration with a 15-km resolution in its uniform "core" centered over North America, providing meteorological inputs to the AURAMS simulations at both 42- and 15-km resolutions.

The observational data used for model evaluation in this study include $O_3$, bulk and speciated $PM_{2.5}$ mass, and precipitation chemistry from various monitoring networks over North America, such as National Air Pollution Surveillance (NAPS), the Aerometric Information Retrieval Systems (AIRS), Interagency Monitoring of Protected Visual Environments (IMPROVE), the Canadian Air and Precipitation Monitoring Network (CAPMoN), and the U.S. National Acid Deposition Program (NADP). The air concentration measurements include both continuous (available hourly, e.g., $O_3$ and bulk $PM_{2.5}$) and filter-based (e.g., speciated PM, usually 24-h samples available one in 3 or 6 days); the precipitation chemistry measurements vary between daily and weekly samples.

## 85.3 Results and Discussions

The analysis periods considered here are from July 7 to August 31 of 2004 and 2007 (allowing a 7-day model spin-up for the ICARTT 2004 simulation). The analysis is focused on the 15-km resolution model runs. As shown in Gong et al. [4] the marked difference between the two summers is reflected in modeled temperature, being considerably higher for the 2007 BAQSMet period than the 2004 ICARTT period over the study area. The wetter summer of 2004 over the eastern North America is also evidenced by the higher total precipitation amounts observed at the CAPMoN and NADP sites over the July–August period in 2004 compared to the same period in 2007.

Model predicted $O_3$ and $PM_{2.5}$ concentrations are compared with hourly observations at the NAPS and AIRS sites. Table 85.1 presents model-observation comparison statistics over all sites within the 15-km model domain. It shows that overall, the model over-predicted daily maximum ozone for both study periods; the over prediction is higher for the 2004 summer period than the 2007 period while the opposite was found in Gong et al [4], which may be attributed to the difference in simulation configuration. Breaking down by networks, the model bias is higher for the AIRS (U.S.) sites than at the NAPS (Canadian) sites overall. Contrasting to an on-average higher $O_3$ level in the summer of 2007 than 2004, the overall $PM_{2.5}$ levels are higher for the 2004 summer period over the study area. The model is shown to under-predict daily mean $PM_{2.5}$ concentrations, with a negative mean bias significantly greater for the 2004 summer period than for the same period in 2007. Again, breaking down by networks, the under-prediction is much greater at the AIRS sites, while at the NAPS site the model actually over-predicted the daily mean $PM_{2.5}$ for the 2007 period.

Model-predicted $PM_{2.5}$ components are evaluated with the filter measurements from the NAPS, AIRS, and IMPROVE networks (Fig. 85.1). The IMPROVE sites are mostly located in rural areas, while the AIRS (STN) sites are mostly located in commercial and residential areas. Several points are evident from Fig. 85.1. The average sulfate concentration observed at the AIRS/STN sites (within the 15-km model domain) is higher for the summer of 2007 than 2004 while the opposite is true at the IMPROVE sites. For the 2004 summer period the observed sulfate concentrations are overall comparable at both the AIRS/STN and the IMPROVE sites, while for the 2007 summer period the observed sulfate concentrations are, on average, considerably higher at the AIRS/STN sites than at the IMPROVE sites. The model is seen to under-predict sulfate concentrations on average at both the

**Table 85.1** Averaged evaluation statistics (mean, mean bias, normalized mean bias, correlation coefficient, and root-mean-square-error) for daily 1-h maximum $O_3$ (ppbv) and daily mean $PM_{2.5}$ ($\mu g\ m^{-3}$) at the NAPS and AIRS network sites

| | Daily 1-h $O_3$ maximum | | | | | | Daily mean $PM_{2.5}$ | | | | | |
|---|---|---|---|---|---|---|---|---|---|---|---|---|
| | M (obs) | M (mod) | MB | NMB | R | RMSE | M (obs) | M (mod) | MB | NMB | R | RMSE |
| 2004 | 51.2 | 55.9 | 4.7 | 0.10 | 0.62 | 13.5 | 13.4 | 11.8 | −1.9 | −0.12 | 0.64 | 7.6 |
| 2007 | 55.9 | 58.8 | 2.9 | 0.06 | 0.67 | 13.0 | 12.4 | 11.8 | −0.6 | 0.01 | 0.68 | 6.6 |

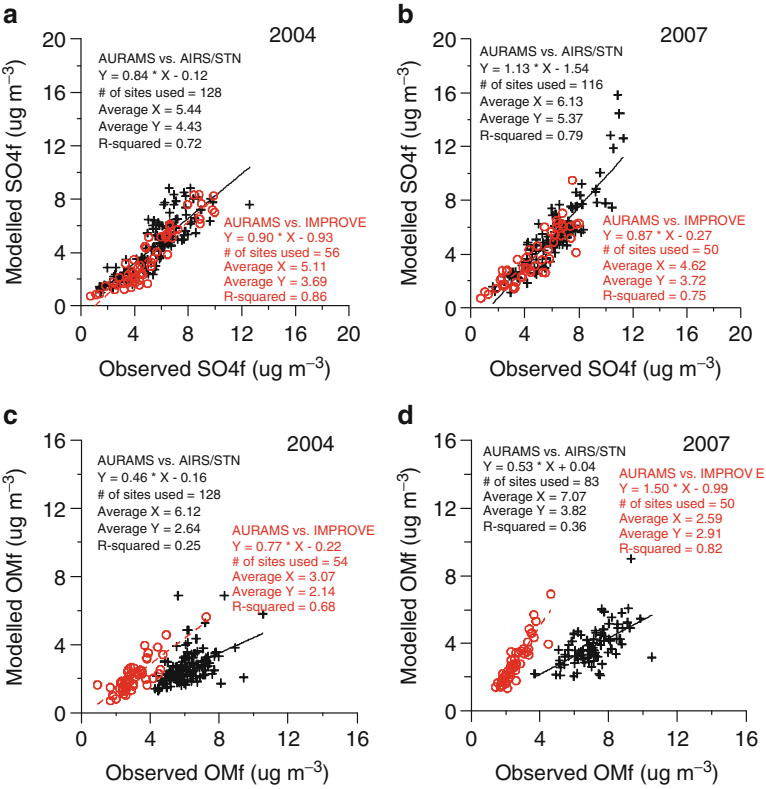


**Fig. 85.1** Model-observation comparison for the speciated $PM_{2.5}$ components at AIRS/STN (*pluses*) and IMPROVE (*circles*) sites: (**a**) and (**b**) are for fine sulfate for the two periods respectively (as indicated), and (**c**) and (**d**) are for organic matters; an OC-to-OM conversion factor of 1.4 is used for the observations from both networks

AIRS/STN and IMPROVE sites for both summer periods, with relatively more significant under-prediction at the IMPROVE sites. For the organic aerosol (OA) component, the observed concentrations are significantly higher at the AIRS/STN sites than at the mostly rural IMPROVE sites; the model, on average, under-predicts OA at these sites except for at the IMPROVE sites for the 2007 summer period. The under-prediction is particularly significant at the STN sites.

## 85.4 Conclusions and Further Work

While further analysis is underway, the comparative evaluation of model simulations for the two summer periods thus far has shown that, although the model is capable of capturing some of the meteorological impacts on air quality

over the study region, there are several areas needing further investigation. For example, the general over-prediction of $O_3$ and PM sulfate in near-source areas points to emission and source representation; there is an indication that anthropogenic OA (both primary and secondary) is underrepresented and the biogenic OA formation may be overrepresented in the model. The current SOA scheme in the model is being updated with better representation of SVOC/IVOC.

**Acknowledgments** The authors wish to acknowledge Canadian National Atmospheric Chemistry Database and various agencies/networks in U.S. and Canada for making data available.

## References

1. Côté J et al (1998) The operational CMC/MRB global environmental multiscale (GEM) model. Part 1: design considerations and formulation. Mon Wea Rev 126:1373–1395
2. Fehsenfeld FC et al (2006) International consortium for atmospheric research on transport and transformation (ICARTT) North America to Europe – overview of the 2004 summer field study. J Geophys Res 111:D23–S01. doi:10.1029/2006JD007829
3. Gong W et al (2006) Cloud processing of gases and aerosols in a regional air quality model (AURAMS). Atmos Res 82:248–275
4. Gong W et al (2010) Evaluation of a regional air-quality model (AURAMS) for two field campaign periods over south-eastern Canada and U.S. northeast: impact of meteorology on air quality. Extended abstract for 12th AMS Conference on Atmospheric Chemistry
5. Makar PA et al (2006) Heat flux, urban properties, and regional weather. Atmos Environ 40:2750–2766
6. Makar PA et al (2010) Mass tracking for chemical analysis: the causes of ozone formation in southern Ontario during BAQS-Met 2007. Atmos Chem Phys 10:14241–14312
7. McKeen S et al (2005) Assessment of an ensemble of seven real-time ozone forecasts over Eastern North America during the summer of 2004. J Geophys Res 110:D21307. doi:10.1029/2005JD005858
8. Smyth SC et al (2009) A comparative performance evaluation of the AURAMS and CMAQ air quality modelling systems. Atmos Environ 43:1059–1070

## Questions and Answers

**Elisabetta Angelino**: Are there any emission estimates from inventories to evaluate the potential influence, in addition to meteorological factors, of emission trends from 2004 to 2007 on model performance differences that you have shown for the two simulated periods?

**Wanmin Gong**: The model runs were conducted with U.S. and Canadian 2005 anthropogenic emission inventories for both simulated periods. This is the closest inventory year to both simulated periods. The real emission for the two periods would no doubt be different and some of the differences may be due to, for example, the NOx budget trading program for the power generation sector in north-eastern U.S. A main focus of this study is to see how much of the observed

difference in regional $O_3$ and $PM_{2.5}$ between the two periods can be explained by meteorology alone. A previous sensitivity study with a simple adjustment to major-point emissions, to reflect the changes due to the U.S. EPA NOx budget trading program, showed limited influence on the regional $O_3$ levels for the study periods. Further study may be pursued by using satellite information to obtain better estimates of the emission changes between the two periods to evaluate the potential influence on the model performance.

# Chapter 86
# Dynamic Evaluation of Long-Term Air Quality Model Simulations over the Northeastern U.S.

**Christian Hogrefe, Kevin Civerolo, Winston Hao, Eric E. Zalewsky, Jia-Yeong Ku, P. Steven Porter, S. T. Rao, and Gopal Sistla**

**Abstract** Dynamic model evaluation assesses a modeling system's ability to reproduce changes in air quality induced by changes in meteorology and/or emissions. In this paper, we illustrate various approaches to dynamic model evaluation utilizing 18 years of air quality simulations performed with the regional-scale MM5/SMOKE/CMAQ modeling system over the Northeastern U.S. for the time period 1988–2005. A comparison of observed and simulated weekly cycles in elemental carbon (EC) and organic carbon (OC) concentrations shows significant differences, indicating potential problems with the magnitude and temporal allocation of traffic-related emissions and the split between primary and secondary organic aerosols. A comparison of the observed and simulated interrelationships between temperature and ozone over the 18-year simulation period reveals that the high end of the modeled ozone concentration distribution is less influenced by interannual variability in the high end of the temperature distribution as compared to the observations.

**Keywords** Model evaluation • Weekday-weekend effect • Long-term modelling

C. Hogrefe (✉)
New York State Department of Environmental Conservation, Albany, NY, USA

Atmospheric Sciences Research Center, University at Albany, Albany, NY, USA
e-mail: chogrefe@asrc.cestm.albany.edu

K. Civerolo • W. Hao • E.E. Zalewsky •
J.-Y. Ku • G. Sistla
New York State Department of Environmental Conservation, Albany, NY, USA

P.S. Porter
University of Idaho, Idaho Falls, ID, USA
e-mail: porter@if.uidaho.edu

S.T. Rao
AMAD/NERL, U.S. Environmental Protection Agency, Research Triangle Park, NC, USA
e-mail: rao.st@epa.gov

D.G. Steyn and S. Trini Castelli (eds.), *Air Pollution Modeling and its Application XXI*,
NATO Science for Peace and Security Series C: Environmental Security 4,
DOI 10.1007/978-94-007-1359-8_86, 

## 86.1 Introduction

Regional-scale photochemical modelling systems are routinely used to support air quality planning activities. Often, model evaluation focuses on comparing predictions from the base case scenario against observations. While such comparisons can help build confidence in the performance of the modelling system, they can leave several key questions unanswered: how well does the modelling system capture the impacts of projected changes in emissions? How well does the modelling system capture the effects of meteorological variability on pollutant concentrations, a question of particular importance when using regional-scale models to assess the effects of climate change? These questions are at the core of "dynamic model evaluation", a concept defined by Gilliland et al. [2] and integrated into an overall model evaluation framework by Dennis et al. [1]. In this paper, we present some illustrative examples for dynamic model evaluation using results from air quality simulations over the North eastern U.S. covering an 18 year period from 1988 to 2005.

## 86.2 Modeling System, Observations, and Method of Analysis

The model simulations analyzed here have been described in greater detail in Hogrefe et al. [3, 4] and Pierce et al. [5]. The following is a brief summary of the model set-up used for the simulations analyzed in this study. The MM5 meteorological model was used to simulate meteorological conditions over the Northeastern U.S. for the time period from January 1, 1988 to December 31, 2005 using two-way nested grids with 36 and 12 km grid cell sizes. Emission inventories were compiled from a variety of sources as described in Hogrefe et al. [3] and processed by the SMOKE system. Air quality simulations were performed with the Community Multiscale Air Quality (CMAQ) model, version 4.6. As described in Hogrefe et al. [4], chemical boundary conditions for the 36 km grid were extracted from archived monthly-mean fields of global chemistry simulations performed for the 1988–2005 time period with the ECHAM5-MOZART modelling system as part of the RETRO project [6].

Hourly ozone ($O_3$) observations from 1988 to 2005 were obtained from the U.S. EPA Air Quality System (AQS). Only sites located within the 12 km CMAQ modelling domain were included in the analysis. After screening for data completeness, 90 $O_3$ monitors were selected for the analysis. Hourly temperature observations for 1988–2005 were obtained from the Data Support Section at the National Center for Atmospheric Research (NCAR-DSS). To analyze the observed and simulated relationships between temperature and $O_3$, the closest temperature monitor was selected for each of the 90 $O_3$ sites described above. To analyze 2000–2005 CMAQ predictions of Elemental Carbon (EC) and organic carbon (OC), filter-based 24-h average concentrations were obtained from AQS for 27 Chemical Speciation Network (CSN) monitors located in the 12 km CMAQ domain.

## 86.3 Results and Discussion

As pointed out by Pierce et al. [5], the pronounced differences in anthropogenic emissions between weekdays and weekends offer an excellent opportunity for dynamic model evaluation. While Pierce et al. [5] examined weekend/weekday (WEWD) differences in observed and simulated concentrations of $O_3$ and its precursors, here we focus on WEWD differences in concentrations of carbonaceous fine particles. Figure 86.1 presents averaged weekly cycles of observed and simulated concentrations of EC and OC based on all available data at the 27 CSN sites from 2000 to 2005. The observed EC concentrations show a marked decline on weekends, decreasing from a weekday average of about 0.7 μg/m$^3$ to a weekend average of about 0.55 μg/m$^3$, a reduction of more than 20%. A majority of this reduction likely is due to reduced diesel truck traffic on weekends. The CMAQ predictions also show a decrease of EC concentrations on weekends, but the magnitude of this decrease (from about 0.85 μg/m$^3$ to about 0.8 μg/m$^3$) is much smaller than that observed. This underestimation may be indicative of problems with either the magnitude or the temporal allocation of diesel truck emissions. The differences between observed and simulated weekly cycles are even more pronounced for OC. While the observations display little systematic WEWD differences, the weekly cycle of the simulated OC concentrations does show a decrease on weekends, closely resembling the weekly cycle of the simulated EC concentrations. A possible explanation for the discrepancies could be a different split between primary and secondary OC. Specifically, the observed total OC concentrations may contain a larger portion of secondary OC than the simulated total OC concentrations. Since biogenic emissions can be a significant contributor to secondary OC and are not expected to exhibit a regular weekly cycle, the absence of a pronounced WEWD differences in the observed OC concentrations supports this hypothesis. Further support comes from the model's underestimation of observed total OC

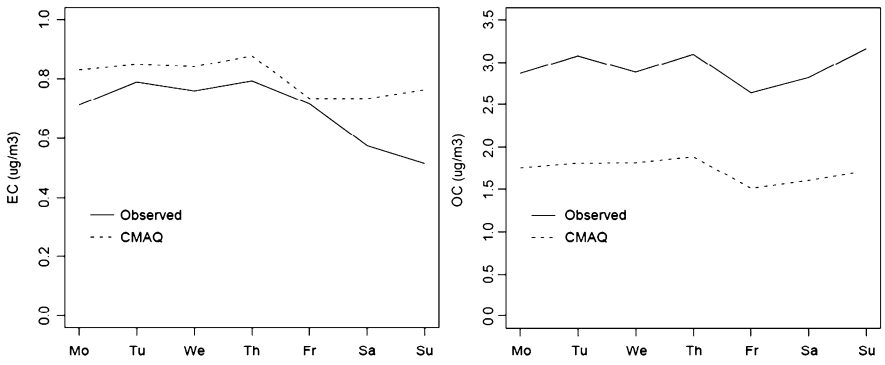


**Fig. 86.1** Average weekly cycle of observed and simulated EC (*left*) and OC (*right*) concentrations

concentrations and from the fact that the model simulated weekly cycle of OC closely resembles that of EC, a purely primary component. In summary, this comparison of the observed and simulated weekly cycles of EC and OC provides an illustration where dynamic evaluation can provide a starting point for further diagnostic studies aimed at improving the model's response to emission changes.

From a dynamic model evaluation perspective, it is also of interest to examine how well the model can capture the interrelationships between meteorological and air quality variables. As an illustration, we compared the relationship between summertime temperature and $O_3$ anomalies for both observations and model simulations. To this end, anomalies for each variable were computed by first rank-ordering each year's May-September distribution of daily maximum temperature and daily maximum 8-h $O_3$ at each site and then, for each given percentile and each site, subtracting the site- and percentile-specific 18-year mean value from the value for a given year. Figure 86.2 displays a comparison of the observed and simulated relationship between summertime temperature and $O_3$ anomalies. The figure depicts box-whisker plots of the anomalies in the 95th percentile of summertime 8-h daily maximum $O_3$ concentrations as a function of the anomalies in the 95th percentile of summertime daily maximum temperature. The figure illustrates that for summers when the observed anomaly of the 95th temperature percentile is greater than +3°C, the distribution of anomalies of the 95th $O_3$ percentile has a median value of +22 ppb. Conversely, for summers when the observed anomaly of the 95th temperature percentile is less than −3°C, the distribution of anomalies of the 95th $O_3$ percentile has a median value of −8 ppb. The corresponding modeled

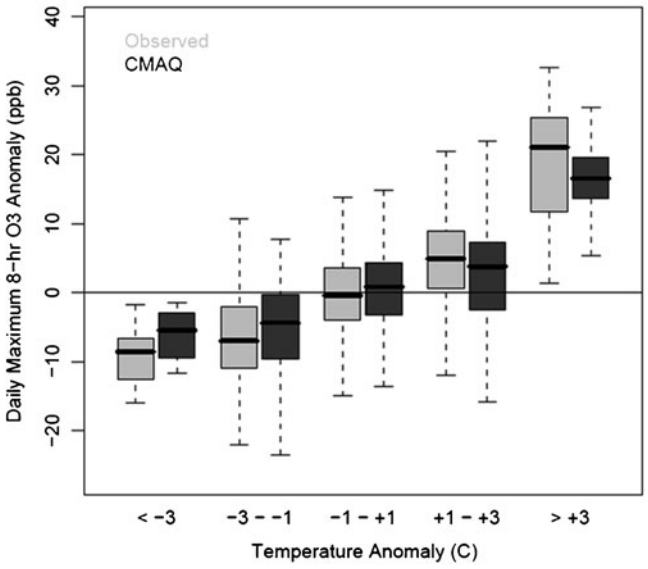


**Fig. 86.2** Relationship between ozone and temperature anomalies for observations and simulations calculated as described in the text

values are +17 ppb and −5 ppb, respectively, indicating that the high end of the modeled $O_3$ distribution appears to be less influenced by interannual variability in the high end of the temperature distribution than the high end of the observed $O_3$ distribution.

## 86.4 Summary and Outlook

The dynamic evaluation examples presented in this study indicate potential problems with the magnitude and temporal allocation of traffic emissions and the split between primary and secondary organic aerosols in the 1988–2005 MM5/CMAQ simulations analyzed here. Also, the modeling system did not fully capture the relationship between the high end of the summertime temperature and $O_3$ distributions. As discussed by Hogrefe et al. [4], key uncertainties affecting the long-term regional-scale simulations, such as the ones analyzed in this study, are estimates of sector-specific, spatially-resolved long-term emission trends and the specification of lateral boundary conditions. The examples presented in this study also highlight opportunities for further dynamic evaluation, such as examining potential changes in photochemical regime over time and additional analyses of the interrelationships between climate and air quality variables. Finally, long-term simulations, such as the one presented here, have a number of potential applications, including tracking the effects of emission reductions, health impact studies, investigating the interactions between climate change and air quality, and testing assumptions about emissions and boundary conditions.

## References

1. Dennis R, Fox T, Fuentes M, Gilliland A, Hanna S, Hogrefe C, Irwin J, Rao ST, Scheffe R, Schere K, Steyn D, Venkatram A (2010) A framework for evaluating regional-scale numerical photochemical modeling systems. Environ Fluid Mech 10:471–489. doi:10.1007/s10652-009-9163-2
2. Gilliland A, Hogrefe C, Pinder R, Godowitch J, Foley K, Rao ST (2008) Dynamic evaluation of regional air quality models: Assessing changes in $O_3$ stemming from changes in emissions and meteorology. Atmos Environ 42:5110–5123
3. Hogrefe C, Lynn B, Goldberg R, Rosenzweig C, Zalewsky EE, Hao W, Doraswamy P, Civerolo K, Ku J-Y, Sistla G, Kinney PL (2009) A combined model-observation approach to estimate historic gridded fields of $PM_{2.5}$ mass and species concentrations. Atmos Environ 43:2561–2570
4. Hogrefe C, Hao W, Zalewsky EE, Ku J-Y, Lynn B, Rosenzweig C, Schultz MG, Rast S, Newchurch MJ, Wang L, Kinney PL, Sistla G (2010) An analysis of long-term regional-scale ozone simulations over the Northeastern United States: variability and trends. Atmos Chem Phys Discuss 10:23045–23090
5. Pierce T, Hogrefe C, Rao ST, Porter PS, Ku J-Y (2010) Dynamic evaluation of a regional air quality model: assessing the weekly cycle in the observations and model outputs. Atmos Environ 44:3583–3596. doi:10.1016/j.atmosenv.2010.05.046

6. RETRO final report (2007) REanalysis of the TROpospheric chemical composition over the past 40 years – A long-term global modeling study of tropospheric chemistry. In: Schulz MG (ed) Reports on Earth System Science, Max Planck Institute for Meteorology, Hamburg, Report No. 48/2007, ISSN 1614–1199

## Questions and Answers

**Questioner Name**: Volker Matthias

**Q**: Was the model nudged with respect to temperature also on the inner grid and in the boundary layer? Did you investigate the effect of grid resolution on the ozone variability?

**A**: Temperature, wind speed, and moisture values were nudged on both grids, but no nudging for temperature and moisture was performed within the boundary layer. To date we have not yet performed a detailed analysis of the impact of grid resolution on the simulated ozone variability.

# Chapter 87
# Aerosol Analysis and Forecast in the ECMWF Integrated Forecast System: Evaluation by Means of Case Studies

**Alexander Mangold, Hugo De Backer, Andy Delcloo, Bart De Paepe, Steven Dewitte, Isabelle Chiapello, Yevgeny Derimian, Meloe Kacenelenbogen, Jean-Francois Léon, Nicolas Huneeus, Michael Schulz, Darius Ceburnis, Colin O'Dowd, Harald Flentje, Stefan Kinne, Angela Benedetti, Jean-Jacques Morcrette, and Olivier Boucher**

**Abstract** A near real-time assimilation and forecast system of aerosols has been developed by integration in the ECMWF IFS code within the GEMS project. The GEMS aerosol modeling system is novel as it is the first aerosol model fully coupled to a NWP model with data assimilation. Aerosol optical depth (AOD) data of the MODIS instrument on Terra and Aqua satellites was assimilated. The performance of the aerosol model was evaluated by the means of case studies. The assimilation of MODIS AOD improved the subsequent aerosol predictions when compared with observations, in particular concerning correlations and AOD peak values. The assimilation is less effective in correcting a positive or a negative bias.

A. Mangold • H. De Backer • A. Delcloo (✉) • B. De Paepe • S. Dewitte
Observations Department, Royal Meteorological Institute, Ringlaan 3, B-1180 Ukkel, Belgium
e-mail: andy.delcloo@meteo.be

I. Chiapello • Y. Derimian • J.-F. Léon
Laboratoire d'Optique Atmospherique, Villeneuve d'Ascq, France

M. Kacenelenbogen
ORAU/NASA Ames Research Center, Moffett Field, California, USA

N. Huneeus • M. Schulz
Laboratoires des Sciences du Climat et de l'Environnement, Gif-sur-Yvette, France

D. Ceburnis • C. O'Dowd
Environmental Change Institute, National University of Ireland, Galway, Ireland

H. Flentje
Deutscher Wetterdienst, Hohenpeissenberg, Germany

S. Kinne
Max-Planck Institute for Meteorology, Hamburg, Germany

A. Benedetti • J.-J. Morcrette
European Centre for Medium-range Weather Forecasts, Reading, UK

O. Boucher
Met Office Hadley Centre, Exeter, UK

D.G. Steyn and S. Trini Castelli (eds.), *Air Pollution Modeling and its Application XXI*, NATO Science for Peace and Security Series C: Environmental Security 4,
DOI 10.1007/978-94-007-1359-8_87, 

**Keywords** Aerosol modeling • AOD • PM2.5 • Angström exponent

## 87.1 Introduction

Within the European Commission's Framework Programme 6 project GEMS (Global and regional Earth-system Monitoring using Satellite and in-situ data; [3]), near real-time assimilation and forecasts of aerosols have been developed by integration in the ECMWF (European Centre for Medium-Range Weather Forecast) Integrated Forecast System (IFS). The GEMS project represents an unprecedented effort to model atmospheric aerosols in the context of operational numerical weather prediction (NWP) taking an advantage of state-of-the-art meteorological information and data assimilation techniques.

Here, we evaluate the performance of the aerosol model before and after assimilation by means of case studies. Case studies examined were: (i) the summer heat wave in Europe in August 2003, characterized by forest fire aerosol and conditions of high temperatures and stagnation, favoring photochemistry and secondary aerosol formation and, (ii) a large Saharan dust event in the beginning of March 2004. Two simulations with the aerosol model are considered: first, the free running forward model with no assimilation of any aerosol related data (hereafter named DIRECT; [4]), and second, the analysis version with assimilation of MODIS total AOD data at 550 nm over ocean and land (hereafter named ASSIM; [1]).

## 87.2 Aerosol Model System and Evaluation Data

The aerosol forward model contains five aerosol types: sea salt (SS), desert dust (DD), organic matter (OM), black carbon (BC), and a sulfate-related variable (SU). Total column aerosol optical depth (AOD) is calculated at 469, 550, 670, 865, 1240, 1640, and 2130 nm. Partial AODs for SS, DD, OM, BC, and SU are calculated at 550 nm. In addition, for each of the five aerosol types, the mass mixing ratio of each size bin on each of the 60 height levels is available. Model resolution is T*L*159L60 (1.125° × 1.125° grid, 60 height levels). The aerosol assimilation scheme (ASSIM) is part of the meteorological 4D-Var assimilation system employed operationally at ECMWF. The ASSIM simulation assimilates total aerosol optical depth data at 550 nm from MODIS (MODerate resolution Imaging Spectroradiometer) on board of Terra and Aqua satellites (data collection 5). The total aerosol mixing ratio, defined as the sum of all aerosol species size bins, is introduced as control variable.

The AERONET network [2] of ground-based sunphotometer measurements provides observations of total AOD and its spectral dependence. The spectral dependence defines the Angström exponent, an indicator for the overall aerosol size. Measured particulate mass concentrations (PM) are obtained from the French air

quality monitoring network. PM analyzed within this study represent particles at the ground level with an aerodynamic diameter lower than 2.5 $\mu$m (PM2.5), measured continuously using a Tapered Element Oscillating Microbalance (TEOM).

## 87.3 Air Pollution During the August 2003 Heat Wave in Europe

For comparisons with the model simulations, AERONET AOD data from the French sites in Lille, Dunkerque and Toulon are available. In addition, PM2.5 measurements are available for Lille, Calais (50 km from Dunkerque, same model grid cell), and Marseille (60 km from Toulon, same model grid cell).

The aerosol model reproduces reasonably well the day-to-day variability in the observed PM2.5 concentrations. After assimilation, the relative increase from the average PM2.5 concentrations before to the average level during the heat wave period is well simulated.

The DIRECT simulation overestimates PM2.5 in Lille and Calais and is very close to the observations in Marseille. ASSIM introduces an additional overestimation, now also for Marseille. This is mainly due to increased $SO_4$ concentrations in the ASSIM version compared to the DIRECT run. Simulated BC and OM concentrations do not contribute distinctly to the simulated PM2.5 concentrations.

The aerosol model agrees also reasonably well with the day-to-day variability in observed AOD. Observed AOD during the heat wave was high with some peaks greater than 0.6. The DIRECT simulation is in good agreement with the overall AOD level, however, there are mismatches between simulated and observed peaks (timing, both over- and underestimation). After assimilation some peaks are better matched, mainly due to increased model sulfate AOD.

## 87.4 Saharan Dust Event 2004

Between 03 and 10 March 2004, a major dust storm swept over large parts of Western Africa and the Atlantic. Time series of observed and simulated (total and partial) AOD at two AERONET sites (Agoufou and Capo Verde) are displayed in Fig. 87.1. The assimilation of MODIS AOD improves the model performance.

Both simulations overestimate the Angström exponent at Agoufou (see Fig. 87.2), whereas at the more distant station El Arenosillo the Angström exponent is better reproduced. The better performance in El Arenosillo reveals that both the DIRECT and the ASSIM simulation overestimate the fine-mode aerosol.

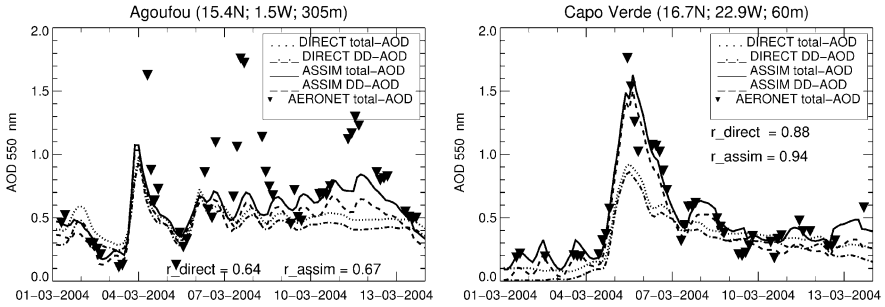


**Fig. 87.1** Time series of observed and simulated (total and partial) AOD for March 2004 at Agoufou and Capo Verde; the linear correlation coefficients for both simulations are given in the graphs

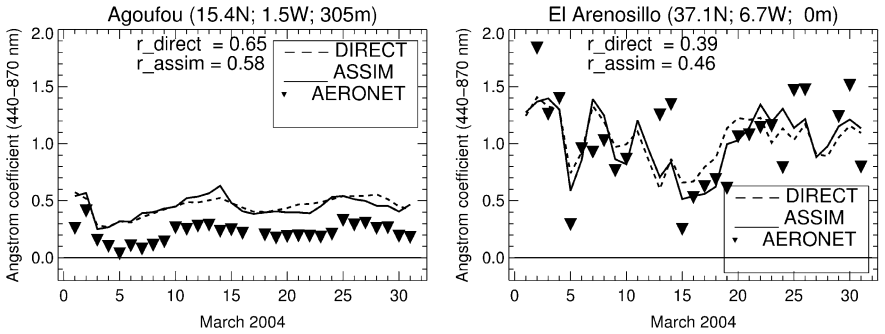


**Fig. 87.2** Angström exponent for March 2004 at Agoufou and El Arenosillo; the linear correlation coefficients for both simulations are given in the graphs

**Acknowledgments** At LOA, D. Tanré is thanked for his helpful contribution to the analysis of AERONET data for the pollution aerosol case study. We also thank P. Goloub, D. Tanré, and V. E. Cachorro, who are the principal investigators of the AERONET sites used for this study. In particular, we are grateful to A. Hollingsworth who initiated and led the GEMS project. GEMS was funded by the EC's framework programme 6, contract no. 516099.

## References

1. Benedetti A et al (2009) Aerosol analysis and forecast in the European Centre for medium-range weather forecasts integrated forecast system: 2. Data assimilation. J Geophys Res 114: D13205. doi:10.1029/2008JD011115
2. Holben BN et al (2001) An emerging ground-based aerosol climatology: aerosol optical depth from AERONET. J Geophys Res 106(D11):12067–12097
3. Hollingsworth A (2008) Toward a monitoring and forecasting system for atmospheric composition: the GEMS project. Bull Am Meteorol Soc 89(8):1147–1164
4. Morcrette J-J (2009) Aerosol analysis and forecast in the European Centre for medium-range weather forecasts integrated forecast system: forward modeling. J Geophys Res 114:D06206. doi:10.1029/2008JD011235

# Chapter 88
# Objective Discrimination and Pooling Models in the Ensemble

**Eugene Genikhovich, Tatiana Pavlova, and Alexander Ziv**

**Abstract** Data assimilating and pooling the model predictions in the multi-model ensemble, described in this paper, are based on the techniques of approximation and regularization of multidimensional vectors in the linear Euclidean space with the use of the non-orthogonal vector basis. This approach has been successfully applied to (i) the time series of the annual temperatures averaged over the globe and northern hemisphere corresponding to the last 100 years, and (ii) the fields of concentrations of atmospheric pollutants over Europe. Quantitative estimates of the efficiency of the proposed technique are presented in the paper.

## 88.1 Introduction

Multi-model ensembles are widely used in the numerical weather prediction, climate and air pollution modeling to reproduce the spreading of relevant characteristics that takes place in the atmosphere due to the instability resulting from the chaotic nature of atmospheric processes. All members in the ensemble are usually considered as "equal in rights" and the resulting ensemble estimates are usually obtained as mean values of the results generated with each model from the ensemble; medians, which are robust estimates of mean values, are also used there, especially in the air pollution modeling [7]. Recent publications (e.g. [2]) have thrown doubts on the validity of this kind of the "model democracy". Indeed, some of the models could be characterized by much larger errors than others. An approach to the objective discrimination and pooling the models in the multi-model ensemble is discussed in this paper.

The methodology in use in this paper is close to this one employed by Strauss et al [8] and Tippett et al [9] (in relation to the climate modeling) and by Mallet and

E. Genikhovich (✉) • T. Pavlova • A. Ziv
Voeikov Main Geophysical Observatory, 7 Karbyshev St., 194021 St. Petersburg, Russia
e-mail: ego@main.mgo.rssi.ru

D.G. Steyn and S. Trini Castelli (eds.), *Air Pollution Modeling and its Application XXI*, NATO Science for Peace and Security Series C: Environmental Security 4,
DOI 10.1007/978-94-007-1359-8_88, 

Sportisse [3] and Mallet et al [4] (in relation to the dispersion modeling) though our approach seems to be different.

## 88.2 Mathematical Formalism

Following to publication by Genikhovich et al [1] let us consider the data set, generated by each of the models included in the ensemble, as a N-dimensional vector $X_k = \{X_{k1}, X_{k2}, \ldots X_{kN}\}$ representing this model (for the sake of brevity this vector will be referring to as to corresponding model). All models $X_k$ ($k = 1, 2, \ldots K$) are included in one ensemble, and it means that their components $X_{kn}$ corresponding to the same "n" have similar physical meaning and, therefore, could be compared with the same "observed value" $F_n$ that forms the observational vector F.

Let us consider now the problem of the best-fit approximation of F using vectors $X_k$ together with the "unity vector" E as a non-orthogonal basis $\boldsymbol{B}$:

$$F = w_0 E + \sum_{(K')} w_k X_k \tag{88.1}$$

The weights $w_0$, $w_1$, $w_2$.... are determined to minimize the distance $\delta^2 = \delta^2_{\min}$ from F to the subspace spanned over the basis $\boldsymbol{B}$ where

$$\delta^2 = \sum_{n=1}^{N} \left(w_0 + \sum_{(K')} w_k x_{kn} f_n\right)^2 \tag{88.2}$$

Here, K′ is the number of vectors forming the basis $\boldsymbol{B}$. In the simplest case, when K′ = K, the problem of minimizing $\delta^2$ is, generally speaking, not well-posed because some of the vectors $X_k$ could be close to being linearly dependent. To regularize it, one can "try" different K′ and for each K′ determine the subset of the vectors $\{X_k\}$ that minimizes the value of $\delta^2_{\min}(K')$ in Eq. 88.2 corresponding to given K′. Such a procedure should be brought to a stop when increasing K′ would not result in the "noticeable" decreasing of $\delta^2_{\min}(K')$ (more rigorously, it means that this decreasing is not "statistically significant"). As a result, the subset of K′ models is determined, which are included in Eq. 88.1. These models are rearranged in the simply ordered set accordingly to their "efficiency" in reduction of $\delta^2_{\min}(K')$, and the weights $w_k$ are determined that minimize Eq. 88.2. It could be understood as an objective discrimination of the models under consideration. Eq. 88.1 can be used to combine or "pool" the model predictions in order to ensure the best performance of the ensemble predictions.

For practical applications the coefficients $w_i$ in Eq. 88.1 are determined using the method of supervised learning usually applied in pattern recognition. Accordingly, the observational vector F should be transformed in two subsets called the training

("dependent") data, F′, and validation ("independent") data, F″. The above described procedure is actually performed only with the training data set to select the models sought and determine corresponding weights $w_k$. Then the performance of the resulting model given by Eq. 88.1 is tested upon the independent data set to check the efficiency of the regularization.

Formally, this procedure is identical to the stepwise regression but it would not require any assumptions about the statistical properties of processed data; consequently, $\delta$ characterizes the root mean squared error (RMSE) and that coefficients of the multiple determination or correlation could be used to describe the decreasing of the distance given by Eq. 88.2.

## 88.3 Results and Discussion

Two model ensembles used in this work corresponded to (i) the time series of the annual globally averaged temperatures for the last 135 years, and (ii) the fields of concentrations of atmospheric pollutants over Europe. The climate ensemble in use was described by Meehl et al [5]; 17 models from this ensemble were listed by Genikhovich et al [1]. Empirical annual mean global temperatures covering years from 1871 to 2005 were taken from Met Office Hadley Centre observations datasets [6]. The years 1871–1985 were attributed to the learning set, and the rest was used for validation. It turned out that one, starting with 17 models, could select just two models with weights $w_0 = 5.8°C$; $w_1 = 0.39$ and $w_2 = 0.22$. Pooling these models with Eq. 88.1 resulted, for the independent data set, in $\delta = 0.18$; if one would use the ensemble average, the corresponding value is equal to 0.70. Increasing the number of models lead to instability of $w_i$ and worsened the RMSE. One can conclude from these results that the number if models included in this ensemble seems to be excessive (probably because the predictions with different models are closely correlated).

The same approach was used to analyze the fields of ozone and nitrogen dioxide concentrations obtained in the framework of GEMS project. The data set included concentrations modeled and measured at 178 European monitoring stations in 2003. The number of the models in the ensemble was equal to 5 for ozone and to 6 for $NO_2$. The learning data set was constructed using either (i) 50% of the stations available (with multiple sampling of stations based on bootstrap) or (ii) first 8 months of the year. It turned out that, for ozone, when using one "best performing" model ($K'' = 1$), the relative error $R = RMSE/RMSE_{min}$ in the cases (i) and (ii) is equal to 1.04 and 1.03 where $RMSE_{min} = \underbrace{\min}_{K'} \delta(K')$. If $K'' = 2$, practically $R = 1$ in both cases. It is worth mentioning that the ensemble average and median correspond to 1.13. Similar results were obtained for $NO_2$.

The developed method could be instrumental in reducing the errors of the climate projections for the twenty-first century and improving quality of numerical forecasts of the air pollution over Europe.

**Acknowledgments** This work was partially funded by the Russian Foundation for Basic Research (grant # 08-05-00569-a). We would like to acknowledge the participants of the project GEMS for kindly providing all necessary data sets.

## References

1. Genikhovich EL, Pavlova TV, Kattsov VM (2010) On combining climate models in ensembles. Proc Main Geophys Observatory 561:28–46 (in Russian)
2. Knutti R (2010) The end of model democracy? Clim Change 102(3–4):395–404. doi:10.1007/s10584-010-9800-2
3. Mallet V, Sportisse B (2006) Ensemble-based air quality forecasts: a multimodel approach applied to ozone. J Geophys Res 111:D18302.1–D18302.11. doi:10.1029/2005JD006675
4. Mallet V, Stoltz G, Mauricette B (2009) Ozone ensemble forecast with machine learning algorithms. J Geophys Res 114:D05307.1–D05302.13
5. Meehl GA, Covey C, Delworth T, Latif M, McAvaney B, Mitchell JFB, Stouffer RJ, Taylor KE (2007) The WCPR CMIP3 multimodel dataset: a new era in climate change research. Bull Am Meteorol Soc 88:1383–1394. doi:10/1175/BAMS-88-9-1383
6. Met Office Hadley Centre observations datasets. http://www.cru.uea.ac.uk/cru/data/temperature/; http://hadobs.metoffice.com/hadcrut3/diagnostics/global
7. Riccio A, Guinta G, Galmarini S (2007) Seeking for the rational basis of the median model: the optimal combination of multi-model ensemble results. Atmos Chem Phys 7:6085–6098, www.atmos-chem-phys.net/7/6085/2007
8. Strauss D, Shukla J, Paolino D, Schubert S, Suarez M, Pegion P, Kumar A (2003) Predictability of the seasonal mean atmospheric circulation during autumn, winter, and spring. J Climate 16:3629–3649
9. Tippett MK, DelSole T, Mason SJ, Barnston AG (2008) Regression-based method for finding coupled patterns. J Climate 21:4384–4398

# Chapter 89
# Implementation and Evaluation of a Comprehensive Emission Model for Europe

**Johannes Bieser, A. Aulinger, V. Matthias, and M. Quante**

**Abstract** Temporal and spatial distributed emissions are an essential input parameter for Chemical Transport Models (CTM). In order to obtain consistent emissions for long-term CTM runs the US EPA emission model SMOKE has been adapted and modified. The modified version of the SMOKE emission model (SMOKE-EU) uses official and publicly available data sets and statistics to create emissions of CO, NOx, SO2, NH3, PM2.5, PM10, NMVOC. Currently it supports several photochemical mechanisms and a PM2.5 split. Additionally emissions of benzo[a]pyrene have been modelled. The temporal resolution of the emissions is 1 h. The resolution of the surrogates used for spatial disaggregation is $1 \times 1$ km$^2$. Vertical distribution is done via plume rise calculations. The area covered by the emission model is Europe including eastern Russia, North Africa and Turkey the currently implemented datasets allow for the calculation of emissions between 1970 and 2020. Emissions for the year 2000 on a $54 \times 54$ km$^2$ domain were evaluated by comparison to datasets from three commonly used emission models. Additionally SMOKE/EU emissions were used as input for the CMAQ4.6 CTM and the calculated air concentrations of Ozone, NH4, NO3 and SO4 were compared to EMEP measurements. O3: (NMB 0.71) (SD 0.68) (F2 0.83) (CORR 0.55) 48 Stations (hourly). NH4: (NMB 0.25) (SD 1.01) (F2 0.55) (CORR 0.53) 8 Stations (daily). NO3: (NMB 0.42) (SD 0.60) (F2 0.40) (CORR 0.45) 7 Stations (daily). SO4: (NMB 0.34) (SD 0.84) (F2 0.65) (CORR 0.55) 21 Stations (daily). Abbreviations: Normalized Mean Bias (NMB), Standard Deviation (SD), Factor of 2 (F2),

J. Bieser (✉) • M. Quante
Helmoltz Zentrum Geesthacht, Institute for Coastal Research, D-21502 Geesthacht, Germany

Institute of Ecology and Environmental Chemistry, Leuphana University Lüneburg, D-21335 Lüneburg, Germany
e-mail: johannes.bieser@gkss.de

A. Aulinger • V. Matthias
Helmoltz Zentrum Geesthacht, Institute for Coastal Research, D-21502 Geesthacht, Germany
e-mail: Volker.matthias@gkss.de

D.G. Steyn and S. Trini Castelli (eds.), *Air Pollution Modeling and its Application XXI*, NATO Science for Peace and Security Series C: Environmental Security 4,
DOI 10.1007/978-94-007-1359-8_89, 

Correlation (CORR). Using three different emission datasets as input for CMAQ showed that the SMOKE-EU model produces results comparable to those of commonly used European emissions data sets.

**Keywords** Emissions • Emission modelling

## 89.1 Introduction

Chemistry transport models (CTMs) are used for a variety of purposes (air quality modelling, source attribution, assessment of abatement strategies, etc.) with modeling domains reaching from global coverage down to local scales. In addition to the meteorological data, lack of knowledge on emissions introduce a major uncertainty to the CTM modeling results [1, 9, 20, 23].

Besides proprietary emissions models which are not publicly available, there are several public models. Each of these models has its own restrictions, e.g. compatibility to a certain CTM, temporal coverage, spatial resolution for regional modelling or the focus on a single nation or region. Given the variety of emission models available for Europe the question arises "What benefit can be gained by an additional model?". The rational for this emission model is to provide a flexible tool capable of creating consistent high resolution emission datasets for long term CTM runs over Europe based only on open source data. Flexibility means that the model can be easily altered concerning the input data and output format and that new species or different photochemical splits can be implemented with a minimum amount of work. Consistency requires that emissions for each year are calculated using similar input data and the same algorithms. This consistency in approach is in contrast to many emission models, which use the best available data for each new report year, with report years usually being every 5 or 10 years. Such an approach leads to a steady improvement of the emission datasets but comes at the cost of compatibility with older datasets since these older report years are not compatible with the new methodologies. The model introduced in this paper is specifically designed for long-term CTM runs and thus needs to overcome these problems.

## 89.2 Model Overview

The emission model SMOKE is the official emission model of the Unites States Environmental Protection Agency (US EPA) and is one of the most used emission models worldwide [11, 13, 24]. SMOKE was originally created by the MCNC Environmental Modeling Center (EMC) and developed further by the US EPA. It is the official emission model of the Models-3 Community Modelling and Analysis System (CMAS) and creates emission data suitable for CMAQ [5, 6]. Anthropogenic emissions are calculated using the 'Top-Down' methodology while biogenic

emissions are calculated by the Bottom-Up model BEIS3 ([8, 21]; Pierce et. al. 16]). Although SMOKE is highly specialized for usage with officially reported data in the US, there have been several successful attempts to use it for other regions. In Europe, for example, SMOKE has been adapted to use the national emission inventories of Spain and the UK [3, 28].

The SMOKE emissions model follows a modular setup. Area, point, mobile and biogenic sources are calculated by different modules and merged into a single output file. In order to run SMOKE, four kinds of data are needed for the different species: The bulk emission inventory, spatial surrogates, speciation profiles, and temporal profiles. For plume rise calculations and biogenic emissions certain meteorological input data are needed additionally (e.g. temperature, radiation, wind, humidity).

### *89.2.1 Modifications*

Since the SMOKE model has been under development for over a decade, it is highly specialized on the usage of official data of the US. Thus, this model setup is not directly compatible to European data reporting schemes and several adjustments need to be made for the use of SMOKE for Europe (SMOKE-EU).

In order to achieve a high spatial resolution SMOKE uses emission aggregates on county basis and distributes them using static surrogates for each region. This is done by the *Grdmat* module which creates a single, static gridding matrix for each year. When used with European emissions aggregated on the national level these static surrogates lead to a static spatial distribution for each country over the whole year. This is a sound assumption for sources that are spatially static like for example mobile emissions which are connected to the road network throughout the year. For emissions that are influenced by local events, such as combustion for heating, static surrogates in combination with large or inhomogeneous regions can lead to an unrealistic emission distribution. This is due to the fact that the spatial distribution of heating demand is not static throughout the year but changing depending on the temperature. Furthermore the temporal disaggregation in SMOKE is done via monthly, weekly and hourly profiles. This can lead to strong emission changes between the last day of a month and the first day of the next month. In order to overcome these restrictions of SMOKE, in SMOKE-EU a new module has been introduced [2]. The new module uses external data, temperature in this case, to create new gridding matrices for each day of the year. This leads to a more realistic spatial and temporal disaggregation of the emissions.

### *89.2.2 Datasets*

The bulk emission inventory is created from two pan-European emission inventories. Point sources are taken from the European Pollutants Emission

Register (EPER) [7] and are merged with the annual national total emissions of the European Monitoring and Evaluation Program (EMEP) [26, 27].

These annual total emissions are disaggregated in time and space using a variety of datasets. The temporal distribution is done via sectoral emission profiles from the LOTOS-EUROS emission model [4]. The vertical distribution is calculated via plume rise algorithms using average stack data for different industrial sectors [17]. The chemical speciation for compatibility with the photochemical mechanisms used by CTMs is done with NMVOC split factors obtained from Passant [15]. The spatial disaggregation is done with the help of spatial surrogates. The proxies used as spatial surrogates to disaggregate the national total emissions to the emissions model grid, are applied following Maes [12]. Data used for spatial surrogates are population density, land use, vegetation maps, road and railway networks as well as statistical data.

## 89.3 Comparison of Calculated Concentrations to Observations

The CTM CMAQ4.6 of the US EPA was used to simulate atmospheric concentrations of air pollutants for the year 2000 [25]. The spatial resolution is $54 \times 54$ km$^2$ with 30 vertical layers, the photochemical mechanism used is CB-IV. Meteorological fields are taken from the COSMO-CLM model [18, 19]. Monthly average boundary conditions were derived from the MOZART global model [10, 14]. With this setup, four CMAQ runs using different emission datasets were calculated. The calculated atmospheric concentrations in the lowest model layer were compared to observations from EMEP measurement stations. Six different compounds are used for comparison, three gaseous species ($NO_2$ $SO_2$, $O_3$) and three aerosol components ($SO_4$, $NH_4$, $NO_3$). Ozone concentrations are given as hourly values while all other values are reported as daily averages.

It could be shown that the vertical distribution has a strong influence on the simulated $SO_4$ and $SO_2$ concentrations. Generally, $SO_2$ emissions in higher altitudes have lead to higher $SO_4$ concentrations near the surface and a better agreement with observations. The largest differences between the four CTM runs were found for $NH_4$ and $NO_3$ concentrations. $NH_4$ was systematically overestimated while $NO_2$ was strongly underestimated over the Spanish peninsula. Ozone concentrations which are strongly influenced by the meteorology were almost identical for all datasets.

## 89.4 Conclusions

The US-EPA SMOKE emission model has been successfully adopted and modified to use publicly available pan-European datasets in order to create high resolution emission data for Europe. Several pre-processors were developed

which transform these datasets to create the input data necessary to run the SMOKE for Europe (SMOKE-EU) model.

CMAQ has been used to calculate atmospheric concentrations of air pollutants using the four different emission datasets. These are the TNO-GEMS dataset created by TNO, a dataset from IER purchased by GKSS and the official gridded EMEP emissions provided by the MSC-W. Comparison of simulated values with observations from EMEP measurement stations showed that each of the four CTM runs produced sound results.

By comparison with other emission datasets for the years 2000 and 2003 it could be shown that the project to create high resolution European emission data with the use of open source data only was successful. Emission data created by SMOKE-EU will now be used for European long-term CTM runs for the timespan 1970–2010. Being a very flexible tool, SMOKE-EU will be further enhanced in the future. Improvements planned are different temporal profiles for each country, implementation of further photochemical mechanisms and the implementation of additional species (benzo[a]pyrene, mercury).

## References

1. Andersson C, Langner J (2005) Inter-annual variations of ozone and nitrogen dioxide over Europe during 1958–2003 Simulated with a regional CTM. Water Air Soil Pollut 7:15–23
2. Bieser J, Aulinger A, Matthias V, Quante M, Builtjes P (2010) SMOKE for Europe – adaptation, modification and evaluation of a comprehensive emission model for Europe. GMDD 3(3):949–1007
3. Borge R, Lumbreras J, Encarnacion R (2008) Development of a high-resolution emission inventory for Spain using the SMOKE modelling system: a case study for the years 2000 and 2010. Environ Modell Softw 23:1026–1044
4. Builtjes PJH, van Loon M, Schaap M, Teeuwisse S, Visschedijk AJH, Bloos JP (2003) Abschlussbericht zum FE-Vorhaben 298 41 252: "Modellierung und Prüfung von Strategien zur Verminderung der Belatung durch Ozon" Contribution of TNO-MEP. TNO-report R2003/166
5. Byun DW, Ching JKS (1999) Science algorithms of the EPA Models-3 community multi-scale air quality (CMAQ) modeling system. EPA/600/R-99/030, US EPA National Exposure Research Laboratory, Research Triangle Park
6. Byun DW, Schere (2006) Review of the governing equations, computational algorithms, and other components of the Models-3 community multiscale air quality (CMAQ) modeling system. Appl Mech Rev 59(2):51–77
7. European Commission (2000) Commission Decision 2000/479/EC of 17 July 2000 on the implementation of a European pollutant emission register (EPER) according to Article 15 of council directive 96/61/EC concerning integrated pollution prevention and control (IPPC). Off J Eur Commun L 192:36–43
8. Guenther A, Geron C, Pierce T, Lamb B, Harley P, Fall R (2000) Natural emissions of non-methane volatile organic compounds, carbon monoxide, and oxides of nitrogen from North America. Atmos Environ 34:2205–2230
9. Hanna SR, Davis JM (2001) Uncertainties in predicted ozone concentrations due to input uncertainties for the UAM-V photochemical grid model applied to the July 1995 OTAG domain. Atmos Environ 35(5):891–903

10. Horowitz LW, Walters S, Mauzerall DL, Emmons LK, Rasch PJ, Granier C, Tie X, Lamarque J-F, Schultz MG, Tyndall GS, Orlando JJ, Brasseur GP (2003) A global simulation of tropospheric ozone and related tracers: description and evaluation of MOZART, version 2. J Geophys Res 108:4784. doi:10.1029/2002JD002853
11. Houyoux MR et al (2000) Emission inventory development and processing for the seasonal model for regional air quality (SMRAQ) project. J Geophys Res 105(D7):9079–9090
12. Maes J, Vliegen J, van de Vel K, Janssen S, Deutsch F, de Ridder K, Mensink C (2009) Spatial surrogates for the disaggregation of CORINAIR emission inventories. Atmos Environ 43:1246–1254
13. MCNC-environmental modeling center: sparse matrix operational kernel emissions modeling system, http://envpro.ncsc.org/products/smoke/. Accessed 8 May 2008
14. Niemeier U, Granier C, Kornblueh L, Walters S, Brasseur GP (2006) Global impact of road traffic on atmospheric chemical composition and on ozone climate forcing. J Geophys Res 111 (D09):301. doi:10.1029/2005JD006407
15. Passant N (2002) Speciation of UK emissions of non-methane volatile organic compounds, AEA Technology, AEAT/R/ENV/0545, Feb 2002
16. Pierce T, Geron C, Bender L, Dennis R, Tonnesen G, Guenther A (1998) Influence of increased isoprene emissions on regional ozone modeling.J Geophys Res 103:25611–25629
17. Pregger T, Friedrich R (2009) Effective pollutant emission height for atmospheric transport modelling based on real-world information. Environ Pollut 157:552–560
18. Rockel B, Geyer B (2008) The performance of the regional climate model CLM in different climate regions, based on the example of precipitation. Meteorol Z 17(4):487–498
19. Rockel B, Will A, Hense A (2008) The regional climate model COSMO-CLM (CCLM). Meteorol Z 17:347–348
20. Russell D (2000) NARSTO critical review of photochemical models and modelling. Atmos Environ 34(12–14):2261–2282
21. Schwede D, Pouliot G, Pierce T (2005) Changes to the biogenic emissions inventory system version 3 (BEIS3). In: 4th CMAS Models-3 users' conference, Chapel Hill, 26–28 Sept 2005
22. Sedac (2010) Gridded population of the world version 3, http://sedac.ciesin.columbia.edu/gpw/global.jsp. Accessed 1 Jan 2010
23. Sofiev M, Miranda A I, Sokhi R (2009) Review of the capabilities of meteorological and chemistry-transport models for describing and predicting air pollution episodes, (WMO/TD-No. 1502), Technical report, COST 728 and GURME, Geneva.
24. UNC Carolina Environmental Program (2005) sparse matrix operator kernel emissions (SMOKE) Modeling system
25. U.S. Environmental Protection Agency (2009) community multiscale air quality modeling system, http://www.epa.gov/asmdnerl/models3/. Accessed 12 Aug 2009
26. Vestreng V, Mareckova K, Kakareka S, Malchykhina A, Kukharchyk T (2007) Inventory review 2007. Emission data reported to LRTAP convention and NEC directive. MSC-W Technical report 1 Jul 2007
27. Webdab (2010) http://www.ceip.at/emission-data-webdab/emissions-used-in-emep-models/. Accessed 1 Jan 2010
28. Yu Y, Sokhi RS, Kitwiroon N, Middleton DR, Fisher B (2008) Performance characteristics of MM5-SMOKE-CMAQ for a summer photochemical episode in southeast England, United Kingdom. Atmos Environ 42:4870–4883

# Chapter 90
# A Wintertime Local-to-Regional Scale Test Case Study of SILAM Model

**Riinu Ots, Ardi Loot, and Marko Kaasik**

**Abstract** The SILAM model (version 4.5.4) is applied for retrospective modelling of wintertime deposition fluxes of fly ash and sulphate near Estonian oil-shale-based industrial complex. The fluxes are validated against snow-based deposition measurements that have been carried out during nine winters since 1985. Also, the data from the Lahemaa (Estonia) and Virolahti (Finland) EMEP stations are applied for regional-scale validation. In this test case SILAM tends to systematically underestimate the deposition of fly ash and overestimate the deposition of sulphate at distances up to 30 km from the pollution sources. Overestimation of sulphate is severe during recent decade, whereas at more remote (100 km) EMEP stations the fluxes are nearly correct. As SILAM is basically developed and validated for meso-scale applications, some scale-dependent effects near the sources may appear. The recent changes in oil shale combustion technology may also play a role in increasing overestimation trend for sulphate.

**Keywords** Atmospheric deposition • Fly ash • Sulphate

## 90.1 Models and Methods

This is a local-to-regional scale case study aimed at validating the SILAM air quality modelling system [4] with secondary goal to understand more deeply the processes of transport and deposition of admixtures emitted from high industrial stacks.

The Eulerian kernel [5] of SILAM model, version 4.5.4, was applied for fly ash and sulphate dispersion and deposition computations (SILAM calculates the conversion of $SO_2$ to sulphate; all $SO_2$ is assumed to be converted in deposition process). To enhance the near-source performance, the thermal plume rise based on formulae by Briggs [1]

R. Ots • A. Loot • M. Kaasik (✉)
Institute of Physics, University of Tartu, Riia 142, 51014 Tartu, Estonia
e-mail: marko.kaasik@ut.ee

D.G. Steyn and S. Trini Castelli (eds.), *Air Pollution Modeling and its Application XXI*,
NATO Science for Peace and Security Series C: Environmental Security 4,
DOI 10.1007/978-94-007-1359-8_90, 

was included into SILAM code. The modelling domain includes Estonia and southernmost part of Finland with grid resolution nearly 3.3 km. The HIRLAM meteofields from BaltAN65+ reanalysis ([2], roughly 11 km grid resolution) were applied for years until 2005 and Estonian ETB-HIRLAM forecast data (3.3 km grid) for later years except 2009/2010, when the ETA HIRLAM (11 km grid) was applied due to technical reasons. The emission data are gathered from national inventories (since 1994) and review papers of national spread for earlier years.

The validation method is based on snow samples taken from the neighbourhood of two oil-shale-fired thermoelectric power plants (150–250 m stacks, 3 GW in total) and industrial enterprises nearby, most of samples closer than 30 km to the sources. The samples from natural snow cover (known duration) have been analysed for anions, cations and (in some winters) for suspended mineral matter. The fly ash load was estimated from calcium, based on known 22% calcium content of the ash [3]. The samples from winters 1984/1985, 1986/1987, 1993/1994, 1995/1996, 1998/1999, 2001/2002, 2002 (November–December), 2007/2008, 2008/2009 and 2009/2010 include 585 days of snow accumulation in total. Also, the daily-based sulphate deposition fluxes from Lahemaa and Virolahti EMEP stations (about 100 km from main sources, respectively to west and to north) are applied.

## 90.2 Results

The sample-wise deposition fluxes (modelled *vs*. measured) of fly ash and sulphate are presented in Figs. 90.1 and 90.2 respectively. The linear regression gives nearly two-fold underestimation for fly ash. Power regression gives better fit with slightly

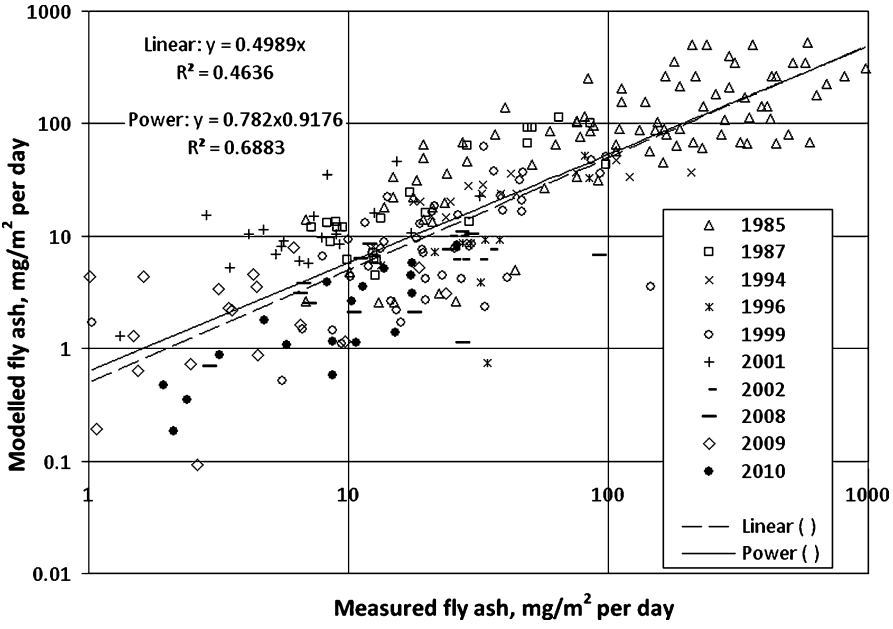


**Fig. 90.1** Modelled *versus* measured sample-wise deposition fluxes of fly ash

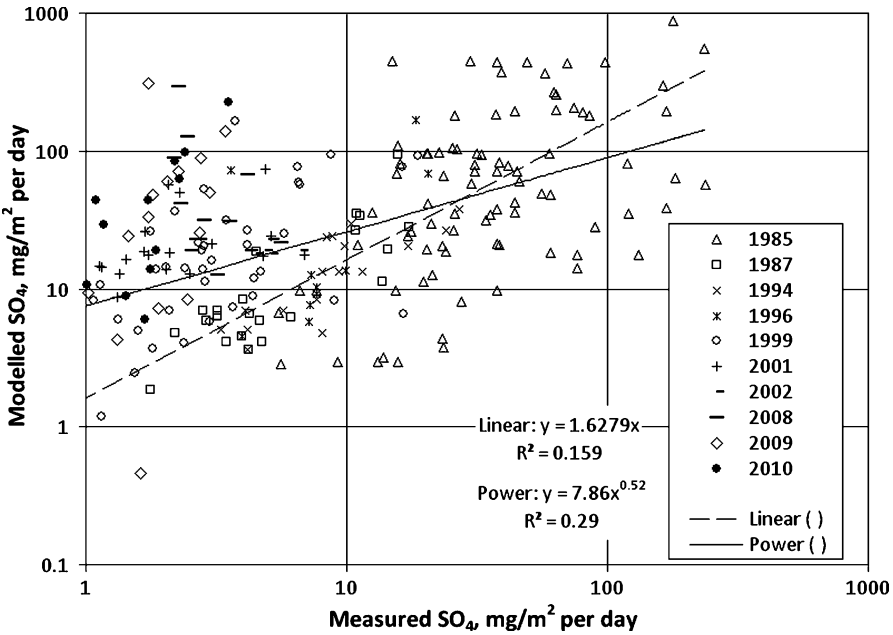


**Fig. 90.2** Modelled *versus* measured sample-wise deposition fluxes of sulphate ion

**Table 90.1** Yearly fit parameters for modelled *versus* measured deposition fluxes of sulphate ion (intercept forced to zero). Year indicates the end of snow cover, when samples were collected

| Year | 1985 | 1987 | 1994 | 1996 | 1999 | 2001 | 2002 | 2008 | 2009 | 2010 |
|---|---|---|---|---|---|---|---|---|---|---|
| Sites | 87 | 22 | 17 | 10 | 44 | 19 | 11 | 11 | 18 | 18 |
| Days | 99 | 94 | 27 | 69 | 66 | 68 | 16 | 12 | 42 | 92 |
| Slope | 1.60 | 2.50 | 1.44 | 4.53 | 3.78 | 4.98 | 7.44 | 21.7 | 28.3 | 33.24 |
| $R^2$ | 0.049 | 0.181 | 0.596 | 0.394 | 0.230 | 0.183 | −0.109 | −0.145 | 0.042 | 0.547 |

weaker dependence than linear: fit is almost perfect for small deposition fluxes and two-fold underestimation occurs for highest ones. For sulphate the different regression types give very different fit with rather poor determination coefficients: the data points are so scattered that it is useless to analyse all the data together. The yearly-based slope (Table 90.1) shows increasing overestimation in time, but years 2001 and forward, seem rather unreliable due to poor determination coefficients in general and even negative slope in 2008. The winter ending in 2010, with exceptionally stable snow cover during more than 90 days, was an exception with well-determined fit, but exposes the highest overestimation rate.

Year-wise comparison of modelled and measured deposition fluxes of sulphur in two EMEP stations gives us nearly perfect slope 1.07, rather small intercept −0.74 mg/m$^2$ per day, most probably representing the background flux, reliable determination coefficient 0.82 and no evident trend in time. However, EMEP data from most recent years, 2009 and 2010, are not available yet. This fair fit agrees with earlier European-scale validations of SILAM.

## 90.3 Discussion and Conclusions

It seems that SILAM, initially designed for meso-scale applications, has problems reproducing the local-scale processes with sulphuric compounds near the sources. According to the SILAM results, mainly the washout processes are responsible on deposition fluxes of SOx. Thus, the washout calculated by SILAM may be too fast due to inadequate description of processes occurring with freshly emitted sulphur dioxide.

On the other hand, there is obvious trend for much higher overestimation for recent years. There may appear discrepancies due to dramatically decreased emissions (thus, lower concentrations in the air, affecting the saturation processes) and remarkable changes in oil shale combustion technology within recent decade. Partial transition from pulverised oil shale combustion to the circulating fluidised bed technology has reduced the ratio of fly ash *vs*. sulphuric emissions. In general, deposition fluxes are found following the dramatic decrease of emissions during last 25 years, when the oil-shale-fired power plants in Estonia were converted from major European scale emitters into pollution sources of local-to-regional importance.

**Acknowledgments** This study is funded by Estonian National Targeted Financing Project SF0180038s08 and the Estonian Science Foundation, research grant No. 7005.

## References

1. Briggs G (1984) Plume rise and buoyancy effects. In: Randerson D (ed) Atmospheric science and power production, US Department of Energy
2. Luhamaa A, Kimmel K, Männik A, Rõõm R (2011) High resolution re-analysis for the Baltic Sea region during 1965–2005 period. Clim Dyn 36(3–4):727–738. doi:10.1007/s00382-010-0842-y
3. Pets LI, Vaganov PA, Knoth J, Haldna ÜL, Schwenke H, Schnier C, Juga RJ (1985) Microelements in oil-shale ash of the Baltic thermoelectric power plant. Oil Shale 2(4):379–390
4. Sofiev M, Siljamo P, Valkama I, Ilvonen M, Kukkonen J (2006) A dispersion modelling system SILAM and its validation against ETEX data. Atmos Environ 40:674–685
5. Sofiev M, Galperin M, Genikhovich E (2008) Construction and evaluation of Eulerian dynamic core for the air quality and emergency modeling system SILAM. In: Borrego C, Miranda AI (eds) NATO Science for peace and security, vol C, Environmental security. Air pollution modelling and its application, XIX. Springer, Dordrecht, pp 699–701

# Chapter 91
# Air Pollution Dispersion Modeling Around Thermal Power Plant Šoštanj in Complex Terrain: Model Validation and Regulatory Planning

**Marija Zlata Božnar, Boštjan Grašič, and Primož Mlakar**

**Abstract** Performance and efficiency of the general purpose air-pollution dispersion modeling system based on Lagrangian particle model Spray is evaluated on highly complex terrain over Šaleška region. The evaluation is made to determine if modeling system complies with the requirements of the Slovenian legislation for industrial air pollution control which requires efficient modeling systems for small domains over complex terrain. Evaluation has proved that the modeled concentrations show significant agreement in time and place with the observations. After this proof was available the model was used for regulatory planning of the new block stack.

**Keywords** Air pollution modeling • Lagrangian particle dispersion model • Compley terrain • Model validation • Regulatory planning

## 91.1 Introduction

Most of the industry and power plants in Slovenia are placed in very complex terrain. The evaluation of the air pollution effects of these sources is therefore a considerable challenge that requires the usage of the most advanced numerical models that have prior proven successful validation in similar conditions. In the case of Šoštanj the validation was done on a set of historical data from the measuring campaign held on the same location in 1991.

Šoštanj Thermal Power Plant is Slovene biggest thermal power plant that burns local coal. The TPP is in the process of building new block that will substitute several older ones and therefore reduce the emissions of the pollutants in the air.

For the new block the study had to answer the question of the optimal height and configuration (stand alone stack or combined cooling tower with stack inside) for

M.Z. Božnar (✉) • B. Grašič • P. Mlakar
MEIS d.o.o., Mali Vrh pri Šmarju 78, SI-1293 Šmarje-Sap, Slovenia
e-mail: marija.zlata.boznar@meis.si; bostjan.grasic@meis.si; primoz.mlakar@meis.si

D.G. Steyn and S. Trini Castelli (eds.), *Air Pollution Modeling and its Application XXI*, NATO Science for Peace and Security Series C: Environmental Security 4,
DOI 10.1007/978-94-007-1359-8_91, 

the given planned emission parameters and with strict respecting of the required ambient air quality in the plant's vicinity according to the European legislation.

This is not a simple question as the TPP is placed in the relatively closed basin with high hills around. The TPP is placed at the border of the basin, just next to the hills. The area is characterized by weak winds, several calm periods and often winter thermal inversions.

## 91.2 Models Used

The studies were done with numerical Lagrangian particle model Spray [11] coupled with the Surfpro turbulence pre-processor [10] and Minerve [4] 3D mass consistent wind field model based on diagnostic measurements that include vertical wind profile measurements and several ground level meteorological measurements.

## 91.3 Models Evaluation

The main goal of the study is qualitative evaluation of a modeling system by using operational configuration of both input data and model parameters and selecting a testing period with very complex dispersion conditions. Such validation improves the understanding of the quality of modeling results that can be achieved in presented conditions. It also gives new ideas for better evaluations and better understanding of some results that can be sometimes underestimated by certain statistical evaluations.

For evaluation data is used from experimental campaign performed around the Šoštanj Thermal Power Plant during the spring of 1991 [5]. The database consists of very high ambient concentrations over complex terrain due to the absence of desulphurization plants. Three weeks of data exist that include meteorological measurements and measurements of $SO_2$ on several stations in the TPP vicinity, one SODAR and automated emission measurements in all TPP stacks.

The simulation is performed for the full duration of campaign. To outline the model behavior in complex conditions a particular situation during 1st and 2nd of April 1991 (including accumulation and convective mixing) is used for detailed demonstration.

Measurements during this demonstrated period show that wind speeds were very low and winds change direction rapidly. Consequently the plume is spread in all directions. At the positions of air quality measuring stations statistical indexes are computed between measured and reconstructed $SO_2$ concentrations.

Comparison showed that air pollution events with wind blowing directly from the TPP towards the ambient air quality station are correctly reconstructed, while others reconstructed $SO_2$ concentrations are in overall underestimated relative to the measured ones, but the overall pattern of peaks measured is well reproduced.

One of the possible reasons is relatively small domain that in most complex cases of night accumulation below the inversion layer enables some of the polluted masses to escape out of domain and morning wind direction complete changes could not bring that back. Relatively small domain was chosen because of the terrain complexity and because of the need of as good as possible ambient concentrations reconstruction in the TPP vicinity. Detail case by case and numerical evaluation is given in [7, 8]. It can also be compared with past validations of the same models and campaign data [2, 3].

## 91.4 Regulatory Planning

After the models suite was successfully validated on historical Šoštanj experimental campaign data, it was used to determine the appropriate height and configuration of the stack for the new Block 6.

Several different configurations and heights were tested in combination with existing Block 5. The studies were done on more recent meteorological measurements. These data include 1 year of measurements elaborated in half hour intervals. Measurements were taken at one SODAR and ten ground level meteorological stations in the basin and on the hills near by TPP. FAIRMODE guidelines were followed [6]. Special conditions due to combined cooling tower were taken into account [1, 9].

It was calculated that the configuration of combined cooling tower with stack inside is preferable solution. The combined cooling tower will be 157 m high.

Detail evaluation was in addition focused on the influence of air pollution during the episodes of northern winds that move plume directly toward the hills that are the closest to the TPP.

## 91.5 Conclusions

Slovene complex terrain requires the usage of most advance numerical models to determine correctly the local impact of industrial emissions on ambient air.

Several data sets exist on Slovene territory that enables evaluation of models performances. The most complete data set is Šoštanj experimental campaign from 1991. Using this data Lagrangian particle model Spray was successfully validated and after validation it was used for regulatory planning of the new Block 6 of Šoštanj TPP. Validation of models in similar conditions before the regulatory usage is mandatory [6]. And model should be fit to the purpose (development and validation made for similar scale of domain, similar terrain and meteorological conditions).

**Acknowledgments** The study was partially financed by the Slovenian Research Agency, Project No. L1-2082 and Ministry of Higher Education, Science and Technology of Republic of Slovenia, Grant No. 3211-05-000552.

## References

1. Anfossi D, Richiardone R, Bonino G (1979) An application of a plume rise model for multiple sources to the cooling tower plumes of John E Amos power plant. Nuovo Cimento C 2 (4):488–497
2. Božnar M, Brusasca G, Cavicchioli C, Faggian P, Finardi S, Minella M, Mlakar P, Morselli MG, Sozzi R (1994) Model evaluation and application of advanced and traditional Gaussian models on the experimental Šoštanj (Slovenia, 1991) campaign. In: Cuvelierv C (ed) Workshop on intercomparison of advanced practical short-range atmospheric dispersion model, Manno, 1993, Proceedings of the workshop, European Commission, pp 112–121
3. Božnar M, Brusasca G, Cavicchioli C, Faggian P, Finardi S, Mlakar P, Morselli MG, Sozzi R, Tinarelli G (1994) Application of advanced and traditional diffusion models to an experimental campaign in complex terrain. In: Baldsano et al. JM (ed) 2nd international conference on air pollution, Barcelona, 1994, Air Pollution II, vol 1, Computer Simulation, Southampton, Boston, Computational Mechanics Publisher, pp 159–166
4. Desiato F, Finardi S, Brusasca G, Morselli MG (1998) TRANSALP 1989 Experimental campaign – Part I: simulation of 3-D Flow with diagnostic wind field models. Atmos Environ 32(7):1141–1156
5. Elisei G, Bistacchi S, Bocchiola G, Brusasca G, Marcacci P, Marzorati A, Morselli MG, Tinarelli G, Catenacci G, Corio V, Daino G, Era A, Finardi S, Foggi G, Negri A, Piazza G, Villa R, Lesjak M, Božnar M, Mlakar P, Slavic F (1992) Experimental campaign for the environmental impact evaluation of Šoštanj thermal power plant, progress report. CISE Technology innovative, Milano, Italia, ENEL S.p.A, CRAM-Servizio Ambiente, Milano, Italy, C.I.S.E. Technology innovative S.p.A, Milano, Italy, Institute Jozef Stefan, Ljubljana
6. FAIRMODE (2009) Guidance on the use of models for the European Air Quality Directive, (FAIRMODE – Forum for Air Quality Modelling in Europe) ETC/ACC report, Version 5.1, http://fairmode.ew.eea.europa.eu/fol404948/guidance-document/Model_guidance_document_v5_1.pdf/download. Accessed 20 Jun 2010
7. Grašič B, Božnar MZ, Mlakar P (2007) Re-evaluation of the Lagrangian particle modelling system on an experimental campaign in complex terrain. Nuovo Cimento C 30 (6):557–575
8. Grašič B, Mlakar P, Božnar MZ, Tinarelli G (2008) Enhanced evaluation of a Lagrangian-particle air pollution model based on a Šaleška region field data set. In: Brebbia CA, Longhurst JWS (ur) Air pollution XVI: [reviewed papers accepted for the sixteenth international conference on modelling, monitoring and management of air pollution held in Skiathos, Greece, September 2008], (WIT transactions on ecology and the environment, vol 116). Southampton, WIT, cop. 2008, pp 39–48
9. Marzorati A (1992) Cooling towers study. ENEL, Milan
10. Silibello C (2006) SURFPRO (SURrface-atmosphere interFace PROcessor) User's guide. ARIANET report R2006.06
11. Tinarelli G, Anfossi D, Bider M, Ferrero E, Trini Castelli S (2000) A new high performance version of the Lagrangian particle dispersion model SPRAY, some case studies. In: Gryning SE, Batchvarova E (eds) Air pollution modelling and its applications XIII. Kluwer/Plenum, New York, pp 499–507

# Part V
# Aerosols in the Atmosphere

# Chapter 92
# Will Pollution Reduce Precipitation?

**Andrea I. Flossmann and Wolfram Wobrock**

**Abstract** The results of parcel model studies seem to indicate that increasing particulate pollution and decreasing solubility suppresses rain formation. In individual and short time cloud simulations this behaviour was confirmed in our 3D model studies. However, taking into account entire cloud fields over longer periods of time yields the strong spatial and temporal variability of the results with isolated regions of inverse correlation of the effects. Even though in general the expected behaviour was found, after several hours of simulation, the integrated precipitation of the more polluted cases caught up. This suggests that a changing pollution will affect the spatial and temporal pattern of precipitation, but will probably not reduce the overall long term precipitation amount which might be entirely governed by the moisture state of the atmosphere.

**Keywords** Clouds • Aerosol particles • Pollution

## 92.1 Introduction

Still in the 1970s, the community of the cloud physicists was well separated from the community of the aerosol physicists. It was commonly understood that clouds were determined by the sounding and water vapour supply and that saturation was mostly maintained. Aerosol particles were mainly related to health problems.

However, even at that time the role of particles in cloud nucleation was known already for about a 100 years from scientists like Aitken and Wilson (for a review see [7]). But first attempts of planned weather modification to make use of this

A.I. Flossmann (✉) • W. Wobrock
Laboratoire de Météorologie Physique, Clermont Université,
Université Blaise Pascal, F-63000 Clermont-Ferrand, France

CNRS, INSU, UMR 6016, LaMP, F-63177 Aubière, France
e-mail: a.flossmann@opgc.univ-bpclermont.fr

D.G. Steyn and S. Trini Castelli (eds.), *Air Pollution Modeling and its Application XXI*,
NATO Science for Peace and Security Series C: Environmental Security 4,
DOI 10.1007/978-94-007-1359-8_92, 

knowledge were only started in the middle of the 1950s. In particular the role of silver iodide on the formation of the ice phase was used for hail prevention (see [2] for a review of cloud seeding).

In the 1980s the first models were designed to put together the different pieces and obtain an overall picture of the importance of aerosol particle loading for the formation and evolution of the cloud. It became possible not only to study the role of the particles in the formation of a cloud, but also to study the cleaning capacity of the cloud in the overall pollution problem. A scientific review of the aerosol pollution impact on precipitation can be found in Levin and Cotton [5]. Also, the removal of accidental releases of particles by rain was an important issue [2].

In general, these studies seem to indicate that an increase of particulate pollution in the atmosphere suppresses precipitation formation. Often, these results were obtained by modelling exercises in an individual cloud using a simple dynamical framework. The following study aims to investigate the validity of the simple "air parcel" type assumption, in focussing on the particular role of supersaturation in a bin resolved microphysics model and a 3-D dynamics of an entire cloud.

## 92.2 The Model

The 3D model with detailed (bin) microphysics used herein couples the 3D non-hydrostatic model of Clark and Hall [1] with the Detailed Scavenging Model DESCAM [3, 4] for the microphysical package. It follows 5 density distribution function: the number distribution function for the aerosol particles $f_{AP}(m_{AP})$, for drops $f_d(m)$ and for the ice particles $f_i(m_i)$, as well as the mass density distribution function for aerosol particles in the drops $g_{AP,d}(m)$and in the ice crystals $g_{AP,i}(m_i)$ (Fig. 92.1).

A discussion of the different processes considered in the microphysics code can be found in Flossmann and Wobrock [3], and the coupling with the 3-D code is discussed in Leroy et al. [4].

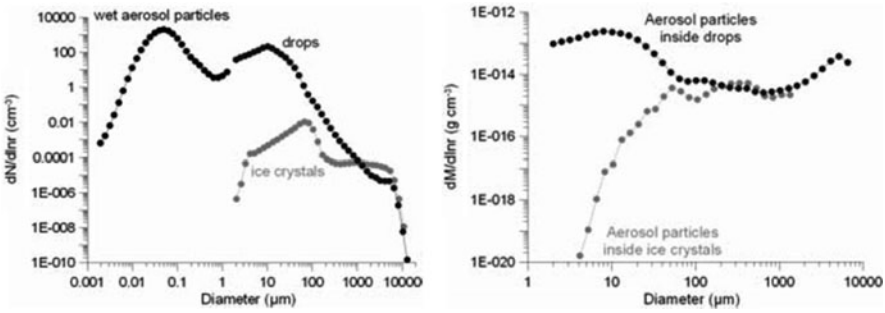


**Fig. 92.1** The grid resolution of the different distribution functions treated by DESCAM 3D

## 92.3 Results

### *92.3.1 In-Cloud Dynamics of a Single Cloud*

As was already shown in Leroy et al. [4], even the evolution of an individual cloud is far from being adiabatic.

The figures below show the Crystal-Face cloud simulated by them and indicate the complex dynamics, giving rise to rather different life histories of the individual "air parcels" making up the cloud.

### *92.3.2 In-Cloud Dynamics of a Cloud Field*

We note from Fig. 92.2 the complex structure of an individual cloud. In an entire cloud field, as modelled by Planche et al. [6] for the COPS field campaign, the situation is equally complex, as shows the Fig. 92.3.

We note that in the complex cloud field about 85% of the parcels experience one, two, three, or more periods of subsaturation, while only 15% of the parcels stay always supersaturated after passing cloud base, as is suggesting the rising air parcel concept.

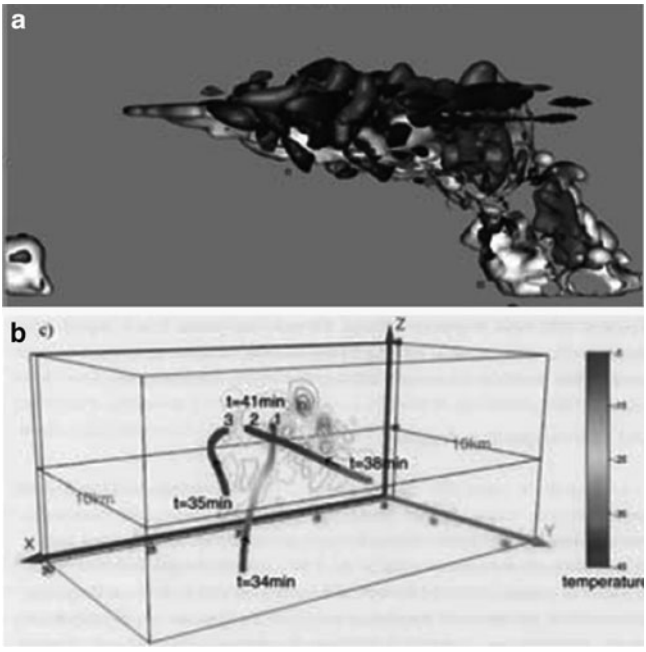


**Fig. 92.2** (**a**) Simulation of a Crystal-Face convective cloud (situation after precipitation formation): *medium*: updrafts $> 8\ \mathrm{m\ s^{-1}}$; *dark*: downdrafts $> 8\ \mathrm{m\ s^{-1}}$; *light*: cloud water $> 0.03\ \mathrm{g\ m^{-3}}$, (**b**) Life history of 3 neighbouring points ending in the anvil at 11 km altitude

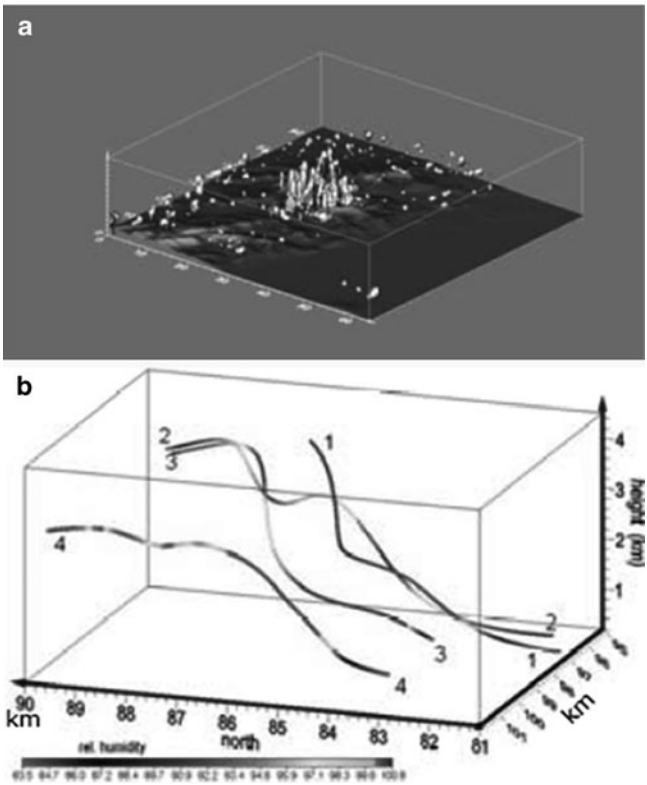


**Fig. 92.3** (**a**) Cloud field over complex *terrainwhite*: cloud water, *grey*: rain water, (**b**) *medium*: supersaturated; *dark*: outside cloud; *light grey*: still in cloud

We note that the most probable supersaturation is a function of the total number of particles available and their composition: $S_{mean,min} = 0.05\%$ for polluted all soluble particles and $S_{mean,max} = 0.5\%$ for clean mostly insoluble particles. The influence of the initial aerosol particle spectrum propagates to the precipitation on the ground.

### *92.3.3 Precipitation for a Single Cloud*

Figure 92.4 indicates the sensitivity of a single cloud with respect to the initial pollution of the boundary layer.

We note that a highly polluted boundary layer is able to suppress precipitation entirely in the model. However, this result applies to an individual cloud and for the lifetime of an individual cloud [4].

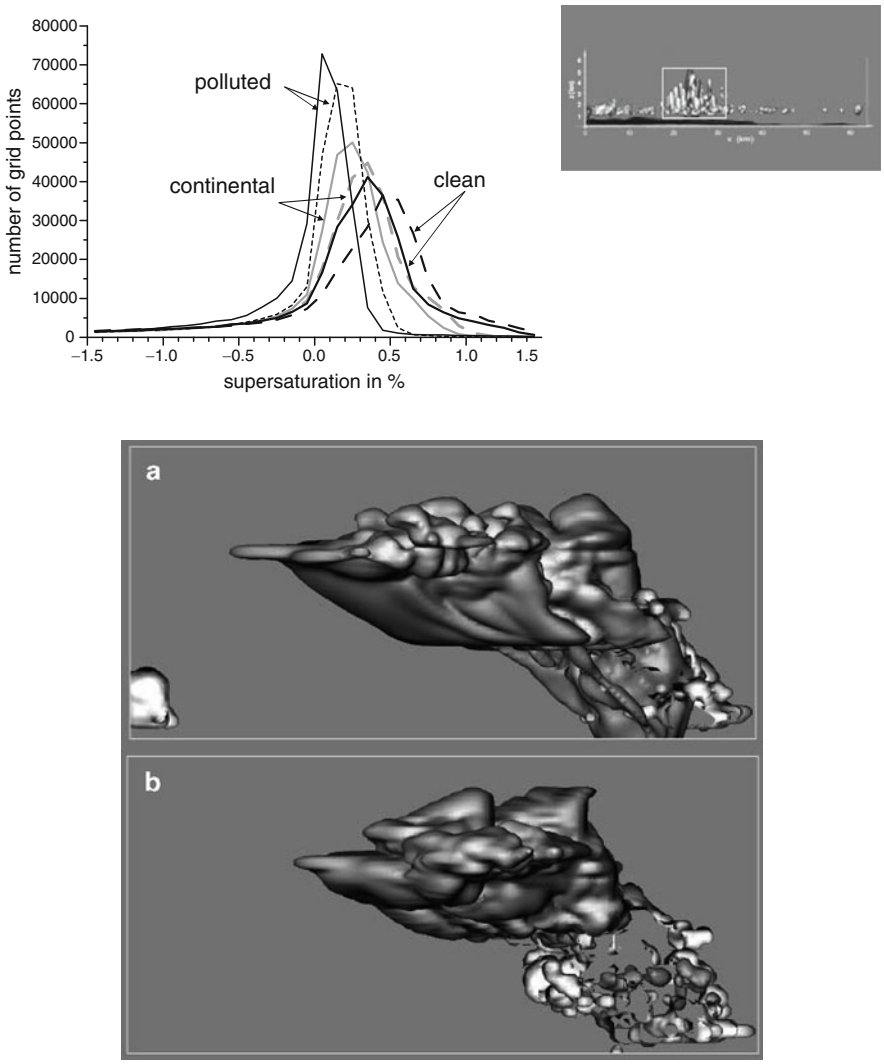


**Fig. 92.4** Role of aerosol concentration and composition for supersaturation in the white box of the cloud field (*solid line* pertains to complete soluble particles); *dashed curve* to particles with 0.01% solubility [6]. (**a**) Clean boundary layer: $N_{AP} \approx 400$ cm$^{-3}$; Cloud drops (*light grey*): 0.01 g m$^{-3}$; Raindrops (*medium grey below*): 1 g m$^{-3}$; Ice crystals (*medium high*): 0.01 g m$^{-3}$, (**b**) Polluted boundary layer: $N_{AP} \approx 6{,}500$ cm$^{-3}$; Cloud drops (*light grey*): 0.01 g m$^{-3}$; Raindrops (*medium grey below*): 0.03 g m$^{-3}$; Ice crystals (*medium grey high*): 0.01 g m$^{-3}$

### *92.3.4 Precipitation of a Cloud Field as a Function of Time*

Figure 92.5 shows the result of a cloud field that remained stagnant over the Cevennes Mountains in the south of France. It depicts the difference of rain for a simulation initialized with a rather clean spectrum and one with a polluted one.

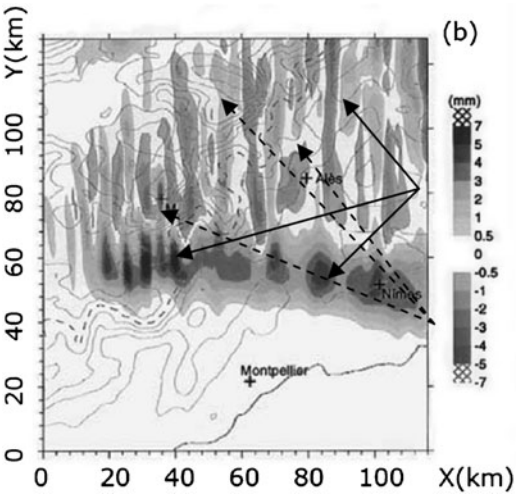


**Fig. 92.5** Difference of precipitation between the continental particle spectrum and a polluted particle spectrum: in the southern part: more rain for continental case; negative values in the mountains: more rain for polluted case

**Table 92.1** Evolution with time of the total integrated amount of rain for the different cases considered

| Simulation time (h) | Mixed phase continental case (700 $cm^{-3}$) | Mixed phase polluted case (2,400 $cm^{-3}$) | Difference (mixed cont.− mixed poll.) in % |
|---|---|---|---|
| 2 | 7.1 | 5.7 | −20 |
| 3 | 30.9 | 26.4 | −15 |
| 4 | 62.3 | 54.3 | −13 |

We note that not at all locations the cleaner case gives more precipitation, but that at some location the more polluted one rains more. Globally, if averaged over the entire domain, the text book results come out again, however, the difference between the two cases decreases with time (Table 92.1).

### *92.3.5 Precipitation of a Cloud Field as a Function of Particle Number*

For the COPS field campaign we have varied the number of particles in the boundary layer as already discussed in Fig. 92.3. The resulting pattern for the integrated amount of rain on the ground can be found in Fig. 92.6.

We note that, globally, decreasing pollution increases the total amount of precipitation and the total watered surface. But locally, the tendency can be opposite. Table 92.2 summarizes the properties for the three cases:

Table 92.3 shows the results if only solubility is varied.

We note that globally decreasing solubility increases the total amount of precipitation and the total watered surface. However, the effect is much weaker than the influence of the number concentration. However, locally (not shown), we have also an inverse behaviour [6].

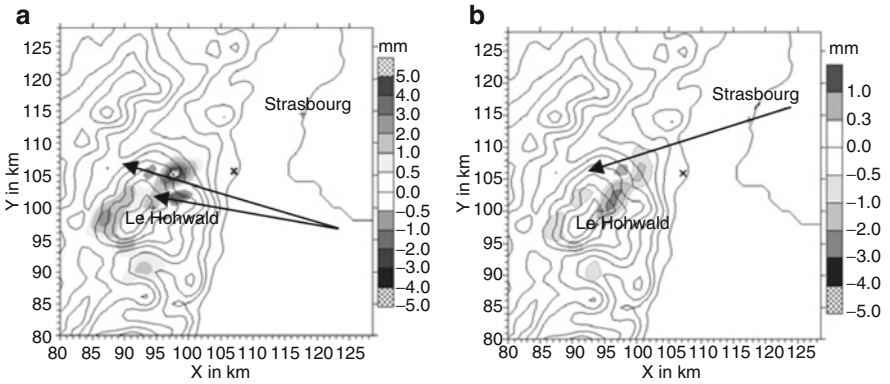


**Fig. 92.6** (**a**) Difference continental – polluted (all values positive except *2* marked places), (**b**) Difference continental – clean (all values negative except *1* marked place)

**Table 92.2** Variables for the cumulative rain on the ground as a function of initial aerosol particle number

| | Continental $\varepsilon = 1$ | Clean $\varepsilon = 1$ | Polluted $\varepsilon = 1$ |
|---|---|---|---|
| Rain max. (mm) | 7.42 | 8.02 | 6.39 |
| Mean rain (mm) | 1.74 | 2.00 | 1.31 |
| Rain area ($km^2$) | 337 | 344 | 307 |
| Total rain (Mt) | 0.59 | 0.69 | 0.40 |

**Table 92.3** Variables for the cumulative rain on the ground as a function of initial aerosol particle solubility

| | Continental $\varepsilon = 1$ | Continental $\varepsilon = 0.5$ | Continental $\varepsilon = 0.05$ |
|---|---|---|---|
| Rain max. (mm) | 7.42 | 7.52 | 7.68 |
| Mean rain (mm) | 1.74 | 1.80 | 1.93 |
| Rain area ($km^2$) | 337 | 335 | 339 |
| Total rain (Mt) | 0.59 | 0.60 | 0.65 |

## 92.4 Conclusion

From the simulations we noted that inside cloud (LWC $> 0.1$ g $m^{-3}$) about 20% of the area is subsaturated. The most probable supersaturation in clouds increases with decreasing total number concentration and decreasing solubility. Varying particle number concentration can suppress precipitation for individual clouds. For cloud fields and longer simulations times, we note a strong temporal and spatial variability. Some locations show an inverse behaviour from the overall trend at some time. The differences seem to decrease in the course of time.

We can conclude that the air parcel concept generally over predicts the reaction of the cloud to the initial parameters. The complex dynamics and microphysics

installs a non-linear feedback. Great caution is, thus, advised before making climate relevant conclusions.

For the time being, we can state, that pollution can suppress precipitation, but more research is needed to confirm the behavior for longer periods and larger scales.

One hypothesis seems to impose itself: precipitation is mainly determined by water vapor availability; pollution might only influence the spatial and temporal variation. This hypothesis needs to be validated in the future.

## References

1. Clark TL, Hall WD (1991) Multi-domain simulations of the time dependent Navier-Stokes equation: benchmark error analysis of some nesting procedures. J Comput Phys 92:456–481
2. Cotton WR, Pielke RA (1992) Human impacts on weather and climate. Cambridge University Press, Cambridge, 288 pp
3. Flossmann AI, Wobrock W (2010) A review of our understanding of the aerosol – cloud interaction from the perspective of a bin resolved cloud scale modelling, accepted. Atmos Res. doi:10.1016/j.atmosres.2010.05.008
4. Leroy D, Wobrock W, Flossmann AI (2009) The role of boundary layer aerosol particles for the development of deep convective clouds: a high-resolution 3D model with detailed (bin) microphysics applied to CRYSTAL-FACE. Atmos Res 91(1):62–78. doi:10.1016/j.atmosres.2008.06.001
5. Levin Z, Cotton WR (eds) (2009) Aerosol pollution impact on precipitation, a scientific review. Springer, Dordrecht, 386 pp
6. Planche C, Wolfram W, Andrea IF, Frédéric T, Van Joël B, Yves P, Martin H (2010) The influence of aerosol particle number and hygroscopicity on the evolution of convective cloud systems and their precipitation: A numerical study based on the COPS observations on 12 August 2007. Atmos Res 98(1):40–56. doi:10.1016/j.atmosres.2010.05.003
7. Pruppacher HR, Klett JD (1997) Microphysics of clouds and precipitation, 2nd edn. Kluwer Academic, Dordrecht, 954 p

## Questions and Answers

**Questioner Name**: Akula Venkatram

**Q**: The common understanding of cloud physics suggests that increasing CCN increases precipitation. Your talk suggests that increasing aerosols decreases precipitation. Could you explain this discrepancy?

**A**: It depends on the size of aerosol particles that are added. Large particles (added e.g. during seeding attempts) can potentially increase precipitation. Small particles (as in pollution episodes) seem rather to reduce precipitation.

**Q**: Considering the complexity of cloud physics, how do you explain the good comparison between model estimates and observation?
**A**: Thank you. Small scale cloud models have significantly evolved during the years. Provided they have good input data, they can do a good job, on reasonable time scales.

**Questioner Name**: Joakim Klausner

**Q**: How important were ice clouds in the simulations for the COPS experiment?
**A**: For the case presented, ice was not important. Cloud top was low and the clouds were basically liquid. However, the model considers the ice phase.

**Questioner Name**: Tony Dore

**Q**: Does the dissolution of gases into cloud droplets have an important influence on modifying aerosol properties and the potential to modify long term precipitation?
**A**: Dissolution of gases and subsequent chemical reactions add to the processing of aerosol particles. After evaporation, particles are generally larger and more soluble.

# Chapter 93
# Aerosol Simulation with Fully Coupled "Online" Meteorology-Chemistry Model WRF/Chem over Europe: Preliminary Results

**Paolo Tuccella, Gabriele Curci, and Guido Visconti**

**Abstract** The new generation fully coupled "online" WRF/Chem model is implemented over Europe on a coarse grid and validated against ground-based observations of meteorological variables and atmospheric composition. Anthropogenic emissions are derived from the EMEP database. We studied its sensitivity to "Dudhia" and "Goddard" short waves radiation schemes. The model satisfactory reproduces the observed meteorological fields, particularly with the Goddard scheme. For chemical variable, they are not much difference between the two scheme. Ozone ($O_3$) daily maximum is reproduced with a correlation of 0.81 and an root mean square error (RMSE) of 23 $\mu g/m^3$. Nitrogen dioxide ($NO_2$) is overestimated by a factor of 2, and reproduced with a correlation of 0.47. Particulate matter shows poor correlation with observations, however the model captures the magnitude of $PM_{2.5}$ concentrations (bias $-10\%$, RMSE 7 $\mu g/m^3$). Simulated $PM_{10}$ is affected by a too strong local dust source over dry areas.

**Keywords** Urban and regional air quality modelling • Aerosol particles • Air quality forecasting

## 93.1 Introduction

In recent years, aerosols have received much attention by scientific community. Anthropogenic aerosol particles play a key role in Earth climate because they act on radiation budget (direct effects) and on properties and distribution of clouds (indirect effect) [7]. Moreover, they are responsible for cardiopulmonary diseases [6]. Chemistry-Transport Models (CTM) are recognized as very useful tools for

P. Tuccella (✉) • G. Curci • G. Visconti
CETEMPS – Dip. Fisica, Università degli Studi dell'Aquila, Via Vetorio,
67010 Coppito, L'Aquila, Italy
e-mail: paolo.tuccella@aquila.infn.it; gabriele.curci@aquila.infn.it

D.G. Steyn and S. Trini Castelli (eds.), *Air Pollution Modeling and its Application XXI*,
NATO Science for Peace and Security Series C: Environmental Security 4,
DOI 10.1007/978-94-007-1359-8_93, 

studying aerosol distribution and planning emission reduction strategies for abatement of PM concentrations

In CTMs commonly the chemical processes are solved independently by meteorological model, whose output feeds the transport and chemistry. The decoupling between these two components leads to a loss of information, because of physical and chemical processes occurring on a time scale much smaller than the output time of the meteorological model [3]. WRF/Chem is a coupled "online" model where the chemistry is fully consistent with meteorological processes.

In this work, we report on a first validation of a European implementation of the WRF/Chem model [2, 3] and its sensitivity to two different short waves (SW) radiation schemes.

## 93.2 Model Setup

In this study the version 3.1.1 of WRF/Chem is implemented over Europe. Two simulations are conducted in July 2007 on a grid that extends from 35°N at 57°N in latitude and from 15°W at 27°E in longitude with a horizontal resolution of 30 Km and with 28 vertical levels which extend to ~20 Km. The initial and boundary meteorological conditions are provided by ECMWF analyses with a resolution of 0.5° every 6 h.

The configuration of WRF/Chem is shown in Table 93.1. Previous studies and sensitivity tests indicate that the combination of schemes for surface layer and PBL adopted in this work produces the best results [8]. The two simulations presented here differ only for SW radiation scheme. In first we use the Dudhia scheme [3], in second the finest Goddard scheme [2].

The main step for implementation of WRF/Chem over Europe is the development of an inventory of anthropogenic emissions of $NO_x$, VOCs, CO, $SO_x$, $NH_3$ and aerosol mass. We used the EMEP inventory [9], which provides total annual emission of trace

**Table 93.1** WRF/Chem configuration. The simulations differ only for SW radiation scheme

| Physical process | WRF/Chem option |
|---|---|
| Microphysics | Lin |
| Long-wave radiation | RRTM |
| Short-wave radiation | Dudhia in first simulation, Goddard in second |
| Surface layer | Monin-Obukhov |
| Land-surface model | Noah LSM |
| Boundary layer scheme | MYNN Level 2.5 PBL |
| Cumulus parameterization | Grell-Devenyi |
| Photolysis scheme | Madronich |
| Chemistry model | RADM2 |
| Aerosol model | MADE/SORGAM |

gases and particulate matter over Europe with a resolution of 50 Km for several types of sources (SNAP sectors). The procedure followed to build the emissions interface with model is similar to that illustrated by Bessagnet et al. [1]. Total amount of NMVOC emissions is disaggregated into several species using speciation coefficients for each SNAP sector [5]. Aggregation of NMVOC species into RADM2 emissions species is done following a reactivity-weighting procedure [4].

Elemental carbon and organic carbon emissions are taken from 2000 total annual data emissions provided by the Laboratoire d'Aerologie (www.aero.obs-mip.fr). Biogenic emissions are calculated on line by WRF/Chem with a module based on the Guenther scheme [10]. Dust and sea salt emissions [10] are included in the simulations.

## 93.3 Results for July 2007

Each simulation is compared against meteorological (hourly temperature, wind speed, wind direction and relative humidity) and chemical (hourly O3 and daily mean NO2, PM2.5 and PM10) ground-based observations. We use the NOAA (www.ncdc.noaa.gov/oa/climate/isd/index.php) and EMEP (www.emep.int) databases. Table 93.2 we show statistics of comparison.

The temperature is simulated with a mean CC of 0.86 and both configurations have a negative small bias. The smallest NMBE and RMSE are produced by Goddard scheme being about −2% and 3°C, respectively. The wind speed is over predicted in all simulations by ~50%. The best CC (0.55) is showed by Goddard model configuration and the best RMSE (2.17 m/s) by Dudhia. The predicted relative humidity has a positive bias; the best statistical indices are found in second simulation, 0.67 for CC and 15.89% for RMSE.

Better meteorological performances of Goddard scheme are not reflected in all chemical variables. The simulations have the same mean statistic for $O_3$. The hourly

**Table 93.2** Comparison of meteorological and chemical ground-based observations with WRF/Chem simulations for July 2007 over Europe, with two different short-wave (*SW*) radiation schemes. CC is the correlation coefficient, MNBE is the mean normalized bias error, and RMSE is the root mean square error

| | | Dudhia SW | | | Goddard SW | | |
|---|---|---|---|---|---|---|---|
| Variables | Station | CC | MNBE | RMSE | CC | MNBE | RMSE |
| T | 355 | 0.86 | −5.78 | 3.24°C | 0.86 | −2.17 | 2.93 |
| WS | 342 | 0.53 | 53.79 | 2.17 m/s | 0.55 | 60.21 | 2.19 m/s |
| RH | 348 | 0.64 | 22.06 | 17.31% | 0.67 | 17.75 | 15.98% |
| $O_3$ | 84 | 0.74 | 39.51 | 22.28 μg/m$^3$ | 0.74 | 39.67 | 21.98 μg/m$^3$ |
| $O_3$ peak | 84 | 0.81 | 2.51 | 22.95 μg/m$^3$ | 0.81 | 2.67 | 22.51 μg/m$^3$ |
| $NO_2$ | 18 | 0.47 | 107.68 | 1.53 μNg/m$^3$ | 0.46 | 97.30 | 1.42 μNg/m$^3$ |
| $PM_{2.5}$ | 15 | 0.27 | −4.55 | 7.09 μg/m$^3$ | 0.29 | −9.16 | 7.13 μg/m$^3$ |
| $PM_{10}$ | 22 | 0.05 | 31.71 | 11.72 μg/m$^3$ | 0.05 | 33.36 | 12.00 μg/m$^3$ |

data are reproduced with a CC of 0.74 and a RMSE of about 22 μg/m$^3$; the maximum ozone has a CC of 0.81 and a RMSE of about 23 μg/m$^3$. $NO_2$ is overestimated by about a factor of 2. The $PM_{2.5}$ mass simulated has a CC of 0.27 and 0.29 for Dudhia and Goddard, respectively; 9 stations out of 15 have the CC greater than 0.20 with a maximum value of 0.70. The NMBE is negative. The $PM_{10}$ has very low mean CC (0.05). The bias is very high, about +30%. This is mainly due to overestimation of soil dust flux calculated by the model at some locations. Discarding stations strongly affected by local dust source, we obtain a MNBE as low as 5–6%, but no improvement in CC.

The future developments will focus on the improvement of PM simulation, also through comparison with measurements of aerosols speciation, a longer-term validation and tests on the aerosol-cloud feedback.

## References

1. Bessagnet B, Hodzic A, Vautard R, Beekmann M, Cheinet S, Honoré C, Liousse C, Rouil L (2004) Aerosol modeling with CHIMERE-preliminary evaluation at the continental scale. Atmos Environ 38:2803–2817. doi:10.1016/j.atmosenv.2004.02.034
2. Fast JD, Gustafson WI Jr, Easter RC, Zaveri RA, Barnard JC, Chapman EG, Grell GA, Peckham SE (2006) Evolution of ozone, particulate, and aerosol direct radiative forcing in the vicinity of Houston using a fully coupled meteorology-chemistry-aerosol model. J Geophys Res 111:D21305. doi:10.1029/2005JD006721
3. Grell GA, Peckham SE, McKeen S, Schmitz R, Frost G, Skamarock WC, Eder B (2005) Fully coupled "online" chemistry within the WRF model. Atmos Environ 39:6957–6975. doi:10.1016/j.atmosenv.2005.04.027
4. Middleton P, Stockwell WR, Carter WP (1990) Aggregation and analysis of volatile organic compound emissions for regional modelling. Atmos Environ 24:1107–1133
5. Passant N (2002) Speciation of UK emissions of NMVOC. AEA Technology, AEAT/ENV/0545
6. Pope CA (2000) Review: Epidemiological basis for particulate air pollution health standards. Aerosol Sci Technol 32:4–14
7. Rosenfeld D, Lohmann U, Raga GB, O'Dowd CD, Kulmala M, Fuzzi S, Reissell A, Andreae MO (2008) Flood or drought: how do aerosols affect precipitation? Science 321:1309–1313. doi:10.1126/science.1160606
8. Tuccella P (2009) Processi di retroazione nel sistema aerosol-nubi: prima applicazione a livello europeo del modello accoppiato meteorologia-chimica WRF/Chem, Degree thesis in Physics, Università degli Studi dell'Aquila
9. Verstreng V (2003) Review and revision. Emission data reported to CLRTAP. Tech. Rep., EMEP MSC-W, http://www.emep.int
10. WRF/Chem version 3.1 user's guide. http://ruc.noaa.gov/wrf/WG11/

## Questions and Answers

**Questioner Name**: S. T. Rao

**Q**: Do you have any explanations for your disagreements between simulated and observed pollutants (e.g., $O_3$, $NO_2$, PM)?

**A**: They are many reasons to explain the disagreements among observations and simulated gas phase species. They are mainly due to errors in estimation of emissions, parameterization of dry deposition and PBL mixing.
Further analysis demonstrates that the $PM_{2.5}$ negative bias is ascribable to underestimation of organic mass and primary $PM_{2.5}$.

# Chapter 94
# Human Health Impacts of PM2.5 and $NO_x$ Transport Air Pollution in Belgium

**Hans Michiels, Felix Deutsch, Leo De Nocker, Steven Broekx, Leen Van Esch, and Luc Int Panis**

**Abstract** This paper seeks to calculate marginal external costs from human health impacts of transport air pollution. We focus on PM2.5 and $NO_x$ emissions in Belgium. Our analysis builds upon the widely used impact pathway approach. The great novelty compared to previous work is that both future emissions and background concentrations are modelled now, taking into account different destinations of a tonne of emitted pollutant now versus in the future. Moreover, the model allows for demographic evolution. We find similar results from two separate exercises: one for Belgian and one for Flemish PM2.5 and $NO_x$ emissions.

**Keywords** Human health • Transport • Air pollution • Marginal external cost

## 94.1 Methodology

### *94.1.1 General Idea*

External costs are the result of damages from a particular economic activity, not accounted for in market prices. As long as these costs are not internalized (i.e., included in prices), there will be a loss of welfare. The external cost level is a relevant indicator for society as it indicates which policy measures deserve priority. In this paper, we only discuss marginal external cost (MEC) numbers. The result is a cost in EUR/tonne emission.

H. Michiels (✉) • F. Deutsch • L. De Nocker • S. Broekx • L. Van Esch • L. Int Panis
Vito NV (Flemish Institute for Technological Research), Boeretang 200,
Mol 2400, Belgium
e-mail: hans.michiels@vito.be

D.G. Steyn and S. Trini Castelli (eds.), *Air Pollution Modeling and its Application XXI*,
NATO Science for Peace and Security Series C: Environmental Security 4,
DOI 10.1007/978-94-007-1359-8_94, 

We decided to follow the impact pathway approach (IPA), as developed in [2]. This method consists of five steps, starting from emissions and concentrations, over exposure and impacts, till monetization. In this paper, transport emissions from a source area (Belgium or Flanders) were taken as a starting point and total concentration levels were calculated in the considered grid (see Sect. 1.2) by using one of the air quality models BelEUROS or IFDM-RIO. After that, the exposed population (split per age class) was taken into account, and these results were used in order to calculate the impact levels and external costs.

Aiming at calculating a marginal external cost figure, it was a useful first step to run two scenarios: one with all emissions (from all sectors) being default, the other with a marginal change in transport emissions for one pollutant. For each of these two cases, we were able to follow the IPA, and compare the total external cost. As a last step, the external cost difference between the two scenarios was divided by the original marginal change of transport emissions, in order to get to a MEC figure expressed in EUR/tonne.

### *94.1.2 New Insights*

The approach followed is new in a couple of senses.

From now on, realistic predictions for future European emissions were included, based on IIASA. So, background emissions were assumed to be dependent on the timeframe considered. Secondly, specific Belgian air quality models were used to model dispersion. It is to say, the BelEUROS model is particularly suited to predict the concentrations in neighbouring regions and the formation of secondary pollutants (ozone, secondary particles). The IFDM-RIO model, on the other hand, is ideal for simulating air quality impacts from transport PM2.5 on a very detailed level (individual houses). Thirdly, estimation of demographic exposure was optimized by using a European population map, extrapolated till 2030. These exposure numbers took into consideration both population growth and evolution over the age classes [6]. What was modelled then are the effects of Belgian or Flemish transport emissions (depending on the exercise) on the population of Belgium and the surrounding areas (i.e., 'hot spot' defined in BelEUROS). This area comprises Belgium, Luxemburg and the Netherlands, Southwestern UK, Northern France and Western Germany. Impacts beyond this grid were assumed to be negligible and therefore ignored. Finally, the use of concentration-response (CR) functions was fine-tuned for the specific Belgian/Flemish incidence and relative risk numbers. Moreover, the monetization of some health end points is updated in order to be more in line with current practice [3, 5].

## 94.2 Results

### *94.2.1 Two Examples*

One exercise was conducted in the light of the LIMOBEL project [6], where emissions of transport in Belgium were evaluated. Within the framework of this project, we exclusively used the BelEUROS model to simulate air quality.

This contrasts with the exercise performed for MIRA [1], where only Flemish emissions was focused on and both the BelEUROS ($NO_x$) and the IFDM-RIO model (PM2.5) were used. Furthermore, the specification of the $NO_x$ emission sectors included in this project was slightly different from the one used under Limobel. Finally, regarding PM2.5, the grid resolution was far more detailed (individual house level) than in BelEUROS (15 × 15 km) and a distinction was made for different road types.

### *94.2.2 MEC for Emissions of PM2.5 and $NO_X$*

In the figures below, the *L* and *M* denote values extracted from the LIMOBEL and MIRA project, respectively. The MEC of PM2.5 is provided for an average (A) of all transport modes and road segments, and separate modes like urban (U), highway (H) and rural (R) roads, inland navigation (N) and railway transport (r). No distinction between modes and road types was made for emissions of $NO_x$.

See Fig. 94.1, left-hand side. The total MEC was shown to be largest for transport on urban roads (ca. 465 kEUR for emissions in 2007), mainly because of higher population densities. Furthermore, the MEC from the Limobel project was found be the lowest in all cases. We presume that the combination of a coarser grid resolution and a lower average population density (compared to Flanders) in the source area are the most important explanations for this difference. In addition, our models predicted a slight increase in the future MEC, particularly due to population growth. Finally, it was found that the majority of the external costs from PM2.5 impacts the area where it is emitted (Belgium for L, Flanders for M), i.e. domestic effects are found to be larger than effects on foreign areas. The numbers displayed here are in line with the results from some recent European studies [4], although not completely based on the same assumptions.

The right-hand side of Fig. 94.1 illustrates the MEC for emissions of $NO_x$. $NO_x$ emissions seem to result in an external benefit in 2007 (e.g., −4.2 kEUR for Limobel), independent of the exercise considered. This was predicted to be no longer the case for emissions in 2020 and 2030, due to altered background emissions. Furthermore, only modest differences were shown to arise between the

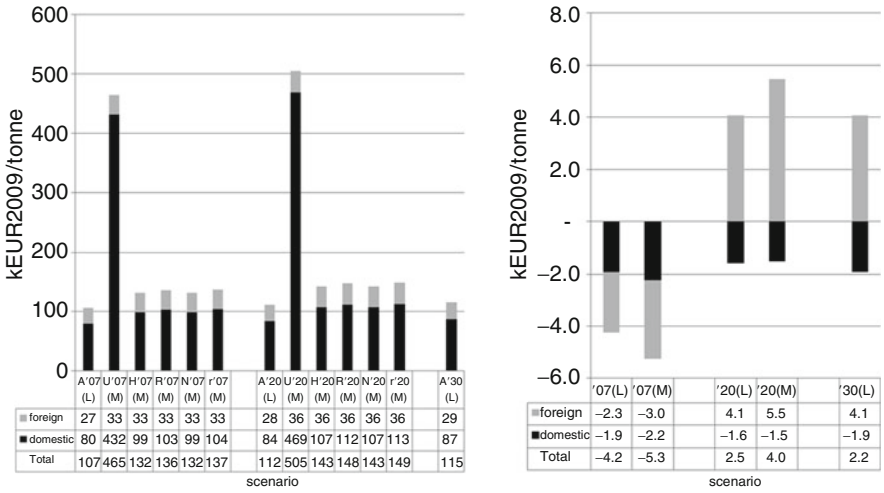


**Fig. 94.1** Marginal external costs from emissions of PM2.5 (*left*) and $NO_x$ (*right*) in 2007 ('07), 2020 ('20) and 2030 ('30)

two exercises, completely attributable to dissimilarities in model setup, explained in Sect. 2.1. Finally, the effect of $NO_x$ emissions was in all cases shown to be greater on foreign areas than on domestic areas, which contrasts with the impacts of PM2.5. This could be attributed to the nonlinear reactions of $NO_x$ emissions with the complex background concentrations, which implies the interactions taking more time and the effects taking place further from the emission source.

It is nice to know that $NO_x$ emissions influence both ozone and secondary particle formation. Taking into account the specific Belgian air conditions (low ratio VOC/$NO_x$), impacts of $NO_x$ through ozone were found to result definitely (today and in the near future) in an external benefit. Impacts of $NO_x$ through the formation of secondary particles (mainly nitrate aerosols), on the other hand, were revealed to result in an external cost. The reason for the expected increase in MEC over the years principally lies in the increasing level of nitrate aerosol formation, while the level of ozone degradation remains more or less the same.

## References

1. De Nocker L, Michiels H, Deutsch F, Lefebvre W, Buekers J, Torfs R (2010) MIRA O&O – Externe Kosten van luchtverontreiniging en broeikasgassen: kengetallen. Study carried out for MIRA, 143 pp
2. ExternE (2005) Externalities of energy, Methodology 2005 update. European Commission, Directorate-General for Research, Institut für Energiewirtschaft und Rationelle Energieanwendung – IER, Universität Stuttgart, Stuttgart, 270 pp
3. Franckx L, Van Hyfte A, Bogaert S, Vermoote S, Hunt A (2009) Reële Milieugerelateerde Gezondheidskosten in Vlaanderen – Eindrapport, 06/12038/RD, 208 pp

4. IMPACT (2008) Handbook on Estimation of External Costs in the Transport Sector. Internalisation Measures and Policies for All External Costs of Transport (IMPACT). Maibach M et al., CE Delft, 336 pp
5. Máca V, Ščasný M (2009) New energy externalities developments for sustainability. A review of monetary values for health end-points, transferability of these values and the effect of adjusted values on the external costs. Technical paper No. 4.2a – RS 1d, 40 pp
6. Michiels H, Int Panis L, De Vlieger I, Mayeres I (2010). Limobel – Long Run Impacts of Policy Packages on Mobility in Belgium. External Environmental Cost Model for Transport (Task 4.6). Study carried out for the Belgian Federal Public Planning Service, Science Policy, 44 pp

## Questions and Answers

**Questioner Name**: Mykola Biliaiev, Bernad Fisher

**Q**: I was surprised that for PM2.5 the effect of domestic emissions was much larger than that from foreign sources (PM2.5 is usually thought to be a regional pollutant). Is secondary particulate included within PM2.5 concentrations?

**A**: We did not compute the effects of Belgian and foreign emissions on PM2.5 concentrations in Belgium. The model setup was designed the other way around, i.e. we wanted to get an idea of the impact of Belgian (or Flemish) emissions on Belgium and the surrounding areas. From this perspective, a share of ca. 25% (except for urban roads) of domestic emissions impacting foreign areas seems reasonable to us, taking into account the size and location of Belgium (Flanders). Nitrate and sulphate particle concentrations were indeed included in these calculations.

**Questioner Name**: Ivanka Stajner

**Q**: Analysis examined impact of $NO_x$ on ozone and PM. Would direct wealth impact of $NO_x$ change the results, especially the marginal benefit of $NO_x$ emissions?

**A**: The impact analysis was restricted to concentrations of PM and ozone because these are the only pollutants for which the size of the effects is broadly accepted in Europe [2]. It was simply not possible to extract reliable CR functions from literature for other pollutants (e.g., $NO_2$) resulting from emissions of $NO_x$.

**Questioner Name**: Henk Eskes

**Q**: What is the mean cost for driving a car for 1 year?

**A**: Let's multiply the numbers found in this paper (MIRA) by the European emission standard levels for euro 3 and euro 4 diesel and petrol passenger cars (ca. 70% of all kilometres in Belgium were driven by these vehicles in 2007). The combined external cost to human health due to PM and $NO_x$ air pollution in 2007 then amounts to 161, 81, −16 and −8 euro/year for a euro 3 and euro 4 diesel and a euro 3 and euro 4 petrol vehicle, respectively. We assumed an average of 20,000 km/year and used the split over the road types observed in 2007.

**Questioner Name**: Sotiris Vardoulakis

**Q**: What was the metric used to quantify the health impacts of air pollution (deaths brought forwards, years of life lost)?

**A**: Concerning mortality impacts of PM and ozone concentrations, we indeed used the number of years of life lost (YOLL). However, other impacts besides mortality were examined as well, which are usually expressed in cases (e.g., the number of cardiac hospital admissions) or days (e.g., the number of days with lower respiratory symptoms).

# Chapter 95
# Effects of Airborne Particles on Cloud Formation and Precipitation: A Modeling Study

**Stavros Solomos, Jonilda Kushta, and George Kallos**

**Abstract** The amount, size distribution and chemical properties of cloud condensation nuclei (CCN), depend on the type of the prevailing air mass and also on local production and transportation of natural and anthropogenic particles. The aerosol properties vary in both space and time and impose significant amount of uncertainty on atmospheric research and also on future climatic projections. Cloud microphysics are very complex in nature and most of the times it is difficult to separate and identify the links and feedbacks between air quality and atmospheric processes under real atmospheric conditions. This presentation focuses on the interactions between air quality, clouds and precipitation for the area of greater Mediterranean. Mixtures of Saharan desert dust with sea-salt or with particles of anthropogenic origin, mainly sulphates and nitrates, may lead to the formation of new aerosols with different physiochemical properties. The effectiveness of airborne particles to act as CCN is examined towards their chemical composition and size distribution. Several modeling experiments, in-situ and airborne observations are analyzed and first results on the role of natural and anthropogenic particles on cloud formation and precipitation are discussed.

**Keywords** Aerosols • CCN • Clouds and precipitation

S. Solomos • J. Kushta • G. Kallos (✉)
School of Physics, Atmospheric Modeling and Weather Forecasting Group,
University of Athens, University Campus Bldg PHYS-5, 15784 Athens, Greece
e-mail: stavros@mg.uoa.gr; kallos@mg.uoa.gr

D.G. Steyn and S. Trini Castelli (eds.), *Air Pollution Modeling and its Application XXI*,
NATO Science for Peace and Security Series C: Environmental Security 4,
DOI 10.1007/978-94-007-1359-8_95, 

## 95.1 Introduction

Airborne particles of natural or anthropogenic origin, may act as efficient Cloud Condensation Nuclei (CCN), depending on their concentrations, their size distributions and their chemical composition. Some particles – such as mineral dust – may also act as Ice Nuclei (IN) and contribute in the formation of ice particles in high clouds. Apart from the ability of aerosol particles to form cloud droplets, they do also interfere with atmospheric conditions by altering the radiation pattern as they can absorb and scatter at both shortwave and longwave parts of the radiation spectrum. Describing the precipitation mechanism under real atmospheric conditions is a complicated issue since precipitation may differ from one area to another depending on the type of clouds, local circulations, topography and also land use. The complexity of the above processes and the possible interactions and feedbacks that interfere in the system, indicate the need for an integrated modeling approach in order to examine the impacts of air quality on meteorology and vice versa. The present work focuses on investigating the effects of aerosols on cloud processes and precipitation for an isolated cloud system and for a specific system over eastern Mediterranean with the use of the integrated atmospheric model ICLAMS [3, 5]. The model includes full description of natural particles cycle in the atmosphere, explicit cloud droplet nucleation scheme and calculation of dust radiative effects.

## 95.2 Model Results

For the single cloud run we considered two distinctive distributions of airborne particles namely the "pristine" and "hazy" scenarios as seen in Fig. 95.1a. The "pristine" scenario is representative of a remote area with a relatively clean atmosphere of total 100 particles $cm^{-3}$, while the "hazy" scenario assumes a total of 1,500 particles $cm^{-3}$. Such high aerosol concentrations can be found near urban areas or industrial zones and are also typical during intense episodes of dust advection. As seen in Fig. 95.1b, the "pristine" scenario produced overall more rain due to the increased autoconversion rates of cloud droplets to rain droplets. The "hazy" cloud inhibited rain production during the early stages of cloud development since the increased number of CCN had to compete for the available amount of vapour and only a few managed to grow up to rain sizes. Moreover, as illustrated in Fig. 95.2, changing the surface properties resulted in substantially different spatial distribution of precipitation. These results indicate the need for an integrated air quality – meteorology modelling approach in order to resolve such processes.

The second test case describes the combination of a low pressure system and a dust storm reaching the coastline of Israel on 29 January 2003. We performed several experimental runs concentrating mostly on the amount of available airborne particles that could be activated as CCN or IN for the particular case. We examined

**Fig. 95.1** (**a**) Aerosol distribution (**b**) 1 h accumulated precipitation integrated over the domain

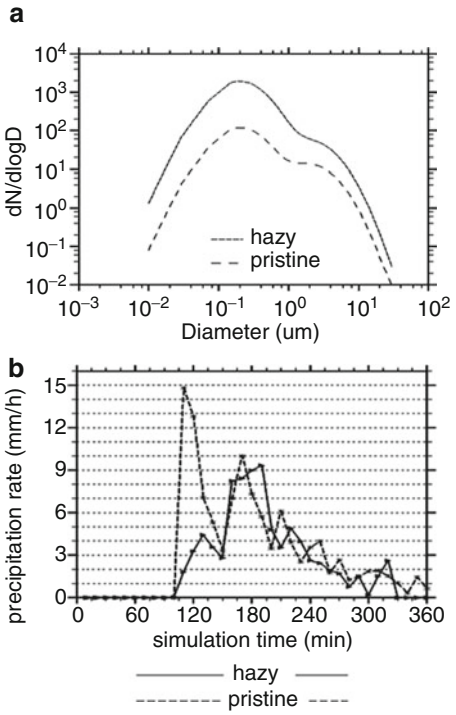


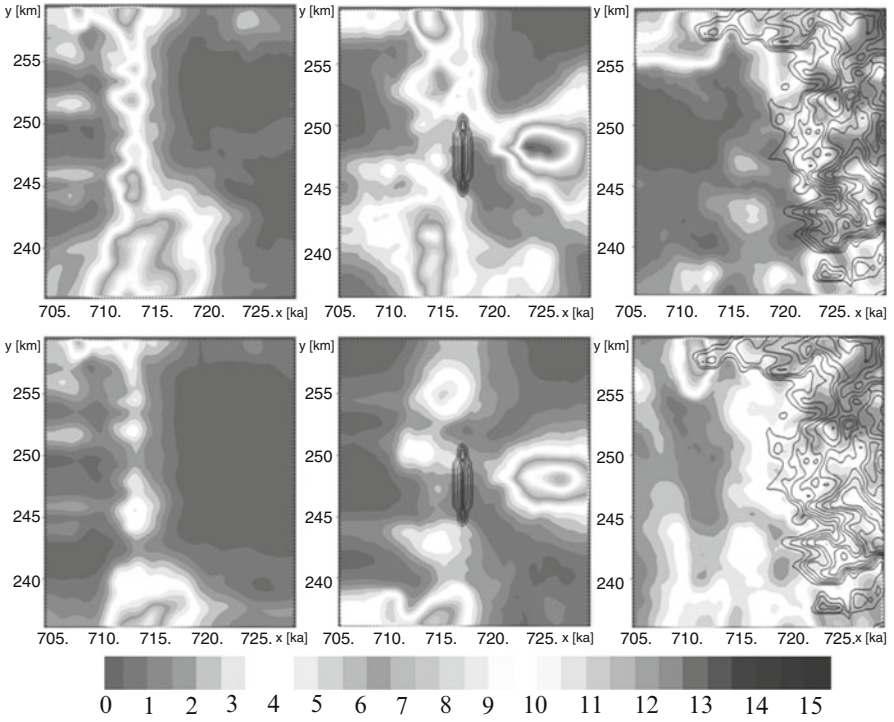


**Fig. 95.2** Accumulated precipitation (mm) after 4 h of model simulation. *First row*: clean aerosol. *Second row*: polluted aerosol. *First column*: flat terrain. *Second column*: artificial obstacle vertical to the general flow. *Third column*: complex topography

both the effects of aerosols on the precipitation reaching the ground and also the effects on the microphysical structure inside the clouds. All runs were executed with the exactly identical configuration except from the options regarding the interaction between airborne particles and meteorology. Advection of dust particles from the northern African coast and the interaction with a cyclonic system over Eastern Mediterranean is evident in Fig. 95.3a, b. As discussed in [4] the aerosol particles during this particular test case were a mixture of dust and sea-salt within the lowest 2 km of the atmosphere. The number concentration of modeled dust and sea salt particles was tested against aircraft observations and the results

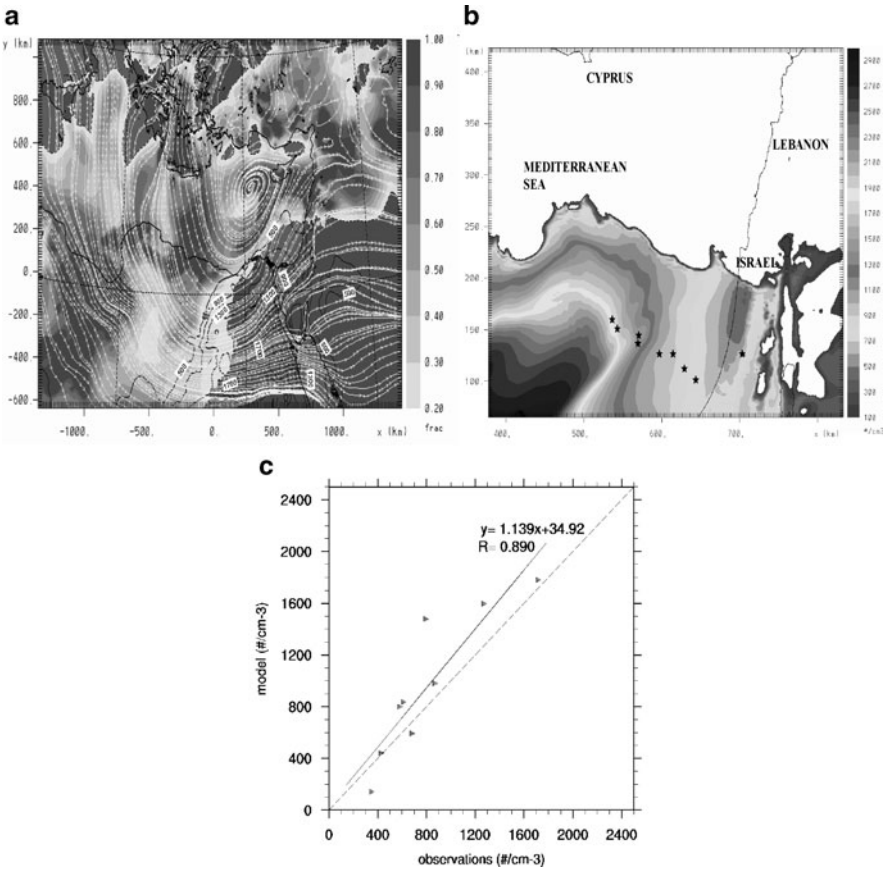


**Fig. 95.3** (**a**) Cloud cover percentage (*grayscale*), near surface streamlines and dustload (line contours in mg $m^{-2}$) on 28 January 2003, 1,100 UTC (**b**) Modeled dust number concentration (# $cm^{-3}$) at 538 m height on 28 January 2003, 09:20 UTC. Black stars indicate the locations of the aircraft measurements (**c**) Comparison of aircraft measurements of natural particles with modeled dust and salt concentrations. The solid line indicates the linear regression line while the dotted line indicates the y = x line

**Table 95.1** Model characteristics for nine aerosol scenarios

| Aerosol cases | Aerosol-cloud interaction | Aerosol-radiation interaction |
|---|---|---|
| Case1 (passive tracers) | NO | NO |
| Case2 (only radiation interaction) | NO | YES |
| Case3 (constant air mass – "pristine") | YES | NO |
| Case4 (constant air mass – "hazy") | YES | NO |
| Case5 (Prognostic air mass – 1% hygroscopic dust) | YES | YES |
| Case6 (Prognostic air mass – 5% hygroscopic dust) | YES | YES |
| Case7 (Prognostic air mass – 10% hygroscopic dust) | YES | YES |
| Case8 (Prognostic air mass – 30% hygroscopic dust) | YES | YES |
| Case9 (Prognostic air mass – 5% hygroscopic dust + IN $\times$ 10) | YES | YES |

are illustrated in Fig. 95.3c. The concentrations of modelled particles inside the dust layer were in good agreement with airborne measurements with a correlation coefficient of 0.89. These results indicate that the model was able to reproduce the horizontal and vertical structure of the dust storm qualitatively and quantitatively. The estimated aerosol concentration is then used for the calculation of the number of CCN that will activate for the formation of cloud droplets. Nine scenarios regarding the aerosol composition were performed (Table 95.1) and the modeled 24-h accumulated precipitation on 29 January 2003 was tested against ground measurements from 86 measuring stations over North Israel.

The model bias for each case is shown in Fig. 95.4a. As it is seen in this figure, the model exhibited significant sensitivity to the variations in the percentage of dust particles that can be activated as CCN and IN. In general, model results with prognostic aerosol treatment were closer to the observations than those of the control run and the model bias for these cases was improved by almost 40%. Also, assuming a constant prescribed air mass type did not improve the model results. The average bias for all thresholds was also calculated for each one of the nine cases and is illustrated at Fig. 95.3b. Cases one to four exhibited more or less the same biases. This is probably explained from the use of constant prescribed air mass properties for these runs. However, including the radiative dust effects (Case2) slightly improved the model results. The accumulated precipitation for the eighth case was clearly underestimated due to the increased number of CCN that delayed the initiation of precipitation and resulted in the enhancement of ice concentrations. Most of these clouds evaporated before they managed to precipitate and the accumulated precipitation was underestimated. The model results were significantly improved for the remaining prognostic aerosol cases (five, six, seven and nine) with average biases of 0.84, 0.84, 0.96 and 0.94 respectively. These findings imply that a more detailed representation of the atmospheric composition and of the aerosol-cloud–radiation feedbacks can provide some insight in the processes involved in the formation of clouds and precipitation.

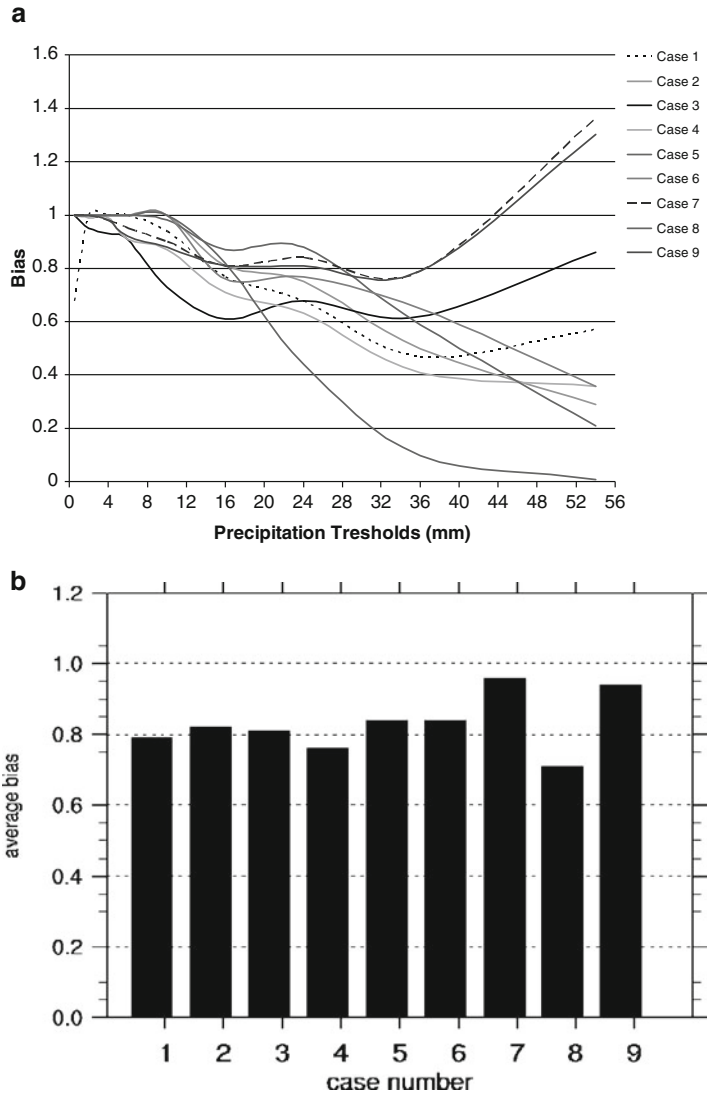


**Fig. 95.4** (**a**) Bias of the 24 h accumulated precipitation for each precipitation threshold and for nine scenarios of aerosol composition (**b**) Average bias of the 24 h accumulated precipitation for nine scenarios of aerosol composition

## 95.3 Concluding Remarks

The relatively high numbers of aerosols that are commonly found at areas downwind of mega-cities or during intense dust events have a strong impact on rain distribution. However, it is not clear whether such increased concentrations of particles will have a positive or a negative feedback in precipitation amounts. Physically based

aerosol-cloud parameterizations are expected to explicitly resolve such interactions over complex terrain. During this modeling study the effects of aerosol on precipitation were not monotonic. Comparison between modeled and observed accumulated precipitation for various scenarios of atmospheric composition indicated a non-linear response of precipitation amounts to aerosol properties. In general, treatment of the aerosols as CCN and IN in a forecasting mode, improved the model performance in comparison to the runs considering a constant atmospheric composition all over the domain.

**Acknowledgments** This work has been supported by the EU Program CIRCE IP, # 036961

## References

1. Astitha M, Kallos G (2008) Gas-phase and aerosol chemistry interactions in South Europe and the Mediterranean Region. Special Issue on "Physics-Chemistry Interactions from the Air Quality Perspective" Environ Fluid Mech
2. Astitha M, Kallos G, Spyrou C, O'Hirok W, Lelieveld J, Denier van der Gon HAC (February 2010) Chemically aged and mixed aerosols over the Central Atlantic Ocean – potential impacts
3. Kallos G, Solomos S, Kushta J (2009) Air quality – meteorology interaction processes in the ICLAMS modeling system. In: 30th NATO/CCMS international technical meeting on air pollution modeling and its applications. May, 2009, San Francisco
4. Levin Z, Teller A, Ganor E, Yin Y (2005) On the interactions of mineral dust, sea-salt particles and clouds a measurement and modeling study from the Mediterranean Israeli Dust Experiment campaign. J Geophys Res 110:D20202
5. Solomos S, Kallos G, Kushta J, Astitha M, Tremback C, Nenes A, Levin Z (2011) An integrated modeling study on the effects of mineral dust and sea salt particles on clouds and precipitation. Atmos Chem Phys 11:873–892. doi:10.5194/acp-11-873-2011

## Questions and Answers

**Questioner Name**: Akula Venkatram

**Q**: In the first part of the paper you showed comparison between model estimates and observations of PM. Could you explain why the comparison is so good considering the inherent complexity of cloud processes and the uncertainty in model inputs?

**A**: The relatively good correlation between modeled and measured PM is probably attributed to the increased resolution of the model (that is $3 \times 3$ km in the region of comparison) and to the use of a high resolution reanalysis dataset ($15 \times 15$ km with 3 h time interval) as initial and boundary conditions. The prevailing atmospheric conditions during the case study were adequately reproduced during the experimental runs. This leads to improved representation of the production/transportation/deposition processes of PM and probably explains the good performance of the model on predicting the PM concentrations.

**Questioner Name**: Pavel Kishcha

**Q**: How were dust particles coated by sea-salt included in the model? Could you elaborate on this?

**A**: In order to keep the model complexity at a reasonable level and also be able to evaluate the results, the amount of salt-coated dust particles was prescribed for each one of the various model scenarios. The partitioning between soluble and insoluble particles is mostly based on previous work by [1, 2]. These particles were then treated as a separate aerosol mode in the cloud nucleation routine and the number of activated cloud droplets was computed at each time step.

# Chapter 96
# Simulation of the Indirect Radiative Forcing of Climate Due to Aerosols by the Two-Way Coupled WRF-CMAQ over the Eastern United States

**Shaocai Yu, Rohit Mathur, Jonathan Pleim, David Wong, Annmarie G. Carlton, Shawn Roselle, S.T. Rao, and Yang Shao**

**Abstract** In this study, the shortwave cloud forcing (SWCF) and longwave cloud forcing (LWCF) are estimated with the newly developed two-way coupled WRF-CMAQ over the eastern United States. Preliminary indirect aerosol forcing has been successfully implemented in WRF-CMAQ. The comparisons with the observed $PM_{2.5}$ at the AIRNow sites indicates that the models captured a majority of observed daily $PM_{2.5}$ within a factor of 2, but generally underestimated the observations in the high $PM_{2.5}$ concentration range. The domain means of CERES satellite observations, WRF-CMAQ/CAM and WRF-CMAQ/RRTMg for SWCF (LWCF) are −48.1 (31.9), −31.9 (22.6), −19.8 (15.5) watts $m^{-2}$, respectively. This means that the WRF-CMAQ model generally underestimated the cloud field for the 12-km resolution simulations.

**Keywords** Indirect aerosol forcing • Two-way • WRF-CMAQ

## 96.1 Introduction

Aerosol particles can influence the Earth's climate both directly by scattering and absorption of incoming solar radiation and terrestrial outgoing radiation, and indirectly by affecting cloud radiative properties through their role as cloud condensation nuclei (CCN) [1, 2]. The IPCC [3] concludes that increasing concentrations of the long-lived greenhouse gases have led to a combined radiative forcing

S. Yu (✉) • R. Mathur • J. Pleim • D. Wong • A.G. Carlton • S. Roselle • S.T. Rao
Atmospheric Modeling and Analysis Division, National Exposure Research Laboratory, U.S. Environmental Protection Agency, Research Triangle Park, NC 27711, USA
e-mail: mathur.rohit@epa.gov; pleim.jon@epa.gov; rao.st@epa.gov

Y. Shao
NRC/Environmental Science Division, NERL, U.S. EPA, Research Triangle Park, NC 27711, USA

D.G. Steyn and S. Trini Castelli (eds.), *Air Pollution Modeling and its Application XXI*, NATO Science for Peace and Security Series C: Environmental Security 4,
DOI 10.1007/978-94-007-1359-8_96, 

+2.63 [±0.26] W $m^{-2}$, and the total direct aerosol radiative forcing is estimated to be −0.5 [±0.4] W $m^{-2}$, with a *medium-low* level of scientific understanding, while the radiative forcing due to the cloud albedo effect (also referred to as first indirect), is estimated to be −0.7 [−1.1, +0.4] W $m^{-2}$, with a *low* level of scientific understanding. Clearly, the great uncertainty in the indirect aerosol forcing for the assessment of climate forcing by anthropogenic aerosols must be reduced.

## 96.2 The Modeling System and Observational Databases

The two-way coupled WRF-CMAQ modeling system was developed by linking the Weather Research and Forecasting (WRF) model and Community Multiscale Air Quality (CMAQ) model. In this system, radiative effects of absorbing and scattering aerosols and the cloud droplets diagnosed from the activation of CMAQ-predicted aerosol particles interact with the WRF radiation calculations, resulting in a "two-way" coupling between atmospheric dynamic and chemical modeling components [4, 5]. Figure 96.1a shows a schematic coupling for the WRF and CMAQ modeling system. A flow diagram for calculation of indirect aerosol forcing in the two-way coupled WRF-CMAQ model is shown in Fig. 96.1b. Specifically, the cloud droplet number concentrations [6] are diagnosed from the activation of CMAQ-predicted aerosol particles. The resulting cloud droplet number is used to calculate variations in droplet effective radius, which in turn allows us to estimate aerosol effects on cloud optical depth and microphysical process rates for indirect aerosol forcing by tying a two-moment treatment of cloud water (cloud water mass and cloud droplet number) to precipitation (the Lin cloud microphysics scheme) and two radiation schemes (RRTMg and CAM) in the WRF. The $PM_{2.5}$ data from the AIRNow and shortwave cloud forcing (SWCF) and longwave cloud forcing (LWCF) data from CERES satellite were used to evaluate the model performance.

## 96.3 Results and Discussions

The scatterplot of $PM_{2.5}$ concentrations between model and observations in Fig. 96.2 indicates that the model captured a majority of observed daily $PM_{2.5}$ within a factor of 2, but generally underestimated the observations in the high $PM_{2.5}$ concentration range. The domain means ± standard deviation of observations, WRF-CMAQ/CAM and WRF-CMAQ/RRTMg for $PM_{2.5}$ concentrations are 13.9 ± 7.9, 10.2 ± 6.7, and 9.5 ± 5.9 μg $m^{-3}$, respectively. The comparisons of $PM_{2.5}$ chemical composition at the IMPROVE sites (no shown here) indicate that WRF-CMAQ/CAM and WRF-CMAQ/RRTMg underestimated observed $SO_4^{2-}$ by −26% and −23%, respectively, and underestimated observed OC by −25% and −26%, respectively, mainly leading to the general underestimation of $PM_{2.5}$. One of the reasons for the underestimation of $SO_4^{2-}$ is due to the fact that the model generally

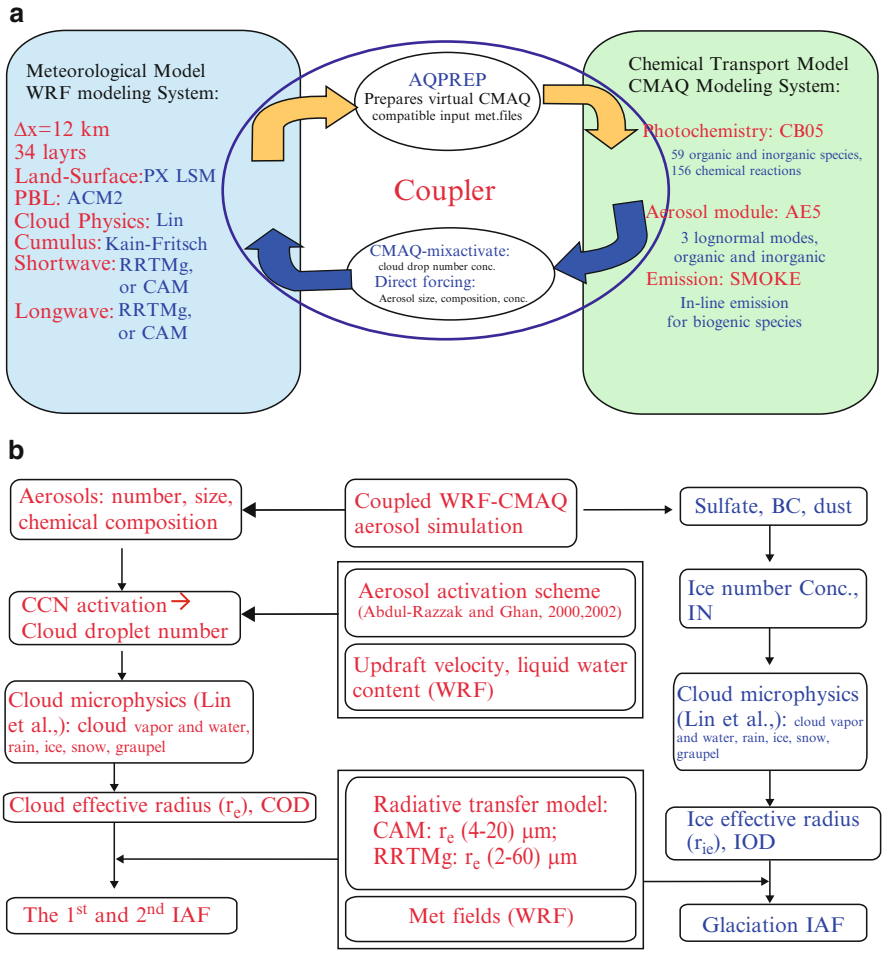


**Fig. 96.1** (**a**) The two-way coupled WRF-CMAQ modeling system, (**b**) Flow diagram for calculation of indirect aerosol forcing (IAF)

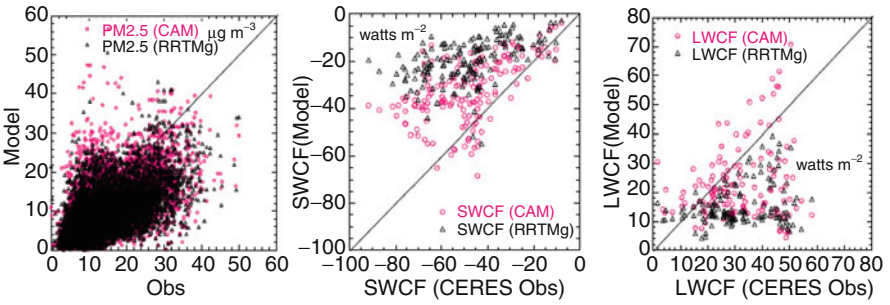


**Fig. 96.2** Comparison of modeled (Two-way coupled WRF-CMAQ) and observed $PM_{2.5}$, SWCF and LWCF for two radiation schemes (RRTMg and CAM) over the eastern US for August of 2006

underestimated the cloud field as analyzed below, which caused underestimation of aqueous $SO_4^{2-}$ production.

The domain means ± standard deviation of CERES satellite observations, WRF-CMAQ/CAM and WRF-CMAQ/RRTMg for SWCF (LWCF) are $-48.1 \pm 17.6$ ($31.9 \pm 12.4$), $-31.9 \pm 13.3$ ($22.6 \pm 12.3$), $-19.8 \pm 9.0$ ($15.5 \pm 7.1$) watts $m^{-2}$, respectively (see Fig. 96.2 for scatterplots). The consistent underestimations of both SWCF and LWCF by the models indicated that the WRF-CMAQ model generally underestimated the cloud field, although the WRF-CMAQ/CAM produced more cloud than the WRF-CMAQ/RRTMg. One of the reasons for the underestimation of cloud is that the subgrid convective clouds do not include aerosol effects because the model simulations were run at 12 km resolution. On the other hand, CAM and RRTMg radiation schemes used different parameterizations to calculate the optical properties of cloud, in part, leading to the different results for WRF-CMAQ/CAM and WRF-CMAQ/RRTMg. More studies and tests are needed although preliminary indirect aerosol forcing has been successfully implemented in the two-way coupled WRF-CMAQ.

## References

1. Yu SC (2000) The role of organic acids (formic, acetic, pyruvic and oxalic) in the formation of cloud condensation nuclei (CCN): a review. Atmos Res 53:185–217
2. Yu SC, Saxena VK, Zhao Z (2001) A comparison of signals of regional aerosol-induced forcing in eastern China and the southeastern United States. Geophys Res Lett 28:713–716
3. Intergovernmental Panel on Climate Change (IPCC) (2007) Climate change 2007: The physical science basis, contribution of working group I to the fourth assessment report of the intergovernmental panel on climate change. Cambridge University Press, New York
4. Mathur R et al (2010) The WRF-CMAQ integrated on-line modeling system. In: Steyn DG, Rao ST (eds) Development, testing and initial application, air pollution modeling and its application XX. Springer, Dordrecht, pp 155–159. doi:10.1007/978-90-481-3812-8
5. Pleim J et al (2008) In: Borrego C, Miranda AI (eds) Two-Way coupled meteorology and air quality modeling, *air pollution modeling and its application XIX*. Springer, Dordrecht, pp 496–504. ISBN 978-1-4020-8452-2
6. Abdul-Razzak H, Ghan SJ (2002) A parameterization of aerosol activation. 3. Sectional representation. J Geophys Res 107(D3):4026. doi:10.1029/2001JD000483

## Questions and Answers

**Questioner Name**: S. Hanna

**Q**: If NWP models are underpredicting the occurrence of subgrid clouds (as in a partly cloudy sky), does this not also imply a bias in prediction of radiative effects?

**A**: Yes, this will lead a bias in prediction of radiative effects. This is one of issues we try to understand. Hopefully, we can improve this in the future.

**Questioner Name**: A. Venketram

**Q**: Why do the two radiation schemes produce different water contents?

**A**: One of the reasons is that CAM and RRTMg radiation schemes used different parameterizations to calculate the optical properties of cloud, in part, leading to the different results for WRF-CMAQ/CAM and WRF-CMAQ/RRTMg.

# Chapter 97
# Assessing the Anthropogenic Fugitive Dust Emission Inventory and Temporal Allocation Using an Updated Speciation of Particulate Matter

**George Pouliot, Heather Simon, Prakash Bhave, Daniel Tong, David Mobley, Tom Pace, and Thomas Pierce**

**Abstract** Crustal materials are mainly emitted by anthropogenic and windblown fugitive dust, but also may potentially include some fly ash and industrial process emissions which are chemically similar to crustal emissions. Source apportionment studies have shown that anthropogenic fugitive dust emissions contribute on the order of 5–20% of $PM_{2.5}$ (particulate matter with an aerodynamic diameter less than 2.5 μm) and 40–60% of $PM_{10}$ (particulate matter with an aerodynamic diameter less than 10 μm) in urban areas that either have been or potentially may be unable to attain the National Ambient Air Quality Standards (NAAQS) for $PM_{2.5}$ and/or $PM_{10}$. On the other hand, air quality models suggest vastly higher contributions from current fugitive dust emission inventories, with contributions ranging from 50% to 80% for $PM_{2.5}$ and 70–90% for $PM_{10}$. This paper uses an improved speciation of PM to include, in addition to the current species, eight trace metals as well as separate non-carbon organic matter to assess potential improvements to the emission estimates of anthropogenic fugitive dust (unpaved and paved road dust, dust from highway, commercial and residential construction and agricultural tilling).

**Keywords** Air pollution • Air quality modeling • Emission inventories • Particulate matter

G. Pouliot (✉) • H. Simon • P. Bhave • D. Mobley • T. Pierce
Atmospheric Modeling and Analysis Division, National Exposure Research Laboratory, Office of Research and Development, U.S. Environmental Protection Agency, Research Triangle Park, NC 27711, USA
e-mail: pouliot.george@epa.gov; mobley.david@epa.gov; pierce.tom@epa.gov

D. Tong
Air Resources Laboratory, National Oceanic and Atmospheric Administration, Silver Spring, MD, USA

T. Pace
Air Quality Modeling Group, Office of Air Quality Planning and Standards, U.S. Environmental Protection Agency, Research Triangle Park, NC 27711, USA

D.G. Steyn and S. Trini Castelli (eds.), *Air Pollution Modeling and its Application XXI*, NATO Science for Peace and Security Series C: Environmental Security 4,
DOI 10.1007/978-94-007-1359-8_97, 

## 97.1 Introduction

The NARSTO 2005 assessment report stressed that emissions are at the cornerstone of air quality management decision-making. While the United States Environmental Protection Agency (EPA), Office of Air Quality Planning and Standards (OAQPS) bears the responsibility for maintaining the National Emissions Inventory (NEI) for traditional anthropogenic sources (e.g., electrical generating units and mobile sources), many nontraditional emission categories (such as fugitive dust) remain poorly characterized. Fugitive dust categories of interest include unpaved and paved road dust, dust from highway, commercial and residential construction and agricultural tilling. Of these, unpaved roads are the highest single emissions category, accounting for about one third of non-windblown fugitive dust emissions. This is followed in importance by dust from tilling, quarrying and other earthmoving. Area source fugitive dust emissions are currently estimated in the NEI on a county-level annual basis with little information about temporal allocation. For instance, the current temporal allocation assumes no monthly variability and no weekday/weekend variation. In essence, each day is represented identically throughout the year. In addition, in the NEI there is no adjustment for local source removal due to small scale turbulence. For modeling applications a transportable fraction, as proposed by [3], is commonly applied on a per county basis to both $PM_{10}$ and $PM_{2.5}$. An example modeling application is EPA's Transport Rule (Docket ID EPA-HQ-OAR-2009-0491).This transportable fraction represents the portion of emitted PM which becomes entrained and dispersed throughout the model grid cell.

This paper summarizes two phases to improve the fugitive dust emission estimates used in chemical transport modeling. The first phase involves improvements to the transportable fraction applied to the gridded emission inventory field and improvements to the temporal allocation of the fugitive dust emissions. The second phase involves a new speciation of $PM_{2.5}$ from all sources that tracks eight trace metals. These trace metals are then modeled in a chemical transport model and compared with ambient measurements. This new speciation allows for better source attribution of measured trace metals to help determine emission inventory improvement at the source classification code (SCC) code level rather than at broader sector levels.

## 97.2 Improvements to the Inventory

The transportable fraction represents the fraction of the emission estimate that is transported beyond the local environment from which it was generated due to the effects of land cover. Thus a dense forest would have a small fraction compared to shrubland. In [3], the transportable fraction is calculated on a per county basis for 3 RPOs using the BELD2 county-level land use information. The western states, (WRAP and CENRAP) are calculated using a different land use database North

**Table 97.1** BELD3 categories, capture fraction class, and transportable fraction

| BELD3 category | Capture fraction class | Transportable fraction |
|---|---|---|
| USGS_urban | Urban | 0.50 |
| USGS_drycrop | Grass | 0.75 |
| USGS_irrcrop | Grass | 0.75 |
| USGS_cropgrass | Grass | 0.75 |
| USGS_cropwdlnd | Grass | 0.75 |
| USGS_grassland | Grass | 0.75 |
| USGS_shrubland | Water/Barren | 1.00 |
| USGS_shrubgrass | Grass | 0.75 |
| USGS_savanna | Grass | 0.75 |
| USGS_decidforest | Forest | 0.05 |
| USGS_evbrdleaf | Forest | 0.05 |
| USGS_coniferfor | Forest | 0.05 |
| USGS_mxforest | Forest | 0.05 |
| USGS_water | Water/Barren | 1.00 |
| USGS_wetwoods | Forest | 0.05 |
| USGS_sprsbarren | Water/Barren | 0.00 |
| USGS_woodtundr | Grass | 0.75 |
| USGS_mxtundra | Water/Barren | 1.00 |
| USGS_snowice | Water/Barren | 1.00 |
| All agriculture classes | Grass | 0.75 |
| All tree classes | Forest | 0.05 |

American Landcover Dataset 2000 [2]. In this paper, we have recalculated the transportable fraction at a 1 km resolution using the newer BELD3 database for all of the Contiguous US (CONUS). The transportable fraction is calculated for five broad land use categories (Forest, Urban, Sparsely wooded & grass, Agricultural, and Water/Barren). Table 97.1 shows the mapping of the BELD3 land use types to the five broad land use categories and the associated capture fraction. This provides a consistent method across the lower 48 states as well as a more accurate representation of the land cover.

Another improvement to the methodology is to modify the temporal activity factors used in the emissions processing. The source categories of emissions from fugitive dust include unpaved road dust, paved road dust, commercial construction, residential construction, road construction, agricultural tilling, livestock operations, and mining and quarrying. For each of these categories, revisions are made to the monthly, weekly, and daily temporal profiles. The rationale for these temporal allocation changes is that we have activity factors for associated sectors that differ from the activity factors that have been assumed for the fugitive dust emissions. An example of this is agricultural tilling. We have a temporal profile for the combustion emissions of agricultural equipment in the non-road mobile source sector that is different than the fugitive dust emissions from agricultural tilling. We harmonized the temporal factors for each the fugitive dust sectors with other components of the emission inventory and processing platform where appropriate and summarize our proposed changes. See [4] for a table of changes to the temporal allocation.

We also updated the speciation of $PM_{2.5}$ from all sources including the dust sources. These updates to the speciation of $PM_{2.5}$ were made possible as a result of the work of [5]. In that work, an inventory for trace metals from $PM_{2.5}$ was derived using EPA's SPECIATE database and ground-based measurements in the CONUS. Composite $PM_{2.5}$ profiles containing the trace metals were then mapped to all available source classification codes. The miscellaneous component of $PM_{2.5}$ was broken down into 14 components. These 14 components are: Water, Chloride, Sodium, Ammonium, Non-Carbon Organic Matter, Calcium, Silicon, Magnesium, Manganese, Aluminium, Iron, Titanium, Potassium, and PMother. With this new speciation, we are now able to view the emission inventory in much more detail. We can see which SCCs are associated with particular trace metals. For example, 89% of silicon inventory in the unadjusted 2002 NEI is dominated by six sources: agricultural tilling, unpaved road dust, external combustion boilers, paved road dust, construction, and mining and quarrying. Of these six sources, all but external combustion boilers are in the area source fugitive dust inventory.

## 97.3 Results and Discussion

CMAQv4.7.1 [1] was used to study the impact of the changes to the emissions processing on the model results. We ran three versions of the chemical transport model: (1) without any area source fugitive dust sources but including the revised speciation; (2) with area source fugitive dust sources and the revised speciation but no temporal or spatial updates from phase 1; and (3) with all the changes in phase 1 and phase 2. We then compared the trace metals to the observed metals at IMPROVE and CSN monitoring sites for January and July 2002.

By revising the speciation profiles from $PM_{2.5}$ to include trace metals that are readily measured at monitoring locations, we are able to study the impact of changes to the emission inventory processing (temporal and spatial allocation), and begin to make improvements to our emission inventory. Using silicon as an example, we see that the model has a high bias for silicon in the winter by a significant factor. We can then go to our inventory by SCC code and trace metals to see that the high bias in the winter is due to at least two causes: overestimates of silicon from the electric utility sector and from fugitive dust. We can then look for improvements to specific sectors by reviewing the methods and assumptions associated with a particular SCC. For silicon, we see that agricultural tilling is overestimated in the winter probably because the inventory estimates poorly accounts for the meteorological effects of snow and rainfall on agriculture tilling. We plan to modify the emission estimates for this sector significantly by accounting for meteorological effects in the emission processing.

## 97.4 Summary

This paper summarizes initial work to improve the speciation of the particulate matter in order to assess potential improvements to the emission estimates of anthropogenic fugitive dust (unpaved and paved road dust, dust from highway, commercial and residential construction and agricultural tilling). We included proposed changes to the fugitive dust emission processing as well as the method by which we plan to ascertain which components of the emission inventory can be improved using a detailed speciation of $PM_{2.5}$ in a chemical transport model. Updates to CMAQ to incorporate these changes will be included in the next release of CMAQ.

## References

1. Byun D, Schere K (2006) Review of the governing equations, computational algorithms, and other components of the models-3 community multiscale air quality modeling system. Appl Mech Rev 59:51–77
2. Latifovic R, Zhu Z-L, Cihlar J, Giri C (2002) Land cover of North America 2000. Natural resources Canada, Canada centre for remote sensing. US Geological Service EROS Data Center
3. Pace TG (2005) Methodology to estimate the transportable fraction (TF) of fugitive dust emissions for regional and urban scale air quality analyses. U.S. EPA, Research Triangle Park, August
4. Pouliot G, Simon H, Bhave P, Tong D, Mobley D, Pace T, Pierce T (2010) Assessing the anthropogenic fugitive dust inventory and temporal allocation using an updated speciation of particulate matter. 19th Annual International Emission Inventory Conference, San Antonio, 27–30 Sept 2010
5. Reff A, Bhave PV, Simon H, Pace TG, Pouliot GA, Mobley JD, Houyoux M (2009) Emissions inventory of $PM_{2.5}$ trace elements across the United States. Environ Sci Technol 43(15):5790–5796

## Questions and Answers

**Q**: Have you looked at the species composition of the dust in the samples to see if that suggests the dust source and if that coincides with your assumption about the main sources? *(Jeff Weil)*

**A**: We have not done that analysis yet, but it is in our work plan.

**Q**: The model has a large positive bias in PM2.5 estimates in winter and a large negative bias during summer. Does this suggest that meteorology plays a major role in creating these biases? *(Akula Venkatram)*

**A**: The new $PM_{2.5}$ speciation has allowed us to more specifically identify the PM components with the highest bias. We have found that the positive wintertime bias is dominated by soil while the negative summertime bias is dominated by organic carbon and non-carbon organic matter. We are in the process of investigating the causes of these very different biases.

# Chapter 98
# Improvements to Wintertime Particulate-Matter Forecasting With GEM-MACH15

**Michael D. Moran, Paul A. Makar, Sylvain Ménard, Radenko Pavlovic, Mourad Sassi, Paul-André Beaulieu, David Anselmo, Curtis J. Mooney, Wanmin Gong, Craig Stroud, Sunling Gong, and Junhua Zhang**

**Abstract** Elevated levels of $PM_{2.5}$ have been observed in North America in all seasons, underlining the need for year-round air-quality (AQ) forecasts. Wintertime AQ forecasting, however, poses unique challenges given well-known seasonal variations in emissions, meteorology, chemistry, and removal processes. In the case of $PM_{2.5}$, both systematic and episodic overpredictions have been noted in the wintertime for current AQ forecast models, including Environment Canada's GEM-MACH15 AQ forecast model. GEM-MACH15 is the regional forecasting configuration of the multi-scale, in-line AQ model GEM-MACH. Performance evaluations of GEM-MACH15 predictions for several recent winter periods have pointed to several sources of forecast error, including the spatial and temporal allocation of primary $PM_{2.5}$ emissions and the treatment of vertical diffusion. This paper describes recent improvements to input emissions for the GEM-MACH15 modelling system and their resulting impacts on forecast performance.

## 98.1 Introduction

Environment Canada (EC), Canada's federal ministry of the environment, has issued national AQ forecasts operationally since 2001, beginning with daily 48 h $O_3$ forecasts and then adding $PM_{2.5}$ and $PM_{10}$ forecasts in 2003. In late 2009 EC replaced its existing operational AQ forecast model, CHRONOS, with a new AQ forecast model called GEM-MACH15. As described by Moran et al. [4] and Anselmo et al. [1],

M.D. Moran (✉) • P.A. Makar • W. Gong • C. Stroud • S. Gong • J. Zhang
Air Quality Research Division, Environment Canada, Toronto, ON, Canada
e-mail: mike.moran@ec.gc.ca; wanmin.gong@ec.gc.ca

S. Ménard • R. Pavlovic • M. Sassi • P.-A. Beaulieu • D. Anselmo
Air Quality Modelling Applications Section, Environment Canada, Montreal, Canada

C.J. Mooney
Air Quality Science Unit, Environment Canada, Edmonton, AB, Canada

D.G. Steyn and S. Trini Castelli (eds.), *Air Pollution Modeling and its Application XXI*,
NATO Science for Peace and Security Series C: Environmental Security 4,
DOI 10.1007/978-94-007-1359-8_98, 

GEM-MACH15 has an improved chemistry package compared to CHRONOS and is run with a continental North American domain having 15-km horizontal grid spacing vs. the 21-km grid spacing used by CHRONOS. GEM-MACH15's hourly $O_3$, $PM_{2.5}$, and $NO_2$ predictions for summer 2008, winter 2008/09, and summer 2009 were found to be superior on balance to those of CHRONOS, leading to the decision to replace CHRONOS. Immediately upon its operational implementation in mid November 2009, however, GEM-MACH15 $PM_{2.5}$ forecasts were found to be unrealistically high for some Canadian cities.

Hourly $PM_{2.5}$, $O_3$, and $NO_2$ point forecasts from CHRONOS or GEM-MACH15 are used to produce city-specific hourly forecasts of Canada's new national Air Quality Health Index (AQHI: [5]). Intermittent GEM-MACH15 $PM_{2.5}$ overpredictions in late November 2009 in six Canadian cities (Quebec City and Montreal, Quebec; Ottawa, Ontario; Saskatoon, Saskatchewan; and Calgary and Edmonton, Alberta) resulted in AQHI forecasts of extremely unhealthy conditions for these cities that did not actually occur. This problem was not identified during the GEM-MACH15 evaluation and acceptance process, but it needed to be fixed as soon as possible because it rendered the model guidance suspect. The remainder of this paper describes the problem investigation, the solution, and the outcome.

## 98.2 Problem Investigation

Wintertime meteorological conditions in mid- and northern latitudes include cold temperatures, reduced solar radiation, widespread snowcover, strong surface inversions, shallow boundary layers, and light winds, all factors that may affect air quality via their influence on dispersion, chemistry, or removal processes. For example, Mathur et al. [3] found that the U.S. Eta-CMAQ AQ forecast model has a systematic $PM_{2.5}$ overprediction in the winter that they ascribed to a combination of uncertainties in primary PM emissions and in model representations of chemistry and boundary-layer mixing. They also presented results for a wintertime regional $PM_{2.5}$ episode in eastern North America in February 2005.

Figure 98.1 shows time series of hourly $PM_{2.5}$ surface concentration predicted by the operational GEM-MACH15 model for the 180-h period from November 18–25, 2009 for six selected Canadian cities. These time series display pronounced variability, including what appear to be synoptic fluctuations (e.g., Vancouver, Toronto) and diurnal periodicity (e.g., Montreal, Quebec City). Two of these cities, Vancouver and Toronto, were predicted to have peak $PM_{2.5}$ concentrations in the 45–55 $\mu g\ m^{-3}$ range during this week whereas the other four cities had very high predicted peak $PM_{2.5}$ concentrations in the 160–250 $\mu g\ m^{-3}$ range. The forecasts of such elevated $PM_{2.5}$ levels turned out to be false alarms when compared to hourly $PM_{2.5}$ measurements made for the same period by TEOM instruments. For example, the predicted maximum $PM_{2.5}$ concentration of 251 $\mu g\ m^{-3}$ for Saskatoon was much

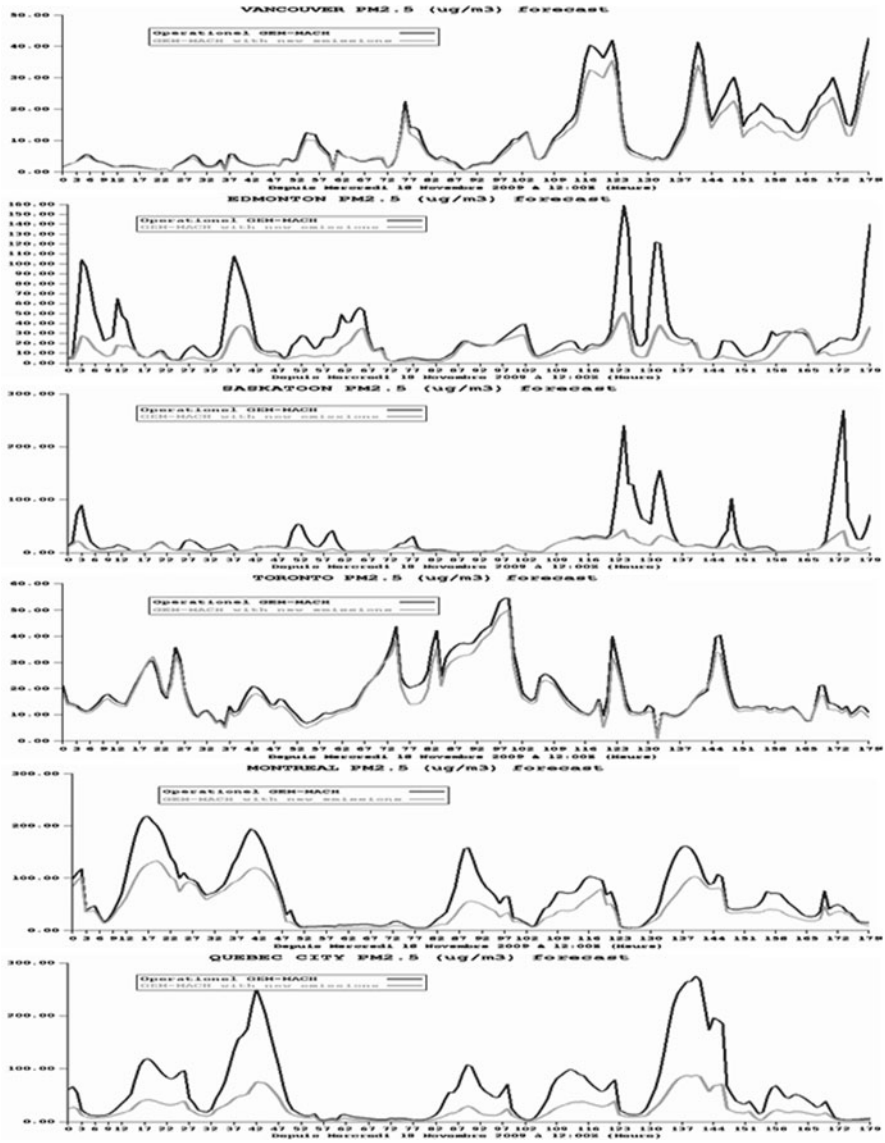


**Fig. 98.1** Time series of hourly surface $PM_{2.5}$ concentration (μg $m^{-3}$) predicted by GEM-MACH15 for the 180 h period from Nov. 18, 2009, 12 UTC to Nov. 26, 00 UTC for six Canadian cities (starting from the *top*: Vancouver, *BC*; Edmonton, *AB*; Saskatoon, *SK*; Toronto, *ON*; Montreal, *QC*; Quebec City, *QC*) for the operational version of GEM-MACH15 (*heavy line*) and an emissions sensitivity run (*light line*)

higher than the observed maximum concentration of 9 μg $m^{-3}$. For Montreal and Quebec City, the observed maximum values of 40 and 53 μg $m^{-3}$ were elevated but were still much lower than the predicted maximum values of 160 and 270 μg $m^{-3}$, respectively.

A detailed examination of the GEM-MACH15 $PM_{2.5}$ predictions provided useful information. First, it was found, particularly in western Canada, that the overpredictions were associated with isolated "hot spots" that were as small as one or two grid cells in size and associated with cities (e.g., Saskatoon). Second, two sensitivity tests in which (1) point-source emissions were turned off (can contribute to hot spots) and (2) aqueous-phase chemistry was turned off (important pathway for sulphate formation) had very little impact, but a third sensitivity test in which area-source emissions were turned off caused the spurious peaks in Fig. 98.1 to vanish. And third, the two PM species that were the largest contributors to the spurious $PM_{2.5}$ peaks were crustal material and primary organic matter, both inert species associated with primary PM emissions.

## 98.3 Solution and Results

The above findings all suggested a direct causal link to the primary $PM_{2.5}$ emissions used by GEM-MACH15. As well, the GEM-MACH15 anthropogenic emissions files were considerably newer than those being used by CHRONOS. One difference between the two sets of files was that the CHRONOS emissions files were based on the 2000 Canadian and 2001 U.S. emissions inventories (with modifications made to U.S. point sources to account for the reductions associated with the NOx SIP Call) whereas the GEM-MACH15 emissions files were based on newer national emissions inventories, namely the 2006 Canadian and 2005 U.S. inventories. A second difference was that a new set of Canadian spatial surrogate fields was used with the SMOKE emissions processing system (e.g., [2]) to spatially disaggregate the Canadian emissions to the GEM-MACH15 grid. The next step was to review how the GEM-MACH15 emissions files had been prepared in order to identify possible improvements.

First, in terms of how the two sets of spatial surrogates were different, some of the Canadian spatial surrogate fields used for CHRONOS were based on labour-force statistics from the 2001 Canadian census, which were reported by place of *residence,* whereas the comparable statistics used for GEM-MACH15 came from the 2006 Canadian census and were reported by place of *work*. In principle the latter tabulation should provide more realistic spatial surrogates for industrial emissions since such emissions are clearly associated with the location of industrial facilities and not with the locations of the residences of the workers at those facilities. In practice, however, many workers do administrative or clerical jobs in head offices or regional offices that are usually located in urban centres rather than co-located with the industrial facilities associated with the process or combustion emissions of interest.

This problem was addressed in an *ad hoc* fashion for the spatial surrogate fields associated with heavy construction, upstream oil and gas (UOG), and mining, three industrial sectors with large primary PM emissions whose operations are unlikely to be located in large cities. These surrogate fields were recalculated by first setting the fractional contribution of selected major urban areas in each province to zero and

then re-normalizing the fields to unity. The result was to limit the association of sector emissions with sector workplaces located outside the cities of Vancouver, Calgary, Edmonton, Saskatoon, Regina, Winnipeg, Toronto, Ottawa, Montreal, and Quebec City. Second, the monthly temporal profiles used for these three sectors were also reviewed and were found to be overweighted in the wintertime. New profiles with lower wintertime weights were substituted.

Third, one other important primary PM emissions source sector in Canada is residential wood combustion (RWC). The spatial surrogate that is used for RWC is the intersection of forest land cover with dwelling density, which is likely overweighted in urban areas, where RWC is less common and also less likely to be used for space heating, and which does not account for geographic variations in mean temperature (since colder areas are likely to have higher RWC emissions). A more realistic spatial surrogate for RWC that had been developed based on two direct surveys was available for the province of Quebec, and this surrogate was adopted for this province. And fourth, 2006 RWC emissions for Quebec were 33% higher than 2005 emissions, but an independent estimate was much closer to the 2005 emissions total so the 2005 value was used in place of the 2006 value.

2006 Canadian emissions were then reprocessed with SMOKE v2.3 for the GEM-MACH15 grid after incorporating these four changes. Figure 98.2 shows the impact of this reprocessing on primary $PM_{2.5}$ emissions in select regions of western and eastern Canada. In western Canada the largest $PM_{2.5}$ emissions reduction occurred in three cities (Calgary, Edmonton, Saskatoon), smaller reductions occurred in surrounding suburban and rural areas, and increases occurred in other rural areas associated with UOG and mining. Note that the emissions total did not change, just the distribution. In southern Quebec, the new spatial surrogate for RWC had the biggest impact: large decreases can be seen for Ottawa-Gatineau, Montreal, and Quebec City, but the pattern of decreases and increases is complex.

The impact of these emissions changes can be seen in Fig. 98.1. For Vancouver and Toronto, which are located in provinces in which the contribution of heavy construction, UOG, and mining to total primary $PM_{2.5}$ emissions is relatively small,

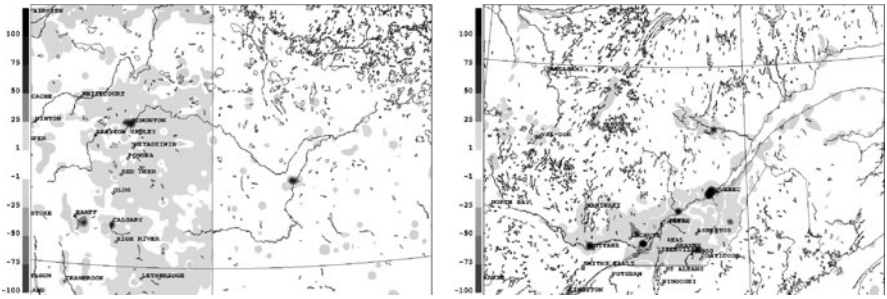

**Fig. 98.2** Difference between operational vs. reprocessed primary $PM_{2.5}$ emissions (g $s^{-1}$) for a February weekday at 20 UTC for southern Alberta and southern Saskatchewan (*left panel*) and at 03 UTC for eastern Ontario, southern Quebec, Maine, and New Brunswick (*right panel*). Lightest shade indicates an increase for reprocessed emissions, others a decrease

$PM_{2.5}$ concentrations were reduced by less than 15%. For Edmonton and Saskatoon, however, which are located in provinces where these three industrial sectors make a large contribution to primary $PM_{2.5}$ emissions, decreases in $PM_{2.5}$ concentration by factors as large as 3–6 are evident. And for Montreal and Quebec City, reductions as large as a factor of 3 can be seen. However, despite these improvements, predicted $PM_{2.5}$ concentrations are still biased high for all six cities but the magnitude of the bias has decreased in all six cities

## 98.4 Conclusions

The details and specifics of this case study do suggest some general conclusions. First, the meteorological conditions that often prevail in the winter and that reduce atmospheric dispersion, chemistry, or removal in effect enhance the local impact of primary PM emissions, thus making any weaknesses in emissions inventories or emissions processing more noticeable. Second, as illustrated in this paper, some of the details of emissions inventories and emissions processing can have very large impacts on AQ forecasts, so that further attention to these details may be required, including provision of emissions by more detailed source type and development of improved spatial and temporal surrogates. And third, as noted by Mathur et al. [3], model process representations for wintertime conditions may also need to be improved. The treatment of boundary-layer processes is one obvious candidate. Another candidate in the current version of GEM-MACH15 does not consider the meteorological modulation of fugitive PM emissions by snow cover, soil wetness, and precipitation. Thus while the emissions processing modifications discussed in this paper have resulted in improved GEM-MACH15 wintertime $PM_{2.5}$ forecasts, more improvements are definitely possible.

## References

1. Anselmo D, Moran MD, Ménard S, Bouchet V, Makar P, Gong W, Kallaur A, Beaulieu P-A, Landry H, Stroud C, Huang P, Gong S, Talbot D (2010) A new Canadian air quality forecast model: GEM-MACH15. 12th AMS conference on atmospheric chemistry, 17–21 Jan Atlanta, 6 pp. See http://ams.confex.com/ams/pdfpapers/165388.pdf
2. CEP (2006) SMOKE User Manual Version 2.3. Carolina Environmental Program. University of North Carolina, Chapel Hill, Available online at http://www.smoke-model.org/version2.3/index.cfm
3. Mathur R, Yu S, Kang D, Schere KL (2008) Assessment of the wintertime performance of developmental particulate matter forecasts with the Eta-Community multiscale air quality modeling system. J Geophys Res 113:D02303. doi:10.1029/2007JD008580
4. Moran MD, Ménard S, Talbot D, Huang P, Makar PA, Gong W, Landry H, Gravel S, Gong S, Crevier L-P, Kallaur A, Sassi M (2010) Particulate-matter forecasting with GEM-MACH15, a new Canadian air-quality forecast model. In: Steyn DG, Rao ST (eds) Air pollution modelling and its application XX. Springer, Dordrecht, pp 289–292

5. Stieb DM, Burnett RT, Smith-Doiron M, Brion O, Hyun Shin H, Economou V (2008) A new multipollutant, no-threshold air quality health index based on short-term associations observed in daily time-series analyses. J Air Waste Manage Assoc 58:435–450

## Questions and Answers

**Questioner Name**: J. Kukkonen (FMI)

**Q**: You presented a health index for air pollution effects. Such indices could potentially be very useful. However, the values of the index seem to be determined mainly by $NO_2$ concentrations, although there is ample evidence of the more important effects of $PM_{2.5}$. Could you elaborate on which studies (e.g., epidemiological ones) the equation was based on?

**A**: The primary evidentiary basis for the Canadian Air Quality Health Index (AQHI) is a time-series analysis of air pollution and mortality in Canadian cities described by Stieb et al. [5]. Note that (a) this index accounts for the additive effects of multiple pollutants and (b) co-variances between different pollutants can be significant. The AQHI has been formulated so that the contributions of $O_3$ and $PM_{2.5}$ are independent of the contribution of $NO_2$. Moreover, $NO_2$ itself may not be a causal agent but rather a marker for other pollutants that are likely associated with emissions from traffic.

**Questioner Name**: S. Lee (CSIRO)

**Q**: After modification of the Canadian $PM_{2.5}$ emissions, how did the false alarm rate of AQHI improve?

**A**: The false alarm rate for AQHI values of seven or higher (high health risk) was reduced in the six Canadian cities where pronounced episodic wintertime overpredictions of $PM_{2.5}$ concentration had been observed. Statistical measures such as correlation coefficient, mean bias, and unbiased RMSE also improved in eastern and western Canada for wintertime $PM_{2.5}$ forecasts.

# Chapter 99
# Improved CTM Boundary Conditions Using DREAM Desert Dust Forecasts: A Case Study over the Po Valley

**Claudio Carnevale, Giovanna Finzi, Enrico Pisoni, Marialuisa Volta, Pavel Kishcha, Gabriele Curci, and P. Alpert**

**Abstract** The Po Valley in Northern Italy is frequently affected by high PM10 concentrations, where both natural and anthropogenic sources play a significant role. This work was aimed at giving a proper account of the contribution of Saharan dust to air quality in the Po Valley. This was carried out by improving the boundary conditions of the mesoscale 3D deterministic Transport Chemical Aerosol Model (TCAM) on large-scale transport of Saharan dust, daily predicted over the Mediterranean region. A case study of the integration of the TCAM and DREAM models was implemented over the Po Valley. The results show that the use of improved boundary conditions leads TCAM to better performances, both in terms of correlation and mean errors: TCAM was able to more accurately reproduce high PM10 concentrations observed in the Po Valley during particular dust events.

**Keywords** Aerosol modeling • Chemical transport model • Saharan dust

## 99.1 Introduction

As a result of the rather ambitious goal for PM10 fixed by European Directives, the impact of natural sources on the PM10 levels requires deep investigation. In recent years a number of experimental studies have been performed to investigate the

C. Carnevale (✉) • G. Finzi • E. Pisoni • M. Volta
Faculty of Engineering, Department of Information Engineering,
University of Brescia, Brescia, Italy
e-mail: Carneval@ing.unibs.it

P. Kishcha • P. Alpert
Department of Geophysics and Planetary Sciences, Tel-Aviv University, Tel-Aviv 69978, Israel

G. Curci
CETEMPS, Department of Physics, University of L'Aquila, L'Aquila, Italy
e-mail: gabriele.curci@aquila.infn.it

D.G. Steyn and S. Trini Castelli (eds.), *Air Pollution Modeling and its Application XXI*,
NATO Science for Peace and Security Series C: Environmental Security 4,
DOI 10.1007/978-94-007-1359-8_99, 

impact of Saharan dust transport on PM10 levels in the Euro-Mediterranean basin [3, 6, 10]. This work is aimed at evaluating the impact of Saharan dust on PM10 records in the Po Valley. This was carried out by improving the boundary conditions of the mesoscale multiphase Transport Chemical Aerosol Model (TCAM) [1] on large-scale transport of Saharan dust, using DREAM dust concentration computed over the Mediterranean region from the Tel-Aviv University weather research center [4]. In fact, multiphase models, simulating the physical-chemical processes involving secondary pollutants in the troposphere, are key tools to evaluate the effectiveness of emission control strategies and so to improve air quality. Due to the complexity of the phenomena involved in the formation and accumulation of aerosol, these models require very detailed input in terms of meteorological fields, emission sources and boundary conditions. In particular, boundary condition fields give the mesoscale models information about the pollutant fluxes incoming in the domain, assuming a very important role in the correct representation of large scale phenomena like Saharan dust transport.

## 99.2 TCAM model

TCAM [1] is a 3-D multiphase Eulerian model. It is a part of the Gas Aerosol Modeling Evaluation System (GAMES) [12] which also includes the meteorological pre-processor PROMETEO and the emission processor POEM-PM [2]. TCAM solves time by time a PDE system which describes the horizontal/vertical transport, the multiphase chemical reactions and the gas to particle conversion phenomena using a splitting operator technique. The horizontal transport is solved by a chapeau function approximation and the non linear Forester filter, while the vertical transport PDE system is solved by an hybrid implicit/explicit scheme. The gas chemistry is described by the COCOH97 scheme. The ODE chemical kinetic system is solved by means of the Implicit-Explicit Hybrid (IEH) solver, which splits the species in fast and slow ones, according to their reaction rates. The system of fast species is solved by means of the implicit Livermore Solver for Ordinary Differential Equations (LSODE) implementing an Adams predictor/corrector method in the non-stiff case, and the Backward Differentiation Formula method in the stiff case. The slow species system is solved by the Adams-Bashfort method.

## 99.3 DREAM Desert Dust Forecasts

DREAM is a model designed to predict the atmospheric cycle of mineral dust aerosol [5, 7]. It solves the Euler-type partial differential nonlinear equation for dust mass continuity. The NCEP/Eta regional atmospheric model drives the aerosol. During the model integration, calculation of the surface dust injection fluxes is made over the model cells declared as deserts. Once injected into the air, dust

aerosol is driven by the atmospheric model variables: by turbulence in the early stage of the process when dust is lifted from the ground to the upper levels; by winds in the later phases of the process when dust travels away from the sources; and finally, by thermodynamic processes and rainfall of the atmospheric model and land cover features which provide wet and dry deposition of dust over the Earth surface. A detailed set of eight particle size classes with effective size between 0.1 and 7.1 μm (0.15, 0.25, 0.45, 0.78, 1.3, 2.2, 3.8, and 7.1 μm) is used [4]. At Tel-Aviv University, since the year 2006, DREAM has been producing daily forecasts of 3-D distribution of dust concentrations over the Mediterranean model domain 20°W–45°E, 15°N–50°N with horizontal resolution 0.3° and 24° vertical levels [8, 9] (http://wind.tau.ac.il/dust8/dust.html).

## 99.4 The Case Study

The impact of the DREAM dust boundary condition has been evaluated for performing a simulation over a Northern Italy domain for the period 15 May–30 June 2007. The TCAM domain (Fig. 99.1a) has been split on a regular horizontal grid with resolution of 10 km, and on 11 terrain following vertical layers ranging from 20 to 4,000 m above ground level. The emission fields were estimated by POEM-PM preprocessor starting from the regional emission inventory collected by ISPRA (Italian Agency for Environmental Protection and Research), while the meteorological fields are computed by means of MM5 model. Two different boundary condition configurations have been tested. In the first case, Chimere CTM [11] simulations have been performed on a European scale domain at an horizontal resolution of 0.5° × 0.5° (Fig. 99.1b) in the frame of QUITSAT project (www.quitsat.it).

The simulation outputs have been interpolated over the bound of TCAM grid and adapted to meet TCAM chemical and size requirements. In the second configuration, the Chimere output has been integrated with the finer resolution outputs of DREAM model (0.1° × 0.1°, Fig. 99.1b). The integration has been performed updating the dust aerosol species in Chimere with DREAM model results, after a spatial and temporal interpolation. The size characterization derived by experimental profiles [3] has been used to characterize DREAM model results. The validation of TCAM simulation results has been performed comparing computed and observed PM10 daily mean concentration in 102 monitoring stations selected to cover all the emission and meteorological regimes of the domain. The use of the DREAM dust forecasts to improve boundary conditions allows TCAM to reach better performances both in terms of normalized mean absolute error (NMAE) and correlation coefficient (Fig. 99.2). In particular, the NMAE shows a significant decreasing due to reduction of the model underestimation and the correlation coefficient median increases with respect to the results computed only with Chimere boundary conditions.

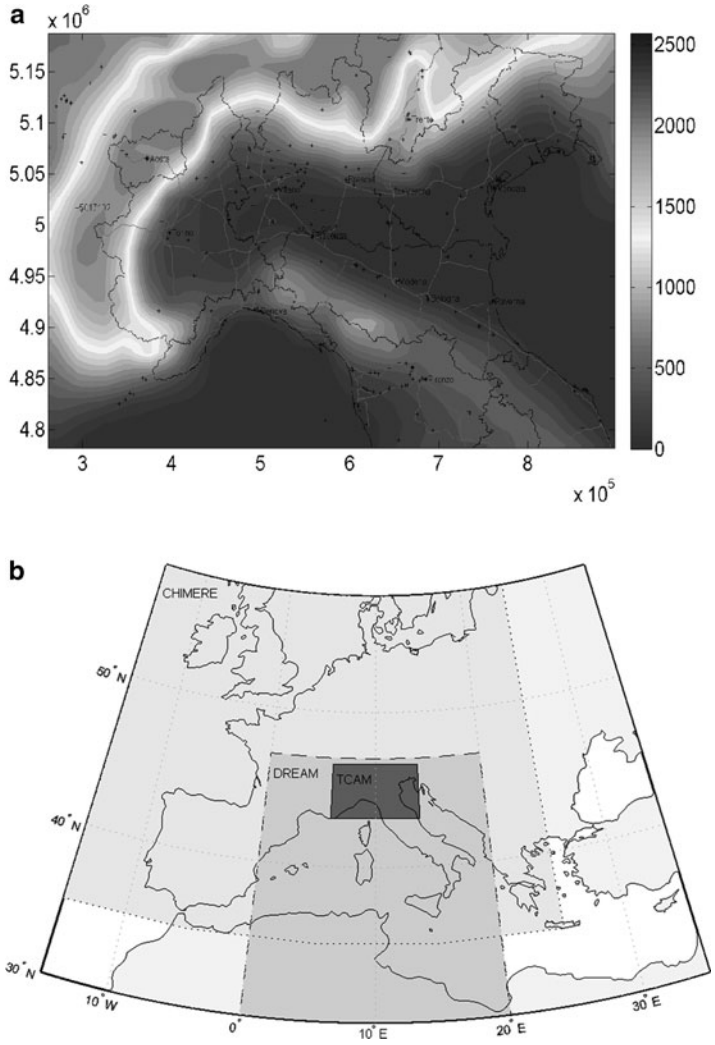


**Fig. 99.1** (**a**) TCAM simulation domain topography, and (**b**) TCAM and Chimere domains. The area of DREAM data used is also presented

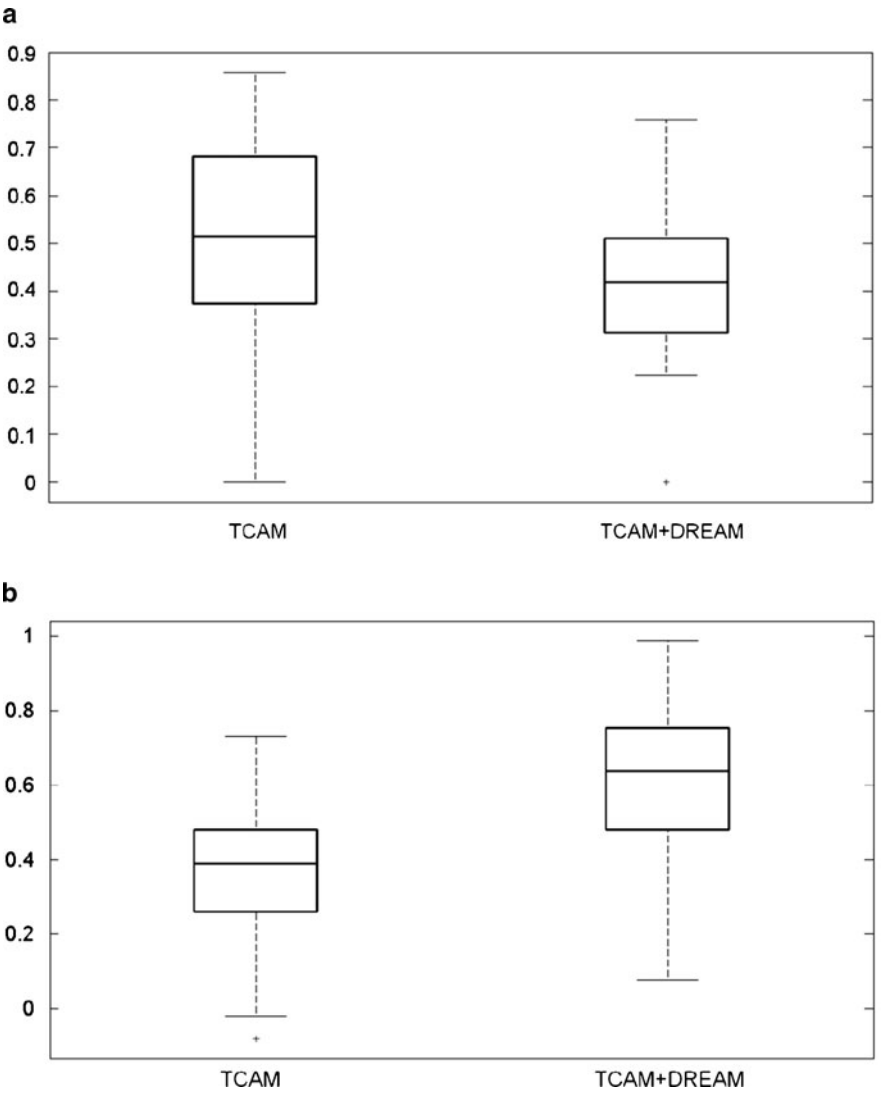


**Fig. 99.2** (**a**) PM10 24 h mean NMAE and (**b**) correlation coefficient for the two tested configuration

**Acknowledgments** The research co-operation between Tel Aviv and Brescia Universities was enhanced and supported by COST ES602 action. The TCAM model simulations have been performed in the frame of the Pilot Project QUITSAT funded by Italian Space Agency.

## References

1. Carnevale C, Decanini E, Volta M (2008) Design and validation of a multiphase 3D model to simulate tropospheric pollution. Sci Total Environ 390:166–176
2. Carnevale C, Gabusi V, Volta M (2006) POEM-PM: an emission model for secondary pollution control scenarios. Environ Modell Softw 21:320–329
3. Gobbi GP, Barnaba F, Ammannato L (2007) Estimating the impact of Saharan dust on the year 2001 PM10 record of Rome, Italy. Atmos Environ 41:261–275
4. Kishcha P, Nickovic S, Ganor E, Kordova L, Alpert P (2008) Saharan dust over the Eastern Mediterranean: model sensitivity. Air pollution modelling and its applications XIX. Chapter 4.2, Springer, ISSN: 1874–6519, doi: 10.1007/978-1-4020-8453-9_39, pp 358–366
5. Kishcha P, Alpert P, Shtivelman A, Krichak SO, Joseph JH, Kallos G, Katsafados P, Spyrou C, Gobbi GP, Barnaba F, Nickovic S, Perez C, Baldasano JM (2007) Forecast errors in dust vertical distributions over Rome (Italy): multiple particle size representation and cloud contributions. J Geophys Res 112:D15205. doi:10.1029/2006JD007427
6. Masson O, Piga D, Guarriaran R, D'Amico D (2010) Impact of exceptional Saharan dust outbreak in France: PM10 and artificial radionuclides concentrations in air in dust deposit. Atmos Environ 44:2478–2486
7. Nickovic S, Kallos G, Papadopoulos A, Kakaliagou O (2001) A model for prediction of desert dust cycle in the atmosphere. J Geophys Res 106(D16):18113–18129
8. Papayannis A, Zhang HQ, Amiridis V, Ju HB, Chourdakis G, Georgoussis G, Perez C, Chen HB, Goloub P, Mamouri RE, Kazadzis S, Paronis D, Tsaknakis G, Baldasano JM (2007) Extraordinary dust event over Beijing, China, during April 2006: Lidar, Sun photometric, satellite observations and model validation. Geophys Res Let 34:L07806. doi:10.1029/2006GL029125
9. Perez C, Nickovic S, Baldasano JM, Sicard M, Rocadenbosch F, Cachorro VE (2006) A long Saharan dust event over the western Mediterranean: Lidar, Sun photometer observations, and regional dust modeling. J Geophys Res 111:D15214. doi:10.1029/2005JD006579
10. Rodriguez S, Querol X, Alastuey A, Kallos G, Kakaliagou O (2001) Saharan dust contributions to PM10 and TSP levels in Southern and Eastern Spain. Atmos Environ 35:2433–2447
11. Schmidt H, Derognat C, Vautard R, Beekman M (2001) A comparison of simulated and observed ozone mixing ratios for the summer of 1998 in Western Europe. Atmos Environ 35:6277–6297
12. Volta M, Finzi G (2006) GAMES, a comprehensive gas aerosol modelling evaluation system. Environ Modell Softw 21:587–594

## Questions and Answers

**A. Kerschbaumer**: Have you validate the DREAM model predictions?
**C. Carnevale**: DREAM has been using for several years for producing operational dust forecasts at two Mediterranean dust prediction centers: at the Barcelona Supercomputer Center, Spain, and at Tel-Aviv University, Israel. Several publications on

the DREAM model validation against lidar measurements, AERONET data, and PM10 measurements are available (see e.g. [5, 8, 9]).

**S. Finardi**: Did you verify if the dust plume trajectory and surface concentration fields produced by TCAM with boundary conditions from DREAM were coincident or similar to those produced by the original dream simulation?
**C. Carnevale**: The point has been addressed. Our analysis shows that, in the two models, the patterns of dust vertical columns are quite similar, even though sometimes both vertical distributions and ground level concentrations could differ due to different meteorological input.

**E. Ferrero**: Is it possible to distinguish the particulates coming from dust in the model and in the measurements?
**C. Carnevale**: In the TCAM model an aerosol chemical species (desert dust) that follow the lifecycle and the dynamics of DREAM boundary conditions is included. Unfortunately, in the measurement a detailed chemical characterization of PM is difficult to achieve and it is only available in a limited number of monitoring stations and days.

# Chapter 100
# Desert Dust Particle Distribution: From Global to Regional Scales

**Marina Astitha, Alexander de Meij, Jos Lelieveld, and Andrea Pozzer**

**Abstract** Atmospheric particulate matter, notably desert dust, can have important impacts on air quality and climate. In this work we present a new parameterization scheme of dust production in the atmospheric chemistry general circulation model EMAC. The new scheme extends previous dust emission parameterizations, making use of online vegetation, meteorological and soil particle size distribution fields basic to the simulation of dust emissions. It aims at a more detailed and accurate representation of the dust production worldwide and in specific targeted regions. Data from satellites and in situ measurements are used to evaluate the model performance showing the first preliminary results of the new implementation.

## 100.1 Introduction

With a wide range of potential effects on radiative transfer, atmospheric dynamics and chemistry [1], desert dust production and distribution are important processes to represent in global and regional models. Implementing a dust emission parameterization in an atmospheric chemistry model is associated with uncertainties and assumptions, especially when covering all the arid areas in the world. The work presented here has two main objectives: (1) to present the new physical parameterization of the dust production that has been incorporated in the atmospheric chemistry general circulation model EMAC (ECHAM5/Messy1 Atmospheric Chemistry);

M. Astitha (✉) • A. de Meij • A. Pozzer
Energy, Environment and Water Research Centre, The Cyprus Institute,
Athalassa Campus, Nicosia, Cyprus
e-mail: m.astitha@cyi.ac.cy

J. Lelieveld
Energy, Environment and Water Research Centre, The Cyprus Institute,
Athalassa Campus, Nicosia, Cyprus

Max Planck Institute for Chemistry, Becherweg 27, 55128 Mainz, Germany

D.G. Steyn and S. Trini Castelli (eds.), *Air Pollution Modeling and its Application XXI*,
NATO Science for Peace and Security Series C: Environmental Security 4,
DOI 10.1007/978-94-007-1359-8_100, 

(2) to assess the model performance over designated areas by running it in relatively high spatial resolution (~1.1° lat/long). The on-line calculation of all relevant parameters by a general circulation model and using this resolution allow the investigation of desert dust intrusions in sub-regions close to the regional scale. Among the improvements of the new parameterization we show a more realistic spatial and temporal distribution of the emitted dust. Products from the MODIS and MISR satellite instruments as well as in situ measurements of dust particle distributions and concentrations are used to assess the model performance and suggest possible additional improvements to the parameterization scheme.

## 100.2 Description of the Dust Production Scheme in the EMAC Model

The ECHAM5/MESSy Atmospheric Chemistry model (EMAC) is used for the implementation of a new dust production scheme. The EMAC model is a combination of the ECHAM5 general circulation model [4] and the Modular Earth Submodel System [2]. The EMAC model was run with a spectral resolution of T106 (~1.1° × 1.1°) and 31 vertical levels up to 10 hPa.

The methodology followed in this work is based on a selection of previous dust emission schemes for regional and global modelling systems. Dust particles are injected in the atmosphere through saltation and sandblasting processes [3]. The previously adopted dust production scheme in the EMAC model was presented by Stier et al. [5]. In brief, the previous scheme included three pre-calculated tables of clay content, emission source strength factors (kg $s^2$ $m^{-5}$) and a threshold wind friction velocity (m $s^{-1}$) to represent the entire globe. The modeled temperature and precipitation fields were used to adjust the soil wetness and the vertical dust flux for coarse mode particles as calculated with the diagnosed wind speed at 10 m, the threshold velocity and the emission source strength factor from the pre-calculated tables.

For the new implementation, we have tested two different formulations of the online dust production and injection into the atmosphere. Both formulations use as input fields the following data: geographical sources of dust based on the Olson global ecosystem biomes, clay content of the soil and the rooting depth. The schemes also use online meteorological fields from the atmospheric model: temperature, relative humidity, soil moisture and the surface friction velocity. The difference between the two implementations concerns the soil size distribution characterization. In the first scheme we assume that the optimum size for saltation is 70 μm and the soil size distribution at the source follows a tri-modal distribution. In the second scheme we have introduced an explicit size distribution of the soil based on the Zobler soil type categorization, thus allowing each grid cell to be represented by fractions of particle sizes (7 types from coarse to fine). Both schemes use the same size distribution for the transport of the soil particles once they are injected into the atmosphere.

They are grouped in 8-size bins from 0.2 to 20 μm in diameter and the 8 size bins are then grouped into the accumulation and coarse insoluble modes used for all aerosol physical and chemical processes in the EMAC model.

## 100.3 Results and Discussion

The implementation of the new dust emission schemes shows important differences with the default version of dust production in the model. Figure 100.1 shows the differences in the emission flux for April 2000. Dust covered areas not present or with low intensity in the previous scheme, such as Australia, Northern and South-plementation. Sources over Northern and Central Africa are shown to have higher intensity and the Asian deserts appear to have more spatial heterogeneity than previously. Both simulations were performed with T106 spatial resolution (~1.1°).

For testing the two new formulations of the dust production scheme, we performed annual simulations for 2000 using the T106 resolution. Starting with a qualitative approach, we have used MODIS and MISR products (aerosol optical depth and Angstrom coefficients) for April and May 2000, which allows us to locate the source regions of natural dust emissions. In Fig. 100.2 the results for April 2000 are presented. In general MODIS Terra Level 3 Aerosol Optical Depth (AOD) over Middle East, Central Africa, Central America, India and China are high. High AOD values (>1.0) are observed over Mali, Niger, Algeria, Libya and Chad, which corroborate the observed AODs by MISR. In general the model results (Fig. 100.3b) show similar patterns as the MODIS and MISR images, except for some regions where the model calculates higher values than the two instruments.

A first quantitative comparison was realized with the use of annual observations in several locations worldwide, as they appear in Stier et al. [5]. Figure 100.3a shows

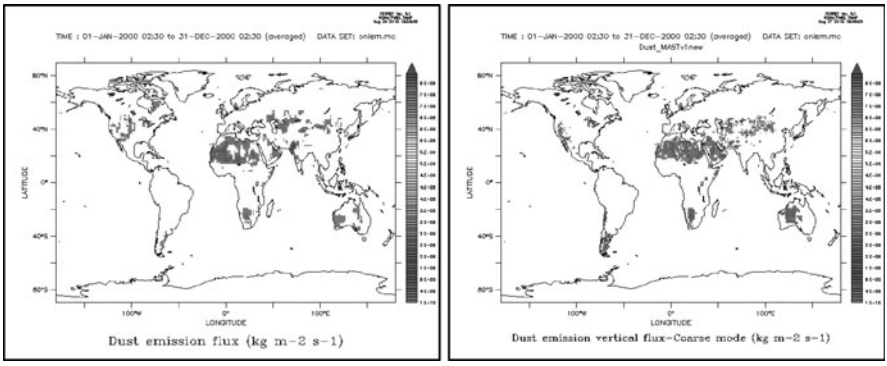


**Fig. 100.1** Dust emission fluxes for 2000 (annual average) for the default scheme (*left*) and the first version of the new dust scheme (*right*). These values refer to the coarse mode

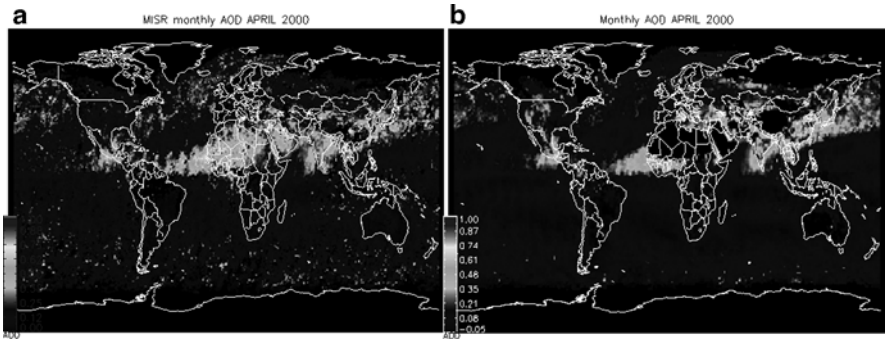


**Fig. 100.2** Monthly average AOD for April 2000 from: (**a**) MISR, (**b**) MODIS (on Terra)

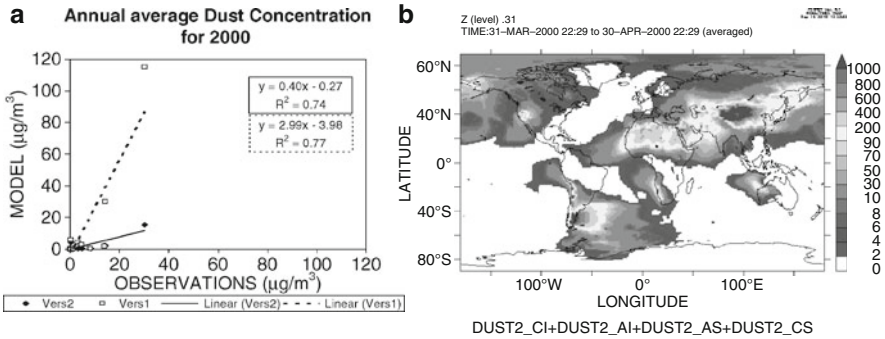


**Fig. 100.3** (**a**) Comparison between the two dust production schemes (the observations are taken from [5]). (**b**) Average dust concentration near the surface for April 2000 from dust scheme version 2

the comparison of the two new dust schemes with the observations for 2000, indicating an overestimation of the observations for the first implementation and an underestimation for the second. This work, as part of an on-going development of the new dust emission scheme in the EMAC model, has showed preliminary results that are promising and require future steps for assessing and improving the model's performance.

**Acknowledgments** This work has been supported by the European Research Council (C8 project).

## References

1. Forster P et al (2007) Changes in atmospheric constituents and in radiative forcing. In: Climate change 2007.The physical science basis. Cambridge University Press, Cambridge/New York
2. Jockel P, Sander R, Kerkweg A, Tost HJ, Lelieveld J (2005) Technical note: the modular earth submodel system (MESSy) a new approach towards earth system modeling. Atmos Chem Phys 5:433–444

3. Marticorena B, Bergametti G, Aumont B, Callot Y, N'Doume C, Legrand M (1997) Modeling the atmospheric dust cycle: 2. Simulation of Saharan dust sources. J Geophys Res 102 (D4):4387–4404
4. Roeckner E et al (2006) Sensitivity of simulated climate to horizontal and vertical resolution in the ECHAM5 atmosphere model. J Climate 19:3371–3791. doi:10.1175/JCLI3824.1
5. Stier P, Feichter J, Kinne S, Kloster S, Vignati E, Wilson J, Ganzeveld L, Tegen I, Wener M, Balkanski Y, Schulz M, Boucher O (2005) The aerosol-climate model ECHAM5-HAM. Atmos Chem Phys 5:1125–1156. doi:1680-7324/acp/2005-5-1125
6. Spyrou C, Mitsakou C, Kallos G, Louka P, Vlastou G (2010) An improved limited area model for describing the dust cycle in the atmosphere. J Geophys Res 115(D17211). doi:10.1029/2009JD013682
7. Tegen I, Harrison SP, Kohfeld K, Prentice IC, Coe M, Heimann M (2002) Impact of vegetation and preferential source areas on global dust aerosol: Results from a model study. J Geophys Res 107(D21):4576. doi:10.1029/2001JD000963
8. White BR (1979) Soil transport by winds on Mars. J Geophys Res 84:4643–4651
9. Zender CS, Bian H, Newman D (2003) Mineral dust entrainment and deposition (DEAD) model: Description and 1990s dust climatology. J Geophys Res 108(D14):4416. doi:10.1029/2002JD002775

## Questions and Answers

**Questioner Name**: Akula Venkatram

**Q**: You make a distinction between horizontal and vertical dust fluxes. How do you define these fluxes and how are these fluxes used in the air quality model?

**A**: The horizontal and vertical fluxes of dust particles are calculated based on the theory of White [8]. The relationship used, assumes linearity between the vertical mass flux and the horizontally saltating mass flux which is a result of microphysical saltation models and wind tunnel studies. The parameterization used to calculate the vertical dust fluxes allows for the computation of emissions of dust particles which are used as input to the air quality model. This parameterization has already been implemented in dust models by various researchers in the past ([3, 6, 7, 9] among others).

**Questioner Name**: Pavel Kishcha

**Q**: How are soluble and insoluble dust particles defined in the model? Is there interaction between dust particles in the model?

**A**: Dust is emitted in the model as insoluble particles. The particles in the insoluble mode are transformed to the soluble mode by condensation of sulphate on their surface [5]. The interaction between dust particles exists in the repartition between the modes through coagulation/condensation processes.

# Chapter 101
# Study of Vertical Transport of Marine Aerosol Using an Unsteady 2D Model

**Gilles Tedeschi and J. Piazzola**

**Abstract** The Marine Aerosol Concentration Model is presented. It is a two-dimensional unsteady model describing the evolution of aerosol concentration in the marine coastal area. It is validated with the help of experimental data measured in the Mediterranean coastal zone. Then, it is used to quantify the effect of the thermal stability on aerosol concentration measured at 10 m height in the MABL.

**Keywords** Marine aerosol • Transport modeling

## 101.1 Introduction

Marine aerosols constitute one of the most significant part to the global aerosol field. The marine aerosol is thus of major importance to Earth's radiative balance and climate system at global scale. At a more regional or local scale, it will have a significant contribution to the electromagnetic propagation in the MABL or impact on ecosystems and vegetation in coastal area. The vertical transport is an important process involved in the concentration of marine aerosol particles in the atmosphere, but models commonly used do not take thermal stability effects into account. The present study focuses then on this last point, with the help of a new model. The Marine Aerosol Concentration Model (MACMod) is tested by comparison with concentrations measured during experimental campaigns held in the coastal Mediterranean area, for various stability conditions. Then, it is used to calculate the concentration of aerosol downwind the shoreline, for several values of radius, wind speed and Air-Sea Temperature Difference. The influence of the various parameters is analyzed and the under or over-concentrations (compared to neutral case) is quantified. It is found that

G. Tedeschi (✉) • J. Piazzola
LSEET Laboratory, University of Toulon-Var,
Av. G. Pompidou, 83162 La Valette du Var, France
e-mail: tedeschi@univ-tln.fr

D.G. Steyn and S. Trini Castelli (eds.), *Air Pollution Modeling and its Application XXI*,
NATO Science for Peace and Security Series C: Environmental Security 4,
DOI 10.1007/978-94-007-1359-8_101, 

the thermal stability has an increased effect for low wind speeds. The 10 m height concentration of submicronic and supermicronic aerosol behaves in an opposite way: when the concentration of the former is increased for stable conditions, it is decreased for the latter. This could explain some apparently surprising experimental results. Above 10 m/s, the thermal stability effect is lowered. These results will be, in the future, used to correct and improve parametric models, better estimate sea-salt particle deposition onto coastal vegetation, as well as the amount of condensation nuclei produced by the marine surface.

## 101.2 The Marine Aerosol Concentration Model (MACMod)

MACMod is a two-dimensional unsteady model describing the evolution of aerosol concentration in the marine coastal area. The equation for the concentration is integrated over a cartesian grid (regular in the horizontal direction and stretched in the vertical direction), using the finite volume method. The environmental data such as the wind velocity, the friction velocity and the air and sea temperatures, can be either pre-computed with a meteorological model for a real case modelling, issued from a theoretical parameterisation (this will be the case for the present study) or chosen constant. They also can be updated regularly with time (especially for the meteorological model). Subroutines are developed for each physical processes, such as the aerosol source function, aerosol deposition on the marine surface, gravitational settling or turbulent dispersion. Various laws can be chosen by the user for the different subroutines, allowing comparisons between them. The specificity of both the surf zone and the open ocean is taken into account. The model can be initialized in the whole domain either with an empirical particle vertical for a real case modeling or with a clear atmosphere for a theoretical case. Each physical processes involved in the production and transport of marine aerosols in coastal areas are included in the model inside separate subroutines called by the main program.

## 101.3 Comparison with Experimental Data

The field campaigns took place in the Mediterranean coastal zone, close to Toulon city in Southern France, in December 2000, May 2007 and May 2008. Two different locations were used for the PMS probes. The first one was at the scientific station of Porquerolles island, the second was on board of the oceanographic vessel “Atalante”. Four different cases have been analysed, in order to have various conditions of stability and fetch length. Wind speeds are ranging from 10 to 16 m/s. An example of comparison between modeled and measured concentrations is shown on Fig. 101.1. The general shapes of experimental and computed curves are similar, with aerosol concentration spectra of the same order. Results simulated with MACMod are coherent with the reality. Nevertheless, some differences between both datasets appear.

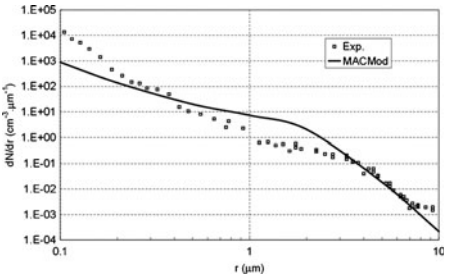


**Fig. 101.1** Comparison between experimental and computed concentrations for the 18 May 2008

For the smallest particles (radii less than 0.2–0.3 μm), the modelled concentrations are lower than the measured ones. That can be easily explained by the fact that in reality submicronic continental particles are advected from long distances upwind, whereas only marine aerosols are taken into account in the modelling and not the additional concentration (the atmosphere is supposed to be clean at the computational domain inlet). For radii between 0.8 and 3 μm, the modelled concentrations are greater than measured ones. This result has been also observed by *Vignati et al*. (2001) and is due to Monahan formula for the flux production at the surface which overestimates it for this range of radii. As we will rather deal with concentration ratios and not absolute values, it will not change the analysis.

## 101.4 Concentration Calculated with MACMod

The stability of atmospheric layers depends classically on the potential temperature vertical gradient $\partial\theta/\partial z$. When its value is positive, a mass of air climbing adiabatically to an upper layer will be cooler and more dense than the surrounding air and then will tend to come back to its previous height (stability case). At the opposite, when the gradient is negative, the climbing air will be warmer than the surrounding air and then will tend to continue to climb (instability case). Close to the sea surface the potential temperature can be assimilated to the temperature (moreover when using differences). The air at the surface is supposed to be at the same temperature as the sea and the "engine" of thermal stability will be thus the temperature difference between air (at a reference height $Z$) and sea (ASTD). A negative value of the ASTD, generating thermal instability, will produce a higher vertical turbulent dispersion of aerosols. The aerosol particles being carried up with buoyancy, the concentration level should be then lower close to the sea surface and higher in the upper layers, compared to the neutral case. A positive value of the ASTD will involve the opposite phenomena. The marine aerosols produced by the sea will remain close to the surface, with lower concentration in the upper layers.

The horizontal (in the $x$ direction) extension of the calculation domain is 100 km, divided in $nx = 400$ cells of $\Delta x = 250$ m length. In the vertical ($z$) direction, the extension is 600 m, divided in $nz = 25$ cells, stretched close to the sea surface. After a few hours of simulated time, an equilibrium is reached and the results are analysed

for this steady state. The final time of the simulation depends on the steadiness of the calculation, which is determined for the lower layers (below 150 m). A matrix of numerical runs has been defined, for a wind speeds range between 5 and 15 m/s, a radii range between 0.1 and 10 μm, and for three ASTD values (−5 K, 0 K, +5 K) corresponding to unstable, neutral and stable cases. For each run, the horizontal profile (at 10 m ASL) and two vertical profiles (at 10 and 50 km offshore) have been more specifically extracted from the steady-state concentration data.

An example of result is shown on Fig. 101.2, for a radius r = 1 μm and a 10 m wind speed $U_{10}$ = 10 m/s. More the case stable is and more the aerosol cloud needs time to climb and to be mixed. As it can been seen on Fig. 101.2 (vertical profiles of the concentration for a 50 km offshore distance), the vertical aerosol distribution is better mixed when thermal instability occurs. The aerosol particles are drawn upward and the concentration close to the sea surface mechanically decreases. The aerosol are dispersed vertically in the atmosphere, more efficiently for unstable and neutral cases.

The concentration ratio (stable and unstable to neutral) at 10 m height allows to quantify the over- or the under-concentration compared to the neutral case. In this example, after a stabilization distance around 20–30 km, it tends to a constant value and the concentration is found 20% higher for the stable case (than neutral one) and 10% lower for the unstable case. The whole results are summarized on Fig. 101.3, which presents the concentration at 50 km offshore for the stable (Fig. 101.3 left) and unstable (Fig. 101.3 right) cases divided by the neutral one, for several wind speeds.

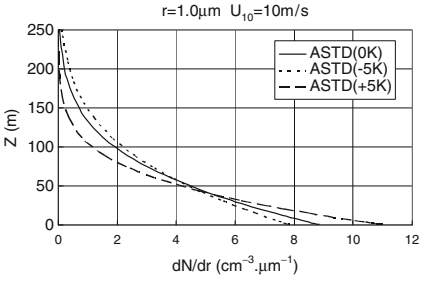


**Fig. 101.2** Concentration vertical profiles for $U_{10}$ = 10 m/s and r = 1 μm at 50 km offshore

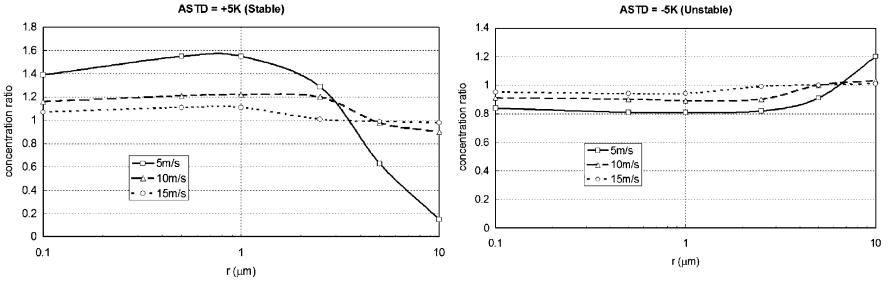


**Fig. 101.3** Concentration ratios (to neutral case) at 50 km offshore as functions of aerosol radius, for stable case (*left*), and unstable case (*right*)

For a low wind speed, the effect of the thermal (un)stability will be the more increased (compared to high wind speed) as the mechanical turbulence is low. For submicronic particles an over-concentration around 40–60% is found in the stable case and a under-concentration around 20% in the unstable case. For a positive ASTD the aerosols are less mixed in the vertical direction and tend to stay close to the sea surface, their concentration will be higher than in the neutral case. For a negative ASTD and an increased turbulent dispersion, the particles will be drawn upward and the concentration at a 10 m height will be lower. For micronic particles, the ratio behaves in the opposite way. For stable case, the layer in which aerosols are trapped becomes very thin and few aerosols reach the 10 m height. The ratio falls thus quickly to a few percent when the radius grows. When the flow is unstable, the layer grows up to values greater than 10 m but keeps not too high. The concentration at 10 m is thus larger than for the neutral case and the ratio is found close to (and sometimes greater than) 1 for largest particles. For moderate and high wind speeds, the effect of thermal stability is less significant (than for low speed). The mechanical turbulence tends to smooth the thermal instabilities and the vertical profiles for concentration are close. For submicronic particles the over-concentration is around 20% in the stable case and the under-concentration is around 10% in the unstable case, for $U_{10} = 10$ m/s. For $U_{10} = 15$ m/s, no significant over- or under-concentration is found and the ratios remain close to 1 whatever the radius is.

## Questions and Answers

**Questioner Name**: Jeff Weil

**Q**: Does your model account for waves and breaking waves on the production of white caps (white cap area / total surface area), on the surface roughness height, and the turbulence / surface stress especially at high winds (>10.15 m/s)?

**A**: We are currently working on the dependence of white caps on the wave field, but it is not yet implemented in the model. For the surface roughness height and stress at high winds, the problem is that we want to keep the model quite fast to use, which would not be the case if these processes were directly taken into account. So, we intend to use an aero/hydrodynamics model to pre-calculate the vertical fluxes for a certain amount of typical situations and to use it to correct the classical aerosol emission fluxes. The vertical area where the atmospheric field is modified by waves (vertical deviation, rotor) will be replaced by an equivalent box. Of course, as a "flat surface" will be still used for the ocean, the layers very close to the water would be only represent a mean situation.

**Questioner Name**: Gabriele Curci

**Q**: The "Monahan" model is used as a kind of reference also in your study. "Monahan" is widely used because relatively easy to implement into 3D-Eulerian model. Your model might be very difficult for this application, because its grid changes with wind direction on a very long horizontal scale.

**A**: the grid in the model is constant in the horizontal direction and does not change with wind direction. The horizontal scale here is limited to a few tens of kilometres, and the wind direction is supposed to be lightly varying.

**Questioner Name**: Steven Hanna

**Q**: The dispersion solution over water seems to be similar for aerosols over land. Did you also study the emissions over water and their dependence on wind speed?

**A**: In this study, the sea salt emission flux is modelled by the "Monahan" formula, which has been especially developed for aerosols over water. It already depends on wind speed and no additional study has been held about this dependence in the present paper.

# Chapter 102
# Comparing Monitoring-Based and Modeling-Based Approaches for Evaluating Black Carbon Contributions from a U.S. Airport

**Saravanan Arunachalam, Alejandro Valencia, Dongmei Yang, Neil Davis, Bok Haeng Baek, Robin E. Dodson, Andres E. Houseman, and Jonathan I. Levy**

**Abstract** Black carbon (BC) is a key component of fine particulate matter that is emitted from aircraft and other combustion sources at airports. Understanding the contribution of aviation activity to ambient BC is important given the projected growth in aviation transport and decrease in emissions from other anthropogenic

S. Arunachalam (✉)
Institute for the Environment, University of North Carolina at Chapel Hill, 137 E. Franklin St., #648A, Chapel Hill, NC 27599–6116, USA
e-mail: sarav@email.unc.edu

A. Valencia
Institute for the Environment, University of North Carolina at Chapel Hill, 137 E. Franklin St., #673, Chapel Hill, NC 27599–6116, USA

D. Yang
Institute for the Environment, University of North Carolina at Chapel Hill, 137 E. Franklin St., #668, Chapel Hill, NC 27599–6116, USA

N. Davis
Institute for the Environment, University of North Carolina at Chapel Hill, 137 E. Franklin St., #665, Chapel Hill, NC 27599–6116, USA

B.H. Baek
Institute for the Environment, University of North Carolina at Chapel Hill, 137 E. Franklin St., #651, Chapel Hill, NC 27599–6116, USA

R.E. Dodson
Silent Spring Institute, 29 Crafts Street, Newton, MA 02458, USA

A.E. Houseman
Center for Environmental Health and Technology, The Warren Alpert Medical School of Brown University, 121 South Main Street, Room 217, Providence, RI 02903, USA

Boston University School of Public Health, 715 Albany Street, T4W, Boston, MA 02118–2526, USA

J.I. Levy
Boston University School of Public Health, 715 Albany Street, T4W, Boston, MA 02118–2526, USA

D.G. Steyn and S. Trini Castelli (eds.), *Air Pollution Modeling and its Application XXI*, NATO Science for Peace and Security Series C: Environmental Security 4,
DOI 10.1007/978-94-007-1359-8_102, 

sources, but there are limitations in the various approaches conventionally used for source attribution. In this study, we evaluate three contrasting approaches to assess the contribution of aviation activity to BC concentrations near a small regional airport in Rhode Island, USA. First, we apply a previously developed regression model utilizing continuous BC concentrations measured at five monitoring sites and predictors such as real-time flight activity (departures and arrivals) and meteorological data, including mixing height, wind speed and direction. Second, we used AERMOD to model all airport sources of BC. Third, we used the Community Multiscale Air Quality (CMAQ) model, a comprehensive chemistry-transport air quality model. We included emissions estimates of all airport activity using an enhanced representation within the lowest 10,000 ft. inclusive of the landing and takeoff (LTO) cycle (the lowest 3,000 ft.) in the modeling system, along with other emissions from all other background sources. Median contribution estimates from the regression model indicate that flight activity contribute to approximately 24–28% of the observed BC concentrations at these five locations. The CMAQ and AERMOD based results show a much smaller contribution, in the range of 2–5% of the observed BC concentrations. We present possible explanations for these discrepancies, using a detailed analysis at different temporal scales at all five locations, and consider possible refinements to each approach. Our findings help to highlight the strengths and weaknesses of various source attribution approaches in the context of aviation emissions and other settings where it is of interest to infer local contributions to ambient concentrations.

**Keywords** Black carbon • Providence • Airport • CMAQ • AERMOD • Aircraft emissions

## 102.1 Introduction

Black carbon (BC) is a key component of fine particulate matter that is emitted from aircraft and other combustion sources at airports. Understanding the contribution of aviation activity to ambient BC is important given the projected growth in aviation transport and decrease in emissions from other anthropogenic sources. However, there are several limitations in the various approaches conventionally used for source attribution. In this study, we compare and contrast airport contributions to BC concentrations using source-based air quality models and statistical models.

## 102.2 Modeling Approach

For this study, we chose the T.F. Green (PVD) airport in Providence, Rhode Island. This airport was chosen since we had activity data to estimate emissions. Further, based upon a field study in 2005, we had hourly BC concentrations at five different locations in and around the airport (See Fig. 102.1). We used the Federal Aviation

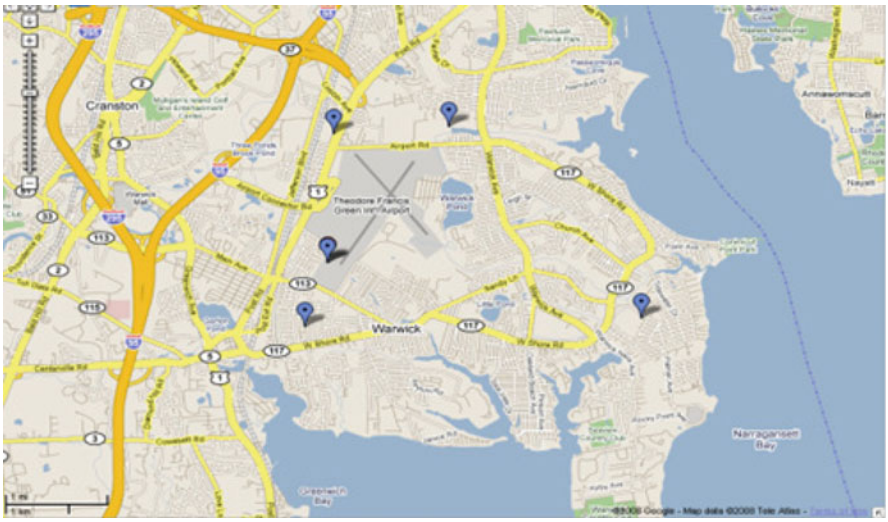


**Fig. 102.1** PVD airport layout showing monitoring locations.

Administration's Emissions Dispersion Modeling System (EDMS) to prepare an airport-level emission inventory that included both commercial aircraft and all other stationary and onroad sources within the airport. Aircraft emissions were modeled within the Landing and Takeoff (LTO) cycle in the lowest 3-km in the model, and we used EDMS2Inv [3] to process them through SMOKE for use in CMAQ at 4-km resolution. We performed air quality modeling using the Community Multiscale Air Quality (CMAQ) model and the AERMOD models. Using CMAQ, we performed two simulations – one using all emissions sources including airport-level emissions for the T.F. Green (PVD) airport in Providence, Rhode Island, and the second without the airport level emissions. The air quality modeling application is described in detail in Arunachalam et al. [1, 2].

To compare and contrast the source-based detailed modeling approach from CMAQ and AERMOD described above with a statistical approach, we applied a previously-developed regression model [4] utilizing continuous BC concentrations measured at five monitoring sites [5] and predictors such as real-time flight activity (departures and arrivals) and meteorological data, including mixing height, wind speed and direction.

## 102.3 Results

Figure 102.2 shows the distribution of hourly BC concentrations from observations at the five sites, along with predicted values from AERMOD, CMAQ (difference of the two simulations) and the regression model-based percent contribution to the observed values.

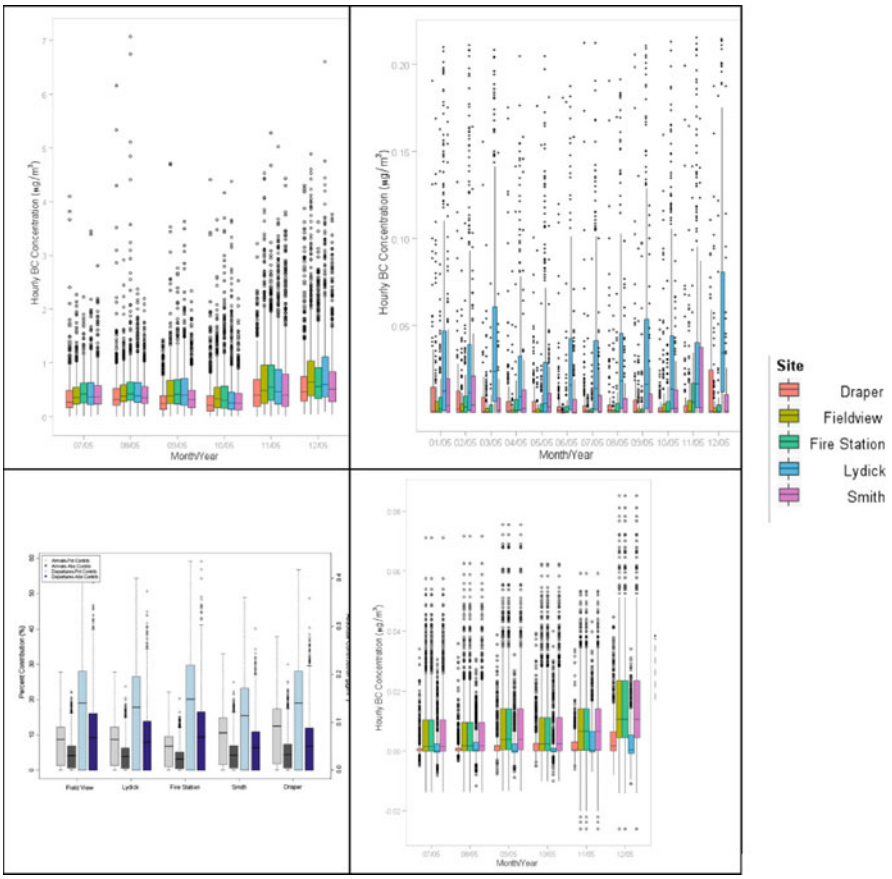


**Fig. 102.2** Distribution of BC concentrations at the five sites: observed (*top left*), AERMOD (*top right*), regression model outputs [3] (*bottom left*) and CMAQ predicted contributions from PVD sources (*bottom right*)

## 102.4 Discussion

CMAQ base model performance (not shown here) at upwind and downwind sites demonstrated reasonable performance, thus indicating capability of model to pick daily variability in concentrations. Median contribution estimates from the regression model indicate that flight activity contribute to approximately 24–28% of the observed BC concentrations at these five locations. From this model, we observe that departures contribute more than arrivals, there is not much intra-site variability, and use of hourly concentrations in regression model limits causal connections. CMAQ and AERMOD based results, however, show a much smaller contribution, in the range of 2–5% of the observed BC concentrations. The CMAQ grid-cell containing three sites (Fire Station, Fieldview and Smith) show the highest

concentrations. AERMOD shows more variability in the concentrations than CMAQ and regression model. AERMOD predicts higher contributions from Lydic than at other locations. It should be noted that AERMOD predictions are missing contributions from regional background. To further study this relative underestimate of AERMOD based concentrations, we instrumented AERMOD to predict concentrations at elevated flagpole receptors. These receptors at heights of 2–16 m showed higher concentrations aloft (12–14 m) than at surface, indicating the presence of the plume aloft rather than at the surface in AERMOD.

Both approaches, i.e., analytical and source-based modeling (AERMOD and CMAQ) show ability to assess contributions from LTO activity, although regression model seems to overestimate impacts compared to source-based models. Our findings help to highlight the strengths and weaknesses of various source attribution approaches in the context of aviation emissions and other settings where it is of interest to infer local contributions to ambient concentrations.

**Acknowledgments** This work was funded by the Partnership for Air Transportation Noise and Emissions Reduction (PARTNER) under grants to UNC and Harvard University. The Air Quality project is managed by Christopher Sequeira. Any opinions, findings, and conclusions or recommendations expressed in this material are those of the author(s) and do not necessarily reflect the views of PARTNER and its sponsors. PARTNER is funded by FAA, NASA, and Transport Canada. Concentration data were collected as part of Community Assessments grant from the U.S. Environmental Protection Agency's National Air Toxics Monitoring Program received by the Rhode Island Department of Environmental Management.

## References

1. Arunachalam S et al (2008) An improved method to represent aviation emissions in air quality models and their impacts on air quality. In: Proceedings of the 13th conference on aviation, range and aerospace meteorology, New Orleans, 22 Jan 2008
2. Arunachalam S et al (2011) Effect of chemistry-transport model scale and resolution on population exposure to PM2.5 from aircraft emissions during landing and takeoff. Atmos Environ 45(19):3294–3300
3. Baek BH et al (2007) Development of an interface for EDMS. In: Proceedings of the 16th annual emissions inventory conference – Emissions inventories: integration, analyses and communication, Raleigh, May 2007
4. Dodson R et al (2009) An analysis of continuous black carbon concentrations in proximity to an airport and major roadways. Atmos Environ 43(24):3764–3773
5. Rhode Island Department of Environmental Management (2008) Characterization of ambient air toxics in neighborhoods abutting T. F. Green airport and comparison sites, Final report, April 2008

# Part VI
# Interactions Between Air Quality and Climate Change

# Chapter 103
# Modelling the Impact of Climate Change on Air Pollution over Europe Using the MATCH CTM Linked to an Ensemble of Regional Climate Scenarios

**Joakim Langner, Magnuz Engardt, and Camilla Andersson**

**Abstract** We used an off-line, regional, model of atmospheric transport and chemistry, CTM, to investigate current and future levels of near-surface ozone and deposition of oxidized nitrogen in Europe. To assess changes in concentrations and deposition due to climate change, the CTM was run with recent (2000) emissions using meteorology from a regional climate model simulating control (1990–2009) and future (2030–2049) climates. The sensitivity to the choice of global climate model was explored by using output from a range of global climate models as forcing to the regional climate model. The analysis shows that results are more robust for surface ozone than for deposition of oxidized nitrogen with increase in summer surface ozone simulated over southern and western Europe. The analysis presented clearly demonstrates the need of exploring a range of different climate scenarios before drawing conclusions on the possible implications of climate change for future regional air pollution.

**Keywords** Ozone • Nitrogen deposition • Chemical transport model • Eulerian

## 103.1 Introduction

The emission, atmospheric transport, chemical and physical conversion and deposition of air pollutants is strongly dependent on meteorological processes in the atmosphere. This strong link is evidenced by substantial variability in observed concentrations and deposition of air pollutants on time scales ranging from hours to years. Model studies also confirm the importance of meteorological variability on both short and longer time scales, e.g. Andersson et al. [2]. It is therefore natural to hypothesize that changes in climate on global and regional scales will result in

J. Langner (✉) • M. Engardt • C. Andersson
Swedish Meteorological and Hydrological Institute, Norrköping, SE-601 76, Sweden
e-mail: joakim.langner@smhi.se

D.G. Steyn and S. Trini Castelli (eds.), *Air Pollution Modeling and its Application XXI*, NATO Science for Peace and Security Series C: Environmental Security 4,
DOI 10.1007/978-94-007-1359-8_103, 

changes in the distribution and deposition of air pollutants both globally and on continental scales. This topic has been the focus of several model studies over the last 10 years. The European situation has been the theme in a range of studies using the regional CTM MATCH [1, 4, 7, 8].

Most, if not all studies so far have been restricted to use just a few (in most cases only one or two) scenarios for the future evolution of the climate. Results from recent co-ordinated climate modelling projects such as CMIP3 [10] and ENSEMBLES [3] demonstrate that the spread in simulated climate change is substantial between contemporary coupled atmosphere-ocean general circulation models, AOGCMs, using the same future greenhouse gas forcing scenario. The differences between the different global climate models are carried over to the regional scale when using regional climate models, RCMs, to depict further details in the climate change signal. In order to approach more robust conclusions about the impact of climate change on future air pollution it is therefore important to include a range of climate scenarios based on different global models in the design of model studies. Here we present for the first time preliminary results from model simulations of future air pollution and deposition over Europe using an ensemble of regional climate scenarios.

## 103.2 Methods

### *103.2.1 Ensemble of Climate Scenarios*

This study relies on a comprehensive ensemble of regional climate scenarios for Europe prepared at the SMHI Rossby Centre trough dynamical downscaling of a range of global GCM runs. Details on the ensemble, it's quality and the RCM used for downscaling can be found in Kjellström et al. [6]. The ensemble was designed to assess the importance of three key sources of uncertainty that affect future climate projections from coupled climate models;

- Uncertainties associated with the greenhouse gas emissions scenarios used to force the models,
- Uncertainties related to the model formulations, and
- Uncertainties related to natural variability, i.e. addressing the uncertainty arising from our inability to predict climate change on decadal time scale.

In order to address these uncertainties the ensemble includes downscaled scenarios using data from several GCMs run for the same greenhouse gas emission scenario; the same GCMs run for different emission scenarios and also a set of model runs using the same GCM/emission scenario combination but with slightly different pre-industrial initial conditions leading to different timing of the simulated climate change. For the CTM modelling presented here we have utilized data from five scenarios of the ensemble, including full 3D model states for every 6 h over a simulated period of 1950–2100. Some characteristics of the AOGCMs used are

**Table 103.1** AOGCMs used in this study. TXX denotes the truncation number, where XX is the maximum number of waves resolved in the horizontal along a latitude circle. In levels, A/O signifies the number of levels in the vertical in the atmosphere/ocean. References for the models can be found in [10]

| Model | Country | Atm. res. | Ocean res. | Levels |
|---|---|---|---|---|
| CNRM-CM3 | France | T63 | 0.5–2° × 2° | A31, O29 |
| ECHAM5/MPI-OM | Germany | T63 | 1.5° × 1.5° | A31, O40 |
| HadCM3 | UK | 2.5° × 3.75° | 1.25° × 1.25° | A19, O20 |

given in Table 103.1. The scenarios from the GCMs were all downscaled with the same RCM, RCA3 [5], to a horizontal resolution of 0.44° × 0.44°. Results for the A1B emission scenario was used for all models. Three different realisations with different initial conditions were used from the ECHAM5 model.

### *103.2.2 CTM Model Setup*

The regional CTM MATCH was used in the study. MATCH is a three-dimensional, Eulerian, off-line, CTM developed at the Swedish Meteorological and Hydrological Institute (SMHI). The model structure, boundary layer parameterisation, advection scheme and numerical treatment were given in Robertson et al. [11]. The dry deposition of gases and aerosols is calculated using a resistance approach depending on land surface type. The wet scavenging is assumed to be proportional to the precipitation intensity for most gaseous and aerosol components. For $O_3$, hydrogen peroxide ($H_2O_2$) and $SO_2$ in-cloud scavenging is calculated assuming Henry's law equilibrium. The chemical scheme in MATCH, based on Simpson et al. [12], considers more than 60 species including relevant sulphur- and nitrogen-containing pollutants as well as all important oxidants. The implementation was described in Langner et al. [9], and extensions were described in Andersson et al. [2]. Important model parameters, such as dry deposition velocities, scavenging coefficients and chemical boundary concentrations, are also tabulated in Andersson et al. [2].

The model domain covers Europe and part of the North Atlantic with a horizontal resolution of 0.44° × 0.44°. In the vertical direction, the model domain reach 5–6 km above the surface using 15 model levels, the lowest model layer is ~60 m thick, increasing to ~700 m in layer 15. The temporal resolution of the meteorological input data is 6 h, interpolated to 1 h inside MATCH; the overall model time step is 10 min.

Anthropogenic emissions of oxidised nitrogen, sulphur dioxide, ammonia, non-methane hydrocarbons and carbon monoxide valid for the year 2000 and needed as input to the CTM were interpolated to the appropriate MATCH grid from the 50 × 50 $km^2$ Co-operative Programme for Monitoring and Evaluation of the Long-Range Transmission of Air Pollutants in Europe (EMEP) "expert" emissions model [13]. $NO_x$ emissions from soils were not included, but natural emissions of isoprene were calculated on-line in the CTM using the meteorological input. The emission fields for the two sets of experiments were identical from year to year in the simulations. This means that meteorological variability was the only factor driving the interannual variability and trends in the model simulations.

## 103.3 Results and Discussion

In order to evaluate the model performance comparisons were made to measured wet deposition and air concentrations of sulphur and nitrogen compounds from EMEP stations across Europe. Since we compare model results using driving meteorology from climate models we restrict the comparison to multi-year annual averages as we cannot expect a good correspondence between model and measurements for individual years. Here we used observations from the time period 1995–2005 centred on the emission year, since trends in anthropogenic emissions become more important when extending the observation period far from the year of emission used in the model simulation. We also put a restriction on data coverage of observations so that only stations with at least 8 years of data and 80% data coverage were included in the analysis.

Table 103.2 shows average statistics for sulphur and nitrogen compounds. The performance using meteorological input downscaled from different global models is quite similar. It is evident that the correlation is better for air concentrations than for deposition. This could partly be related to known deficiencies in the control climate of the GCMs (Lind and Kjellström 2008). They generally exhibit a too zonal circulation over Europe giving rise to a biased precipitation distribution which affects the horizontal distribution of wet deposition Overall bias is however

**Table 103.2** Average statistics comparing model results for the simulation period 1990–2009 to observations in the period 1995–2005

| | Air concentrations ug S/N $m^{-3}$ | | | | | Wet dep. mg N/S $m^{-2}$ $year^{-1}$ | | |
|---|---|---|---|---|---|---|---|---|
| | $SO_2$ | $NO_2$ | $SO_4^{2-}$ | NHx | NOy | SOx | NOx | NHx |
| *Mean* | | | | | | | | |
| Observations | 1.04 | 2.08 | 0.77 | 1.16 | 0.42 | 444 | 319 | 371 |
| CNRM A1B | 0.74 | 1.22 | 1.10 | 1.00 | 0.46 | 538 | 338 | 329 |
| HADLEY A1B | 0.74 | 1.29 | 1.02 | 0.97 | 0.44 | 565 | 351 | 363 |
| ECHAM5 A1B-1 | 0.68 | 1.24 | 0.88 | 0.87 | 0.39 | 537 | 349 | 351 |
| ECHAM5 A1B-2 | 0.69 | 1.24 | 0.92 | 0.91 | 0.41 | 533 | 342 | 342 |
| ECHAM5 A1B-3 | 0.68 | 1.23 | 0.90 | 0.88 | 0.39 | 523 | 341 | 344 |
| *Bias %* | | | | | | | | |
| CNRM A1B | −27 | −41 | 42 | −13 | 8 | 21 | 6 | −11 |
| HADLEY A1B | −29 | −38 | 33 | −16 | 4 | 27 | 10 | −1 |
| ECHAM5 A1B-1 | −34 | −40 | 14 | −24 | −8 | 20 | 9 | −5 |
| ECHAM5 A1B-2 | −33 | −40 | 19 | −21 | −3 | 20 | 7 | −7 |
| ECHAM5 A1B-3 | −34 | −40 | 16 | −24 | −7 | 17 | 6 | −7 |
| *Spatial corr.* | | | | | | | | |
| CNRM A1B | 0.70 | 0.75 | 0.67 | 0.88 | 0.81 | 0.54 | 0.41 | 0.61 |
| HADLEY A1B | 0.70 | 0.75 | 0.70 | 0.90 | 0.80 | 0.54 | 0.41 | 0.61 |
| ECHAM5 A1B-1 | 0.70 | 0.75 | 0.72 | 0.88 | 0.81 | 0.51 | 0.44 | 0.61 |
| ECHAM5 A1B-2 | 0.70 | 0.75 | 0.71 | 0.90 | 0,80 | 0.52 | 0.45 | 0.62 |
| ECHAM5 A1B-3 | 0.69 | 0.75 | 0.71 | 0.87 | 0.81 | 0.48 | 0.43 | 0.60 |
| *# stations* | 67 | 54 | 56 | 23 | 23 | 62 | 62 | 62 |

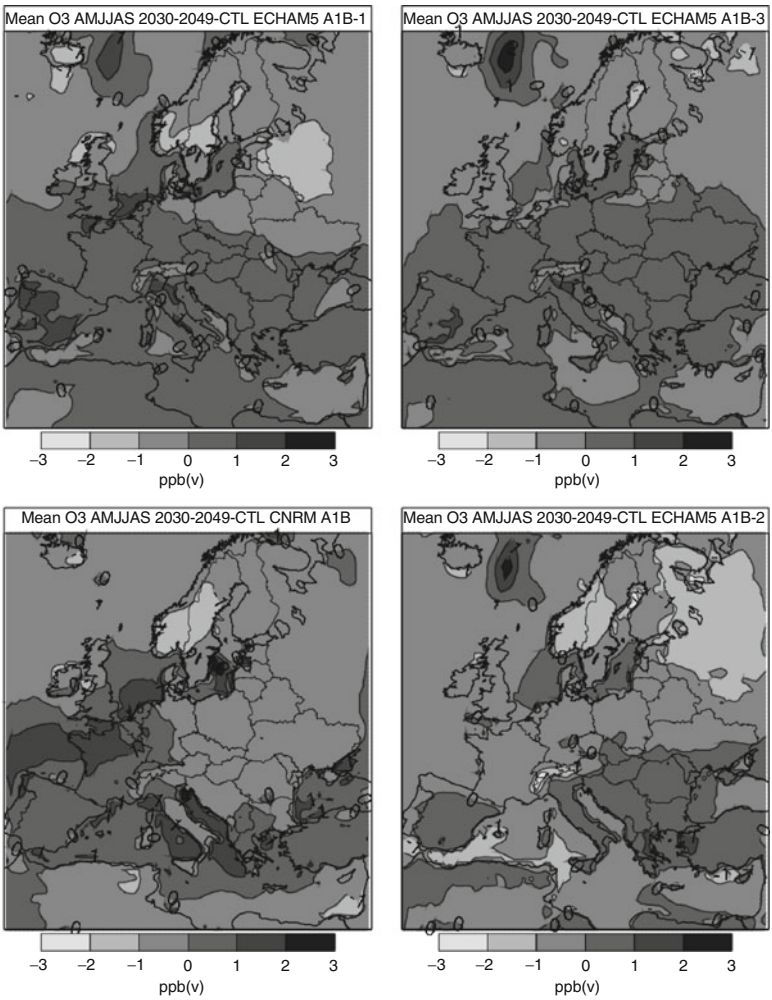


**Fig. 103.1** Change in surface ozone concentration, Apr–Sep daily mean between control period (1990–2009) and scenario period (2030–2049) using meteorological data from four different global model runs downscaled with RCA3. Units: (ppb(v))

lower for wet deposition than for $SO_2$ and $NO_2$ and lowest for inorganic aerosol components of sulphate, nitrate and ammonium. This feature has been observed also in previous model evaluations and is attributed partly to the still rather low horizontal and vertical resolution used in the CTM. Overall the comparison with observations is similar to what is achieved using observed meteorological data for specific years to drive the MATCH CTM.

Figures 103.1 and 103.2 show simulated changes in average surface ozone concentration during summer and annual total (wet + dry) deposition oxidized nitrogen, $NO_x$, between the scenario period, 2030–2049 and the control period,

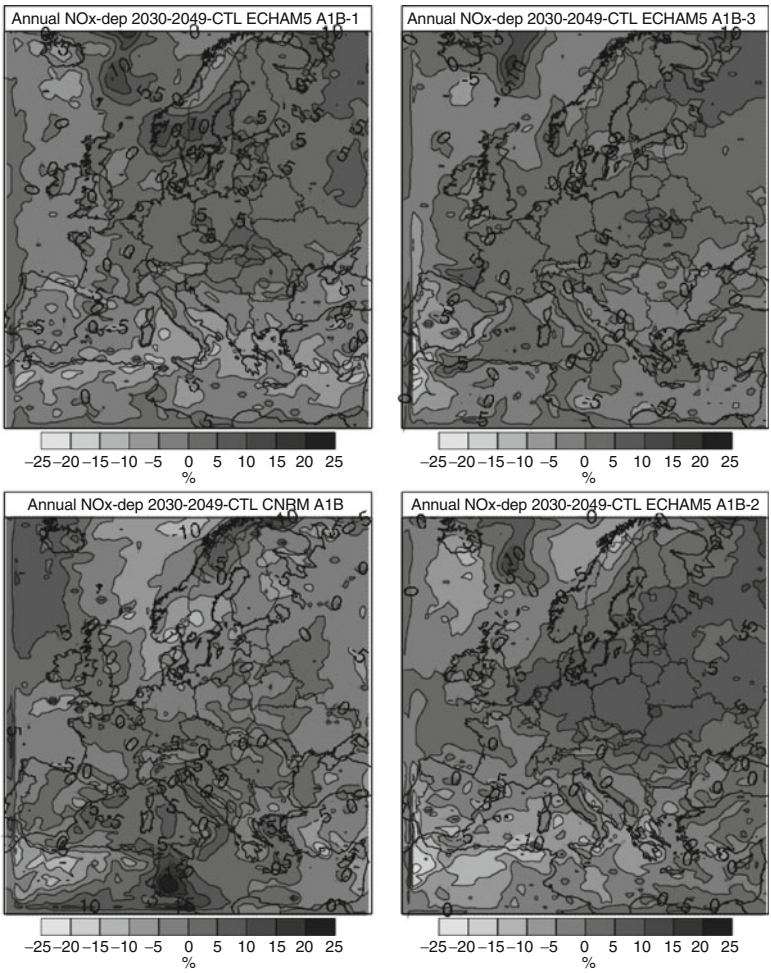


**Fig. 103.2** Change in annual NOx deposition change between control period (1990–2009) and scenario period (2030–2049) using meteorological data from four different global model runs downscaled with RCA3. Units: %

1990–2009. Due to space limitations results are shown for the scenarios based on the CNRM-CM3 model and the ECHAM5 model. For the ECHAM5 case we show the three different scenarios with different initial conditions to illustrate the uncertainty due to natural variability.

Although we are looking at a period quite near in the future the results for ozone are quite robust with generally higher concentrations simulated for the future in southern and western parts of Europe and lower towards the north-east. The increase is in the range of 1–2 ppb(v). It is clear though from the results forced by the different ECHAM5 scenarios that natural variability is important. One of the scenarios

shows small changes while the two others show similar and larger changes. Currently we have no way of saying that one of these three scenarios is more probable than the other.

The results for deposition of oxidized nitrogen is not as robust as for ozone. Here the climate models clearly behave differently. The three ECHAM5 based scenarios look quite similar with an increase in deposition in central and north-eastern Europe and a decrease in the south while the scenario based on CNRM shows a scattered increase in southern and western Europe and a decrease in the north-east.

So far the analysis is preliminary. Remaining work include calculating significance statistics for the simulated changes and analysing also results for periods towards the end of the century when the climate change signal is expected to be stronger. However, the analysis presented so far clearly demonstrates the need of exploring a range of different climate scenarios before drawing conclusions on the possible implications of climate change for future regional air pollution.

**Acknowledgments** This work was supported by Swedish EPA under the CLEO programme - Climate Change and Environmental Objectives and The Nordic Council of Ministers under the project – Robustness of predictions of climate change impact on dispersion and effects of airborne pollutants in northern Europe. Climate scenario results were kindly provided in a suitable format for use in MATCH by the SMHI Rossby Centre.

## References

1. Andersson C, Engardt M (2009) European ozone in a future climate – the importance of changes in dry deposition and isoprene emissions. J Geophys Res. doi:10.1029/2008JD011690
2. Andersson C, Langner J, Bergström R (2007) Interannual variation and trends in air pollution over Europe due to climate variability during 1958–2001 simulated with a regional CTM coupled to the ERA-40 reanalysis. Tellus 59B:77–98
3. Hewitt CD, Griggs DJ (2004) Ensembles-based predictions of climate changes and their impacts. EOS 85:566
4. Hole L, Engardt M (2008) Climate change impact on atmospheric nitrogen deposition in Northwestern Europe: a model study. Ambio 37(1):9–17
5. Kjellström E, Bärring L, Gollvik S, Hansson U, Jones C, Samuelsson P, Rummukainen M, Ullerstig A, Willén U, Wyser K (2005) A 140-year simulation of the European climate with the new version of the Rossby Centre regional atmospheric climate model (RCA3). SMHI report, RMK No. 108, Swedish Meteorological and Hydrological Institute, Norrköping, 54 pp
6. Kjellström E, Nikulin G, Hansson U, Strandberg G, Ullerstig A (2011) 21st century changes in the European climate: uncertainties derived from an ensemble of regional climate model simulations. Tellus 63(A):24–40
7. Langner J, Andersson C, Engardt M (2009) Atmospheric input of nitrogen to the Baltic Sea basin: present situation, variability due to meteorology and impact of climate change. Boreal Environ Res 14:1239–6095
8. Langner J, Bergström R, Foltescu VL (2005) Impact of climate change on surface ozone and deposition of sulphur and nitrogen in Europe. Atmos Environ 39:1129–1141
9. Langner J, Bergström R, Pleijel K (1998) European scale modeling of sulphur, oxidized nitrogen and photochemical oxidants. Model development and evaluation for the 1994 growing season. SMHI report, RMK No. 82, Swedish Meteorological and Hydrological Institute, Norrköping, 71 pp

10. Meehl GA, Stocker TF, Collins WD, Friedlingstein P, Gaye AT, Gregory JM, Kitoh A, Knutti R, Murphy JM, Noda A, Raper SCB, Watterson IG, Weaver AJ, Zhao Z-C (2007) Global climate projections. In: Solomon S, Qin D, Manning M, Chen Z, Marquis M, Averyt KB, Tignor M, Miller HL (eds) Climate change 2007: the physical science basis. Contribution of working Group I to the fourth assessment report of the intergovernmental panel on climate change. Cambridge University Press, Cambridge/New York
11. Robertson L, Langner J, Engardt M (1999) An Eulerian limited-area atmospheric transport model. J Appl Meteorol 38:190–210
12. Simpson D, Andersson-Sköld Y, Jenkin ME (1993) Updating the chemical scheme for the EMEP MSC-W oxidant model: current status, EMEP MSC-W Note 2/93. Norwegian Meteorological Institute, Oslo, 33 pp
13. Vestreng V (2003) Inventory review. Emission data reported to CLRTAP, MSC-W status report 2003. EMEP/MSC-W Note 1/2003. Norwegian Meteorological Institute, Oslo, 134 pp

## Questions and Answers

**Questioner Name**: Pius Lee

**Q**: The ensemble presented consists of many members. Can you kindly point us to the spread you expect the members can capture given that the ensemble members are a range of rather different models with presumably different physical schemes and dynamic characteristics?

**A**: We think we capture a substantial part of the spread with the current ensemble. Ongoing coordinated efforts in the international climate modelling community, e.g. CORDEX, will provide new information on this in the coming years.

**Questioner Name**: Nick Savage

**Q**: Your ensemble only sampled uncertainty from the different GCMs. Have you considered using multiple RCMs and/or multiple CTMs?

**A**: We plan to use multiple CTMs in a recently started project funded by the Nordic council of ministers, NMR.

**Questioner Name**: Gabriele Curci

**Q**: From results of all these scenarios is there any suggestion on what we (as society) should do next, to limit climate change and related problems?

**A**: Reduced emissions of greenhouse gases is the obvius need. A personal view is that taxes on greenhouse gas emissions is a very efficient measure to take.

**Questioner Name**: Sebnem Aksoyoghi

**Q**: Land use might be quite different in 100 years. This would lead to different natural emissions, deposition, etc. How do you deal with it in your future scenario calculations?

**A**: So far these changes were not included either in the GCM/RCM or CTM. It is expected to be included in future GCM/RCM studies.

**Questioner Name**: S.T. Rao

**Q**: Have you examined how well these models have simulated changes (anomalies over decadal time scales) using historical periods?

**A**: Results for historic periods have been evaluated, e.g. Andersson et al. [2], Tellus. Disentangling effects of emission changes and climate variability requires model simulations including emission trends and such simulations were not done so far with the present model system.

**Q**: How did you define the atmospheric lifetimes of secondary pollutants?

**A**: Turnover times were calculated as the ratio of the total mass in the model domain divided by total loss fluxes (deposition plus chemistry).

**Questioner Name**: Ken Schere

**Q**: To maintain large-scale pattern fidelity from GCM to RCM, did you consider to use data assimilation (nudging, 3D-var) in the RCM in addition to boundary forcing?

**A**: Nudging or 3D-var was not used so far in the RCM simulations. We try to avoid using too large RCM domains in order to constrain the simulations.

**Q**: Did you consider an additional regional CTM model run, where you scaled the anthropogenic emissions to the emission scenario used in the GCM run, to look at the combined impacts of climate and emissions change?

**A**: Indeed, we plan such simulations in the near future.

# Chapter 104
# Urban Impact on Air Quality in RegCM/CAMx Couple for MEGAPOLI Climate Change Study in High Resolution

**Tomas Halenka, Peter Huszar, and Michal Belda**

**Abstract** For the purpose of qualifying and quantifying the climate forcing due to atmospheric chemistry/aerosols on regional scale, the regional climate model RegCM3 has been coupled with the chemistry/aerosol model CAMx. Experiments with the couple have been run for EC FP7 project MEGAPOLI assessing the impact of the megacities and industrialized areas on climate. New domain have been settled in 10 km resolution including all the European "megacities" regions, i.e. London metropolitan area, Paris region, industrialized Ruhr area, Po valley etc. TNO emissions are adopted to resolve urban areas. A sensitivity test of the resolution effect is presented to reveal whether the concept of effective emission indices could help to parameterize the urban plume effects in lower resolution models. The sensitivity test to switch on/off Paris area emissions is analysed as well.

**Keywords** Regional climate modeling • Air quality modeling • Urban impact

## 104.1 Coupling of Chemistry and Climate

The information on climate change at regional and local scale is fundamental in the assessment of climate change impacts and the role of local processes. Thus, dynamical downscaling becomes the most convenient tool taking into account processes significantly affected by topography and land use of the region being studied. This is especially true when estimating the impacts of climate change on air-quality and vice-versa, because not only topographic features but regionally extremely varying emissions play significant role. In Europe the need for high

T. Halenka (✉) • P. Huszar • M. Belda
Department of Meteorology and Environment Protection, Charles University,
V Holesovickach 2, 180 00 Prague, Czech Republic
e-mail: tomas.halenka@mff.cuni.cz

D.G. Steyn and S. Trini Castelli (eds.), *Air Pollution Modeling and its Application XXI*,
NATO Science for Peace and Security Series C: Environmental Security 4,
DOI 10.1007/978-94-007-1359-8_104, 

resolution studies is particularly important with respect to complex terrain of the territory; that is why 10 km resolution has been introduced in the EC FP6 project CECILIA [3]. The main aim of the project dealing with climate change impacts and vulnerability assessment in targeted areas of Central and Eastern Europe was the application of regional climate modelling at a resolution of 10 km for local impact studies in key sectors of the region, among others in air quality issues in urban and industrialized areas. The driving chemistry is based on whole Europe simulation by Krüger et al. [6] and Katragkou et al. [5].

To study these effects requires coupling of regional climate models with an atmospheric chemistry/aerosols model to assess the climate forcing to the chemical composition of the atmosphere and its feedback to the radiation, eventually other components of the climate system. In this study climate is calculated using model RegCM [2, 7], while chemistry is solved by model CAMx from ENVIRON Int. Corp. [1], with CB-IV gas phase chemistry mechanism option, wet deposition of gases and particles.

New domain have been settled for an application of the couple in framework of EC FP7 project MEGAPOLI. The main goal of the project is to study the interactions between a climate change and an urban environment. For this purpose we have setup the domain in 10 km resolution including all the European "megacities" regions, i.e. London metropolitan area, Paris region, industrialized Ruhr area, Po valley etc. There is critical issue of the emission inventories available for 10 km resolution including the urban hot-spots, TNO emissions [8] are adopted to resolve the urban areas.

## 104.2 Resolution Sensitivity

A test of the sensitivity with respect to the model resolution was performed comparing the results at 50 km grid to the results at 10 km grid. This was done to assess the effects of nonlinearity of chemical reactions with different concentrations in the input for the model in different resolutions. Actually, this concept has been addressed in project QUANTIFY and we have made some tests there for ship emissions [4]. The question raised here is whether similar concept can be valid for urban plume.

Some comparisons are presented in Figs. 104.1 and 104.2. It should be mentioned that for 50 km run the TNO emissions from 10 km run are merged together, i.e. basically representing original EMEP values, and the results from 10 km grid are rescaled to 50 km grid. In Fig. 104.1 it can be seen for ozone that there is certain effect of the nonlinear chemistry in some urban areas, especially in summer (Paris, London), but the positive differences seem to be connected mostly with elevation patterns. In Fig. 104.2 there are results for black carbon presented, higher positive differences are connected to London, Paris and Po-valley area in winter season.

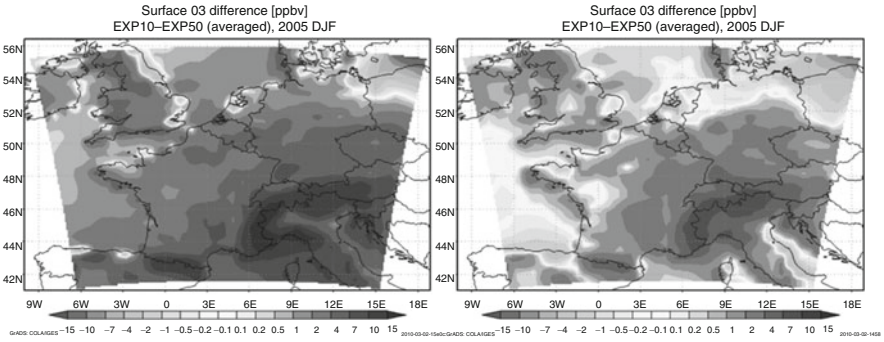


**Fig. 104.1** The difference in surface concentrations of ozone (ppbv) between 10 and 50 km experiments for winter season (*left panel*) and summer season (*right panel*)

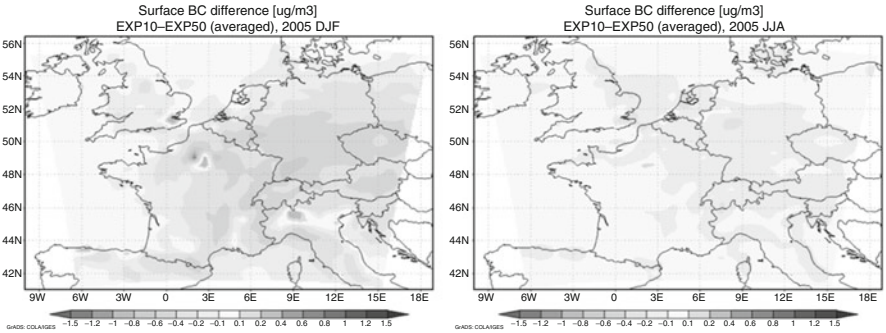


**Fig. 104.2** The difference in surface concentrations of black carbon (μg/m$^3$) between 10 and 50 km experiments for winter season (*left panel*) and summer season (*right panel*)

## 104.3 Sensitivity to Urban Areas

A sensitivity experiment was performed to see the effect of urban areas by means of simple method of switching the urban area emissions on and off. We have made this exercise for Paris region. The results of this simplified experiment are presented in Fig. 104.3. A quite spread negative effect can be seen in winter, during summer this negative effect is localized closely to Paris, with positive effect remotely.

## 104.4 Concluding Remarks

This is a preliminary study for urban areas interaction with a climate change. Further experiments will follow with emission scenario applied in the urban areas included into the MEGAPOLI project. Two way couple has been prepared to assess the real interaction of the "megacities" with climate. The resolution sensitivity results suggest implementation of effective emissions used before for ship plumes.

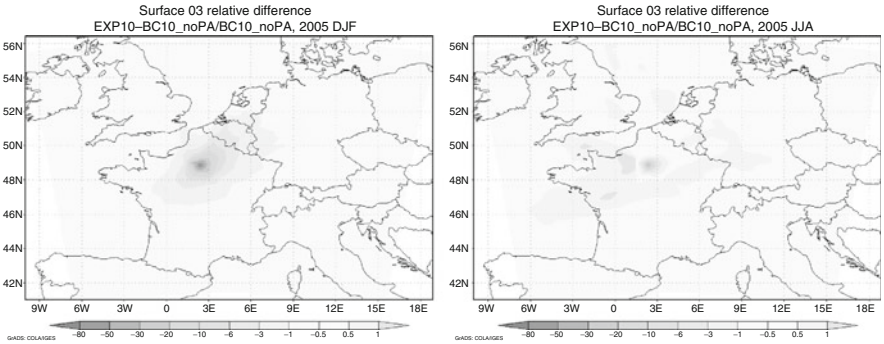


**Fig. 104.3** The relative difference in surface concentrations against background (no Paris emissions) for ozone (%) in 10 km resolution for winter season (*left panel*) and summer season (*right panel*)

**Acknowledgments** This work is supported in framework of EC FP7 MEGAPOLI project (grant agreement n°212520) with local support under MSMT project 7E09089 as well as under local support of Research Plan of MSMT under No. MSM 0021620860. The model development is based on previous support of the grant of Programme Informacni spolecnost, No. 1ET400300414.

## References

1. ENVIRON Corporation (2006) CAMx users' guide, version 4.40
2. Giorgi F, Huang Y, Nishizawa K, Fu C (1999) A seasonal cycle simulation over eastern Asia and its sensitivity to radiative transfer and surface processes. J Geophys Res 104:6403–6423
3. Halenka T (2008) Regional climate modeling activities in CECILIA project: Introduction. IDOJARAS, 112:3–4, III-IX
4. Huszar P, Cariolle D, Paoli R, Halenka T, Belda M, Schlager H, Miksovsky J, Pisoft P (2010) Modeling the regional impact of ship emissions on NOx and ozone levels over the Eastern Atlantic and Western Europe using ship plume parameterization. Atmos Chem Phys 10 (14):6645–6660
5. Katragkou E, Zanis P, Tegoulias I, Melas D, Kioutsioukis I, Krüger BC, Huszar P, Halenka T, Rauscher S (2010) Decadal regional air quality simulations over Europe in present climate: near surface ozone sensitivity to external meteorological forcing. Atmos Chem Phys 10:11805–11821
6. Krüger BC, Katragkou E, Tegoulias I, Zanis P, Melas D, Coppola E, Rauscher S, Huszar P, Halenka T (2008) Regional decadal photochemical model calculations for Europe concerning ozone levels in a changing climate. Quart J Hung Meteorol Serv Idojaras 112(3–4):285–300
7. Pal JS, Giorgi F, Bi X, Elguindi N, Solmon F, Gao X, Rauscher SA, Francisco R, Zakey A, Winter J, Ashfaq M, Syed FS, Bell JL, Diffenbaugh NS, Karmacharya J, Konaré A, Martinez D, da Rocha RP, Sloan LC, Steiner AL (2007) Regional climate modeling for the developing world: the ICTP RegCM3 and RegCNET. Bull Am Meteorol Soc 88(9):1395–1409
8. Denier van der Gon HAC, Visschedijk AJH, Van der Brugh H (2009) Gridded European emission data for the projection years 2010, 2015 and 2020 based on IIASA GAINS NEC scenarios. TNO-034-UT-2009-02306_RPT-ML

# Chapter 105
# Impact of Climate Change on Ozone Pollution in the Lower Fraser Valley, Canada

**Christian Reuten, Bruce Ainslie, Peter Jackson, Ian McKendry, and Douw Steyn**

**Abstract** Assuming steady emissions and background concentrations, we investigate how changes of synoptic meteorology alone in future climates affect ozone episodes in the Lower Fraser Valley, Canada. We perform synoptic typing of combined sea-level pressure and 500 hPa geopotential heights for June to September for 1961–2000 from NCEP reanalysis. Five clusters provide a qualitatively good representation of typical synoptic conditions and stratify exceedance days into one cluster with more than half of all exceedances. Independent cluster analyses for climate model output from CGCM3.1 T63 1961–2000 control runs and 2046–2065 SRES A1B scenario runs give clusters qualitatively similar to NCEP. When CGCM output is mapped to the NCEP clusters, the CGCM control run cluster frequencies are almost identical to NCEP frequencies, while CGCM 2046–2065 output shows only small frequency changes. However, CGCM predicts substantial increases in daily maximum temperatures in the Lower Fraser Valley across all five clusters. An analysis of exceedance probabilities suggests that the predicted temperature increase will more than double the number of exceedance days per year.

**Keywords** Climate change • Ozone • CGCM • NCEP

C. Reuten (✉) • B. Ainslie • D. Steyn
Department of Earth and Ocean Sciences, The University of British Columbia, Vancouver, BC, Canada
e-mail: creuten@gmail.com; dsteyn@eos.ubc.ca

P. Jackson
Natural Resources & Environmental Studies Institute, University of Northern BC, Prince George, BC, Canada

I. McKendry
Department of Geography, The University of British Columbia, Vancouver, BC, Canada

D.G. Steyn and S. Trini Castelli (eds.), *Air Pollution Modeling and its Application XXI*, NATO Science for Peace and Security Series C: Environmental Security 4,
DOI 10.1007/978-94-007-1359-8_105, 

## 105.1 Introduction

Tropospheric ozone concentrations experienced at a specific location arise from the interaction of local emissions of ozone precursors; the local background concentration of ozone and its precursors; and meteorological conditions which control local ozone production and advection. McKendry et al. [2] demonstrated that a previous version of the Canadian GCM had difficulties reproducing past synoptic circulation patterns. We apply a similar approach for the latest version of the GCM and explore how future climate-change scenarios may influence the atmospheric controls on tropospheric ozone production at a coastal location in the Pacific Northwest of North America. We assume steady future emissions and background concentrations because of the large uncertainties in their predictions.

## 105.2 Data and Methods

Our study region is the Lower Fraser Valley (LFV) on the west coast of Canada, which includes the city of Vancouver and its satellite communities (pop. two million). To characterize the local meteorological and ozone conditions, we use station temperatures at Abbotsford Airport (YXX) and hourly ozone measurements from a monitoring station at the edge of the urbanized region (Surrey East), and from 2 semi-rural up-valley (and generally downwind) stations (Chilliwack and Hope).

Ongoing policy efforts in the region to reduce precursor emissions have resulted in substantial reductions in the number of exceedances since the 1980s. As a result, we restrict our analysis to the 1991–2008 period, when the ozone record is more stationary. We use the Canada Wide Standard (CWS) to characterize ozone exceedances. This standard requires 3-year running averages of the fourth highest annual value of the 8-h maxima to not exceed 65 ppb. Based on this metric, Hope has been intermittently out of compliance during our study period, Chilliwack has been mostly in compliance but close to the standard, and Surrey East has been substantially below.

To characterize large-scale meteorological conditions, we use sea-level pressure (SLP) and 500 hPa geopotential height (GPH) output from National Center for Environmental Prediction and National Center for Atmospheric Research (NCEP/NCAR) Reanalysis [1] at $2.5^\circ \times 2.5^\circ$ resolution over the North Pacific (110–157.5° W, 40–62.5° N). The study of future climate is performed with SLP and 500 hPa GPH output from Canadian Centre for Climate Modelling and Analysis (CCCMA) CGCM3.1 T63 (roughly 2.8° resolution), interpolated to the NCEP grid. Daily maximum temperatures at the CGCM grid point closest to YXX, roughly 100 km east from YXX, are used for temperature calibrations.

In order to examine the association between local ozone concentrations and synoptic patterns, a circulation-to-environment approach [3] is adopted whereby summertime (June 1 – September 30) daily synoptic patterns are sorted into a small

number of clusters and the associated daily maximum 8-h ozone concentrations from the three monitoring stations are analyzed. Before clustering, we perform a principle component analysis on combined SLP-GPH daily fields over the control period 1961–2000 for both NCEP and CGCM output and over the future period 2046–2065 for CGCM output for the SRES A1B CO2 emissions scenario. Next, we apply k-means clustering with a Euclidean distance metric, random initial seeding, and 100 repetitions, on the six first EOF components. We find that sorting the EOF loadings into five clusters produces a set of synoptic patterns that are distinct, complete, easy-to-interpret, and which clearly separate exceedance from non-exceedance days.

## 105.3 Results and Discussion

Figure 105.1 shows the result of independent clustering for five clusters in descending order of frequencies for NCEP 1948–2008, CGCM 1961–2000, and CGCM 2046–2065. The CGCM control-run clusters very closely resemble the NCEP clusters. For future CGCM output, clusters 2 and 3 have swapped their frequencies compared to the control run but otherwise remain very similar; the SLP characteristics in cluster 4 have changed, while clusters 1 and 5 remain very similar.

This good qualitative agreement between NCEP and CGCM suggests using NCEP clusters as a basis and to map CGCM output onto the nearest cluster. Figure 105.2 shows the resulting frequencies. CGCM 1961–2000 output has very similar frequencies to NCEP. CGCM 2046–2065 produces the same order of clusters as NCEP. The frequency of cluster 3, which contains most exceedances (Fig. 105.3), does not change. Clusters 2 and 4 contain roughly equal shares of the remaining exceedances. The slight future increase in the frequency of cluster 2 is therefore roughly balanced by a similar decrease in the frequency of cluster 4. Overall, the small future changes in cluster frequencies will likely not lead to any substantial changes in the occurrence of exceedances.

However, future temperatures increase substantially in all five clusters. Therefore, despite very similar large-scale weather patterns, increases in ozone exceedances can be expected from temperature enhancement. Ozone exceedances occur only on days with YXX daily maximum temperatures exceeding about 27°C. Historical meteorological and ozone observations for the period 1991–2000 show an average of 3.34 exceedances per year. We assign YXX temperatures to intervals with equal number of observations, beginning with the largest observed temperature and compute for each interval the probability of ozone exceedances based on observed ozone measurements. Temperatures at the CGCM grid point nearest to YXX are colder, probably because the area represented by the CGCM grid point consists mostly of elevated terrain while YXX is only 60 m ASL. We recalibrate the temperature intervals for the CGCM output over 1991–2000 such that the interval boundaries of YXX and CGCM correspond to the same percentiles. Using the recalibrated CGCM temperature intervals and the YXX exceedance probabilities

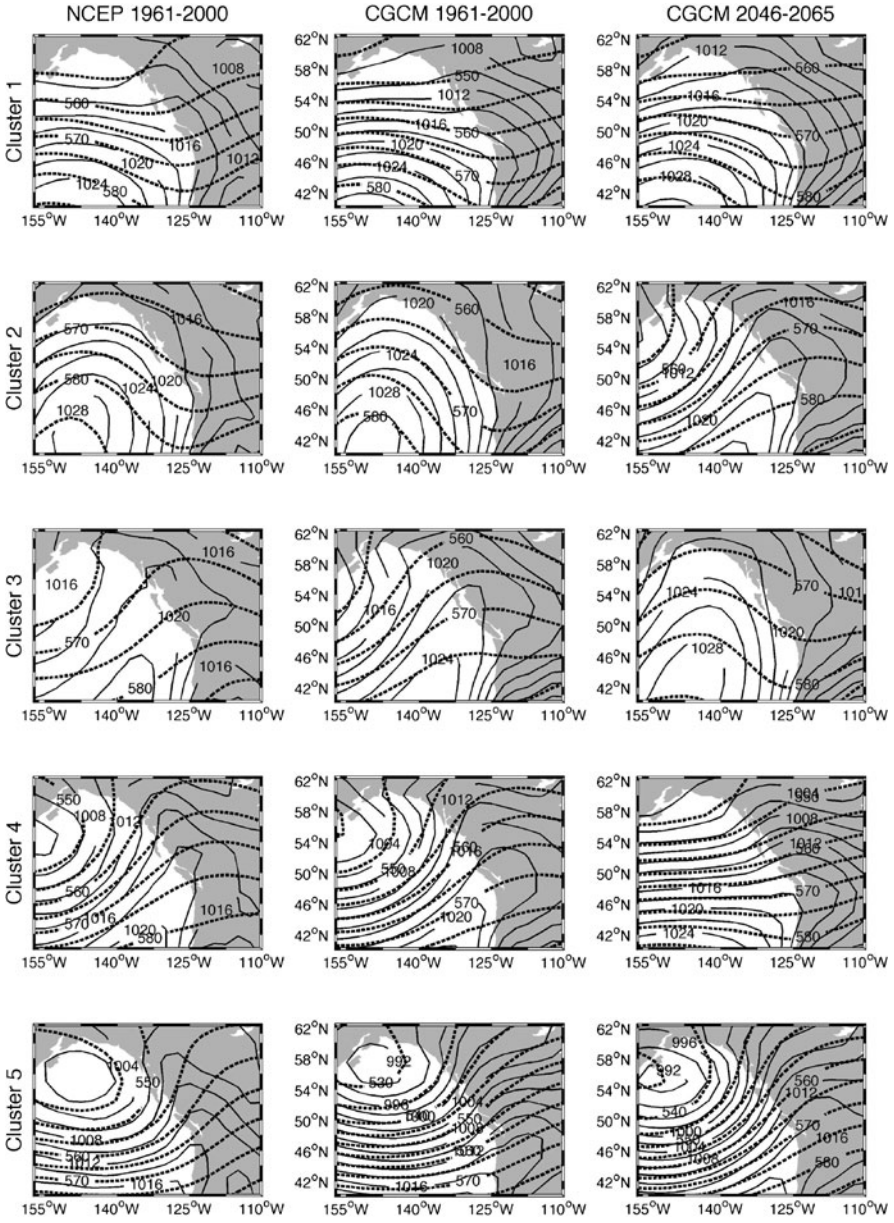


**Fig. 105.1** Composite clusters of sea-level pressure (*thin solid lines*, in hPa, contours every 2 hPa) and 500-hPa geopotential height (*thick dashed line*, in dm, contours every 5 dm) in decreasing order from *top* (*cluster 1*) to *bottom* (*cluster 5*) for NCEP 1961-2000 (*first column*), CGCM 1961-2000 (*second column*), CGCM 2046-2065 (*third column*)

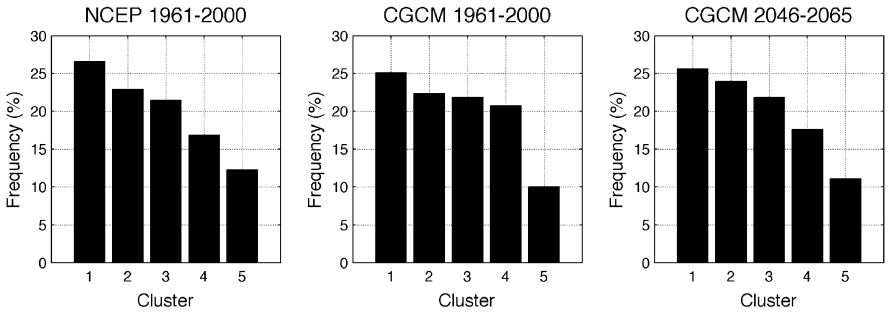


**Fig. 105.2** Frequencies of occurrence of clusters 1–5 determined from NCEP 1961–2000 (*first column* in Fig. 105.1). As labeled from *left* to *right*: original NCEP 1961–2000 frequencies, and frequencies when CGCM output is mapped to these clusters for CGCM 1961–2000 and CGCM 2046–2065 runs

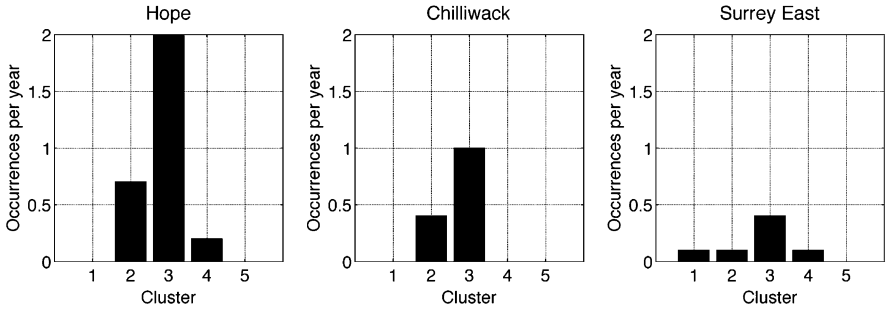


**Fig. 105.3** Occurrences of ozone exceedances per year over the period 1991–2000 by location as labeled

for 2046–2065 CGCM temperatures gives 7.1 (±0.3; standard deviation of spread from using 20–60 observations per interval) exceedances per year. This large value (compared to 3.34 in 1991–2000) implies that, in the absence of other dominating effects, there is a potential for the eastern part of the LFV to be permanently out of compliance with CWS by the middle of this century.

## 105.4 Conclusions

Analysis from the CGCM3.1 2046–2065 SRES A1B scenario suggests that the frequency of occurrence of synoptic patterns, associated with summertime elevated ozone concentrations in the LFV, will not change substantially in the future. However, in this region local meso-scale circulation patterns are extremely important in influencing episodic ozone concentrations. Such circulations patterns, while driven by the larger synoptic conditions, are not resolved in the CGCM3.1 model output.

While it remains to be seen how these local circulations patterns will be affected under future climate scenarios, the general trend in increased surface temperatures suggests that climate change will have a potentially serious effect on summertime ozone concentrations in the LFV.

**Acknowledgments** We are grateful to Derek van der Kamp for providing us with his earlier R code and sharing his experience. Metro Vancouver provided the air-quality data and CCCMA the CGCM output. NCEP/NCAR Reanalysis data was provided by the Physical Sciences Division in the Earth and System Research Laboratory of the National Oceanic & Atmospheric Administration. Funding for the research was derived from NSERC grants to Douw Steyn and Peter Jackson and from the British Columbia Clean Air Research Fund supported by the Fraser Basin Council, Fraser Valley Regional District, and Metro Vancouver.

## References

1. Kalnay E et al (1996) The NCEP/NCAR 40-year reanalysis project. Bull Am Meteorol Soc 77:437–471
2. McKendry IG, Steyn DG, McBean GA (1995) Validation of synoptic circulation patterns predicted by the Canadian climate centre global circulation model for Western North America. Atmos Ocean 33(4):809–825
3. Stahl K, Moore RD, McKendry IG (2006) The role of synoptic-scale circulation in the linkage between large-scale ocean-atmosphere indices and winter surface climate in British Columbia, Canada. Int J Climatol 26:541–560

## Question and Answer

**Questioner Name**: Christian Hogrefe

**Q:** Did the sequence of synoptic patterns change between the GCM Base and Control runs? If so, would this be expected to affect ozone?

**A:** The sequence of synoptic types within an episode has a fairly strong influence on ozone levels. We did investigate the sequence, by performing a rather messy type sequence analysis. While the outcome was fairly complicated, it seems that the sequences were generally preserved.

# Chapter 106
# Impact of Global Warming on the Regional Climate Adjacent to the Great Lake Biwa

**Takehide Hama, Shigeto Kawashima, and Koji Sato**

**Abstract** We tried to simulate local climatic elements (temperature, wind speed and wind direction) in a lake watershed by using the turbulence closure model. The study site is Lake Biwa watershed, which is the largest lake in Japan and the most important water resource for 12 million people in Kinki region including Osaka and Kyoto Prefectures. The lake watershed is surrounded by mountains and covered mainly by lake, forest, and paddy field. Then, we conducted scenario analysis of global warming by rising the surface temperature of the lake according to IPCC reports and estimated the impact of global warming on the regional climate adjacent to the great Lake Biwa. In addition, we selected some local areas, which are typical land use, in the watershed and conducted sensitivity analysis for global warming in the local areas. The effect of global warming on the lake watershed appears clearer in the daytime, when wind speed in the upper boundary is higher. In this case, the energy from the great lake may be rapidly distributed to the surrounding region.

**Keywords** Lake watershed • Regional climate • Global warming • Turbulence closure model • Simulation

## 106.1 Introduction

It is one of the most important issues to evaluate the impact of global warming on energy and material balances in hydrological watershed, especially lake watersheds. It is complicated to evaluate the impact on a lake watershed because

T. Hama (✉) • S. Kawashima
Graduate School of Agriculture, Kyoto University, 606-8502 Kyoto, Japan
e-mail: hama@kais.kyoto-u.ac.jp

K. Sato
Nomura Research Institute, Limited, Tokyo 240-0005, Japan

D.G. Steyn and S. Trini Castelli (eds.), *Air Pollution Modeling and its Application XXI*,
NATO Science for Peace and Security Series C: Environmental Security 4,
DOI 10.1007/978-94-007-1359-8_106, 

a large lake has large energy capacity and functions as a buffer for daily variations in energy in the watershed.

We tried to simulate climatic parameters (temperature, wind speed and wind direction) in a lake watershed by using the turbulence closure model [4].

## 106.2 Materials and Methods

### *106.2.1 Study Site*

The study watershed is located around Lake Biwa, which is the largest freshwater lake in Japan. The watershed is about 3,800 $km^2$ and surrounded by mountains. The Lake Biwa is about 670 $km^2$ and located in the center of the watershed.

The watershed has been affected by Asian monsoon climate on a large scale. The local climate in the watershed is roughly characterized by three types of climate: the first climate is that in the northwestern part of the watershed affected by the Japan Sea and has high rainfall or snow in summer and in winter; the second is in the southwestern part affected by the Seto Island Sea and has low rainfall or snow throughout the year; and the third is eastern part affected by the Pacific Ocean and has high rainfall in summer and low rainfall or snow in winter.

### *106.2.2 Meteorological Data*

Meteorological data was obtained from the 8 points around the lake, among which 1 point (Oshinohara) was set by us and the other 7 points were set by JMA, Japan [2]. We used the data on water temperature of the lake provided by LBERI, Japan [3] and the data on wind speed and direction on the vertical and upper boundary of analysis region provided by NOAA/NCEP, USA [5].

### *106.2.3 Model and Simulation*

We have computed distribution of air temperature and wind speed and direction in the local region around the Lake Biwa by using mesoscale meteorological model.

The basic equations to calculate atmospheric motion are as follows. These three equations are mass conservation equation, Navier-Stokes equation, thermal diffusion equation, respectively;

$$\frac{\mathrm{D}U_i}{\mathrm{D}x_i} = 0 \tag{106.1}$$

$$\frac{\mathrm{D}U_i}{\mathrm{D}x_i} = -\frac{1}{\rho}\frac{P}{x_i} + \nu\frac{\partial^2 U_i}{\partial {x_k}^2} - \varepsilon_{ijk} f_k U_i + \mathrm{g}_i \tag{106.2}$$

$$\frac{\mathrm{D}\Theta}{\mathrm{D}x_i} = \alpha\frac{\partial^2 \Theta}{\partial {x_i}^2} \tag{106.3}$$

where $U$ is wind speed, ρ is air density, $P$ is pressure, ν is kinetic viscosity coefficient, ε is Eddington's epsilon, $f$ is Coriolis parameter, g is gravity acceleration, Θ is potential temperature, α is thermal diffusion coefficient. $x_i$ ($i = 1 - 3$) and $t$ represent special coordinate and time, respectively. Then, the Navier-Stokes equation was developed for the turbulence simulation by Reynolds averaging. In addition, we have used the Level 2.5 model developed by Mellor and Yamada [4] to close the Reynolds-averaged Navier-Stokes equation.

Analysis region was the lake and its surroundings. The horizontal area was 57.6 km in east-west direction (from 135.8° to 136.4° east latitude) × 67.2 km in north-south direction (from 34.9° to 35.5° north latitude). The vertical range was from the surface of the ground to an altitude of 2 km.

Analysis period was 1 day. We selected 2 days, February 20th and July 28th in 2004, for the simulation as representative weather conditions in winter and summer.

We assumed that the differential terms on temperature and wind equaled to zero in lateral direction. We applied the meteorological data by NCEP to the upper boundary of the analysis region.

Heat condition on the surface of the ground was calculated from heat balance. Land surface was characterized by 7 parameters such as albedo, roughness length, and thermal conductivity and categorized into 16 types such as paddy field area, forest area and urban area.

The meteorological values in a steady state after temporary initial condition and iterative calculation were used as initial condition for the simulation.

We simulated the meteorological change in the lake watershed in two types of scenario by using the meteorological model. One scenario assumes the rising of the temperature of lake water related with global warming. The other assumes the increase of the urban area related with development of rural area. We considered impact of global warming on the lake watershed by increasing initial water temperature. The increment of the water temperature was set to 2.4°C (low level), 4°C (middle level), and 6°C (high level) by reference to the IPCC scenarios [1]. In addition, we considered impact of urbanization on the lake watershed by changing forest and farming areas to urban area.

## 106.3 Results and Discussion

### *106.3.1 Lake Warming Scenario*

Figure 106.1 shows the difference distribution of temperature in the lake watershed on the lake water warming scenario from the current state. Center of the map with about 3°C higher temperature is the lake area.

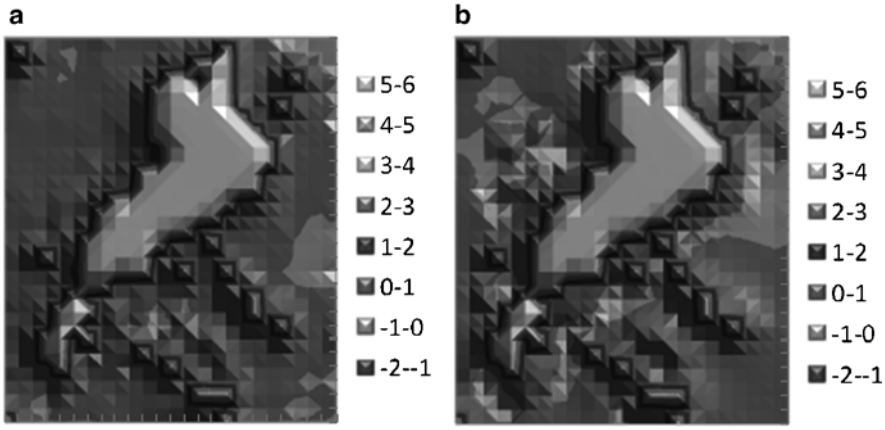


**Fig. 106.1** The difference distribution of temperature (°C) in the lake watershed at noon on the lake warming scenario (middle level = 4°C up) from the current state; on a sunny day (**a**) in summer (July 28th) and (**b**) in winter (Feb 20th)

In summer, higher temperature was seen in the lakeside area and mountain area, especially in the southeast. This tendency was also seen at night. Whereas, lower temperature (negative values), that suggests the area has inverse response to the lake water warming, was seen in the east.

Clearer difference was seen in winter than in summer. Lower temperature was seen in many areas around the lake.

Wind speed from land to the lake was increased at many areas by the lake warming. Wind speed in the daytime in summer was increased at many areas except in the east. On the other hand, wind speed in winter was decreased in the daytime and increased in nighttime. It was suggested that additional heat in the lake on the lake warming scenario was delivered to west-side area of the lake by the wind in the east in summer, whereas heat was delivered to northeast-side area by the wind in the southwest direction in winter.

### *106.3.2 Urbanizing Scenario*

Figure 106.2 shows the difference distribution of temperature in the lake watershed on the urbanizing scenario from the current state.

Temperature was increased in many areas both in summer and winter with increase of urban area. The amount of increase in temperature in the nighttime was larger than in the daytime.

Contrast to temperature, wind speed was decreased on the urbanizing scenario. The amount of decrease in wind speed in the nighttime was larger than in the daytime.

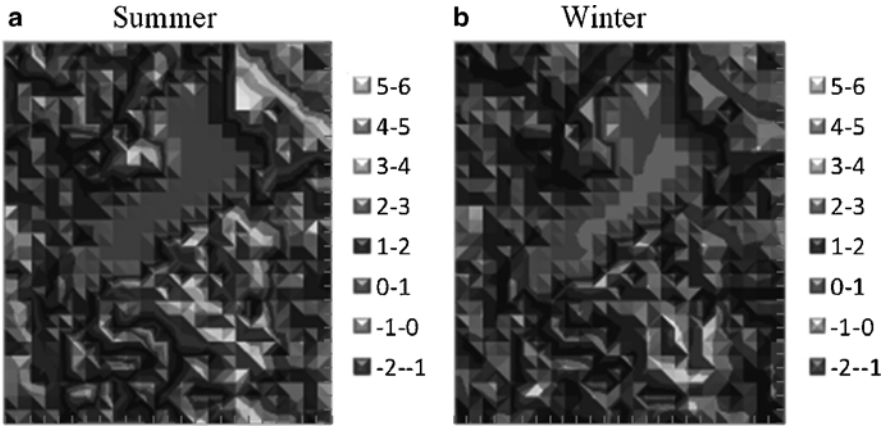


**Fig. 106.2** The difference distribution of the surface temperature (°C) in the lake watershed at midnight on the urbanizing scenario from the current state; (**a**) in summer (July 28th) and (**b**) in winter (Feb 20th)

## 106.4 Summary

The effect of global warming on the lake watershed appears clearer in the daytime, when wind speed in the upper boundary is higher. In this case, the energy from the great lake may be rapidly distributed to the surrounding region. Whereas, the effect of global warming appears only in some local areas in winter night because wind is not strong enough to distribute the additional energy. It is suggested that the effect of global warming on the lake watershed in macroscopic may be depend not only on the energy level stored in the lake, but also on the energy redistribution system of the adjacent region.

## References

1. IPCC (Intergovernmental Panel on Climate Change) (2007) The fourth assessment report
2. JMA (Japan Meteorological Agency) (2010) http://www.jma.go.jp/
3. LBERI (Lake Biwa Environmental Research Institute), Shiga Prefecture, Japan (2010) http://www.lberi.jp/
4. Mellor GL, Yamada T (1982) Development of a turbulence closure model for geophysical fluid problems. Rev Geophys Space Phys 20:851–875
5. NOAA/NCEP (National Oceanic and Atmospheric Administration/National Centers for Environmental Prediction), USA (2010) http://www.ncep.noaa.gov/

# Part VII
# Air Quality and Human Health

# Chapter 107
# Advancing Exposure Science and Its Applications

**Lawrence W. Reiter**

**Abstract** The mission of most environmental organizations around the world is to safeguard human health and the environment. In the United States, air quality management practice relies on the ambient concentrations of pollutants of concern and the success of a regulatory strategy is assessed by determining whether pollutant emissions have been reduced and ambient concentration levels have decreased. Some countries (e.g. United Kingdom) assess the success of their regulatory strategy by determining whether exposure reduction have occured. Exposure is defined as the contact of a stressor with a receptor for a given duration of time. It is now well-recognized that ambient concentrations and human exposure levels are not the same. Hence, it is important to better understand exposure levels since exposure is the link between environmental pollution and human and ecosystem health. Exposure science deals with comprehensive understanding of the relationship among pollutant emissions, pollutant transport and fate, pollutant levels that people breathe in and stressor levels to sensitive ecosystems, and associates health effects. Given the increasing complexity of current and emerging environmental problems, exposure science must play a pivotal role in developing and implementing most meaningfull and cost-effective emission control policies. Theis paper provides exposure framework to identify and minimize exposures to harmful pollutants, thereby better protectinf human ecosystem health.

**Keywords** Air quality modeling • Air quality and human health • Exposure modeling • Epidemiological analysis

L.W. Reiter (✉)
National Exposure Research Laboratory, U.S. Environmental Protection Agency,
Research Triangle Park, NC 27711, USA
e-mail: sanders.carola@epa.gov

D.G. Steyn and S. Trini Castelli (eds.), *Air Pollution Modeling and its Application XXI*,
NATO Science for Peace and Security Series C: Environmental Security 4,
DOI 10.1007/978-94-007-1359-8_107, 

## 107.1 Introduction

In an effort to protect public health from the impacts of air pollution, many environmental agencies in the world implement rules/regulations to reduce emissions for various sectors to maintain ambient air quality at acceptable levels. The implicit assumption here is that when ambient concentrations are maintained at regulated levels, human health is adequately protected. Often times, human exposure to harmful air pollutants is not directly assessed/considered but is based on epidemiology studies which use ambient concentrations as the surrogate for exposure. However, we know that for many air pollutants spatial and temporal variability of both the receptors and the pollutants can affect the utility of ambient concentration measurements as a surrogate for exposure. In epidemiology studies this can result in exposure misclassifications which "...blunt the sensitivity of epidemiologic studies for detecting the effects of environmental agents..." [1]. To fully assess the nature and magnitude of an air pollution problem it is important to explicitly consider exposure in understanding the health impacts of air pollutants along with their sources. "Our understanding of exposure-response relationships can be no more accurate than our characterization of exposure. Perhaps, the greatest current limitation to estimating multipollutant effects is the uncertainty regarding personal exposures of multiple pollutants, taking into consideration the complicated differences in the time-activity patterns of individuals or special subgroups" [2].

## 107.2 Exposure

The U.S. Environmental Protection Agency's National Exposure Research Laboratory (NERL) has recently developed a Conceptual Framework for Exposure Science [3]. Under this Framework, exposure is defined as the contact of a stressor with a receptor for a specific duration of time (Fig. 107.1).

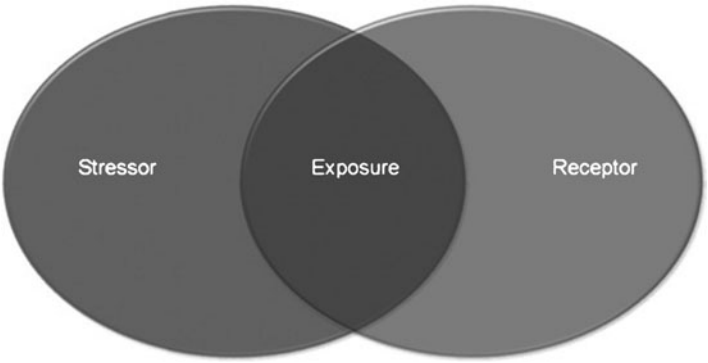


**Fig. 107.1** Conceptual diagram which illustrates exposure

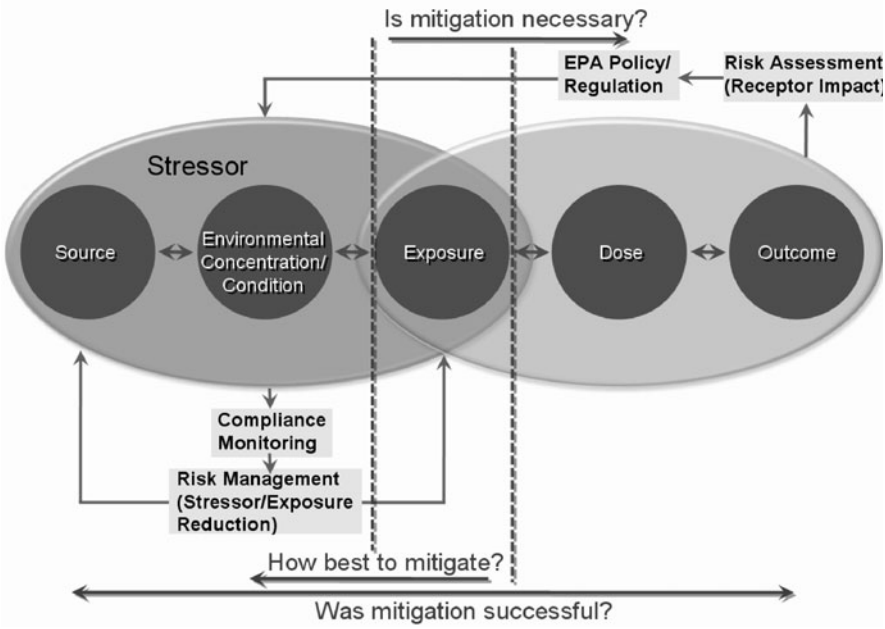


**Fig. 107.2** Framework for exposure science

For exposure to occur, the stressor and receptor must come together at the same time and in the same place. The actual exposure is described in terms of magnitude, frequency and duration of contact.

The goal of exposure science is to characterize, forecast and manage exposures. Figure 107.2 overlays the concept of stressor and receptor on the source-to-outcome framework. This figure demonstrates the pivotal role exposure plays in environmental management practices including risk assessment (Is mitigation necessary?), risk management (How best to mitigate?), and accountability (Was mitigation successful?).

The objectives of this paper are to (1) illustrate the need for developing innovative approaches for exposure prediction, (2) examine various alternative exposure metrics for health data analysis, and (3) assess the benefits of using various levels of detail in air quality modeling for exposure and health studies.

## 107.3 Air Quality Exposure Metrics

Epidemiology studies aimed at understanding the relationships between air pollution and human health have utilized a variety of exposure metrics to characterize air quality (Fig. 107.3). As reviewed by Jerrett et al. [4], "there has been limited effort

| | |
|---|---|
| **Proximity Models** | Use proximity to pollution sources to estimate exposure |
| **Interpolation Models** | Use geostatistical methods to develop continuous pollutant surface concentrations over an area using monitoring data from the area |
| **Land-Use Regression Models** | Use least-squares regression to predict continuous pollutant surface concentrations using monitoring data and area specific variables (i.e., traffic volume, land-use type and altitude) |
| **Dispersion Models** | Use deterministic processes (i.e., Gaussian Plume equations) to develop continuous pollutant surfaces concentrations using data on emissions, meteorology, and topography |
| **Integrated Meteorological-Emission Models** | Use emission data coupled with meteorological and chemical modules to simulate dynamics of atmospheric pollutants, and |
| **Hybrid Exposure Models** | Combine information from personal or regional monitoring or models with other exposure metrics |

**Fig. 107.3** Models used to better characterize air quality (Adapted from Jerrett et al. [4])

to compare and evaluate formally the relative accuracy of results produced by the existing air pollution models. Such an evaluation requires that the models be implemented with the same population over the same spatiotemporal domain."

NERL has recently implemented a series of studies to evaluate various metrics being used for characterizing air quality and exposure with the hypothesis that better definition of air quality/exposure data will enable us to better discern a health effect (Fig. 107.4). The most resource-intense metric is the exposure surface based on regional and urban air quality models (e.g. CMAQ and AERMOD) and exposure models (e.g. SHEDS and APEX). Given uncertainties in air quality models, the modelled air quality surfaces can be bias-corrected using appropriate data fusion techniques [5, 6]. This paper presents some preliminary data on the merits of different exposure metrics based on studies being carried out in Atlanta, Georgia and New York State.

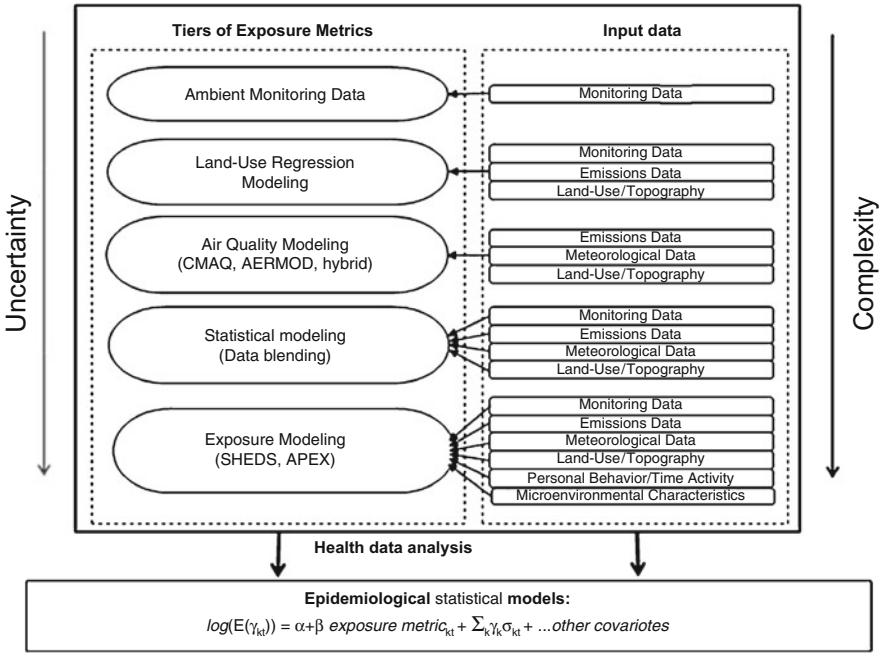


**Fig. 107.4** Tiers of exposure metrics used to support epidemiologic research

The Atlanta study is considering exposure metrics such as central city monitoring data, AERMOD model estimates of pollutant concentrations, combined regional and urban modeling estimates of pollutant levels, and exposure model estimates together with emergency department visits over the 1999–2002 period. The risks calculated from different metrics, presented in Fig. 107.5, reveal that the use of data from a central city monitoring site is inadequate to detect health signals. Air quality models can help better discern the relationships between air quality and human health.

The New York State study is examining whether refining exposure metrics can help reduce exposure misclassification and improve our ability to discern health signals. To this end, ambient ozone concentration surfaces were generated over five summers for the 2001–2005 period using three techniques; kriging observations, adjusting the bias of CMAQ ozone estimates, and modelling exposure by accounting for factors such as infiltration of pollutants into buildings and daily activity patterns of individuals (Fig. 107.6).

The early results of epidemiologic analysis of respiratory-related hospital admissions in New York, provided in Fig. 107.7, indicate that associations between ozone and respiratory-related hospital admissions are stronger with improved exposure characterization (i.e., using bias-corrected ozone concentration surfaces and exposure surfaces), resulting in significant risk as compared to insignificant risk using monitoring data alone.

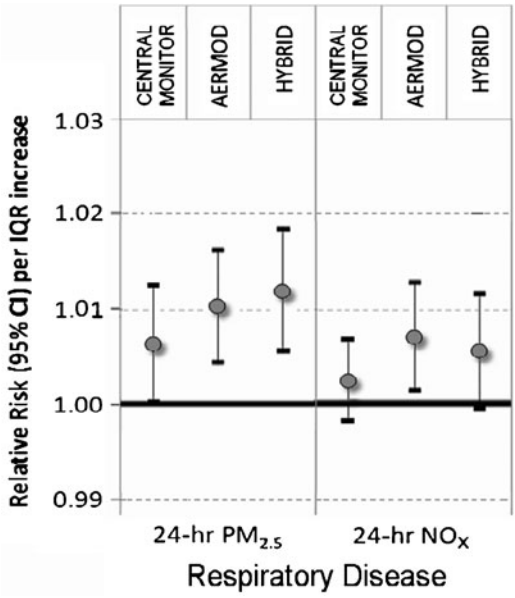


**Fig. 107.5** Preliminary results of epidemiologic analysis of emergency department data in Atlanta [7]

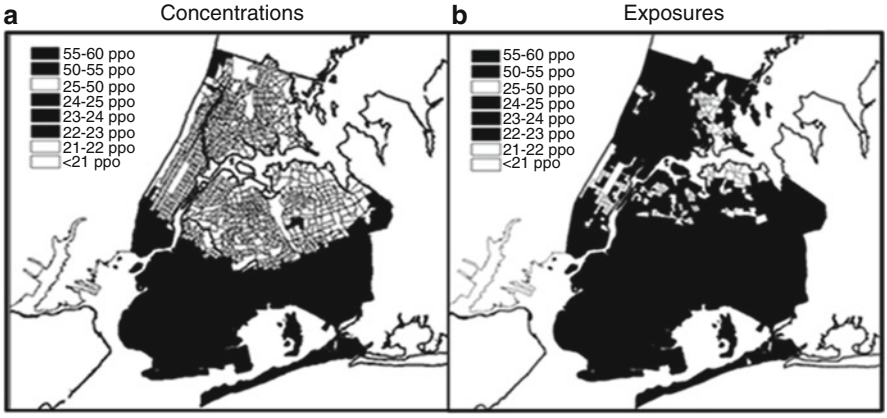


**Fig. 107.6** Spatial maps of modelled ambient concentrations (**a**) and exposure (**b**) in New York [5, 6]

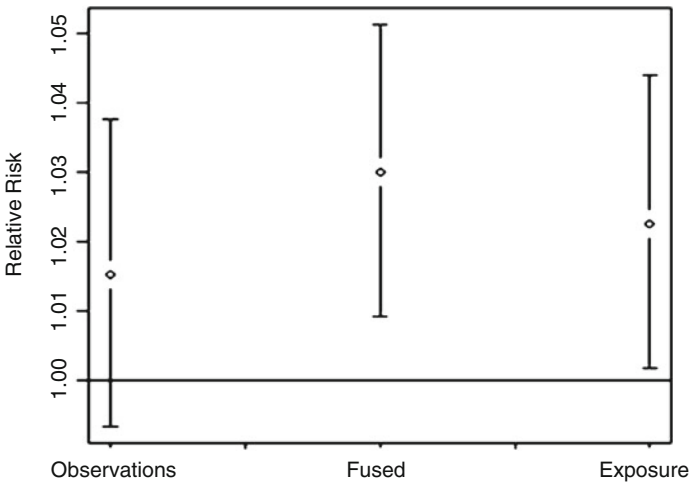


**Fig. 107.7** Preliminary results of epidemiologic analysis of hospital admissions in New York [5, 6]

## 107.4 Summary

Since environmental managers and health scientists rely on the ambient concentrations in managing air quality, it is important that we have a better understanding of human exposure to air contaminants to adequately protect human health. To this end, the following factors that impact exposures need to be incorporated into air quality models.

- Local sources (mobile, area and point) on outdoor residential concentrations
- Local meteorology on outdoor residential concentrations and infiltration rates
- Housing type and house operations on infiltration and indoor concentration
- Locations and Activities on personal exposure

The air pollution modeling community must be fully engaged in:

- Advancing the use of exposure science in the air quality standard setting and standard implementation process
- Improving characterization of ambient air quality with high spatial and temporal resolutions
- Developing an integrated modeling system that can be operationally applied in air quality management practices (e.g., standard setting, standard implementation, risk mitigation, accountability)
- Streamlining and integrating air quality and exposure information to optimally assess exposures (reduce exposure misclassification) and make models accessible to multiple users.

## References

1. Zeger SL, Duncan T, Dominici F, Samet JM, Schwartz J, Dockery D, Cohen A (2000) Exposure measurement error in time-series studies of air pollution: concepts and consequences. Environ Health Perspect 108:419–426
2. Mauderly JL, Burnett RT, Castillejos M, Özkaynak H, Samet JM, Stieb DM, Vedal S, Wyzga RE (2010) Is the air pollution health research community prepared to support a multipollutant air quality management framework? Inhal Toxicol 22(S1):1–19
3. Environmental Protection Agency (2009) A conceptual framework for the US EPA's National Exposure Research Laboratory. Environmental Protection Agency, EPA/600/R–09/003
4. Jerrett M, Arain A, Kanaroglou P, Beckerman B, Potoglou D, Sahsuvaroglu T, Morrison J, Giovis C (2005) A review and evaluation of intraurban air pollution exposure models. J Exposure Anal Environ Epidemiol 15:185–204
5. Garcia VC, Crooks J, Gego E, Lin S, Rao ST (2010) Characterizing the exposure of regional-scale air quality in the northeastern United States. Presented at the ITM 2010: 31st NATO/SPS international technical meeting on air pollution modeling and its application, Torino, 27 Sept–01 Oct 2010
6. Garcia V, Foley K, Gego E, Holland D, Rao ST (2010) A comparison of statistical techniques for combining modeled and observed concentrations to create high-resolution air quality surfaces. Air Waste Manage Assoc 60:586–595
7. Isakov V, Touma J, Valari M, Özkaynak H, Sarnat SE, Sarnat J, Kewada P, Mulholland J (2010) Development and evaluation of alternative metrics of ambient air pollution exposure for use in epidemiologic studies. Presented at the ITM 2010: 31st NATO/SPS international technical meeting on air pollution modeling and its application, Torino, 27 Sept–01 Oct 2010

# Chapter 108
# An Investigation of the Impacts of Aviation Emissions on Future Air Quality and Health

**Saravanan Arunachalam, Matthew Woody, Bok Haeng Baek, Uma Shankar, and Jonathan I. Levy**

**Abstract** Recent estimates of the growth in demand for aviation indicate that passenger counts may double or even triple by the year 2025, with a corresponding projected increase in emissions from the aviation sector. This would contribute to approximately proportional increases in concentrations and health effects if other factors were unchanging, but background emissions from non-aviation anthropogenic sources are generally expected to decrease due to several emissions control measures that are likely to be in place, and population size and age distribution will change over time. In this study, we evaluated changes in air quality and health risk due to growth in aviation activities from the year 2005 to 2025, focusing on 99 major U.S. airports with aircraft activity data for landing and takeoff (LTO) based on Terminal Area Forecasts (TAFs) developed for a sample growth scenario under the Next Generation Air Transportation System (NextGen) for 2025. We performed

S. Arunachalam (✉)
Institute for the Environment, University of North Carolina at Chapel Hill, 137 E. Franklin St., #648A, Chapel Hill, NC 27599–6116, USA
e-mail: sarav@email.unc.edu

M. Woody
Institute for the Environment, University of North Carolina at Chapel Hill, 137 E. Franklin St., #658, Chapel Hill, NC 27599–6116, USA

B.H. Baek
Institute for the Environment, University of North Carolina at Chapel Hill, 137 E. Franklin St., #651, Chapel Hill, NC 27599–6116, USA

U. Shankar
Institute for the Environment, University of North Carolina at Chapel Hill, 137 E. Franklin St., #644, Chapel Hill, NC 27599–6116, USA

J.I. Levy
Boston University School of Public Health, 715 Albany Street, T4W, Boston, MA 02118–2526, USA

D.G. Steyn and S. Trini Castelli (eds.), *Air Pollution Modeling and its Application XXI*, NATO Science for Peace and Security Series C: Environmental Security 4,
DOI 10.1007/978-94-007-1359-8_108, 

four annual simulations using the MM5-SMOKE-CMAQ modeling system for the year 2005 and 2025, with and without aircraft emissions. We obtained non-aviation emissions for 2005 from EPA's 2005 National Emissions Inventory (NEI), and projected these to the year 2025. In performing the health risk analyses, we applied the EPA's Speciated Modeled Attainment Test (SMAT) to the CMAQ results, and compared the air quality and health risk results on a pre-SMAT and post-SMAT basis. Our findings illustrated that each of the time-varying components – background concentrations, emissions, and population patterns – contributes significantly to growth in projected health risks over time, with significant differences in trends by particle constituent and region of the country. The relative importance of various particle constituents also depended significantly on the SMAT process, although secondary sulfate and nitrate particles dominated health risk in all scenarios. These conclusions provide an indication of the factors influencing health risk over time and the resulting areas in which interventions may be most effective.

**Keywords** CMAQ • Aviation emissions • $PM_{2.5}$ • Health risk analysis • SMAT

## 108.1 Introduction

Aviation is a vital component of the U.S.'s infrastructure and usage is projected to grow steadily over the next 20 years. The Federal Aviation Administration (FAA) projects U.S. passenger enplanements to grow at an average annual rate of 2.5% between 2011 and 2030. While an important mode of transportation, aircraft activities affect air quality due to emissions of CO, $NO_x$, Volatile Organic Compounds (VOCs), $SO_x$, $PM_{2.5}$, and numerous hazardous air pollutants. In light of the projected growth of aircraft usage and emissions, coupled with the expectation that background emissions from non-aviation anthropogenic sources will decrease due to several emissions control measures that are likely to be in place as well as population size and age distribution changes over time, it is critical to understand the effects of aircraft on air quality from both an environmental and public health perspective. Here we present an investigation of the simulated impacts of aviation emissions on current (2005) and future year (2025) air quality, using the CMAQ model. We focus on $PM_{2.5}$, with the goal of quantifying the contribution of aviation emissions during landing and takeoff (LTO) activities on ambient $PM_{2.5}$ concentrations in a current and future year and its impact on public health.

## 108.2 Modeling Approach

We performed MM5-SMOKE-CMAQ modeling to estimate the effects of current and future aircraft emissions on air quality within the continental U.S. Four annual modeling simulations were performed at a 36-km horizontal

grid resolution with 21 vertical layers. Meteorological inputs based on 2005 conditions were held constant across all model scenarios. Current year non-aviation emissions were estimated using the EPA's 2005 NEI and by excluding the NEI reported emissions from commercial aircraft. Future year non-aviation emissions were interpolated from EPA's 2020 and 2030 projections of the 2005 NEI, which include existing or planned emission control programs for various sectors on the national and state level.

Aircraft emissions data, based on Landing and Takeoff (LTO) cycles of commercial aircraft below 10,000 ft, were generated from a research version of EDMS, processed through the EDMS2Inv tool [1], and input into SMOKE. Aircraft emission estimates included CO, total organic gases (TOG), $NO_x$, $SO_x$, primary elemental carbon, and hazardous air pollutants (HAPS). Current year emissions estimates were based on hourly National Aerospace Standards (NAS) activity data from 99 major airports for February 19, 2004 and scaled up to compute an annual inventory [2]. Specific annual scaling factors were applied to each airport based on flight schedules [2]. Future year aviation estimates were scaled up using air traffic data based on the FAA TAFs for February 19, 2025. This future year estimate represents a scenario with no mitigation strategies, policies, or changes in technology and considers only growth in aviation activity. However, actual 2025 aircraft emissions are expected to be lower due to advanced technologies, alternative fuels, and changes in operational procedures that are likely to be implemented by 2025.

Prior to performing the health impact analysis, CMAQ results were post-processed using SMAT. SMAT takes the speciated components of $PM_{2.5}$ from CMAQ for each of the model years and computes species-specific relative reduction factors and uses them in conjunction with ambient data from Federal Reference Method (FRM), STN and IMPROVE monitors to compute future year design values. SMAT thus applies modeling data in a relative sense rather than an absolute sense to investigate air quality changes between two scenarios.

Premature mortality associated with $PM_{2.5}$ concentrations were then calculated using pre- and post-SMAT CMAQ outputs. A concentration-response function of a 1% increase in mortality per $\mu g/m^3$ increase in annual average $PM_{2.5}$ concentrations was applied to population estimates for 2005 and 2025 based on 2000 Census data, focusing on individuals age 25 and older given. To determine populations within each census tract, we used projections from Woods and Poole [3], which provided county-resolution population estimates by age group, and we developed scaling factors from 2000 to 2005 and from 2000 to 2025 which were applied to census blocks by age group. We extracted age-specific mortality rates by county from CDC WONDER, using data from 1999 to 2005, and determined mortality rates by grid cell using population weighting. We assumed that age-specific mortality rates would not change over time, but projected demographic changes in the population could lead to changes in the per capita mortality rates.

Combining this information, we estimated the population mortality risk under various combinations of 2005 and 2025 emissions, background concentrations, and population/baseline mortality rate data.

## 108.3 Results

CMAQ modeling results indicated that, on an annual average basis in the continental U.S., 2005 aircraft emissions increased $PM_{2.5}$ concentrations by 0.0037 μg/m$^3$ (0.05% of total $PM_{2.5}$) and 2025 aircraft emissions increased $PM_{2.5}$ concentrations by 0.0127 μg/m$^3$ (0.21%). Nitrate aerosol was the largest speciated contributor in both years, contributing on average 0.0019 μg/m$^3$ (0.16%) and 0.0074 μg/m$^3$ (0.85%), respectively. Conversely, post-SMAT results indicated that 2005 aircraft emissions increased $PM_{2.5}$ concentrations by 0.0024 ug/m$^3$ (0.03%) while 2025 aircraft emissions increased concentrations by 0.0096 ug/m$^3$ (0.11%). Sulfate was the largest speciated component in both years, contributing on average 0.0010 ug/m$^3$ (0.05%) and 0.0032 ug/m$^3$ (0.15%), respectively.

Based on post-SMAT results, the $PM_{2.5}$-related public health impacts of aviation emissions are projected to increase from approximately 75 deaths per year in 2005 to approximately 560 deaths per year in 2025, a factor of 7.5 increase. The factor of 7.5 increase can be explained by a factor of 2.1 increase attributable to emissions growth, a factor of 2.3 increase attributable to changing background concentrations, and a factor of 1.5 increase attributable to population growth and increased per-capita mortality rates. In both years and across all scenarios, the health risks are dominated by ammonium nitrate and ammonium sulfate, with a greater relative contribution from ammonium nitrate in 2025. Health risk estimates are appreciably different pre-SMAT, though the growth in health risks over time and the relative importance of various factors are qualitatively similar. Pre-SMAT, the estimated public health impacts are approximately 180 deaths per year in 2005 and 970 deaths per year in 2025, a factor of 5.4 increase. The factor of 5.4 increase is attributable to a factor of 2.0 increase due to emissions growth, a factor of 1.8 increase due to changing background concentrations, and a factor of 1.5 increase due to population growth (versus the factors of 2.1, 2.3, and 1.5 reported previously). The reduction in estimated health impacts post-SMAT is largely attributable to significant reductions in ammonium nitrate; ammonium sulfate health risks are increased by 24% in 2005 and by 102% in 2005 post-SMAT, whereas ammonium nitrate health risks are decreased by 73% in 2005 and 65% in 2025. We present in Fig. 108.1, the ratio of 2025 to 2005 based changes in health risk as a function of each of the three factors, and segregated by regions within the U.S.

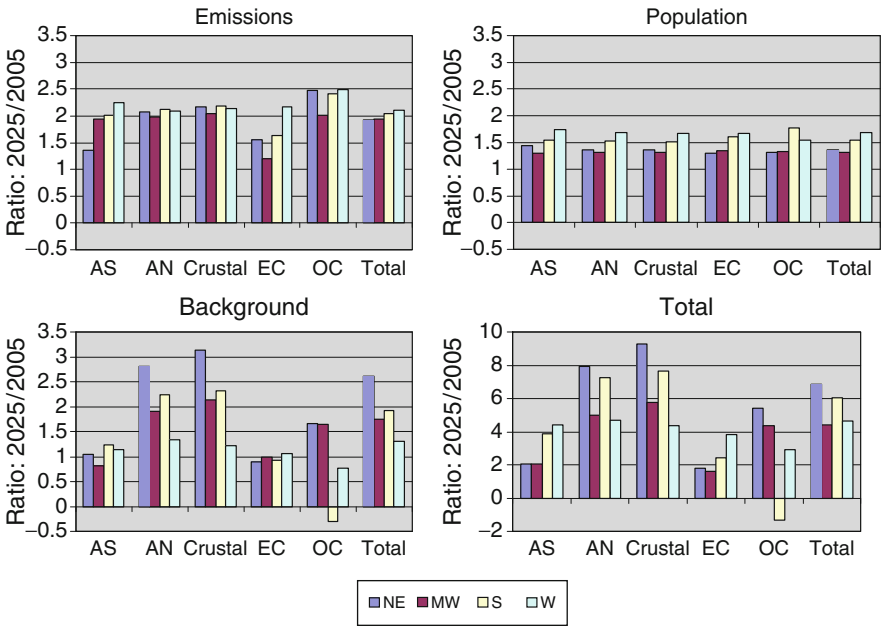


**Fig. 108.1** 2025 to 2005 ratios by each of emissions, population, background factors and total

## 108.4 Discussion

SMAT results can have important implications when considering health impacts from $PM_{2.5}$ speciated components. Furthermore, analyses demonstrate that changing aircraft emissions, background conditions, and population patterns all make significant contributions to health risk trajectories over time. PM-related health impacts are anticipated to grow significantly over time, even if emissions per aircraft did not change due to an increase in the number of aircraft, increase in population size and aging population, and the influence of control strategies on background concentrations. Goals and targets for aircraft emission control strategies related to public health risks need to keep these factors in mind, as various mitigation options may need to be considered depending upon the desire to stabilize emissions vs. stabilizing health impacts.

**Acknowledgments** We would like to acknowledge the University of Tennessee for providing GEOS-Chem based initial and boundary conditions for CMAQ. This work was funded by the Partnership for Air Transportation Noise and Emissions Reduction (PARTNER) under grants to UNC and Harvard University. The Air Quality project is managed by Christopher Sequeira. Any opinions, findings, and conclusions or recommendations expressed in this material are those of the author(s) and do not necessarily reflect the views of PARTNER and its sponsors. PARTNER is funded by FAA, NASA, and Transport Canada.

## References

1. Baek BH et al (2007) Development of an interface for EDMS. In: Proceedings of the 16th annual emissions inventory conference – Emissions inventories: integration, analyses and communication, Raleigh, NC, May 2007
2. CSSI (2009) JPDO – NextGen – TDM23: investigation of aviation emissions for future aviation activity scenario. Technical Directive Memorandum B-002-023
3. Woods and Poole (2008) Complete economic and demographic data source. Available at: http://www.woodsandpoole.com. Accessed on 15 Sept 2009

## Questions and Answers

**Questioner Name**: Bernard Fisher

**Q**: How would your conclusions change if ground transportation sources were included in aviation emissions? A secondary comment is that $NO_2$ is the pollutant of concern in Europe, because of a strict annual average limit value, so a comparative study in Europe might conclude that aviation was more significant.

**A**: In our current modeling, the ground transportation sources or ground support equipment (GSEs) were not included as part of the aircraft emissions at the study airports. Had we included those emissions, we expect the air quality and health impacts from aviation to be marginally higher, but would not change the overall conclusions regarding the trajectory of the health risks from this study.

While we did include $NO_2$ emissions from aircraft, and the model was run as a one-atmosphere model to predict both gas-phase and PM species, the focus of this study has been on fine particulate matter. We agree that for a comparative study, the impact of aviation on $NO_2$-based health impacts may be higher in Europe, given the tighter form of the European standards.

# Chapter 109
# Nitrogen Deposition in the UK: The Influence of Grid-Space and Time on the Exceedance of Critical Loads and Levels

**Anthony James Dore, Małgorzata Werner, Stephen Hallsworth, Jane Hall, Christopher Dore, Maciej Kryza, Ron Smith, Ulrike Dragosits, Sim Tang, Massimo Vieno, and Mark Sutton**

**Abstract** Atmospheric transport models may be applied to run historic emissions scenarios, which are important in order to assess the correlation between monitored change in ecosystem health and biodiversity and changes in nitrogen inputs. The ability of models to calculate the response of nitrogen deposition to future emissions scenarios is of importance for policy makers to assess the benefits of implementing controls on atmospheric nitrogen emissions. Here we apply a relatively simple Lagrangian model, the Fine Resolution Atmospheric Multi-pollutant Exchange (FRAME) model to estimate the spatial distribution of nitrogen deposition in the UK, past and estimated future changes and the exceedance of critical loads. A second important issue concerns the grid resolution of the model simulation. We consider the difference in environmental impact criteria obtained with model simulations at 5 km and 1 km.

**Keywords** Nitrogen • Critical level • Critical load • Eutrophication

A.J. Dore (✉) • S. Hallsworth • R. Smith • U. Dragosits • S. Tang • M. Sutton
Centre for Ecology and Hydrology, Edinburgh, Scotland, UK
e-mail: todo@ceh.ac.uk

M. Werner • M. Kryza
Department of Climatology and Atmospheric Protection,
University of Wrocław, Wroclaw, Poland

J. Hall
Centre for Ecology and Hydrology, Bangor, Wales, UK

C. Dore
AETHER ltd,

M. Vieno
School of Geosciences, University of Edinburgh, Edinburgh, Scotland, UK

D.G. Steyn and S. Trini Castelli (eds.), *Air Pollution Modeling and its Application XXI*,
NATO Science for Peace and Security Series C: Environmental Security 4,
DOI 10.1007/978-94-007-1359-8_109, 

## 109.1 Model Description

FRAME is a Lagrangian model using straight line trajectories with a 1° angular resolution which runs at either a 1 km or a 5 km resolution over the British Isles and 50 km resolution over Europe with a fine vertical grid spacing (1 m at the surface). Area emissions are injected into sector dependent levels and point source emissions are treated with a plume rise routine. Vertical diffusion in the air column is calculated using K-theory eddy diffusivity. Wet deposition is calculated using a 'constant drizzle' approximation driven by an annual rainfall map. Five land classes are considered and a vegetation specific canopy resistance parameterisation is employed to calculate dry deposition of $SO_2$, $NO_2$ and $NH_3$. The model chemistry includes gas phase and aqueous phase reactions of oxidised sulphur and oxidised nitrogen as well as aerosol formation.

The model was found to give a good representation of aerosol and gas concentrations of nitrogen compounds as well as wet deposition when compared with measurements from the UK national monitoring networks for the year 2007 [1]. Table 109.1 illustrates the correlation with annually averaged measurements for the year 2007.

## 109.2 Results

$NO_x$ emissions in the UK were at a maximum of 951 Gg N in 1970 and fell to 378 by 2005, with a further decrease to 243 Gg N forecast by 2020. The significant reduction (of 46%) in $NO_x$ emissions occurred, in particular from passenger cars due to the introduction of three-way-catalysts as well as a number of increasingly stringent emissions standards. These large decreases in emissions have not been matched by similar changes for $NH_3$ which decreased from 315 Gg N in 1990 to 259 in 2005 and are forecast to fall to 222 Gg by 2020. For reduced nitrogen, the smaller reduction in emissions (of 18%) has been driven primarily by a decrease in

**Table 109.1** Statistics for model correlation with annual average measurements of wet deposition and air concentrations for the year 2007 (*N* number of samples; $R^2$ determination coefficient, *NMB* normalised mean bias; % percentage of modelled points less than twice and greater than half the measured value)

| | N | $R^2$ | NMB | % |
|---|---|---|---|---|
| $NH_4^+$ wet dep | 38 | 0.66 | 0.06 | 71 |
| $NO_3^-$ wet dep | 38 | 0.65 | 0.27 | 79 |
| $NH_3$ concentration | 90 | 0.50 | 0.18 | 69 |
| $NO_2$ concentration | 26 | 0.93 | −0.13 | 100 |
| $NH_4^+$ concentration | 30 | 0.89 | −0.23 | 67 |
| $NO_3^-$ concentration | 30 | 0.89 | 0.02 | 87 |
| $HNO_3$ concentration | 30 | 0.57 | −0.03 | 72 |

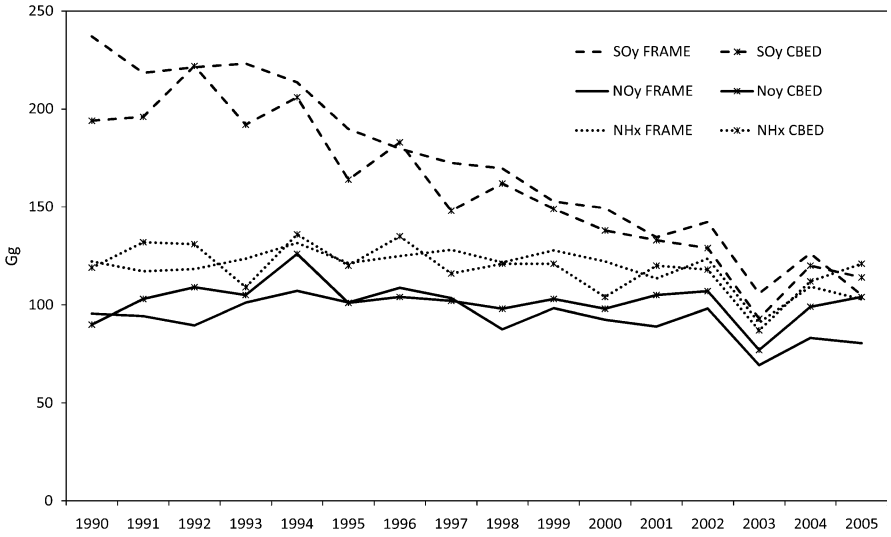


**Fig. 109.1** Trend in total UK nitrogen and sulphur wet deposition between 1990 and 2005 calculated by FRAME and by CBED (Gg)

livestock numbers and N fertiliser application rates, changes to animal diet and improvements to manure management.

The model was applied to make 16 simulations of annual deposition, using meteorological data and emissions for each of the years 1990–2005. These results were used to calculate the trend in total deposition of nitrogen and sulphur to the UK. In Fig. 109.1, the modelled national wet deposition budgets are compared with those from the Concentration Based Estimated Deposition (CBED; [2]). CBED combines measured concentrations of ions in precipitation from 38 national monitoring sites with a map of annual precipitation to generate interpolated maps of wet deposition for the UK and budgets of total national deposition. Due to its simple representation of meteorology, the FRAME model is less sensitive to meteorological changes than is apparent with CBED. Wet deposition of sulphur shows a clear downwards trend during the 15 year time period, driven by major decreases in national emissions of approximately 80% during this time period. Wet deposition of both oxidized and reduced nitrogen however show only minor downward trends which are partially masked by inter-annual meteorological variability.

For oxidized nitrogen, deposition is not controlled only by UK emissions. Increases in emissions from international shipping during this period are thought to partially off-set the reductions in UK emissions. Secondly, atmospheric chemical reaction rates are known not to respond linearly to emissions changes [3]. The major decrease in $SO_2$ concentrations during this period is believed to have resulted in less depletion of atmospheric oxidants, maintaining the rate of nitrate aerosol production despite lower $NO_x$ emissions.

The rates of change of nitrogen deposition in the UK can be estimated by the model for a longer 50 year time period, using historical emissions estimates back to 1970

and projected forward to 2020. Calculation of exceedance of critical loads [4] showed that the percentage area of ecosystems with exceedance of the critical load for acid deposition in the UK has decreased significantly. Smaller changes have occurred for exceedance of critical loads for nitrogen deposition, in particular with a high percentage of unmanaged woodland retaining exceeded deposition levels (Fig. 109.2).

FRAME was also run using a 1 km resolution for the model grid. The spatial separation of agricultural source regions from Natura 2000 sites was significantly improved at the finer resolution. An improved correlation with measurements of ammonia concentrations at nature sites and reduced overestimate was evident from the 1 km simulation, as compared to the 5 km simulation. An assessment of the exceedance of the critical level for ammonia concentration (1 μg $m^{-3}$ for bryophytes and lichens, 3 μg $m^{-3}$ for other vegetation) was undertaken. The results (Table 109.2) suggest that a fine resolution simulation is necessary to assess critical level exceedance. With the 5 km resolution data, there was a tendency for the agricultural source regions and the sensitive nature sites to be mixed into the same

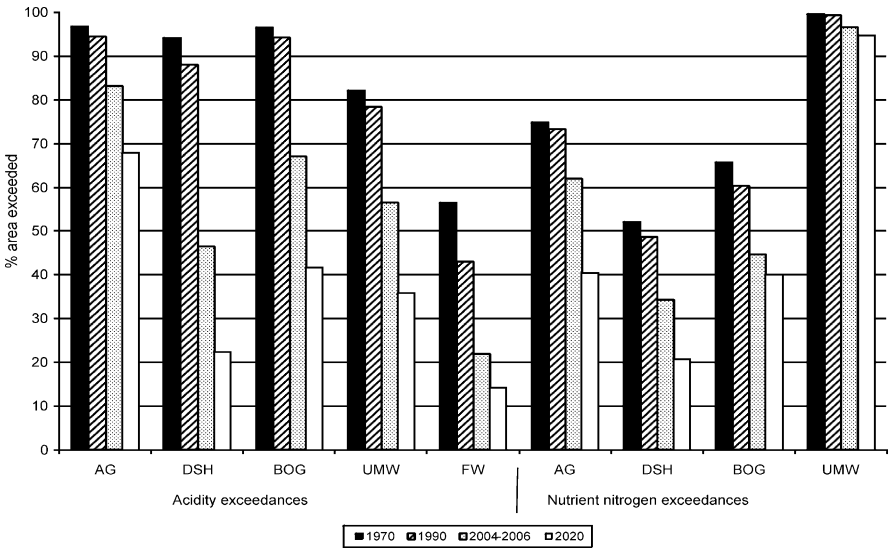


**Fig. 109.2** The percentage of system area in the UK with exceedance of critical loads for deposition of acidity and nitrogen during 1970–2020 (*AG* acid grassland, *DSH* dwarf shrub heath, *BOG* bog, *UMW* unmanaged woodland, *FW* freshwater)

**Table 109.2** Percentage area of UK Natura 2000 special area of conservation network exceeding the 1 and 3 μg $NH_3$ $m^{-3}$ critical levels for 5 km and 1 km simulations

| % area exceedance | 5 km | 1 km |
|---|---|---|
| 1 μg $m^{-3}$ critical level | 40% | 21% |
| 3 μg $m^{-3}$ critical level | 2.2% | 0.9% |

model grid square, resulting in an over-estimate of the area exceeding the critical level. Preliminary results also show that in hill areas, a fine resolution (1 km) representation of precipitation can lead to improved estimates of nitrogen deposition in sensitive upland ecosystems.

**Acknowledgments** This work was supported by the Natural Environment Research Council and the Department for the Environment, Food and Rural Affairs.

## References

1. Dore AJ, Vieno M, Tang YS, Dragosits U, Dosio A, Weston KJ, Sutton MA (2007) Modelling the atmospheric transport and deposition of sulphur and nitrogen over the United Kingdom and assessment of the influence of SO2 emissions from international shipping. Atmos Environ 41(11):2355–2367. doi:10.1016/j.atmosenv.2006.11.013
2. Fowler D, Smith RI, Müller JBA, Hayman G, Vincent KJ (2005) Changes in atmospheric deposition of acidifying compounds in the UK between 1986 and 2001. Environ Pollut 137:15–25
3. Matejko M, Dore AJ, Hall J, Dore CJ, Błaś M, Kryza M, Smith R, Fowler D (2009) The influence of long term trends in pollutant emissions on deposition of sulphur and nitrogen and exceedance of critical loads in the United Kingdom. Environ Sci Policy 12:882–896
4. Hall J, Ullyett J, Heywood E, Broughton R, Fawehinmi J (2003) Preliminary assessment of critical loads exceedance. Addendum to status of UK critical loads-methods, data and maps

## Questions and Answers

**Questioner Name**: Bruce Benby

**Q**: Did you assess differences in the 5 km and 1 km simultions (e.g. by aggregating the 1 km to 5 km)? Perhaps this affects the results.

**A**: Averaged nationally, the 1 km and 5 km simulations produced only small differences in ammonia gas concentrations. However in the 1 km simulation, the more highly resolved spatial separation of ammonia emissions from acid gas emissions resulted in slower formation of ammonium aerosol and, on average, lower wet deposition of ammonium. The 1 km data was therefore aggregated to 5 km resolution to test the influence of grid resolution of deposition data on exceedance of the critical load for nitrogen deposition.

**Questioner Name**: Clement Mensink

**Q**: Does your model include any background contributions and if so, what is the amount of this contribution?

**A**: Boundary conditions for the UK simulation were generated with a European scale simulation running on the EMEP 50 km resolution grid. Land emission sources from other European countries were found to contribute 27% to $NO_y$ deposition and 30% to $NH_x$ deposition in the UK.

# Chapter 110
# Modelling of Particulate Matter: A Detailed Analysis of Sources and Abatement Strategies

**Peter Builtjes, Wolfram Jörss, Rainer Stern, and Jochen Theloke**

**Abstract** The effectivity of abatement strategies concerning elevated PM 10 and PM 2.5 levels in Germany have been determined by establishing detailed emission data bases reflecting the strategies, and using CTM's to calculate the resulting concentrations up to the year 2020. The concentrations have been weighted by population density, and the uncertainty of the calculated yearly averaged concentrations have been estimated to be +/− 30%.

**Keywords** Particulate matter • Emissions • Abatement strategies

## 110.1 Introduction

Observed concentrations of PM10 and PM2.5 over large parts of Europe exceed the current EU-limit values. The limit value for PM10 is that daily averaged concentrations of 50 μgr/m$^3$ should not be exceeded more than 35 days a year. The limit value for PM 2.5 that holds everywhere will be an annual average value of 25 μgr/m$^3$. There is a more stringent PM 2.5 limit value for the annual average value for the urban background. At a concentration of 22 μgr/m$^3$, as observed over the

P. Builtjes (✉)
Freie Universität Berlin, Berlin, Germany

TNO, P.O. Box 8005, 3508 TA Utrecht, The Netherlands
e-mail: peter.builtjes@tno.nl

W. Jörss
IZT, Germany

R. Stern
Freie Universität Berlin, Berlin, Germany

J. Theloke
IER, Germany

D.G. Steyn and S. Trini Castelli (eds.), *Air Pollution Modeling and its Application XXI*, NATO Science for Peace and Security Series C: Environmental Security 4,
DOI 10.1007/978-94-007-1359-8_110, 

years 2008–2010, every measure has to be taken to lower the concentration to 18 by 2015. When the observed concentration is between 18 and 22, the concentration should be reduced by 20%, and with 15% between 13 and 18. It seems that this so-called Average Exposure Indicator-AEI- is less stringent than the PM10 limit value.

The question was raised whether, with the help of chemical transport models, it can be assessed which are the causes of the current concentrations of PM and what the effectivity of proposed abatement strategies is, and whether limit values will be exceeded still in the future.

## 110.2 Structure of the Study and Main Results

In order to address this question, the 3-D Eulerian chemical transport model, REMCALGRID (RCG), has been used for modelling PM10 and PM2.5 concentrations and its precursors over Europe, with a focus on Germany.

First, a detailed anthropogenic emission data base for primary PM10 and PM2.5 and the secondary aerosol precursors ($NO_x$, $SO_2$, $NH_3$, NMVOC) has been set up over Europe on grids of 0.0625 lat $\times$ 0.125 long, about 7 $\times$ 8 $km^2$ for the base year 2005 and over Germany on grids of 1/60 lat $\times$ 1/60 long, about 1.2 $\times$ 1.8 $km^2$. The European emission data base has been based on the EMEP-emissions, the German emissions are based on the so-called Central System Emissions (ZSE) of the German Environmental Protection Agency (UBA).

As a first step, the calculated concentrations with RCG of PM10 and PM2.5 have been compared to the observations over Germany in 2005, the base year of the study. In order to get a feeling of the bandwith/uncertainty of the model results, the following approach has been chosen. First, model runs have been carried out using a prognostic (COSMO) and a diagnostic (TRAMPER) meteorological driver which contain different descriptions of the mixing height and the friction velocities. Second, estimates have been made of the uncertainty of the anthropogenic emissions. And finally, also runs have been performed using two other CTM's: COSMO-MUSCAT of the IfT in Leipzig and the LOTOS-EUROS of TNO. In this way an estimate of the bandwidth of calculated concentrations could be determined. The absolute uncertainty in comparison to observations was of the order of 30% (2-$\sigma$ level), the relative uncertainty (differences between scenario-runs) was about 20%.

As expected, the model results show a fair agreement with the observations for inorganic aerosols, but a general underestimation of both PM10, and – to a lesser extent- of PM 2.5.

Calculations have been carried out with the RCG-model over Europe on grids of 0.25 $\times$ 0.5, with a one-way nesting over Germany of 0.0625° latitude $\times$ 0.125° longitude to make a detailed assessment of the emissions contributing to the PM 2.5 and PM 10 concentrations. A major problem in analysing the results of all these runs is how the results can be presented in such a way that generic pictures can be derived. The decision has been made to focus on annual averaged values of PM10 and PM2.5, and to make a distinction in different classes of population density.

In this way also a weighting with population density- a first step in the direction of exposure- has become possible. Four population density classes have been defined, going from rural to densily populated areas with more than 950 inhabitants/km$^2$.

Model runs have been performed by reducing emissions in a systematic way (by %) by species; $SO_2$, $NO_x$, NMVOC, Primary PM10 and $NH_3$-emissions, and by ten source categories (SNAP-codes). When all anthropogenic German emissions are set to zero, the PM10 concentrations drop in agglomeration areas to a level of about 14 µgr/m$^3$, which is 63% of the base concentration, in rural areas to a level of about 7 µgr/m$^3$ which is 49% of the base case.

Furthermore, the results show that in the dense population areas about 2/3 of the concentrations are due to primary PM-emissions, which is only 1/3 in rural areas. Concerning source categories, the major contribution in dense population areas comes from traffic and industry, in rural areas from agriculture. Reducing $NH_3$ emissions has a large impact, especially in rural areas. Furthermore, the impact on PM10 concentration of reducing $NH_3$ is strongly non-linear. Setting the reduction in PM-concentration in rural areas at 1.00 for 5% decrease of $NH_3$-emissions, this factor increases to 1.12 at 25% reduction, and until 1.34 at 50% reduction, 1.72 at 75% and 2.75 at 100% reduction.

These results show the large impact and large non-linearity of $NH_3$ on the PM-concentrations in rural areas, and the large impact of primary PM emissions on the concentrations in urban areas.

The analysis and the ranking of the effectivity of a large number of proposed abatement strategies has been performed. For this analysis emissions have been determined over Europe and in Germany for the years 2010, 2015 and 2020 under the so-called CLE-Current Legislation Scenario. The results show that, although substantial concentration reductions will occur, the limit values will still be exceeded in 2020. Consequently, for the year 2020 also a so-called MFR-Maximum Feasible Reduction-scenario, so a scenario with a stronger abatement than the CLE-scenario, has been defined, as well as a still further going climate scenario. Only under such a climate scenario, the limit values might be reached in 2020. Figure 110.1 shows the calculated concentration reduction in PM10 for the different population density areas (BVK1 is rural, BVK 4 is densily populated) as well as averaged over Germany (DEU) and averaged over the AEI-Stations.

The MFR-scenario contains numerous individual abatement measures, with their own PM10 or precursor reductions. Calculations have been performed to assess the impact of the different abatement measures. Starting from CLE, traffic and agriculture have the largest reduction potential, both in dense population areas (traffic 26% of the potential, agriculture 20%) and in rural areas (agriculture 47%, traffic 18%) when set to zero.

Finally two hypothetical scenario calculations have been performed. In the first one all small wood burning facilities have been replaced by oil burning facilities. This scenario results in a reduction of PM10 concentration which is for rural areas 63%, and in dense population areas 87% of what is achievable going from CLE to MFR. A second hypothetical scenario is the reduction of the current meat consumption in Germany to the amount that is needed per person, which is about 50–60 gr

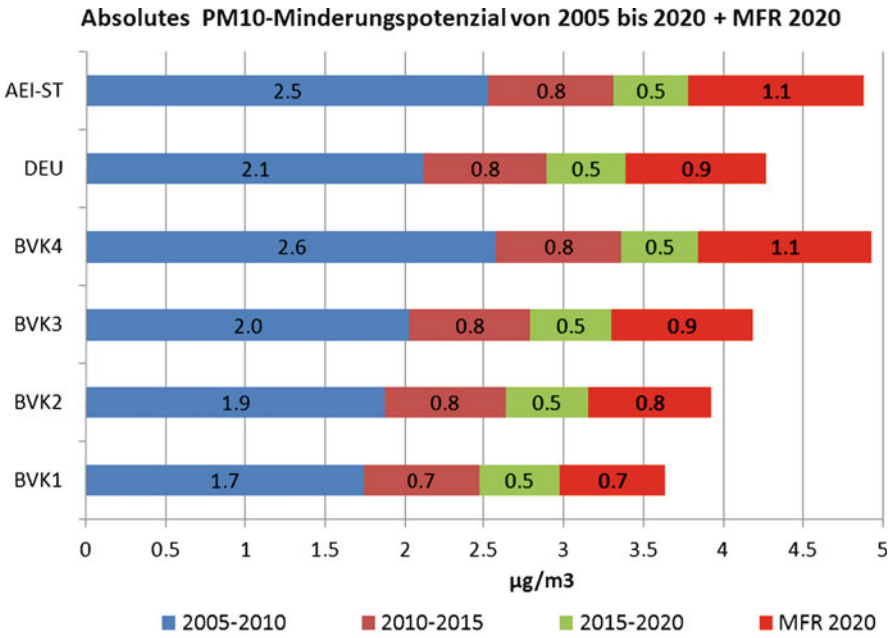


**Fig. 110.1** Calculated annual average PM10-concentration decreases in Germany (µg/m$^3$) due to the CLE-emissions development from 2005 to 2020 and due to the additional MFR-scenario for four population classes (BVK1 rural until BVK4 agglomeration areas), Germany (DEU) and 36 urban background stations (AEI-stations)

meat per day. This scenario results in rural areas in a PM-reductions of 42%, in dense populated areas of 36% of what is achievable from CLE to MFR. Both hypothetical scenarios show the large impact on PM concentrations by changes in individual life-style.

**Acknowledgments** The project has been funded by the German UBA, see www.parest.de

## Questions and Answers

**Questioner Name**: Stijn Jansen.

**Q**: A relative uncertainty of 20% is suggested for scenario differences. How do you arrive at these values?

**A**: Using different CTM's with different meteorological input the same reference scenario's have been calculated and the ranking by the different models have been compared, resulting in this 20% value.

**Questioner Name**: Christian Hogrefe

**Q**: It is important to give uncertainty values for the calculated concentrations and the relative uncertainties, but aren't they different for the different emission reductions?

**A**: I do agree with your remark/question. The uncertainty due to for example aNH3-emission reduction will be larger than due to a NOx- or PPM emission reduction.

# Chapter 111
# Development and Evaluation of Alternative Metrics of Ambient Air Pollution Exposure for Use in Epidemiologic Studies

**Vlad Isakov, James Crooks, Joe Touma, M. Valari, Halûk Özkaynak, Stefanie Ebelt Sarnat, Jeremy Sarnat, Priya Kewada, and James Mulholland**

**Abstract** Population-based epidemiologic studies of air pollution have traditionally relied upon imperfect surrogates of personal exposures, such as area-wide ambient air pollution levels based on readily available outdoor concentrations from central monitoring sites. This practice may introduce exposure misclassification in epidemiologic analyses for pollutants that are spatially heterogeneous, including those associated with traffic emissions (i.e., carbon monoxide, elemental carbon, nitrogen oxides, and particulate matter). To investigate the potential impact of misclassification within observed health risk estimates, U.S. EPA in collaboration with Emory University is developing and evaluating several tiers of exposure metrics for ambient traffic-related and regional pollutants that vary in their approaches for modeling pollutant spatial heterogeneity. The following tiers of exposure metrics are examined: (1) central site monitoring data, (2) local scale modeling (AERMOD), and (3) combined regional and local scale modeling. Each metric is applied in two extensive, ongoing epidemiologic studies conducted by Emory University to examine ambient air pollution and acute morbidity in Atlanta, GA. We hypothesize that using the more refined exposure estimates will provide greater power to detect epidemiologic associations of interest, particularly for

V. Isakov (✉) • J. Crooks • J. Touma • M. Valari
Atmospheric Modeling and Analysis Division, National Exposure Research Laboratory, Office of Research and Development, U.S. EPA, Research Triangle Park, Durham, NC 27711, USA
e-mail: isakov.vlad@epa.gov

H. Özkaynak
Office of Research and Development, U.S. EPA, Research Triangle Park, Durham, NC 27711, USA

S.E. Sarnat • J. Sarnat • P. Kewada
Emory University, Atlanta, GA, USA

J. Mulholland
Georgia Institute of Technology, Atlanta, GA, USA

D.G. Steyn and S. Trini Castelli (eds.), *Air Pollution Modeling and its Application XXI*, NATO Science for Peace and Security Series C: Environmental Security 4,
DOI 10.1007/978-94-007-1359-8_111, 

heterogeneous, traffic-related pollutants. This research will be useful for improving exposure assessment in future air pollution epidemiology studies, by providing alternative methods as well as by providing a further understanding of to the situations that might require refined exposure metrics.

**Keywords** Air pollution • Epidemiologic studies • Exposure • Air quality modeling

## 111.1 Introduction

Recent studies [1] have shown that more narrowly defining the geographic domain of the study populations and the improvements in the corresponding ambient PM concentrations, lead to stronger associations between ambient concentrations and hospital admissions and mortality records. To meet these needs, researchers are now beginning to use air quality dispersion models to support air pollution exposure and health studies [2–4]. There are many advantages to using air quality models over traditional approaches used by epidemiologist such using ambient measurement. The direct use of monitoring data inherently assumes that they are representative of the air quality over a broad area. However, there is increasing evidence that the monitoring network is not capturing the sharp gradients in exposure due to high concentrations near, for example, major roadways [5]. Monitoring networks are sparse in both space and time, are costly to maintain, and are often designed purposely to avoid detecting highly localized sources. Air quality models, on the other hand, have a long history of use in air pollution regulations and thus are widely available and supported by regulatory agencies and a large user community. Here, the hybrid modeling approach [3] was used to estimate air quality model concentrations.

Here we explore the associations between traffic-related ($NO_x$) and regional ($PM_{2.5}$) pollutants and two acute adverse health Emergency Department (ED) and Implanted Cardio Defibrillator (ICD) studies collected in Atlanta, Georgia during 1999–2002. We also compare the resulting hybrid model concentration estimates with available ambient monitoring data. Evaluation is critical for any air quality model application. However, evaluating spatially- and temporally-resolved model concentrations in a large urban area is a challenge because observations are usually not available at this level.

## 111.2 Atlanta Modeling Study

The Atlanta study area is centered on downtown and extends to a 100 km in all directions in order to include the impacts from a majority of emission sources. For this paper, we have focused on two air pollutants: particulate matter at 2.5 μm

or less ($PM_{2.5}$) and nitrogen oxides ($NO_x$). These pollutants were selected because of health outcomes based on previous known associations: respiratory disease hospitalization and mortality ($PM_{2.5}$ and $NO_x$) and cardiovascular disease hospitalization and mortality ($PM_{2.5}$). Also, these pollutants represent different pattern of spatial and temporal structure (e.g. $PM_{2.5}$ is mostly regional, while $NO_x$ has both local and regional components).

Pollutant specific local-scale air concentrations were first estimated using the EPA's AERMOD dispersion model which uses information on local emission sources and local meteorological conditions to provide hourly and annual average concentrations at multiple receptors. To estimate the total air concentrations, an estimate of the regional background concentrations is needed. Here we used a statistical approach based on ambient monitoring data to obtain these estimates [6]. Daily and annual average air quality model simulations during 4 years (1999–2002) were made to coincide with available health outcomes.

## 111.3 Results

Figure 111.1 shows the relative contribution of local and regional average daily modeled concentrations at all 225 receptors. For PM2.5 (Fig. 111.1a) the contribution of the AERMOD dispersion model to the total concentrations is small. As seen in the monitoring data, this pollutant is driven primarily by regional sources. The hybrid concentration reflects the influence of the estimated regional background concentration.

We examined the relationship between daily modeled air pollution concentrations and ED visits for respiratory and cardiovascular disease using Poisson generalized linear models [1]. In our analysis, we assumed that greater levels of refinement in air quality model concentrations used as metrics of exposure would result in reduced exposure measurement error. Thus, differences in estimated relative risks when different air pollution exposure metrics are used may serve to illustrate the relative degree of exposure error. According to this assumption, if the health outcome is caused by the exposure, using a more accurate measure of exposure should typically result in less bias towards the null. Comparing observed relative risks may, therefore, provide a means of evaluating this error. In Fig. 111.2, we compare the relative risks using different measures of exposure using different air quality concentration estimates (central monitoring site, AERMOD and hybrid model). We anticipated that the hybrid model, which accounts for greater levels of spatio-temporal heterogeneity throughout our large modeling domain compared to that from a central monitoring site, will have the strongest associations with the health outcomes.

Preliminary results suggest that the effect of improved spatiotemporal heterogeneity on the observed relative risk estimates depend on the pollutant by outcome of

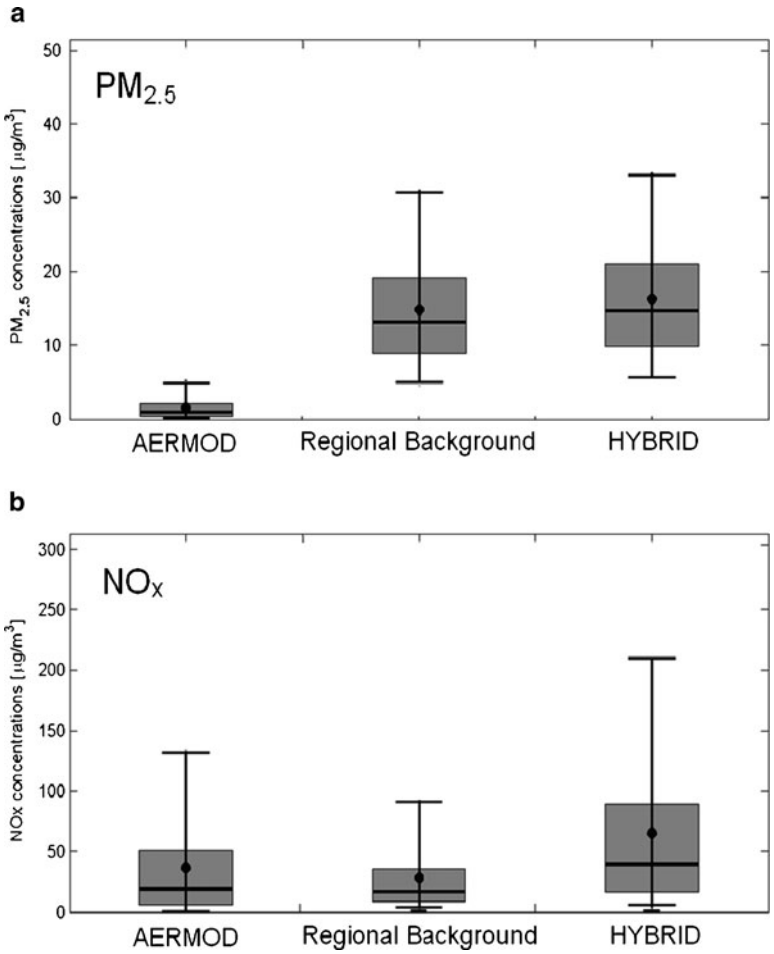


**Fig. 111.1** Relative contributions of local and regional signals in (**a**) $PM_{2.5}$ and (**b**) $NO_x$ concentrations in Atlanta based on daily average estimates at 225 zip code receptors

interest, as expected. For spatially homogeneous pollutants (i.e., $PM_{2.5}$), relative risk estimates, in particular, for respiratory ED visits, were generally higher using model based metrics. For spatially heterogeneous pollutants (i.e., CO and $NO_2$), estimated associations also varied but to a lesser extent.

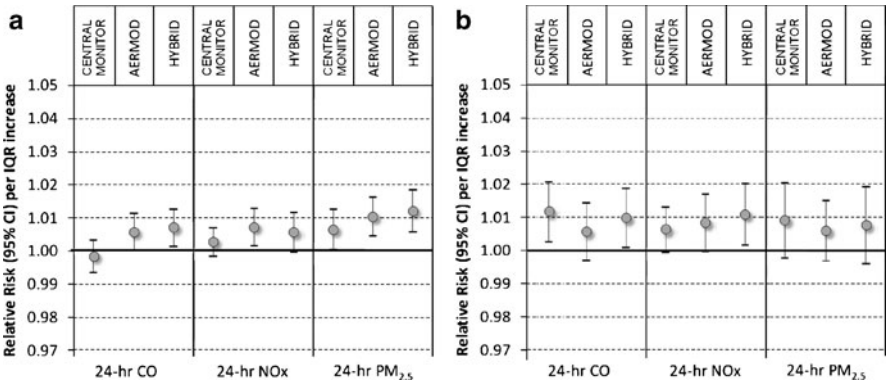


**Fig. 111.2** Mean Results of the epidemiologic analysis for (**a**) respiratory and (**b**) cardiovascular disease

**Disclaimer** This paper has been subjected to Agency review and approved for publication. Approval does not signify that the contents reflect the views of the Agency nor does mention of trade names or commercial products constitute endorsement or recommendation for use.

## References

1. Sarnat SE, Klein M, Sarnat JA, Flanders WD, Waller LA, Mulholland JA, Russell AG, Tolbert PE (2010) An examination of exposure measurement error from air pollutant spatial variability in time-series studies. J Expo Sci Environ Epidemiol 20:135–146
2. Özkaynak H, Palma T, Touma J, Thurman J (2008) Modeling population exposures to outdoor sources of hazardous air pollutants. J Expo Sci Environ Epidemiol 18:45–58
3. Isakov V, Touma J, Burke J, Lobdell D, Palma T, Rosenbaum A, Özkaynak H (2009) Combining regional and local scale air quality models with exposure models for use in environmental health studies. J Air Waste Manage Assoc 59:461–472
4. Georgopoulos P, Wang S, Vyas V, Sun Q, Burke J, Vedantham R, McCurdy T, Özkaynak H (2005) A source-to-dose assessment of population exposures to fine PM and ozone in Philadelphia, PA, during a summer 1999 episode. J Expos Anal Environ Epidemiol 2005 (15):439–457
5. Zhou Y, Levy JI (2007) Factors influencing the spatial extent of mobile source air pollution impacts: a meta analysis. BMC Public Health 89:1–11
6. Wade KS, Mulholland JA, Marmur A, Russell AG, Hartsell EE, Edgerton E, Klein M, Waller L, Peel JL, Tolbert PE (2006) Effect of instrument precision and spatial variability on the assessment of the temporal variation of ambient air pollution in Atlanta, Georgia. J Air Waste Manage Assoc 56:876–888

## Questions and Answers

**B. Denby**: Have you considered using individual sources for the risk assessment instead of total concentrations?
**V. Isakov**: The main objective of this study was to examine the relationship between daily modeled air pollution concentrations and ED visits for respiratory and cardiovascular disease and to compare the relative risks using different measures of exposure. Therefore, we did not consider using individual sources for the risk assessment.

**S. Vardoulakis**: Have you controlled for confounding and correlation between pollutants emitted from common sources in your epidemiological time-series analysis?
**V. Isakov**: The epidemiologic analysis was conducted for each pollutant separately using Poisson generalized linear models as described in [1].

# Chapter 112
# Sub-grid Variability and Its Impact on Air Quality Exposure Assessment

**Bruce Rolstad Denby, Massimo Cassiani, Jan Horálek, Peter de Smet, and Frank de Leeuw**

**Abstract** Long term exposure estimates over large areas can be made using a combination of air quality models and population density data. However, the grid resolution of such models is often limited to 25–50 km and there may be a significant level of unresolved variability within the grids that will impact on the exposure estimates. In this paper the sub-grid variability is assessed using air quality monitoring (AirBase) and population data, concentrating on the covariance of concentration and population, which is the defining term in estimating sub-grid population exposure. The error that occurs when calculating the urban background exposure is assessed. The assessment shows that the error made in the exposure calculation for all of Europe is small for typical CTM resolutions of 50 km. The error is largest for $NO_2$, where the average European urban background exposure is underestimated by 16%. Particulate matter is also underestimated, but only by 6%. Conversely, estimates of ozone exposure (SOMO35) are overestimated by a factor of 15%.

**Keywords** Sub-grid variability • Exposure • Air quality modelling

## 112.1 Introduction

The health impacts of air pollution have been investigated in a number of studies. Many of these studies make use of gridded air quality data either directly from models, e.g. CAFÉ [4], or using a combination of models and monitoring,

B.R. Denby (✉) • M. Cassiani
Norwegian Institute for Air Research (NILU), Kjeller, Norway
e-mail: bruce.denby@nilu.no

J. Horálek
The Czech Hydro-Meteorological Institute (CHMI), Prague, Czech Republic

P. de Smet • F. de Leeuw
The Netherlands Environmental Assessment Agency (PBL), The Hague, The Netherlands

D.G. Steyn and S. Trini Castelli (eds.), *Air Pollution Modeling and its Application XXI*,
NATO Science for Peace and Security Series C: Environmental Security 4,
DOI 10.1007/978-94-007-1359-8_112, 

e.g. Fiala et al. [3], to estimate the static population exposure for all of Europe. When finite grid resolutions are used the question arises:

> *What is the error in the exposure calculation when using finite gridded concentration data and can a correction be implemented to account for this?*

Though grid resolution may have an impact on the physical and chemical descriptions of the models themselves, the subject of this study is the effect of grid resolution on the exposure estimates. Since regional scale chemical transport models (CTMs) do not capture the same spatial variability as the population, sub-grid variability (SGV) will also contribute to the exposure estimate. To deal with this question various schemes have been employed, e.g. CityDelta [2], that parameterize the 'urban increment'. This represents the concentration difference between urban and regional areas and is employed to improve the population exposure estimates in urban areas. An alternative to implementing an 'urban increment' is to simply increase the model resolution to better represent the population variability, though this is highly impractical on continental scales for long term assessments.

In actual fact, it is not necessary to increase the model resolution to resolve the concentration and population *variability* in an urban area. It is sufficient to resolve the *covariance* of the population and concentration fields. In other words, it is not necessary to increase a models resolution to improve the population exposure estimate if the population or concentration fields are uncorrelated since enhancing the model resolution will not improve the population exposure estimate.

To address this, a study has been carried out to quantify SGV, including parameterisations that can be used to estimate it. In this paper however we present just one aspect of the study, quantifying the total error when estimating European wide population weighted concentrations. This is achieved using air quality monitoring and population density data then calculating their covariance at varying spatial resolutions, to show how the total exposure estimate is dependent on resolution.

## 112.2 Method

The discretised population exposure (or population weighted concentration) $C_{pw,j}$ over any defined area $A_j$ (index $j$) for a given period of time is defined as:

$$C_{pw,j} = \frac{\sum_{i}^{n} c_i p_i}{\sum_{i}^{n} p_i} \tag{112.1}$$

where $c_i$ is the spatially distributed concentration within a specified sub-area $i$, $p_i$ is the total population within that sub-area and there are $n$ discrete sub-areas within

the area $A_j$. $C_{pw,j}$ is used in exposure studies since it represents the average concentration that members of a population are exposed to. Since most epidemiological studies are carried out based on ambient air concentrations representative of larger urban areas we consider the sub-areas $i$ to be some kilometers in size. In this study $3 \times 3$ km$^2$ is the smallest resolution assessed. The area $A_j$ over which $C_{pw,j}$ is calculated can be representative of a typical grid square in a regional or global CTM, usually in the range of 25–200 km.

Equation 112.1 can be rewritten in terms of the mean concentration $C_j$ and the mean population $P_j$ in the area $A_j$ as follows:

$$C_{pw,j} = C_j\left(1 + \frac{\mathrm{cov}_j(c,p)}{C_j P_j}\right) = C_j\left(1 + COV_{CP,j}\right) \tag{112.2}$$

Here we have substituted the discretised covariance function ($cov_j$) into Eq. 112.1. Equation 112.2 written in this form implies a 'covariance correction factor' ($\mathrm{COV_{CP,j}}$) for each of the $j$ grid cells based on the covariance of population and concentration. Knowledge of this correction factor will indicate the 'increment' needed to the mean concentration ($C_j$) for each grid square $j$. If there is no covariance between population and concentration then this factor is 0. However, some degree of covariance is expected as many of the emission sources are directly related to population density.

$COV_{CP}$ can be directly assessed using available monitoring (AirBase) and population data with the application of spatial statistical methods. This involves determination of the accumulated cross-variogram, which provides the covariance of two spatially distributed data fields, for a range of effective grid resolutions.

Monitoring data for $NO_2$, $PM_{10}$ and the ozone indicator SOMO35 have been extracted from AirBase [1] for use in the assessment. Only regional and (sub)urban background stations have been used in the study and population data at a resolution of $3 \times 3$ km$^2$ is used as representative for these background stations.

## 112.3 Results

In Fig. 112.1 the total covariance correction factor, as function of grid resolution, are shown for $NO_2$, $PM_{10}$ and SOMO35. The curves provide the empirical relationship between the total covariance correction factor (as in Eq. 112.2 but additionally assessed over the whole domain) and the grid resolution. This factor represents the error made in calculating the total population weighted concentration for any given grid resolution. For example, at 50 km the correction factor for $NO_2$ is 16%, for $PM_{10}$ this is just 6%. For SOMO35 the correction factor is negative at −15%.

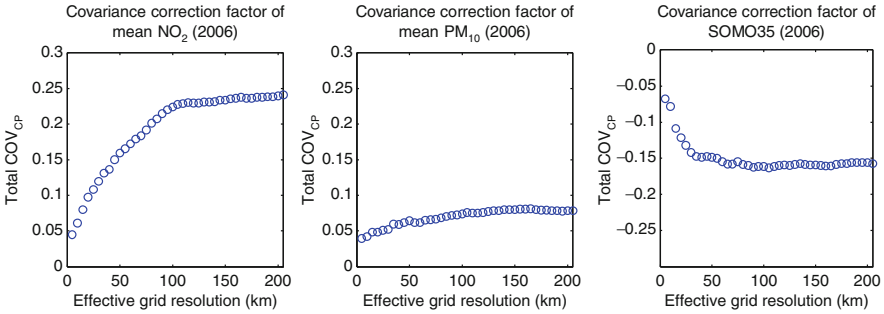


**Fig. 112.1** Total covariance correction factor ($COV_{CP}$) for $NO_2$, $PM_{10}$ and SOMO35 as a function of effective grid resolution (km). Scales are the same in all cases but note that the values are negative for SOMO35

## 112.4 Conclusion

In this paper, the first part of a study assessing sub-grid variability and its impact on European wide exposure estimates is shown. These results indicate that a small but significant error in the population weighted concentrations can result due to the use of finite grid sizes. It is shown that the sub-grid covariance is the defining factor in determining this error and an assessment of this has been made using monitoring and population data for $NO_2$, $PM_{10}$ and the ozone indicator SOMO35. The following conclusions can be made:

- The $NO_2$ covariance correction factor (16% at 50 km; 23% at 100 km) is more strongly dependent on grid resolution than is the $PM_{10}$ factor. This is due to the relatively high correlation between $NO_2$ concentrations ($NO_x$ emissions) and population density.
- The $PM_{10}$ covariance correction factor (6% at 50 km; 8% at 100 km) shows a weak dependence on grid resolution. This is due to the spatial homogeneity of $PM_{10}$ concentrations.
- SOMO35 shows a negative correlation, likely due to $NO_x$ titration in urban areas, and as such ozone exposure estimates will be overestimated by 15% when finite grids of 50 km or more are used.
- Significant variability in the covariance correction factors will occur from grid to grid, but most 'gridded' covariance correction factors were found to be $< -0.5|$ for all compounds.

The results presented in this paper are the first part of a wider study. In addition to the results presented here a simple paramaterisation for the sub-grid covariance has been developed that is based on the covariance of population density with emission and altitude data at 3–5 km resolution. This parameterisation has been applied to 50 km resolution model data (Unified EMEP model) for the entire EMEP domain to determine the total impact of SGV on exposure estimates. The results

from this further work have shown that the impact of SGV may be more significant than is indicated by the assessment presented here, which is based on monitoring with a limited spatial coverage. This further assessment implies that the total error made in exposure estimates may be twice that presented here.

## References

1. AirBase (2010), European air quality database. http://air-climate.eionet.europa.eu/databases/airbase/
2. Amann M, J Cofala, A Gzella, C Heyes, Z Klimont, W Schöpp (2007) Estimating concentrations of fine particulate matter in urban background air of European cities. IIASA Interim Report IR-07-001. http://www.iiasa.ac.at/rains/reports/IR-07-001-citydelta.pdf
3. Fiala J et al (2009) Spatial assessment of PM10 and ozone concentrations in Europe (2005). EEA Technical report No 1/2009. http://air-climate.eionet.europa.eu/reports/EEA_TR_1_2009_Spatial_AQ_assessment_2005
4. IIASA (2005) CAFE Scenario Analysis Report Nr. 6, "A final set of scenarios for the Clean Air For Europe (CAFE) programme".. http://ec.europa.eu/environment/air/cafe/activities/pdf/cafe_scenario_report_6.pdf

## Questions and Answers

**Questioner Name**: Peter Builtjes

**Q**: Are the covariance correction factors stable in time, so they can be applied for scenarios?

**A**: $NO_2$ and $PM_{10}$ are both stable in time, i.e. there is little variation from year to year. The ozone indicator SOMO35 is less stable as it may be more sensitive to variable meteorology. The method is suitable for scenarios because the parameterization used is based on emission and population distributions. If these change with the scenarios then so will the parameterized covariance correction factors.

**Questioner Name**: Jeff Weil

**Q**: Is your study/analysis based on a static or "non-moving" population exposure? A mobile population that commutes from a rural area (e.g. with low pollution) to an urban area (e.g. with high pollution) and moving from grid or sub-grid to another would make the calculation of exposure more complicated and would require a different analysis, would it not?

**A**: The study is based on a static population. It is true that introducing mobility would make the analysis more complicated, as it would for any exposure study. There are however elements in this study that could be applied to a 'work' and 'home' analysis, but that would require significantly more information on the work and home address of all citizens in Europe. To my knowledge this information is not currently available.

**Questioner Name**: Jaakko Kukkonen

**Q:** In a previous study we found that population exposure for $PM_{2.5}$ was increased substantially, by an order of magnitude, when the modelling using a regional scale model at 10 km resolution was replaced by a local scale model on a resolution of 1 km. Is this comparable with your results?

**A**: I have not seen this study but it seems strange that such a large increase in exposure would occur with the change in resolution when 80% or so of the $PM_{2.5}$ concentrations in Helsinki come from the regional background, which would be quite homogenous.

**Answer post conference**: I have since seen this study and understand why this would be the case. Firstly it is only the primary $PM_{2.5}$ emissions that are dealt with in that study and that will lead to enhanced exposure because emissions of primary $PM_{2.5}$ are related to traffic and domestic heating, which are both highly correlated with population. Secondly, the two different types of models are not necessarily comparable. Thirdly, that was a modelling study only, with no observational element. The analysis presented here is based directly on observed concentrations. I have since seen another analysis for Helsinki where this large change in calculated exposure with enhanced resolution does not occur. This was based on the local scale model only, which infers that the two models were not comparable. This more recent result from Helsinki does agree with the results found here, indicating a covariance correction factor of around 0.04 at a resolution of 6.4 km, very similar to the $PM_{10}$ results presented here.

# Chapter 113
# Cost-Effective Plans to Mitigate Air Quality Effects on Human Health in Northern Italy

**Claudio Carnevale, Giovanna Finzi, Enrico Pisoni, Marialuisa Volta, and Fabian Wagner**

**Abstract** The use of modeling to support environmental authorities to plan air quality control policies is now quite widespread in different parts of Europe. At the sub-national level the most common way to face the problem is through the scenario analysis approach, using Chemical Transport Models to assess the impact of emission reductions on pollution concentrations. In this paper a multi-objective approach to define air quality policies is proposed. The considered objective function is a vector including an Air Quality Index and an Internal Costs Index. In this work the Air Quality Index (AQI) is the yearly mean PM10 concentration over the study domain. It is estimated processing source-receptor models linking emission and concentrations over the domain cells, taking into account nonlinear phenomena and using Artificial Neural Networks (ANNs). The ExternE methodology is then applied to estimate health impacts and external costs of optimal control policies up to 2020. The data used to identify the source-receptor models has been provided by a set of 10 simulations computed through the TCAM (Transport Chemical Aerosol) model. The Internal Cost Index (CI) describes the costs to implement a particular emission reduction policy. This index is computed by means of ANNs linking emission reductions and their relative implementation costs, for different CORINAIR macro sectors. Simulations with IIASA's GAINS model have been used to calibrate the emission-to-cost model. The solutions of the decision problem represent cost-effective policies at the sectoral level. The methodology is applied to Northern Italy, one of the most polluted areas in Europe, to select optimal control policies up to 2020.

C. Carnevale • G. Finzi • E. Pisoni (✉) • M. Volta
Faculty of Engineering, Department of Information Engineering
University of Brescia, Brescia, Italy
e-mail: enrico.pisoni@ing.unibs.it

F. Wagner
International Institute for Applied Systems Analysis, APD Program, Laxenburg, Austria

D.G. Steyn and S. Trini Castelli (eds.), *Air Pollution Modeling and its Application XXI*,
NATO Science for Peace and Security Series C: Environmental Security 4,
DOI 10.1007/978-94-007-1359-8_113, 

**Keywords** Integrated assessment models • Multi-objective problem

## 113.1 Introduction

Air quality management faces the trade-off between environmental benefits on the one hand and costs to reduce these impacts on the other. Multi-objective methods (e.g. [5]) can be used to address this dilemma by expressing both costs and impacts in the same metric and optimizing a joint objective function. Other methodologies available in literature are include scenario analysis [4], cost-benefit and cost-effectiveness approach [1].

In this work a multi-objective approach is presented that uses neural networks both to describe air quality and technology cost objectives. This approach also takes into account nonlinearities in secondary pollution formation and accumulation (through the use of neural networks). The system works at a sub-national scale for Northern Italy, i.e. considers local features that usually are not completely described at internationally relevant spatial resolutions (e.g. 50 km × 50 km in the EMEP model).

## 113.2 The Multi-Objective Approach and the Neural Network-Based Cost Functions

In our approach the optimal control of the exposure of humans to particulate matter is described by minimizing a joint function of both air quality indicators and emission abatement costs. This is implemented optimizing emission reduction rates (decision variables) through a two-objective mathematical programming algorithm.

The problem can be formalized as follows:

$$\min_{\vartheta} J(\vartheta) = \min_{\vartheta} \left[AQI(E(\vartheta)); CPI(E(\vartheta))\right]$$
$$\vartheta \in \Theta$$

where $E$ represents the precursor emissions for the reference case, $\vartheta$ are the decision variables (namely the emission reductions) constrained to assume values in the feasible range $\Theta$, $AQI(E(\vartheta))$ and $CPI(E(\vartheta))$ are the Air Quality Index and Policy Cost Index respectively, both depending on precursor emissions and emission reductions. The Air Quality Index has been already described through neural networks in previous work [3]. Here this Index is described as external costs due to PM10 concentrations, in particular associated to the Years Of Lost Life (YOLL) index [2]. In this work neural networks have been also identified and validated to describe the link between emission reductions and costs. In particular a neural network has been created for each CORINAIR macrosector, starting from input-output data derived

by the deterministic cost module implemented in GAINS [1]. The multi-objective optimization approach, based on the two set of neural networks, has been solved for the Northern Italy case study.

## 113.3 Results

This section shows both the results of the validation of the emission-cost neural networks, and the Pareto curve obtained solving the multi-objective problem. Figure 113.1 shows a comparison of the emission-cost deterministic model (left) and neural network model (right) variability, showing a good capacity of the neural networks to describe the deterministic model patterns.

In terms of optimization results, Fig. 113.2 (left) shows the efficient solutions computed for the Northern Italy domain. Internal costs span from 0 to roughly 2.6 Billions of Euro, while External Costs (related to YOLL) from 4.8 to 3 Billions of Euro.

Figure 113.2 (right) shows the internal and external costs, for the different points of the Pareto Curve (10 points) obtained performing a difference between point j (with j = 2:10) of the curve and the base case cost (j = 1, that is to say the first point, to the left, of the Pareto Curve). This to be able to consider relative values of costs, less affected by uncertainties. This analysis stresses it is profitable, from a societal point of view, to act on emission reductions to improve air quality; this is true from point 2 to 7 of the Pareto Curve (Fig. 113.2, right), while from point 8 Internal Costs start to be higher than External Costs, meaning that from this point internal costs are overcoming benefits.

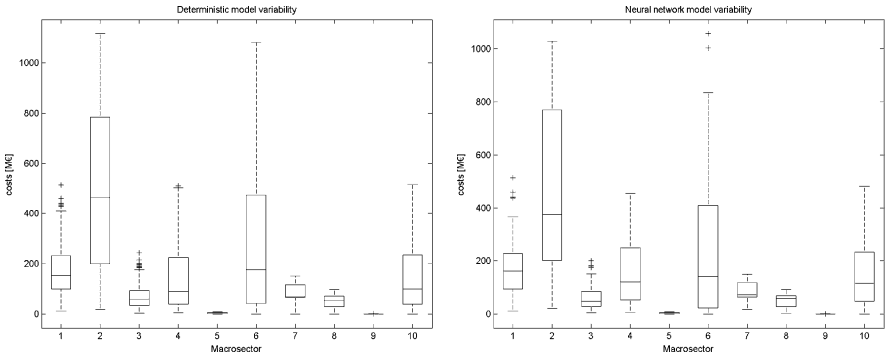


**Fig. 113.1** Variability of deterministic (*left*) and artificial neural network based (*right*) model costs, for the different Corinair macrosectors (representation through standard box-plot, describing 25th, 50th, 75th percentiles, and outliers)

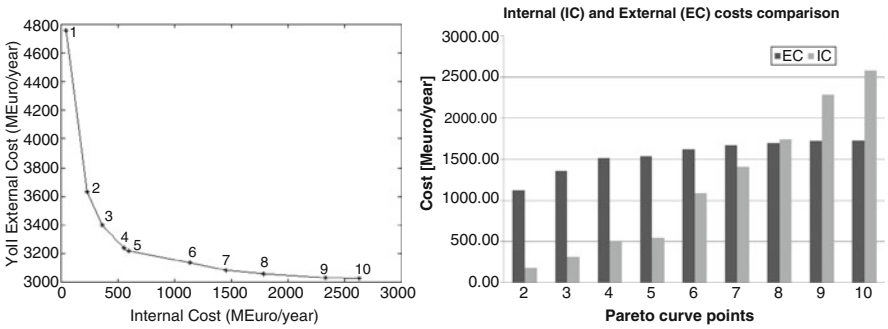


**Fig. 113.2** Pareto curve (*left*), obtained for the optimization procedure, considering internal cost (*x-axis*) and external (*YOLL, y-axis*) costs as objectives. Comparison of internal (*IC*) and external (*EC*) costs (*right*), for the different points of the Pareto curve. Numbers from 1 to 10 (on the Pareto curve, to the left, and on x-axis, to the right) represent points on the Pareto curve

## 113.4 Conclusions

In this work a multi-objective approach, based on neural network to describe both Air Quality Index and Cost Index, has been presented and applied over Northern Italy, to reduce PM10 exposure. In particular the contribution of this paper is mainly (1) the identification and validation of the Internal Cost Index based on a neural network system, and (2) the assessment of the solution of the optimization problem, in terms of trade-offs between internal and external costs. The proposed approach can be used to suggest to Environmental Authorities effective emission reduction priorities to improve air quality.

**Acknowledgments** The TCAM model simulations used to identify ANNs for the Air Quality Index have been performed in the frame of the Pilot Project QUITSAT (QUalità dell'aria mediante l'Integrazione di misure da Terra, da SAtellite e di modellistica chimica multifase e di Trasporto – contract I/035/06/0 – http://www.quitsat.it), funded by Italian Space Agency.

## References

1. Amann M, Cofala J, Heyes C, Klimont Z, Mechler R, Posch M, Schoopp W (2004) The RAINS model. Documentation of the model approach prepared for the RAINS peer review 2004. Tech. rep., International Institute for Applied Systems Analysis
2. Bickel P, Friedrich R (2005) ExternE: externalities of energy, methodology 2005 update. Tech. Rep., IER, University of Stuttgart. Bickel and Friedrich
3. Carnevale C, Finzi G, Pisoni E, Volta M (2009) Neuro-fuzzy and neural network systems for air quality control. Atmos Environ 43:4811–4821
4. Cuvelier C et al (2007) City-Delta: a model intercomparison study to explore the impact of emission reductions in European cities in 2010. Atmos Environ 41(1):189–207
5. Pisoni E, Carnevale C, Volta M (2009) Multi-criteria analysis for PM10 planning. Atmos Environ 43:4833–4842

## Questions and Answers

**B. Fisher**: From your experience of generating cost vs benefit curves, is there always an optimal point which a rational decision maker would choose? The curve could be almost linear making it difficult to come to one best decision.
**C. Carnevale**: In our experience (and for our particular study domain) the Pareto curve often shows peculiar (nonlinear) behavior, with a first part of the Curve with high air quality index decreasing with relatively low cost and, and a second part of the curve with very little further enhancement with high costs. So even if it is not possible to find a "rational" point for the decision maker, it is however possible to identify Pareto Curve "areas" that are more favorable than others.

# Chapter 114
# Enhanced Aerosol Formation and Nutrient Deposition by Ship Emissions in North Sea Coastal Regions

**Volker Matthias, Ines Bewersdorff, Armin Aulinger, and Markus Quante**

**Abstract** This study investigates the impact of ship emissions on secondary aerosol formation in coastal areas of the North Sea under conditions of the year 2000. The regional chemistry transport model CMAQ is used with different emission data sets as input to study their impact on aerosol concentrations. It is shown that the largest effect occurs in summer, when sulphate, nitrate and ammonium concentrations may be increased by more than 50% in large areas of Denmark and Northern Germany. The use of sulphur reduced fuels results in a significant reduction of sulphate aerosols. However at the same time, nitrate aerosol concentrations increase.

**Keywords** Aerosol • Sulphate • Ship emissions • CMAQ model

## 114.1 Introduction

As a consequence of the global distribution of manufacturing sites and the increasing international division of labour, ship traffic is steadily increasing and is becoming more and more important as an origin of air pollution. This concerns both, direct particle emissions and secondary aerosol formation from gaseous precursors, particularly sulphur oxides and nitrogen oxides.

The southern North Sea with the large harbours in Rotterdam and Hamburg is one of the regions with the highest ship traffic in the world. For the estimation of the ship emissions in this region a bottom-up approach on the basis of ship movement data together with average engine loads and emission factors available in literature is used to generate a ship emission inventory that is of sufficient spatial resolution to

V. Matthias (✉) • I. Bewersdorff • A. Aulinger • M. Quante
Helmholtz-Zentrum Geesthacht GmbH, Institute of Coastal Research,
Max-Planck-Strasse 1, 21502 Geesthacht, Germany
e-mail: volker.matthias@hzg.de

D.G. Steyn and S. Trini Castelli (eds.), *Air Pollution Modeling and its Application XXI*,
NATO Science for Peace and Security Series C: Environmental Security 4,
DOI 10.1007/978-94-007-1359-8_114, 

investigate coastal gradients in aerosol concentrations. This inventory serves as input for the Models-3 Community Multiscale Air Quality modelling system (CMAQ), a state-of-the-art Eulerian chemistry transport model.

## 114.2 Model System

### *114.2.1 Emissions*

Ship emissions were derived out of a database purchased from Lloyd's Marine Intelligence Unit (LMIU). It contains vessel characteristics and vessel movements of all commercial vessels equal to or greater than 100 gross tonnages (GT). Emission factors (power-based in g/kWh) used in this study are obtained from Cooper and Gustafsson [3]. The procedure how to obtain the ship emission dataset is as follows. The vessel movement database provides the basis for calculating the routes of the vessels. It is assumed that all vessels take the shortest routes between two ports at sea. The travelling time is distributed equally to all passed grid boxes on their route. The ship emissions per grid box and time step are calculated for the different pollutants by means of the corresponding emission factors and the engine power of the particular vessel.

Land based emission data for the nitrogen, sulphur and volatile organic compounds as well as for aerosol particles was provided by IER Stuttgart based on EMEP area emissions and EPER point source emissions [4].

### *114.2.2 Chemistry Transport Model*

CMAQ version 4.6 [2] is set up on a $54 \times 54$ km$^2$ grid ($81 \times 90$ grid cells) for Europe and on a $18 \times 18$ km grid ($55 \times 58$ grid cells) for the greater North Sea area. Thirty vertical layers up to 100 hPa (approx. 15 km altitude) are used. The CBM IV chemical mechanism [5] with aerosol and aqueous chemistry extensions is used. The aerosol is represented by three log-normal size modes [1] and it includes secondary inorganic aerosols as sulphate ($SO_4$), ammonium ($NH_4$) and nitrate ($NO_3$), sea salt (NaCl), organic carbon and elemental carbon. The model is driven by meteorological fields that were derived from MM5 [6] model runs that were driven by ERA40 6-hourly global reanalysis data on a $1^\circ \times 1^\circ$ grid. We used four dimensional data assimilation of the ERA40 fields in MM5. The boundary conditions for the CMAQ simulations were taken from MOZART [7,10] model results for the year 2000.

To investigate the contribution of ship emissions to air pollution in coastal areas four different model runs with hourly output for the complete year 2000 were performed with CMAQ, one model run including all land-based emissions and the

ship emissions ("incl. ships"), a reference model run just including the land-based emissions ("no ships") and two model runs where the sulphur emissions in the North and Baltic Seas were reduced by 45% ("low sulf") and 96% ("low sulf 0.1"). This corresponds to the case that all ships in the North and Baltic Sea use sulphur reduced fuels with 1.5% sulphur as it is required since November 2007 and 0.1% sulphur which will be the sulphur limit value in 2015 [8]. The typical sulphur content of residual oils that are mainly used by large ocean going vessels is 2.7%. The seasonal impact is considered by comparing monthly average concentrations for January and July.

## 114.3 Results

Caused by the higher oxidation capacity of the atmosphere, the increase of the secondary aerosol concentration is higher in summer than in winter. Figure 114.1 shows the relative increase of the nitrate, sulphate and ammonium aerosol concentrations due to ship emissions in July. Higher nitrate values are mainly seen over land, in the coastal areas of Germany and in Denmark. Higher sulphate values are more clearly connected with the shipping routes. Smaller areas of the German coast and again complete Denmark suffer from an increase in sulphate aerosols by more than 50%. Although ammonia is not emitted by ships, ammonium aerosol concentrations are also increased by 20–50% in large parts of Germany and Denmark. This is due to the secondary aerosol formation mechanism in polluted areas. Particulate nitrate exists as part of ammonium nitrate aerosols ($NH_4NO_3$). These can only be formed if gaseous ammonia ($NH_3$) is available, and this largely depends on the sulphate concentrations. Atmospheric ammonia is first used to neutralize sulphate and form ammonium sulphate aerosol ($(NH_4)_2SO_4$). Particulate nitrate can only exist if excess ammonia would be available.

The relative increase of nitrate, sulphate and ammonium aerosol particles in July for the case that ship fuels contain 45% less sulphur are shown in Fig. 114.2.

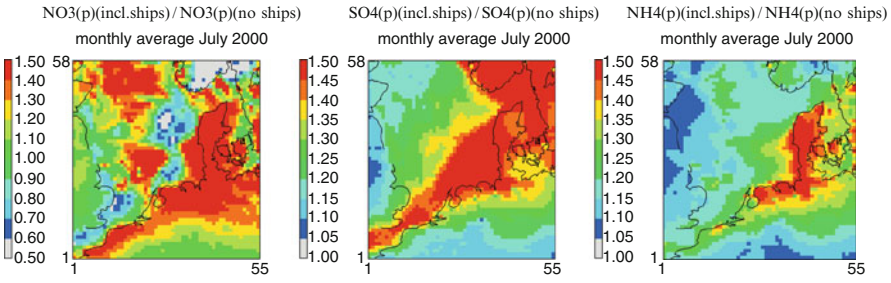


**Fig. 114.1** Monthly averaged increase in secondary aerosol concentrations caused by ship emissions in July 2000 (nitrate (*left*), sulphate (*middle*) and ammonium (*right*))

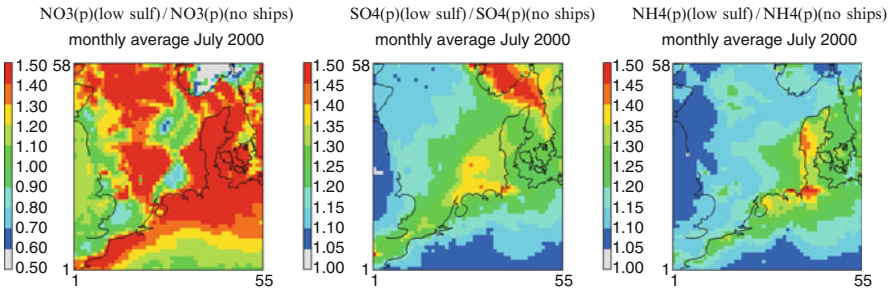


**Fig. 114.2** Monthly averaged increase in secondary aerosol concentrations caused by ship emissions if ships use sulphur reduced fuels in July 2000 (nitrate (*left*), sulphate (*middle*) and ammonium (*right*))

As intended, the sulphate concentrations are significantly reduced, a reduction is also visible for ammonium. Nitrate is slightly increased, although one might have expected from the interplay between sulphate, nitrate and ammonium that significantly more nitrate can be formed if sulphate is reduced (see e.g. [9]).

The 45% decrease in ship-based sulphur emissions leads to a reduction of the additional atmospheric $SO_2$ from ships by 42%, averaged over the whole year and the entire inner model domain. At the same time, additional sulphate aerosols decrease by 38% and additional ammonium aerosols by 20%. Nitrate aerosols were 7% higher compared to the standard run with sulphur rich ship fuels.

## References

1. Binkowski F, Roselle S (2003) Models-3 community multiscale air quality (CMAQ) model aerosol component. 1. Model description. J Geophys Res 108(D6):4183
2. Byun D, Ching JKS (1999) Science algorithms of the EPA Models-3 community multiscale air quality modelling system. Office of Research and Development Washington DC, EPA report, EPA/600/R-99/030
3. Cooper DA, Gustafsson T (2004) Methodology for calculating emissions from ship: 1. Update of emission factors. SMHI Swedish Metrological and Hydrological Institute, Norrköping
4. Friedrich R, Reis S (2004) Emissions of air pollutants. Springer, Berlin/Heidelberg/New York
5. Gery MW, Whitten GZ, Killus JP, Dodge MC (1989) A photochemical kinetics mechanism for urban and regional scale computer modelling. J Geophys Res 94:12925–12956
6. Grell GA, Dudhia J, Stauffer DR (1995) A description of the fifth-generation penn state/NCAR mesoscale model MM5. NCAR Technical Note, NCAR/TN 398 + STR. Boulder
7. Horowitz LW, Walters S, Mauzerall DL, Emmons LK, Rasch PJ, Granier C, Tie X, Lamarque J-F, Schultz MG, Tyndall GS, Orlando JJ, Brasseur GP (2003) A global simulation of tropospheric ozone and related tracers: description and evaluation of MOZART, version 2. J Geophys Res 108(D24):4784
8. IMO (2008) Amendments to the annex of the protocol of 1997 to amend the international convention for the prevention of pollution from ships, 1973, as modified by the protocol of 1978 relating thereto (MARPOL Annex VI). http://www.imo.org/includes/blastDataOnly.asp/data_id%3D23760/176%2858%29.pdf

9. Lauer A, Eyring V, Corbett JJ, Wang CF, Winebrake JJ (2009) Assessment of near-future policy instruments for oceangoing shipping: impact on atmospheric aerosol burdens and the earth's radiation budget. Environ Sci Technol 43(15):5592–5598
10. Niemeier U, Granier C, Kornblueh L, Walters S, Brasseur GP (2006) Global impact of road traffic on atmospheric chemical composition and on ozone climate forcing. J Geophys Res 111:D09301

## Questions and Answers

**Questioner Name**: Tony Dore

**Q**: You mentioned that there is discussion within the shipping industry as to whether they can meet the commitment to 0.1% sulphur content fuel by 2015. Is it realistic to practice fuel switching for ships traveling in and out of the SECA area?

**A**: Already today ships have different kinds of fuels on board, low sulphur fuel to be used inside the SECA and standard heavy fuel oil with on average 2.7% sulphur content outside the SECA. It is difficult to judge from $SO_2$ and particulate sulphate observations at land whether ships really use sulphur reduced fuel or not. However, ship fuels are examined on a random basis at berth and ship owners have to pay high penalties when they do not follow the IMO regulations.

**Questioner Name**: S. Arunachalam

**Q**: Did you include sea salt emissions in this CMAQ application and what was the effect of these on the overall results?

**A**: Yes, sea salt emissions are included. In CMAQ they are calculated with a standard wind velocity dependent parameterization. Sea salt contributes significantly to PM10 concentrations in coastal regions. In our study the effect of ship emissions on the secondary aerosol components nitrate, ammonium and sulphate was investigated. In the North Sea region, these components sum up to the largest part of the harmful PM2.5 aerosol mass.

# Chapter 115
# Multi-objective Optimization of Emission Parameters for Air Pollution Models

**Volodymyr Nochvai**

**Abstract** Optimization algorithms for control of industrial emission parameters with environmental and economic criteria are considered. Combination of the vector relaxation with external penalty function methods is used for multi-objective optimization. The optimization algorithms are developed for air quality management in decision support information systems and to generate some necessary emission scenarios in integrated air pollution models too.

**Keywords** Multi-objective optimization • Air pollution model • Source-receptor relationship • Emission parameters • Cost functions • Constraints • Penalty functions

The source-receptor relationship is an important concept in air quality modeling [13, 15]. Determination of source-receptor matrix is an important intermediate step for solving optimization problems: either the minimization of environmental impact under defined abatement costs or inverse modeling to determine sources from given measurements.

There is a difficulty in calculation for the nonlinear case of the relationship because of nonlinear chemical reactions and "cross-sensitivity" interactions between the impacts of multiple emission sources. The investigations of these problems are mainly provided as sensitivity analyses in the numerical models of photochemical formation of the pollution fields [5, 11, 16].

The usual tasks of multi-objective optimization relating to air pollution are both minimizing of environmental cost functions (air quality damage) and the control cost [4, 6–8, 12]. Control variables may differ depending on the characteristics of

V. Nochvai (✉)
Pukhov Institute for Modeling in Energy Engineering, National Academy of Science Ukraine, General Naumov Str., 15, 03164 Kiev, Ukraine
e-mail: volivn@ukr.net; fhvortex@yahoo.com

D.G. Steyn and S. Trini Castelli (eds.), *Air Pollution Modeling and its Application XXI*, NATO Science for Peace and Security Series C: Environmental Security 4,
DOI 10.1007/978-94-007-1359-8_115, 

the target functions: percentage of the pollution abatement factor (cleaning or not producing) [4, 8, 12], stack height [8], emission rates [10], production level of the controlled sources [7]. The coordinates of sources are the control parameters in optimal facility location and urban planning [1, 12].

A comprehensive problem formulation should consider each emission source as a control variable separately. But usually this is not possible for regions with a large number of stationary and mobile sources of emissions yet and leads to an unfeasible computational problem due to the high number of control variables resulting from this hypothesis. For this reason some authors consider a common percentage of reduction for groups of pollutant activities as control variables [4]. But the spatial characteristics of impacts are quite significant for the tasks of urban air quality management. It is very important to have an ability of managing spatial characteristics of the emission parameters. Therefore, the approach proposed here is the spatial grouping of emission sources on the grid which covers the controlled area. The urban area is divided into zones depending on the emission condition. Atmospheric loads are caused mainly by road traffic and less by industrial sources. Emission sources are grouped as point and area ones on city's domain. For example, the Kyiv-city's domain is presented as a cell grid of 17 × 15, with size of each cell of 2 × 2 km [14]. The cell size conditioned by accuracy of available emission data. Emission from each cell was estimated on the base of traffic volume on roads within each cell and district averaged emissions of stationary sources which were not accounted as point sources. Among point sources, 16 high stationary sources were selected for emission modeling separately.

Generalized criteria for $n_c$-cost functions with a given vector of preference $\rho$ is defined as follows:

$$F(Q) = \sum_{i=1}^{n_c} \rho_i w_i(Q) \rightarrow min,$$

where

$$Q = \left\{Q_s{}^j\right\}, \quad 0 \le Q_s^{j\min} \le Q_s{}^j \le Q_s^{j\max}$$

is the vector of control variables: emission rates of $j$-pollutant from $s$- source, $s = \{1, \ldots, n\}$.

Constraints for $j$-pollutant concentration ($Y^j{}_k$) near surface in an area $k$:

$$Y_k^j \le c_{kd}^j$$

$\tilde{n}^j{}_{kd}$ denotes the admissible level of air pollution in $k$-zone

Equivalent set of objective function can be obtained with transformation:

$$w_i(f_i(Q)) = \begin{cases} \dfrac{f_i^o - f_i(Q)}{f_i^o}, \forall i \in MaxF, \\ \dfrac{f_i(Q) - f_i^o}{f_i^o}, \forall i \in MinF. \end{cases}$$

We can proceed to the unconstrained optimization using penalty functions method:

$$F(Q_1, Q_2, \ldots, Q_n) = f(Q_1, Q_2, \ldots, Q_n) + H_j(Q_1, Q_2, \ldots, Q_n)$$

$$f(Q_1, Q_2, \ldots, Q_n) = \sum_{i=1}^{\mathrm{n_c}} \rho_i w_i(Q).$$

Since start point for optimization lies out of admissible domain external Penalty functions are used:

$$H_j(Q_1, Q_2, \ldots, Q_n) = \sum_k \alpha_k \delta_{kj}(Q_1, Q_2, \ldots, Q_n),$$

$$\delta_{kj} = \frac{Y_k^j}{c_{kd}^j},$$

$$\alpha_k(Q_1, Q_2, \ldots, Q_n) = \left\{ \begin{array}{l} 0, if\ \delta_{kj}(Q_1, Q_2, \ldots, Q_n) \le 1 \\ \alpha_k, if\ \delta_{kj}(Q_1, Q_2, \ldots, Q_n) > 1 \end{array} \right\}.$$

As is proved particularly in [9], the method converges to a local minimum under the condition of continuity of functions.

To solve the optimization problem we can use sensitivity of the functional $F(Q_1, Q_2, \ldots, Q_n)$ to changing of control parameters $Q$ that can be expressed [13] as source-receptor relationship $\frac{\partial F}{\partial Q}$ (for linear case $\frac{F}{Q}$).

As we have the vector of control variables, we can write it in the form of source-receptor matrix: $\frac{\partial F(Q_1, Q_2, \ldots, Q_n)}{\partial Q_s^j}$.

Using the penalty function consistently we move from one point to another until we get an acceptable solution. The coordinates of consequent points are computed through the iterative process [3]:

$$Q_s^{j(m+1)} = \max\left\{0; Q^{jm}{}_s + \lambda' \sum_{i=1}^{\mathrm{n_c}} \rho_i \frac{\partial w_i(Q^m)}{\partial Q_s^j} + \lambda \sum_k \alpha_k \frac{\partial \delta_{kj}(Q^m)}{\partial Q_s^j}\right\}.$$

Factors $\lambda'$ and $\lambda$ regulate the step size. Multiplier $\alpha_k$ can be calculated with Arrow-Hurwicz formula [2]:

$$\alpha_k{}^{(m)} = \max\left\{0; \quad \alpha_k^{(m-1)} + r\delta_{kj}\right\},\ r > 0.$$

Combination of the vector relaxation with external penalty function methods is used for multi-objective optimization. Compromise settlement can be obtained where the minimum $k_0$ of weighted loss with all criteria does not exceed:

$$\rho_i w_i(Q) \le k_{0\min}, i = 1..n_c, Q \in A.$$

The components of source-receptor matrix $\frac{\partial \delta_{kj}(Q)}{\partial Q_s^j}$ can be evaluated for $k$-receptor from $s$-source ($s = 1..n$) with an Air pollution model in forward mode ($n$ - runs): $\Delta Q_s^j \rightarrow \Delta Y_k^j$ as a solution of the transport equation; or just with one run of the model in backward mode [13] as a solution of adjoint equations [12].

Optimization model reveals emission sources that make the most contribution to the pollution of the target zones or the whole region for the given meteorological conditions by gradient of sensitivity function. Emission parameters are changed also by gradient of other introduced functionals.

The optimization model can be used for urban emission parameter control with numerical air pollution models. The model of multi-objective optimization is developed for both the decision making in information systems for air quality management and generating some necessary emission scenarios in integrated air pollution models too.

## References


1. Afshartous D, Guan Y, Mehrotra A (2009) US coast guard air station location with respect to distress calls: a spatial statistics and optimization based methodology. Eur J Oper Res 196:1086–1096
2. Arrow KJ, Hurwicz L, Uzawa H (1958) Studies in linear and non-linear. Programming. Stanford University Press, Stanford
3. Bejko IV, Nochvai VI (2008) Modeling and optimization of emission processes parameters in urban atmosphere. J "Math comput model". Series: Physics and mathematic – Kamyanets-Podilsky, vol 1, pp 25–32 (in Ukrainian)
4. Carnevale C, Pisoni E, Volta M (2008) A multi-objective nonlinear optimization approach to designing effective air quality control policies. Automatica 44:1632–1641
5. Hakami A, Odman MT, Russell AG (2004) Non-linearity in atmospheric response: a direct sensitivity analysis approach. J Geophys Res 109:D15303
6. Holnicki P (2006) On the real-time emission control – case study application. Control Cybern 235:351–367
7. Holnicki P, Sokolowski J, Zochowski A (1987) Diferential stability of solutions to air quality control problems in urban area. Appl Math 32(3):240–253
8. Ismael A, Vaz F, Ferreira EC (2009) Air pollution control with semi–infinite programming. Appl Math Model 33:1957–1969
9. Izmailov AF (2006) Sensitivity in optimization, Moscow (in Russian)
10. Makowski M (2008) Multi-objective decision support including sensitivity analysis. International Institute for Applied Systems Analysis, Laxenburg, pp 21–22
11. Mallet V, Sportisse B (2005) A comprehensive study of ozone sensitivity with respect to emissions over Europe with a chemistry-transport model. J Geophys Res 110(D22)
12. Marchuk GI (1986) Mathematical models in environmental problems. Elsevier, Amsterdam
13. Seibert P, Frank A (2004) Source-receptor matrix calculation with a Lagrangian particle dispersion model in backward mode. Atmos Chem Phys 4:51–63. doi:10.5194/acp-4-51-2
14. Shavrina AV, Sosonkin MG, Veles AA et al (2008) Integrated modeling of surface and tropospheric ozone for Kyiv city. In: Barnes I, Kharytonov MM (eds) Simulation and assessment of chemical processes in a multiphase environment, vol 25, NATO science for peace and security series C: environmental security. Springer, Dordrecht, pp 345–357

15. Tong D, Muller N, Kan H, Mendelsohn R (2009) Using air quality modeling to study source-receptor relationships between nitrogen oxides emissions and ozone exposures over the United States. Environ Int Nov 35(8):1109–17
16. Zhang Y, Bischof C, Easter R, Wu P (2005) Sensitivity analysis of photochemical indicators for $O_3$ chemistry using automatic differentiation. J Atmos Chem 51:1–41

## Question and Answer

**Questioner Name**: Prof. D. Steyn

**Q**: How do you account for meteorological variability in your optimization approach?

**A**: The emission parameters optimization is based on the calculation of the gradients of the cost functionals. The transition to the subsequent iteration point of the optimization algorithm is performed with the calculation of the gradient direction according to the objective functions and their weights. Moreover, the penalty functions turns the gradient in the direction of the admissible domain, if constrains for allowable concentration in the specified areas are not complied. This direction is determined by calculating of the source-receptor matrix in an air pollution model for given meteorological conditions which are defined on the basis of measurements and meteorological models calculations. The elements of the matrix express the sensitivity function for concentration in a given zone to the emissions change under the given conditions for particular terrain characteristics and weather parameters. Therefore, the accuracy of the optimization problem solution is determined, also, by the accuracy of the air pollution models and meteorological models used.

# Chapter 116
# Characterizing the Exposure of Regional-Scale Air Quality in the Northeastern United States

**Valerie C. Garcia, J. Crooks, E. Gego, S. Lin, and S.T. Rao**

**Abstract** The Clean Air Act (CAA) requires that the United States (U.S.) Environmental Protection Agency (EPA) set National Ambient Air Quality Standards (NAAQS) for pollutants considered harmful to human health and the environment. Previous research has shown that high ambient ozone levels are harmful to human health (e.g., Bell ML, Dominici F, Samet JM, Epidemiology, 16(4):436–445, 2005; Ito K, De Leon SF, Lippmann M, Epidemiology, 16(4):446–457, 2005, [4]). While ozone is not directly emitted, the formation of ozone is driven by chemical interactions in the presence of sunlight involving nitrogen oxides ($NO_x$) and volatile organic compounds. Prevailing weather conditions in the Northeastern U.S. transport the relatively long-lived $NO_x$ (NO and $NO_2$) and the secondarily-formed ozone downwind, contributing to pollutant levels at locations much farther from the emission source regions. In this study, we investigate associations between polluted air parcels transported from the Ohio River Valley (ORV) in the Midwestern U.S. and respiratory-related hospital admissions in New York State (NYS). We also examine whether better characterization of exposure in an epidemiology model would improve the discernment of this health signal.

**Keywords** Accountability • Ozone • Health effects • Transport

V.C. Garcia (✉) • J. Crooks • S.T. Rao
Atmospheric Modeling and Analysis Division, U.S. Environmental Protection Agency, Raleigh, NC, USA
e-mail: garcia.val@epa.gov

E. Gego
Gego and Associates, Idaho Falls, ID, USA

S. Lin
New York State Department of Health, Albany, NY, USA

D.G. Steyn and S. Trini Castelli (eds.), *Air Pollution Modeling and its Application XXI*, NATO Science for Peace and Security Series C: Environmental Security 4,
DOI 10.1007/978-94-007-1359-8_116, 

## 116.1 Approach

Back-trajectories were performed from several sites within NYS for ten summers (June, July and August) from 1997 to 2006 to identify days that the air parcel passed through the Ohio River Valley (ORV) area within 48 h back in time. The ORV zone was defined as a boundary encompassing relatively high-emitting power plants in the Midwestern United States (Fig. 116.1).

The ORV zone variable and daily maximum 8-h average (8-h DMA) ozone concentrations were then used as the main health effects variables in a Generalized Additive Model (GAM; Eq. 116.1) to investigate potential associations between these two variables and respiratory-related hospital admissions in NYS.

$$\begin{aligned} Y_t \sim \text{ Poisson } (\mu_t)\text{Ln}(\mu_t) = {} & \beta_0 + \beta_1 \text{SMA}_t + \beta_2 \text{ORV}_t + s_3(\text{maxtemp}_t) \\ & + s_4(\text{dewpoint}_t) + \beta_5 \text{holiday}_t + \beta_6 \text{dow}_t \\ & + \beta_7 \text{year}_t + s_8(\text{Date}_{t-\text{year}}) \end{aligned} \qquad (116.1)$$

Where $\beta_0$ is the natural log of the baseline predicted number of hospital admissions per day per region; $\beta_1 \text{SMA}_t$ is the 3-day simple moving average of the 8-h DMA ozone concentration for each day and region; ($\beta_2 \text{ORV}_t$ ) is a dichotomous variable used to identify days that the air parcel passed through the ORV bounded zone versus days it did not; $s_3(\text{maxtemp}_t)$ is a spline function applied to the average maximum temperature for each day and region (degrees of freedom (df) optimized by the model at ~2.5 per year); $s_4(\text{dewpoint}_t)$ is a spline function applied to the average dew point for each day and region (df optimized at ~3.0 per year); $\beta_5 \text{holiday}_t$ is a dichotomous variable used to indicate holidays; $\beta_6 \text{dow}_t$ is the day-of-week included to account for the delay in admissions over the weekend and other weekday effects; $\beta_7 \text{year}_t$ accounts for inter-annual variability; and $s_8(\text{Date}_{\text{t-year}})$ is a spline function applied to account for autocorrelation in the model (df set at 3.0 per summer).

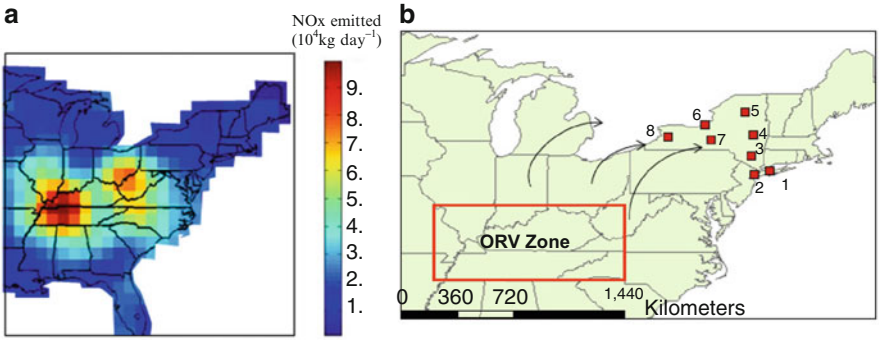


**Fig. 116.1** (**a**) Relatively high NOx emissions (July 1997 shown) originating from power plants in the ORV area; and (**b**) boundaries drawn for identifying days when the air parcel passed through the ORV zone using back-trajectories. Arrows represent transport of pollution into NYS; red squares indicate starting locations of back-trajectories for each numbered NYS region

In addition to the averaged observations, two other approaches were used to define ozone exposure in the GAM: (1) A multiplicative adjusted bias approach [3] was applied to combine Community Multiscale Air Quality model output and observed ozone concentrations; and (2) output from the Stochastic Human Exposure and Dose Simulation (SHEDS) model. The SHEDS model provides estimates of individual exposure by accounting for infiltration of pollutants into buildings and daily activity patterns, such as commuting and time spent indoors. For this portion of the study, the three metrics of ozone exposure were applied to five summers (2001–2005) and four counties in the New York City Metro Area. The study time period and domain were selected because of the availability of model estimates and the large number of hospital admissions available for these four counties. For this second phase of the study, risk was calculated for five metrics (same-day, lag 1 day, lag 2 days, lag 3 days and 3-day SMA) for each data type (averaged observations, combined modeled and measured values, and exposure model output). All other variables in the GAM remained the same.

## 116.2 Data

Eight-hour DMA ozone concentrations were calculated from measurements obtained from the EPA's Air Quality System database (http://www.epa.gov/oar/data/aqsdb.html) and averaged for each NYS region. Health data were obtained from the NYS Statewide Planning & Research Cooperative (SPARCS). These data included daily hospital admissions for respiratory-related diseases, including asthma, chronic bronchitis, chronic obstructive pulmonary disease (COPD), emphysema, and pneumonia and influenza. Daily hospital admissions were summed for each region and matched to daily ozone concentrations. Back-trajectories from selected sites in eight meteorological regions were computed using the HYSPLIT (HYbrid Single-Particle Lagrangian Integrated Trajectory) model [2] for 48 h back in time beginning at 1,800 UTC at a height of 500 m, producing 920 (10 years $\times$ 92 days) trajectories for each site.

## 116.3 Results

The results of the GAM indicate that the risk of being admitted to the hospital for a respiratory-related illness on those days that air parcels are transported from the ORV is elevated in NYS Regions [2, 3] and 6. In addition, the risk of respiratory-related hospital admission from exposure to ozone is elevated in NYS Regions 2 and 4 (Fig. 116.2).

The results in Fig. 116.3 indicate that the combined air quality data does add information relevant for discerning associations between ozone and respiratory-related hospital admissions. Note that the lag 1 day, lag 2 days and 3-day SMA all

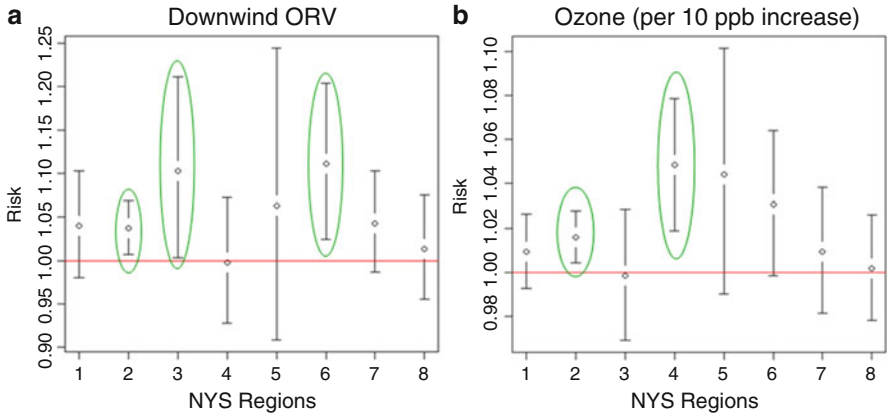


**Fig. 116.2** Risk calculated for the two explanatory variables; (**a**) ORV indicator variable and (**b**) 8-h DMA ozone concentrations. Ovals highlight significant findings

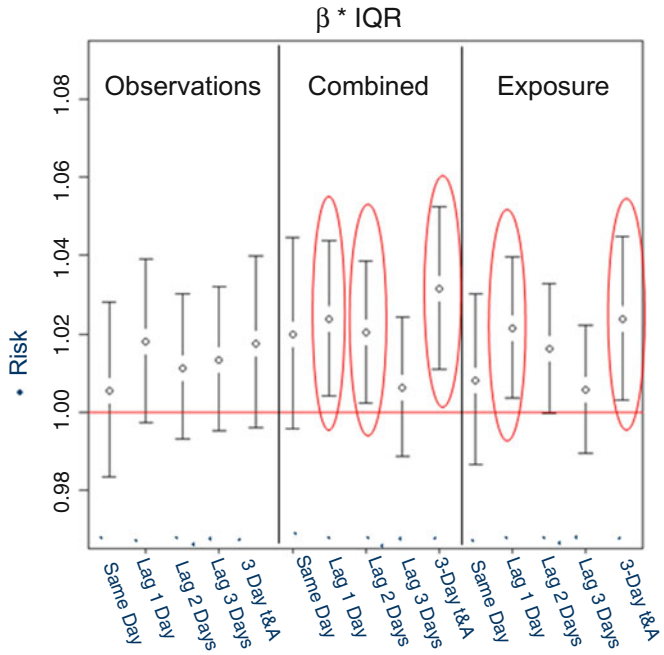


**Fig. 116.3** Risk and 95th percentile confidence intervals calculated by applying averaged observations, combined model and observations, and exposure model output in the GAM. Coefficients are multiplied by the inter-quartile range to account for the varying distributions of the three datasets. Ovals highlight significant findings

produce significant risk (i.e., confidence intervals are above the 1.0 line) as compared to using observations alone. Hence, among the metrics considered here, the use of the enhanced ozone concentration surfaces (combined and exposure model output) resulted in a significant finding for the lag 1 day, lag 2 days, and 3-day SMA metrics, where no significant association was seen with observations alone.

**Acknowledgments** This document has been subjected to Agency review and approved for publication. Approval does not signify that the contents reflect the views of the Agency nor does mention of trade names or commercial products constitute endorsement or recommendation for use.

## References

1. Bell ML, Dominici F, Samet JM (2005) A meta-analysis of time-series studies of ozone and mortality with comparison to the national morbidity, mortality, and air pollution study. Epidemiology 16(4):436–445
2. Draxler RR, Hess GD (1997) Description of the HYSPLIT_4 modeling system, NOAA technical memorandum ERL ARL-224, NOAA Air Resources Laboratory, Silver Spring, MD, http://www.arl.noaa.gov/ready/hysplit4.html.
3. Garcia VC, Foley KL, Gego E, Holland DM, Rao ST (2010) A comparison of statistical techniques for combining modeled and observed concentrations to create high-resolution ozone air quality surfaces. J Air Waste Manage Assoc 60:586–595
4. Ito K, De Leon SF, Lippmann M (2005) Associations between ozone and daily mortality: analysis and meta-analysis. Epidemiology 16(4):446–457

# Chapter 117
# Development and Evaluation of Land-Use Regression Models Using Modeled Air Quality Concentrations

**Vlad Isakov, Markey Johnson, Joe Touma, and Halûk Özkaynak**

**Abstract** Land-use regression (LUR) models have emerged as a preferred methodology for estimating individual exposure to ambient air pollution in epidemiologic studies in absence of subject-specific measurements. Although there is a growing literature focused on LUR evaluation, further research is needed to identify strengths and limitations of LUR modeling and strategies for improvement. In particular, LUR models have several limitations and among these are the needs for comprehensive monitoring data from a large number of sites, and the inability to link sources of emissions with measured elevated concentrations. In contrast, air quality models are designed to provide this linkage and have a long history of use by regulatory agencies in developing pollution mitigation strategies. Thus, the linkage of LUR techniques with available air quality modeling tools may benefit evaluation and enhancement of LUR techniques. In this study, we evaluated the fitted LUR models in several different ways and examined the implications of alternate LUR development strategies on model performance for benzene, particulate matter (PM2.5), and nitrogen oxides (NOx).

**Keywords** Air pollution • Epidemiology • Land-use regression • Air quality modeling

V. Isakov (✉) • J. Touma
Atmospheric Modeling and Analysis Division, National Exposure Research Laboratory, Office of Research and Development, U.S. EPA, Research Triangle Park, Durham, NC 27711, USA
e-mail: isakov.vlad@epa.gov

M. Johnson
Air Health Science Division, Water Air and Climate Change Bureau, Health Canada, Ottawa, ON K1A 0K9, Canada

H. Özkaynak
Office of Research and Development, U.S. EPA, Research Triangle Park, Durham, NC 27711, USA

D.G. Steyn and S. Trini Castelli (eds.), *Air Pollution Modeling and its Application XXI*, NATO Science for Peace and Security Series C: Environmental Security 4,
DOI 10.1007/978-94-007-1359-8_117, 

## 117.1 Introduction

There is a growing body of literature linking proximity to roadways and traffic intensity with adverse respiratory health effects [1]. Pollutants of interest include nitrogen dioxide ($NO_2$), fine particular matter ($PM_{2.5}$), and elemental carbon (EC) since each has been linked to vehicular emissions and respiratory health. Land-use regression (LUR) models have emerged as a preferred methodology for estimating individual exposure to ambient air pollution in epidemiologic studies in absence of subject-specific measurements. Despite their advantages of being easy to apply, simple, practical, and widely used by researchers, LUR models have several limitations. Among these are that they require accurate monitoring data and at a large number of sites, especially in highly-industrialized urban areas with many types of emission sources. In these areas, monitoring data collection is expensive and time consuming. Other limitations are: (1) these models are typically not transferable from one urban area to the another; (2) they lack the ability to connect specific sources of emissions to concentrations for developing pollution mitigation strategies; and (3) they are not typically designed to address multi-pollutant aspects of air pollution (e.g., they usually deal with one pollutant at a time). LUR methodology, however, is relatively new and many of these issues are currently being examined or addressed. In contrast, air quality models have been used for many years in air quality management but only more recently applied in exposure assessments to provide improved spatial exposure estimates [2]. Recent developments include the hybrid air quality modeling that combines dispersion models to provide local-scale concentrations with photochemical grid models to provide regional background concentrations Isakov et al. [3].

## 117.2 Methods

First, we predicted air quality concentrations of $PM_{2.5}$, $NO_x$, and benzene using hybrid modeling techniques based on CMAQ and AERMOD model results. $PM_{2.5}$ was selected as a criteria pollutant that is mostly regional and is largely formed in the atmosphere due to secondary reactions. $NO_x$ was selected because it is strongly influenced by local combustion sources. Benzene was selected as representative of air toxics pollutants that are mostly emitted from mobile sources. We focused on a 20 by 20 km area that includes the impacts from a majority of emission sources. Next, we used these modeled concentrations to develop and evaluate LUR models. The LUR models were then evaluated to examine the implications of varying the number of training sites (25, 50, 75, 100, 125, 150, 200, and 285 sites) used to build the models on LUR fit and performance.

Spatially-resolved hourly concentrations for multiple pollutants were estimated based on a hybrid air quality model approach using the AERMOD dispersion model to predict local concentration gradients (e.g., within a few meters to few kilometers

from the source) and the CMAQ regional model to provide concentrations due to photochemical reactions and transport from sources outside the domain, e.g., background [3].

To build a LUR model, the measured values of air quality concentrations at sampling locations are regressed against GIS variables [4]. The dependent variables for LUR development were modeled pollutant concentrations generated by air quality models. The independent variables were traffic data, emission source information, and land-use variables. Two-month (July–August of 2001) summer time average of hourly modeled concentrations of $PM_{2.5}$, $NO_x$, and benzene were estimated at 318 census block group centroids in New Haven, CT. These receptors can be viewed as pseudo-monitoring sites (instead of field measurements) for the purpose of their use in the LUR model.

## 117.3 Results

The LUR models for benzene, $NO_x$, and $PM_{2.5}$ were similar in terms of general model characteristics and performance. Benzene models typically had the greatest number of independent predictors per model, followed by $NO_x$ and $PM_{2.5}$. We then evaluated the fitted LUR models using various approaches, including LOOCV and Hold-Out evaluation. Finally, we examined whether the LUR models performed similarly for different pollutants. For this comparison, we used the following evaluation metrics: predicted versus observed correlation (adjusted model $R^2$) and "Mean Residuals", calculated as mean predicted minus observed concentrations. The results of model performance or explanatory power of LUR models (measured by adjusted model $R^2$ values) in training datasets are shown in Fig. 117.1. Mean and variability in adjusted $R^2$ values (shown here as mean and the inter-quartile range or 25th–75th percentiles of the mean adjusted $R^2$ values derived from 100 different iterations) for LUR models were inversely associated with the number of sites in the training set. Mean adjusted $R^2$ values for benzene ranged from 0.89 for training datasets with 25 sites to 0.67 for training datasets with 285 sites.

For $NO_x$, mean adjusted $R^2$ values ranged from 0.79 for training datasets with 25 sites to 0.63 for those with 285 sites. Mean adjusted $R^2$ values for $PM_{2.5}$ ranged from 0.83 for training datasets with 25 sites to 0.59 for training datasets with 285 sites. Mean standardized prediction residuals approached zero and root mean square of standardized prediction residuals approached one as the number of training sites used to develop the models increased. These results were consistent for all three pollutants. Figure 117.1 also shows the results from evaluation of LUR models based on the correlations between observed and predicted pollutant concentrations at test sites that were not used for model development. Although adjusted $R^2$ values for LUR models in the training datasets decreased with number of training sites used to develop the models, model performance and robustness in the test datasets used for hold-out evaluation improved with increased number of training sites. Specifically, the correlation between observed pollutant concentrations and

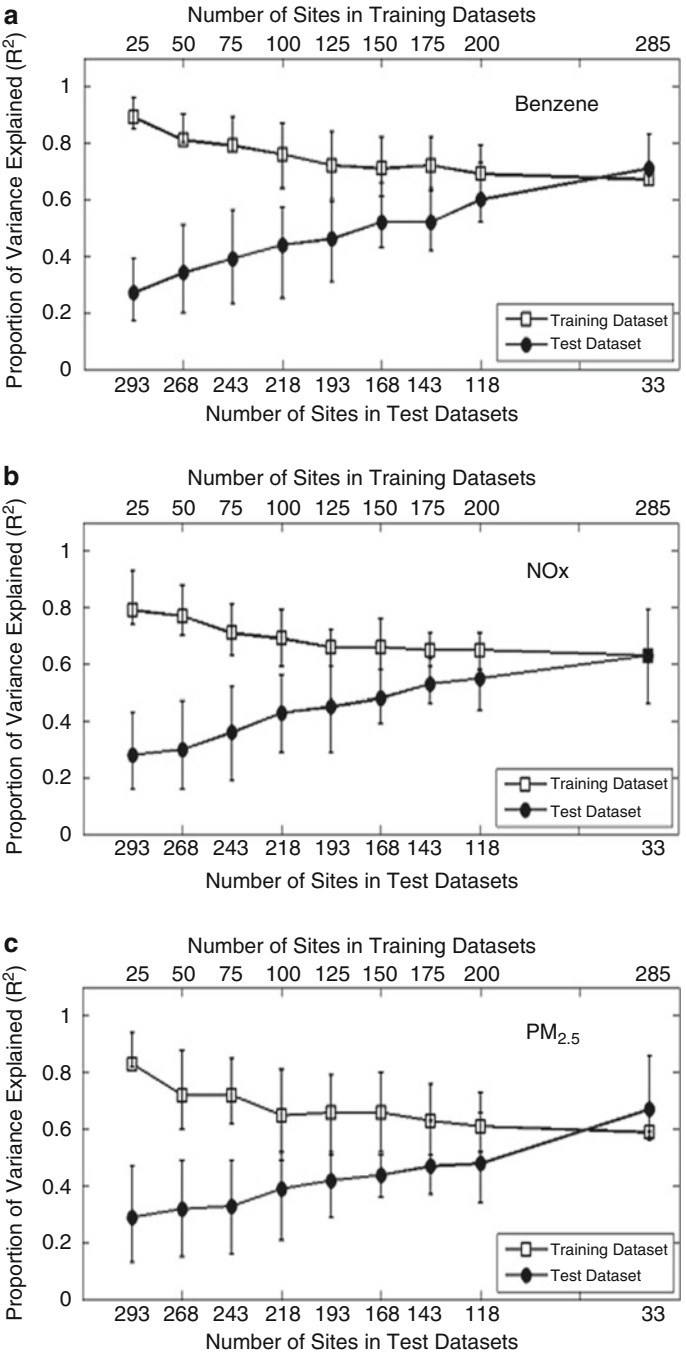


**Fig. 117.1** Mean and inter-quartile range of adjusted $R^2$ values for LUR models as a function of number of sites in both training (upper horizontal axis) and test datasets (lower horizontal axis) for (**a**) Benzene, (**b**) NOx and (**c**) $PM_{2.5}$

LUR estimates in sites that were not used to develop the models (adjusted $R^2$ predicted versus observed in the test dataset) was positively associated with number of training sites used to develop the models. The adjusted $R^2$ for LUR models in the training datasets and adjusted $R^2$ for predicted versus observed in test datasets began to converge at approximately 125 sites. These results were observed in LUR models for benzene, $NO_x$, and $PM_{2.5}$.

## 117.4 Summary

In this study we linked land-use regression modeling approaches with combined regional-local scale air quality models in order to evaluate and improve LUR techniques. The air quality modeling results were first evaluated against available monitoring data to assure their reliability and later used to develop and evaluate LUR models in a hierarchical fashion using an iterative site selection approach. We evaluated the fitted LUR models in several different ways and examined the implications of varying the number of training sites used to develop the LUR models on LUR model performance for multiple pollutants.

Our results confirm the challenges facing the LUR community when attempting to fit empirical response surfaces to spatially and temporally varying urban pollution levels. Even at the 2-month averaging periods considered in this initial research, it is clear that complex emissions and atmospheric processes due to meteorological, transport, diffusion and chemical mechanisms can substantially limit the predictive power of most straightforward LUR based models. Clearly, the greater the number of sites selected for building these models (e.g., above $N = 100$) the fit of these models can improve up to a certain level. Unfortunately, the locations where these sites are selected within the airshed could introduce additional uncertainties and potential for exposure misclassification in community based air pollution epidemiology studies. We have shown that the ambient concentration prediction errors greatly increase (nearly double) over the wide range and type of LUR models we evaluated. The variations that we observed in LUR model performance (e.g., across different models, pollutants and sample sizes) are most likely reflected in the diverse range of LUR model fits reported in the published literature, especially for $NO_x$ and $PM_{2.5}$.

Based on these results, future work should examine best ways to augment basic LUR models with site-specific source-receptor information generated from air quality models. Despite their known limitations (e.g., need for detailed emissions and meteorological information and uncertainties due to model inputs, algorithms and outputs), air quality models have several features that can be useful in improving LUR model applications. For example, air quality models can reliably provide temporal (hourly) and spatial (at hundreds of locations) estimates, and have a long history of use by regulatory agencies in multi pollutant mitigation strategies. Air quality models are also based on physical and chemical principles, are widely used and tested in permit applications, and are readily and freely available with extensive

user support tools, such as user's guides and manuals. Air quality models often undergo extensive peer review so model improvements are continuously made to enhance scientific credibility.

**Disclaimer** This document has been subjected to Agency review and approved for publication. Approval does not signify that the contents reflect the views of the Agency nor does mention of trade names or commercial products constitute endorsement or recommendation for use.

## References

1. Health Effects Institute (2010) Traffic-related air pollution: a critical review of the literature on emissions, exposure, and health effects. Special Report #17, 2010–01–12. Available on-line at: http://pubs.healtheffects.org/view.php?id=334
2. Jerrett M, Arain A, Kanaroglou P, Beckerman B, Potoglou D, Sahsuvaroglu T, Morrison J, Giovis C (2005) A review and evaluation of intraurban air pollution exposure models. J Expo Anal Environ Epidemiol 15:185–204
3. Isakov V, Touma J, Burke J, Lobdell D, Palma T, Rosenbaum A, Özkaynak H (2009) Combining regional and local scale air quality models with exposure models for use in environmental health studies. J Air Waste Manage Assoc 59:461–472
4. Johnson M, Isakov V, Touma J, Mukerjee S, Özkaynak H (2010) Evaluation of land use regression models used to predict air quality concentrations in an urban area. Atmos Environ 44:3660–3668

# Chapter 118
# Pollen Dispersal and Hybridization Model for Risk Assessment of Genetically Modified Crops

**Shigeto Kawashima and Takehide Hama**

**Abstract** In recent years, an attention to the gene flow problem of dispersal of artificially modified genes to the natural environment by airborne pollen is increasing rapidly. Especially for wind-pollinated crop, there is a possibility that pollen diffuses quite widely depending on meteorological conditions. In order to deal with such problems, it is necessary to develop the model that can estimate the pollen dispersal and the hybridization mating appropriately. In this paper, I present an aerobiological mechanistic model for assessing pollen dispersal and hybridization using hourly data. This model considers hourly change of the meteorological conditions and daily change of biological conditions. And it was constructed for estimating the spatial distribution of hybridization percentage in a recipient field. The effectiveness of the model was certified by the field experiments. The model was constructed in consideration of physical processes and biological processes. The algorithms presented here can be applied to estimate the total pollen deposition and hybridization mating for many kinds of plants.

**Keywords** Transgenic crops • Pollen dispersal • Hybridization • Modeling • Simulation • Meteorological effect • Risk assessment

## 118.1 Introduction

The safety and impact on the environment of transgenic crops are important issues. Losey et al. [5] first suggested that pollen from transgenic Bt (Bacillus thuringiensis) corn (Zea mays L.) might kill nontarget insects, a potentially significant problem. In recent years, an attention to the gene flow problem of dispersal of artificially modified genes to the natural environment by airborne pollen is

S. Kawashima (✉) • T. Hama
Kyoto University, Kitashirakawa Oiwakechou, Sakyo, Kyoto, Japan
e-mail: sig@kais.kyoto-u.ac.jp

D.G. Steyn and S. Trini Castelli (eds.), *Air Pollution Modeling and its Application XXI*, NATO Science for Peace and Security Series C: Environmental Security 4,
DOI 10.1007/978-94-007-1359-8_118, 

increasing rapidly (e.g., [1, 3]). Pollen dispersal in relation to crop breeding has been studied for various crops (e.g., [4, 8]). Especially for wind-pollinated crop, there is a possibility that pollen diffuses quite widely depending on meteorological conditions [2, 6, 7].

In Japan, it becomes most emergent issue to assess the co-existence of GMO crops and non-GMO crops for rice that is the key crop in our country. Then we surveyed the hybridization level, meteorological condition and phenological data for the rice plant, and developed the forecasting model of hybrid ratio by using biological and environmental data. In this model, we aimed to trace the actual phenomena of hybridization in detail, and combined to estimate hybrid percentage in the rice field. The process of pollen emission from the male flower, the process of the diffusion of pollen by wind, the process of hybridization mating are modeled respectively independently, and finally united to make simulation model. The physical correctness in the diffusion process are cared to keep. Hybridization experiment was carried out by using an actual rice field to acquire the value of the parameter used and the verification data of the model.

## 118.2 Materials and Methods

### *118.2.1 Outline of the Field Experiment*

Two sets of experiments were executed in the rice field of the National Institute for Agro-Environmental Sciences. The size of donor field is 19 m by 2 m, and the size of recipient field is 19 m by 17 m. Donor area was arranged to be the windward of the recipient field for the prevailing wind in the flowering season of rice. Hourly airborne pollen was surveyed using Hirst type pollen sampler in the center of the experimental field. Meteorological observation system was set up in the field. Air temperature, relative humidity, wind speed, wind direction and precipitation were observed and recorded during the experiment. The number of newly flowered ears in each day was surveyed in ten individuals for each kind. Hybridization percentage was measured by sampling the rice seeds after harvest. We distinguish the presence of hybrid by using xenia phenomenon that appeared in the albumen color of rice seed. The hybridization percentages were estimated for 975 individuals for each field experiment.

### *118.2.2 Model Descriptions*

(a) Outline of the pollen dispersal and hybridization model
The experimental field was overlayed with orthogonal grid system of 0.5 m interval. The dispersal and deposition of pollen emitted from each grid square are estimated by using an appropriate solution of diffusion equation. Observed hourly meteorological data and estimated number of emitted pollen

were used to this calculation. The depositions of donor pollen in the recipient field for each hour were totaled by repeated calculation for all source grids square of donor. The spatial distribution of the donor pollen and the flowering rate of recipient were used to estimate the distribution of hybrid probability in the recipient field. Spatial distribution of hybrid percentage was calculated by summing up the hourly distribution of hybrid probability throughout the flowering period.

(b) Pollen emission sub-model
The amount of pollen emitted from the donor vegetation of a unit area in a unit time is estimated by using the following equation.

$$P = aF\ dT/dt \tag{118.1}$$

where, $P$ is the amount of pollen emitted from the donor vegetation of a unit area in a unit time, $F$ is the flowering intensity of the donor vegetation, $T$ is air temperature, $t$ is time, $a$ is constant parameter.

(c) Pollen diffusion sub-model
Pollen dispersion from a unit area is estimated by the plume equation that is a typical solution of the diffusion equation. The basic expression of the plume equation is shown as follows.

$$X(x,y,z) = \frac{P}{2\pi\bar{u}\sigma_y\sigma_z}\exp\left[-\frac{1}{2}\left(\frac{y^2}{\sigma_y^2}+\frac{z^2}{\sigma_z^2}\right)\right] \tag{118.2}$$

where, $X$ is pollen concentration at the point $(x,y,z)$, $u$ is wind speed, $\sigma_y$ is diffusion parameter in horizontal direction $(y)$, $\sigma_z$ is diffusion parameter in vertical direction $(z)$. In our calculation, we assumed as $\sigma = \sigma_y = \sigma_z$, and $\sigma^2 = 2\,k\,x/u$. $k$ is diffusion coefficient in air.

(d) Hybridization estimation sub-model
At first, one ear of rice is thought. The hybridization probability of this ear is simply assumed as follows,

$$h = D/(R+D) \tag{118.3}$$

where, $D$ is donor pollen concentration around the female flower of the recipient, $R$ is recipient pollen concentration around the female flower of the recipient.

## 118.3 Results

Changes of hybridization ratio with distance from the donor field in the former experiment with early-ripening rice are shown in Fig. 118.1. Black squares with a solid line show simulated hybridization ratios; white squares show observed ratios. Although the ratios of hybridization are comparatively higher in the area near the

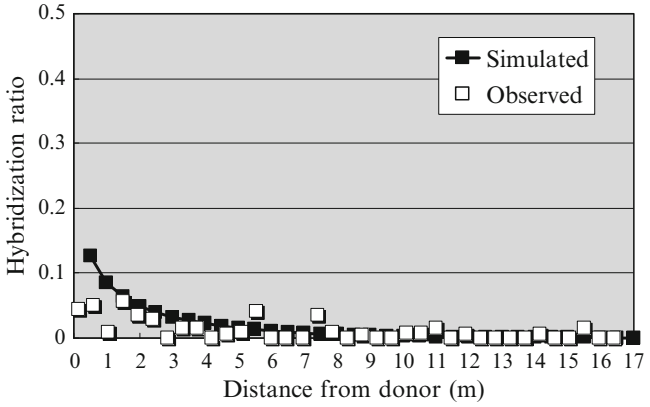


**Fig. 118.1** Changes of hybridization ratio with distance from the donor field in the former experiment with early-ripening rice

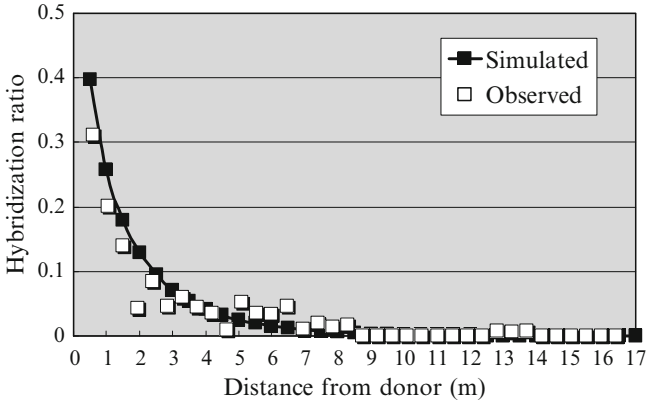


**Fig. 118.2** Changes of hybridization ratio with distance from the donor field in the latter experiment with late-ripening rice

donor, it became smaller values in the recipient field generally. Simulation reproduced this fact well. Changes of hybridization ratio with distance from the donor field in the latter experiment with late-ripening rice are shown in Fig. 118.2. The ratios of hybridization are high in general in the latter experiment, and it became very high in the area near the donor in the recipient field. Simulation reproduced the variation pattern of the hybridization ratio with distance from the donor very well. The validity of the "Pollen dispersion hybridization model" constructed by considering the biological and physical processes was verified based on the comparison with two experimental results.

## 118.4 Discussion and Conclusion

A mechanistic model that considers hourly change of the meteorological conditions and daily change of biological conditions was constructed for estimating the spatial distribution of hybridization percentage in a recipient field. The effectiveness of the model was certified by the field experiments. The algorithms presented here can be applied to estimate the total pollen deposition and hybridization mating for many kinds of plants. We will accumulate the hybridization data for many kinds of crops under various meteorological conditions, and perform analyses based on the comparison between the forecast values of models and the observed data. Further experiments must be performed and mechanistic simulations must be used in order to determine how the deposited pollen count leeward of a field varies as the size of the field changes.

## References

1. Gliddon CJ (1999) Gene flow and risk assessment. In: Lutman PJW (ed) Gene flow and agriculture. Relevance for transgenic crops. Proceedings of a conference, University of Keele. British Crop Protection Council, Farnham, Surrey, pp 49–56
2. Kawashima S, Matsuo K, Du M, Oka M, Daido H, Takahashi Y, Kobayashi T, Inoue S, Yonemura S (2002) Relationship between percentage of wind-pollinated maize hybrids and distance from donor pollen source. Jpn J Palyn 48:1–12
3. Kwon YW, Kim DS, Yim K-O (2001) Herbicide-resistant genetically modified crop: assessment and management of gene flow. Weed Biol Manage 1:96–107
4. Lavigne C, Klein EK, Couvet D (2002) Using seed purity data to estimate an average pollen mediated gene flow from crops to wild relatives. Theor Appl Genet 104:139–145
5. Losey JE, Raynor LS, Carter ME (1999) Transgenic pollen harms monarch larvae. Nature 399:214
6. Louette D, Charrier A, Berthand J (1997) In situ conservation of maize in Mexico: genetic diversity and maize seed management in a traditional community. Econ Bot 51:20–38
7. Quist D, Chapela IH (2001) Transgenic DNA introgressed into traditional maize landraces in Oaxaca, Mexico. Nature 414:541–543
8. Richards CM, Church S, McCauley DE (1999) The influence of population size and isolation on gene flow by pollen in silene alba. Evolution 53:63–73

# Chapter 119
# The Impact of the Urban Air Pollution on the Human Health: A Case-Study in Turin

**Valeria Garbero*, A. Montalto, N. Lazovic, Pietro Salizzoni, S. Berrone, and Lionel Soulhac**

**Abstract** An integrated methodology evaluating the impact of the urban air pollution on human health is presented. From traffic emission data, background pollution level and meteorological data the pollutant concentration distribution within the street network is calculated by the urban scale dispersion model SIRANE and the potential health impact on population is evaluated by the traditional toxicological approach.

**Keywords** Air pollution • Dispersion model • Risk assessment

## 119.1 Introduction

The problem of atmospheric pollution in urban areas gives rise to increased concern. Appropriate tools to manage and control the urban air quality and suitable methodologies to quantify the impact of air pollution on human health become essential.

* Supported by Regione Piemonte via the project AirToLyMi (CIPE Grant 2006)

V. Garbero* (✉)
DIMAT, Politecnico di Torino, Corso Duca degli Abruzzi 24, Torino, Italy

Golder Associates, S.r.l. Via Banfo 43, Torino, Italy
e-mail: valeria.garbero@polito.it

A. Montalto
DITER, Politecnico di Torino, Corso Duca degli Abruzzi 24, Torino, Italy

N. Lazovic
Golder Associates, S.r.l. Via Banfo 43, Torino, Italy

P. Salizzoni • L. Soulhac
LMFA, Ecole Centrale de Lyon, Ecully, France

S. Berrone
DIMAT, Politecnico di Torino, Corso Duca degli Abruzzi 24, Torino, Italy

D.G. Steyn and S. Trini Castelli (eds.), *Air Pollution Modeling and its Application XXI*, NATO Science for Peace and Security Series C: Environmental Security 4,
DOI 10.1007/978-94-007-1359-8_119, 

The operational urban dispersion model SIRANE has been applied to the city Turin, in order to evaluate the population exposure to the urban air pollution and estimate the associated health risks.

## 119.2 Methods

SIRANE assumes the decomposition between the external atmospheric flow and the urban canopy flow. The external flow is described following the similarity theory and the pollutant dispersion above roof level is modelled by means of a Gaussian model. The urban geometry is described as a simplified network of street segments connected by nodes representing the street intersections. Each street segment is represented as a box and a mass balance is computed within the box, taking into account inward and outward pollutant fluxes as well as the pollutant sources within it, in order to calculate the pollutant concentration in the street. A detailed description of the model can be found in Soulhac [2] and Soulhac et al. [3, 4]. The input data required to calculate the pollutant concentration in the street are the urban network geometry, the meteorological data, the background concentration and the traffic emission data.

The study area consists of the central neighbourhoods of Turin and the domain geometry is represented as a street network. The pollutants considered in the study are $NO_2$, $PM_{10}$ and benzene ($C_6H_6$).

The hourly meteorological data refer to the year 2004 and were measured at the meteorological station in Via della Consolata, Turin, whereas the estimation of the background concentration was inferred from the hourly concentration measured at an urban background monitoring station in Turin. The vehicular emissions are calculated combining the traffic flux data referred to 2004 (5 T data) and the emission factors of the vehicle fleet in Turin (ACI data), obtained by the COPERT methodology for each studied pollutant. Different scenarios of vehicle fleet corresponding to different years, past (2004), present (2007) and future, are taken into account in order to evaluate the impact of the renewal of the vehicle fleet on the air quality and human health. The future scenario considers replacements of vehicles characterized by old technologies (<euro 3) with the newer ones (>euro3).

The human health risk assessment consists of evaluating the intake of pollutants via the inhalation exposure pathway for two different receptors, resident adult and resident child; in this preliminary study, we assume that the receptors are exposed to the long-term averaged concentration C computed as the UCL95 of the annual mean concentration calculated by SIRANE over the domain and that $C_{indoor} = C_{outdoor} = C$. A less conservative estimate of C is the mean of the annual mean concentration weighted on the number of exposed population. The chronic daily intake is calculated as follows:

$$CDI = \frac{C \times IR \times ED \times EF}{BW} \times \frac{1}{AT}$$

**Table 119.1** Exposure factors (APAT)

| Exposure factors | Symbol | UM | Adult | Child |
|---|---|---|---|---|
| Body weight | BW | kg | 70 | 15 |
| Average exposure time for carcinogenic chemical | ATc | year | 70 | 70 |
| Average exposure time for non carcinogenic chemical | ATn | year | ED | ED |
| Exposure duration | ED | year | 24 | 6 |
| Exposure frequency | EF | day/year | 350 | 350 |
| Exposure daily frequency | EF | h/day | 24 | 24 |
| Inhalation rate | IR | $m^3/h$ | 0.9 | 0.7 |

**Table 119.2** Toxicological parameters of the chemicals

| | Symbol | UM | $PM_{10}$ | $NO_2$ | $C_6H_6$ |
|---|---|---|---|---|---|
| Reference dose | RfD | mg/kg-day | $1.1 \cdot 10^{-2}$ | $1.1 \cdot 10^{-2}$ | $8.6 \cdot 10^{-3}$ |
| Slope factor | SF | $[mg/kg\text{-}day]^{-1}$ | – | – | $2.7 \cdot 10^{-2}$ |

The exposure factors provided by APAT [1] are described in Table 119.1.

The potential for non-carcinogenic effects of a chemical is evaluated by comparing the exposure level with a reference dose (RfD); if this ratio of exposure to toxicity, which is called hazard quotient (HQ = CDI/RfD), is <1 no adverse health effects occur. For carcinogens, risks are estimated as the incremental probability of an individual developing cancer over a lifetime as a result of exposure to the carcinogenic chemical (R = CDI × SF). The toxicological parameters are described in Table 119.2 and have been inferred from the Air Quality values imposed by EU legislation for $PM_{10}$ and $NO_2$ (D.M. 60/02) and from ISS-ISPESL (Italian Health Institute) database for benzene.

## 119.3 Results

The model SIRANE has been validated by comparing the hourly evolution of the simulated concentrations with those measured at three monitoring stations (Consolata, Madama Cristina, Rivoli) in 2004. The agreement has been evaluated by the BOOT statistical parameters and is rather good.

The population exposure is represented in Fig. 119.1 as number of inhabitants exposed to the concentration of $NO_2$, $PM_{10}$ and $C_6H_6$.

The hazard quotient and the risk calculated for the receptors, adult and child resident, concern $NO_2$, $PM_{10}$ and $C_6H_6$ and are presented for the different scenarios in Table 119.3. The values show that carcinogenic and non carcinogenic risks are higher than acceptable level and that the renewal of the vehicle fleet determined a 10% reduction of the risks from 2004 to 2007 and could be further reduced (20%) in the future scenario.

The study presents an integrated methodology to evaluate the impact of air pollution on human health and shows the capabilities of the urban dispersion

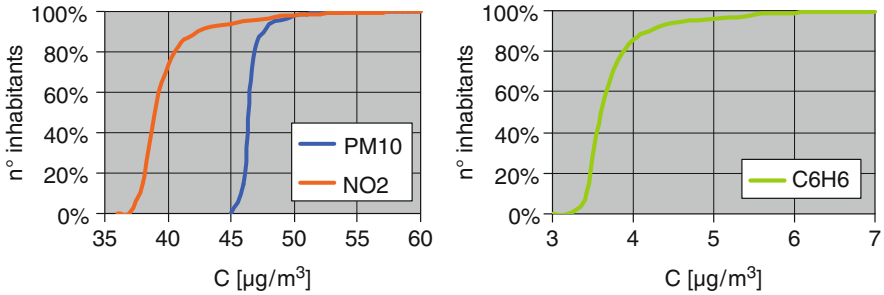


**Fig. 119.1** Exposed population to the $NO_2$ and $PM_{10}$ concentrations respectively

**Table 119.3** Hazard quotient and risk in the different scenarios

| | | 2004 | | 2007 | | Future | |
|---|---|---|---|---|---|---|---|
| | | HI | R | HI | R | HI | R |
| | Mean | 1.22 | – | 1.10 | – | 0.98 | – |
| $PM_{10}$ | UCL95 | 1.28 | – | 1.15 | – | 1.02 | – |
| | Mean | 1.06 | – | 0.96 | – | 0.70 | – |
| $NO_2$ | UCL95 | 1.23 | – | 1.11 | – | 0.78 | – |
| | Mean | 0.09 | $2.1 \cdot 10^{-5}$ | 0.06 | $1.4 \cdot 10^{-5}$ | 0.02 | $5.4 \cdot 10^{-6}$ |
| $C_6H_6$ | UCL95 | 0.13 | $3.0 \cdot 10^{-5}$ | 0.08 | $1.9 \cdot 10^{-5}$ | 0.03 | $7.4 \cdot 10^{-6}$ |
| | Mean | **2.37** | $\mathbf{2.1 \cdot 10^{-5}}$ | **2.12** | $\mathbf{1.4 \cdot 10^{-5}}$ | **1.70** | $\mathbf{5.4 \cdot 10^{-6}}$ |
| Σ | UCL95 | **2.63** | $\mathbf{3.0 \cdot 10^{-5}}$ | **2.34** | $\mathbf{1.9 \cdot 10^{-5}}$ | **1.83** | $\mathbf{7.4 \cdot 10^{-6}}$ |
| | Mean | 4.43 | – | 4.00 | – | 3.55 | – |
| $PM_{10}$ | UCL95 | 4.63 | – | 4.16 | – | 3.70 | – |
| | Mean | 3.83 | – | 3.49 | – | 2.53 | – |
| $NO_2$ | UCL95 | 4.45 | – | 4.03 | – | 2.84 | – |
| | Mean | 0.34 | $7.8 \cdot 10^{-5}$ | 0.21 | $4.9 \cdot 10^{-5}$ | 0.08 | $2.0 \cdot 10^{-5}$ |
| $C_6H_6$ | UCL95 | 0.47 | $1.1 \cdot 10^{-4}$ | 0.29 | $6.8 \cdot 10^{-5}$ | 0.12 | $2.7 \cdot 10^{-5}$ |
| | Mean | **8.60** | $\mathbf{7.8 \cdot 10^{-5}}$ | **7.71** | $\mathbf{4.9 \cdot 10^{-5}}$ | **6.16** | $\mathbf{2.0 \cdot 10^{-5}}$ |
| Σ | UCL95 | **9.55** | $\mathbf{1.1 \cdot 10^{-4}}$ | **8.48** | $\mathbf{6.8 \cdot 10^{-5}}$ | **6.65** | $\mathbf{2.7 \cdot 10^{-5}}$ |

model SIRANE to investigate the effects, associated to management strategies, traffic plans and emission reduction policies, on air quality. SIRANE can be an important tool for Public Authority decision maker.

## References

1. APAT (2008) Criteri metodologici per l'applicazione dell'analisi di rischio ai siti contaminati
2. Soulhac L (2002) Manuale di utilizzo del modello SIRANE. École centrale de Lyon, Université Claude Bernard-Lyon, Centre National de la Recherche Scientifique, Lyon
3. Soulhac L, Garbero V, Salizzoni P, Mejean P, Perkins RJ (2009) Pollutant dispersion in street intersections. Atmos Environ 43:2981–2996
4. Soulhac L, Perkins RJ, Salizzoni P (2008) Flow in a street canyon for any external wind direction. Bound-Lay Meteorol 127(1):97–110

# Chapter 120
# A New Canadian Modeling Platform for Policy Emission Reduction Scenarios: Year 2006 Configuration

**Sophie Cousineau, Didier Davignon, Jack Chen, Annie Duhamel, Samuel Gilbert, Valérie Ménard, Radenko Pavlovic, Jacinthe Racine, Mourad Sassi, and Mehrez Samaali**

**Abstract** The Air Quality Modeling and Application Section of Environment Canada (EC) is transitioning its policy modeling platform from base year 2002 to base year 2006. The motivation behind this transition is to take into account the latest technological and scientific information upon which sound advice can be given to policy management. The latest data available at the beginning of the transition process includes 2006 emission inventories, 2006 meteorology inputs, and latest tools such as the meteorological and chemical transport models, interpolators, etc. The development of such a modeling platform encompasses the meteorology generation and interpolation, the emissions inventory and processing tools, post-processing of the modeling outputs, preparation of inputs for health and environmental benefits valuation models as well as the performance verification. The new system also addresses some of the technical weaknesses of the previous platform such as portability for different users, domain nesting capabilities, flexibility in emissions scenarios, more robust post-processing tools and better system diagnostic tools (reporting, error traceability). These changes will facilitate easier exchange of scenario configurations, data and results, allowing for improved coordination and collaboration between EC modelers. This paper provides an overview of the new policy modeling platform. It first outlines the general model configuration follow by preliminary results of the 2006 annual base case evaluation.

**Keywords** Modeling • Policy • Scenario • Evaluation • Platform • Air quality

S. Cousineau (✉) • D. Davignon • J. Chen • A. Duhamel • S. Gilbert • V. Ménard • R. Pavlovic • J. Racine • M. Sassi • M. Samaali
Air Quality Modeling Applications Section, Environment Canada, Montreal, QC, Canada
e-mail: sophie.cousineau@ec.gc.ca; didier.davignon@ec.gc.ca

D.G. Steyn and S. Trini Castelli (eds.), *Air Pollution Modeling and its Application XXI*, NATO Science for Peace and Security Series C: Environmental Security 4,
DOI 10.1007/978-94-007-1359-8_120, 

## 120.1 Methodology

Policy scenario analyses most often consist of comparisons of a reference case with a second predicted simulation that is referred to as a "scenario case". Model input meteorology is generally the same for both the reference and scenario cases. The reference case often represents present-day conditions, thus all input fields are from the best available estimates for the given time period. The resulting simulation output may then be compared to ground measurements during the same time period, and statistics generated to evaluate the model's performance. The scenario case usually involves a perturbation to the input emissions used in the reference case in order to understand the model's or atmosphere's sensitivity to a given pollutant, or to predict the air quality impacts that would result from a proposed or projected change in emissions. The results of a scenario analysis are most often presented as the difference in the model-predicted atmospheric conditions between the simulation with the modified emission fields (i.e. the scenario) and the reference case. When evaluating the impact of any proposed air quality management or regulatory action on future conditions, the emissions for the reference case are produced using emission projections that will occur in the absence of the proposed action. This is often referred to as a "business-as-usual" (BAU) case. The emissions for the scenario are then generated using future emission levels representative of the proposed regulatory action. The impact on air quality of Canada's proposed regulatory framework for air emissions is compared against a BAU case for a selected future year.

## 120.2 Modelling Platform Description and Configuration

The production of a single scenario run implies the use of a complete modeling platform. The heart of the system is the AURAMS model developed at Environment Canada. This system allows the study of interactions between nitrogen oxides ($NO_x$), volatile organic compounds (VOCs), ammonia ($NH_3$), ozone ($O_3$) and primary and secondary particulate matter (PM). AURAMS is an off-line chemical transport model. The system is composed of three major components: a meteorological driver, an emission processor, and the chemical transport model. The meteorological driver is the Global Environment Mesoscale (GEM) model [1, 2] which is the Canadian meteorological forecast model. For this modeling platform, GEM 3.3.2 with physics version 4.7.2 was used. Daily 30-hour analysis cycles were run for year 2006. The modeling domain of GEM uses a variable resolution global grid with a finer 15-km uniform resolution core over the North American continent. To account for different horizontal and vertical coordinate systems, GEM meteorological outputs are pre-processed with an in-house interpolator to generate meteorological files as input to AURAMS. The Canadian 2006 comprehensive Criteria Air Contaminants (CAC) emission inventory (version 2) and the United-States 2005 National Emission Inventory (NEI, version 5) are used as the anthropogenic

emissions for the current 2006 modeling platform. Mexican inventory for year 1999 is also included for parts of Mexico in the modeling domain. Canadian emission inventory is based on the National Pollutant Release Inventory (NPRI) section of Environment Canada. United-States and Mexican anthropogenic emissions were obtained from the Environmental Protection Agency (EPA) (http://www.epa.gov/ttn/chief/emch/index.html). These inventories include emissions for $NO_x$, VOC, $NH_3$, carbon monoxide (CO), oxides of sulphur ($SO_x$) and primary PM with an aerodynamic diameter less than or equal to 10 μm and 2.5 μm (PM10 and PM2.5). The inventories are provided for different source type such as stationary, mobile and point sources.

AURAMS treats gas-phase species and particulate-matter (PM) formation and evolution with time, as well as their interactions through gaseous, aqueous and heterogeneous and physical reactions [3]. Forty-two gas-phase species are included and up to eight chemical components are considered to contribute to secondary PM formation in the atmosphere. PM sizes are represented as sectional distribution with 12 size-bins, from 0.01 to 41 μm in Stokes diameter; PM components are assumed to be internally mixed within each size bin. PM chemistry is represented by the following chemical components: sulphate (p-$SO_4$), nitrate (p-$NO_3$), ammonium (p-$NH_4$), elemental carbon (EC), primary and secondary organic carbon (POM and SOM), crustal material (CM) and sea salt. Current platform transition coincides with the transition of AURAMS from version 1.3.1 (2005) to version 1.4.0 (2009). This model transition includes new features, options, improvements, bug-fixes and optimizations. New features of interest of AURAMS model for the modeling platform are the options for the chemical lateral boundary conditions (CLBC) and the associated chemical initialization. The modeling domain of the new platform covers most of the North American continent with a 45-km grid resolution. Two nested domain are also established at 22.5-km grid resolution covering Eastern and Western Canada. Grid points are co-located between coarser and higher resolution grids to minimize interpolation errors. Additional levels of higher resolution grids at 3-km can be used following specific policy requests.

## 120.3 Evaluation and Perspective

Preliminary evaluation of the 2006 modeling platform for Canada was conducted for ozone ($O_3$) and fine particulate matter ($PM_{2.5}$). Observation data were provided by the National Air Pollution Surveillance Network (NAPS) of Canada and were included in a geo-referenced verification database developed in-house. In the verification database, model results were imported and paired corresponding to each observation station by time and location. Observations are available on an hourly basis for approximately 150 stations for $PM_{2.5}$, and 190 stations for $O_3$. The number of paired-data exceeds 1.5 and 1.2 millions respectively for $O_3$ and $PM_{2.5}$. Most stations in Canada are located in the southern part of the country, where most of the population lives. Moreover, around 85% of the stations are located within 4 of the 10

**Table 120.1** Model performance statistics for hourly ozone and PM2.5 averaged over 2006 annual simulation

| | | | Average | | Standard deviation | | | | | |
|---|---|---|---|---|---|---|---|---|---|---|
| | Region | #stations | obs | mod | obs | mod | Corr | RMSE | Mean bias | Mean error |
| PM2.5 | BC | 43 | 6.23 | 9.33 | 6.30 | 17.26 | 0.11 | 17.98 | 3.10 | 8.65 |
| | AB | 27 | 5.74 | 8.67 | 6.28 | 8.40 | 0.24 | 9.65 | 2.93 | 6.09 |
| | ON | 39 | 7.76 | 9.04 | 7.07 | 9.71 | 0.41 | 9.49 | 1.28 | 5.89 |
| | QC | 22 | 7.83 | 8.91 | 7.84 | 8.62 | 0.37 | 9.29 | 1.08 | 5.66 |
| | Canada | 152 | 6.79 | 8.54 | 6.81 | 11.57 | 0.24 | 12.06 | 1.75 | 6.41 |
| Ozone | BC | 37 | 20.45 | 28.48 | 12.80 | 19.13 | 0.32 | 20.94 | 8.03 | 14.63 |
| | AB | 26 | 25.56 | 23.90 | 14.20 | 18.85 | 0.56 | 16.05 | −1.66 | 12.28 |
| | ON | 45 | 26.73 | 24.22 | 14.89 | 17.52 | 0.59 | 15.14 | −2.51 | 12.00 |
| | QC | 50 | 23.94 | 21.70 | 12.72 | 13.22 | 0.44 | 13.91 | −2.23 | 11.19 |
| | Canada | 191 | 24.58 | 24.42 | 13.47 | 16.30 | 0.44 | 15.91 | −0.16 | 12.10 |

provinces of Canada, namely British-Columbia (BC), Alberta (AB), Ontario (ON) and Québec (QC). General statistics are presented only for these 4 provinces in Table 120.1. The model tends to generally overestimate the observed values for $PM_{2.5}$ and underestimate the $O_3$ values. This is generally true for all provinces, except for BC where some meteorological conditions, in a particular urban area, create abnormally high values for both $O_3$ and $PM_{2.5}$. This is also reflected in the high root mean square error (RMSE) values and the poor correlation values.

Further analyses are in preparation to refine the performance evaluation and it includes the elaboration of the seasonal and monthly statistics, the evaluation of precipitation chemistry and particulate matter chemical components. Finally the comparison of the new platform performance versus the previous one will be of the highest importance, in order to show the increase value of the development of the new Canadian 2006 policy modeling platform.

## References

1. Côté J, Desmarais J-G, Gravel S, Méthot A, Patoine A, Roch M, Staniforth A (1998) The operational CMC/MRB Global Environmental Multiscale (GEM) model. Part 1: design considerations and formulation. Mon Weather Rev 126:1373–1395
2. Côté J, Desmarais J-G, Gravel S, Méthot A, Patoine A, Roch M, Staniforth A (1998) The operational CMC-MRB Global Environment Multiscale (GEM) model. Part II: results. Mon Weather Rev 126:1397–1418
3. Gong W, Dastoor AP, Bouchet VS, Gong S, Makar PA, Moran MD, Pabla B, Ménard S, Crevier L-P, Cousineau S, Vankatesh S (2006) Cloud processing of gases and aerosols in a regional air quality model (AURAMS). Atmos Res 82:248–275

# Chapter 121
# flexRISK – Flexible Tools for Assessment of Nuclear Risk in Europe

**Delia Arnold, Klaus Gufler, Wolfgang Kromp, Helga Kromp-Kolb, Gabriele Mraz, Petra Seibert, Steven Sholly, Philipp Sutter, and Antonia Wenisch**

**Abstract** flexRISK studies the geographical distribution of the risk due to severe accidents in nuclear facilities, especially nuclear power plants (NPP) in Europe. Starting with source terms and accident frequencies, the large-scale dispersion of radionuclides in the atmosphere is simulated for about 1,000 meteorological situations. Together with the subsequent calculation of resulting radiation doses the consequences of severe accidents can be estimated. In this contribution, a description of the flexRISK project is provided.

**Keywords** FLEXPART • Nuclear risk assessment

## 121.1 Introduction

After a long break in the construction of new nuclear power plants in most countries, since a few years, licensing procedures for new plants have been started in several European countries, and also some developing countries increase their efforts to embark on a nuclear energy path. Also, many aging plants continue to

D. Arnold (✉)
Institute of Meteorology, University of Natural Resources and Life Sciences, Vienna, Austria

Institute of Energy Technologies, Technical University of Catalonia, Diagonal 647, 08028 Barcelona, Spain
e-mail: delia.arnold@boku.ac.at

K. Gufler • W. Kromp • S. Sholly
Department of Civil Engineering and Natural Hazards, Institute of Safety and Risk Sciences, University of Natural Resources and Life Sciences, Vienna, Austria

H. Kromp-Kolb • P. Seibert
Institute of Meteorology, University of Natural Resources and Life Sciences, Vienna, Austria

G. Mraz • P. Sutter, • A. Wenisch
Austrian Institute of Ecology, Vienna, Austria

D.G. Steyn and S. Trini Castelli (eds.), *Air Pollution Modeling and its Application XXI*, NATO Science for Peace and Security Series C: Environmental Security 4,
DOI 10.1007/978-94-007-1359-8_121, 

operate, often with life-time extensions up to 60 years and power uprating. Severe accidents, continue to carry the potential for widespread contamination.

## 121.2 The flexRISK Project

Considering this context, flexRISK [3] (continuation of the RISKMAP project [5]) aims at studying the geographical distribution in Europe of the consequences of severe accidents in nuclear facilities providing a flexible set of tools, for the present situation as well as foreseeable developments, according to the state-of-the-art knowledge. To achieve this three main work areas have been defined:

## 121.3 Definition of Source Terms and Accident Frequencies

Source terms and accident frequencies for different reactors or reactor types are defined on the base of available technical literature. For each reactor unit, two representative release scenarios are selected. Where no detailed information is available, generic assumptions are made. For each, the timing of the release, effective release heights, and release fractions for nuclide groups such as noble gases, iodine-caesium, etc. are specified. Source terms and emission inventories are in a tabular form used for the following dispersion and dose calculations.

## 121.4 Atmospheric Dispersion Modelling

Atmospheric dispersion is simulated for a large number of representative meteorological situations within a 10 year period for the defined scenarios and all nuclear power plant sites in Europe. The latest version of the state-of-the-art transport and dispersion model FLEXPART [7] is applied to produce contamination patterns of the ground and near-surface concentrations of relevant radionuclides. Several preliminary decisions regarding both meteorological data and set-up of the dispersion model have been made:

1. *Meteorological input data*. ERA40 and ERA-Interim datasets from the European Centre for Medium-Range Weather Forecasts (ECMWF) were considered. ERA-Interim has higher horizontal and vertical resolution, better data assimilation and a more recent model system than ERA-40. As washout of radionuclides is very important in such a study, averaged total precipitation obtained from both data sets has been compared with gridded precipitation observations [4]. The total precipitation from the ERA-interim data deviates less from the measurements for an overlapping period of 10 years (from 1990 to 2002) which supports the decision of taking ERA-Interim to drive FLEXPART.

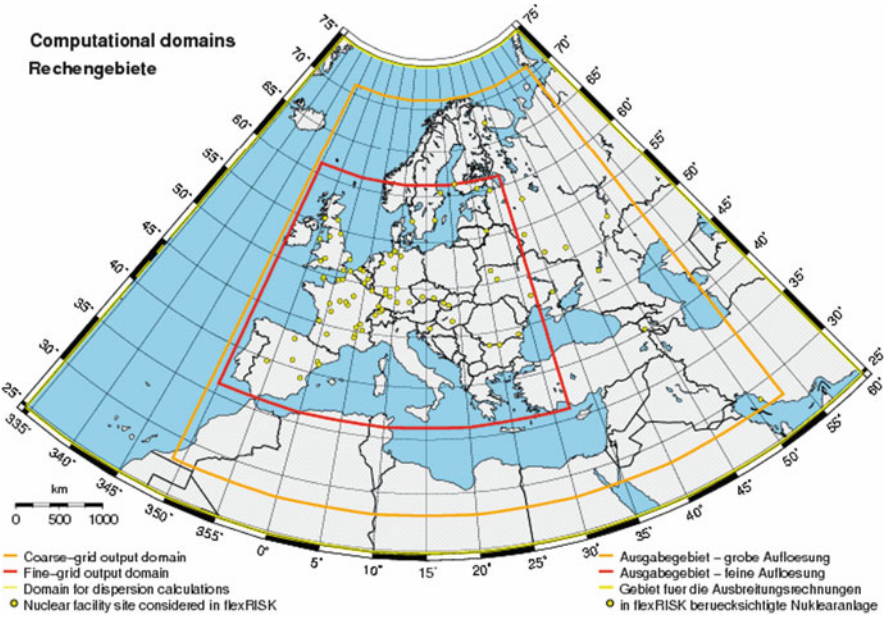


**Fig. 121.1** Map with the three domains used in flexRISK. The computational domain (*yellow line*) for the dispersion calculations. The region for evaluation of the results in a $1 \times 1^\circ$ grid (*in orange*), and the smallest domain (*red line*)

2. *Computational domains*. Two domains will be used to collect gridded output (Fig. 121.1). An outer domain with a horizontal resolution of $1^\circ \times 1^\circ$ and an inner one covering most of central and western Europe, with a finer horizontal grid size. Both domains will have a common vertical resolution of two layers to allow a more accurate calculation of the dose due to cloudshine.
3. *Computational species*. Two different species of radionuclides will be transported, radionuclides attached to aerosol and noble gases.

Since the large number of FLEXPART runs is computationally expensive and it produces large output the FLEXPART code has been also modified.

## 121.5 Dose Calculations

Radiation doses will be derived from the dispersion calculations with a dose model, and will be compared with, inter alia, limits of the Austrian intervention regulations. As a first step to define the radionuclides that contribute most (up to 95%) to the dose and thus, to be considered, test runs with the COSYMA [2] code to assess radiological impact have been performed with release scenarios from US EPR final safety report AREVA 2009 [1] and radioactive inventories described in the Germany's radiation protection commission's "Guide for protection in radiological

emergencies" [6]. The tests included the most probable early release scenario from AREVA 2009 (Release Category 304) under different stability classes, with and without precipitation, and an unlikely early release scenario but with the maximum activity released (Release Category 802). The output provided the percentage contributions of all major radionuclides to different organ and effective 7-day doses and, in one case, also the 1-year doses at a distance of 28 and 155 km from the release point. These tests have lead to a final set of 15 radionuclides (Ca-134 Ca-136 Ca-137 I-131 I-132 I-133 I-135 Ke-88 Rb-88 Ru-103 Ru-106 Sr-89 SR-91 Te-132 Xe-135) which will be considered.

**Acknowledgments** flexRISK is funded by the Austrian Climate and Energy Fund in the framework of "NEW ENERGIES 2020". The computational results presented have been achieved [in part] using the Vienna Scientific Cluster (VSC).

## References

1. AREVA (2009), U.S. EPR Final safety report
2. COSYMA: Code System from Maria (1995) Methods for assessing radiological impact of accidents, EUR 16240 EN, PC COSYMA version 2.0. National Radiological protection Board, 6Forshungszentrum Karlsruhe GmbH
3. flexRISK (2010). http://flexrisk.boku.ac.at/
4. Haylock MR, Hofstra N, Klein Tank AMG, Klok EJ, Jones PD, New M (2008) A European daily high-resolution gridded dataset of surface temperature and precipitation. J Geophys Res (Atmospheres) 113: D20119, doi: 10.1029/2008JD10201
5. RISKMAP (1998). http://www.umweltbundesamt.at/umweltschutz/kernenergie/akw/riskmap/
6. SSK (2003) Leitfaden für den Fachberater Strahlenschutz der Katastrophenschutleitung bei kerntechnischen Notfällen. SSK des BM für Umwelt, Naturschutz und Reaktorsicherheit, Heft 37
7. Stohl A, Forster C, Frank A, Seibert P, Wotawa G (2005) Technical note: the Lagrangian particle dispersion model FLEXPART version 6.2. Atmos Chem Phys 5:2461–2474

# Chapter 122
# Novel Approaches for Estimating Human Exposure to Air Pollutants

**Tim Watkins, Lisa Baxter, Haluk Özkaynak, Vlad Isakov, and David Mobley**

**Abstract** Numerous health studies have used measurements from a few central-site ambient monitors to characterize air pollution exposures. Relying on solely on central-site ambient monitors does not account for the spatial-heterogeneity of ambient air pollution patterns, the temporal variability in ambient concentrations, nor the influence of infiltration and indoor sources. Central-site monitoring becomes even more problematic for certain air pollutants that exhibit significant spatial-heterogeneity. Improving characterization of air pollution exposures involves novel approaches to estimating ambient concentrations, a better understanding of the personal-ambient relationship, and personal exposure modeling. Estimates of ambient concentrations and human exposure estimates have been enhanced by utilizing both measurements and modeling tools. Statistical interpolation techniques and passive monitoring methods can provide additional spatial resolution in ambient concentration estimates. In addition, spatio-temporal models, which integrate GIS data and other factors, such as meteorology, have also been developed to produce more resolved estimates of ambient concentrations. Hybrid modeling approaches, which integrate regional scale models with local scale dispersion models, provide

T. Watkins (✉)
Environmental Public Health Division, National Health and Environmental Effects Research Laboratory, Office of Research and Development, U.S. EPA, Research Triangle Park, NC 27711, USA

L. Baxter
Human Exposure and Atmospheric Sciences Division, National Exposure Research Laboratory, Office of Research and Development, U.S. EPA, Research Triangle Park, NC 27711, USA

H. Özkaynak
Office of Research and Development, U.S. EPA, Research Triangle Park, NC 27711, USA

V. Isakov • D. Mobley
Atmospheric Modeling and Analysis Division, National Exposure Research Laboratory, Office of Research and Development, U.S. EPA, Research Triangle Park, NC 27711, USA
e-mail: isakov.vlad@epa.gov; mobley.david@epa.gov

D.G. Steyn and S. Trini Castelli (eds.), *Air Pollution Modeling and its Application XXI*, NATO Science for Peace and Security Series C: Environmental Security 4,
DOI 10.1007/978-94-007-1359-8_122, 

new alternatives for characterizing ambient concentrations. Estimating actual personal exposures requires an understanding of factors that impact personal-ambient relationships. Publically available data on housing characteristics (e.g., age and size of home) and commuting patterns can be utilized to understand these personal-ambient relationships. In addition, personal exposure modelling approaches are being developed, such as the Stochastic Human Exposure and Dose Simulation (SHEDS) model, which provides estimates of population exposures, and the Exposure Model for Individuals (EMI), which provide individual specific estimates of exposure. Many of these exposure characterization approaches are currently being applied and evaluated in epidemiological investigations. This paper describes the novel exposure assessment approaches discussed above and will briefly present results from the application of these tools. In addition, the paper will discuss ongoing and future applications of these approaches to evaluate their use in health studies.

**Keywords** Air pollution • Epidemiologic studies • Exposure • Air quality modeling

## 122.1 Introduction

Numerous health studies have used measurements from a few central-site ambient monitors to characterize air pollution exposures. Relying solely on central-site ambient monitors does not account for the spatial–heterogeneity of ambient air pollution patterns, the temporal variability in ambient concentrations, or the influence of infiltration and indoor sources [1–4]. Central-site monitoring becomes even more problematic for certain PM components (e.g., metals) or size fractions (e.g., coarse, ultrafine) that exhibit significant spatial-heterogeneity. When central site monitoring is used as a surrogate for air pollution exposure, it does not take into account the spatial–heterogeneity pattern, particularly for certain PM components and size fractions. This variation may be influenced by meteorology as well as emissions from both regional and local sources. In addition, using central site monitors does not reflect the important contributors to human exposures, such as the influence of residential ventilation or indoor sources. Given that people spend the majority of their time indoors, the infiltration of outdoor air indoors and indoor sources can greatly affect the personal-ambient exposure relationship. Improving air pollution exposure characterization will result in more accurate risk estimates of associated health effects to inform future development of NAAQS and other air pollution regulations.

Improving characterization of air pollution exposures involves novel approaches to estimating ambient concentrations, a better understanding of the personal-ambient relationships, and personal exposure modeling. Various exposure characterization approaches are currently being applied and evaluated in several epidemiological investigations supported by the USEPA (Fig. 122.1).

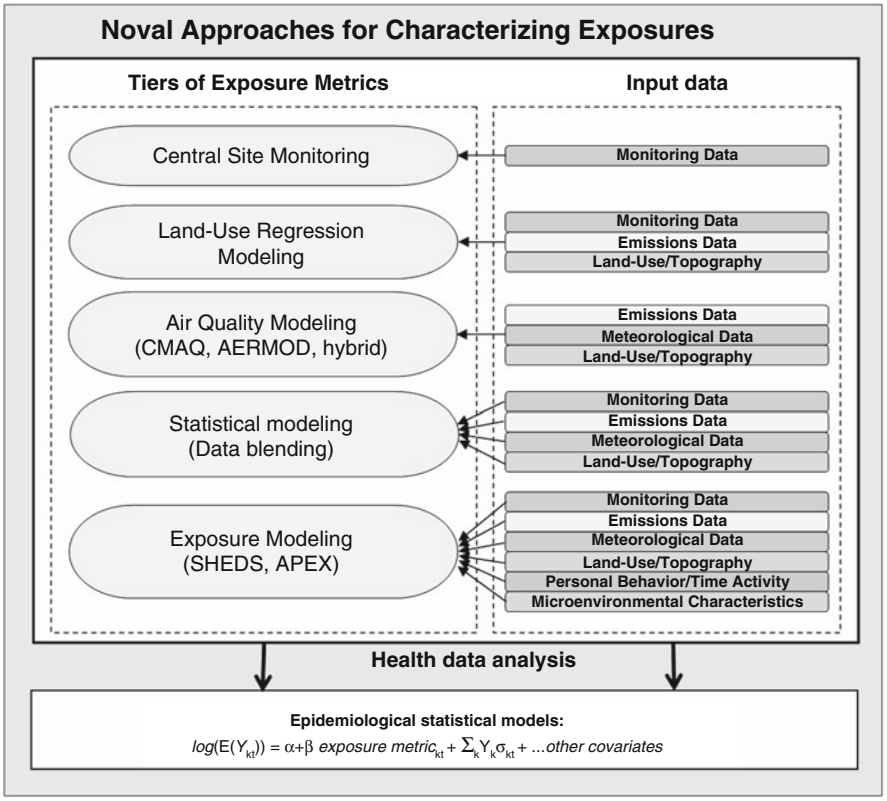


**Fig. 122.1** Various approaches to characterize air pollution exposures for use in environmental health studies

## 122.2 Novel Approaches for Estimating Exposures

Estimates of ambient concentrations have been enhanced by utilizing both measurements and modeling tools. Statistical interpolation techniques and passive monitoring methods can provide additional spatial resolution in ambient concentration estimates. In addition, spatio-temporal models, which integrate GIS data and other factors, such as meteorology, have been developed to produce more resolved estimates of ambient concentrations. Models, such as the Community Multi-Scale Air Quality (CMAQ) model, estimate ambient concentrations by combining information on meteorology, source emissions, and chemical-fate and transport [5]. In addition, hybrid modeling approaches, which integrate regional scale models (such as CMAQ) with local scale dispersion models, provide new alternatives for characterizing ambient concentrations. Publically available data on housing characteristics and commuting patterns can be utilized to understand the personal-ambient exposure relationships. The age and size of the home will affect the proportion of

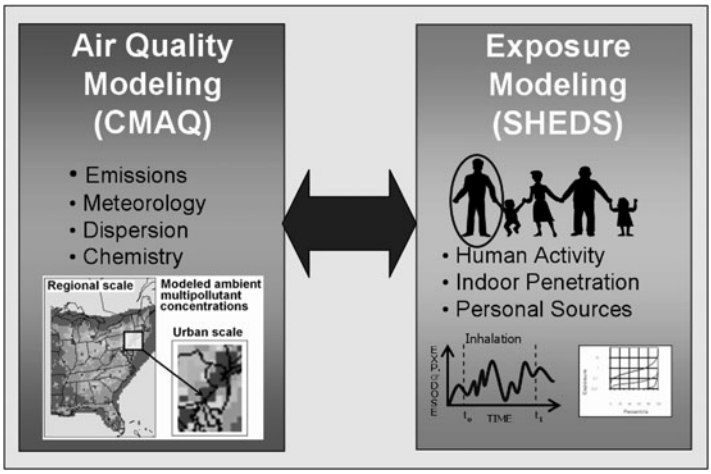


**Fig. 122.2** Integrated air quality and exposure modeling

personal exposure due to ambient air, and commuting patterns will influence how representative an ambient monitor is to ambient exposure. Since publically available data are limited, estimating personal exposure modeling approaches, such as the Stochastic Human Exposure and Dose Simulation Model (SHEDS), are being developed [6, 7]. The SHEDS model is a population exposure model that calculates distribution of exposures within the study population. An integrated air quality and exposure modeling system provides the means to predict the distribution of exposures for the population of interest in various microenvironments by linking air quality modeling information to SHEDS (Fig. 122.2). The integrated modeling system could be also operationally applied in air quality management practices such as standard setting, standard implementation, risk mitigation, accountability [8, 9].

Improved models of ambient concentrations could be utilized in the reanalysis of existing PM health studies leading to more precise and potentially larger health effect estimates. In addition, studies have observed significant heterogeneity in PM-health effects across locations. One potential reason is that while PM mass concentrations may be similar across locations, the composition may be very different, making the understanding of sources very important. Another potential reason for the observed variability may be due to the geographic differences in the personal-ambient exposure relationships necessitating a better understanding of personal exposures. Additional model development is recommended for estimating personal exposures to PM species and specific sources and in developing an individual specific exposure model for use in cohort health studies.

**Disclaimer** This paper has been subjected to Agency review and approved for publication. Approval does not signify that the contents reflect the views of the Agency nor does mention of trade names or commercial products constitute endorsement or recommendation for use.

## References

1. Fuentes M, Song HR, Ghosh S, Holland D, Davis J (2006) Spatial association between speciated particulate matter and mortality. Biometrics 62:855–863
2. Gryparis A, Coull B, Schwartz J, Suh H (2007) Semiparametric latent variable regression models for spatiotemporal modeling of mobile source particles in the greater Boston area. Appl Stat 56(2):183–209
3. Jerrett M, Burnett RT, Ma R, Arden Pope III CA, Krewski D, Newbold KB, Thurston G, Shi Y, Finkelstein N, Calle EE, Thun MJ (2005) Spatial analysis of air pollution and mortality in Los Angeles. Epidemiology 16(6):727–736
4. Sarnat SE, Coull B, Schwartz J, Gold DR, Suh HH (2006) Factors Affecting the Association between Ambient Concentrations and Personal Exposures to Particles and Gases. Environ Health Perspect 114:649–654
5. Byun DW, Schere K (2006) Review of the governing equations, computational algorithms, and other components of the Models-3 Community Multiscale Air Quality (CMAQ) modeling system. Appl Mech Rev 59:51–77
6. Burke JM, Zufall MJ, Özkaynak H (2001) A population exposure model for particulate matter: case study results for $PM_{2.5}$ in Philadelphia, PA. J Expo Anal Environ Epidemiol 11:470–489
7. Ozkaynak HA, Palma T, Touma JS, Thurman J (2007) Modeling population exposures to outdoor sources of hazardous air pollutants. J Expo Sci Environ Epidemiol 18:45–58
8. Isakov V, Graham S, Burke J, Özkaynak H (2006) Linking air quality and exposure models. EM Magazine, 26–29 Sept 2006
9. Isakov V, Touma J, Burke J, Lobdell D, Palma T, Rosenbaum A, Özkaynak H (2009) Combining regional- and local-scale air quality models with exposure models for use in environmental health studies. J Air Waste Manage Assoc 59:461–472

# Chapter 123
# Air Quality Trends in the U.S. Rocky Mountain Area

**Steven R. Hanna, Dan Jaffe, P. Steven Porter, and Douglas Blewitt**

**Abstract** This study is attempting to identify and quantify trends over the past 20 years in measured air quality in the U.S. Rocky Mountain area, including the states of Colorado, New Mexico, South Dakota, Utah, and Wyoming. Long-term well-maintained air sampling sites in the area include those from the IMPROVE and CASTNET monitoring networks, which were intentionally located in remote areas. Analysis of the observations from the ten available sites in the region focuses on ozone, fine particulates, sulfates and nitrates. Statistical trend analysis methods have been applied to the CASTNET ozone sites, with the conclusion that there is no consistent trend found at a majority of the sites. At the Mesa Verde site, there is a significant upwards trend in ozone, as well as a downwards trend in sulfates, with the latter due to emission controls in that area. Preliminary analyses of monthly mean MDA8 ozone at collocated sites at Rocky Mountain NP have revealed biases in that are being investigated further.

**Keywords** Air quality trends • Ozone • CASTNET • Rocky Mountains

S.R. Hanna (✉)
Hanna Consultants, Kennebunkport, ME, USA
e-mail: hannaconsult@roadrunner.com

D. Jaffe
Northwest Air Quality, Seattle, WA, USA

P.S. Porter
University of Idaho, Idaho Falls, ID, USA
e-mail: porter@if.uidaho.edu

D. Blewitt
Air Quality Resources Management, Wellfleet, MA, USA

D.G. Steyn and S. Trini Castelli (eds.), *Air Pollution Modeling and its Application XXI*,
NATO Science for Peace and Security Series C: Environmental Security 4,
DOI 10.1007/978-94-007-1359-8_123, 

## 123.1 Introduction

The objective is to identify and quantify trends in air quality measured by the IMPROVE (Interagency Monitoring of Protected Visual Environments, see http://vista.cira.colostate.edu/improve) and CASTNET (Clean Air Status and Trends Network, see www.epa.gov/castnet) sampling networks in the U.S. mountain states (Colorado, New Mexico, South Dakota, Utah and Wyoming). The current paper concerns an analysis of CASTNET and Wyoming DEQ ozone monitoring data and CASTNET and IMPROVE sulfate, nitrate and fine mass data to determine if statistically significant trends have occurred over the period of record (since 1989). The observations indicate that, in the past 20 years, concentrations of several pollutants, such as ozone, are sometimes close to the National Ambient Air Quality Standard (NAAQS) at these mountain state sites. Various scientific reasons have been advanced for the observed relatively high ozone concentrations (e.g., advection from far upwind source regions, stratospheric intrusions associated with vertical mixing in frontal zones, and local sources) but our current study is mainly concerned with the trends in the observed concentrations.

Increases in "background" ozone concentrations in the Western U.S. have been shown by Jaffe and Ray [3]. Cooper et al. [1] show that there is a correlation between increased ozone in the mid-troposphere in the Western U.S. and emissions in Eastern Asia. The latter study hypothesizes that ozone is transported across the Pacific Ocean from China and other major Asian source regions.

A recent special issue of the *Journal of the Air and Waste Management Association* contains several papers on the analysis of air pollutants in the Western Mountain states. For example, Rodriguez et al. [4] discuss the regional impacts of oil and gas development on ozone formation. The Wyoming DEQ [5] hosted a workshop on "The Upper Green River Ozone Study", and several relevant presentations are posted on their website. The analysis in the current paper includes trends from one of those WYDEQ sites.

## 123.2 CASTNET, IMPROVE, and WYDEQ Observations Archive

For each of the CASTNET sites in the western mountain states, ozone, gaseous and particulate nitrate, particulate sulfate concentrations and meteorology were downloaded. Several IMPROVE sites collect PM observations in the five states, and 1-day averages are recorded once every 3 days. IMPROVE air quality variables that are the initial focus of the trend study are fine PM mass, fine aerosol NO3, fine aerosol SO4, fine aerosol TOC, fine aerosol soil, coarse mass, and aerosol extinction. The Wyoming DEQ network air quality observations were downloaded from their web site. All data were placed in a master archive that allows the authors to efficiently carry out a variety of analyses, including time series plots and statistical analyses.

## 123.3 Results for Ozone

Ozone trends were analyzed at CASTNET sites, using a combination of "look and see" tables and plots of the observations, and statistical analyses of trends.

***Trend Plots*** The scientific issues and the difficulties in applying statistical methods can be seen by plotting the observations and "looking" at the magnitudes and distributions of the observations. For example, Fig. 123.1 contains plots of the observed ozone at the CASTNET sites for the periods of record. The points are 3-year running means of the fourth highest Maximum Daily Averaged 8-hour (MDA8) ozone concentration for each year. The regulations are based on that measure. Figure 123.1 illustrates that the different sites tend to have different total sampling times. Further, there seems to be an elevation dependency, with the lower sites having the lowest concentrations. It is also seen that there are many sites with MDA8 exceeding 70 ppb for many days during each year. If the ozone NAAQS is further lowered, more of these rural sites will exceed the standard. The figure also shows the presence of long-term cycles with periods extending over several years.

The peaks around 2002–2004 in Fig. 123.1 have been postulated to be partly due to the many forest fires and resulting dense clouds of pollutants during that period [2]. The data show that extreme events such as high MDA8 have a large year-to-year variability. For example, at the Centennial site, the number of days in a year with MDA8 exceeding 70 ppb varies from 0 to 32.

Plots were made of daily MDA8 ozone observations from the past 5–10 years at the special WYDEQ sites in the Green River Basin. They are separate from the national CASTNET and IMPROVE network. Similar to the CASTNET sites, most

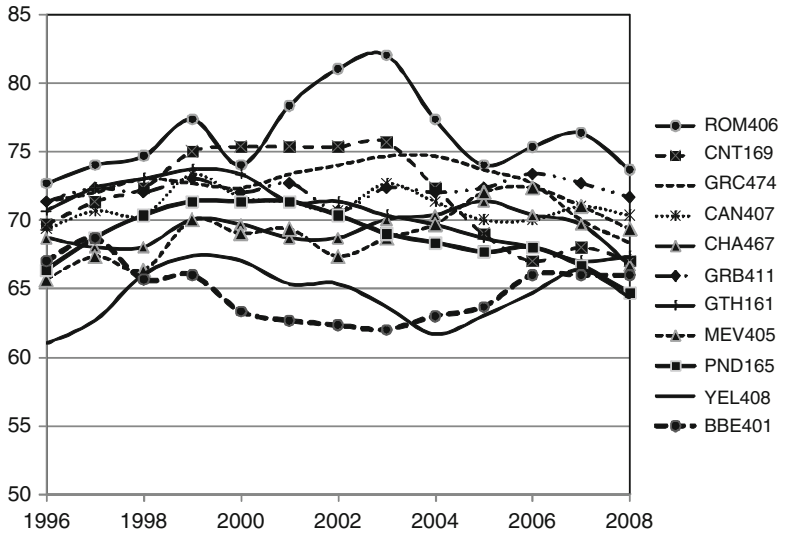


**Fig. 123.1** Three year running mean of fourth highest MDA8 $O_3$ value at CASTNET sites

of these sites do not have a significant trend. Many have several days exceeding 75 ppb and a few days exceeding 100 ppb. The isolated highest values tend to occur in the late winter or early spring of each year.

***Statistical Trend Analyses*** The trends in the ozone data were analyzed using the Ordinary Linear Regression (OLR) and the Theil method. Using a P value of 0.1 or less, four sites show significant increases in ozone (Great Basin, Grand Canyon, Lassen, Mesa Verde and Rocky Mountain 406). Increases of approximately 0.1–0.3 ppb/year are found. The results using OLR and Thiel's method are very consistent in most cases, with only small differences in the trend estimate and P value. Mesa Verde shows the largest trend (0.3 ppb/year) and a very robust P value, $<0.1$ for both OLR and Theil's method. However, several of the CASTNET sites show no significant trend and some show decreases in ozone. It cannot be concluded that there is a consistent long term ozone trend at these sites.

It is interesting that multiyear cycles are usually found in these ozone time series. Can they be explained by other variables, such as meteorology? Our analysis shows that meteorology may at first appear to explain variations in ozone at one site, but then not at another site. For example, the ozone concentration decreases after 2003 at Centennial and increases during the same time period at Mesa Verde.

## 123.4 Results for Sulfate, Nitrate and Fine Mass

Because visibility is a concern in these states, some particulate components of air pollution were analyzed. Time series plots of annual mean sulfate and nitrate for the Mesa Verde IMPROVE site showed that sulfate concentrations are decreasing (see Fig. 123.2) while nitrate levels are increasing. Although further investigation is

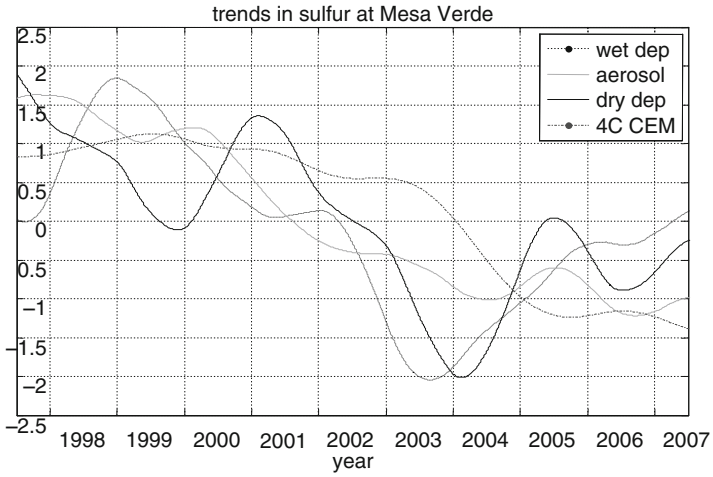


**Fig. 123.2** Low frequency variation in sulfur at the Mesa Verde CASTNET site

warranted, this is consistent with decreasing power plant emissions of $SO_2$ in the area and a change in the particulate chemistry leading to increased nitrate concentrations.

Time series plots of fine mass (with a running 3 year smoothing) at several IMPROVE sites were analyzed. Most did not show a significant trend. A large increase in 2002–2003 at most sites may be due to widespread forest fires.

## 123.5 Biases and Uncertainties in Ozone at Collocated Sites

Two of the sites in the western mountain sites are collocated – ROM206 and ROM406, in Rocky Mountain National Park. Ozone observed at these ROM NP collocated sites sometimes showed a bias, and the issue is currently being investigated by the EPA and National Park Service (NPS) operators.

**Acknowledgments** This research was supported by the American Petroleum Institute, with Ms. Cathe Kalisz as program manager.

## References

1. Cooper OR et al (2010) Increasing springtime ozone mixing ratios in the free troposphere over western North America. Nature 463:344–348
2. Jaffe DA, Hafner W, Chand D, Westerling A, Spracklen D (2008) Influence of fires on O3 concentrations in the Western UW. Environ Sci Technol 42(16):5885–5891
3. Jaffe D, Ray J (2007) Increase in surface ozone at rural sites in the western US. Atmos Environ 41:5452–5463
4. Rodriguez MA, Barna MG, Moore T (2009) Regional impacts of oil and gas development on ozone formation in the Western U.S. J Air Waste Manage Assoc 59:1111–1118
5. Wyoming DEQ (2009) Proceedings, workshop on upper green river ozone study, Laramie, 8–9 Dec 2009. http://deq.state.wy.us/aqd/Ozone%20%Technical%20Forum.asp

# Chapter 124
# The Potential of Biofumigation in Solving Air Pollution in Developing Countries

**Mohamed Fathy M. Salem**

**Abstract** Biofumigation is a sustainable strategy to manage soil-borne pathogens, nematodes, insects, and weeds instead of methyl Bromide in developing countries including Egypt. Initially it was defined as the pest suppressive action of decomposing Brassica tissues, but it was later expanded worldwide to include animal and plant residues. Most data on the efficacy of biofumigation are from in vitro studies using fungal pathogens. Biofumigation also attracted the interest of nematologists, and plant pathologists. Moreover, this is a new trend to find out a substitute for Methyl Bromide that was banned worldwide since 2005, and no one interested in that time to find new and environmentally safe compounds that can work efficiently like the Methyl bromide did. We face this ecological problem in Egypt. However, concerns about the negative impact of synthetic nematicides on the environment and on general public health led to a re-evaluation of these products. For example, high use of the soil fumigant methyl bromide and resulting contamination of ground, surface and drinking water in The Netherlands led to a ban on its use in the 1980s. Later, methyl bromide was listed as an ozone depleting compound at the 4th meeting of the Montreal Protocol in Copenhagen, 1992, and in accordance with the US Clean Air Act its use as a fumigant is now banned in several nations. In last two decades, there is a worldwide awareness and interest to Air Pollution problems. In 1992 methyl bromide (MB) was added as controlled substance to the Montreal Protocol. The problem in developing countries including Egypt is more difficult to solve, as there is still a weak and not rigid environmental laws to respect and there is no multiple alternatives to follow by our Egyptian farmers. On the other hand, the developed countries must phase out most uses by 1 January 2005, with the possibility of critical use exemptions where alternatives have yet to be implemented. All the signed parties could not resolve differences in opinion on the amount

M.F.M. Salem (✉)
Department of Environmental Biotechnology, Genetic Engineering and Biotechnology Research Institute (GEBRI), Minufiya University, P.O. Box 79, Sadat City, Egypt
e-mail: salemkairo@gmail.com

D.G. Steyn and S. Trini Castelli (eds.), *Air Pollution Modeling and its Application XXI*, NATO Science for Peace and Security Series C: Environmental Security 4,
DOI 10.1007/978-94-007-1359-8_124, 

and time period for these critical use exemptions which led to the scheduling of the first Extraordinary Meeting of the Parties (ExMOP1) in March 2004. They accord together to the amount of MB for most of the CUEs for 2005, the level of production necessary to satisfy the CUEs (taking stocks into account), and conditions for granting and reporting on CUEs. One of the most relevant to replace this toxic compound is biofumigation. Biofumigation refers to the suppression of soil-borne pests and pathogens by biocidal compounds released by Brassicaceous green manure and rotation crops when glucosinolates (GSLs) in their tissues are hydrolysed. We studied the effect of different brassicaceous green manure on the biological environment in soil and in their ecosystem. We concluded that, biofumigation can easily replace the mis/excessive use of methyl bromide and with some subsidizes programs for the poor farmers in developing countries. We have to enhance and encourage poor farmers especially in developing countries to make greater reductions in MB consumption. We have to mention that, with this climate change problem, we have to focus on this modifications in developing countries which focusing in their economics on agriculture and hence using this methyl bromide with weak control measures and hence we have to force them to use this safe, environmentally-friendly measures like biofumigation. Moreover, we have to add this item as an extension to the Montreal Protocol in 1992, and COP10. Finally, I invite the European Community to modify this Regulation (EC) 2037/2000 on 'Substances that Deplete the Ozone Layer', by using this biofumigation as an alternative measure to control this fatal problem. Finally, I encourage the UNEP to find out and to finance an innovative program for the new alternatives for this highly toxic compound especially for those farmers and consumers in the developing countries.

**Keywords** Air pollution • Methyl bromide • Montreal protocol • Biofumigation • Developing countries • Egypt • Organic farming • Ozone depletion potential • UNEP

## 124.1 Introduction

In many parts of the developing world, pesticide poisoning, air pollution and toxicity causes more deaths than infectious and epidemic diseases. Use of chemical pesticides is poorly regulated and often very dangerous to those people in the developing countries all over the world; their easy availability also makes them a popular method of self-harm. In 1985, the UN Food and Agriculture Organization (FAO) produced a voluntary code of conduct for the pesticide industry in an attempt to limit the harmful effects of pesticides. Unfortunately, a lack of adequate government regulations in the developing world makes this code ineffective, and thousands of deaths continue today. World Health Organization who has recommended that access to highly toxic pesticides be restricted-where this has been done, suicide rates have fallen. Since an Essential Drugs List was established

in 1977, use of a few essential drugs has rationalized drug use in many regions. An analogous Minimum Pesticides List would identify a restricted number of less dangerous pesticides to do specific tasks within an integrated pest management system. Use of safer pesticides should result in fewer deaths, just as the change from barbiturates to benzodiazepines has reduced the number of deaths from pharmaceutical self-poisoning. (Eddleston et al. 2002). Hundreds of active ingredients and tens of thousands of formulations are used to control agricultural pests and disease-carrying vectors (Meister Publishing Company 1999). More than 1·5 million tones of pesticides are manufactured every year, producing a business worth US$30 billion. The widespread adoption of pesticides during the 1950s was associated with increased crop yields, opening up of new agricultural land, and reductions in incidence of vector-borne diseases. However, increasing pest resistance has resulted in lower yields and a resurgence of vector-borne diseases such as malaria. At the same time, the many health and environmental costs of intensive pesticide use have become starkly apparent. Methyl bromide (bromomethane, MeBr) has been used widely since the 1940s as an effective preplant soil fumigant for controlling nematodes, plant pathogens, weeds and insects (UNEP 1995; Noling and Becker 1994). Fumigant use is vital for the economic viability of many crops, including strawberries, tomatoes, peppers, eggplants, tobacco, ornamentals, nursery stock, vines, and turf (Anderson and Lee-Bapty 1992; NAPIAP 1993; Ferguson and Padula 1994). The total global sales of MeBr were $7.16 \times 107$ kg in 1992, about 75% of which was used as a preplant soil fumigant (UNEP 1995). Methyl bromide is also widely used as a structural and commodity fumigant, as well as for quarantine or regulatory purposes (Anderson and Lee-Bapty 1992; NAPIAP 1993; Ferguson and Padula 1994; UNEP 1995). Its success as a fumigant is largely due to its wide spectrum of activity against pests at many stages of life, its ability to penetrate the fumigated zones, and the ease of application. Because of its high volatility, it leaves very low residue levels in the soil that may be phytotoxic or accumulated in plants, a problem commonly associated with the use of many other modern pesticides. In 1991, MeBr was identified as a potential ozone depleting compound (Chakrabarti and Bell 1993). In 1992, on the Fourth Conference of the Parties to the Montreal Protocol, MeBr was officially added to the list of ozone-depleting chemicals, with its production suggested to be frozen at the 1991 level, effective from 1995. The inclusion of MeBr in the ozone-depleting chemicals list naturally brought this fumigant within the scope of the U.S. Environmental Protection Agency (EPA) Clean Air Act, which has an amendment that mandates discontinuation of any chemical with an ozone depletion potential (ODP) greater than 0.2 at the beginning of 2001. The ODP index for MeBr was determined to be 0.60–70 in 1992 (UNEP 1995); the ODP estimate was reduced to 0.4 in 1998. In March 1993, EPA announced that MeBr was scheduled for a phaseout in the United States by the year 2001 (USEPA 1993). This date was later changed to 2005 (USEPA 2000). During the past decade, there has been an increased research effort devoted to understanding the effects of halogenated gases emitted into the atmosphere on the depletion of the stratospheric

ozone layer. According to the Ozone Assessment Synthesis Panel of the United Nations Environmental Programme (UNEP), the hole in the Antarctic ozone layer is due primarily to increases in chlorine- and bromine-containing chemicals in the atmosphere. Even though most of the ozone loss is due to chlorinated compounds (90–95%; Watson et al. 1992), attention has been focused more recently on MeBr because stratospheric bromine is believed to be 40 times more efficient than chlorine in breaking down ozone on a per atom basis (Wofsy et al. 1975). Although the largest effects from ozone-depleting gases have been observed in the southern hemisphere, there are indications that atmospheric ozone is also decreasing in the northern hemisphere. There is a great deal of uncertainty in estimates of the global MeBr budget. In the early 1990s, the ocean was viewed as a net source of MeBr. More recent global balances account for larger sinks than sources (Yvon-Lewis and Butler 1997), with the ocean acting as a net sink of MeBr, the magnitude of which is being refined (Lobert et al. 1997; King et al. 2000). Soil fumigation is thought to contribute 32 Gg year$^{-1}$ (1 Gg is equivalent to 1,000 metric tons) of MeBr to the atmosphere, or _20% of the total MeBr source (Yvon-Lewis and Butler 1997). The oceans represent the largest known source of atmospheric MeBr, followed by fumigation (Butler 2000). Other natural sources of atmospheric MeBr include biomass burning and production by plants, salt marshes, and fungi (Butler 2000). In recent global budgets, only 60% of the MeBr sinks were accounted for by the quantified source terms, and the "missing source" outweighed all other sources in the budget (Butler 2000). Agricultural use of MeBr, including soil fumigation, may be responsible for 3–10% of stratospheric ozone depletion (USDA 2001). The relative significance of each global source of MeBr, including that from agricultural uses, needs to be better quantified to assist in developing rational national and worldwide policy.

## 124.2 Egyptian Pharaohs and Biofumigation

The ancient Greeks called watercress; they believed it could brighten their intellect, hence their proverb "Eat watercress and get wit." Hippocrates, the father of medicine, is thought to have decided on the location for his first hospital because of its proximity to a stream so he could use only the freshest watercress to treat his patients. Philosopher and statesman Francis Bacon (1561–1626) claimed it could restore a youthful bloom to women. Romans and Anglo Saxons ate it to prevent baldness. The Egyptian Pharoahs served freshly squeezed watercress juice to their slaves each morning and afternoon in order to increase their productivity. We have to mention that the Egyptian Pharaohs kept their wheat and barley for many several years by mixing it with white mustard as antifungal and antimicrobial activities by the mechanism of its biofumigation power.

## 124.3 Conclusions and Future Research Work for Developing Countries

In conclusion, biofumigation using Brassica tissues or other sources of organic material appears as a promising strategy for the management of soil-borne diseases, pests and weeds especially in those developing countries. There are many benefits of amending soil with these organic matter include increase the soil fertility, enhance the soil suppressions against many plant pathogens and nematodes. Moreover, improvements in the soil nutrient status and water-holding capacity, and an increase in the presence and activity of beneficial soil microorganisms (biocontrol agents) including those that are antagonistic to both soil-borne plant pathogens and plant-parasitic nematodes as well. In addition, it may provide a use for agroindustrial and some kind of municipal "waste" products (Lazarovits et al. 2001).

The mechanisms of pest and pathogen control by biofumigation are still largely unknown and studied worldwide in different lab and research institutes. Although the production of biocidal gases is undoubtedly important, several researchers have indicated that other mechanisms are also likely to play an important role (Bending and Lincoln 1999; Potter et al. 1998). In fact, few studies have compared the efficacy of biofumigation under plastic to trap gases, and biofumigation without plastic. In one study, biofumigation with manure under plastic to control M. incognita in tomato only gave a slight reduction in root-galling indices compared to biofumigation without plastic, and M. incognita soil populations were controlled to very similar levels by both methods (Bello 1998).This can be managed and adapted in different developing countries instead of using Methyl Bromide and this technique is still cheap and eco-friendly, and can widespread in different regions worldwide. Researches on optimizing the methods to apply biofumigant materials under different soil types and climates in those developing countries are likely to enhance this strategy. Also, we have to develop or identify certain crop varieties with high biofumigant activity those are resistant, non-hosts, or trap crops for the locally occurring target nematodes and soil-borne plant pathogens are likely to enhance the potential of this strategy in different regions worldwide to be an eco-friendly management. We are planning to widespread this methodology of biofumigation by adding certain strategies like production suppressive compost that can contain a chitin and this will enhance the production of chitinolytic fungi and bacteria that can control the widespread of both the soil-borne plant pathogens and the target nematode in the same time. This we can call Double Target Control Strategy (DTCS). It is unlikely that biofumigation alone will provide sufficient or satisfied levels of nematode control over multiple seasons, but advantages include that this method is also useful to manage other soil-borne problems, and that it can easily be combined with other strategies such as soil solarization, production of different compost types like mentioned before and the use of resistant varieties.

## 124.4 Recent Training and Innovative Knowledge for the Developing Countries by the Technical Assistance with the UNEP

Introducing a new agricultural technology to farmers in the developing countries including Egypt requires a well coordinated research and development efforts through multidisciplinary approach. I mean by a multidisciplinary approach is to solve the problem of find out the new, safer, cheap, and feasible, with a subsidy program for the farmers in the developing countries like Egypt, and Africa countries. This will be done through problem solving approaches that involve drawing appropriately from multiple disciplines to redefine the Mt.Br contamination problems outside of normal boundaries and reach solutions based on a new understanding of complex situations. I invite the World society to start a global initiative to work together and to solve this problem with an efficient ways.

**Acknowledgments** I would like to thank Professor Douw Steyn, Atmospheric Science Department of Earth and Ocean Sciences, University of British Columbia for his kind support and sincere efforts to attend this International meeting in Italy. I appreciate all his assistance. Also, I would like to thank Dr. Silvia Trini Castelli, ISAC-CNR, UOS Torino, Corso Fiume 4, 10133-Torino, Italy for their support with Italian Embassy in Cairo.

## References

Andersen SO, Lee-Bapty S (1992) Technology and economic assessment of methyl bromide uses, alternatives and substitutes. In: Methyl bromide: its atmospheric science, technology and economics. United Nations Environment Programme, Nairobi, June 1992. Global Biogeochem Cycles 10:175–190

Bello A (1998) Biofumigation and integrated crop management. In: Bello A, González JA, Arias M, Rodríguez-Kábana R (eds) Alternatives to methyl bromide for the Southern European countries. Consejo Superior de Investigaciones Científicas, Direction General XI European Communities, Valencia, pp 99–126

Bello A, Arias M, López-Pérez JA, García-Álvarez A, Fresno J, Escuer M, Arcos SC, Lacasa A, Sanz R, Gómez P, Díez-Rojo MA, Piedra Buena A, Goitia C, de la Horra JL, Martínez C (1998) Biofumigation, fallow, and nematode management in vineyard replant. Nematropica 34(1)

Butler JH (1995) Methyl bromide under scrutiny. Nature 376:469–470

Chakrabarti B, Bell CH (1993) The methyl bromide issue. Chem Ind 24:992–995

Chakrabarti B, Wontner-Smith T, Bell CH (1995) Reducing methyl bromide emissions from soil fumigation in greenhouses. In: Proceedings of the annual international research conference on methyl bromide alternatives and emissions reductions, San Diego, 6–8 Nov 1995, Methyl bromide alternatives outreach, Fresno, pp 25-1–25-3

Eddleston ML, Szinicz EP, Buckley N (2002) Oximes in acute organophosphorus pesticide poisoning: a systematic review of clinical trials. Q J Med 95:275–283

Ferguson W, Padula A (1994) Economic effects of banning methyl bromide for soil fumigation. Agricultural Economic Report 677. USDA Economic Research Service, USDA, Washington, DC

Gary BD, Lincoln SD (1999) Inhibition of soil nitrifying bacteria communities and their activities by glucosinolate hydrolysis products. Soil Biol Biochem 32(8–9):1261–1269, 1 Aug 2000

Harvey SG, Hannahan HN, Sams CE (2002) Indian mustard and allyl isothiocyanate inhibit *Sclerotium rolfsii*. J Am Soc Hortic Sci 127:27–31

Lazarovits G, Tenuta M, Conn KL (2001) Organic amendments as a disease control strategy for soil borne diseases of high-value agricultural crops. Australas Plant Path 30(2):111–117

Lobert JM, Yvon-Lewis SA, Butler JH, Montzka SA, Myers RC (1997) Undersaturation of CH3Br in the Southern Ocean. Geophys Res Lett 24:171–172

NAPIAP (The National Agricultural Pesticide Impact Assessment Program) (1993) The biologic and economic assessment of methyl bromide. USDA-NAPIAP, Washington, DC

Noling JW, Gilreath JP (2000) Propargyl bromide and other fumigants for nematode control. In: USDA-ARS methyl bromide alternatives newsletter, Jan 2000. http://www.ars.gov/is/np/mba/jan00/nema.htm

Potter MJ, Davies KA, Rathjen AJ (1998) Suppressive impact of glucosinolates in Brassica vegetative tissues on root lesion nematodes (Pratylenchus neglectus). J Chem Ecol 24:67–80

UNEP (1995) Report of the methyl bromide technical option committee. UNEP, Kenya

UNEP (1998) Report of the methyl bromide technical option committee. UNEP, Kenya

United States Environmental Protection Agency (USEPA) (1993) Protection of stratospheric ozone. Fed Reg 58:15014–15049

United States Environmental Protection Agency (USEPA) (2002) The phase-out of methyl bromide. http:// www.epa.gov/spdpublic/mbr/

U.S. Department of Agriculture (USDA) (2001) Atmospheric impact of agricultural use of methyl bromide. Methyl Bromide Altern 7:1–2

Watson RT, Albritton DL, Andersen SO, Lee-Bapty S (1992) Methyl bromide: its atmospheric science, technology, and economics. United Nations Environment Programme, Ozone Secretariat, Nairobi

Wofsy SC, McElroy MB, Yung YL (1975) Chemistry of atmospheric bromine. Geophys Res Lett 2(6):215–218. CODEN: GPRLAJ; ISSN: 0094–8276

Yates SR, Gan J, Papiernik SK (2003) Environmental fate of methyl bromide as a soil fumigant. Rev Environ Contam Toxicol 177:45–122

Yvon-Lewis SA, Butler JH (1997) The potential effect of oceanic biological degradation on the lifetime of atmospheric CH3Br. Geophys Res Lett 24:1227–1230

# Author Index


**A**
Achilli, M., 133–136
Ainslie, B., 641–646
Aksoyoglu, S., 155–158
Alessandrini, S., 45–48
Alpert, P., 299–303, 599–603
Andersson, C., 627–633
Anfossi, D., 45–48
Anselmo, D., 591–596
Antonopoulos, S., 309–314
Appel, K.W., 227–230, 439–444, 505–510
Arnold, D., 269–272, 737–740
Arunachalam, S., 619–623, 663–667
Astitha, M., 359–364, 607–610
Aulinger, A., 533–537, 699–702
Austin, G.L., 285–288

**B**
Baek, B.H., 619–623, 663–667
Baklanov, A., 359–364
Balanzino, A., 293–296
Balk, T., 239–242, 359–364
Baltensperger, U., 155–158
Banzhaf, S., 193–197, 459–464
Bash, J., 169–173
Bassoukos, T., 239–242
Batchvarova, E., 499–502
Baxter, L., 741–744
Beauharnois, M., 411–415
Beaulieu, P.-A., 591–596
Becagli, S., 299–303
Bedogni, M., 133–136
Beevers, S., 199–202
Bélair, S., 93–96
Belayev, N.N., 88–90
Belda, M., 637–640
Benbouta, N., 93–96
Benedetti, A., 525–528
Benson, V., 213–218
Bergström, R., 627–629
Bermúdez, J.L., 275–278
Berrone, S., 729–732
Bertari, R., 133–136
Bewersdorff, I., 699–702
Bhave, P., 585–589
Bieser, J., 533–537
Biliaiev, M.M., 87–91
Binkowski, F., 175–178
Błaś, M., 279–283
Blewitt, D., 747–751
Blommaert, F., 147–151
Bloss, W.J., 63–67
Bodnar, M.Z., 69–72
Bommarito, C., 300–302
Borrego, C., 3–6, 161–166
Boucher, O., 525–528
Bourgouin, P., 93–96, 309–314
Boy, M., 359–364
Božnar, M.Z., 69–72, 543–545
Bozzano, R., 299–303
Brechler, J., 137–140
Briganti, G., 491–498
Bright, V.B., 63–67
Broekx, S., 565–568
Builtjes, P., 347–350, 459–464, 467–470, 675–678
Bullock, O.R. Jr., 175–178
Byun, D., 187–192, 341–345, 379–383

**C**
Cacciari, A., 107–110
Cai, X., 51–54, 63–67



D.G. Steyn and S. Trini Castelli (eds.), *Air Pollution Modeling and its Application XXI*, NATO Science for Peace and Security Series C: Environmental Security 4,
DOI 10.1007/978-94-007-1359-8, © Springer Science+Business Media B.V. 2012

Calori, G., 491–498
Canepa, E., 299–303
Cappelletti, A., 491–498
Carissimo, B., 39–43, 75–79
Carlton, A.G., 579–582
Carnevale, C., 107–110, 599–603, 693–696
Carvalho, A., 161–166
Casares, J.J., 161–166, 275–278, 305–308, 407–410
Cassiani, M., 98–100, 687–691
Castelli, S.T., 9–13
Cats, G., 119–122
Causà, M., 293–296
Ceburnis, D., 525–528
Celis, D., 147–151
Chai, T., 187–192
Chang, J., 479–482
Chemel, C., 427–430
Chen, J., 733–736
Chiapello, I., 525–528
Civerolo, K., 519–523
Claeys, N., 205–209
Colle, B., 411–415
Cooter, E., 169–173, 213–218
Corti, A., 453–457
Cosemans, G., 81–85, 147–151
Cousineau, S., 733–736
Crooks, J., 681–685, 711–715
Croteau, G., 309–314
Cucurull, L., 391–396
Curci, G., 397–401, 559–562, 599–603
Curier, L., 221–225
Cuvelier, C., 485–488
Czader, B., 341–345

**D**
Daggupaty, S.M., 257–260
D'Allura, A., 199–202
Davidson, P., 379–383
Davignon, D., 733–736
Davis, N., 619–623
De Backer, H., 315–319, 525–528
Deckmyn, A., 315–319
Delcloo, A.W., 315–319, 525–528
de Leeuw, F., 687–691
De Maerschalck, B., 15–19, 27–31
de Meij, A., 485–488, 607–610
Demerjian, K.L., 411–415
Denby, B.R., 687–691
De Nocker, L., 565–568
De Paepe, B., 525–528
Derimian, Y., 525–528
de Smet, P., 687–691
Deutsch, F., 205–209, 565–568
Dewitte, S., 525–528
Dickerson, P., 379–383
DiMego, G., 391–396
Di Nicolantonio, W., 107–110
Dios, M., 275–278, 305–308
Dirks, K.N., 285–288
di Sarra, A., 299–303
D'Isidoro, M., 373–377
Dodson, R.E., 619–623
Doraiswamy, P., 411–415
Dore, A.J., 279–283, 427–430, 669–673
Douros, I., 21–24
Dragosits, U., 669–673
Draxler, R., 379–383
Duhamel, A., 733–736
Dupont, E., 39–43

**E**
Eben, K., 359–364
Eder, B., 439–444, 505–510
Ek, N., 93–96
Elangasinghe, M.A., 285–288
Elbern, H., 161–166
Engardt, M., 627–633
Epitropou, V., 239–242
Erickson, M., 411–415
Ermakova, T., 385–389
Eskes, H., 221–225, 347–350

**F**
Ferrero, E., 45–48, 97–100, 293–296
Fierens, F., 205–209
Finardi, S., 199–202, 289–291, 321–324, 359–364, 491–498
Finzi, G., 107–110, 599–603, 693–696
Fisher, B., 427–430
Flentje, H., 525–528
Flossmann, A.I., 549–556
Foley, K.M., 447–450
Foret, G., 315–319
Francis, X.V., 427–430
Freitas, S.R., 251–255
Fuka, V., 137–140

**G**
Gadzhev, G.K., 263–267
Galmarini, S., 419–425, 505–510
Ganev, K.G., 263–267

Garbero, V., 729–732
Garcia, V.C., 353–357, 711–715
Gauger, T., 467–470
Gauthier, J.-P., 93–96
Gauthier, N., 93–96
Geertsema, G., 119–122
Gégo, E.L., 353–357, 711–715
Genikhovich, E., 529–531
Georgieva, E., 485–488
Georgiev, G.J., 263–267
Giambini, P., 453–457
Gilbert, S., 733–736
Gilliam, R., 175–178
Giostra, U., 98–100
Gong, S., 513–517, 591–596
Gong, W., 513–517, 591–596
Grašič, B., 69–72, 543–545
Gravel, S., 513–517
Griffiths, S., 427–430
Gryning, S.-E., 499–502
Gufler, K., 737–740
Guler, M., 103–106

**H**
Haeni, C., 155–158
Hakkarainen, J., 385–389
Halenka, T., 637–640
Hall, J., 669–673
Hallsworth, S., 669–673
Halmer, G., 21–24
Hama, T., 647–651, 723–727
Hamdi, R., 315–319
Hanna, S.R., 479–482, 747–751
Hao, W., 411–415, 519–523
Hayman, G.D., 427–430
Hendriks, E., 467–470
He, Q., 213–218
Hirtl, M., 359–364
Hogrefe, C., 353–357, 411–415, 519–523
Hogue, R., 93–96
Holly, M., 93–96
Honoré, C., 199–202, 367–370
Horálek, J., 687–691
Houseman, A.E., 619–623
Huneeus, N., 525–528
Hu, R.-M., 427–430
Huszar, P., 637–640

**I**
Im, U., 103–106
İncecik, S., 103–106, 119–122
Ionov, D., 245–249
Isakov, V., 681–685, 717–722, 741–744

**J**
Jackson, P., 641–646
Jaffe, D., 747–751
Jakobs, H., 359–364
Jaňour, Z., 113–118
Janssen, S., 15–19, 27–31, 147–151, 205–209
Jing, Q., 33–37
Johnson, M., 717–722
Jörss, W., 675–678
José, R.S., 359–364
Jurčáková, K., 113–118

**K**
Kaasik, M., 539–542
Kacenelenbogen, M., 525–528
Kalenderski, S.D., 333–338
Kallos, G., 327–332, 359–364, 571–577
Kang, D., 447–450
Karatzas, K., 239–242, 359–364
Kawashima, S., 647–651, 723–727
Kazakevitch, M.I., 88–90
Keller, J., 155–158
Kellnerová, R., 113–118
Kerschbaumer, A., 459–464, 467–470
Kewada, P., 681–685
Kharytonov, M.M., 87–91
Khrutch, V.K., 88–90
Kim, H.-C., 187–192, 341–345
Kim, S., 341–345
Kindap, T., 103–106
Kinne, S., 525–528
Kioutsioukis, I., 359–364
Kishcha, P., 299–303, 599–603
Kitada, T., 233–238
Klein, T., 359–364
Knoth, O., 473–476
Kondragunta, S., 341–345
Kromp-Kolb, H., 737–740
Kromp, W., 737–740
Kryza, M., 279–283, 669–673
Kuenen, J., 199–202
Ku, J.-Y., 411–415, 519–523
Kukačka, L., 113–118
Kukkonen, J., 239–242, 359–364
Kushta, J., 327–332, 571–577

**L**
Langner, J., 627–633
Lazovic, N., 729–732
Lee, D.-G., 341–345
Lee, P., 187–192
Lefebre, F., 205–209
Lefebvre, W., 81–85, 147–151, 205–209
Lehtinen, K.E.J., 359–364
Lelieveld, J., 607–610
Léon, J.-F., 525–528
Leroux, A., 93–96
Leroy, D., 550–552
Levitin, Y., 125–130
Levy, J.I., 619–623, 663–667
Lien, F.-S., 93–96
Lin, S., 711–715
Longo, K.M., 251–255
Loot, A., 539–542

**M**
Maiheu, B., 15–19, 27–31
Ma, J., 257–260
Makarova, M., 245–249
Makar, P.A., 513–517, 591–596
Malherbe, L., 367–370
Manders, A., 193–197
Mangold, A., 525–528
Manikin, G., 391–396
Markakis, K., 103–106
Marri, P., 491–498
Martins, H., 3–6, 161–166
Mathur, R., 175–178, 227–230, 447–450, 505–510, 579–582
Matthias, V., 499–502, 533–537, 699–702
Maurizi, A., 373–377
McKendry, I., 641–646
McQueen, J., 187–192, 379–383, 391–396
Meagher, J., 379–383
Melas, D., 103–106
Meleux, F., 367–370
Ménard, S., 591–596
Ménard, V., 733–736
Mensink, C., 15–19, 147–151
Mercier, G., 93–96
Michiels, H., 565–568
Milliez, M., 39–43, 75–79
Miloshev, N.G., 263–267
Miranda, A.I., 3–6, 161–166, 359–364
Mircea, M., 289–291, 321–324, 491–498
Mlakar, P., 69–72, 543–545
Mobley, D., 585–589, 741–744
Montalto, A., 729–732
Monteiro, A., 161–166, 359–364
Montpetit, J., 309–314
Mooney, C.J., 591–596
Moran, M.D., 513–517, 591–596
Morcrette, J.-J., 525–528
Mortarini, L., 97–100
Moussiopoulos, N., 21–24
Mraz, G., 737–740
Mulholland, J., 681–685
Musson-Genon, L., 39–43, 75–79

**N**
Nanni, A., 285–288
Napelenok, S.L., 447–450
Ngan, F., 187–192, 341–345
Nickovic, S., 299–303
Nikolova, I., 27–31
Nochvai, V., 705–708

**O**
Oderbolz, D., 155–158
Odman, M.T., 103–106
O'Dowd, C., 525–528
Ots, R., 539–542
Özkaynak, H., 681–685, 717–722, 741–744

**P**
Paales, M., 433–437
Pabla, B., 513–517
Pace, G., 491–498
Pace, T., 585–589
Panis, L.I., 565–568
Pankratz, D., 33–37
Pavlova, T., 529–531
Pavlovic, R., 591–596, 733–736
Pederzoli, A., 289–291, 321–324, 491–498
Peelaerts, W., 205–209
Pensieri, S., 299–303
Pernigotti, D., 485–488
Perrussel, O., 199–202
Peuch, V.-H., 359–364
Piazzola, J., 613–617
Pierce, B., 341–345
Pierce, T., 439–444, 447–450, 505–510, 585–589
Pirovano, G., 293–296
Pisoni, E., 107–110, 599–603, 693–696
Pleim, J., 169–173, 175–178, 579–582
Podrascanin, Z.M., 143–146
Porter, P.S., 353–357, 519–523, 747–751

Potempski, S., 419–425
Pouliot, G., 505–510, 585–589
Poupkou, A., 103–106, 359–364
Pournazeri, S., 33–37
Pozzer, A., 607–610
Prank, M., 386, 433–437
Prevot, A.S.H., 155–158
Princevac, M., 33–37
Prodanova, M., 263–267

**Q**
Quante, M., 499–502, 533–537, 699–702
Qu, Y., 75–79

**R**
Racine, J., 733–736
Radice, P., 199–202
Rajkovic, B., 143–146
Rakitin, A., 245–249
Ran, L., 213–218
Rao, S.T., 353–357, 447–450, 505–510, 519–523, 579–582, 711–715
Rappenglueck, B., 341–345
Reimer, E., 359–364, 459–464
Reisin, T.G., 9–13
Reiter, L.W., 655–661
Renner, E., 181–184, 473–476
Reuten, C., 641–646
Riva, G.M., 293–296
Robarge, W.P., 171–173
Rodríguez, A., 161–166, 275–278, 305–308, 407–410
Rompaey, H.V., 147–151
Roselle, S., 175–178, 505–510, 579–582
Russo, F., 373–377

**S**
Saavedra, S., 161–166, 275–278, 305–308, 407–410
Salem, M.F.M, 753–758
Salizzoni, P., 453–457, 729–732
Samaali, M., 733–736
Sändig, B., 181–184
Sarnat, J.,681–685
Sarnat, S.E., 681–685
Sarwar, G., 227–230
Sassi, M., 591–596, 733–736
Sato, K., 647–651
Sauter, F., 193–197
Saylor, R., 187–192
Schaap, M., 193–197, 221–225, 347–350, 359–364, 459–464
Schere, K., 227–230, 505–510
Schicker, I., 269–272
Schroedner, R., 473–476
Schultz, D.M., 359–364
Schulz, M., 525–528
Segers, A., 347–350
Seibert, P., 269–272, 737–740
Sferlazzo, D., 300–302
Shankar, U., 663–667
Shao, Y., 579–582
Sholly, S, 737–740
Silibello, C., 491–498
Simon, H., 585–589
Singhal, N., 285–288
Singh, V., 107–110
Sistla, G., 411–415, 519–523
Sleeuwaert, F., 147–151
Smalla, A., 473–476
Smith, R., 669–673
Soares, J., 385–389
Sofiev, M., 359–364, 385–389, 403–406, 433–437
Sokhi, R.S., 359–364, 427–430
Solomos, S., 327–332, 571–577
Songeur, C., 367–370
Soto, B., 275–278
Souders, M., 411–415
Soulhac, L., 453–457, 729–732
Souto, J.A., 161–166, 275–278, 305–308, 407–410
Stajner, I., 187–192, 379–383
Starobinets, B., 299–303
Stein, A., 187–192
Stern, R., 459–464, 675–678
Steyn, D.G., 333–338, 641–646
Stoll, J., 473–476
Streets, D., 175–178
Stroud, C., 513–517, 591–596
Strunk, A., 161–166
Sutter, P., 737–740
Sutton, M., 669–673
Sutton, P., 427–430
Swart, D., 221–225, 347–350
Syrakov, D.E., 263–267
Szykman, J.J., 353–357

**T**
Tampieri, F., 373–377
Tang, S., 669–673
Tang, Y., 187–192

Tarvainen, V., 359–364
Tassone, C., 391–396
Tayanc, M., 103–106
Tchepel, O., 161–166
Tedeschi, G., 613–617
Theloke, J., 199–202, 675–678
Thunis, P., 485–488
Timmermans, R., 221–225, 347–350
Tinarelli, G., 9–13
Todorova, A.D., 263–267
Tong, D., 187–192, 585–589
Topçu, S., 103–106
Toros, H., 119–122
Torres, C., 275–278, 305–308
Touma, J., 681–685, 717–722
Trudel, S., 93–96
Tsegas, G., 21–24
Tsidulko, M., 187–192, 391–396
Tuccella, P., 559–562

**U**
Udisti, R., 299–303
Ulke, A.G., 251–255
Ung, A., 367–370
Uzbasich, M., 199–202

**V**
Valari, M., 681–685
Valencia, A., 619–623
van der Gon, H.D., 199–202
van der Swaluw, E., 193–197, 459–464
van de Vel, K., 147–151
Van Esch, L., 565–568
Vankerkom, J., 15–19, 27–31, 205–209
Van Langenhove, H., 315–319
Van Looy, S., 205–209
Van Mierlo, T., 205–209
Veldeman, N., 205–209
Venkatram, A., 33–37
Vieno, M., 669–673
Vincent, K.J., 427–430
Vira, J., 403–406, 433–437
Visconti, G., 559–562
Visschedijk, A., 199–202
Vitali, L., 491–498
Volta, M., 107–110, 599–603, 693–696
Vos, P., 27–31

**W**
Wagner, F., 693–696
Walker, J., 169–173
Watkins, T., 741–744
Weil, J.C., 57–60
Wenisch, A., 737–740
Werner, M., 279–283, 669–673
Wobrock, W., 549–556
Wolke, R., 473–476
Wong, D., 175–178, 579–582
Woody, M., 663–667
Wright, R.D., 427–430

**Y**
Yang, D., 619–623
Yee, E., 93–96
Yenigün, O., 103–106
Yu, S., 579–582

**Z**
Zaganescu, C., 93–96
Zaidi, H., 39–43
Zalewsky, E.E., 519–523
Zanini, G., 289–291, 321–324, 491–498
Zhang, J., 513–517, 591–596
Zhang, X., 39–43
Zhu, Y., 391–396
Ziv, A., 529–531